R-08-56

Compilation of data used for the analysis of the geological and hydrogeological DFN models

Site descriptive modelling SDM-Site Laxemar

Jan Hermanson, Aaron Fox, Johan Öhman
Golder Associates

Ingvar Rhén, SWECO

August 2008

Svensk Kärnbränslehantering AB
Swedish Nuclear Fuel
and Waste Management Co
Box 250, SE-101 24 Stockholm
Tel +46 8 459 84 00

ISSN 1402-3091
SKB Rapport R-08-56

Compilation of data used for the analysis of the geological and hydrogeological DFN models

Site descriptive modelling SDM-Site Laxemar

Jan Hermanson, Aaron Fox, Johan Öhman
Golder Associates

Ingvar Rhén, SWECO

August 2008

Keywords: Flow log, Fracture, Fracture domain, Hydraulic, Outcrop.

Appendices 1, 3–5, 7 are available on the enclosed CD.

Abstract

This report provides an overview and compilation of the various data that constitutes the basis for construction of the geological and hydrogeological discrete feature network (DFN) models as part of model version SDM-Site Laxemar. This includes a review of fracture data in boreholes and in outcrop. Furthermore, the basis for the construction of limeament maps is given as well as a review of the hydraulic test data from cored and percussion-drilled boreholes. An emphasis is put on graphical representation of borehole logs in the form of composites of geological, hydrogeological and even hydrogeochemical data in the case of cored boreholes. One major contribution is a compilation of characteristics of minor local deformation zones (MDZs) identified in cored boreholes. Basic orientation data and fracture intensity data are presented as a function of depth for individual boreholes. The coupling between hydrogological data and geological data is further refined in plots of Posiva flow log (PFL) data vs. geological single hole interpretation data.

Sammanfattning

Denna rapport ger en överblick och sammanställning av olika typer av data som utgör basen för byggandet av geologiska och hydrogeologiska diskreta spricknätverksmodeller (DFN) inom ramen för modellversion SDM-Site Laxemar. Detta inkluderar en sammanställning av sprickdata karterade i borrhål och i häll. Vidare presenteras underlaget för framtagandet av lineamentskartor liksom en genomgång av resultat från hydrauliska tester genomförda i kärnborrhål och i hammarborrade borrhål. En tyngdpunkt är lagd på den grafiska återgivningen av borrhålsdata i form av kompositplottar av geologisk, hydrogeologisk, och även hydrogeokemisk information i fallet med kärnborrhål. Ett viktigt bidrag är en redovisning av karakteristik hos tolkade mindre lokala deformationszoner (MDZs) tolkade i kärnborrhål. Grundläggande data på sprickorienteringar och sprickintensitet redovisas som funktion av djupet. Kopplingen mellan hydrogeologiska och geologiska data förfinas ytterligare genom plottar där data från Posiva flödeslogg (PFL) korsplottas mot data från den geologiska enhålstolkningen.

Contents

1 Introduction

The Swedish Nuclear Fuel and Waste Management Company (SKB) is undertaking site characterization at two different locations, Forsmark and Laxemar, with the objective of finding a site for a repository for spent nuclear fuel. The site characterization program is built upon the development of site descriptive models (SDM) that utilize data available up to the data freeze date.

The geological model is composed of three main components: the rock domain model, the deformation zone model, and the geological DFN model. The deformation zone model aims to define the larger structural features in the model volume, while the aim of the geological DFN model is to provide a statistical description of the features below the resolution threshold for the definition of deterministic deformation zones and fractures. This involves an important interaction between the models, as primary data need to be addressed in the appropriate manner. Moreover, other disciplines are dependent on the assumptions made in the overall geological modelling work.

Similarly, an important component of the hydrogeological modelling is the hydraulic DFN model, which constitutes a foundation for the ensuing hydrogeological flow modelling. Furthermore, the hydraulic DFN model is an important basis for assessments of bedrock solute transport, and also for purposes of designing the layout of the repository.

Previous experience of the modelling process shows that the input data used for the geological and hydraulic DFN model are of vital importance in the interaction between downstream modellers such as hydrogeology/rock mechanics and transport/design. To further simplify the interaction process between the various disciplines involved it was decided to compile a description of the input data into this separate document, which acts a basis for the SDM-Site Laxemar geological DFN (GeoDFN) and hydraulic DFN (HydroDFN) models and associated reports.

2 Objective and scope

The main objective of the data compilation report is to compile and present the geologic and hydraulic data that will be used in the analysis and parameterisation of the SDM Laxemar discrete-fracture network models. A secondary objective is to present an overview of the primary data (fractures, rock types, faults, and model area hydraulic features) that are available to model teams for model version SDM-Site Laxemar.

The intention is that the data compilation report (DCR) will present the data that will be used in the development of the geological and hydraulic DFN models in a clear and concise format, such that reviewers and model users have a useful reference with which to evaluate the discipline-specific model reports. The DCR will present data and basic descriptive statistics for data sources available up to the data freeze date for model version SDM-Site Laxemar.

The report is written in support of the SDM-Site Laxemar DFN modelling and as such contains a limited amount of data analyses. Hence, the geological DFN modelling teams will base their models on this set of data for their analysis and presentation of DFN parameters. However, unlike the modelling process employed in Forsmark, a fracture domain concept will not be presented as part of this document and prior to the analysis of fracture statistics. The fracture domains at Laxemar will be presented as a possible component of the SDM-Site Laxemar geological DFN in that method-specific report /La Pointe et al. 2008/.

No geological DFN modelling work was performed during modelling stage 2.1 /SKB 2006b/. In the SDM-Site Laxemar DFN models, all the Laxemar data available from previous data freezes will be incorporated in the modelling process. The original intention was that no data made available after the data freeze Laxemar 2.3 (August 31, 2007) were to be used. However, in several cases, updated interim models (RD, DZ) necessary for DFN parameterisation that arrived after data freeze Laxemar 2.3 were used. The rationale behind this decision is presented in Chapter 3.

NB. Data from borehole KLX27A became available after data freeze Laxemar 2.3 and has been used solely in the ensuing RD and DZ modelling, but not in the GeoDFN and HydroDFN modelling. Included here only for reasons of completeness.

2.1 Definitions

The following definitions are terms that are crucial to geological modelling at Laxemar. The definitions below are based on the guidelines provided in /Munier and Hermanson 2001/ and /Munier et al. 2003/. The general terms used in these previous reports have been updated to better reflect the site-specific geologic environment at Laxemar and the needs of other scientific disciplines for site modelling.

Rock unit (RU)

A rock unit is defined primarily on the basis of the composition, grain size and inferred relative age of the dominant rock type. Other geological features including the degree of bedrock homogeneity, the degree and style of ductile deformation, the occurrence of early-stage alteration (albitisation) that affects the composition of the rock and anomalous fracture frequency also help define rock units. Both dominant rock type and subordinate rock types are defined for the rock units. The term rock unit is used in the bedrock mapping work at the surface (2D) and in conjunction with the single-hole interpretation work (essentially 1D). In the latter work, rock units are referred to as RUxx, where the name of the rock unit is coupled to a single borehole. Thus, there is no unique name for the rock units valid throughout the site.

Rock domain (RD)

A rock domain refers to a rock volume in which rock units that show specifically similar composition, grain size, degree of bedrock homogeneity, and degree and style of ductile deformation have been combined and distinguished from each other. The occurrence of early-stage alteration (albitisation) is also used as a help to distinguish rock domains. The term rock domain is used in the 3D geometric modelling work. The different rock domains at Laxemar are referred to as RSMxxx. The recognition of rock domains as defined here aims primarily to meet the needs of thermal modelling and rock mechanics modelling.

Deformation zone (DZ)

A deformation zone is a general term that refers to an essentially 2D structure along which there is a concentration of brittle, ductile or combined brittle and ductile deformation. The term fracture zone is used to denote a brittle deformation zone without any specification whether there has or has not been a shear sense of movement along the zone. A fracture zone that shows a shear sense of movement is referred to as a fault zone. In the single-hole interpretation work, deformation zones are referred to as DZxx, where the name is coupled to a single borehole.

In accordance with the methodology adopted by SKB for single-hole interpretation work, which is also implicit in the methodology for geological modelling /Munier et al. 2003, p. 37/, each deformation zone identified during the single-hole interpretation is referred to as a *possible* deformation zone. This approach has been adopted to permit alternative interpretations, for example that concentrations of fractures are clusters related to a particular lithology rather than to previously unmapped (minor) deformation zones.

Table 2-1 presents a terminology for brittle structures based on trace length and thickness /Andersson et al. 2000/. The borders between the different structures are only approximately located. The estimated length of a zone takes account of the continuation of a zone outside the model volumes. Furthermore, the total length of zones, which consist of different segments or contain splays or attached branches, is accounted for in the classification of the zone according to length.

Based on the scale of the structure and bearing in mind the resolution scale of the current modelling work, a distinction is made between:

- *Deformation zones longer than 1,000 m*, are modelled deterministically and are included in the deformation zone block models. The letter prefixes NS, NE, EW and NW provide an indication of the strike of the steeply dipping zones. They are used as simple guidelines without any coupling to the dip of the zones, i.e. they do not follow the right-hand-rule. Deformation zones recognized in the single-hole interpretation that have an inferred thickness greater than 10 m, but have not been linked to other features such as surface lineaments or to other borehole intercepts, have been modelled as circular disks. The disc geometry has a standard 564 m radius based on an equivalent area to a 1,000 m × 1,000 m square and an applied inferred true thickness and orientation. This series of modelled zones have been named following the original ESHI source data, namely borehole and deformation zone number from the ESHI to facilitate traceability KLX*xx*_DZ*xx*.
- Minor deformation zones (MDZ), which have been recognized in the single-hole interpretation and have an inferred true thickness less than 10 m, but have not been directly linked to larger zones treated as minor deformation zones, are included in the stochastic DFN modelling.

The term deformation zone is used at all stages in the geological work − bedrock surface mapping, single-hole interpretation and 3D modelling.

Table 2-1. Terminology and geometrical description of the brittle structures in the bedrock based on /Andersson et al. 2000/. The boundaries between the different structures are approximate.

Terminology	Length	Thickness	Geometrical description
Regional deformation zone	> 10 km	> 100 m	Deterministic
Local major deformation zone	1 km–10 km	5 m–100 m	Deterministic
Local minor deformation zone	10 m–1 km	0.1–5 m	Stochastic
Fracture	< 10 m	< 0.1 m	Stochastic

Fracture domain (FD)

A fracture domain refers to a rock volume outside deformation zones in which rock units show similar fracture characteristics. Fracture domains at Laxemar are defined on the basis of the single-hole interpretation and its modifications and extensions.

The term fracture domain is used in the first instance as a basis for the discrete fracture network modelling work (geological DFN). The different fracture domains at Laxemar are referred to as FSM_XXXXX. The recognition of fracture domains as defined here is also of relevance to colleagues working in the disciplines of hydrogeology, hydrogeochemistry and rock mechanics.

The fracture data associated with deformation zones (either the regional DZ simulated deterministically or the MDZ simulated stochastically) are excluded from the fracture domains for the purpose of initial assessment of fracture domain characteristics (e.g. relative fracture intensity). In the ensuing geological DFN analysis the minor local deformation zones are reintroduced, but are represented by a single fracture.

The full description of the identification of fracture domains at Laxemar and their implementation in the geological DFN modelling is given in /La Pointe et al. 2008/.

Discrete fracture network (geological DFN)

A discrete fracture network model or geological DFN involves a description of the fracturing in the bedrock on the basis of a statistical model, which provides geometries, directions and spatial distributions for the fractures within defined fracture domains.

2.2 Model volumes

Regional model volume for deterministic modelling

The (Simpevarp) regional model area at the ground surface that is used for the model version SDM-Site Laxemar is shown in Figure 2-1. This area extends downwards to an elevation of –2,100 m and up to +100 m relative to mean sea level. This volume remains unchanged and identical to that used in model version 0 /SKB 2002/. The coordinates below (eastings, northings; in metres) define the four corners of the regional model area in the RT90 (RAK) coordinate system:

- SW corner – (1539000, 6360000)
- NW corner – (1539000, 6373000)
- SE corner – (1560000, 6373000)
- NE corner – (1560000, 6360000).

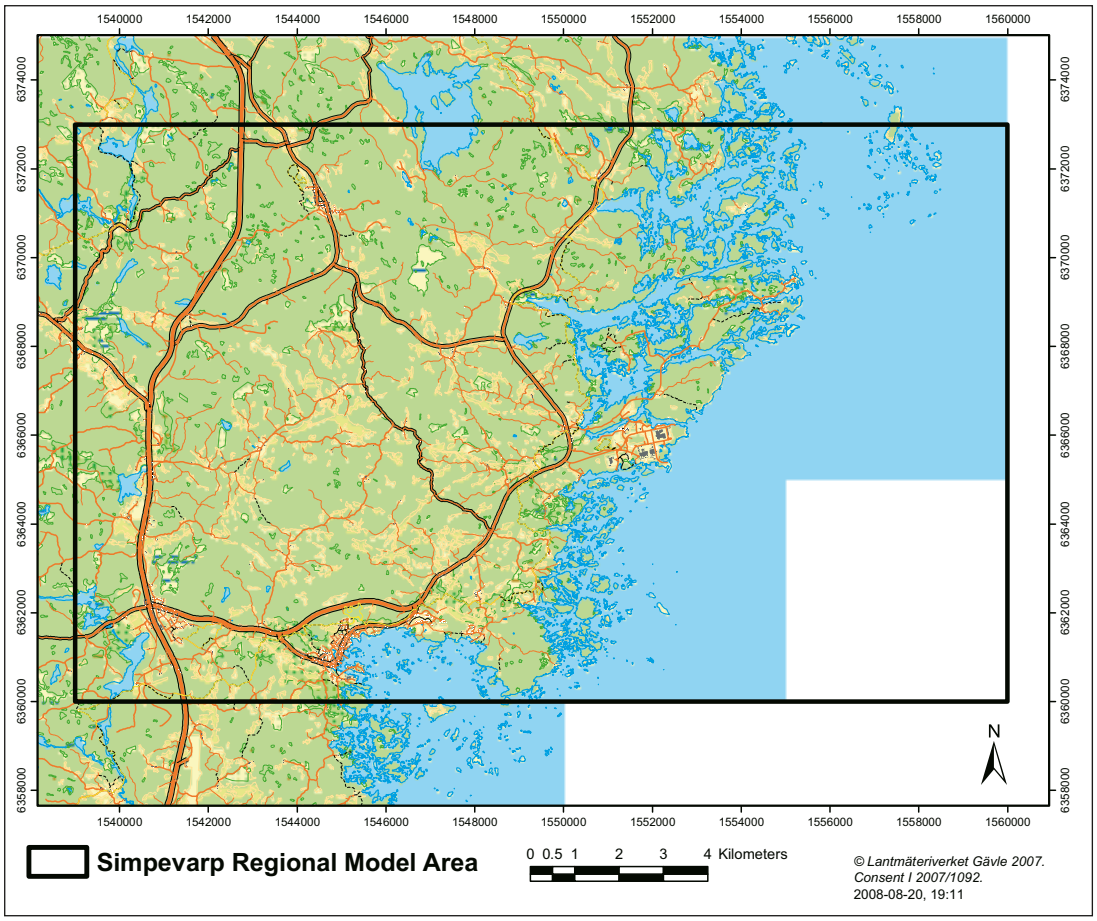

Figure 2-1. *Definition of the Simpevarp regional model area which is employed in the SDM-Site Laxemar modelling.*

Local model volume for deterministic modelling

The local model volume for SDM-Site Laxemar, cf. Figure 2-2, is focused on the Laxemar subarea, and particularly on the southern and south-western parts to which the investigations were focused during recent site investigations. The local-scale models of rock domains and deformation zones are integrated (at the boundaries) with those of the regional scale model. The SDM-Site Laxemar local scale model area has been extended southwards compared to model version 2.1 to incorporate a greater volume of the quartz monzodiorite. The coordinates for the SDM-Site Laxemar local model area are:

- 1546150, 6368200 (unchanged from Laxemar model stage 2.1)
- 1550390, 6368200 (unchanged from Laxemar model stage 2.1)
- 1546150, 6364250 (new southern boundary)
- 1550390, 6364250 (new southern boundary).

The geological SDM-Site DFN model will be established only within the local model area boundary.

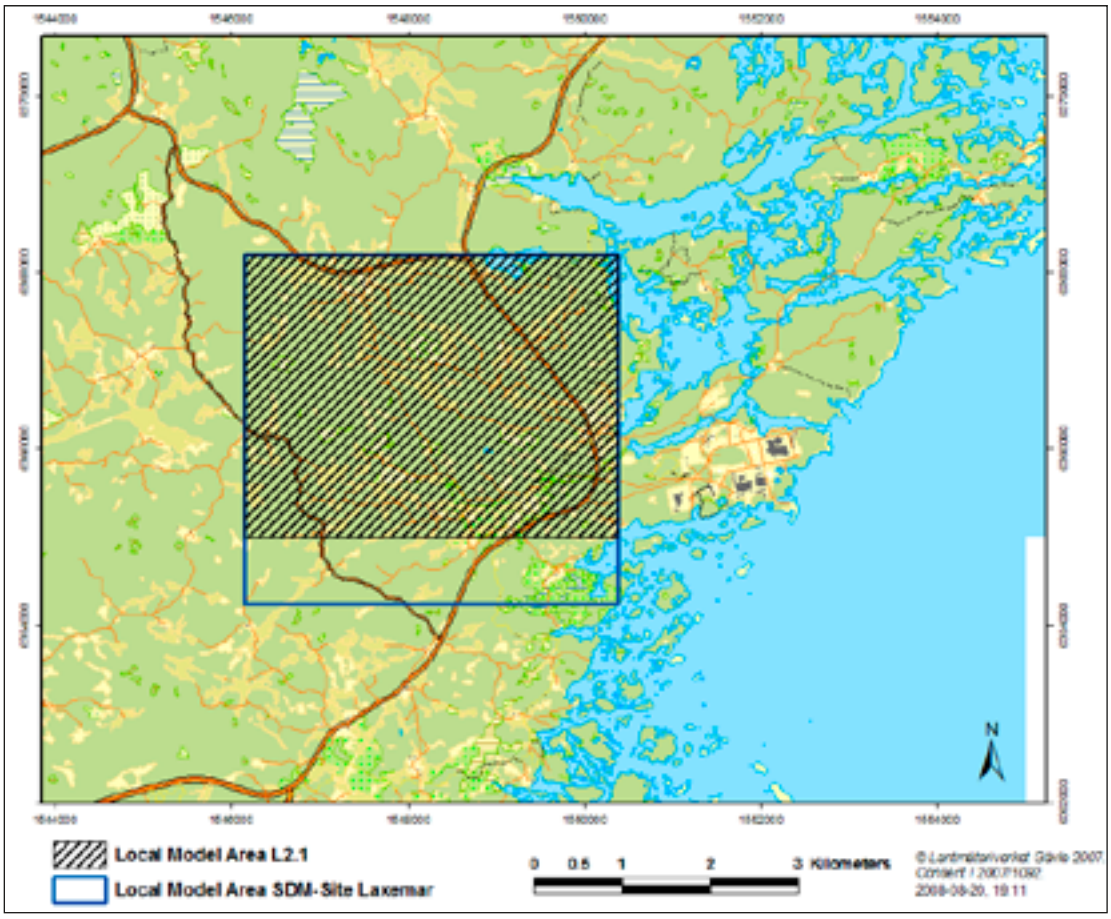

Figure 2-2. *Local model area used in the Geological Laxemar SDM Site models.*

3 Available primary data

3.1 Input data

The DFN modelling work is conducted on quality-checked data from Laxemar that are stored in the SKB database SICADA and the SKB Geographic Information System spatial database (SDE) at the date of data freeze Laxemar 2.3 (August 31, 2007).

However, during the autumn of 2007, updates to single-hole interpretations (SHI) and the deformation zone model were performed after the specified data freeze date for the SDM-Site Laxemar modelling. Both data elements (SHIs and the DZ model) are integral input data in the DFN analyses; the updates could not have been excluded from the DFN analysis without having a detrimental effect on the site descriptive modelling process.

In order to perform the DFN analysis on schedule, using a clearly defined data set, while still incorporating the updated SHI and DZ model results, a new fixed date for data delivery to the DFN analysis was established (October 18, 2007). This date coincides with the first interim delivery of the SDM Site Laxemar deformation zone model. Since this date, new updates to the deformation zone model have been presented, but this information has not entered into the DFN analysis.

Due to the inherent lower quality of information about fractures available in percussion-drilled boreholes, the geological DFN analysis is focused on data collected from cored boreholes. Data from percussion boreholes have mainly been used by the Geology team to identify of rock units and deformation zones,

3.1.1 Geology

The geological DFN analysis focuses on fracture data from surface and subsurface investigations. However, as the DFN is an integral part of the whole geological model, geological data that help build the Rock Domain model and the Deformation Zone model are also used in the DFN analysis as background information (primarily in the identification and delineation of fracture domains). However, this report only contains data that are intended as input to the calculation of geological DFN parameters as well as selected information used in the hydro DFN parameterization. Geological information available to the DFN model teams include:

- Surface data, including the fractures mapped in detail on various outcrops across the Laxemar local model area, are used primarily in the development of fracture orientation and size models. Surface fracture data are also used in conjunction with cored borehole fracture records to delineate fracture domains (FSMs), to assess the spatial distribution of fractures at small (5–10 m scales), and to determine the size-intensity scaling properties of fractures within the local model area. Surface data sources are described in detail in Chapter 4.
- Fracture and lithology data from cored boreholes are used primarily in the construction of the fracture orientation, intensity, scaling, and spatial location models. Cored borehole fracture data, especially fracture frequency and orientation, serves also as key indicators of potential fracture domain boundaries or transitions. More than 20 km of cored boreholes have been drilled in the Laxemar subarea, of which 18 km have been logged through both detailed core mapping (Boremap) and borehole televiewer (BIPS). A composite log of Boremap/BIPS data, extended single-hole interpretations, Posiva flow log anomaly maps, injection tests, water chemistry and packer positions for all cored boreholes up until Laxemar data freeze 2.3 are presented in Appendix 2 (the corresponding compilation for percussion boreholes is provided in Appendix 6). A brief summary, along with basic descriptive statistics, is presented in Chapter 5.

- Linked lineaments derived from both regional geophysics (airborne gravity, magnetic, electrical, LIDAR and coordinated lineaments) and local (high-resolution ground magnetic lineaments) are used as components in the coupled size-intensity DFN models. Specifically, this data set is used, along with outcrop fracture data, to establish the scaling exponent for a power law (Pareto) size distribution. Linked lineament data are presented in Chapter 6.
- Fracture data collected from the walls of the access tunnel of the Äspö Hard Rock Laboratory will not be used in the direct parameterisation, neither the hydraulic nor the geologic DFN models. The Äspö HRL exists in a rock volume that is both compositionally different and spatially isolated (by the Äspö shear zone) from the Laxemar subarea. However, it is possible that Äspo data may be used in verification simulations or model benchmarking. Therefore it has been included in the DCR. Äspö tunnel data are presented in Section 5.3.

Data from the percussion-drilled boreholes have primarily been used in the interpretation of rock units and deformation zones in the single-hole interpretations, in the construction of the rock domain (RD) models, and as additional evidence of the existence of a deterministically-modelled deformation zone. Percussion borehole data will not used directly in the SDM Laxemar DFN models. Therefore they are not included in this data compilation. However, the associated WellCAD logs for percussion boreholes are provided in Appendix 6 for reasons of completeness.

The sources and delivery date for the used geological data are given in Table 3-1.

3.1.2 Hydrogeology

The compilation below, and account provided in Chapter 7, does not represent an exhaustive list of all hydraulic data that are available for the model version SDM-Site Laxemar, but lists the main hydrogeological data that are to be used in developing the HydroDFN model

The following sources of data are available:

- PFL-f (Posiva Flow Log, feature) properties in relation to the geological single hole interpretation.
- Over view of hydraulic single hole tests in cored and percussion boreholes.

3.2 Errors and omissions in primary data

The basic assumption for all site characterisation modelling efforts is that primary data extracted from official SKB sources (RVS, SICADA, and SDE-GIS) have been quality-checked, validated, and approved for use. However, it is possible that additional errors or oversights may be noted during the modelling work. In that specific case, model teams are obligated to formally report any errors detected. Error reporting should be conducted in accordance with the steering document SDP-517, version 3.0, "*Hantering av fel i primärdata*", and submitted electronically to data.error@skb.se. The error(s) must be documented in a special error report; the form for handling data is presented as Appendix 1.

In the case of serious errors and omissions, a formal discrepancy report, constructed according to procedure SD-006, should be submitted. Modellers are also encouraged to check the official SICADA error list on a regular basis.

Table 3-1. Geological data sources in SICADA and SDE-GIS.

Data type	SICADA/SDE table/ filename	SICADA/SDE delivery reference	Date	Comment
Cored borehole fractures	p_fract_core_ESHI	SICADA_07_350_2	20071022	Only data from cored boreholes in Laxemar have been used according to the specifications in Chapter 4
Single hole interpretation	p_eshi	SICADA_07_350_2	20071022	
Borehole definitions of modeled DZ	DZ_intercepts_Lax_2-3_071018.xls	Direct download from SIMON	20071116	The Laxemar 2.3 interim deformation zone definitions available at SIMON
Linked lineaments	SDEADM_GV_LX_GEO_5566 SDEADM_GV_LX_GEO_5567	Direct download from SDE	20071019	Lineaments > 1,000 m Lineaments < 1,000 m
Detailed Trench outcrop fractures	SDEADM_GOL_SM_GEO_4751_VIEW SDEADM_GOL_SM_GEO_4753_VIEW SDEADM_GOL_SM_GEO_4755_VIEW SDEADM_GOL_SM_GEO_4757_VIEW SDEADM_GOL_SM_GEO_4759_VIEW SDEADM_GOL_SM_GEO_4760_VIEW SDEADM_GOL_SM_GEO_4762_VIEW SDEADM_GOL_SM_GEO_4764_VIEW SDEADM_GOL_SM_GEO_4766_VIEW SDEADM_GOL_SM_GEO_4767_VIEW	Direct download from SDE	20071019	ASM000114 ASM000115 ASM000116 ASM000117 ASM000118 ASM000119 ASM000120 ASM000121 ASM000122 ASM000123
Linked detailed outcrop fractures	ASM000208_hand_linked_Clip (pending SDE) ASM000209_hand_linked_Clip (pending SDE) ASM100234_hand_linked_Clip (pending SDE) ASM100235_hand_linked_Clip (pending SDE)	Product of this report	20080206	Pending SDE name and delivery number
Detailed outcrop fractures	SDEADM_GOL_LX_GEO_4125_VIEW SDEADM_GOL_LX_GEO_4126_VIEW SDEADM_GOL_SM_GEO_4224_VIEW SDEADM_GOL_SM_GEO_4641_VIEW	Direct download from SDE	20071019	ASM000208 ASM000209 ASM100234 ASM100235
Local model area	SDEADM_SKB_LX_ADM_5301	Direct download from SDE	20071020	

4 Fracture data in boreholes

4.1 Data input

The geological and geophysical data used in the SDM-Site Laxemar DFN modeling work comprise all data that have been acquired from Laxemar, i.e. data that were already available at the Laxemar 1.2 data freeze (November 1, 2004) plus new data that that were available before the SDM-Site Laxemar data freeze (August 31, 2007) as well as updates in the single-hole interpretation and developments in the deformation zone model up until October 18, 2007, when the interim SDM-Site DZ model was delivered. However, data from cored borehole KLX27A, which was drilled during the fall of 2007, will not be used in the DFN modelling work while the relevant geological and hydraulic data is not available in time. The locations of the boreholes used in the geological and hydraulic DFN analyses are presented below in Figure 4-1.

Between the data freezes for SDM Laxemar 1.2 and SDM-Site Laxemar (data freeze for model version 2.3), some 40 new cored boreholes were drilled across the Laxemar subarea:

- Boreholes with lengths between 400–1,000 m: KLX07A, KLX08, KLX09, KLX10, KLX11A, KLX12A, KLX13A, KLX15A, KLX16A, KLX17A, KLX18A, KLX19A, KLX20A, KLX21B (and KLX27A, NB. Data from this borehole became available after data freeze L2.3 and has been used solely in the ensuing RD and DZ modelling, but not in DFN modelling. Included here for reasons of completeness).
- Boreholes with lengths shorter than 200 m: KLX07B, KLX09B, KLX09C, KLX09D, KLX09E, KLX09F, KLX09G, KLX10B, KLX10C, KLX11B, KLX11C, KLX11D, KLX11E, KLX11F, KLX14A, KLX22A, KLX22B, KLX23A, KLX23B, KLX24A, KLX25A, KLX26A, KLX26B, KLX28A and KLX29A.

The primary site investigation objectives of the longer boreholes were either to penetrate and characterize modelled deformation zones, or to characterize the bedrock between deterministic deformation zones. All of the shorter boreholes, with the exception of KLX07B and KLX14A, were designed for either DFN analysis (KLX9B–F /Hartley et al. 2007/ and KLX11B–F) or were carried out as components of the Minor Deformation Zone (MDZ) project (KLX22A–KLX29A) /Olsson et al. 2007/. Standard geological and geophysical log data and extended single-hole interpretations (ESHI) exist in SICADA for all these boreholes. The geological and geophysical logging of site investigation cored boreholes is controlled by the following method description (MD) documents:

- Borehole televiewer mapping (BIPS): (SKB MD 222.006, SKB Internal document).
- Borehole radar mapping: (SKB MD 252.020, SKB Internal document).
- Borehole geophysics (other than radar): (SKB MD 221.003, SKB Internal document).
- BOREMAP protocol: (SKB MD 143.006, SKB Internal document).
- Geological Single Hole Interpretation (SHI) protocol: (SKB MD 810.003, SKB Internal document).

A complete listing of the authoritative method-specific documents (‘P-reports’) for all new cored boreholes used in the geological and hydrological DFN modelling work is presented in Chapter 8 of this report. In general, the single-hole interpretation summary report has been considered authoritative. However, for several boreholes (KLX15A, KLX16A, KLX17A, and KLX21B), an SHI summary report was not completed. For those holes, the BOREMAP summary report is given as the formal reference.

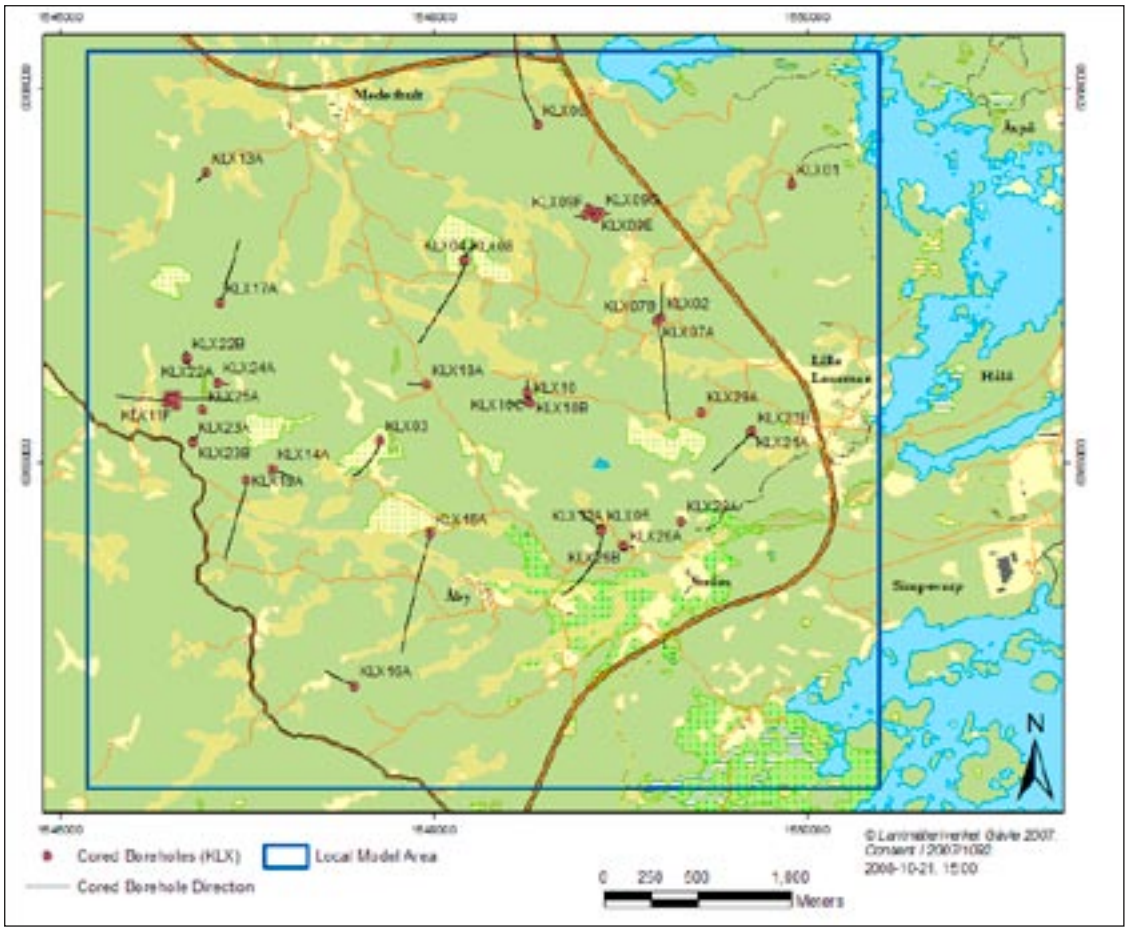

Figure 4-1. *Locations of drill sites and boreholes in the Laxemar local model area for which data were available to model version SDM-Site Laxemar.*

The fracture data available for DFN analysis are listed in Table 4-1. Borehole fracture data have been included in the DFN analysis with the following assumptions:

1. All mapped fractures in the cored boreholes are natural fractures; the assumption is that drilling-induced features have been detected and removed during the borehole mapping process.
2. Fractures that are mapped in BOREMAP as visible in BIPS can be used for orientation analyses.
3. Fractures that are mapped in BOREMAP as not visible BIPS are more uncertain and should not be used for orientation analyses, but can and should be used in the analysis of fracture intensity, scaling, and spatial location.
4. Fractures that reside outside the limits of identified deformation zones (i.e. deterministic and minor deformation zones identified through extended single hole interpretation, cf. Section 4.3) are included in the DFN analysis.
5. No distinction is made between fractures that are mapped as sealed and open; the final DFN model presents a statistical description that describes all fractures regardless of aperture.

Assumptions 2 and 3 are taken in the context of /Munier and Stigsson 2007/, who recommend avoiding the usage of fractures not visible in BIPS when possible due to substantial uncertainty in their assigned orientations.

Table 4-1. Borehole fracture data population, subdivided by fracture visibility in borehole image logs (BIPS).

IDCODE	Visible in BIPS					Not visible in BIPS							
	Sealed	Open	Partly open	Unidentified	sum	Sealed	Open	Partly open	Unidentified	Sum	Missing orientation	Inside DZs	Borehole total
KLX02	301	471	28		800	187	325	18		530	165	1,575	3,070
KLX03	2,089	284	2		2,375	920	125	1		1,046	110	857	4,388
KLX04	2,309	826	8		3,143	660	291	3		954	103	1,298	5,498
KLX05	1,753	209	1		1,963	1,371	74			1,445	61	70	3,539
KLX06	1,741	388	11		2,140	1,184	135			1,319	247	1,661	5,367
KLX07A	2,182	668	5		2,855	779	200	1		980	108	2,622	6,565
KLX07B	438	226	2		666	114	54	1		169	36	503	1,374
KLX08	1,691	945	2		2,638	728	320	5		1,053		1,605	5,296
KLX09	1,861	546	1		2,408	488	348	2		838	10	1,406	4,662
KLX09B	255	120			375	97	32			129	25	80	609
KLX09C	368	169	3		540	94	42			136	31	64	771
KLX09D	327	164	2		493	132	48	2		182	59	181	915
KLX09E	333	124			457	133	44			177	32	355	1,021
KLX09F	330	123	2		455	219	68	1		288	10	289	1,042
KLX09G	274	88	1		363	121	26			147		318	828
KLX10	1,943	880	4		2,827	958	503	1		1,462	21	1,291	7,947
KLX10B	149	86	3		238	15	10			25	28	341	746
KLX10C	495	131	1		627	56	31			87	30	821	1,784
KLX11A	2,757	368		1	3,126	884	249			1,133	4	1,095	6,860
KLX11B	172	91			263	90	35			125	1	55	660
KLX11C	210	95			305	106	35			141			682
KLX11D	318	131			449	58	18			76		154	886
KLX11E	171	102			273	174	37			211		171	968
KLX11F	194	86			280	88	17			105	5	23	604
KLX12A	851	560	3		1,414	903	514			1,417	49	121	4,981
KLX13A	1,175	702	3		1,880	395	259			654	25	1,177	5,095
KLX14A	259	271			530	261	78			339	48	589	2,116
KLX15A	1,937	871	5		2,813	1,145	447	3		1,595	31	1,079	7,989
KLX16A	1,199	504	5		1,708	549	132			681	22	1,546	5,147
KLX17A	2,174	509	3		2,686	690	156	2	1	849	65	868	5,829
KLX18A	1,179	583	4		1,766	526	218			744		548	4,389
KLX19A	731	295	1		1,027	552	167			719	35	941	3,737
KLX20A	532	243			775	570	150			720	9	794	3,261
KLX21B	2,141	616	4		2,761	805	211			1,016	29	2,094	7,536
KLX22A	326	225			551	102	33			135		8	1,054
KLX22B	313	194			507	101	39			140		22	1,003
KLX23A	97	42			139	26	8			34	3	31	283
KLX23B	40	26			66	14	11			25		24	166
KLX24A	314	238	2		554	173	66			239		91	1,363
KLX25A	143	70			213	85	16			101	1	32	518
KLX26A	188	213	1		402	146	84			230	7	173	1,256
KLX26B	93	223	1		317	13	16			29			599
KLX28A	217	109			326	33	21			54	12	171	726
KLX29A	171	131	1		303	53	9			62	15	83	657

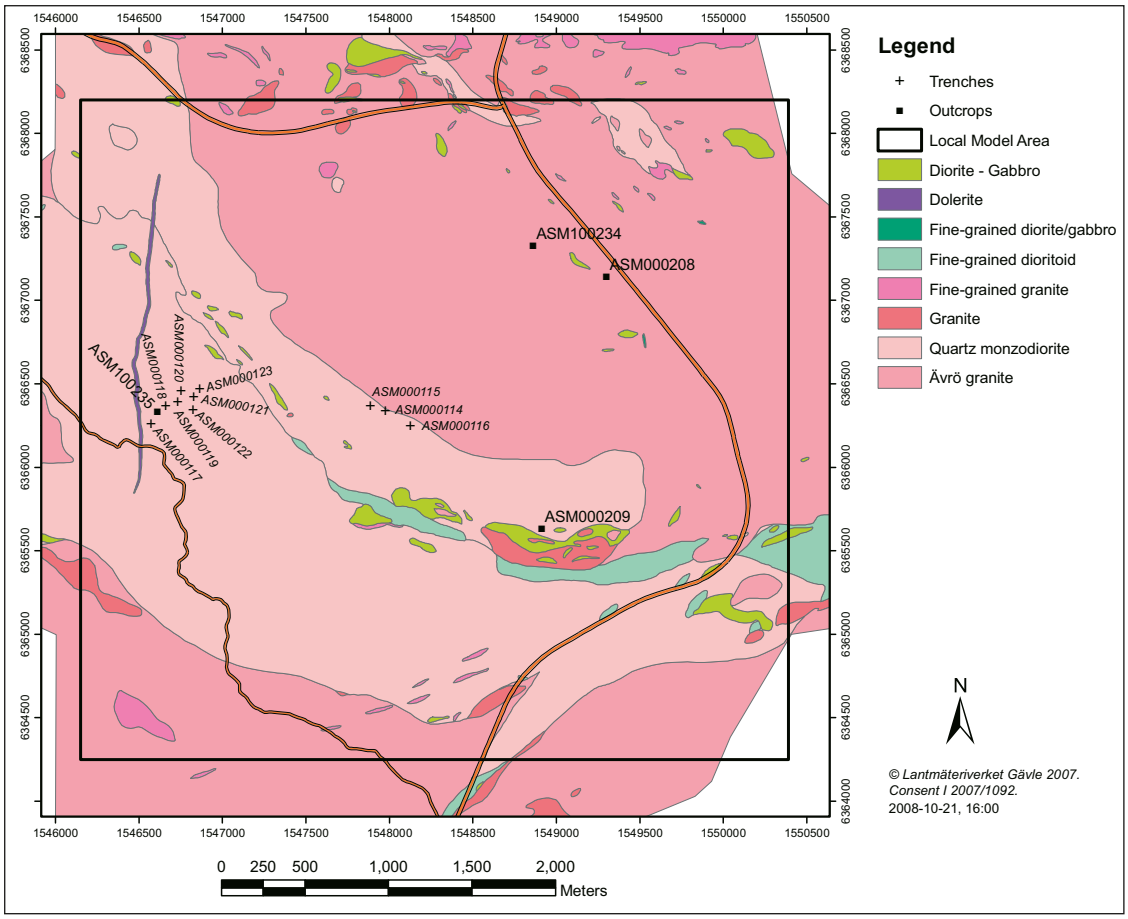

Figure 4-2. *Locations of detailed fracture mapped outcrops and trenches overlying bedrock lithology in the Laxemar local model area. Coordinates are given in the RT90 (RAK) coordinate system.*

4.2 Borehole composite logs

In each of the cored boreholes geological and hydrogeological data have been compiled into composite logs. The composite log compilation presents data graphically in a simple and intuitive manner. The composite logs contain Boremap data, rock and ESHI units, results of single-hole hydraulic tests and some selected chemistry data important for the hydrogeological evaluation (see Chapter 5). An example composite log is presented in Figure 4-3; composite logs for each borehole are presented in Appendix 2.

4.3 Modifications of single hole interpretation in connection with geological modelling work

The modification and updating of the single-hole interpretation in connection with the SDM-Site Laxemar modelling work comprised the following two activities:

- Subdivision of the Ävrö granite into two sub-varieties: Ävrö quartz monzodiorite, which is a relatively quartz-poor rock, and Ävrö granodiorite, which is a relatively quartz-rich rock.
- Identification of minor deformation zones (MDZ) in the cored boreholes KLX02 (200–1,000 m), KLX03, KLX04, KLX05, KLX06, KLX07A, KLX07B and KLX08.

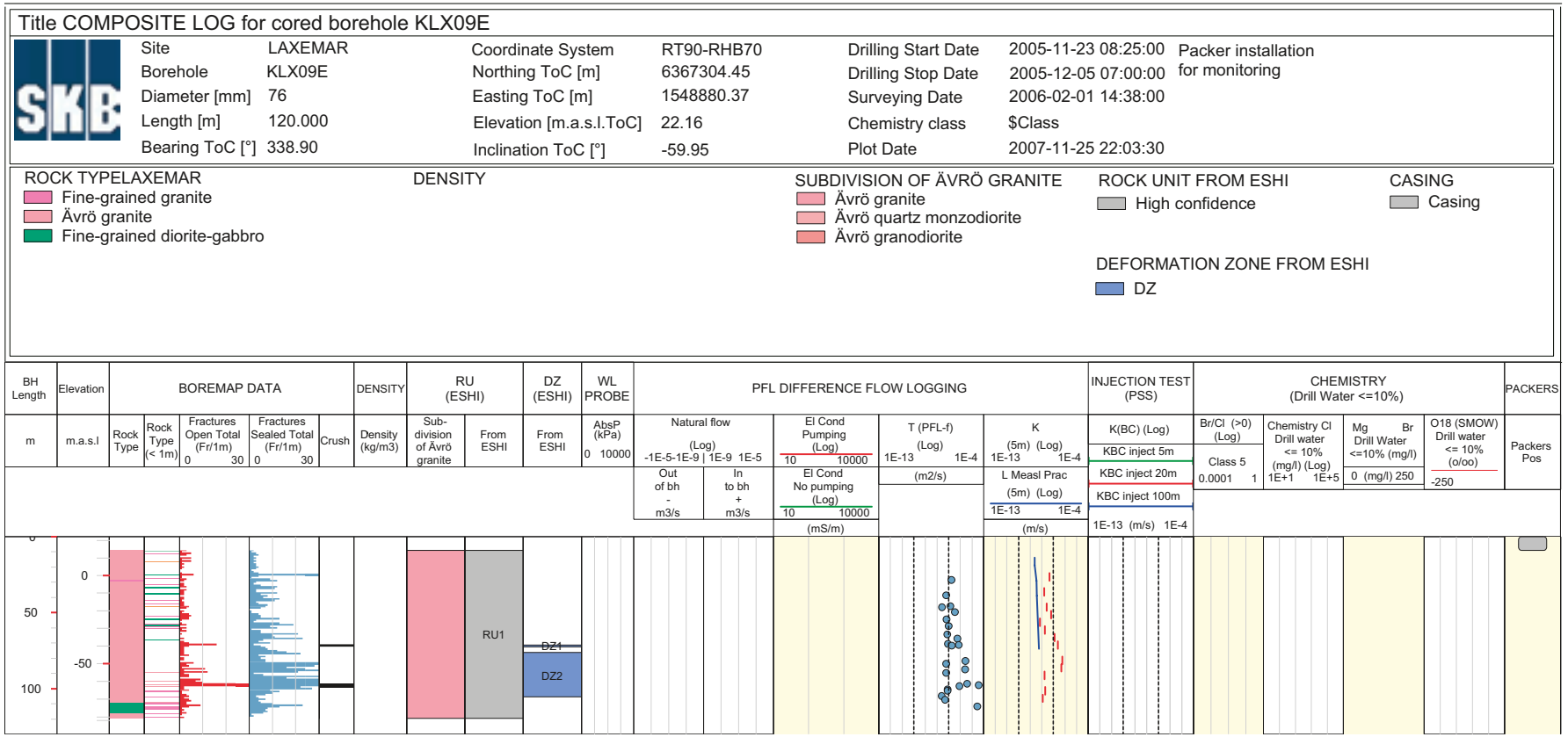

Figure 4-3. *Example of KLX09E composite log of borehole data (all cored boreholes presented in Appendix 2).*

4.3.1 Subdivision of the Ävrö granite

As has been stated in all previous SDM reports, i.e. model versions Simpevarp 1.1 and 1.2 /SKB 2004, 2005/, and Laxemar 1.2 /SKB 2006a/, and also in the geological background report /Wahlgren et al. 2006/, the Ävrö granite concept represents a suite of lithologies with a large compositional variation. The variation in rock compositions within the Ävrö granite made the property assignment for rock domain RSMA01 difficult, and also impaired the effective handling of this rock domain in the thermal, rock mechanical and hydrogeologic models.

A subdivision of the Ävrö granite has therefore been carried out in all cored and percussion boreholes (including the Simpevarp subarea) in which Ävrö granite constitutes an important rock type. An evaluation of available geological data, supported by thermal and rock mechanical data from the Laxemar 1.2 modelling stage, indicated that a density of 2,710 kg/m^3 should be used as a threshold value to separate the quartz poor Ävrö quartz monzodiorite from the quartz richer Ävrö granodiorite. This subdivision results in the need for a re-assessment of rock domains and rock units in all boreholes; rocks can now be classified as being dominated by either Ävrö quartz monzodiorite or Ävrö granodiorite, or separated into separate and different rock units.

4.3.2 Identification of minor deformation zones (MDZ)

Beginning with cored borehole KLX09, the identification of minor deformation zones was included as part of the standard geologic single hole interpretation. Since fractures that are related to deformation zones will not be used in the parameterisation of the DFN model, it was necessary to re-evaluate earlier single-hole interpretations (cored boreholes KLX02 to KLX08) to determine if minor deformation zones were present. In the case MDZ were found in these boreholes, the single-hole interpretations were adjusted in SICADA to exclude fractures related to them.

The single-hole interpretation update was a two stage process. The first stage comprised a desktop study of photographs of core boxes, existing single-hole interpretations, Boremap/BIPS mappings, borehole radar data and geophysical borehole logs. The goal of this first stage was to address the potential existence of deformation zones that were considered too minor to be included in the original single-hole interpretation. Seventy-four candidate minor deformation zones were identified in the desktop study.

The second step of the single-hole interpretation update was to confirm or reject each candidate minor deformation zone through a physical inspection of the associated drill core. Out of the seventy-four identified minor deformation zones, thirty-five minor deformation zones were confirmed during the physical analysis of the drill core. These interpreted minor deformation zones were then described according to the same procedure as deformation zones in the method description (SKB MD 810.003, version 3.0).

The updates of the single-hole interpretations have been delivered to the SICADA database as “extended single-hole interpretations”, abbreviated ESHI. In order to avoid confusion as to whether an extended single-hole interpretation exists for a given borehole when extracting data from SICADA, it was decided to store all single-hole interpretations, regardless of whether or not an ESHI was carried out, in the same data tables in SICADA. All analyses and evaluations that are carried out in conjunction with the SDM-Site Laxemar modeling will utilize the extended single-hole interpretation as existing in SICADA. The basic results correlating to the latter database entries are provided in Appendix 3.

4.4 Fracture frequency distribution for each borehole

Fracture data for the DFN analysis takes into account the location of deformation zones and minor deformation zones as defined by the extended single-hole interpretation. For the purpose of comparing fracture frequency over defined vertical depth intervals between boreholes the following approach has been adopted:

- Fracturing within the borehole intersection length for each mapped deformation zone and minor deformation zone has been removed from the data set (marked grey in figures below).
- Fracture data have been plotted relative to elevation (m.a.s.l.) at a constant scale.
- The frequencies of open and sealed fractures are plotted separately.

Fracture frequency as a function of depth for individual boreholes is presented in Appendix 4. Fracture frequency has been calculated as an average linear fracture intensity (P10 in 1 m long bins using a 5 m long moving window. However, it is difficult to compare relative fracture frequencies between boreholes of different orientation unless an orientation bias correction is adopted. Below follows two examples of orientation bias corrected graphs, cf. Figure 4-4:

1. (Left) A moving average of Terzaghi-weighted fracture frequency assuming a 5 m moving average elevation window for open and sealed fracture intensity in 1 m long borehole length intervals outside of identified deformation zones and minor deformation zones.
2. (Right) A graph of cumulative Terzaghi-weighted fracture intensity (CFI) versus elevation, normalized by the length of the borehole outside of deformation zones mapped in RVS.

The moving average plot is useful for visual comparison between different boreholes of the relationship between open and sealed fractures and to inspect the variability of fracture frequency as a function of depth. The second plot of cumulative intensity is useful for observing gradual changes in open and sealed fracture intensity, as well as for delineating sharp potential lithostratigraphic or fracture domain boundaries.

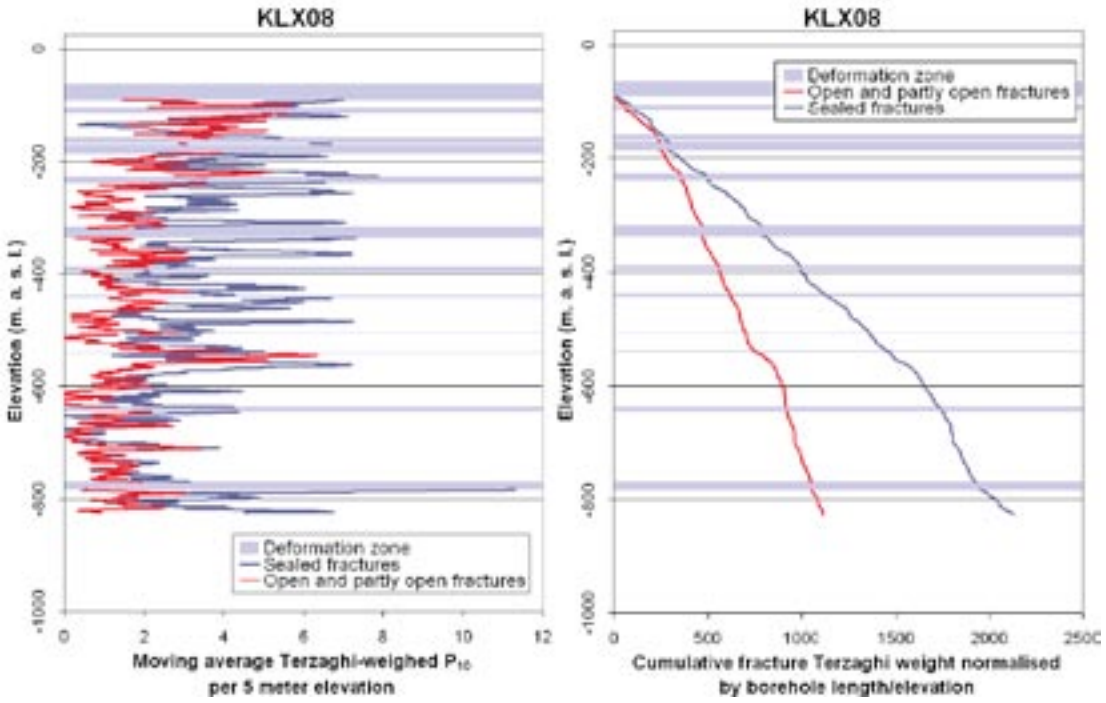

Figure 4-4. *Left: Moving average of Terzaghi-weighted fracture frequency over 5 m elevation intervals for open and sealed fractures, excluding deformation zones. Right: Cumulative Terzaghi-weighted fracture intensity (CFI) versus elevation, normalized by borehole length. Data presented is from cored borehole KLX08.*

The absolute intensity values presented in both types of plots are affected by the value of the Terzaghi correction used to compensate for orientation bias; a maximum Terzaghi weight of 7 was used for all calculations. The absolute intensity values are also affected by the decision to normalize as a function of elevation, rather than by measured borehole length. Complete plots for all cored boreholes in Laxemar are given in Appendix 4.

Initial qualitative analyses indicate that fracture frequency is highly variable in borehole sections between interpreted deformation zones. Furthermore, the frequency of open fractures is substantially lower than the sealed fracture frequency and there can be significant spatial variability in fracture intensity. In general, the total fracture frequency does not decrease systematically as a function of depth. However, open fracture frequency is generally higher in the upper 200 m of the rock mass.

4.5 Fracture orientation from boreholes

Fracture orientation is best addressed using only fractures mapped in BOREMAP as 'visible in BIPS'. The uncertainty in orientation of fractures that are only observed in the drill core during Boremap activities possess uncertainty in their orientations that has been deemed too great for use in DFN parameterisation /Munier and Stigsson 2007/.

Fracture orientations are presented, both in this report and in the DFN model reports, using equal-area (Schmidt) stereonets in a lower hemispherical projection /Schmidt 1917/. Data is displayed either as point plots of pole vector intersections with the sphere, or as pole density plots using Kamb or Fisher /Fisher 1953/ contouring. Kamb contouring /Kamb 1959/ has the advantage that pole clusters are independent of sample size and can be compared directly between boreholes or sections, given that the same Terzaghi correction and intervals of standard deviation are used as shown in Figure 4-5. Contour plots for all boreholes of all fractures (regardless of aperture) and of just open fractures separately, are presented in Appendix 5a.

A comprehensive visualization of specific variations in orientation along boreholes have been processed for all cored boreholes in vertical depth intervals (elevation, m.a.s.l.) and are presented in Appendix 5b. An example of Fisher contours for 30 m vertical depth sections along borehole KLX07B are presented in Figure 4-6. It is clear that variation is large between different depth intervals where no clear indications can be seen of consistent changes of dominating fracture orientations with increasing depth. It seems that a few dominating orientations in SH, NS, NNE, WNW and E-W occur throughout the Laxemar volume but in variable relative intensity between boreholes and borehole sections.

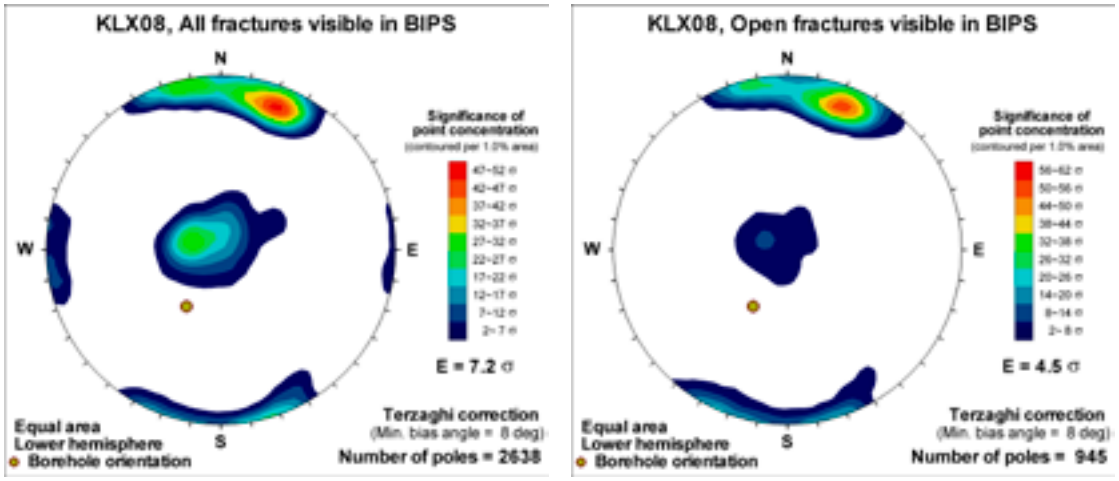

Figure 4-5. *Borehole fracture orientations in KLX08 plotted on a lower hemisphere, equal area Schmidt projection using Kamp contouring. Fracture data is Terzaghi corrected. Complete coverage for all KLX boreholes is provided in Appendix 5a.*

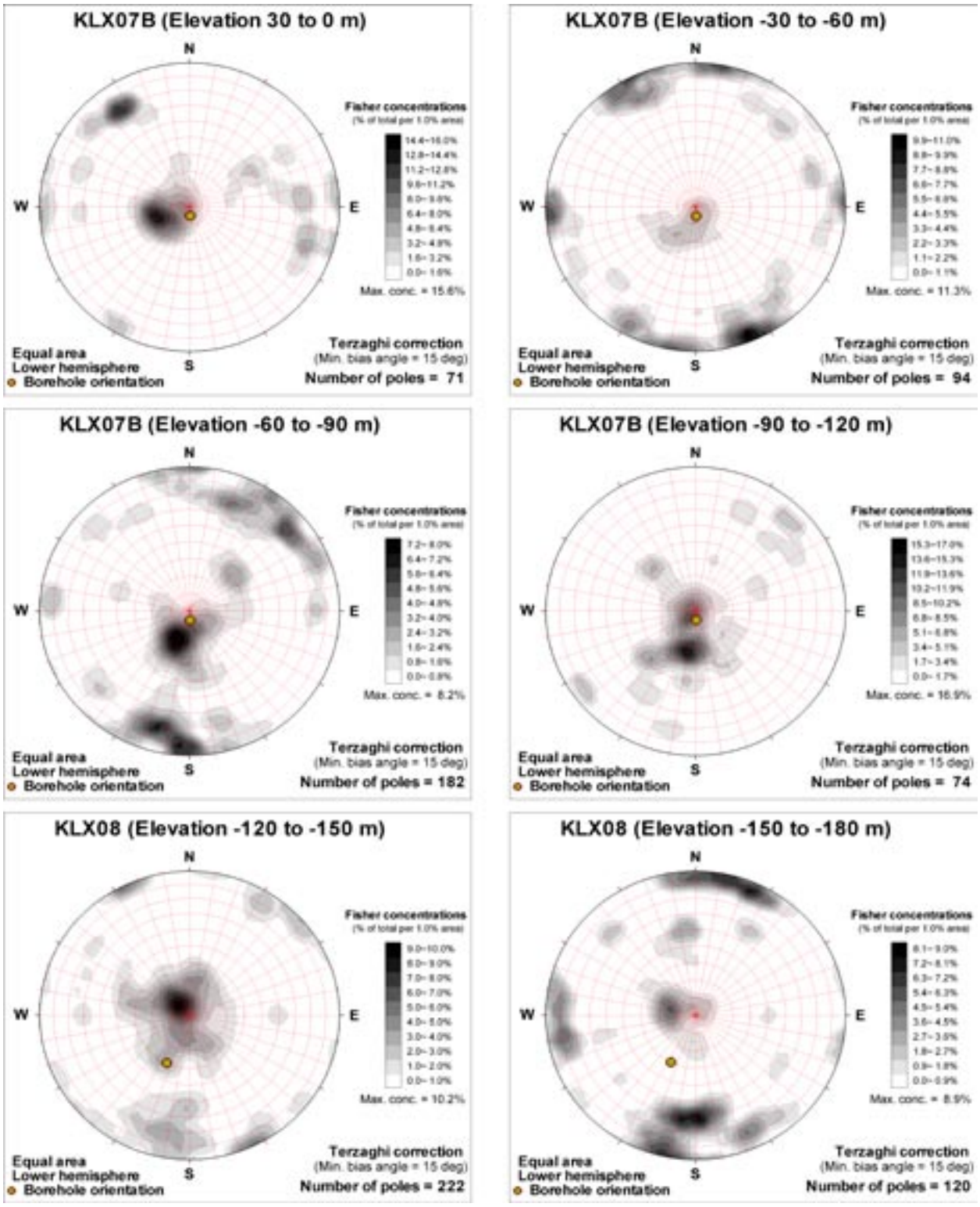

Figure 4-6. *Example plot of fracture orientations in 30 m elevation bins for cored borehole KLX08. Fisher concentrations are shown as a percentage of the total number of poles per 1.0% of the stereonet area. Complete coverage for all Laxemar cored boreholes is provided in Appendix 5b.*

As a further qualitative analysis of the depth-dependency of fracture orientation with depth, a series of Terzaghi-corrected fracture orientation density plots (functionally a kernel density) have been created; an example is presented below as Figure 4-7. In Figure 4-7, elevation (as a vertical depth) has been plotted against the frequency of fracture strike (left) and dip (right) in 5 degree intervals. Fracture strike and dip intensities are averaged over a 10 m elevation window. Figure 4-7 suggests that there is no clear systematic change of fracture strike as a function of depth.

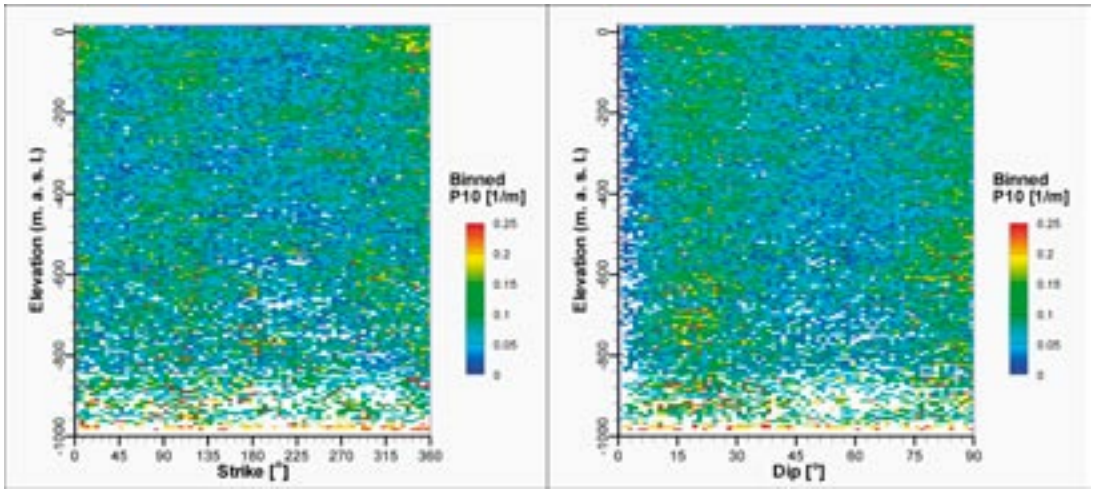

Figure 4-7. *Illustration of fracture orientation density as a function of depth. The plot illustrates the Terzaghi- corrected fracture intensity for all KLX boreholes, averaged over 10 m elevation intervals).*

5 Fracture data from surface outcrops

5.1 Data input

The surface data set for the SDM Site Laxemar geological and hydrological DFN modelling efforts consists of lithologic and structural geologic maps of bedrock exposures within the Laxemar local model domain, and completed prior to the Laxemar 2.3 data freeze.

There are two basic surface fracture data sources:

Detail-mapped outcrops (Section 5.2): These are rectilinear-shaped bedrock exposures created by the removal of several meters of overburden. Detail-mapped outcrops generally have a surface area between 200 and 600 m^2, and, after mapping was completed, were used as drilling pads for percussion and cored boreholes. Mapping efforts focused on describing the orientation, size, morphology, and properties of outcrop fractures, with a secondary focus on bedrock lithology and alteration. Only fractures with a visible surface trace length longer that 0.5 m were mapped. However, on some outcrops, additional fracture mapping was performed on intersecting scanlines. Fractures down to a visible surface trace length of 0.2 m were mapped where they intersected the scanlines.

Trench maps (Section 5.2.2): In 2006 and 2007, additional surface mapping was completed along narrow strips of cleared land (hereafter referred to as 'trenches') across the Laxemar local model area. The goals of the trench mapping studies were to investigate the surface extent of potential deformation zones identified by LIDAR and regional geophysics, and to provide additional data coverage for rock domain and DFN modelling efforts.

Figure 5-1. *Map illustrating the locations of outcrops and trenches mapped in the Laxemar area.*

Outcrop mapping data is available from several sources:

- Parameter tables (*p_area_map, p_line_map*) in SKB's SICADA database.
- As GIS feature classes in SKB's SDE geospatial database.
- As non-rectified digital photographs, taken at both high and low angles relative to the outcrop surface. These photographs are useful primarily for qualitative analyses and site descriptions; without rectification, mapping or data analysis is difficult to impossible.
- Orthorectified photo collages (trenches): The photo collages consist of series of digital photographs, taken from vertical to near vertical orientations, and stitched together electronically. The resulting collage is then orthorectified and oriented in the RT-90 (RAK) coordinate system.

5.2 Detailed fracture outcrop mapping

Detailed outcrop fracture and lithologic maps were created for four outcrops within the Laxemar sub-region. Example outcrop maps are presented below as Figure 5-3 and Figure 5-4.

The four outcrops mapped in detail were:

- ASM000208 – /Cronquist et al. 2004/. The mapping domain encompassed an approximately 331 m^2 area, within which 1,034 fractures within the size range (0.5–10 m) were mapped. This resulted in an average of 3.1 fracture traces per square meter of bedrock mapped. Four basic rock types were present in the mapped area of this outcrop; Ävrö granite (granite to quartz monzodiorite, generally porphyritic), fine- to medium-grained granite, diorite/gabbro, and fine-grained mafic rock.
- ASM000209 – /Cronquist et al. 2004/. The mapping domain encompassed an area of approximately 442 m^2, within which 1,030 fractures within the size range (0.5–10 m) were mapped. This resulted in an average of 2.3 fracture traces per square meter of bedrock mapped. Three basic rock types were present in the mapped area of this outcrop: Ävrö granite (granite to quartz monzodiorite, generally porphyritic), fine- to medium-grained granite, and diorite/gabbro.
- ASM100234 – /Forssberg et al. 2005/. The mapping domain encompassed an approximately 479 m^2 area, within which 1,128 fractures within the size range (> 0.5 m) were mapped. This resulted in an average of 2.4 fractures per square meter of bedrock mapped. Four basic rock types were present in the mapped area of this outcrop; Ävrö granite (granite to quartz monzodiorite, generally porphyritic), fine- to medium-grained granite, pegmatite, and fine-grained mafic rock.
- ASM100235 – /Cronquist et al. 2006/. The mapping domain encompassed an approximately 333 m^2, within which 1,028 fractures within the size range (> 0.5 m) were mapped.

Table 5-1. Descriptive statistics of fractures identified during the detailed outcrop mapping.

Outcrop IDCODE	# of traces	Tracelength				Outcrop area (m^2)	P_{21} (1/m)
		Total	Mean	Median	Std. Dev.		
ASM000208	1,034	1,327.42	1.26	1.01	0.85	330.70	4.01
ASM000209	1,030	1,484.41	1.44	1.04	1.19	442.10	3.36
ASM100234	1,128	1,789.68	1.59	1.15	1.37	478.60	3.74
ASM100235	1,028	1,337.34	1.30	1.04	0.83	332.60	4.02

Figure 5-2. *View of outcrops ASM100234 (top) and ASM100235 (bottom), cf. Figure 5-1.*

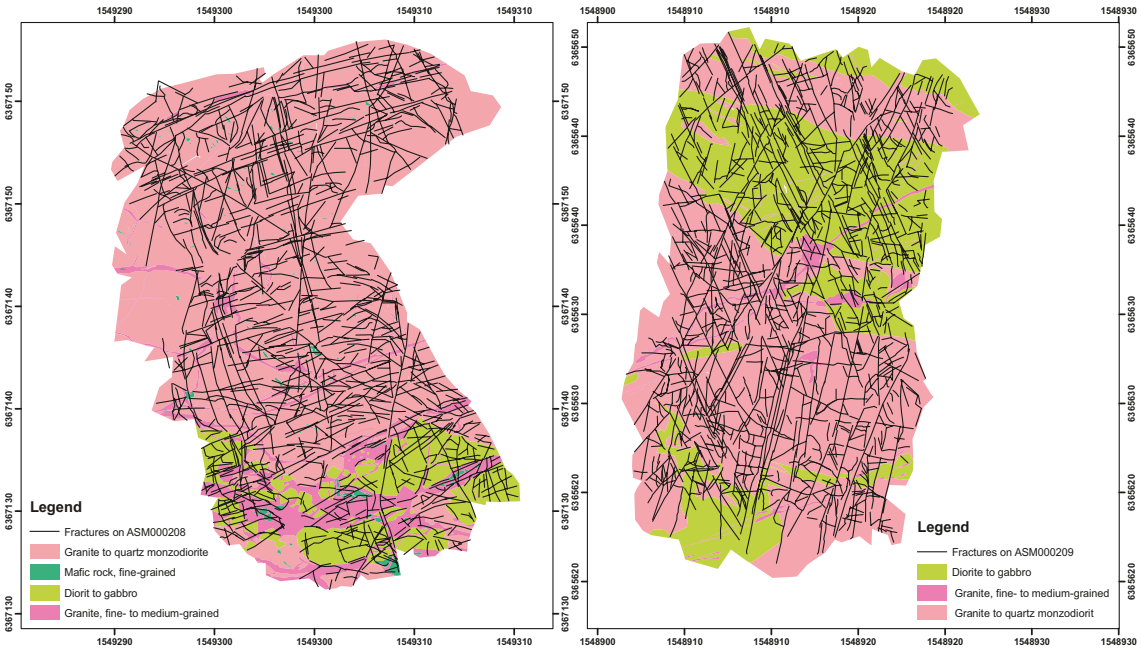

Figure 5-3. *Fracture traces and bedrock lithologies on outcrops ASM000208 and ASM000209, cf. Figure 5-1.*

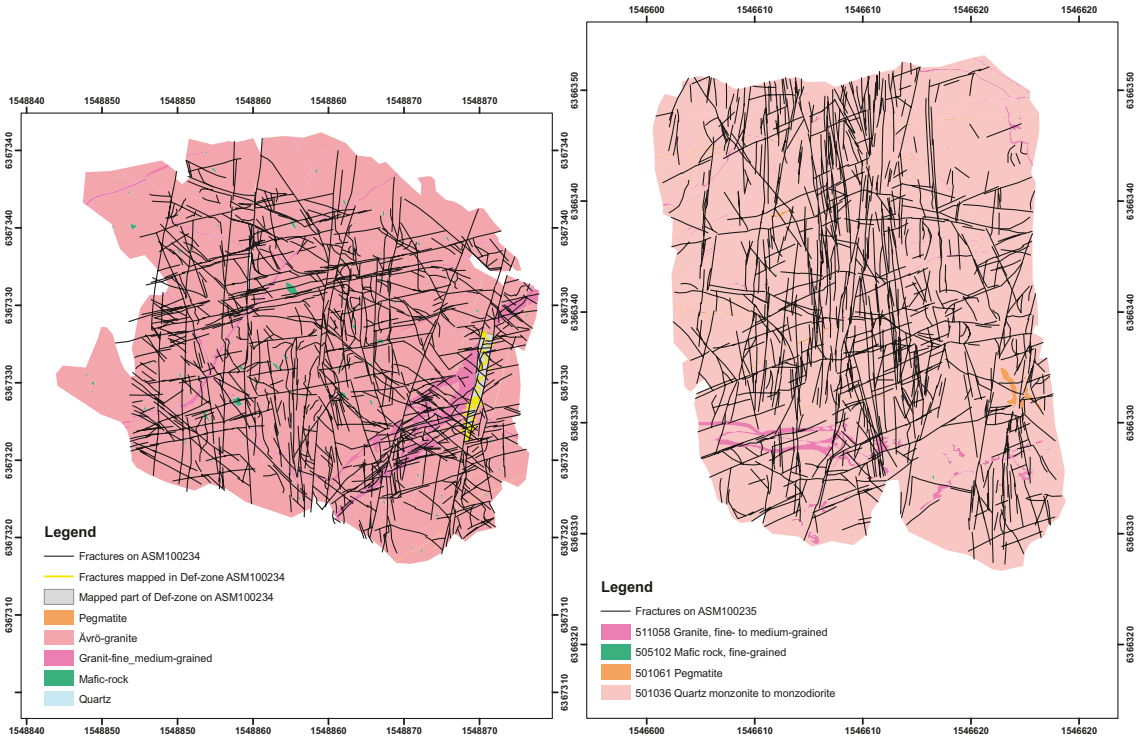

Figure 5-4. *Fracture traces and bedrock lithologies of outcrops ASM100234 and ASM100235, cf. Figure 5-1.*

GIS data files for all mapped outcrops are as follows (note the name given is the SDE feature class ID):

Outcrop Mapping Limits (polygon shapefiles)

- SDEADM_GOL_LX_GEO_2347 (ASM000208)
- SDEADM_GOL_LX_GEO_2356 (ASM000209)
- SDEADM_GOL_SM_GEO_3570 (ASM100234)
- SDEADM_GOL_SM_GEO_3690 (ASM100235)

Outcrop Fractures (unlinked; polyline shapefiles)

- SDEADM_GOL_LX_GEO_4125_VIEW (ASM000208)
- SDEADM_GOL_LX_GEO_4126_VIEW (ASM000209)
- SDEADM_GOL_SM_GEO_4224_VIEW (ASM100234)
- SDEADM_GOL_SM_GEO_4641_VIEW (ASM100235)
- SICADA tables p_area_map and p_line_map

Outcrop Fractures (linked)

Note that, as of early February 2008, these features had not yet been delivered to SKB and placed in SDE. As such, they represent an interim delivery product.

- ASM000208_hand_linked_Clip.shp
- ASM000209_hand_linked_Clip.shp
- ASM100234_hand_linked_Clip.shp
- ASM100235_hand_linked_Clip.shp

5.2.1 Linked outcrop data

The fracture trace data provide indispensable information for the parameterization of fracture size distribution in DFN modelling. Past DFN models at Forsmark and Laxemar-Simpevarp have assumed that fracture centre locations can be approximated as a three-dimensional Poisson point process. However, some specific trace data reveal spatial patterns in outcrop which deviate from the Poissonian assumption. One such particular spatial pattern may be described as “sequentially located traces (i.e. closely located trace endpoints) with similar orientations” (Figure 5-5a). It is possible that such fractures may form a well-connected structure below the ground surface (Figure 5-5b), even though the traces are not actually connected in the outcrop surface.

Failure to represent this type of possibly connected structures in fracture network modelling may have severe implications on downstream modelling of different processes; e.g. resulting in underestimation of the risk of the development of planes of failure or connectivity along flow paths (Figure 5-5c). The goal of the linking efforts were to provide a more reasonable definition of fractures at the outcrop scale, where the length of the surface traces directly affects the final size model parameterization in the geological DFN. This is also consistent with the procedure used in lineament interpretation /Triumf and Thunehed 2007/.

The details of the linking process will be described in detail in the method-specfic DFN report /La Pointe et al. 2008/. An example outcrop of linked traces is presented in Figure 5-6.

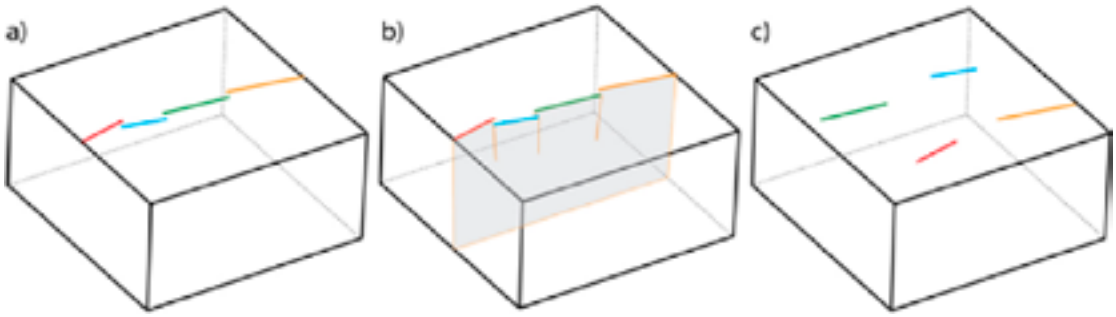

Figure 5-5. *Conceptual figure: a) a hypothetical set of sequentially located traces with similar orientations observed in the field, b) possible underground connectivity of fracture planes, with implications for downstream modelling, e.g. hydrological or rock-mechanical properties of the fracture system, and c) illustration of the error resulting from failure to represent this spatial aspect in DFN modelling.*

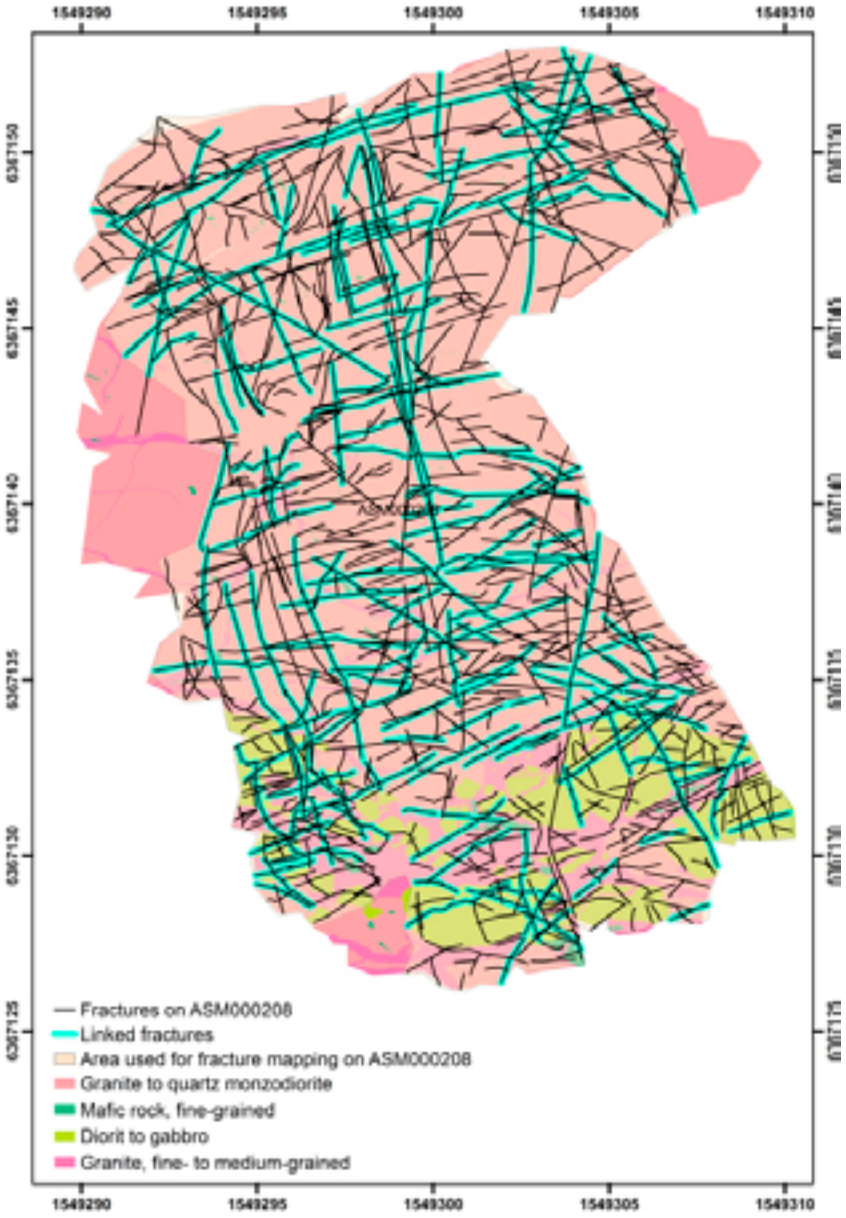

Figure 5-6. *Illustration of linked fractures (blue) on outcrop ASM000208.*

5.2.2 Trenches

In 2006 and 2007, additional surface mapping was done along narrow strips of cleared land across the Laxemar local model region. The goal was to investigate the surface extent of potential deformation zones identified from LIDAR and regional geophysics, as well as to provide additional data coverage for rock domain and DFN modelling efforts. The mapping results are presented in detail in /Forssberg et al. 2007/.

In brief, this investigation was performed using the same methodology as for the detailed fracture outcrops with slight differences in detail, namely:

- Along each strip, fracture traces were measured within a 1 m wide corridor.
- Truncation of traces was set to 1 m trace length.
- Trace length of traces > 1 m which had at least one end within the 1 m wide band was measured in its full length also extending outside the 1 m wide band.

The trench data consisted primarily of fracture orientation, trace length and bedrock mapping (lithology) data. Trench SDE data sources are listed below. The trench fracture and lithology maps are presented as Figure 5-9 through Figure 5-11.

Trench Mapping Limits / Bedrock Lithology

- SDEADM_GOL_SM_GEO_4740 -- ASM000114 fracture scanline limits
- SDEADM_GOL_SM_GEO_5343 -- ASM000114 outcrop limits and lithology
- SDEADM_GOL_SM_GEO_4742 -- ASM000115 fracture scanline limits
- SDEADM_GOL_SM_GEO_4720 -- ASM000115 outcrop limits and lithology
- SDEADM_GOL_SM_GEO_4723 -- ASM000116 outcrop limits and lithology
- SDEADM_GOL_SM_GEO_4745 -- ASM000117 fracture scanline limits
- SDEADM_GOL_SM_GEO_4746 -- ASM000118 fracture scanline limits
- SDEADM_GOL_SM_GEO_4727 -- ASM000118 outcrop limits and lithology
- SDEADM_GOL_SM_GEO_4747 -- ASM000119 fracture scanline limits
- SDEADM_GOL_SM_GEO_4729 -- ASM000119 outcrop limits and lithology
- SDEADM_GOL_SM_GEO_4748 -- ASM000120 fracture scanline limits
- SDEADM_GOL_SM_GEO_4731 -- ASM000120 outcrop limits and lithology
- SDEADM_GOL_SM_GEO_4749 -- ASM000121 fracture scanline limits
- SDEADM_GOL_SM_GEO_4733 -- ASM000121 outcrop limits and lithology
- SDEADM_GOL_SM_GEO_4750 -- ASM000122 fracture scanline limits
- SDEADM_GOL_SM_GEO_4735 -- ASM000122 outcrop limits and lithology
- SDEADM_GOL_SM_GEO_4739 -- ASM000123 fracture scanline limits
- SDEADM_GOL_SM_GEO_4737 -- ASM000123 outcrop limits and lithology

Fracture Maps

- SDEADM_GOL_SM_GEO_4751_VIEW -- ASM000114 outcrop fractures
- SDEADM_GOL_SM_GEO_4752 -- ASM000114 fractures with shear indicators
- SDEADM_GOL_SM_GEO_4753_VIEW -- ASM000115 outcrop fractures
- SDEADM_GOL_SM_GEO_4754 -- ASM000115 fractures with shear indicators
- SDEADM_GOL_SM_GEO_4755_VIEW -- ASM000116 outcrop fractures
- SDEADM_GOL_SM_GEO_4756 -- ASM000116 fractures with shear indicators
- SDEADM_GOL_SM_GEO_4757_VIEW-- ASM000117 outcrop fractures
- SDEADM_GOL_SM_GEO_4758 -- ASM000117 fractures with shear indicators
- SDEADM_GOL_SM_GEO_4759_VIEW -- ASM000118 outcrop fractures
- SDEADM_GOL_SM_GEO_4760_VIEW -- ASM000119 outcrop fractures

- SDEADM_GOL_SM_GEO_4761 -- ASM000119 fractures with shear indicators
- SDEADM_GOL_SM_GEO_4762_VIEW -- ASM000120 outcrop fractures
- SDEADM_GOL_SM_GEO_4763 -- ASM000120 fractures with shear indicators
- SDEADM_GOL_SM_GEO_4764_VIEW -- ASM000121 outcrop fractures
- SDEADM_GOL_SM_GEO_4765 -- ASM000121 fractures with shear indicators
- SDEADM_GOL_SM_GEO_4766_VIEW -- ASM000122 outcrop fractures
- SDEADM_GOL_SM_GEO_4767_VIEW -- ASM000123 outcrop fractures
- SDEADM_GOL_SM_GEO_4768 -- ASM000123 fractures with shear indicators

Figure 5-7. *Overview of trenches ASM100114 (left) from the central part of Laxemar and ASM100118 (right) from the western part of Laxemar.*

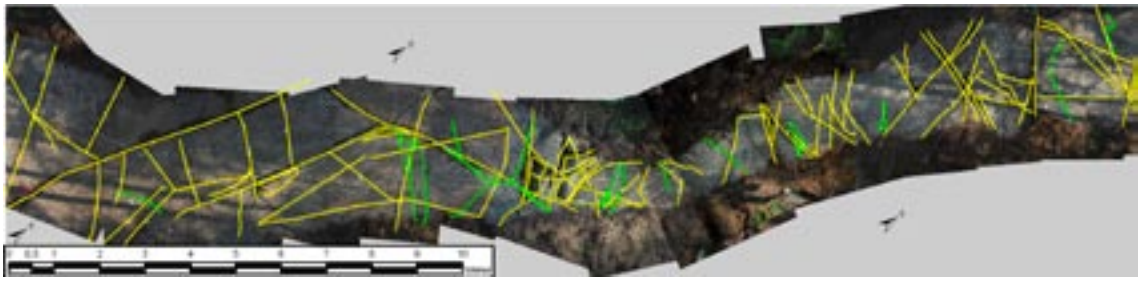

Figure 5-8. *Rectified images of trench ASM100119 (selected part of the trench).*

5.2.3 West area

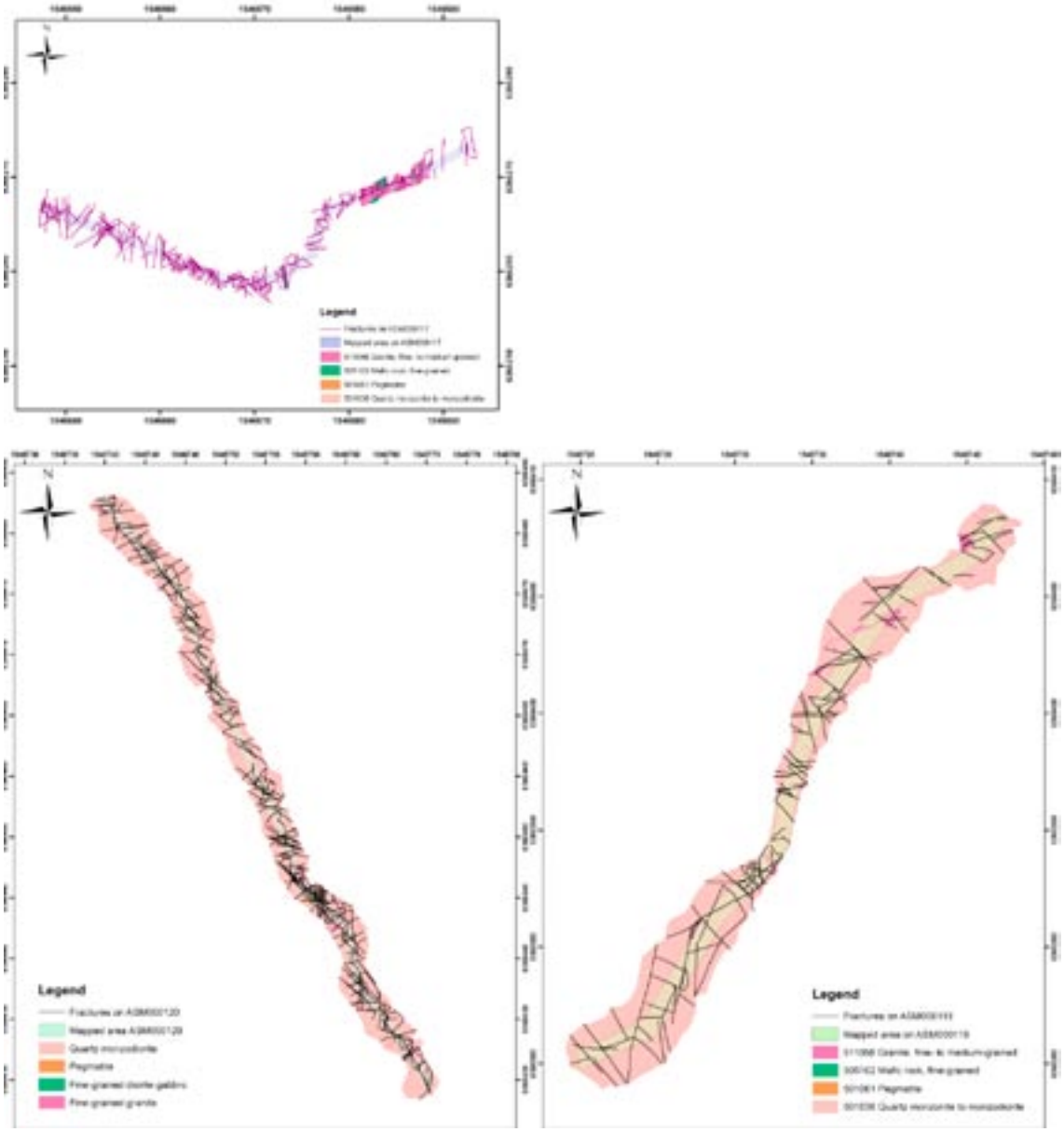

Figure 5-9. *Mapped fracture traces and lithologies on trenches in the west part of the Laxemar subarea. Figure illustrates trenches ASM00117, ASM00120 and ASM00119, respectively.*

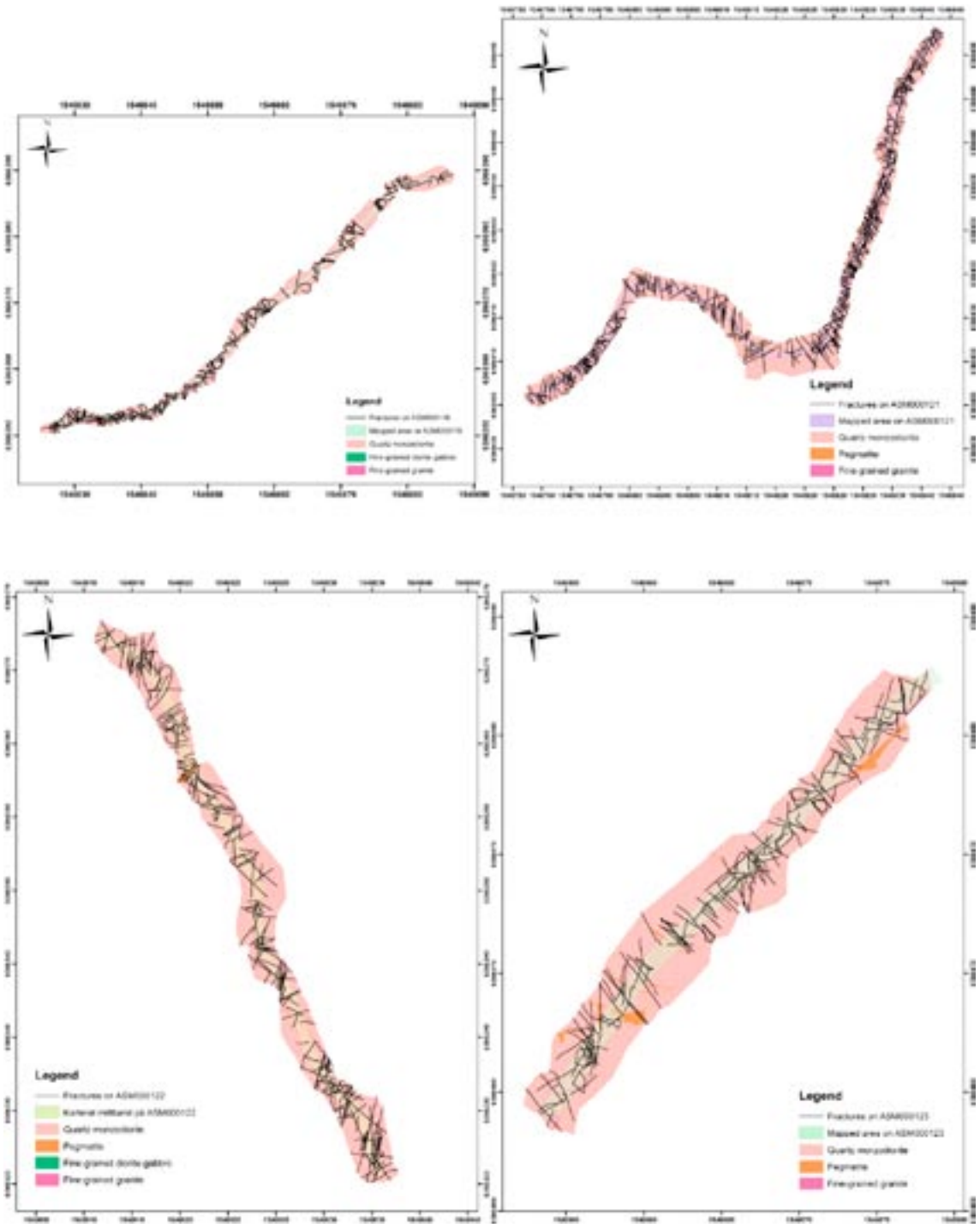

Figure 5-10. *Mapped fracture traces and bedrock lithologies for trenches in the west part of the Laxemar subarea. Trenches ASM00118, ASM00121, ASM00122, and ASM00123, respectively.*

5.2.4 Central area

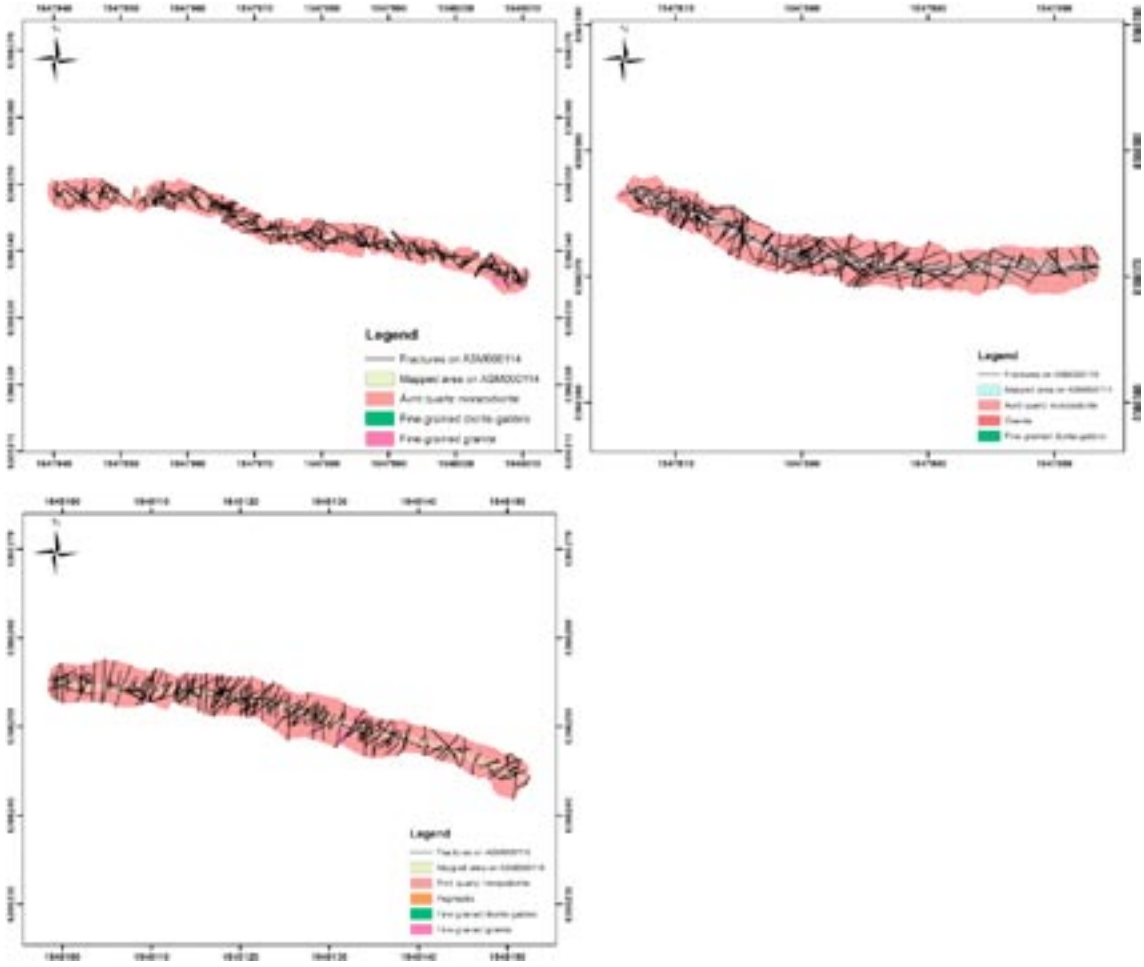

Figure 5-11. Mapped fracture traces and bedrock lithologies of trenches in the central part of the Laxemar subarea. Trenches ASM00114, ASM00115 and ASM00116, respectively.

5.3 Äspö HRL tunnel data

5.3.1 Purpose for usage of data outside local model domain

The geological DFN parameterisation is heavily dependent on observed data on fracture orientations, intensity and size. Fracture size is not possible to observe directly, but it can be estimated through the study of the length distribution of fracture traces. The primary data used for size estimation are the detail fracture-mapped outcrops (Section 5.2) and the regional and local lineament maps (Chapter 6). However, both data sources have a significant weakness; horizontal sampling planes (the ground surface) are biased against intersections with subhorizontal fractures.

In previous modelling efforts in Simpevarp and Laxemar it has been noted that sub-horizontal fractures occur at a relatively high intensity in most boreholes. The sub horizontal fractures are not as abundant on the detailed fracture outcrops available in Laxemar.

The Äspö Hard Rock Laboratory (Äspö HRL) provides a unique opportunity to potentially investigate subhorizontal fractures. The access tunnel to the laboratory has been mapped in detail by geologists during construction. The maps of the tunnel walls can be unfolded to geometrically simulate a series of trace planes. Although the Äspö HRL is located in a different geologic regime than the Laxemar subarea (i.e. on the other side of the Äspö shear zone and in a different set of rock domains), it is constructed and accessed through bedrock lithologies that have undergone similar tectonic histories to those inside the Laxemar subarea. Therefore, they can provide a useful "reality check" in relation to the subhorizontal size and intensity models calculated using outcrop and lineament data.

5.3.2 Data used

Database linked to the CAD files created by VBB 1995 (both 2D map cell data and 3D tunnel-folded traces, documented in "rpt9551.doc")

- PANEL.DBF
- FRAC3D.DBF
- FRACTURE.DBF
- FRZON3D.DBF

Trace data

It was decided to use combined data from the two databases FRACTURE.DBF and FRAC3D.DBF (referring to 2D, respectively, 3D CAD files). The fracture ID [Tunnel_name-section_length-fracture_number] was used to link information between the two databases. These databases have been processed such that each trace mapped over multiple map cell sections in TMS has been joined to a single trace with unique properties and assigned to a single tunnel section. The trace orientation data and records of multiple traces with identical properties (NOF) are taken from FRACTURE.DBF (as it is unavailable in FRAC3D.DBF). However, it was decided not to use the parameter "LENGTH" in FRACTURE.DBF in this analysis, as its definition is "the distance between the two endpoints of a trace" (i.e. not the integrated length along the visible intersection between the tunnel wall and the fracture). Instead, trace length was taken as the parameter LTOT in FRAC3D.DBF, which is a summed length along the trace exposed to the ideal tunnel wall (based on the 3D tunnel-folded CAD drawings). The reason for using LTOT in preference of LENGTH is that there are geometrical cases where the distance between the endpoints poorly relates to the radius of the real fracture. The relation between LENGTH and LTOT is shown in Figure 5-12. It can be noted that some values are equal to zero, and therefore it was decided to apply a trace length truncation threshold for the data set (see below).

Deformation zone data

Deformation zones are available as closed tunnel-intersection areas in FRZON3D.DBF. These are areas with such high fracture intensity that, during the tunnel construction phase, it was generally considered too time consuming to map the traces therein. However, this study targets the background fracturing, and therefore it is essential to exclude any traces that may be part of deformation zones. In order to distinguish such traces, the deformation zone areas in FRZON3D.DBF were projected to the tunnel section floor (i.e. collapsed vertically), as well as the 3D trace coordinates in FRAC3D.DBF. Projected traces falling partly inside the projected deformation zone areas are classified as a population of traces "possibly influenced by deformation zone". This projection step may somewhat overestimate the number of traces assumed influenced by deformation zones; however, data are fairly abundant and it avoids some difficulties caused by the complexity of 3D geometry. The TBM tunnel is intersected by two minor zones. By visual inspection it was decided to assume that no traces relate to these zones.

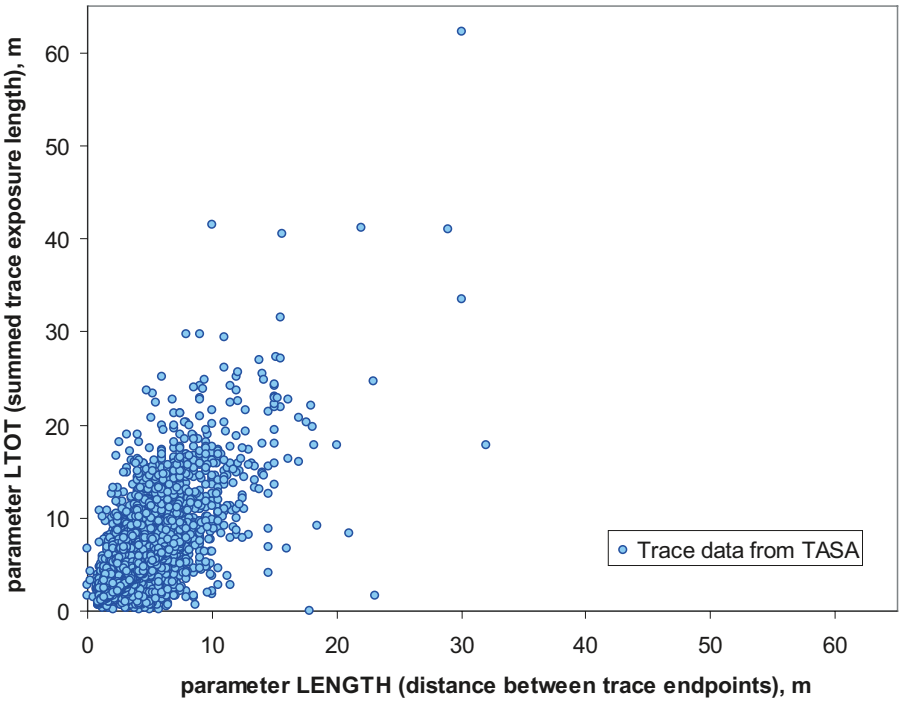

Figure 5-12. *Crossplot between the parameters LENGTH and LTOT. LTOT reflects a summed length along the fracture exposure in the tunnel wall, and is therefore considered better represent the underlying fracture radius. Note also that e.g. a trace has been mapped with LENGTH = 17.8 m, and LTOT = 0.0 m, which depends on low quality of the data.*

Orientation and trace length threshold

In the tunnel section of the TBM there are no traces recorded shorter than 1.3 m. In the TASA data there is a small population of traces equal to or shorter than 1 m. Fracture orientation of TASA is visualized in terms of contour plots for different classes of LTOT in Figure 5-13. The group of traces equal to or shorter than 1 m appears to have somewhat different orientation distribution compared to the longer traces. This may relate to errors in mapping or be due to the small sample size. However, in order to delimit these possible deviations traces longer than 1 m where chosen for further analysis.

In Figure 5-14 fracture orientation is presented for each tunnel leg according to the colour scheme at the top of the figure. Each tunnel leg with similar main orientation was colour coded with blue (SE), green (N-S), red (E-W), orange (SW) and yellow (TBM).

By visual inspection of the contour plots in Figure 5-13 there appears to be three dominant fracture orientations; NW, NNE, and SH. In comparison between the TASA entry tunnel, TASA spiral, and TBM tunnel data, cf. Figure 5-14, the intensity of the NNE and subhorizontal orientations seems to decrease with depth, while the NW trend seems to grow more intensive at depth. However, before such conclusions can be drawn, consideration must also be taken to the sampling bias associated with different tunnel orientations. Legs 1 and 3 are “semi-parallel” to the entry tunnel, while Leg 2 is orthogonal; yet, as can be clearly seen in Figure 5-14, Leg 2 is the tunnel orientation that exposes the strongest concentrations of the NNE and SH orientations. Therefore, the suspected trends in data cannot be explained by difference in sampling bias.

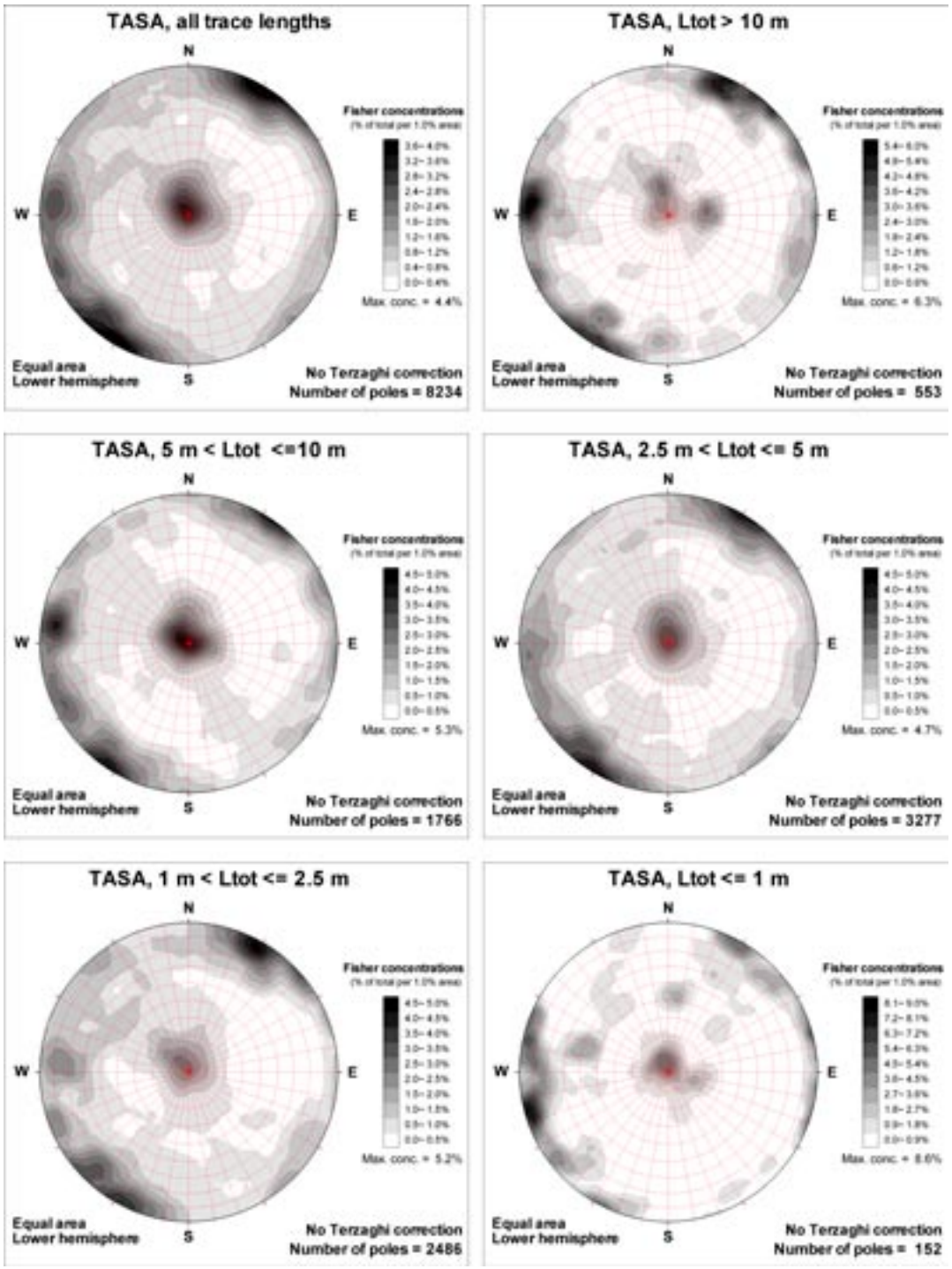

Figure 5-13. *Fracture orientation of fractures in TASA, classified in terms of fracture length, L***TOT***. Traces partly inside deformation zones are excluded.*

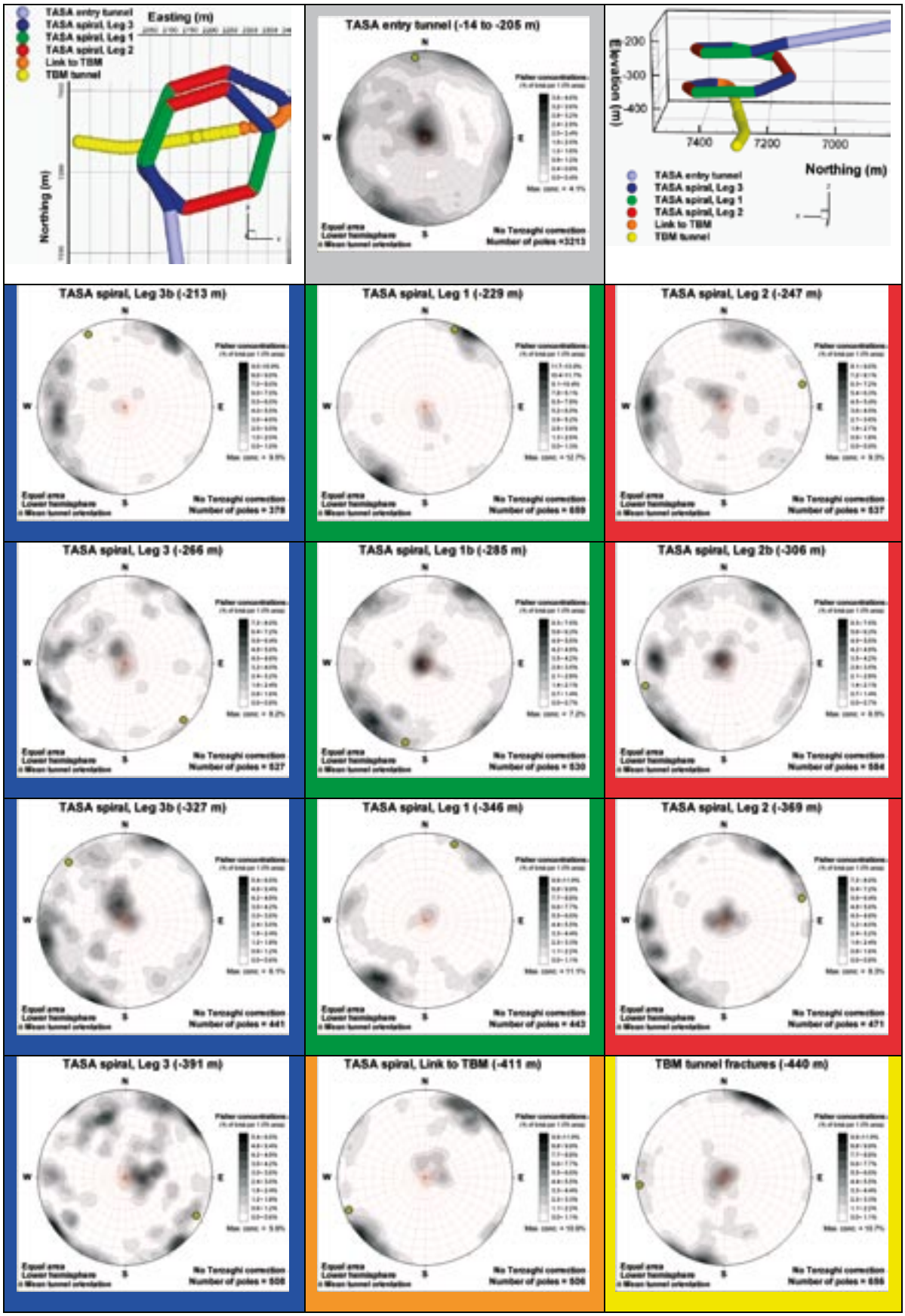

Figure 5-14. *Fracture orientation with depth for each data subgroup. All data included.*

It appears that the NW orientation is strongest in Leg 1 and in the TBM tunnel (although Leg 1 and the TBM are almost orthogonal). Legs 2 and 3 exposures show almost equally strong NNE and NW orientations. The gently dipping fractures are fairly evident in all data subgroups. Most striking is the absence of NNE in the TBM tunnel. One would perhaps suspect the NNE set to be particularly well-exposed in the TBM tunnel, considering its sampling orientation. However, possibly the absence of recorded NNE traces in the TBM tunnel is a consequence of sampling bias relating to the difference in tunnel construction technique. Perhaps faint NNE traces tend to be opened or revealed by blasting, but remain undetected in a smooth bored tunnel wall. Overall, the data sub-division by elevation decreases the sample sizes to such an extent that, with its inherent increase in dispersion of orientation, it is difficult to observe any obvious trend with depth.

Overview of trace length over depth for gently dipping fractures

The trace length distribution (LTOT) are illustrated in Figure 5-15 for fractures dipping less than 45 degrees in order to present a view on size trends with depth for fractures that should be less biased than vertical fractures due to the gently dipping tunnel.

It appears that the average length of traces are different in the TBM from the rest of the HRL, which may be explained by the smoother surfaces experienced in the drilled tunnel compared to the ordinary drill and blast access ramp and spiral part of the HRL. The conclusion is that fewer small fractures are observed; with perhaps also fewer engineered fractures, in the TBM. On the other hand traces appear to exhibit more or less similar mean lengths in the TASA entry and spiral sections. It also appears that trace length does not change systematically over depth, given the explanation of the traces in the TBM sections.

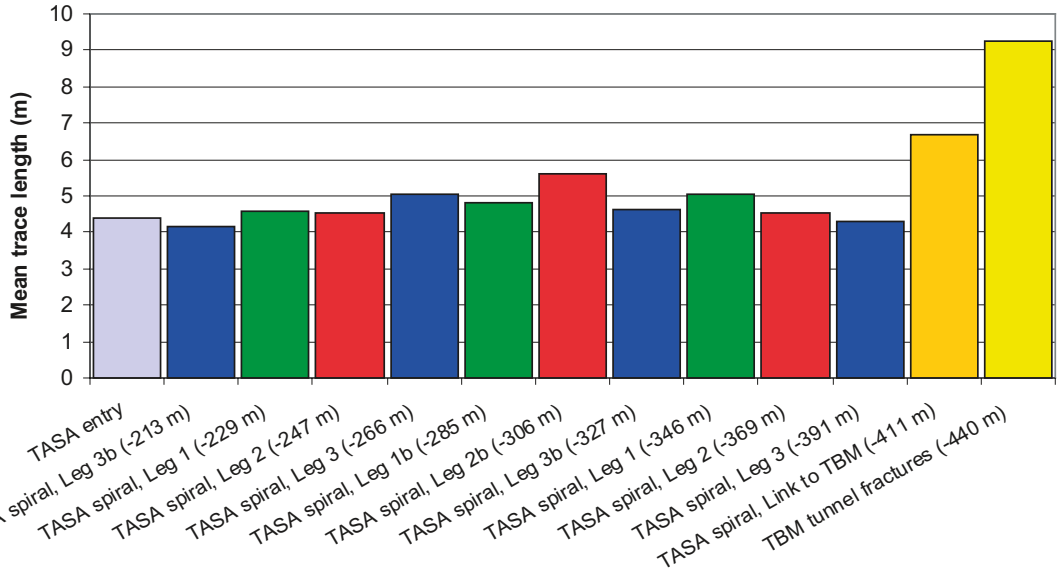

Figure 5-15. *Histogram representation of mean trace length for different tunnel sections shows longer mean trace lengths at depth. Does it mean longer traces at depth, or absence of short traces at depth, or perhaps a change in mapping methodology? Colour coding according to Figure 5-14.*

6 Lineaments

For the purpose of statistical modelling of fractures over a large range of scales, lineaments that represent a size fraction larger than what can normally be observed in outcrop are very useful. In previous model versions several lineament studies based on topographical and airborne geophysics have provided the framework of large scale structures in the Oskarshamn region, for example by /Triumf 2004/. New LIDAR and ground magnetic data have been processed by /Mattson and Triumf 2007/ to a detailed linked lineament map over the central parts of Laxemar. The methodology used for performing the linking process between LIDAR and ground magnetic lineaments are described in the previous geological model versions fro Laxemar and by /Triumf 2004/.

In short, the available coverage of the detailed linked lineament map is shown in Figure 6-1. LIDAR covers the majority of the Laxemar local model area except for the southern boundary.

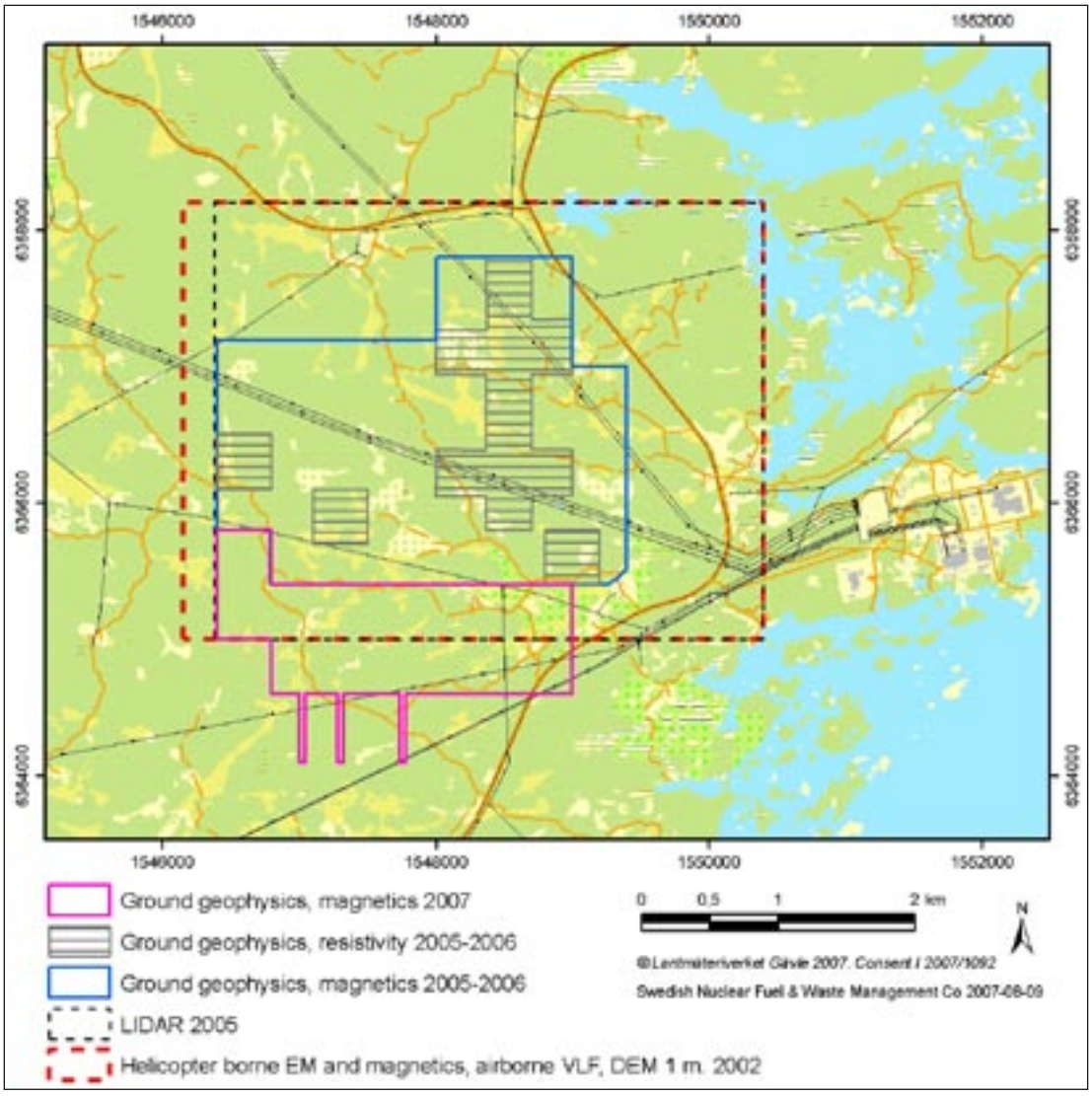

Figure 6-1. *Areal coverage of the detailed ground magnetic measurements and LIDAR used for the evaluation of linked lineaments over Laxemar. From /Mattsson and Triumf 2007/.*

The ground magnetic survey has a complete coverage in the central parts of Laxemar, and was extended also into the south during 2007, but covers less surface area than LIDAR. All generations of magnetic and topographical surveys, including LIDAR was used to analyze lineaments, and to finally produce the linked lineament map.

The surface traces of the linked lineament map, illustrated in Figure 6-2, along with their associated attribute table, is intended to be used in the construction of the coupled size-intensity models of the geological DFN. Data for linked lineament traces are taken from SDE, and consists of the following single feature class:

- SDEADM_GV_LX_GEO_5567.

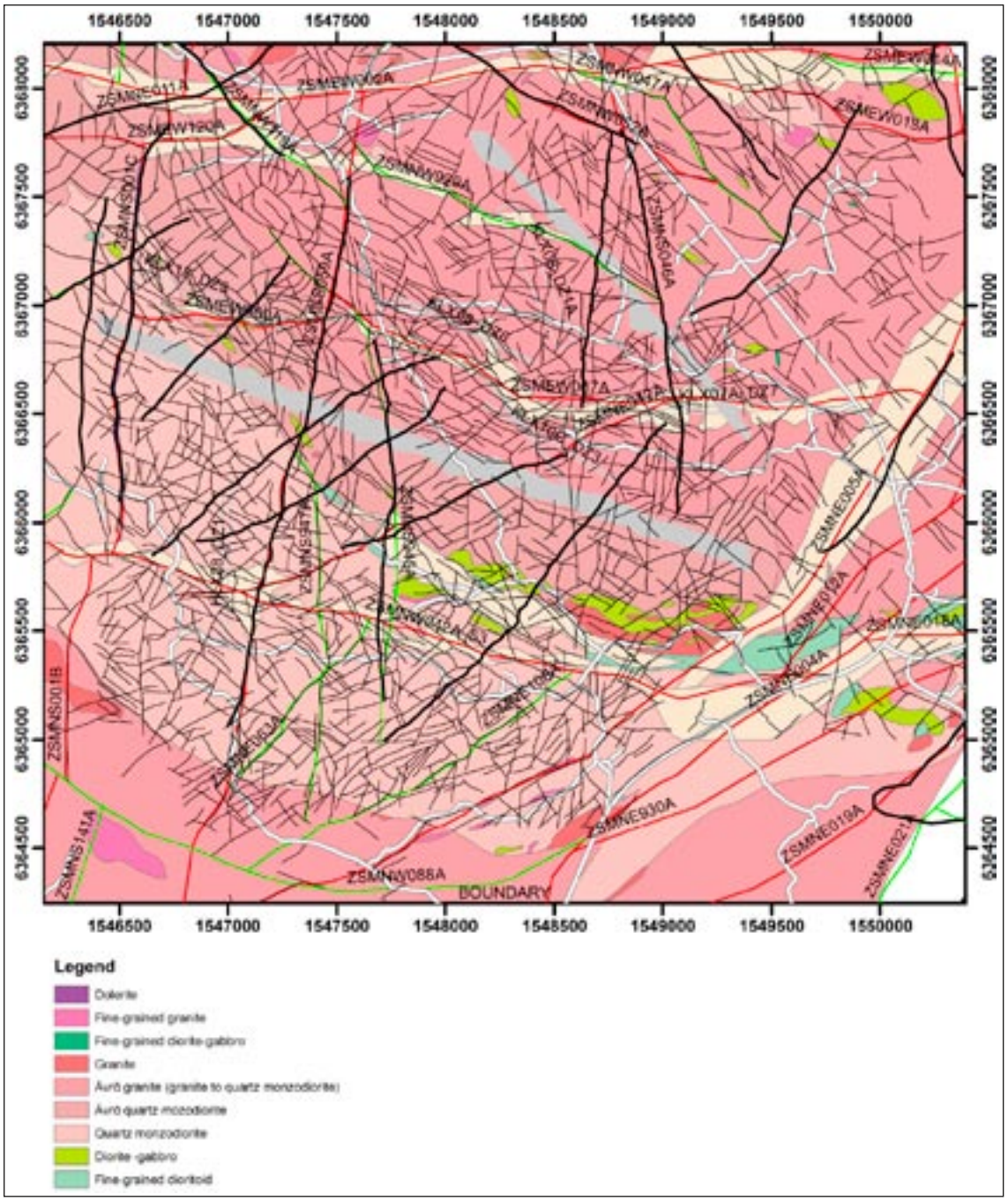

Figure 6-2. *The linked lineament map over the Laxemar local model area, including the preliminary deformation zone model and the bedrock map over Laxemar.*

7 Compilation of hydrogeological data

7.1 Available hydrogeological data and data selection

The main data for HydroDFN modelling are the PFL data (Posiva Flow Log). More specifically it is the interpretation of properties from the hydraulic features; PFL-f data, that is most important. These hydraulically conductive features are mainly coupled to single fractures but may in some cases be connected to a crush zone. The other set of PFL data are PFL-s; the PFL data for 5 m sections. Field data are found in /Ludvigson and Hansson 2002, Kristiansson et al. 2006, Kristiansson 2006, Kyllönen and Leppänen 2007, Pöllänen 2007abc, Pöllänen and Sokolnicki 2004, Pöllänen et al. 2007, 2008, Rouhiainen 2000, Rouhiainen and Sokolnicki 2005, Rouhiainen and Pöllänen 2003ab, 2004, Rouhiainen et al. 2005, Sokolnicki 2006, Sokolnicki and Rouhianien 2005abc, Sokolnicki and Pöllänen 2005, 2007, Sokolnicki and Väisäsvaara 2006, Sokolnicki and Kristiansson 2006, 2007, Väisäsvaara 2006, 2007, Väisäsvaara and Pekkanen 2006, Väisäsvaara et al. 2006abc, 2007/.

In this report all PFL-f data are shown together with geological interpretation of the core holes. NB. In the statistics shown in this chapter, all PFL-f data are included (i.e. also interpreted deformation zones are included in the data).

7.2 Borehole overview

7.2.1 Core-drilled boreholes

Most available single-hole hydraulic data are presented in Appendix 2 and 6. In Appendix 7 PFL-f data (transmissivity and orientation of features) are shown in relation to the geological single-hole interpretation. In this section some of the PFL-f and geological characteristics in the PFL-s measured sections are shown for the individual boreholes KLX02 through KLX29A. (NB. Hydraulic data from KLX27A are not yet available, and are consequently not part of this compilation). The PFL-s measured borehole length is used to extract fracture and crush data as it covers the borehole length where PFL-f features are defined. Generally the PFL-s measured borehole length is almost the same as the geologically mapped borehole length.

7.2.2 Percussion-drilled boreholes

Most available single-hole hydraulic data are presented in Appendix 2. These data are not commented in detail in this report as they are not used for the HydroDFN modelling.

7.3 Summary and discussion

Some selected mean values are given above as an overview. It should however be kept in mind that these figures and plots in Section 7.2 represent the entire measured borehole lengths and includes all deformation zones. Depth trends are present to a small extent concerning open fractures and depth trends are clearly present concerning PFL-f features.

The mean frequency of open fractures within PFL-s measured intervals are for Certain/ Probable/Possible/ Certain+Probable+Possible: 0.40/0.87/1.36/2.63 (frequency: m^{-1}), respectively. There are very few fractures mapped as partly open in the boreholes (mean per borehole: c 6 partly open fractures and 727 open fractures (Certain+Probable+Possible)). Inclusion of open fractures, partly open fractures and crush zones (assuming 40 fractures/m in crush zone) increases the mean frequency of total open fractures within PFL-s measured interval to 2.91 m^{-1}.

Boreholes KLX02 and KLX10B seem to constitute extremes among the boreholes looking at some plots (KLX02: Figure 7-1, KLX10B: Figure 7-1 through Figure 7-4). However, KLX02 was drilled before PLU and was subsequently re-mapped down to c 1,000 m borehole length and essentially only fractures mapped as certain or possible are in the database. Looking at the total fracture frequency (All open, partly open and crush zone fractures (40 fractures/m assumed for crush zones)), results from KLX02 do not differ significantly from the other cored boreholes. KLX10B differs from other boreholes concerning open fractures but it is a very short borehole and the data is from borehole length 10.7–43.5 m, i.e. relatively close to the surface.

The mean of the proportions between Certain/Probable/Possible/ for open fractures within PFL-s measured interval are: 0.11/0.34/0.55. (Mean proportion: No of Certain open fracture/ Total No. of open fractures , etc)

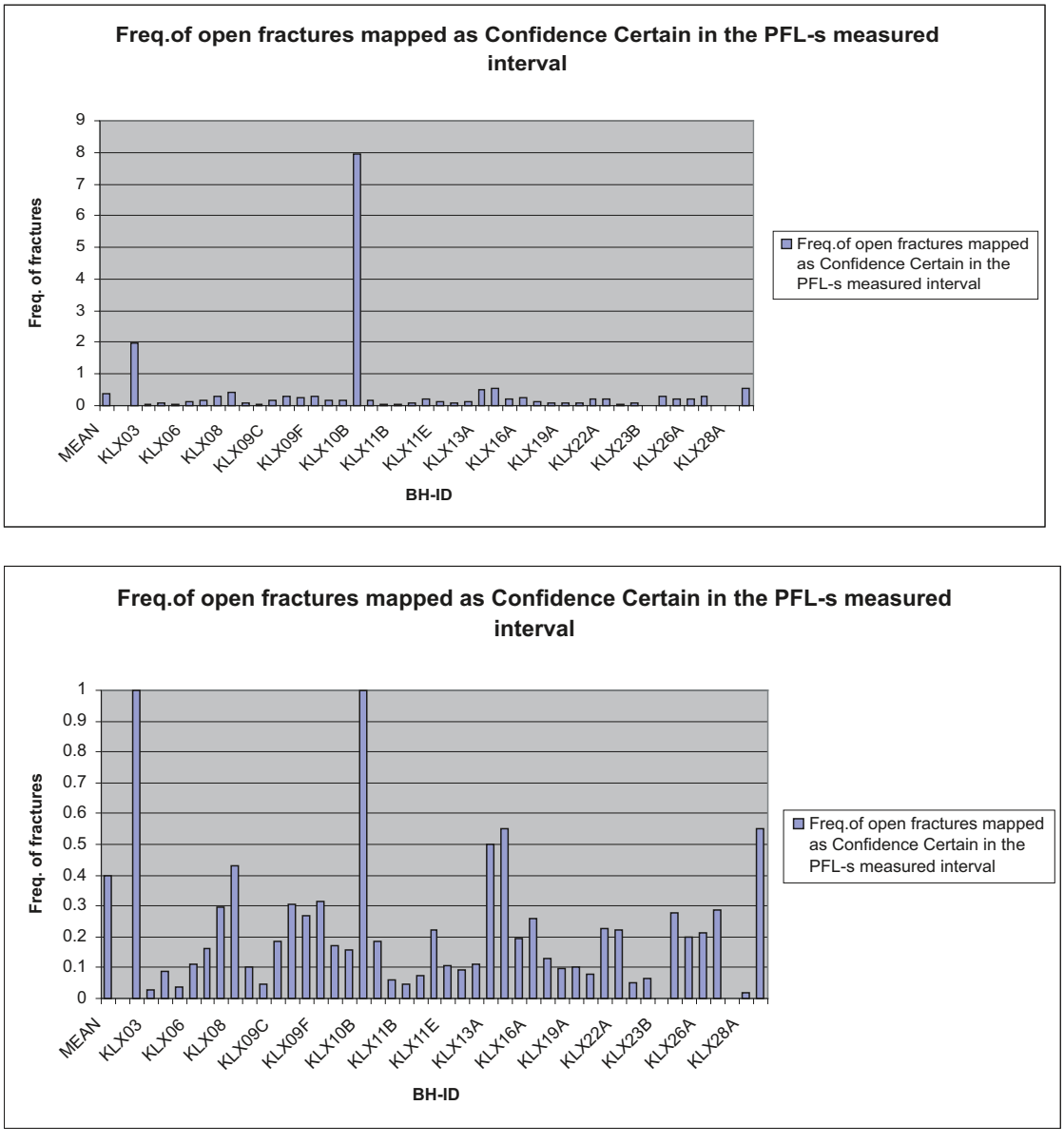

Figure 7-1. *Frequency of mapped open fractures attributed confidence level "certain". Boreholes KLX02 through KLX29A (KLX27A data not included). (Top: vertical scale set to showing all data. Bottom: Limited vertical scale to better visualise data.)*

The frequency of PFL-f features within PFL-s measured interval is 0.30 m^{-1}. That is, c. every tenth open fracture has a transmissivity T > c 10^{-9} m^2/s (=approximate measurement limit for the PFL).

Along the boreholes the mean frequency of crush zones is 0.029 m^{-1}, and.45% of all crush zones have one or several PFL-f features associated with the crush zone. Approximately 9% of the PFL-f are within crush zones.

Approximately 31% of all PFL-f are within deformation zones defined in the geological single-hole interpretation.

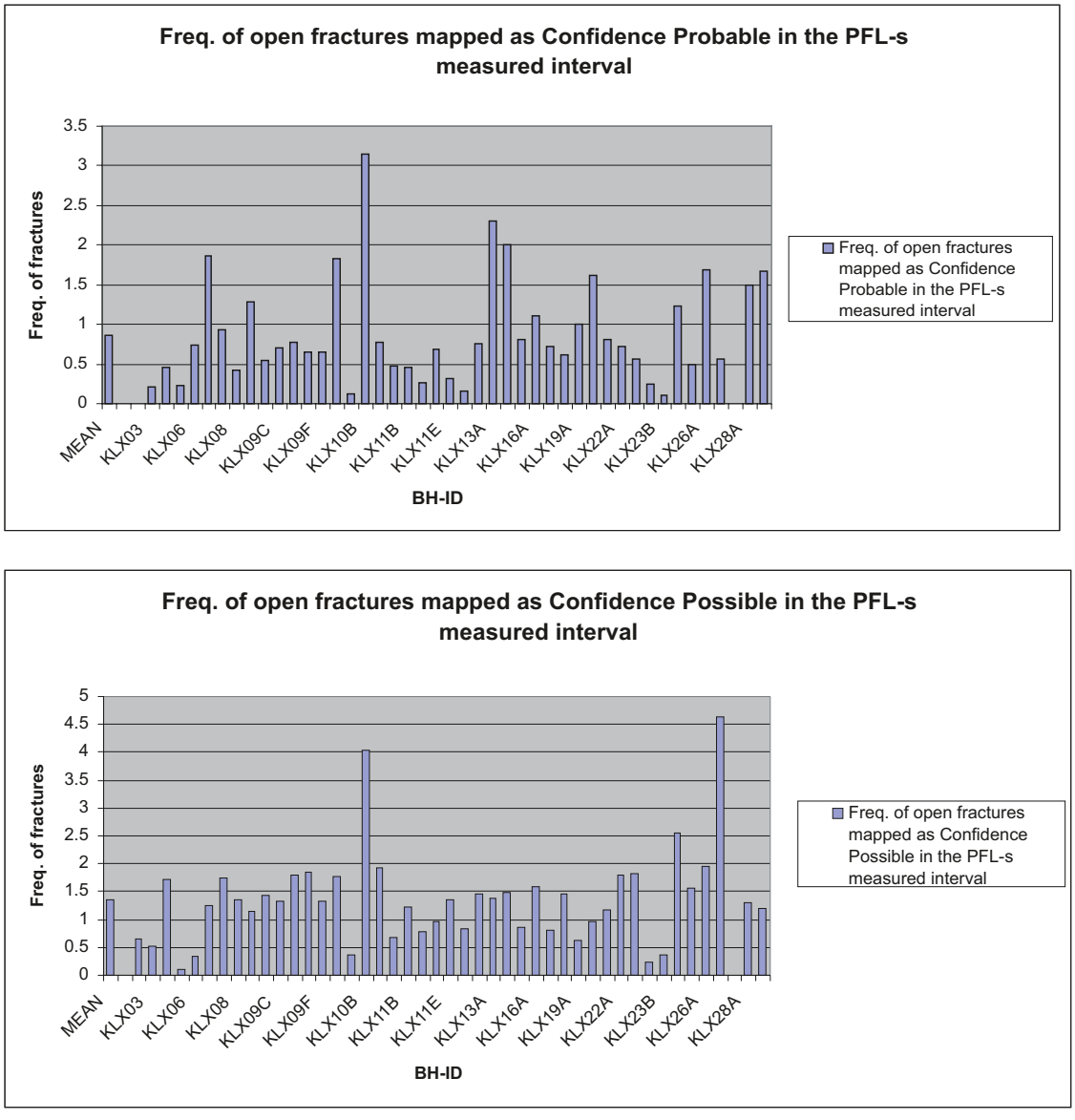

Figure 7-2. *Frequency of mapped open fractures attributed confidence level "probable and possible". Boreholes KLX02 through KLX29 (KLX27A data not included).*

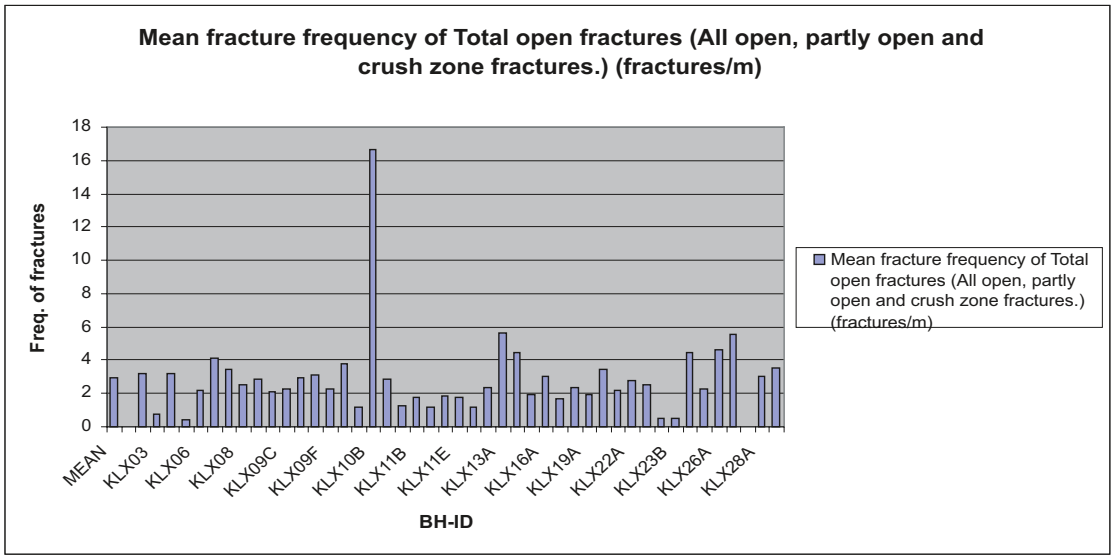

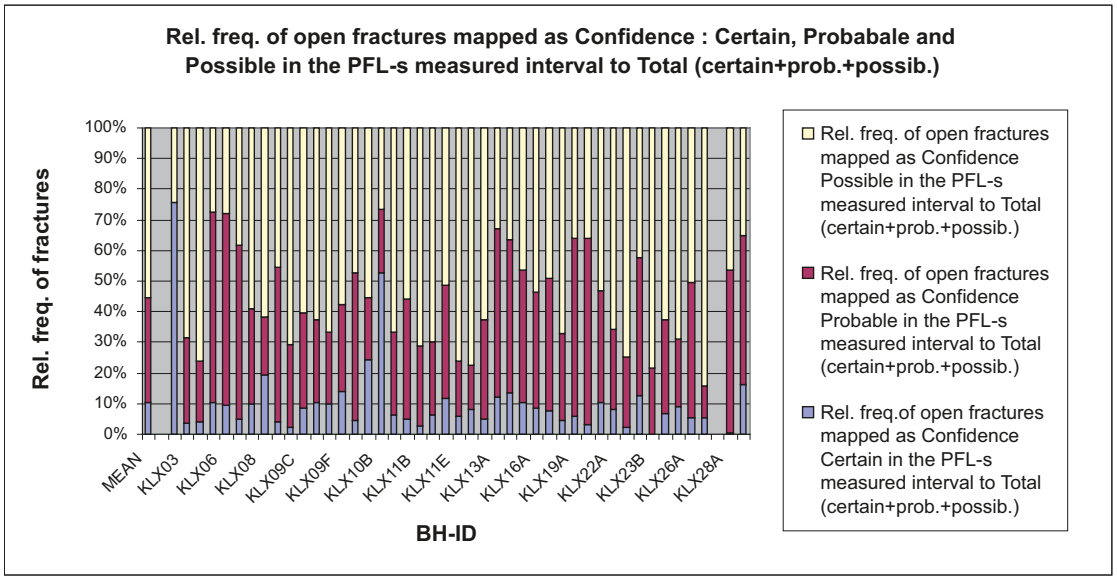

Figure 7-3. *Top: Frequency of Mean fracture frequency of Total open fractures (All open, partly open and crush zone fractures, 40 fractures/m assumed for crush zones). Boreholes KLX02 through KLX29A (KLX27A data not included). Bottom: Relative frequency of mapped open fractures attributed confidence level "certain, probable and possible". Boreholes KLX02 through KLX29A (KLX27A data not included).*

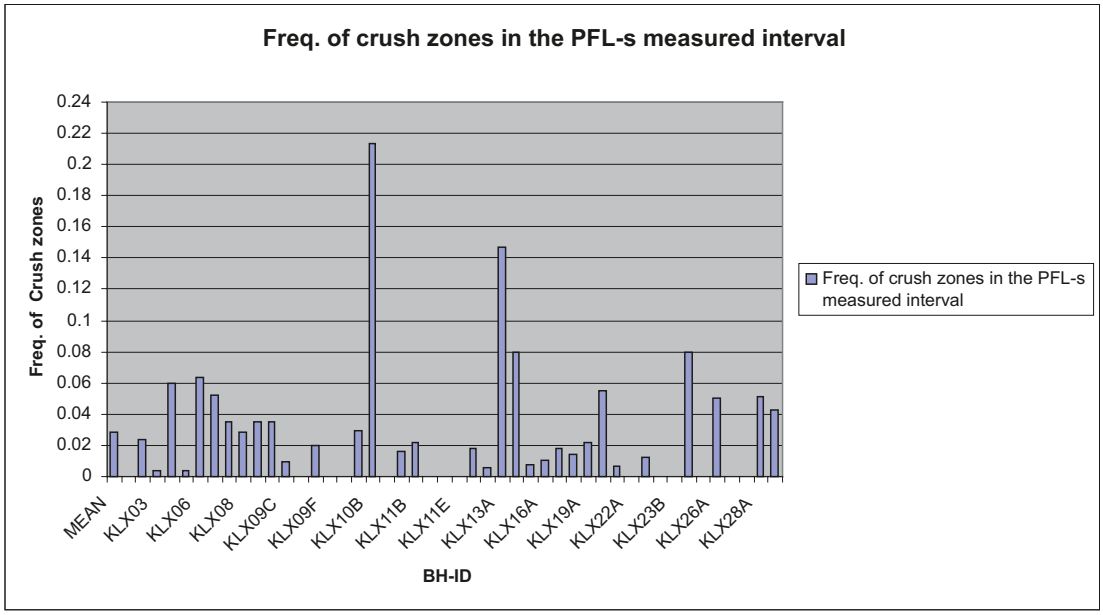

Figure 7-4. *Frequency of crush zones. Boreholes KLX02 through KLX29A (KLX27A data not included).*

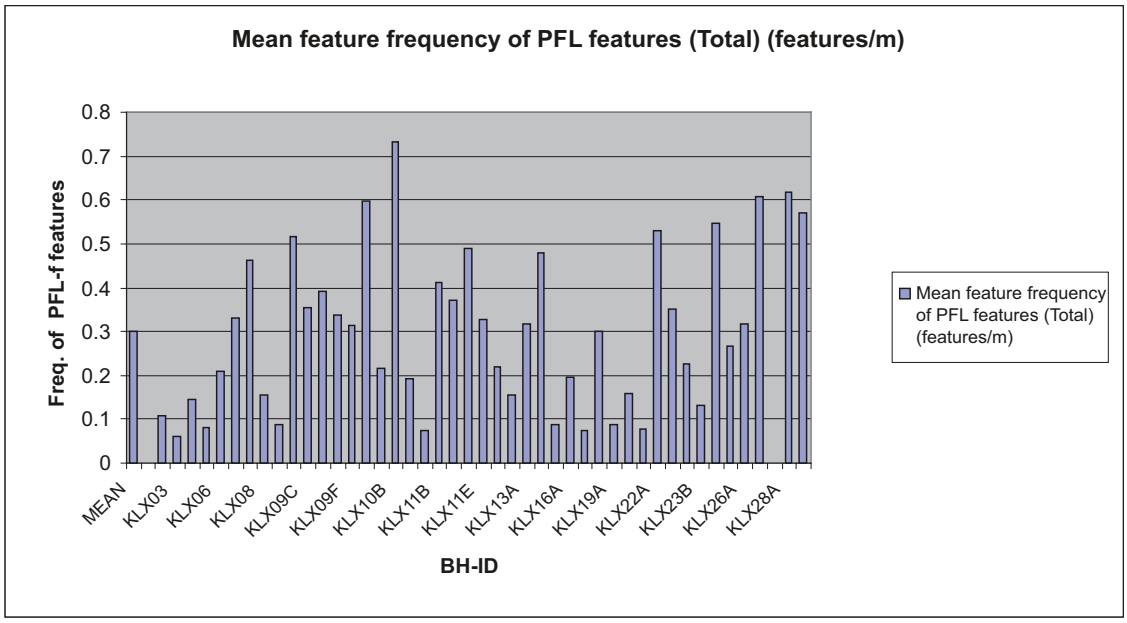

Figure 7-5. *Frequency of PFL-features. Boreholes KLX02 through KLX29A (KLX27A data not included).*

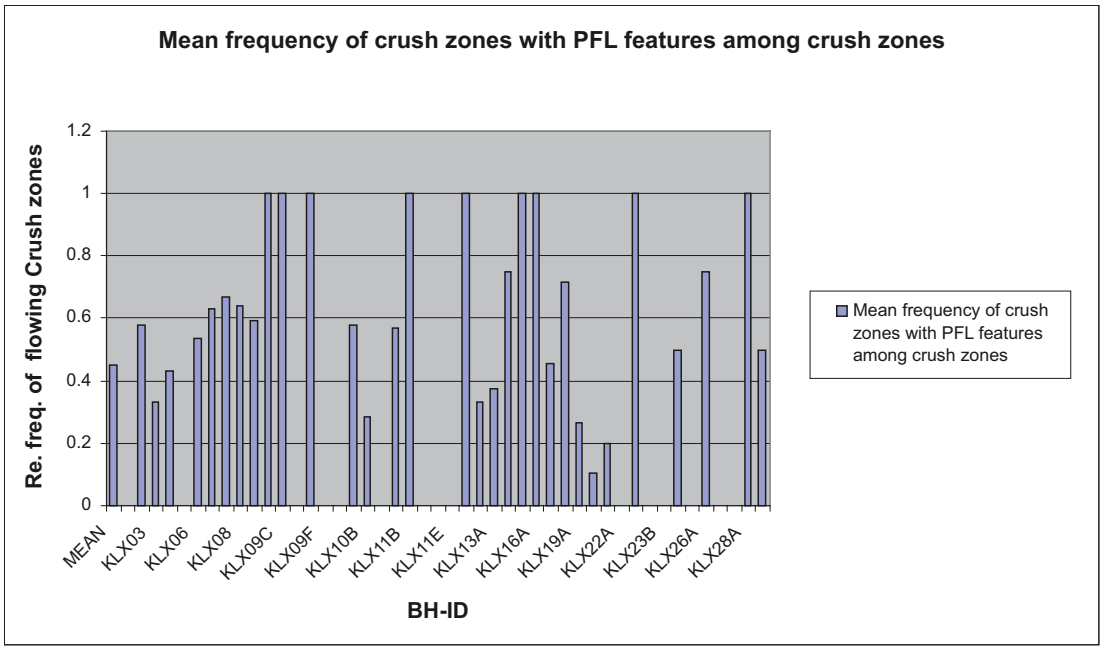

Figure 7-6. *Relative frequency of crush zones with PFL-f ((No. of crush zones with PFL-f) / (Total No. of crush zones)). Boreholes KLX02 to KLX29A (KLX27A data not included).*

8 References

Andersson J, Ström A, Svemar C, Almén K-E, Ericsson L, 2000. Vilka krav ställer djupförvaret på berget? Geovetenskapliga lämplighetsindikatorer och kriterier för lokalisering och platsutvärdering. SKB R-00-15, Svensk Kärnbränslehantering AB.

Carlsten S, Hultgren P, Mattsson H, Stanfors R, Wahlgren C-H, 2006a. Geological single-hole interpretation of KLX06, HLX13, HLX17 and HLX28. Oskarshamn site investigation. SKB P-06-129, Svensk Kärnbränslehantering AB.

Carlsten S, Wahlgren C-H, Hultgren P, Mattsson H, Stanfors R, 2006b. Geological single-hole interpretation of KLX07A, KLX07B, HLX34 and HLX35. Oskarshamn site investigation. SKB P-06-175, Svensk Kärnbränslehantering AB.

Carlsten S, Stråhle A, Hultgren P, Mattsson H, Stanfors R, Wahlgren C-H, 2006c. Geological single-hole interpretation of KLX08. Oskarshamn site investigation. SKB P-06-176, Svensk Kärnbränslehantering AB.

Carlsten S, Mattsson K-J, Curtis P, Hultgren P, Stanfors R, Thunehed H, Wahlgren C-H, 2007a. Geological single-hole interpretation of KLX22A-B, KLX23A-B, KLX24A, KLX25A and KLX26A-B. Oskarshamn site investigation. SKB P-07-66, Svensk Kärnbränslehantering AB.

Carlsten S, Stråhle A, Hultgren P, Thunehed H, Stanfors R, Wahlgren C-H, 2007b. Geological single-hole interpretation of KLX09 and HLX37. Oskarshamn site investigation. SKB P-07-67, Svensk Kärnbränslehantering AB.

Carlsten S, Stråhle A, Hultgren P, Mattsson H, Wahlgren C-H, 2007c. Geological single-hole interpretation of KLX18A and KLX20A. Oskarshamn site investigation. SKB P-07-70, Svensk Kärnbränslehantering AB.

Carlsten S, Mattsson K-J, Stråhle A, Curtis P, Hultgren P, Mattsson H, Stanfors R, Wahlgren C-H, 2007d. Geological single-hole interpretation of KLX28A and KLX29A. Oskarshamn site investigation. SKB P-07-153, Svensk Kärnbränslehantering AB.

Carlsten S, Mattsson K-J, Stråhle A, Curtis P, Hultgren P, Mattsson H, Stanfors R, Wahlgren C-H, 2007e. Geological single-hole interpretation of KLX14A and HLX43. Oskarshamn site investigation. SKB P-07-155, Svensk Kärnbränslehantering AB.

Carlsten S, Stråhle A, Hultgren P, Mattsson H, Stanfors R, Wahlgren C-H, 2007f. Geological single-hole interpretation of KLX13A, HLX39 and HLX41. Oskarshamn site investigation. SKB P-07-156, Svensk Kärnbränslehantering AB.

Carlsten S, Mattsson K-J, Stråhle A, Hultgren P, Mattsson H, Wahlgren C-H, 2007g. Geological single-hole interpretation of KLX19A and HLX38. Oskarshamn site investigation. SKB P-07-161, Svensk Kärnbränslehantering AB.

Cronquist T, Forssberg O, Maersk Hansen L, Jonsson A, Koyi S, Leiner P, Sävås J, Vestgård J, 2004. Detailed fracture mapping of two outcrops at Laxemar. Oskarshamn site investigation. SKB P-04-274, Svensk Kärnbränslehantering AB.

Cronquist T, Forssberg O, Hansen L, Koyi S, Vestgård J, Wikholm M, 2006. Detailed outcrop mapping on drillsite KLX11. Oskarshamn site investigation. SKB P-06-06, Svensk Kärnbränslehantering AB.

Fisher R, 1953. Dispersion on a sphere, Royal Society of London Proceedings 217: 295–305.

Forssberg O, Cronquist T, Hansen L, Vestgård J, 2005. Detailed outcrop mapping at drill site of KLX09 in Laxemar. Oskarshamn site investigation. SKB P-05-260, Svensk Kärnbränslehantering AB.

Forssberg O, Cronquist T, Vestgård J, Bergkvist L, Hermanson J, Öhman J, Pettersson A, Koyi S, Bergman T, 2007. Detailed outcrop mapping in trenches. Oskarshamn site investigation. SKB P-07-29, Svensk Kärnbränslehantering AB.

Hartley L, Jackson P, Joyce S, Roberts D, Shevelan J, Swift B, Gylliing B, Marsic N, Hermanson J, Öhman J, 2007. Hydrogeological pre-modelling exercises. Assessment of impact of the Äspö Hard Rock Laboratory. Sensitivities of palaeo-hydrogeology. Development of a local near-surface Hydro-DFN for KLX09B–F. Site descriptive modelling SDM-Site Laxemar. SKB R-07-57, Svensk Kärnbränslehantering AB.

Kamb W B, 1959. Ice petrofabric observations from Blue Glacier, Washington, in relation to theory and experiments, J. Geophys. Res. 64, pp. 1891–1919.

Kristiansson S, 2006. Oskarshamn site investigation. Difference flow logging of borehole KLX20A. Subarea Laxemar. SKB P-06-183, Svensk Kärnbränslehantering AB.

Kristiansson S, Pöllänen J, Väisäsvaara J, Kyllönen H, 2006. Oskarshamn site investigation. Difference flow logging of borehole , KLX22A-B, KLX23A-B, KLX24A, KLX25A, Subarea Laxemar. SKB P-06-246, Svensk Kärnbränslehantering AB.

Kyllönen H, Leppänen H, 2007. Oskarshamn site investigation. Difference flow logging of borehole KLX19A. Subarea Laxemar. SKB P-07-20, Svensk Kärnbränslehantering AB.

La Pointe P, Fox A, Hermanson J, Öhman J, 2008. Geological discrete fracture network model for the Laxemar site. Site Descriptive Modelling, SDM Site Laxemar. SKB R-08-55, Svensk Kärnbränslehantering AB.

Ludvigson J-E, Hansson K, 2002. Methodology study of Posiva difference flow meter in borehole KLX02 at Laxemar. SKB R-01-52. Svensk Kärnbränslehantering AB.

Mattson H, Triumf C-A, 2007. Detailed ground geophysics at Laxemar, spring 2007. Magnetic total field. Oskarshamn site investigation. SKB P-07-168, Svensk Kärnbränslehantering AB.

Mattsson K-J, Dahlin P, 2007. Boremap mapping of telescopic drilled borehole KLX15A. Oskarshamn site investigation. SKB P-07-157, Svensk Kärnbränslehantering AB.

Mattsson K-J, Dahlin P, 2007. Boremap mapping of telescopic drilled borehole KLX17A. Oskarshamn site investigation. SKB P-07-158, Svensk Kärnbränslehantering AB.

Mattsson K-J, Dahlin P, Lundberg E, 2007. Boremap mapping of telescopic drilled borehole KLX16A. Oskarshamn site investigation. SKB P-07-211, Svensk Kärnbränslehantering AB.

Mattsson K-J, Dahlin P, Lundberg E, 2007. Boremap mapping of telescopic drilled borehole KLX21B. Oskarshamn site investigation. SKB P-07-218, Svensk Kärnbränslehantering AB.

Munier R, Hermanson J, 2001. Metodik för geometrisk modellering Presentation och administration av platsbeskrivande modeller. SKB R-01-15, Svensk Kärnbränslehantering AB.

Munier R, Stenberg L, Stanfors R, Milnes A-G, Hermanson J, Triumf C-A, 2003. Geological Site Descriptive Model. A strategy for the model development during site investigations. SKB R-03-07, Svensk Kärnbränslehantering AB.

Munier R, Stigsson M, 2007. Implementation of uncertainties in borehole geometries and geological orientation data in SICADA. SKB R-07-19, Svensk Kärnbränslehantering AB.

Olsson T, Stanfors R, Sigurdsson O, Erlström M, 2007. Identification and characterization of minor deformation zones based on lineament interpretation. Oskarshamn site investigation. SKB P-06-282, Svensk Kärnbränslehantering AB.

Schmidt W, 1917. Statistische Methoden beim Gefugestudium Kristalliner Schiefer: Kaiserliche Akademie der Wissenhaften in Wien, Sitzungsberichte, Mathematisch-Naturwissenschaftliche Klasse, Abtheilung 1, v. 126, p. 515–538.

SKB, 2002. Simpevarp – site descriptive model version 0. SKB R-02-35, Svensk Kärnbränslehantering AB.

SKB, 2004. Preliminary site description Simpevarp area – version 1.1. SKB R-04-25, Svensk Kärnbränslehantering AB.

SKB, 2005. Preliminary site description Simpevarp subarea – version 1.2. SKB R-05-08, Svensk Kärnbränslehantering AB.

SKB, 2006a. Preliminary site description Laxemar subarea – version 1.2. SKB R-06-10, Svensk Kärnbränslehantering AB.

SKB, 2006b. Preliminary site description Laxemar stage 2.1. Feedback for completion of the site investigation including input from safety assessment and repository engineering. SKB R-06-110, Svensk Kärnbränslehantering AB.

Triumf C-A, 2004. Joint interpretation of lineaments. Oskarshamn site investigation. SKB P-04-49, Svensk Kärnbränslehantering AB.

Triumf C-A, Thunehed H, 2007. Coordinated lineaments longer than 100 m at Laxemar, Identification of lineaments from LIDAR data and co-ordination with lineaments in other topographic and geophysical data, Oskarshamn site investigation. SKB P-06-262, Svensk Kärnbränslehantering AB.

Wahlgren C-H, Hermanson J, Forssberg O, Curtis P, Triumf C-A, Drake H, Tullborg E-L, 2006. Geological description of rock domains and deformation zones in the Simpevarp and Laxemar subareas. Preliminary site description Laxemar subarea – version 1.2. SKB R-05-69, Svensk Kärnbränslehantering AB.

Väisäsvaara J, 2006. Oskarshamn site investigation. Difference flow logging of borehole KLX14A. Subarea Laxemar. SKB P-06-318, Svensk Kärnbränslehantering AB.

Väisäsvaara J, Pekkanen J, 2006. Oskarshamn site investigation. Difference flow logging of borehole KLX13A. Subarea Laxemar. SKB P-06-245, Svensk Kärnbränslehantering AB.

Väisäsvaara J, Heikkinen P, Kristiansson S, Pöllänen J, 2006a. Oskarshamn site investigation. Difference flow logging of borehole KLX09. Subarea Laxemar. SKB P-06-164, Svensk Kärnbränslehantering AB.

Väisäsvaara J, Heikkinen P, Kristiansson S, Pöllänen J, 2006b. Oskarshamn site investigation. Difference flow logging of borehole KLX12A. Subarea Laxemar. SKB P-06-185, Svensk Kärnbränslehantering AB.

Väisäsvaara J, Leppänen H, Kristiansson S, Pöllänen J, 2006c. Oskarshamn site investigation. Difference flow logging of borehole KLX09G, KLX10B and KLX10C. Subarea Laxemar. SKB P-06-229, Svensk Kärnbränslehantering AB.

Väisäsvaara J, 2007. Oskarshamn site investigation. Difference flow logging of borehole KLX16A. Subarea Laxemar. SKB P-07-87, Svensk Kärnbränslehantering AB.

Väisäsvaara J, Kristiansson S, Sokolnicki M, 2007. Oskarshamn site investigation. Difference flow logging of borehole KLX11A. Subarea Laxemar. SKB P-07-24, Svensk Kärnbränslehantering AB.

Appendix 1

Procedure for reporting errors in primary data in site modelling

Företagsintern

Rutin

DOKUMENTID	VERSION	STATUS	REG.NR	SIDA
1095416	1.0	Godkänt	SD-141	1(4)
FÖRFATTARE Göran Rydén			SKAPAD DEN 2008-02-15	
GRANSKAD AV Karl-Erik Almén Niklas Heneryd			GRANSKAD DATUM 2008-03-26 2008-04-08	
GODKÄND AV Ebbe Eriksson			GODKÄND DATUM 2008-04-14	

SD-141 Hantering av fel i primärdata

Innehållsförteckning

Svensk Kärnbränslehantering AB
Box 250, 101 24 Stockholm
Besöksadress Blekholmstorget 30
Telefon 08-459 84 00 Fax 08-661 57 19
www.skb.se
556175-2014 Säte Stockholm

1. Syfte

Syftet med rutinen är att beskriva hur fel i primärdata skall rapporteras och åtgärdas inom SKB, samt informera om felen och hur de har blivit åtgärdade. SD-141 är kopplat till SDK-508 Hantering av primärdata vid platsundersökningar, SD-112 Inlagring och utleverans av data, SD-113 GIS - Inlagring och utleverans av data och SDTD-217 Hantering av data vid Äspölaboratoriet.

2. Omfattning

Rutinen gäller för projekt och undersökningar inom SKB som lagrar primärdata i databaserna SICADA och SDE(GIS), även för modeller och tolkningar. Den gäller inte för avvikelser som omhändertas i SD-006 Hantering av avvikelser och förbättringsförslag.

3. Definitioner

Primärdata	Data och metadata som lagras i databaserna SICADA och SDE(GIS).
Fel	Med fel avses oklarheter eller fel i kvalitetssäkrade primärdata.
Kvalitetssäkrade data	Data kontrollerad och signerad av ansvarig.
Låsta primärdata	Lagrad primärdata som ej är tillgängliga för utvärdering eller bearbetning.
SICADA BugReport	Sicadas ärendehanteringssystem.
Dataägare	Projektledare och efter projektslut ansvarig linjechef.

Se även SD-127 Definitioner av begrepp i Ledningssystemet.

4. Ansvar och befogenheter

V-Informationshantering funktion datahantering	ansvarar för registrering av upptäckta fel samt att meddela den som är ansvarig för att åtgärda felet samt att ge information så att berörda kan ta del av fel samt återrapportering när rapporterat fel är åtgärdat.
Verksamhetsansvarig	har det övergripande ansvaret för att enhetens inrapporterade fel blir åtgärdade.
Aktivitetsledare/koordinator /ämnesansvarig	ansvarar för att låsa felaktiga primärdata.
Informationsförvaltare	befogenhet att låsa felaktiga primärdata
Användare av data	var och en som använder data skall med hjälp av bugglistan regelbundet bevaka rapporterade fel i primärdata. Ansvarar för att rapportera upptäckta fel. Analys eller vidare arbete med dessa data får ej ske utan dataägarens medgivande.

Operatör	lagrar data i Sicada eller Gis
Metodansvarig	är ansvarig för metodenbeskrivningen

Den som får ett fel tilldelat sig för åtgärd skall snarast möjligt åtgärda felet, dokumentera åtgärder samt återrapportera till funktion Datahantering när åtgärden är utförd.

5. Genomförande

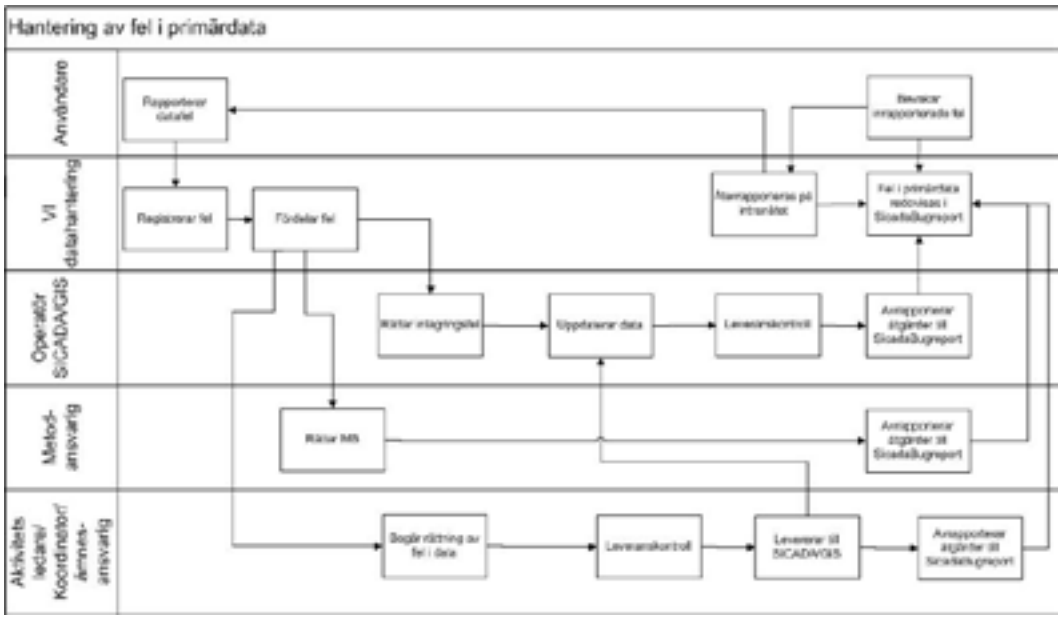

5.1 Upptäckt och inrapportering

Den som upptäcker fel i primärdata skall inrapportera felet till SICADA BugReport. Om den som rapporterar fel inte har tillgång till BugReport skall rapportering ske till epost-adressen data.error@skb.se. VI datahantering redovisar fel och dess åtgärder i en exposevy på intranät. Exposevyn hittas på VI:s sida om SICADA. Detta är enda ordinarie informationskanalen till berörda om fel i primärdata och rättning av primärdata.

Vid inrapporteringen skall tydligt dokumenteras vilken primärdatamängd som felet finns i, samt beskriva felet. Vidare skall om möjligt felets påverkan på projektet bedömas och biläggas dokumentationen.

Systematiska fel samt fel som bedöms som allvarliga skall även generera avvikelse enligt rutin SD-006 Hantering av avvikelser och förbättringsförslag.

5.2 Hantering av fel i primärdata

För varje upptäckt fel skall ansvarig person inom ansvarig enhet identifieras, och kontaktas för att felet skall åtgärdas.

- Om felet orsakats av felaktig handhavande vid inlagring i databaser så överlämnas det normalt till databasoperatör som ska rätta felet i databaserna.
- Om felet härrör från en inlevererad datamängd så överlämnas felet till ansvarig aktivitetsledare/koordinator/ämnesansvarig.
- Om felet orsakas av metodfel eller systemfel överlämnas det till metodansvarig för åtgärd.

Den som får i uppgift att åtgärda ett fel skall göra detta så snart som möjligt. Rättning av fel har hög prioritet.
Primärdata som är rapporterade som fel skall låsas i databaserna vid behov.

5.3 Rättning och frisläppande av data

Rättning av fel skall ske enligt normala rutiner för hantering och inlagring av data. Se SDK-508 Hantering av primärdata vid platsundersökningar, SD-112 Inlagring och utleverans av data, SD-113 GIS - Inlagring och utleverans av data eller SDTD-217 Hantering av data vid Äspölaboratoriet. Hur felet åtgärdats skall dokumenteras och samlas i SICADA BugReport. Om felet kan finnas på andra data skall även dessa data kontrolleras. Återrapportering och information till användare om åtgärdade fel sker genom uppvisning av buggar på en expose-vy på intranätet. Information till berörda om allvarliga fel i primärdata kan även rapporteras via e-post.

När det uppstår tveksamhet i samband med bedömningen av ett förmodat fel i primärdata skall ämnesansvariga kontaktas. Berörd aktivitetsledare och ämnesansvarig/koordinator behandlar då ärendet gemensamt och avgör vilka åtgärder som skall vidtas.

När data rättas och ingår i en P-rapport skall rapporten uppdateras enligt rutin SDK-107 Framtagande och hantering av P-rapporter.

6. Dokumenthantering

Dokumentationen hanteras enligt VI dokumenthanteringsplan SKBdoc id: 1068702

7. Referenser

SDK-508 Hantering av primärdata vid platsundersökningar
SD-112 Inlagring och utleverans av data
SD-113 GIS - Inlagring och utleverans av data
SD-006 Hantering av avvikelser och förbättringsförslag
SDK-107 Framtagande och hantering av P-rapporter
SDTD-217 Hantering av data vid Äspölaboratoriet

Revisionsförteckning

Version	Datum	Revideringen omfattar	Utförd av	Granskad	Godkänd
1.0	2008-	Ersätter SDK-517. Rutinen är helt omarbetad.	Göran Rydén		

Appendix 2

WellCad plots for geological, hydrogeological and hydrochemical data – Cored boreholes

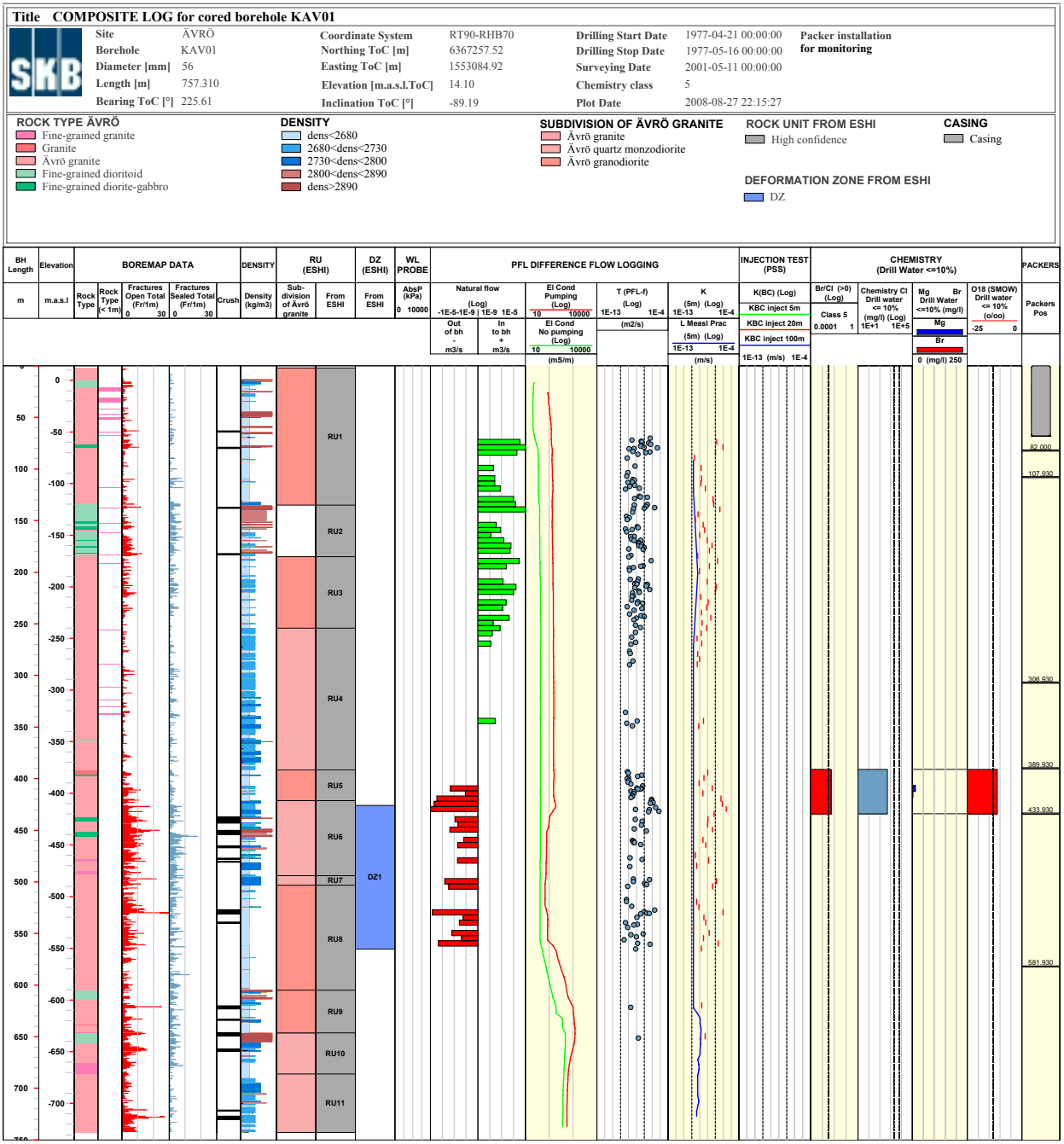

Title COMPOSITE LOG for cored borehole KAV04A

Site	ÄVRÖ	**Coordinate System**	RT90-RHB70	**Drilling Start Date**	2003-12-10 13:55:00	**Packer installation for monitoring**	
Borehole	KAV04A	**Northing ToC [m]**	6366795.76	**Drilling Stop Date**	2004-05-03 14:53:00		
Diameter [mm]	76	**Easting ToC [m]**	1552475.00	**Surveying Date**	2003-11-04 14:30:00		
Length [m]	1004.000	**Elevation [m.a.s.l.ToC]**	10.35	**Chemistry class**	5		
Bearing ToC [°]	77.03	**Inclination ToC [°]**	-84.90	**Plot Date**	2008-08-27 22:15:27		

ROCK TYPE ÄVRÖ
- Fine-grained granite
- Pegmatite
- Granite
- Ävrö granite
- Quartz monzodiorite
- Diorite / Gabbro
- Fine-grained dioritoid
- Fine-grained diorite-gabbro

DENSITY
- dens<2680
- 2680<dens<2730
- 2730<dens<2800
- 2800<dens<2890
- dens>2890

SUBDIVISION OF ÄVRÖ GRANITE
- Ävrö granite
- Ävrö quartz monzodiorite
- Ävrö granodiorite

ROCK UNIT FROM ESHI
- High confidence

CASING
- Casing

DEFORMATION ZONE FROM ESHI
- DZ

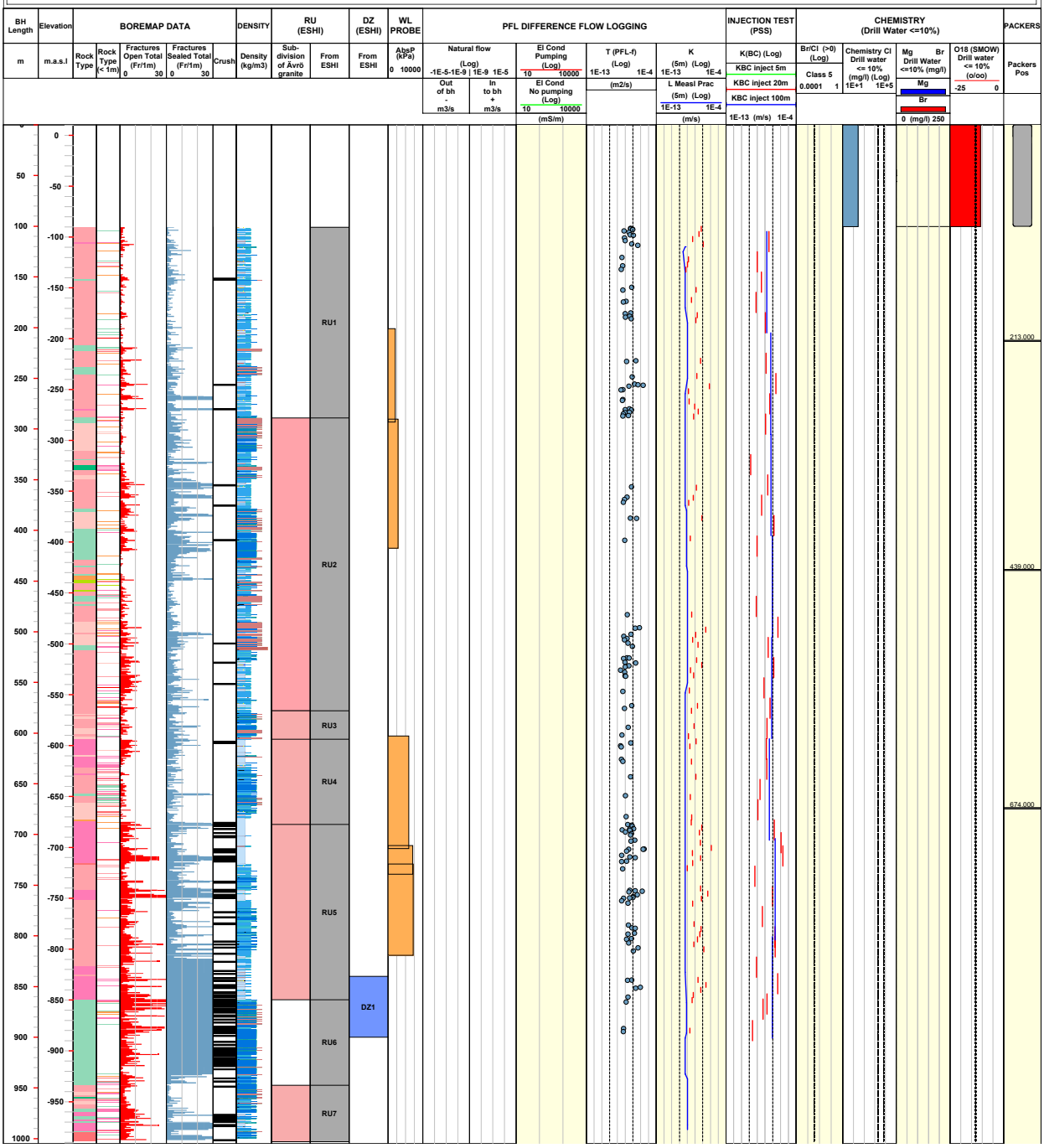

Title COMPOSITE LOG for cored borehole KAV04B

Site	ÄVRÖ	**Coordinate System**	RT90-RHB70	**Drilling Start Date**	2004-05-12 07:20:00	**Packer installation for monitoring**	
Borehole	KAV04B	**Northing ToC [m]**	6366795.64	**Drilling Stop Date**	2004-05-18 07:31:00		
Diameter [mm]	76	**Easting ToC [m]**	1552474.47	**Surveying Date**	2004-05-25 10:15:00		
Length [m]	101.030	**Elevation [m.a.s.l.ToC]**	10.35	**Chemistry class**	$Class		
Bearing ToC [°]	134.27	**Inclination ToC [°]**	-89.83	**Plot Date**	2008-08-31 22:34:28		

ROCK TYPE ÄVRÖ
- Fine-grained granite
- Granite
- Ävrö granite

DENSITY
- dens<2680
- 2680<dens<2730

SUBDIVISION OF ÄVRÖ GRANITE
- Ävrö granite
- Ävrö quartz monzodiorite
- Ävrö granodiorite

ROCK UNIT FROM ESHI
- High confidence

CASING
- Casing

DEFORMATION ZONE FROM ESHI
- DZ

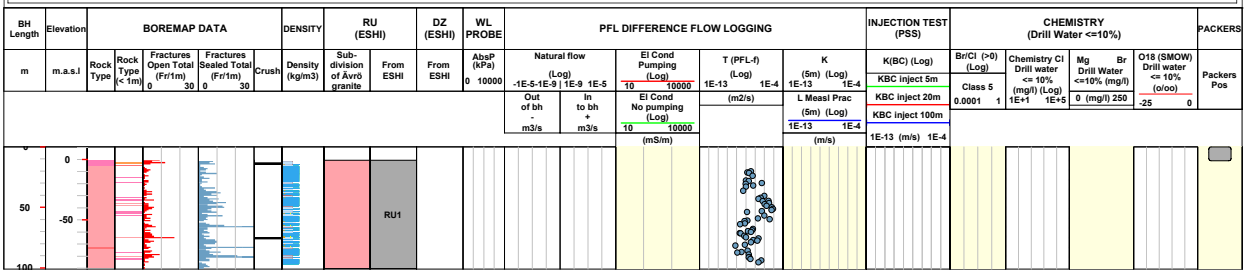

Title COMPOSITE LOG for cored borehole KAV01

Site	ÄVRÖ	Coordinate System	RT90-RHB70	Drilling Start Date	1977-04-21 00:00:00	Packer installation for monitoring	
Borehole	KAV01	Northing ToC [m]	6367257.52	Drilling Stop Date	1977-05-16 00:00:00		
Diameter [mm]	56	Easting ToC [m]	1553084.92	Surveying Date	2001-05-11 00:00:00		
Length [m]	757.310	Elevation [m.a.s.l.ToC]	14.10	Chemistry class	5		
Bearing ToC [°]	225.61	Inclination ToC [°]	-89.19	Plot Date	2008-08-27 22:15:27		

ROCK TYPE ÄVRÖ
- Fine-grained granite
- Granite
- Ävrö granite
- Fine-grained dioritoid
- Fine-grained diorite-gabbro

DENSITY
- dens<2680
- 2680<dens<2730
- 2730<dens<2800
- 2800<dens<2890
- dens>2890

SUBDIVISION OF ÄVRÖ GRANITE
- Ävrö granite
- Ävrö quartz monzodiorite
- Ävrö granodiorite

ROCK UNIT FROM ESHI
- High confidence

CASING
- Casing

DEFORMATION ZONE FROM ESHI
- DZ

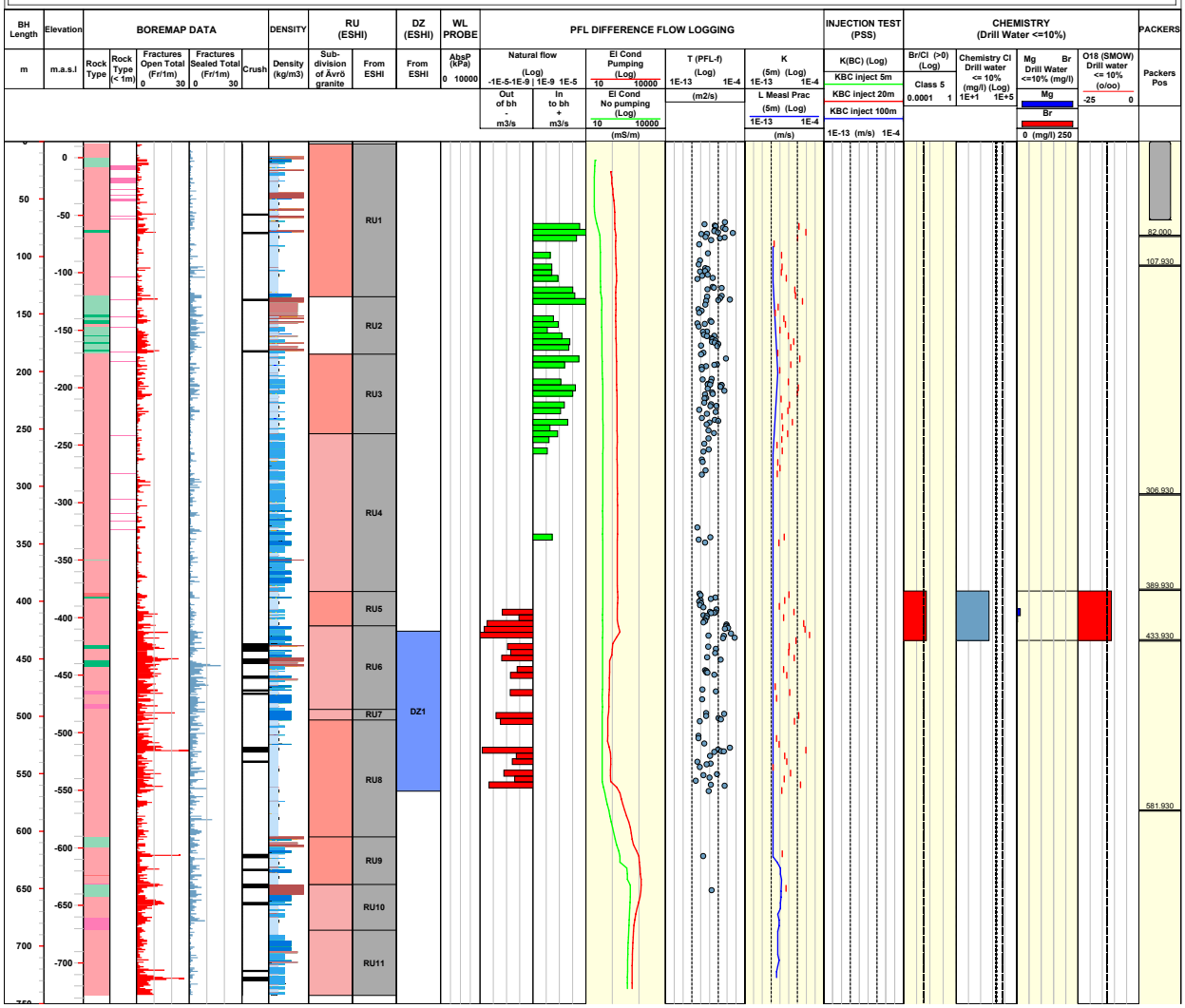

Title COMPOSITE LOG for cored borehole KLX01

Site	LAXEMAR	Coordinate System	RT90-RHB70	Drilling Start Date	1987-12-05 00:00:00	**Packer installation for monitoring**	
Borehole	KLX01	Northing ToC [m]	6367485.52	Drilling Stop Date	1987-12-15 00:00:00		
Diameter [mm]	56	Easting ToC [m]	1549923.09	Surveying Date	2001-05-11 00:00:00		
Length [m]	1077.990	Elevation [m.a.s.l.ToC]	16.77	Chemistry class	$Class		
Bearing ToC [°]	348.73	Inclination ToC [°]	-85.29	Plot Date	2007-11-25 22:03:30		

ROCK TYPE LAXEMAR
- Fine-grained granite
- Pegmatite
- Ävrö granite
- Diorite / Gabbro
- Fine-grained diorite-gabbro

DENSITY
- unclassified
- dens<2710
- 2710<dens<2820
- 2820<dens<2930
- dens>2930

SUBDIVISION OF ÄVRÖ GRANITE
- Ävrö granite
- Ävrö quartz monzodiorite
- Ävrö granodiorite

ROCK UNIT FROM ESHI
- Medium confidence
- High confidence

DEFORMATION ZONE FROM ESHI
- DZ

CASING
- Casing

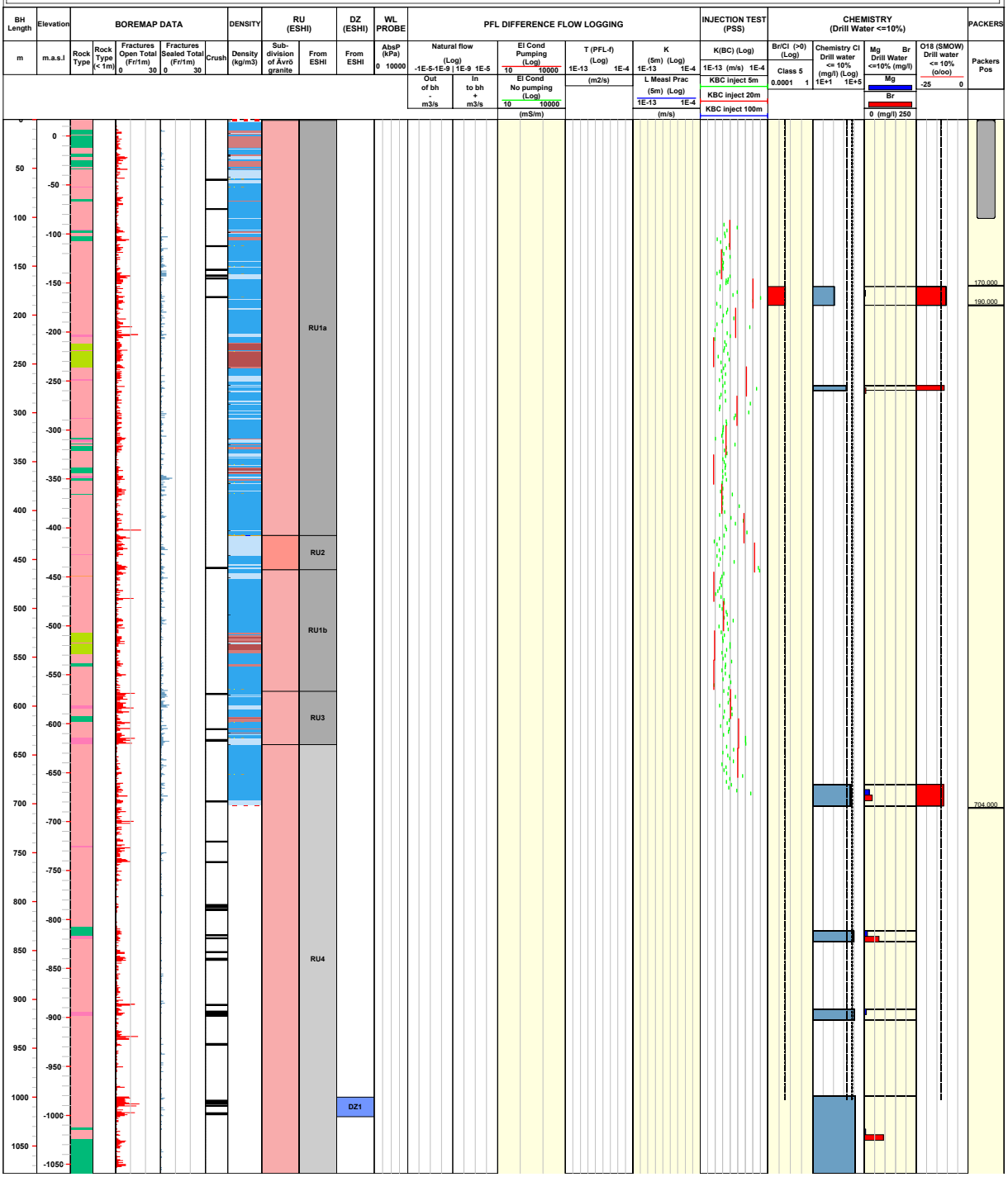

Title COMPOSITE LOG for cored borehole KLX02

Site	LAXEMAR	**Coordinate System**	RT90-RHB70	**Drilling Start Date**	1992-08-15 00:00:00	**Packer installation for monitoring**	
Borehole	KLX02	**Northing ToC [m]**	6366768.99	**Drilling Stop Date**	1992-09-05 00:00:00		
Diameter [mm]	76	**Easting ToC [m]**	1549224.09	**Surveying Date**	2001-05-11 00:00:00		
Length [m]	1700.500	**Elevation [m.a.s.l.ToC]**	18.40	**Chemistry class**	5		
Bearing ToC [°]	357.30	**Inclination ToC [°]**	-84.99	**Plot Date**	2008-08-18 22:12:45		

ROCK TYPE LAXEMAR
- Fine-grained granite
- Ävrö granite
- Fine-grained dioritoid
- Fine-grained diorite-gabbro

DENSITY
- dens<2680
- 2680<dens<2730
- 2730<dens<2800
- 2800<dens<2890
- dens>2890

SUBDIVISION OF ÄVRÖ GRANITE
- Ävrö granite
- Ävrö quartz monzodiorite
- Ävrö granodiorite

ROCK UNIT FROM ESHI
- High confidence

CASING
- Casing

DEFORMATION ZONE FROM ESHI
- DZ

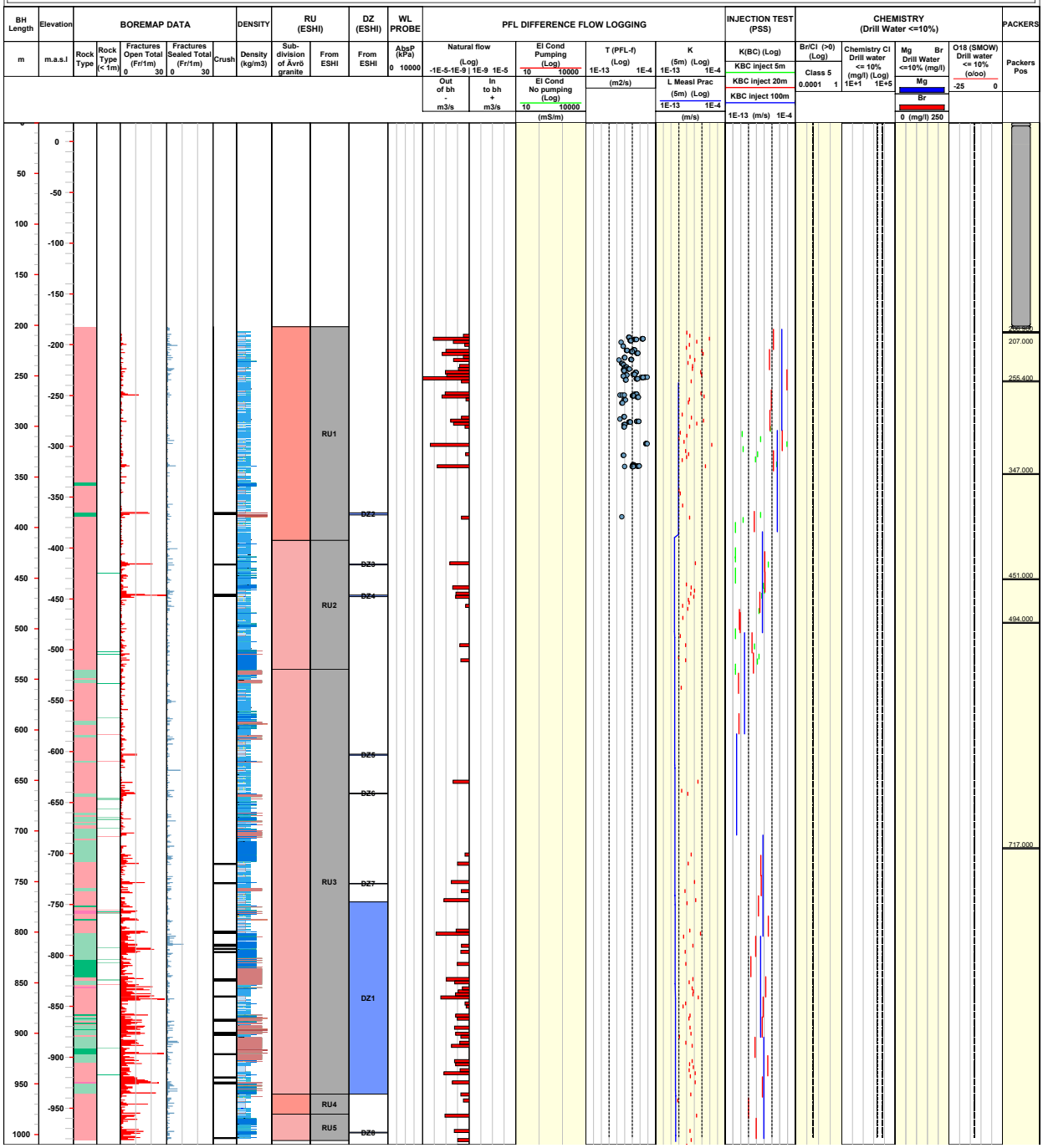

Title COMPOSITE LOG for cored borehole KLX03

Site	LAXEMAR	**Coordinate System**	RT90-RHB70	**Drilling Start Date**	2004-05-28 18:00:00	**Packer installation for monitoring**
Borehole	KLX03	**Northing ToC [m]**	6366112.59	**Drilling Stop Date**	2004-09-07 09:00:00	
Diameter [mm]	76	**Easting ToC [m]**	1547718.93	**Surveying Date**	2004-05-13 14:55:00	
Length [m]	1000.420	**Elevation [m.a.s.l.ToC]**	18.49	**Chemistry class**	5	
Bearing ToC [°]	199.04	**Inclination ToC [°]**	-74.92	**Plot Date**	2008-08-18 22:12:45	

ROCK TYPE LAXEMAR
- Fine-grained granite
- Ävrö granite
- Quartz monzodiorite
- Diorite / Gabbro
- Fine-grained dioritoid
- Fine-grained diorite-gabbro

DENSITY
- dens<2680
- 2680<dens<2730
- 2730<dens<2800
- 2800<dens<2890
- dens>2890

SUBDIVISION OF ÄVRÖ GRANITE
- Ävrö granite
- Ävrö quartz monzodiorite
- Ävrö granodiorite

ROCK UNIT FROM ESHI
- High confidence

CASING
- Casing

DEFORMATION ZONE FROM ESHI
- DZ

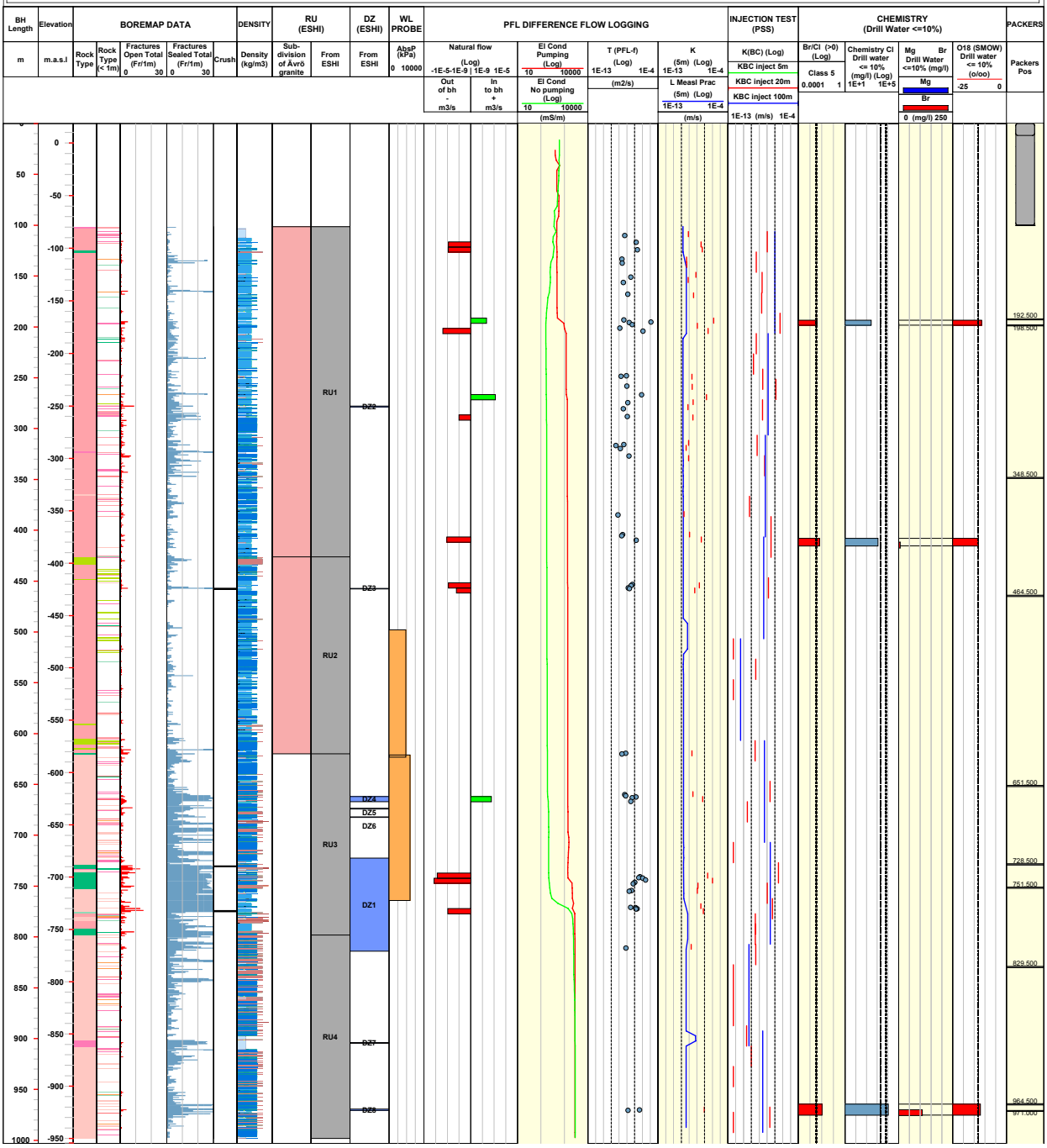

Title COMPOSITE LOG for cored borehole KLX04

Site	LAXEMAR	**Coordinate System**	RT90-RHB70	**Drilling Start Date**	2004-03-13 11:00:00	**Packer installation for monitoring**	2005-01-29 00:00:00
Borehole	KLX04	**Northing ToC [m]**	6367077.19	**Drilling Stop Date**	2004-06-28 10:12:00		
Diameter [mm]	76	**Easting ToC [m]**	1548171.94	**Surveying Date**	2004-02-19 13:10:00		
Length [m]	993.490	**Elevation [m.a.s.l.ToC]**	24.09	**Chemistry class**	5		
Bearing ToC [°]	0.93	**Inclination ToC [°]**	-84.75	**Plot Date**	2008-08-18 22:12:45		

ROCK TYPE
- Fine-grained granite
- Granite
- Ävrö granite
- Quartz monzodiorite
- Diorite / Gabbro
- Fine-grained dioritoid
- Fine-grained diorite-gabbro

DENSITY
- dens<2680
- 2680<dens<2730
- 2730<dens<2800
- 2800<dens<2890
- dens>2890

SUBDIVISION OF ÄVRÖ GRANITE
- Ävrö granite
- Ävrö quartz monzodiorite
- Ävrö granodiorite

ROCK UNIT FROM ESHI
- High confidence

CASING
- Casing

DEFORMATION ZONE FROM ESHI
- DZ

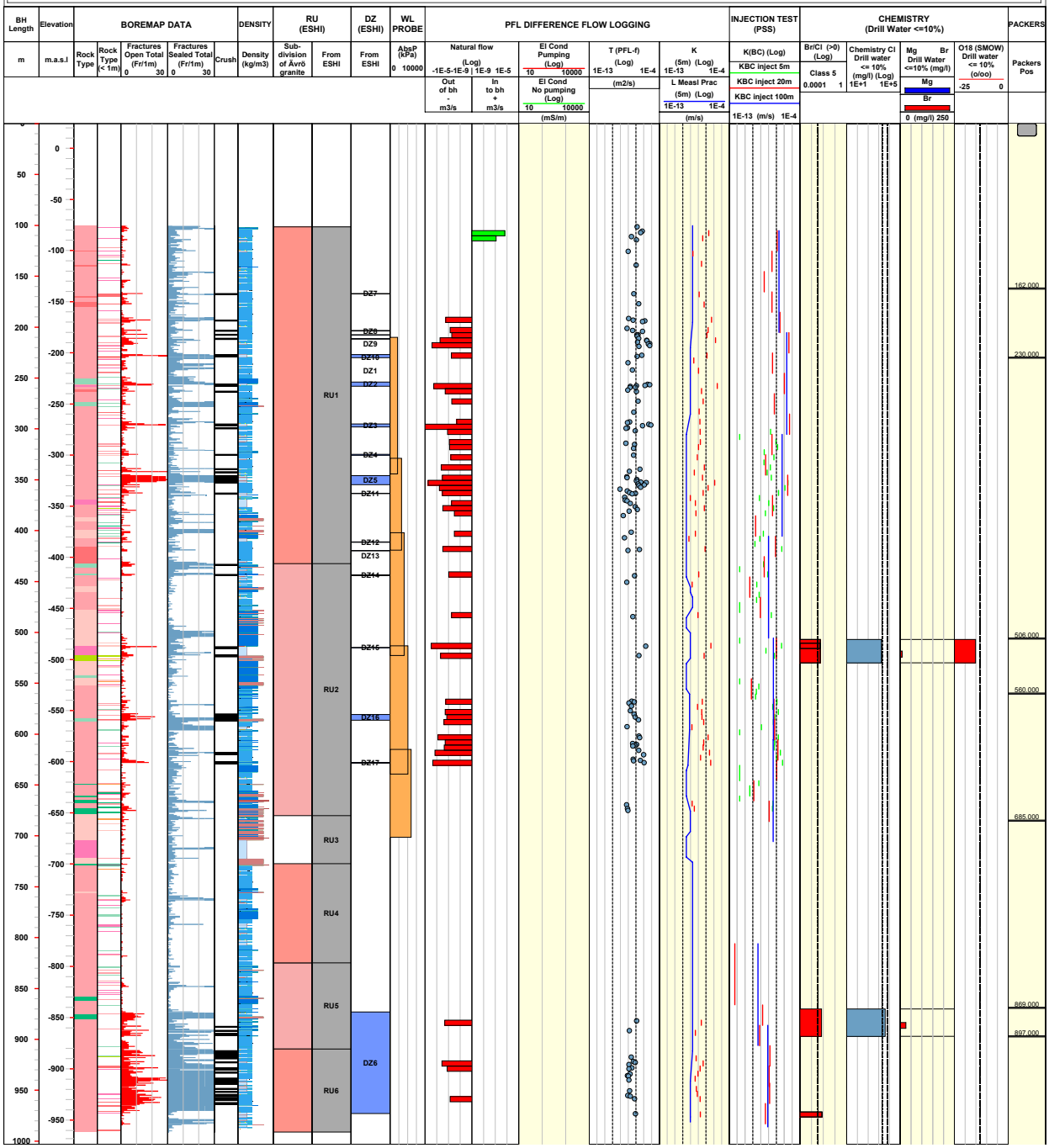

Title COMPOSITE LOG for cored borehole KLX05

Site	LAXEMAR	**Coordinate System**	RT90-RHB70	**Drilling Start Date**	2004-10-01 14:00:00	**Packer installation for monitoring**	
Borehole	KLX05	**Northing ToC [m]**	6365633.34	**Drilling Stop Date**	2005-01-22 13:45:00		
Diameter [mm]	76	**Easting ToC [m]**	1548909.41	**Surveying Date**	2004-08-27 11:15:00		
Length [m]	1000.160	**Elevation [m.a.s.l.ToC]**	17.63	**Chemistry class**	5		
Bearing ToC [°]	190.19	**Inclination ToC [°]**	-65.21	**Plot Date**	2008-08-18 22:12:45		

ROCK TYPE LAXEMAR
- Fine-grained granite
- Pegmatite
- Granite
- Ävrö granite
- Quartz monzodiorite
- Diorite / Gabbro
- Fine-grained dioritoid
- Fine-grained diorite-gabbro

DENSITY
- dens<2680
- 2680<dens<2730
- 2730<dens<2800
- 2800<dens<2890
- dens>2890

SUBDIVISION OF ÄVRÖ GRANITE
- Ävrö granite
- Ävrö quartz monzodiorite
- Ävrö granodiorite

ROCK UNIT FROM ESHI
- High confidence

CASING
- Casing

DEFORMATION ZONE FROM ESHI
- DZ

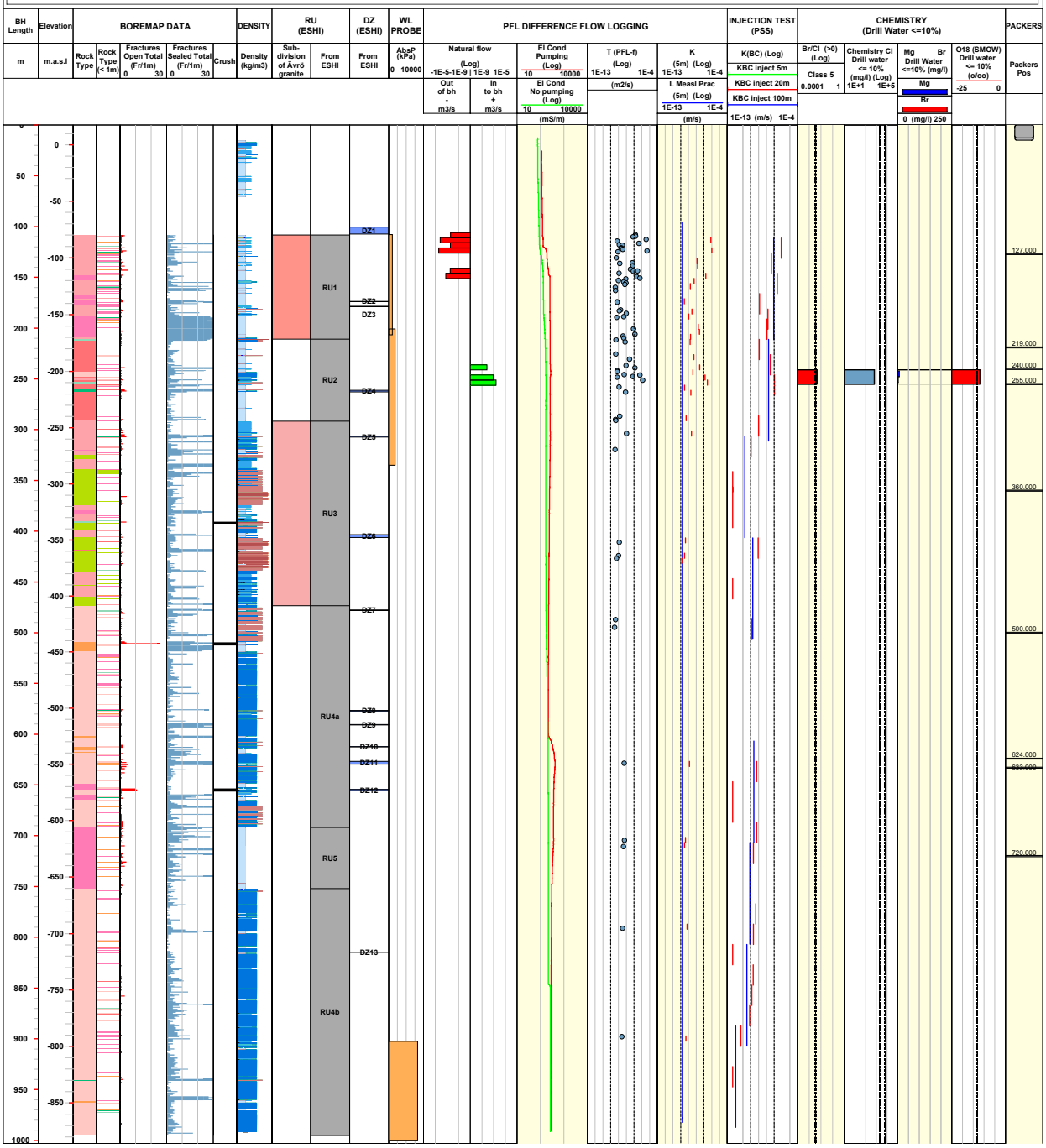

Title COMPOSITE LOG for cored borehole KLX06

Site	LAXEMAR	**Coordinate System**	RT90-RHB70	**Drilling Start Date**	2004-08-25 17:00:00	**Packer installation for monitoring**	
Borehole	KLX06	**Northing ToC [m]**	6367806.64	**Drilling Stop Date**	2004-11-25 11:30:00		
Diameter [mm]	76	**Easting ToC [m]**	1548566.88	**Surveying Date**	2004-08-13 10:00:00		
Length [m]	994.940	**Elevation [m.a.s.l.ToC]**	17.68	**Chemistry class**	5		
Bearing ToC [°]	329.65	**Inclination ToC [°]**	-65.19	**Plot Date**	2008-08-18 22:12:45		

ROCK TYPE LAXEMAR
- Fine-grained granite
- Granite
- Ävrö granite
- Fine-grained dioritoid
- Fine-grained diorite-gabbro

DENSITY
- dens<2680
- 2680<dens<2730
- 2730<dens<2800
- 2800<dens<2890
- dens>2890

SUBDIVISION OF ÄVRÖ GRANITE
- Ävrö granite
- Ävrö quartz monzodiorite
- Ävrö granodiorite

ROCK UNIT FROM ESHI
- High confidence

CASING
- Casing

DEFORMATION ZONE FROM ESHI
- DZ

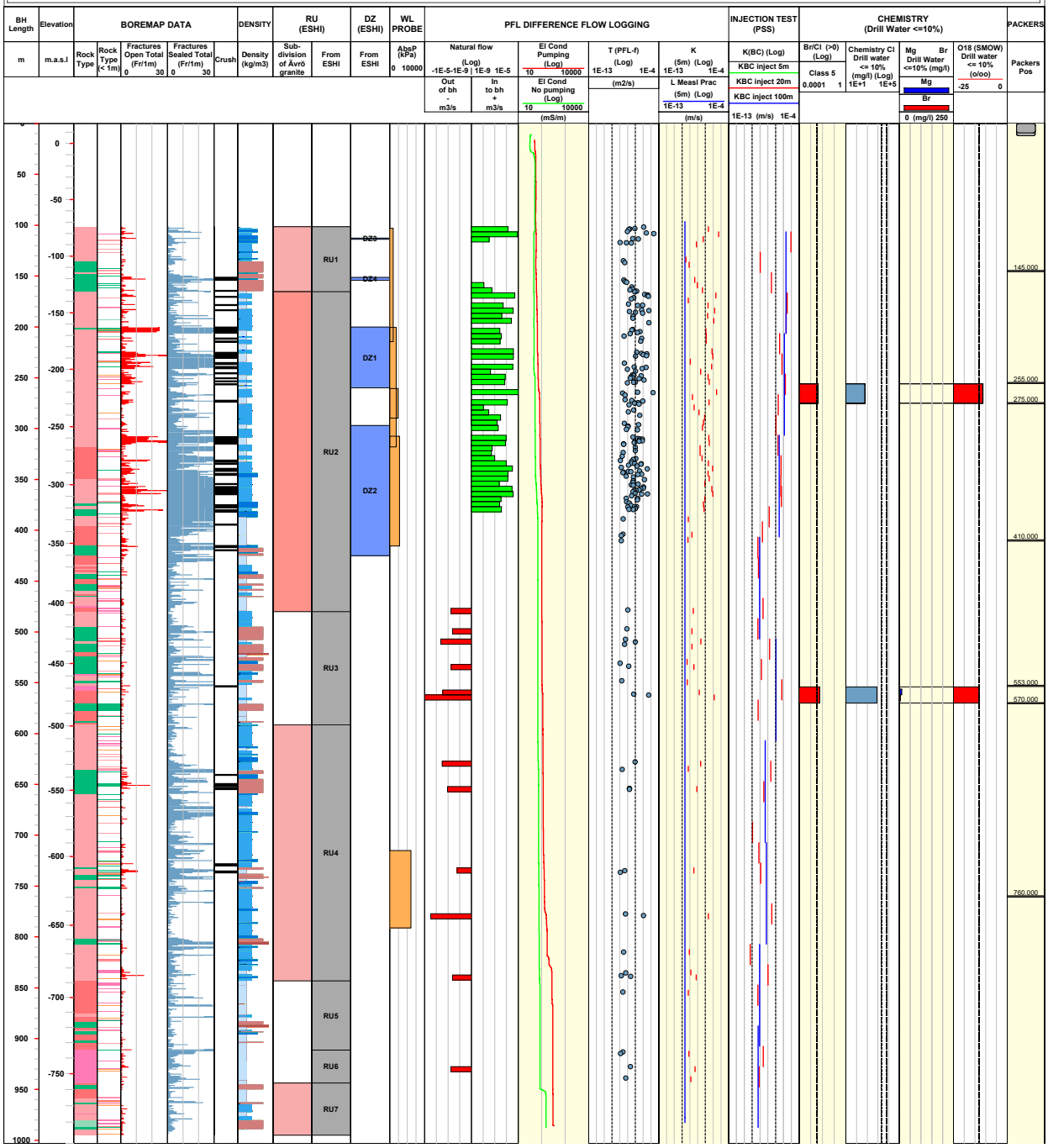

Title COMPOSITE LOG for cored borehole KLX07A

Site	LAXEMAR	**Coordinate System**	RT90-RHB70	**Drilling Start Date**	2005-01-06 14:00:00	**Packer installation for monitoring**	
Borehole	KLX07A	**Northing ToC [m]**	6366752.09	**Drilling Stop Date**	2005-05-04 10:00:00		
Diameter [mm]	76	**Easting ToC [m]**	1549206.86	**Surveying Date**	2005-05-23 10:20:00		
Length [m]	844.730	**Elevation [m.a.s.l.ToC]**	18.47	**Chemistry class**	5		
Bearing ToC [°]	174.18	**Inclination ToC [°]**	-60.03	**Plot Date**	2008-08-18 22:12:45		

ROCK TYPE LAXEMAR
- Fine-grained granite
- Ävrö granite
- Fine-grained diorite-gabbro

DENSITY
- dens<2680
- 2680<dens<2730
- 2730<dens<2800
- 2800<dens<2890

SUBDIVISION OF ÄVRÖ GRANITE
- Ävrö granite
- Ävrö quartz monzodiorite
- Ävrö granodiorite

ROCK UNIT FROM ESHI
- High confidence

CASING
- Casing

DEFORMATION ZONE FROM ESHI
- DZ

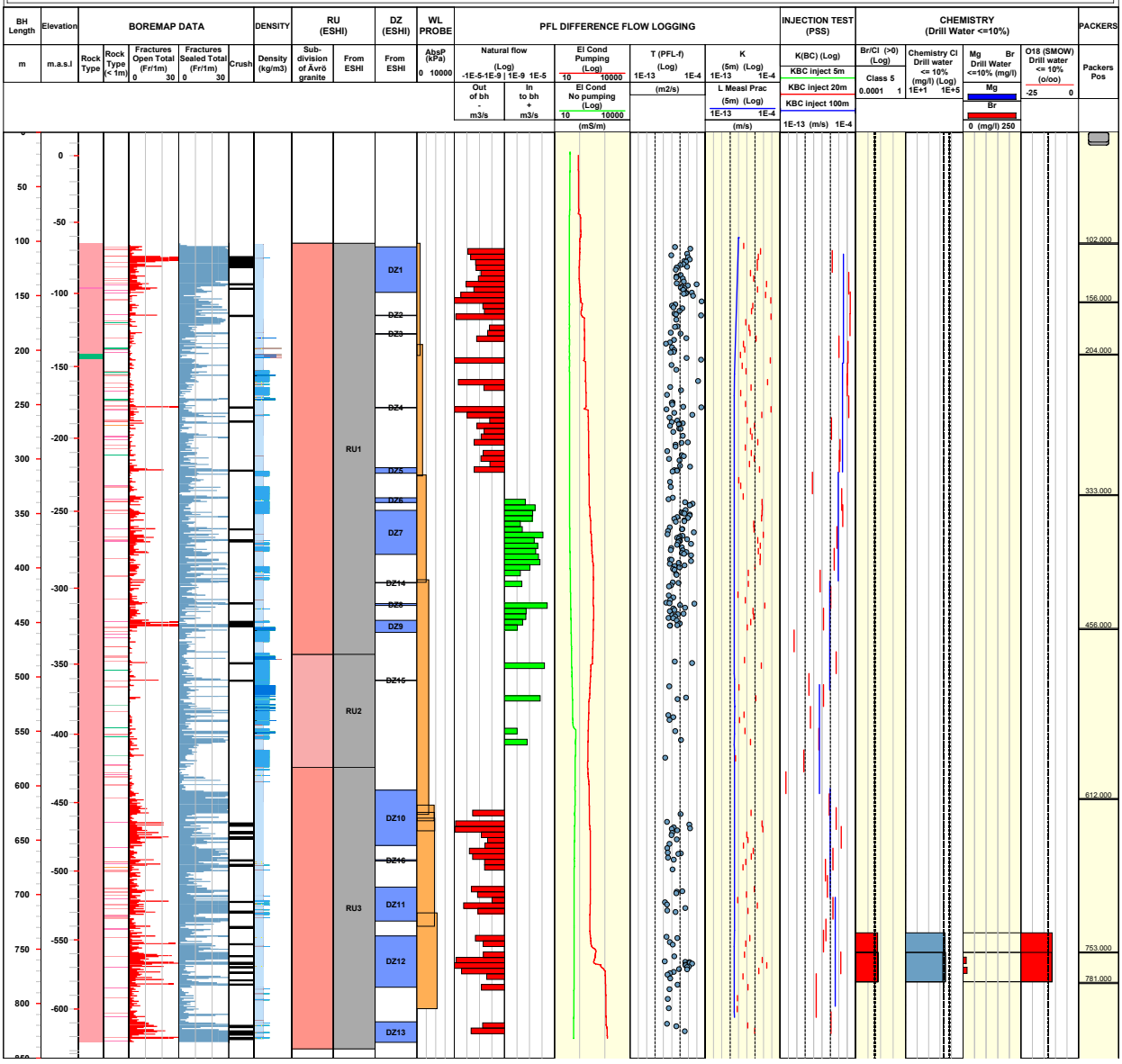

Title COMPOSITE LOG for cored borehole KLX07B

Site	LAXEMAR	**Coordinate System**	RT90-RHB70	**Drilling Start Date**	2005-05-23 18:00:00	**Packer installation for monitoring**	
Borehole	KLX07B	**Northing ToC [m]**	6366753.14	**Drilling Stop Date**	2005-06-03 08:00:00		
Diameter [mm]	76	**Easting ToC [m]**	1549206.76	**Surveying Date**	2005-06-07 15:55:00		
Length [m]	200.130	**Elevation [m.a.s.l.ToC]**	18.38	**Chemistry class**	3		
Bearing ToC [°]	174.33	**Inclination ToC [°]**	-85.14	**Plot Date**	2008-08-18 22:12:45		

ROCK TYPE LAXEMAR
- Ävrö granite
- Fine-grained diorite-gabbro

DENSITY
- dens<2680
- 2680<dens<2730
- 2730<dens<2800
- 2800<dens<2890
- dens>2890

SUBDIVISION OF ÄVRÖ GRANITE
- Ävrö granite
- Ävrö quartz monzodiorite
- Ävrö granodiorite

ROCK UNIT FROM ESHI
- High confidence

CASING
- Casing

DEFORMATION ZONE FROM ESHI
- DZ

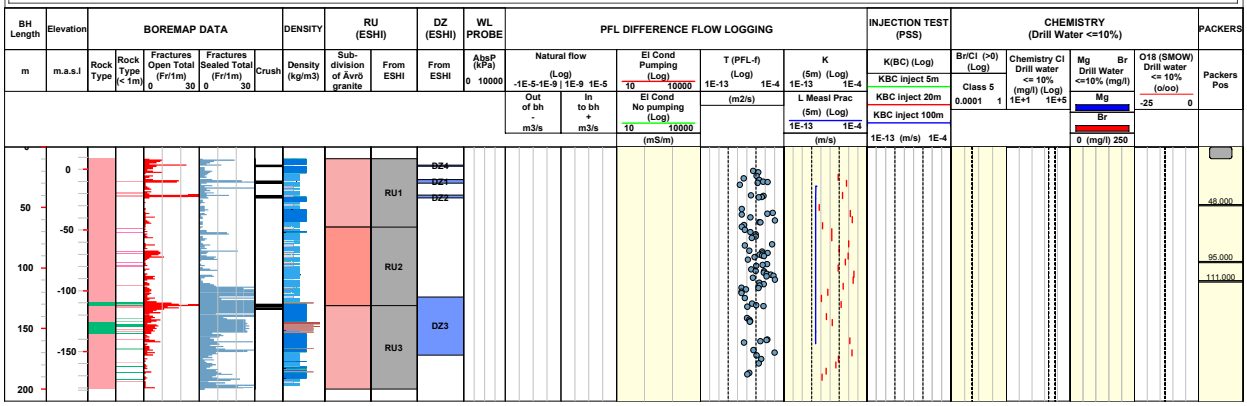

Title COMPOSITE LOG for cored borehole KLX08

Site	LAXEMAR	**Coordinate System**	RT90-RHB70	**Drilling Start Date**	2005-04-04 13:30:00	**Packer installation for monitoring**	
Borehole	KLX08	**Northing ToC [m]**	6367079.10	**Drilling Stop Date**	2005-06-13 14:00:00		
Diameter [mm]	76	**Easting ToC [m]**	1548176.71	**Surveying Date**	2005-01-26 11:25:00		
Length [m]	1000.410	**Elevation [m.a.s.l.ToC]**	24.31	**Chemistry class**	5		
Bearing ToC [°]	199.17	**Inclination ToC [°]**	-60.50	**Plot Date**	2008-08-18 22:12:45		

ROCK TYPE LAXEMAR
- Fine-grained granite
- Ävrö granite
- Quartz monzodiorite
- Diorite / Gabbro
- Fine-grained dioritoid
- Fine-grained diorite-gabbro

DENSITY
- dens<2680
- 2680<dens<2730
- 2730<dens<2800
- 2800<dens<2890
- dens>2890

SUBDIVISION OF ÄVRÖ GRANITE
- Ävrö granite
- Ävrö quartz monzodiorite
- Ävrö granodiorite

ROCK UNIT FROM ESHI
- High confidence

CASING
- Casing

DEFORMATION ZONE FROM ESHI
- DZ

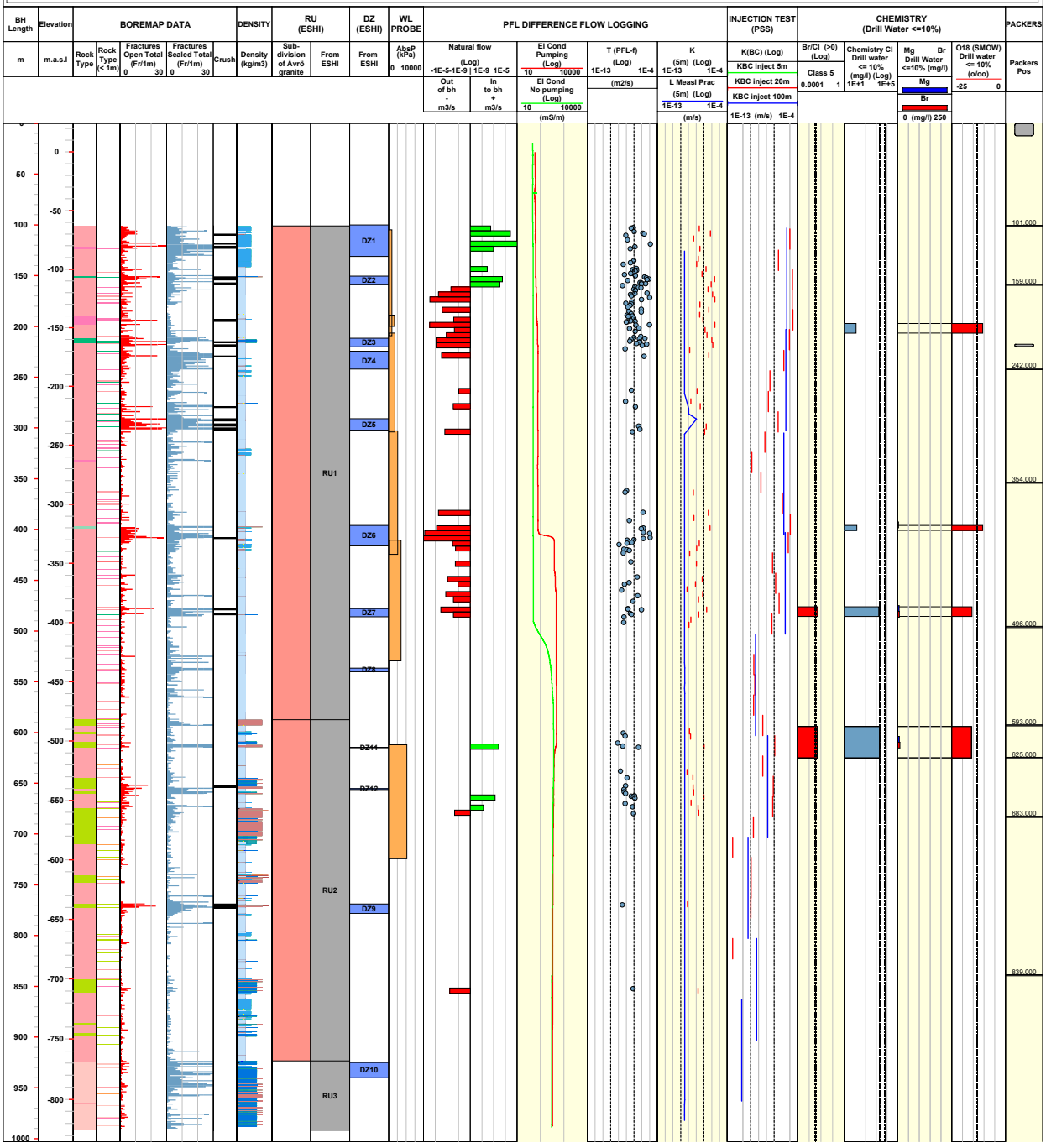

Title COMPOSITE LOG for cored borehole KLX09

Site	LAXEMAR	**Coordinate System**	RT90-RHB70	**Drilling Start Date**	2005-08-26 09:30:00	**Packer installation for monitoring**	
Borehole	KLX09	**Northing ToC [m]**	6367323.45	**Drilling Stop Date**	2005-10-15 12:00:00		
Diameter [mm]	76	**Easting ToC [m]**	1548863.18	**Surveying Date**	2005-06-14 13:25:00		
Length [m]	880.380	**Elevation [m.a.s.l.ToC]**	23.45	**Chemistry class**	3		
Bearing ToC [°]	267.41	**Inclination ToC [°]**	-84.93	**Plot Date**	2008-08-18 22:12:45		

ROCK TYPE LAXEMAR
- Fine-grained granite
- Ävrö granite
- Quartz monzodiorite
- Diorite / Gabbro
- Fine-grained dioritoid
- Fine-grained diorite-gabbro

DENSITY
- dens<2680
- 2680<dens<2730
- 2730<dens<2800
- 2800<dens<2890
- dens>2890

SUBDIVISION OF ÄVRÖ GRANITE
- Ävrö granite
- Ävrö quartz monzodiorite
- Ävrö granodiorite

ROCK UNIT FROM ESHI
- High confidence

CASING
- Casing

DEFORMATION ZONE FROM ESHI
- DZ

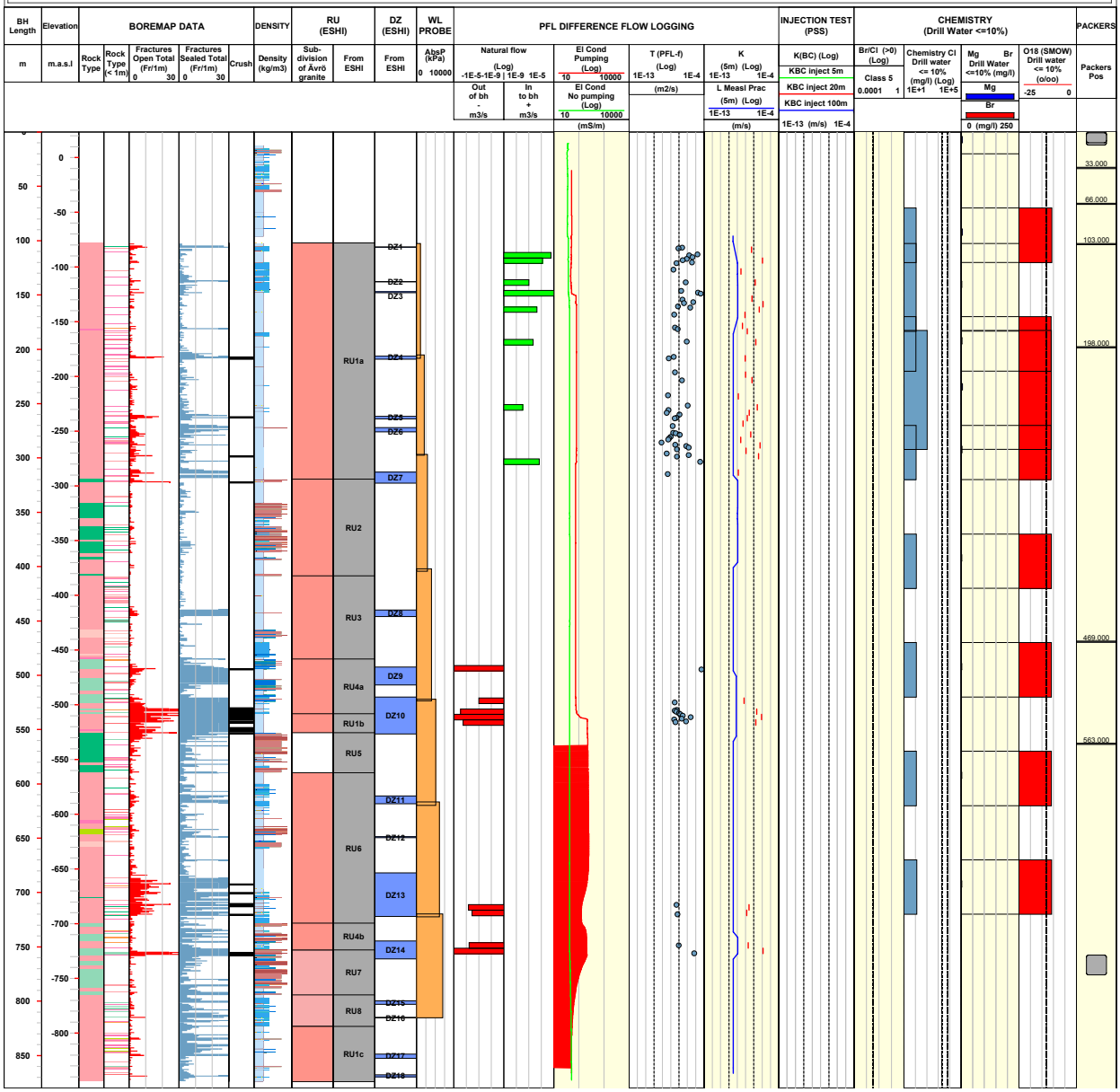

Title COMPOSITE LOG for cored borehole KLX09B

Site	LAXEMAR	**Coordinate System**	RT90-RHB70	**Drilling Start Date**	2006-01-16 14:00:00	**Packer installation for monitoring**	
Borehole	KLX09B	**Northing ToC [m]**	6367329.07	**Drilling Stop Date**	2006-01-26 12:00:00		
Diameter [mm]	76	**Easting ToC [m]**	1548859.01	**Surveying Date**	2006-02-01 14:42:00		
Length [m]	100.220	**Elevation [m.a.s.l.ToC]**	23.62	**Chemistry class**	$Class		
Bearing ToC [°]	21.25	**Inclination ToC [°]**	-89.82	**Plot Date**	2008-08-18 22:12:45		

ROCK TYPE LAXEMAR
- Fine-grained granite
- Ävrö granite
- Fine-grained diorite-gabbro

DENSITY
- dens<2680
- 2680<dens<2730
- 2730<dens<2800
- 2800<dens<2890
- dens>2890

SUBDIVISION OF ÄVRÖ GRANITE
- Ävrö granite
- Ävrö quartz monzodiorite
- Ävrö granodiorite

ROCK UNIT FROM ESHI
- High confidence

CASING
- Casing

DEFORMATION ZONE FROM ESHI
- DZ

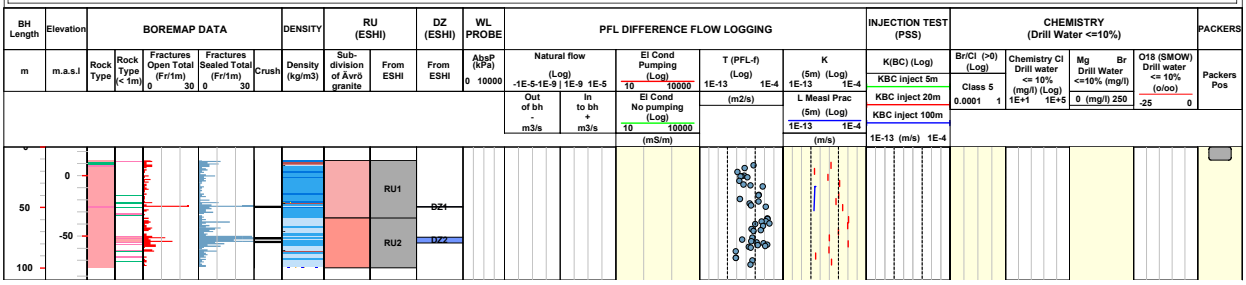

Title **COMPOSITE LOG for cored borehole KLX09C**

Site	LAXEMAR	**Coordinate System**	RT90-RHB70	**Drilling Start Date**	2006-01-07 11:00:00	**Packer installation**	
Borehole	KLX09C	**Northing ToC [m]**	6367353.43	**Drilling Stop Date**	2006-01-15 12:00:00	**for monitoring**	
Diameter [mm]	76	**Easting ToC [m]**	1548838.82	**Surveying Date**	2006-02-01 15:12:00		
Length [m]	120.050	**Elevation [m.a.s.l.ToC]**	23.75	**Chemistry class**	$Class		
Bearing ToC [°]	160.39	**Inclination ToC [°]**	-59.51	**Plot Date**	2008-08-18 22:12:45		

ROCK TYPE LAXEMAR
- Fine-grained granite
- Ävrö granite

DENSITY

SUBDIVISION OF ÄVRÖ GRANITE
- Ävrö granite
- Ävrö quartz monzodiorite
- Ävrö granodiorite

ROCK UNIT FROM ESHI
- High confidence

CASING
- Casing

DEFORMATION ZONE FROM ESHI
- DZ

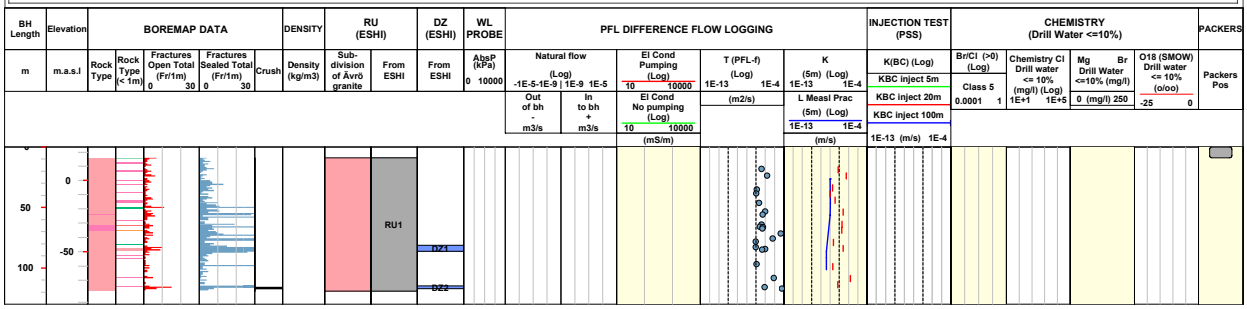

Title COMPOSITE LOG for cored borehole KLX09D

Site	LAXEMAR	**Coordinate System**	RT90-RHB70	**Drilling Start Date**	2005-11-05 06:00:00	**Packer installation for monitoring**	
Borehole	KLX09D	**Northing ToC [m]**	6367336.99	**Drilling Stop Date**	2005-11-17 14:00:00		
Diameter [mm]	76	**Easting ToC [m]**	1548878.22	**Surveying Date**	2006-02-01 14:31:00		
Length [m]	121.020	**Elevation [m.a.s.l.ToC]**	23.10	**Chemistry class**	$Class		
Bearing ToC [°]	270.15	**Inclination ToC [°]**	-60.24	**Plot Date**	2008-08-18 22:12:45		

ROCK TYPE LAXEMAR
- Fine-grained granite
- Ävrö granite
- Fine-grained diorite-gabbro

DENSITY
- dens<2680
- 2680<dens<2730
- 2730<dens<2800
- 2800<dens<2890
- dens>2890

SUBDIVISION OF ÄVRÖ GRANITE
- Ävrö granite
- Ävrö quartz monzodiorite
- Ävrö granodiorite

ROCK UNIT FROM ESHI
- High confidence

CASING
- Casing

DEFORMATION ZONE FROM ESHI
- DZ

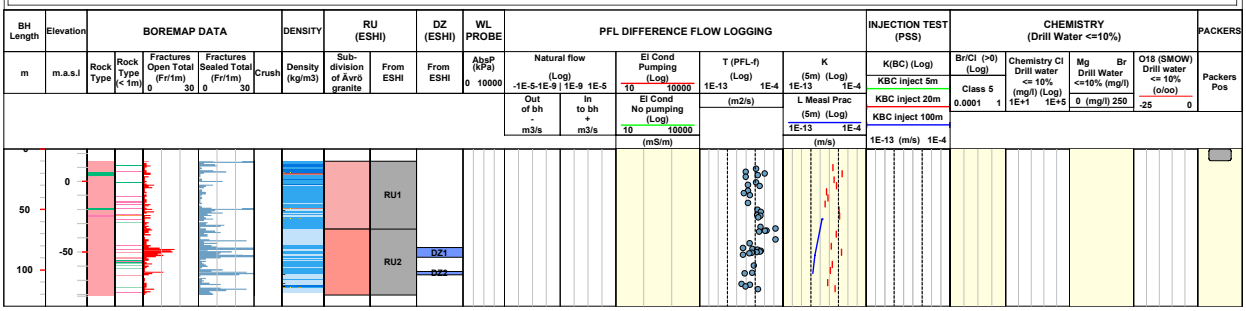

Title **COMPOSITE LOG for cored borehole KLX09E**

Site	LAXEMAR	**Coordinate System**	RT90-RHB70	**Drilling Start Date**	2005-11-23 08:25:00	**Packer installation**	
Borehole	KLX09E	**Northing ToC [m]**	6367304.45	**Drilling Stop Date**	2005-12-05 07:00:00	**for monitoring**	
Diameter [mm]	76	**Easting ToC [m]**	1548880.37	**Surveying Date**	2006-02-01 14:38:00		
Length [m]	120.000	**Elevation [m.a.s.l.ToC]**	22.16	**Chemistry class**	$Class		
Bearing ToC [°]	338.90	**Inclination ToC [°]**	-59.95	**Plot Date**	2008-08-18 22:12:45		

ROCK TYPE LAXEMAR
- Fine-grained granite
- Ävrö granite
- Fine-grained diorite-gabbro

DENSITY

SUBDIVISION OF ÄVRÖ GRANITE
- Ävrö granite
- Ävrö quartz monzodiorite
- Ävrö granodiorite

ROCK UNIT FROM ESHI
- High confidence

CASING
- Casing

DEFORMATION ZONE FROM ESHI
- DZ

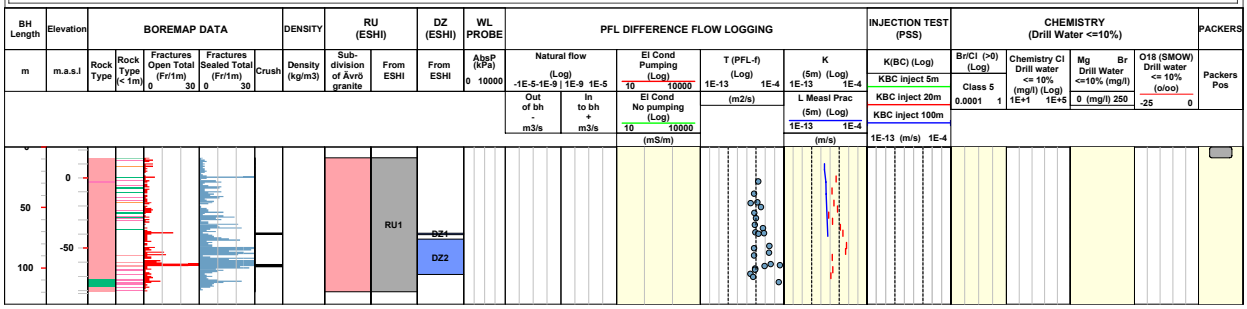

Title COMPOSITE LOG for cored borehole KLX09F

Site	LAXEMAR	**Coordinate System**	RT90-RHB70	**Drilling Start Date**	2005-12-06 09:00:00	**Packer installation for monitoring**	
Borehole	KLX09F	**Northing ToC [m]**	6367318.02	**Drilling Stop Date**	2006-01-06 13:00:00		
Diameter [mm]	76	**Easting ToC [m]**	1548817.27	**Surveying Date**	2006-02-01 14:05:00		
Length [m]	152.300	**Elevation [m.a.s.l.ToC]**	19.57	**Chemistry class**	$Class		
Bearing ToC [°]	90.67	**Inclination ToC [°]**	-59.73	**Plot Date**	2008-08-18 22:12:45		

ROCK TYPE LAXEMAR
- Fine-grained granite
- Granite
- Ävrö granite
- Fine-grained diorite-gabbro

DENSITY
- dens<2680
- 2680<dens<2730
- 2730<dens<2800
- 2800<dens<2890
- dens>2890

SUBDIVISION OF ÄVRÖ GRANITE
- Ävrö granite
- Ävrö quartz monzodiorite
- Ävrö granodiorite

ROCK UNIT FROM ESHI
- High confidence

CASING
- Casing

DEFORMATION ZONE FROM ESHI
- DZ

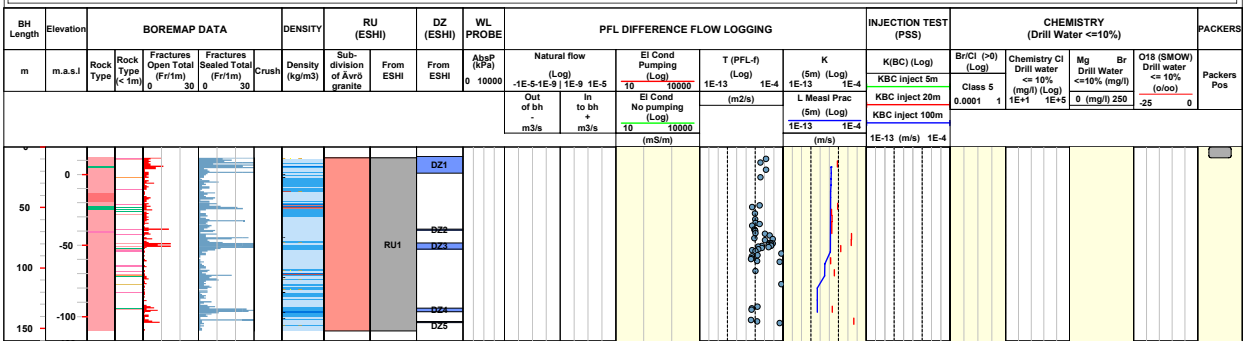

Title COMPOSITE LOG for cored borehole KLX09G

Site	LAXEMAR	**Coordinate System**	RT90-RHB70	**Drilling Start Date**	2006-01-27 16:00:00	**Packer installation for monitoring**	
Borehole	KLX09G	**Northing ToC [m]**	6367330.09	**Drilling Stop Date**	2006-02-03 12:00:00		
Diameter [mm]	76	**Easting ToC [m]**	1548905.77	**Surveying Date**	2006-02-07 14:50:00		
Length [m]	100.100	**Elevation [m.a.s.l.ToC]**	19.63	**Chemistry class**	$Class		
Bearing ToC [°]	85.41	**Inclination ToC [°]**	-61.07	**Plot Date**	2008-08-18 22:12:45		

ROCK TYPE LAXEMAR
- Fine-grained granite
- Ävrö granite
- Fine-grained diorite-gabbro

DENSITY
- dens<2680
- 2680<dens<2730
- 2730<dens<2800
- 2800<dens<2890

SUBDIVISION OF ÄVRÖ GRANITE
- Ävrö granite
- Ävrö quartz monzodiorite
- Ävrö granodiorite

ROCK UNIT FROM ESHI
- High confidence

CASING
- Casing

DEFORMATION ZONE FROM ESHI
- DZ

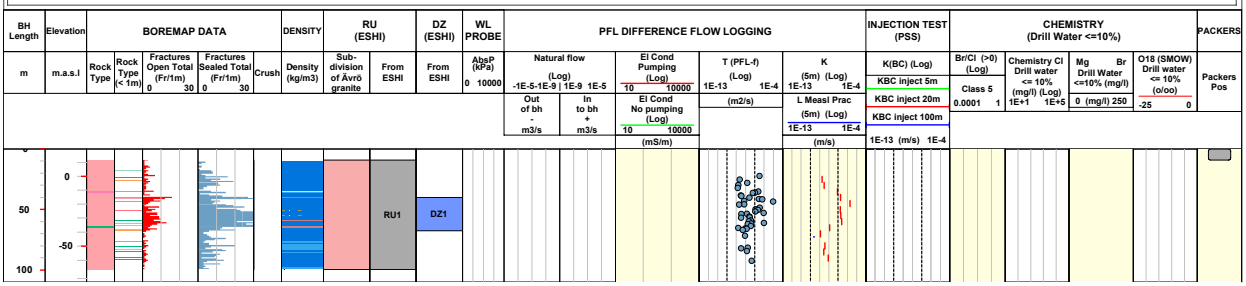

Title COMPOSITE LOG for cored borehole KLX10

Site	LAXEMAR	**Coordinate System**	RT90-RHB70	**Drilling Start Date**	2005-06-18 08:00:00	**Packer installation for monitoring**
Borehole	KLX10	**Northing ToC [m]**	6366319.38	**Drilling Stop Date**	2005-10-15 07:40:00	
Diameter [mm]	76	**Easting ToC [m]**	1548515.23	**Surveying Date**	2005-06-07 11:10:00	
Length [m]	1001.200	**Elevation [m.a.s.l.ToC]**	18.28	**Chemistry class**	5	
Bearing ToC [°]	250.80	**Inclination ToC [°]**	-85.18	**Plot Date**	2008-08-18 22:12:45	

ROCK TYPE LAXEMAR
- Fine-grained granite
- Ävrö granite
- Quartz monzodiorite
- Diorite / Gabbro
- Fine-grained dioritoid
- Fine-grained diorite-gabbro

DENSITY
- dens<2680
- 2680<dens<2730
- 2730<dens<2800
- 2800<dens<2890
- dens>2890

SUBDIVISION OF ÄVRÖ GRANITE
- Ävrö granite
- Ävrö quartz monzodiorite
- Ävrö granodiorite

ROCK UNIT FROM ESHI
- High confidence

CASING
- Casing

DEFORMATION ZONE FROM ESHI
- DZ

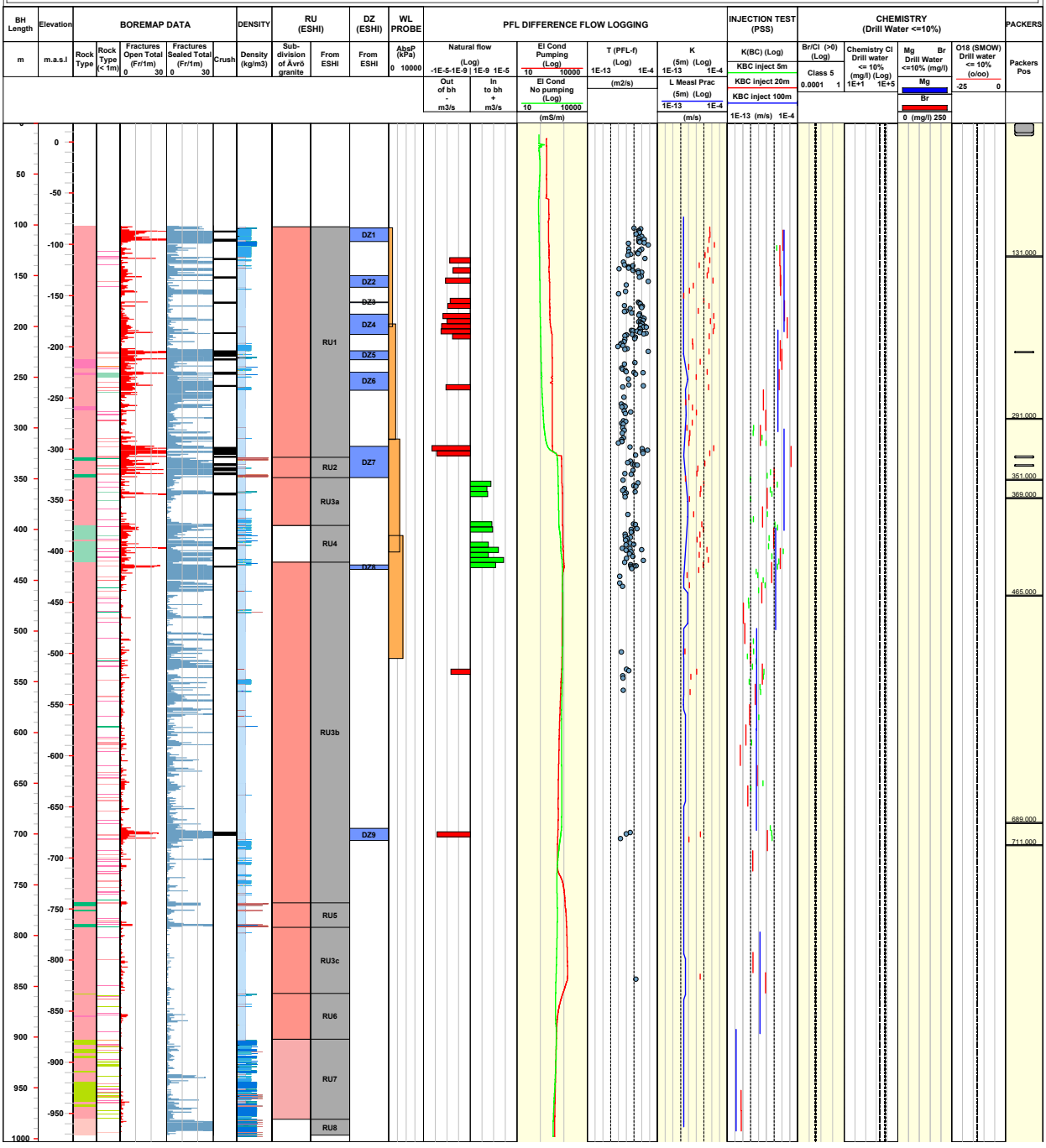

Title COMPOSITE LOG for cored borehole KLX10B

Site	LAXEMAR	**Coordinate System**	RT90-RHB70	**Drilling Start Date**	2006-02-08 16:35:00	**Packer installation for monitoring**	
Borehole	KLX10B	**Northing ToC [m]**	6366316.49	**Drilling Stop Date**	2006-02-14 06:55:00		
Diameter [mm]	76	**Easting ToC [m]**	1548525.15	**Surveying Date**	2006-04-03 09:25:00		
Length [m]	50.250	**Elevation [m.a.s.l.ToC]**	18.15	**Chemistry class**	$Class		
Bearing ToC [°]	170.33	**Inclination ToC [°]**	-59.96	**Plot Date**	2008-08-18 22:12:45		

ROCK TYPE LAXEMAR
- Fine-grained granite
- Ävrö granite

DENSITY
- dens<2680
- 2680<dens<2730
- 2730<dens<2800

SUBDIVISION OF ÄVRÖ GRANITE
- Ävrö granite
- Ävrö quartz monzodiorite
- Ävrö granodiorite

ROCK UNIT FROM ESHI
- High confidence

CASING
- Casing

DEFORMATION ZONE FROM ESHI
- DZ

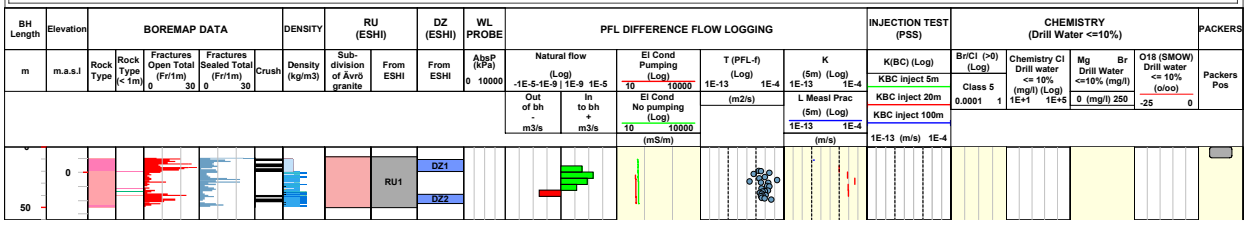

Title COMPOSITE LOG for cored borehole KLX10C

Site	LAXEMAR	**Coordinate System**	RT90-RHB70	**Drilling Start Date**	2006-02-15 14:38:00	**Packer installation for monitoring**	
Borehole	KLX10C	**Northing ToC [m]**	6366372.07	**Drilling Stop Date**	2006-02-28 07:22:00		
Diameter [mm]	76	**Easting ToC [m]**	1548506.94	**Surveying Date**	2006-04-03 09:35:00		
Length [m]	146.250	**Elevation [m.a.s.l.ToC]**	16.94	**Chemistry class**	1		
Bearing ToC [°]	352.43	**Inclination ToC [°]**	-60.02	**Plot Date**	2008-08-18 22:12:45		

ROCK TYPE LAXEMAR
- Ävrö granite
- Fine-grained dioritoid
- Fine-grained diorite-gabbro

DENSITY
- dens<2680
- 2680<dens<2730
- 2730<dens<2800
- 2800<dens<2890

SUBDIVISION OF ÄVRÖ GRANITE
- Ävrö granite
- Ävrö quartz monzodiorite
- Ävrö granodiorite

ROCK UNIT FROM ESHI
- High confidence

CASING
- Casing

DEFORMATION ZONE FROM ESHI
- DZ

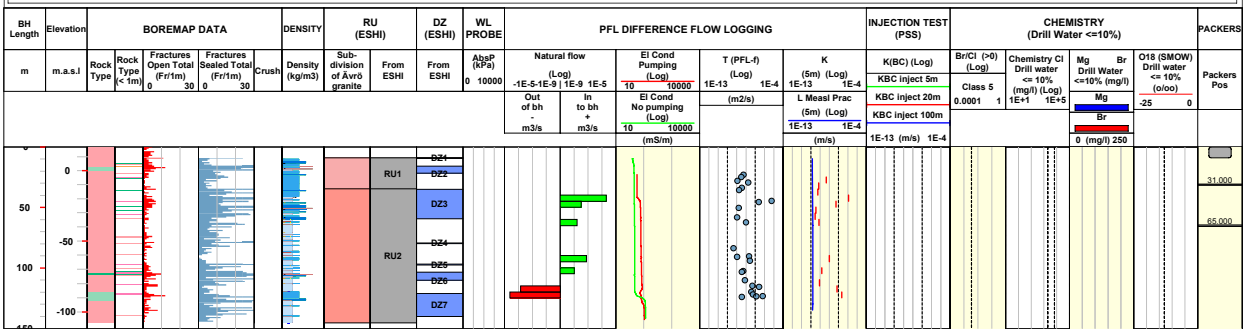

Title COMPOSITE LOG for cored borehole KLX11A

Site	LAXEMAR	**Coordinate System**	RT90-RHB70	**Drilling Start Date**	2005-11-24 06:00:00	**Packer installation for monitoring**	
Borehole	KLX11A	**Northing ToC [m]**	6366339.72	**Drilling Stop Date**	2006-03-02 11:00:00		
Diameter [mm]	76	**Easting ToC [m]**	1546608.49	**Surveying Date**	2005-11-09 10:15:00		
Length [m]	992.290	**Elevation [m.a.s.l.ToC]**	27.14	**Chemistry class**	5		
Bearing ToC [°]	89.84	**Inclination ToC [°]**	-76.76	**Plot Date**	2008-08-18 22:12:45		

ROCK TYPE LAXEMAR
- Fine-grained granite
- Pegmatite
- Quartz monzodiorite
- Fine-grained diorite-gabbro

DENSITY
- dens<2680
- 2680<dens<2730
- 2730<dens<2800
- 2800<dens<2890
- dens>2890

SUBDIVISION OF ÄVRÖ GRANITE

ROCK UNIT FROM ESHI
- High confidence

CASING
- Casing

DEFORMATION ZONE FROM ESHI
- DZ

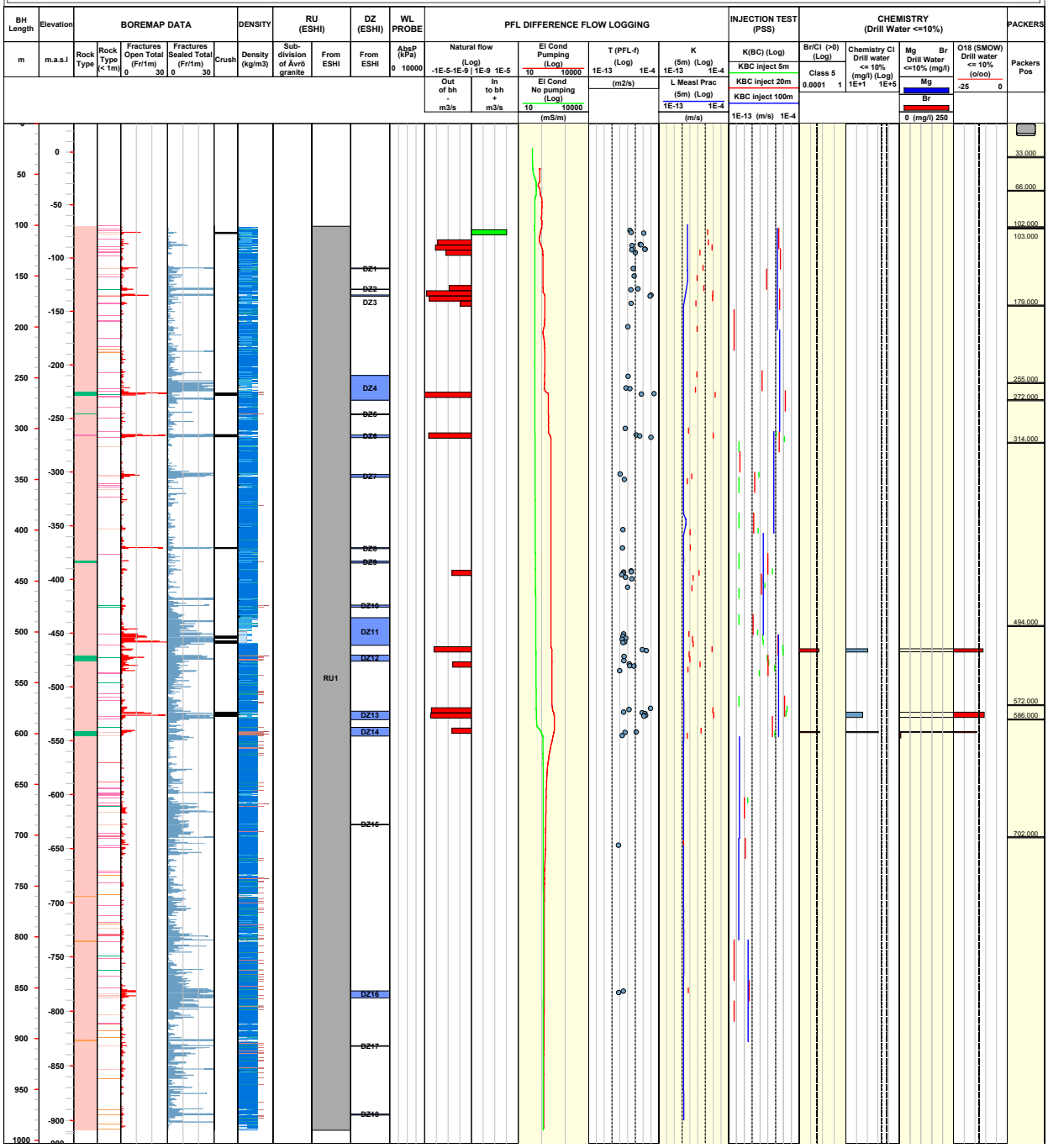

Title COMPOSITE LOG for cored borehole KLX11B

Site	LAXEMAR	**Coordinate System**	RT90-RHB70	**Drilling Start Date**	2006-04-22 16:00:00	**Packer installation for monitoring**	
Borehole	KLX11B	**Northing ToC [m]**	6366339.51	**Drilling Stop Date**	2006-04-28 08:50:00		
Diameter [mm]	76	**Easting ToC [m]**	1546604.89	**Surveying Date**	2006-05-09 09:25:00		
Length [m]	100.200	**Elevation [m.a.s.l.ToC]**	27.27	**Chemistry class**	$Class		
Bearing ToC [°]	136.16	**Inclination ToC [°]**	-89.92	**Plot Date**	2008-08-18 22:12:45		

ROCK TYPE LAXEMAR
- Fine-grained granite
- Quartz monzodiorite

DENSITY
- dens<2680
- 2680<dens<2730
- 2730<dens<2800
- 2800<dens<2890

SUBDIVISION OF ÄVRÖ GRANITE

ROCK UNIT FROM ESHI
- High confidence

CASING
- Casing

DEFORMATION ZONE FROM ESHI
- DZ

BH Length	Elevation	BOREMAP DATA					DENSITY	RU (ESHI)		DZ (ESHI)	WL PROBE	PFL DIFFERENCE FLOW LOGGING				INJECTION TEST (PSS)	CHEMISTRY (Drill Water <=10%)				PACKERS
m	m.a.s.l	Rock Type	Rock Type (< 1m)	Fractures Open Total (Fr/1m) 0 30	Fractures Sealed Total (Fr/1m) 0 30	Crush	Density (kg/m3)	Sub-division of Ävrö granite	From ESHI	From ESHI	AbsP (kPa) 0 10000	Natural flow (Log) -1E-5 1E-9 | 1E-9 1E-5	El Cond Pumping (Log) 10 10000	T (PFL-f) (Log) 1E-13 1E-4	K (5m) (Log) 1E-13 1E-4	K(BC) (Log)	Br/Cl (>0) (Log)	Chemistry Cl Drill water <= 10% (mg/l) (Log) 1E+1 1E+5	Mg Br Drill Water <=10% (mg/l)	O18 (SMOW) Drill water <= 10% (o/oo)	Packers Pos
												Out of bh - m3/s | In to bh + m3/s	El Cond No pumping (Log) 10 10000 (mS/m)	(m2/s)	L Meas Prac (5m) (Log) 1E-13 1E-4 (m/s)	KBC inject 5m | KBC inject 20m | KBC inject 100m 1E-13 (m/s) 1E-4	Class 5 0.0001 1	(mg/l) (Log)	0 (mg/l) 250	-25 0	

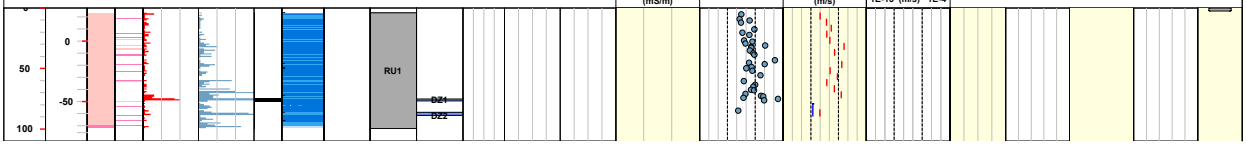

Title **COMPOSITE LOG for cored borehole KLX11C**

Site	LAXEMAR	**Coordinate System**	RT90-RHB70	**Drilling Start Date**	2006-03-30 06:00:00	**Packer installation**	
Borehole	KLX11C	**Northing ToC [m]**	6366350.26	**Drilling Stop Date**	2006-04-05 14:30:00	**for monitoring**	
Diameter [mm]	76	**Easting ToC [m]**	1546586.89	**Surveying Date**	2006-04-06 11:45:00		
Length [m]	120.150	**Elevation [m.a.s.l.ToC]**	27.19	**Chemistry class**	$Class		
Bearing ToC [°]	159.34	**Inclination ToC [°]**	-60.72	**Plot Date**	2008-08-18 22:12:45		

ROCK TYPE LAXEMAR
Quartz monzodiorite

DENSITY

SUBDIVISION OF ÄVRÖ GRANITE

ROCK UNIT FROM ESHI
High confidence

CASING
Casing

DEFORMATION ZONE FROM ESHI
DZ

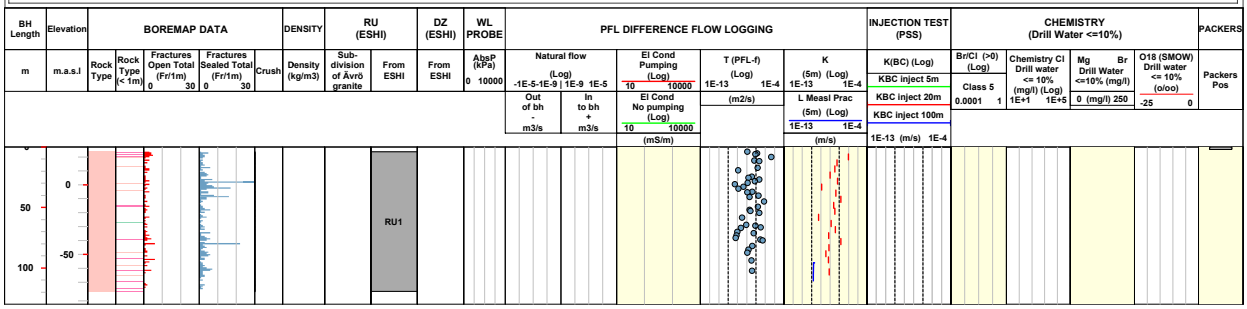

Title COMPOSITE LOG for cored borehole KLX11D

Site	LAXEMAR	**Coordinate System**	RT90-RHB70	**Drilling Start Date**	2006-04-06 06:00:00	**Packer installation for monitoring**	
Borehole	KLX11D	**Northing ToC [m]**	6366357.37	**Drilling Stop Date**	2006-04-13 08:00:00		
Diameter [mm]	76	**Easting ToC [m]**	1546631.42	**Surveying Date**	2006-05-09 10:30:00		
Length [m]	120.350	**Elevation [m.a.s.l.ToC]**	25.57	**Chemistry class**	$Class		
Bearing ToC [°]	268.70	**Inclination ToC [°]**	-58.99	**Plot Date**	2008-08-18 22:12:45		

ROCK TYPE LAXEMAR
- Fine-grained granite
- Quartz monzodiorite

DENSITY

SUBDIVISION OF ÄVRÖ GRANITE

ROCK UNIT FROM ESHI
- High confidence

CASING
- Casing

DEFORMATION ZONE FROM ESHI
- DZ

BH Length	Elevation	BOREMAP DATA					DENSITY	RU (ESHI)		DZ (ESHI)	WL PROBE	PFL DIFFERENCE FLOW LOGGING				INJECTION TEST (PSS)	CHEMISTRY (Drill Water <=10%)				PACKERS
m	m.a.s.l	Rock Type	Rock Type (< 1m)	Fractures Open Total (Fr/1m) 0 30	Fractures Sealed Total (Fr/1m) 0 30	Crush	Density (kg/m3)	Sub-division of Ävrö granite	From ESHI	From ESHI	AbsP (kPa) 0 10000	Natural flow (Log) -1E-5 1E-9 1E-9 1E-5		El Cond Pumping (Log) 10 10000	T (PFL-f) (Log) 1E-13 1E-4	K (5m) (Log) 1E-13 1E-4	K(BC) (Log)	Br/Cl (>0) (Log)	Chemistry Cl Drill water <= 10% (mg/l) (Log) 1E+1 1E+5	Mg Br Drill Water <=10% (mg/l)	O18 (SMOW) Drill water <= 10% (o/oo)	Packers Pos
												Out of bh - m3/s	In to bh + m3/s	El Cond No pumping (Log) 10 10000 (mS/m)	(m2/s)	L Meas Prac (5m) (Log) 1E-13 1E-4 (m/s)	KBC inject 5m KBC inject 20m KBC inject 100m 1E-13 (m/s) 1E-4	Class 5 0.0001 1	0 (mg/l) 250	-25 0	

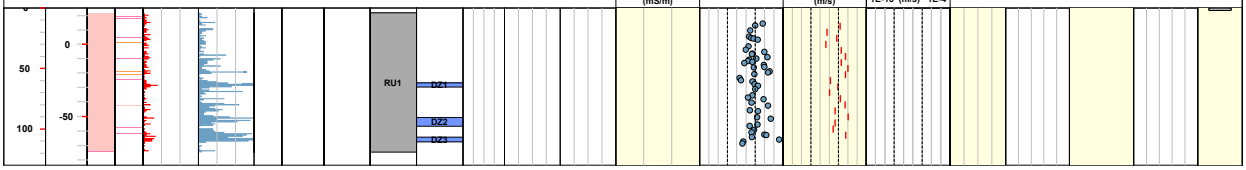

Title **COMPOSITE LOG for cored borehole KLX11F**

Site	LAXEMAR	**Coordinate System**	RT90-RHB70	**Drilling Start Date**	2006-03-14 06:00:00	**Packer installation**	
Borehole	KLX11F	**Northing ToC [m]**	6366314.09	**Drilling Stop Date**	2006-03-17 18:00:00	**for monitoring**	
Diameter [mm]	76	**Easting ToC [m]**	1546577.96	**Surveying Date**	2006-04-06 11:40:00		
Length [m]	120.050	**Elevation [m.a.s.l.ToC]**	24.47	**Chemistry class**	$Class		
Bearing ToC [°]	88.61	**Inclination ToC [°]**	-61.13	**Plot Date**	2008-08-18 22:12:45		

ROCK TYPE LAXEMAR
- Fine-grained granite
- Quartz monzodiorite

DENSITY

SUBDIVISION OF ÄVRÖ GRANITE

ROCK UNIT FROM ESHI
- High confidence

CASING
- Casing

DEFORMATION ZONE FROM ESHI
- DZ

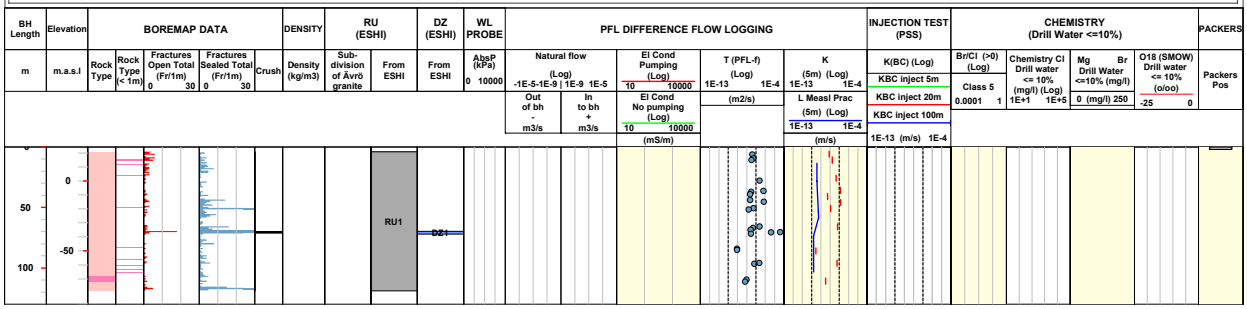

Title COMPOSITE LOG for cored borehole KLX12A

Site	LAXEMAR	**Coordinate System**	RT90-RHB70	**Drilling Start Date**	2005-11-10 09:30:00	**Packer installation for monitoring**	
Borehole	KLX12A	**Northing ToC [m]**	6365630.78	**Drilling Stop Date**	2006-03-04 14:48:00		
Diameter [mm]	76	**Easting ToC [m]**	1548904.44	**Surveying Date**	2005-10-31 12:15:00		
Length [m]	602.290	**Elevation [m.a.s.l.ToC]**	17.74	**Chemistry class**	5		
Bearing ToC [°]	315.92	**Inclination ToC [°]**	-75.30	**Plot Date**	2008-08-27 22:15:27		

ROCK TYPE LAXEMAR
- Fine-grained granite
- Ävrö granite
- Quartz monzodiorite
- Diorite / Gabbro
- Fine-grained dioritoid
- Fine-grained diorite-gabbro

DENSITY
- dens<2680
- 2680<dens<2730
- 2730<dens<2800
- 2800<dens<2890
- dens>2890

SUBDIVISION OF ÄVRÖ GRANITE
- Ävrö granite
- Ävrö quartz monzodiorite
- Ävrö granodiorite

ROCK UNIT FROM ESHI
- High confidence

CASING
- Casing

DEFORMATION ZONE FROM ESHI
- DZ

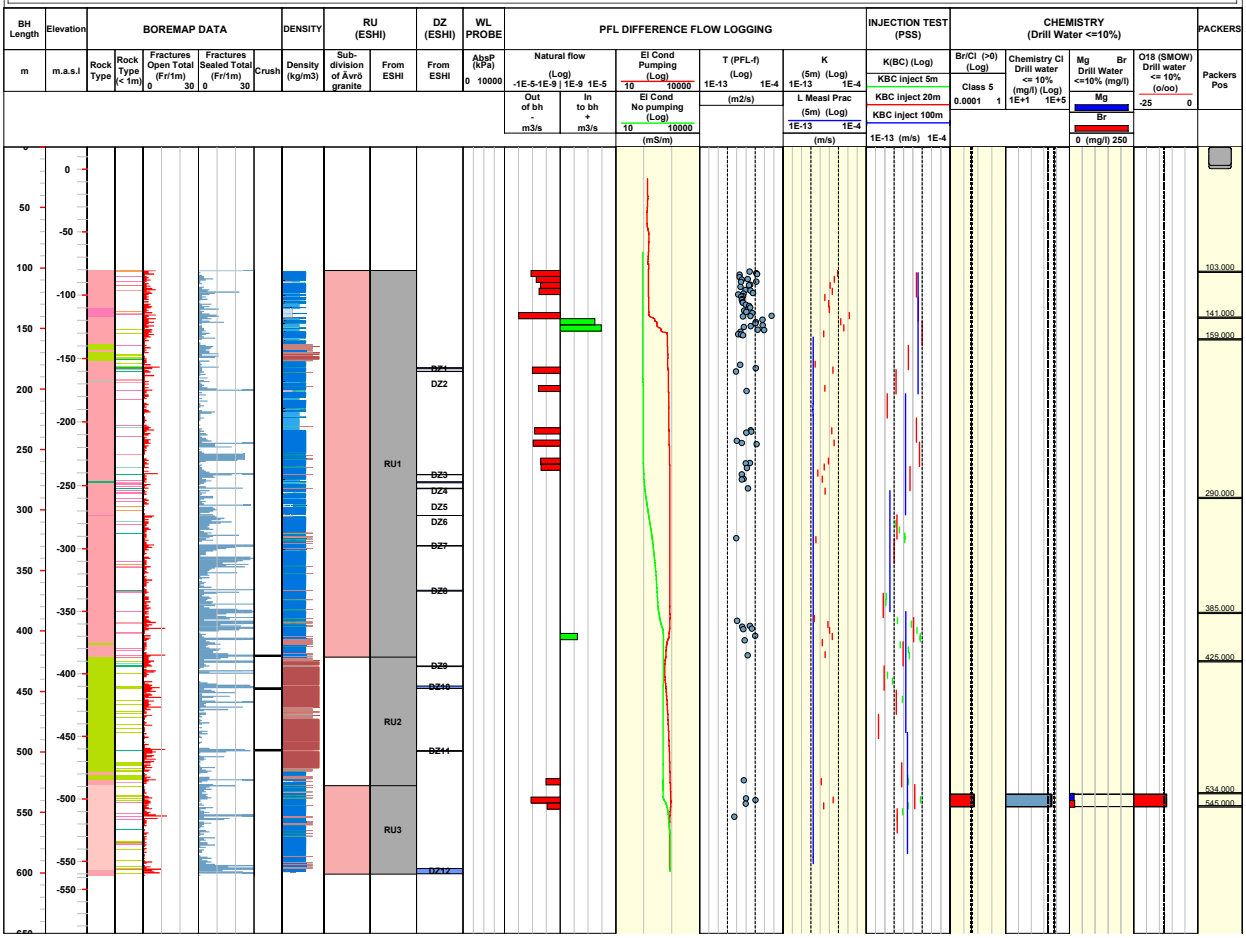

Title COMPOSITE LOG for cored borehole KLX13A

Site	LAXEMAR	**Coordinate System**	RT90-RHB70	**Drilling Start Date**	2006-05-19 14:02:00	**Packer installation for monitoring**	
Borehole	KLX13A	**Northing ToC [m]**	6367547.14	**Drilling Stop Date**	2006-08-16 09:02:00		
Diameter [mm]	76	**Easting ToC [m]**	1546787.36	**Surveying Date**	2006-04-03 10:15:00		
Length [m]	595.850	**Elevation [m.a.s.l.ToC]**	24.15	**Chemistry class**	5		
Bearing ToC [°]	224.48	**Inclination ToC [°]**	-82.23	**Plot Date**	2008-08-18 22:12:45		

ROCK TYPE LAXEMAR
- Fine-grained granite
- Ävrö granite
- Diorite / Gabbro
- Fine-grained diorite-gabbro

DENSITY
- dens<2680
- 2680<dens<2730
- 2730<dens<2800
- 2800<dens<2890
- dens>2890

SUBDIVISION OF ÄVRÖ GRANITE
- Ävrö granite
- Ävrö quartz monzodiorite
- Ävrö granodiorite

ROCK UNIT FROM ESHI
- High confidence

CASING
- Casing

DEFORMATION ZONE FROM ESHI
- DZ

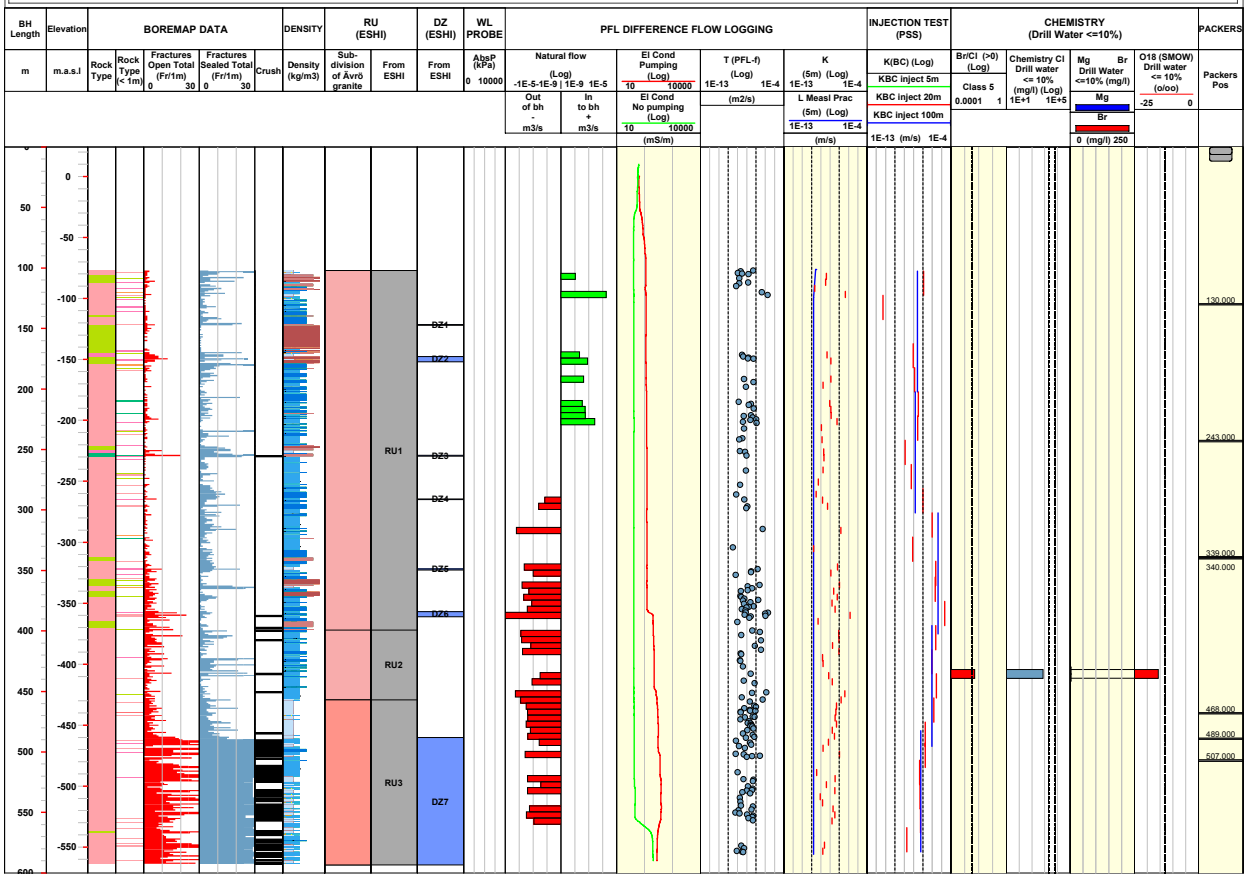

Title COMPOSITE LOG for cored borehole KLX14A

Site	LAXEMAR	**Coordinate System**	RT90-RHB70	**Drilling Start Date**	2006-08-19 08:00:00	**Packer installation for monitoring**	
Borehole	KLX14A	**Northing ToC [m]**	6365959.69	**Drilling Stop Date**	2006-09-04 15:22:00		
Diameter [mm]	76	**Easting ToC [m]**	1547146.87	**Surveying Date**	2006-09-11 14:55:00		
Length [m]	176.270	**Elevation [m.a.s.l.ToC]**	16.35	**Chemistry class**	1		
Bearing ToC [°]	111.95	**Inclination ToC [°]**	-49.95	**Plot Date**	2008-08-18 22:12:45		

ROCK TYPE LAXEMAR
- Dolerite
- Fine-grained granite
- Quartz monzodiorite

DENSITY
- dens<2680
- 2680<dens<2730
- 2730<dens<2800
- 2800<dens<2890

SUBDIVISION OF ÄVRÖ GRANITE

ROCK UNIT FROM ESHI
- High confidence

CASING
- Casing

DEFORMATION ZONE FROM ESHI
- DZ

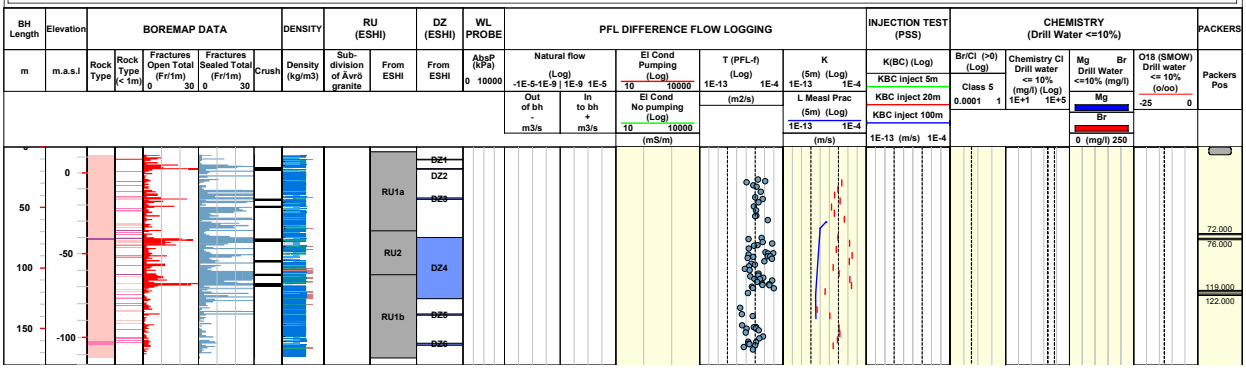

Title COMPOSITE LOG for cored borehole KLX15A

Site	LAXEMAR	**Coordinate System**	RT90-RHB70	**Drilling Start Date**	2007-01-17 10:30:00	**Packer installation for monitoring**	
Borehole	KLX15A	**Northing ToC [m]**	6365614.17	**Drilling Stop Date**	2007-02-25 20:00:00		
Diameter [mm]	76	**Easting ToC [m]**	1547987.47	**Surveying Date**	2007-01-02 12:45:00		
Length [m]	1000.430	**Elevation [m.a.s.l.ToC]**	14.59	**Chemistry class**	5		
Bearing ToC [°]	198.83	**Inclination ToC [°]**	-54.41	**Plot Date**	2008-08-24 22:12:09		

ROCK TYPE LAXEMAR
- Fine-grained granite
- Pegmatite
- Granite
- Ävrö granite
- Quartz monzodiorite
- Fine-grained diorite-gabbro

DENSITY
- dens<2680
- 2680<dens<2730
- 2730<dens<2800
- 2800<dens<2890
- dens>2890

SUBDIVISION OF ÄVRÖ GRANITE
- Ävrö granite
- Ävrö quartz monzodiorite
- Ävrö granodiorite

ROCK UNIT FROM ESHI
- High confidence

CASING
- Casing

DEFORMATION ZONE FROM ESHI
- DZ

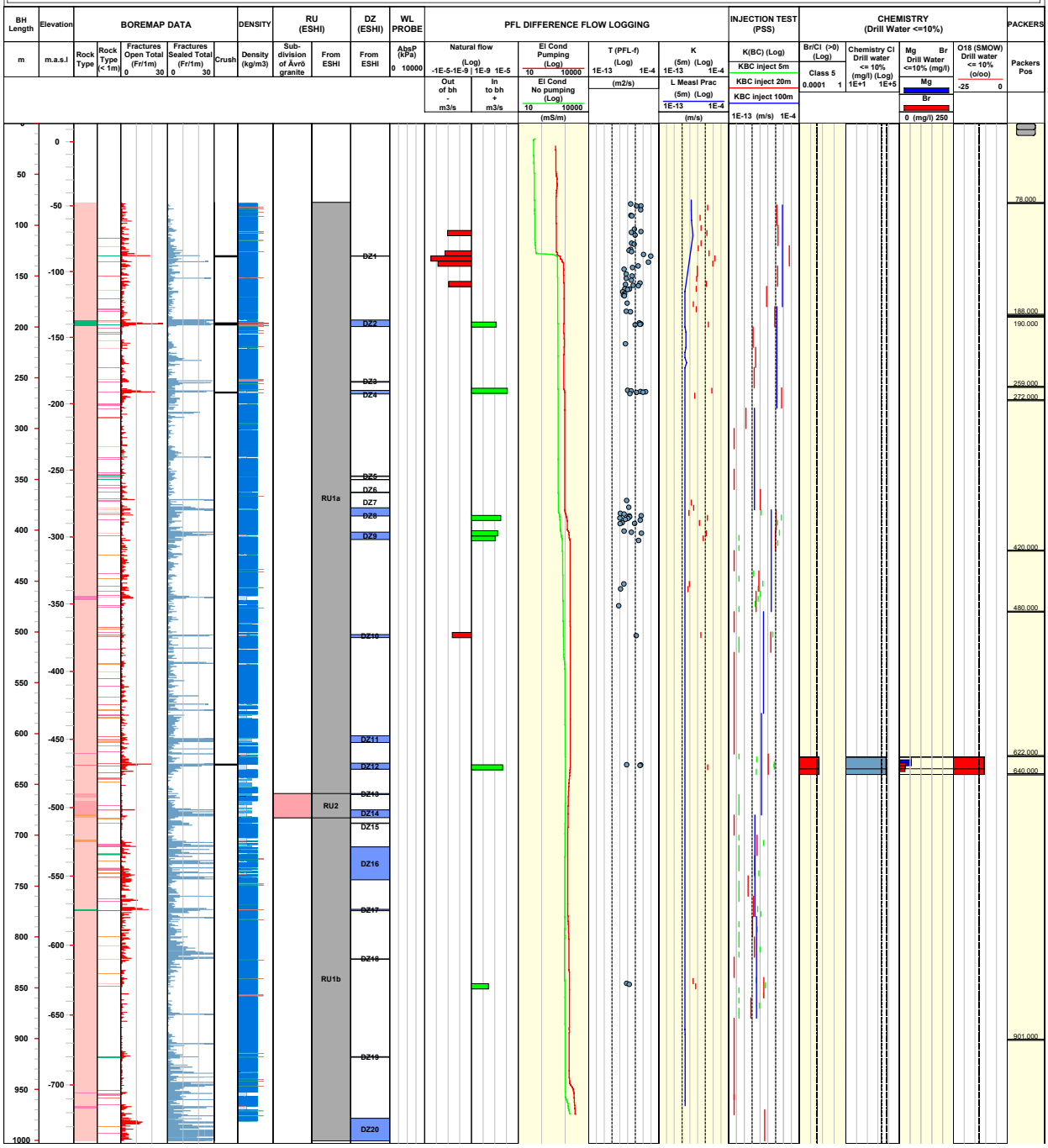

Title COMPOSITE LOG for cored borehole KLX16A

Site	LAXEMAR	**Coordinate System**	RT90-RHB70	**Drilling Start Date**	2006-11-28 13:00:00	**Packer installation for monitoring**	
Borehole	KLX16A	**Northing ToC [m]**	6364797.69	**Drilling Stop Date**	2007-01-09 13:00:00		
Diameter [mm]	76	**Easting ToC [m]**	1547584.06	**Surveying Date**	2007-01-17 12:30:00		
Length [m]	433.550	**Elevation [m.a.s.l.ToC]**	18.85	**Chemistry class**	3		
Bearing ToC [°]	294.37	**Inclination ToC [°]**	-64.97	**Plot Date**	2008-08-24 22:12:09		

ROCK TYPE LAXEMAR
- Fine-grained granite
- Pegmatite
- Granite
- Quartz monzodiorite
- Fine-grained dioritoid
- Fine-grained diorite-gabbro

DENSITY
- dens<2680
- 2680<dens<2730
- 2730<dens<2800
- 2800<dens<2890
- dens>2890

SUBDIVISION OF ÄVRÖ GRANITE

ROCK UNIT FROM ESHI
- High confidence

CASING
- Casing

DEFORMATION ZONE FROM ESHI
- DZ

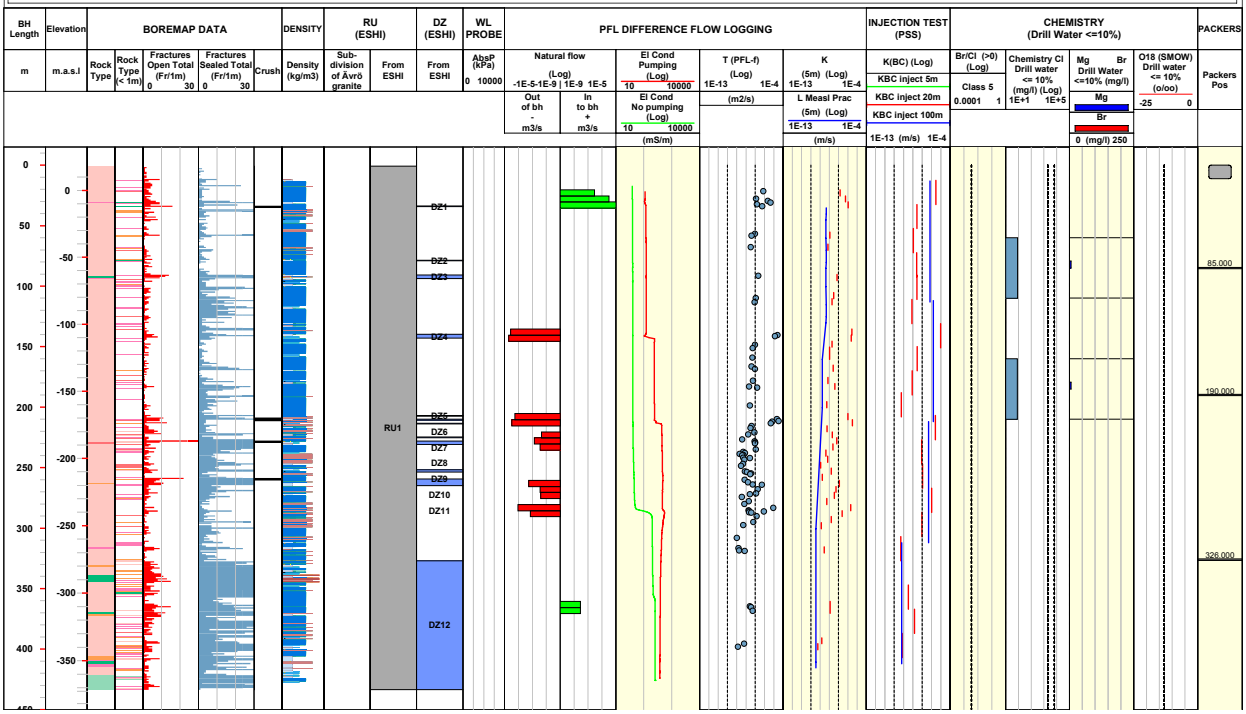

Title COMPOSITE LOG for cored borehole KLX17A

Site	LAXEMAR	**Coordinate System**	RT90-RHB70	**Drilling Start Date**	2006-09-13 06:00:00	**Packer installation for monitoring**	
Borehole	KLX17A	**Northing ToC [m]**	6366848.75	**Drilling Stop Date**	2006-10-23 09:30:00		
Diameter [mm]	76	**Easting ToC [m]**	1546862.09	**Surveying Date**	2006-08-16 16:03:00		
Length [m]	701.080	**Elevation [m.a.s.l.ToC]**	27.63	**Chemistry class**	5		
Bearing ToC [°]	11.21	**Inclination ToC [°]**	-61.33	**Plot Date**	2008-08-24 22:12:09		

ROCK TYPE LAXEMAR
- Fine-grained granite
- Ävrö granite
- Diorite / Gabbro
- Fine-grained diorite-gabbro

DENSITY
- dens<2680
- 2680<dens<2730
- 2730<dens<2800
- 2800<dens<2890
- dens>2890

SUBDIVISION OF ÄVRÖ GRANITE
- Ävrö granite
- Ävrö quartz monzodiorite
- Ävrö granodiorite

ROCK UNIT FROM ESHI
- High confidence

CASING
- Casing

DEFORMATION ZONE FROM ESHI
- DZ

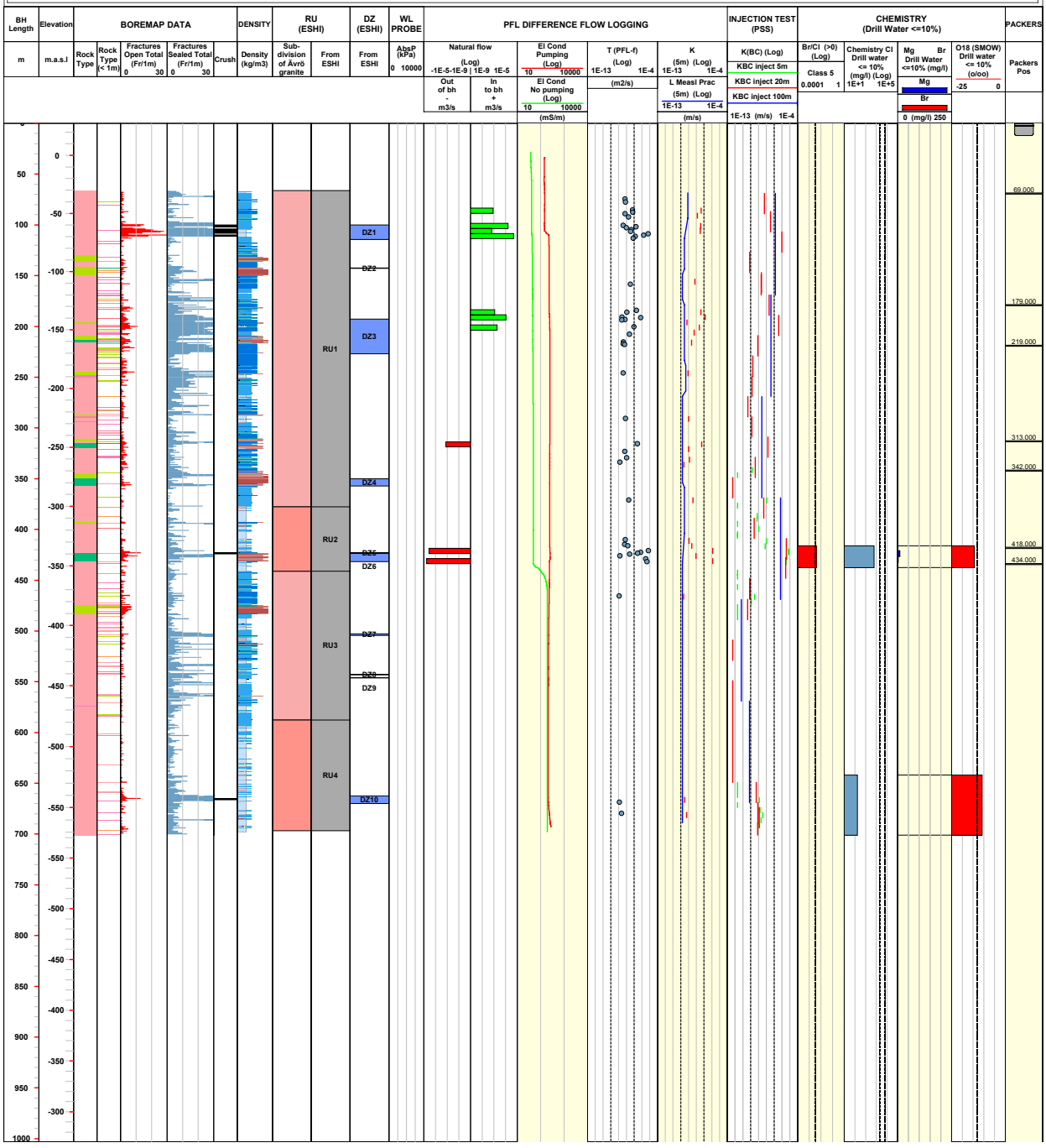

Title COMPOSITE LOG for cored borehole KLX18A

Site	LAXEMAR	**Coordinate System**	RT90-RHB70	**Drilling Start Date**	2006-03-29 10:00:00	**Packer installation for monitoring**	
Borehole	KLX18A	**Northing ToC [m]**	6366413.39	**Drilling Stop Date**	2006-05-02 12:22:00		
Diameter [mm]	76	**Easting ToC [m]**	1547966.35	**Surveying Date**	2006-02-22 11:15:00		
Length [m]	611.280	**Elevation [m.a.s.l.ToC]**	21.01	**Chemistry class**	5		
Bearing ToC [°]	271.40	**Inclination ToC [°]**	-82.10	**Plot Date**	2008-08-24 22:12:09		

ROCK TYPE LAXEMAR
- Fine-grained granite
- Ävrö granite
- Diorite / Gabbro
- Fine-grained diorite-gabbro

DENSITY
- dens<2680
- 2680<dens<2730
- 2730<dens<2800
- 2800<dens<2890
- dens>2890

SUBDIVISION OF ÄVRÖ GRANITE
- Ävrö granite
- Ävrö quartz monzodiorite
- Ävrö granodiorite

ROCK UNIT FROM ESHI
- High confidence

CASING
- Casing

DEFORMATION ZONE FROM ESHI
- DZ

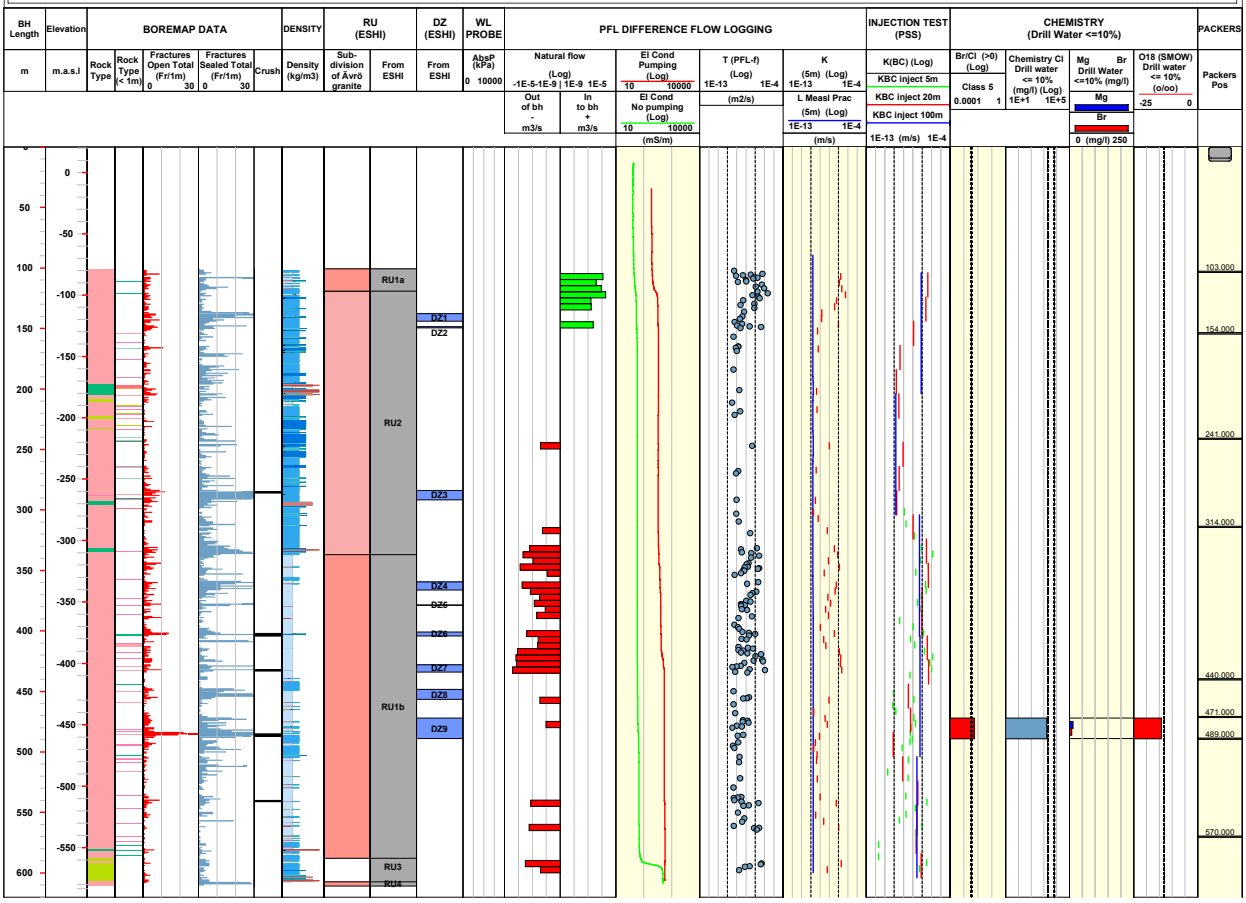

Title COMPOSITE LOG for cored borehole KLX19A

Site	LAXEMAR	**Coordinate System**	RT90-RHB70	**Drilling Start Date**	2006-06-03 11:00:00	**Packer installation**	
Borehole	KLX19A	**Northing ToC [m]**	6365901.42	**Drilling Stop Date**	2006-09-20 17:27:00	**for monitoring**	
Diameter [mm]	76	**Easting ToC [m]**	1547004.62	**Surveying Date**	2006-05-22 13:39:00		
Length [m]	800.070	**Elevation [m.a.s.l.ToC]**	16.87	**Chemistry class**	5		
Bearing ToC [°]	197.13	**Inclination ToC [°]**	-57.54	**Plot Date**	2008-08-24 22:12:09		

ROCK TYPE LAXEMAR
- Dolerite
- Fine-grained granite
- Pegmatite
- Quartz monzodiorite
- Fine-grained diorite-gabbro

DENSITY
- dens<2680
- 2680<dens<2730
- 2730<dens<2800
- 2800<dens<2890
- dens>2890

SUBDIVISION OF ÄVRÖ GRANITE

ROCK UNIT FROM ESHI
- High confidence

CASING
- Casing

DEFORMATION ZONE FROM ESHI
- DZ

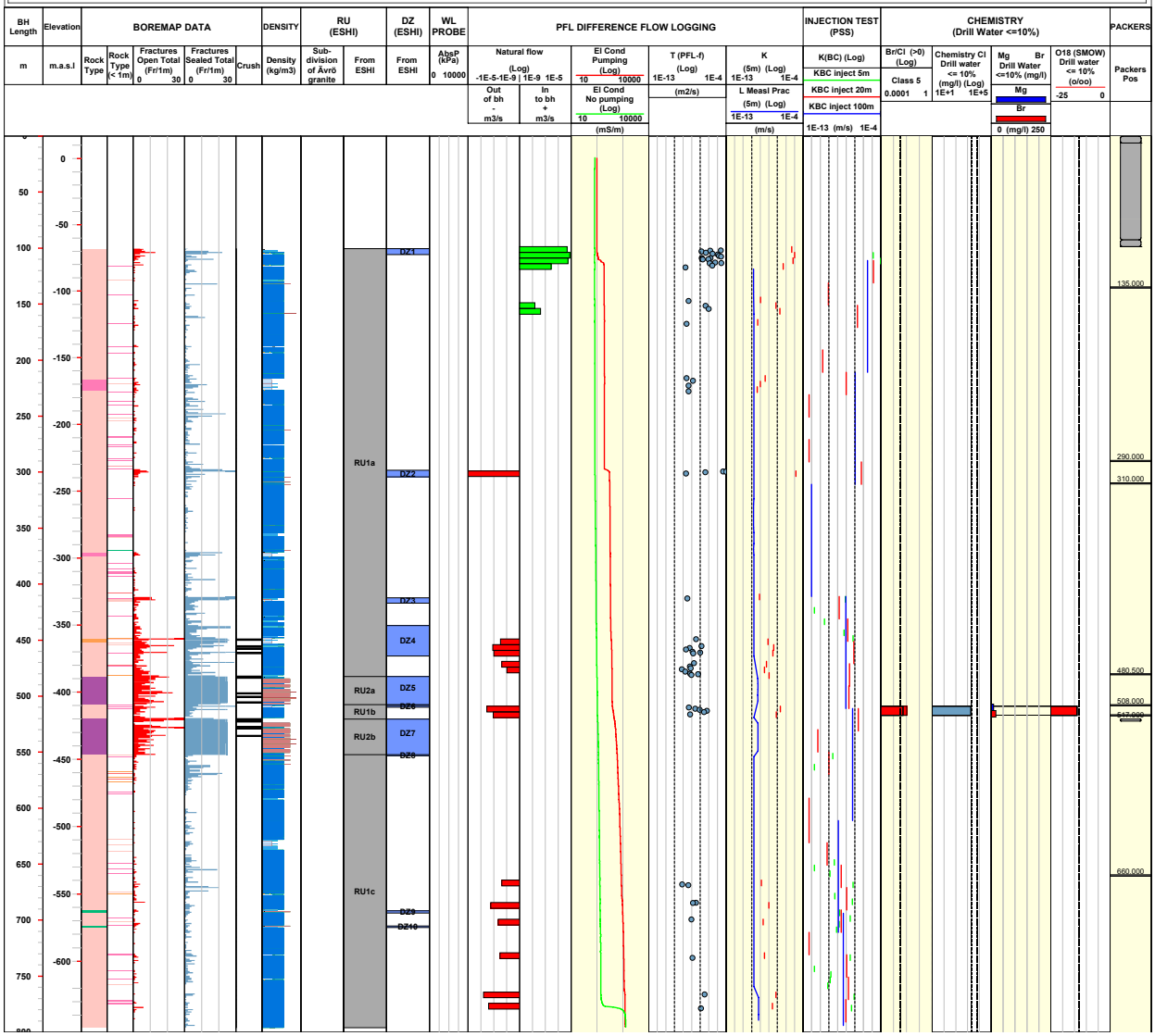

Title COMPOSITE LOG for cored borehole KLX20A

Site	LAXEMAR	**Coordinate System**	RT90-RHB70	**Drilling Start Date**	2006-03-25 06:00:00	**Packer installation for monitoring**	
Borehole	KLX20A	**Northing ToC [m]**	6366334.57	**Drilling Stop Date**	2006-04-24 13:20:00		
Diameter [mm]	76	**Easting ToC [m]**	1546604.89	**Surveying Date**	2006-05-09 09:15:00		
Length [m]	457.920	**Elevation [m.a.s.l.ToC]**	27.24	**Chemistry class**	5		
Bearing ToC [°]	270.60	**Inclination ToC [°]**	-50.02	**Plot Date**	2008-08-24 22:12:09		

ROCK TYPE LAXEMAR
- Dolerite
- Fine-grained granite
- Quartz monzodiorite
- Fine-grained diorite-gabbro

DENSITY
- dens<2680
- 2680<dens<2730
- 2730<dens<2800
- 2800<dens<2890
- dens>2890

SUBDIVISION OF ÄVRÖ GRANITE
- Ävrö granite
- Ävrö quartz monzodiorite
- Ävrö granodiorite

ROCK UNIT FROM ESHI
- High confidence

CASING
- Casing

DEFORMATION ZONE FROM ESHI
- DZ

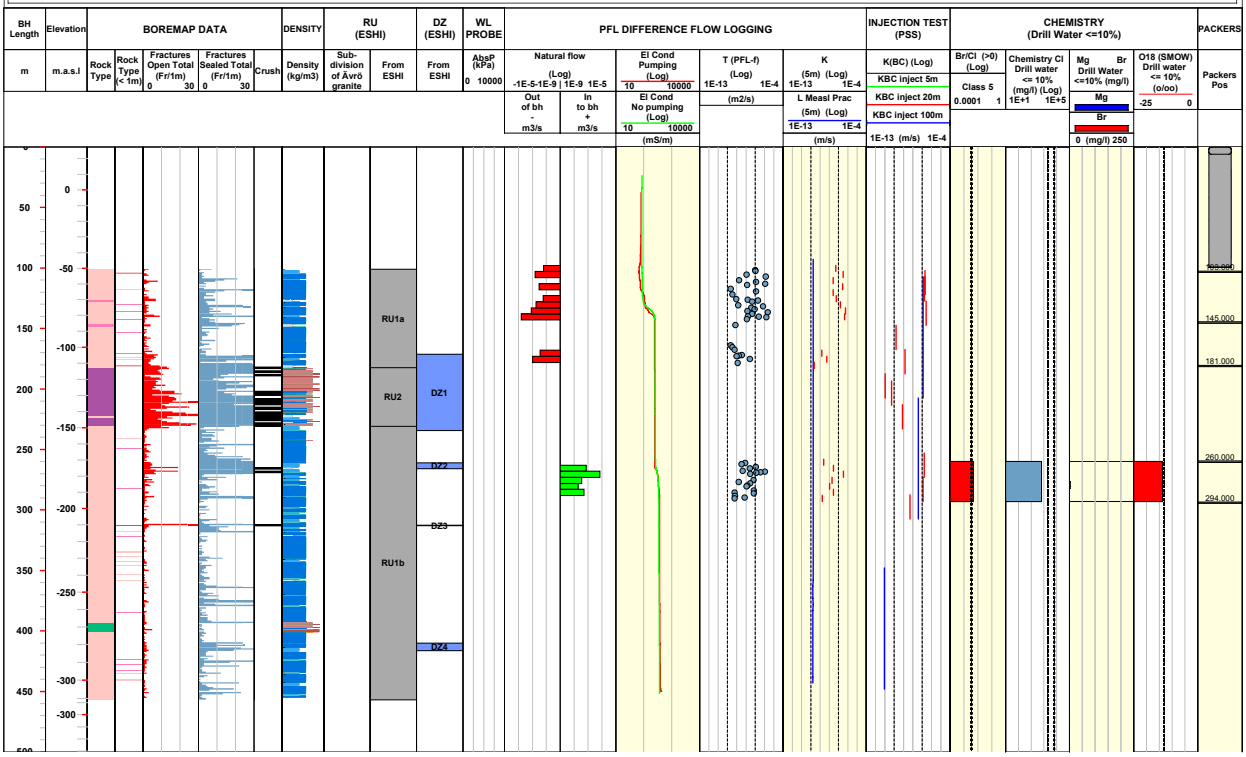

Title COMPOSITE LOG for cored borehole KLX21B

Site	LAXEMAR	**Coordinate System**	RT90-RHB70	**Drilling Start Date**	2006-10-12 08:00:00	**Packer installation for monitoring**	
Borehole	KLX21B	**Northing ToC [m]**	6366164.00	**Drilling Stop Date**	2006-11-29 10:30:00		
Diameter [mm]	76	**Easting ToC [m]**	1549715.10	**Surveying Date**	2006-09-27 11:15:00		
Length [m]	858.780	**Elevation [m.a.s.l.ToC]**	10.68	**Chemistry class**	3		
Bearing ToC [°]	225.05	**Inclination ToC [°]**	-70.85	**Plot Date**	2008-08-24 22:12:09		

ROCK TYPE LAXEMAR
- Fine-grained granite
- Ävrö granite
- Quartz monzodiorite
- Diorite / Gabbro
- Fine-grained dioritoid
- Fine-grained diorite-gabbro

DENSITY
- dens<2680
- 2680<dens<2730
- 2730<dens<2800
- 2800<dens<2890
- dens>2890

SUBDIVISION OF ÄVRÖ GRANITE
- Ävrö granite
- Ävrö quartz monzodiorite
- Ävrö granodiorite

ROCK UNIT FROM ESHI
- High confidence

CASING
- Casing

DEFORMATION ZONE FROM ESHI
- DZ

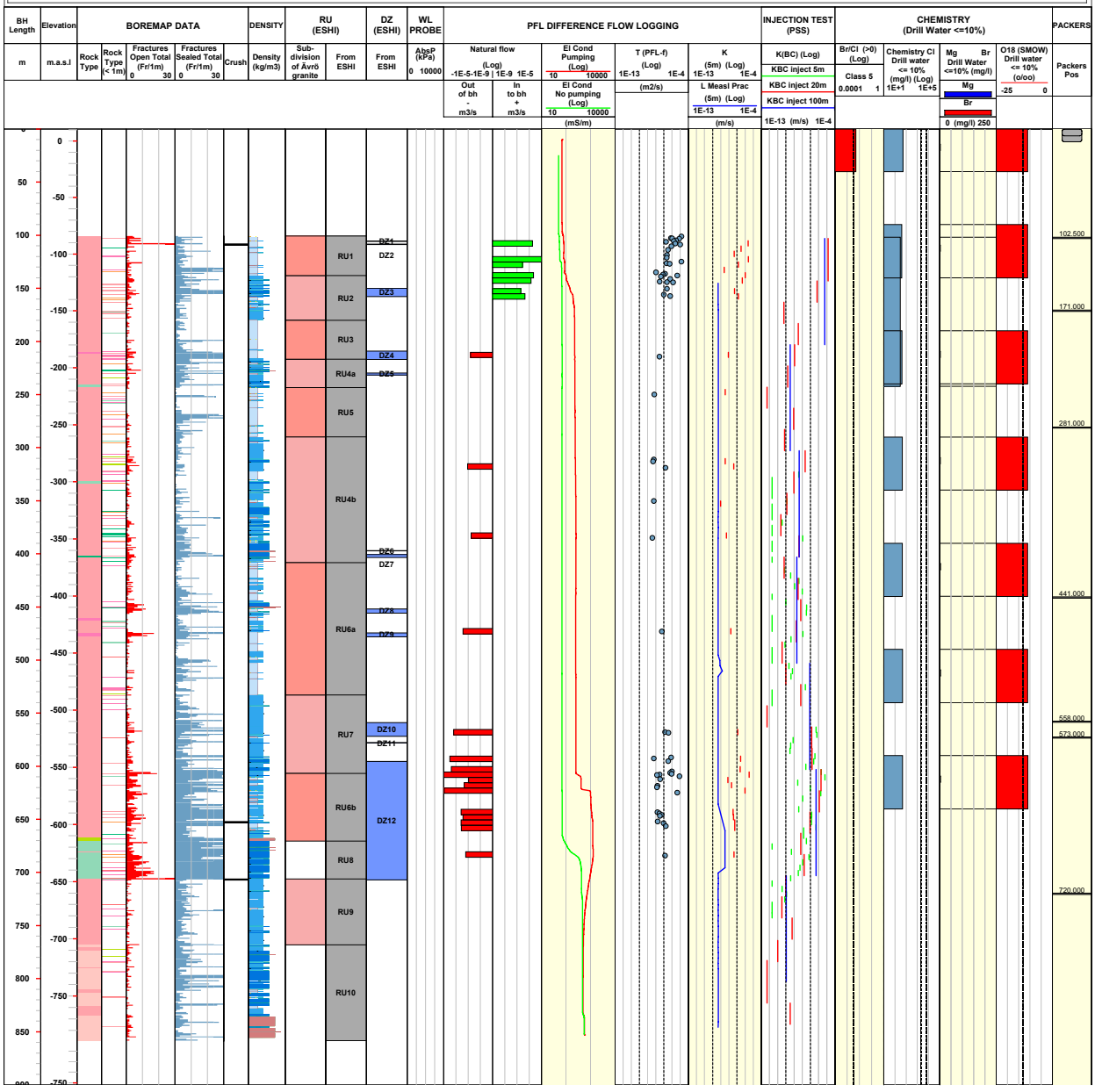

Title COMPOSITE LOG for cored borehole KLX22A

Site	LAXEMAR	**Coordinate System**	RT90-RHB70	**Drilling Start Date**	2006-05-05 12:00:00	**Packer installation for monitoring**	
Borehole	KLX22A	**Northing ToC [m]**	6366548.35	**Drilling Stop Date**	2006-05-12 13:40:00		
Diameter [mm]	76	**Easting ToC [m]**	1546688.60	**Surveying Date**	2006-08-03 10:51:00		
Length [m]	100.450	**Elevation [m.a.s.l.ToC]**	21.97	**Chemistry class**	$Class		
Bearing ToC [°]	179.19	**Inclination ToC [°]**	-60.33	**Plot Date**	2008-08-24 22:12:09		

ROCK TYPE LAXEMAR
- Fine-grained granite
- Quartz monzodiorite
- Fine-grained diorite-gabbro

DENSITY
- dens<2680
- 2680<dens<2730
- 2730<dens<2800
- 2800<dens<2890

SUBDIVISION OF ÄVRÖ GRANITE
- Ävrö granite
- Ävrö quartz monzodiorite
- Ävrö granodiorite

ROCK UNIT FROM ESHI
- High confidence

CASING
- Casing

DEFORMATION ZONE FROM ESHI
- DZ

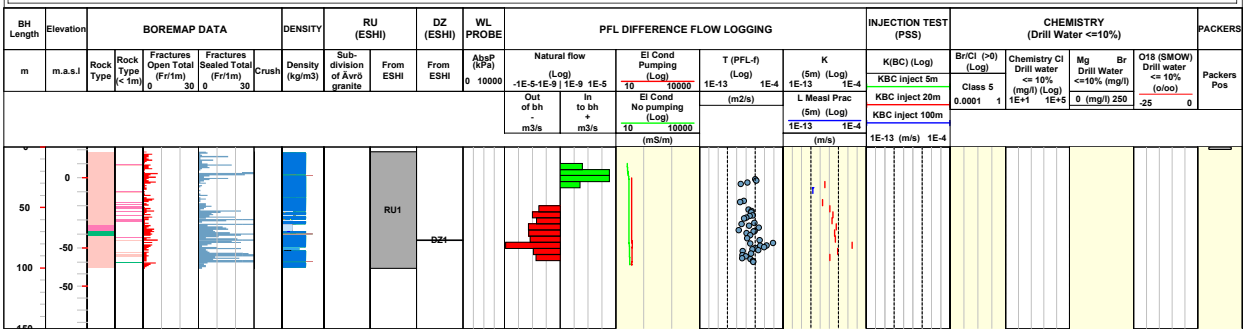

Title COMPOSITE LOG for cored borehole KLX22B

Site	LAXEMAR	**Coordinate System**	RT90-RHB70	**Drilling Start Date**	2006-05-13 09:13:00	**Packer installation for monitoring**	
Borehole	KLX22B	**Northing ToC [m]**	6366553.13	**Drilling Stop Date**	2006-05-18 13:03:00		
Diameter [mm]	76	**Easting ToC [m]**	1546685.41	**Surveying Date**	2006-08-03 10:46:00		
Length [m]	100.250	**Elevation [m.a.s.l.ToC]**	21.58	**Chemistry class**	$Class		
Bearing ToC [°]	343.97	**Inclination ToC [°]**	-61.24	**Plot Date**	2008-08-24 22:12:09		

ROCK TYPE LAXEMAR
- Fine-grained granite
- Quartz monzodiorite
- Fine-grained diorite-gabbro

DENSITY
- dens<2680
- 2680<dens<2730
- 2730<dens<2800
- 2800<dens<2890
- dens>2890

SUBDIVISION OF ÄVRÖ GRANITE
- Ävrö granite
- Ävrö quartz monzodiorite
- Ävrö granodiorite

ROCK UNIT FROM ESHI
- High confidence

CASING
- Casing

DEFORMATION ZONE FROM ESHI
- DZ

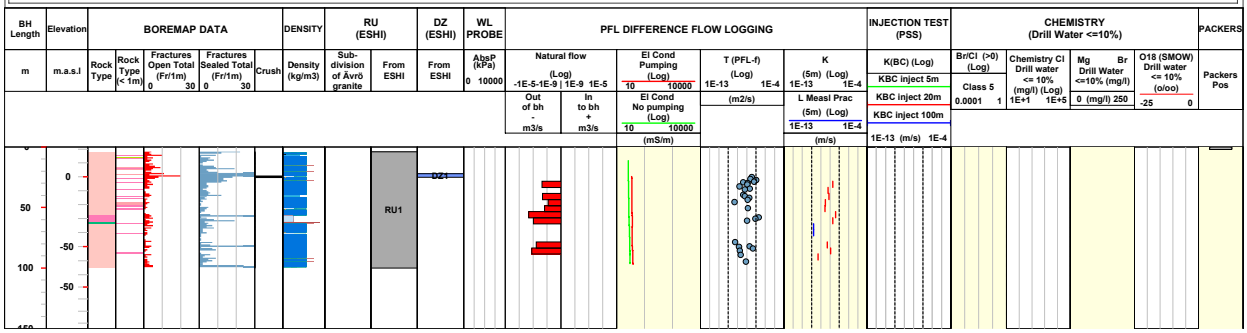

Title COMPOSITE LOG for cored borehole KLX23A

Site	LAXEMAR	**Coordinate System**	RT90-RHB70	**Drilling Start Date**	2006-05-21 10:27:00	**Packer installation for monitoring**	
Borehole	KLX23A	**Northing ToC [m]**	6366106.89	**Drilling Stop Date**	2006-05-27 07:45:00		
Diameter [mm]	76	**Easting ToC [m]**	1546715.74	**Surveying Date**	2006-08-07 10:28:00		
Length [m]	100.150	**Elevation [m.a.s.l.ToC]**	22.26	**Chemistry class**	1		
Bearing ToC [°]	28.73	**Inclination ToC [°]**	-61.35	**Plot Date**	2008-08-24 22:12:09		

ROCK TYPE LAXEMAR
- Quartz monzodiorite

DENSITY
- dens<2680
- 2680<dens<2730
- 2730<dens<2800

SUBDIVISION OF ÄVRÖ GRANITE
- Ävrö granite
- Ävrö quartz monzodiorite
- Ävrö granodiorite

ROCK UNIT FROM ESHI
- High confidence

CASING
- Casing

DEFORMATION ZONE FROM ESHI
- DZ

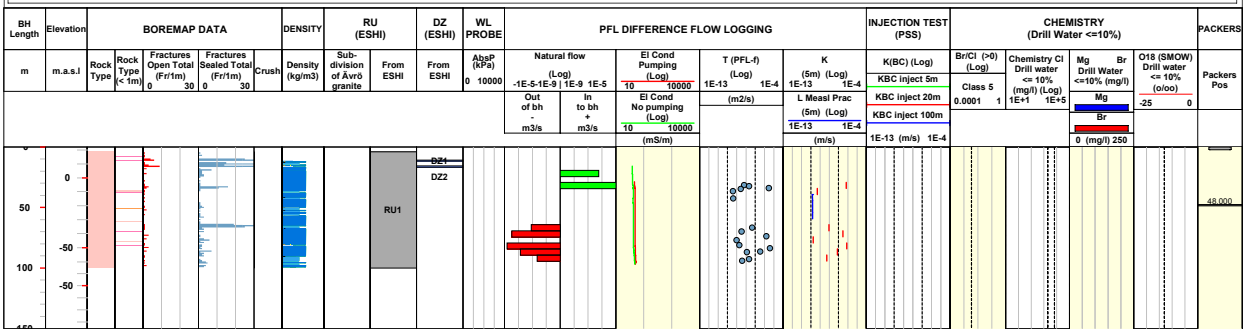

Title **COMPOSITE LOG for cored borehole KLX23B**

Site	LAXEMAR	**Coordinate System**	RT90-RHB70	**Drilling Start Date**	2006-05-28 13:55:00	**Packer installation for monitoring**	
Borehole	KLX23B	**Northing ToC [m]**	6366101.90	**Drilling Stop Date**	2006-05-31 11:15:00		
Diameter [mm]	76	**Easting ToC [m]**	1546717.33	**Surveying Date**	2006-08-04 11:00:00		
Length [m]	50.270	**Elevation [m.a.s.l.ToC]**	22.32	**Chemistry class**	$Class		
Bearing ToC [°]	121.36	**Inclination ToC [°]**	-60.84	**Plot Date**	2008-08-24 22:12:09		

ROCK TYPE LAXEMAR
- Quartz monzodiorite

DENSITY
- dens<2680
- 2680<dens<2730
- 2730<dens<2800

SUBDIVISION OF ÄVRÖ GRANITE
- Ävrö granite
- Ävrö quartz monzodiorite
- Ävrö granodiorite

ROCK UNIT FROM ESHI
- High confidence

CASING
- Casing

DEFORMATION ZONE FROM ESHI
- DZ

BH Length	Elevation	BOREMAP DATA					DENSITY	RU (ESHI)		DZ (ESHI)	WL PROBE	PFL DIFFERENCE FLOW LOGGING					INJECTION TEST (PSS)	CHEMISTRY (Drill Water <=10%)				PACKERS
m	m.a.s.l	Rock Type	Rock Type (< 1m)	Fractures Open Total (Fr/1m) 0 30	Fractures Sealed Total (Fr/1m) 0 30	Crush	Density (kg/m3)	Sub-division of Ävrö granite	From ESHI	From ESHI	AbsP (kPa) 0 10000	Natural flow (Log) -1E-5-1E-9	1E-9 1E-5	El Cond Pumping (Log) 10 10000	T (PFL-f) (Log) 1E-13 1E-4	K (5m) (Log) 1E-13 1E-4	K(BC) (Log)	Br/Cl (>0) (Log)	Chemistry Cl Drill water <= 10% (mg/l) (Log) 1E+1 1E+5	Mg Br Drill Water <=10% (mg/l) 0 (mg/l) 250	O18 (SMOW) Drill water <= 10% (o/oo) -25 0	Packers Pos
												Out of bh - m3/s	In to bh + m3/s	El Cond No pumping (Log) 10 10000 (mS/m)	(m2/s)	L Measl Prac (5m) (Log) 1E-13 1E-4 (m/s)	KBC inject 5m KBC inject 20m KBC inject 100m 1E-13 (m/s) 1E-4	Class 5 0.0001 1				

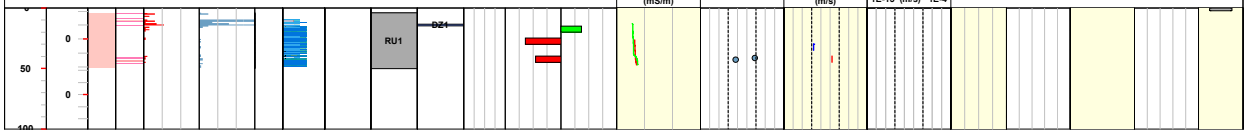

Title COMPOSITE LOG for cored borehole KLX24A

Site	LAXEMAR	**Coordinate System**	RT90-RHB70	**Drilling Start Date**	2006-06-14 11:00:00	**Packer installation for monitoring**	
Borehole	KLX24A	**Northing ToC [m]**	6366423.35	**Drilling Stop Date**	2006-06-29 08:45:00		
Diameter [mm]	76	**Easting ToC [m]**	1546853.80	**Surveying Date**	2006-08-03 12:21:00		
Length [m]	100.170	**Elevation [m.a.s.l.ToC]**	21.29	**Chemistry class**	1		
Bearing ToC [°]	98.41	**Inclination ToC [°]**	-59.14	**Plot Date**	2008-08-24 22:12:09		

ROCK TYPE LAXEMAR
- Fine-grained granite
- Quartz monzodiorite

DENSITY
- dens<2680
- 2680<dens<2730
- 2730<dens<2800
- 2800<dens<2890

SUBDIVISION OF ÄVRÖ GRANITE

ROCK UNIT FROM ESHI
- High confidence

CASING
- Casing

DEFORMATION ZONE FROM ESHI
- DZ

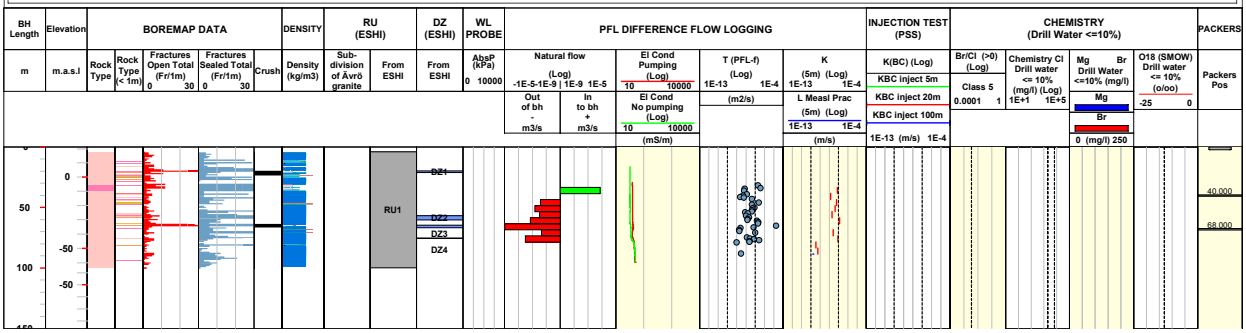

Title COMPOSITE LOG for cored borehole KLX25A

Site	LAXEMAR	**Coordinate System**	RT90-RHB70	**Drilling Start Date**	2006-07-01 14:00:00	**Packer installation for monitoring**	
Borehole	KLX25A	**Northing ToC [m]**	6366274.74	**Drilling Stop Date**	2006-07-04 14:00:00		
Diameter [mm]	76	**Easting ToC [m]**	1546769.66	**Surveying Date**	2006-08-03 11:48:00		
Length [m]	50.240	**Elevation [m.a.s.l.ToC]**	22.84	**Chemistry class**	$Class		
Bearing ToC [°]	145.73	**Inclination ToC [°]**	-59.45	**Plot Date**	2008-08-24 22:12:09		

ROCK TYPE LAXEMAR
Quartz monzodiorite

DENSITY
2730<dens<2800
2800<dens<2890

SUBDIVISION OF ÄVRÖ GRANITE

ROCK UNIT FROM ESHI
High confidence

CASING
Casing

DEFORMATION ZONE FROM ESHI
DZ

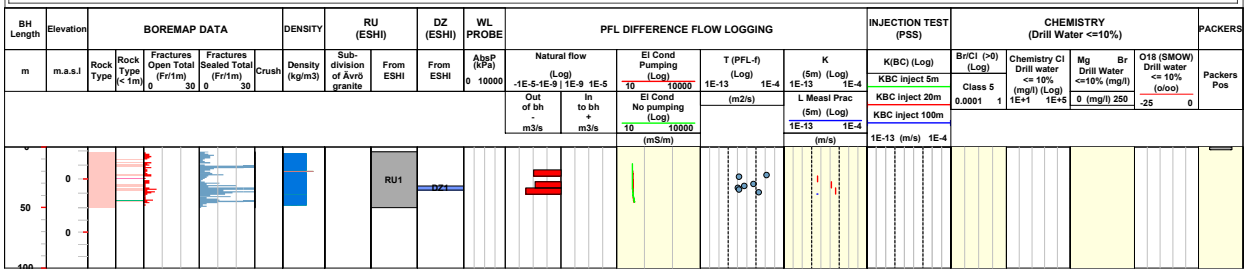

Title COMPOSITE LOG for cored borehole KLX26A

Site	LAXEMAR	**Coordinate System**	RT90-RHB70	**Drilling Start Date**	2006-08-03 06:00:00	**Packer installation for monitoring**	
Borehole	KLX26A	**Northing ToC [m]**	6365546.49	**Drilling Stop Date**	2006-08-11 11:00:00		
Diameter [mm]	76	**Easting ToC [m]**	1549029.90	**Surveying Date**	2006-09-12 11:30:00		
Length [m]	101.140	**Elevation [m.a.s.l.ToC]**	15.63	**Chemistry class**	1		
Bearing ToC [°]	93.47	**Inclination ToC [°]**	-60.44	**Plot Date**	2008-08-24 22:12:09		

ROCK TYPE LAXEMAR
- Fine-grained granite
- Ävrö granite
- Quartz monzodiorite
- Diorite / Gabbro
- Fine-grained diorite-gabbro

DENSITY
- dens<2680
- 2680<dens<2730
- 2730<dens<2800
- 2800<dens<2890
- dens>2890

SUBDIVISION OF ÄVRÖ GRANITE
- Ävrö granite
- Ävrö quartz monzodiorite
- Ävrö granodiorite

ROCK UNIT FROM ESHI
- High confidence

CASING
- Casing

DEFORMATION ZONE FROM ESHI
- DZ

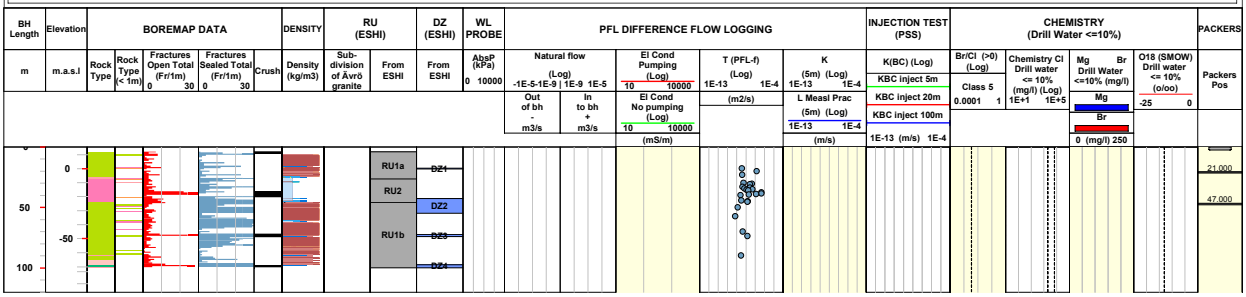

Title COMPOSITE LOG for cored borehole KLX26B

Site	LAXEMAR	**Coordinate System**	RT90-RHB70	**Drilling Start Date**	2006-08-12 09:00:00	**Packer installation for monitoring**	
Borehole	KLX26B	**Northing ToC [m]**	6365550.66	**Drilling Stop Date**	2006-08-17 07:15:00		
Diameter [mm]	76	**Easting ToC [m]**	1549025.61	**Surveying Date**	2006-09-12 11:25:00		
Length [m]	50.370	**Elevation [m.a.s.l.ToC]**	15.82	**Chemistry class**	$Class		
Bearing ToC [°]	137.42	**Inclination ToC [°]**	-60.00	**Plot Date**	2008-08-24 22:12:09		

ROCK TYPE LAXEMAR
- Fine-grained granite
- Diorite / Gabbro

DENSITY
- dens<2680
- 2730<dens<2800
- 2800<dens<2890
- dens>2890

SUBDIVISION OF ÄVRÖ GRANITE
- Ävrö granite
- Ävrö quartz monzodiorite
- Ävrö granodiorite

ROCK UNIT FROM ESHI
- High confidence

CASING
- Casing

DEFORMATION ZONE FROM ESHI
- DZ

BH Length	Elevation	BOREMAP DATA					DENSITY	RU (ESHI)		DZ (ESHI)	WL PROBE	PFL DIFFERENCE FLOW LOGGING					INJECTION TEST (PSS)	CHEMISTRY (Drill Water <=10%)				PACKERS
m	m.a.s.l	Rock Type	Rock Type (< 1m)	Fractures Open Total (Fr/1m) 0 30	Fractures Sealed Total (Fr/1m) 0 30	Crush	Density (kg/m3)	Sub-division of Ävrö granite	From ESHI	From ESHI	AbsP (kPa) 0 10000	Natural flow (Log) -1E-5-1E-9	1E-9 1E-5	El Cond Pumping (Log) 10 10000	T (PFL-f) (Log) 1E-13 1E-4	K (5m) (Log) 1E-13 1E-4	K(BC) (Log) KBC inject 5m KBC inject 20m KBC inject 100m 1E-13 (m/s) 1E-4	Br/Cl (>0) (Log) Class 5 0.0001 1	Chemistry Cl Drill water <= 10% (mg/l) (Log) 1E+1 1E+5	Mg Br Drill Water <=10% (mg/l) 0 (mg/l) 250	O18 (SMOW) Drill water <= 10% (o/oo) -25 0	Packers Pos
												Out of bh - m3/s	In to bh + m3/s	El Cond No pumping (Log) 10 10000 (mS/m)	(m2/s)	L Measl Prac (5m) (Log) 1E-13 1E-4 (m/s)						
0 50	0							RU1a RU2 RU1b														22.000 46.000

Title COMPOSITE LOG for cored borehole KLX27A

Site	LAXEMAR	**Coordinate System**	RT90-RHB70	**Drilling Start Date**	2007-10-08 14:00:00	**Packer installation for monitoring**	
Borehole	KLX27A	**Northing ToC [m]**	6365608.29	**Drilling Stop Date**	2007-11-21 11:30:00		
Diameter [mm]	76	**Easting ToC [m]**	1546742.63	**Surveying Date**	2007-09-07 13:30:00		
Length [m]	650.560	**Elevation [m.a.s.l.ToC]**	16.98	**Chemistry class**	5		
Bearing ToC [°]	0.73	**Inclination ToC [°]**	-65.36	**Plot Date**	2008-08-24 22:12:09		

ROCK TYPE LAXEMAR
- Fine-grained granite
- Quartz monzodiorite
- Fine-grained diorite-gabbro

DENSITY
- dens<2680
- 2680<dens<2730
- 2730<dens<2800
- 2800<dens<2890

SUBDIVISION OF ÄVRÖ GRANITE
- Ävrö granite
- Ävrö quartz monzodiorite
- Ävrö granodiorite

ROCK UNIT FROM ESHI
- High confidence

CASING
- Casing

DEFORMATION ZONE FROM ESHI
- DZ

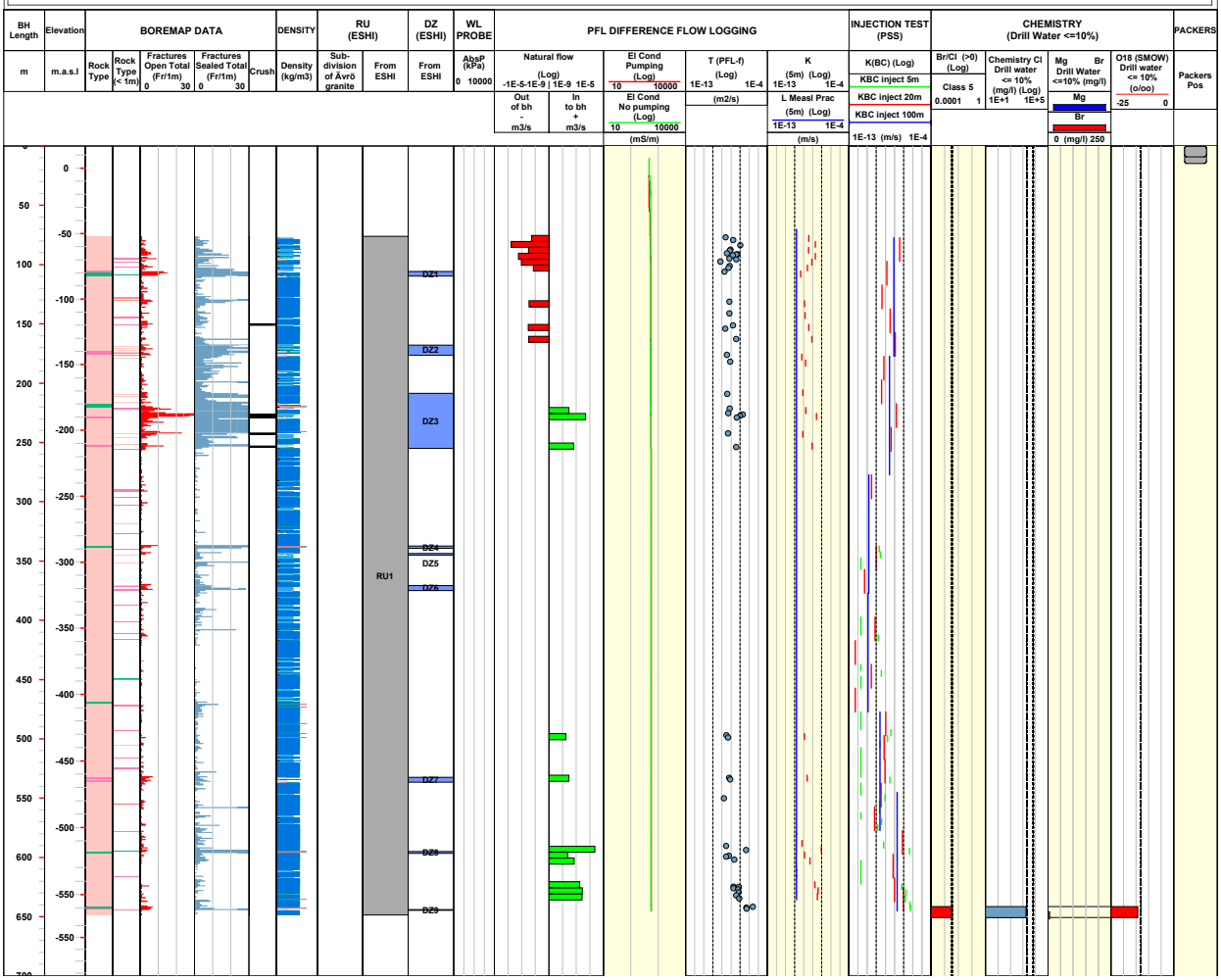

Title **COMPOSITE LOG for cored borehole KLX28A**

Site	LAXEMAR	**Coordinate System**	RT90-RHB70	**Drilling Start Date**	2006-09-14 16:00:00	**Packer installation for monitoring**	
Borehole	KLX28A	**Northing ToC [m]**	6365682.22	**Drilling Stop Date**	2006-09-20 08:55:00		
Diameter [mm]	76	**Easting ToC [m]**	1549333.71	**Surveying Date**	2006-09-27 14:45:00		
Length [m]	80.230	**Elevation [m.a.s.l.ToC]**	10.05	**Chemistry class**	$Class		
Bearing ToC [°]	189.70	**Inclination ToC [°]**	-60.05	**Plot Date**	2008-08-24 22:12:09		

ROCK TYPE LAXEMAR
- Fine-grained granite
- Ävrö granite
- Fine-grained diorite-gabbro

DENSITY
- dens<2680
- 2680<dens<2730
- 2730<dens<2800
- 2800<dens<2890

SUBDIVISION OF ÄVRÖ GRANITE
- Ävrö granite
- Ävrö quartz monzodiorite
- Ävrö granodiorite

ROCK UNIT FROM ESHI
- High confidence

CASING
- Casing

DEFORMATION ZONE FROM ESHI
- DZ

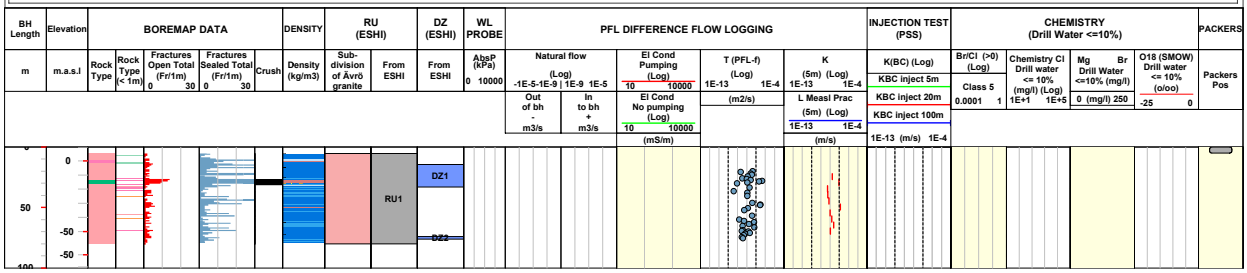

Title COMPOSITE LOG for cored borehole KLX29A

Site	LAXEMAR	**Coordinate System**	RT90-RHB70	**Drilling Start Date**	2006-09-09 10:00:00	**Packer installation for monitoring**	
Borehole	KLX29A	**Northing ToC [m]**	6366264.54	**Drilling Stop Date**	2006-09-13 11:40:00		
Diameter [mm]	76	**Easting ToC [m]**	1549443.99	**Surveying Date**	2006-09-25 10:40:00		
Length [m]	60.250	**Elevation [m.a.s.l.ToC]**	13.63	**Chemistry class**	$Class		
Bearing ToC [°]	321.21	**Inclination ToC [°]**	-60.90	**Plot Date**	2008-08-24 22:12:09		

ROCK TYPE LAXEMAR
- Ävrö granite
- Fine-grained diorite-gabbro

DENSITY
- dens<2680
- 2680<dens<2730
- 2730<dens<2800
- 2800<dens<2890
- dens>2890

SUBDIVISION OF ÄVRÖ GRANITE
- Ävrö granite
- Ävrö quartz monzodiorite
- Ävrö granodiorite

ROCK UNIT FROM ESHI
- High confidence

CASING
- Casing

DEFORMATION ZONE FROM ESHI
- DZ

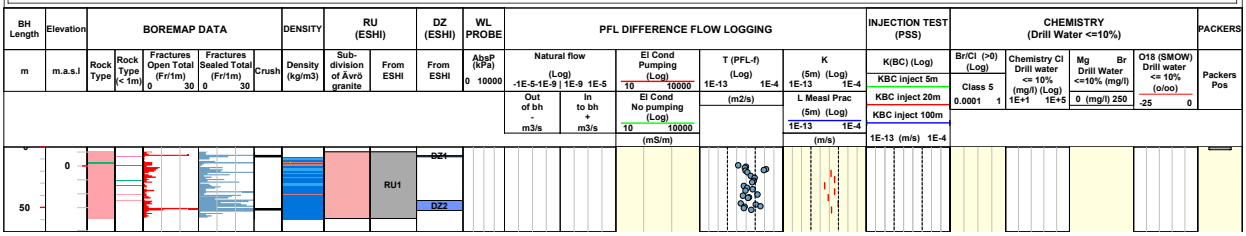

Title COMPOSITE LOG for cored borehole KSH01A

Site	SIMPEVARP	**Coordinate System**	RT90-RHB70	**Drilling Start Date**	2002-10-07 16:00:00	**Packer installation for monitoring**	
Borehole	KSH01A	**Northing ToC [m]**	6366013.45	**Drilling Stop Date**	2002-12-18 21:10:00		
Diameter [mm]	76	**Easting ToC [m]**	1552442.98	**Surveying Date**	2003-11-06 13:20:00		
Length [m]	1003.000	**Elevation [m.a.s.l.ToC]**	5.32	**Chemistry class**	5		
Bearing ToC [°]	173.60	**Inclination ToC [°]**	-80.43	**Plot Date**	2008-08-27 22:15:27		

ROCK TYPE SIMPEVARP
- Fine-grained granite
- Pegmatite
- Granite
- Ävrö granite
- Quartz monzodiorite
- Diorite / Gabbro
- Fine-grained dioritoid
- Fine-grained diorite-gabbro

DENSITY

SUBDIVISION OF ÄVRÖ GRANITE
- Ävrö granite
- Ävrö quartz monzodiorite
- Ävrö granodiorite

ROCK UNIT FROM ESHI
- High confidence

CASING
- Casing

DEFORMATION ZONE FROM ESHI
- DZ

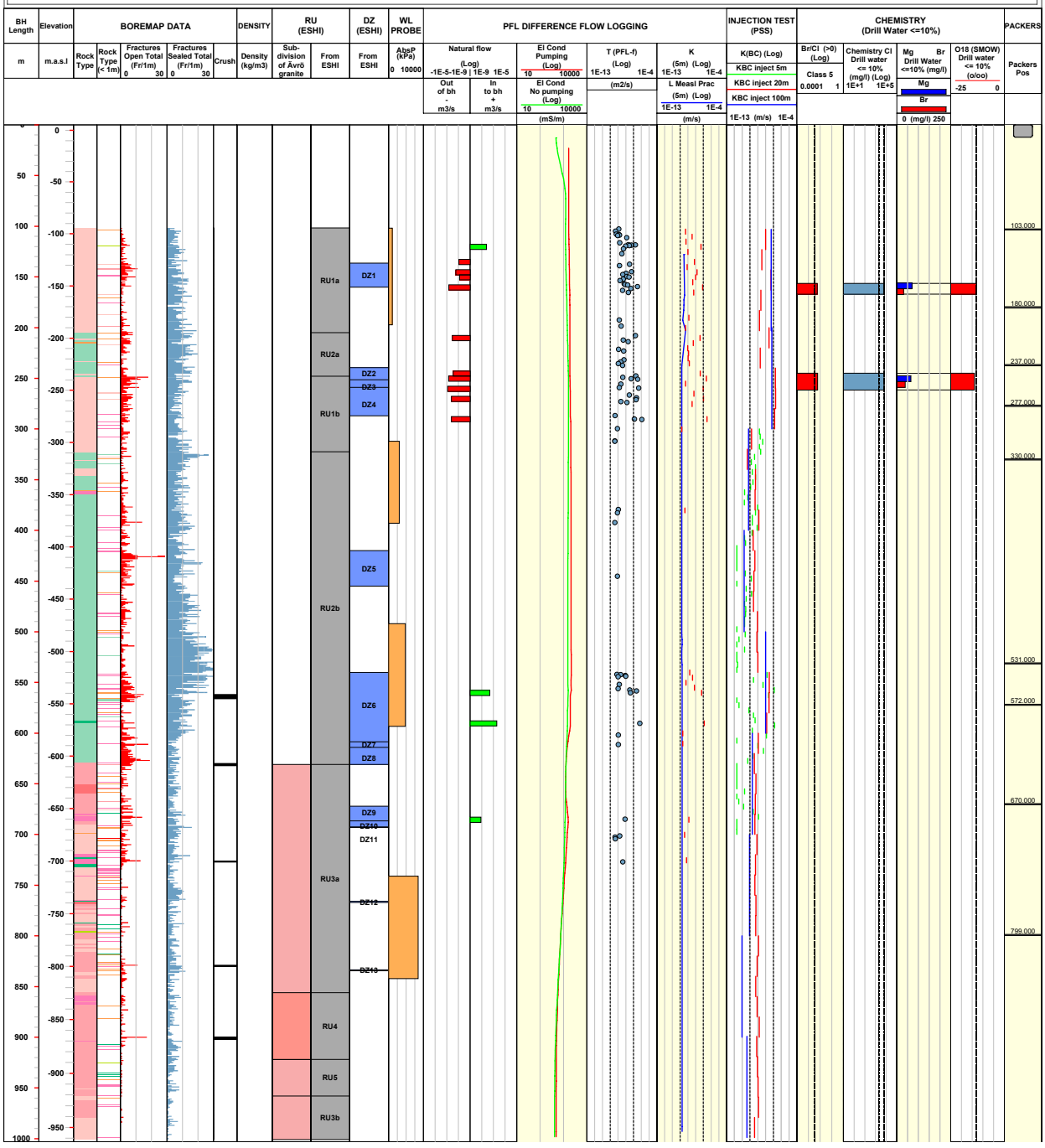

Title **COMPOSITE LOG for cored borehole KSH01B**

Site	SIMPEVARP	**Coordinate System**	RT90-RHB70	**Drilling Start Date**	2003-01-17 12:00:00	**Packer installation**	
Borehole	KSH01B	**Northing ToC [m]**	6366014.04	**Drilling Stop Date**	2003-01-27 19:00:00	**for monitoring**	
Diameter [mm]	76	**Easting ToC [m]**	1552442.89	**Surveying Date**	2003-01-29 09:30:00		
Length [m]	100.250	**Elevation [m.a.s.l.ToC]**	5.20	**Chemistry class**	$Class		
Bearing ToC [°]	177.76	**Inclination ToC [°]**	-87.87	**Plot Date**	2008-08-31 22:34:28		

ROCK TYPE SIMPEVARP
- Quartz monzodiorite

DENSITY

SUBDIVISION OF ÄVRÖ GRANITE
- Ävrö granite
- Ävrö quartz monzodiorite
- Ävrö granodiorite

ROCK UNIT FROM ESHI
- High confidence

CASING
- Casing

DEFORMATION ZONE FROM ESHI
- DZ

BH Length	Elevation	BOREMAP DATA					DENSITY	RU (ESHI)		DZ (ESHI)	WL PROBE	PFL DIFFERENCE FLOW LOGGING					INJECTION TEST (PSS)	CHEMISTRY (Drill Water <=10%)				PACKERS
m	m.a.s.l	Rock Type	Rock Type (< 1m)	Fractures Open Total (Fr/1m) 0 30	Fractures Sealed Total (Fr/1m) 0 30	Crush	Density (kg/m3)	Sub-division of Ävrö granite	From ESHI	From ESHI	AbsP (kPa) 0 10000	Natural flow (Log) -1E-5 1E-9	1E-9 1E-5	El Cond Pumping (Log) 10 10000	T (PFL-f) (Log) 1E-13 1E-4	K (5m) (Log) 1E-13 1E-4	K(BC) (Log)	Br/Cl (>0) (Log)	Chemistry Cl Drill water <= 10% (mg/l) (Log) 1E+1 1E+5	Mg Br Drill Water <=10% (mg/l)	O18 (SMOW) Drill water <= 10% (o/oo)	Packers Pos
												Out of bh - m3/s	In to bh + m3/s	El Cond No pumping (Log) 10 10000 (mS/m)	(m2/s)	L Meas Prac (5m) (Log) 1E-13 1E-4 (m/s)	KBC inject 5m KBC inject 20m KBC inject 100m 1E-13 (m/s) 1E-4	Class 5 0.0001 1		0 (mg/l) 250	-25 0	

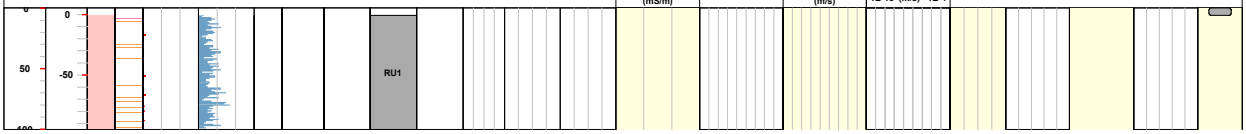

Title COMPOSITE LOG for cored borehole KSH02

Site	SIMPEVARP	**Coordinate System**	RT90-RHB70	**Drilling Start Date**	2003-01-28 07:00:00	**Packer installation for monitoring**	
Borehole	KSH02	**Northing ToC [m]**	6365658.33	**Drilling Stop Date**	2003-06-11 15:10:00		
Diameter [mm]	76	**Easting ToC [m]**	1551528.93	**Surveying Date**	2003-11-24 11:40:00		
Length [m]	1001.110	**Elevation [m.a.s.l.ToC]**	5.48	**Chemistry class**	5		
Bearing ToC [°]	330.68	**Inclination ToC [°]**	-85.62	**Plot Date**	2008-08-27 22:15:27		

ROCK TYPE SIMPEVARP
- Fine-grained granite
- Pegmatite
- Fine-grained dioritoid
- Fine-grained diorite-gabbro

DENSITY
- dens<2680
- 2680<dens<2730
- 2730<dens<2800
- 2800<dens<2890
- dens>2890

SUBDIVISION OF ÄVRÖ GRANITE
- Ävrö granite
- Ävrö quartz monzodiorite
- Ävrö granodiorite

ROCK UNIT FROM ESHI
- High confidence

CASING
- Casing

DEFORMATION ZONE FROM ESHI
- DZ

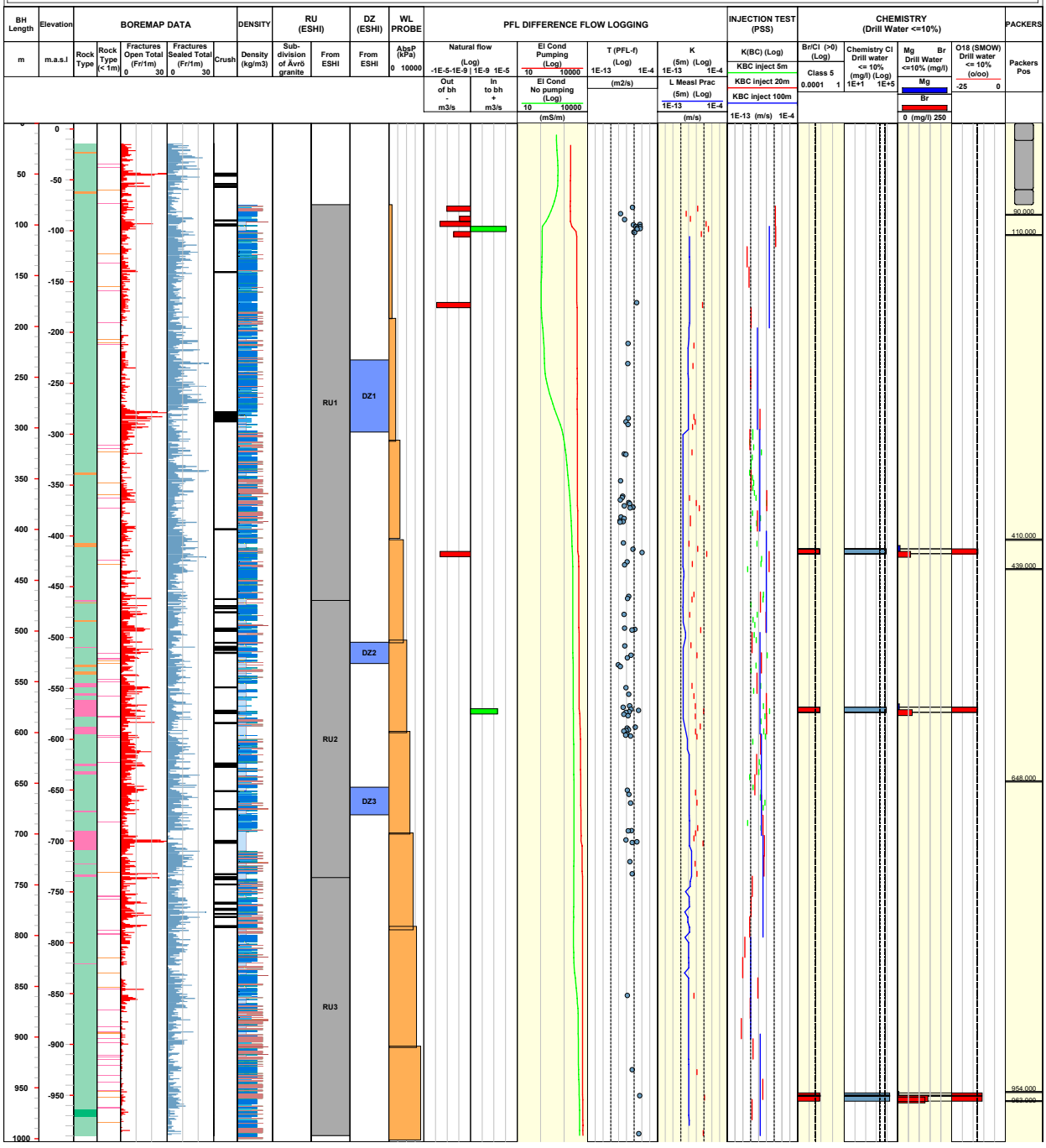

Title COMPOSITE LOG for cored borehole KSH03A

Site	SIMPEVARP	**Coordinate System**	RT90-RHB70	**Drilling Start Date**	2003-09-11 12:45:00	**Packer installation for monitoring**
Borehole	KSH03A	**Northing ToC [m]**	6366018.66	**Drilling Stop Date**	2003-11-07 08:30:00	
Diameter [mm]	76	**Easting ToC [m]**	1552711.17	**Surveying Date**	2004-05-26 10:20:00	
Length [m]	1000.700	**Elevation [m.a.s.l.ToC]**	4.15	**Chemistry class**	3	
Bearing ToC [°]	125.80	**Inclination ToC [°]**	-59.20	**Plot Date**	2008-08-27 22:15:27	

ROCK TYPE SIMPEVARP
- Fine-grained granite
- Pegmatite
- Granite
- Ävrö granite
- Quartz monzodiorite
- Diorite / Gabbro

DENSITY
- dens<2680
- 2680<dens<2730
- 2730<dens<2800
- 2800<dens<2890
- dens>2890

SUBDIVISION OF ÄVRÖ GRANITE
- Ävrö granite
- Ävrö quartz monzodiorite
- Ävrö granodiorite

ROCK UNIT FROM ESHI
- High confidence

CASING
- Casing

DEFORMATION ZONE FROM ESHI
- DZ

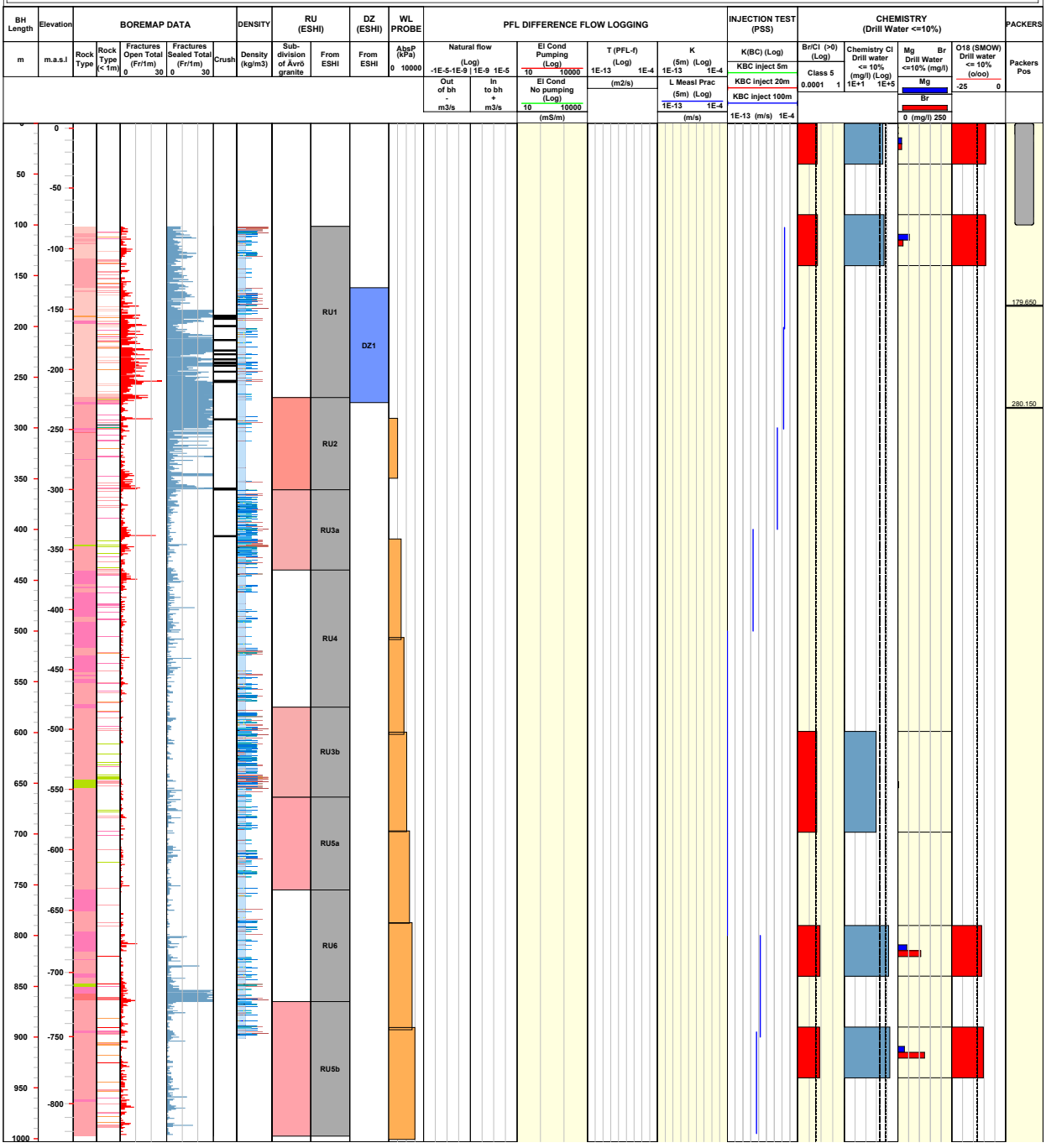

Title **COMPOSITE LOG for cored borehole KSH03B**

Site	SIMPEVARP	**Coordinate System**	RT90-RHB70	**Drilling Start Date**	2003-11-21 10:50:00	**Packer installation for monitoring**	
Borehole	KSH03B	**Northing ToC [m]**	6366018.98	**Drilling Stop Date**	2003-11-26 20:20:00		
Diameter [mm]	76	**Easting ToC [m]**	1552710.70	**Surveying Date**	2004-05-26 10:10:00		
Length [m]	100.860	**Elevation [m.a.s.l.ToC]**	4.08	**Chemistry class**	$Class		
Bearing ToC [°]	128.54	**Inclination ToC [°]**	-64.30	**Plot Date**	2008-08-31 22:34:28		

ROCK TYPE SIMPEVARP
- Ävrö granite
- Quartz monzodiorite

DENSITY
- dens<2680
- 2680<dens<2730
- 2730<dens<2800
- 2800<dens<2890
- dens>2890

SUBDIVISION OF ÄVRÖ GRANITE
- Ävrö granite
- Ävrö quartz monzodiorite
- Ävrö granodiorite

ROCK UNIT FROM ESHI
- High confidence

CASING
- Casing

DEFORMATION ZONE FROM ESHI
- DZ

BH Length	Elevation	BOREMAP DATA					DENSITY	RU (ESHI)		DZ (ESHI)	WL PROBE	PFL DIFFERENCE FLOW LOGGING					INJECTION TEST (PSS)	CHEMISTRY (Drill Water <=10%)				PACKERS
m	m.a.s.l	Rock Type	Rock Type (< 1m)	Fractures Open Total (Fr/1m) 0 30	Fractures Sealed Total (Fr/1m) 0 30	Crush	Density (kg/m3)	Sub-division of Ävrö granite	From ESHI	From ESHI	Abs P (kPa) 0 10000	Natural flow (Log) -1E-5-1E-9	1E-9 1E-5	El Cond Pumping (Log) 10 10000	T (PFL-f) (Log) 1E-13 1E-4	K (5m) (Log) 1E-13 1E-4	K(BC) (Log)	Br/Cl (>0) (Log)	Chemistry Cl Drill water <= 10% (mg/l) (Log)	Mg Br Drill Water <=10% (mg/l)	O18 (SMOW) Drill water <= 10% (o/oo)	Packers Pos
												Out of bh - m3/s	In to bh + m3/s	El Cond No pumping (Log) 10 10000 (mS/m)	(m2/s)	L Measl Prac (5m) (Log) 1E-13 1E-4 (m/s)	KBC inject 5m KBC inject 20m KBC inject 100m 1E-13 (m/s) 1E-4	Class 5 0.0001 1	1E+1 1E+5	0 (mg/l) 250	-25 0	

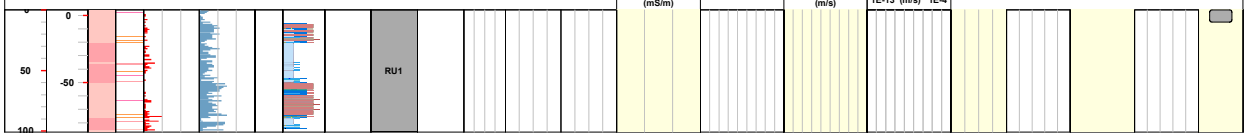

Appendix 3

Description and orientation of local minor deformation zones (MDZ) identified in cored boreholes in Laxemar

- Use the appendices for presentation of results in the form of tables and/or graphs (see Chapter 5 above).

A3.1 Description and orientation of local minor deformation zones (MDZ) identified in cored boreholes in Laxemar

In the cored boreholes in Laxemar, deformation zones have been identified through the extended single hole interpretation (ESHI) /Carlsten et al. 2006abc, 2007a–g)/ where a general description of each identified zone is given. Some of these deformation zones have later been examined in more detail in the context of the analysis of regional and local major deformation zones and are part of the deterministically modeled deformation zones in the RVS model. However, most of the identified deformation zones are considered to be local minor deformation zones which are less than 1,000 m in surface length and will not be modeled deterministically.

The analysis below presents a complementary assessment of the orientation and the true thickness of the deformation zones in the Laxemar area that was not modeled deterministically. The analysis is based on the individual intercepts in each borehole.

The analysis was made for several forthcoming purposes;

- Borehole-wise correlation of individual deformation zones to hydraulic anomalies.
- Analysis of the aggregated orientation statistics of local minor deformation zones for usage in the GeoDFN model parameterization.
- Provision of the true deformation zone thickness for the analysis of a possible true thickness – deformation zone length relationship.

A3.1.1 Analysis of orientation

In the ESHI deformation zones have been identified by type and geological character over a certain section length in the borehole. In general three types of deformation zones exist; ductile, ductile-brittle and brittle deformation zones. The character is described based on visible inspection of the core in combination with underlying geophysical data and BIPS. Orientation of the zones is not given.

Based on the ESHI, orientation data from the borehole mapping is used to determine the most likely orientation of the zone. The relevant orientation data types are selected based on the zone type:

- Brittle zones are analyzed based on fracture orientation and the orientations of the upper and/or lower contacts of identified crush zones and/or mapped sealed fracture networks.
- Ductile zones are analyzed based on mapped ductile structures. The analyzed ductile parameters are; foliation, mylonitic structures or ductile and brittle-ductile shear zones.
- Ductile/brittle zones are analyzed from a combined assessment of the above mentioned data and characteristics. The assumption is that the brittle features in these zones are normally due to reactivation along the older ductile structures.

In addition to mapped core data, radar reflections have been used when observed in close vicinity of, or within the boundaries of a given zone.

The interpretation of orientation is based on the stereonets through the identification of a visible cluster, or a group of observations as best judged by the geologist. Radar observations are always used as part of the analysis but are not plotted in stereonets as they often are defined only by an angle to the borehole, or several possible orientations for each reflector. The selection is illustrated with a circle and a calculated mean pole as shown in Figure A3-1a and b. The mean orientation is based only on the datatype where the blue circle is present.

In case the analyses rely on a single observation (i.e. one reflector or a single fracture etc) the zone is oriented like that observation and no specific circle or mean pole are marked in the stereonet.

In some cases the orientation of near by larger zones or lithologies are judged to override the implications of the zone data.

Each MDZ is presented by:

- The ESHI zone description.
- Orientation data presented in up to four stereoplots. The data is visualized by the poles (trend/plunge) of the planar structures.
- Additional comments to the interpretation of orientation, if present.
- The assessed orientation (*strike/dip*, applying the 'right hand rule').
- A summary table revealing the main source of data used for the orientation interpretation as well as which data sources verify or contradict the interpretation (U*sed, Verify and Contradict*).
- The certainty of the interpretation (*Certain, Probable, Uncertain and Very uncertain)*. The certainty is a subjective measure assessed based on the amount of information supporting the interpretation, the prescence of contradicting observations, and the general orientation pattern in data (i.e. clusters versus large variation in orientations).
- The calculated true thickness (see below).

A3.1.2 Calculation of true thickness

The apparent thickness (ds) can be extracted from the upper and lower limit in the *ESHI* (borehole length) and is the identical to true thickness only in the case when a zone is intersected perpendicularly by a borehole. However, true thickness (t) can easily be calculated from the apparent thickness and the angular difference between the zone normal and the borehole axis.

$t = ds\ (s \cdot p)$ (Figure A3-2)

Where:
s is the unit length vector along the borehole axis,
p is the unit length normal vector to the deformation zone.

True thickness is presented as part of the deformation zone summary table for each analysed MDZ.

Eleven MDZs do not contain any relevant data for an assessment of zone orientation. Ten of these are defined as ductile zones in the ESHI but contain no ductile descriptors. One is defined as a brittle zone and contains no brittle information. Seven of the zones are from KLX05 and four zones are from KLX12A.

Table A3-1 shows a summary table of the estimated orientations, apparent and true thicknesses for each MDZ. Deterministically modeled deformation zones which intersect boreholes have been name tagged for completeness of the ESHI deformation zone logs. However, no orientation assessment has been performed for these deformation zones.

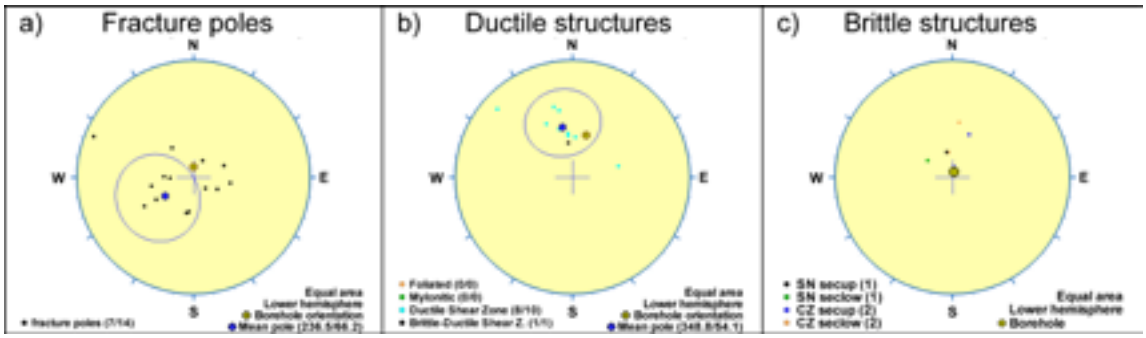

Figure A3-1. *Example of plots illustrating the different data types. SN = Sealed network, CZ = crush zone, secup = upper contact, seclow = lower contact. The blue circle marks the data used for orienting the zone.*

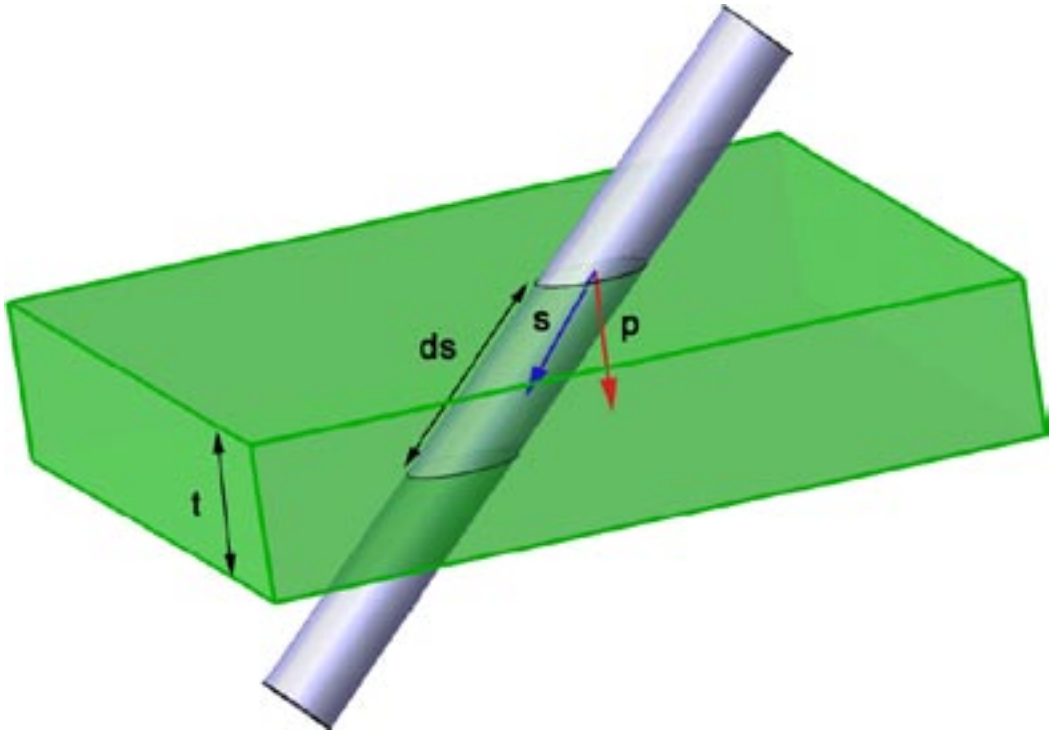

Figure A3-2. *Illustration of the parameters used for the calculation of the true thickness.*

Table A3-1. Summary of analyzed deformation zones.

ID	ESHI-DZ	Model zone name	Certainty	From length	To length	Z type	Mean orientation		Thickness	
							strike	dip	apparent	true
KLX01	DZ1	EW007A		1,000	1,020					
KLX02	DZ1	NE107 + NW928A		770	960					
KLX02	DZ2		Probable	385.45	387.63	Brittle	58	51	2.2	1.5
KLX02	DZ3		Probable	436.1	436.9	Brittle	57	52	0.8	0.5
KLX02	DZ4		Certain	466.6	468.25	Brittle	11	62	1.6	0.8
KLX02	DZ5		Probable	624.1	625	Brittle	17	77	0.9	0.2
KLX02	DZ6		Very uncertain	662.5	663.4	Brittle	43	30	0.9	0.8
KLX02	DZ7		Certain	751.55	752.25	Brittle	80	34	0.7	0.6
KLX02	DZ8		Uncertain	997.8	998.4	Brittle	327	24	0.6	0.5
KLX03	DZ1	EW946A, Klx03_dz1b, Klx03_dz1c		722.5	814					
KLX03	DZ2		Probable	277.9	278.7	Brittle	16	24	0.8	0.7
KLX03	DZ3		Probable	457.2	457.6	Brittle	4	22	0.4	0.4
KLX03	DZ4		Uncertain	662	667.1	Brittle	326	28	5.1	4.9
KLX03	DZ5		Uncertain	673.4	674.1	Brittle	311	14	0.7	0.7
KLX03	DZ6		Uncertain	681.9	682.4	Brittle	312	14	0.5	0.5
KLX03	DZ7		Uncertain	903.9	904.7	Brittle	76	78	0.8	0.1
KLX03	DZ8		Probable	969.3	970.5	Brittle	334	13	1.2	1.2
KLX04	DZ5	ZSMEW007A		346	355					
KLX04	DZ6	ZSMNW928A, Klx04_dz6b, Klx04_dz6c		873	973					
KLX04	DZ1		Probable	227	230	Brittle	163	43	3.0	2.3
KLX04	DZ2		Probable	254	258	Brittle	313	18	4.0	3.7
KLX04	DZ3		Certain	295	298	Brittle	120	22	3.0	2.9
KLX04	DZ4		Certain	325	326	Brittle	169	10	1.0	1.0
KLX04	DZ7		Uncertain	167	167.4	Brittle	97	6	0.4	0.4
KLX04	DZ8		Probable	203.35	203.75	Brittle	30	25	0.4	0.4
KLX04	DZ9		Probable	207.35	207.75	Brittle	45	9	0.4	0.4
KLX04	DZ10		Probable	211.1	211.75	Brittle	6	37	0.7	0.5
KLX04	DZ11		Probable	363.25	363.6	Brittle	204	21	0.4	0.3

ID	ESHI-DZ	Model zone name	Certainty	From length	To length	Z type	Mean orientation		Thickness	
							strike	dip	apparent	true
KLX04	DZ12		Certain	411.05	411.5	Brittle	121	34	0.4	0.4
KLX04	DZ13		Certain	419.62	419.95	Brittle	77	31	0.3	0.3
KLX04	DZ14		Probable	443.8	444	Brittle	349	17	0.2	0.2
KLX04	DZ15		Very uncertain	514.7	515.2	Brittle	89	78	0.5	0.1
KLX04	DZ16		Probable	580.7	586.2	Brittle	279	18	5.5	5.1
KLX04	DZ17		Probable	627.56	628.5	Brittle	115	6	0.9	0.9
KLX05	DZ1	No data		100.5	107.5	Brittle			7.0	
KLX05	DZ2	No data		173.82	173.92	Brittle			0.1	
KLX05	DZ3		Probable	178.7	178.78	Ductile	210	7	0.1	0.1
KLX05	DZ4	No data		261.23	263	Ductile			1.8	
KLX05	DZ5	No data		306.41	307.27	Ductile			0.9	
KLX05	DZ6		Certain	403.4	406.1	Ductile	101	22	2.7	1.9
KLX05	DZ7		Probable	477.5	478.1	Ductile	25	20	0.6	0.5
KLX05	DZ8	No data		576.6	577.6	Ductile			1.0	
KLX05	DZ9	No data		590.35	590.85	Ductile			0.5	
KLX05	DZ10		Certain	612.34	612.54	Ductile/brittle	214	64	0.2	0.1
KLX05	DZ11		Uncertain	626.73	629.43	Ductile/brittle	204	60	2.7	1.0
KLX05	DZ12	No data		654.4	655.5	Ductile			1.1	
KLX05	DZ13		Probable	814.7	814.86	Ductile	273	63	0.2	0.1
KLX06	DZ1	NW052A		200	260					
KLX06	DZ2	EW002A		297	425					
KLX06	DZ3		Certain	112.7	113.9	Brittle	247	10	1.2	1.0
KLX06	DZ4		Certain	151.43	154	Brittle	292	30	2.6	1.6
KLX07A	DZ1	EW007A		105	147					
KLX07A	DZ2	EW007A		167.9	168.3					
KLX07A	DZ3		Uncertain	184.8	185.4	Brittle	295	7	0.6	0.5
KLX07A	DZ4		Very uncertain	252.5	253.1	Brittle	180	60	0.6	0.3
KLX07A	DZ5		Probable	308	313	Brittle	244	57	5.0	4.6
KLX07A	DZ6		Probable	335.6	340	Brittle	239	30	4.4	4.1
KLX07A	DZ7	Klx07a_dz7		347	387.5					
KLX07A	DZ8		Probable	432.6	434.5	Brittle	270	43	1.9	1.9
KLX07A	DZ9	Klx07a_dz9		448	459					

ID	ESHI-DZ	Model zone name	Certainty	From length	To length	Z type	Mean orientation		Thickness	
							strike	dip	apparent	true
KLX07A	DZ10	Klx07a_dz10		604	654.7					
KLX07A	DZ11	Klx07a_dz11		693	724.2					
KLX07A	DZ12	Klx07a_dz12		737.9	785					
KLX07A	DZ13	Klx07a_dz13		816.8	835.5					
KLX07A	DZ14		Probable	413.4	413.73	Brittle	268	37	0.3	0.3
KLX07A	DZ15		Certain	502.9	503.5	Brittle	225	78	0.6	0.4
KLX07A	DZ16		Probable	667.95	669	Brittle	264	38	1.0	1.0
KLX07B	DZ1		Probable	27	30	Brittle	254	20	3.0	2.9
KLX07B	DZ2		Probable	39.7	42	Brittle	225	47	2.3	1.7
KLX07B	DZ3	EW007A		124	172	Brittle				
KLX07B	DZ4		Probable	14.9	15.97	Ductile/brittle	193	75	1.1	0.3
KLX08	DZ1	Klx08_dz1		100	131	Brittle				
KLX08	DZ2		Probable	150.32	159	Brittle	328	29	8.7	8.3
KLX08	DZ3	EW007A		211.5	220					
KLX08	DZ4	EW007A		224.5	242					
KLX08	DZ5	EW007A		291	302					
KLX08	DZ6	Klx08_dz6		396	416					
KLX08	DZ7	EW946A		478	486	Brittle				
KLX08	DZ8		Uncertain	536.5	540	Brittle	301	30	3.5	3.5
KLX08	DZ9		Probable	769	778	Brittle	248	59	9.0	6.3
KLX08	DZ10	Klx08_dz10		925	940	Brittle				
KLX08	DZ11		Very uncertain	614.45	615	Brittle	303	33	0.5	0.5
KLX08	DZ12		Very uncertain	655.3	656.15	Brittle	65	25	0.9	0.6
KLX09	DZ1		Probable	105.8	106	Ductile/brittle	354	36	0.2	0.2
KLX09	DZ2		Uncertain	137.6	138	Brittle	273	19	0.4	0.4
KLX09	DZ3		Probable	147	148	Brittle	102	18	1.0	0.9
KLX09	DZ4		Certain	206	209	Brittle	280	29	3.0	2.6
KLX09	DZ5		Probable	261.8	264	Brittle	334	11	2.2	2.2
KLX09	DZ6		Probable	272	276	Brittle	322	11	4.0	4.0
KLX09	DZ7		Very uncertain	313	323.2	Brittle	357	12	10.2	10.2
KLX09	DZ8		Probable	440	446	Brittle	268	6	6.0	5.9
KLX09	DZ9		Probable	492.4	509	Brittle	320	26	16.6	6.2

ID	ESHI-DZ	Model zone name	Certainty	From length	To length	Z type	Mean orientation		Thickness	
							strike	dip	apparent	true
KLX09	DZ10	Klx09_dz10		520	554					
KLX09	DZ11		Probable	611	618.3	Brittle	60	24	7.3	6.8
KLX09	DZ12		Probable	648.6	649.6	Brittle	97	31	1.0	0.8
KLX09	DZ13	EW007A, NW928A		682	722					
KLX09	DZ14		Probable	744.5	761	Brittle	193	50	16.5	9.0
KLX09	DZ15		Uncertain	799.6	803	Brittle	200	40	3.4	2.4
KLX09	DZ16		Uncertain	815	815.25	Brittle	288	43	0.3	0.2
KLX09	DZ17		Probable	848.7	852.6	Brittle	5	77	3.9	1.3
KLX09	DZ18		Uncertain	867.8	869.7	Brittle	256	41	1.9	1.4
KLX09B	DZ1		Probable	49.14	49.65	Brittle	300	21	0.5	0.5
KLX09B	DZ2		Certain	74.55	79.3	Ductile/brittle	336	23	4.8	4.4
KLX09C	DZ1		Probable	81.3	86.3	Ductile/brittle	300	19	5.0	4.6
KLX09C	DZ2		Probable	114.85	117	Brittle	322	27	2.2	1.9
KLX09D	DZ1		Uncertain	81.4	89.52	Ductile/brittle	4	11	8.1	7.6
KLX09D	DZ2		Very uncertain	101.15	104	Brittle	51	9	2.8	2.5
KLX09E	DZ1		Probable	71.2	72.35	Brittle	113	83	1.1	0.6
KLX09E	DZ2	Klx09E_dz2		76.15	105.45					
KLX09F	DZ1	Klx09F_dz1		7.86	21.7					
KLX09F	DZ2		Probable	67.9	68.75	Brittle	12	17	0.8	0.6
KLX09F	DZ3		Probable	79.45	84.4	Ductile/brittle	312	13	5.0	3.8
KLX09F	DZ4		Probable	133.1	136.2	Brittle	319	30	3.1	1.7
KLX09F	DZ5		Probable	144.32	145.07	Brittle	134	84	0.8	0.3
KLX09G	DZ1	NS046A		40.02	67.52	Brittle				
KLX10	DZ1	NE942A		103	116.3					
KLX10	DZ2	NE942A		150	161.5					
KLX10	DZ3		Very uncertain	176	176.7	Brittle	150	55	0.7	0.3
KLX10	DZ4	NE942A		188	208					
KLX10	DZ5	NE942A		224	232.7					
KLX10	DZ6	NE942A		245	263					
KLX10	DZ7	NE942A		318	349					
KLX10	DZ8		Probable	435	439.2	Brittle	142	29	4.2	3.5
KLX10	DZ9	EW946A		694.4	706.4	Brittle				

ID	ESHI-DZ	Model zone name	Certainty	From length	To length	Z type	Mean orientation		Thickness	
							strike	dip	apparent	true
KLX10B	DZ1	NE942A		10.35	20.35	Ductile				
KLX10B	DZ2		Probable	39.2	46.6	Brittle	192	62	7.4	4.3
KLX10C	DZ1		Certain	8.65	9.5	Brittle	111	24	0.9	0.8
KLX10C	DZ2		Uncertain	15.9	21.6	Brittle	225	19	5.7	3.9
KLX10C	DZ3	Klx10C_dz3		35	59.3					
KLX10C	DZ4		Probable	79.45	79.7	Brittle	113	37	0.3	0.2
KLX10C	DZ5		Probable	96.9	97.6	Brittle	263	76	0.7	0.2
KLX10C	DZ6		Probable	103.5	110.1	Brittle	108	38	6.6	6.4
KLX10C	DZ7	Klx10C_dz7		121	140					
KLX11A	DZ1		Certain	142.25	142.9	Ductile/brittle	169	28	0.7	0.6
KLX11A	DZ2		Probable	162.75	163.26	Ductile/brittle	134	37	0.5	0.5
KLX11A	DZ3		Probable	168.7	169.9	Ductile/brittle	238	41	1.2	1.0
KLX11A	DZ4	/Viola et al. NGU 2007/		247.67	272	Ductile/brittle	15	81	24.3	3.7
KLX11A	DZ5		Uncertain	285.4	286.4	Ductile/brittle	57	33	1.0	0.7
KLX11A	DZ6		Certain	306.22	308.78	Ductile/brittle	210	34	2.6	2.4
KLX11A	DZ7		Probable	345.3	348.03	Ductile/brittle	246	49	2.7	2.0
KLX11A	DZ8		Probable	417.26	418.1	Brittle	90	39	0.8	0.6
KLX11A	DZ9		Probable	430.56	432.2	Ductile	130	23	1.6	1.6
KLX11A	DZ10		Very uncertain	473.62	475.7	Ductile	257	35	2.1	1.7
KLX11A	DZ11	Klx11A_dz11		486.1	513.15					
KLX11A	DZ12	EW946A		522.85	528.66					
KLX11A	DZ13		Probable	577.9	586.16	Brittle	171	15	8.3	8.2
KLX11A	DZ14		Certain	593.9	602.27	Ductile	153	25	8.4	8.2
KLX11A	DZ15		Very uncertain	689.06	689.86	Brittle	181	30	0.8	0.8
KLX11A	DZ16		Probable	853	860	Ductile/brittle	184	67	7.0	4.8
KLX11A	DZ17		Probable	906.84	907.6	Ductile/brittle	219	76	0.8	0.4
KLX11A	DZ18		Certain	974.1	975.2	Ductile/brittle	208	75	1.1	0.6
KLX11B	DZ1		Probable	75.18	76.87	Brittle	197	25	1.7	1.5
KLX11B	DZ2		Probable	86.3	88.7	Brittle	352	63	2.4	1.1
KLX11D	DZ1		Probable	61.93	65.36	Brittle	3	67	3.4	2.8
KLX11D	DZ2		Probable	90.44	97.7	Brittle	15	81	7.3	5.0
KLX11D	DZ3		Probable	106.67	110.6	Brittle	130	17	3.9	2.7

ID	ESHI-DZ	Model zone name	Certainty	From length	To length	Z type	Mean orientation		Thickness	
							strike	dip	apparent	true
KLX11E	DZ1		Uncertain	15.56	20.05	Brittle	334	33	4.5	3.2
KLX11E	DZ2		Probable	39	61.42	Ductile	236	35	22.4	9.6
KLX11E	DZ3		Uncertain	74.11	74.53	Brittle	171	37	0.4	0.3
KLX11E	DZ4		Probable	112.48	114.8	Brittle	78	71	2.3	1.8
KLX11F	DZ1		Probable	69.6	72	Brittle	200	28	2.4	2.4
KLX12A	DZ1	No data		182.5	183.2	Ductile			0.7	
KLX12A	DZ2	No data		185.4	185.7	Ductile			0.3	
KLX12A	DZ3		Certain	270.7	271.05	Ductile	67	26	0.4	0.3
KLX12A	DZ4	No data		276.6	277.7	Ductile			1.1	
KLX12A	DZ5		Certain	282	282.4	Ductile	100	20	0.4	0.4
KLX12A	DZ6	No data		304.41	304.45	Ductile			0.0	
KLX12A	DZ7		Very uncertain	329.39	329.85	Brittle	239	81	0.5	0.0
KLX12A	DZ8		Probable	366.41	366.99	Ductile	257	12	0.6	0.5
KLX12A	DZ9		Probable	428.95	429.4	Ductile	41	31	0.4	0.4
KLX12A	DZ10		Probable	445.6	447.55	Ductile/brittle	143	54	1.9	1.0
KLX12A	DZ11		Probable	498.85	499.54	Ductile	26	46	0.7	0.6
KLX12A	DZ12		Certain	596.5	600.8	Ductile	61	42	4.3	3.7
KLX13A	DZ1		Certain	146.8	147.4	Ductile/brittle	293	71	0.6	0.3
KLX13A	DZ2		Certain	173.2	177.45	Brittle	33	36	4.3	3.5
KLX13A	DZ3		Probable	254.9	255.6	Ductile/brittle	151	25	0.7	0.6
KLX13A	DZ4		Certain	291	291.3	Ductile	237	32	0.3	0.3
KLX13A	DZ5		Uncertain	348.75	349.5	Ductile/brittle	348	61	0.8	0.4
KLX13A	DZ6		Probable	384	388.2	Brittle	336	33	4.2	3.8
KLX13A	DZ7	EW120A		488	593.30					
KLX14A	DZ1		Uncertain	10.11	10.61	Ductile/brittle	176	33	0.5	0.5
KLX14A	DZ2		Probable	17.83	18.3	Brittle	155	18	0.5	0.4
KLX14A	DZ3		Probable	42.07	43.35	Ductile/brittle	230	35	1.3	1.2
KLX14A	DZ4	NS059A		74.67	125.35					
KLX14A	DZ5		Probable	138.1	138.9	Brittle	28	78	0.8	0.4
KLX14A	DZ6		Probable	162.07	163.82	Ductile	72	4	1.8	1.2
KLX15A	DZ1		Certain	130.15	130.36	Ductile/brittle	102	8	0.2	0.1
KLX15A	DZ2		Certain	193.14	199.7	Ductile/brittle	83	20	6.6	3.5

ID	ESHI-DZ	Model zone name	Certainty	From length	To length	Z type	Mean orientation		Thickness	
							strike	dip	apparent	true
KLX15A	DZ3		Certain	253.69	254.37	Ductile/brittle	249	53	0.7	0.6
KLX15A	DZ4		Uncertain	262.35	265.79	Brittle	302	14	3.4	3.1
KLX15A	DZ5		Certain	346.65	347	Ductile/brittle	135	17	0.4	0.2
KLX15A	DZ6		Probable	350.16	350.34	Ductile	80	18	0.2	0.1
KLX15A	DZ7		Probable	362.75	362.95	Brittle	80	23	0.2	0.1
KLX15A	DZ8		Uncertain	377.84	386	Ductile/brittle	130	28	8.2	3.2
KLX15A	DZ9		Very uncertain	401.9	409.1	Ductile/brittle	191	35	7.2	4.3
KLX15A	DZ10		Uncertain	502.5	505.6	Ductile/brittle	89	84	3.1	1.7
KLX15A	DZ11		Very uncertain	602.24	608.72	Brittle	233	84	6.5	3.2
KLX15A	DZ12		Certain	629.1	634.94	Brittle	225	71	5.8	3.3
KLX15A	DZ13		Uncertain	658.91	659.8	Ductile/brittle	87	65	0.9	0.2
KLX15A	DZ14		Very uncertain	675.05	682.68	Brittle	224	72	7.6	4.2
KLX15A	DZ15		Certain	688	688.5	Ductile/brittle	223	85	0.5	0.2
KLX15A	DZ16	NE107A		711.36	743.76					
KLX15A	DZ17		Certain	772.7	774.15	Ductile/brittle	221	12	1.4	1.1
KLX15A	DZ18		Probable	821.63	821.94	Ductile/brittle	205	73	0.3	0.1
KLX15A	DZ19		Certain	917.75	918.46	Ductile/brittle	80	78	0.7	0.3
KLX15A	DZ20	NW042A		978.43	1,000.43	Ductile/brittle				
KLX16A	DZ1		Probable	33.8	34.25	Ductile/brittle	68	47	0.5	0.4
KLX16A	DZ2	No data		78.66	78.98	Ductile			0.3	
KLX16A	DZ3		Very uncertain	90.89	93.72	Brittle	96	18	2.8	2.6
KLX16A	DZ4		Probable	139.9	143	Brittle	112	69	3.1	1.1
KLX16A	DZ5		Probable	207.08	207.22	Ductile/brittle	20	48	0.1	0.1
KLX16A	DZ6		Probable	209.95	210.92	Ductile/brittle	21	72	1.0	0.7
KLX16A	DZ7		Very uncertain	213.33	213.88	Ductile/brittle	49	75	0.5	0.3
KLX16A	DZ8	No data		224.63	225.35	Ductile			0.7	
KLX16A	DZ9	NE107A		228.2	230.9					
KLX16A	DZ10	NE107A		251.85	253.71					
KLX16A	DZ11	NE107A		259.3	265					
KLX16A	DZ12	NE107A		327	433.55					
KLX17A	DZ1	EW900A		100.1	114.3					
KLX17A	DZ2		Certain	142.27	142.86	Ductile	69	10	0.6	0.5

ID	ESHI-DZ	Model zone name	Certainty	From length	To length	Z type	Mean orientation		Thickness	
							strike	dip	apparent	true
KLX17A	DZ3	EW900B		192.7	227	Ductile/brittle				
KLX17A	DZ4		Certain	350.14	357.25	Ductile	79	36	7.1	6.8
KLX17A	DZ5		Probable	422.75	423.67	Ductile/brittle	64	40	0.9	0.8
KLX17A	DZ6		Certain	423.67	431.76	Ductile	69	15	8.1	7.5
KLX17A	DZ7		Uncertain	502.75	504.4	Ductile/brittle	189	77	1.6	0.4
KLX17A	DZ8		Uncertain	542.57	543.3	Brittle	84	22	0.7	0.7
KLX17A	DZ9		Probable	546.05	546.35	Ductile/brittle	181	45	0.3	0.2
KLX17A	DZ10		Uncertain	662.29	670	Brittle	8	39	7.7	4.6
KLX18A	DZ1		Probable	137.8	143.9	Ductile/brittle	147	29	6.1	4.9
KLX18A	DZ2		Probable	148.6	149.4	Ductile/brittle	103	39	0.8	0.6
KLX18A	DZ3	NE944A		283.75	291.6					
KLX18A	DZ4		Probable	359.6	366.2	Ductile/brittle	134	13	6.6	6.2
KLX18A	DZ5		Probable	378.6	378.85	Brittle	92	18	0.3	0.2
KLX18A	DZ6		Probable	401	404.2	Ductile/brittle	49	14	3.2	3.2
KLX18A	DZ7		Certain	428	434	Ductile/brittle	103	35	6.0	4.8
KLX18A	DZ8		Uncertain	448.35	456.55	Ductile/brittle	223	43	8.2	5.1
KLX18A	DZ9	Klx18A_dz9		471.9	488.9					
KLX19A	DZ1		Very uncertain	100.42	105.76	Brittle	225	24	5.3	4.7
KLX19A	DZ2		Probable	298.35	304.2	Brittle	262	73	5.8	4.2
KLX19A	DZ3		Certain	412.15	416.9	Brittle	107	89	4.8	2.6
KLX19A	DZ4	NE942A		437	464.1	Ductile/brittle				
KLX19A	DZ5		Probable	482.6	507.68	Brittle	284	36	25.1	25.1
KLX19A	DZ6		Uncertain	508.4	510	Brittle	65	25	1.6	0.9
KLX19A	DZ7		Uncertain	520.44	552.21	Brittle	40	90	31.8	7.2
KLX19A	DZ8		Probable	552.21	553.1	Ductile/brittle	263	65	0.9	0.7
KLX19A	DZ9		Probable	691.5	693.64	Ductile	92	35	2.1	0.8
KLX19A	DZ10		Probable	705.21	706.6	Ductile	113	20	1.4	0.8
KLX20A	DZ1	NS001C		171.38	234.45	Ductile/brittle				
KLX20A	DZ2		Very uncertain	261	265.9	Ductile/brittle	17	88	4.9	3.3
KLX20A	DZ3		Probable	312.55	313	Brittle	357	81	0.4	0.4
KLX20A	DZ4		Very uncertain	410.1	416.4	Brittle	13	64	6.3	6.0
KLX21B	DZ1		Probable	105.27	105.73	Brittle	136	34	0.5	0.3

ID	ESHI-DZ	Model zone name	Certainty	From length	To length	Z type	Mean orientation		Thickness	
							strike	dip	apparent	true
KLX21B	DZ2		Probable	108.37	108.82	Brittle	128	43	0.4	0.2
KLX21B	DZ3		Certain	150	157.8	Ductile/brittle	114	42	7.8	3.8
KLX21B	DZ4		Probable	209.08	216.82	Brittle	237	25	7.7	6.8
KLX21B	DZ5		Certain	229.7	231.5	Brittle	142	28	1.8	1.2
KLX21B	DZ6		Probable	396.95	397.1	Brittle	209	74	0.2	0.0
KLX21B	DZ7		Probable	400.64	403.49	Brittle	115	50	2.9	0.9
KLX21B	DZ8		Probable	452.06	455.9	Brittle	20	82	3.8	1.1
KLX21B	DZ9		Uncertain	474.41	478.1	Brittle	142	13	3.7	3.0
KLX21B	DZ10	Klx21B_dz10_12		558.9	571.75					
KLX21B	DZ11	Klx21B_dz10_12		577.67	578.06					
KLX21B	DZ12	Klx21B_dz10_12		595.45	706.95					
KLX22A	DZ1		Certain	76.9	77.22	Ductile/brittle	183	38	0.3	0.2
KLX22B	DZ1		Very uncertain	22	25	Brittle	75	29	3.0	3.0
KLX23A	DZ1		Probable	10.75	11.75	Brittle	51	3	1.0	0.9
KLX23A	DZ2		Probable	15.66	16.7	Brittle	123	33	1.0	1.0
KLX23B	DZ1		Uncertain	13.3	14.8	Brittle	223	73	1.5	1.1
KLX24A	DZ1		Probable	19.75	21.2	Brittle	142	28	1.5	1.3
KLX24A	DZ2		Uncertain	56.75	60.25	Ductile/brittle	80	10	3.5	2.8
KLX24A	DZ3		Certain	64.65	66.6	Ductile/brittle	219	34	1.9	1.9
KLX24A	DZ4		Probable	75.25	75.75	Brittle	68	13	0.5	0.4
KLX25A	DZ1		Uncertain	32.1	35.66	Ductile/brittle	275	60	3.6	2.8
KLX26A	DZ1		Probable	17.45	18.1	Ductile/brittle	238	65	0.7	0.4
KLX26A	DZ2		Probable	42.6	54.8	Ductile/brittle	182	76	12.2	8.5
KLX26A	DZ3		Probable	72.3	73.95	Ductile/brittle	217	67	1.7	1.2
KLX26A	DZ4		Certain	97.3	99.8	Ductile/brittle	72	21	2.5	1.8
KLX28A	DZ1		Probable	14.4	33.1	Ductile/brittle	182	33	18.7	12.8
KLX28A	DZ2		Uncertain	74	76.1	Ductile/brittle	135	56	2.1	0.3
KLX29A	DZ1		Probable	7.21	8.02	Brittle	210	15	0.8	0.6
KLX29A	DZ2		Very uncertain	44.05	52.4	Brittle	253	9	8.4	6.5
KLX29A	DZ2		Very uncertain	44.05	52.4	Brittle	253	9	8.4	6.5

KLX02 DZ2 (385.45 to 387.63), brittle zone

Brittle deformation zone characterized by increased frequency of open fractures, a slight increase in sealed fractures and one crush zone (0.58 m borehole length). Decrease in resistivity and magnetic susceptibility. Significant caliper anomalies. One radar reflector at 386.5 m with the orientation 079/38. The host rock is totally dominated by fine-grained diorite-gabbro (505102).

Poles from crush zone

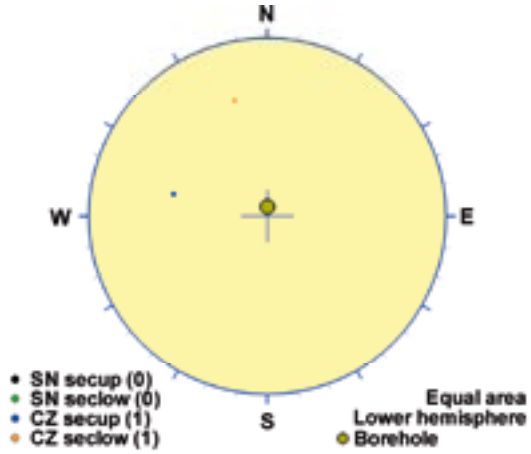

Poles from ductile structures

Data not used

Poles from fractures

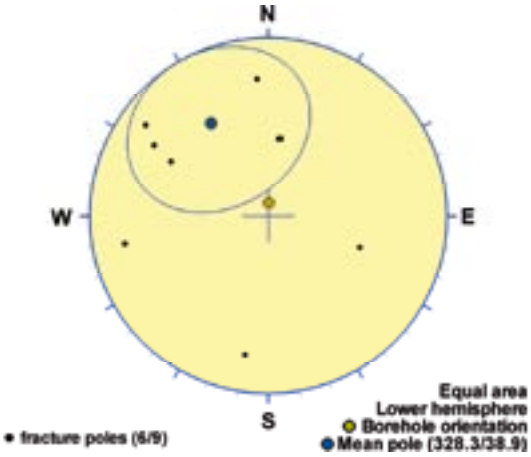

Contours from fractures

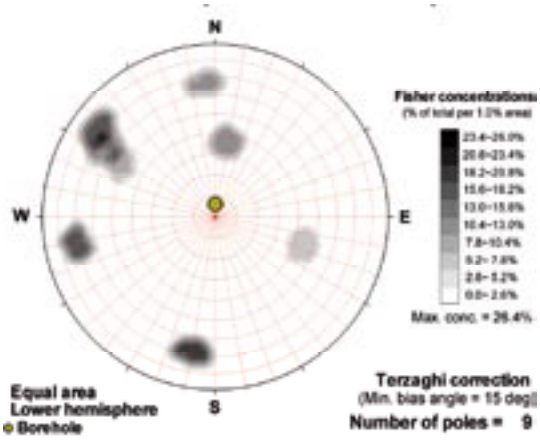

Orientation		Basis for orientation				Certainty	Thickness	
Strike	Dip	Fractures	Crush	Ductile structures	Reflectors	Orientation	Apparent	True
58	51	Used	Verify		Contradict	Probable	2.2 m	1.5 m
Comment:								

KLX02 DZ3 (436.1 to 436.9), brittle zone

Brittle deformation zone characterized by increased frequency of open fractures, a slight increase in sealed fractures, weak red staining and one crush zone (0.47 m borehole length). Decrease in resistivity, magnetic susceptibility and P-wave velocity. One distinct caliper anomaly. The host rock is totally dominated by Ävrö quartz monzodiorite (501046).

Poles from crush zone

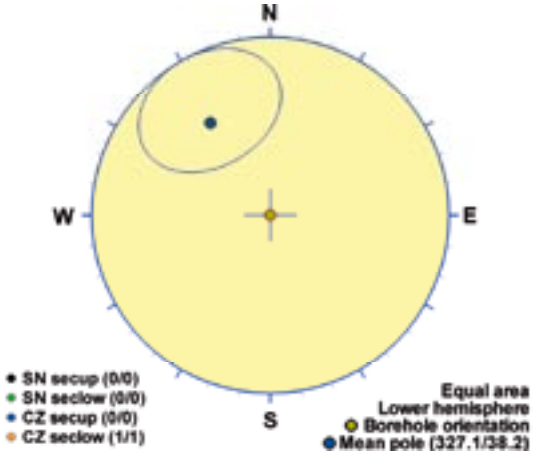

Poles from ductile structures

Data not used

Poles from fractures

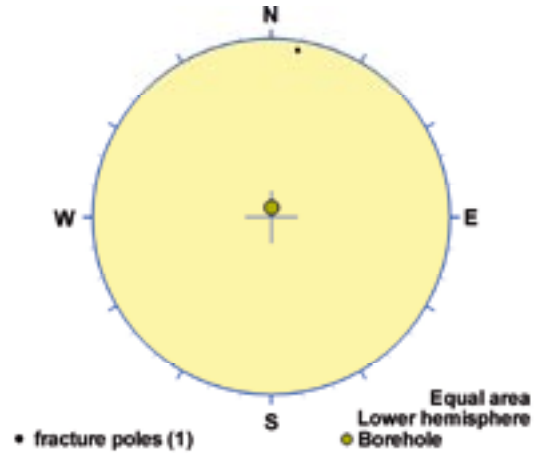

Contours from fractures

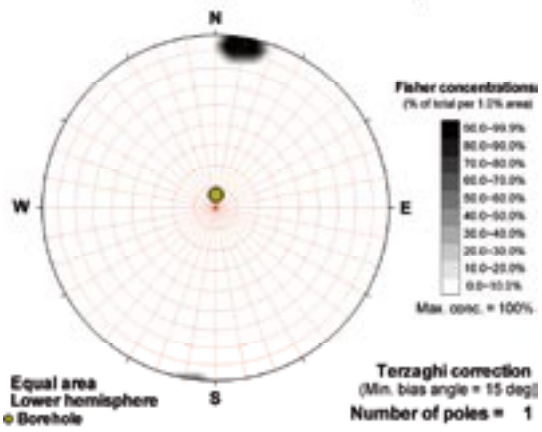

Orientation		Basis for orientation				Certainty	Thickness	
Strike	Dip	Fractures	Crush	Ductile structures	Reflectors	Orientation	Apparent	True
57	52	Contradict	Used			Probable	0.8 m	0.5 m
Comment:								

KLX02 DZ4 (466.6 to 468.25), brittle zone

Brittle deformation zone characterized by increased frequency of open fractures and sealed fractures, medium red staining and two crush zones (with a total borehole length of 0.94 m). Decrease in resistivity, magnetic susceptibility and P-wave velocity. Minor caliper anomalies. One radar reflector at 467,1 m with the orientation 079/90. The host rock is totally dominated by Ävrö granodiorite (501056). Subordinate rock type comprises fine-grained granite (511058).

Poles from crush zone

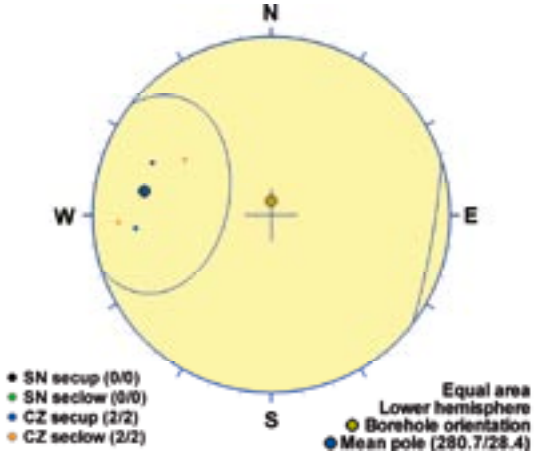

Poles from ductile structures

Data not used

Poles from fractures

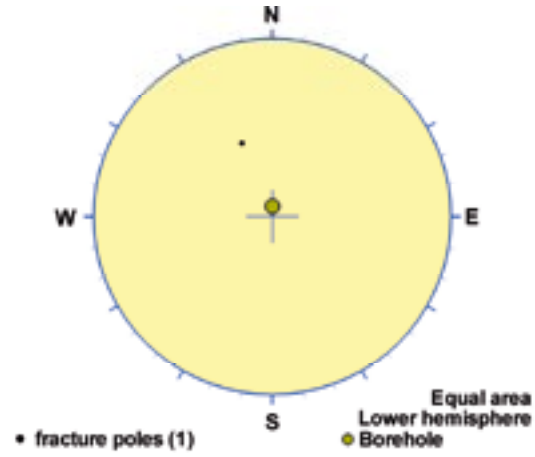

Contours from fractures

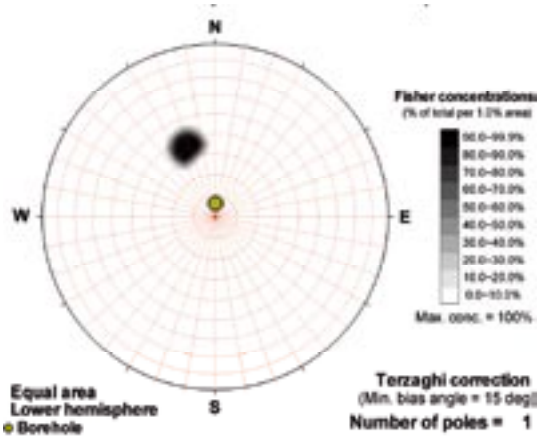

Orientation		Basis for orientation				Certainty	Thickness	
Strike	Dip	Fractures	Crush	Ductile structures	Reflectors	Orientation	Apparent	True
11	62	Contradict	Used			Certain	1.6 m	0.8 m
Comment:								

KLX02 DZ5 (624.1 to 625), brittle zone

Brittle deformation zone characterized by increased frequency of open fractures and faint red staining. Decrease in resistivity, magnetic susceptibility and P-wave velocity. One minor caliper anomaly. The host rock is dominated by Ävrö granodiorite (501056). Subordinate rock type comprises fine-grained granite (511058).

Poles from crush zone

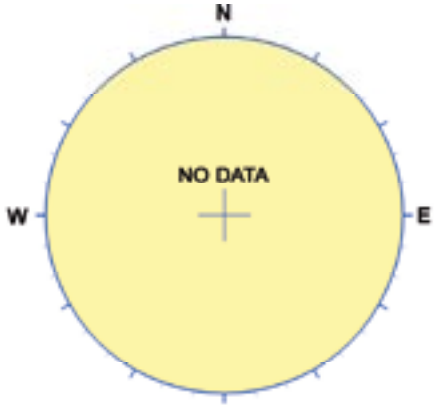

Poles from ductile structures

Data not used

Poles from fractures

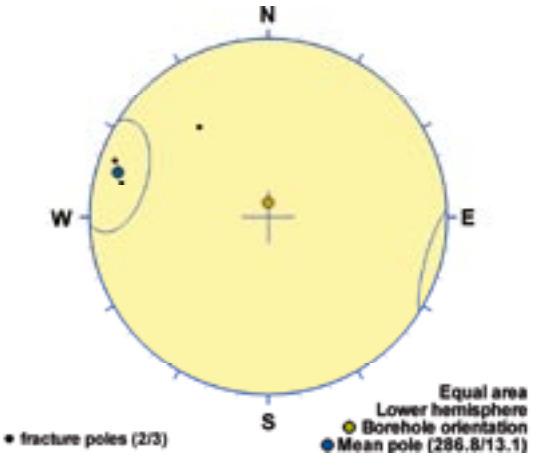

Contours from fractures

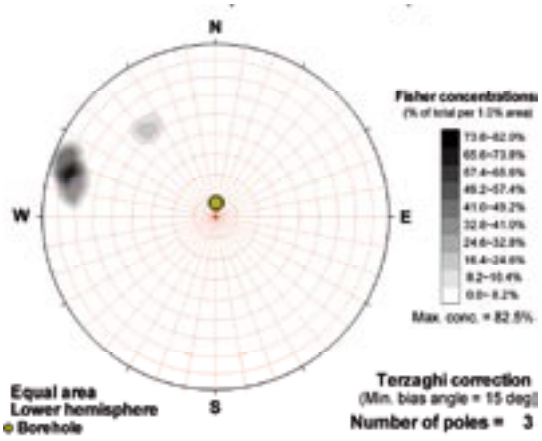

Orientation		Basis for orientation				Certainty	Thickness	
Strike	Dip	Fractures	Crush	Ductile structures	Reflectors	Orientation	Apparent	True
17	77	Used				Probable	0.9 m	0.2 m
Comment:								

KLX02 DZ6 (662.5 to 663.4), brittle zone

Brittle deformation zone characterized by increased frequency of open fractures, a slight increase in sealed fractures and weak red staining. Minor caliper anomalies and partly decreased resistivity. One radar reflector at 663.1 m with the orientation 043/30. The host rock is dominated by Ävrö quartz monzodiorite (501046) and to a lesser extent fine-grained dioritoid (501030).

Poles from crush zone

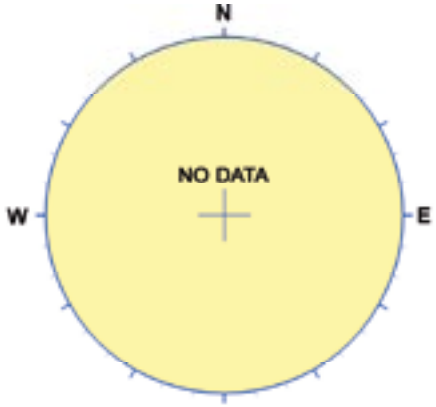

Poles from ductile structures

Data not used

Poles from fractures

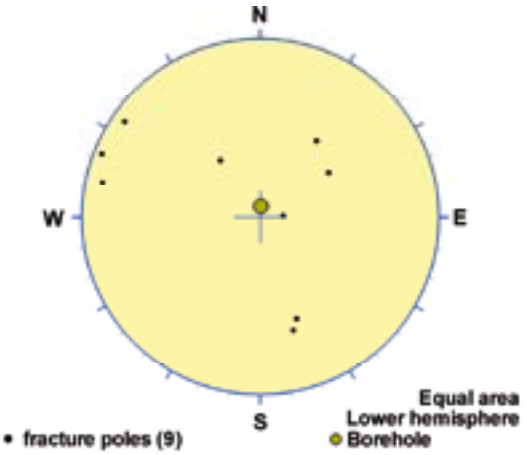

Contours from fractures

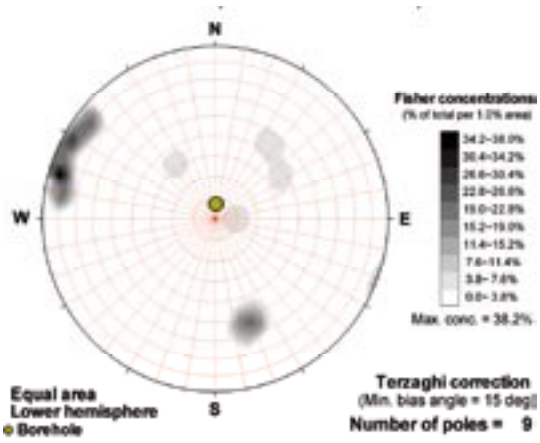

Orientation		Basis for orientation				Certainty	Thickness	
Strike	Dip	Fractures	Crush	Ductile structures	Reflectors	Orientation	Apparent	True
43	30	Verify			Used	Very uncertain	0.9 m	0.8 m
Comment:								

KLX02 DZ7 (751.55 to 752.25), brittle zone

Brittle deformation zone characterized by increased frequency of open fractures, a slight increase in sealed fractures, faint to weak red staining and one crush zone (0.12 m in borehole length). Decrease in resistivity, magnetic susceptibility and P-wave velocity. Minor caliper anomalies. One radar reflector at 752.0 m with the angle 59° to borehole axis. The host rock is totally dominated by Ävrö quartz monzodiorite (501046).

Poles from crush zone

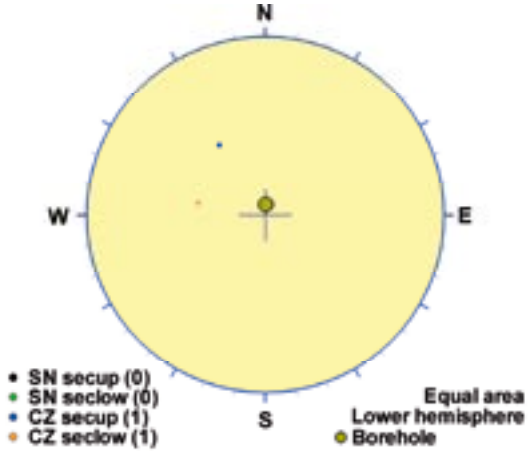

Poles from ductile structures

Data not used

Poles from fractures

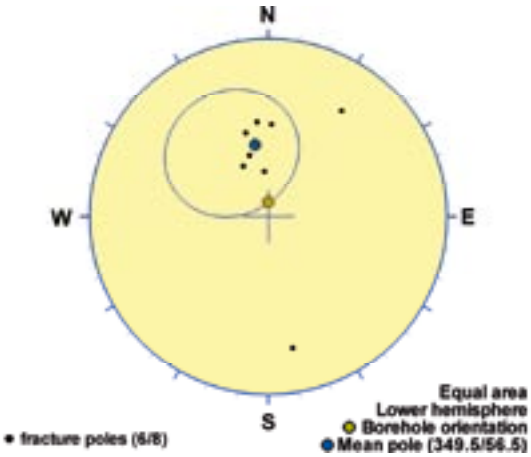

Contours from fractures

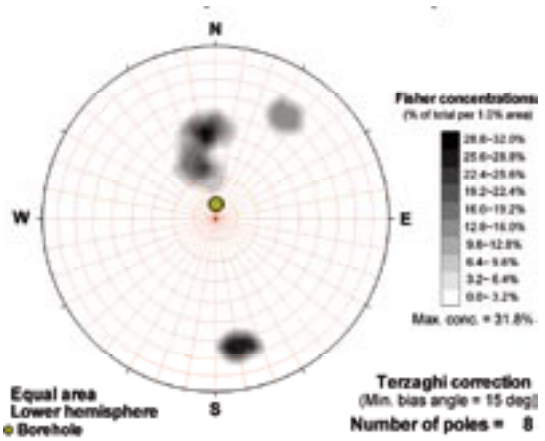

Orientation		Basis for orientation				Certainty	Thickness	
Strike	Dip	Fractures	Crush	Ductile structures	Reflectors	Orientation	Apparent	True
80	34	Used	Verify		Verify	Certain	0.7 m	0.6 m
Comment:								

KLX02 DZ8 (997.8 to 998.4), brittle zone

Brittle deformation zone characterized by increased frequency of open fractures and medium red staining. Decrease in resistivity and minor decrease in magnetic susceptibility. One radar reflector at 998.1 m with the orientation 082/32 or 262/32. The host rock is totally dominated by Ävrö quartz monzodiorite (501046).

Poles from crush zone

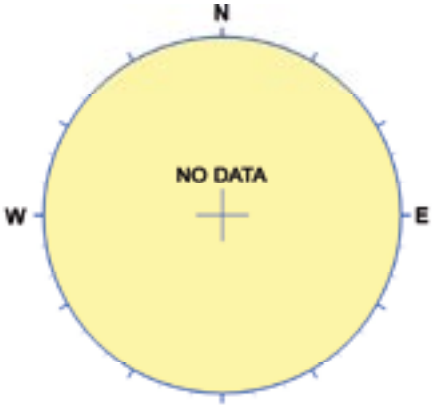

Poles from ductile structures

Data not used

Poles from fractures

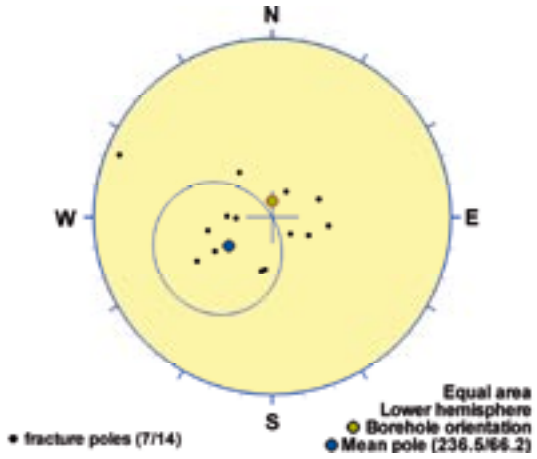

Contours from fractures

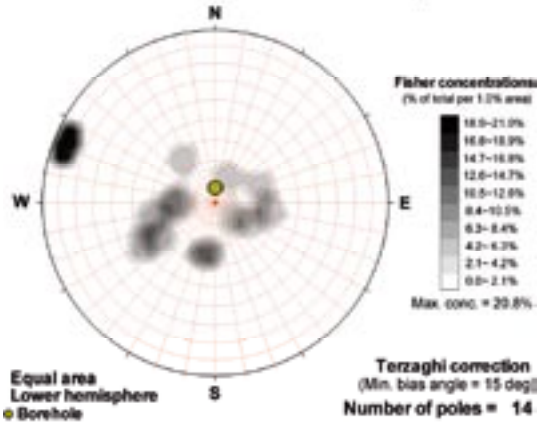

Orientation		Basis for orientation				Certainty	Thickness	
Strike	Dip	Fractures	Crush	Ductile structures	Reflectors	Orientation	Apparent	True
327	24	Used			Contradict	Uncertain	0.6 m	0.5 m
Comment:								

KLX03 DZ2 (277.9 to 278.7), brittle zone

Brittle deformation zone characterized by increased frequency of open and sealed fractures and weak red staining. Decrease in resistivity, magnetic susceptibility and P-wave velocity. The host rock is dominated by Ävrö quartz monzodiorite (501046). Subordinate rock type comprises fine-grained granite (511058).

Poles from crush zone

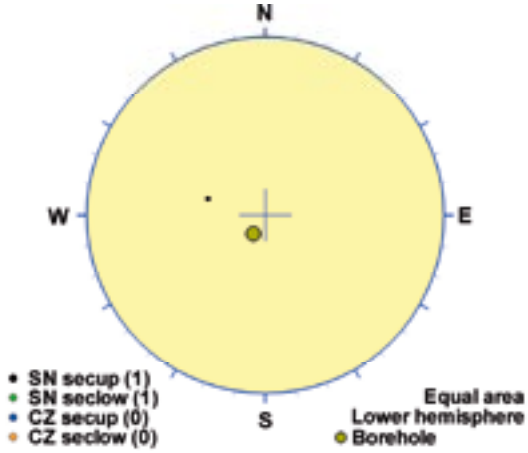

Poles from ductile structures

Data not used

Poles from fractures

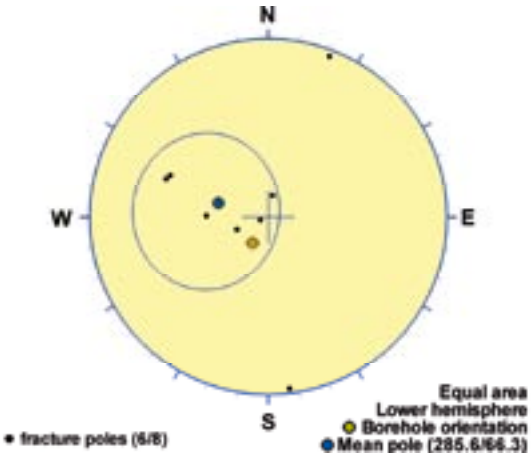

Contours from fractures

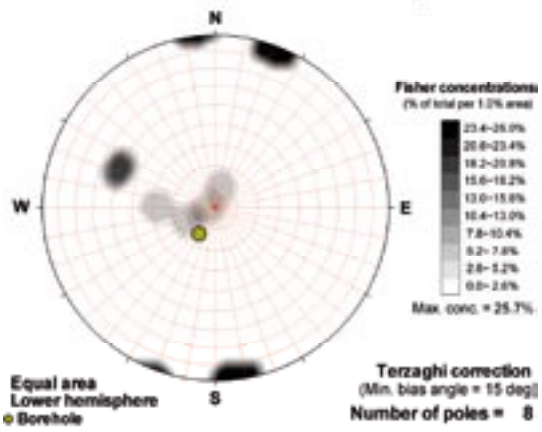

Orientation		Basis for orientation				Certainty	Thickness	
Strike	Dip	Fractures	Crush	Ductile structures	Reflectors	Orientation	Apparent	True
16	24	Used	Verify			Probable	0.8 m	0.7 m
Comment:								

KLX03 DZ3 (457.2 to 457.6), brittle zone

Brittle deformation zone characterized by a crush zone (0.21 m in borehole length) and sealed network. Decrease in resistivity, magnetic susceptibility and P-wave velocity. The host rock is dominated by Ävrö quartz monzodiorite (501046). Subordinate rock type comprises fine-grained granite (511058).

Poles from crush zone

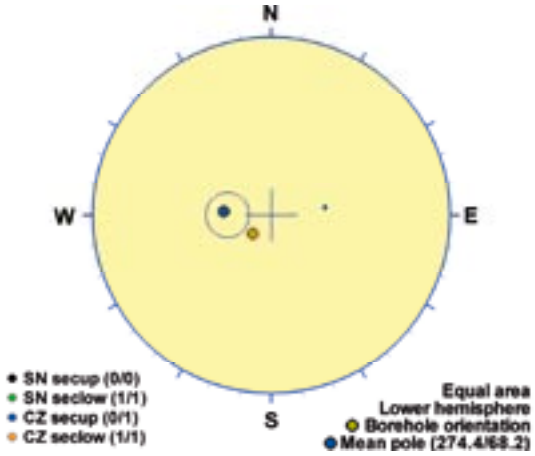

Poles from ductile structures

Data not used

Poles from fractures

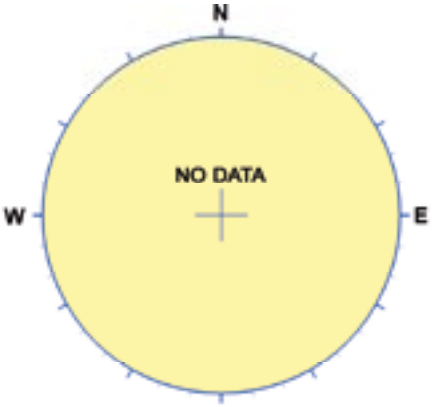

Contours from fractures

Orientation		Basis for orientation				Certainty	Thickness	
Strike	Dip	Fractures	Crush	Ductile structures	Reflectors	Orientation	Apparent	True
4	22		Used			Probable	0.4 m	0.4 m
Comment:								

KLX03 DZ4 (662 to 667.1), brittle zone

Brittle deformation zone characterized by sealed network and increased frequency of open fractures, faint to medium red staining and faint saussuritization. Significant decrease in resistivity and magnetic susceptibility. Two radar reflectors, one at 662.3 m with the orientation 168/45 and one at 664.3 m with the orientation 335/85. The host rock is dominated by quartz monzodiorite (501036). Subordinate rock types comprise granite (501058) and fine-grained granite (511058).

Poles from crush zone

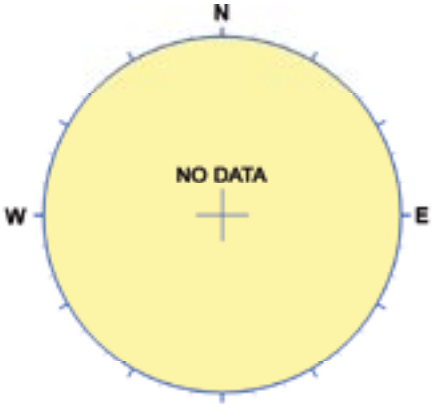

Poles from ductile structures

Data not used

Poles from fractures

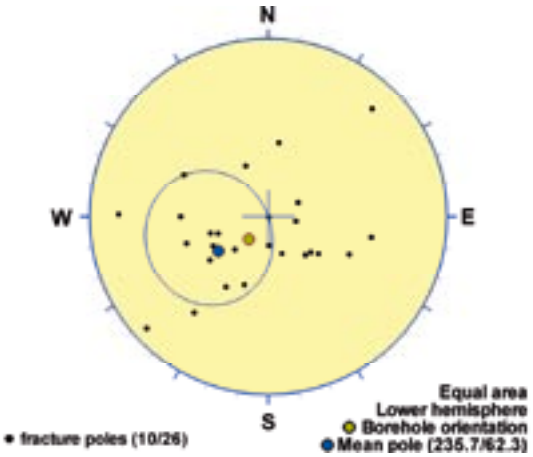

Contours from fractures

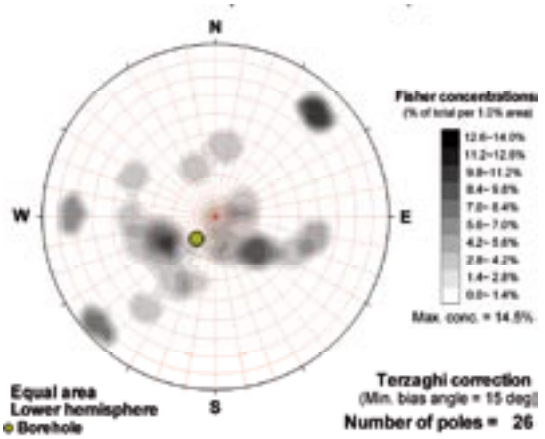

Orientation		Basis for orientation				Certainty	Thickness	
Strike	Dip	Fractures	Crush	Ductile structures	Reflectors	Orientation	Apparent	True
326	28	Used			Contradict	Uncertain	5.1 m	4.9 m
Comment:								

KLX03 DZ5 (673.4 to 674.1), brittle zone

Brittle deformation zone characterized by sealed network and increased frequency of open fractures, weak red staining and weak saussuritization. Decrease in resistivity and magnetic susceptibility. The host rock is totally dominated by quartz monzodiorite (501036).

Poles from crush zone

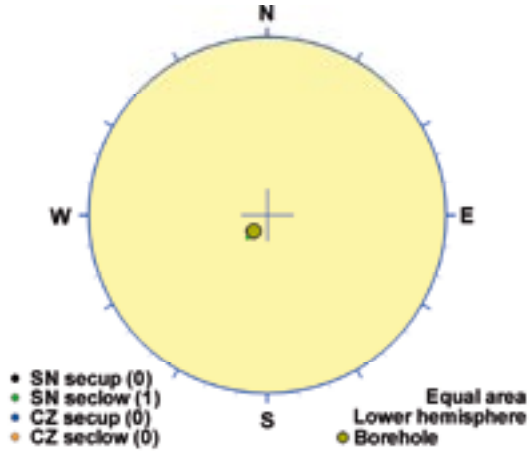

Poles from ductile structures

Data not used

Poles from fractures

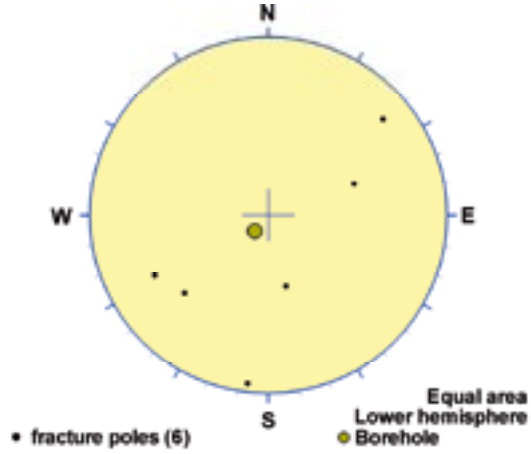

Contours from fractures

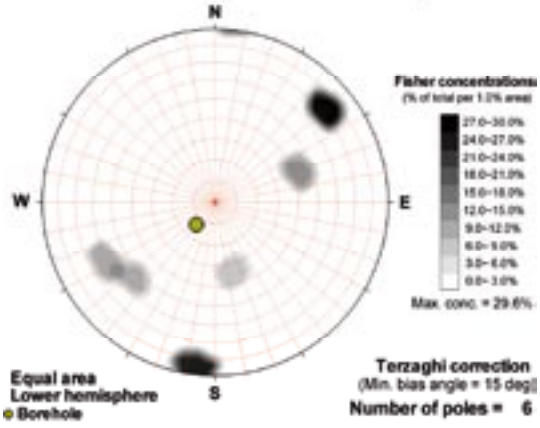

Orientation		Basis for orientation				Certainty	Thickness	
Strike	Dip	Fractures	Crush	Ductile structures	Reflectors	Orientation	Apparent	True
311	14		Used			Uncertain	0.7 m	0.7 m
Comment:								

KLX03 DZ6 (681.9 to 682.4), brittle zone

Brittle deformation zone characterized by sealed network, increased frequency of sealed fracures, a sligth increase in open fractures and medium red staining. Decrease in resistivity and magnetic susceptibility. The host rock is totally dominated by quartz monzodiorite (501036).

Poles from crush zone

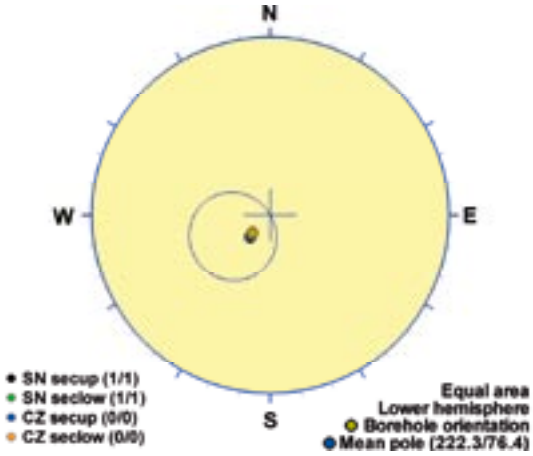

Poles from ductile structures

Data not used

Poles from fractures

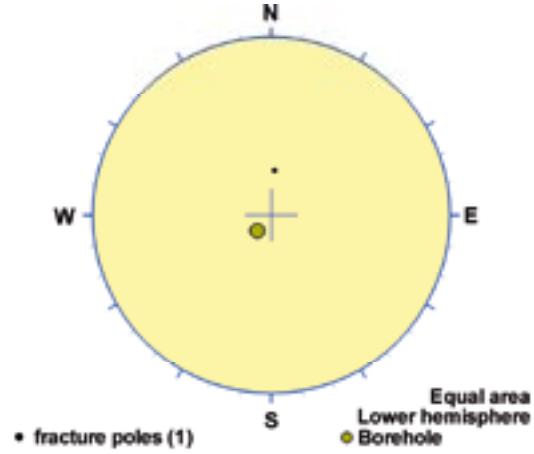

Contours from fractures

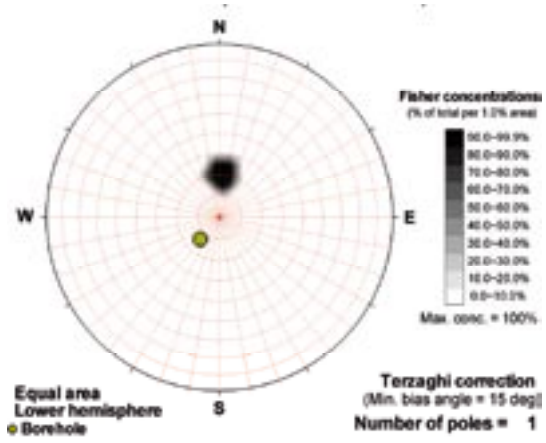

Orientation		Basis for orientation				Certainty	Thickness	
Strike	Dip	Fractures	Crush	Ductile structures	Reflectors	Orientation	Apparent	True
312	14		Used			Uncertain	0.5 m	0.5 m
Comment:								

KLX03 DZ7 (903.9 to 904.7), brittle zone

Brittle deformation zone characterized by sealed network and faint red staining. Distinct caliper anomalies and decreased magnetic susceptibility and resistivity. The host rock is totally dominated by fine-grained granite (511058).

Poles from crush zone

Poles from ductile structures

Data not used

Poles from fractures

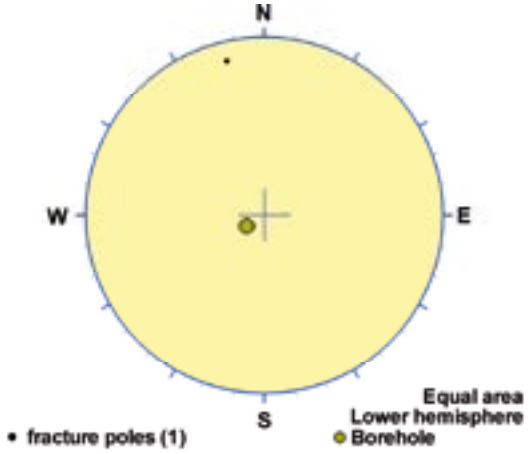

Contours from fractures

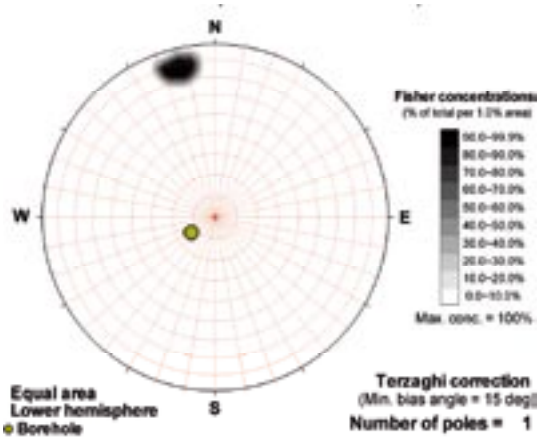

Orientation		Basis for orientation				Certainty	Thickness	
Strike	Dip	Fractures	Crush	Ductile structures	Reflectors	Orientation	Apparent	True
76	78	Used				Uncertain	0.8 m	0.1 m
Comment:								

KLX03 DZ8 (969.3 to 970.5), brittle zone

Brittle deformation zone characterized by sealed network, increased frequency of sealed fractures and open fractures, weak red staining, weak saussuritization and quartz dissolution (0.1 m in borehole length). Significant decrease in resistivity and magnetic susceptibility. One radar reflector at 970.4 m with the angle 90° to borehole axis. The host rock is dominated by quartz monzodiorite (501036). Subordinate rock type comprises fine-grained granite (511058).

Poles from crush zone

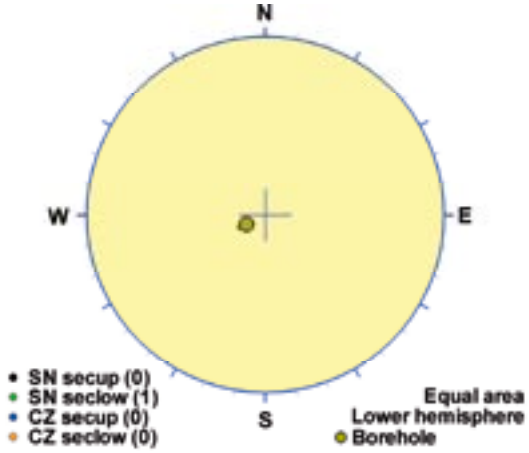

Poles from ductile structures

Data not used

Poles from fractures

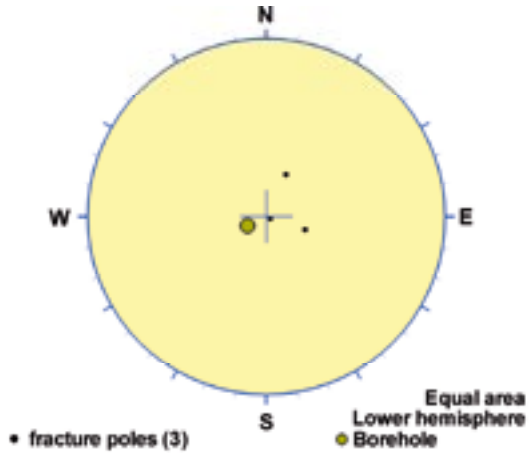

Contours from fractures

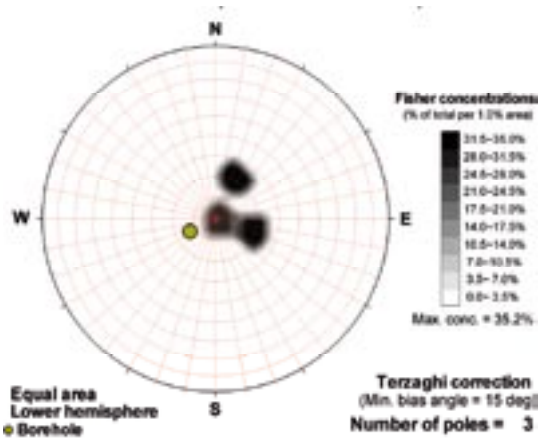

Orientation		Basis for orientation				Certainty	Thickness	
Strike	Dip	Fractures	Crush	Ductile structures	Reflectors	Orientation	Apparent	True
334	13	Verify	Used			Probable	1.2 m	1.2 m
Comment:								

KLX04 DZ1 (227 to 230), brittle zone

Strongly brecciated. Crush and chlorite-healed fractures. Low resistivity, low density, very low susceptibility and caliper anomaly. A borehole radar reflector occurs at 229.1 m with the angle 71º to borehole axis. Seismic reflector with an interpreted intersection depth at 240 m, and an orientation of 295/27. The host rock is dominated by Ävrö granodiorite (501056).

Poles from crush zone

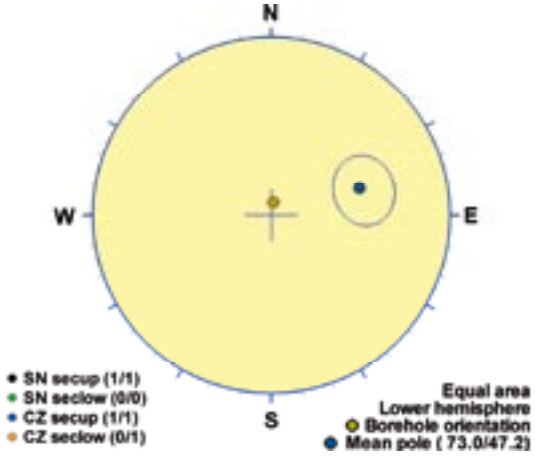

Poles from ductile structures

Data not used

Poles from fractures

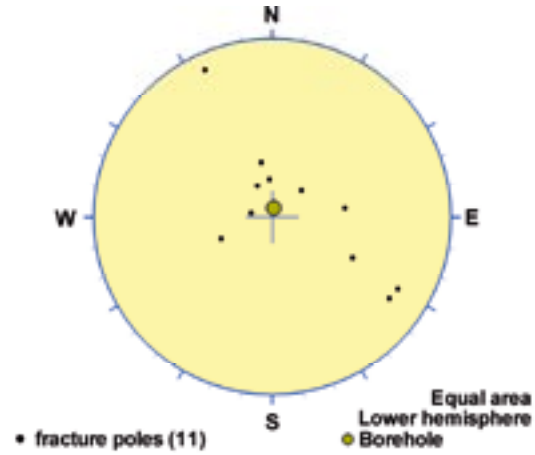

Contours from fractures

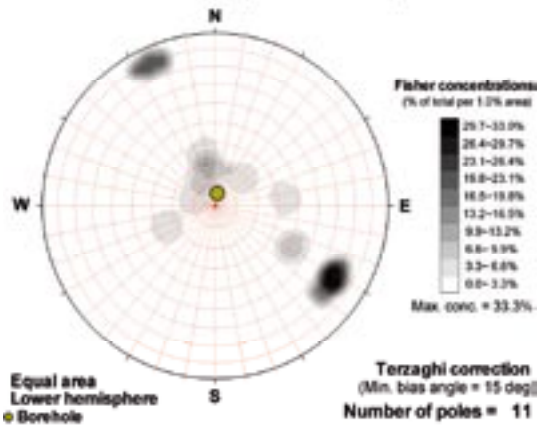

Orientation		Basis for orientation				Certainty	Thickness	
Strike	Dip	Fractures	Crush	Ductile structures	Reflectors	Orientation	Apparent	True
163	43		Used		Contradict	Probable	3 m	2.3 m
Comment:								

KLX04 DZ2 (254 to 258), brittle zone

One meter crush including severe alteration. Reactivated zone. Low resistivity, variable p-wave velocity, low density, low susceptibility and caliper anomaly. One radar reflector with the angle 59º to borehole axis at 255.2 m and one at 258.4 m with the angle 61º to borehole axis. The host rock is dominated by fine-grained dioritoid (501030), Ävrö granodiorite (501056) and fine-grained granite (511058). Subordinate rock type comprises granite (501058).

Poles from crush zone

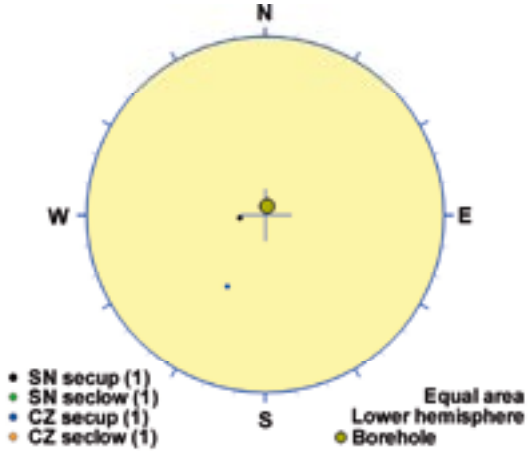

Poles from ductile structures

Data not used

Poles from fractures

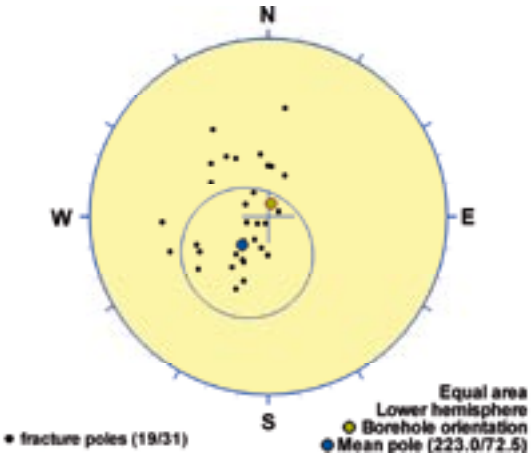

Contours from fractures

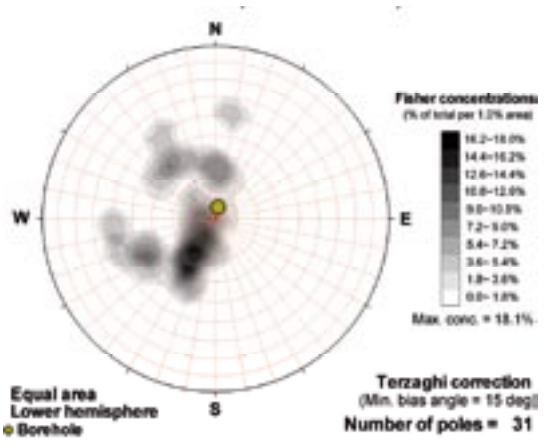

Orientation		Basis for orientation				Certainty	Thickness	
Strike	Dip	Fractures	Crush	Ductile structures	Reflectors	Orientation	Apparent	True
313	18	Used	Verify	Verify	Verify	Probable	4 m	3.7 m
Comment:								

KLX04 DZ3 (295 to 298), brittle zone

Zone core centre at 296-297 m. Low resistivity, low p-wave velocity, low density, very low susceptibility and caliper anomaly. Radar reflectors at 296.8 m and 298.8 m with the angle 70º to borehole axis. Seismic reflector with the orientation 095/20 intersects the borehole at 290 m. The host rock is dominated by Ävrö granodiorite (501056).

Poles from crush zone

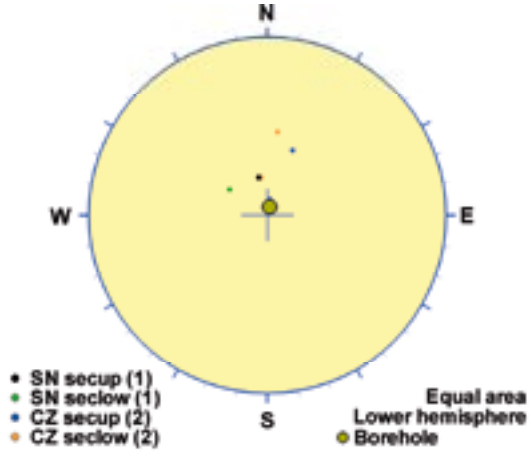

Poles from ductile structures

Data not used

Poles from fractures

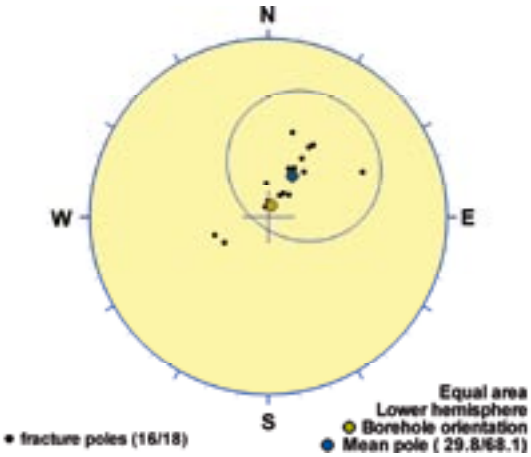

Contours from fractures

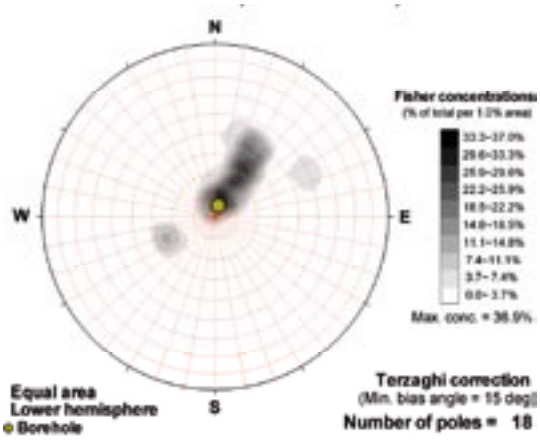

Orientation		Basis for orientation				Certainty	Thickness	
Strike	Dip	Fractures	Crush	Ductile structures	Reflectors	Orientation	Apparent	True
120	22	Used	Verify		Verify	Certain	3 m	2.9 m
Comment:								

KLX04 DZ4 (325 to 326), brittle zone

Brecciated, strongly altered rock. Low resistivity and low susceptibility. One radar reflector at 325.4 m with the angle 89º to borehole axis and one at 327.0 m with the angle 82º. Seismic reflector with orientation of 295/15 intersects the borehole at 330 m. The host rock is dominated by Ävrö granodiorite (501056; indicated by the density log). Subordinate rock type comprises quartz monzodiorite (501036).

Poles from crush zone

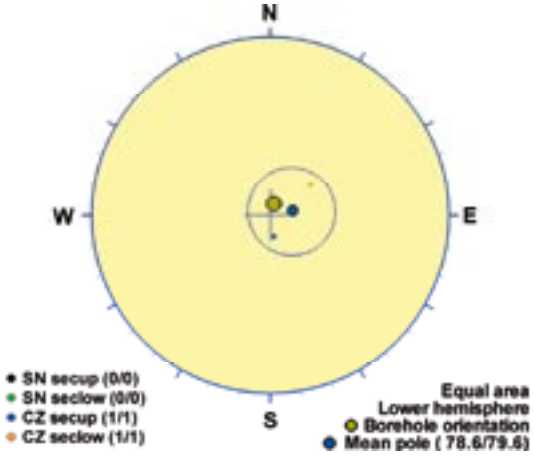

Poles from ductile structures

Data not used

Poles from fractures

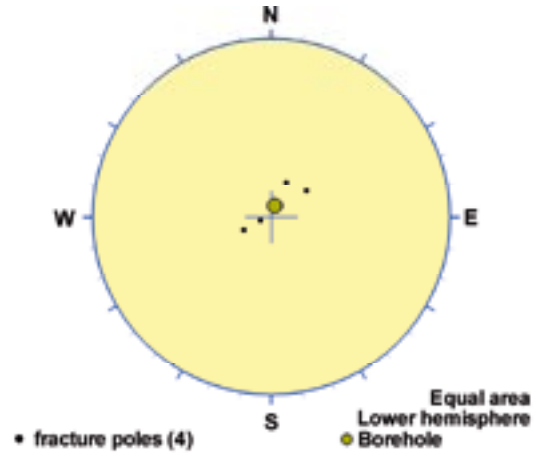

Contours from fractures

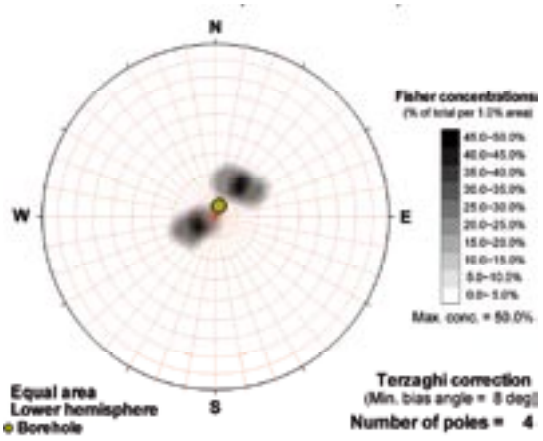

Orientation		Basis for orientation				Certainty	Thickness	
Strike	Dip	Fractures	Crush	Ductile structures	Reflectors	Orientation	Apparent	True
169	10	Used	Verify		Verify	Certain	1 m	1 m
Comment:								

KLX04 DZ7 (167 to 167.4), brittle zone

Brittle deformation zone characterized by a crush zone (0.12 m in borehole length), increased frequency of open fractures and weak red staining. Decrease in resistivity, magnetic susceptibility and P-wave velocity. The host rock is dominated by Ävrö granodiorite (501056). Subordinate rock type comprises granite (501058).

Poles from crush zone

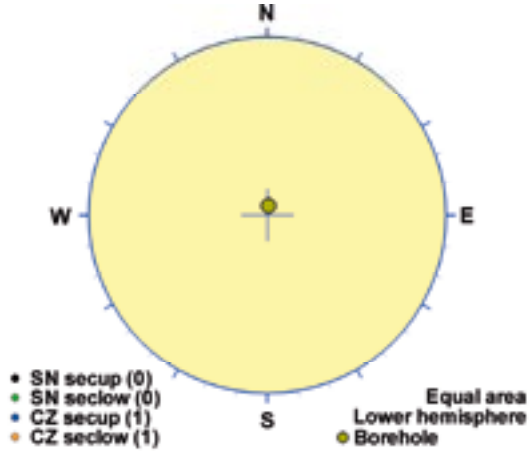

Poles from ductile structures

Data not used

Poles from fractures

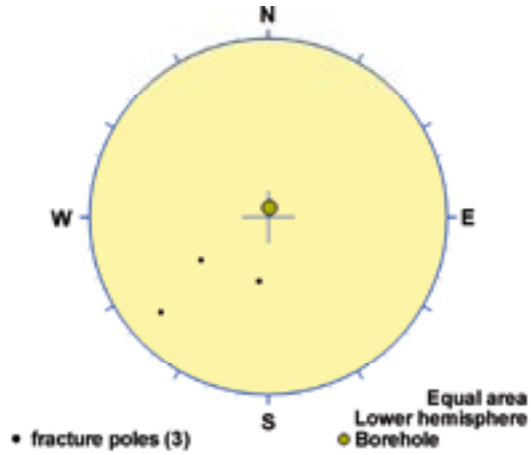

Contours from fractures

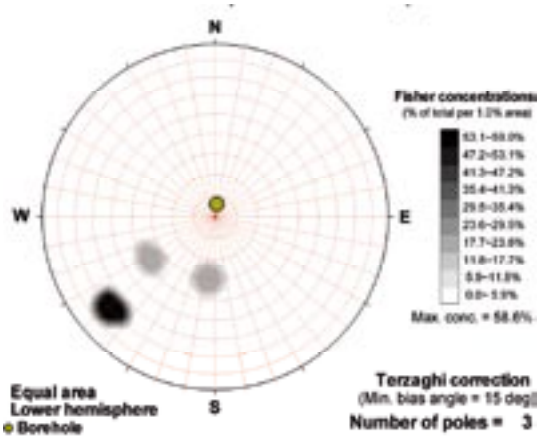

Orientation		Basis for orientation				Certainty	Thickness	
Strike	Dip	Fractures	Crush	Ductile structures	Reflectors	Orientation	Apparent	True
97	6	Contradict	Used			Uncertain	0.4 m	0.4 m
Comment:								

KLX04 DZ8 (203.35 to 203.75), brittle zone

Brittle deformation zone characterized by a crush zone (0.19 m in borehole length), sealed network and faint red staining. Partly decrease in resistivity and magnetic susceptibility. The host rock is totally dominated by Ävrö granodiorite (501056).

Poles from crush zone

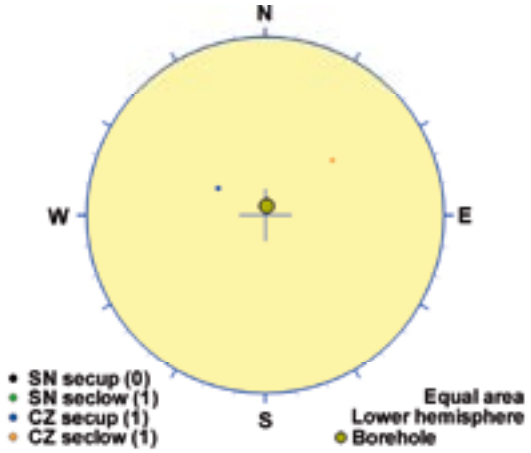

Poles from ductile structures

Data not used

Poles from fractures

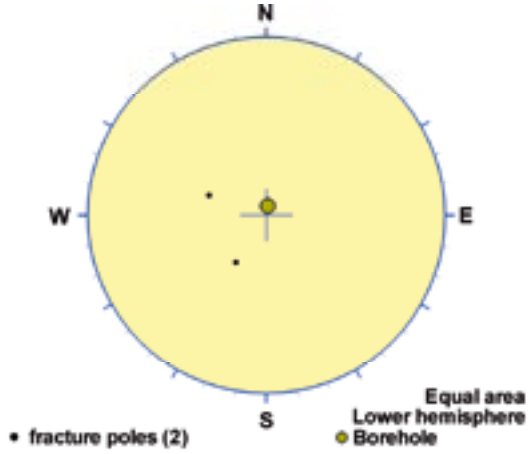

Contours from fractures

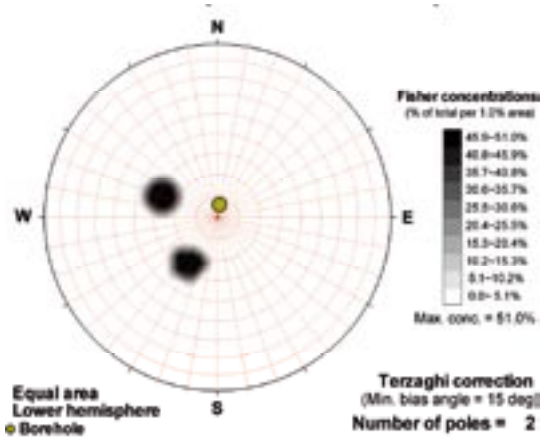

Orientation		Basis for orientation				Certainty	Thickness	
Strike	Dip	Fractures	Crush	Ductile structures	Reflectors	Orientation	Apparent	True
30	25	Verify	Used			Probable	0.4 m	0.4 m
Comment:								

KLX04 DZ9 (207.35 to 207.75), brittle zone

Brittle deformation zone characterized by a crush zone (0.3 m in borehole length), increased frequency of open fractures and faint red staining. Partly decrease in resistivity and magnetic susceptibility. The host rock is dominated by Ävrö granodiorite (501056). Subordinate rock type comprises fine-grained granite (511058).

Poles from crush zone

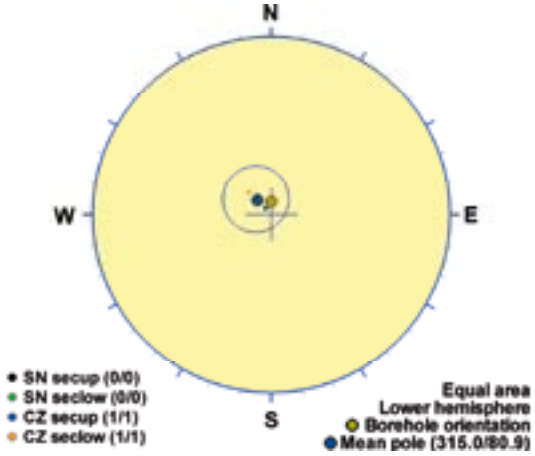

Poles from ductile structures

Data not used

Poles from fractures

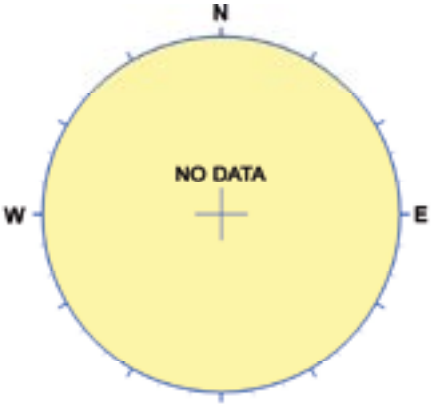

Contours from fractures

Orientation		Basis for orientation				Certainty	Thickness	
Strike	Dip	Fractures	Crush	Ductile structures	Reflectors	Orientation	Apparent	True
45	9		Used			Probable	0.4 m	0.4 m
Comment:								

KLX04 DZ10 (211.1 to 211.75), brittle zone

Brittle deformation zone characterized by a crush zone (0.59 m in borehole length) and weak red staining. Decrease in resistivity and magnetic susceptibility. The host rock is totally dominated by Ävrö granodiorite (501056).

Poles from crush zone

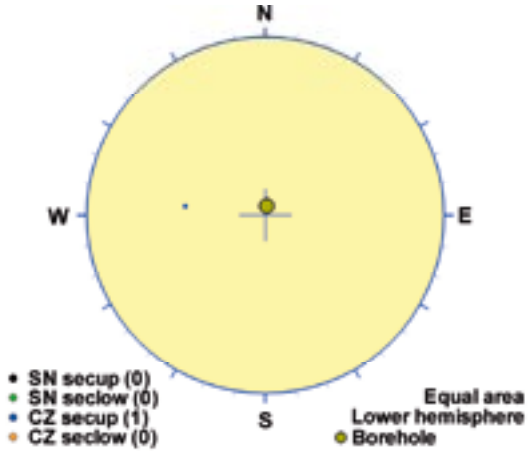

Poles from ductile structures

Data not used

Poles from fractures

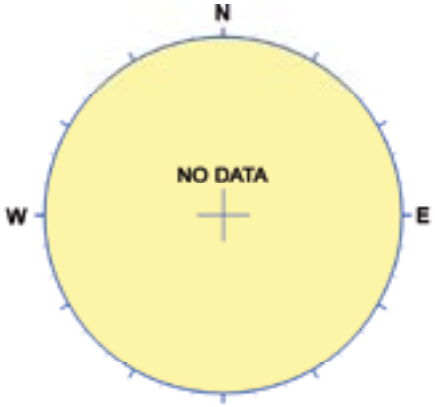

Contours from fractures

Orientation		Basis for orientation				Certainty	Thickness	
Strike	Dip	Fractures	Crush	Ductile structures	Reflectors	Orientation	Apparent	True
6	37		Used			Probable	0.7 m	0.5 m
Comment:								

KLX04 DZ11 (363.25 to 363.6), brittle zone

Brittle deformation zone characterized by a crush zone (0.13 m in borehole length), sealed network, increased frequency of open fractures and faint red staining. Decrease in resistivity, magnetic susceptibility and P-wave velocity. The host rock is totally dominated by Ävrö granodiorite (501056).

Poles from crush zone

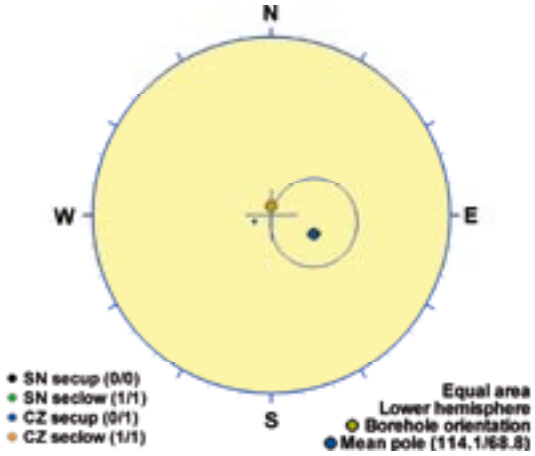

Poles from ductile structures

Data not used

Poles from fractures

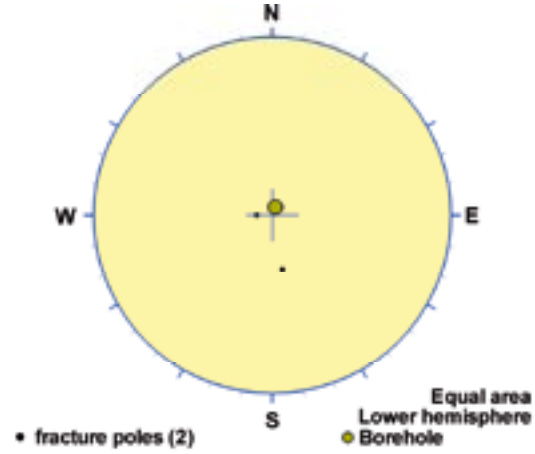

Contours from fractures

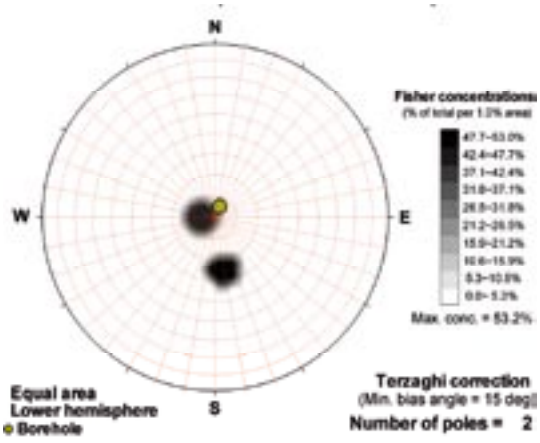

Orientation		Basis for orientation				Certainty	Thickness	
Strike	Dip	Fractures	Crush	Ductile structures	Reflectors	Orientation	Apparent	True
204	21		Used			Probable	0.4 m	0.3 m
Comment:								

KLX04 DZ12 (411.05 to 411.5), brittle zone

Brittle deformation zone characterized by increased frequency of open fractures, sealed network and weak red staining. Partly decrease in resistivity, magnetic susceptibility and P-wave velocity. Host rock is dominated by Ävrö granodiorite (501056) and fine-grained granite (511058). Subordinate rock type comprises fine-grained diorite-gabbro (505102).

Poles from crush zone

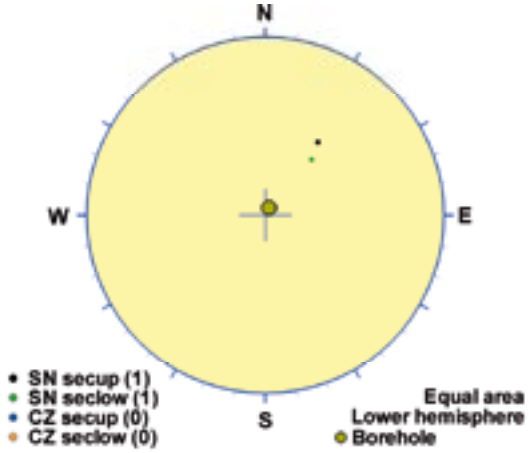

Poles from ductile structures

Data not used

Poles from fractures

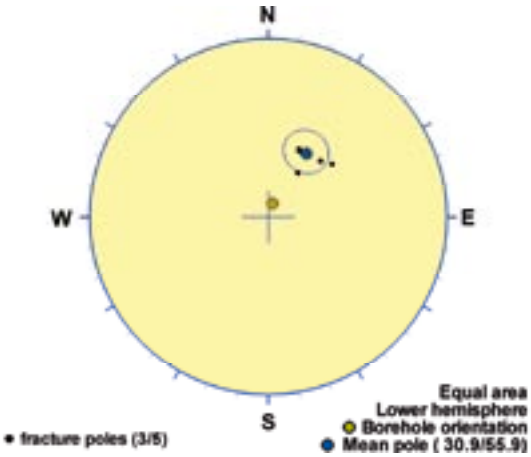

Contours from fractures

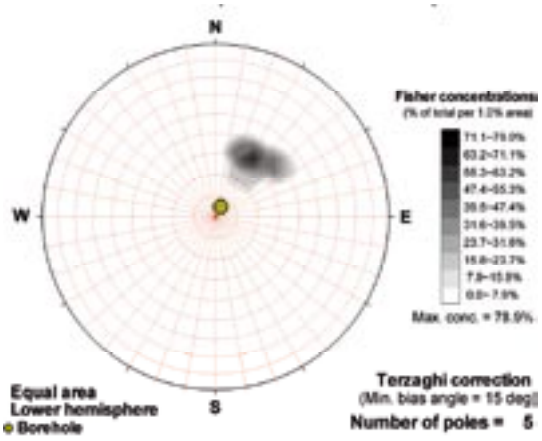

Orientation		Basis for orientation				Certainty	Thickness	
Strike	Dip	Fractures	Crush	Ductile structures	Reflectors	Orientation	Apparent	True
121	34	Used	Verify			Certain	0.4 m	0.4 m
Comment:								

KLX04 DZ13 (419.62 to 419.95), brittle zone

Brittle deformation zone characterized by slight increase in frequency of sealed fractures, sealed network and weak red staining. Decrease in resistivity, magnetic susceptibility and P-wave velocity.The host rock is dominated by granite (501058). Subordinate rock types comprise Ävrö granodiorite (501056) and quartz monzodiorite (501036).

Poles from crush zone

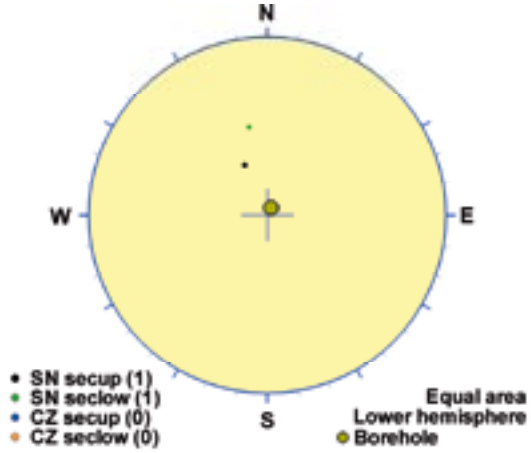

Poles from ductile structures

Data not used

Poles from fractures

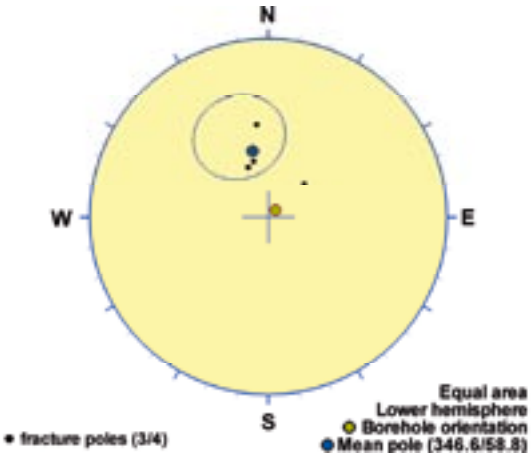

Contours from fractures

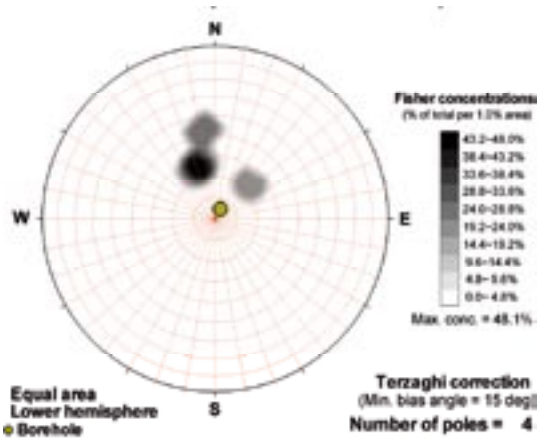

Orientation		Basis for orientation				Certainty	Thickness	
Strike	Dip	Fractures	Crush	Ductile structures	Reflectors	Orientation	Apparent	True
77	31	Used	Verify			Certain	0.3 m	0.3 m
Comment:								

KLX04 DZ14 (443.8 to 444), brittle zone

Brittle deformation zone characterized by a crush zone (0.10 m in borehole length), sealed network, slightly increased frequency of open fractures and faint red staining. Decrease in resistivity, magnetic susceptibility and P-wave velocity. The host rock is dominated by Ävrö quartz monzodiorite (501046) and fine-grained dioritoid (501030).

Poles from crush zone

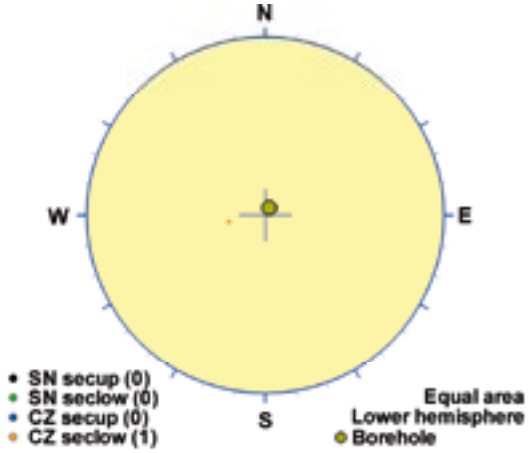

Poles from ductile structures

Data not used

Poles from fractures

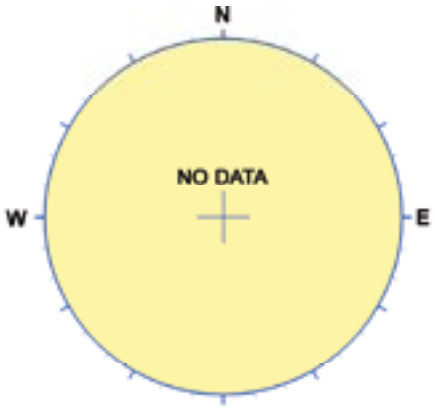

Contours from fractures

Orientation		Basis for orientation				Certainty	Thickness	
Strike	Dip	Fractures	Crush	Ductile structures	Reflectors	Orientation	Apparent	True
349	17		Used			Probable	0.2 m	0.2 m
Comment:								

KLX04 DZ15 (514.7 to 515.2), brittle zone

Brittle deformation zone characterized by a crush zone (0.36 m in borehole length) and faint red staining. Decrease in magnetic susceptibility and P-wave velocity. One radar reflector at 514.7 m with the ngle 29° to borehole axis. The host rock is totally dominated by fine-grained granite (511058).

Poles from crush zone

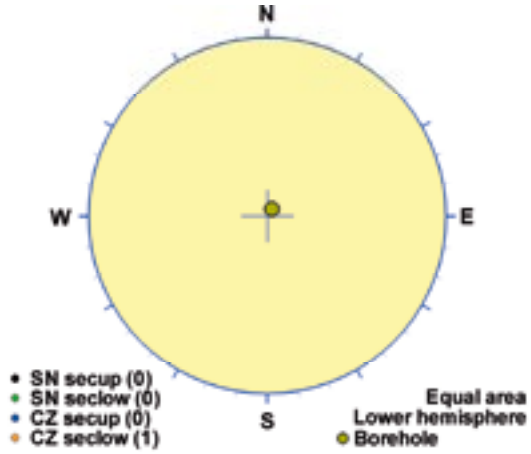

Poles from ductile structures

Data not used

Poles from fractures

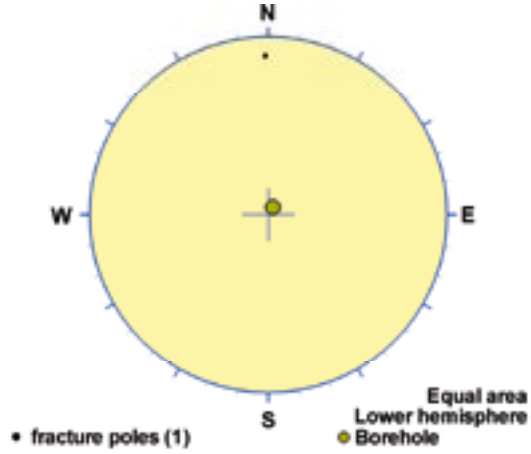

Contours from fractures

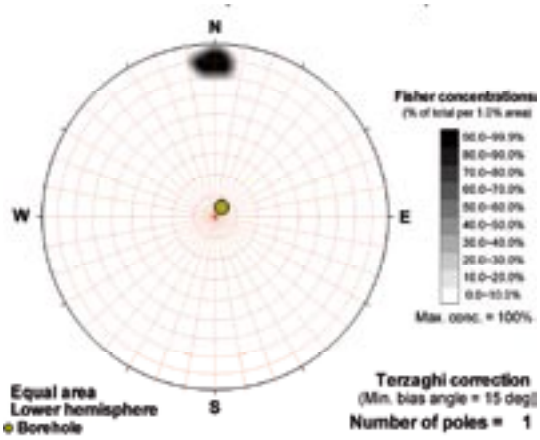

Orientation		Basis for orientation				Certainty	Thickness	
Strike	Dip	Fractures	Crush	Ductile structures	Reflectors	Orientation	Apparent	True
89	78	Contradict	Used			Very uncertain	0.5 m	0.1 m
Comment:								

KLX04 DZ16 (580.7 to 586.2), brittle zone

Brittle deformation zone characterized by four crush zones (with a total borehole length of 1.02 m), sealed network, increased frequency of open fractures and faint to weak red staining. Partly decrease in resistivity, magnetic susceptibility and P-wave velocity. One radar reflector at 584.6 m with the angle 28° to borehole axis. The host rock is domianted by Ävrö quartz monzodiorite (501046) and to a lesser extent fine-grained dioritoid (501030). Subordinate rock types comprise granite (501058) and fine-grained granite (511058).

Poles from crush zone

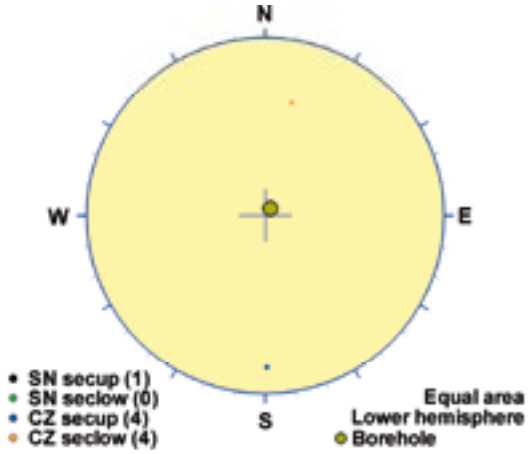

Poles from ductile structures

Data not used

Poles from fractures

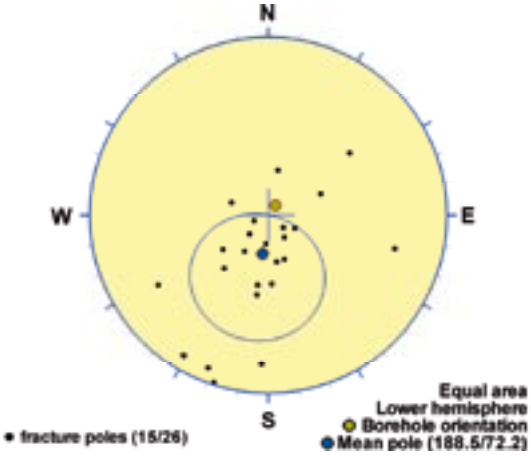

Contours from fractures

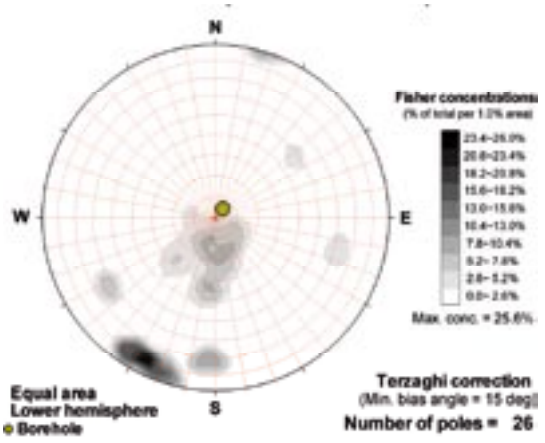

Orientation		Basis for orientation				Certainty	Thickness	
Strike	Dip	Fractures	Crush	Ductile structures	Reflectors	Orientation	Apparent	True
279	18	Used				Probable	5.5 m	5.1 m
Comment:								

KLX04 DZ17 (627.56 to 628.5), brittle zone

Brittle deformation zone characterized by a crush zone (0.63 m in borehole length), faint red staining and quartz dissolution (0.90 m in borehole length). Decrease in resistivity, magnetic susceptibility, P-wave velocity, and one caliper anomaly. The host rock is totally dominated by Ävrö quartz monzodiorite (501046).

Poles from crush zone

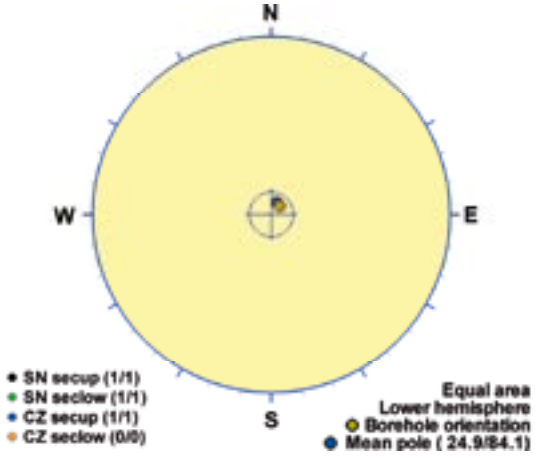

Poles from ductile structures

Data not used

Poles from fractures

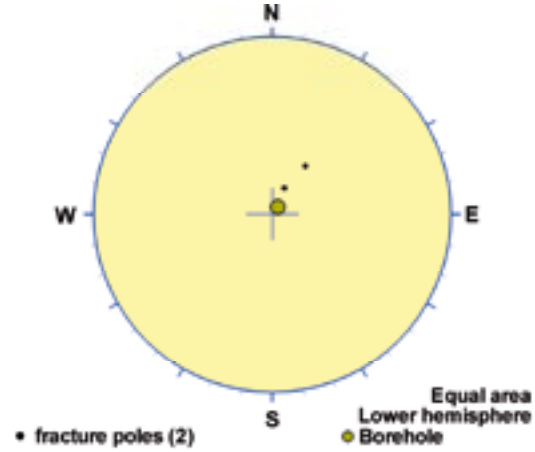

Contours from fractures

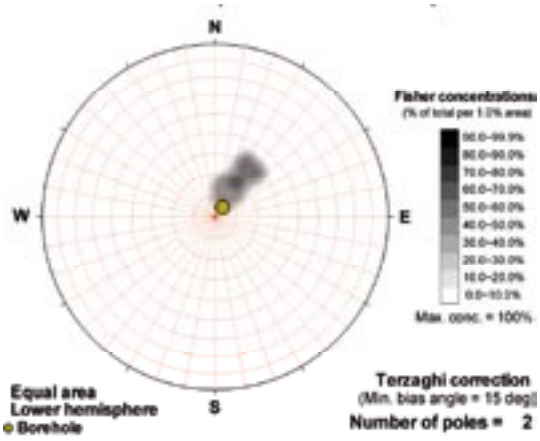

Orientation		Basis for orientation				Certainty	Thickness	
Strike	Dip	Fractures	Crush	Ductile structures	Reflectors	Orientation	Apparent	True
115	6	Verify	Used			Probable	0.9 m	0.9 m
Comment:								

KLX05 DZ3 (178.7 to 178.78), ductile zone

Minor low-grade ductile deformation zone. Strongly foliated to protomylonitic fine-grained diorite-gabbro (505102). Subordinate rock types are Ävrö granodiorite (501056) and fine-grained granite (511058). Minor decrease in resistivity.

Poles from crush zone

Data not used

Poles from ductile structures

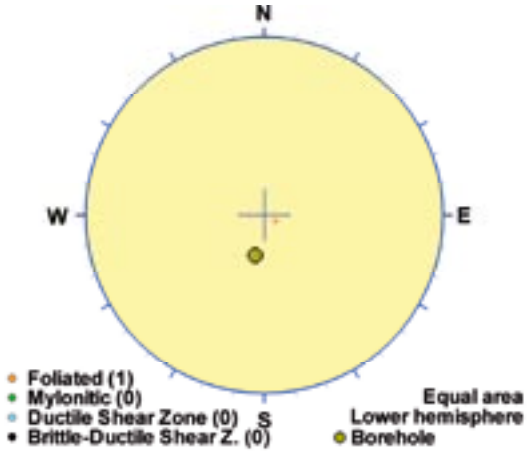

Poles from fractures

Data not used

Contours from fractures

Data not used

Orientation		Basis for orientation				Certainty	Thickness	
Strike	Dip	Fractures	Crush	Ductile structures	Reflectors	Orientation	Apparent	True
210	7			Used		Probable	0.1 m	0.1 m
Comment: One point only								

KLX05 DZ6 (403.4 to 406.1), ductile zone

Minor low-grade ductile deformation zone. Intermediately foliated to protomylonitic Ävrö granodiorite (501056) with subordinate Ävrö quartz monzodiorite (501046). One radar reflector at 403.7 m with the angle 53º to borehole axis. A slight decrease in p-wave velocity. Subordinate rock types comprise diorite/gabbro (501033) and fine-grained granite (511058).

Poles from crush zone

Data not used

Poles from ductile structures

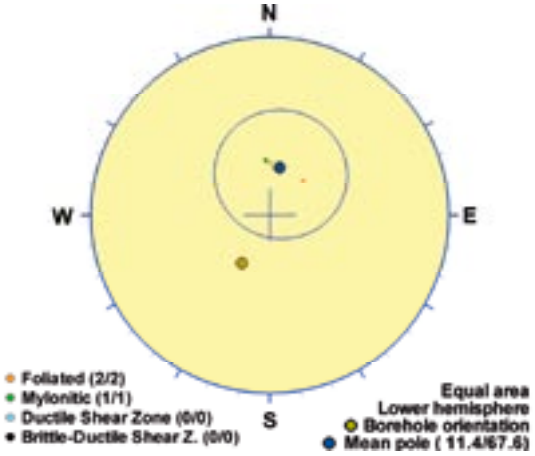

Poles from fractures

Data not used

Contours from fractures

Data not used

Orientation		Basis for orientation				Certainty	Thickness	
Strike	Dip	Fractures	Crush	Ductile structures	Reflectors	Orientation	Apparent	True
101	22			Used	Verify	Certain	2.7 m	1.9 m

Comment: The zone contains plenty of fractures in BIPS, but there is no fracture plot. Therefore only ductile structures are used.

KLX05 DZ7 (477.5 to 478.1), ductile zone

Minor low-grade ductile deformation zone. Intermediately to strongly foliated quartz monzodiorite (501036). One radar reflector at 478.7 m with the angle 72º to borehole axis. No indications in geophysical data. Subordinate rock types comrpise fine-grained granite (511058) and fine-grained dioritoid (501030).

Poles from crush zone

Data not used

Poles from ductile structures

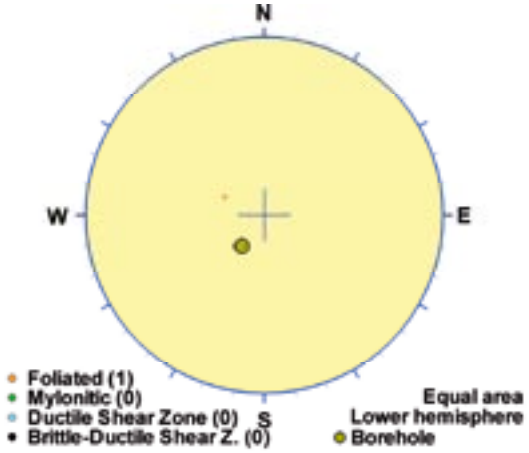

Poles from fractures

Data not used

Contours from fractures

Data not used

Orientation		Basis for orientation				Certainty	Thickness	
Strike	Dip	Fractures	Crush	Ductile structures	Reflectors	Orientation	Apparent	True
25	20		Verify	Used	Verify	Probable	0.6 m	0.5 m

Comment: One point only.

The zone contains plenty of fractures in BIPS, but there is no fracture plot. Therefore only ductile structures are used.

KLX05 DZ10 (612.34 to 612.54), ductile/brittle zone

Minor brittle-ductile deformation zone. Strongly foliated quartz monzodiorite (501036). Significantly decreased resistivity and magnetic susceptibility.

Poles from crush zone

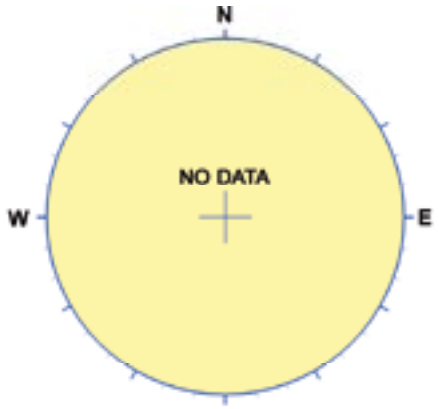

Poles from ductile structures

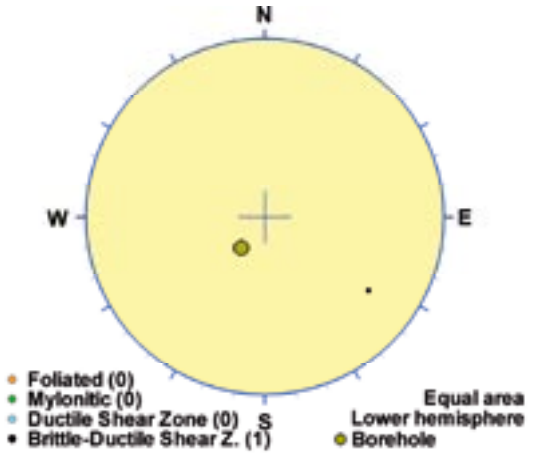

Poles from fractures

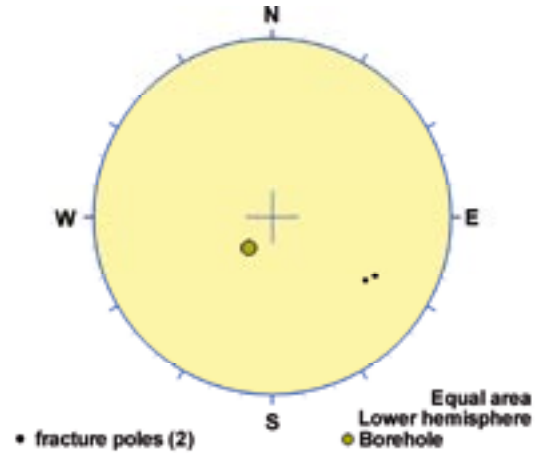

Contours from fractures

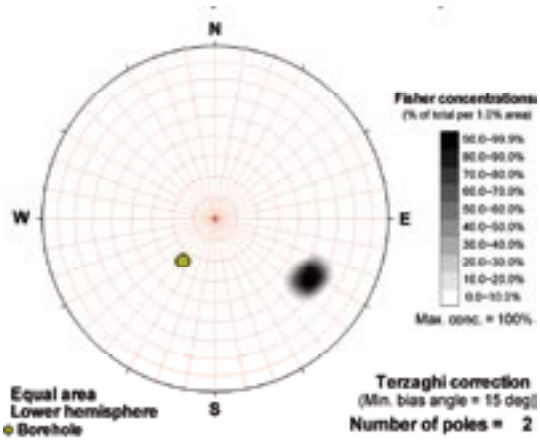

Orientation		Basis for orientation				Certainty	Thickness	
Strike	Dip	Fractures	Crush	Ductile structures	Reflectors	Orientation	Apparent	True
214	64	Verify		Used		Certain	0.2 m	0.1 m
Comment:								

KLX05 DZ11 (626.73 to 629.43), ductile/brittle zone

Inhomogeneous minor brittle-ductile deformation zone. Strongly foliated quartz monzodiorite (501036) with subordinate pegmatite 8501061) and sparse fine-grained granite (511058). Scattered cm-dm thick protomylonitic to mylonitic sections. One oriented radar reflector occurs at 628.3 m with the orientation 325/86 and one non-oriented reflector occurs at 628.9 m with the angle 37° to borehole axis. Significantly decreased resistivity and magnetic susceptibility and minor decrease in P-wave velocity.

Poles from crush zone

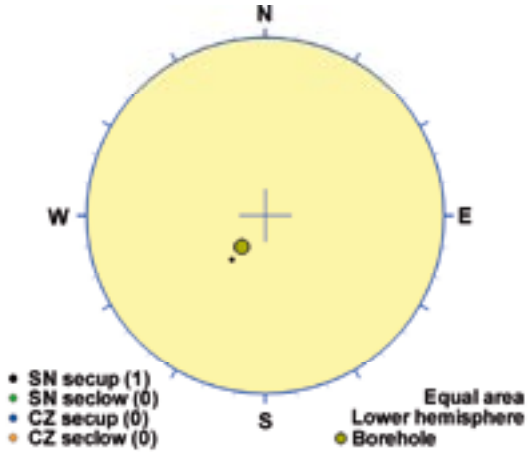

Poles from ductile structures

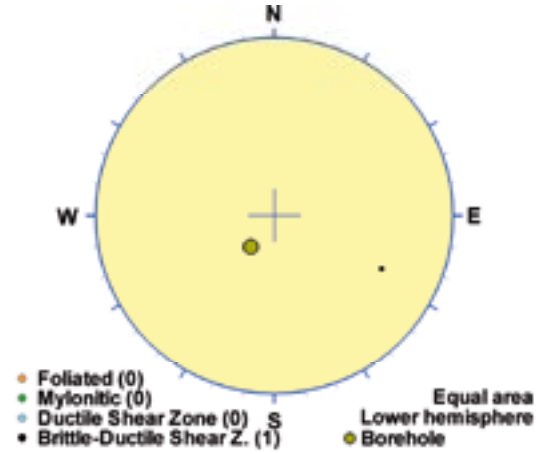

Poles from fractures

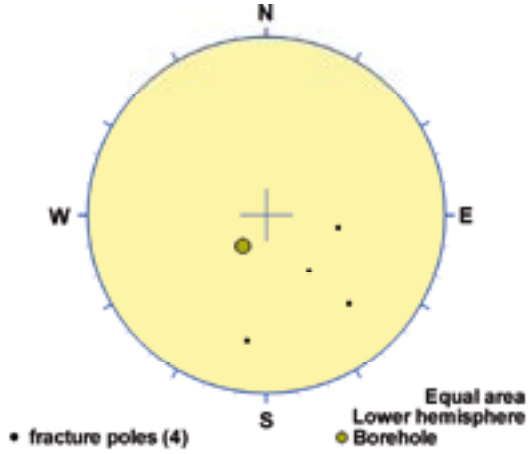

Contours from fractures

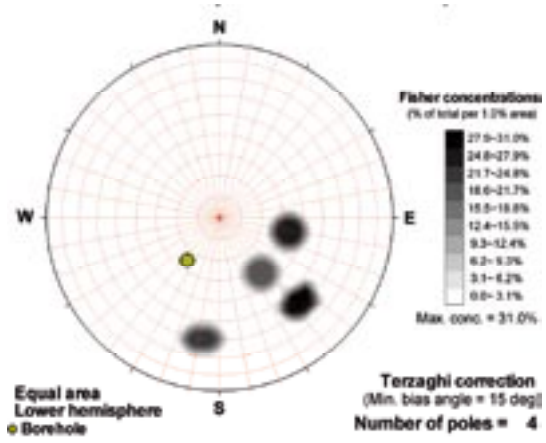

Orientation		Basis for orientation				Certainty	Thickness	
Strike	Dip	Fractures	Crush	Ductile structures	Reflectors	Orientation	Apparent	True
204	60	Verify	Contradict	Used		Uncertain	2.7 m	1 m
Comment:								

KLX05 DZ13 (814.7 to 814.86), ductile zone

Minor low-grade ductile deformation zone. Strongly foliated quartz monzodiorite (501036) and fine-grained granite (511058). Minor decrese in magnetic susceptibility.

Poles from crush zone

Data not used

Poles from ductile structures

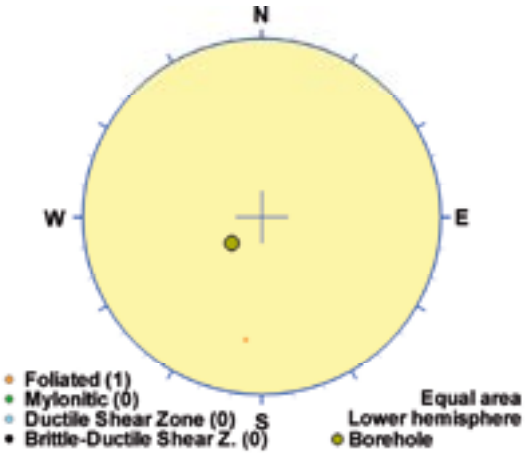

Poles from fractures

Data not used

Contours from fractures

Data not used

Orientation		Basis for orientation				Certainty	Thickness	
Strike	Dip	Fractures	Crush	Ductile structures	Reflectors	Orientation	Apparent	True
273	63			Used		Probable	0.2 m	0.1 m
Comment:								

KLX06 DZ3 (112.7 to 113.9), brittle zone

Brittle deformation zone characterized by increased frequency of open fractures and sealed network. Decrease in resistivity, magnetic susceptibility and P-wave velocity. The host rock is dominated by Ävrö quartz monzodiorite (501046). Subordinate rock type comprises fine-grained granite (511058).

Poles from crush zone

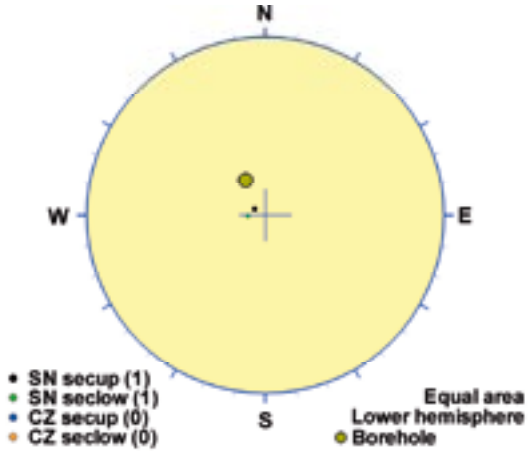

Poles from ductile structures

Data not used

Poles from fractures

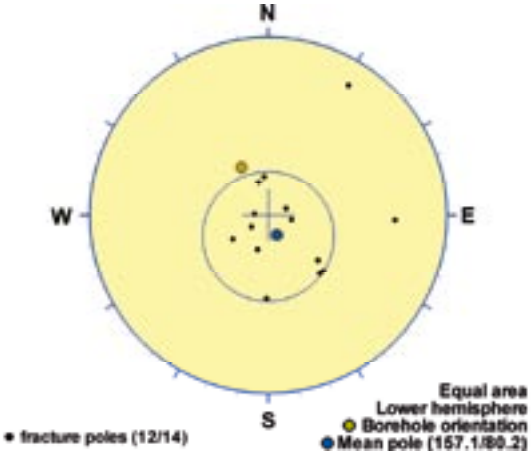

Contours from fractures

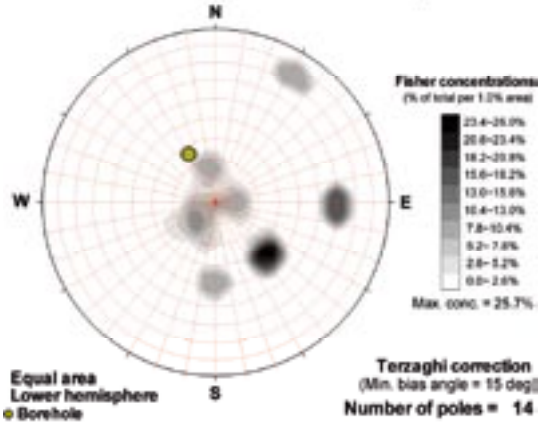

Orientation		Basis for orientation				Certainty	Thickness	
Strike	Dip	Fractures	Crush	Ductile structures	Reflectors	Orientation	Apparent	True
247	10	Used	Verify			Certain	1.2 m	1 m
Comment:								

KLX06 DZ4 (151.43 to 154), brittle zone

Brittle deformation zone characterized by three crush zone (total borehole length 0.38 m), increased frequency of sealed fractures, sealed network and faint to weak red staining. Significant decrease in resistivity, magnetic susceptibility and P-wave velocity. Two radar reflectors, one at 152.3 m with the angle 33° to borehole axis, and one at 154.1 m with the angle 28° to borehole axis. The host rock is totally dominated by fine-grained diorite-gabbro (505102).

Poles from crush zone

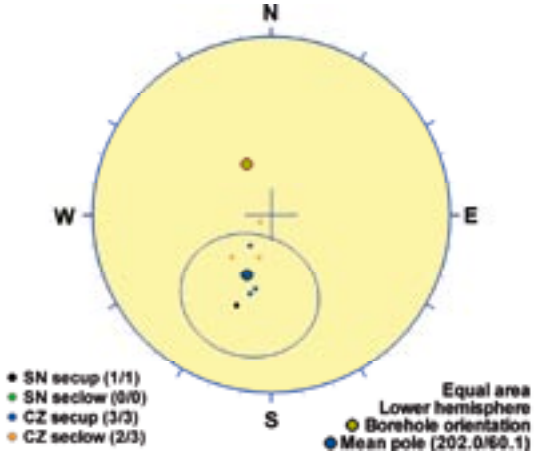

Poles from ductile structures

Data not used

Poles from fractures

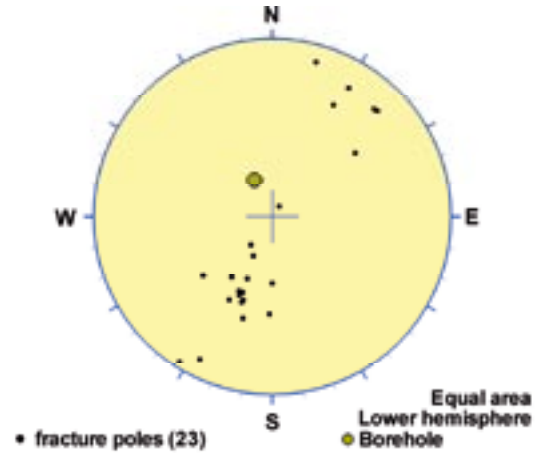

Contours from fractures

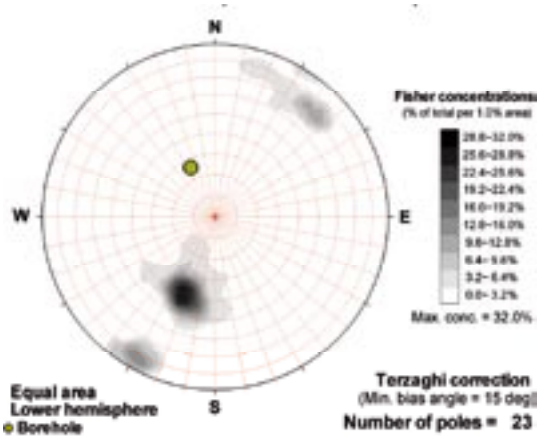

Orientation		Basis for orientation				Certainty	Thickness	
Strike	Dip	Fractures	Crush	Ductile structures	Reflectors	Orientation	Apparent	True
292	30	Verify	Used		Verify	Certain	2.6 m	1.6 m
Comment:								

KLX07A DZ3 (184.8 to 185.4), brittle zone

Minor deformation zone characterized by cataclasite sealed with epidote and chlorite, and fractures sealed with calcite. One non-oriented radar reflector with the angle 47º to borehole axis. Decreased radar amplitude at 185 m. Minor anomalies in p-wave velocity and resistivity loggings. The host rock is totally dominated by Ävrö granodiorite (501056).

Poles from crush zone

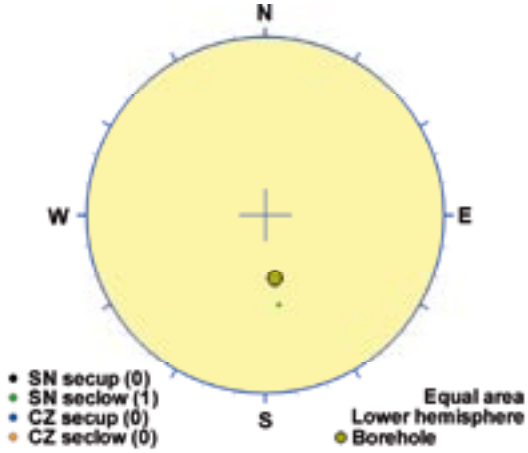

Poles from ductile structures

Data not used

Poles from fractures

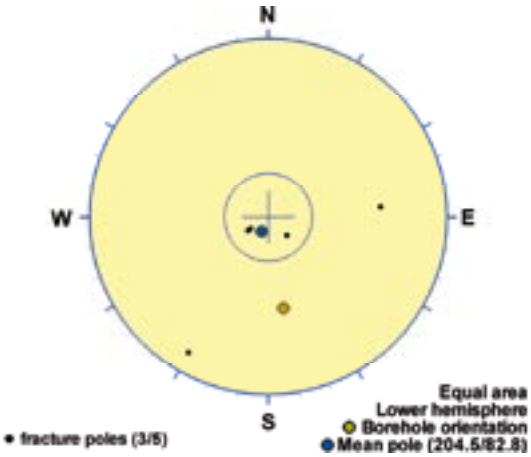

Contours from fractures

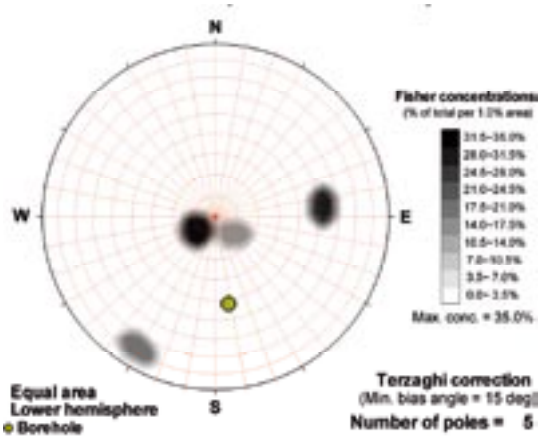

Orientation		Basis for orientation				Certainty	Thickness	
Strike	Dip	Fractures	Crush	Ductile structures	Reflectors	Orientation	Apparent	True
295	7	Used	Contradict		Verify	Uncertain	0.6 m	0.5 m
Comment:								

KLX07A DZ4 (252.5 to 253.1), brittle zone

Minor deformation zone characterized by crush. Chlorite and epidote sealed fractures. Two non-oriented radar reflectors with the angle 40 and 68º to borehole axis. Low resistivity, low p-wave velocity and high caliper anomalies indicate open fractures. The host rock is totally dominated by Ävrö granodiorite (501056).

Poles from crush zone

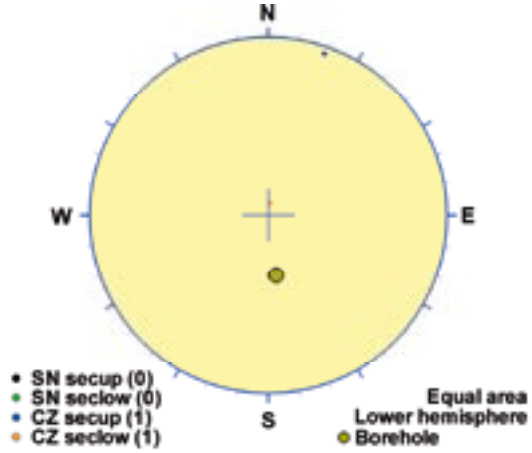

Poles from ductile structures

Data not used

Poles from fractures

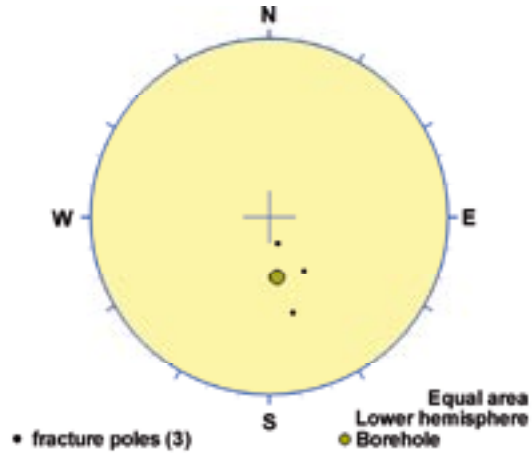

Contours from fractures

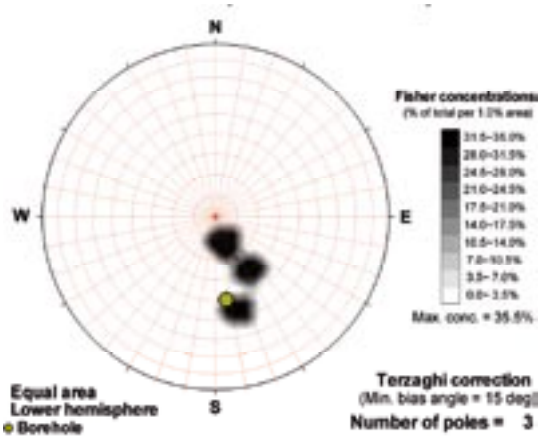

Orientation		Basis for orientation				Certainty	Thickness	
Strike	Dip	Fractures	Crush	Ductile structures	Reflectors	Orientation	Apparent	True
180	60	Used	Contradict			Very uncertain	0.6 m	0.3 m
Comment:								

KLX07A DZ5 (308 to 313), brittle zone

Minor deformation zone characterized by red staining with a central part at 311-312 m comprising epidote sealed cataclasite. Four radar reflectors, two of them oriented. The oriented reflectors are at 311.6 m with the orientation 03/218 and at 311.9 m with the orientation 27/278. The angle to borehole axis is in the interval 48-71º. Geophysical loggings indicate distinct low resistivity, low p-wave velocity and positive caliper anomalies. The host rock is totally dominated by Ävrö granodiorite (501056) with very subordinate fine-grained granite (511058).

Poles from crush zone

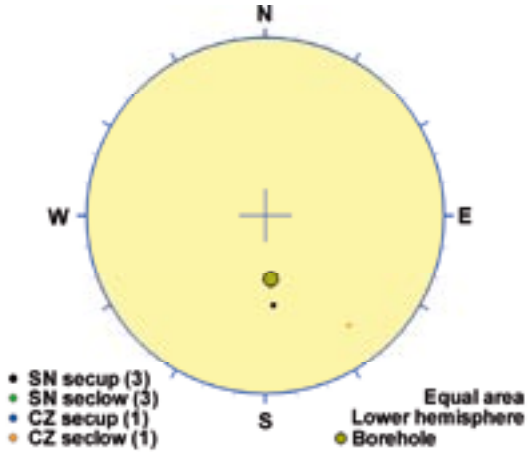

Poles from ductile structures

Data not used

Poles from fractures

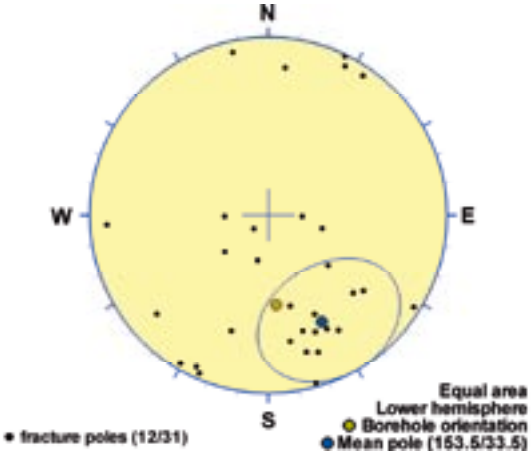

Contours from fractures

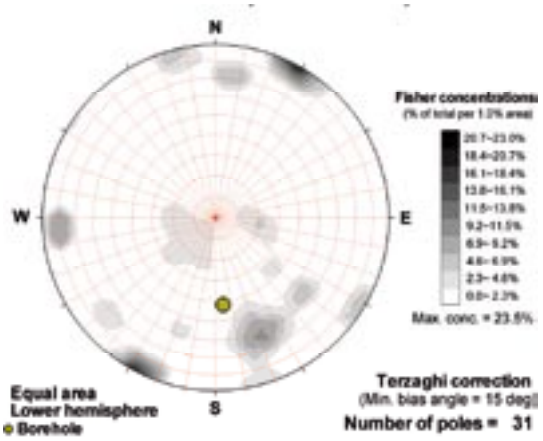

Orientation		Basis for orientation				Certainty	Thickness	
Strike	Dip	Fractures	Crush	Ductile structures	Reflectors	Orientation	Apparent	True
244	57	Used	Verify			Probable	5 m	4.6 m
Comment:								

KLX07A DZ6 (335.6 to 340), brittle zone

Minor deformation zone characterized by inhomogeneous red staining, cataclasite with epidote, chlorite, alternating with more well preserved parts. Three non-oriented radar reflectors are identified. The angle to borehole axis is 12, 70 and 39º. Decreased radar amplitude in the interval 335-340 m, and continues to 340 m. A number of minor low resistivity and low p-wave anomalies occur along the section. The host rock is dominated by Ävrö granodiorite (501056; indicated by the density log). Subordinate rock types comprise fine-grained dioritoid 8501030), fine-grained granite (511058) and granite (501058).

Poles from crush zone

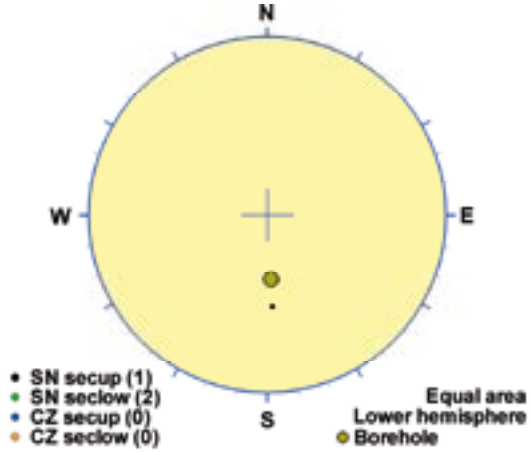

Poles from ductile structures

Data not used

Poles from fractures

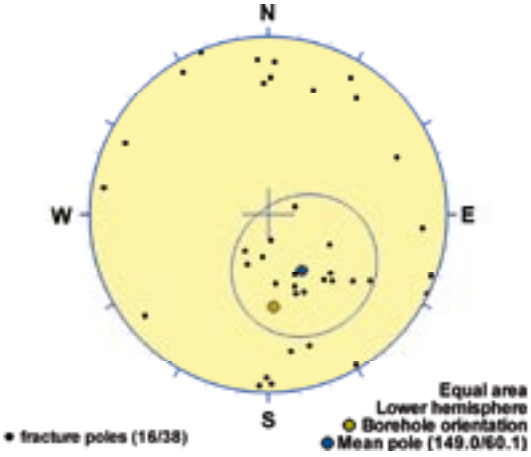

Contours from fractures

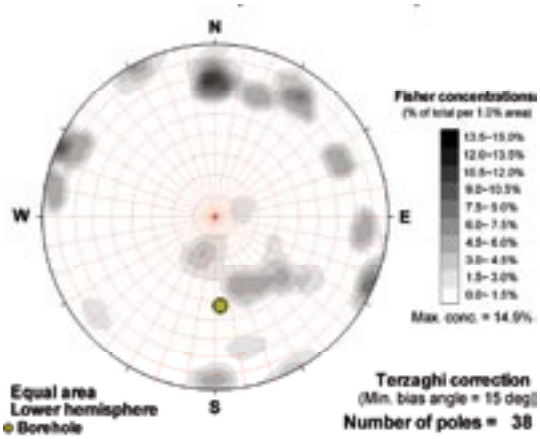

Orientation		Basis for orientation				Certainty	Thickness	
Strike	Dip	Fractures	Crush	Ductile structures	Reflectors	Orientation	Apparent	True
239	30	Used	Verify			Probable	4.4 m	4.1 m
Comment:								

KLX07A DZ8 (432.6 to 434.5), brittle zone

Increased fracture frequency particularly of sealed fractures. Scattered sections of chlorite and epidote sealed cataclasite (1-3 cm wide). Two radar reflectors are identified, one of them is oriented. The angle to borehole axis of the non-oriented reflector is 58º and the reflector at 434.3 m has the orientation 78/252. Low resistivity, low p-wave velocity and positive caliper anomalies. The host rock is totally dominated by Ävrö granodiorite (501056) with subordinate fine-grained granite (511058).

Poles from crush zone

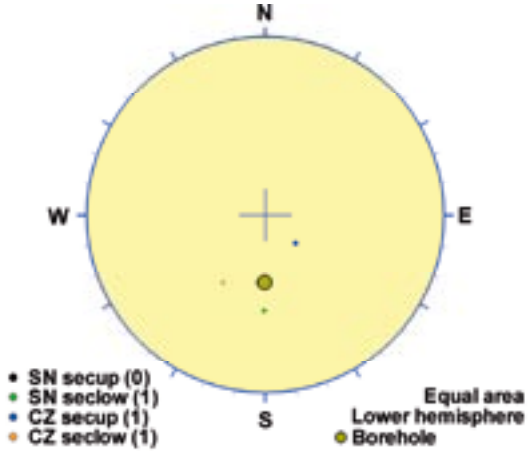

Poles from ductile structures

Data not used

Poles from fractures

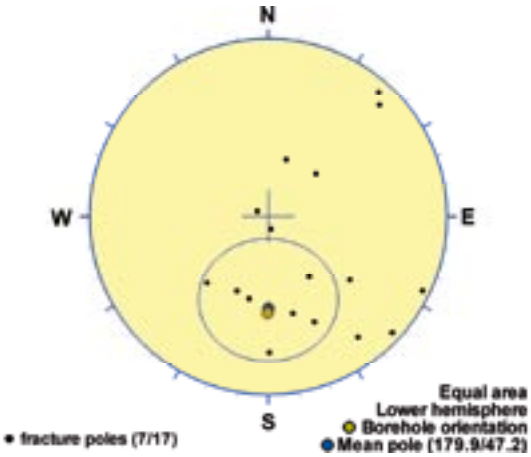

Contours from fractures

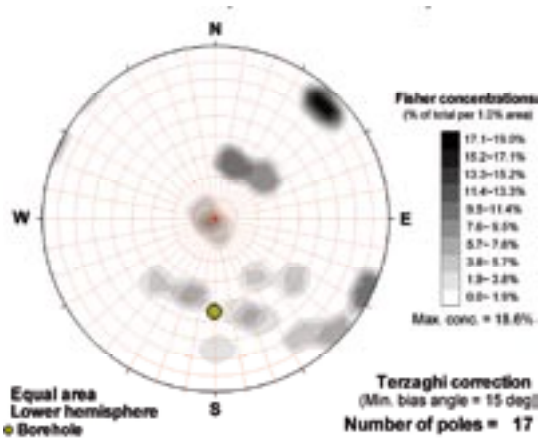

Orientation		Basis for orientation				Certainty	Thickness	
Strike	Dip	Fractures	Crush	Ductile structures	Reflectors	Orientation	Apparent	True
270	43	Used	Verify			Probable	1.9 m	1.9 m
Comment:								

KLX07A DZ14 (413.4 to 413.73), brittle zone

Brittle deformation zone characterized by increased frequency of open fractures, sealed network and weak red staining. Slight decrease in resistivity and magnetic susceptibility. The host rock is totally dominated by Ävrö granodiorite (501056).

Poles from crush zone

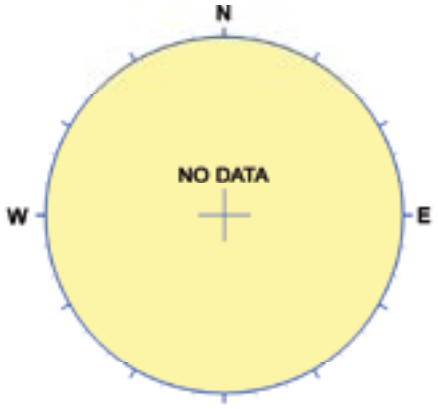

Poles from ductile structures

Data not used

Poles from fractures

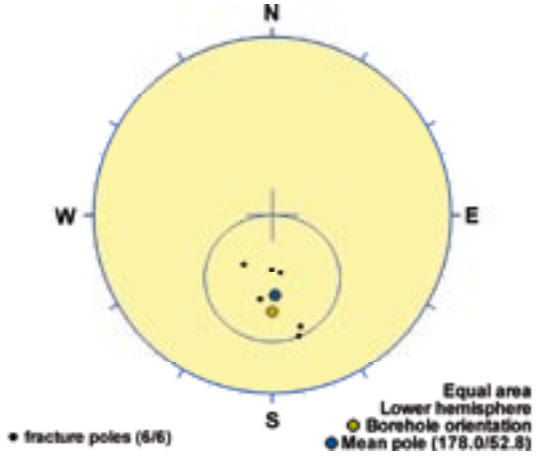

Contours from fractures

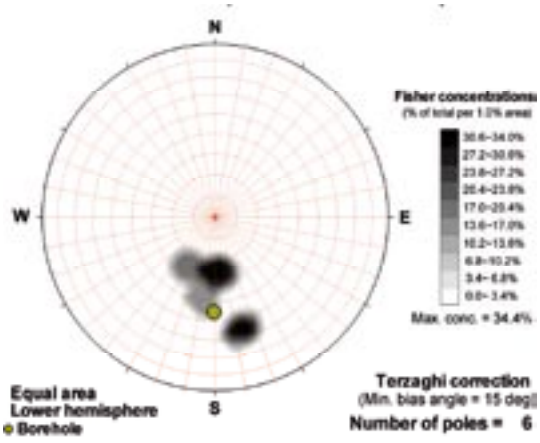

Orientation		Basis for orientation				Certainty	Thickness	
Strike	Dip	Fractures	Crush	Ductile structures	Reflectors	Orientation	Apparent	True
268	37	Used				Probable	0.3 m	0.3 m
Comment:								

KLX07A DZ15 (502.9 to 503.5), brittle zone

Brittle deformation zone characterized by increased frequency of open fractures, one crush zone (0.05 m in borehole length), sealed network, mylonite and weak to medium red staining. No indications in geophysical data. The host rock is totally dominated by Ävrö quartz monzodiorite (501046).

Poles from crush zone

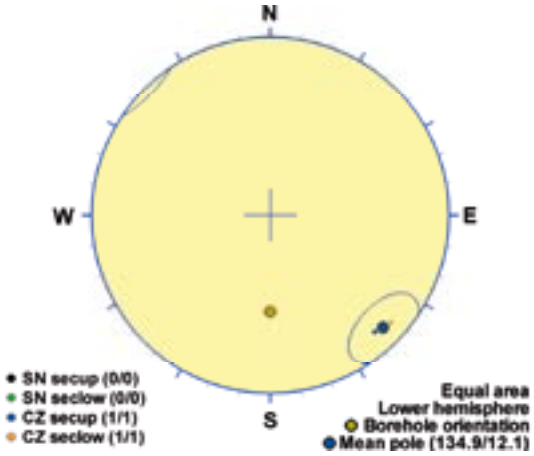

Poles from ductile structures

Data not used

Poles from fractures

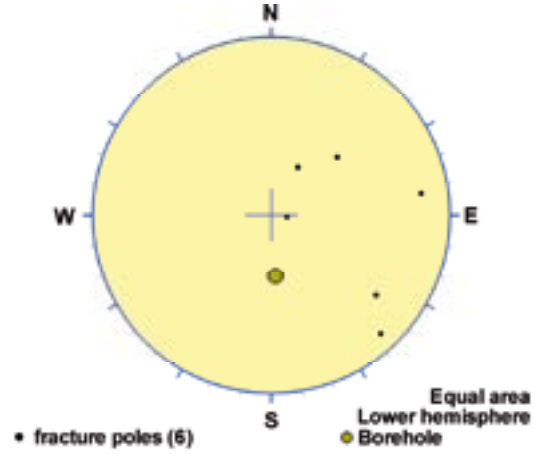

Contours from fractures

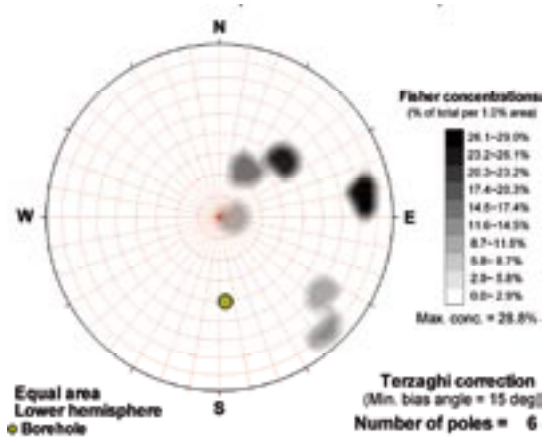

Orientation		Basis for orientation				Certainty	Thickness	
Strike	Dip	Fractures	Crush	Ductile structures	Reflectors	Orientation	Apparent	True
225	78	Verify	Used	Verify		Certain	0.6 m	0.4 m
Comment:								

KLX07A DZ16 (667.95 to 669), brittle zone

Brittle deformation zone characterized by one crush zone (0.48 m in borehole length), sealed network and faint to weak red staining. Minor decrease in resistivity and P-wave velocity. One radar reflector at 668.8 m with the angle 43° to the borehole axis. The host rock is totally dominated by Ävrö granodiorite (501056).

Poles from crush zone

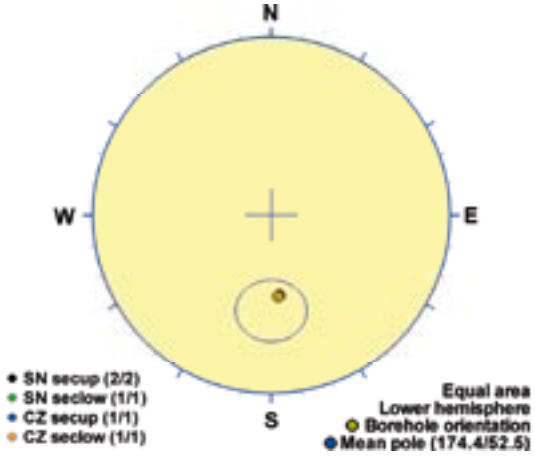

Poles from ductile structures

Data not used

Poles from fractures

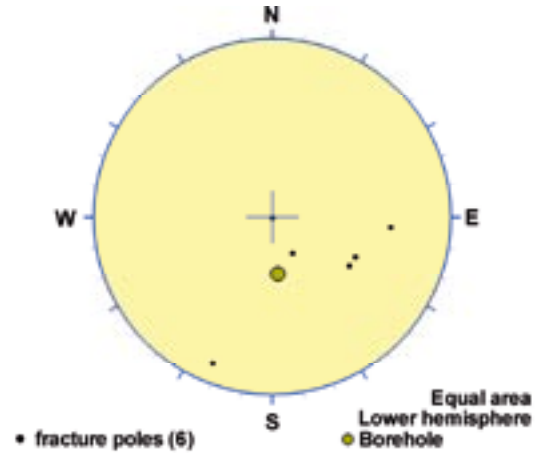

Contours from fractures

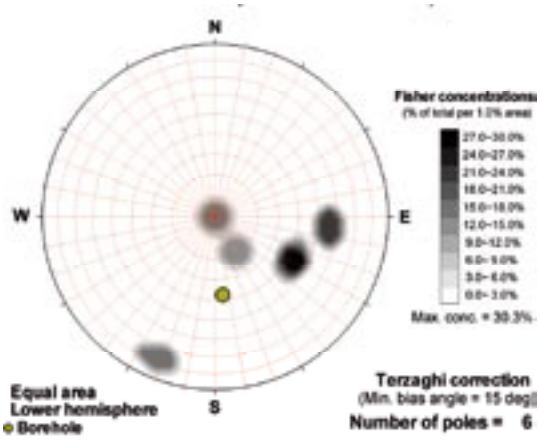

Orientation		Basis for orientation				Certainty	Thickness	
Strike	Dip	Fractures	Crush	Ductile structures	Reflectors	Orientation	Apparent	True
264	38		Used		Verify	Probable	1 m	1 m
Comment: fractures too few and too widespread, why crush supported by reflector is used.								

KLX07B DZ1 (27 to 30), brittle zone

Characterized by increased frequency of open fractures and crush at 28.77-28.89 m and 29.01-29.12 m. Weak red staining. One oriented radar reflector at 28.7 m with the orientation 19/033. Decreased radar amplitude in the interval 25-30 m. There is distinct coincident low resistivity and low p-wave velocity anomalies at the section coordinate ca 28.5 m. There is also a slight increase of the borehole diameter (caliper). The host rock is dominated by Ävrö granodiorite (501056).

Poles from crush zone

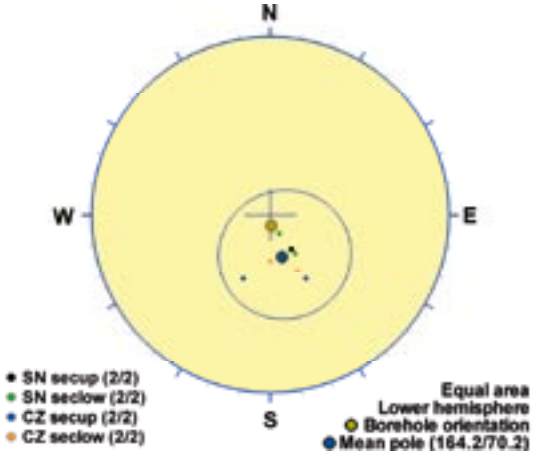

Poles from ductile structures

Data not used

Poles from fractures

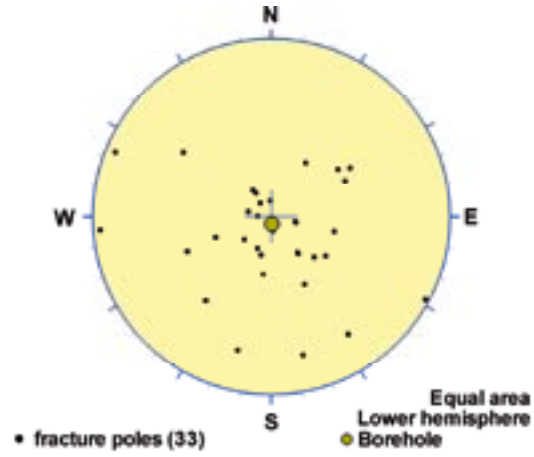

Contours from fractures

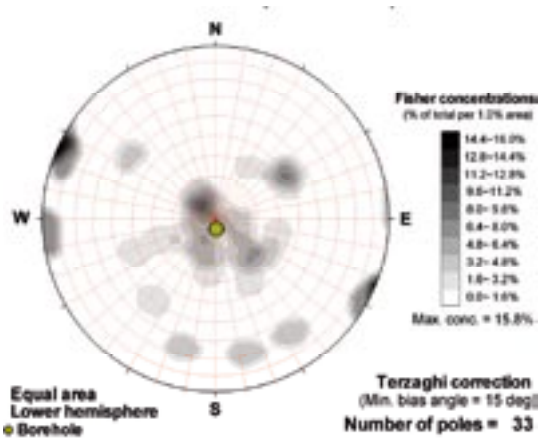

Orientation		Basis for orientation				Certainty	Thickness	
Strike	Dip	Fractures	Crush	Ductile structures	Reflectors	Orientation	Apparent	True
254	20	Verify	Used			Probable	3 m	2.9 m
Comment:								

KLX07B DZ2 (39.7 to 42), brittle zone

Characterized by a crush at 40.52-41.17 m and weak to medium red staining. Two radar reflectors are identified, one of them is oriented. Angle to borehole axis of the nonoriented is 37º and the orientation at 40.9 m is 50/048. Decreased radar amplitude in the interval 40-45 m. There is distinct coincident low resistivity and low p-wave velocity anomalies at the section coordinate ca 40.0 m. There is also a slight increase of the borehole diameter (caliper). The host rock is dominated by Ävrö quartz monzodiorite (501046) with very subordinate fine-grained granite (511058).

Poles from crush zone

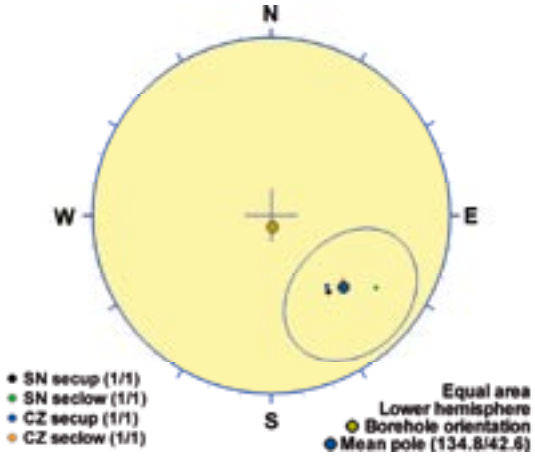

Poles from ductile structures

Data not used

Poles from fractures

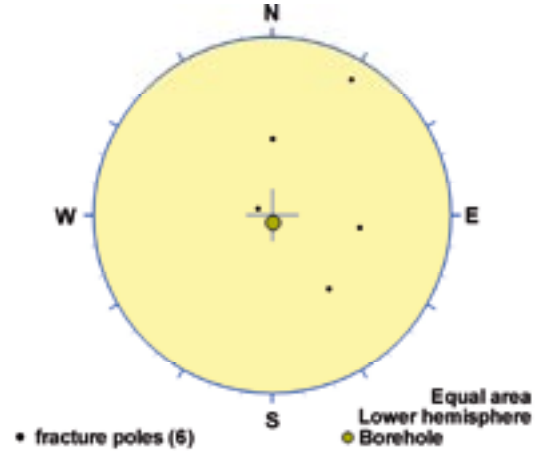

Contours from fractures

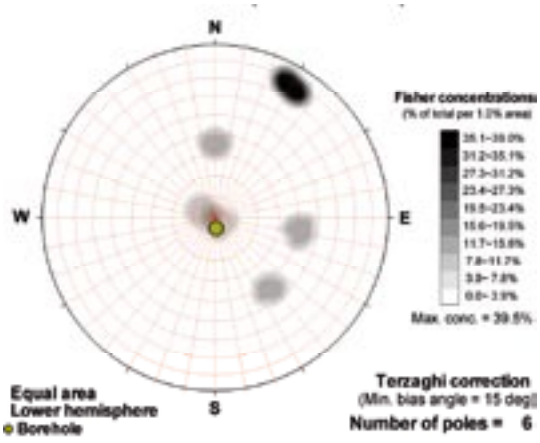

Orientation		Basis for orientation				Certainty	Thickness	
Strike	Dip	Fractures	Crush	Ductile structures	Reflectors	Orientation	Apparent	True
225	47	Verify	Used	Verify		Probable	2.3 m	1.7 m
Comment:								

KLX07B DZ4 (14.9 to 15.97), ductile/brittle zone

Brittle deformation zone characterized by one crush zone (0.24 m in borehole length), increased frequency of open fractures, sealed network, brittle-ductile shear zone and faint red staining. Decreased magnetic susceptibility and minor decrease in resistivity and P-wave velocity. The host rock is totally dominated by Ävrö quartz monzodiorite (501046).

Poles from crush zone

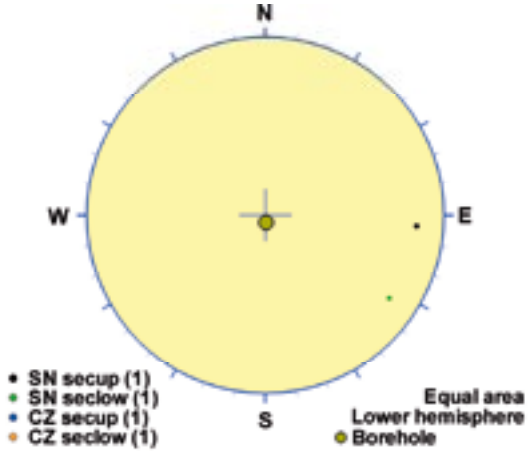

Poles from ductile structures

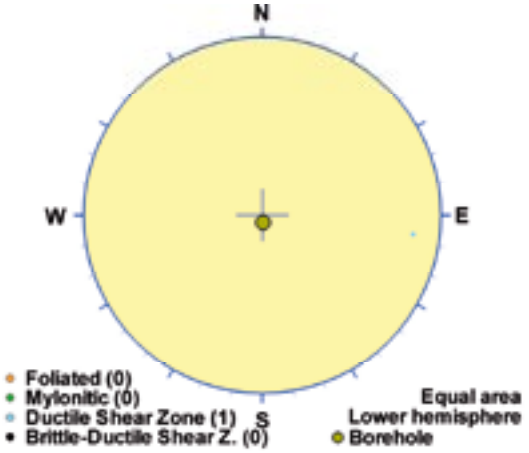

Poles from fractures

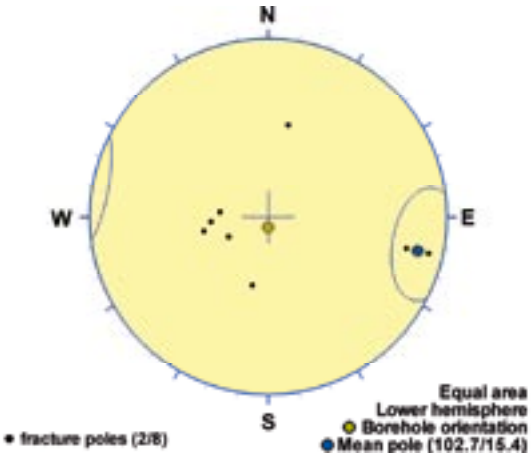

Contours from fractures

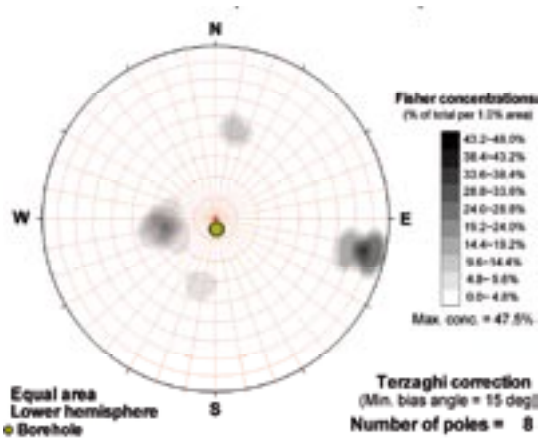

Orientation		Basis for orientation				Certainty	Thickness	
Strike	Dip	Fractures	Crush	Ductile structures	Reflectors	Orientation	Apparent	True
193	75	Used	Verify	Verify		Probable	1.1 m	0.3 m
Comment:								

KLX08 DZ2 (150.32 to 159), brittle zone

Inhomogeneous brittle deformation zone characterized by faint to weak red staining and increased frequency of sealed and open fractures. Six non-oriented radar reflectors occur in the section. Angle to borehole axis varies between 53 and 76º. Decreased radar amplitude between 150 and 160 m. Geophysical loggings indicate general decrease in bulk resistivity and magnetic susceptibility. Several distinct caliper and low p-wave velocity anomalies.The host rock is dominated by Ävrö granodiorite (501056) with subordinate fine-grained diorite-gabbro (505102).

Poles from crush zone

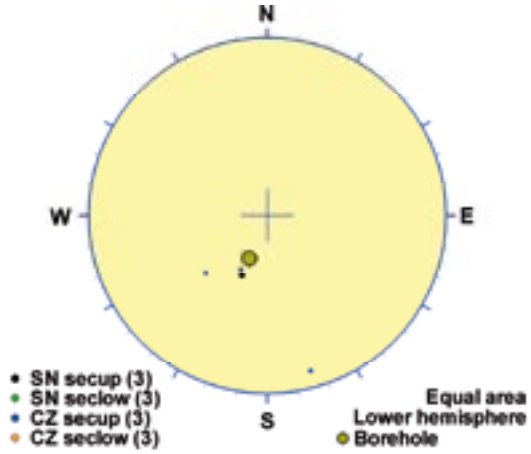

Poles from ductile structures

Data not used

Poles from fractures

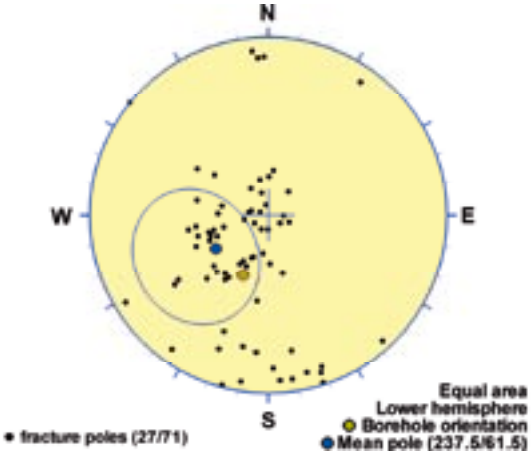

Contours from fractures

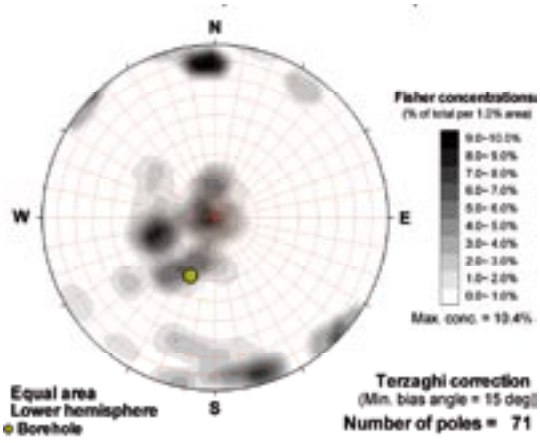

Orientation		Basis for orientation				Certainty	Thickness	
Strike	Dip	Fractures	Crush	Ductile structures	Reflectors	Orientation	Apparent	True
328	29	Used	Verify		Verify	Probable	8.7 m	8.3 m
Comment: fractures scattered								

KLX08 DZ8 (536.5 to 540), brittle zone

Inhomogeneous brittle deformation zone characterized by weak red staining and scattered cm-wide cataclasites. The section 538-539.1 m is characterized by sealed network and cataclasite. Two non-oriented and one oriented radar reflector are identified in the section. Oriented reflector occurs at 537.6 m with the orientation 308/63. The angle to borehole axis of non-oriented reflectors is 51º and 49º. Decreased radar amplitude at 540 m. There is a significant decrease in p-wave velocity in the interval 537-544 m and decreased magnetic susceptibility in interval 536-539 m. At c. 538 m there is one distinct low resistivity anomaly. The host rock is dominated by Ävrö granodiorite (501056) with subordinate fine-grained granite (511058).

Poles from crush zone

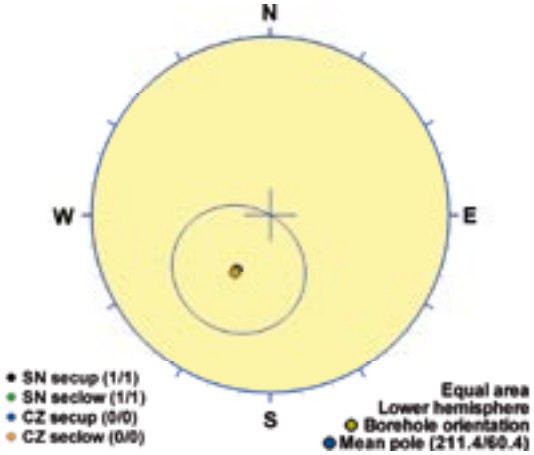

Poles from ductile structures

Data not used

Poles from fractures

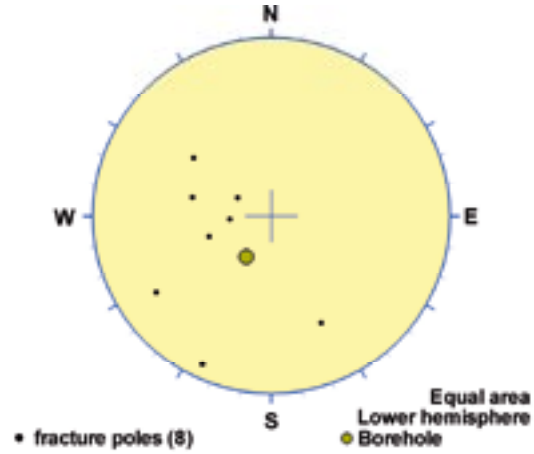

Contours from fractures

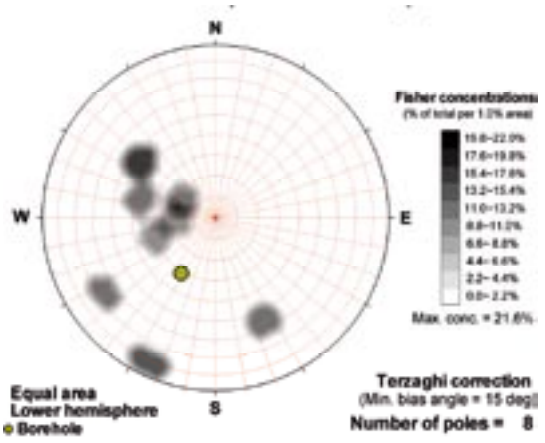

Orientation		Basis for orientation				Certainty	Thickness	
Strike	Dip	Fractures	Crush	Ductile structures	Reflectors	Orientation	Apparent	True
301	30		Used	Contradict	Contradict	Uncertain	3.5 m	3.5 m
Comment: fractures scattered								

KLX08 DZ9 (769 to 778), brittle zone

Inhomogeneous brittle deformation zone characterized by faint to weak red staining and saussuritization, and cataclasite. Crush zones at 769.50-769.56 m, 770.98-771.01 m, 771.58-771.59 m and 771.93-772.07 m. Six non-oriented and one oriented radar reflector are identified in the section. Oriented reflector occurs at 773.4 m with the orientation 223/55. The angle to borehole axis of non-oriented reflectors varies between 30 and 42º. One strong and persistent reflector that intersects the borehole at 775 m with the angle 30º, can be traced at least 40 m away from the borehole. Decreased radar amplitude between 765 and 780 m. The entire section is characterized by low magnetic susceptibility and in the interval c. 760-785 m there is a general decrease in the bulk resistivity. At approximately 772.5 m there are distinct but narrow low resistivity, low p-wave velocity and caliper anomalies. The host rock is dominated by a mixture of Ävrö granodiorite (501056) and diorite/gabbro (501033).

Poles from crush zone

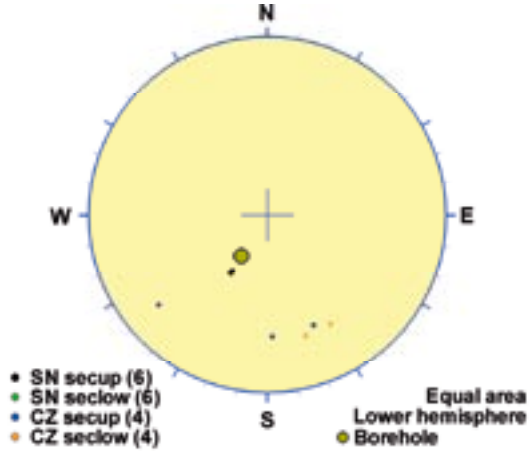

Poles from ductile structures

Data not used

Poles from fractures

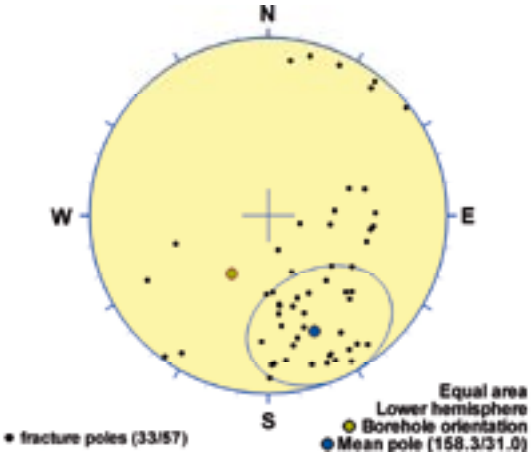

Contours from fractures

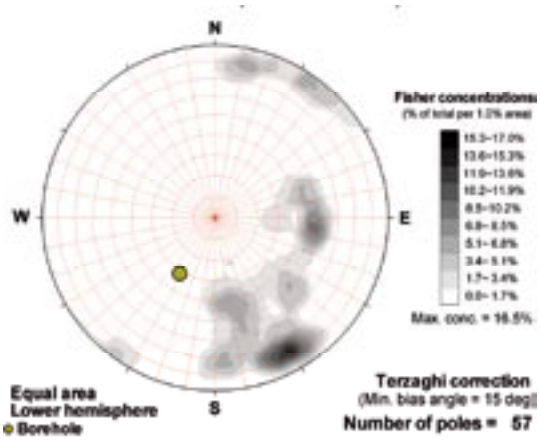

Orientation		Basis for orientation				Certainty	Thickness	
Strike	Dip	Fractures	Crush	Ductile structures	Reflectors	Orientation	Apparent	True
248	59	Used	Verify		Verify	Probable	9 m	6.3 m
Comment:								

KLX08 DZ11 (614.45 to 615), brittle zone

Brittle deformation zone characterized by sealed network, slight increase in frequency of open fractures and faint red staining. Minor decrease in resistivity, magnetic susceptibility, P-wave velocity and caliper anomalies. Three radar reflectors, at 614.5 m, 614.9 m and 615.0 m with the angle 48°, 54° and 16° to borehole axis, respectively. The host rock is dominated by diorite/gabbro (501033) and Ävrö granodiorite (501056).

Poles from crush zone

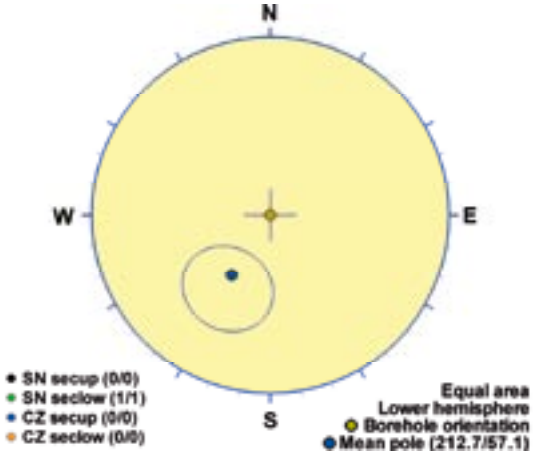

Poles from ductile structures

Data not used

Poles from fractures

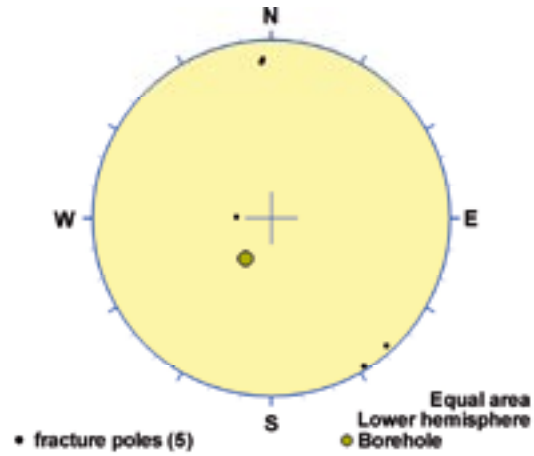

Contours from fractures

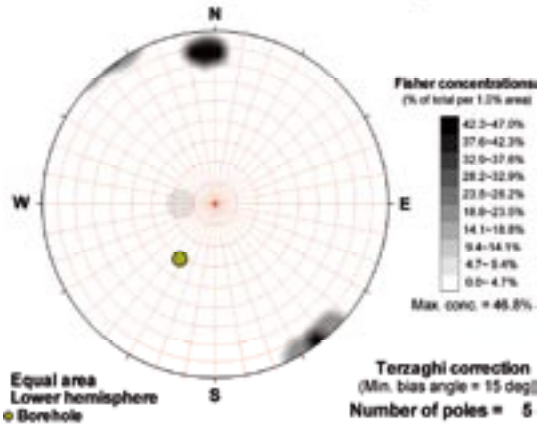

Orientation		Basis for orientation				Certainty	Thickness	
Strike	Dip	Fractures	Crush	Ductile structures	Reflectors	Orientation	Apparent	True
303	33		Used		Contradict	Very uncertain	0.5 m	0.5 m
Comment: fractures scattered								

KLX08 DZ12 (655.3 to 656.15), brittle zone

Brittle deformation zone characterized by increased frequency of open fractures, sealed network, weak red staining and weak saussuritization. Decrease in magnetic susceptibility. Minor decrease in resistivity and P-wave velocity. One radar reflector at 655.5 m with the angle 36° to borehole axis and one at 656.2 m with the orientation 346/72 or 207/44. The host rock is dominated by diorite/gabbro (501033) and Ävrö granodiorite (501056). Subordinate rock type comprises fine-grained granite (511058).

Poles from crush zone

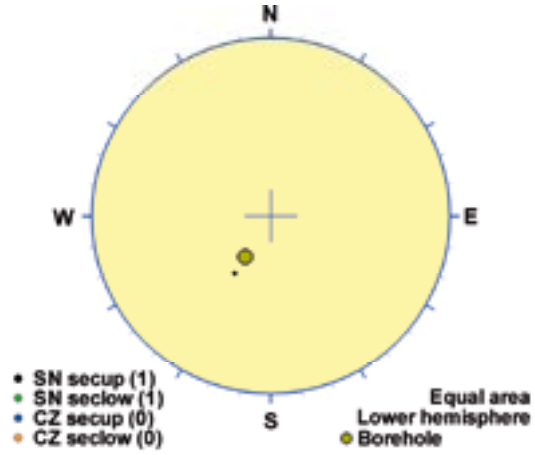

Poles from ductile structures

Data not used

Poles from fractures

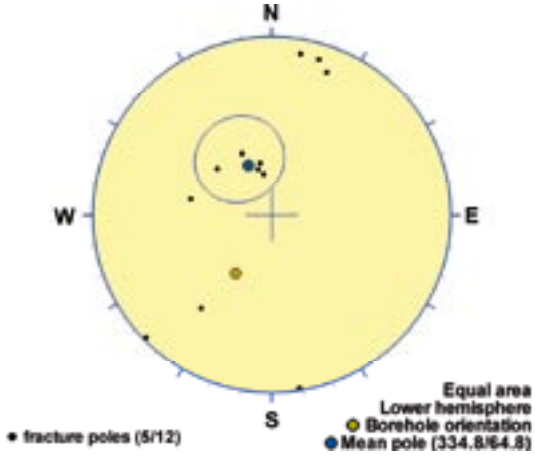

Contours from fractures

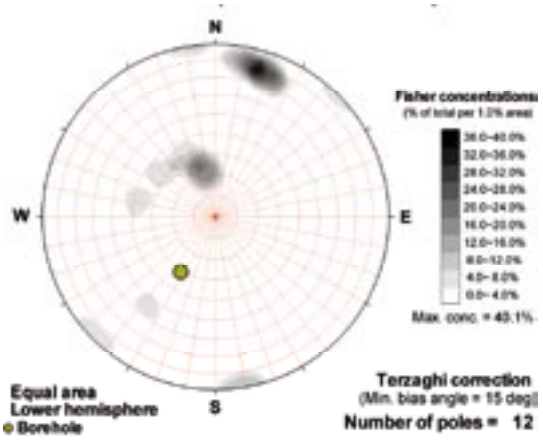

Orientation		Basis for orientation				Certainty	Thickness	
Strike	Dip	Fractures	Crush	Ductile structures	Reflectors	Orientation	Apparent	True
65	25	Used	Contradict		Contradict	Very uncertain	0.9 m	0.6 m
Comment:								

KLX09 DZ1 (105.8 to 106), ductile/brittle zone

Minor brittle and ductile deformation zones including mylonites and cataclasite. Low P-wave velocity, low resistivity and low magnetic susceptibility. One strong and persistent oriented radar reflector occurs at 105.7 m with the orientation 353/39. The host rock is totally dominated by Ävrö granodiorite (501056).

Poles from crush zone

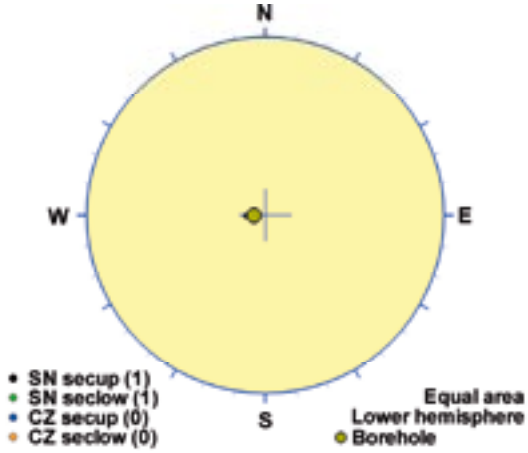

Poles from ductile structures

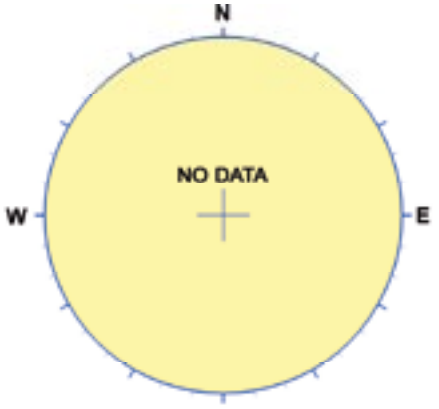

Poles from fractures

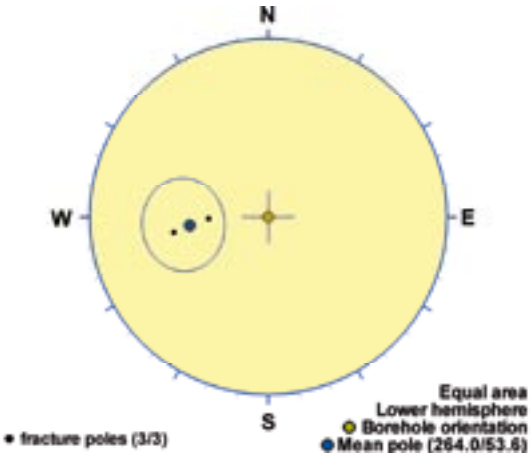

Contours from fractures

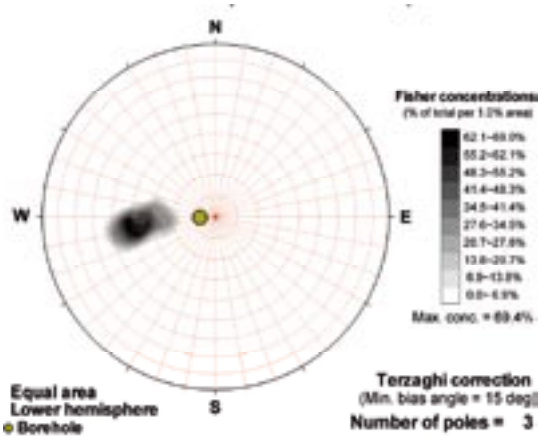

Orientation		Basis for orientation				Certainty	Thickness	
Strike	Dip	Fractures	Crush	Ductile structures	Reflectors	Orientation	Apparent	True
354	36	Used			Verify	Probable	0.2 m	0.2 m
Comment:								

KLX09 DZ2 (137.6 to 138), brittle zone

Red staining and thin cataclastic zones. Low P-wave velocity, low resistivity and low magnetic susceptibility. One non-oriented radar reflector occurs at 138.2 m with the angle 53º to borehole axis. The host rock is totally dominated by Ävrö quartz monzodiorite (501046).

Poles from crush zone

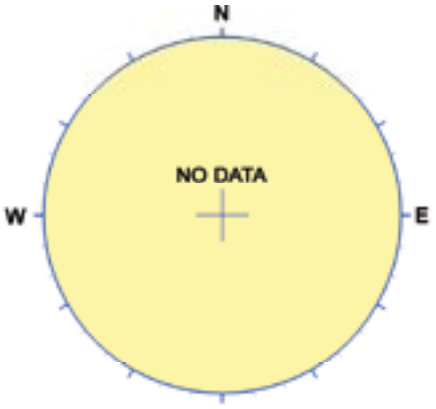

Poles from ductile structures

Data not used

Poles from fractures

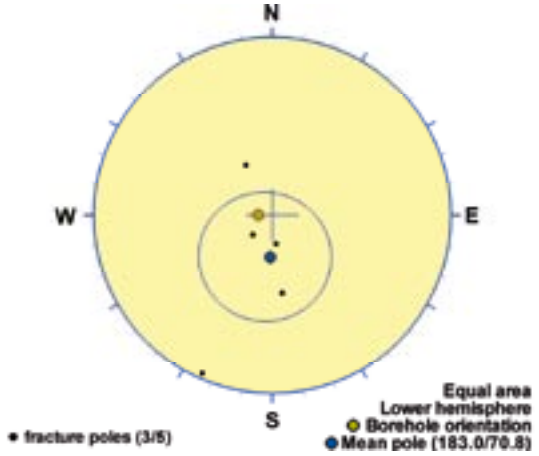

Contours from fractures

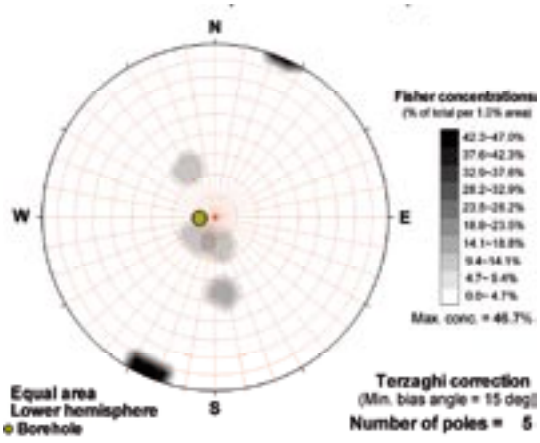

Orientation		Basis for orientation				Certainty	Thickness	
Strike	Dip	Fractures	Crush	Ductile structures	Reflectors	Orientation	Apparent	True
273	19	Used				Uncertain	0.4 m	0.4 m
Comment:								

KLX09 DZ3 (147 to 148), brittle zone

Increased frequency of sealed and open fractures. The section is characterized by red staining. Low P-wave velocity, low resistivity, caliper anomaly and low magnetic susceptibility. The host rock is totally dominated by Ävrö granodiorite (501056). Subordinate rock type is fine-grained granite (511058).

Poles from crush zone

Poles from ductile structures

Data not used

Poles from fractures

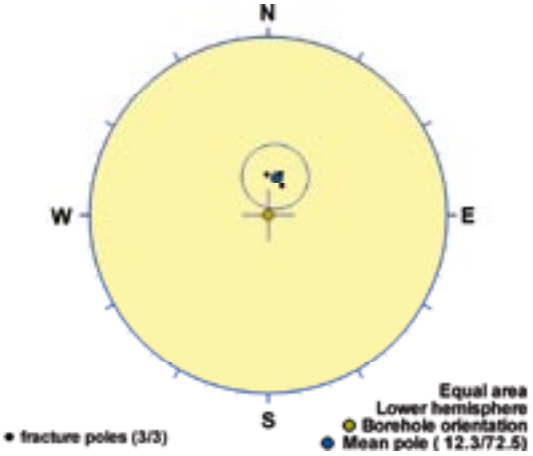

Contours from fractures

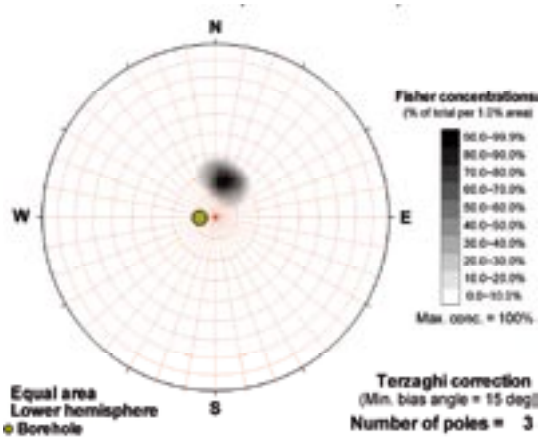

Orientation		Basis for orientation				Certainty	Thickness	
Strike	Dip	Fractures	Crush	Ductile structures	Reflectors	Orientation	Apparent	True
102	18	Used				Probable	1 m	0.9 m
Comment:								

KLX09 DZ4 (206 to 209), brittle zone

Increased frequency of sealed and open fractures and sealed network. Crush rock in the section 207.66-208.14 m. The section is characterized by red staining. Low P-wave velocity, low resistivity and low magnetic susceptibility. One strong and persistent oriented radar reflector occurs at 208.3 m with the orientation 066/46 or 261/42. Two non-oriented radar reflectors at 207.2 m and 208.9 m with the angle 55º and 65º to borehole axis, respectively. The host rock is totally dominated by Ävrö granodiorite (501056). Subordinate rock type is fine-grained granite (511058).

Poles from crush zone

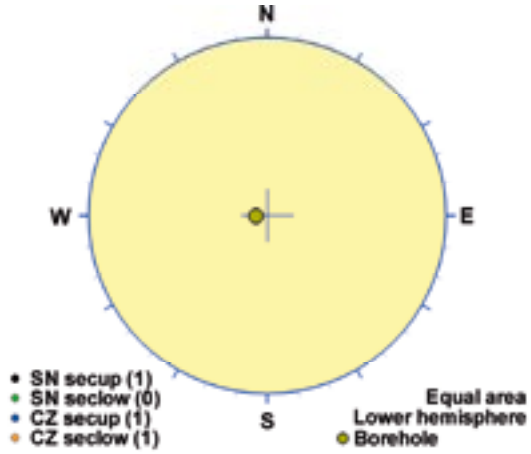

Poles from ductile structures

Data not used

Poles from fractures

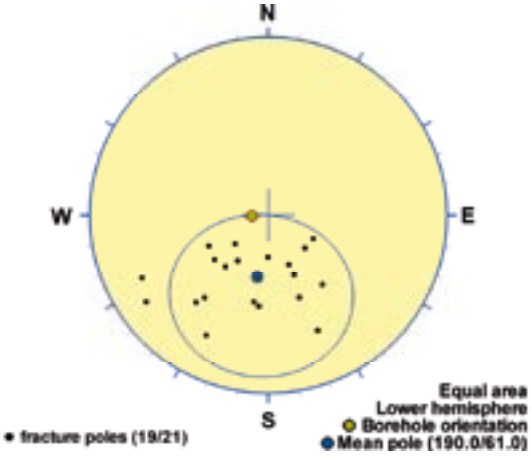

Contours from fractures

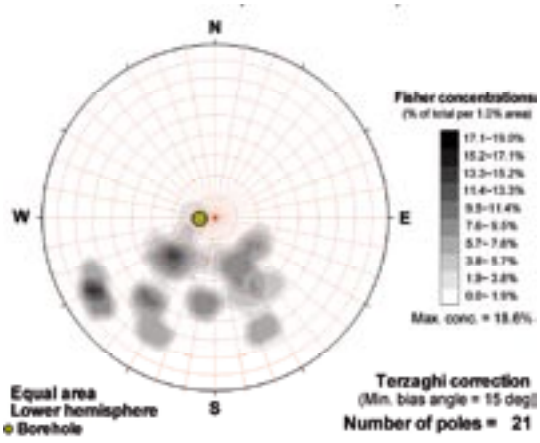

Orientation		Basis for orientation				Certainty	Thickness	
Strike	Dip	Fractures	Crush	Ductile structures	Reflectors	Orientation	Apparent	True
280	29	Used			Verify	Certain	3 m	2.6 m
Comment:								

KLX09 DZ5 (261.8 to 264), brittle zone

Increased frequency of sealed and open fractures and sealed network. The section is characterized by red staining. Crush rock in the section 262.29-262.46 m. Low P-wave velocity, low resistivity and low magnetic susceptibility. One oriented radar reflector occurs at 262.8 m with the orientation 088/22 or 301/26 and one non-oriented at 261.8 m with the angle 67º to borehole axis. The host rock is totally dominated by Ävrö granodiorite (501056).

Poles from crush zone

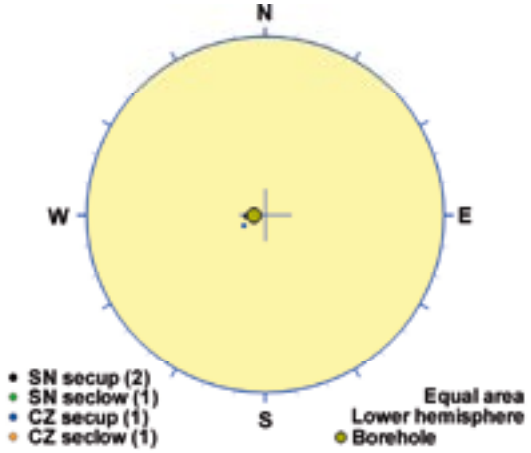

Poles from ductile structures

Data not used

Poles from fractures

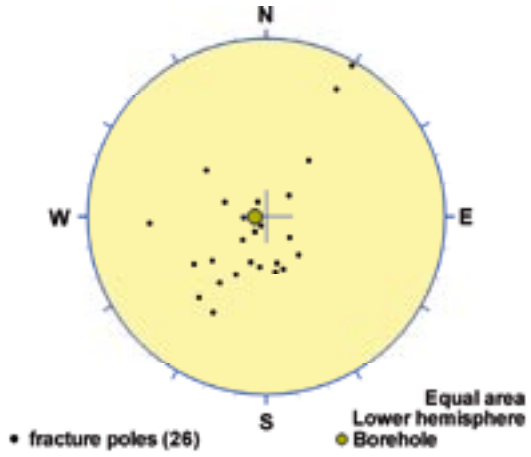

Contours from fractures

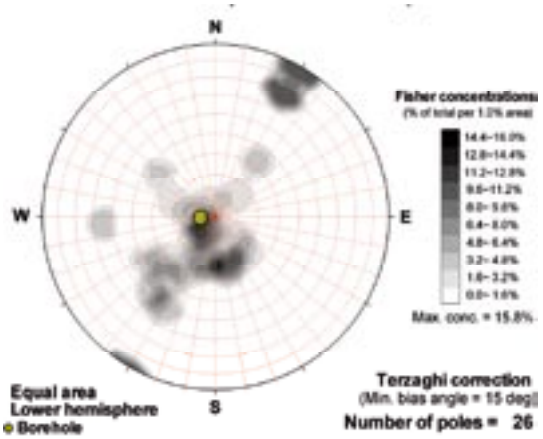

Orientation		Basis for orientation				Certainty	Thickness	
Strike	Dip	Fractures	Crush	Ductile structures	Reflectors	Orientation	Apparent	True
334	11	Verify	Used		Verify	Probable	2.2 m	2.2 m
Comment:								

KLX09 DZ6 (272 to 276), brittle zone

Increased frequency of sealed and open fractures and sealed network. The section is characterized by red staining. Epidote filled fractures and cataclastic bands parallel with core axis. Low P-wave velocity and low magnetic susceptibility. One non-oriented radar reflector occurs at 272.2 m with the angle 62º to borehole axis. The host rock is totally dominated by Ävrö granodiorite (501056). Subordinate rock type is fine-grained granite (511058).

Poles from crush zone

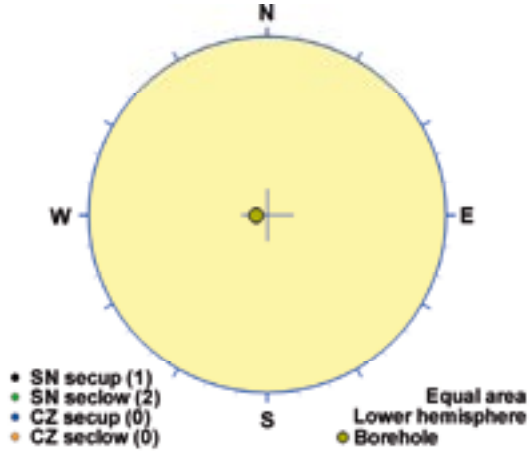

Poles from ductile structures

Data not used

Poles from fractures

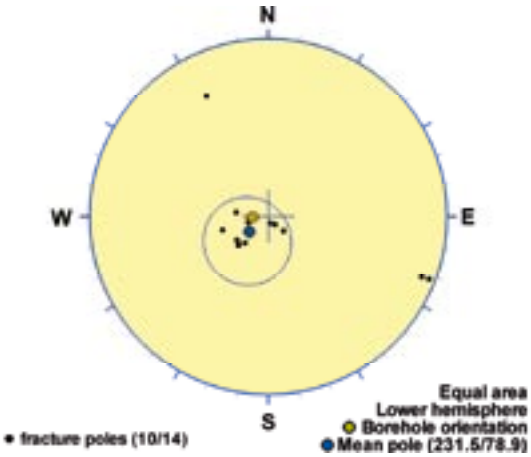

Contours from fractures

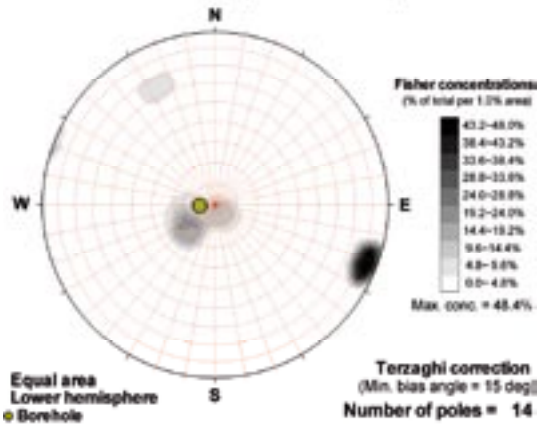

Orientation		Basis for orientation				Certainty	Thickness	
Strike	Dip	Fractures	Crush	Ductile structures	Reflectors	Orientation	Apparent	True
322	11	Used				Probable	4 m	4 m
Comment:								

KLX09 DZ7 (313 to 323.2), brittle zone

Increased frequency of sealed and open fractures and sealed network. Crush rock in the section 322.39-322.90 m. Some fractures with large apertures. The section is characterized by red staining and cataclasite are present. Low P-wave velocity, low resistivity and low magnetic susceptibility. Three non-oriented radar reflectors occur at 315.4 m, 319.8 m and 323.2 m with the angle 45º, 49º and 54º to borehole axis, respectively. The host rock is dominated by Ävrö granodiorite (501056). Fine-grained diorite-gabbro (505102) constitutes an important subordinate rock type. In addition, minor occurrences of fine-grained granite (511058) and pegmatite (501061). .

Poles from crush zone

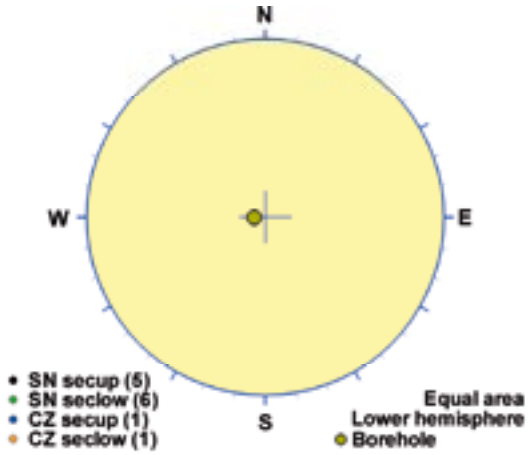

Poles from ductile structures

Data not used

Poles from fractures

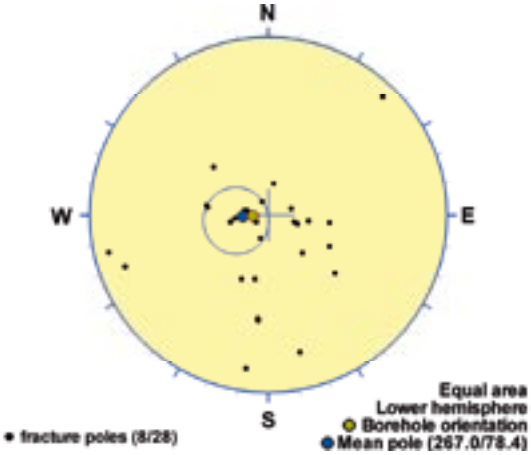

Contours from fractures

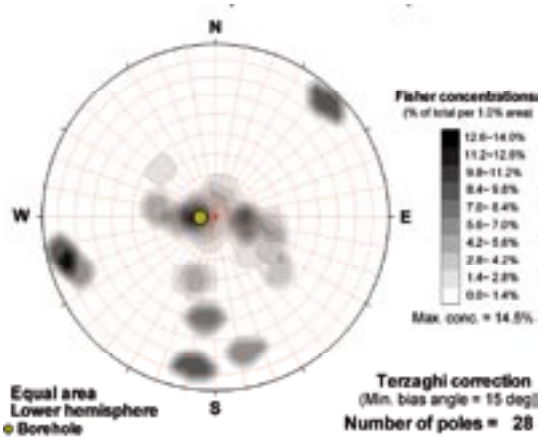

Orientation		Basis for orientation				Certainty	Thickness	
Strike	Dip	Fractures	Crush	Ductile structures	Reflectors	Orientation	Apparent	True
357	12	Used	Verify		Contradict	Very uncertain	10.2 m	10.2 m
Comment:								

KLX09 DZ8 (440 to 446), brittle zone

High frequency of sealed fractures and increased frequency of open fractures and sealed network. The section is characterized by intense red staining and inhomogeneous epidotization (442-443 m) and cataclasite (443.3-443.5 m). Low resistivity and low magnetic susceptibility. Three non-oriented radar reflectors occur at 441.9 m, 442.7 m and 442.7 m with the angle 47º, 68º and 53º to borehole axis, respectively. The host rock is totally dominated by Ävrö granodiorite (501056). Subordinate rock type is fine-grained granite (511058). .

Poles from crush zone

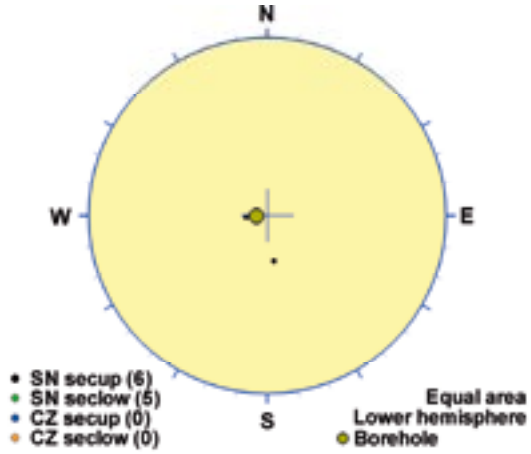

Poles from ductile structures

Data not used

Poles from fractures

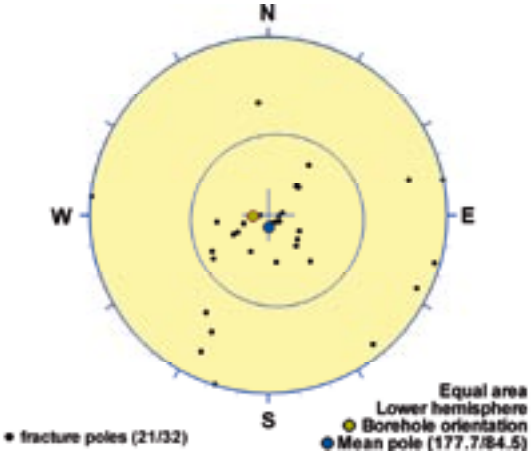

Contours from fractures

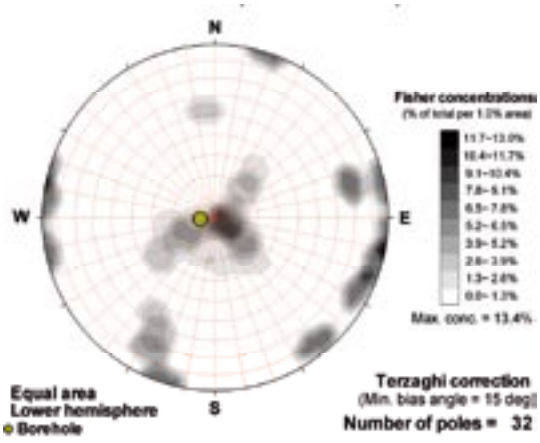

Orientation		Basis for orientation				Certainty	Thickness	
Strike	Dip	Fractures	Crush	Ductile structures	Reflectors	Orientation	Apparent	True
268	6	Used	Verify		Contradict	Probable	6 m	5.9 m
Comment:								

KLX09 DZ9 (492.4 to 509), brittle zone

High frequency of sealed and open fractures and sealed network. Crush rock in the section 494.78-494.84 m. Some fractures with large apertures. The section is characterized by red staining. Low P-wave velocity, low resistivity and low magnetic susceptibility. Three non-oriented radar reflectors occur at 493.6 m, 495.9 m and 500.6 m with the angle 61º, 71º and 25º to borehole axis, respectively. The host rock is dominated by a mixture of Ävrö granodiorite (501056) and fine-grained dioritoid (501030). Subordinate rock types comprise fine-grained granite (511058) and granite (501058).

Poles from crush zone

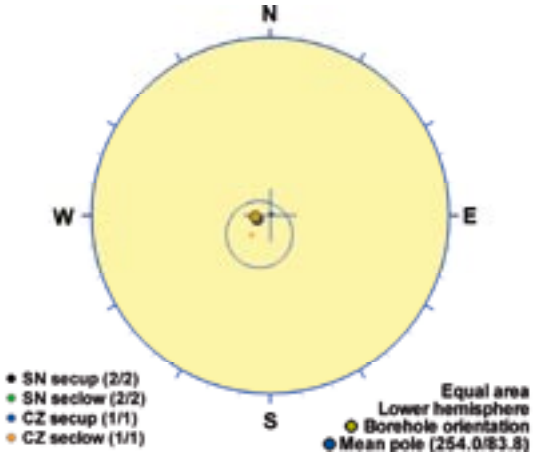

Poles from ductile structures

Data not used

Poles from fractures

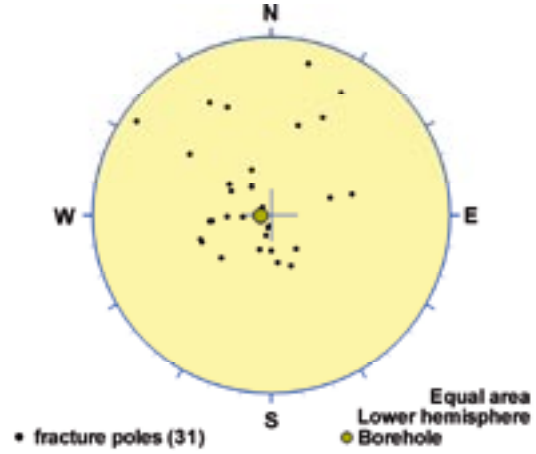

Contours from fractures

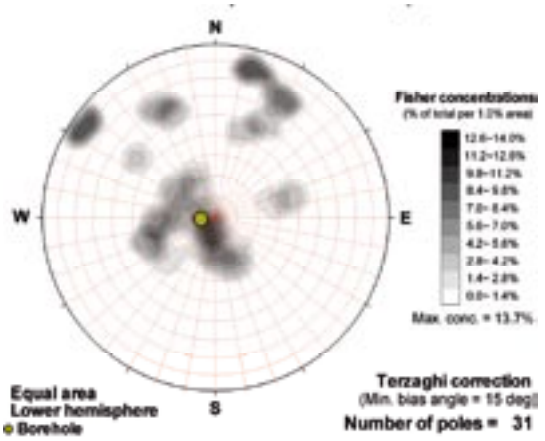

Orientation		Basis for orientation				Certainty	Thickness	
Strike	Dip	Fractures	Crush	Ductile structures	Reflectors	Orientation	Apparent	True
320	26	Verify	Used		Contradict	Probable	16.6 m	6.2 m
Comment: Stucture defined in boremap to (s/d) 320/26. Overrules interpretation above.								

KLX09 DZ11 (611 to 618.3), brittle zone

Increased frequency of sealed and open fractures and sealed network. The section is characterized by inhomogeneous distribution of red staining and cataclastic bands. Low resistivity. Three non-oriented radar reflectors occur at 613.4 m, 614.3 m and 616.5 m with the angle 83º, 38º and 77º to borehole axis, respectively. The host rock is totally dominated by Ävrö granodiorite (501056). Subordinate rock types comprise fine-grained granite (511058) and fine-grained diorite-gabbro (505102).

Poles from crush zone

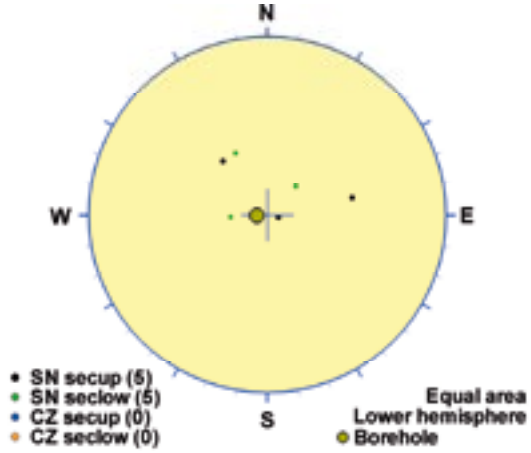

Poles from ductile structures

Data not used

Poles from fractures

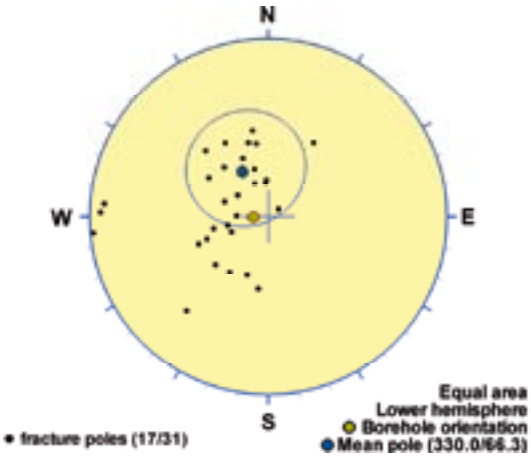

Contours from fractures

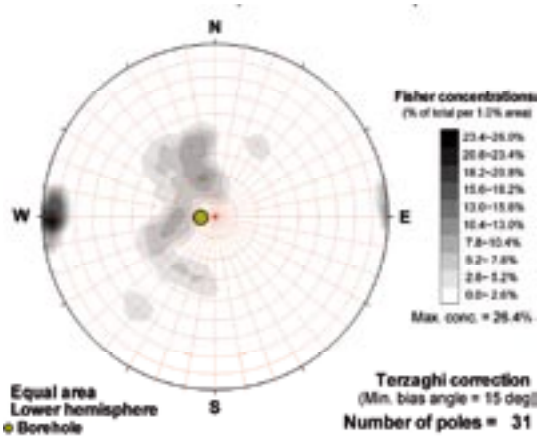

Orientation		Basis for orientation				Certainty	Thickness	
Strike	Dip	Fractures	Crush	Ductile structures	Reflectors	Orientation	Apparent	True
60	24	Used	Verify		Verify	Probable	7.3 m	6.8 m
Comment:								

KLX09 DZ12 (648.6 to 649.6), brittle zone

Increased frequency of sealed fractures. Inhomogeneous distribution of red staining and cataclastic bands in the section. One relatively strong non-oriented radar reflector occurs at 649.7 m with the angle 47º to borehole axis. The host rock is totally dominated by Ävrö granodiorite (501056). Subordinate rock types comprise fine-grained granite (511058) and granite (501058).

Poles from crush zone

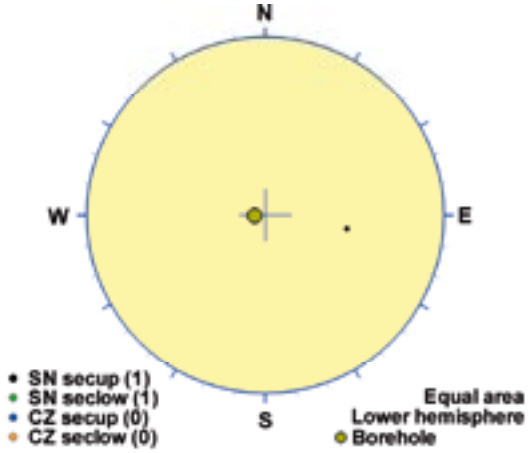

Poles from ductile structures

Data not used

Poles from fractures

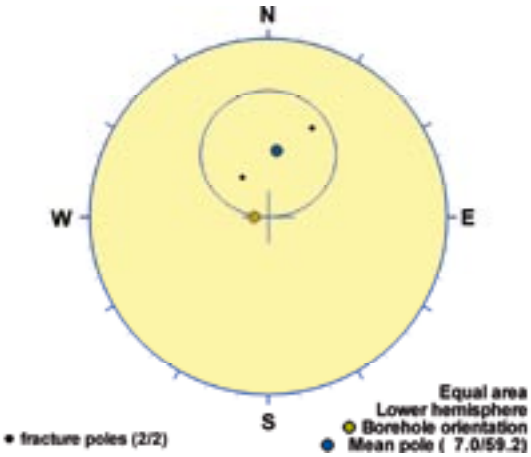

Contours from fractures

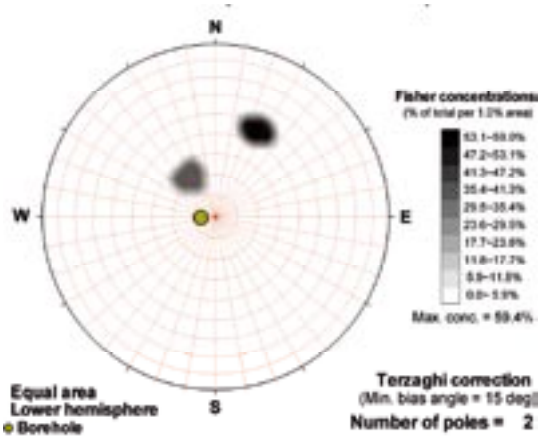

Orientation		Basis for orientation				Certainty	Thickness	
Strike	Dip	Fractures	Crush	Ductile structures	Reflectors	Orientation	Apparent	True
97	31	Used	Contradict		Verify	Probable	1 m	0.8 m
Comment:								

KLX09 DZ14 (744.5 to 761), brittle zone

High frequency of sealed and open fractures and sealed network. Some fractures with large apertures. Three sections with crush rock at 755.83-756.0 m, 756.72-756.80 m and 757.18-757.58 m. Core loss in the interval 756.0-756.2 m. The section is characterized by red staining and scattered cataclastic bands. 754.5-761 m is the most damaged part. Low P-wave velocity, low resistivity, caliper anomaly and low magnetic susceptibility. Four relatively strong and persistent non-oriented radar reflectors occur at 746.2 m, 752.7 m, 754.6 m and 758.5 m with the angles 69º, 41º, 32º and 24º to borehole axis, respectively. The host rock is dominated by a mixture of Ävrö granodiorite (501056) with subordinate Ävrö quartz monzodiorite (501046) and fine-grained dioritoid (501030). Subordinate rock types comprise fine-grained granite (511058), fine-grained diorite-gabbro (505102) and pegmatite (501061).

Poles from crush zone

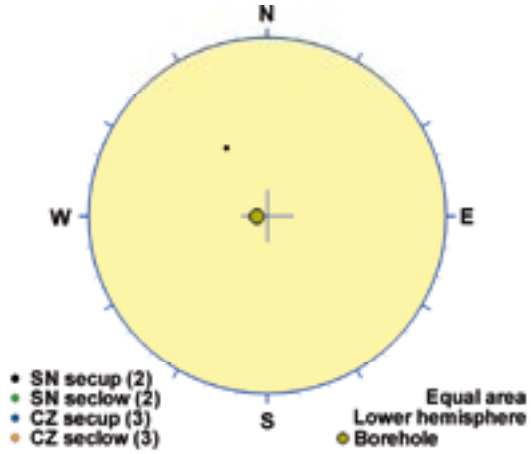

Poles from ductile structures

Data not used

Poles from fractures

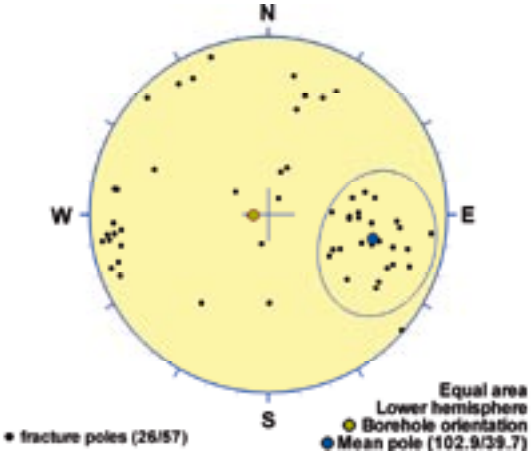

Contours from fractures

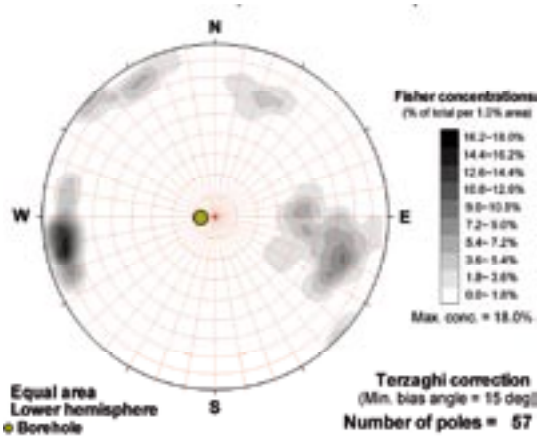

Orientation		Basis for orientation				Certainty	Thickness	
Strike	Dip	Fractures	Crush	Ductile structures	Reflectors	Orientation	Apparent	True
193	50	Used	Verify		Verify	Probable	16.5 m	9 m
Comment: Fractures from BIPS verify the intepretation.								

KLX09 DZ15 (799.6 to 803), brittle zone

Increased distribution of red staining. Strongly quartz and epidote sealed section in the interval 800.60-801.23 m. Strong epidotization in the interval 802.90-803.40 m. Low resistivity and low magnetic susceptibility. The host rock is totally dominated by Ävrö granodiorite (501056). Subordinate rock types comprise fine-grained granite (511058) and fine-grained dioritoid (501030).

Poles from crush zone

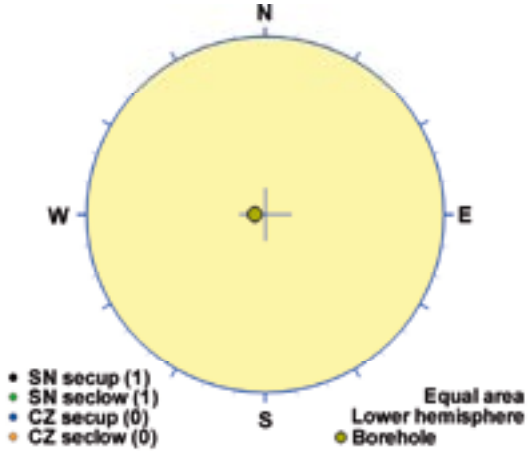

Poles from ductile structures

Data not used

Poles from fractures

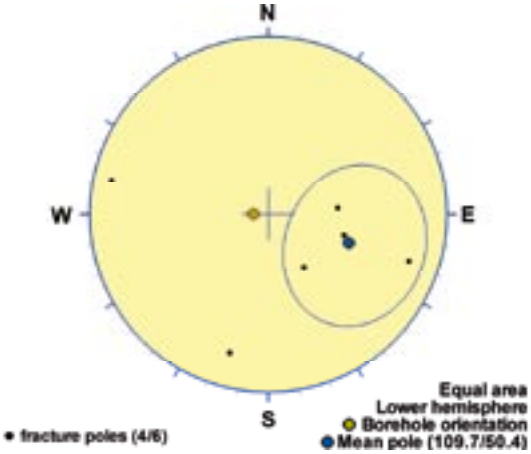

Contours from fractures

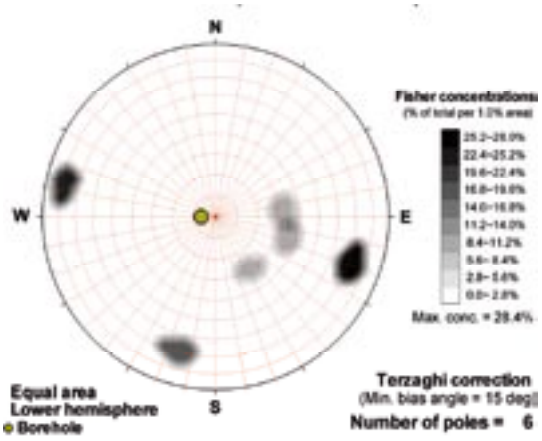

Orientation		Basis for orientation				Certainty	Thickness	
Strike	Dip	Fractures	Crush	Ductile structures	Reflectors	Orientation	Apparent	True
200	40	Used				Uncertain	3.4 m	2.4 m
Comment:								

KLX09 DZ16 (815 to 815.25), brittle zone

Minor deformation zone including red staining and cataclastic bands. Low P-wave velocity, low resistivity and low magnetic susceptibility. One non-oriented radar reflector occurs at 815.0 m with the angle 55º to borehole axis. The host rock is totally dominated by Ävrö granodiorite (501056).

Poles from crush zone

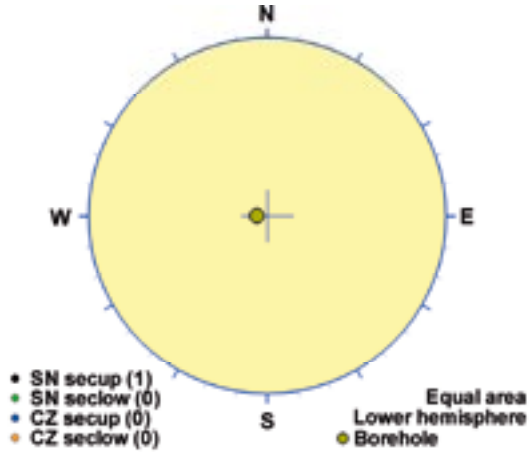

Poles from ductile structures

Data not used

Poles from fractures

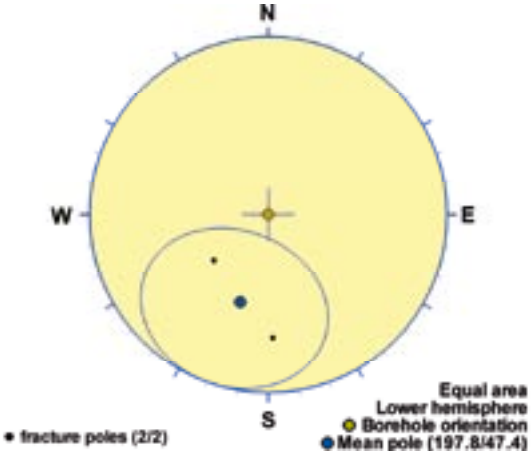

Contours from fractures

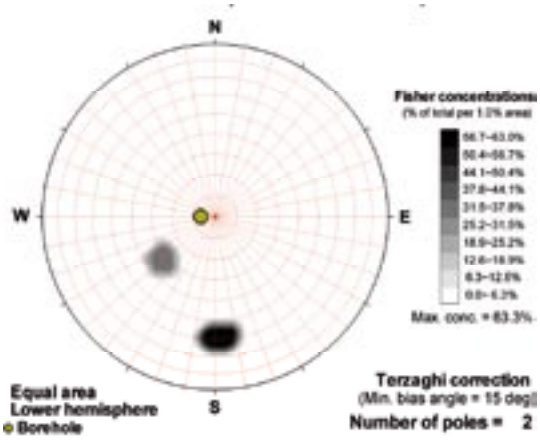

Orientation		Basis for orientation				Certainty	Thickness	
Strike	Dip	Fractures	Crush	Ductile structures	Reflectors	Orientation	Apparent	True
288	43	Used			Verify	Uncertain	0.2 m	0.2 m
Comment:								

KLX09 DZ17 (848.7 to 852.6), brittle zone

Increased distribution of red staining and scattered cataclastic bands. Low resistivity, caliper anomaly and low magnetic susceptibility. One non-oriented radar reflector occurs at 852.1 m with the angle 46º to borehole axis. The host rock is totally dominated by Ävrö granodiorite (501056). Subordinate rock types comprise fine-grained granite (511058).

Poles from crush zone

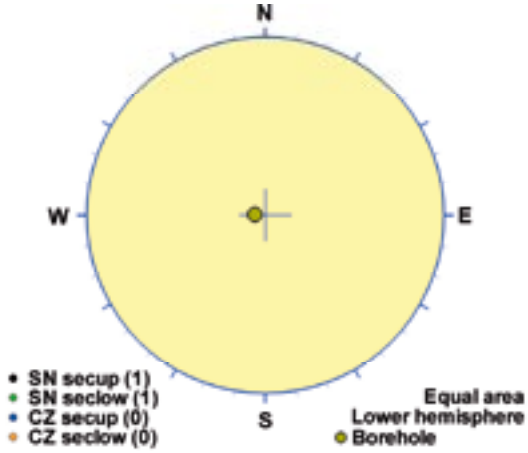

Poles from ductile structures

Data not used

Poles from fractures

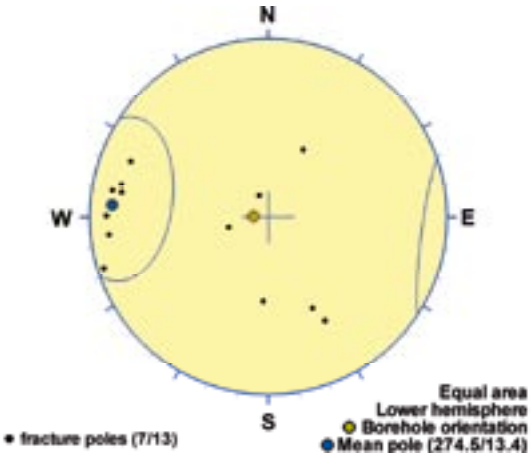

Contours from fractures

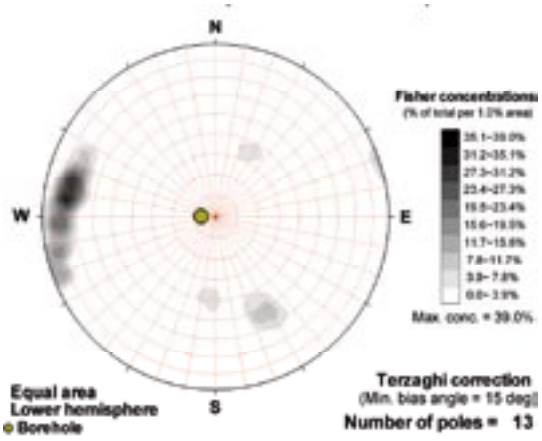

Orientation		Basis for orientation				Certainty	Thickness	
Strike	Dip	Fractures	Crush	Ductile structures	Reflectors	Orientation	Apparent	True
5	77	Used			Contradict	Probable	3.9 m	1.3 m
Comment:								

KLX09 DZ18 (867.8 to 869.7), brittle zone

Increased distribution of red staining, scattered cataclastic bands. Low resistivity and low magnetic susceptibility. The host rock is totally dominated by Ävrö granodiorite (501056). Subordinate rock types comprise fine-grained granite (511058).

Poles from crush zone

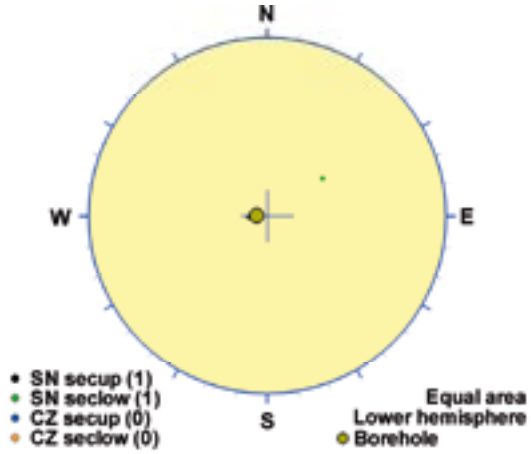

Poles from ductile structures

Data not used

Poles from fractures

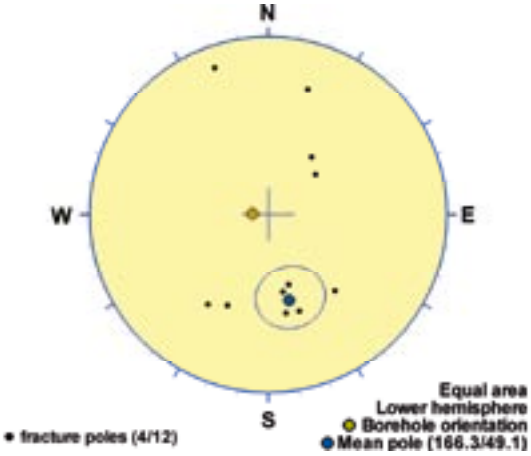

Contours from fractures

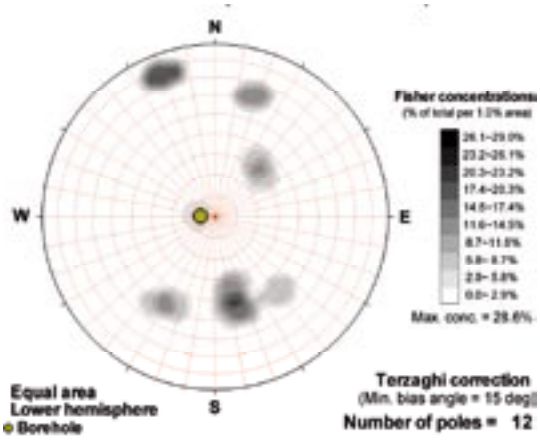

Orientation		Basis for orientation				Certainty	Thickness	
Strike	Dip	Fractures	Crush	Ductile structures	Reflectors	Orientation	Apparent	True
256	41	Used	Contradict			Uncertain	1.9 m	1.4 m
Comment:								

KLX09B DZ1 (49.14 to 49.65), brittle zone

Brittle deformation zone characterized by increased frequency of open and sealed fractures, weak red staining and one crush zone. Decreased resistivity, magnetic susceptibility and partly decreased P-wave velocity. The host rock is dominated by fine-grained granite (511058).

Poles from crush zone

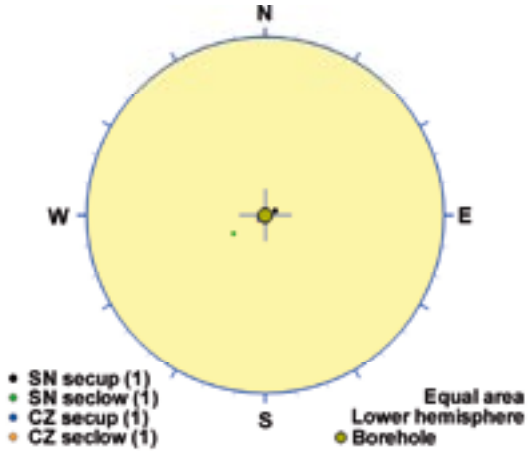

Poles from ductile structures

Data not used

Poles from fractures

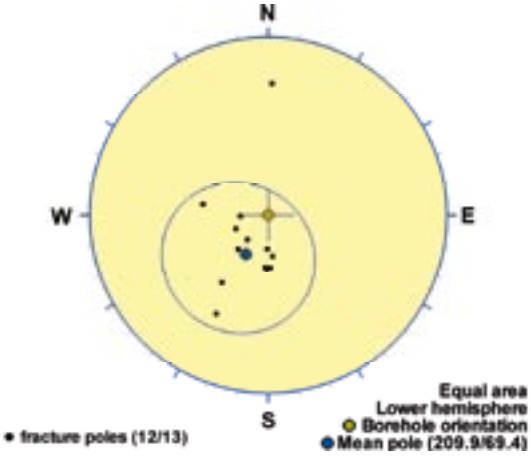

Contours from fractures

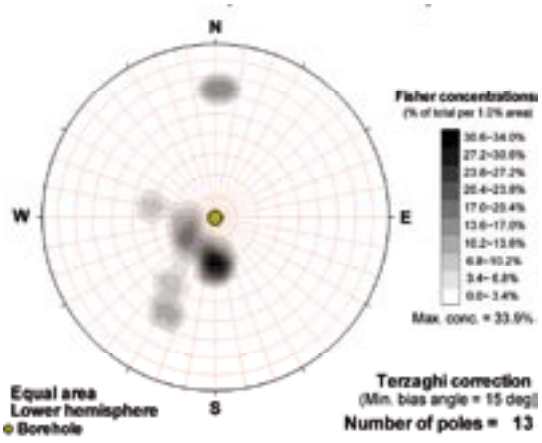

Orientation		Basis for orientation				Certainty	Thickness	
Strike	Dip	Fractures	Crush	Ductile structures	Reflectors	Orientation	Apparent	True
300	21	Used	Verify			Probable	0.5 m	0.5 m
Comment:								

KLX09B DZ2 (74.55 to 79.3), ductile/brittle zone

Inhomogeneous low-grade ductile shear zone overprinted by brittle deformation. Increased frequency of particularly sealed but also open fractures, faint to strong red staining, two crush zones, large apertures, slickensides and mylonitic sections. The most intensely deformed sections (cores) are 74.75-75.06 m and 77.58-78.15 m. Significantly decreased resistivity, magnetic susceptibility and partly decreased P-wave velocity. At c. 78.0 m there is a major drop in fluid water resistivity, which is most likely related to a water bearing structure. One strong radar reflector occurs at 78.9 m with the orientation 288/18 or 108/18. Low radar amplitude at 75-80 m. The host rock is dominated by Ävrö granodiorite (501056). Subordinate rock types comprise fine-grained granite (511058) and fine-grained diorite-gabbro (505102).

Poles from crush zone

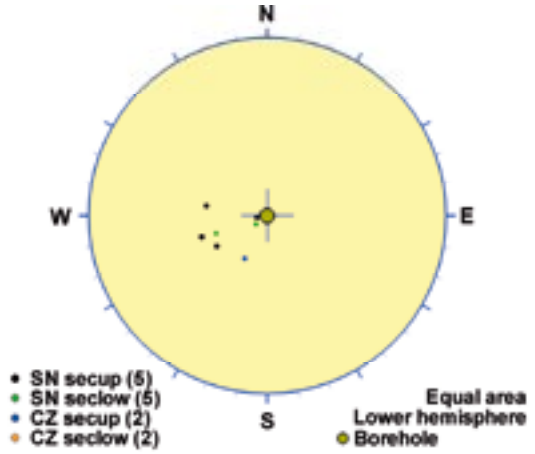

Poles from ductile structures

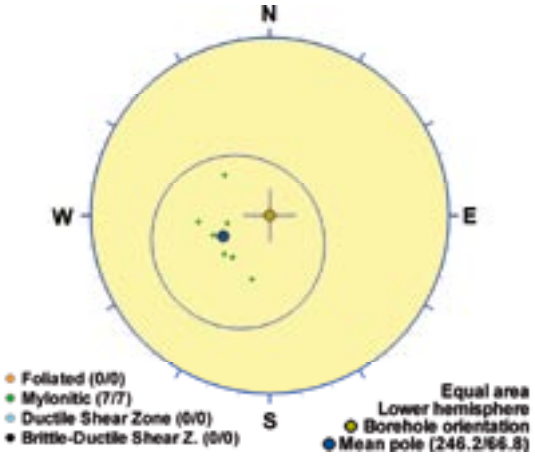

Poles from fractures

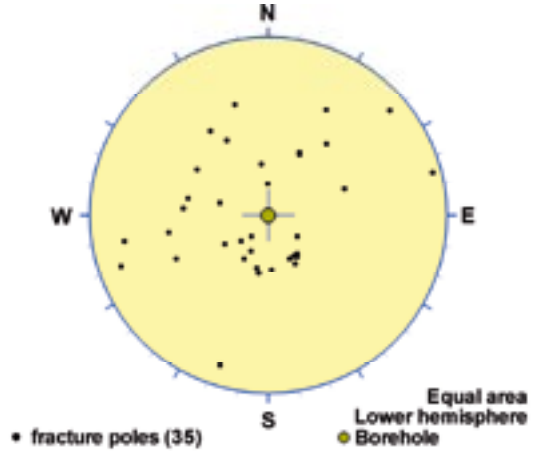

Contours from fractures

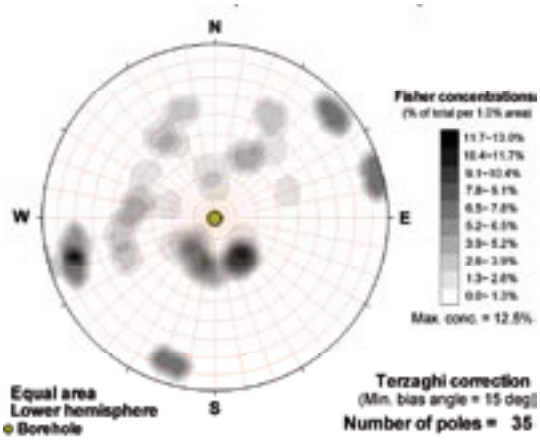

Orientation		Basis for orientation				Certainty	Thickness	
Strike	Dip	Fractures	Crush	Ductile structures	Reflectors	Orientation	Apparent	True
336	23	Verify	Verify	Used	Verify	Certain	4.8 m	4.4 m
Comment:								

KLX09C DZ1 (81.3 to 86.3), ductile/brittle zone

Low grade ductile shear zone overprinted by brittle deformation. Increased frequency of sealed fractures and a slight increase in open fractures, large apertures and mylonitic sections. The most intensely deformed section (core) is 82.81-85.63 m. One non-oriented radar reflector occurs at 82.9 m with the angle 72° to borehole axis and one reflector at 86.3 m with the orientation 238/11 or 253/53. Low radar amplitude at 85-90 m. The host rock is totally dominated by Ävrö granite (501044). Subordinate rock type comprises very sparse occurrence of pegmatite (501061).

Poles from crush zone

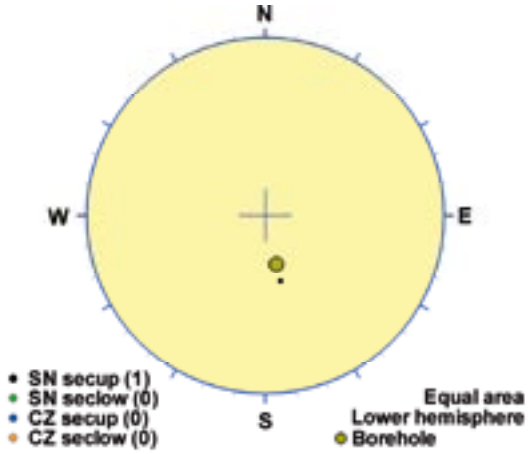

Poles from ductile structures

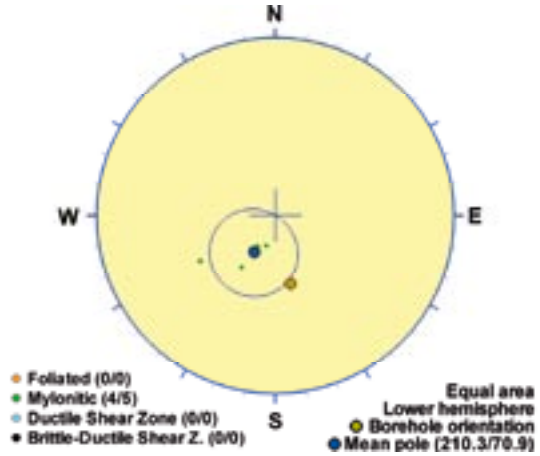

Poles from fractures

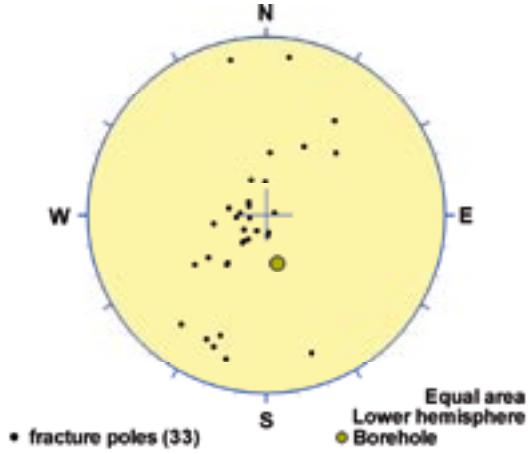

Contours from fractures

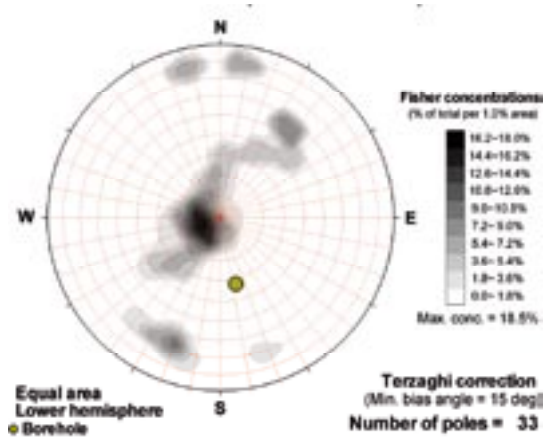

Orientation		Basis for orientation				Certainty	Thickness	
Strike	Dip	Fractures	Crush	Ductile structures	Reflectors	Orientation	Apparent	True
300	19	Verify	Contradict	Used	Contradict	Probable	5 m	4.6 m
Comment:								

KLX09C DZ2 (114.85 to 117), brittle zone

Brittle deformation zone characterized by increased frequency of sealed and open fractures, one crush zone and slickensides. One strong non-oriented radar reflector occurs at 117.4 m (just below DZ2) with the angle 40° to borehole axis. Low radar amplitude occurs at 115-120 m. The host rock is dominated by Ävrö granite (501044). Subordinate rock types comprise fine-grained diorite-gabbro (505102), fine-grained granite (511058) and pegmatite (501061).

Poles from crush zone

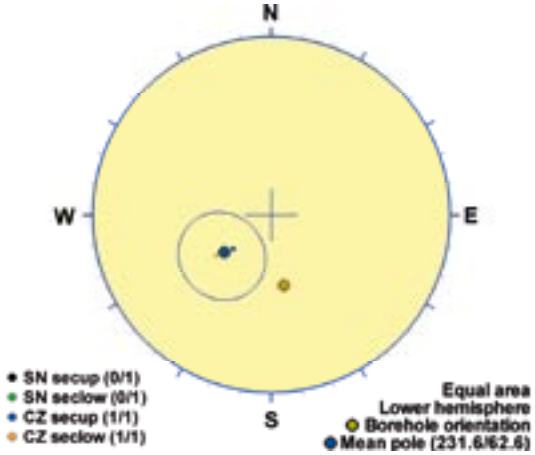

Poles from ductile structures

Data not used

Poles from fractures

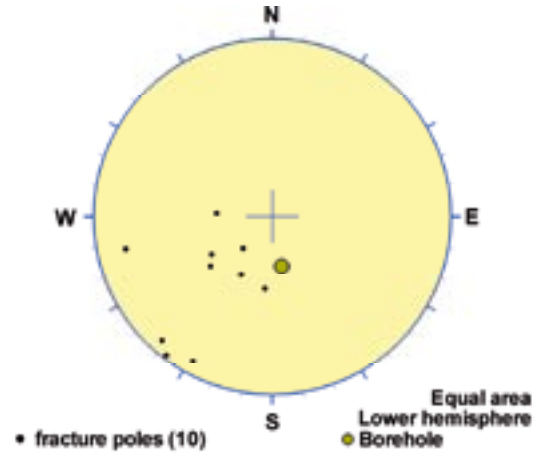

Contours from fractures

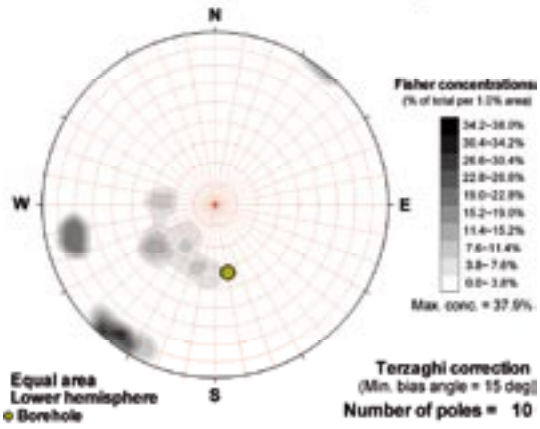

Orientation		Basis for orientation				Certainty	Thickness	
Strike	Dip	Fractures	Crush	Ductile structures	Reflectors	Orientation	Apparent	True
322	27	Verify	Used		Contradict	Probable	2.2 m	1.9 m
Comment:								

KLX09D DZ1 (81.4 to 89.52), ductile/brittle zone

Low grade ductile shear zone overprinted by brittle deformation. Increased frequency of sealed and open fractures, faint to medium red staining, large apertures, slickensides and mylonitic sections. Significantly decreased bulk resistivity and bulk magnetic susceptibility. Partly decreased P-wave velocity. Two non-oriented radar reflectors occur at 83.5 m and 84.0 m with the angle 59° and 26° to borehole axis, respectively. Also, one radar reflector occurs at 88.1 m with the orientation 017/44 or 335/21. Low radar amplitude occurs at 80-90 m. The host rock is dominated by Ävrö granodiorite (501056). Subordinate rock types comprise fine-grained granite (511058) and sparse occurrences of pegmatite (501061) and granite (501058).

Poles from crush zone

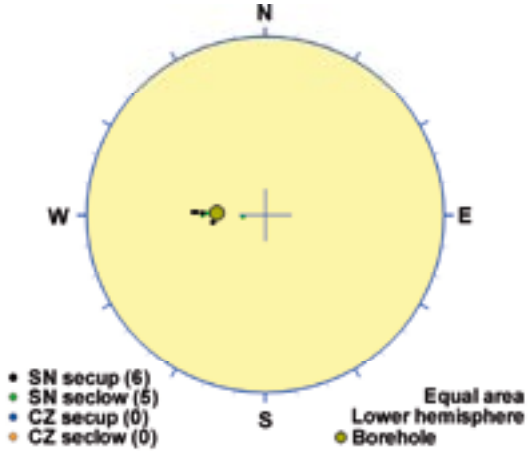

Poles from ductile structures

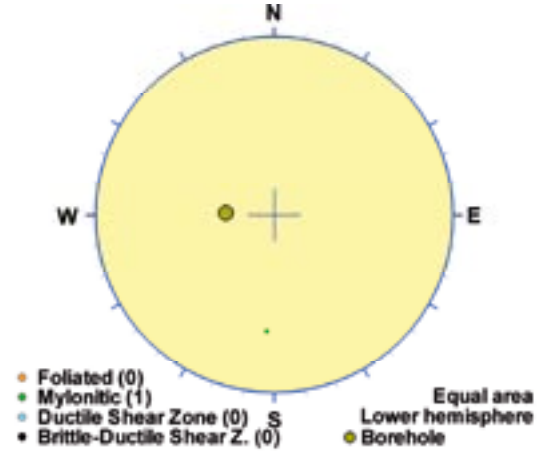

Poles from fractures

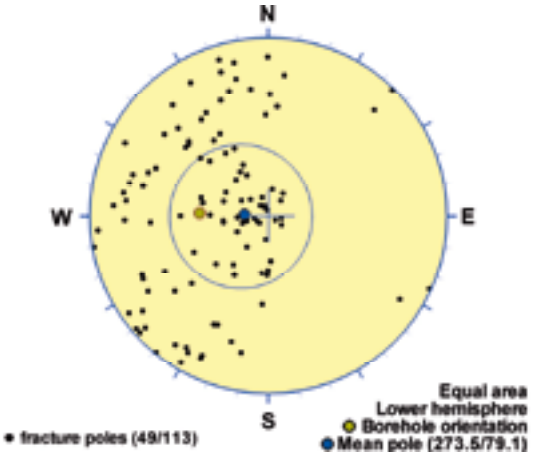

Contours from fractures

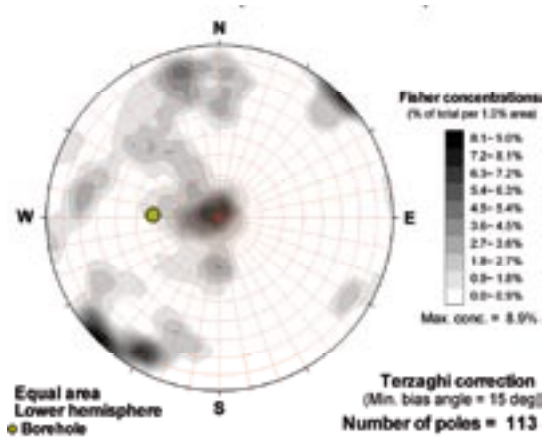

Orientation		Basis for orientation				Certainty	Thickness	
Strike	Dip	Fractures	Crush	Ductile structures	Reflectors	Orientation	Apparent	True
4	11	Used	Verify	Contradict	Contradict	Uncertain	8.1 m	7.6 m
Comment:								

KLX09D DZ2 (101.15 to 104), brittle zone

Brittle deformation zone characterized by increased frequency of sealed fractures and a slight increase in open fractures, medium red staining and slickensides. Significantly decreased resistivity and magnetic susceptibility. One non-oriented radar reflector occurs at 103.9 m with the angle 67° to borehole axis. The host rock is totally dominated by Ävrö granodiorite (501056).

Poles from crush zone

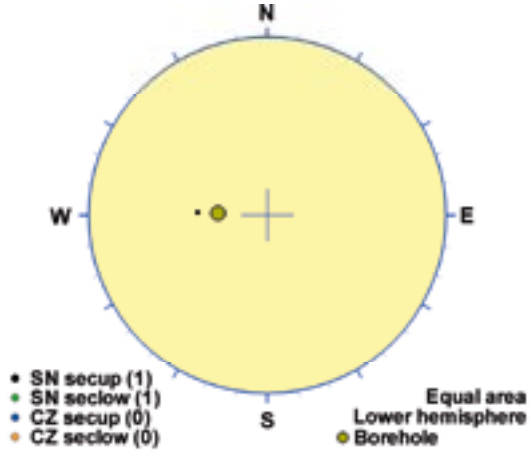

Poles from ductile structures

Data not used

Poles from fractures

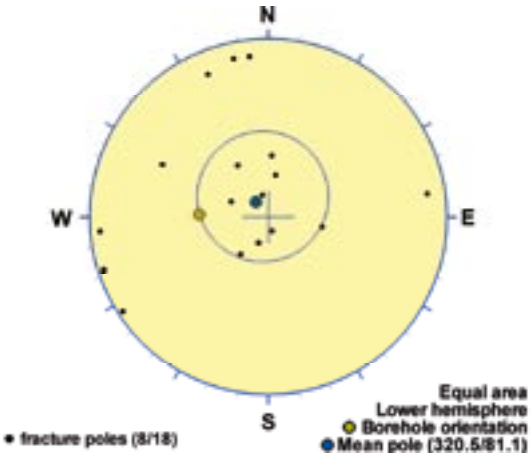

Contours from fractures

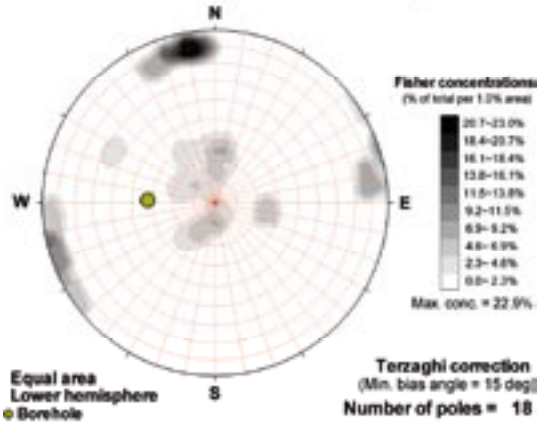

Orientation		Basis for orientation				Certainty	Thickness	
Strike	Dip	Fractures	Crush	Ductile structures	Reflectors	Orientation	Apparent	True
51	9	Used			Verify	Very uncertain	2.8 m	2.5 m
Comment:								

KLX09E DZ1 (71.2 to 72.35), brittle zone

Brittle deformation zone characterized by increased frequency of open fractures and a slight increase in sealed fractures and one crush zone. One non-oriented radar reflector occurs at 71.5 m with the angle 32° to borehole axis. The host rock is totally dominated by Ävrö granite (501044).

Poles from crush zone

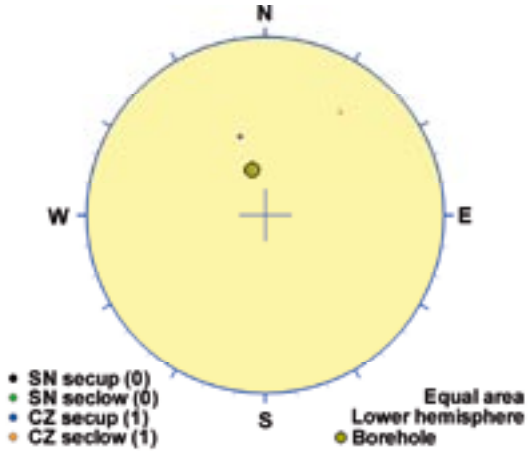

Poles from ductile structures

Data not used

Poles from fractures

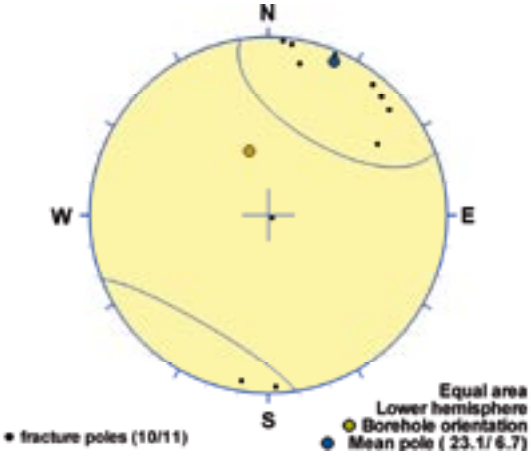

Contours from fractures

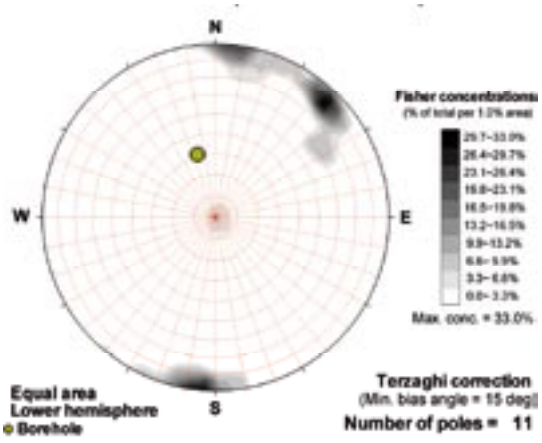

Orientation		Basis for orientation				Certainty	Thickness	
Strike	Dip	Fractures	Crush	Ductile structures	Reflectors	Orientation	Apparent	True
113	83	Used			Verify	Probable	1.1 m	0.6 m
Comment:								

KLX09F DZ2 (67.9 to 68.75), brittle zone

Brittle deformation zone characterized by increased frequency of open fractures, faint to weak red staining and slickensides. Decreased resistivity, magnetic susceptibility and partly decreased P-wave velocity. One strong non-oriented radar reflector at 68.8 m with the anlge 34° to borehole axis. The host rock is dominated by Ävrö granodiorite (501056). Subordinate rock types comprise fine-grained granite (511058).

Poles from crush zone

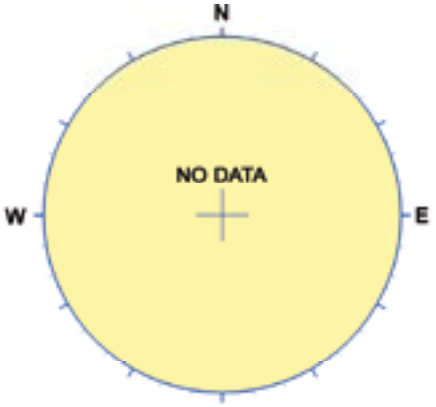

Poles from ductile structures

Data not used

Poles from fractures

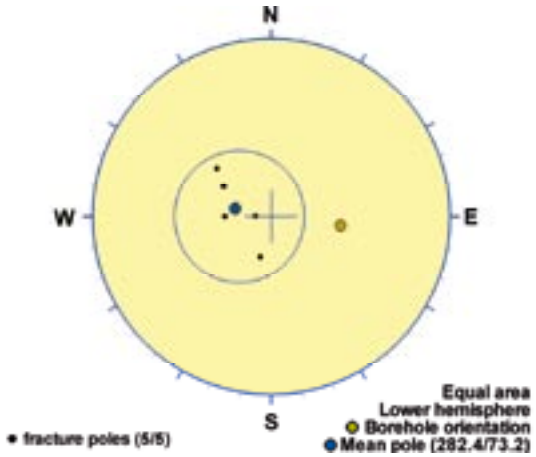

Contours from fractures

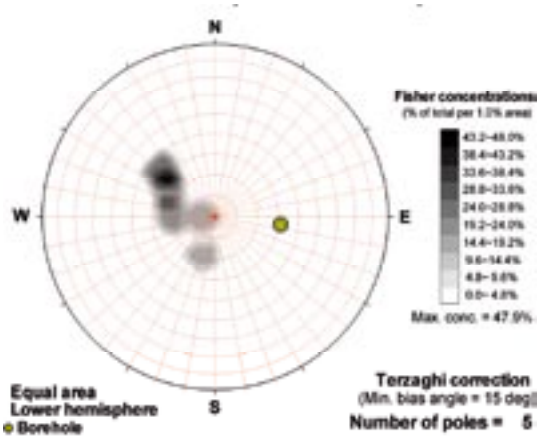

Orientation		Basis for orientation				Certainty	Thickness	
Strike	Dip	Fractures	Crush	Ductile structures	Reflectors	Orientation	Apparent	True
12	17	Used			Contradict	Probable	0.8 m	0.6 m
Comment:								

KLX09F DZ3 (79.45 to 84.4), ductile/brittle zone

Brittle deformation zone overprinting ductile structures. Increased frequency of particularly sealed fractures but also of open fractures, faint to weak red staining, slickensides, mylonitic and brittle-ductile sections. Significantly decreased resistivity and bulk magnetic susceptibility. One minor caliper anomaly but partly increased P-wave velocity. Two non-oriented radar reflectors at 81.1 m and 82.7 m with the angle 59° and 55° to borehole axis, respectively. Low radar amplitude at 75-85 m. The host rock is dominated by Ävrö granodiorite (501056). Subordinate rock types comprise fine-grained granite (511058), fine-grained diorite-gabbro (505102) and very sparse occurrence of pegmatite (501061).

Poles from crush zone

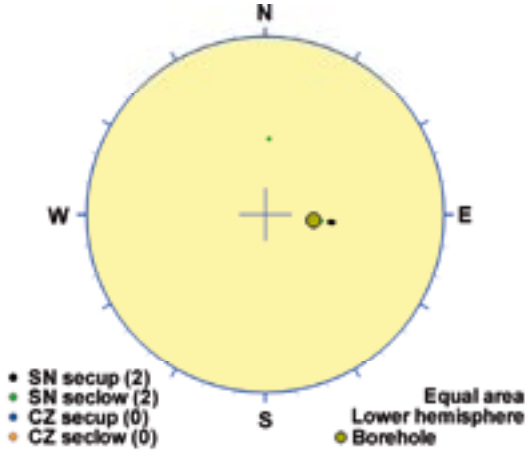

Poles from ductile structures

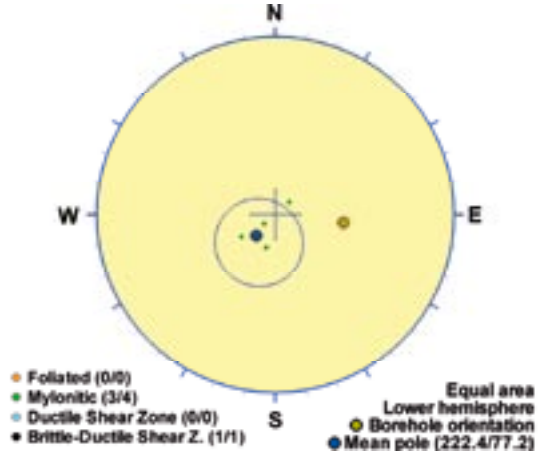

Poles from fractures

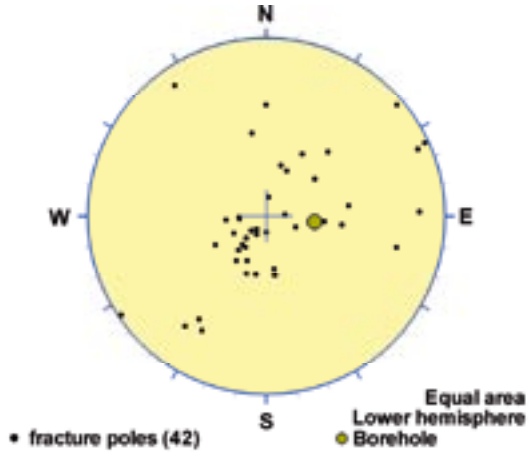

Contours from fractures

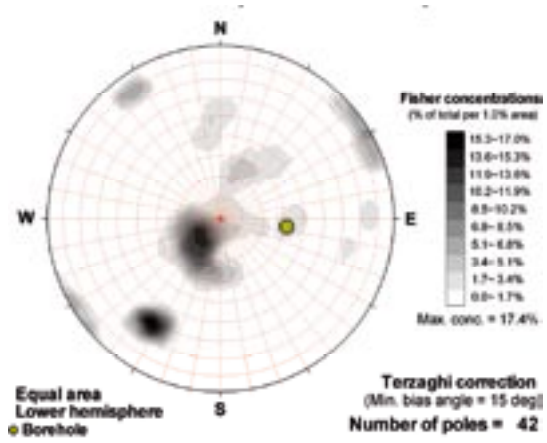

Orientation		Basis for orientation				Certainty	Thickness	
Strike	Dip	Fractures	Crush	Ductile structures	Reflectors	Orientation	Apparent	True
312	13	Verify	Contradict	Used	Verify	Probable	5 m	3.8 m
Comment:								

KLX09F DZ4 (133.1 to 136.2), brittle zone

Brittle deformation zone characterized by increased frequency of sealed fractures and slickensides. Mylonitic and brittle-ductile sections occur. The most intensely deformed section (core) is 134.94-135.80 m. Partly decreased resistivity. Two non-oriented radar reflectors at 133.5 m and 135.5 m with the angle 41° and 42° to borehole axis, respectively. Low radar amplitude at 135 m. The host rock is dominated by Ävrö granodiorite (501056). Subordinate rock type comprises fine-grained diorite-gabbro (505102).

Poles from crush zone

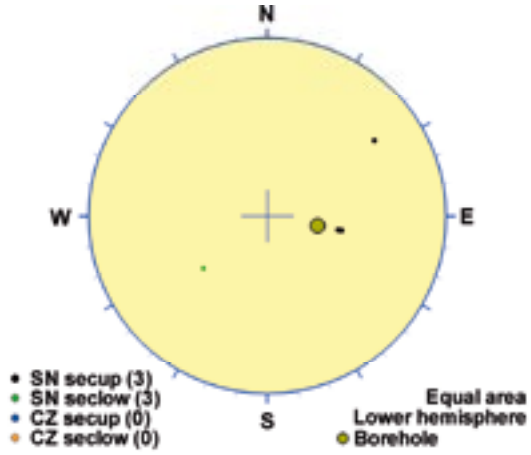

Poles from ductile structures

Data not used

Poles from fractures

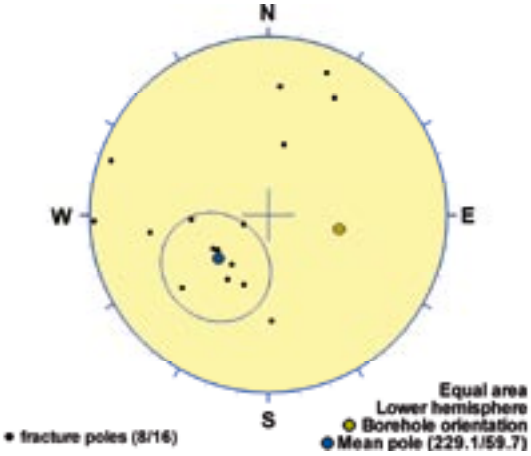

Contours from fractures

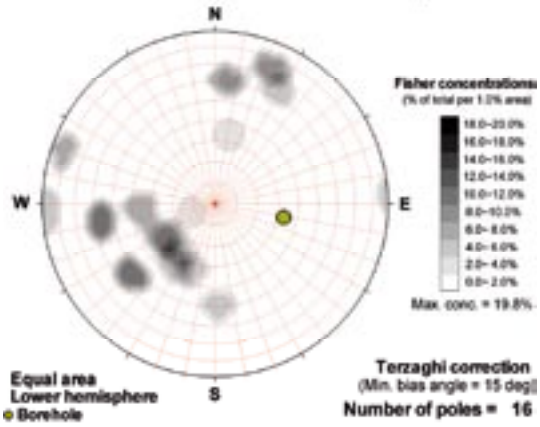

Orientation		Basis for orientation				Certainty	Thickness	
Strike	Dip	Fractures	Crush	Ductile structures	Reflectors	Orientation	Apparent	True
319	30	Used	Verify	Verify	Verify	Probable	3.1 m	1.7 m
Comment:								

KLX09F DZ5 (144.32 to 145.07), brittle zone

Brittle deformation zone characterized by increased frequency of sealed fractures. Decreased resistivity and magnetic susceptibility and caliper anomalies in the section c. 142.5-145.5 m (Note! Also outside zone interval). The host rock is totally dominated by Ävrö granodiorite (501056).

Poles from crush zone

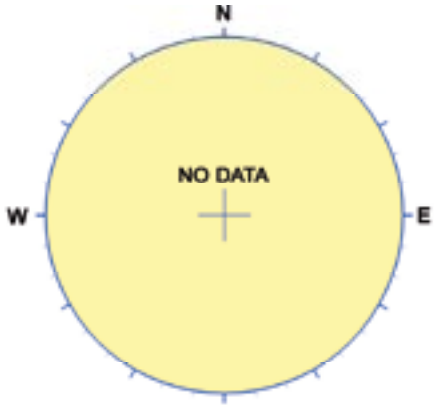

Poles from ductile structures

Data not used

Poles from fractures

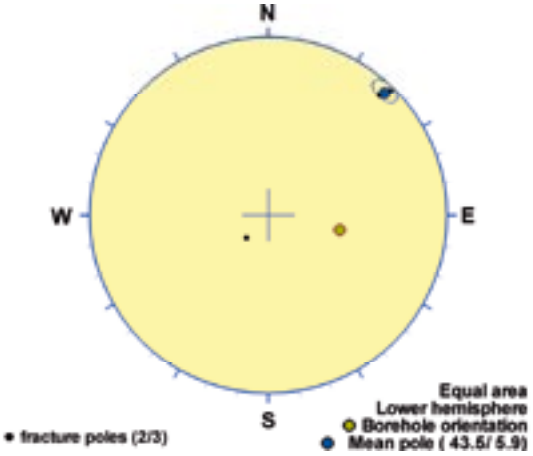

Contours from fractures

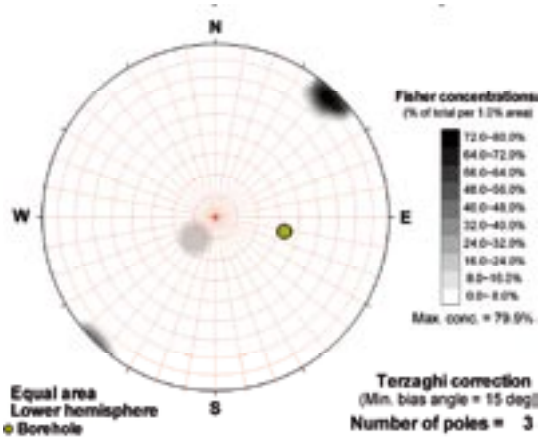

Orientation		Basis for orientation				Certainty	Thickness	
Strike	Dip	Fractures	Crush	Ductile structures	Reflectors	Orientation	Apparent	True
134	84	Used				Probable	0.8 m	0.3 m
Comment:								

KLX10 DZ3 (176 to 176.7), brittle zone

Minor deformation zone characterized by crush. Low electric resistivity and magnetic susceptibility. Minor caliper anomaly. One non-oriented radar reflector occurs at 176.3 m with the angle 75º to borehole axis. The host is dominated by Ävrö granodiorite (501056) with subordinate fine-grained dioritoid (501030).

Poles from crush zone

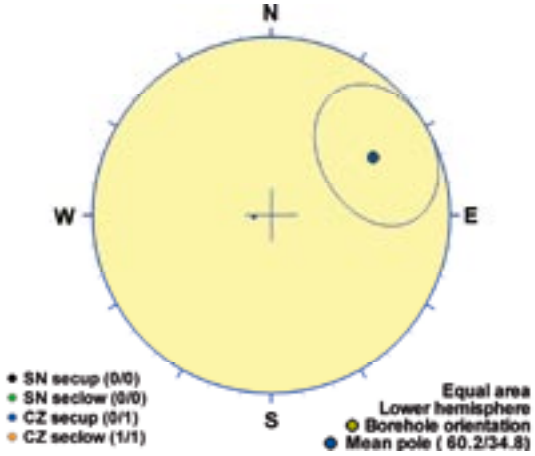

Poles from ductile structures

Data not used

Poles from fractures

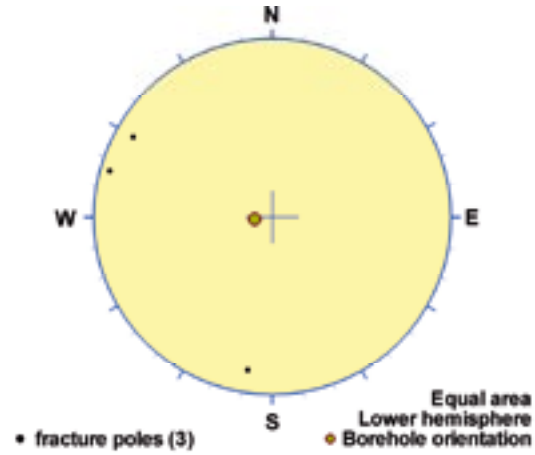

Contours from fractures

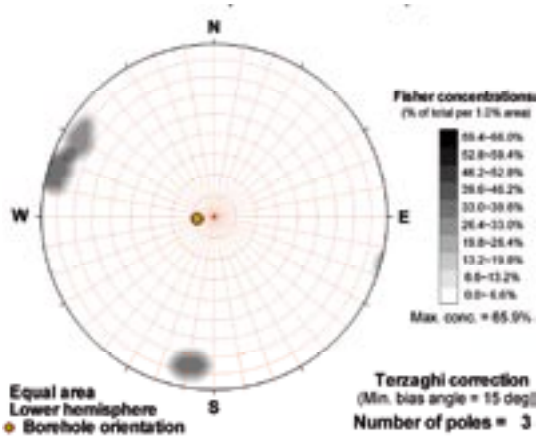

Orientation		Basis for orientation				Certainty	Thickness	
Strike	Dip	Fractures	Crush	Ductile structures	Reflectors	Orientation	Apparent	True
150	55	Contradict	Used		Contradict	Very uncertain	0.7 m	0.3 m
Comment: Low confidence. Crush overrules few fractures, both refuted by refl. Two opposing crush orientations								

KLX10 DZ8 (435 to 439.2), brittle zone

Increased frequency of sealed and open fractures. Some of the latter have large apertures. Crush zone at 436.35-436.44. Weak red staining. Low electric resistivity, P-wave velocity and magnetic susceptibility. One non-oriented radar reflector occurs at 438.6 m with the angle 56º to borehole axis. Low radar amplitude occurs in the interval 435-440 m, i.e. partly outside the deformation zone. The host rock is dominated by Ävrö granodiorite (501056) with subordinate fine-grained granite (511058).

Poles from crush zone

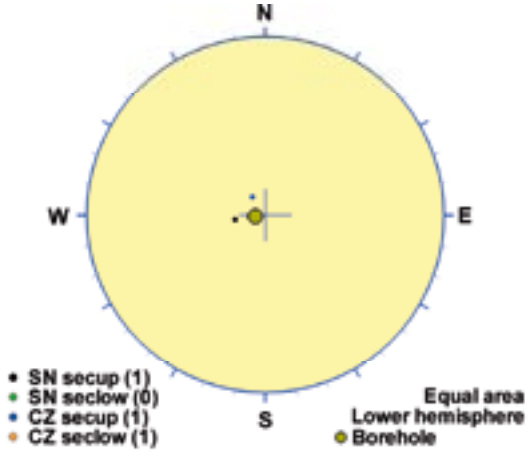

Poles from ductile structures

Data not used

Poles from fractures

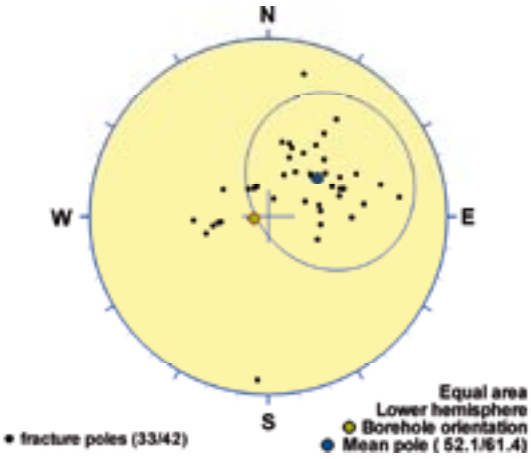

Contours from fractures

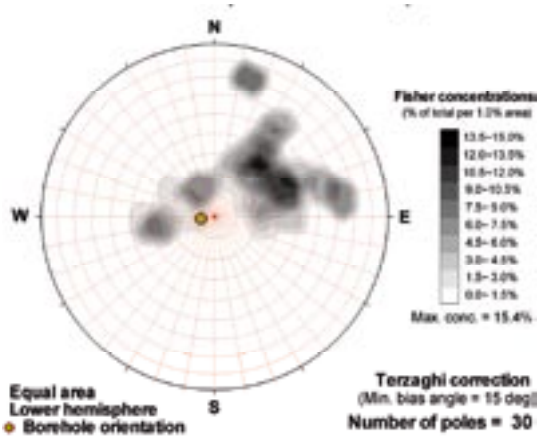

Orientation		Basis for orientation				Certainty	Thickness	
Strike	Dip	Fractures	Crush	Ductile structures	Reflectors	Orientation	Apparent	True
142	29	Used	Contradict		Verify	Probable	4.2 m	3.5 m
Comment:								

KLX10B DZ2 (39.2 to 46.6), brittle zone

Increased frequency of open fractures, partly with large apertures. Low frequency of sealed fractures. Most intense part between 39.96 and 40.32 m. At c 40.4 m there is one distinct caliper anomaly that coincides with decreased resistivity and decreased P-wave velocity. One non-oriented radar reflector at 39.9 m with the angle 51° to borehole axis. Two radar reflectors, one at 41.0 m with the orientation 274/72 or 125/15 and one at 43.6 m with the orientation 131/30. The host rock is dominated by Ävrö quartz monzodiorite (501046).

Poles from crush zone

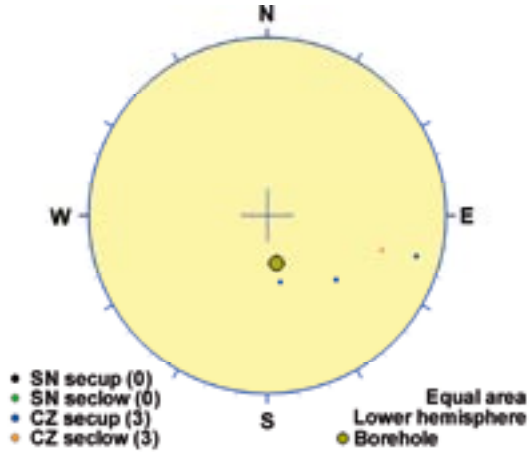

Poles from ductile structures

Data not used

Poles from fractures

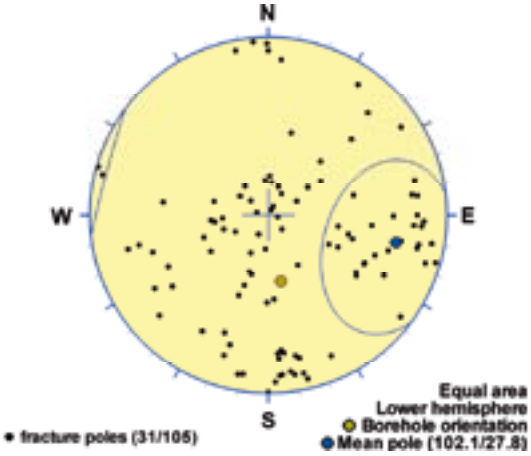

Contours from fractures

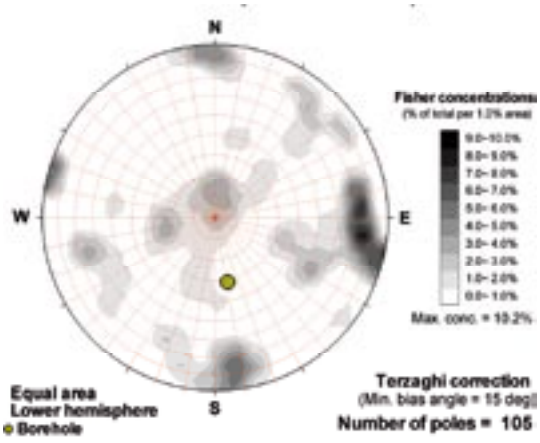

Orientation		Basis for orientation				Certainty	Thickness	
Strike	Dip	Fractures	Crush	Ductile structures	Reflectors	Orientation	Apparent	True
192	62	Used	Verify	Verify	Contradict	Probable	7.4 m	4.3 m
Comment:								

KLX10C DZ1 (8.65 to 9.5), brittle zone

Brittle deformation zone with red staining and increased frequency of open fractures. Section is above BIPS image and geophysical logging data, apart from the caliper log that does not show any anomalies. The host rock is dominated by Ävrö quartz monzodiorite (501046).

Poles from crush zone

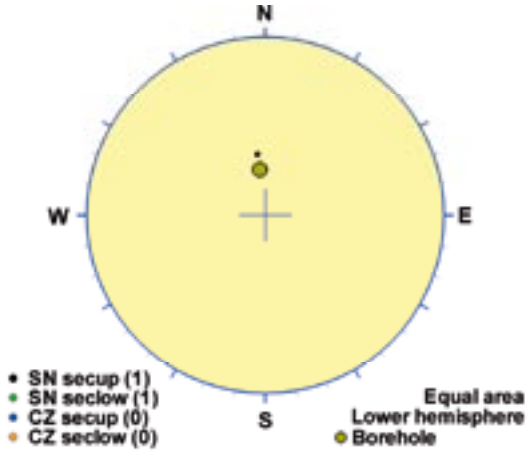

Poles from ductile structures

Data not used

Poles from fractures

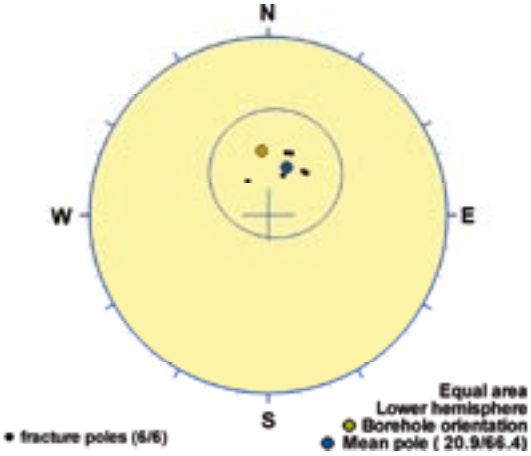

Contours from fractures

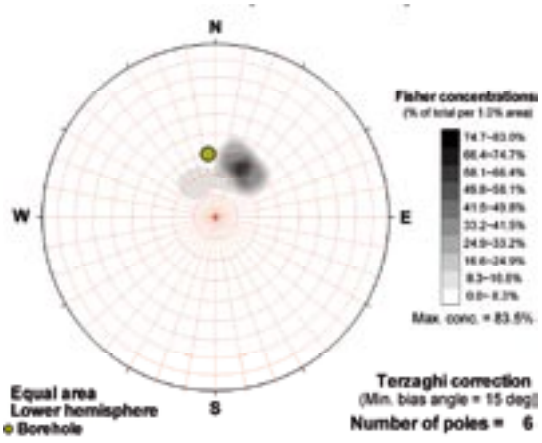

Orientation		Basis for orientation				Certainty	Thickness	
Strike	Dip	Fractures	Crush	Ductile structures	Reflectors	Orientation	Apparent	True
111	24	Used	Verify			Certain	0.8 m	0.8 m
Comment:								

KLX10C DZ2 (15.9 to 21.6), brittle zone

Deformation characterised by medium to strong alteration (chloritization and red staining) and increased frequency of sealed and open fractures. The most intense sections are at 17.18 – 17.35 m and 18.92 – 19.60 m. The entire section is characterized by a major decrease in the bulk resistivity, significantly decreased P-wave velocity and magnetic susceptibility and also caliper anomalies. Two very strong and persistent non-oriented radar reflectors at 16.7 m and 19.4 m with the angle to borehole axis 58° and 55°, respectively. Low radar amplitude at 15-21 m. The host rock is dominated by a mixture of fine-grained dioritoid (501030) and Ävrö quartz monzodiorite (501046). Subordinate rock types are pegmatite (501061) and fine-grained diorite-gabbro (505102).

Poles from crush zone

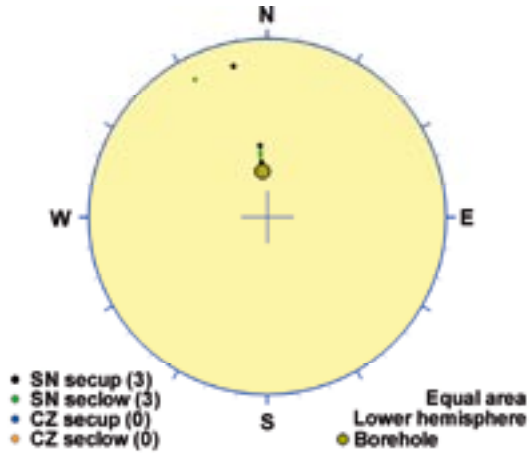

Poles from ductile structures

Data not used

Poles from fractures

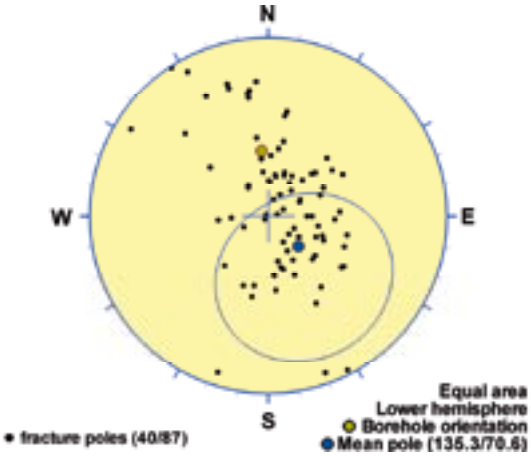

Contours from fractures

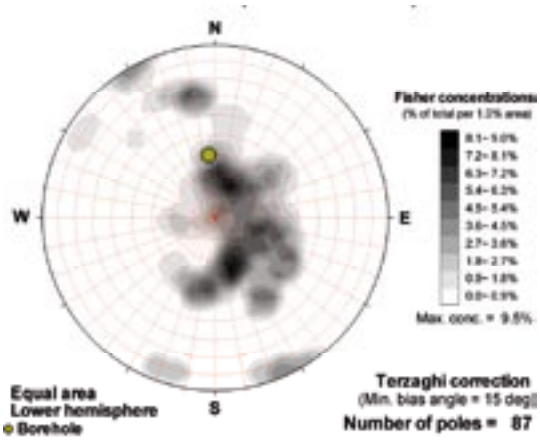

Orientation		Basis for orientation				Certainty	Thickness	
Strike	Dip	Fractures	Crush	Ductile structures	Reflectors	Orientation	Apparent	True
225	19	Used	Contradict			Uncertain	5.7 m	3.9 m
Comment:								

KLX10C DZ4 (79.45 to 79.7), brittle zone

Characterized by sealed network. Partly decreased P-wave velocity in the interval 79.2-80.7 m, and sharp low resistivity anomaly at c 80.0 m. The host rock is dominated by Ävrö granodiorite (501056).

Poles from crush zone

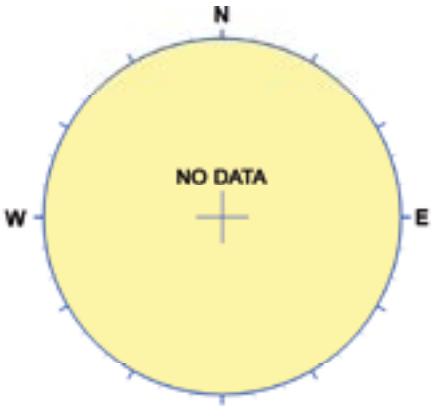

Poles from ductile structures

Data not used

Poles from fractures

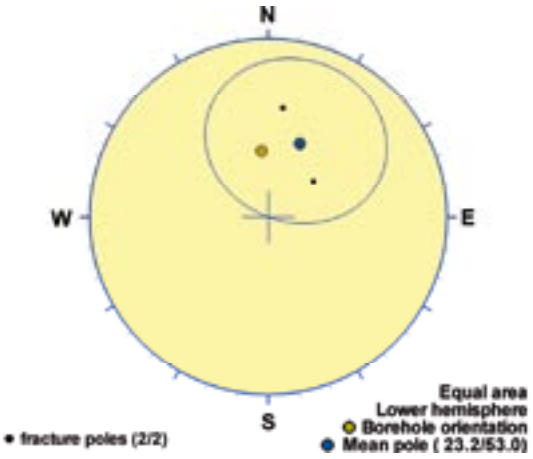

Contours from fractures

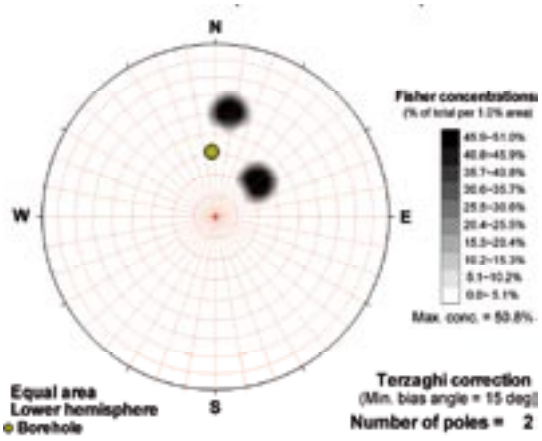

Orientation		Basis for orientation				Certainty	Thickness	
Strike	Dip	Fractures	Crush	Ductile structures	Reflectors	Orientation	Apparent	True
113	37	Used				Probable	0.2 m	0.2 m
Comment:								

KLX10C DZ5 (96.9 to 97.6), brittle zone

Characterized by sealed fracture network. The interval 97.17 – 97.26 m is the most intense section. Red staining. No anomalies in the geophysical logs. The host rock is dominated by Ävrö granodiorite (501056). Subordinate rock type is fine-grained granite (511058).

Poles from crush zone

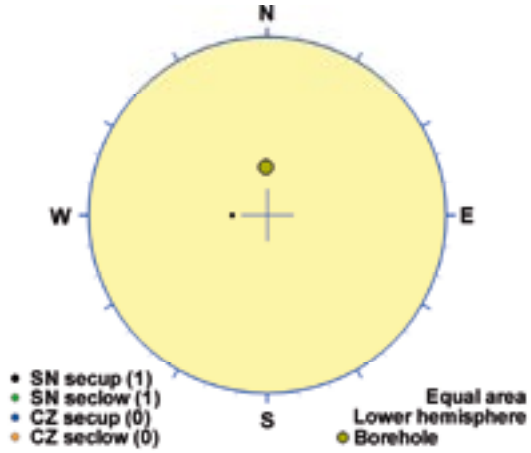

Poles from ductile structures

Data not used

Poles from fractures

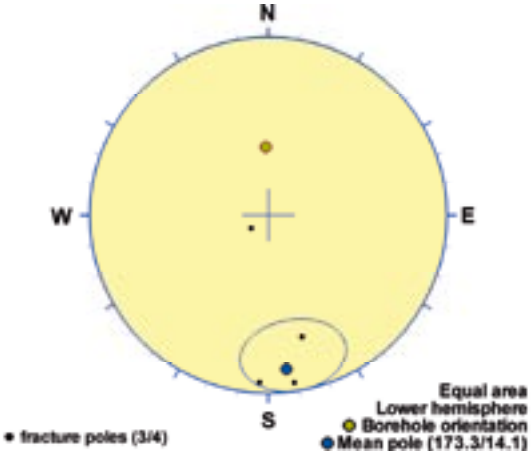

Contours from fractures

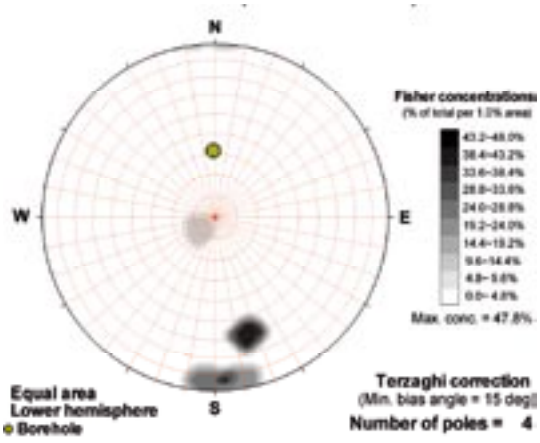

Orientation		Basis for orientation				Certainty	Thickness	
Strike	Dip	Fractures	Crush	Ductile structures	Reflectors	Orientation	Apparent	True
263	76	Used	Contradict			Probable	0.7 m	0.2 m
Comment:								

KLX10C DZ6 (103.5 to 110.1), brittle zone

Inhomogeneous deformation zone. Characterized by sealed fracture network and open fractures. 505102 is foliated. The most intense sections are between 105.50 – 105.74 m and 106.10 – 106.27 m depth. Significant decrease in P-wave velocity and in resistivity along the section 105.5-107.1 m, which coincides with decreased magnetic susceptibility, natural gamma radiation and increased density. One strong and persistent radar reflector at 104.7 m with the orientation 193/25 or 060/71. Two non-oriented radar reflectors at 103.9 m and 105.6 m with the angle to borehole axis 78° and 52°, respectively. Low radar amplitude at 105-108 m.The host rock is dominated by Ävrö granodiorite (501056). Subordinate rock types are fine-grained diorite-gabbro (505102) and very sparse occurrence of fine-grained granite (511058).

Poles from crush zone

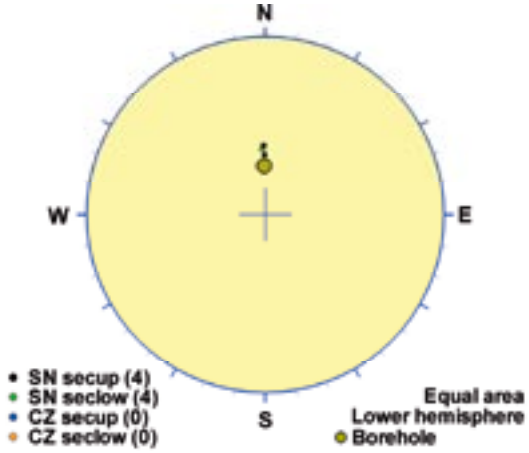

Poles from ductile structures

Data not used

Poles from fractures

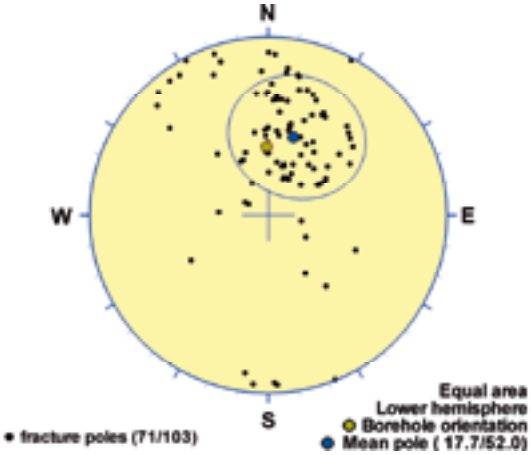

Contours from fractures

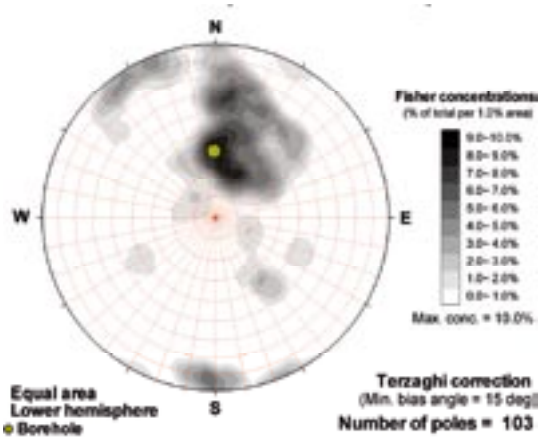

Orientation		Basis for orientation				Certainty	Thickness	
Strike	Dip	Fractures	Crush	Ductile structures	Reflectors	Orientation	Apparent	True
108	38	Used	Verify		Verify	Probable	6.6 m	6.4 m
Comment:								

KLX11A DZ1 (142.25 to 142.9), ductile/brittle zone

Minor low grade ductile shear zone. Increased frequency of open fractures and sealed fractures. Low P-wave velocity, low resistivity and low magnetic susceptibility. One non-oriented radar reflector at 142.2 m with the angle 70° to borehole axis. The host rock is dominated by quartz monzodiorite (501036).

Poles from crush zone

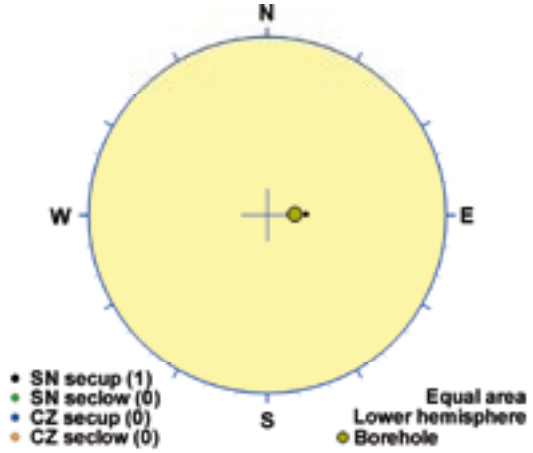

Poles from ductile structures

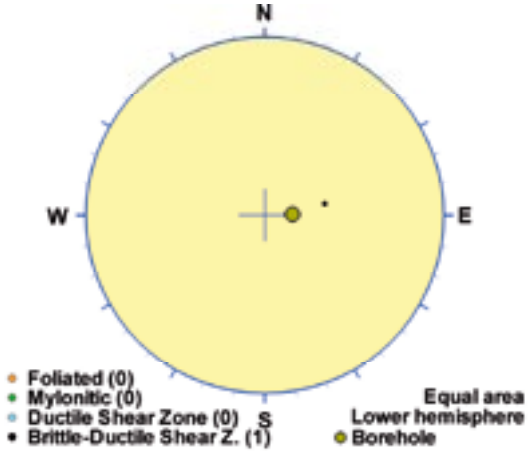

Poles from fractures

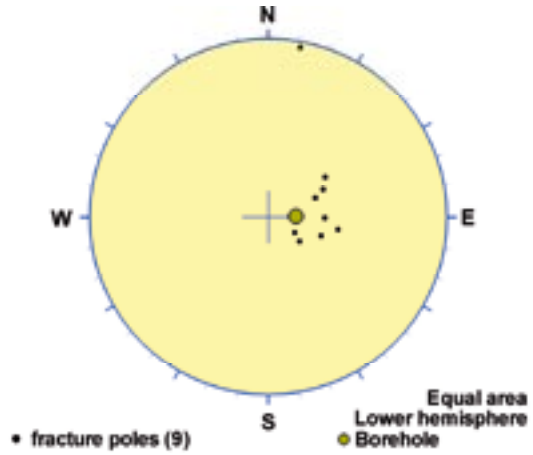

Contours from fractures

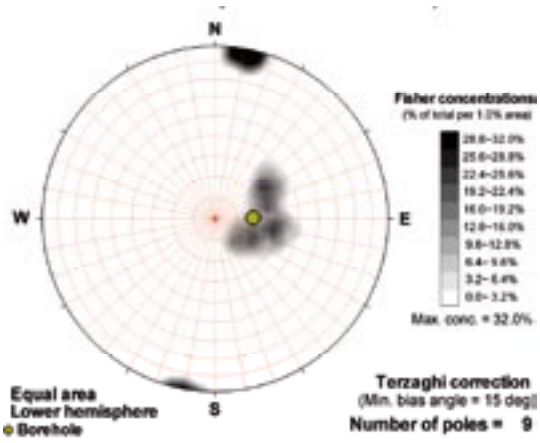

Orientation		Basis for orientation				Certainty	Thickness	
Strike	Dip	Fractures	Crush	Ductile structures	Reflectors	Orientation	Apparent	True
169	28	Verify	Verify	Used	Verify	Certain	0.7 m	0.6 m
Comment:								

KLX11A DZ2 (162.75 to 163.26), ductile/brittle zone

Minor low grade ductile shear zone, overprinted by sealed fractures. Low P-wave velocity, low resistivity and low magnetic susceptibility. One non-oriented radar reflector at 162.5 m (just outside DZ2) with the angle 84° to borehole axis. The host rock is dominated by fine-grained diorite-gabbro (505102).

Poles from crush zone

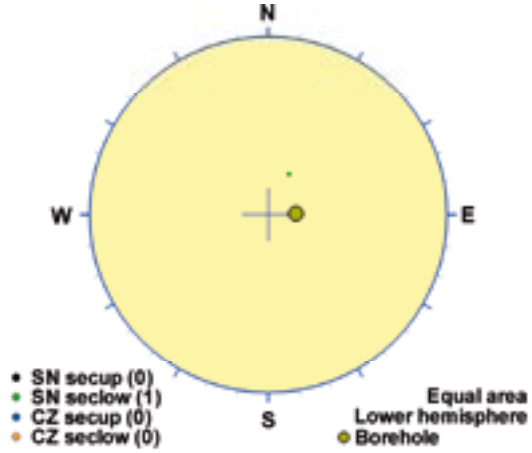

Poles from ductile structures

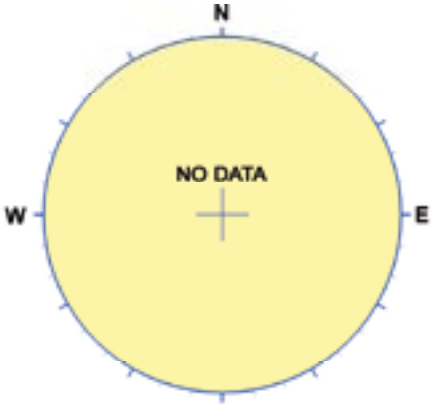

Poles from fractures

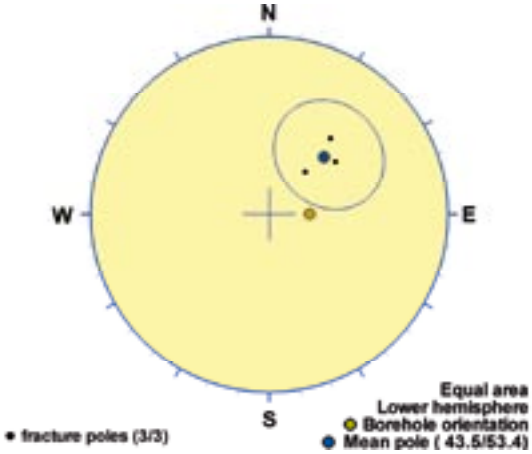

Contours from fractures

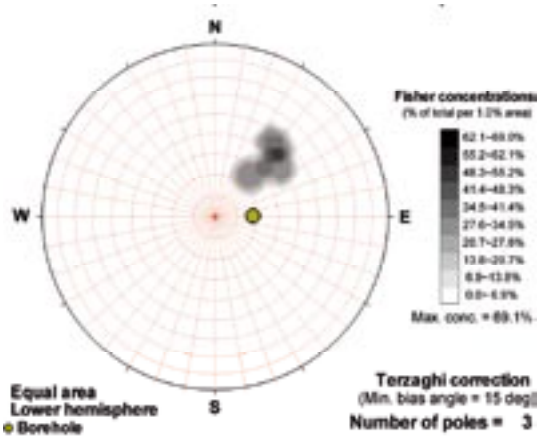

Orientation		Basis for orientation				Certainty	Thickness	
Strike	Dip	Fractures	Crush	Ductile structures	Reflectors	Orientation	Apparent	True
134	37	Used	Verify		Contradict	Probable	0.5 m	0.5 m
Comment:								

KLX11A DZ3 (168.7 to 169.9), ductile/brittle zone

Inhomogeneous, minor low-grade ductile shear zone, with overprint of brittle shear zone. Increased frequency of sealed and open fractures, foliation and mylonites. Low P-wave velocity, low resistivity, caliper anomaly and low magnetic susceptibility. One strong, non-oriented radar reflector at 169.4 m with the angle 78° to borehole axis. The host rock is dominated by quartz monzodiorite (501036). Subordinate rock types are granite (501058) and pegmatite (501061).

Poles from crush zone

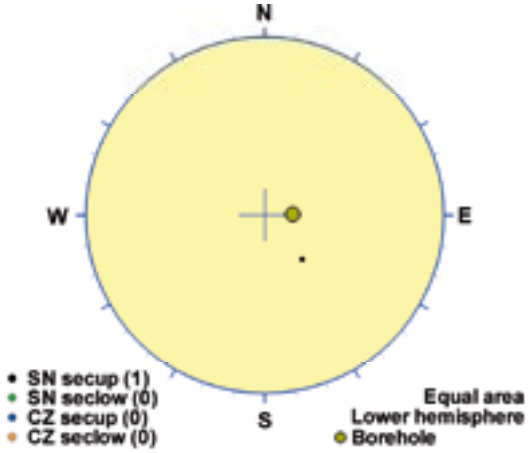

Poles from ductile structures

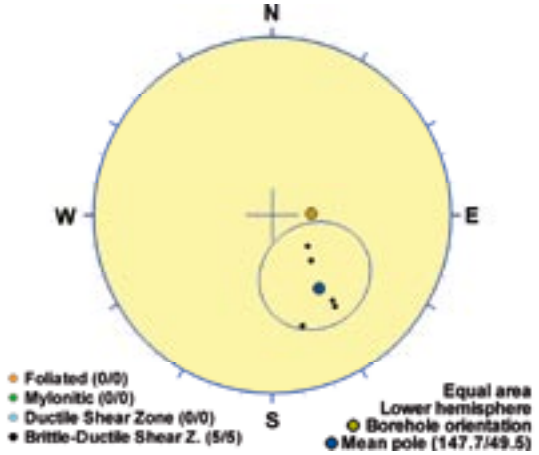

Poles from fractures

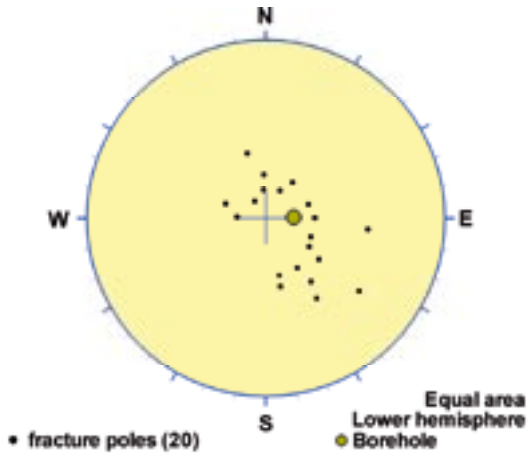

Contours from fractures

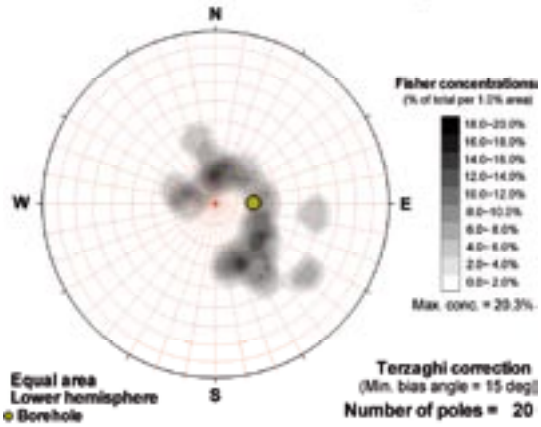

Orientation		Basis for orientation				Certainty	Thickness	
Strike	Dip	Fractures	Crush	Ductile structures	Reflectors	Orientation	Apparent	True
238	41	Verify	Verify	Used	Contradict	Probable	1.2 m	1 m
Comment:								

KLX11A DZ4 (247.67 to 272), ductile/brittle zone

Brittle deformation zone, with a central core (263.82-267.70 m) of a low-grade ductile shear zone. The central part consists of fine-grained diorite-gabbro (505102), with granite veins. The brittle upper part is dominated by one single fracture along the core, which contains sealed network, with prehnite- and quartz-sealed breccias. Low P-wave velocity, low resistivity, caliper anomaly and low magnetic susceptibility. Several non-oriented radar reflectors with angle to borehole axis between 8° and 73° occur within the deformation zone. Also, two oriented radar reflectors occur at 254.3 m with the orientation 095/86 and at 267.7 m with the orientation 185/33 or 102/10.The host rock is dominated by quartz monzodiorite (501036). Subordinate rock types are fine-grained granite (511058), fine-grained diorite-gabbro (505102) and pegmatite (501061).

Poles from crush zone

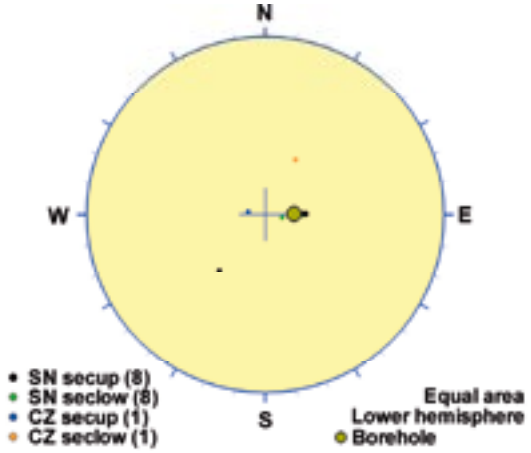

Poles from ductile structures

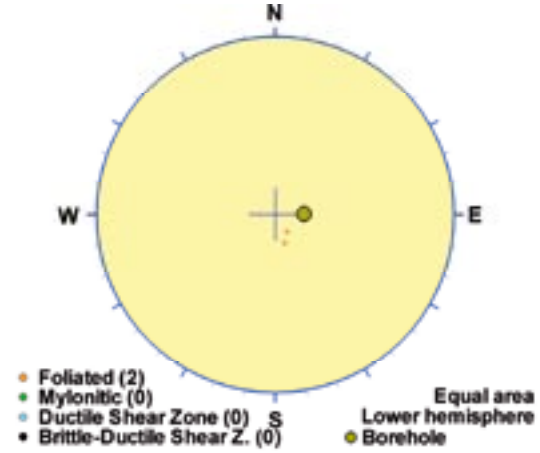

Poles from fractures

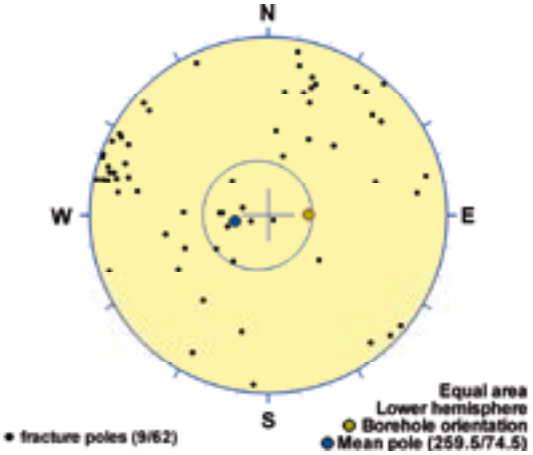

Contours from fractures

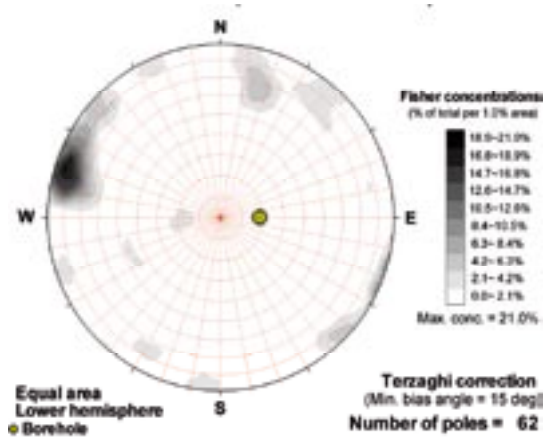

Orientation		Basis for orientation				Certainty	Thickness	
Strike	Dip	Fractures	Crush	Ductile structures	Reflectors	Orientation	Apparent	True
15	81						24.3 m	3.7 m
Comment: Orinentation of the zone is defined in Viola et al., NGU 2007								

KLX11A DZ5 (285.4 to 286.4), ductile/brittle zone

Low-grade ductile shear zone (judged from core). Increased frequency of sealed fractures. Saussuritization occurs in the section. Low P-wave velocity and low resistivity. One non-oriented radar reflector occurs at 285.2 m (just outside DZ5) with the angle 31° to borehole axis. The host rock is dominated by fine-grained diorite-gabbro (505102). Subordinate rock type is quartz monzodiorite (501036).

Poles from crush zone

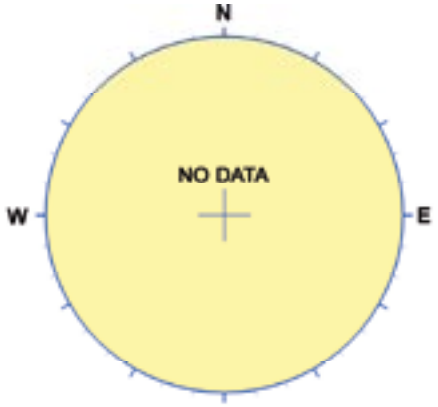

Poles from ductile structures

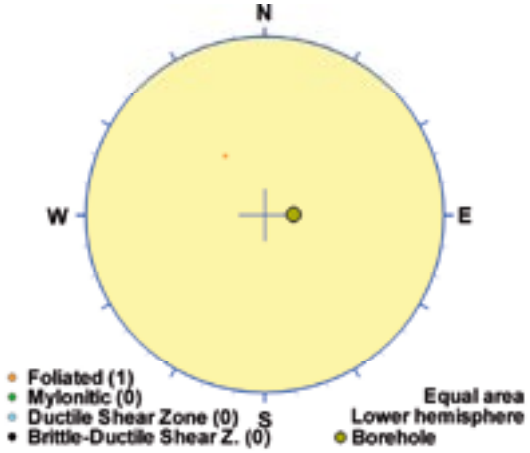

Poles from fractures

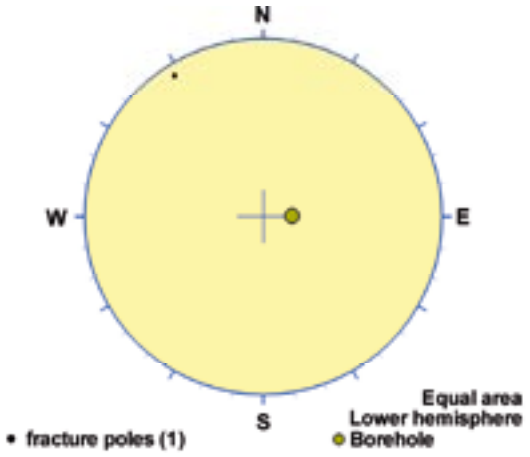

Contours from fractures

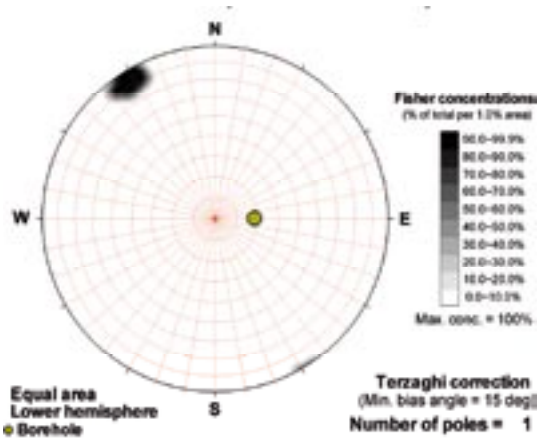

Orientation		Basis for orientation				Certainty	Thickness	
Strike	Dip	Fractures	Crush	Ductile structures	Reflectors	Orientation	Apparent	True
57	33	Contradict		Used	Contradict	Uncertain	1 m	0.7 m
Comment:								

KLX11A DZ6 (306.22 to 308.78), ductile/brittle zone

Low-grade ductile shear zone, with brittle overprinting. Increased frequency of open and sealed fractures. Low P-wave velocity, low resistivity and low magnetic susceptibility. The host rock is dominated by quartz monzodiorite (501036). Subordinate rock types are fine-grained granite (511058) and granite (501058).

Poles from crush zone

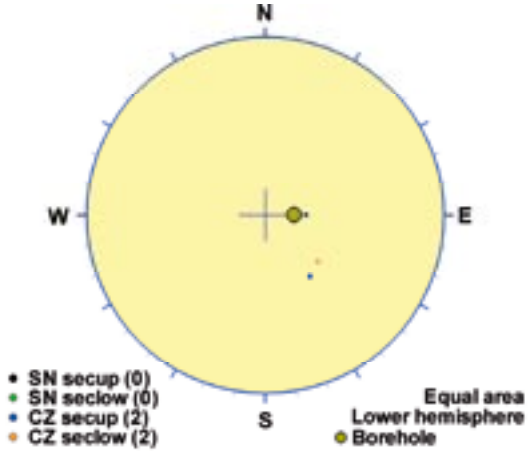

Poles from ductile structures

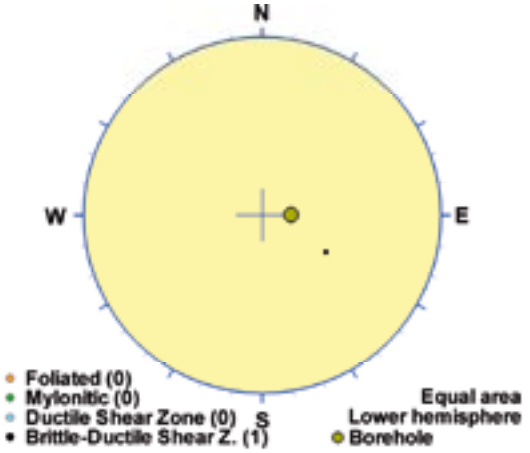

Poles from fractures

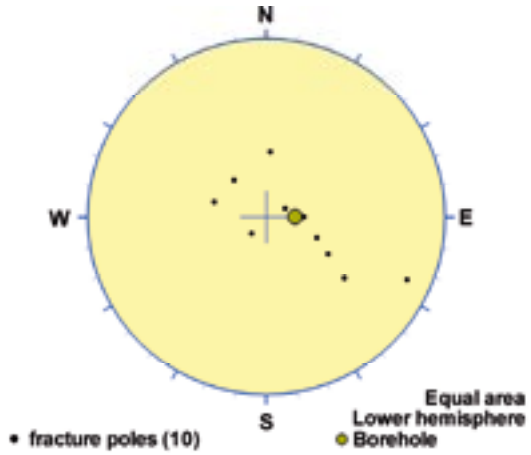

Contours from fractures

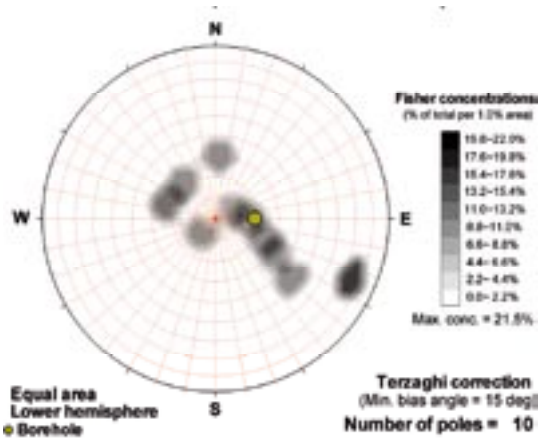

Orientation		Basis for orientation				Certainty	Thickness	
Strike	Dip	Fractures	Crush	Ductile structures	Reflectors	Orientation	Apparent	True
210	34	Verify	Verify	Used		Certain	2.6 m	2.4 m
Comment:								

KLX11A DZ7 (345.3 to 348.03), ductile/brittle zone

Brittle deformation zone, with a central ductile part (346.43-346.72 m), dominated by a sealed breccia. Transition zone is dominated by red staining, breccia and sealed fractures. Low P-wave velocity, low resistivity and low magnetic susceptibility. One non-oriented radar reflector occurs at 346.5 m with the angle 48° to borehole axis, and one rather strong oriented reflector occurs at 345.4 m with the orientation 256/52.The host rock is dominated by quartz monzodiorite (501036).

Poles from crush zone

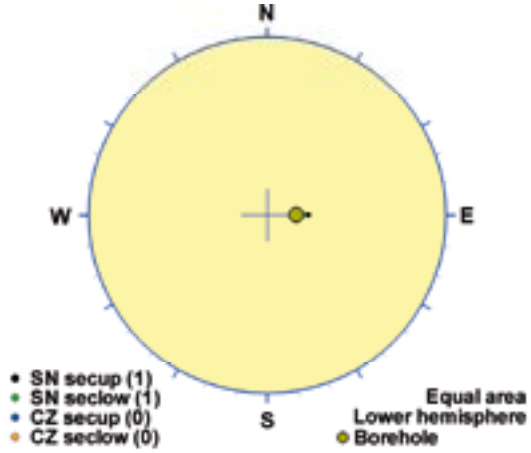

Poles from ductile structures

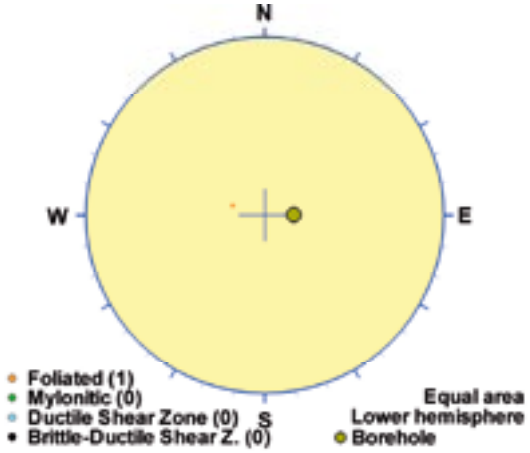

Poles from fractures

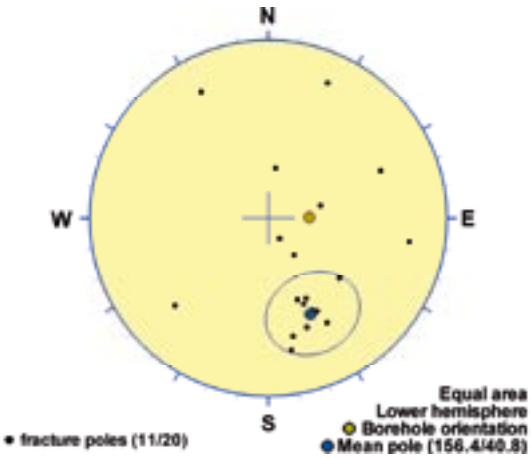

Contours from fractures

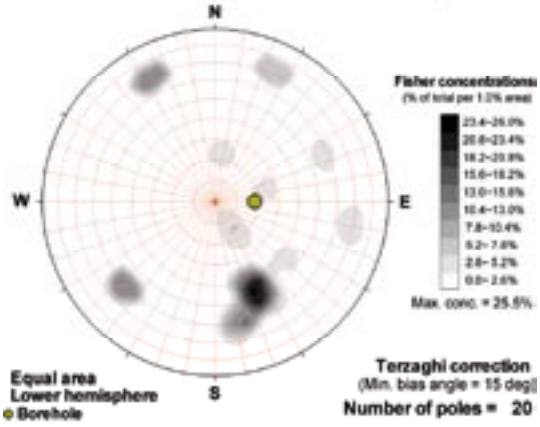

Orientation		Basis for orientation				Certainty	Thickness	
Strike	Dip	Fractures	Crush	Ductile structures	Reflectors	Orientation	Apparent	True
246	49	Used	Contradict	Contradict	Verify	Probable	2.7 m	2 m
Comment:								

KLX11A DZ8 (417.26 to 418.1), brittle zone

Brittle deformation zone, with crush, sealed network and red staining. Low resistivity and caliper anomaly. One oriented radar reflector occurs at 418.3 m (outside DZ8) with the orientation 110/38 or 235/35. The host rock is dominated by quartz monzodiorite (501036).

Poles from crush zone

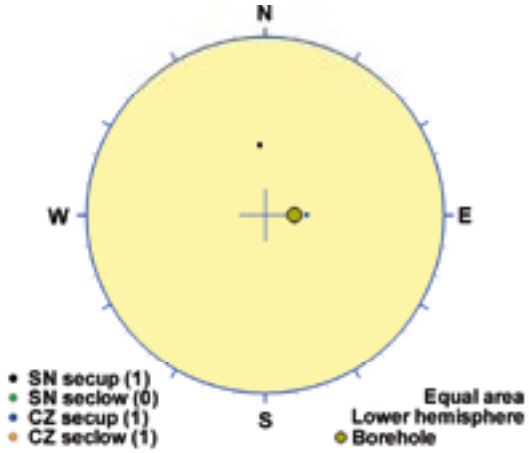

Poles from ductile structures

Data not used

Poles from fractures

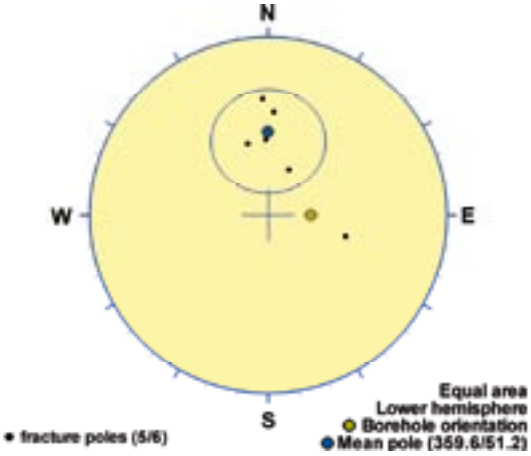

Contours from fractures

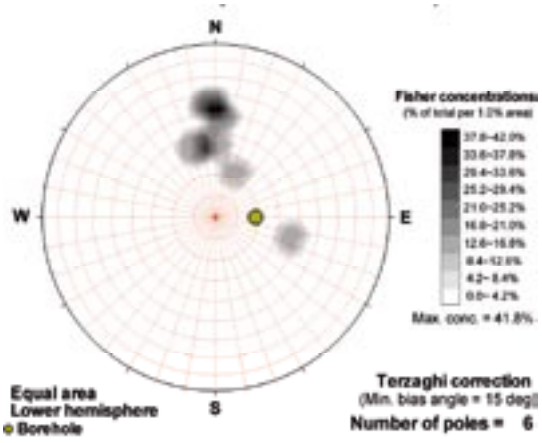

Orientation		Basis for orientation				Certainty	Thickness	
Strike	Dip	Fractures	Crush	Ductile structures	Reflectors	Orientation	Apparent	True
90	39	Used	Verify		Contradict	Probable	0.8 m	0.6 m
Comment: The sealed network data verify the orientation.								

KLX11A DZ9 (430.56 to 432.2), ductile zone

Low-grade ductile shear zone (judged from core) composed of foliated fine-grained diorite-gabbro (505102). Low magnetic susceptibility. One non-oriented radar reflector occurs at 431.2 m with the angle 73° to borehole axis. Subordinate rock type is quartz monzodiorite (501036).

Poles from crush zone

Data not used

Poles from ductile structures

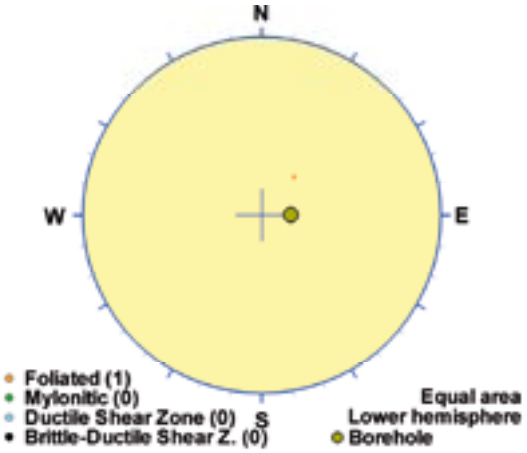

Poles from fractures

Data not used

Contours from fractures

Data not used

Orientation		Basis for orientation				Certainty	Thickness	
Strike	Dip	Fractures	Crush	Ductile structures	Reflectors	Orientation	Apparent	True
130	23			Used	Verify	Probable	1.6 m	1.6 m
Comment:								

KLX11A DZ10 (473.62 to 475.7), ductile zone

Low-grade ductile shear zone, dominated by an altered quartz monzodiorite (501036) at 474.47-475.10 m. Low P-wave velocity, low resistivity and low magnetic susceptibility. One non-oriented radar reflector occurs at 473.8 m with the angle 79° to borehole axis. The host rock is dominated by quartz monzodiorite (501036). Subordinate rock types are fine-grained granite (511058) and fine-grained diorite-gabbro (505102).

Poles from crush zone

Data not used

Poles from ductile structures

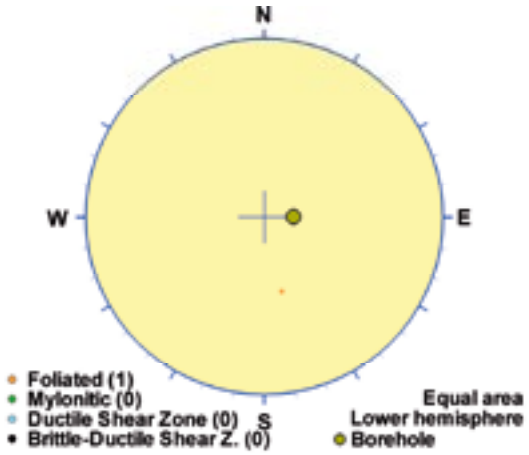

Poles from fractures

Data not used

Contours from fractures

Data not used

Orientation		Basis for orientation				Certainty	Thickness	
Strike	Dip	Fractures	Crush	Ductile structures	Reflectors	Orientation	Apparent	True
257	35			Used	Contradict	Very uncertain	2.1 m	1.7 m
Comment:								

KLX11A DZ13 (577.9 to 586.16), brittle zone

Inhomogeneous brittle deformation zone, with scattered minor cataclasites. Two more intensely deformed sections at 579.66-579.89 m and 582.65-583.10 m, which contains crush. Low P-wave velocity, low resistivity and low magnetic susceptibility. Four non-oriented radar reflectors occur with angles between 48° and 63° to borehole axis. Also, one oriented rather strong radar reflector occurs at 578.9 m with the orientation 081/31 or 213/46. The host rock is dominated by quartz monzodiorite (501036). Subordinate rock types are fine-grained granite (511058), granite (501058) and pegmatite (501061).

Poles from crush zone

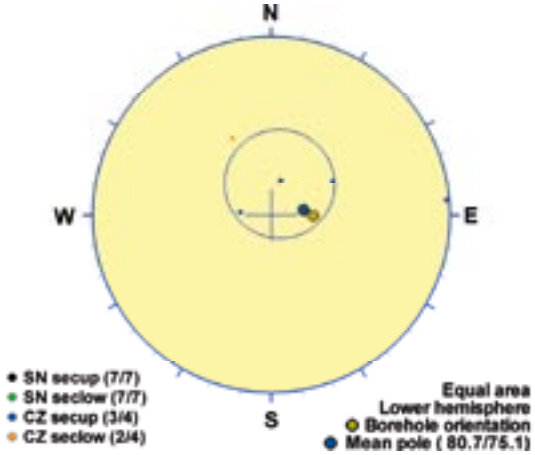

Poles from ductile structures

Data not used

Poles from fractures

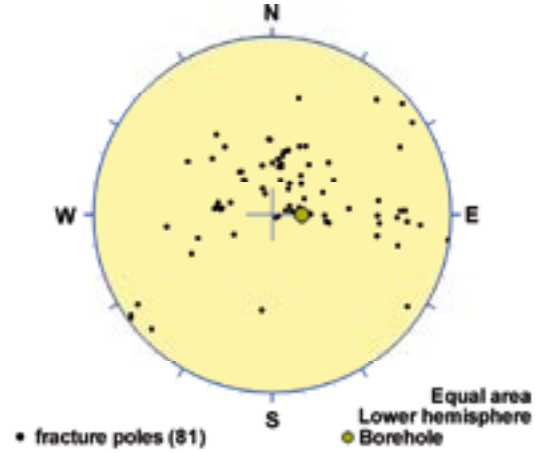

Contours from fractures

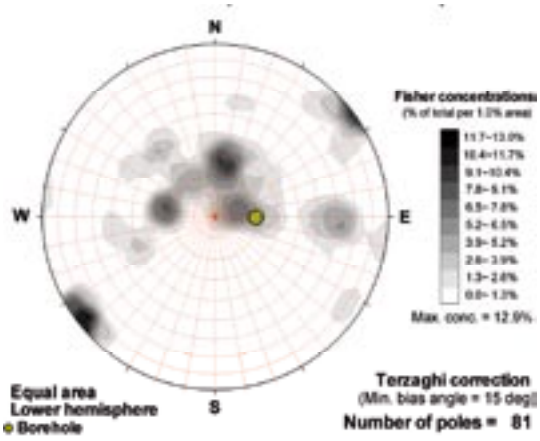

Orientation		Basis for orientation				Certainty	Thickness	
Strike	Dip	Fractures	Crush	Ductile structures	Reflectors	Orientation	Apparent	True
171	15	Verify	Used		Verify	Probable	8.3 m	8.2 m
Comment:								

KLX11A DZ14 (593.9 to 602.27), ductile zone

Low-grade ductile shear zone, particularly developed in fine-grained diorite to gabbro (505102) in the interval 597.70-602.27 m. The quartz monzodiorite (501036) is not affected by the deformation. Low P-wave velocity and low resistivity. Two oriented radar reflectors occur, one strong at 598.6 m with the orientation 200/22 or 137/22, and one at 602.7 m (outside DZ14) with the orientation 030/22 or 186/57. Also, one non-oriented radar reflector occurs at 602.0 m with the angle 59° to borehole axis. The host rock is dominated by fine-grained diorite-gabbro (505102). Subordinate rock types are quartz monzodiorite (501036) and fine-grained granite (511058).

Poles from crush zone

Data not used

Poles from ductile structures

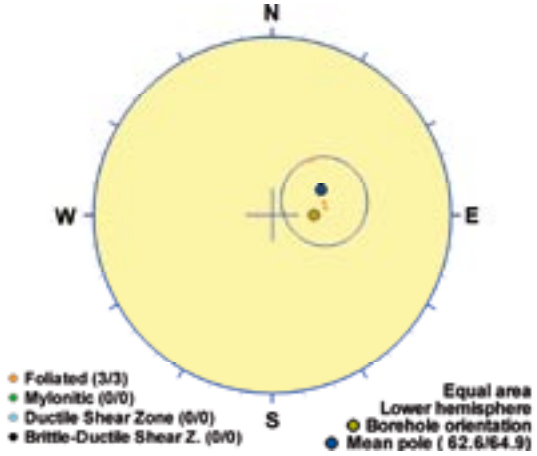

Poles from fractures

Data not used

Contours from fractures

Data not used

Orientation		Basis for orientation				Certainty	Thickness	
Strike	Dip	Fractures	Crush	Ductile structures	Reflectors	Orientation	Apparent	True
153	25			Used	Contradict	Certain	8.4 m	8.2 m
Comment:								

KLX11A DZ15 (689.06 to 689.86), brittle zone

Minor brittle deformation zone, dominated by a central part (689.62-689.69 m) with red staining, sealed fractures and breccia. Low resistivity. One non-oriented radar reflector occurs at 690.1 m (outside DZ15) with the angle 65° to borehole axis. The host rock is dominated by quartz monzodiorite (501036).

Poles from crush zone

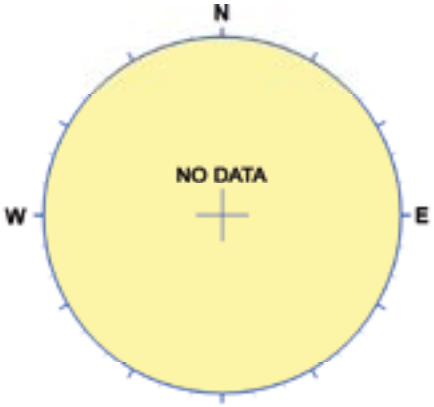

Poles from ductile structures

Data not used

Poles from fractures

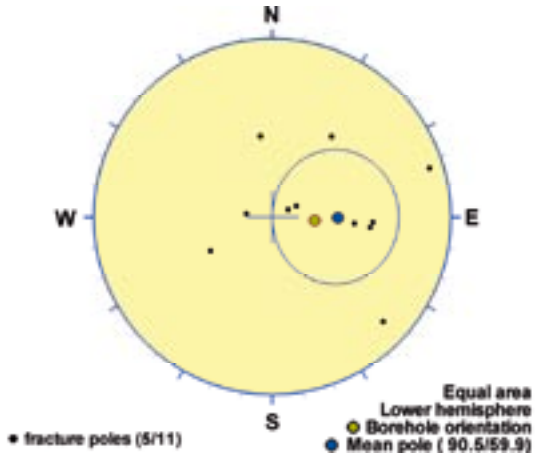

Contours from fractures

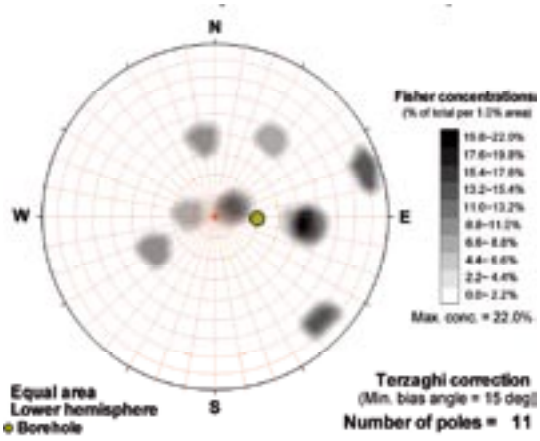

Orientation		Basis for orientation				Certainty	Thickness	
Strike	Dip	Fractures	Crush	Ductile structures	Reflectors	Orientation	Apparent	True
181	30	Used			Contradict	Very uncertain	0.8 m	0.8 m
Comment:								

KLX11A DZ16 (853 to 860), ductile/brittle zone

Scattered sections of brittle/ductile deformation zones with red staining, cataclasites and breccias. Increased frequency of sealed and open fractures. Low resistivity and low magnetic susceptibility. Two oriented radar reflectors occur, one at 854.7 m with the orientation 199/47 or 080/15, and one strong at 855.0 m with the orientation 108/67. Also, four non-oriented radar reflectors occur with angles between 24° and 47° to borehole axis. The host rock is dominated by quartz monzodiorite (501036).

Poles from crush zone

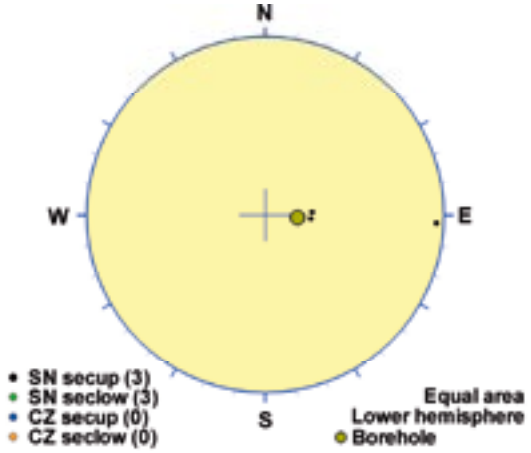

Poles from ductile structures

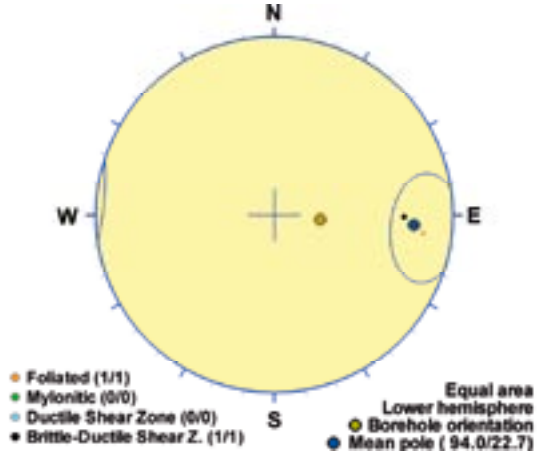

Poles from fractures

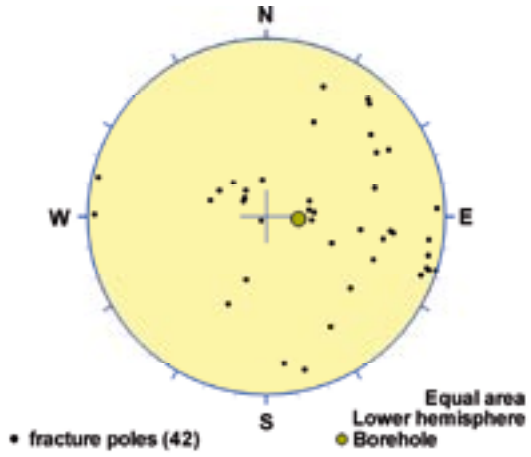

Contours from fractures

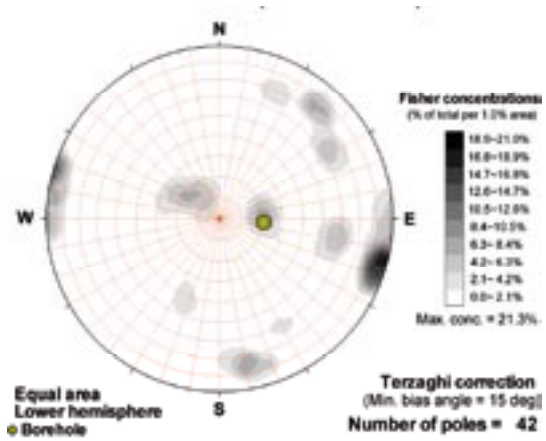

Orientation		Basis for orientation				Certainty	Thickness	
Strike	Dip	Fractures	Crush	Ductile structures	Reflectors	Orientation	Apparent	True
184	67	Verify		Used	Verify	Probable	7 m	4.8 m
Comment:								

KLX11A DZ17 (906.84 to 907.6), ductile/brittle zone

Low-grade ductile shear zone (judged from core). Central brittle part (907.00-907.04 m) with breccia and sealed network. Low resistivity. Two oriented radar reflectors occur, one at 907.3 m with the orientation 054/45, and one at the same borehole length 907.3 m with the orientation 197/63 or 041/24. The host rock is dominated by quartz monzodiorite (501036). Subordinate rock type is fine-grained granite (511058).

Poles from crush zone

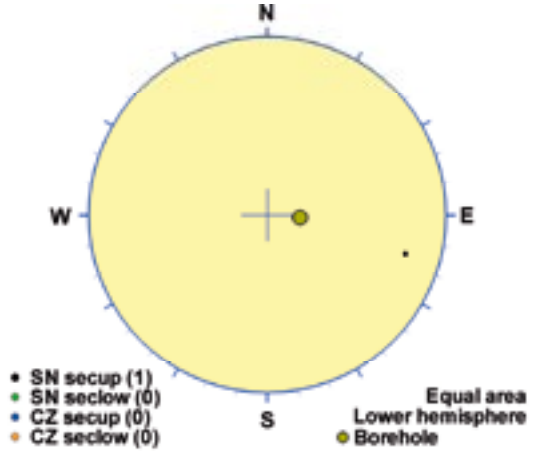

Poles from ductile structures

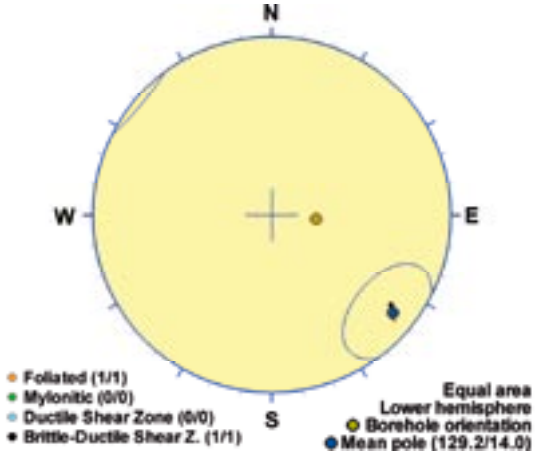

Poles from fractures

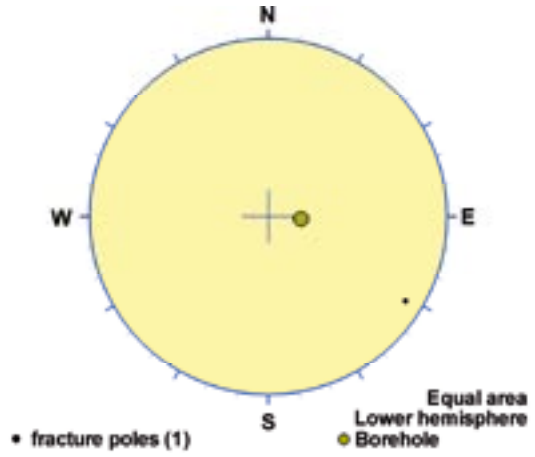

Contours from fractures

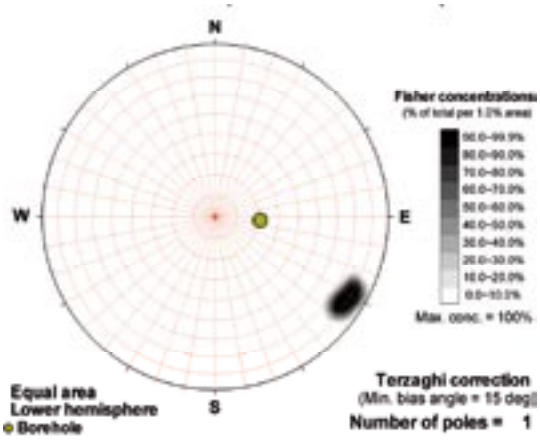

Orientation		Basis for orientation				Certainty	Thickness	
Strike	Dip	Fractures	Crush	Ductile structures	Reflectors	Orientation	Apparent	True
219	76	Verify	Verify	Used	Contradict	Probable	0.8 m	0.4 m
Comment:								

KLX11A DZ18 (974.1 to 975.2), ductile/brittle zone

Low grade ductile shear zone overprinted by brittle epidote-breccia and sealed fractures. Pegmatite dominates the central part. Low P-wave velocity and low magnetic susceptibility. One oriented radar reflector occurs at 975.1 m with the orientation 047/29 or 202/65. The host rock is dominated by quartz monzodiorite (501036). Subordinate rock type is pegmatite (501061).

Poles from crush zone

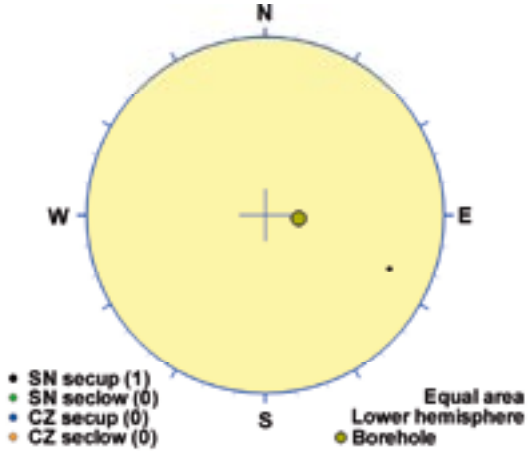

Poles from ductile structures

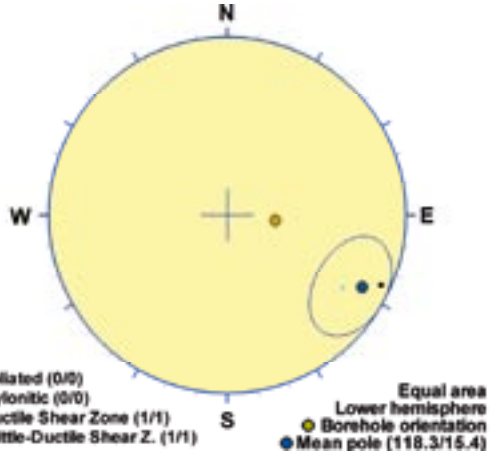

Poles from fractures

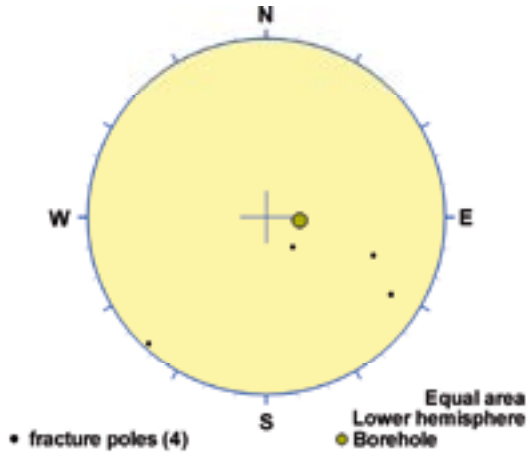

Contours from fractures

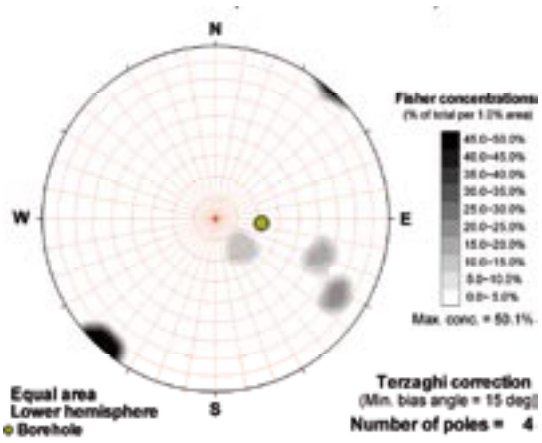

Orientation		Basis for orientation				Certainty	Thickness	
Strike	Dip	Fractures	Crush	Ductile structures	Reflectors	Orientation	Apparent	True
208	75	Verify	Verify	Used	Verify	Certain	1.1 m	0.6 m
Comment:								

KLX11B DZ1 (75.18 to 76.87), brittle zone

Brittle deformation zone characterized by increased frequency of open and sealed fractures, faint red staining, two crush zones and slickensides. Decreased resistivity and magnetic susceptibility. Partly decreased P-wave velocity and minor caliper anomalies. One non-oriented radar reflector at 75.6 m with the angle 66° to borehole axis. The host rock is totally dominated by quartz monzodiorite (501036).

Poles from crush zone

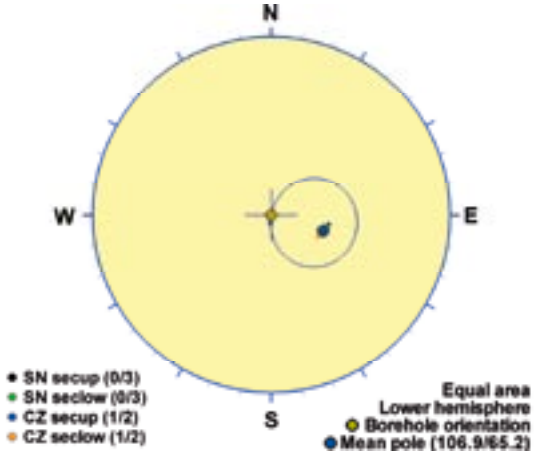

Poles from ductile structures

Data not used

Poles from fractures

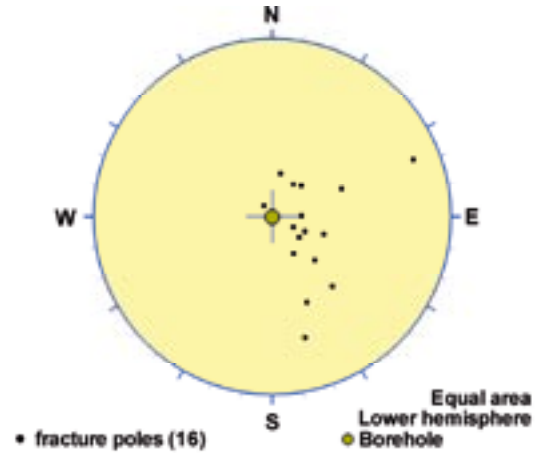

Contours from fractures

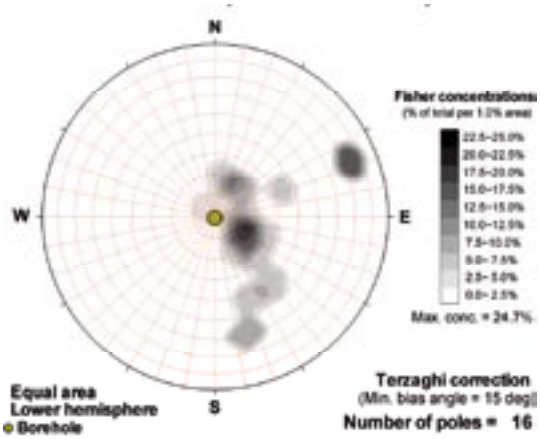

Orientation		Basis for orientation				Certainty	Thickness	
Strike	Dip	Fractures	Crush	Ductile structures	Reflectors	Orientation	Apparent	True
197	25	Verify	Used		Verify	Probable	1.7 m	1.5 m
Comment:								

KLX11B DZ2 (86.3 to 88.7), brittle zone

Brittle deformation zone characterized by increased frequency of sealed fractures, medium red staining, two breccias. Decreased resistivity and magnetic susceptibility. Partly decreased P-wave velocity and minor caliper anomalies. The host rock is totally dominated by quartz monzodiorite (501036).

Poles from crush zone

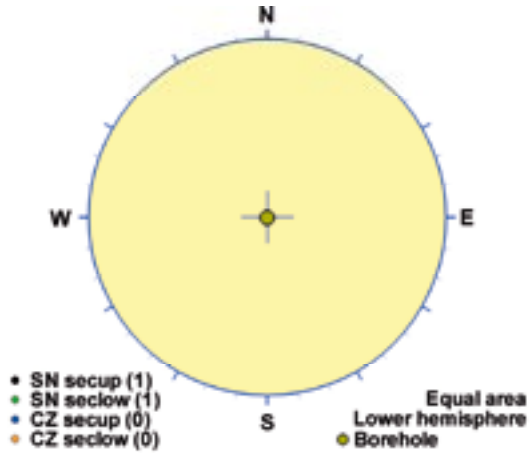

Poles from ductile structures

Data not used

Poles from fractures

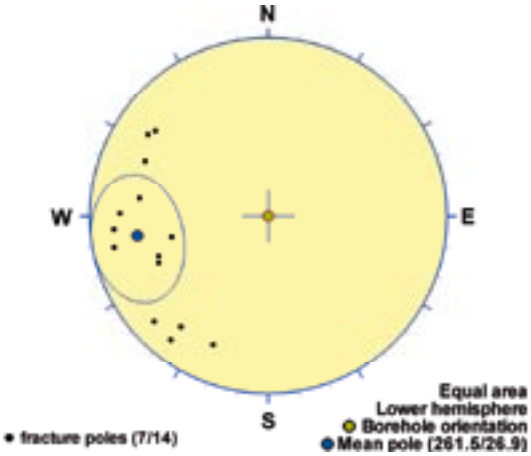

Contours from fractures

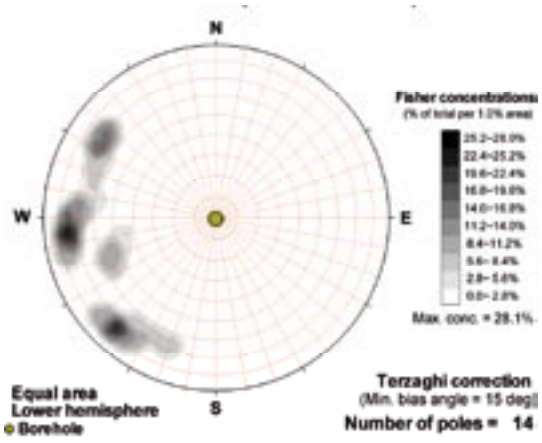

Orientation		Basis for orientation				Certainty	Thickness	
Strike	Dip	Fractures	Crush	Ductile structures	Reflectors	Orientation	Apparent	True
352	63	Used				Probable	2.4 m	1.1 m
Comment:								

KLX11D DZ1 (61.93 to 65.36), brittle zone

Brittle deformation zone characterized by increased frequency of sealed fractures, a slight increase in open fractures and faint to medium red staining. One strong radar reflector at 62.7 m with the orientation 017/70, and one non-oriented radar reflector at 63.8 m with the angle 63° to borehole axis. Low radar amplitude at 60-65 m. The host rock is totally dominated by quartz monzodiorite (501036). Subordinate rock types comprise very sparse occurrences of fine-grained dioritoid (501030) and fine-grained granite (511058).

Poles from crush zone

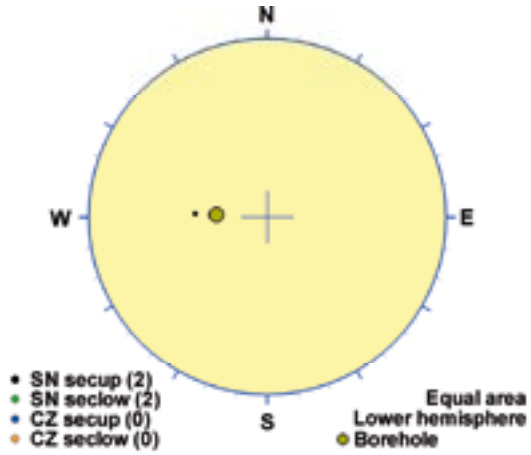

Poles from ductile structures

Data not used

Poles from fractures

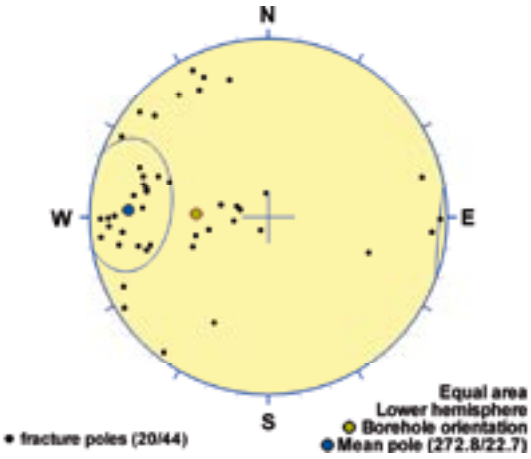

Contours from fractures

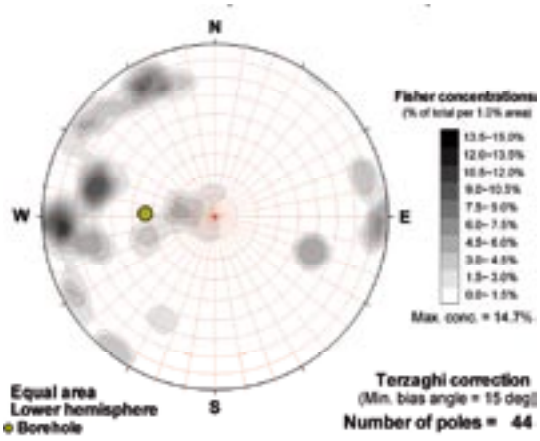

Orientation		Basis for orientation				Certainty	Thickness	
Strike	Dip	Fractures	Crush	Ductile structures	Reflectors	Orientation	Apparent	True
3	67	Used			Verify	Probable	3.4 m	2.8 m
Comment:								

KLX11D DZ2 (90.44 to 97.7), brittle zone

Brittle deformation zone characterized by increased frequency of sealed fractures, a slight increase in open fractures and faint to medium red staining. Three non-oriented radar reflectors at 90.6 m, 95.2 m and 97.1 m with the angle 53°, 42° and 42° to borehole axis, respectively. Low radar amplitude at 90-100 m. The host rock is totally dominated by quartz monzodiorite (501036). Subordinate rock type comprises very sparse occurrence of fine-grained granite (511058).

Poles from crush zone

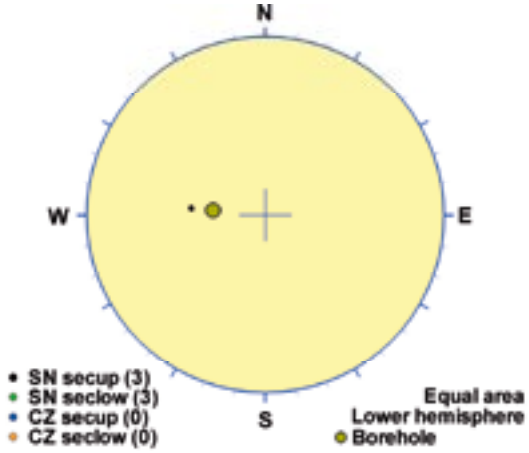

Poles from ductile structures

Data not used

Poles from fractures

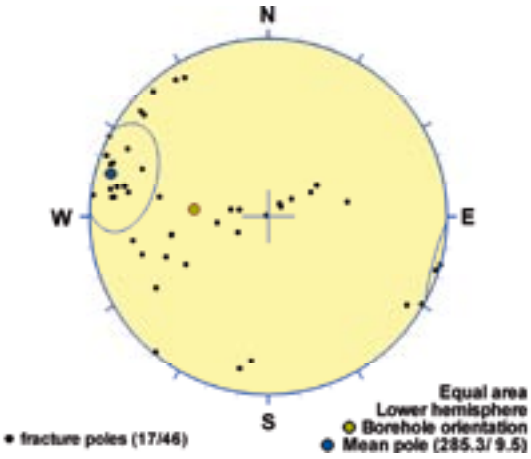

Contours from fractures

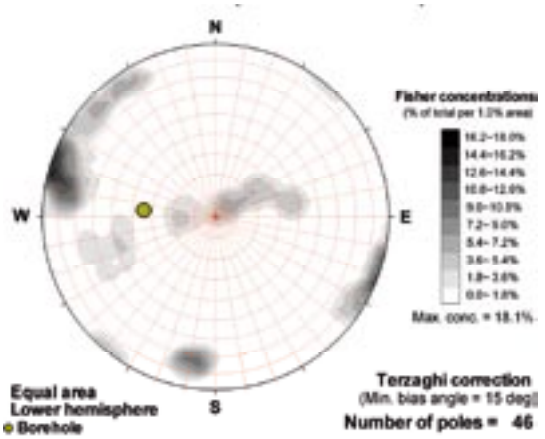

Orientation		Basis for orientation				Certainty	Thickness	
Strike	Dip	Fractures	Crush	Ductile structures	Reflectors	Orientation	Apparent	True
15	81	Used	Contradict		Verify	Probable	7.3 m	5 m
Comment:								

KLX11D DZ3 (106.67 to 110.6), brittle zone

Brittle deformation zone characterized by increased frequency of sealed fractures, a slight increase in open fractures, faint to weak red staining and slickensides. One very strong radar reflector at 107.4 m with the orientation 013/82, and two non-oriented radar reflectors at 107.4 m and 109.5 m, with the angle 37° and 42° to borehole axis, respectively. Low radar amplitude at 105-110 m. The host rock is totally dominated by quartz monzodiorite (501036). Subordinate rock type comprises very sparse occurrence of fine-grained granite (511058).

Poles from crush zone

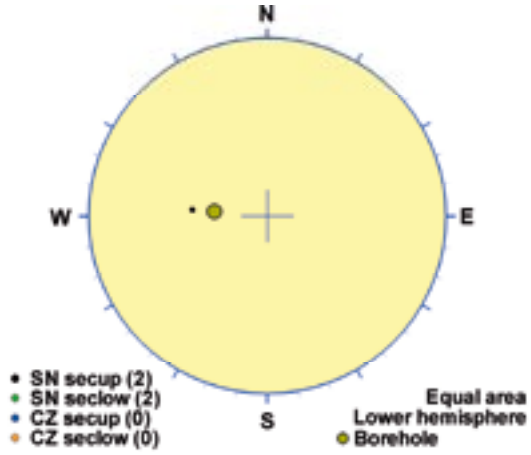

Poles from ductile structures

Data not used

Poles from fractures

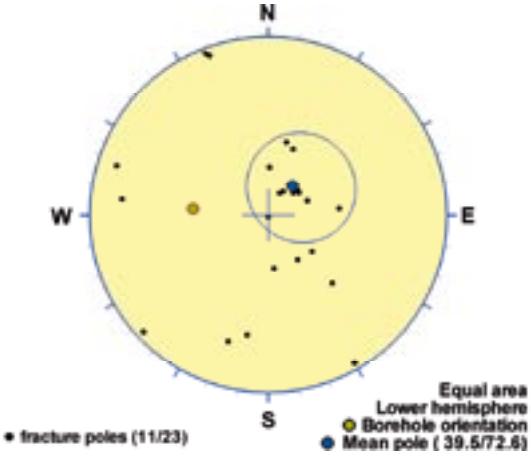

Contours from fractures

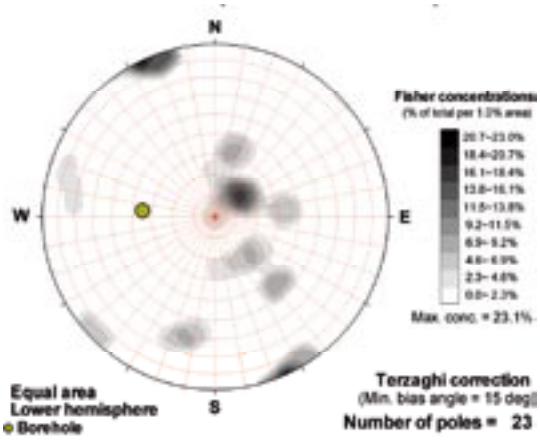

Orientation		Basis for orientation				Certainty	Thickness	
Strike	Dip	Fractures	Crush	Ductile structures	Reflectors	Orientation	Apparent	True
130	17	Used	Contradict		Verify	Probable	3.9 m	2.7 m
Comment:								

KLX11E DZ1 (15.56 to 20.05), brittle zone

Brittle deformation zone characterized by increased frequency of sealed fractures, a slight increase in open fractures, faint to weak saussuritization, faint to weak red staining, one slickenside and apertures up to 10 mm. The brittle deformation is overprinting minor brittle-ductile and ductile shear zones. One radar reflector at 19.4 m with the orientation 162/44 or 018/74, and one non-oriented radar reflector at 16.4 m with the angle 61° to borehole axis. The host rock is totally dominated by quartz monzodiorite (501036). Subordinate rock type comprises sparse occurrence of fine-grained granite (511058).

Poles from crush zone

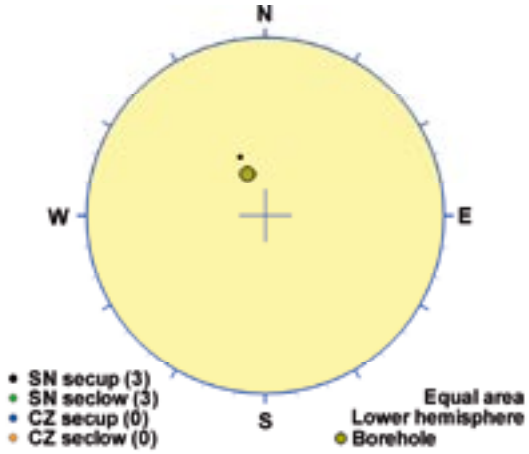

Poles from ductile structures

Data not used

Poles from fractures

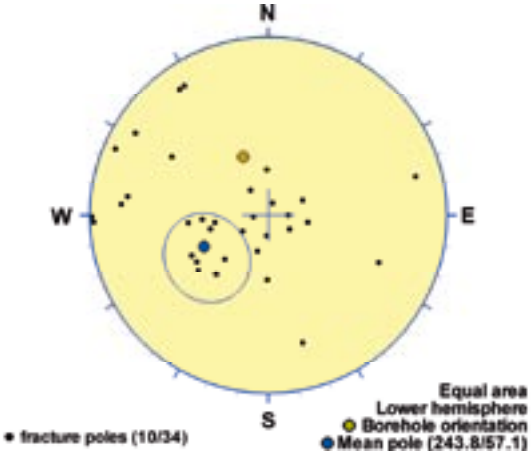

Contours from fractures

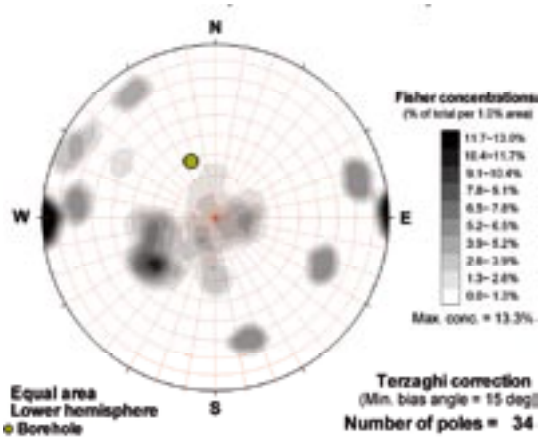

Orientation		Basis for orientation				Certainty	Thickness	
Strike	Dip	Fractures	Crush	Ductile structures	Reflectors	Orientation	Apparent	True
334	33	Used	Contradict	Contradict	Contradict	Uncertain	4.5 m	3.2 m
Comment:								

KLX11E DZ2 (39 to 61.42), ductile zone

Inhomogeneous low-grade ductile deformation zone. Two oriented radar reflectors occur, one at 41.0 m with the orientation 155/45 and one at 55.8 m with the orientation 013/21 or 086/47, the latter of which is strong. Five non-oriented radar reflectors occur with angles between 36° and 65° to borehole axis. The host rock is totally dominated by quartz monzodiorite (501036). Subordinate rock types comprise sparse occurrences of fine-grained granite (511058) and very sparse occurrence of granite (501058).

Poles from crush zone

Data not used

Poles from ductile structures

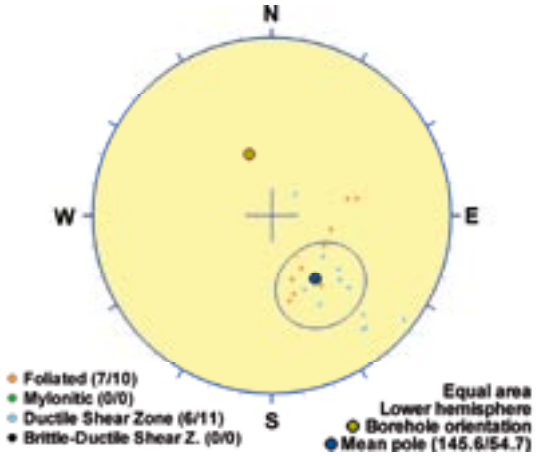

Poles from fractures

Data not used

Contours from fractures

Data not used

Orientation		Basis for orientation				Certainty	Thickness	
Strike	Dip	Fractures	Crush	Ductile structures	Reflectors	Orientation	Apparent	True
236	35			Used	Contradict	Probable	22.4 m	9.6 m
Comment:								

KLX11E DZ3 (74.11 to 74.53), brittle zone

Brittle deformation zone characterized by increased frequency of sealed and open fractures. The host rock is totally dominated by quartz monzodiorite (501036).

Poles from crush zone

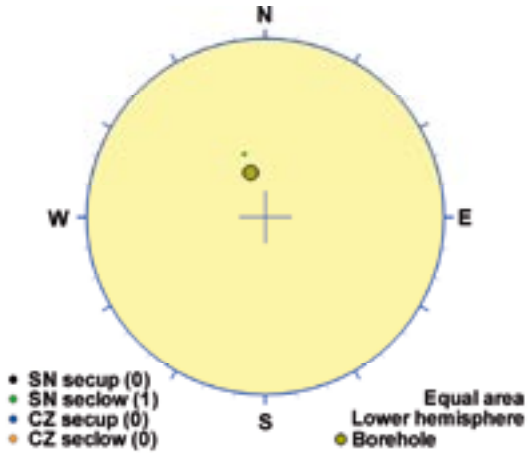

Poles from ductile structures

Data not used

Poles from fractures

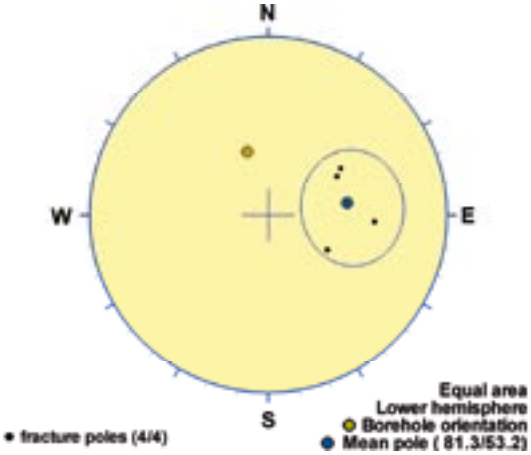

Contours from fractures

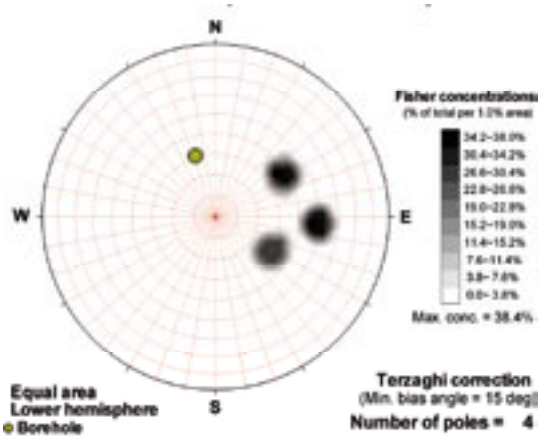

Orientation		Basis for orientation				Certainty	Thickness	
Strike	Dip	Fractures	Crush	Ductile structures	Reflectors	Orientation	Apparent	True
171	37	Used	Contradict			Uncertain	0.4 m	0.3 m
Comment:								

KLX11E DZ4 (112.48 to 114.8), brittle zone

Brittle deformation zone characterized by slight increased frequency of sealed fractures and open fractures, weak to medium red staining and one slickenside. One very strong radar reflector occurs at 113.7 m with the orientation 336/62 or 130/73. Low radar amplitude occurs at 110-115 m. The host rock is totally dominated by quartz monzodiorite (501036).

Poles from crush zone

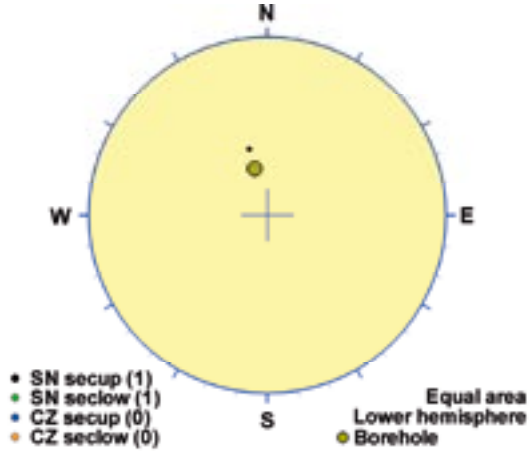

Poles from ductile structures

Data not used

Poles from fractures

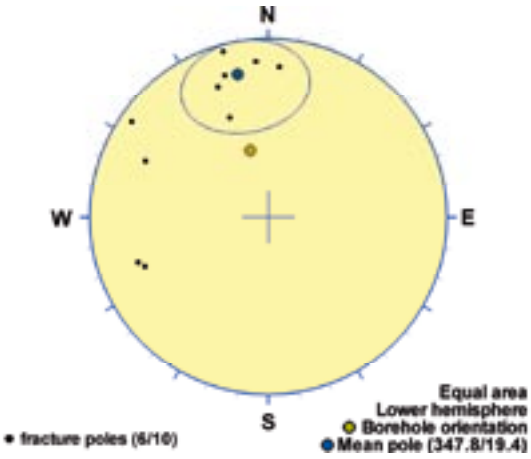

Contours from fractures

Orientation		Basis for orientation				Certainty	Thickness	
Strike	Dip	Fractures	Crush	Ductile structures	Reflectors	Orientation	Apparent	True
78	71	Used	Contradict		Contradict	Probable	2.3 m	1.8 m
Comment:								

KLX11F DZ1 (69.6 to 72), brittle zone

Brittle deformation zone characterized by increased frequency of sealed and open fractures, faint to weak red staining, two crush zones and one slickenside. One non-oriented radar reflector occurs at 70.9 m with the angle 37° to borehole axis. Low radar amplitude at 70 m. The host rock is totally dominated by quartz monzodiorite (501036).

Poles from crush zone

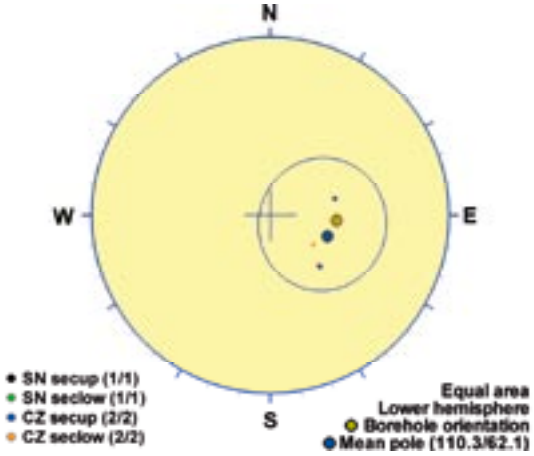

Poles from ductile structures

Data not used

Poles from fractures

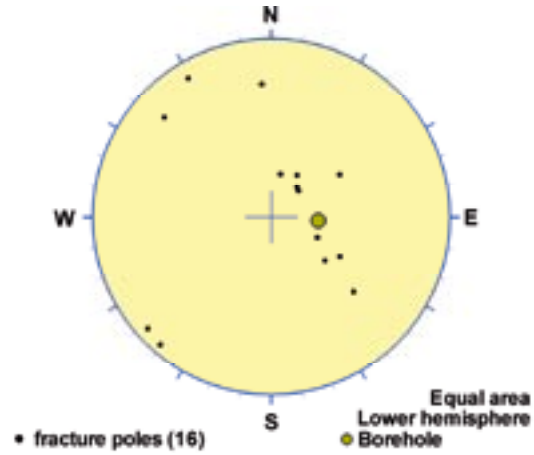

Contours from fractures

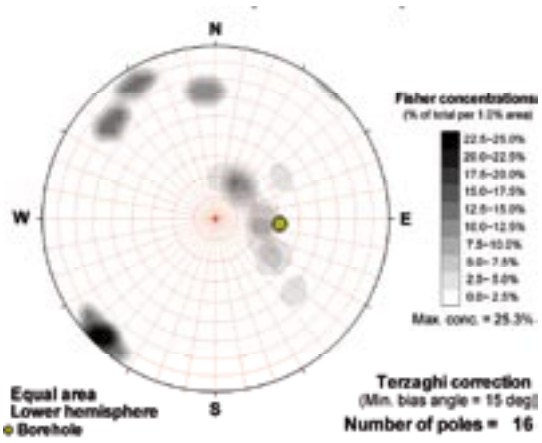

Orientation		Basis for orientation				Certainty	Thickness	
Strike	Dip	Fractures	Crush	Ductile structures	Reflectors	Orientation	Apparent	True
200	28	Verify	Used		Contradict	Probable	2.4 m	2.4 m
Comment:								

KLX12A DZ3 (270.7 to 271.05), ductile zone

Minor low-grade ductile shear zone (judged from core). Low resistivity anomaly and decreased magnetic susceptibility. One radar reflector at 270.9 m with the orientation 351/24 or 085/20. Low radar amplitude at 270-272 m. The host rock is dominated by fine-grained diorite-gabbro (505102).

Poles from crush zone

Data not used

Poles from ductile structures

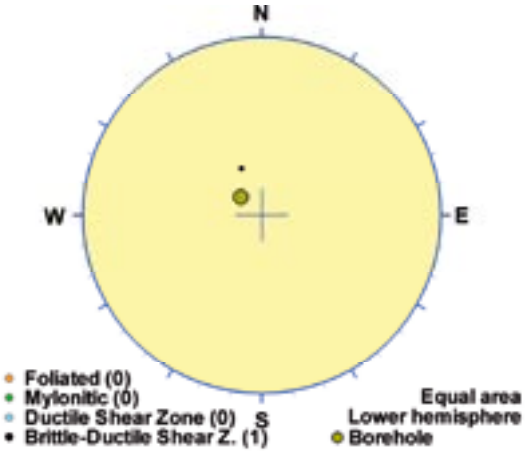

Poles from fractures

Data not used

Contours from fractures

Data not used

Orientation		Basis for orientation				Certainty	Thickness	
Strike	Dip	Fractures	Crush	Ductile structures	Reflectors	Orientation	Apparent	True
67	26			Used	Verify	Certain	0.4 m	0.3 m
Comment:								

KLX12A DZ5 (282 to 282.4), ductile zone

Minor low grade inhomogeneous ductile shear zone (judged from core). Minor low resistivity anomaly and decreased magnetic susceptibility. The host rock is dominated by fine-grained diorite-gabbro (505102).

Poles from crush zone

Data not used

Poles from ductile structures

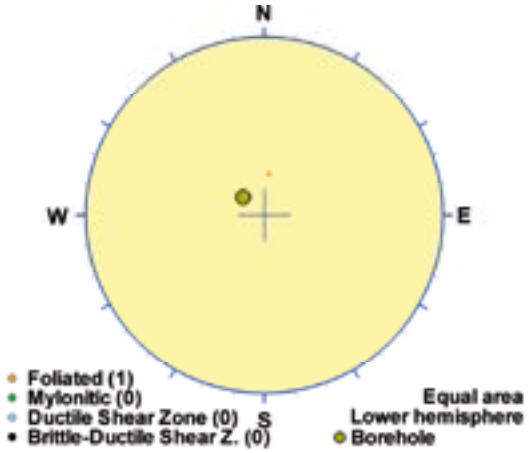

Poles from fractures

Data not used

Contours from fractures

Data not used

Orientation		Basis for orientation				Certainty	Thickness	
Strike	Dip	Fractures	Crush	Ductile structures	Reflectors	Orientation	Apparent	True
100	20			Used		Certain	0.4 m	0.4 m
Comment:								

KLX12A DZ7 (329.39 to 329.85), brittle zone

Minor low grade brittle shear zone (judged from core). Shear zone is subparallel with core. Narrow, low resistivity anomaly and decreased magnetic susceptibility. One non-oriented radar reflector close to the deformation zone at 330.1 m with the angle 15° to borehole axis. The host rock is dominated by Ävrö quartz monzodiorite (501046).

Poles from crush zone

Poles from ductile structures

Data not used

Poles from fractures

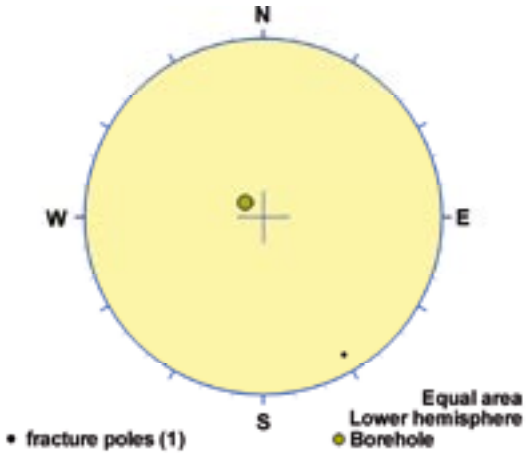

Contours from fractures

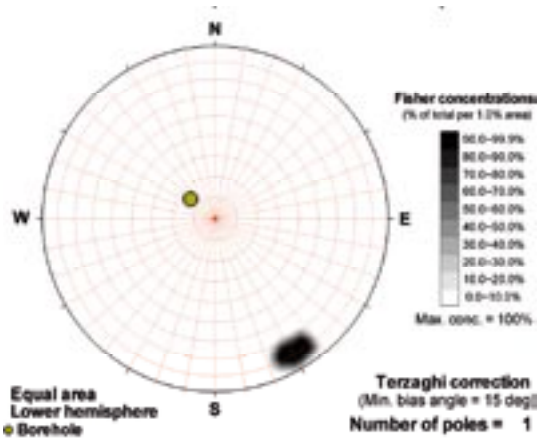

Orientation		Basis for orientation				Certainty	Thickness	
Strike	Dip	Fractures	Crush	Ductile structures	Reflectors	Orientation	Apparent	True
239	81	Used			Verify	Very uncertain	0.5 m	0 m
Comment:								

KLX12A DZ8 (366.41 to 366.99), ductile zone

Minor low grade ductile shear zone (judged from core) in composite dike. Decreased magnetic susceptibility. One non-oriented radar reflector close to the deformation zone at 366.3 m with the angle 75° to borehole axis. The host rock is dominated by fine-grained diorite-gabbro (505102).

Poles from crush zone

Data not used

Poles from ductile structures

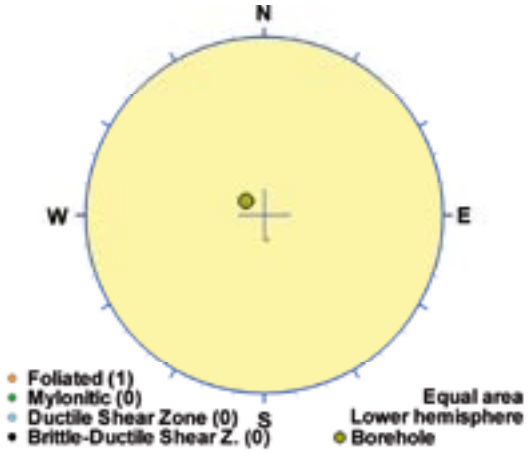

Poles from fractures

Data not used

Contours from fractures

Data not used

Orientation		Basis for orientation				Certainty	Thickness	
Strike	Dip	Fractures	Crush	Ductile structures	Reflectors	Orientation	Apparent	True
257	12			Used	Verify	Probable	0.6 m	0.5 m
Comment:								

KLX12A DZ9 (428.95 to 429.4), ductile zone

Minor low grade ductile shear zone (judged from core) composite dike. Decreased magnetic susceptibility. Low radar amplitude along the deformation zone. The host rock is dominated by fine-grained diorite-gabbro (505102).

Poles from crush zone

Data not used

Poles from ductile structures

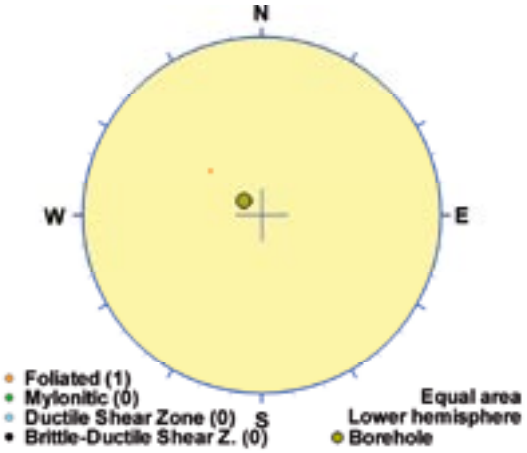

Poles from fractures

Data not used

Contours from fractures

Data not used

Orientation		Basis for orientation				Certainty	Thickness	
Strike	Dip	Fractures	Crush	Ductile structures	Reflectors	Orientation	Apparent	True
41	31			Used		Probable	0.4 m	0.4 m
Comment:								

KLX12A DZ10 (445.6 to 447.55), ductile/brittle zone

Sealed network, inhomogeneously foliated. Low resistivity anomaly. Decreased magnetic susceptibility in the section 446.6-455.6 m, i.e. it continues outside the DZ. One non-oriented radar reflector close to the deformation zone at 447.8 m with the angle 53° to borehole axis. Low radar amplitude along the deformation zone. The host rock is dominated by diorite/gabbro (501033). Subordinate rock type is fine-grained granite (511058).

Poles from crush zone

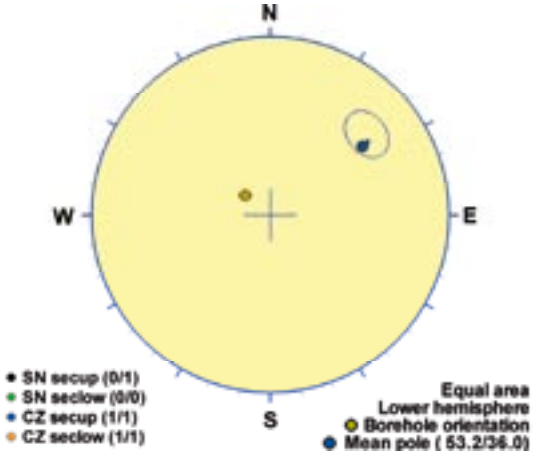

Poles from ductile structures

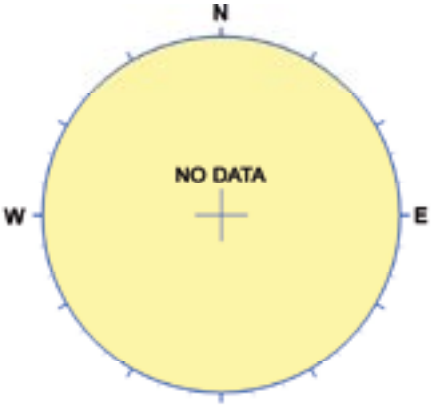

Poles from fractures

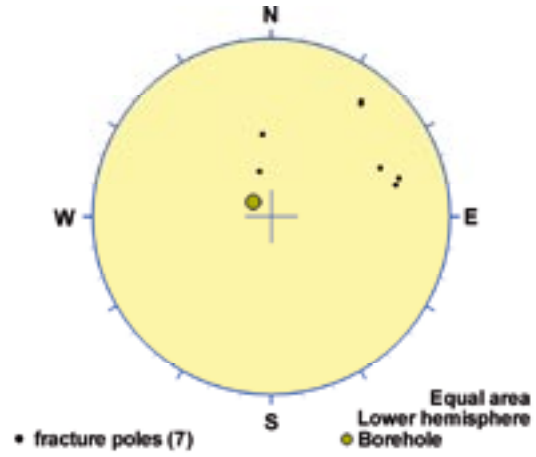

Contours from fractures

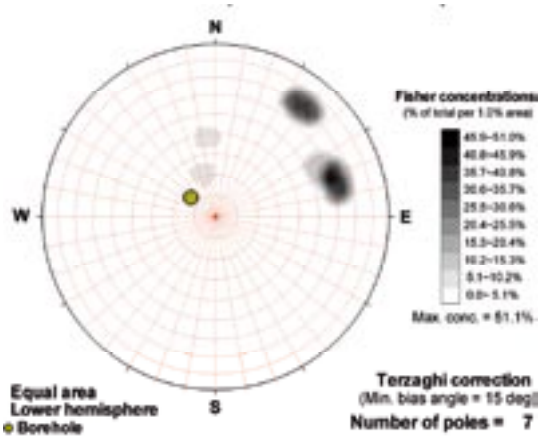

Orientation		Basis for orientation				Certainty	Thickness	
Strike	Dip	Fractures	Crush	Ductile structures	Reflectors	Orientation	Apparent	True
143	54	Verify	Used		Contradict	Probable	1.9 m	1 m
Comment:								

KLX12A DZ11 (498.85 to 499.54), ductile zone

Minor low grade ductile shear zone (judged from core) composite dike. Low resistivity anomaly and decreased magnetic susceptibility. Decreased P-wave velocity. One non-oriented radar reflector close to the deformation zone at 499.6 m with the angle 73° to borehole axis. The host rock is dominated by fine-grained diorite-gabbro (505102). Subordinate rock type is diorite/gabbro (501033).

Poles from crush zone

Data not used

Poles from ductile structures

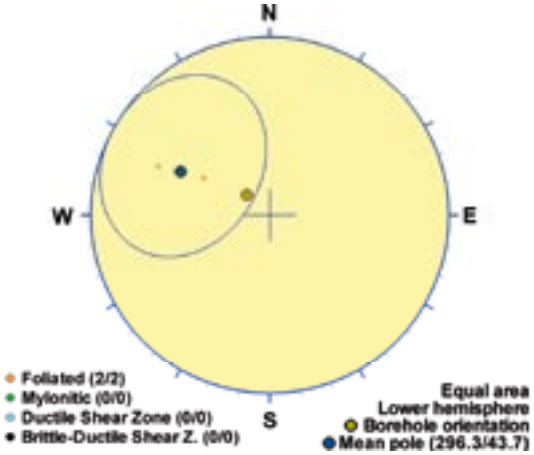

Poles from fractures

Data not used

Contours from fractures

Data not used

Orientation		Basis for orientation				Certainty	Thickness	
Strike	Dip	Fractures	Crush	Ductile structures	Reflectors	Orientation	Apparent	True
26	46		Verify	Used	Verify	Probable	0.7 m	0.6 m
Comment: Several fractures in BIPS, but no stereoplot.								

KLX12A DZ12 (596.5 to 600.8), ductile zone

Minor low grade inhomogeneous ductile shear zone (judged from core). Partly decreased resistivity. One non-oriented radar reflector at 598.0 m with the angle 66° to borehole axis. The host rock is dominated by Ävrö quartz monzodiorite (501046) and quartz monzodiorite (501036). Subordinate rock types are diorite/gabbro (501033), fine-grained granite (511058) and granite (501058).

Poles from crush zone

Data not used

Poles from ductile structures

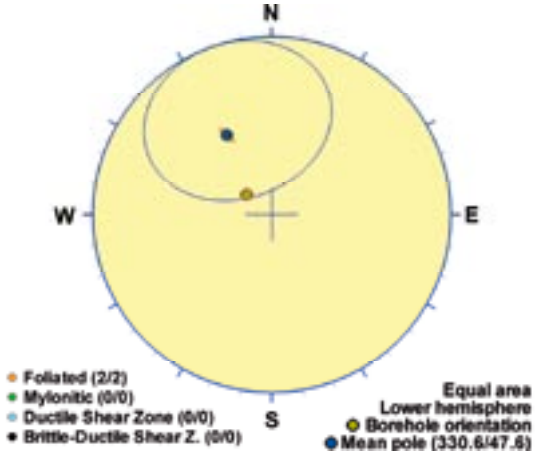

Poles from fractures

Data not used

Contours from fractures

Data not used

Orientation		Basis for orientation				Certainty	Thickness	
Strike	Dip	Fractures	Crush	Ductile structures	Reflectors	Orientation	Apparent	True
61	42			Used	Verify	Certain	4.3 m	3.7 m

Comment: The zone contains plenty of fractures in BIPS, but there is no fracture plot. Therefore only ductile structures are used.

KLX13A DZ1 (146.8 to 147.4), ductile/brittle zone

Brittle-ductile shear zone with increased frequency of sealed fractures and weak alteration. Single distinct low resistivity anomaly that coincides with strong gradient in the density. Decreased magnetic susceptibility. The host rock is dominated by Ävrö quartz monzodiorite (501046) and diorite/gabbro (501033). Subordinate rock types is fine-grained granite (511058).

Poles from crush zone

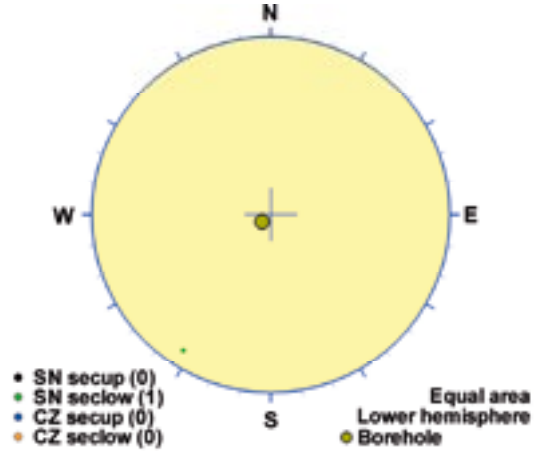

Poles from ductile structures

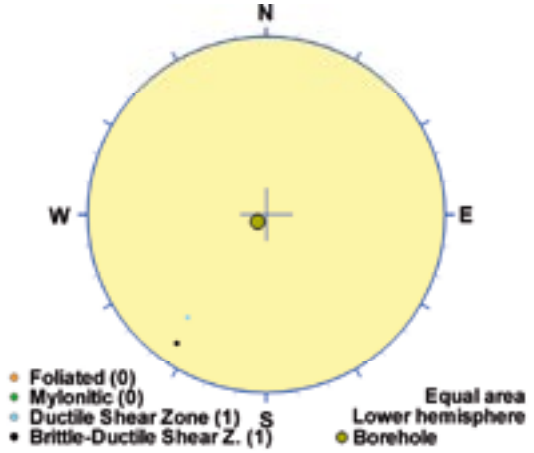

Poles from fractures

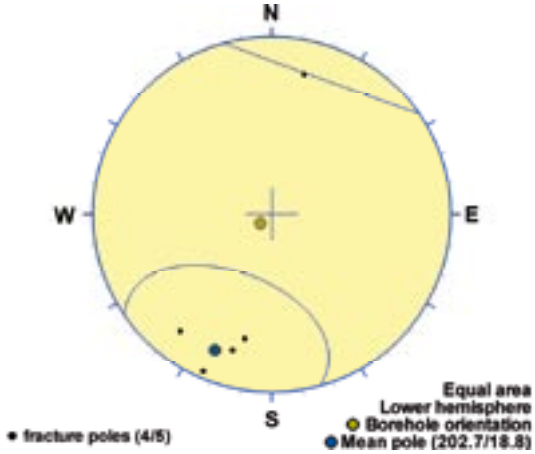

Contours from fractures

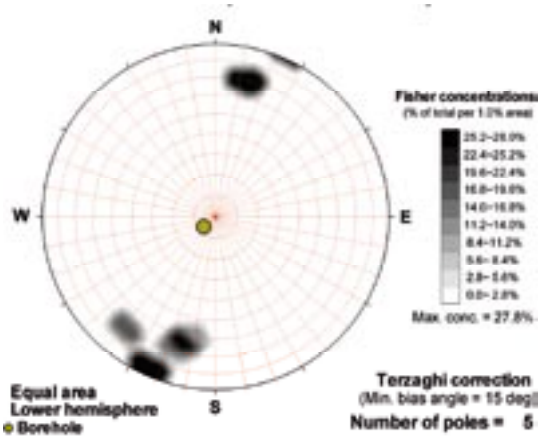

Orientation		Basis for orientation				Certainty	Thickness	
Strike	Dip	Fractures	Crush	Ductile structures	Reflectors	Orientation	Apparent	True
293	71	Used		Verify		Certain	0.6 m	0.3 m
Comment:								

KLX13A DZ2 (173.2 to 177.45), brittle zone

Brittle deformation zone characterized by increased frequency of open and sealed fractures, faint alteration, general decrease in bulk resistivity and partly decreased P-wave velocity. The section displays combination of strong positive and negative anomalies in the density, the natural gamma radiation and the magnetic susceptibility. One oriented radar reflector at 177.5 m (153/37 or 330/50) and one non-oriented at 176.9 m with the angle 56° to borehole axis. Low radar amplitude at 172-176 m. The host rock is dominated by diorite/gabbro (501033). Subordinate rock type is fine-grained granite (511058).

Poles from crush zone

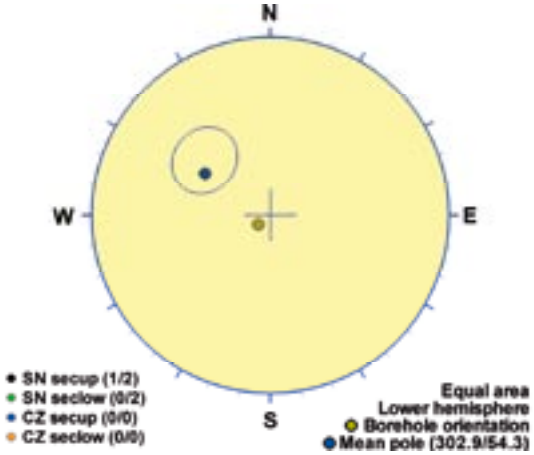

Poles from ductile structures

Data not used

Poles from fractures

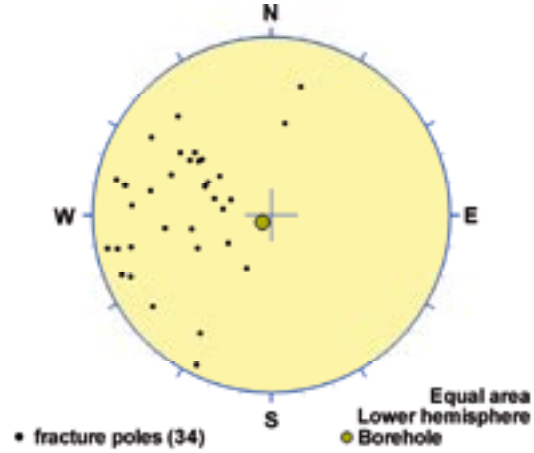

Contours from fractures

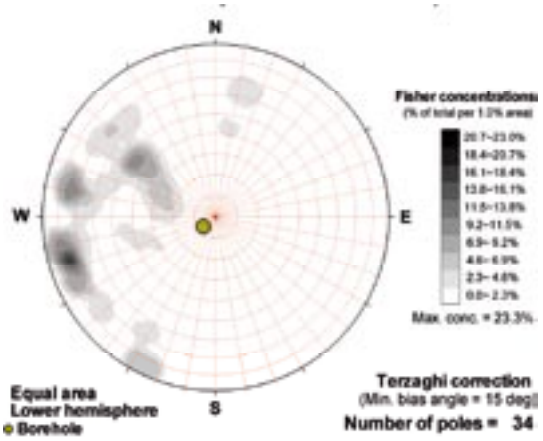

Orientation		Basis for orientation				Certainty	Thickness	
Strike	Dip	Fractures	Crush	Ductile structures	Reflectors	Orientation	Apparent	True
33	36	Verify	Used		Verify	Certain	4.2 m	3.5 m
Comment:								

KLX13A DZ3 (254.9 to 255.6), ductile/brittle zone

Brittle-ductile shear zone (judged from core). Increased frequency of open and sealed fractures. One crush zone at 255.01-255.12 m and weak alteration. Single distinct low resistivity anomaly that coincides with decreased P-wave velocity and strong gradients in the density, the natural gamma radiation and the magnetic susceptibility. One oriented prominent radar reflector at 255.3 m (170/45 or 345/57) and one non-oriented at 255.5 m with the angle 66° to borehole axis. Low radar amplitude at 253-256 m. The host rock is dominated by fine-grained diorite-gabbro (505102). Subordinate rock types are Ävrö granite (501044) and fine-grained granite (511058). Confidence level = 3.

Poles from crush zone

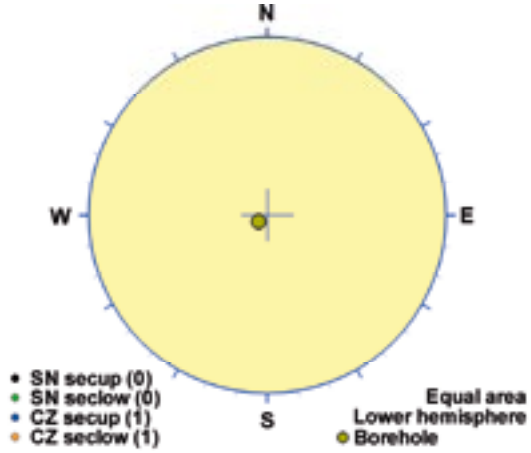

Poles from ductile structures

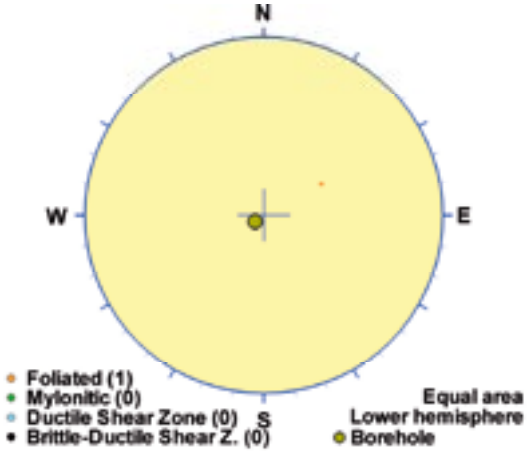

Poles from fractures

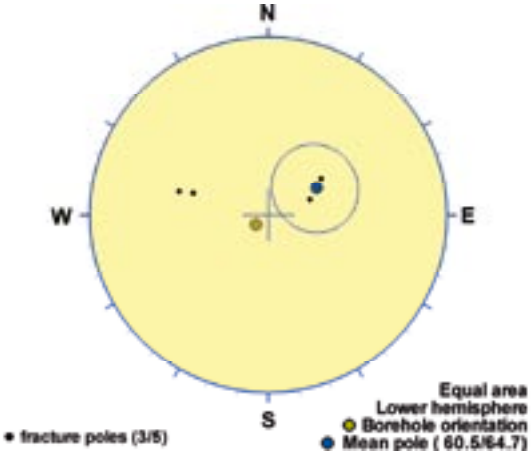

Contours from fractures

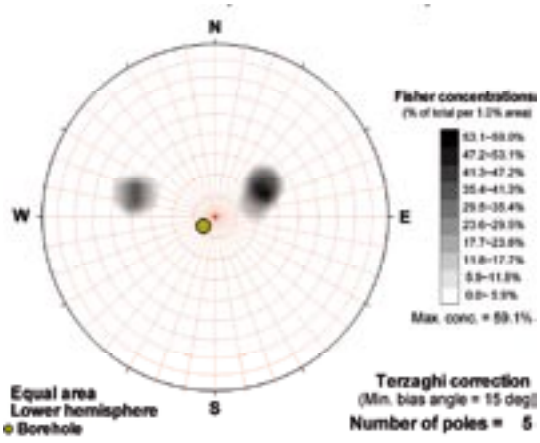

Orientation		Basis for orientation				Certainty	Thickness	
Strike	Dip	Fractures	Crush	Ductile structures	Reflectors	Orientation	Apparent	True
151	25	Used		Verify	Verify	Probable	0.7 m	0.6 m
Comment:								

KLX13A DZ4 (291 to 291.3), ductile zone

Ductile shear zone. Increased frequency of sealed fractures, slight increase of open fractures and weak alteration. Single distinct low resistivity anomaly. The host rock is dominated by Ävrö quartz monzodiorite (501046). Subordinate rock type is fine-grained granite (511058).

Poles from crush zone

Data not used

Poles from ductile structures

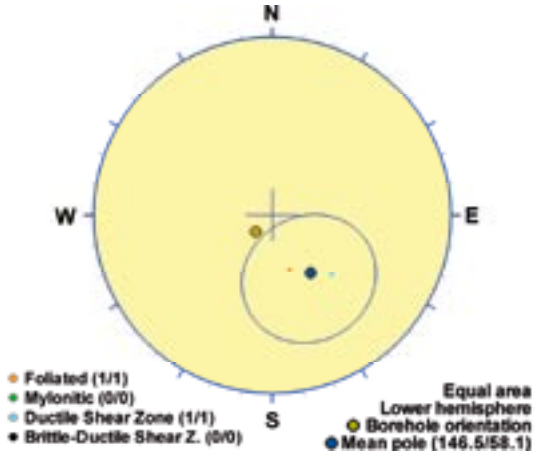

Poles from fractures

Data not used

Contours from fractures

Data not used

Orientation		Basis for orientation				Certainty	Thickness	
Strike	Dip	Fractures	Crush	Ductile structures	Reflectors	Orientation	Apparent	True
237	32			Used		Certain	0.3 m	0.3 m
Comment:								

KLX13A DZ5 (348.75 to 349.5), ductile/brittle zone

Brittle-ductile deformation zone. Increased frequency of sealed fractures and slight increase of open fractures with large apertures. Faint to weak alteration. Single distinct low resistivity anomaly that coincides with decreased P-wave velocity, decreased density, decreased magnetic susceptibility and caliper anomaly. One non-oriented radar reflector at 348.6 m with the angle 39° to borehole axis. The host rock is dominated by fine-grained granite (511058).

Poles from crush zone

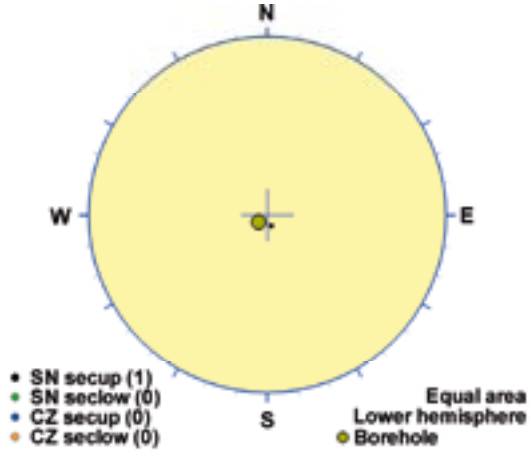

Poles from ductile structures

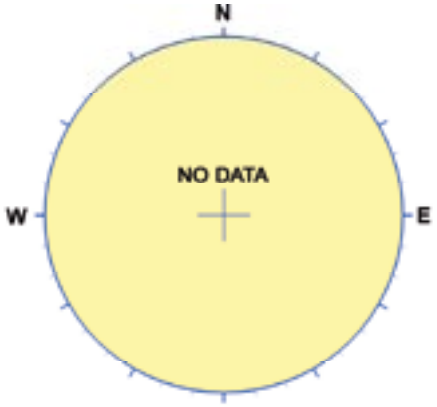

Poles from fractures

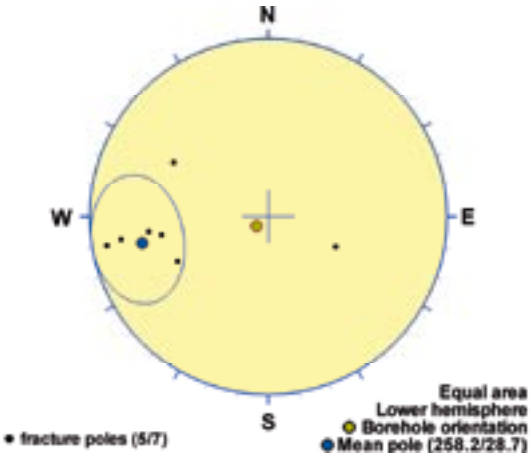

Contours from fractures

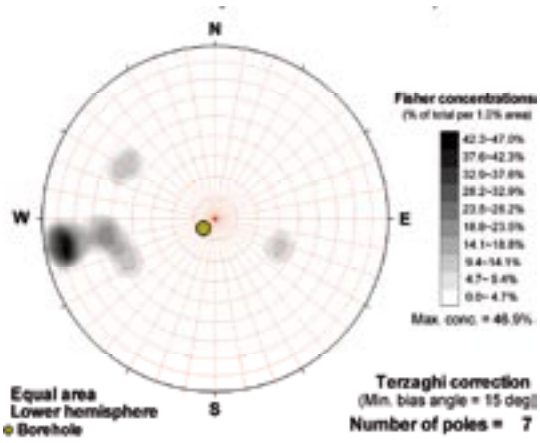

Orientation		Basis for orientation				Certainty	Thickness	
Strike	Dip	Fractures	Crush	Ductile structures	Reflectors	Orientation	Apparent	True
348	61	Used	Contradict		Verify	Uncertain	0.8 m	0.4 m
Comment:								

KLX13A DZ6 (384 to 388.2), brittle zone

Brittle deformation zone characterized by increased frequency of open fractures with large apertures. Crush zone at 387.71-387.82 m. Several low resistivity anomalies, two caliper anomalies and intervals with decreased P-wave velocity. One oriented radar reflector at 385.5 m (150/14) and one non-oriented at 385.0 m with the angle 44° to borehole axis. The host rock is dominated by Ävrö quartz monzodiorite (501046). Subordinate rock types are fine-grained granite (511058) and granite (501058).

Poles from crush zone

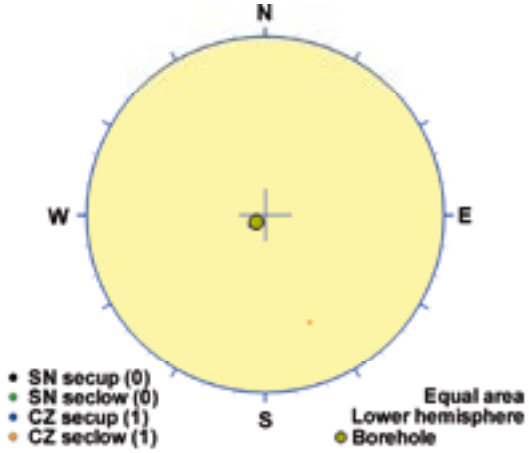

Poles from ductile structures

Data not used

Poles from fractures

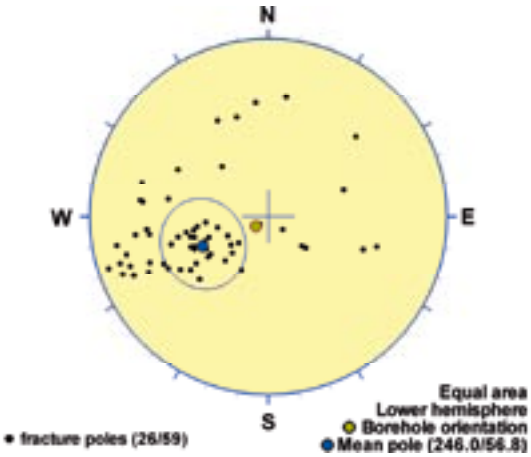

Contours from fractures

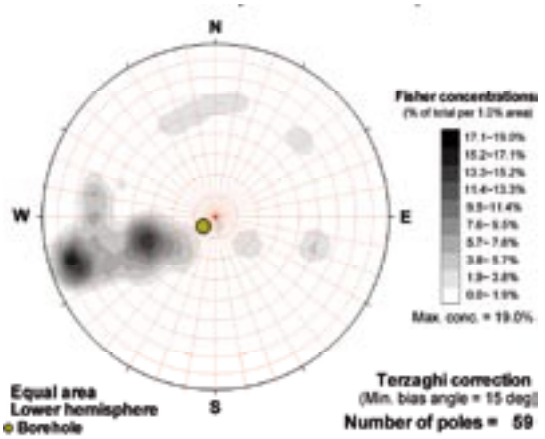

Orientation		Basis for orientation				Certainty	Thickness	
Strike	Dip	Fractures	Crush	Ductile structures	Reflectors	Orientation	Apparent	True
336	33	Used	Contradict		Verify	Probable	4.2 m	3.8 m
Comment:								

KLX14A DZ1 (10.11 to 10.61), ductile/brittle zone

Low-grade ductile shear zone associated with fine-grained diorite-gabbro (505102). Increased frequency of sealed fractures. Decreased magnetic susceptibility and resistivity (no sonic or caliper data available).

Poles from crush zone

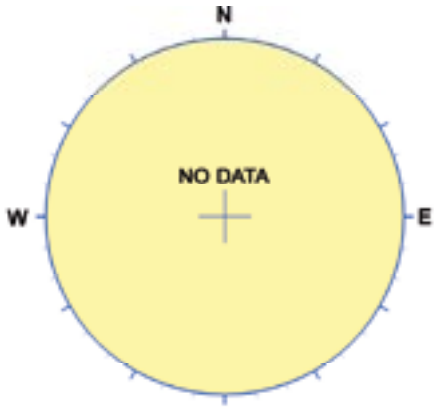

Poles from ductile structures

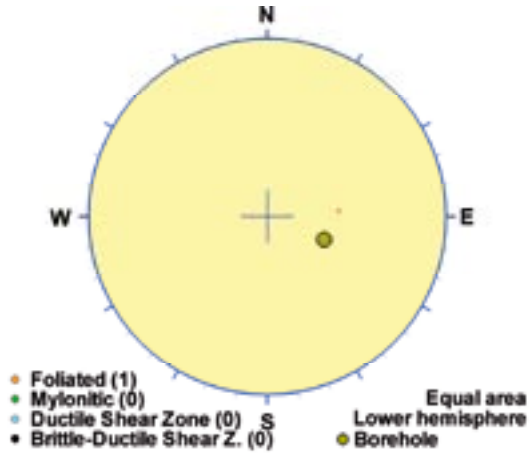

Poles from fractures

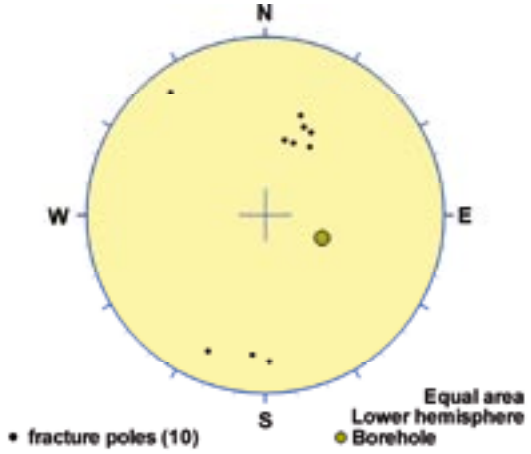

Contours from fractures

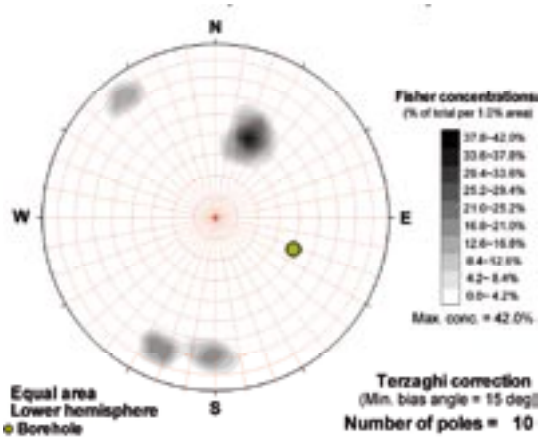

Orientation		Basis for orientation				Certainty	Thickness	
Strike	Dip	Fractures	Crush	Ductile structures	Reflectors	Orientation	Apparent	True
176	33	Contradict	Not Used	Used		Uncertain	0.5 m	0.5 m
Comment:								

KLX14A DZ2 (17.83 to 18.3), brittle zone

Brittle deformation zone characterized by increased frequency of open fractures, crush (0.35 m), faint red staining and slickenside. Decreased magnetic susceptibility and resistivity (no sonic or caliper data available). One radar reflector occurs at 17.9 m with the orientation 186/14. The reflector is prominent and can be observed to a distance of 20 m outside the borehole. The host rock is totally dominated by quartz monzodiorite (501036).

Poles from crush zone

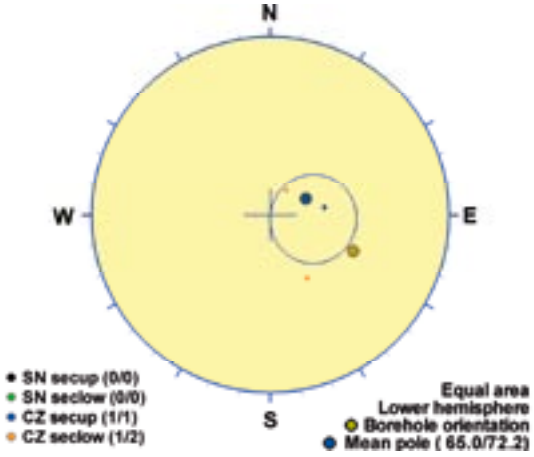

Poles from ductile structures

Data not used

Poles from fractures

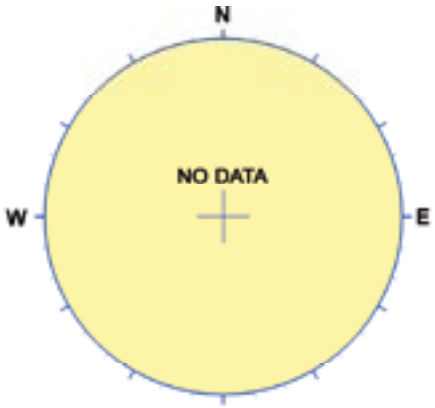

Contours from fractures

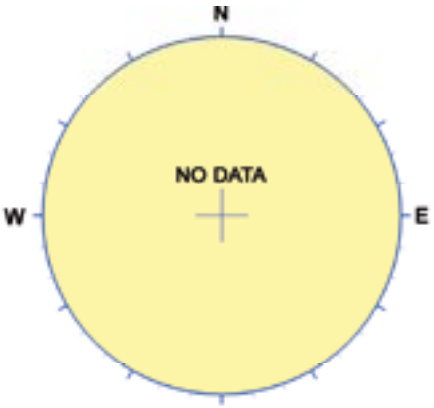

Orientation		Basis for orientation				Certainty	Thickness	
Strike	Dip	Fractures	Crush	Ductile structures	Reflectors	Orientation	Apparent	True
155	18		Used		Verify	Probable	0.5 m	0.4 m
Comment:								

KLX14A DZ3 (42.07 to 43.35), ductile/brittle zone

Brittle-ductile deformation zone characterized by increased frequency of open and sealed fractures and crush (0.3 m). Decreased magnetic susceptibility and resistivity, and slightly decreased P-wave velocity (no caliper data available). One non-oriented radar reflector occurs at 43.1 m with the angle 55° to borehole axis. The host rock is totally dominated by quartz monzodiorite (501036) with subordinate pegmatite (501061).

Poles from crush zone

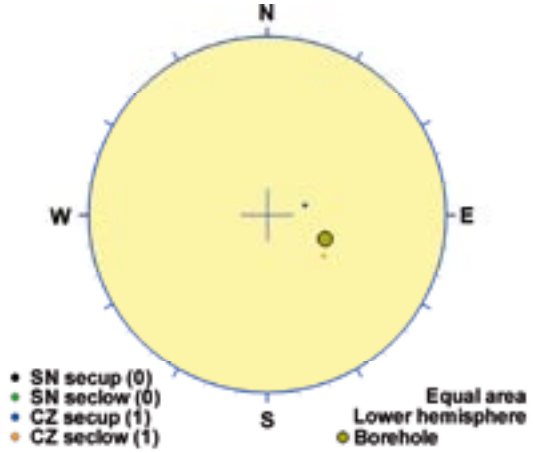

Poles from ductile structures

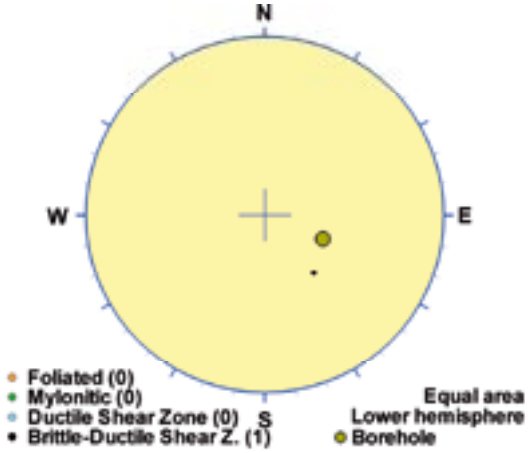

Poles from fractures

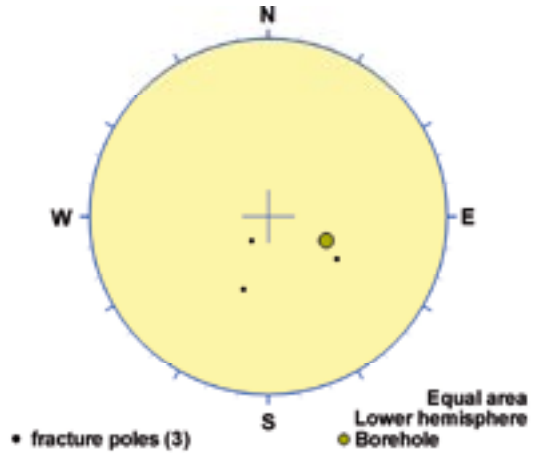

Contours from fractures

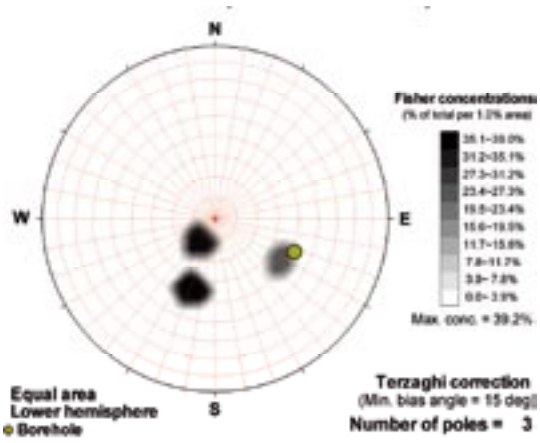

Orientation		Basis for orientation				Certainty	Thickness	
Strike	Dip	Fractures	Crush	Ductile structures	Reflectors	Orientation	Apparent	True
230	35	Verify	Verify	Used	Contradict	Probable	1.3 m	1.2 m
Comment:								

KLX14A DZ5 (138.1 to 138.9), brittle zone

Brittle deformation zone characterized by increased frequency of sealed fractures and a moderate increase in open fractures, slickensides, weak red staining and epidotiztion. The section is characterized by decreased magnetic susceptibility, resistivity and P-wave velocity. The host rock is dominated by quartz monzodiorite with very sparse occurrence of fine-grained granite (511058).

Poles from crush zone

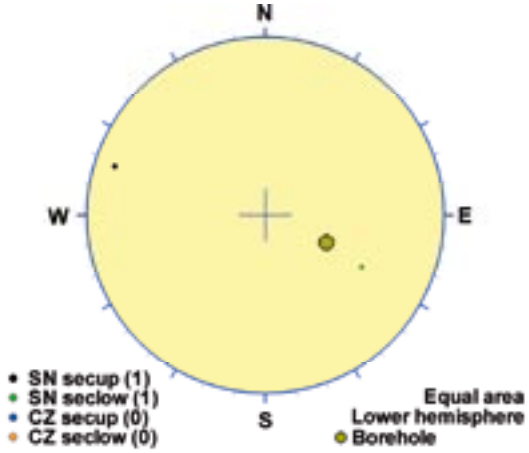

Poles from ductile structures

Data not used

Poles from fractures

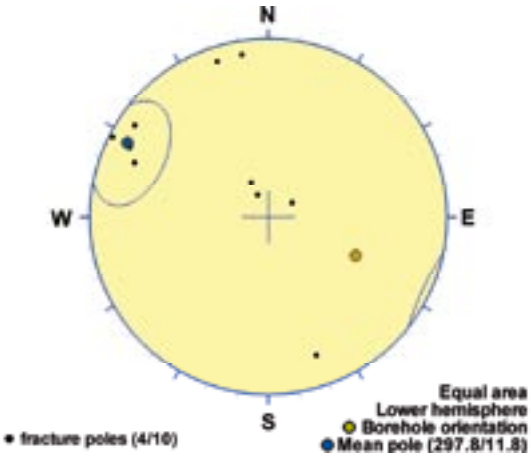

Contours from fractures

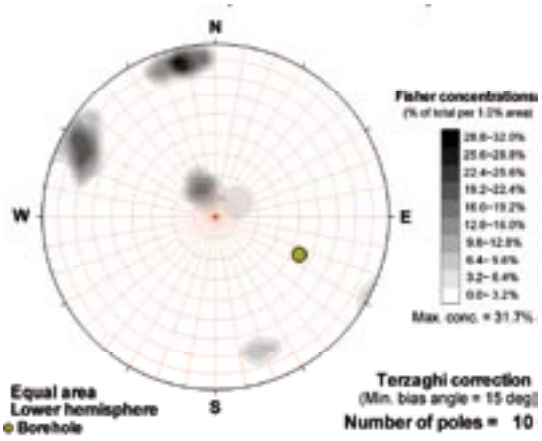

Orientation		Basis for orientation				Certainty	Thickness	
Strike	Dip	Fractures	Crush	Ductile structures	Reflectors	Orientation	Apparent	True
28	78	Used	Verify			Probable	0.8 m	0.4 m
Comment:								

KLX14A DZ6 (162.07 to 163.82), ductile zone

Low-grade ductile shear zone associated with foliated fine-grained granite (511058). The section is characterized by decreased magnetic susceptibility and slightly decreased resistivity. Two non-oriented radar reflectors occur at 162.1 m and 164.9 m with the angle 30° and 36° to borehole axis, respectively. The reflectors are strong and constitute different parts of the same structure. They can be observed to a distance of 25 m outside the borehole. Low radar amplitude occurs in the interval 163-165 m, i.e. partly below DZ6. The host rock is dominated by quartz monzodiorite (501036).

Poles from crush zone

Data not used

Poles from ductile structures

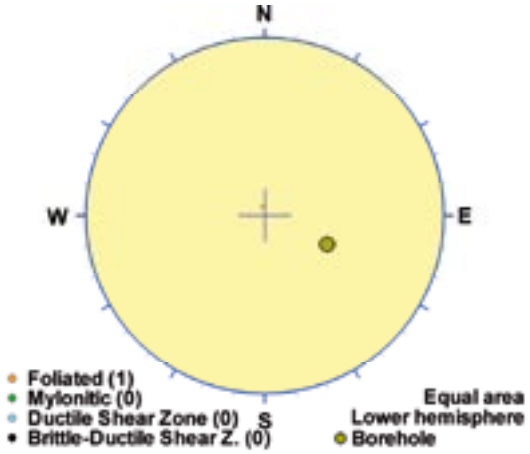

Poles from fractures

Data not used

Contours from fractures

Data not used

Orientation		Basis for orientation				Certainty	Thickness	
Strike	Dip	Fractures	Crush	Ductile structures	Reflectors	Orientation	Apparent	True
72	4			Used	Contradict	Probable	1.8 m	1.2 m
Comment:								

KLX15A DZ1 (130.15 to 130.36), ductile/brittle zone

Minor brittle-ductile shear zone in composite intrusion, including increased frequency of sealed fractures, one crush and faint saussuritization. Significantly decreased P-wave velocity, resistivity and magnetic susceptibility. The caliper mean data indicates decreased borehole diameter in the section. One strong radar reflector occurs at 129.2 m, which is just outside the deformation zone, with the angle 31° to borehole axis. Low radar amplitude occurs in the section 129-131 m. The host rock is dominated by quartz monzodiorite (501036). Subordinate rock type comprises fine-grained diorite-gabbro (505102).

Poles from crush zone

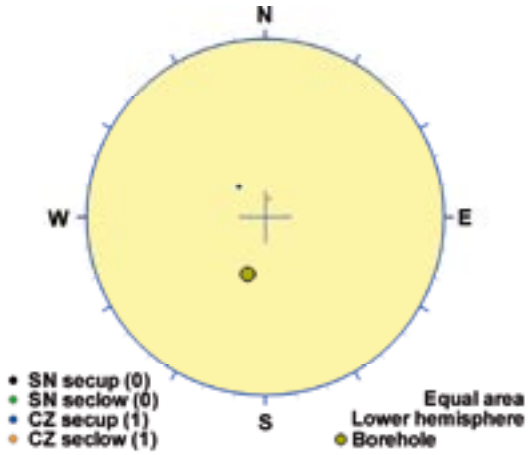

Poles from ductile structures

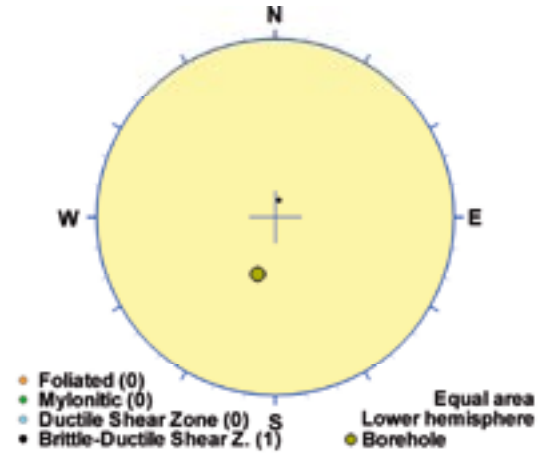

Poles from fractures

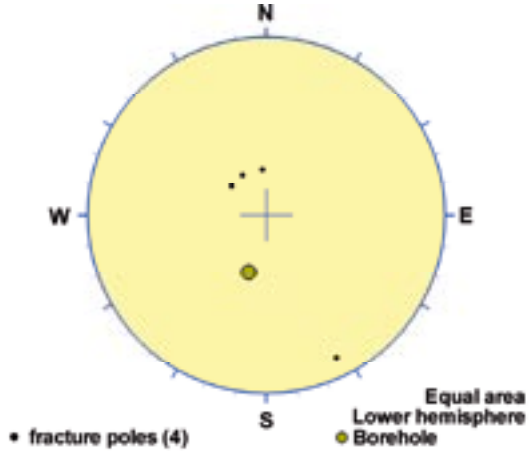

Contours from fractures

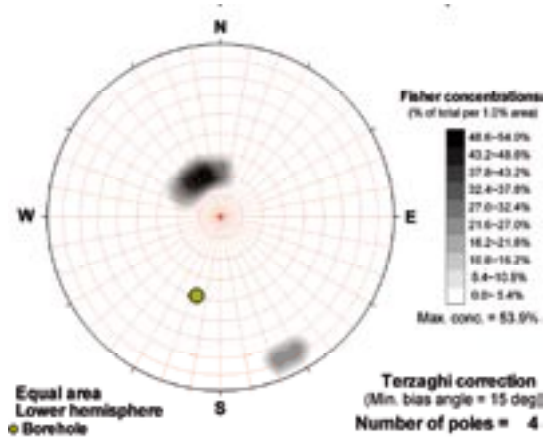

Orientation		Basis for orientation				Certainty	Thickness	
Strike	Dip	Fractures	Crush	Ductile structures	Reflectors	Orientation	Apparent	True
102	8	Verify	Verify	Used	Verify	Certain	0.2 m	0.1 m
Comment:								

KLX15A DZ2 (193.14 to 199.7), ductile/brittle zone

Brittle-ductile shear zone in composite intrusion. Increased frequency of open and sealed fractures, sealed network, two slickensides, two crush and partly weak saussuritization and partly faint epidotization. Significantly decreased resistivity and magnetic susceptibility and partly decreased P-wave velocity along the entire section. The caliper mean data indicates slightly increased borehole diameter. One oriented and two non-oriented radar reflectors occur. The oriented reflector occurs at 195.9 m with the orientation 071/29. The reflector is strong and can be observed to a distance of 30 m outside the borehole. The non-oriented reflectors occur at 196.8 m and 198.7 m with the angle 51° and 46° to borehole axis, respectively. The host rock is dominated by fine-grained diorite-gabbro (505102). Subordinate rock types comprise quartz monzodiorite (501036) and pegmatite (501061).

Poles from crush zone

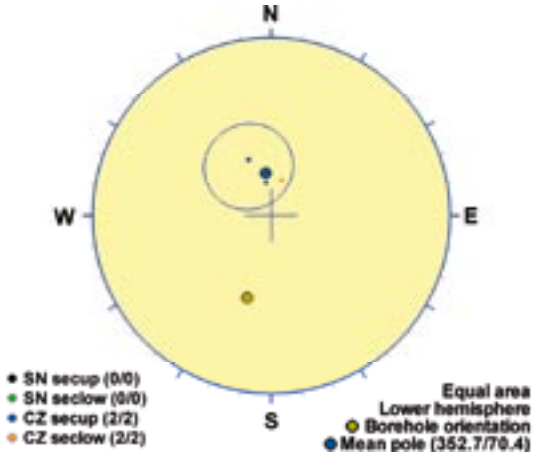

Poles from ductile structures

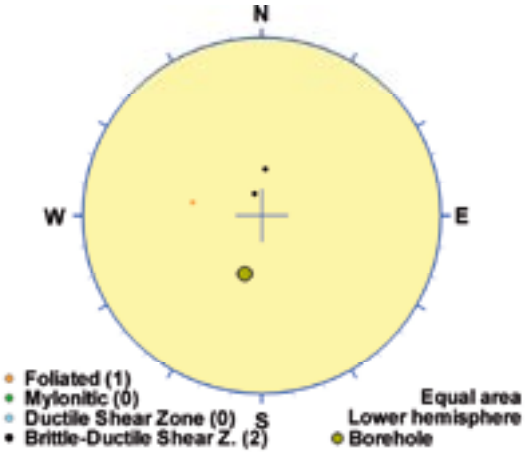

Poles from fractures

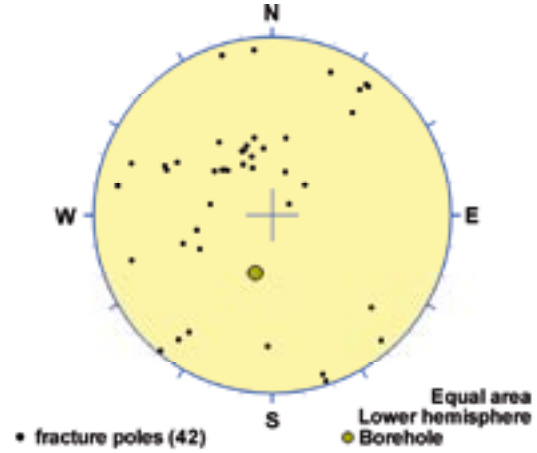

Contours from fractures

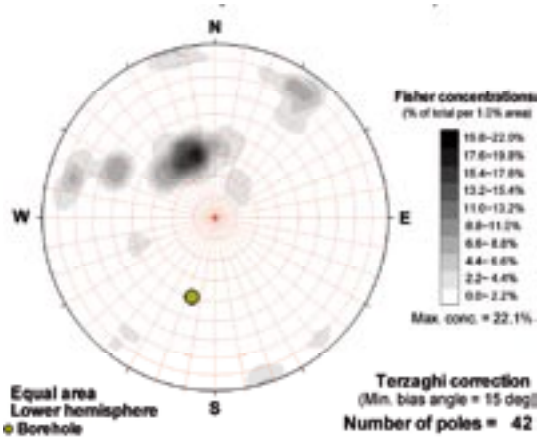

Orientation		Basis for orientation				Certainty	Thickness	
Strike	Dip	Fractures	Crush	Ductile structures	Reflectors	Orientation	Apparent	True
83	20	Verify	Used	Verify	Verify	Certain	6.6 m	3.5 m
Comment:								

KLX15A DZ3 (253.69 to 254.37), ductile/brittle zone

Minor brittle-ductile shear zone characterized by slightly increased frequency of open and sealed fractures. Significantly decreased resistivity and magnetic susceptibility and partly decreased P-wave velocity. One oriented radar reflector occurs at 253.6 m with the orientation 339/38 or 250/59. The reflector is prominent and can be observed to a distance of 15 m outside the borehole. The host rock is dominated by quartz monzodiorite (501036). Subordinate rock type comprises fine-grained granite (511058).

Poles from crush zone

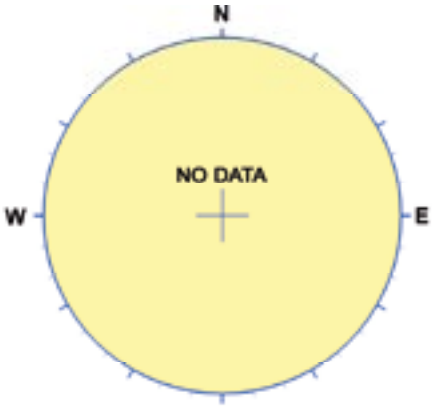

Poles from ductile structures

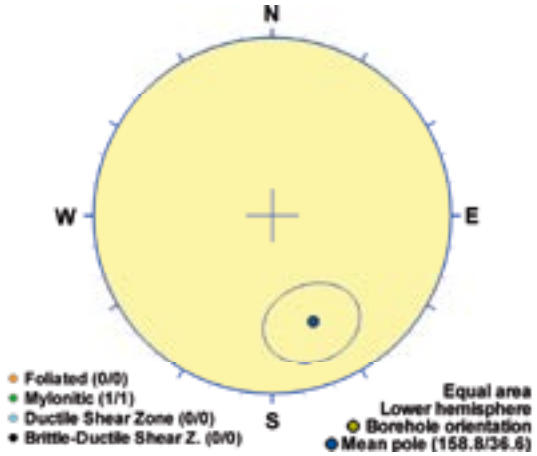

Poles from fractures

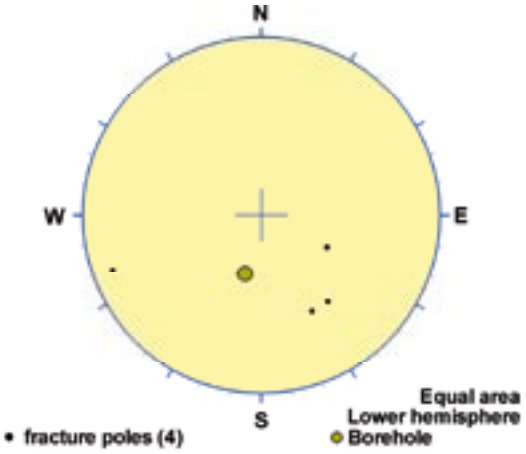

Contours from fractures

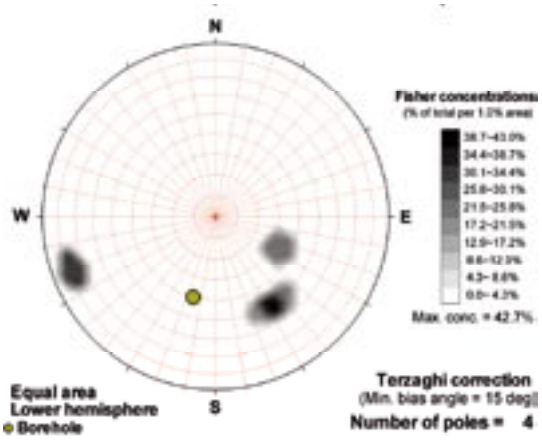

Orientation		Basis for orientation				Certainty	Thickness	
Strike	Dip	Fractures	Crush	Ductile structures	Reflectors	Orientation	Apparent	True
249	53	Verify		Used	Verify	Certain	0.7 m	0.6 m
Comment:								

KLX15A DZ4 (262.35 to 265.79), brittle zone

Brittle deformation zone characterized by increased frequency of open and sealed fractures, sealed network, two crush, apertures 3-10 mm, two slickensides, faint to weak red staining and saussuritization and partly medium epidotization. Significantly decreased resistivity and magnetic susceptibility and partly decreased P-wave velocity. The caliper mean data indicates a significant anomaly at c. 264.6 m. One of the most prominent radar reflectors in the borehole (reflector 66) occurs at 261.3 m, which is immediately above DZ4. The orientation of the reflector is 094/31, and the reflector can be observed to a distance of 30 m outside the borehole. Parts of the reflector (reflector 66xx at 264.2 m, reflector 66xxxx at 264.7 m and reflector 66x at 265.0 m) have been interpreted to intersect within DZ4. Also, one non-oriented radar reflector occurs at 263.0 m with the angle 55° to borehole axis. The host rock is dominated by quartz monzodiorite (501036). Subordinate rock types comprise fine-grained granite (511058) and fine-grained diorite-gabbro (505102).

Poles from crush zone

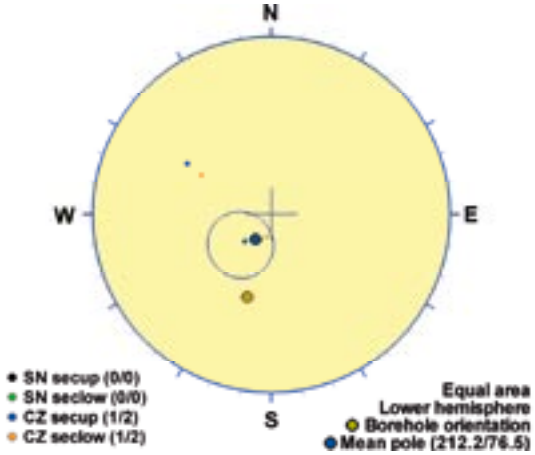

Poles from ductile structures

Data not used

Poles from fractures

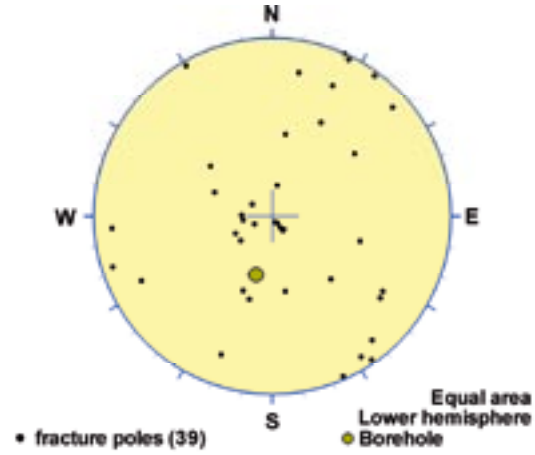

Contours from fractures

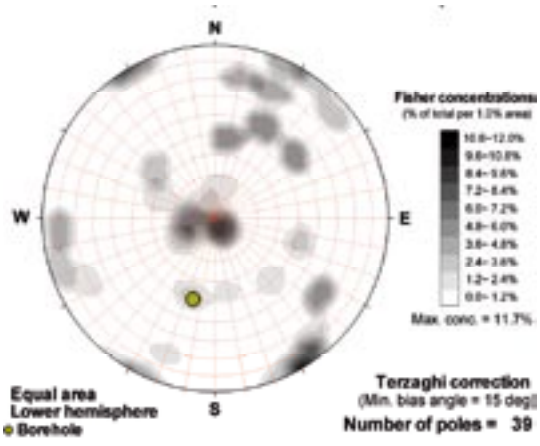

Orientation		Basis for orientation				Certainty	Thickness	
Strike	Dip	Fractures	Crush	Ductile structures	Reflectors	Orientation	Apparent	True
302	14	Verify	Used		Contradict	Uncertain	3.4 m	3.1 m
Comment:								

KLX15A DZ5 (346.65 to 347), ductile/brittle zone

Minor brittle-ductile shear zone in composite intrusion. Weakly red staining. Significantly decreased resistivity and magnetic susceptibility and partly decreased P-wave velocity. Low radar amplitude occurs in the section 346-348 m. The host rock is dominated by quartz monzodiorite (501036). Subordinate rock type comprises fine-grained diorite-gabbro (505102).

Poles from crush zone

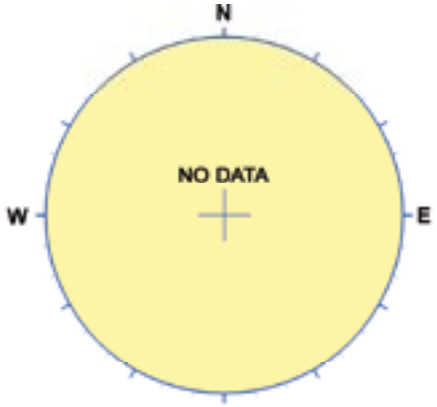

Poles from ductile structures

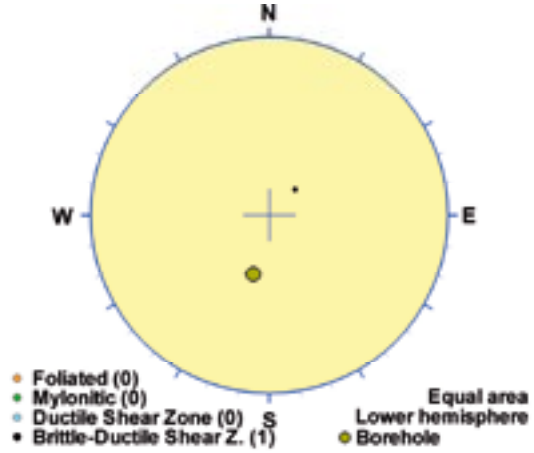

Poles from fractures

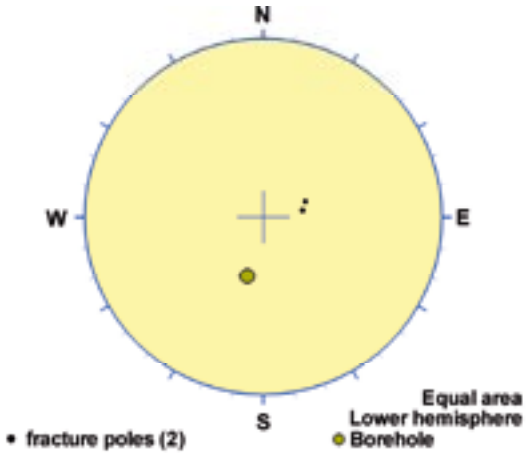

Contours from fractures

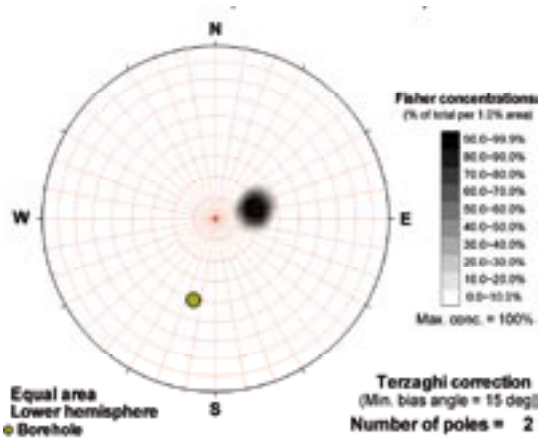

Orientation		Basis for orientation				Certainty	Thickness	
Strike	Dip	Fractures	Crush	Ductile structures	Reflectors	Orientation	Apparent	True
135	17	Verify		Used		Certain	0.4 m	0.2 m
Comment:								

KLX15A DZ6 (350.16 to 350.34), ductile zone

Minor ductile shear zone in composite intrusion. One slickenside and faint saussuritization. There is a minor decrease in magnetic susceptibility and resistivity. The host rock is dominated by quartz monzodiorite (501036). Subordinate rock type comprises fine-grained diorite-gabbro (505102).

Poles from crush zone

Data not used

Poles from ductile structures

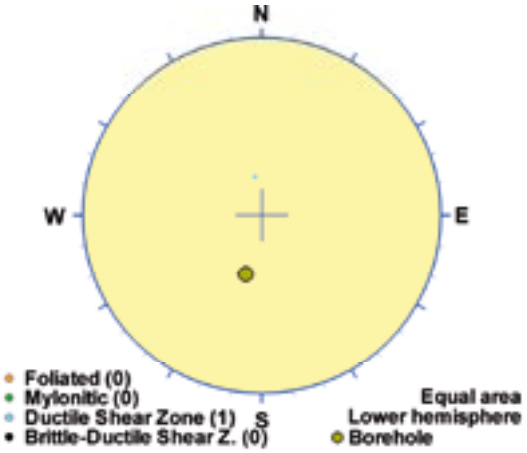

Poles from fractures

Data not used

Contours from fractures

Data not used

Orientation		Basis for orientation				Certainty	Thickness	
Strike	Dip	Fractures	Crush	Ductile structures	Reflectors	Orientation	Apparent	True
80	18			Used		Probable	0.2 m	0.1 m
Comment:								

KLX15A DZ7 (362.75 to 362.95), brittle zone

Minor deformation zone characterized by brecciation. Partly decreased magnetic susceptibility and resistivity. The host rock is dominated Ävrö granite (501044).

Poles from crush zone

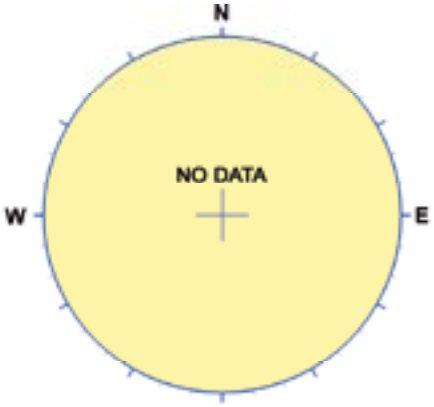

Poles from ductile structures

Data not used

Poles from fractures

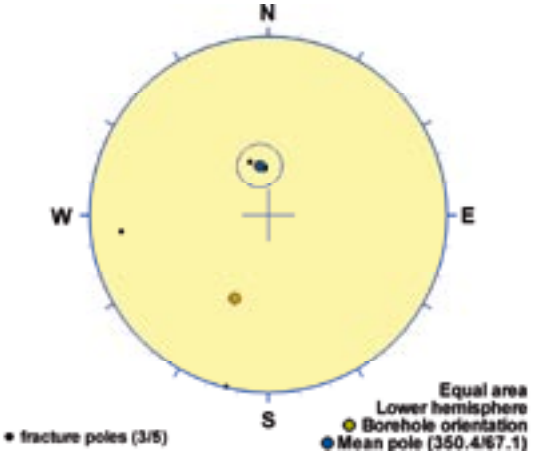

Contours from fractures

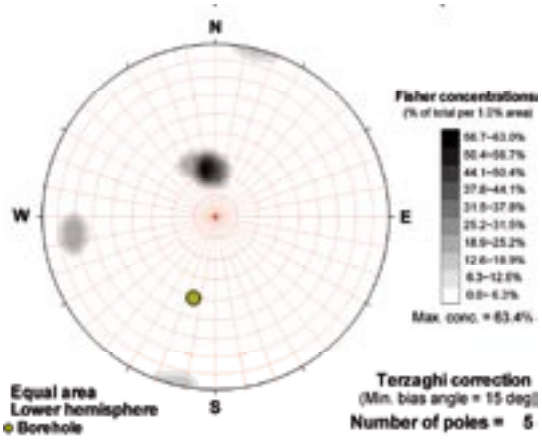

Orientation		Basis for orientation				Certainty	Thickness	
Strike	Dip	Fractures	Crush	Ductile structures	Reflectors	Orientation	Apparent	True
80	23	Used				Probable	0.2 m	0.1 m
Comment:								

KLX15A DZ8 (377.84 to 386), ductile/brittle zone

Inhomogeneous brittle-ductile shear zone. Increased frequency of sealed fractures, slight increase in open fractures, sealed network, cataclasites, breccias, weak to strong red staining and partly weak epidotization. Significant decrease in bulk resistivity and bulk magnetic susceptibility and a minor decrease in P-wave velocity. Three non-oriented radar reflectors occur at 379.5 m, 383.1 m and 385.9 m with the angle 36°, 10° and 34° to borehole axis, respectively. Low radar amplitude occurs in the section 376-383 m. The host rock is dominated by quartz monzodiorite (501036). Subordinate rock types comprise pegmatite (501061) and fine-grained granite (511058).

Poles from crush zone

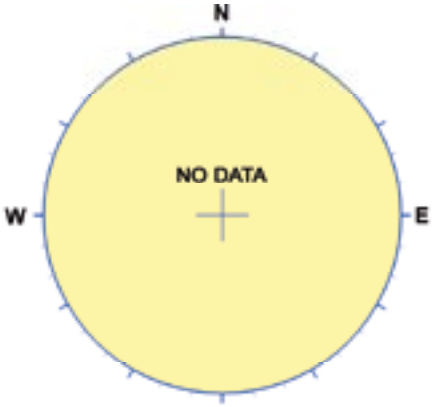

Poles from ductile structures

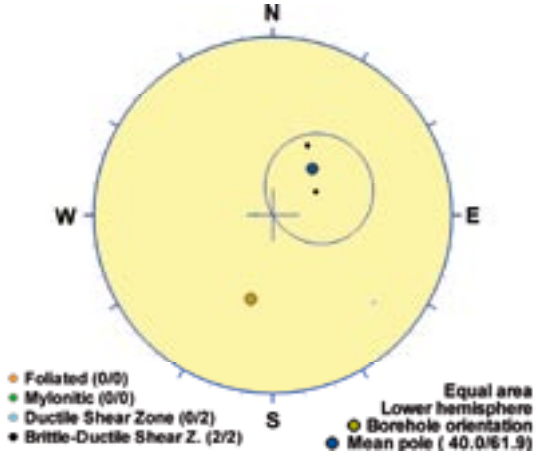

Poles from fractures

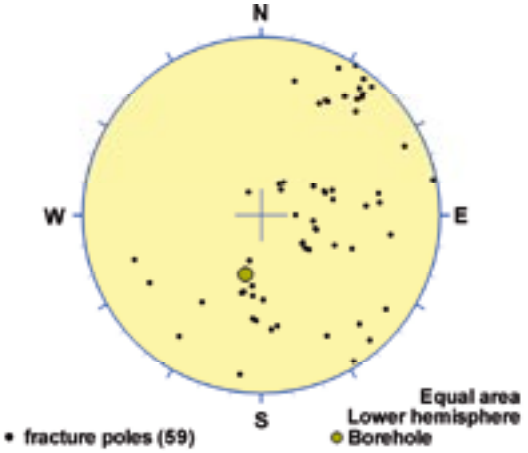

Contours from fractures

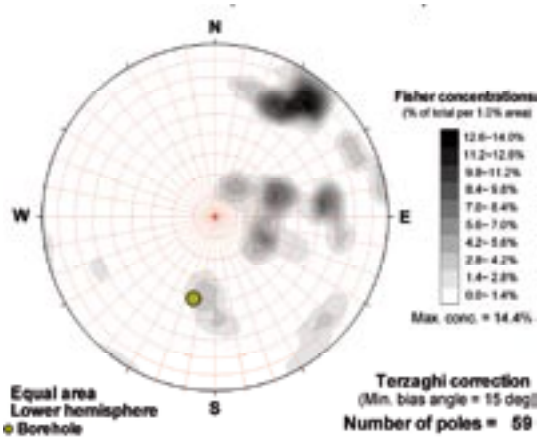

Orientation		Basis for orientation				Certainty	Thickness	
Strike	Dip	Fractures	Crush	Ductile structures	Reflectors	Orientation	Apparent	True
130	28	Verify		Used	Verify	Uncertain	8.2 m	3.2 m
Comment:								

KLX15A DZ9 (401.9 to 409.1), ductile/brittle zone

Brittle-ductile shear zone. Increased frequency of sealed fractures and sealed network, weak to medium red staining and partly weak saussuritization. Significantly decreased resistivity and magnetic susceptibility in the section c. 402.5-403.5 m. Partly decreased P-wave velocity along the entire section of the possible deformation zone. One non-oriented radar reflector occurs at 405.6 m with the angle 63° to borehole axis. The host rock is dominated by quartz monzodiorite (501036). Subordinate rock type comprises fine-grained granite (511058).

Poles from crush zone

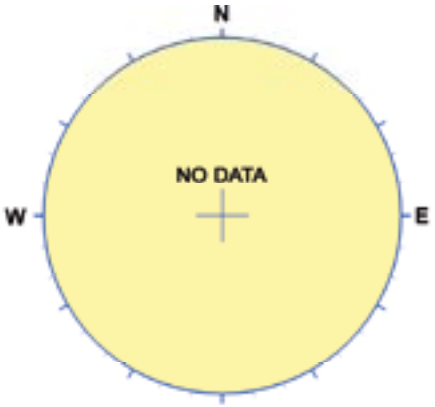

Poles from ductile structures

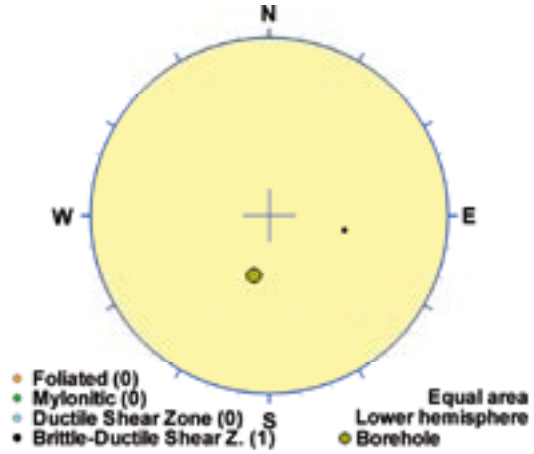

Poles from fractures

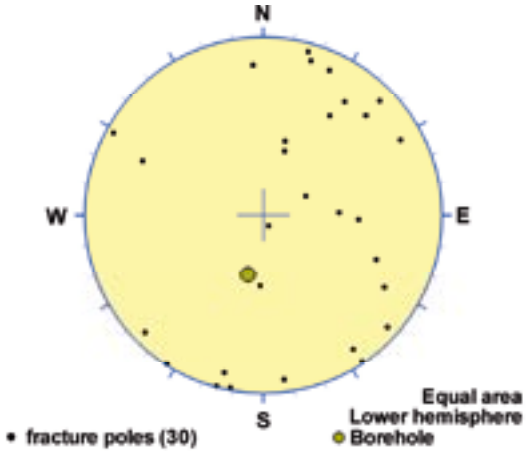

Contours from fractures

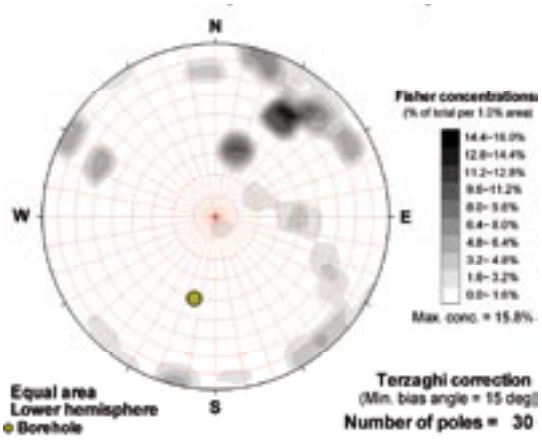

Orientation		Basis for orientation				Certainty	Thickness	
Strike	Dip	Fractures	Crush	Ductile structures	Reflectors	Orientation	Apparent	True
191	35	Verify	Not Used	Used	Contradict	Very uncertain	7.2 m	4.3 m
Comment:								

KLX15A DZ10 (502.5 to 505.6), ductile/brittle zone

Brittle-ductile shear zone. Increased frequency of sealed fractures and sealed network, weak to medium red staining and one slickenside. Significant decrease in resistivity and magnetic susceptibility and a minor decrease in P-wave velocity. Two oriented and two non-oriented radar reflectors occur within DZ10. The oriented reflectors occur at 504.0 m with the orientation 309/33 or 265/29 and at 504.6 m with the orientation 093/14 or 101/86. Both reflectors are strong and can be observed to a distance of 24 m outside the borehole. The non-oriented reflectors occur at 503.8 m and 504.9 m with the angle 56° and 59° to borehole axis, respectively. The host rock is dominated by quartz monzodiorite (501036). Subordinate rock types comprise fine-grained granite (511058) and very sparse occurrence of granite (501058).

Poles from crush zone

Poles from ductile structures

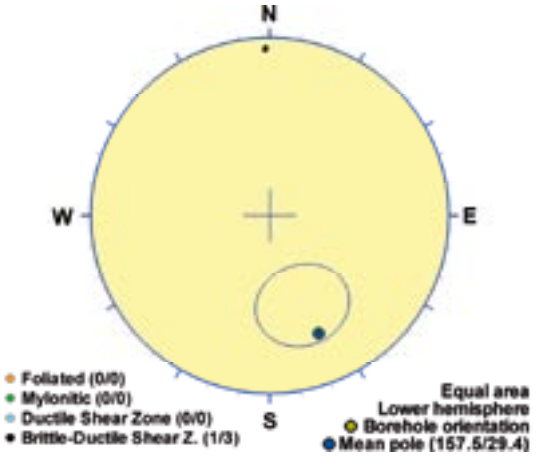

Poles from fractures

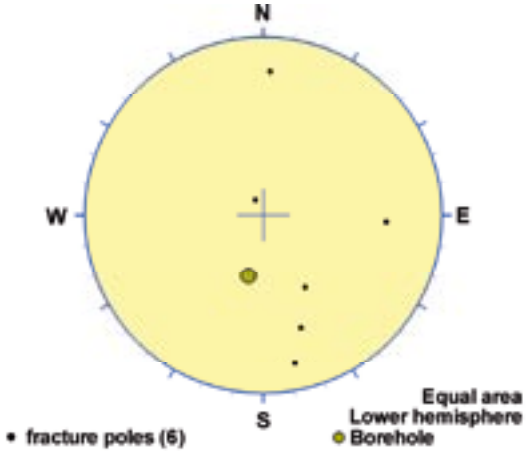

Contours from fractures

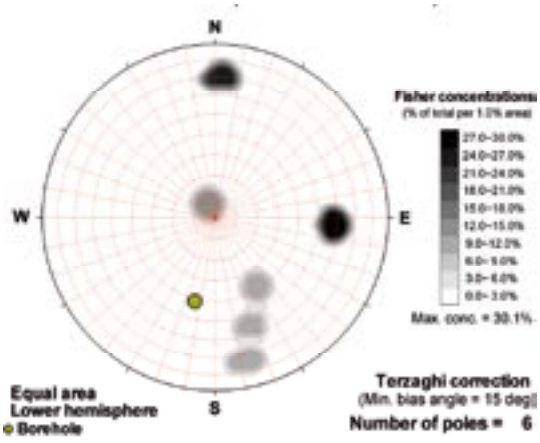

Orientation		Basis for orientation				Certainty	Thickness	
Strike	Dip	Fractures	Crush	Ductile structures	Reflectors	Orientation	Apparent	True
89	84			Used	Verify	Uncertain	3.1 m	1.7 m
Comment:								

KLX15A DZ11 (602.24 to 608.72), brittle zone

Brittle deformation zone characterized by increased frequency of sealed fractures, weak to strong red staining, partly faint epidotization, one cataclasite (2 cm) and one breccia (20 cm). Significant decrease in resistivity and magnetic susceptibility and a minor decrease in P-wave velocity. Three non-oriented radar reflectors occur at 603.0 m, 604.8 m and 605.4 m with the angle 58°, 34° and 50° to borehole axis, respectively. Low radar amplitude occurs in the section 602-608 m. The host rock is dominated by quartz monzodiorite (501036). Subordinate rock types are granite (501058) and pegmatite (501061).

Poles from crush zone

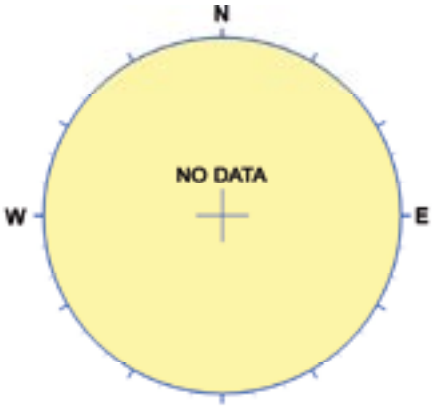

Poles from ductile structures

Data not used

Poles from fractures

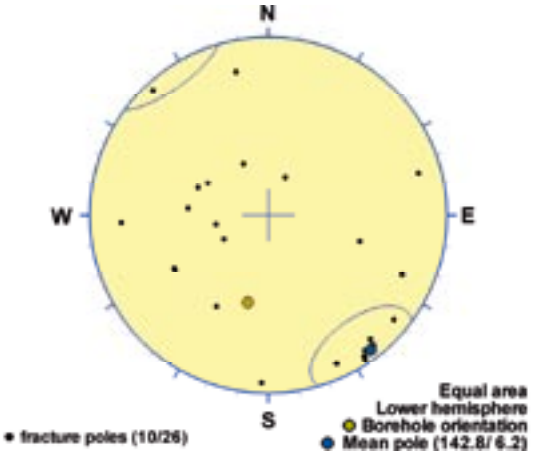

Contours from fractures

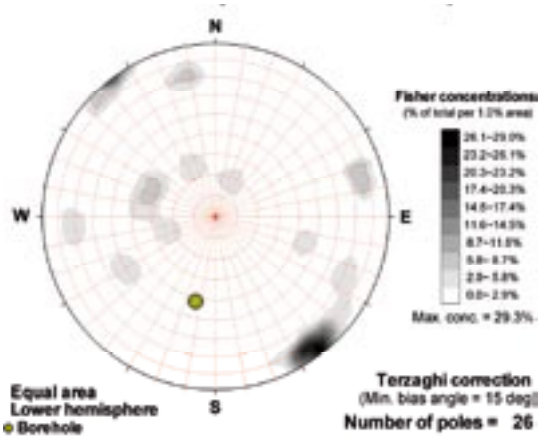

Orientation		Basis for orientation				Certainty	Thickness	
Strike	Dip	Fractures	Crush	Ductile structures	Reflectors	Orientation	Apparent	True
233	84	Used			Contradict	Very uncertain	6.5 m	3.2 m
Comment:								

KLX15A DZ12 (629.1 to 634.94), brittle zone

Brittle deformation zone characterized by increased frequency of open and sealed fractures, sealed network, two crush, weak to medium red staining, partly weak chloritization, weak epidotization and vuggy character in the lower part of the section. Significant decrease in bulk resistivity and bulk magnetic susceptibility and also a major decrease in P-wave velocity. One oriented and two non-oriented radar reflectors occur within the deformation zone. The oriented reflector occurs at 631.1 m with the orientation 004/56 or 225/78. The non-oriented reflectors occur at 630.0 m and 630.5 m with the angle 49° and 37° to borehole axis, respectively. Very low radar amplitude occurs in the section 628-635 m, which is partly above DZ12. The host rock is dominated by quartz monzodiorite (501036). Subordinate rock types comprise granite (501058) and very sparse occurrence of fine-grained granite (511058).

Poles from crush zone

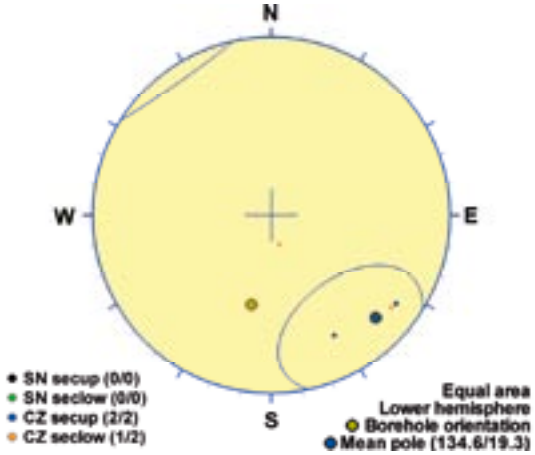

Poles from ductile structures

Data not used

Poles from fractures

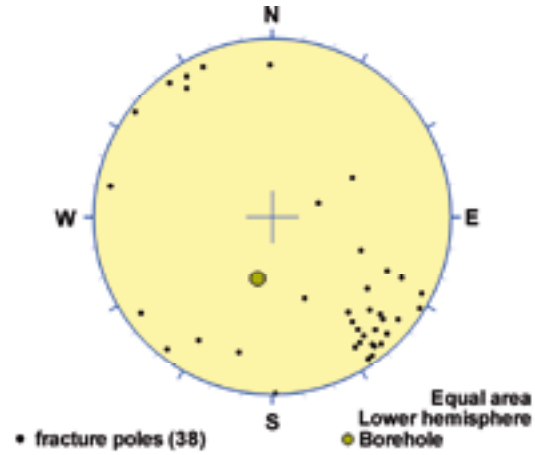

Contours from fractures

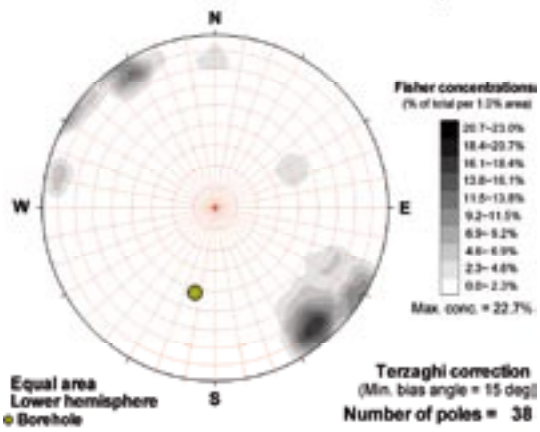

Orientation		Basis for orientation				Certainty	Thickness	
Strike	Dip	Fractures	Crush	Ductile structures	Reflectors	Orientation	Apparent	True
225	71	Verify	Used		Verify	Certain	5.8 m	3.3 m
Comment:								

KLX15A DZ13 (658.91 to 659.8), ductile/brittle zone

Brittle-ductile deformation zone. Faint red staining. There is a minor decrease in magnetic susceptibility and resistivity. One non-oriented radar reflector occurs at 658.9 m with the angle 38° to borehole axis. The host rock is dominated by Ävrö granite (501044). Subordinate rock types comprise quartz monzodiorite (501036) and very sparse occurrence of granite (501058).

Poles from crush zone

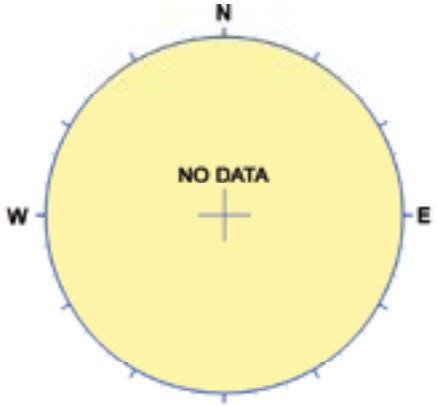

Poles from ductile structures

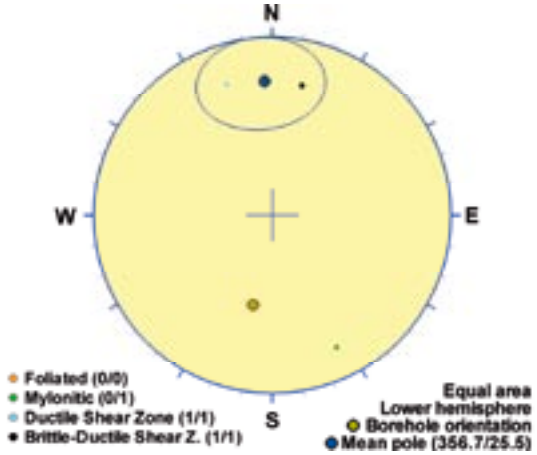

Poles from fractures

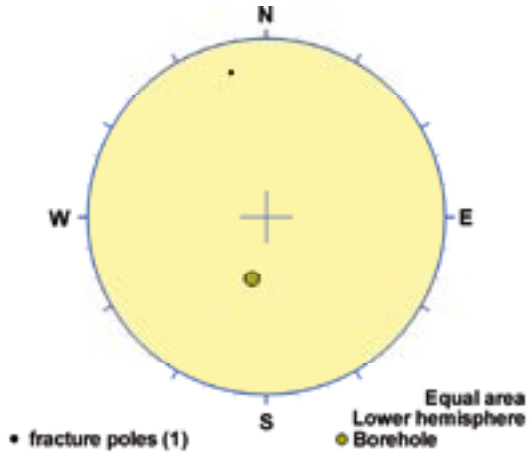

Contours from fractures

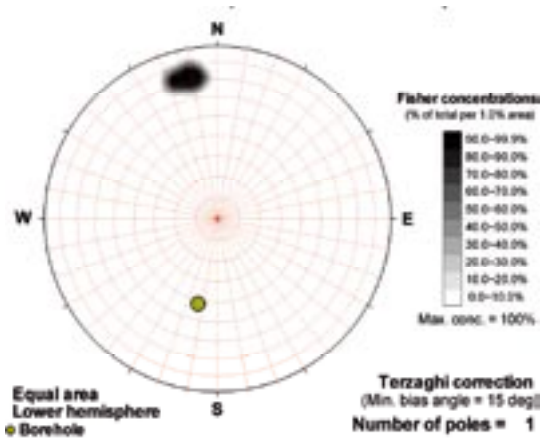

Orientation		Basis for orientation				Certainty	Thickness	
Strike	Dip	Fractures	Crush	Ductile structures	Reflectors	Orientation	Apparent	True
87	65	Verify		Used	Contradict	Uncertain	0.9 m	0.2 m
Comment:								

KLX15A DZ14 (675.05 to 682.68), brittle zone

Brittle deformation zone characterized by increased frequency of sealed fractures and sealed network. Three slickensides, faint to strong red staining and partly faint epidotization. Significantly decreased resistivity and magnetic susceptibility at the two section coordinates 675.5 m and 682.0 m. One strong radar reflector occurs at 681.2 m with the orientation 278/89 or 066/07. The reflector can be observed to a distance of 20 m outside the borehole. Low radar amplitude occurs in the section 680-683 m. The host rock is dominated by Ävrö granite (501044). Subordinate rock types comprise pegmatite (501061), fine-grained granite (511058) and quartz monzodiorite (501036).

Poles from crush zone

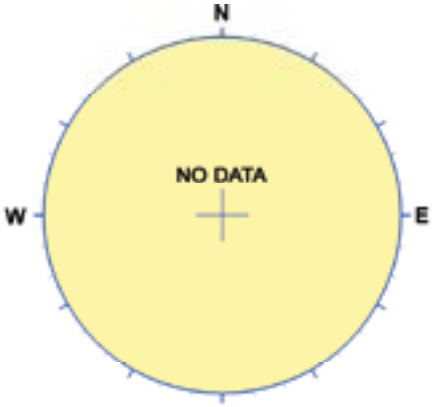

Poles from ductile structures

Data not used

Poles from fractures

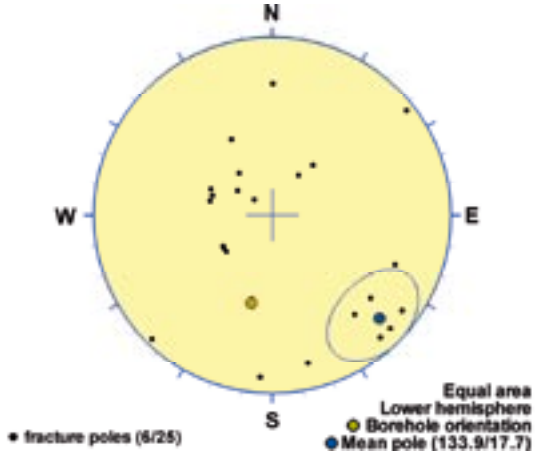

Contours from fractures

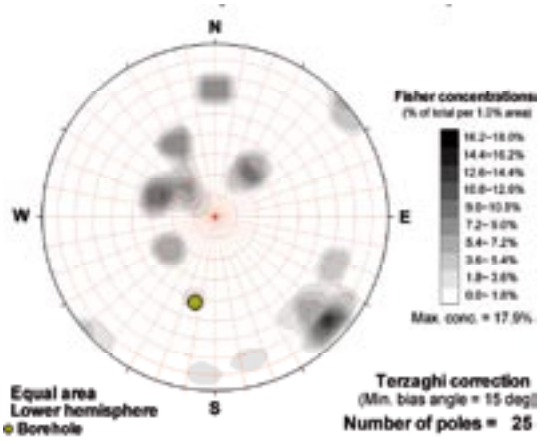

Orientation		Basis for orientation				Certainty	Thickness	
Strike	Dip	Fractures	Crush	Ductile structures	Reflectors	Orientation	Apparent	True
224	72	Used		Verify	Contradict	Very uncertain	7.6 m	4.2 m
Comment:								

KLX15A DZ15 (688 to 688.5), ductile/brittle zone

Minor brittle-ductile shear zone. Moderate increase in sealed fractures. Significantly decreased magnetic susceptibility. The host rock is dominated by quartz monzodiorite (501036). Subordinate rock type comprises pegmatite (501061).

Poles from crush zone

Poles from ductile structures

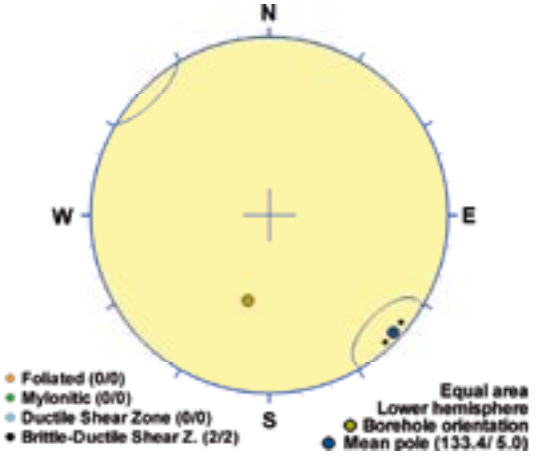

Poles from fractures

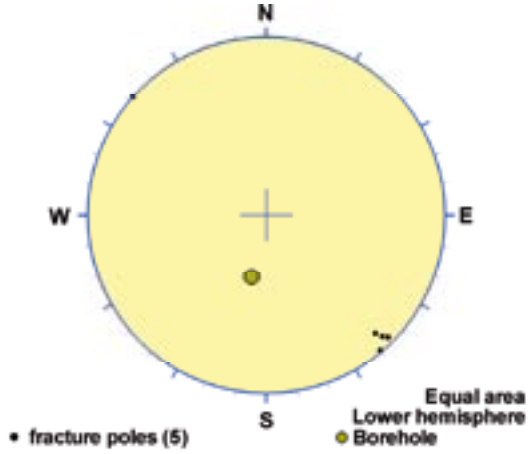

Contours from fractures

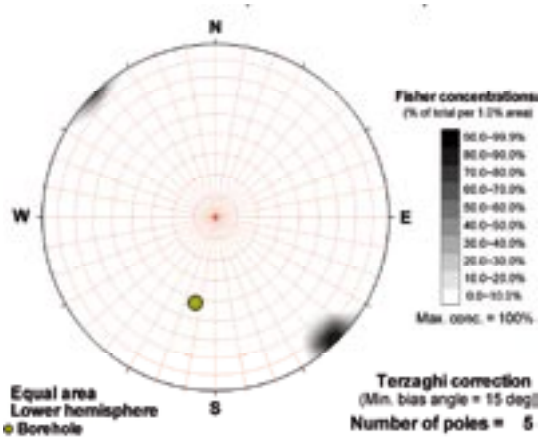

Orientation		Basis for orientation				Certainty	Thickness	
Strike	Dip	Fractures	Crush	Ductile structures	Reflectors	Orientation	Apparent	True
223	85	Verify		Used		Certain	0.5 m	0.2 m
Comment:								

KLX15A DZ17 (772.7 to 774.15), ductile/brittle zone

Brittle-ductile shear zone in composite intrusion. Increased frequency of open and sealed fractures, sealed fracture network and two slickensides. Significantly decreased resistivity and magnetic susceptibility and partly decreased P-wave velocity. One oriented radar reflector occurs at 773.8 m with the orientation 184/06 or 288/84. The reflector is prominent and can be observed to a distance of 25 m outside the borehole. The host rock is dominated by fine-grained diorite-gabbro (505102). Subordinate rock type comprises quartz monzodiorite (501036).

Poles from crush zone

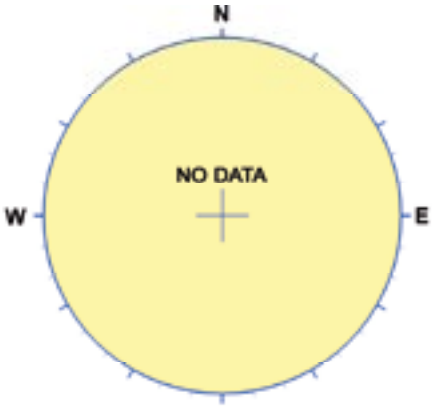

Poles from ductile structures

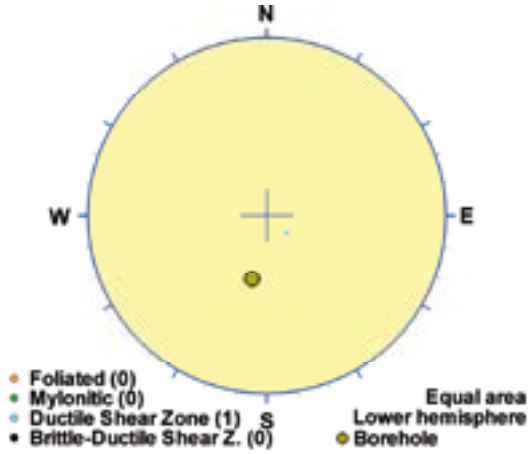

Poles from fractures

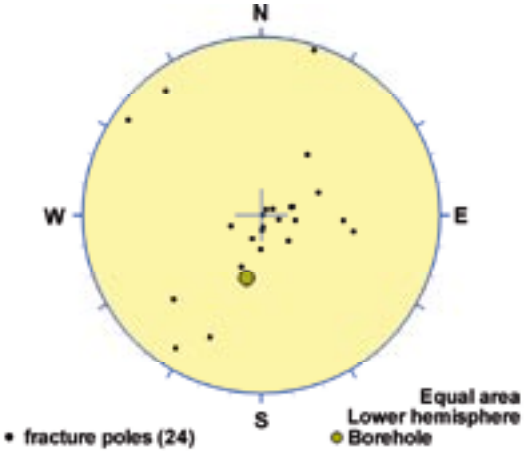

Contours from fractures

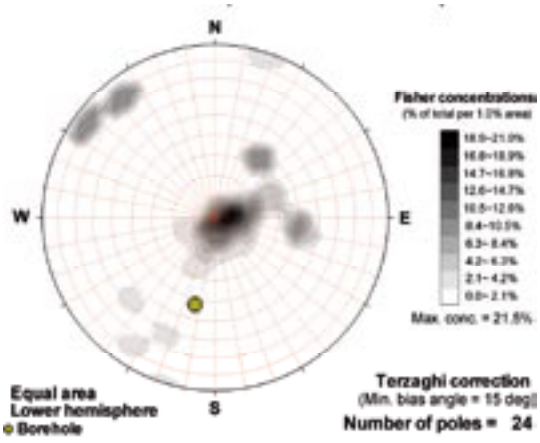

Orientation		Basis for orientation				Certainty	Thickness	
Strike	Dip	Fractures	Crush	Ductile structures	Reflectors	Orientation	Apparent	True
221	12	Verify		Used	Verify	Certain	1.4 m	1.1 m
Comment:								

KLX15A DZ18 (821.63 to 821.94), ductile/brittle zone

Brittle-ductile shear zone. Increased frequency of sealed fractures and sealed network, and slight increase of open fractures and faint epidotization. Significantly decreased resistivity and magnetic susceptibility and partly decreased P-wave velocity. One non-oriented radar reflector occurs at 822.0 m with the angle 69° to borehole axis. The host rock is dominated by quartz monzodiorite (501036).

Poles from crush zone

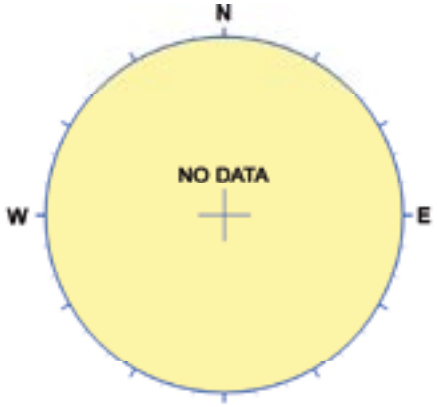

Poles from ductile structures

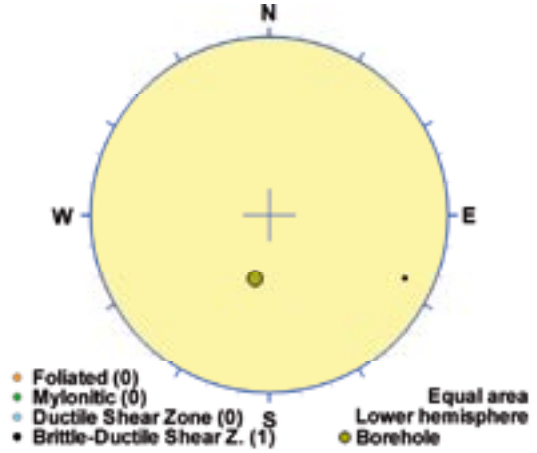

Poles from fractures

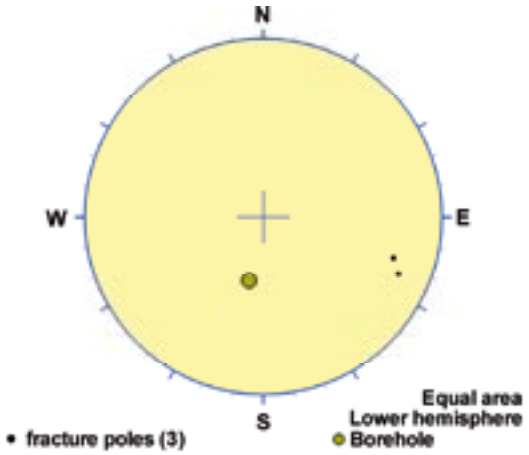

Contours from fractures

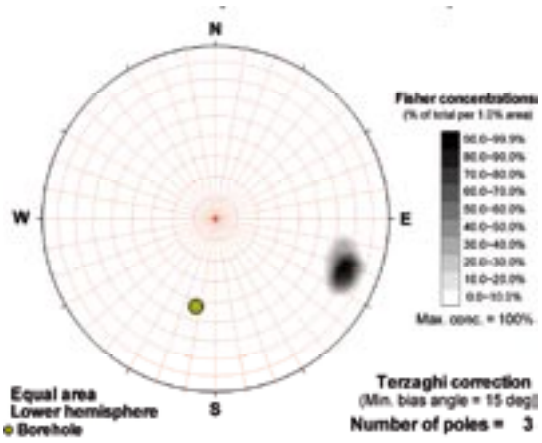

Orientation		Basis for orientation				Certainty	Thickness	
Strike	Dip	Fractures	Crush	Ductile structures	Reflectors	Orientation	Apparent	True
205	73	Verify		Used	Contradict	Probable	0.3 m	0.1 m
Comment:								

KLX15A DZ19 (917.75 to 918.46), ductile/brittle zone

Ductile shear zone in composite intrusion. Increased frequency of sealed fractures and sealed fracture network and one slickenside. Significantly decreased resistivity and magnetic susceptibility and partly decreased P-wave velocity. One of the most prominent radar reflectors in the borehole (reflector 209) occurs at 921.5 m, which is immediately below DZ19. The orientation of the reflector is 088/68 or 077/29, and the reflector can be observed to a distance of 30 m outside the borehole. Parts of the reflector (reflector 209x at 915.6 m, reflector 209xx at 918.9 m and reflector 209xxx at 911.7 m) have been interpreted to intersect close to DZ19. Low radar amplitude occurs in the section 915-920 m, which is partly above and partly below the deformation zone. The host rock is dominated by quartz monzodiorite (501036). Subordinate rock type comprises fine-grained diorite-gabbro (505102).

Poles from crush zone

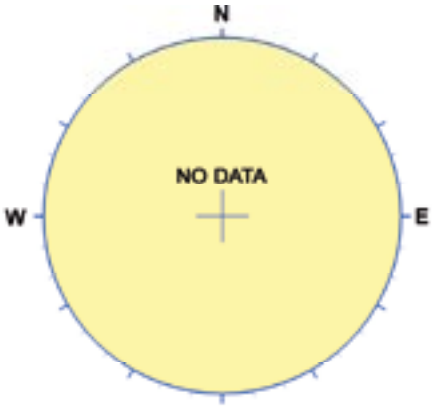

Poles from ductile structures

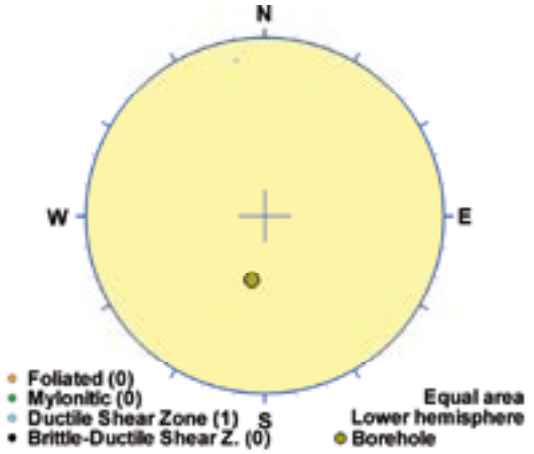

Poles from fractures

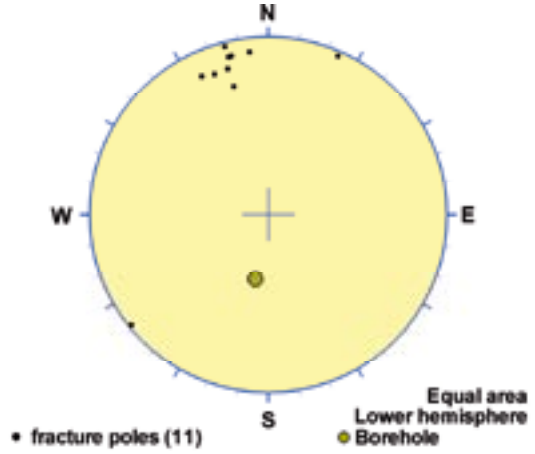

Contours from fractures

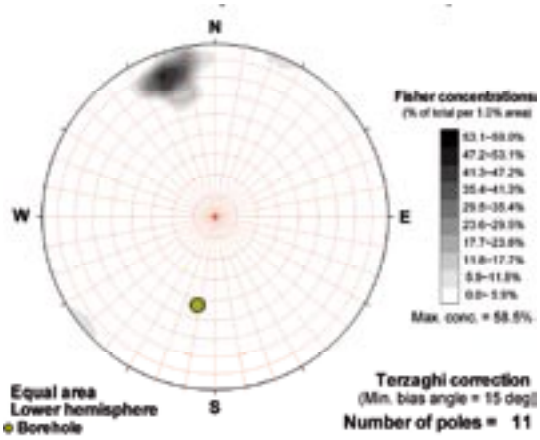

Orientation		Basis for orientation				Certainty	Thickness	
Strike	Dip	Fractures	Crush	Ductile structures	Reflectors	Orientation	Apparent	True
80	78	Verify		Used	Verify	Certain	0.7 m	0.3 m
Comment:								

KLX16A DZ1 (33.8 to 34.25), ductile/brittle zone

Low-grade ductile shear zone in composite intrusion, including crush. Geophysical logs display decreased resistivity, P-wave velocity and magnetic susceptibility. One oriented reflector occurs at 34.2 m with the orientation 324/28. The reflector is of medium strength and can be observed to a distance of 12 m outside the borehole. A non-oriented reflector at 33.3 m exhibits strong character and occurs with the angle 58° to borehole axis. Low radar amplitude occurs at 35 m. The host rock is totally dominated by fine-grained diorite-gabbro (505102). Subordinate rock types include quartz monzodiorite (501036) and fine-grained granite (511058).

Poles from crush zone

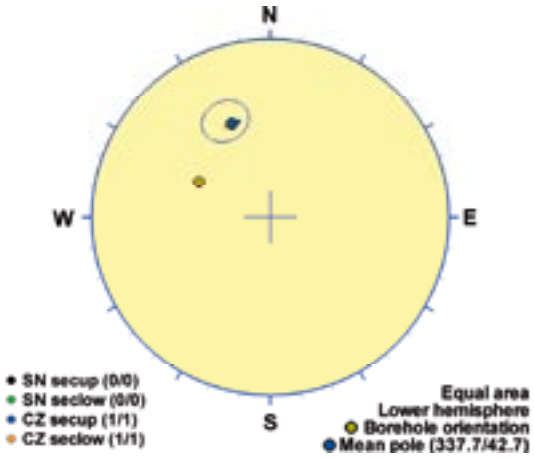

Poles from ductile structures

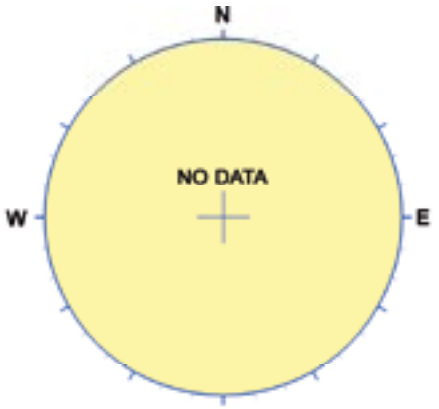

Poles from fractures

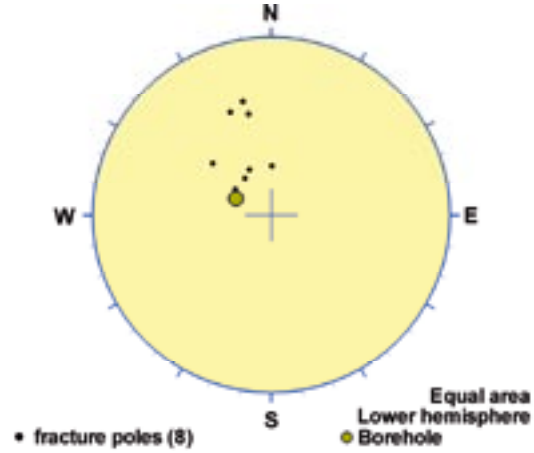

Contours from fractures

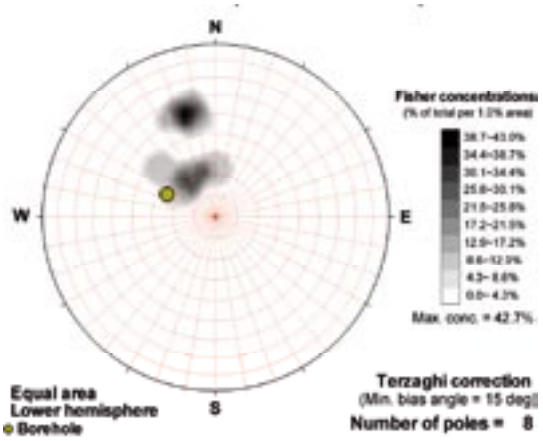

Orientation		Basis for orientation				Certainty	Thickness	
Strike	Dip	Fractures	Crush	Ductile structures	Reflectors	Orientation	Apparent	True
68	47	Verify	Used		Contradict	Probable	0.5 m	0.4 m
Comment:								

KLX16A DZ3 (90.89 to 93.72), brittle zone

Brittle deformation zone characterized by increased frequency of open and sealed fractures, faint red staining, slickensides and apertures =5 mm. The geophysical measurements show significantly decreased resistivity and magnetic susceptibility. There is also partly decreased P-wave velocity and one caliper anomaly. One oriented and two non-oriented radar reflectors occur within DZ3. The oriented reflector occurs at 93.0 m with the orientation 338/27 or 062/36. The radar reflector is strong and can be observed to a distance of 25 m outside the borehole. The non-oriented reflectors occur at 90.7 m and 92.7 m with the angle 63° and 62° to borehole axis, respectively. Low radar amplitude occurs in the interval 90-95 m. The host rock is dominated by fine-grained diorite-gabbro (505102), quartz monzodiorite (501036) and fine-grained granite (511058). Subordinate rock type comprises pegmatite.

Poles from crush zone

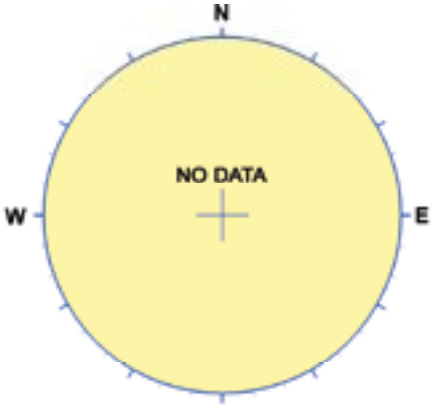

Poles from ductile structures

Data not used

Poles from fractures

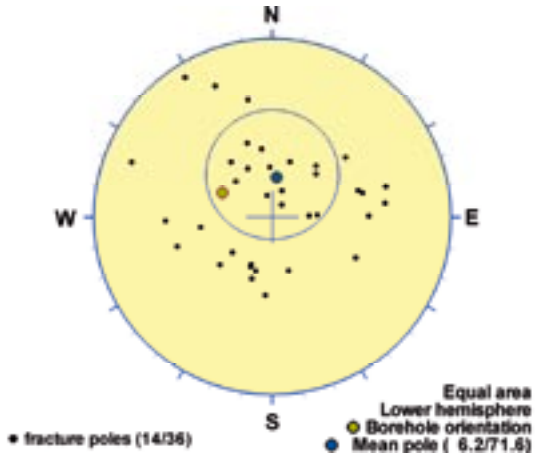

Contours from fractures

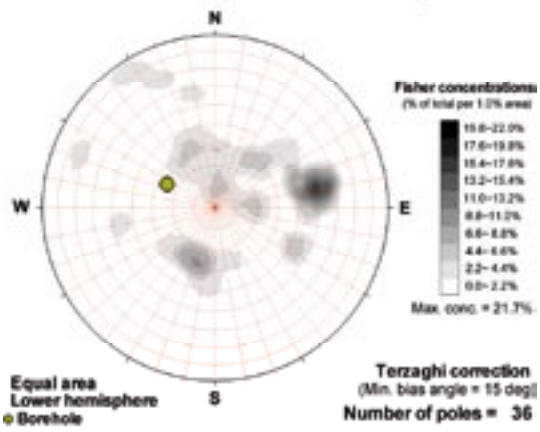

Orientation		Basis for orientation				Certainty	Thickness	
Strike	Dip	Fractures	Crush	Ductile structures	Reflectors	Orientation	Apparent	True
96	18	Used			Contradict	Very uncertain	2.8 m	2.6 m
Comment:								

KLX16A DZ4 (139.9 to 143), brittle zone

Brittle deformation zone characterized by slight increased frequency of open and sealed fractures, apertures =7 mm, faint red staining and chloritization. There is significantly decreased resistivity. There is also partly decreased magnetic susceptibility, P-wave velocity and a few minor caliper anomalies. Three non-oriented radar reflectors occur at 140.7 m, 141.5 m and 143.3 m (just outside DZ4) with the angle 68°, 28° and 34° to borehole axis, respectively. Low radar amplitude occurs in the interval 135-140 m, i.e. partly above DZ4. The host rock is dominated by quartz monzodiorite (501036). Subordinate rock type is fine-grained granite (511058).

Poles from crush zone

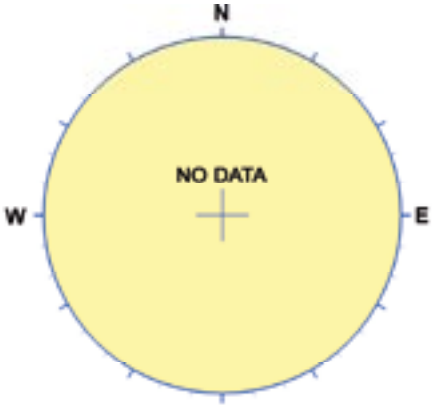

Poles from ductile structures

Data not used

Poles from fractures

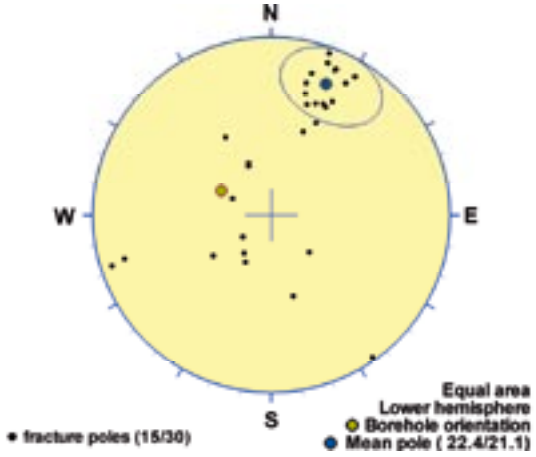

Contours from fractures

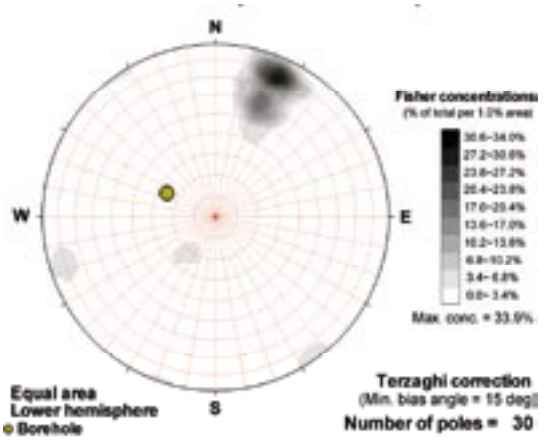

Orientation		Basis for orientation				Certainty	Thickness	
Strike	Dip	Fractures	Crush	Ductile structures	Reflectors	Orientation	Apparent	True
112	69	Used			Verify	Probable	3.1 m	1.1 m
Comment:								

KLX16A DZ5 (207.08 to 207.22), ductile/brittle zone

Low-grade ductile shear zone. Increased frequency of sealed fractures and faint red staining. The DZ is located on a significant negative magnetic susceptibility gradient. There are no other indications in the geophysical logging data. The host rock is totally dominated by quartz monzodiorite (501036).

Poles from crush zone

Poles from ductile structures

Poles from fractures

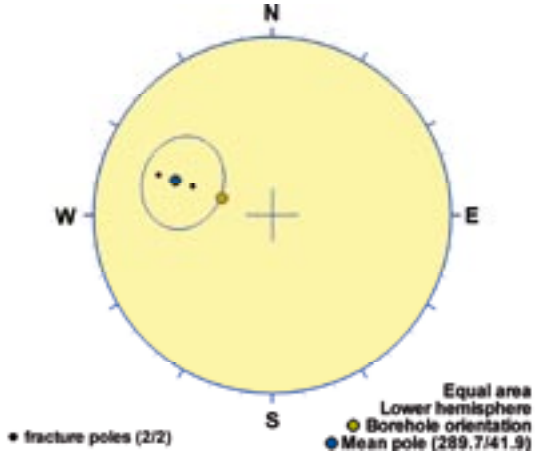

Contours from fractures

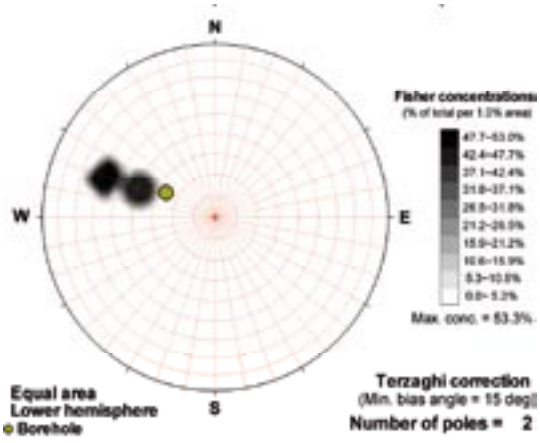

Orientation		Basis for orientation				Certainty	Thickness	
Strike	Dip	Fractures	Crush	Ductile structures	Reflectors	Orientation	Apparent	True
20	48	Used				Probable	0.1 m	0.1 m
Comment:								

KLX16A DZ6 (209.95 to 210.92), ductile/brittle zone

Low-grade ductile shear zone. Increased frequency of sealed and open fractures, slickensides, crush and faint to medium red staining and saussuritization. There is one significant caliper anomaly. The DZ is also characterized by decreased magnetic susceptibility and partly decreased P-wave velocity and resistivity. One oriented radar reflector occurs at 209.9 m with the orientation 008/59 or 143/18. The reflector is strong and can be observed to a distance of 20 m outside the borehole. The host rock is dominated by quartz monzodiorite (501036). Subordinate rock types are granite (501058) and fine-grained granite (511058).

Poles from crush zone

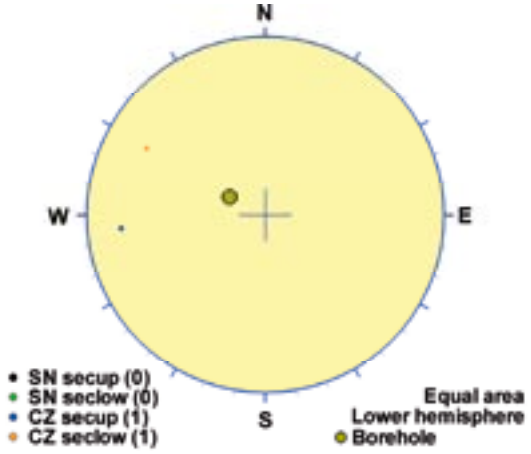

Poles from ductile structures

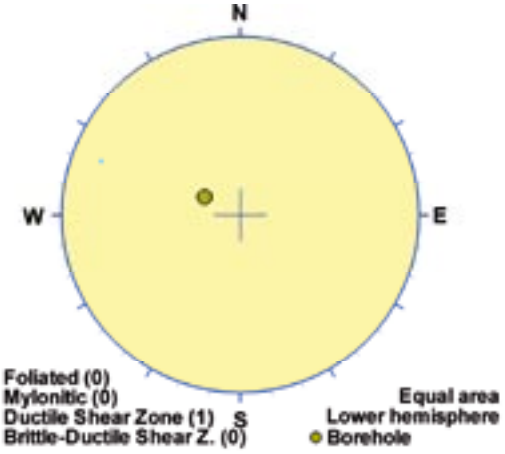

Poles from fractures

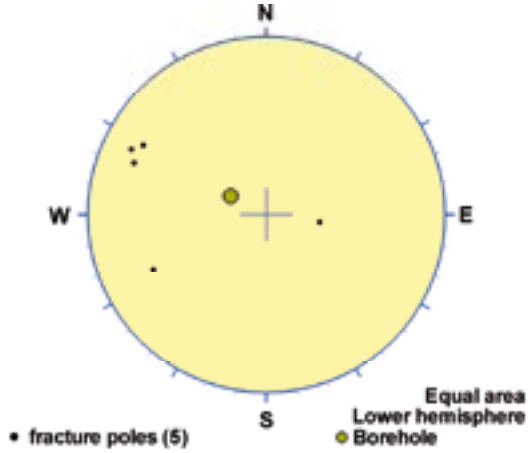

Contours from fractures

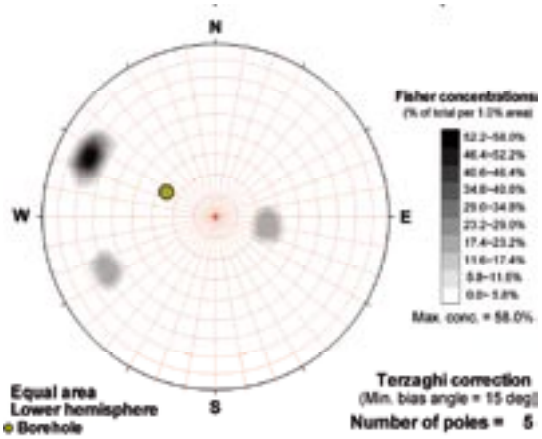

Orientation		Basis for orientation				Certainty	Thickness	
Strike	Dip	Fractures	Crush	Ductile structures	Reflectors	Orientation	Apparent	True
21	72	Verify	Verify	Used	Contradict	Probable	1 m	0.7 m
Comment:								

KLX16A DZ7 (213.33 to 213.88), ductile/brittle zone

Brittle-ductile shear zone. Increased frequency of open fractures. The resistivity is slightly decreased and the magnetic susceptibility is significantly decreased. The host rock is dominated by quartz monzodiorite (501036). Subordinate rock types is pegmatite (501061).

Poles from crush zone

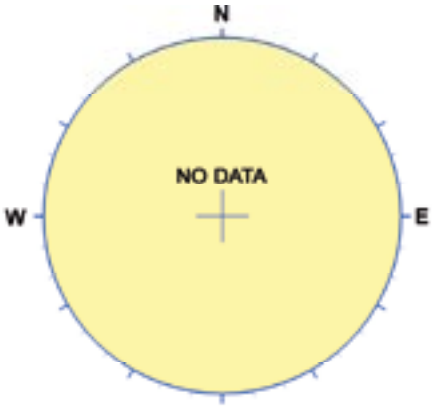

Poles from ductile structures

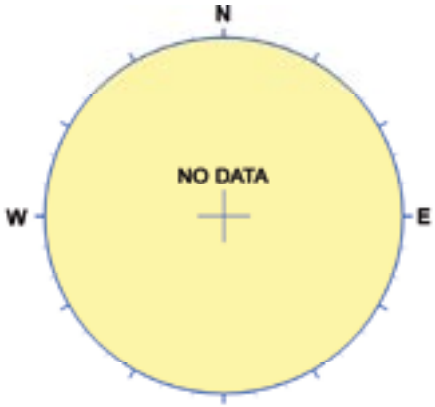

Poles from fractures

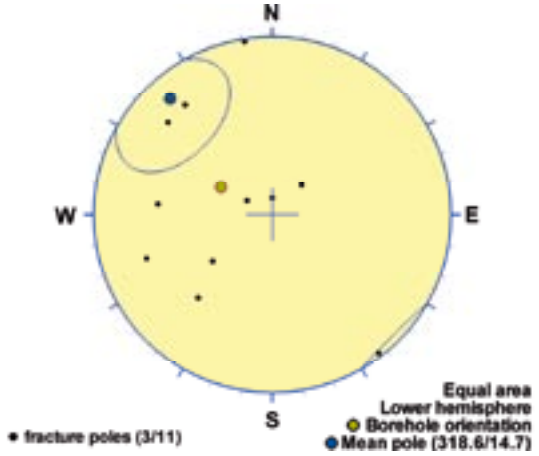

Contours from fractures

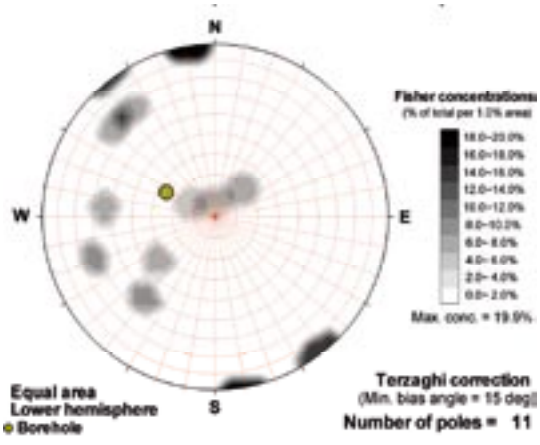

Orientation		Basis for orientation				Certainty	Thickness	
Strike	Dip	Fractures	Crush	Ductile structures	Reflectors	Orientation	Apparent	True
49	75	Used				Very uncertain	0.5 m	0.3 m
Comment:								

KLX16A DZ9 (228.2 to 230.9), ductile/brittle zone

Low-grade ductile shear zone. Increased frequency of open and sealed fractures, apertures =3 mm, minor crush and faint to weak red staining. There is significantly decreased resistivity and magnetic susceptibility. There is also partly decreased P-wave velocity and one minor caliper anomaly. One oriented radar reflector occurs at 230.1 m with the orientation 072/85 or 268/55. The reflector is of medium strength and can be observed to a distance of 10 m outside the borehole. The host rock is dominated by granite (501058) and quartz monzodiorite (501036). Subordinate rock type is fine-grained granite (511058).

Poles from crush zone

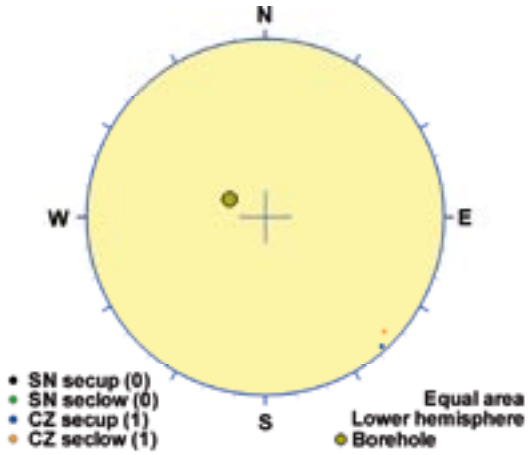

Poles from ductile structures

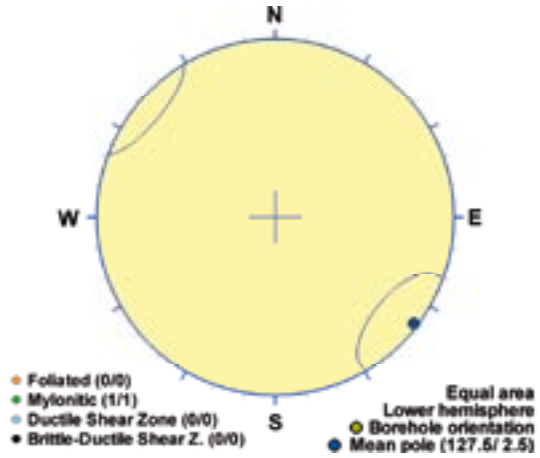

Poles from fractures

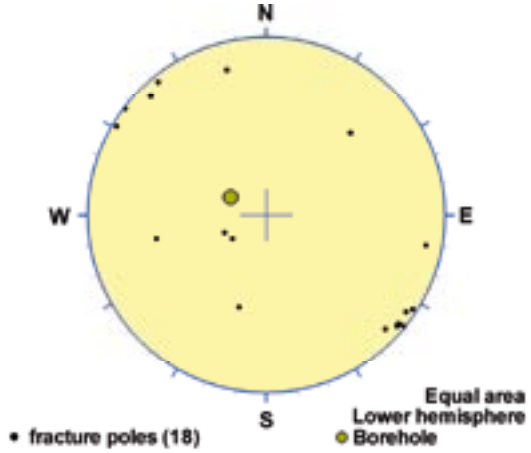

Contours from fractures

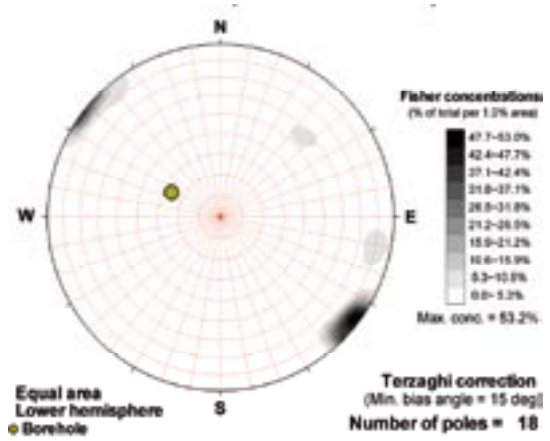

Orientation		Basis for orientation				Certainty	Thickness	
Strike	Dip	Fractures	Crush	Ductile structures	Reflectors	Orientation	Apparent	True
218	88	Verify	Verify	Used		Certain	2.7 m	1 m
Comment:								

KLX17A DZ2 (142.27 to 142.86), ductile zone

Low-grade ductile shear zone in composite intrusion. Moderate increase in sealed fractures and weak epidotization. There are no significant geophysical anomalies in this interval. The host rock is dominated by fine-grained diorite-gabbro (505102). Confidence level = 3.

Poles from crush zone

Data not used

Poles from ductile structures

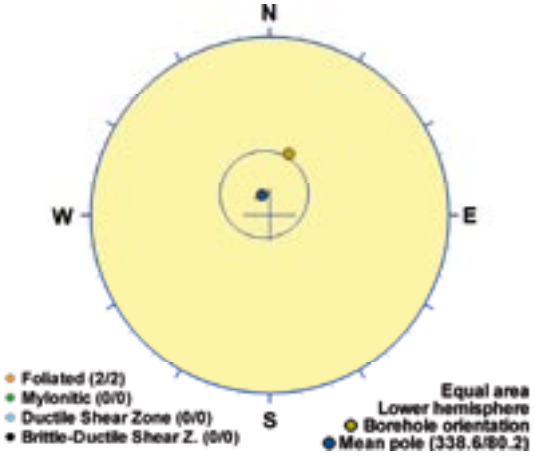

Poles from fractures

Data not used

Contours from fractures

Data not used

Orientation		Basis for orientation				Certainty	Thickness	
Strike	Dip	Fractures	Crush	Ductile structures	Reflectors	Orientation	Apparent	True
69	10			Used		Certain	0.6 m	0.5 m
Comment:								

KLX17A DZ4 (350.14 to 357.25), ductile zone

Low-grade ductile shear zone in composite intrusion. Sealed fractures and slickensides on open fractures. The interval 354-357 m is characterized by a minor decrease in P-wave velocity and resistivity. Four non-oriented radar reflectors occur within DZ4 with an angle from 56° to 86° to borehole axis. The host rock is dominated by fine-grained diorite-gabbro (505102). Subordinate rock types comprise Ävrö quartz monzodiorite (501046) and fine-grained granite (51058). Confidence level = 3.

Poles from crush zone

Data not used

Poles from ductile structures

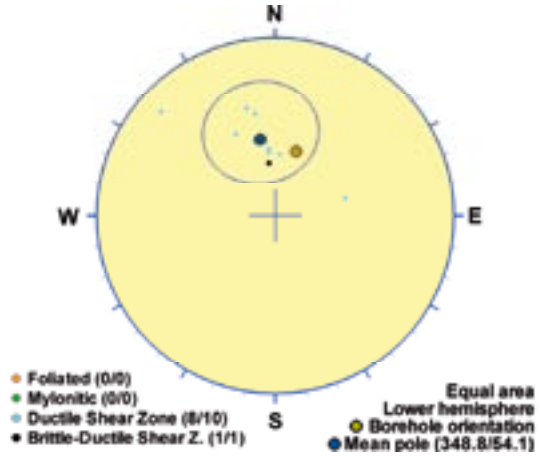

Poles from fractures

Data not used

Contours from fractures

Data not used

Orientation		Basis for orientation				Certainty	Thickness	
Strike	Dip	Fractures	Crush	Ductile structures	Reflectors	Orientation	Apparent	True
79	36			Used	Verify	Certain	7.1 m	6.8 m
Comment:								

KLX17A DZ5 (422.75 to 423.67), ductile/brittle zone

Brittle deformation zone characterized by moderate increase in frequency of both sealed and open fractures, one crush zone, weak foliation and red staining. At c. 423.5 m there is a distinct and sharp decrease in resistivity in combination with a minor caliper anomaly. Two non-oriented radar reflectors occur at 422.7 m and at 423.7 m with the angle 45° and 73° to borehole axis, respectively. Low radar amplitude occurs in the interval 421-431 m, i.e. partly above and below DZ5. The host rock is dominated by Ävrö granodiorite (501056). Subordinate rock type comprises fine-grained diorite-gabbro (505102). Confidence level = 3.

Poles from crush zone

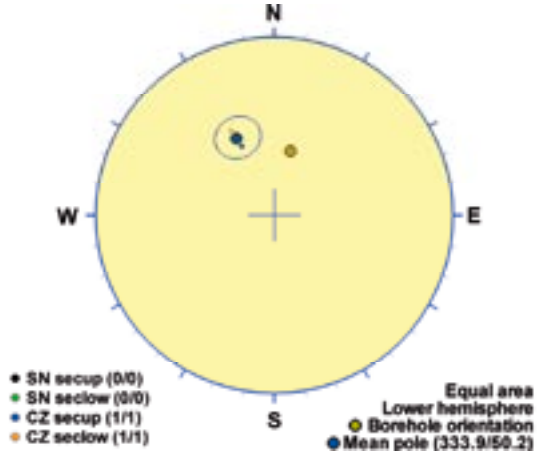

Poles from ductile structures

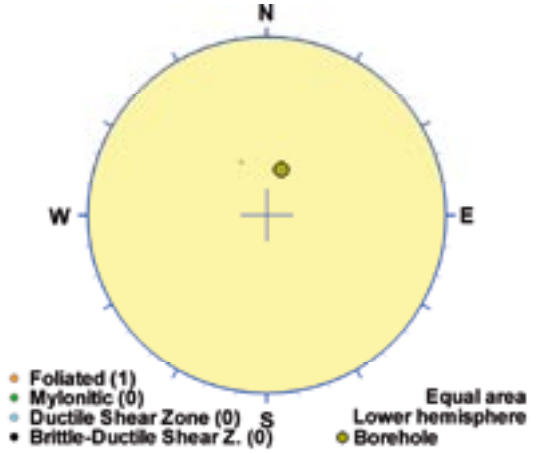

Poles from fractures

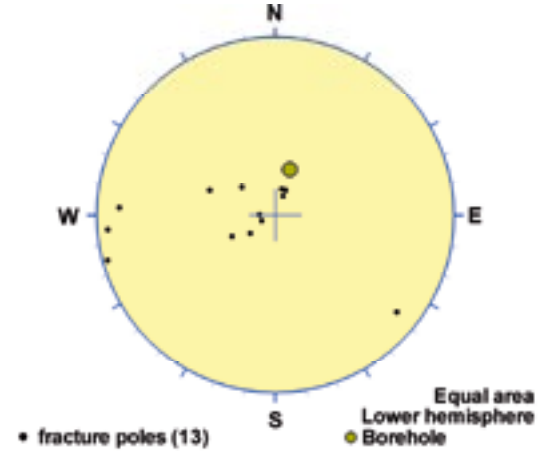

Contours from fractures

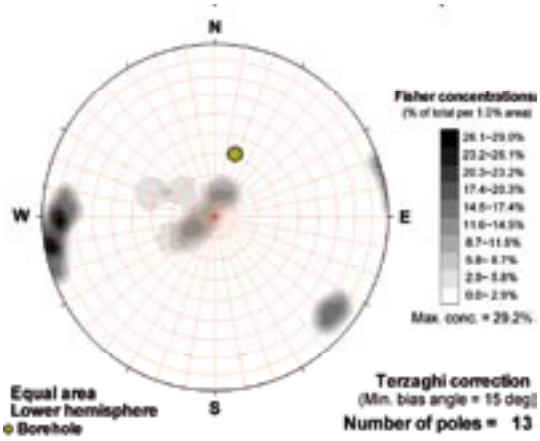

Orientation		Basis for orientation				Certainty	Thickness	
Strike	Dip	Fractures	Crush	Ductile structures	Reflectors	Orientation	Apparent	True
64	40	Contradict	Used	Verify	Verify	Probable	0.9 m	0.8 m
Comment:								

KLX17A DZ6 (423.67 to 431.76), ductile zone

Low-grade ductile shear zone in composite intrusion. Sealed fractures, moderate increase in open fractures and slickensides. The interval is characterized by several minor low resistivity anomalies. One oriented radar reflector occurs at 426.2 m with the orientation 124/45 or 058/23 and one non-oriented radar reflector occurs at 431.6 m with the angle 59° to borehole axis. Low radar amplitude occurs in the interval 421-431 m, i.e. partly above DZ6. The host rock is dominated by fine-grained diorite-gabbro (505102). Subordinate rock type comprises fine-grained granite (511058). Confidence level = 3.

Poles from crush zone

Data not used

Poles from ductile structures

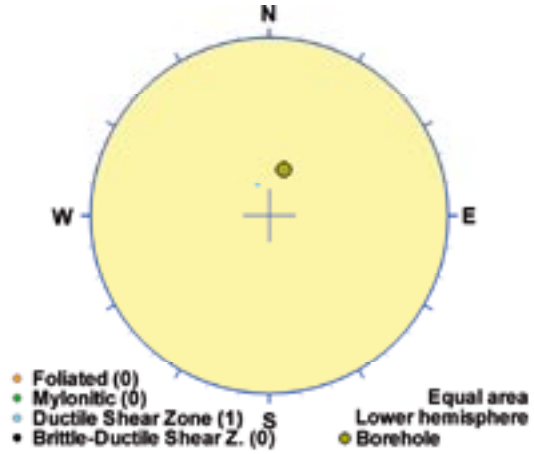

Poles from fractures

Data not used

Contours from fractures

Data not used

Orientation		Basis for orientation				Certainty	Thickness	
Strike	Dip	Fractures	Crush	Ductile structures	Reflectors	Orientation	Apparent	True
69	15			Used	Verify	Certain	8.1 m	7.5 m
Comment:								

KLX17A DZ7 (502.75 to 504.4), ductile/brittle zone

Minor brittle-ductile deformation zone characterized by increased frequency of sealed fractures, sealed network and weak epidotization. At c. 503.9 m there is a minor decrease in resistivity and magnetic susceptibility. Two non-oriented radar reflectors occur at 502.6 m and at 503.4 m with the angle 58° and 30° to borehole axis, respectively. Low radar amplitude occurs in the interval 502-504 m, i.e. partly above DZ7. The host rock is dominated by Ävrö quartz monzodiorite (501046). Confidence level = 3.

Poles from crush zone

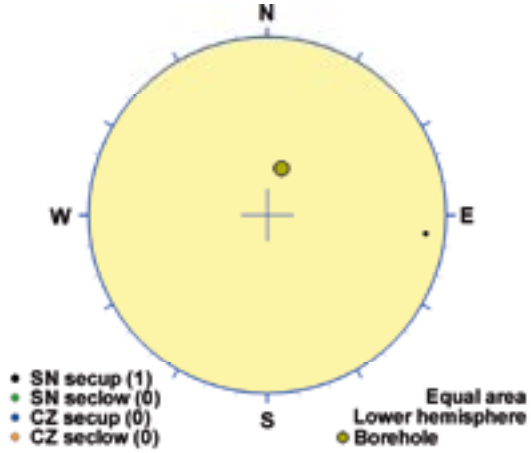

Poles from ductile structures

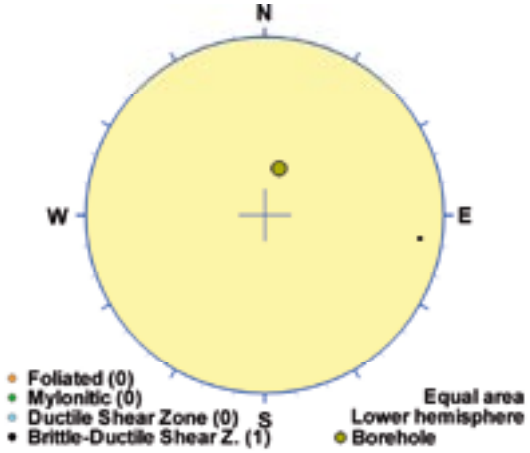

Poles from fractures

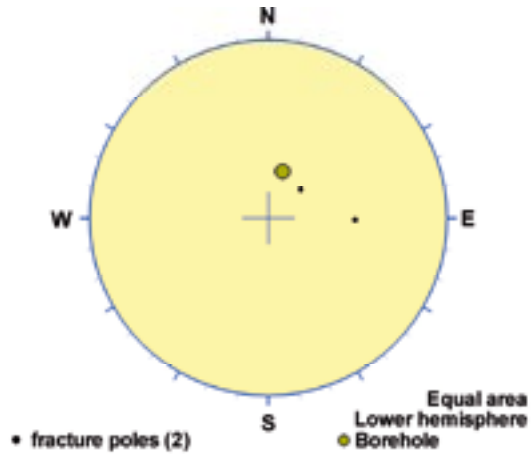

Contours from fractures

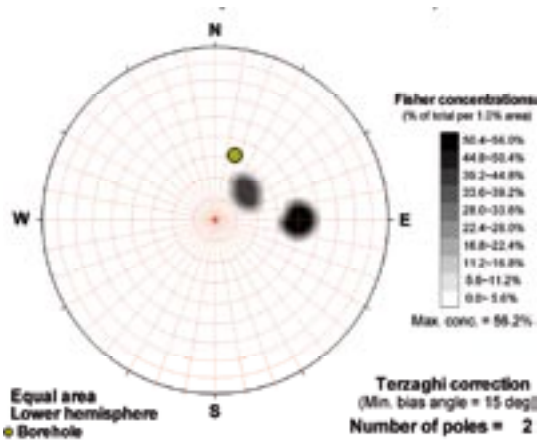

Orientation		Basis for orientation				Certainty	Thickness	
Strike	Dip	Fractures	Crush	Ductile structures	Reflectors	Orientation	Apparent	True
189	77	Contradict	Verify	Used	Contradict	Uncertain	1.6 m	0.4 m
Comment:								

KLX17A DZ8 (542.57 to 543.3), brittle zone

Minor brittle deformation zone characterized by increased frequency of sealed fractures, sealed network, slickensides on open fractures, faint foliation and faint to weak red staining. There are no significant geophysical anomalies in this interval. One non-oriented radar reflector occurs at 543.4 m with the angle 67° to borehole axis. The host rock is dominated by Ävrö quartz monzodiorite (501046). Subordinate rock type comprises diorite/gabbro (501033). Confidence level = 3.

Poles from crush zone

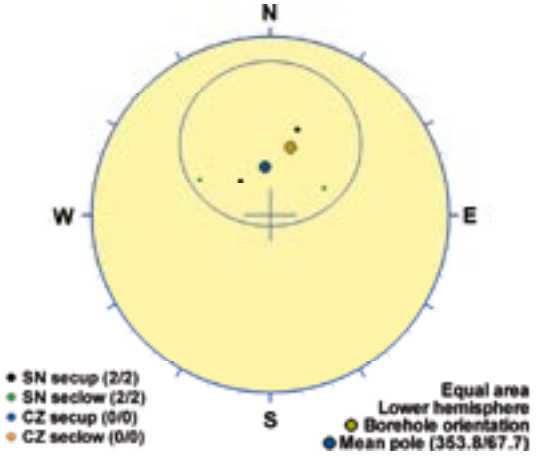

Poles from ductile structures

Data not used

Poles from fractures

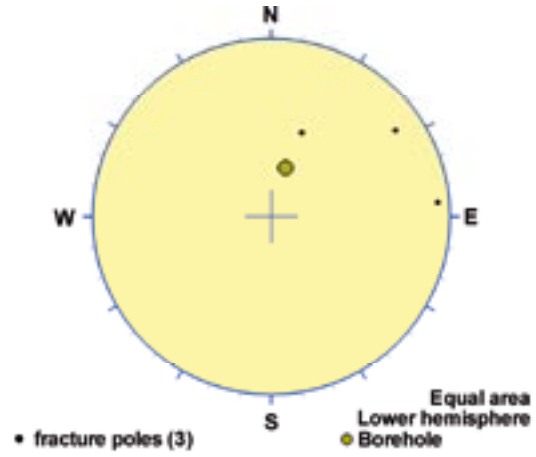

Contours from fractures

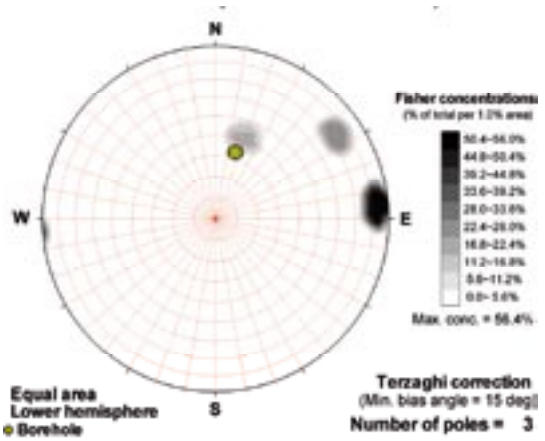

Orientation		Basis for orientation				Certainty	Thickness	
Strike	Dip	Fractures	Crush	Ductile structures	Reflectors	Orientation	Apparent	True
84	22	Contradict	Used		Verify	Uncertain	0.7 m	0.7 m
Comment: Interpretation from the sealed network data.								

KLX17A DZ9 (546.05 to 546.35), ductile/brittle zone

Minor brittle-ductile deformation zone characterized by increased frequency of sealed fractures, sealed network, foliation and weak red staining. There are no significant geophysical anomalies in this interval. The host rock is dominated by Ävrö quartz monzodiorite (501046). Confidence level = 3.

Poles from crush zone

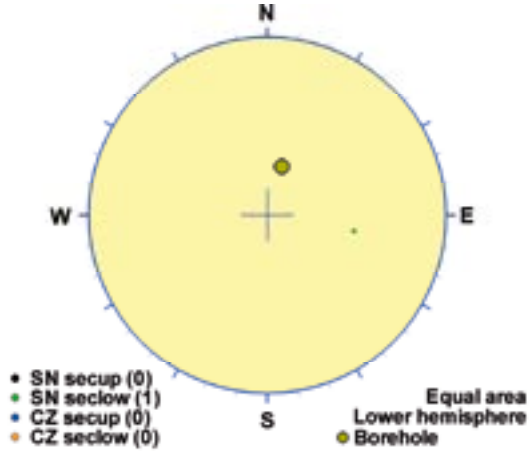

Poles from ductile structures

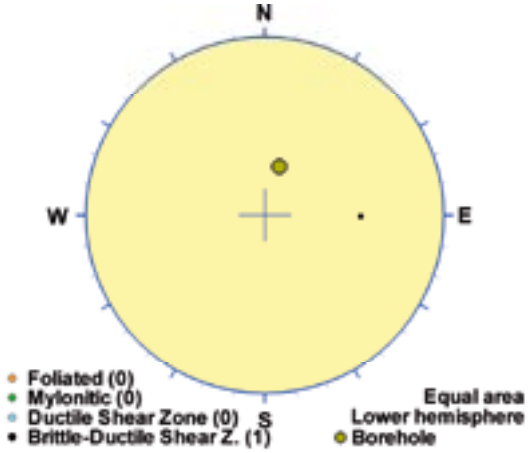

Poles from fractures

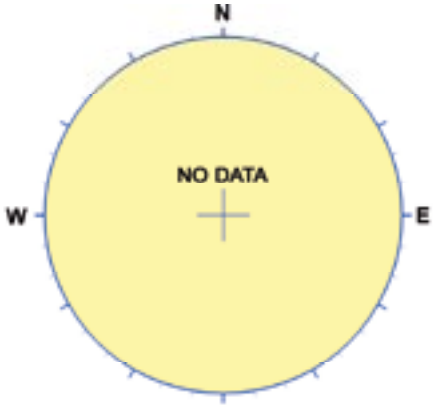

Contours from fractures

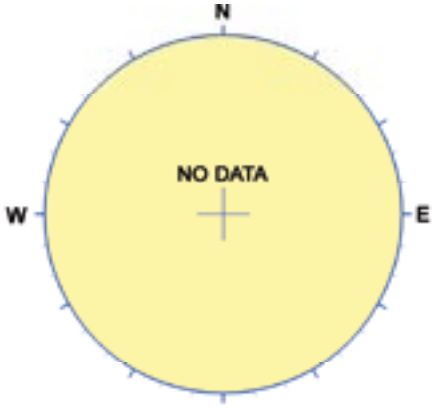

Orientation		Basis for orientation				Certainty	Thickness	
Strike	Dip	Fractures	Crush	Ductile structures	Reflectors	Orientation	Apparent	True
181	45		Verify	Used		Probable	0.3 m	0.2 m
Comment: The sealed network data confirm earlier interpretation.								

KLX17A DZ10 (662.29 to 670), brittle zone

Brittle deformation zone characterized by increase in sealed fractures and sealed network, moderate increase in open fractures, one crush zone, scattered thin brittle-ductile shear zones and cataclasites and weak to medium red staining. The interval is characterized by decreased P-wave velocity, bulk resistivity and magnetic susceptibility. Two non-oriented radar reflectors occur at 667.6 m and at 669.3 m with the angle 31° and 46° to borehole axis, respectively. The host rock is dominated by Ävrö granodiorite (501056). Subordinate rock type comprises fine-grained granite (511058). Confidence level = 3.

Poles from crush zone

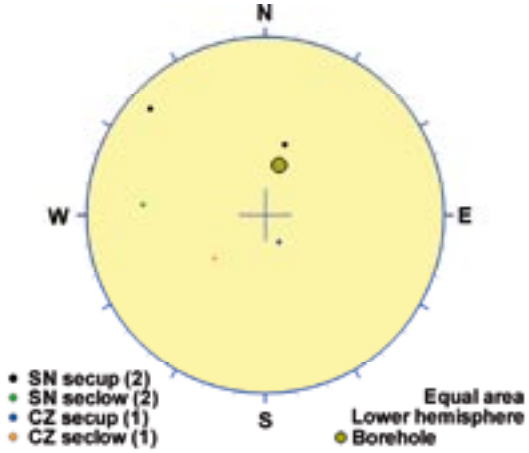

Poles from ductile structures

Data not used

Poles from fractures

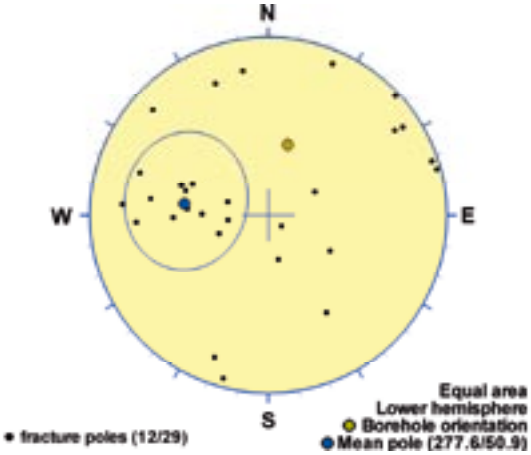

Contours from fractures

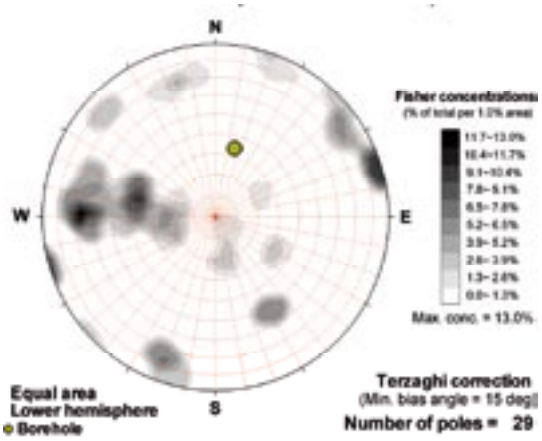

Orientation		Basis for orientation				Certainty	Thickness	
Strike	Dip	Fractures	Crush	Ductile structures	Reflectors	Orientation	Apparent	True
8	39	Used	Verify		Verify	Uncertain	7.7 m	4.6 m
Comment: The sealed network data and data from the crush zones verify AND contradict.								

KLX18A DZ1 (137.8 to 143.9), ductile/brittle zone

Inhomogeneous brittle to brittle-ductile deformation zone. Two 4-7 mm thick cataclasites. Faint to strong red staining. High frequency of sealed fractures and sealed network. Slickensides are observed. Decreased bulk resistivity and magnetic susceptibility. One non-oriented radar reflector occurs at 140.2 m with the angle 62° to borehole axis, and one oriented reflector occurs at 137.2 m with the orientation 129/25 or 333/39. Furthermore, there is one oriented reflector (no. 7x) outside the borehole and probably not intersecting the borehole. The orientation is 114/71 or 299/78. The host rock is dominated by Ävrö quartz monzodiorite (501046). Subordinate rock type is fine-grained granite (511058). Confidence level = 3.

Poles from crush zone

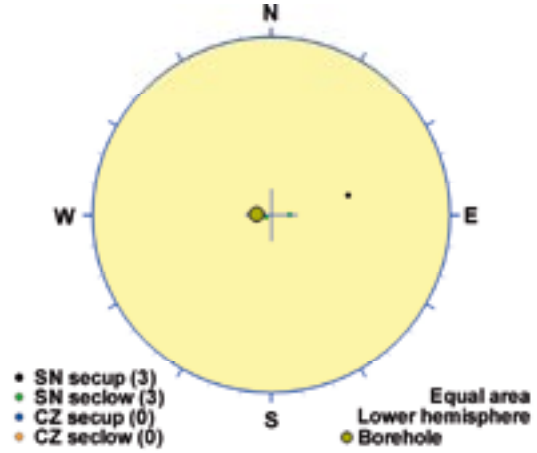

Poles from ductile structures

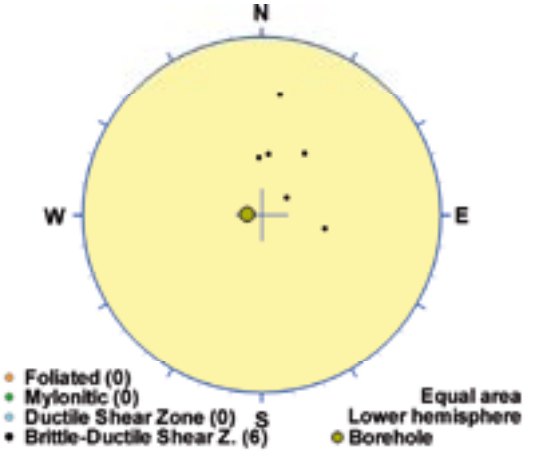

Poles from fractures

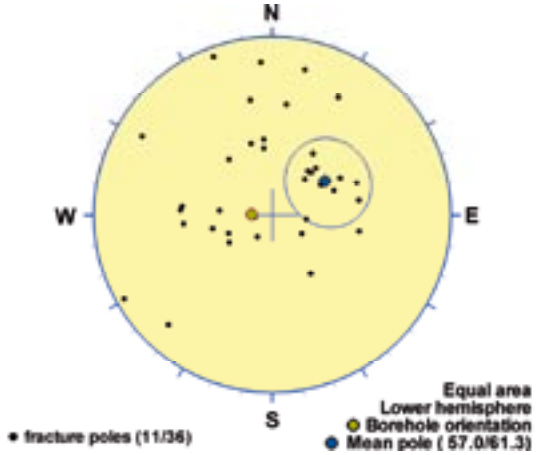

Contours from fractures

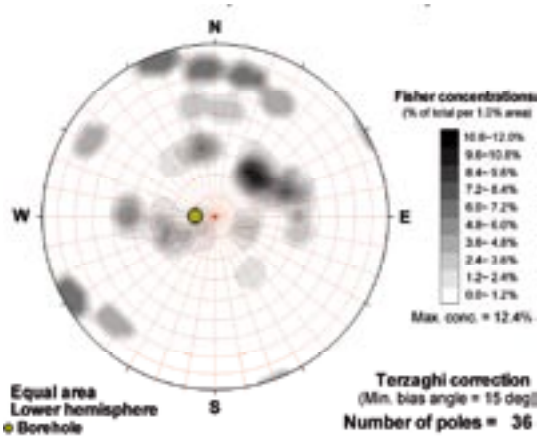

Orientation		Basis for orientation				Certainty	Thickness	
Strike	Dip	Fractures	Crush	Ductile structures	Reflectors	Orientation	Apparent	True
147	29	Used	Verify	Verify	Verify	Probable	6.1 m	4.9 m
Comment:								

KLX18A DZ2 (148.6 to 149.4), ductile/brittle zone

Inhomogeneous brittle to brittle-ductile deformation zone. Faint to medium red staining. High frequency of sealed fractures and sealed network. Slickensides are observed. Distinct low resistivity anomaly and slightly decreased magnetic susceptibility. One rather strong oriented radar reflector at 148.7 m with the orientation 133/26 or 335/40. The host rock is dominated by Ävrö quartz monzodiorite (501046). Confidence level = 3.

Poles from crush zone

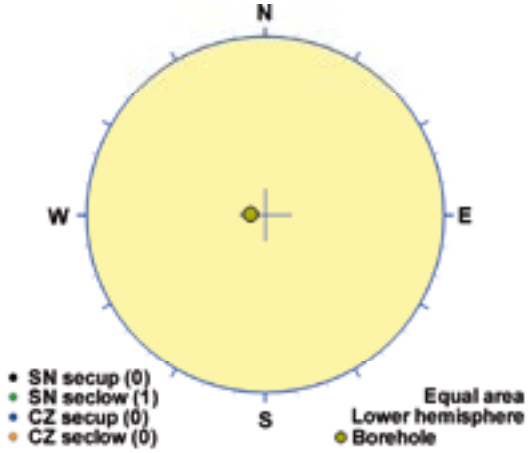

Poles from ductile structures

Poles from fractures

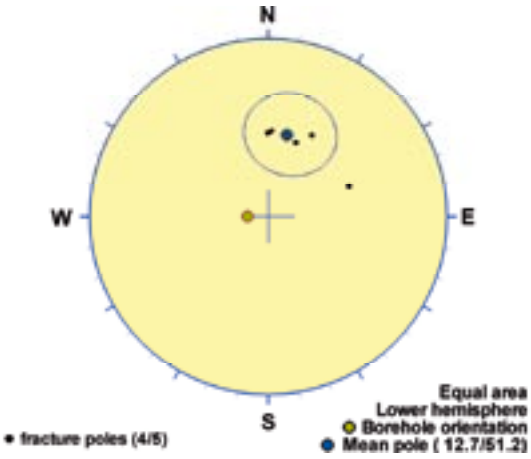

Contours from fractures

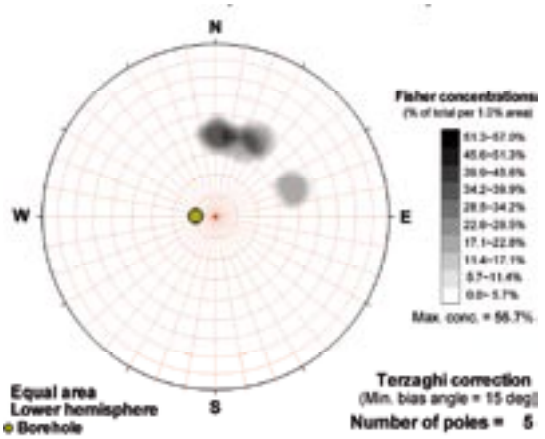

Orientation		Basis for orientation				Certainty	Thickness	
Strike	Dip	Fractures	Crush	Ductile structures	Reflectors	Orientation	Apparent	True
103	39	Used			Verify	Probable	0.8 m	0.6 m
Comment:								

KLX18A DZ4 (359.6 to 366.2 m), ductile/brittle zone

Inhomogeneous brittle to brittle-ductile deformation zone. Eight 4-20 mm thick cataclasites. Faint to medium red staining. High frequency of sealed fractures and sealed network. Slickensides are observed. Several distinct low resistivity anomalies and decreased magnetic susceptibility. Two non-oriented radar reflectors occur at 360.1 m and 362.5 m with the angle 55° and 57° to borehole axis, respectively. The host rock is dominated by Ävrö granodiorite (501056). Confidence level = 2.

Poles from crush zone

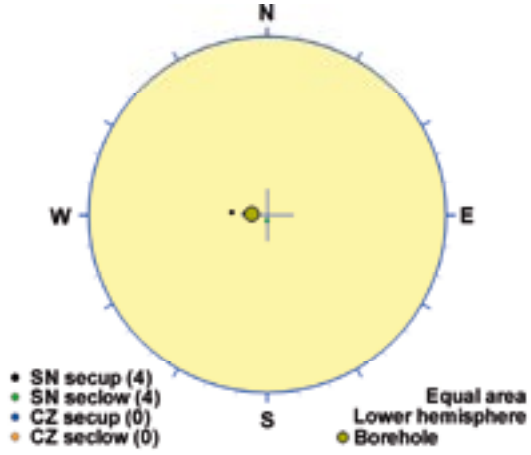

Poles from ductile structures

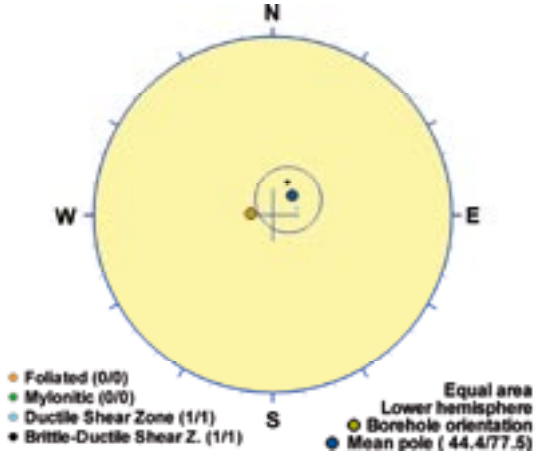

Poles from fractures

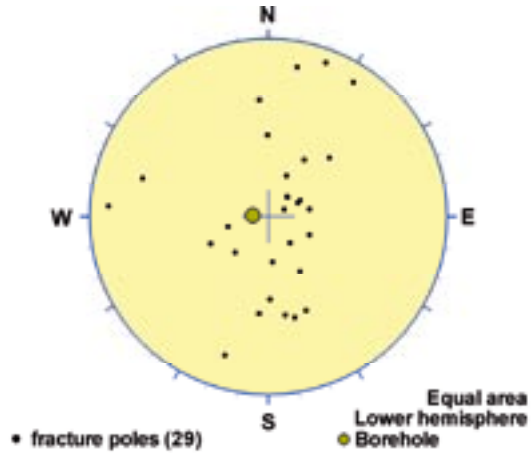

Contours from fractures

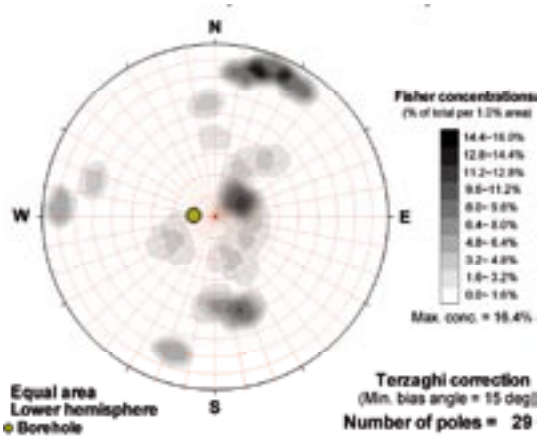

Orientation		Basis for orientation				Certainty	Thickness	
Strike	Dip	Fractures	Crush	Ductile structures	Reflectors	Orientation	Apparent	True
134	13			Used	Contradict	Probable	6.6 m	6.2 m
Comment:								

KLX18A DZ5 (378.6 to 378.85 m), brittle zone

Inhomogeneous brittle deformation zone. One cataclasite (55 mm). Faint red staining is present. High frequency of sealed fractures. One sharp low resistivity anomaly and decreased P-wave velocity and magnetic susceptibility. The host rock is dominated by Ävrö granodiorite (501056). Confidence level = 3.

Poles from crush zone

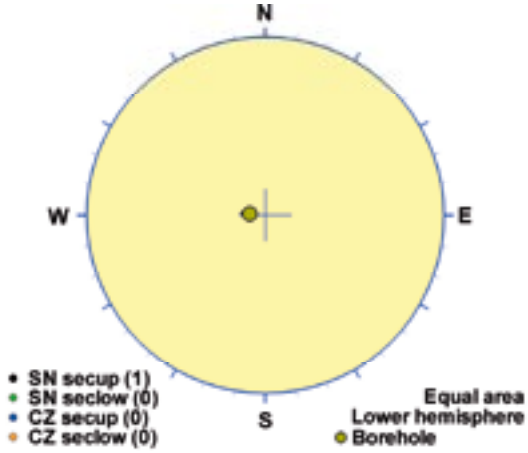

Poles from ductile structures

Data not used

Poles from fractures

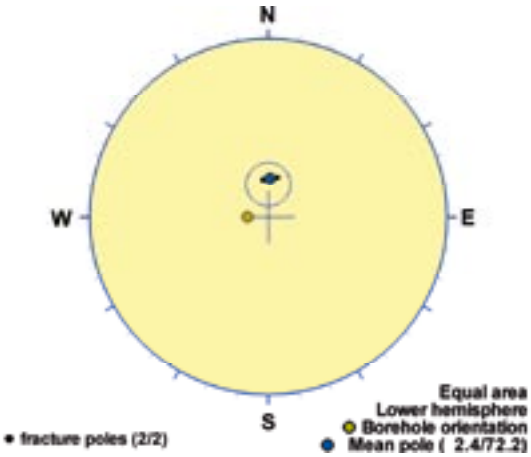

Contours from fractures

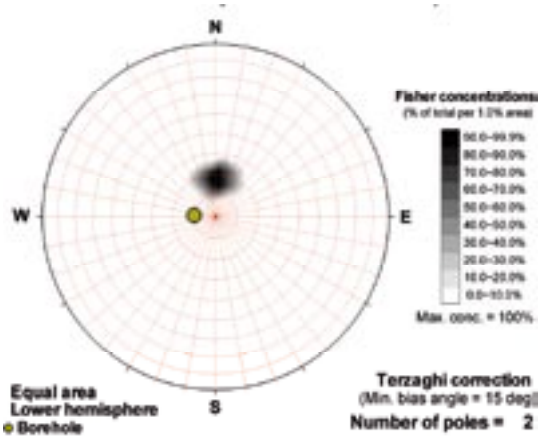

Orientation		Basis for orientation				Certainty	Thickness	
Strike	Dip	Fractures	Crush	Ductile structures	Reflectors	Orientation	Apparent	True
92	18	Used				Probable	0.2 m	0.2 m
Comment:								

KLX18A DZ6 (401 to 404.2), ductile/brittle zone

Inhomogeneous brittle-ductile deformation zone, highly fractured between 402.48 and 403.20 m. High frequency of sealed fractures and moderate increase in open fractures. Minor core loss (5 cm). Weak red staining. Crush zone (0.8 m). Significantly decreased resistivity and magnetic susceptibility. Caliper anomalies and partly decreased P-wave velocity. One non-oriented radar reflector occurs at 401.1 m with the angle 56° to borehole axis, and one strong and persistent oriented reflector occurs at 402.3 m with the orientation 092/30 or 299/35. The host rock is dominated by Ävrö granodiorite (501056). Subordinate rock type is fine-grained diorite-gabbro (505102). Confidence level = 3.

Poles from crush zone

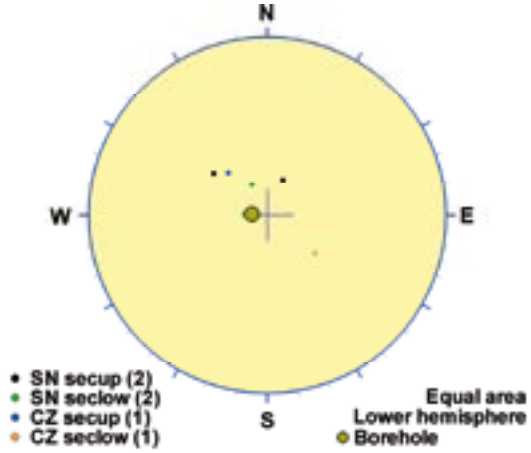

Poles from ductile structures

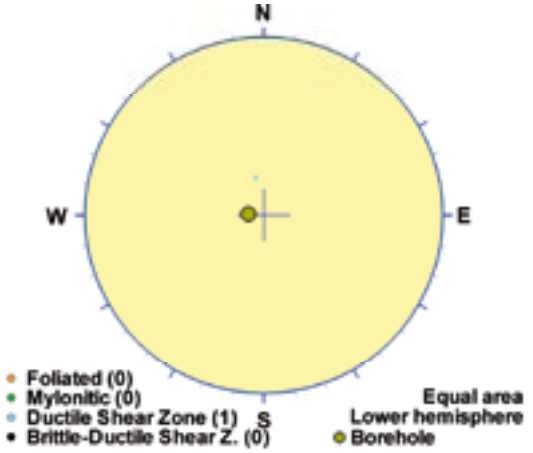

Poles from fractures

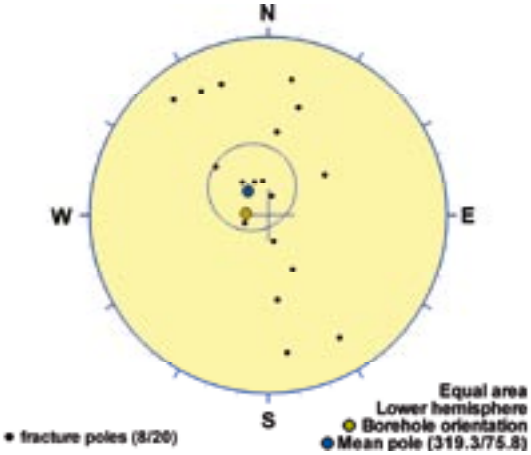

Contours from fractures

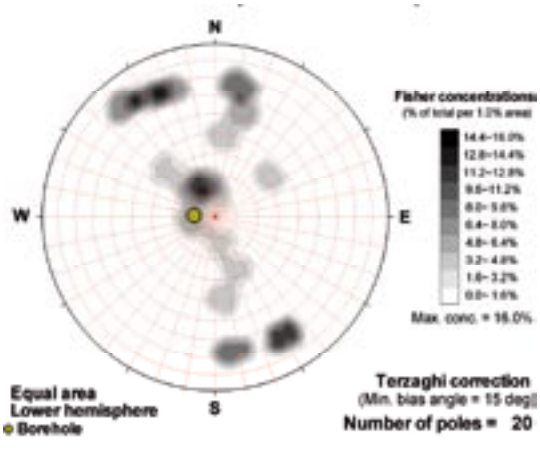

Orientation		Basis for orientation				Certainty	Thickness	
Strike	Dip	Fractures	Crush	Ductile structures	Reflectors	Orientation	Apparent	True
49	14	Used	Verify	Verify	Verify	Probable	3.2 m	3.2 m
Comment:								

KLX18A DZ7 (428 to 434 m), ductile/brittle zone

Inhomogeneous brittle-ductile deformation zone. One cataclasite (13 cm). One crush zone (7 cm). Faint red staining is present. Moderate increase in sealed fractures. Two distinct low resistivity anomalies and decreased magnetic susceptibility. Two non-oriented radar reflectors occur at 431.4 m and 432.6 m with the angle 56° and 57° to borehole axis, respectively. One oriented reflector outside the borehole and probably not reaching the borehole, is interpreted to occur at 432.2 m with the orientation 186/87. The host rock is dominated by Ävrö granodiorite (501056). Subordinate rock type is fine-grained granite (511058). Confidence level = 2.

Poles from crush zone

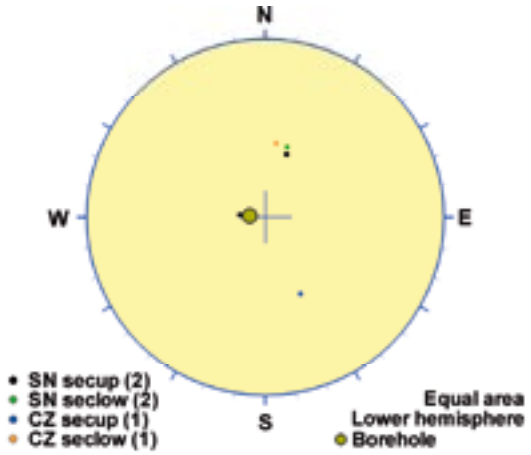

Poles from ductile structures

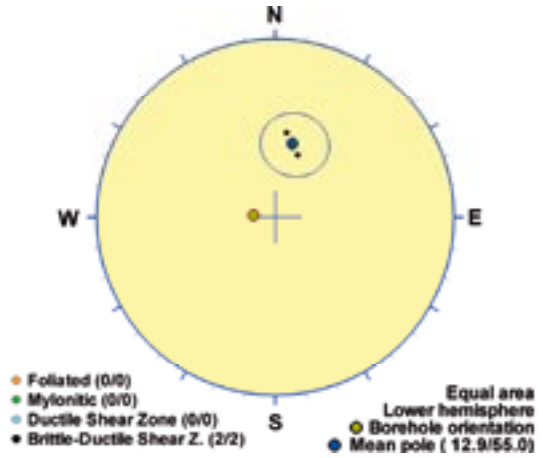

Poles from fractures

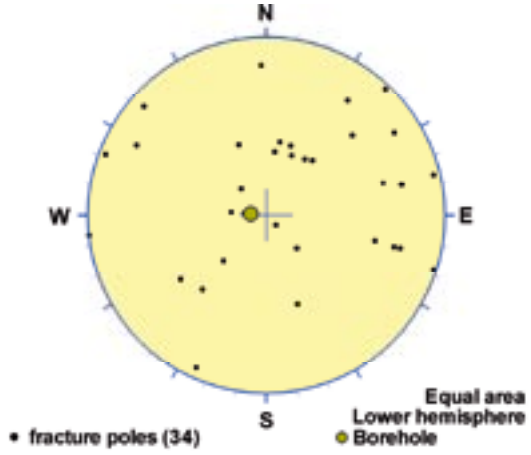

Contours from fractures

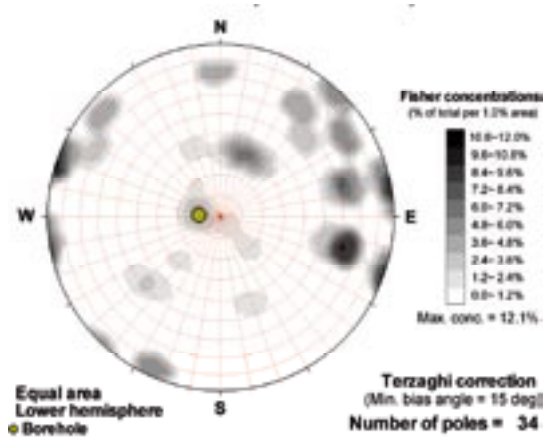

Orientation		Basis for orientation				Certainty	Thickness	
Strike	Dip	Fractures	Crush	Ductile structures	Reflectors	Orientation	Apparent	True
103	35		Verify	Used	Verify	Certain	6 m	4.8 m
Comment:								

KLX18A DZ8 (448.35 to 456.55 m), ductile/brittle zone

Inhomogeneous brittle-ductile deformation zone. High frequency of sealed fractures. One cataclasite (2 cm). Weak red staining. Decreased resistivity and magnetic susceptibility, and partly decreased P-wave velocity. Two non-oriented radar reflectors occur at 448.8 m and 450.2 m with the angle 66° and 47° to borehole axis, respectively. Low radar amplitude in the interval 446-450 m. The host rock is dominated by Ävrö granodiorite (501056). Subordinate rock type is fine-grained granite (511058). Confidence level = 2.

Poles from crush zone

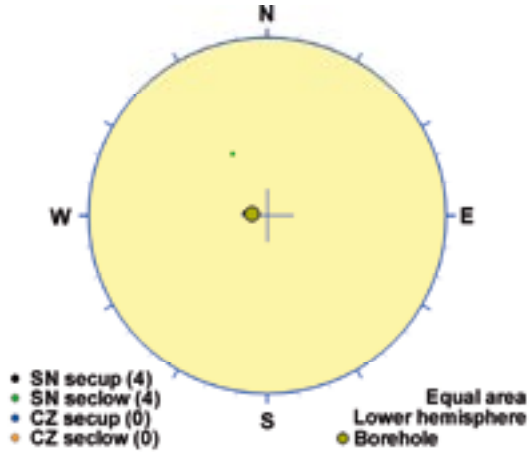

Poles from ductile structures

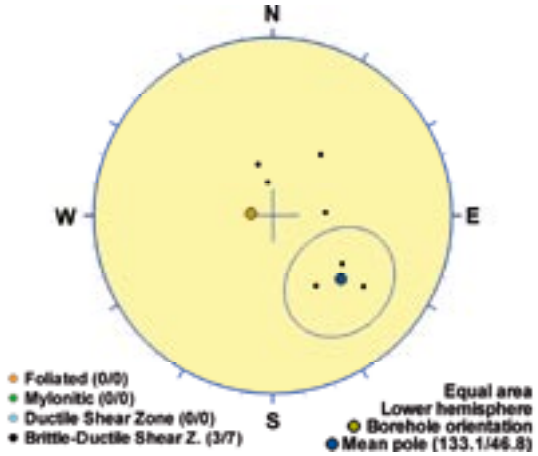

Poles from fractures

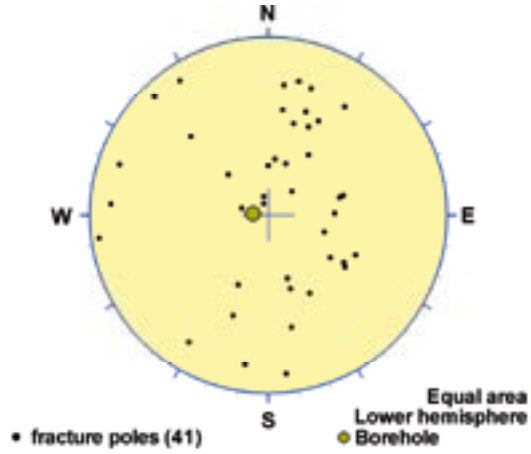

Contours from fractures

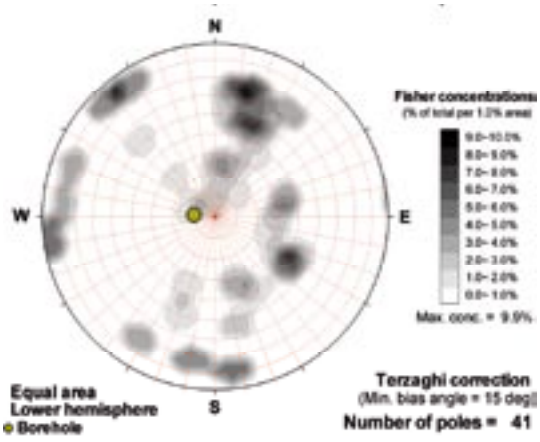

Orientation		Basis for orientation				Certainty	Thickness	
Strike	Dip	Fractures	Crush	Ductile structures	Reflectors	Orientation	Apparent	True
223	43	Verify	Not Used	Used	Contradict	Uncertain	8.2 m	5.1 m
Comment:								

KLX19A DZ1 (100.42 to 105.76), brittle zone

Brittle deformation zone characterized by increased frequency of open and sealed fractures, core loss and faint to medium saussuritization and red staining. Distinctly decreased resistivity, P-wave velocity, magnetic susceptibility, density and caliper anomalies in the interval 104.5-105.5 m. One oriented radar reflector occurs at 103.1 m (111/41 or 110/75) and two non-oriented radar reflectors occur at 103.1 m and 104.8 m with the angle 29° and 57° to borehole axis, respectively. The oriented reflector can be observed to a distance of 16 m outside the borehole, and the upper non-oriented, which exhibits strong character, to a distance of 14 m outside the borehole. Low radar amplitude occurs at 102-105 m. The host rock is totally dominated by quartz monzodiorite (501036), and very sparse occurrence of fine-grained granite (511058).

Poles from crush zone

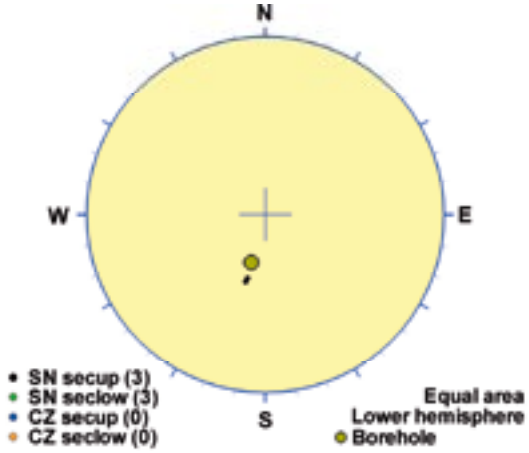

Poles from ductile structures

Data not used

Poles from fractures

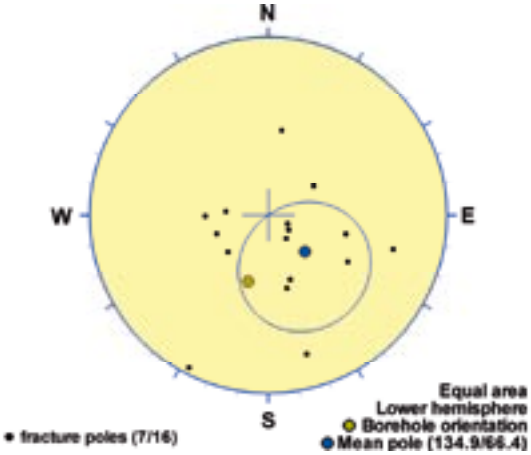

Contours from fractures

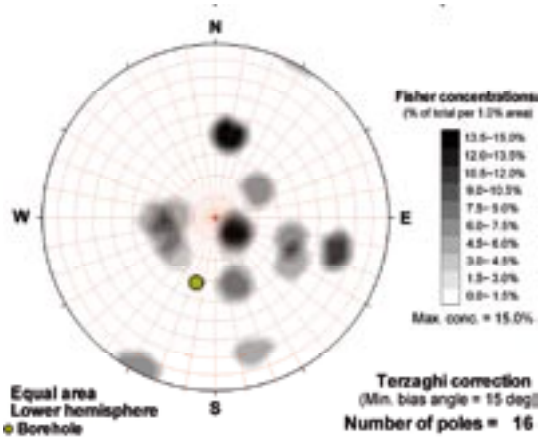

Orientation		Basis for orientation				Certainty	Thickness	
Strike	Dip	Fractures	Crush	Ductile structures	Reflectors	Orientation	Apparent	True
225	24	Used			Contradict	Very uncertain	5.3 m	4.7 m
Comment:								

KLX19A DZ2 (298.35 to 304.2), brittle zone

Brittle deformation zone characterized by increased frequency of open and sealed fractures, faint to weak red staining and saussuritization, core loss and a c. 0.5 dm long sealed breccia in the bottom of the section. Large apertures in open fractures. Distinctly decreased resistivity and P-wave velocity in the interval c. 299-301 m. The entire section is characterized by decreased magnetic susceptibility, increased borehole diameter (caliper) and increased natural gamma radiation. One oriented radar reflector occurs at 299.3 m (277/71 or 050/11) and one non-oriented radar reflector occurs at 301.9 m with the angle 37° to borehole axis. The oriented reflector exhibits strong character and can be observed to a distance of 12 m outside the borehole. The non-oriented, which also exhibits a strong character, can be observed to a distance of 18 m outside the borehole. Low radar amplitude occurs at c. 300 m. The host rock is totally dominated by quartz monzodiorite (501036), and very sparse occurrence of fine-grained granite (511058).

Poles from crush zone

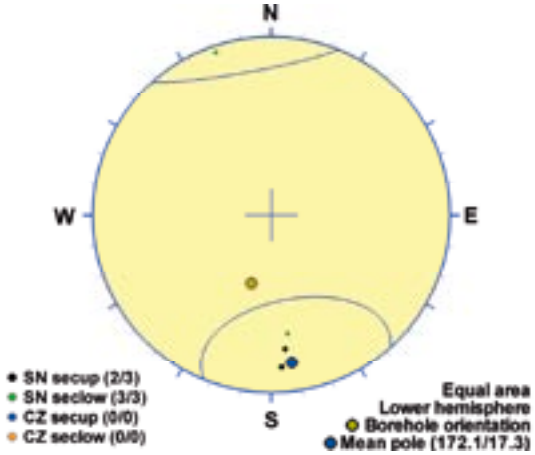

Poles from ductile structures

Data not used

Poles from fractures

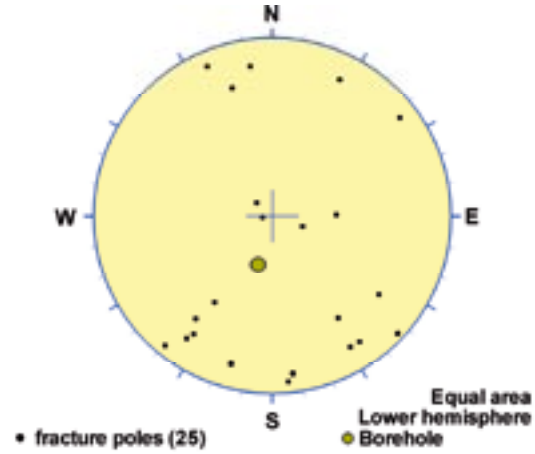

Contours from fractures

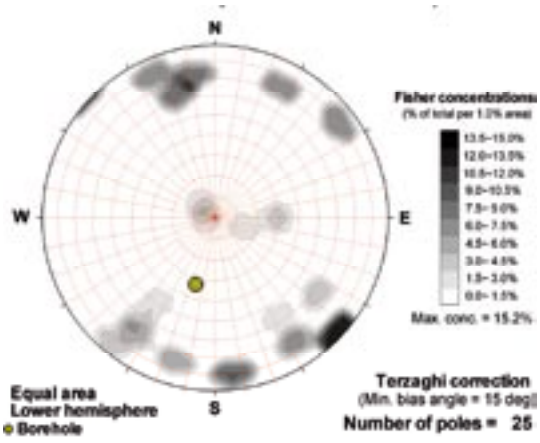

Orientation		Basis for orientation				Certainty	Thickness	
Strike	Dip	Fractures	Crush	Ductile structures	Reflectors	Orientation	Apparent	True
262	73	Verify	Used		Contradict	Probable	5.8 m	4.2 m
Comment:								

KLX19A DZ3 (412.15 to 416.9), brittle zone

Brittle deformation zone characterized by increased frequency of open and sealed fractures, large apertures, weak to medium epidotization and red staining, calcite-healed breccia, slickensides and foliation of medium intensity. Decreased resistivity and P-wave velocity at c. 412-415 m. This interval is also characterized by decreased density and increased natural gamma radiation in combination with decreased magnetic susceptibility, which usually indicates the occurrence of fine-grained granite. One oriented radar reflector occurs at 413.1 m (235/75) and two non-oriented radar reflectors occur at 413.4 m and 416.0 m with the angle 50° and 40° to borehole axis, respectively. The oriented reflector can be observed to a distance of 18 m outside the borehole, and the non-oriented reflectors to a distance of 6 m and 4 m outside the borehole, respectively. The host rock is totally dominated by quartz monzodiorite (501036).

Poles from crush zone

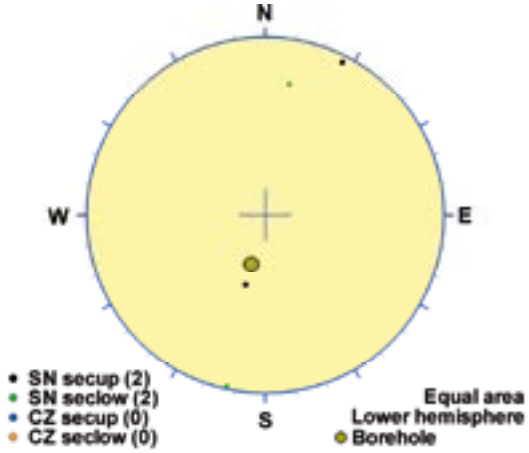

Poles from ductile structures

Data not used

Poles from fractures

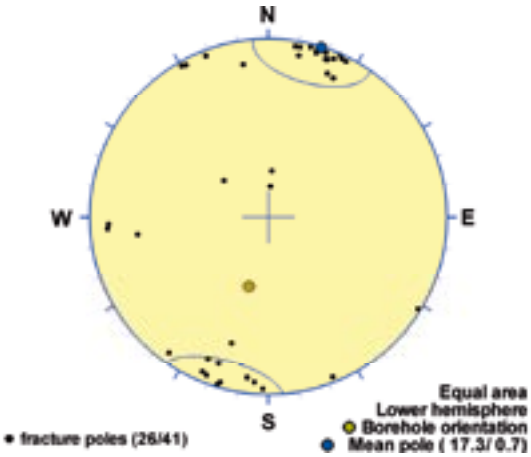

Contours from fractures

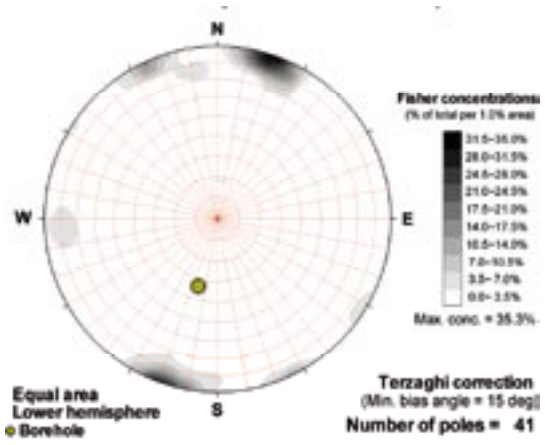

Orientation		Basis for orientation				Certainty	Thickness	
Strike	Dip	Fractures	Crush	Ductile structures	Reflectors	Orientation	Apparent	True
107	89	Used	Verify	Not Used	Verify	Certain	4.8 m	2.6 m
Comment:								

KLX19A DZ5 (482.6 to 507.68), brittle zone

Brittle deformation zone characterized by increased frequency of open and sealed fractures, apertures, six crush zones, core loss and slickensides. The entire section is characterized by a large general decrease in the bulk resistivity and several caliper anomalies. There is also partly decreased P-wave velocity. The magnetic susceptibility is c. 0.012-0.014 SI. Two oriented radar reflectors occur at 494.5 m (039/67 or 047/82) and at 507.1 m (037/70 or 042/79). Both reflectors are very strong and probably indicate the dolerite. Also, reflector 58 at 470.7 m (044/59 or 057/82) probably indicates the upper contact of the same dolerite, even if it is interpreted to intersect above the dolerite section. One non-oriented radar reflector occurs at 501.5 m with the angle 51° to borehole axis. The oriented reflectors can be observed along almost the entire borehole length. The non-oriented reflector can be observed to a distance of 10 m outside the borehole. Extremely low radar amplitude occurs at 481-510 m. The host rock is dominated by dolerite (501027).

Poles from crush zone

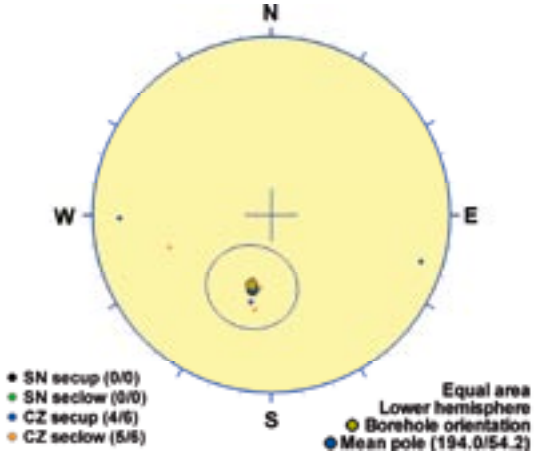

Poles from ductile structures

Data not used

Poles from fractures

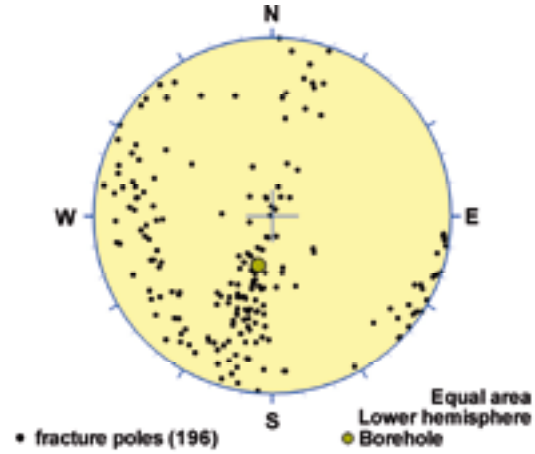

Contours from fractures

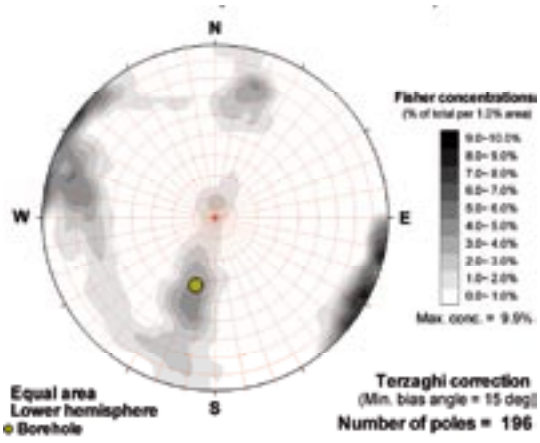

Orientation		Basis for orientation				Certainty	Thickness	
Strike	Dip	Fractures	Crush	Ductile structures	Reflectors	Orientation	Apparent	True
284	36	Verify	Used		Contradict	Probable	25.1 m	25.1 m
Comment: Probably two zones. This zone is probably coupled to nearby dolerite [s/d 045/80]								

KLX19A DZ6 (508.4 to 510), brittle zone

Brittle deformation zone characterized by increased frequency of open and sealed fractures and medium red staining and saussuritization. No significant geophysical anomalies. Two non-oriented radar reflectors occur at 508.5 m with the angle 50° and 30° to borehole axis, respectively. The host rock is dominated by quartz monzodiorite (501036) with subordinate fine-grained granite (511058).

Poles from crush zone

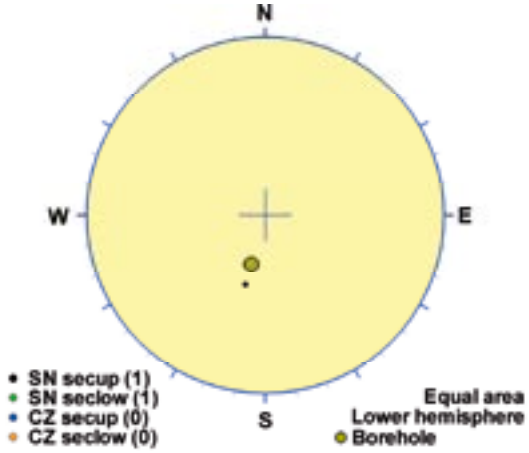

Poles from ductile structures

Data not used

Poles from fractures

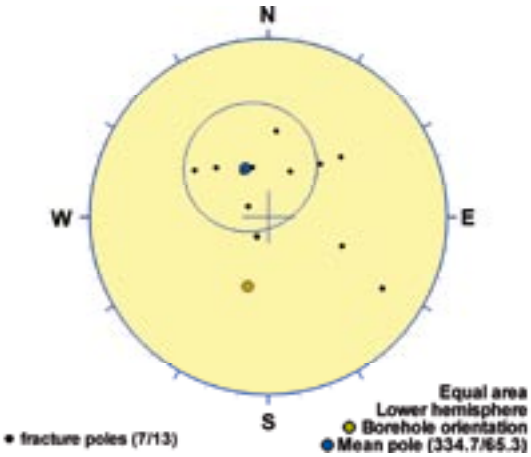

Contours from fractures

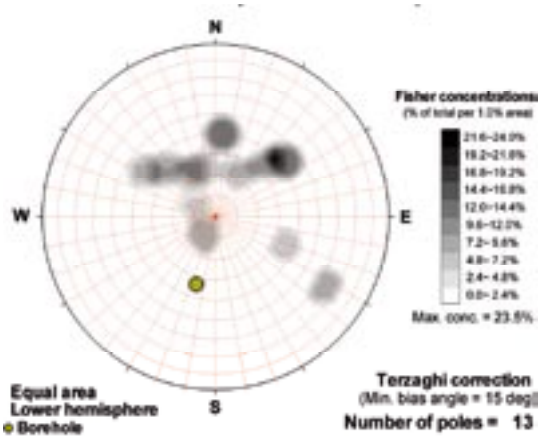

Orientation		Basis for orientation				Certainty	Thickness	
Strike	Dip	Fractures	Crush	Ductile structures	Reflectors	Orientation	Apparent	True
65	25	Used	Contradict			Uncertain	1.6 m	0.9 m
Comment:								

KLX19A DZ7 (520.44 to 552.21), brittle zone

Brittle deformation zone characterized by increased frequency of open and sealed fractures, five crush zones, core loss and slickensides. The entire section is characterized by a large general decrease in the bulk resistivity and several caliper anomalies. There is also partly decreased P-wave velocity. The caliper anomalies and decreased P-wave velocity anomalies are mainly concentrated to the interval c. 520-537 m. The magnetic susceptibility is c. 0.007-0.010 SI. One oriented radar reflector occurs at 543.9 m (031/65). The oriented reflector, which exhibits a strong character, can be observed to a distance of 15 m outside the borehole, from the borehole intersection along the borehole down to the bottom of the borehole. The oriented reflector probably indicates the dolerite. Three non-oriented radar reflectors occur with an angle between 49° and 59° to borehole axis. A fourth non-oriented very strong radar reflector has the angle 7° to borehole axis. It can be observed to a distance of 23 m outside the borehole and is probably a part of the dolerite. Extremely low radar amplitude occurs at 517-552 m. The host rock is dominated by dolerite (501027).

Poles from crush zone

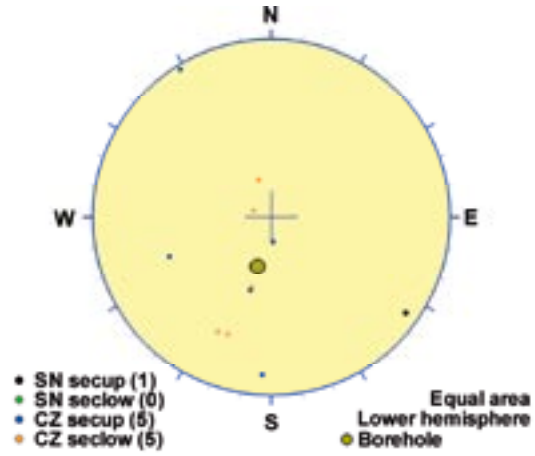

Poles from ductile structures

Data not used

Poles from fractures

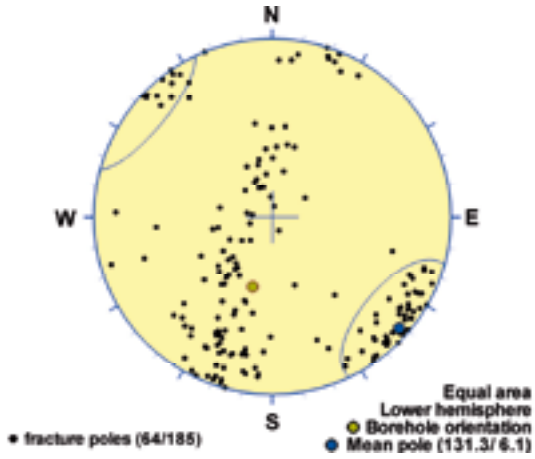

Contours from fractures

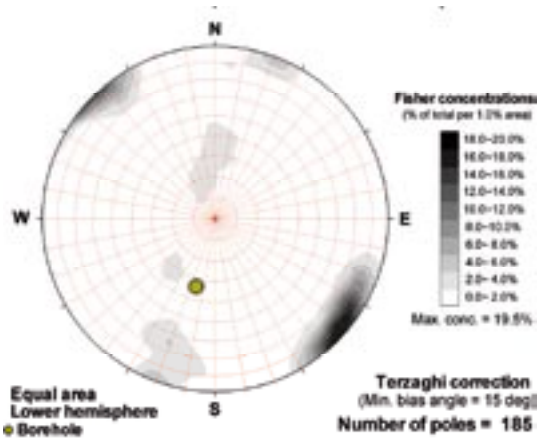

Orientation		Basis for orientation				Certainty	Thickness	
Strike	Dip	Fractures	Crush	Ductile structures	Reflectors	Orientation	Apparent	True
40	90	Verify	Verify		Contradict	Uncertain	31.8 m	7.2 m
Comment: Possibly two zones. Probably coupled to nearby dolerite [s/d 040/90]. Overrules interpretation above.								

KLX19A DZ8 (552.21 to 553.1), ductile/brittle zone

Minor low-grade ductile to brittle-ductile shear zone. Weak saussuritization and faint epidotization and red staining. The interval is characterized by decreased density, magnetic susceptibility, resistivity and partly decreased P-wave velocity. The host rock is dominated by quartz monzodiorite (501036) with subordinate fine-grained granite (511058).

Poles from crush zone

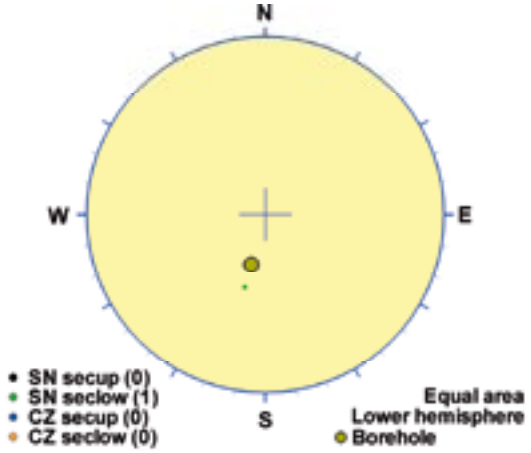

Poles from ductile structures

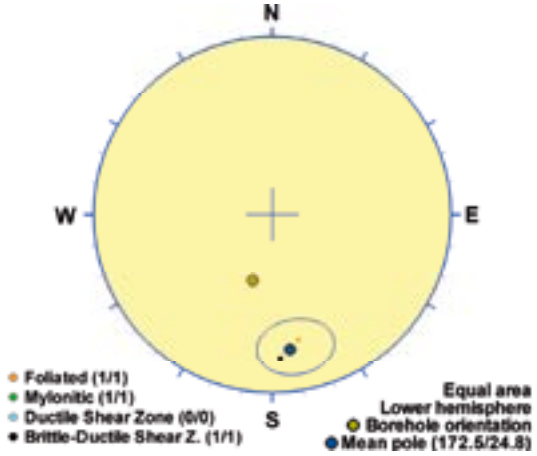

Poles from fractures

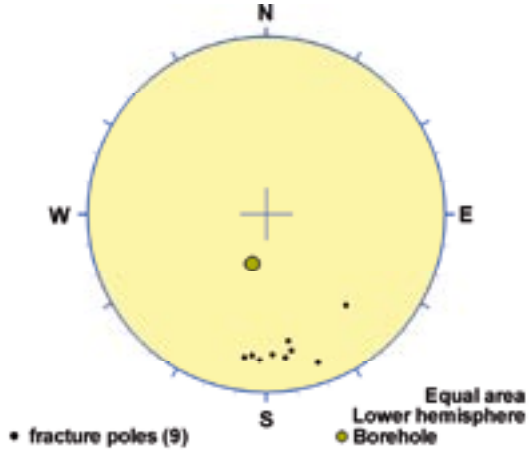

Contours from fractures

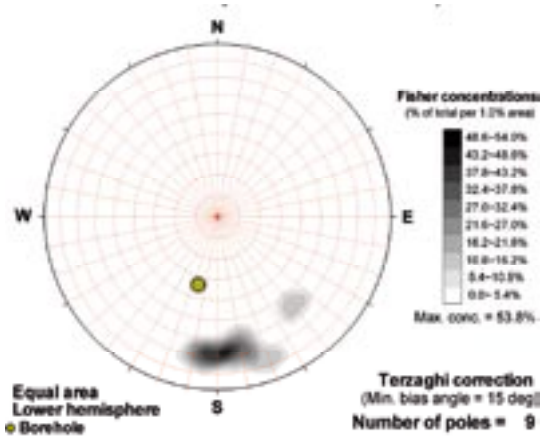

Orientation		Basis for orientation				Certainty	Thickness	
Strike	Dip	Fractures	Crush	Ductile structures	Reflectors	Orientation	Apparent	True
263	65	Verify	Contradict	Used		Probable	0.9 m	0.7 m
Comment:								

KLX19A DZ9 (691.5 to 693.64), ductile zone

Low-grade ductile shear zone in composite intrusion. Faint red staining. The section is characterized by decreased magnetic susceptibility and slightly decreased resistivity. The host rock is dominated by a mixture of fine-grained diorite-gabbro (505102) and fine-grained granite (511058) which most likely explains the large gradients in the density and natural gamma radiation data.

Poles from crush zone

Data not used

Poles from ductile structures

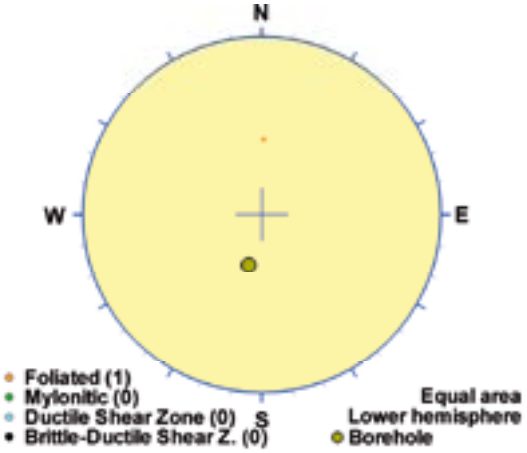

Poles from fractures

Data not used

Contours from fractures

Data not used

Orientation		Basis for orientation				Certainty	Thickness	
Strike	Dip	Fractures	Crush	Ductile structures	Reflectors	Orientation	Apparent	True
92	35			Used		Probable	2.1 m	0.8 m
Comment:								

KLX19A DZ10 (705.21 to 706.6), ductile zone

Low-grade ductile shear zone in composite intrusion. The host rock is dominated by a mixture of fine-grained diorite-gabbro (505102) and fine-grained granite (511058) which most likely explains the large gradients in the density and natural gamma radiation data. One non-oriented radar reflector occurs at 706.2 m with the angle 31° to borehole axis.

Poles from crush zone

Data not used

Poles from ductile structures

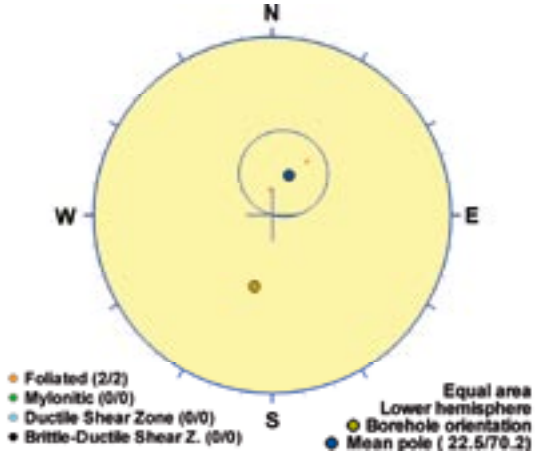

Poles from fractures

Data not used

Contours from fractures

Data not used

Orientation		Basis for orientation				Certainty	Thickness	
Strike	Dip	Fractures	Crush	Ductile structures	Reflectors	Orientation	Apparent	True
113	20			Used	Contradict	Probable	1.4 m	0.8 m
Comment:								

KLX20A DZ2 (261 to 265.9), ductile/brittle zone

Inhomogeneous ductile deformation zone. Faint to weak red staining, silicification, saussuritization and epidotization. Crush zone (7 cm). High frequency of sealed fractures. Moderate frequency of open fractures. Decreased magnetic susceptibility and partly decreased resistivity. Three non-oriented radar reflectors occur at 262.0 m, 262.7 m and 264.3 m with the angle 63°, 21° and 32° to borehole axis, respectively. One oriented reflector occurs at 265.8 m with the orientation 053/87 or 271/48. The host rock is dominated by quartz monzodiorite (501036).

Poles from crush zone

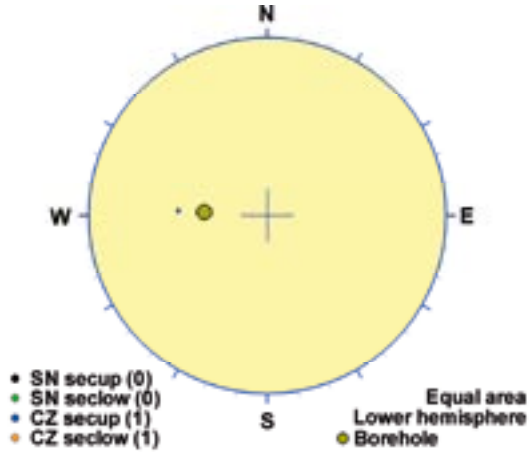

Poles from ductile structures

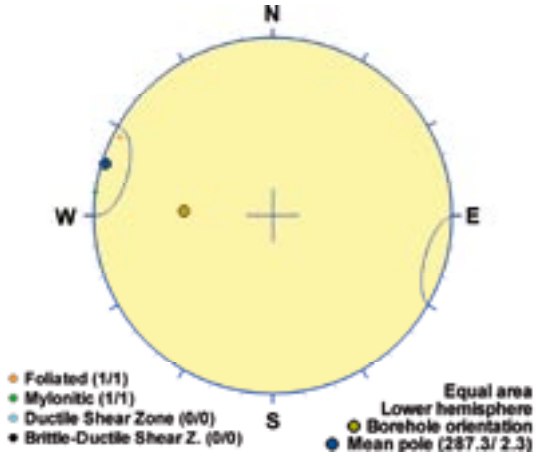

Poles from fractures

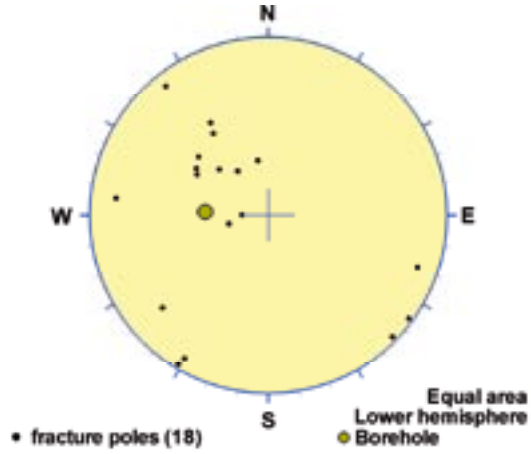

Contours from fractures

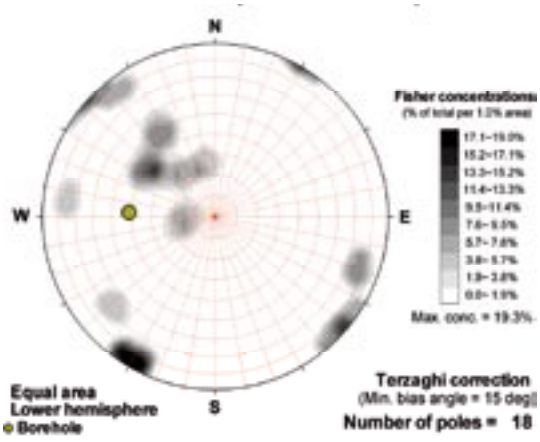

Orientation		Basis for orientation				Certainty	Thickness	
Strike	Dip	Fractures	Crush	Ductile structures	Reflectors	Orientation	Apparent	True
17	88	Contradict	Contradict	Used	Contradict	Very uncertain	4.9 m	3.3 m
Comment:								

KLX20A DZ3 (312.55 to 313), brittle zone

Inhomogeneous brittle deformation zone. Crush zone (0.36 m). High frequency of sealed and open fractures. Major caliper anomaly, low resistivity anomaly and partly decreased magnetic susceptibility. One very strong and persistent oriented reflector occurs at 312.7 m with the orientation 029/78 or 286/23. The host rock is dominated by dolerite (501027). Subordinate rock type is quartz monzodiorite (501036).

Poles from crush zone

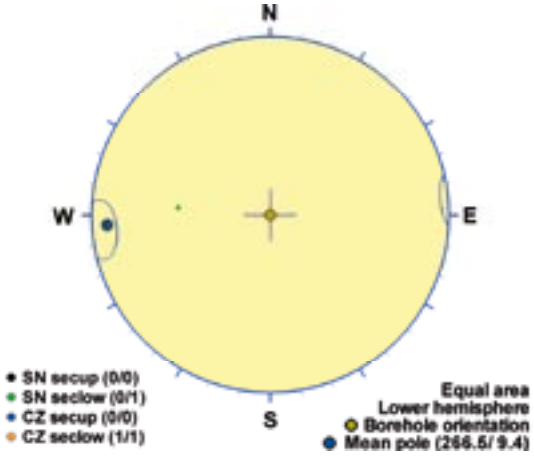

Poles from ductile structures

Data not used

Poles from fractures

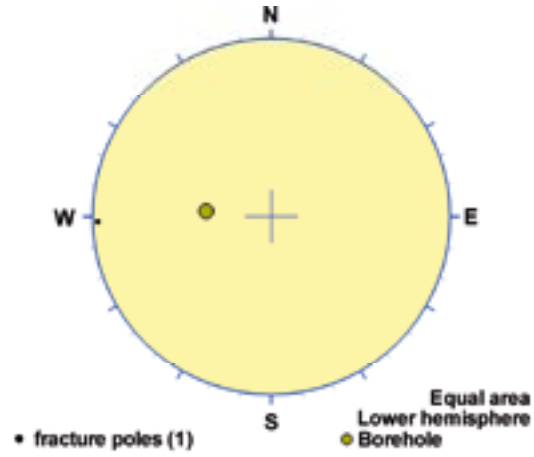

Contours from fractures

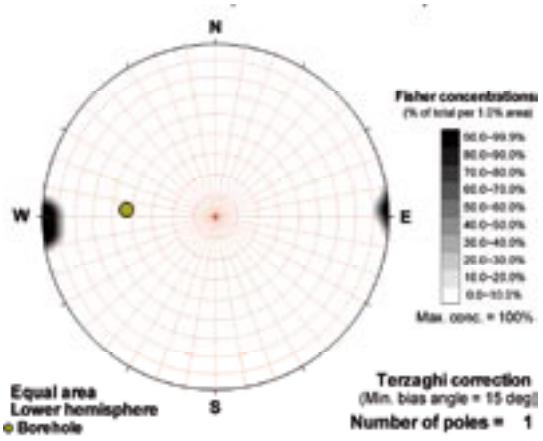

Orientation		Basis for orientation				Certainty	Thickness	
Strike	Dip	Fractures	Crush	Ductile structures	Reflectors	Orientation	Apparent	True
357	81	Verify	Used		Contradict	Probable	0.4 m	0.4 m
Comment:								

KLX20A DZ4 (410.1 to 416.4), brittle zone

Inhomogeneous brittle deformation zone. Breccia (8 mm). Faint to medium red staining, epidotization and saussuritization. High frequency of sealed fractures. Slickenside is observed. Decreased bulk resistivity and magnetic susceptibility, and partly decreased P-wave velocity. One non-oriented radar reflector occurs at 410.5 m with the angle 50° to borehole axis. The host rock is dominated by quartz monzodiorite (501036).

Poles from crush zone

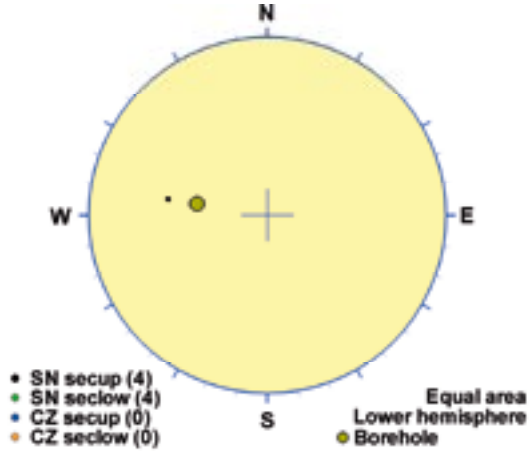

Poles from ductile structures

Data not used

Poles from fractures

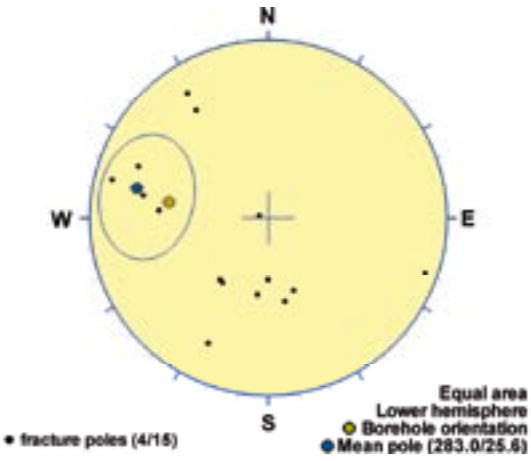

Contours from fractures

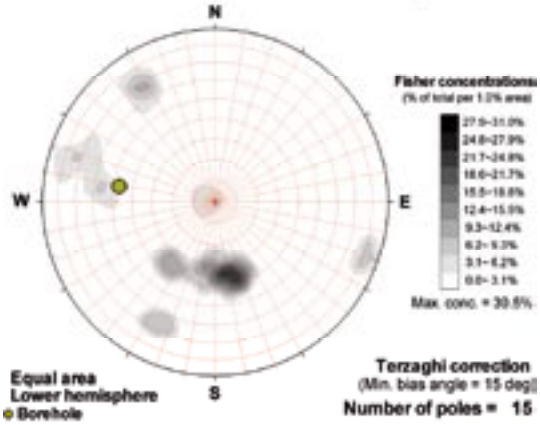

Orientation		Basis for orientation				Certainty	Thickness	
Strike	Dip	Fractures	Crush	Ductile structures	Reflectors	Orientation	Apparent	True
13	64	Used	Verify		Contradict	Very uncertain	6.3 m	6 m
Comment:								

KLX21B DZ1 (105.27 to 105.73), brittle zone

Minor brittle deformation zone which is characterized by a slight increase in open fractures. The host rock is dominated by Ävrö granodiorite (501056). Low electric resistivity. Confidence level = 3.

Poles from crush zone

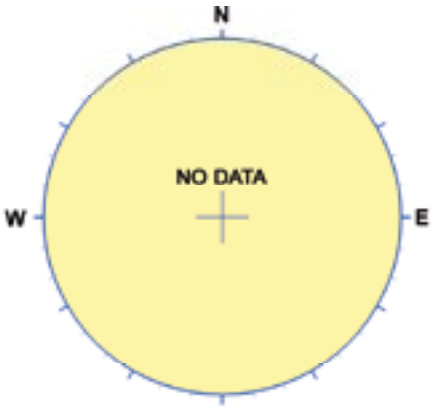

Poles from ductile structures

Data not used

Poles from fractures

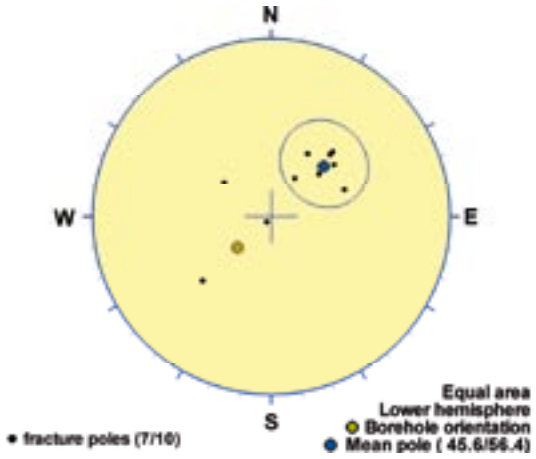

Contours from fractures

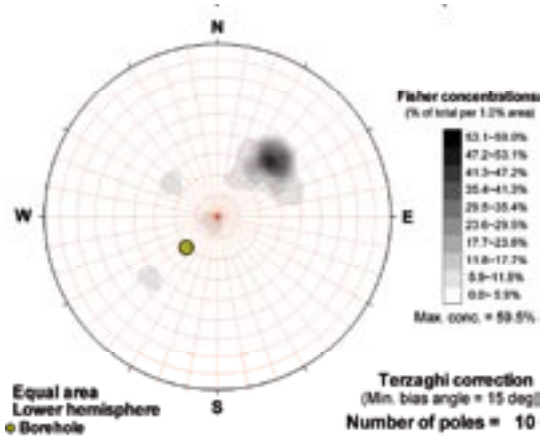

Orientation		Basis for orientation				Certainty	Thickness	
Strike	Dip	Fractures	Crush	Ductile structures	Reflectors	Orientation	Apparent	True
136	34	Used				Probable	0.5 m	0.3 m
Comment:								

KLX21B DZ2 (108.37 to 108.82), brittle zone

Minor brittle deformation zone which is characterized by increased frequency of open and sealed fractures, crush and weak silicification. The host rock is dominated by Ävrö granodiorite (501056). Low resistivity and P-wave velocity, caliper anomaly. Confidence level = 3.

Poles from crush zone

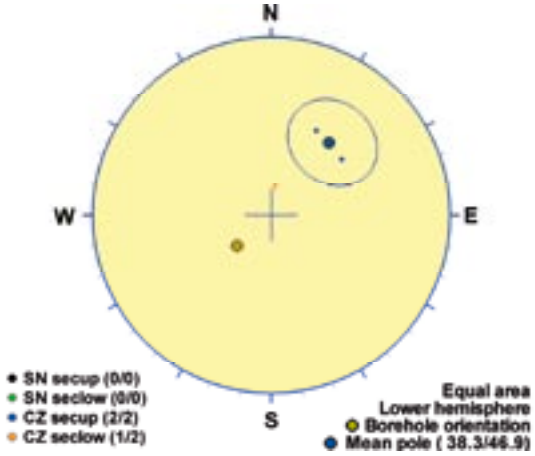

Poles from ductile structures

Data not used

Poles from fractures

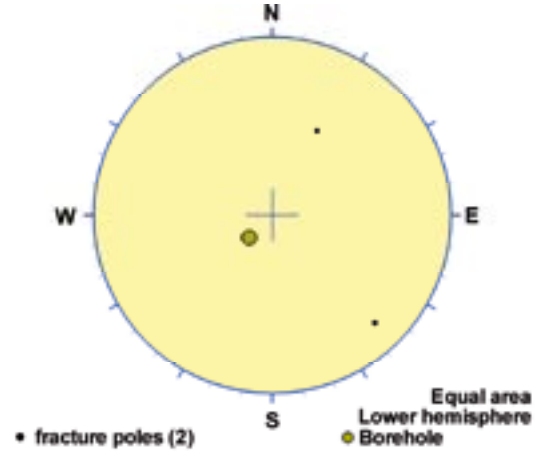

Contours from fractures

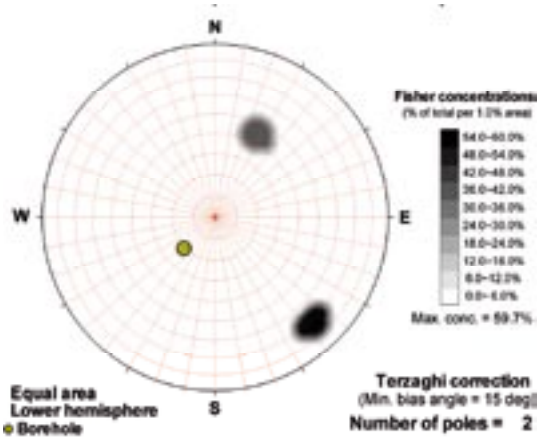

Orientation		Basis for orientation				Certainty	Thickness	
Strike	Dip	Fractures	Crush	Ductile structures	Reflectors	Orientation	Apparent	True
128	43	Verify	Used			Probable	0.4 m	0.2 m
Comment:								

KLX21B DZ3 (150 to 157.8), ductile/brittle zone

Brittle-ductile deformation zone characterized by cataclasites and breccia, weak red staining, inhomogeneous faint epidotization and medium chloritization, increased frequency of sealed fractures and sealed network. The most intensely deformed section is 155.40-156.92 m. Low resistivity, P-wave velocity and magnetic susceptibility, caliper anomalies. One oriented and two non-oriented radar reflectors occur within DZ3. The oriented reflector occurs at 155.8 m with the orientation 111/31 or 302/71. The reflector is strong and can be observed to a distance of 24 m outside the borehole. The non-oriented reflectors occur at 152.0 m and 152.5 m with the angle 44° and 32° to borehole axis, respectively. Low radar amplitude occurs in the interval 135-161 m. The host rock is dominated by Ävrö quartz monzodiorite (501046). Subordinate rock types are fine-grained granite (511058) and granite (501058). Confidence level = 3.

Poles from crush zone

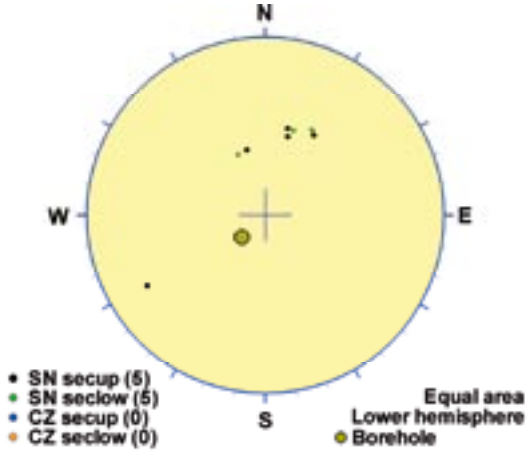

Poles from ductile structures

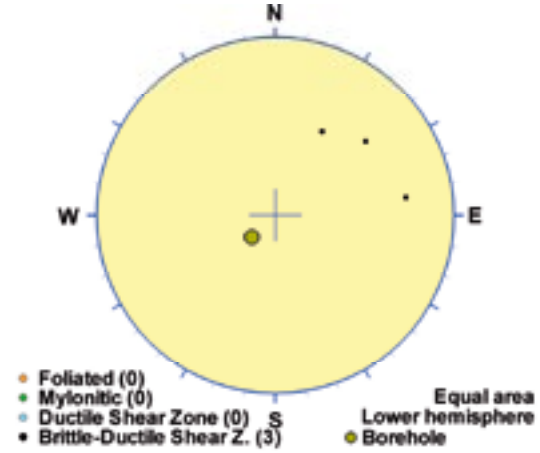

Poles from fractures

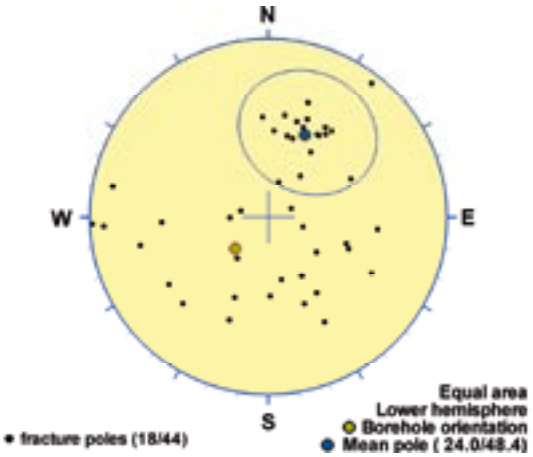

Contours from fractures

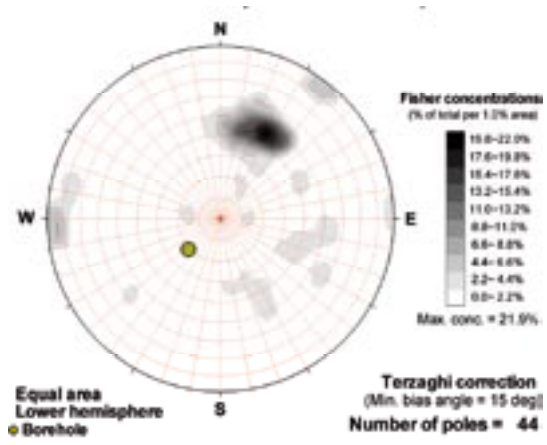

Orientation		Basis for orientation				Certainty	Thickness	
Strike	Dip	Fractures	Crush	Ductile structures	Reflectors	Orientation	Apparent	True
114	42	Used	Verify	Verify	Verify	Certain	7.8 m	3.8 m
Comment:								

KLX21B DZ4 (209.08 to 216.82), brittle zone

Brittle deformation zone characterized by increased frequency of sealed fractures, cataclasites, faint to medium red staining, inhomogeneous faint epidotization, minor saussuritization and slickensides. Low resistivity, P-wave velocity and magnetic susceptibility. One oriented and two non-oriented radar reflectors occur within DZ4. The oriented reflector occurs at 213.5 m with the orientation 118/38. The reflector is medium strong and can be observed to a distance of 10 m outside the borehole. The non-oriented reflectors occur at 209.3 m and 213.9 m with the angle 76° and 39° to borehole axis, respectively. Low radar amplitude occurs in the interval 212-242 m. The host rock is dominated by Ävrö granodiorite (501056). Subordinate rock type is fine-grained granite (511058). Confidence level = 3.

Poles from crush zone

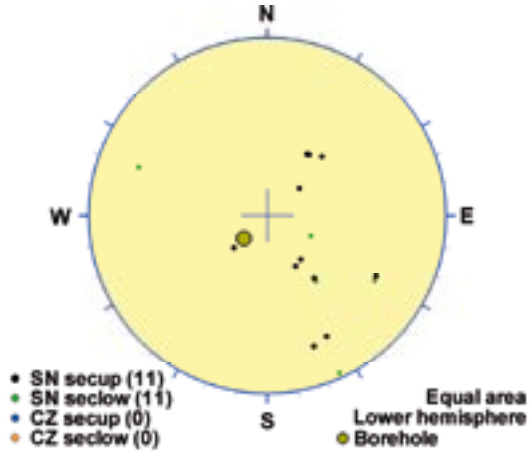

Poles from ductile structures

Data not used

Poles from fractures

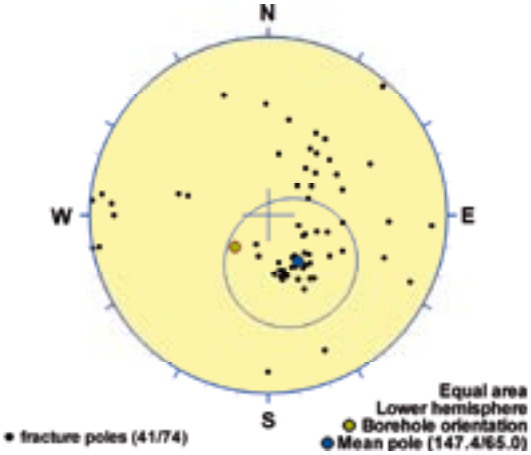

Contours from fractures

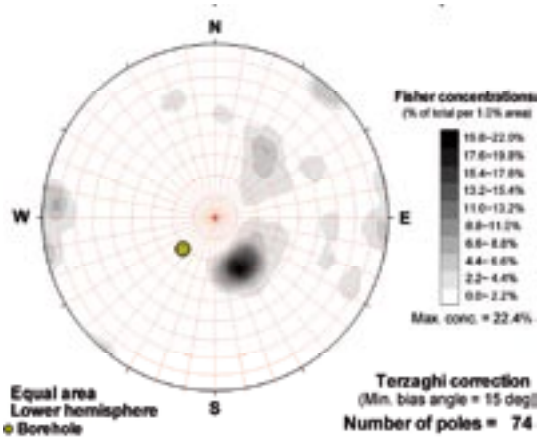

Orientation		Basis for orientation				Certainty	Thickness	
Strike	Dip	Fractures	Crush	Ductile structures	Reflectors	Orientation	Apparent	True
237	25	Used	Verify		Contradict	Probable	7.7 m	6.8 m
Comment:								

KLX21B DZ5 (229.7 to 231.5), brittle zone

Brittle deformation zone characterized by increased frequency sealed fractures, cataclasites, and medium to weak red staining. Low resistivity, P-wave velocity and magnetic susceptibility. One non-oriented reflector occurs at 231.4 m with the angle 50° to borehole axis. Low radar amplitude occurs in the interval 212-242 m. The host rock is dominated by Ävrö quartz monzodiorite (501046). Subordinate rock type is very sparse occurrence of fine-grained granite (511058). Confidence level = 3.

Poles from crush zone

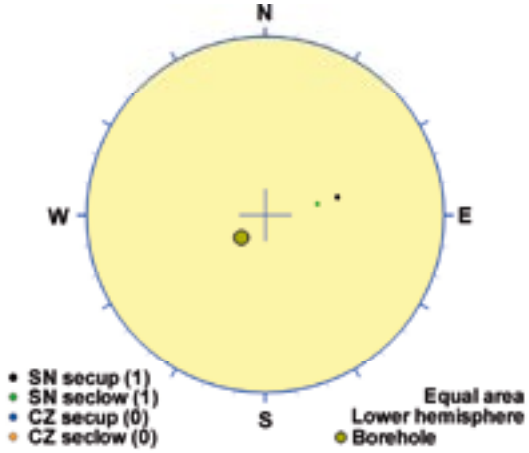

Poles from ductile structures

Data not used

Poles from fractures

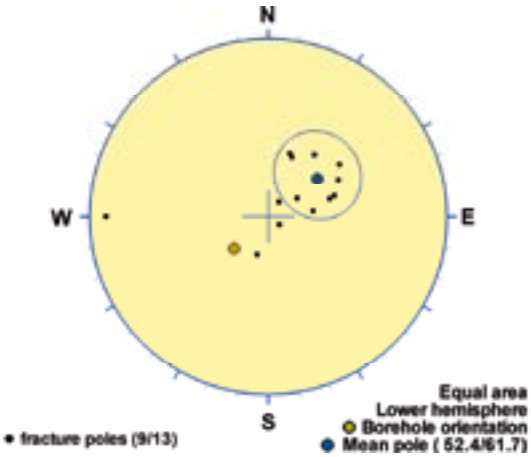

Contours from fractures

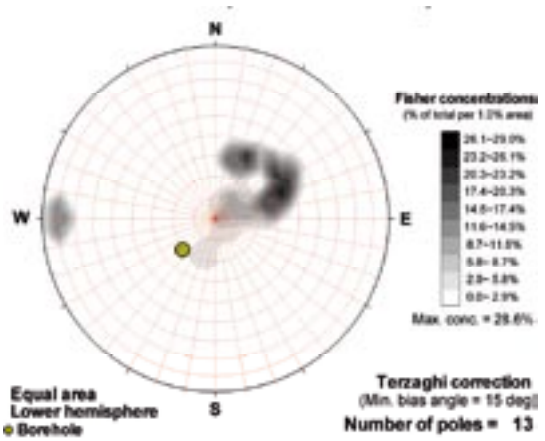

Orientation		Basis for orientation				Certainty	Thickness	
Strike	Dip	Fractures	Crush	Ductile structures	Reflectors	Orientation	Apparent	True
142	28	Used	Verify			Certain	1.8 m	1.2 m
Comment:								

KLX21B DZ6 (396.95 to 397.1), brittle zone

Brittle deformation zone characterized by cataclasites and slickensides. The host rock is dominated by Ävrö quartz monzodiorite (501046). Minor low-resistivity anomaly. Confidence level = 3.

Poles from crush zone

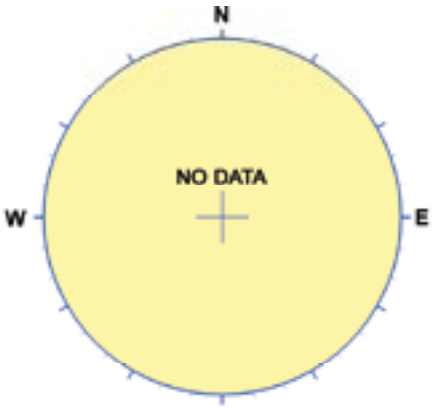

Poles from ductile structures

Data not used

Poles from fractures

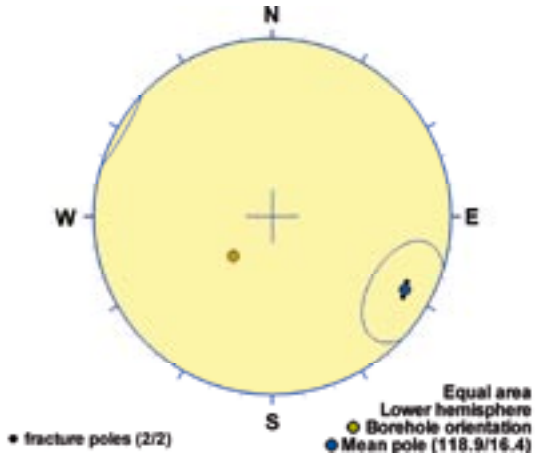

Contours from fractures

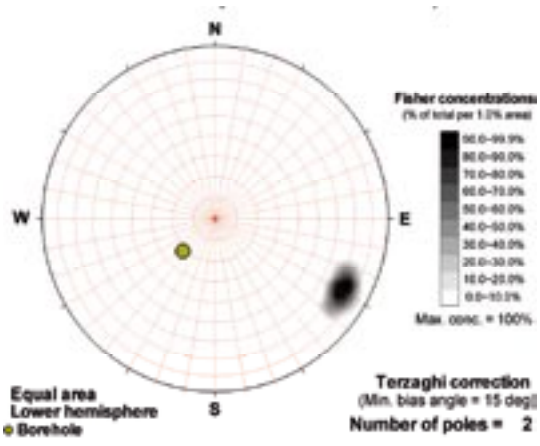

Orientation		Basis for orientation				Certainty	Thickness	
Strike	Dip	Fractures	Crush	Ductile structures	Reflectors	Orientation	Apparent	True
209	74	Used				Probable	0.2 m	0 m
Comment:								

KLX21B DZ7 (400.64 to 403.49), brittle zone

Brittle deformation zone characterized by increased frequency of sealed fractures, cataclasites, weak to medium red staining, inhomogeneous weak epidotization and slickensides. Low resistivity, P-wave velocity and magnetic susceptibility. Two non-oriented reflectors occur at 400.6 m and 403.8 m with the angle 42° and 59° to borehole axis, respectively. The host rock is a mixture of Ävrö quartz monzodiorite (501046) and fine-grained diorite-gabbro (505102). Subordinate rock types are sparse occurrences of fine-grained granite (511058) and pegmatite (501061). Confidence level = 3.

Poles from crush zone

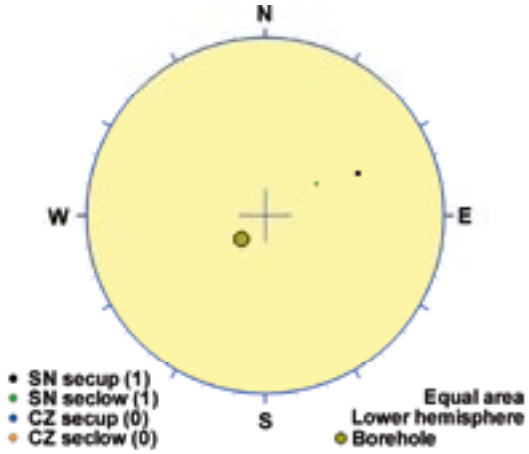

Poles from ductile structures

Data not used

Poles from fractures

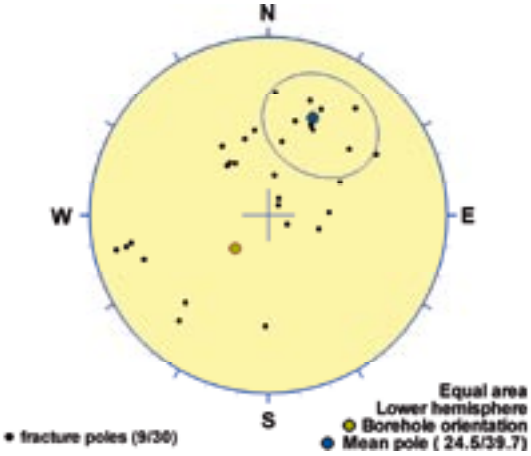

Contours from fractures

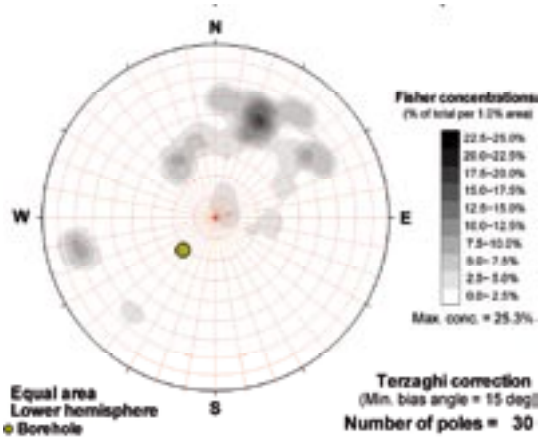

Orientation		Basis for orientation				Certainty	Thickness	
Strike	Dip	Fractures	Crush	Ductile structures	Reflectors	Orientation	Apparent	True
115	50	Used	Verify		Contradict	Probable	2.9 m	0.9 m
Comment:								

KLX21B DZ8 (452.06 to 455.9), brittle zone

Brittle deformation zone characterized by increased frequency of sealed fractures, slight increased frequency of open fractures, cataclasites, faint to medium red staining, minor strong epidotization. Low P-wave velocity and magnetic susceptibility. One oriented and one non-oriented radar reflectors occur within DZ8. The oriented reflector occurs at 454.0 m with the orientation 193/63. The reflector is medium strong and can be observed to a distance of 6 m outside the borehole. The non-oriented reflector occurs at 454.3 m with the angle 50° to borehole axis. The host rock is dominated by Ävrö granodiorite (501056). Subordinate rock type is sparse occurrence of fine-grained granite (511058). Confidence level = 3.

Poles from crush zone

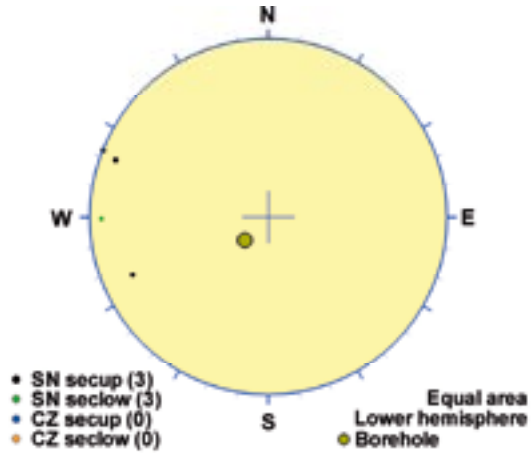

Poles from ductile structures

Data not used

Poles from fractures

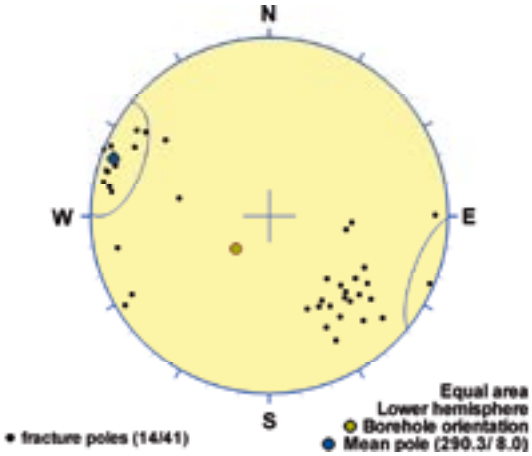

Contours from fractures

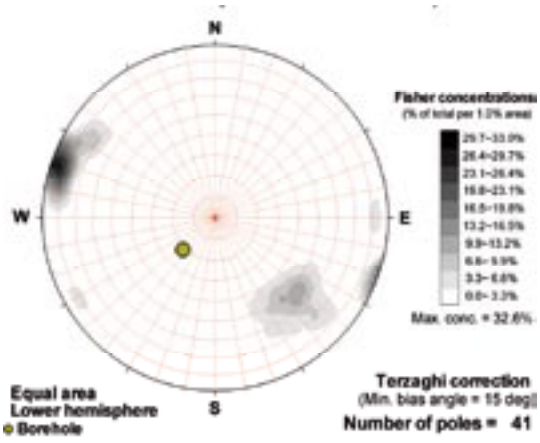

Orientation		Basis for orientation				Certainty	Thickness	
Strike	Dip	Fractures	Crush	Ductile structures	Reflectors	Orientation	Apparent	True
20	82	Used	Verify		Contradict	Probable	3.8 m	1.1 m
Comment:								

KLX21B DZ9 (474.41 to 478.1), brittle zone

Brittle deformation zone characterized by increased frequency of sealed fractures, moderate increase in open fractures and weak red staining. Low resistivity, P-wave velocity and magnetic susceptibility, caliper anomalies. Two non-oriented radar reflectors occur at 475.0 m and 477.5 m with the angle 40° and 49° to borehole axis, respectively. The reflector at 475.0 m is strong and can be observed to a distance of 11 m outside the borehole. Low radar amplitude occurs in the interval 470-476 m. The host rock is dominated by fine-grained granite (511058). Subordinate rock type is Ävrö granodiorite (501056). Confidence level = 3.

Poles from crush zone

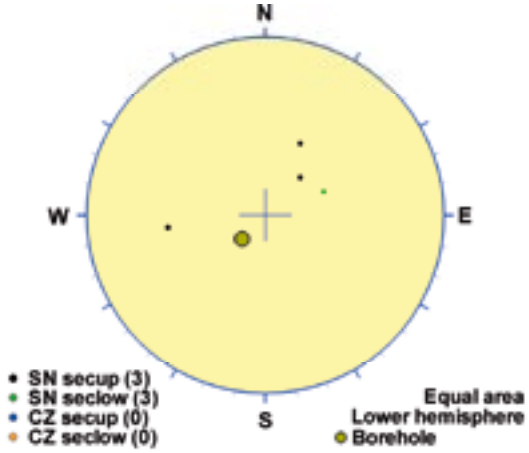

Poles from ductile structures

Data not used

Poles from fractures

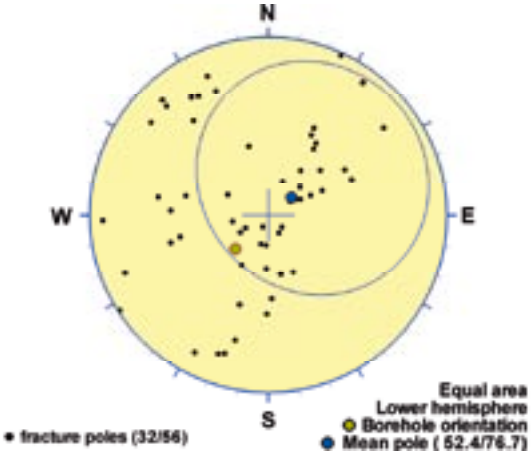

Contours from fractures

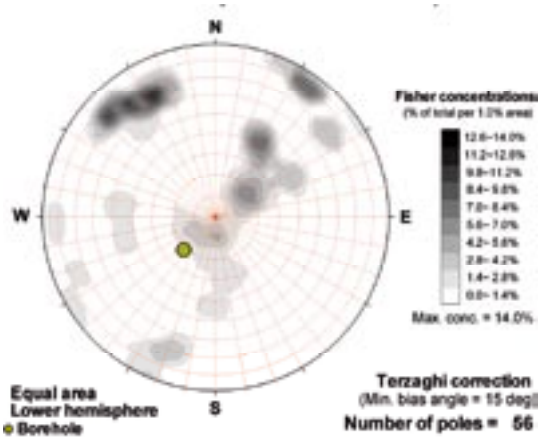

Orientation		Basis for orientation				Certainty	Thickness	
Strike	Dip	Fractures	Crush	Ductile structures	Reflectors	Orientation	Apparent	True
142	13	Used			Verify	Uncertain	3.7 m	3 m
Comment:								

KLX22A DZ1 (76.9 to 77.22), ductile/brittle zone

Minor ductile to brittle-ductile shear zone with increased frequency of sealed fractures, medium red staining and saussuritization and aperture of open fractures. Low magnetic susceptibility, resistivity and P-wave velocity. The host rock is dominated by quartz monzodiorite (501036). Subordinate rock types are fine-grained granite (511058).

Poles from crush zone

Poles from ductile structures

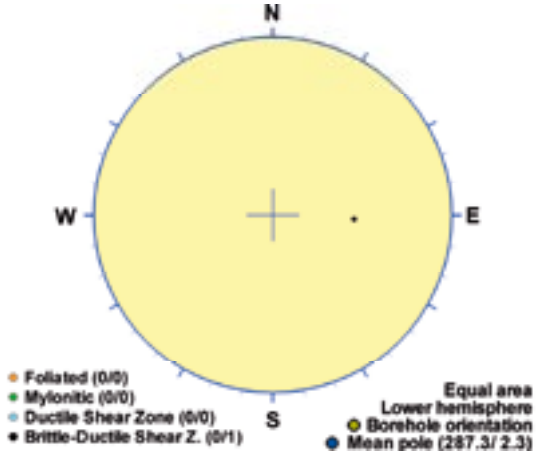

Poles from fractures

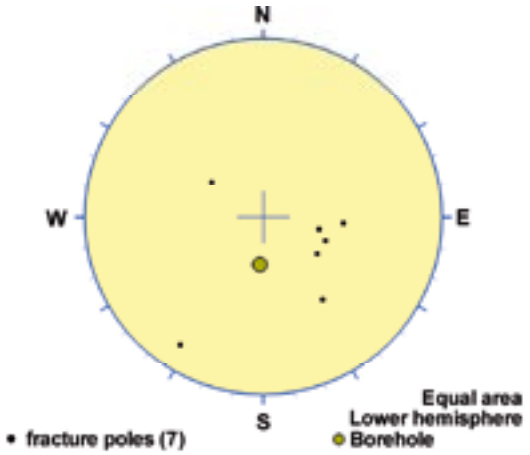

Contours from fractures

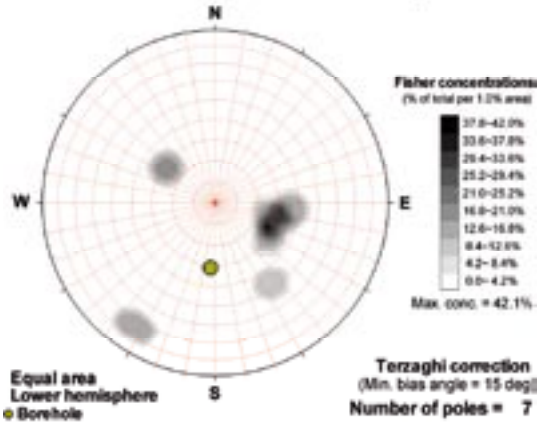

Orientation		Basis for orientation				Certainty	Thickness	
Strike	Dip	Fractures	Crush	Ductile structures	Reflectors	Orientation	Apparent	True
183	38	Verify		Used		Certain	0.3 m	0.2 m
Comment:								

KLX22B DZ1 (22 to 25), brittle zone

Brittle deformation zone characterized by increased frequency of open and sealed fractures, sealed network, minor core loss and crush, and weak to medium red staining, epidotization and saussuritization. Slickensides are documented. Low magnetic susceptibility, resistivity and P-wave velocity. One non-oriented radar reflector occurs at 22.6 m with the angle 32° to borehole axis and one oriented at 25.3 m (just outside the deformation zone) with the orientation 241/31. Both reflectors are medium strong and can be observed to a distance of 9 m outside the borehole. The host rock is dominated by quartz monzodiorite (501036).

Poles from crush zone

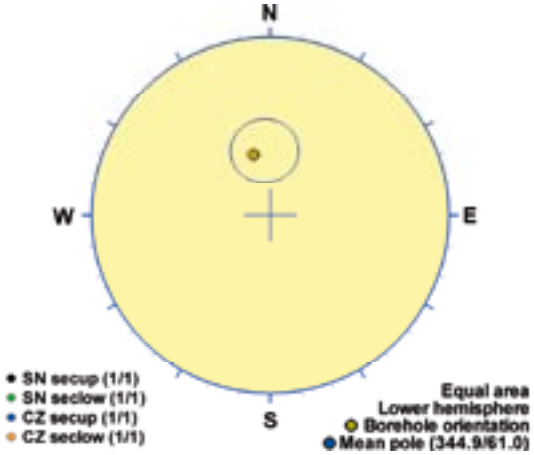

Poles from ductile structures

Data not used

Poles from fractures

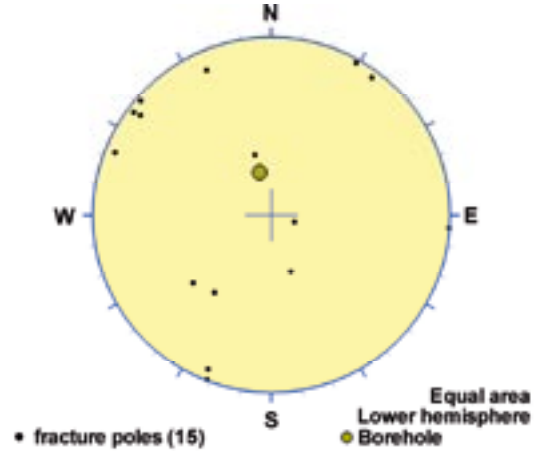

Contours from fractures

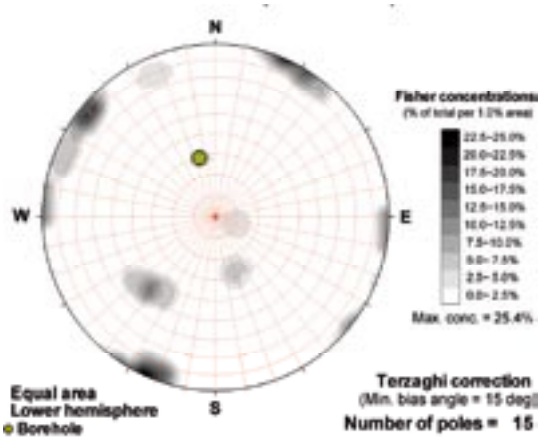

Orientation		Basis for orientation				Certainty	Thickness	
Strike	Dip	Fractures	Crush	Ductile structures	Reflectors	Orientation	Apparent	True
75	29		Used		Contradict	Very uncertain	3 m	3 m
Comment:								

KLX23A DZ1 (10.75 to 11.75), brittle zone

Brittle deformation zone characterized by increased frequency of sealed fractures and a slight increase in open fractures and faint red staining. Low magnetic susceptibility. There is very low radar amplitude from the start of the borehole to 15 m. Two non-oriented radar reflectors occur at 11.4 m and 11.7 m with the angle 61° and 77° to borehole axis, respectively. The latter reflector is strong and can be observed to a distance of 30 m outside the borehole. The host rock is dominated by quartz monzodiorite (501036) and fine-grained granite (511058).

Poles from crush zone

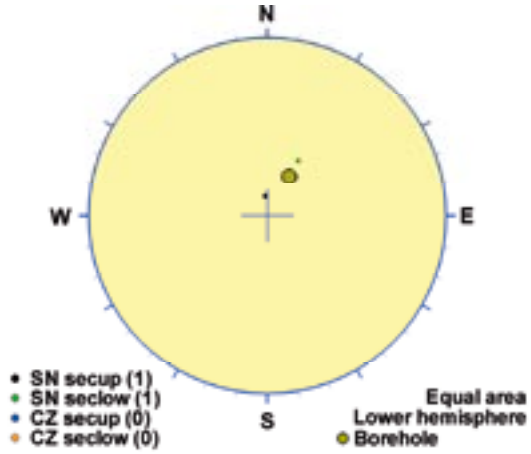

Poles from ductile structures

Data not used

Poles from fractures

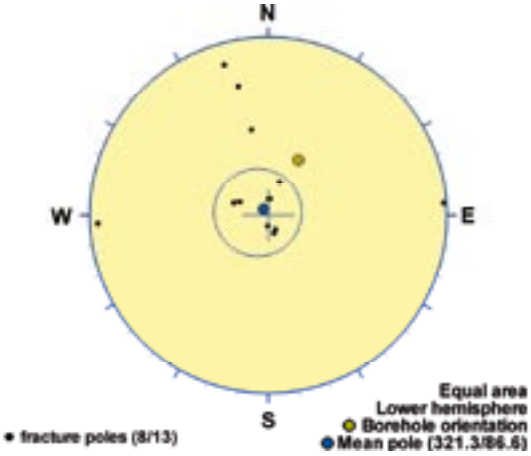

Contours from fractures

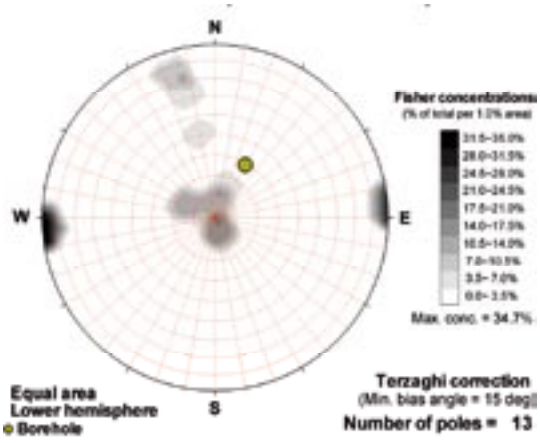

Orientation		Basis for orientation				Certainty	Thickness	
Strike	Dip	Fractures	Crush	Ductile structures	Reflectors	Orientation	Apparent	True
51	3	Used	Verify		Verify	Probable	1 m	0.9 m
Comment:								

KLX23A DZ2 (15.66 to 16.7), brittle zone

Brittle deformation zone characterized by increased frequency of sealed and open fractures and weak red staining. Low magnetic susceptibility, resistivity and P-wave velocity. The host rock is dominated by quartz monzodiorite (501036). Subordinate rock is fine-grained granite (511058).

Poles from crush zone

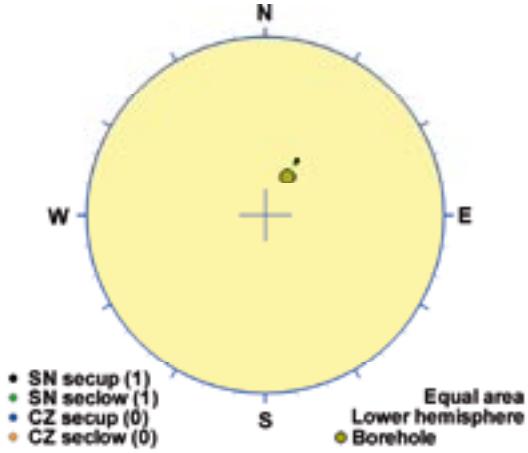

Poles from ductile structures

Data not used

Poles from fractures

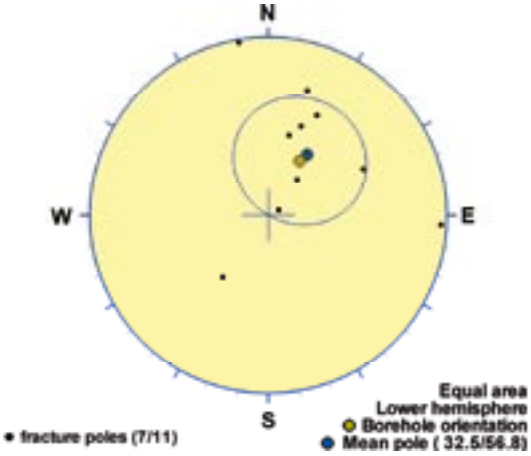

Contours from fractures

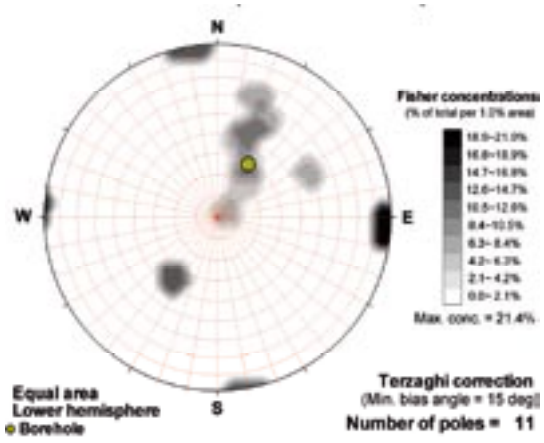

Orientation		Basis for orientation				Certainty	Thickness	
Strike	Dip	Fractures	Crush	Ductile structures	Reflectors	Orientation	Apparent	True
123	33	Used	Verify			Probable	1 m	1 m
Comment:								

KLX23B DZ1 (13.3 to 14.8), brittle zone

Brittle deformation zone characterized by increased frequency of sealed and open fractures, brecciation, apertures in open fractures and medium red staining and weak epidotization. Slickensides are documented. Low magnetic susceptibility, resistivity and P-wave velocity. One non-oriented radar reflector occurs at 13.8 m with the angle 60° to borehole axis. The reflector can be observed to a distance of 4 m outside the borehole. There is very low radar amplitude at 13-15 m. The host rock is dominated by quartz monzodiorite (501036). Subordinate rock is fine-grained granite (511058).

Poles from crush zone

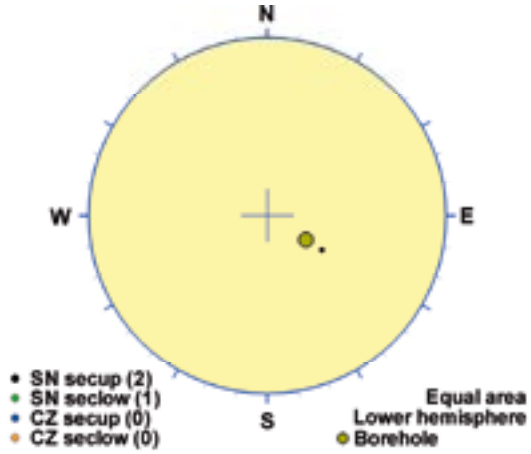

Poles from ductile structures

Data not used

Poles from fractures

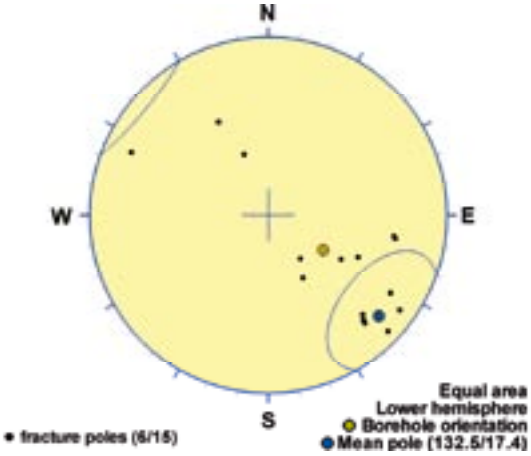

Contours from fractures

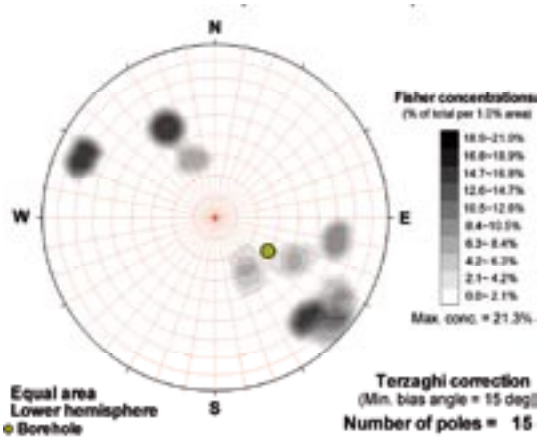

Orientation		Basis for orientation				Certainty	Thickness	
Strike	Dip	Fractures	Crush	Ductile structures	Reflectors	Orientation	Apparent	True
223	73	Used	Contradict		Contradict	Uncertain	1.5 m	1.1 m
Comment:								

KLX24A DZ1 (19.75 to 21.2), brittle zone

Brittle deformation zone characterized by increased frequency of sealed and open fractures, faint red staining, minor crush and slickensides. Low magnetic susceptibility, resistivity and P-wave velocity, two caliper anomalies. Two non-oriented radar reflectors at 20.2 m and 21.4 m with the angle 18° and 63° to borehole axis, respectively. The reflectors can be observed to a distance of 2 m outside the borehole. The host rock is dominated by quartz monzodiorite (501036). Subordinate rock types are pegmatite (501061) and fine-grained granite (511058).

Poles from crush zone

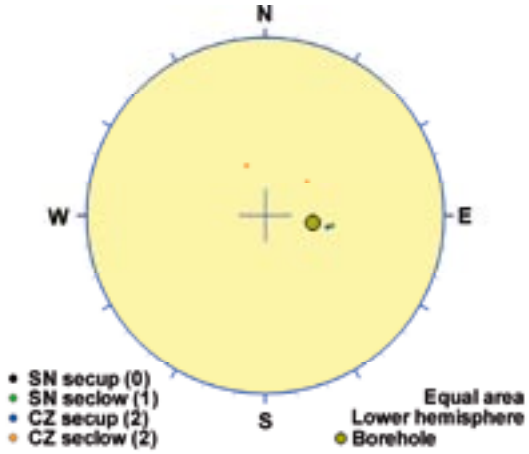

Poles from ductile structures

Data not used

Poles from fractures

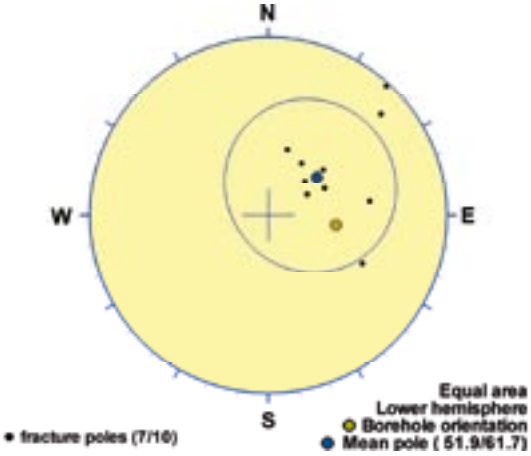

Contours from fractures

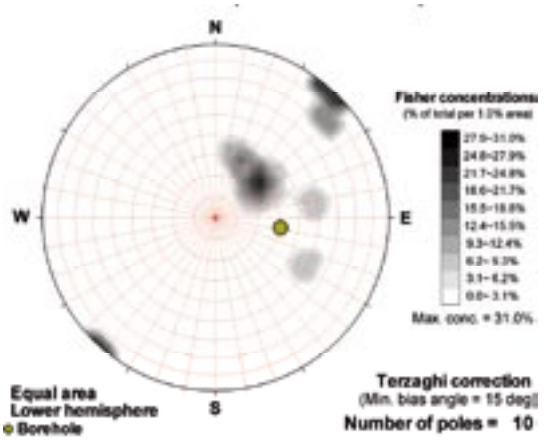

Orientation		Basis for orientation				Certainty	Thickness	
Strike	Dip	Fractures	Crush	Ductile structures	Reflectors	Orientation	Apparent	True
142	28	Used	Verify		Contradict	Probable	1.4 m	1.3 m
Comment:								

KLX24A DZ2 (56.75 to 60.25), ductile/brittle zone

Ductile deformation zone with increased frequency of sealed and open fractures, weak red staining and saussuritization, and slickensides. Low magnetic susceptibility. One non-oriented radar reflector occurs at 56.7 m with the angle 47° to borehole axis. The reflector can be observed to a distance of 3 m outside the borehole. The host rock is dominated by quartz monzodiorite (501036). Subordinate rock types are pegmatite (501061) and fine-grained granite (511058).

Poles from crush zone

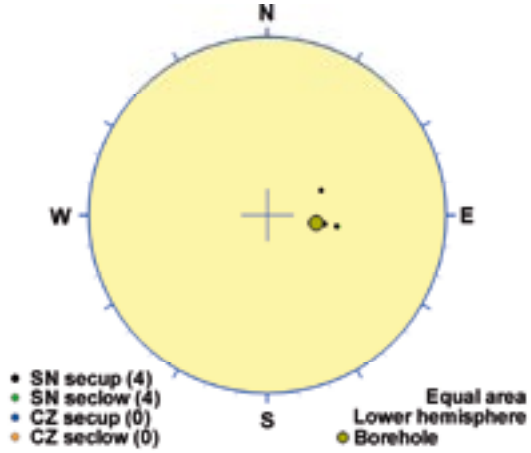

Poles from ductile structures

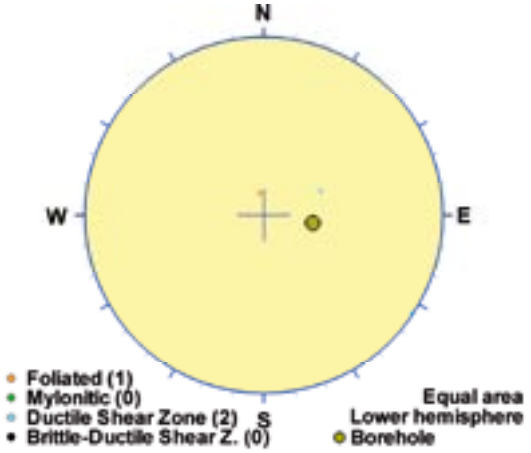

Poles from fractures

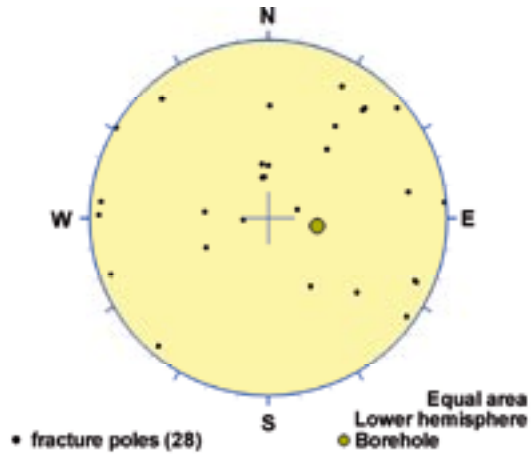

Contours from fractures

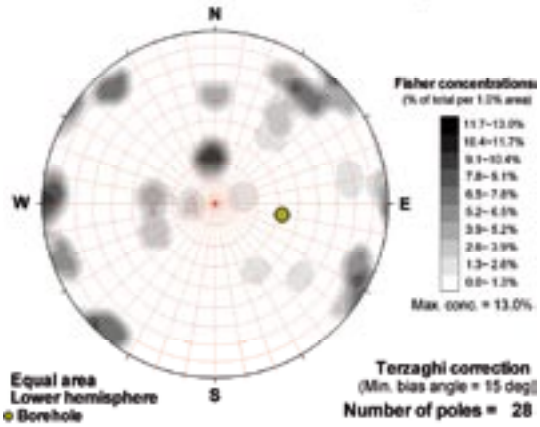

Orientation		Basis for orientation				Certainty	Thickness	
Strike	Dip	Fractures	Crush	Ductile structures	Reflectors	Orientation	Apparent	True
80	10	Verify	Contradict	Used	Contradict	Uncertain	3.5 m	2.8 m
Comment:								

KLX24A DZ3 (64.65 to 66.6), ductile/brittle zone

Brittle-ductile shear zone with increased frequency of both sealed and open fractures, minor crush and core loss, weak red staining and slickensides. Low magnetic susceptibility, resistivity and P-wave velocity, one caliper anomaly. One non-oriented radar reflector occurs at 65.6 m with the angle 82° to borehole axis and one radar reflector occurs at 64.1 m with the orientation 191/17. The oriented radar reflector can be observed to a distance of 9 m outside the borehole. Low radar amplitude at 63-66 m. The host rock is dominated by quartz monzodiorite (501036). Subordinate rock types are pegmatite (501061) and fine-grained granite (511058).

Poles from crush zone

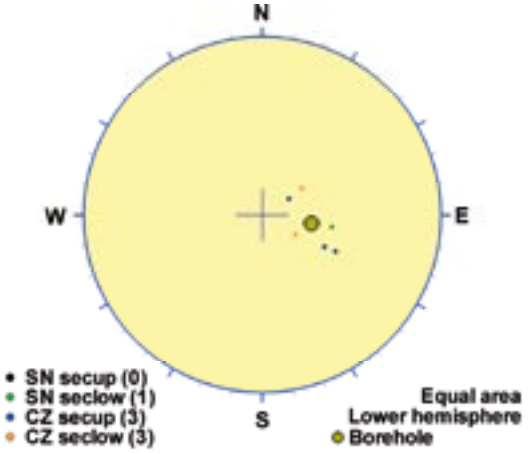

Poles from ductile structures

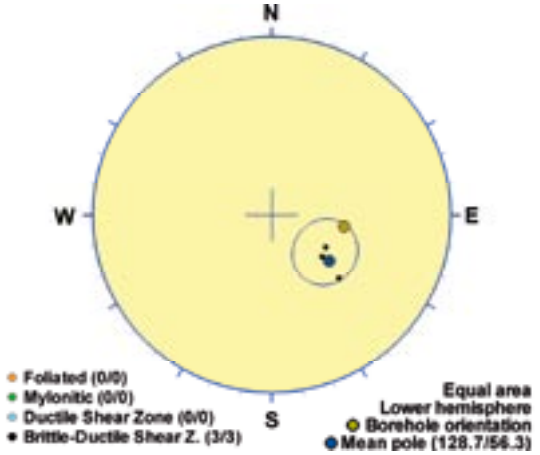

Poles from fractures

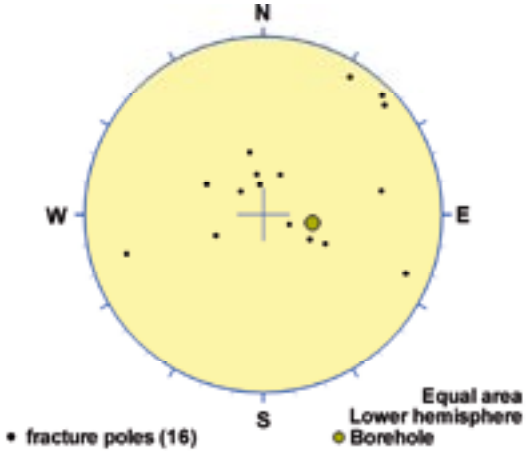

Contours from fractures

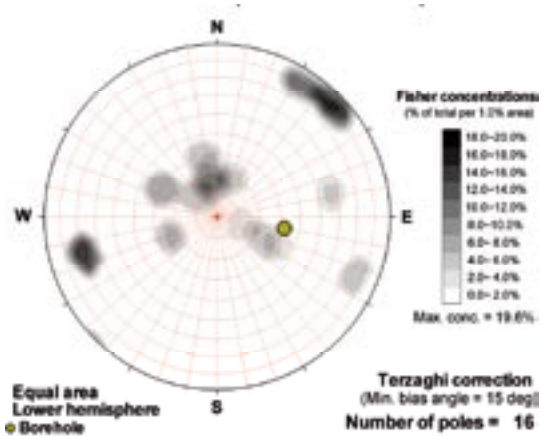

Orientation		Basis for orientation				Certainty	Thickness	
Strike	Dip	Fractures	Crush	Ductile structures	Reflectors	Orientation	Apparent	True
219	34	Verify	Verify	Used	Verify	Certain	1.9 m	1.9 m
Comment:								

KLX24A DZ4 (75.25 to 75.75), brittle zone

Brittle deformation zone, brecciated with increased frequency of sealed fractures, apertures in some open fractures and weak red staining. Low magnetic susceptibility, resistivity and P-wave velocity. Two non-oriented radar reflectors at 73.4 m and 75.3 m with the angle 26° and 45° to borehole axis, respectively. One oriented radar reflector occurs at 74.4 m with the orientation 224/50 or 122/38. The oriented radar reflector can be observed to a distance of 9 m outside the borehole. Decreased radar amplitude at 74-76 m. The host rock is dominated by quartz monzodiorite (501036). Subordinate rock type is pegmatite (501061).

Poles from crush zone

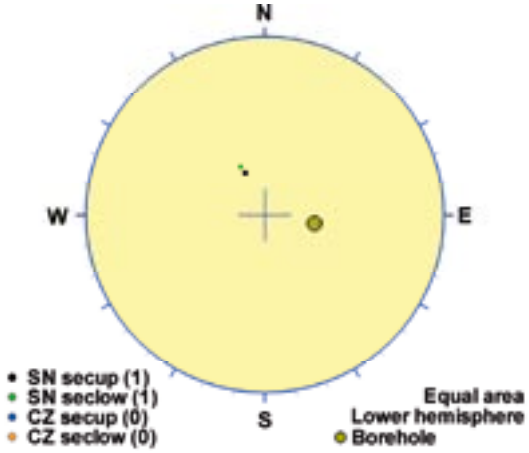

Poles from ductile structures

Data not used

Poles from fractures

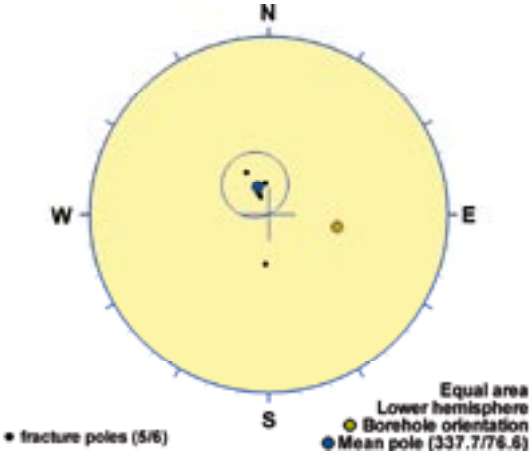

Contours from fractures

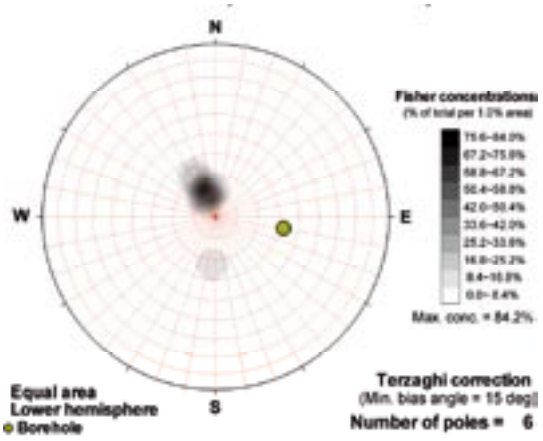

Orientation		Basis for orientation				Certainty	Thickness	
Strike	Dip	Fractures	Crush	Ductile structures	Reflectors	Orientation	Apparent	True
68	13	Used	Verify		Contradict	Probable	0.5 m	0.4 m
Comment:								

KLX25A DZ1 (32.1 to 35.66), ductile/brittle zone

Brittle-ductile shear zone, moderately foliated with increased frequency of sealed and open fractures, apertures in open fractures, faint to weak red staining and weak carbonatization. Low magnetic susceptibility. One non-oriented radar reflector occurs at 34.3 m with the angle 61° to borehole axis. The reflector can be observed to a distance of 5 m outside the borehole. The host rock is dominated by quartz monzodiorite (501036). Subordinate rock type is fine-grained granite (511058).

Poles from crush zone

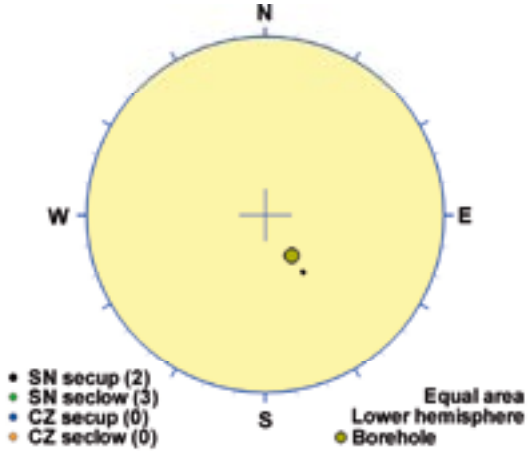

Poles from ductile structures

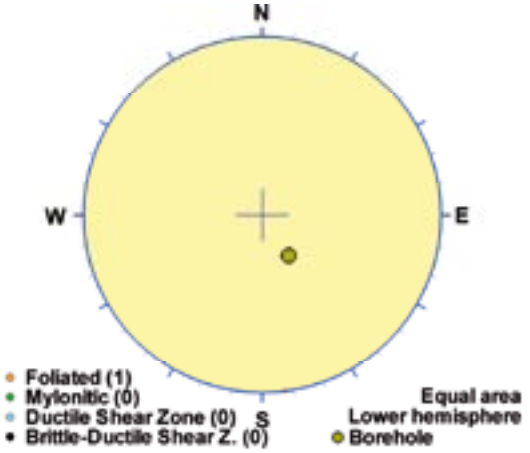

Poles from fractures

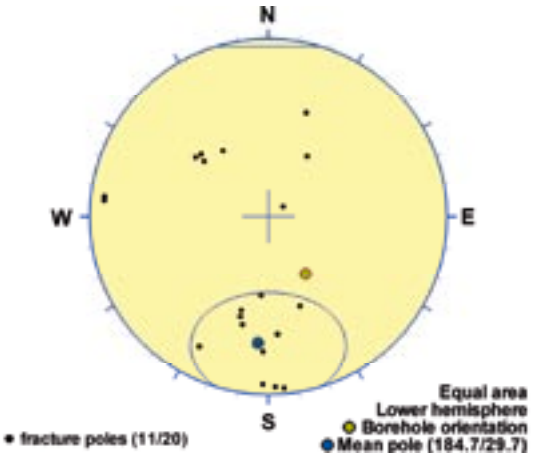

Contours from fractures

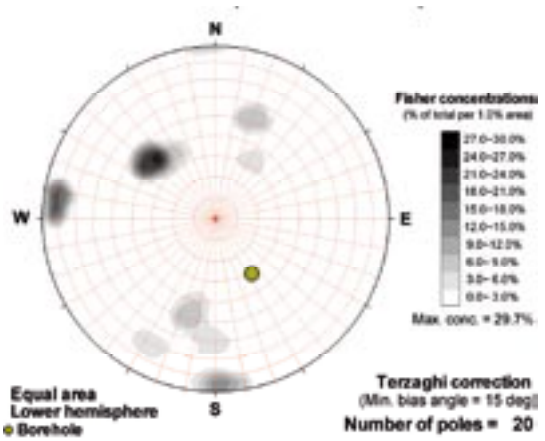

Orientation		Basis for orientation				Certainty	Thickness	
Strike	Dip	Fractures	Crush	Ductile structures	Reflectors	Orientation	Apparent	True
275	60	Used		Verify	Contradict	Uncertain	3.6 m	2.8 m
Comment:								

KLX26A DZ1 (17.45 to 18.1), ductile/brittle zone

Brittle-ductile shear zone, brecciated, with increased frequency of open and sealed fractures, weak epidotization. Low magnetic susceptibility, resistivity and P-wave velocity. One strong radar reflector occurs at 18.6 m with the orientation 121/69 or 264/52. The reflector can be observeded to a distance of 6 m outside the borehole. The host rock is dominated by diorite/gabbro (501033). Subordinate rock type is pegmatite (501061).

Poles from crush zone

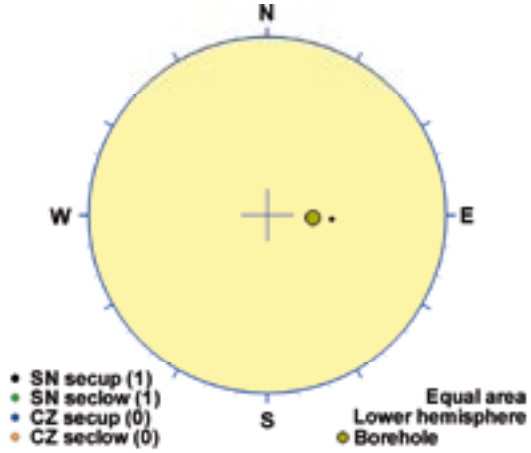

Poles from ductile structures

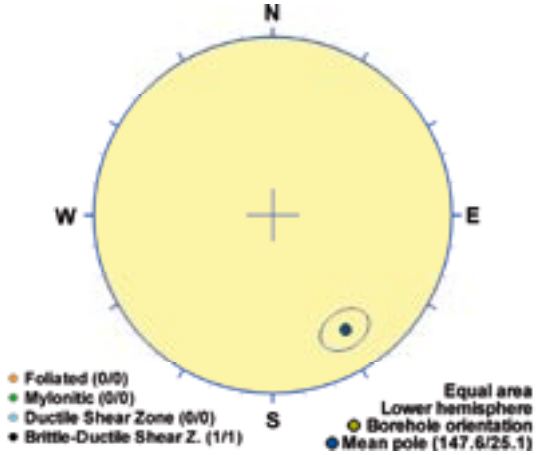

Poles from fractures

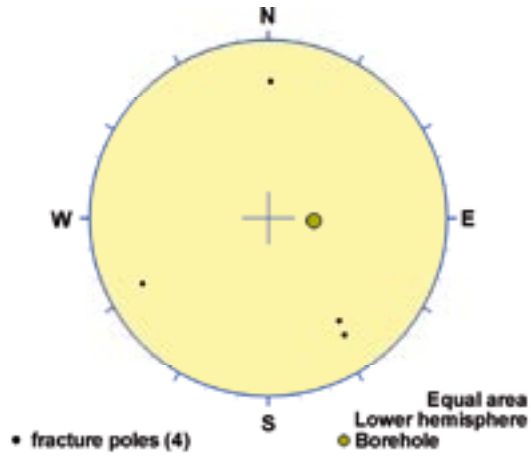

Contours from fractures

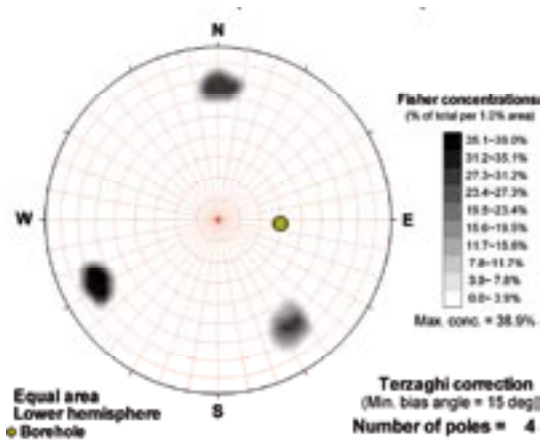

Orientation		Basis for orientation				Certainty	Thickness	
Strike	Dip	Fractures	Crush	Ductile structures	Reflectors	Orientation	Apparent	True
238	65	Verify		Used	Contradict	Probable	0.7 m	0.4 m
Comment:								

KLX26A DZ2 (42.6 to 54.8), ductile/brittle zone

Inhomogeneous brittle-ductile shear zone, partly weakly foliated, with increased frequency of sealed and open fractures, faint red staining and weak epidotization. Low magnetic susceptibility and frequent minor resistivity anomalies. Four non-oriented radar reflectors occur with angles between 26° to 66° to borehole axis. Two oriented radar reflectors occur at 42.2 m with the orientation 122/17 or 200/52 and at 47.4 m with the orientation 103/73. The first one can be observeded to a distance of 18 m outside the borehole and the latter to a distance of 10 m outside the borehole. The host rock is dominated by diorite/gabbro (501033) and fine-grained granite (511058). Subordinate rock types are pegmatite (501061), fine-grained granite (511058) and very sparse quartz monzodiorite (501036).

Poles from crush zone

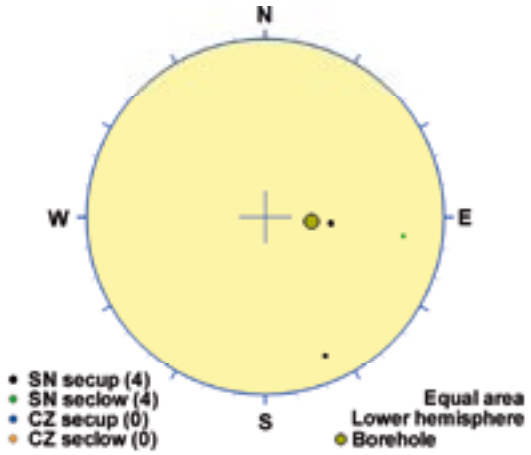

Poles from ductile structures

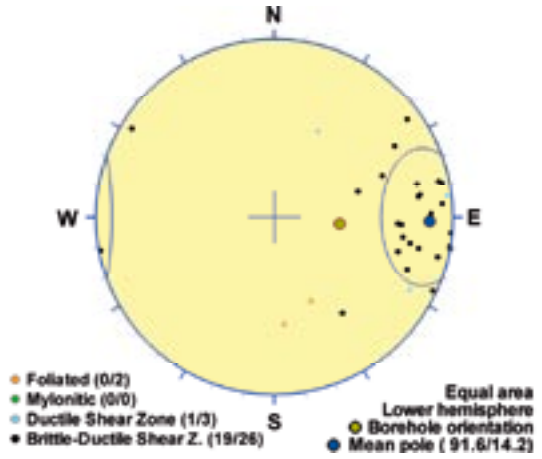

Poles from fractures

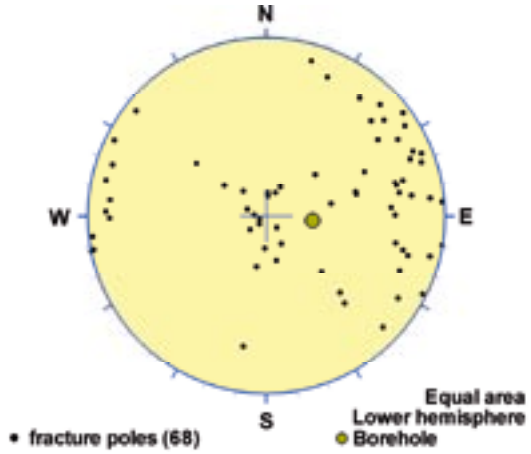

Contours from fractures

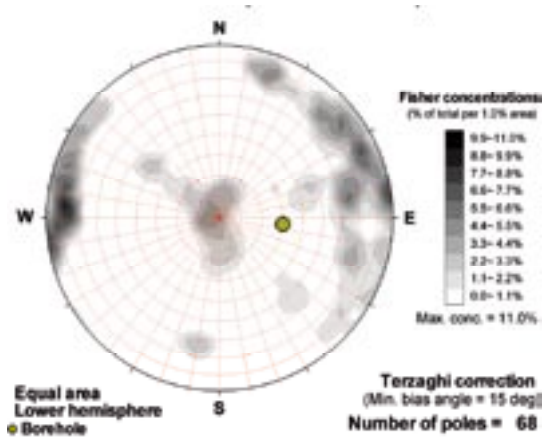

Orientation		Basis for orientation				Certainty	Thickness	
Strike	Dip	Fractures	Crush	Ductile structures	Reflectors	Orientation	Apparent	True
182	76	Verify		Used	Contradict	Probable	12.2 m	8.5 m
Comment:								

KLX26A DZ3 (72.3 to 73.95), ductile/brittle zone

Brittle-ductile shear zone, brecciated, with increased frequency of open and sealed fractures, weak epidotization and crush. Low magnetic susceptibility, resistivity and P-wave velocity, and one caliper anomaly. One rather strong radar reflector occurs at 73.6 m with the orientation 104/32. The reflector can be traced to a distance of 10 m outside the borehole. The host rock is dominated by diorite/gabbro (501033). Subordinate rock type is fine-grained granite (511058).

Poles from crush zone

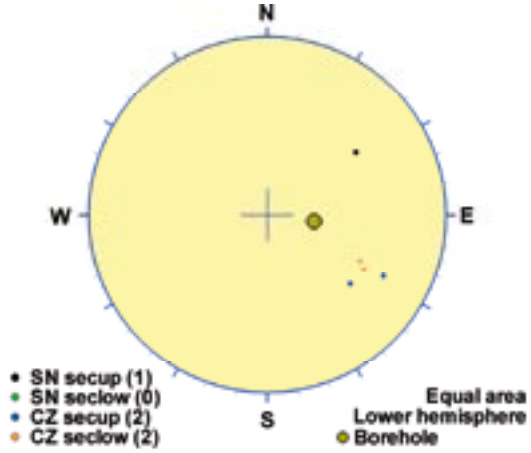

Poles from ductile structures

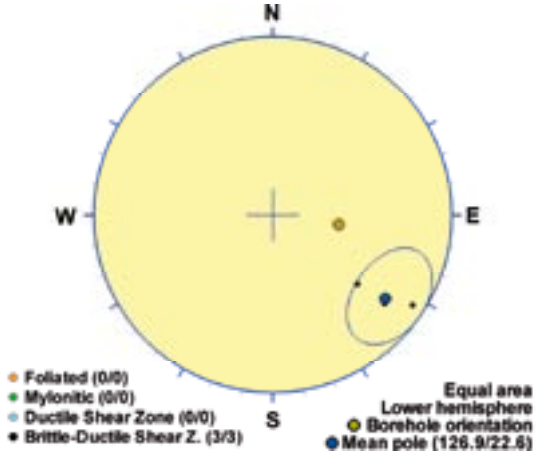

Poles from fractures

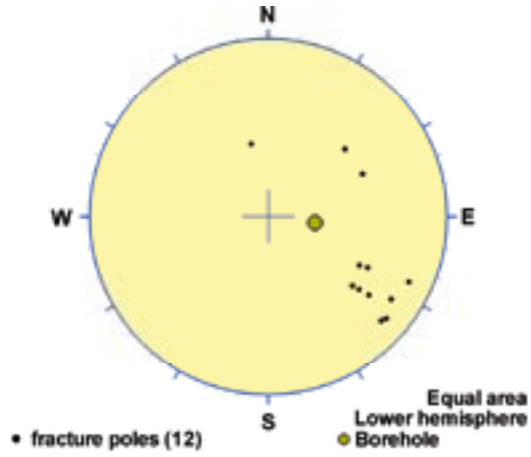

Contours from fractures

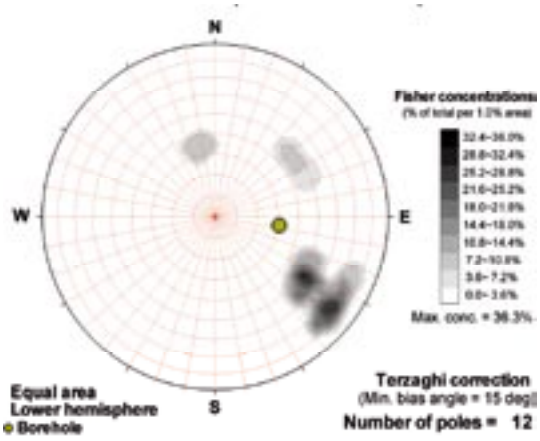

Orientation		Basis for orientation				Certainty	Thickness	
Strike	Dip	Fractures	Crush	Ductile structures	Reflectors	Orientation	Apparent	True
217	67	Verify	Verify	Used	Contradict	Probable	1.7 m	1.2 m
Comment:								

KLX26A DZ4 (97.3 to 99.8), ductile/brittle zone

Ductile shear zone with increased frequency of open and sealed fractures and minor crush. Low magnetic susceptibility, resistivity and P-wave velocity. One non-oriented radar reflector occurs at 99.1 m with the angle 43° to borehole axis. The host rock is dominated by fine-grained diorite-gabbro (505102). Subordinate rock types are quartz monzodiorite (501036) and Ävrö granite (501044).

Poles from crush zone

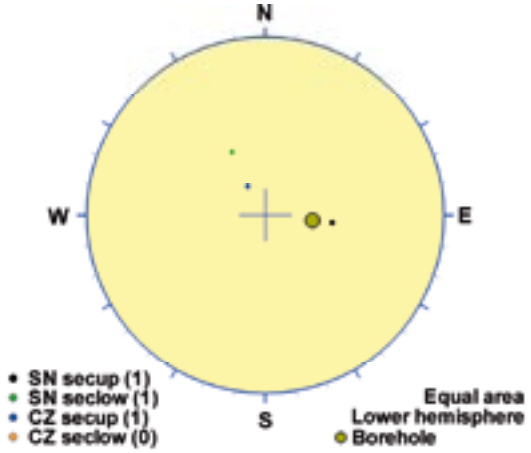

Poles from ductile structures

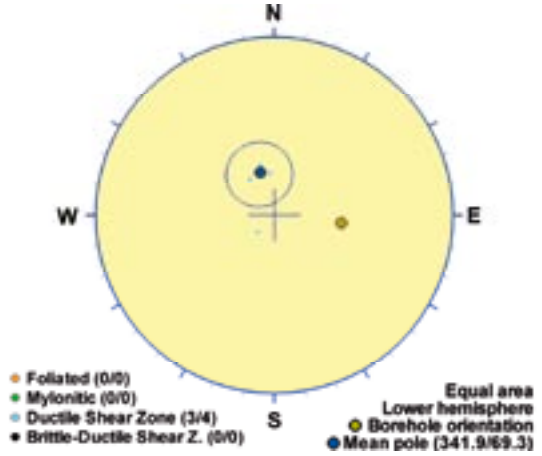

Poles from fractures

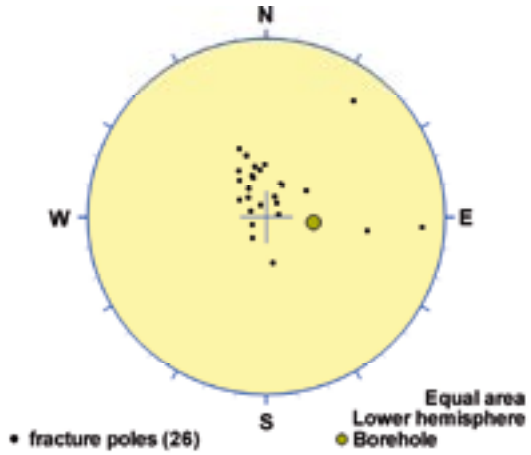

Contours from fractures

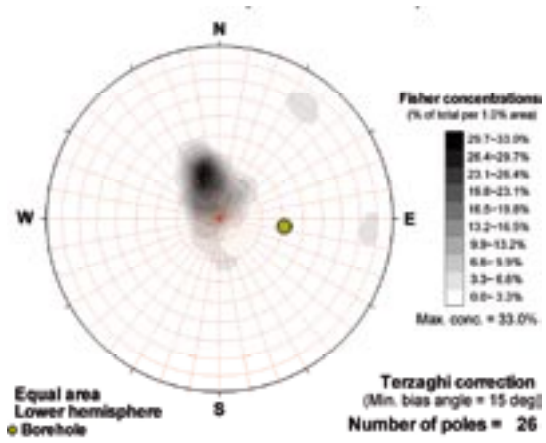

Orientation		Basis for orientation				Certainty	Thickness	
Strike	Dip	Fractures	Crush	Ductile structures	Reflectors	Orientation	Apparent	True
72	21	Verify	Verify	Used	Verify	Certain	2.5 m	1.8 m
Comment:								

KLX28A DZ1 (14.4 to 33.1), ductile/brittle zone

Inhomogeneous brittle-ductile deformation zone characterized by slightly increased frequency of open and sealed fractures, crush zones, cataclasite, slickensides and locally faint to weak red staining. The most intensely deformed part is the section 27.70-30.35 m, which is associated with fine-grained diorite-gabbro (505102). Several distinct low resistivity and decreased P-wave velocity anomalies in the entire section. The core is also characterized by caliper anomalies and decreased magnetic susceptibility. One oriented radar reflector occurs at 27.3 m (096/76) and five non-oriented radar reflectors occur with angle in the interval 43-69° to borehole axis. The oriented reflector can be observed to a distance of 8 m outside the borehole. Low radar amplitude at 13-21 m. The host rock is dominated by Ävrö quartz monzodiorite (501046). Subordinate rock types comprise fine-grained granite (511058) and fine-grained diorite-gabbro (505102), and sparse occurrences of pegmatite (501061), granite (501058) and fine-grained dioritoid (501030).

Poles from crush zone

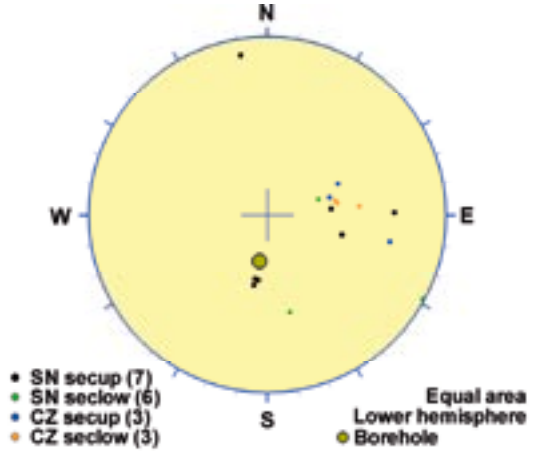

Poles from ductile structures

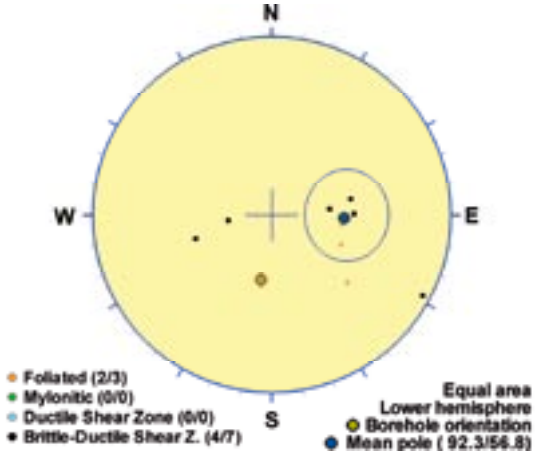

Poles from fractures

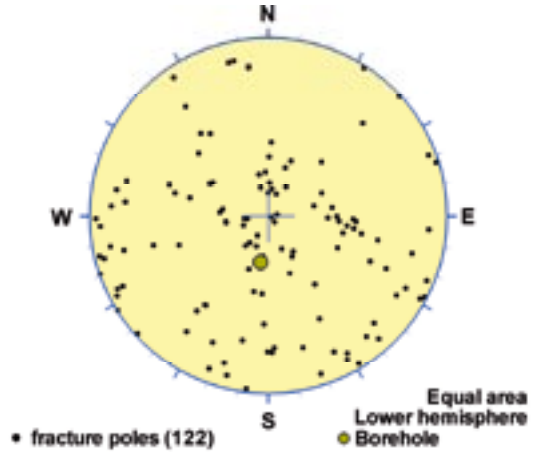

Contours from fractures

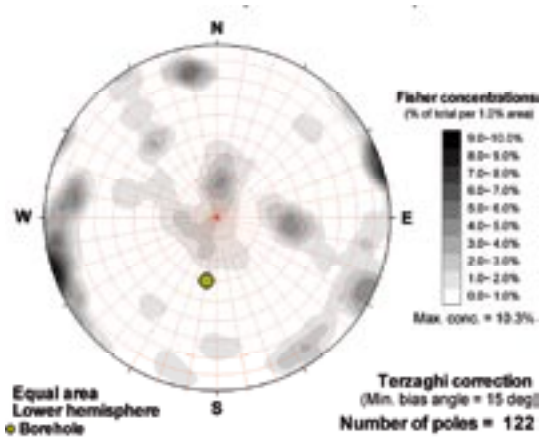

Orientation		Basis for orientation				Certainty	Thickness	
Strike	Dip	Fractures	Crush	Ductile structures	Reflectors	Orientation	Apparent	True
182	33	Verify	Verify	Used	Contradict	Probable	18.7 m	12.8 m
Comment:								

KLX28A DZ2 (74 to 76.1), ductile/brittle zone

Inhomogeneous brittle to ductile deformation zone with weak red staining. No significant anomalies in the geophysical logging data. One non-oriented radar reflector occurs at 76.9 m with the angle 28° to borehole axis. The reflector can be observed to a distance of 18 m outside the borehole. The host rock is dominated by Ävrö quartz monzodiorite (501046) with subordinate occurrence of fine-grained granite (511058).

Poles from crush zone

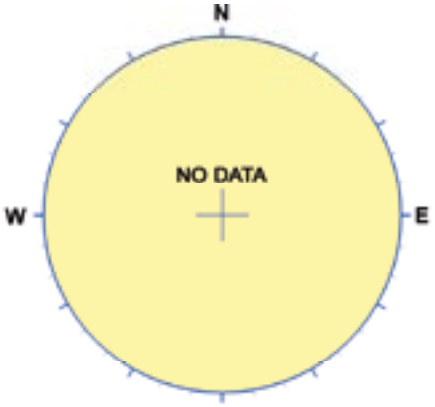

Poles from ductile structures

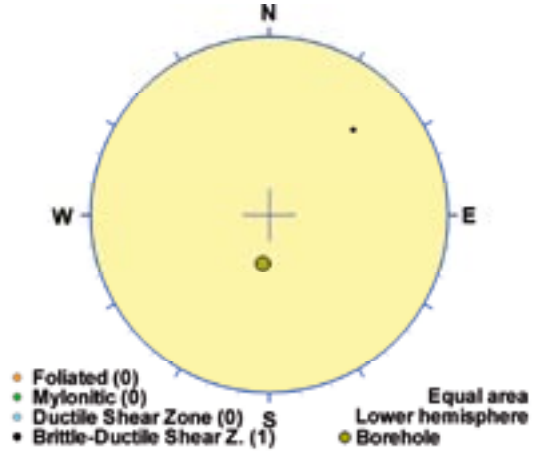

Poles from fractures

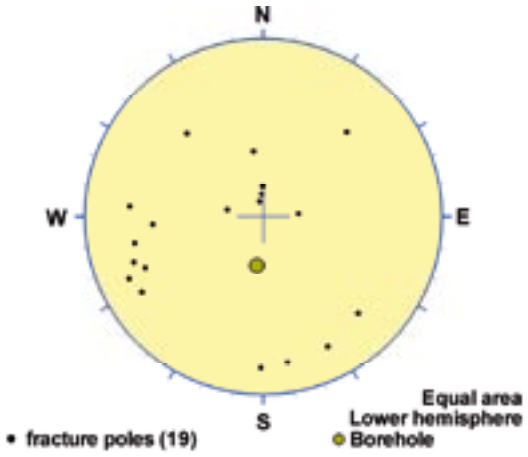

Contours from fractures

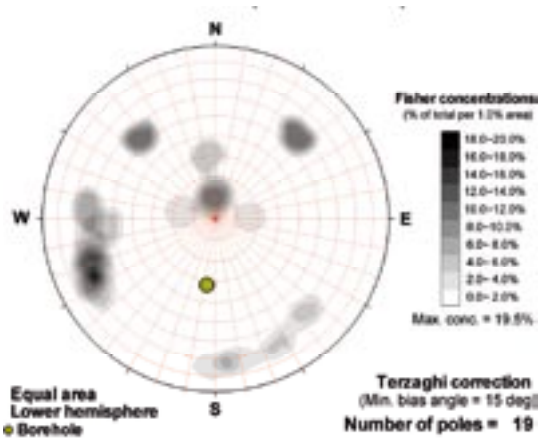

Orientation		Basis for orientation				Certainty	Thickness	
Strike	Dip	Fractures	Crush	Ductile structures	Reflectors	Orientation	Apparent	True
135	56	Contradict		Used	Verify	Uncertain	2.1 m	0.3 m
Comment: One fracture only support the orientation of the ductile structure.								

KLX29A DZ1 (7.21 to 8.02), brittle zone

Brittle deformation zone characterized by increased frequency of open and sealed fractures, minor core loss and crush, and medium to strong red staining. No geophysical logging data available. One non-oriented radar reflector occurs at 8.4 m with the angle 52° to borehole axis. The reflector can observed to a distance of 2 m outside the borehole. Low radar amplitude at 5-8 m. The host rock is dominated by Ävrö quartz monzodiorite (501046) with subordinate occurrence of fine-grained granite (511058).

Poles from crush zone

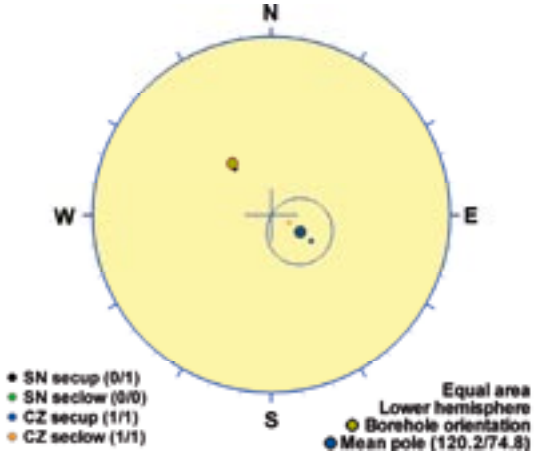

Poles from ductile structures

Data not used

Poles from fractures

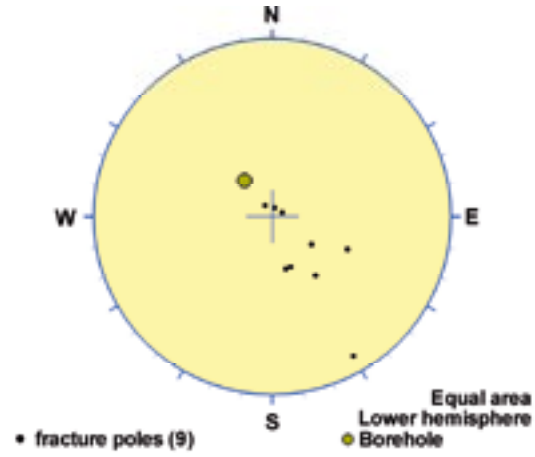

Contours from fractures

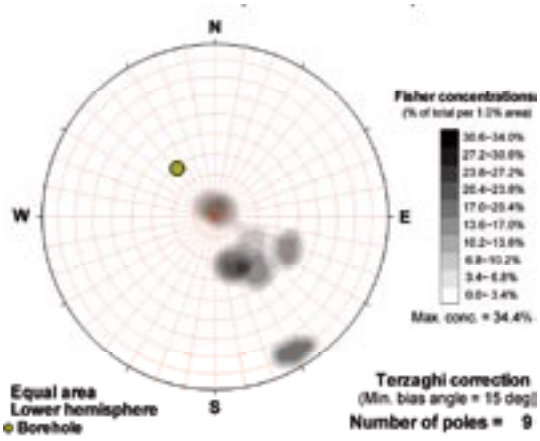

Orientation		Basis for orientation				Certainty	Thickness	
Strike	Dip	Fractures	Crush	Ductile structures	Reflectors	Orientation	Apparent	True
210	15	Verify	Used		Verify	Probable	0.8 m	0.6 m
Comment:								

KLX29A DZ2 (44.05 to 52.4), brittle zone

Inhomogeneous brittle deformation zone characterized by increased frequency of sealed fractures, sealed network, local increased frequency of open fractures, slickensides, minor crush, faint saussuritization, local weak red staining and local weak epidotization. The most intensely deformed parts are located to the sections 44.05-45.10 m and 51.44-52.40 m. The most intensely deformed sections are geophysically characterized by decreased resistivity and magnetic susceptibility; the lowermost also by a caliper anomaly. There are no significant geophysical anomalies outside the most intensely deformed sections. Two non-oriented radar reflectors occur at 44.9 m and 52.1 m with the angle 61° and 59° to borehole axis, respectively. The reflectors can be observed to a distance of 7 m and 6 m outside the borehole, respectively. The host rock is dominated by Ävrö quartz monzodiorite (501046) with subordinate occurrence of fine-grained granite (511058).

Poles from crush zone

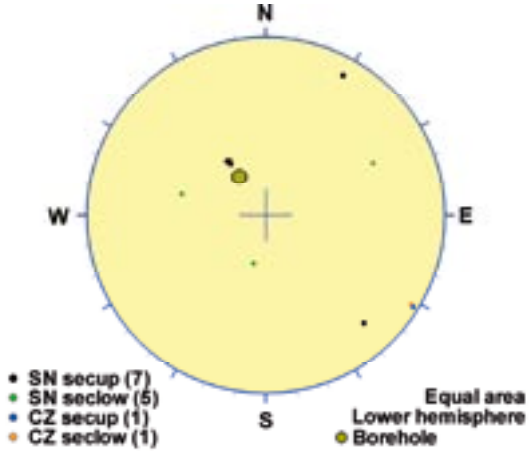

Poles from ductile structures

Data not used

Poles from fractures

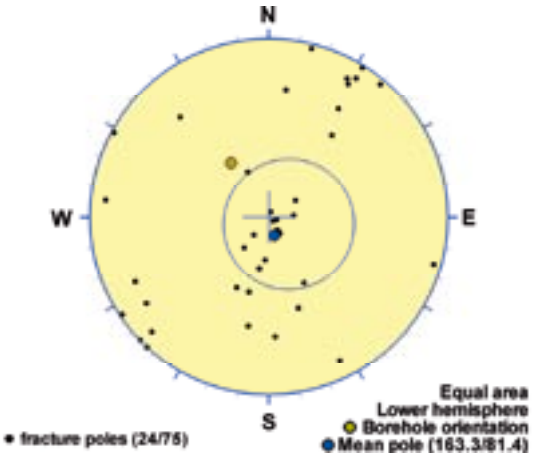

Contours from fractures

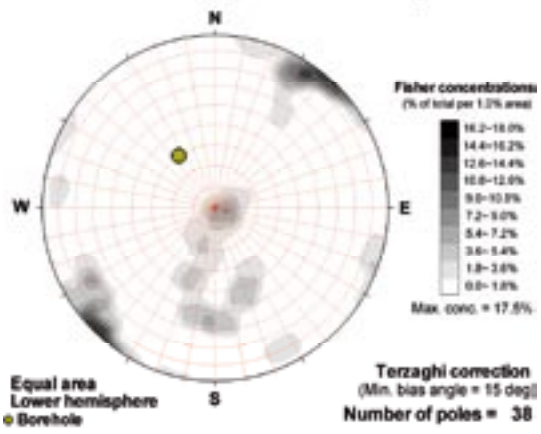

Orientation		Basis for orientation				Certainty	Thickness	
Strike	Dip	Fractures	Crush	Ductile structures	Reflectors	Orientation	Apparent	True
253	9	Used	Contradict		Verify	Very uncertain	8.4 m	6.5 m
Comment: In this case there may be two structures: one as selected, the other the NNE striking subvertical crush zone. Further study recommended.								

Appendix 4

Fracture intensity as a function of depth in cored boreholes

A4.1 Discussion on methods, trends, and heterogeneities in cored borehole fracture intensity data

The description of the spatial variability of fracture intensity is a key parameter in both the geologic and hydraulic DFN models, as well in the geological model in general. It is of principal importance to understand the patterns and trends in the relative intensity of fractures and fracture orientation sets, in order to construct a fracture domain model that best encompasses the spatial variability of fracturing at Laxemar. This appendix summarises fracture information from the cored borehole array at Laxemar in a way that is useful for the qualitative assessment of fracture domains.

Generally speaking, the fracture intensity data at Laxemar reflect two different classes of elevation intervals in the bedrock: short boreholes and deep boreholes. The short cored boreholes extend from near the ground surface to an elevation of approximately –100 m.a.s.l. These boreholes are drilled in multiple directions and at multiple inclinations, and consequently provide excellent coverage of the near-surface fracture environment with minimal orientation bias. The mapped sections of deep cored boreholes begin at an elevation of approximately –100 m.a.s.l. (the upper portions of these boreholes have been completed using percussion drilling.

There are three key limitations to keep in mind in the interpretation of the cored borehole data:

1. The relative paucity of fracture data at sub-repository depths at Laxemar must be taken into consideration before conclusions on fracture intensity trends are drawn. illustrates this problem; there is a steep drop off in the number. It is entirely possible that what appears to be an increase in fracture intensity with depth may actually stem from only a single borehole, which may or may not have an anomalously high or low intensity at that location in the Laxemar model volume. The lack of data at depth results in a much wider confidence interval for the mean fracture intensity; in some cases, the confidence interval of the mean is larger than the potential increase or decrease in fracture intensity as a function of depth. This makes it difficult, if not impossible, in some circumstances to demonstrate a depth trend with any statistical significance.

2. Many boreholes have intentionally been drilled to further investigate deformation zones. Therefore, it is possible to mistake the increase in fracture intensity found around and outside of regional deformation zones for an apparent depth trend.

Section A4.2 illustrates the variability of the intensity of fractures of all orientations as a function of depth on an individual borehole basis. Fracture intensity is plotted as a Terzaghi-compensated linear fracture intensity (P_{10}), with the value of fracture intensity representing a average of P_{10} calculated from 1m intervals in the cored boreholes over a 5 m moving window. Fracture intensity is plotted for both open fractures and sealed fractures. The purple bands on each plot represent the mapped limits of deformation zones identified in the extended single-hole interpretation. Since fractures inside DZ are outside of the scope of the geological DFN, they have been omitted from the plots of intensity versus depth.

The plots on the right side of Section A4.2 represent the cumulative fracture intensity (CFI) as a function of depth. These plots are useful in a qualitative sense; one is not concerned with the magnitude of the cumulative fracture intensity, but rather the slope of the line. Long sections of the curve which are straight represent sections along the borehole in which the average Terzaghi-compensated fracture intensity is stable. Sections of the curve with sharp breaks or changes in slope represent changes in the average fracture intensity, which can occur at the boundary between rock domains, between fracture domains, or at deformation zones.

Generally speaking, a straight line in these curves would represent relatively constant fracture intensity with depth. Lines that curve to the left or right represent an **apparent potential** decrease or increase in fracture intensity with depth.

The CFI plots were constructed by summing the Terzaghi weights for all fractures within a certain elevation range (the CFI plots use 5 m elevation bins), and dividing this sum by the total borehole length within the 5m elevation bin (for a vertical borehole, this would be 5 m, and for an inclined borehole, the length, expressed as ADJ_SECLOW – ADJ_SECUP, would be longer than 5 m).

The plots in Section A4.2 utilise the linear fracture intensity (P_{10}), with a compensation bias for the borehole orientation provided by the Terzaghi correction /Terzaghi 1965/. In summary, Terzaghi weighing compensates for the bias inherent in sampling vertically- to subvertically-dipping fractures with vertical to subvertical boreholes. In this situation, the probability of intersecting horizontally- to subhorizontally-dipping fractures is much higher than the probability of intersecting vertically- to subvertically-dipping fractures. Terzaghi weighing partially compensates for this sampling bias. Fundamentally, a Terzaghi-weighted P_{10} can be used as a rough estimate of volumetric fracture intensity (P_{32}). It is only an estimate, however, as P_{32} is also dependent on fracture size, which is not accounted for using borehole sampling.

It is important to note, however, that the Terzaghi correction has significant limitations. The value of the Terzaghi weight is asymptotic as the β[1] angle (the angle between the borehole axis and the plane of the fracture) approaches zero /Yow 1987/. It is generally accepted /Yow 1987/, /Mauldon and Mauldon 1997/, that a 'blind zone' exists between $\beta = 0°$ and $\beta = 20°$. Within this zone the Terzaghi compensation is generally viewed as inappropriate. This is important, because for the fracture data derived from the cored borehole array at Laxemar, approximately 1/3 of the fractures possess orientations with a β angle less than or equal to 20°. The standard of practice /Yow 1987, Priest 1993/ to address the blind zone is to set a maximum value for the Terzaghi correction; a maximum value of 10 is generally used. For the plots of fracture intensity in Sections A4.2, a bias angle of 8.2 degrees, corresponding to a maximum Terzaghi weight of 7, was used. This implies that, for fractures with a β angle less than 8.2, the intensity may be under-sampled.

In addition, /Davy et al. 2006/ showed that, for fracture networks where fracture size follows a Pareto (power-law) length distribution, the Terzaghi correction will over-estimate the frequency of fractures subparallel to the borehole. Past geological DFN models at Forsmark and Laxemar have demonstrated that a power-law distribution is generally the most appropriate model for fracture sizes.

The end result is that there is uncertainty in using Terzaghi-corrected P_{10} to quantitatively state anything about fracture intensity trends as functions of depth or spatial location. In the geological DFN modelling /La Pointe et al. 2008/, the formal analysis of fracture intensity as a function of depth is conducted using volumetric fracture intensity (P_{32}) specifically to get around these limitations. The Terzaghi-compensated P_{10} values are still quite useful for the qualitative assessment of fracture intensity trends and the delineation of fracture domains. However, the user is encouraged not to use the charts presented in Section A4.2 in quantitative analyses.

[1] The β angle defined here is NOT the same β angle as defined in SICADA; there is no standard as to naming for the angle between the borehole axis and the plane of the fracture. Terzaghi refers to it as α while /Yow 1987/ and /Mauldon and Mauldon 1997/ refer to as β. We utilise the Yow definition.

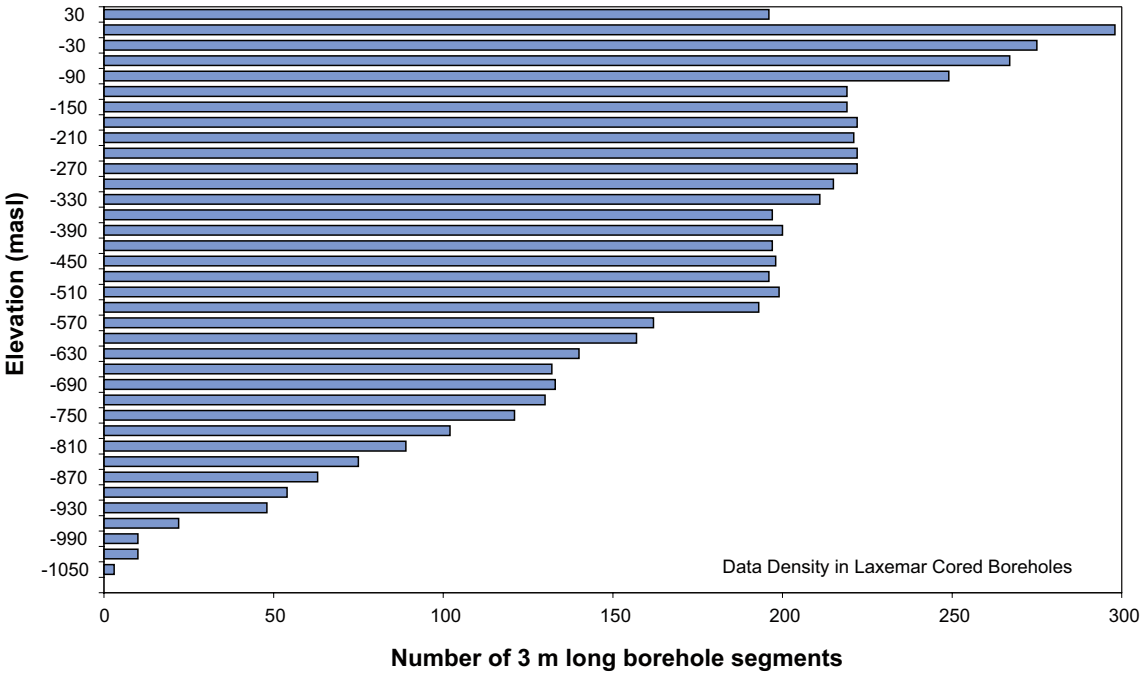

Figure A4-1. *Histogram of cored borehole data density as a function of elevation. Figure charts the number of complete 3m intervals in a 30 m elevation window. Note the lack of data below an elevation of -600 m.a.s.l.*

A4.2 Terzaghi-compensated fracture intensity (P_{10}) as a function of elevation in individual boreholes

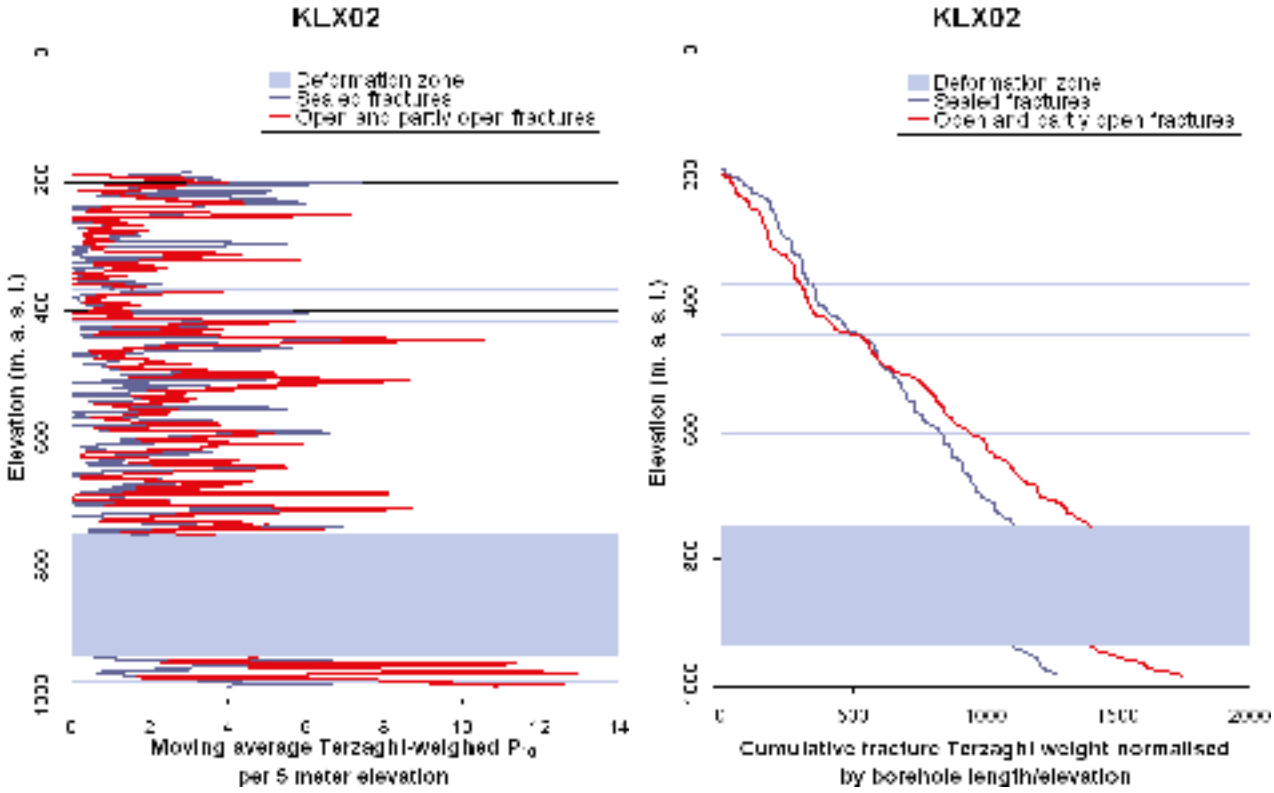

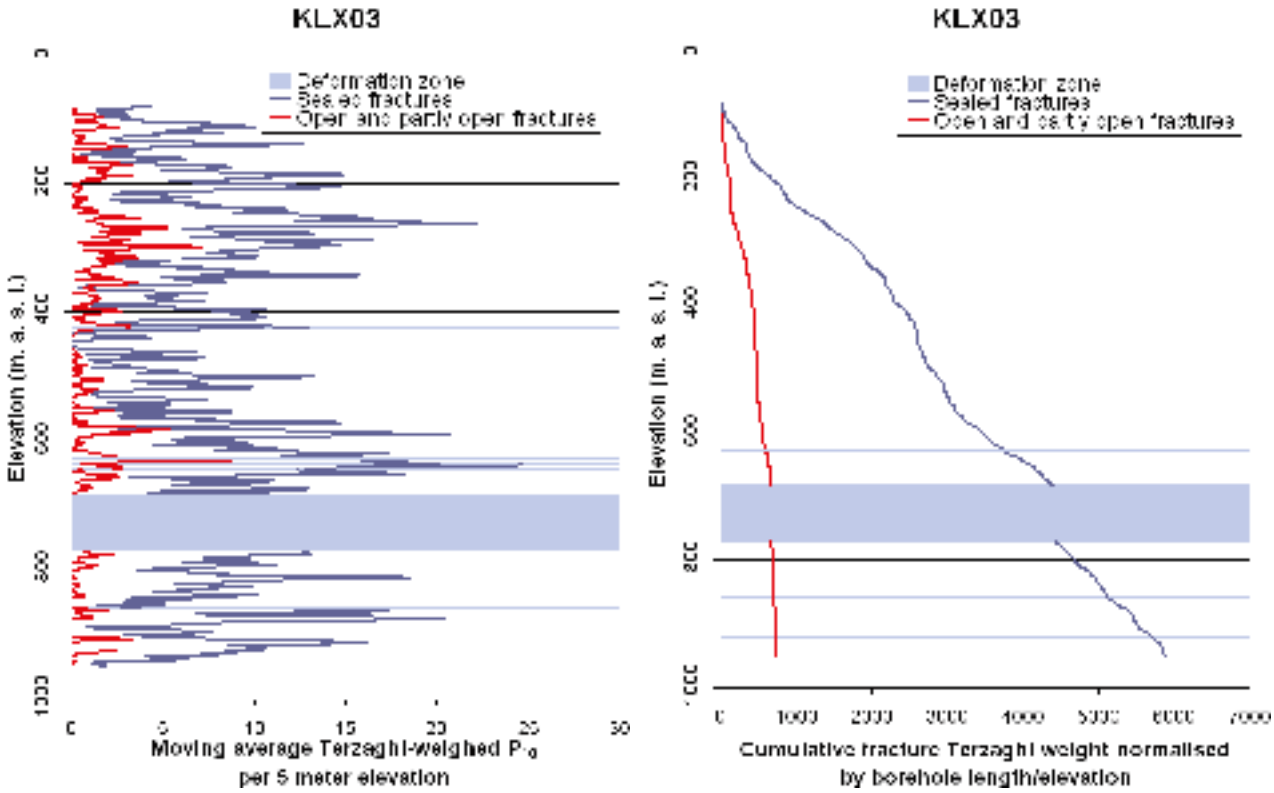

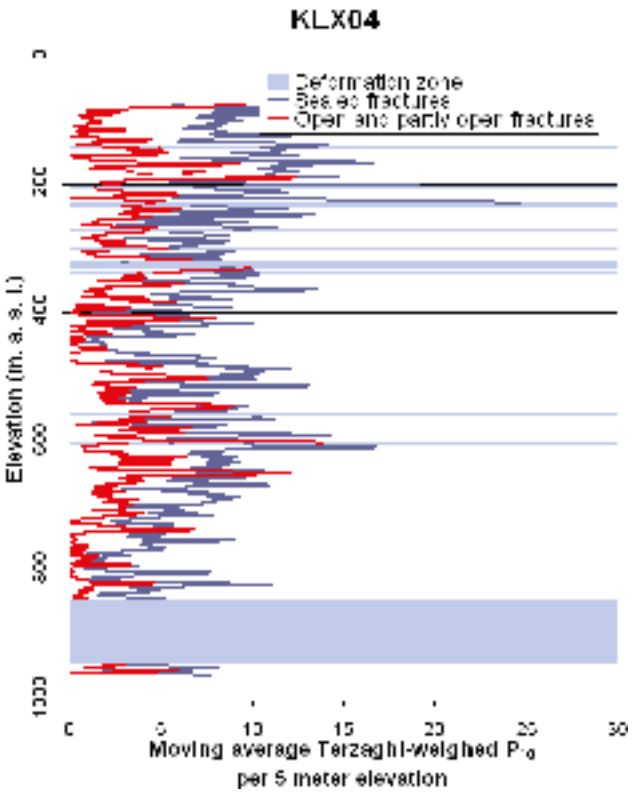
KLX04
Deformation zone
Sealed fractures
Open and partly open fractures
Elevation (m. a. s. l.)
Moving average Terzaghi-weighed P10
per 5 meter elevation

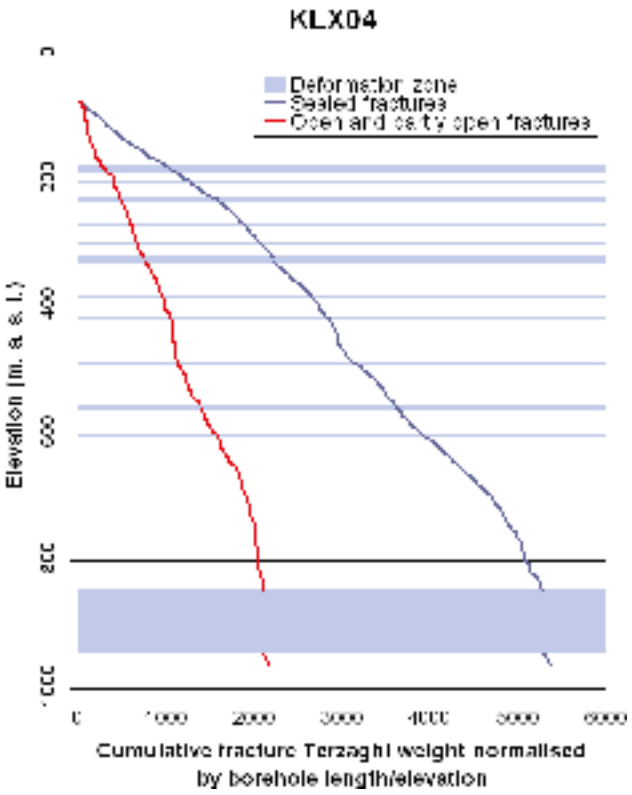
KLX04
Deformation zone
Sealed fractures
Open and partly open fractures
Elevation (m. a. s. l.)
Cumulative fracture Terzaghi weight normalised
by borehole length/elevation

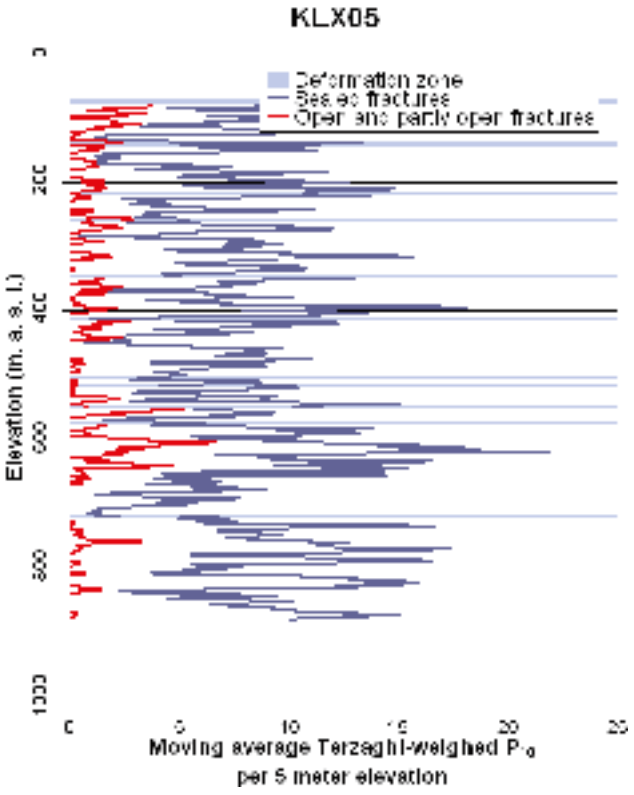
KLX05
Deformation zone
Sealed fractures
Open and partly open fractures
Elevation (m. a. s. l.)
Moving average Terzaghi-weighed P10
per 5 meter elevation

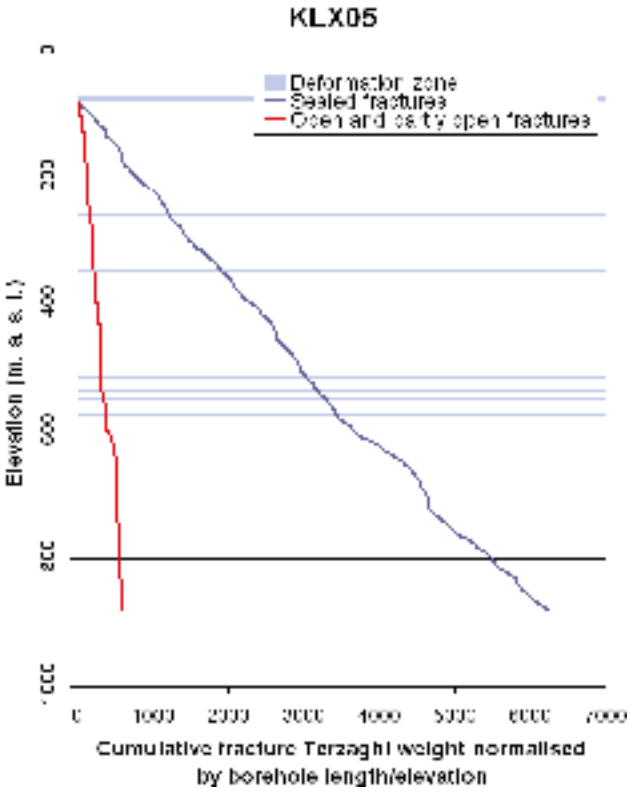
KLX05
Deformation zone
Sealed fractures
Open and partly open fractures
Elevation (m. a. s. l.)
Cumulative fracture Terzaghi weight normalised
by borehole length/elevation

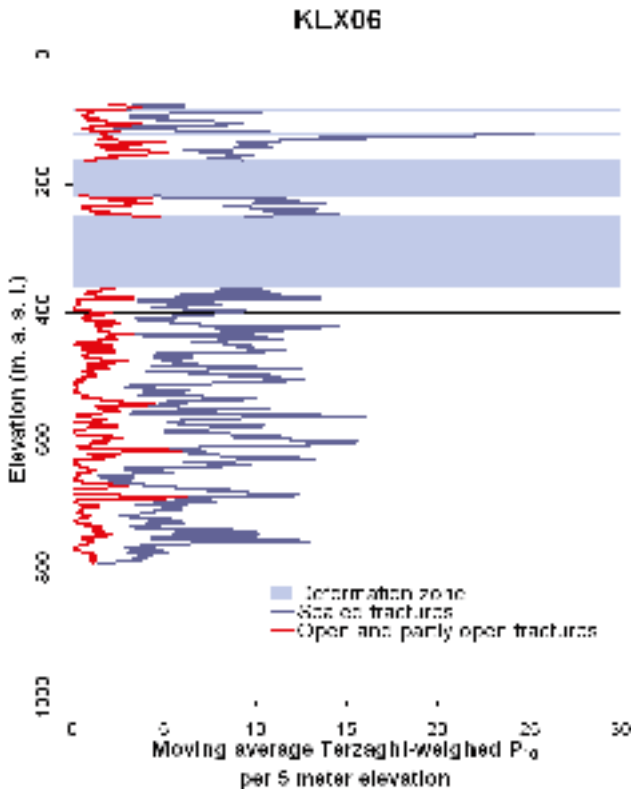
KLX06
Elevation (m. a. s. l.)
Moving average Terzaghi-weighed P10
per 5 meter elevation

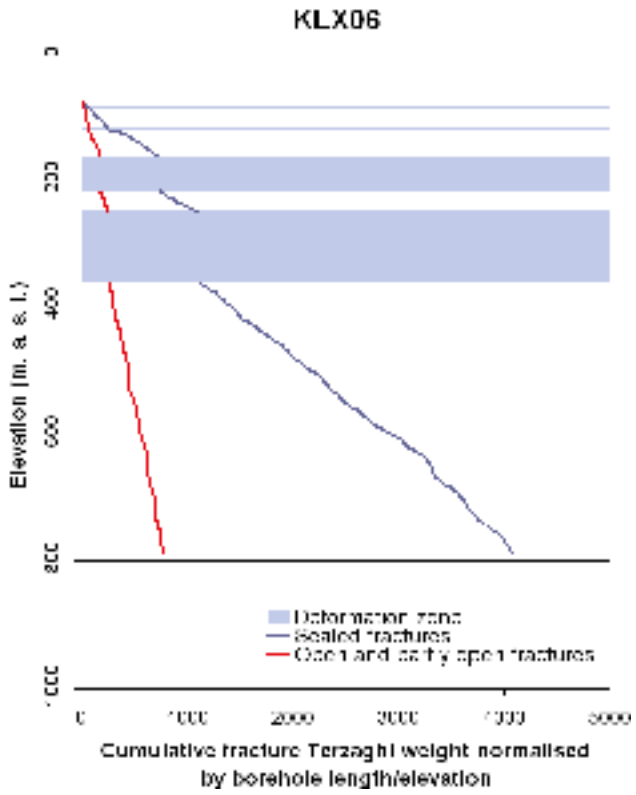
KLX06
Elevation (m. a. s. l.)
Cumulative fracture Terzaghi weight normalised
by borehole length/elevation

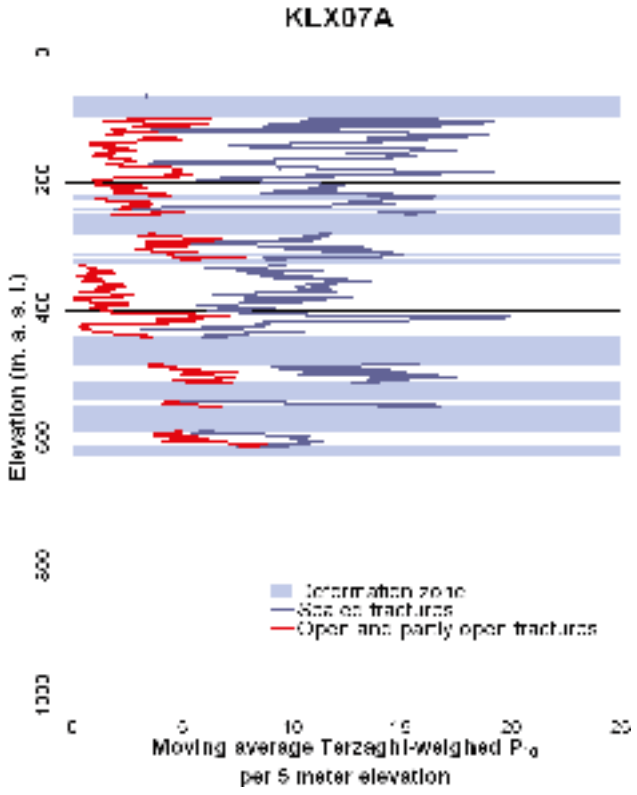
KLX07A
Elevation (m. a. s. l.)
Moving average Terzaghi-weighed P10
per 5 meter elevation

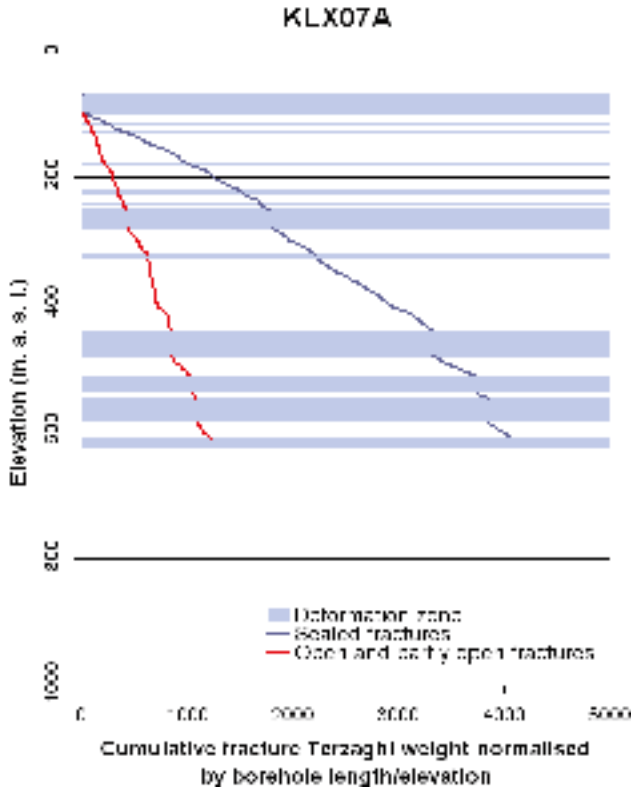
KLX07A
Elevation (m. a. s. l.)
Cumulative fracture Terzaghi weight normalised
by borehole length/elevation

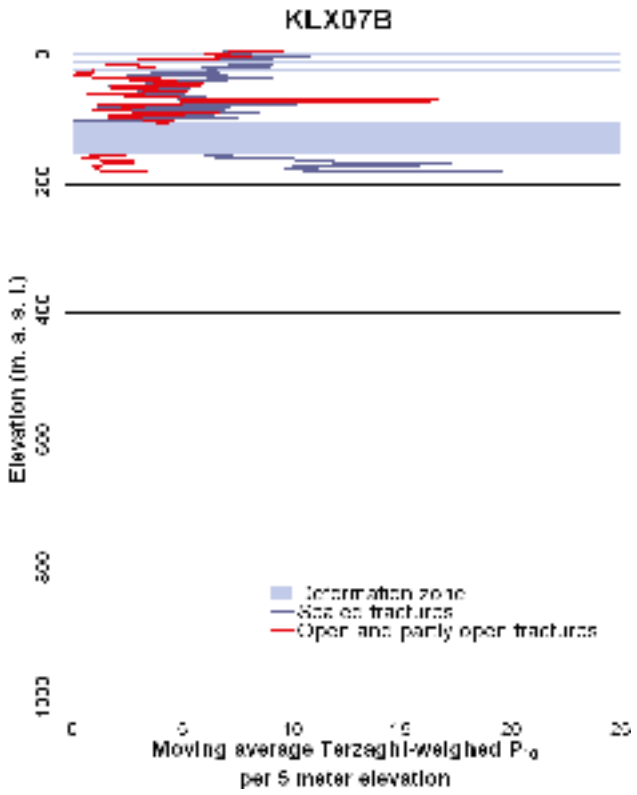
KLX07B
Elevation (m. a. s. l.)
Moving average Terzaghi-weighed P10
per 5 meter elevation

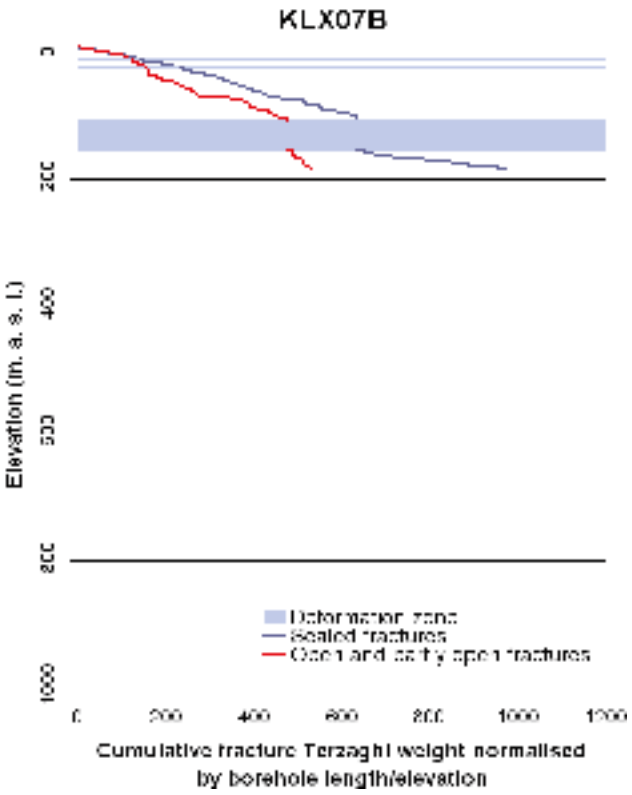
KLX07B
Elevation (m. a. s. l.)
Cumulative fracture Terzaghi weight normalised
by borehole length/elevation

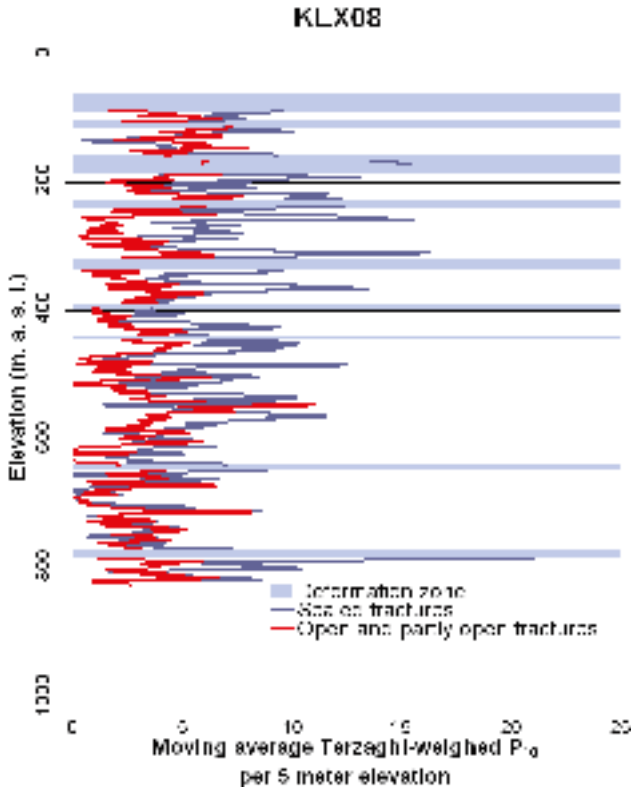
KLX08
Elevation (m. a. s. l.)
Moving average Terzaghi-weighed P10
per 5 meter elevation

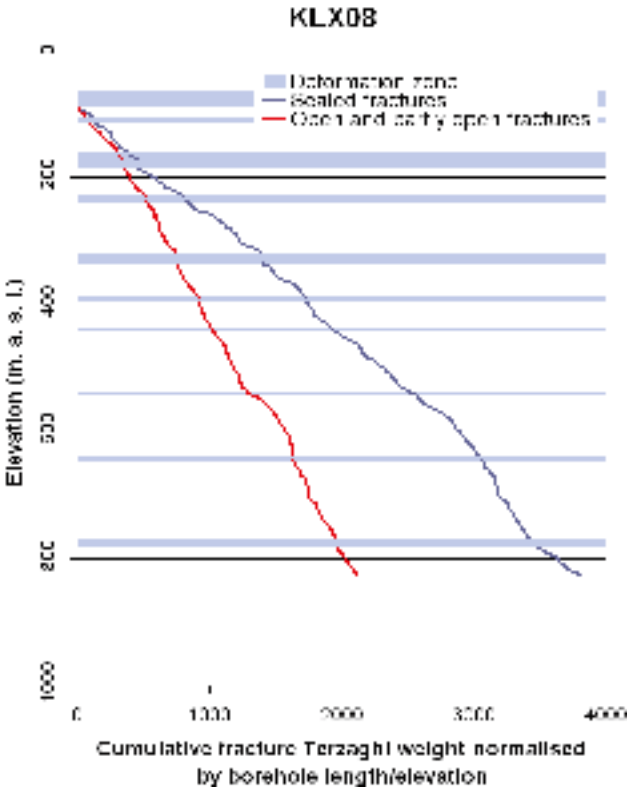
KLX08
Elevation (m. a. s. l.)
Cumulative fracture Terzaghi weight normalised
by borehole length/elevation

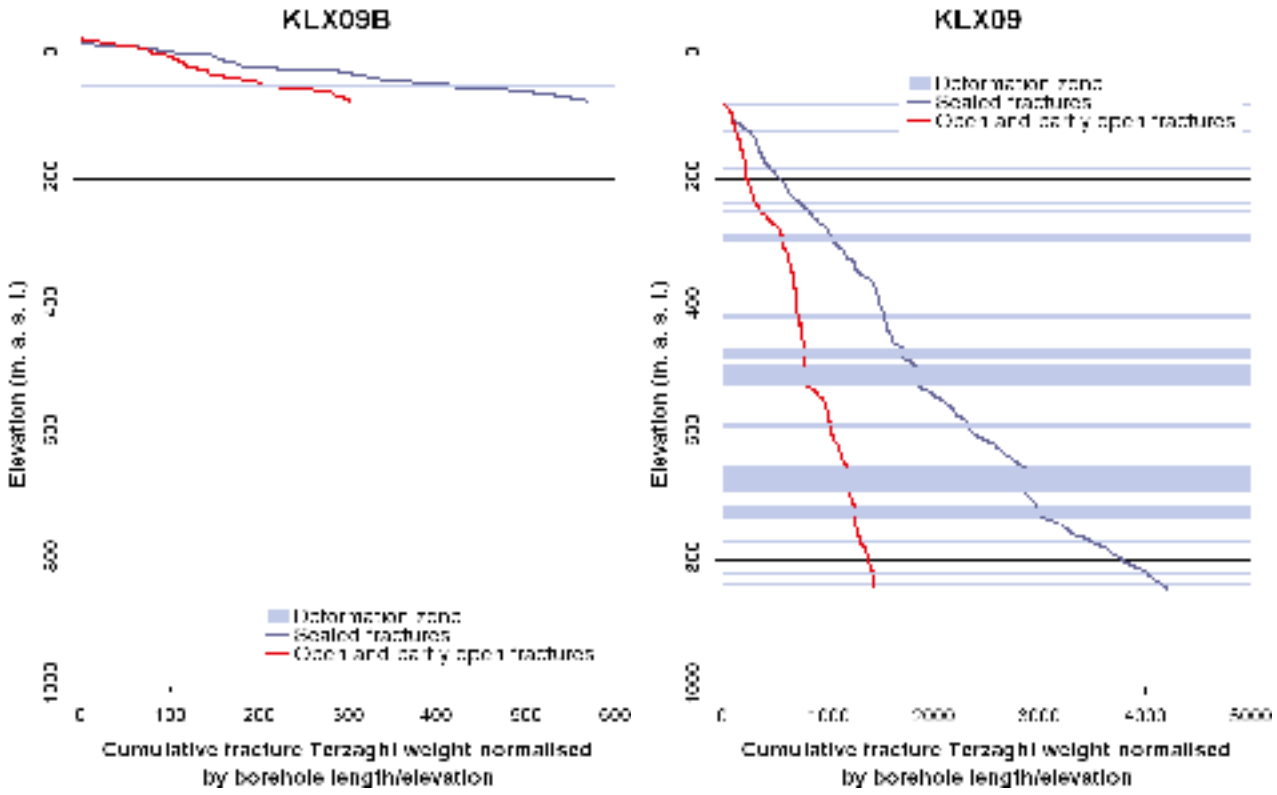
KLX09B
Elevation (m. a. s. l.)
Cumulative fracture Terzaghi weight normalised
by borehole length/elevation
KLX09
Elevation (m. a. s. l.)
Cumulative fracture Terzaghi weight normalised
by borehole length/elevation

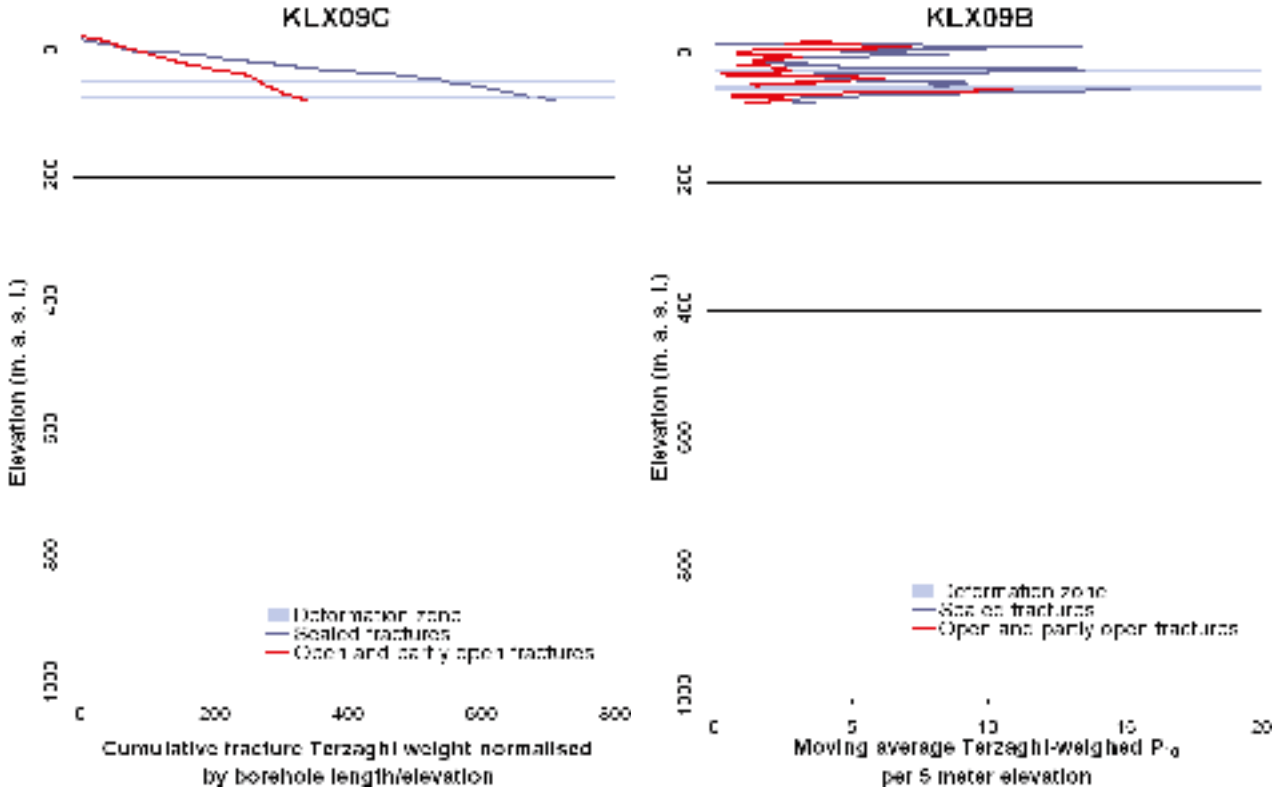
KLX09C
Elevation (m. a. s. l.)
Cumulative fracture Terzaghi weight normalised
by borehole length/elevation
KLX09B
Elevation (m. a. s. l.)
Moving average Terzaghi-weighed P10
per 5 meter elevation

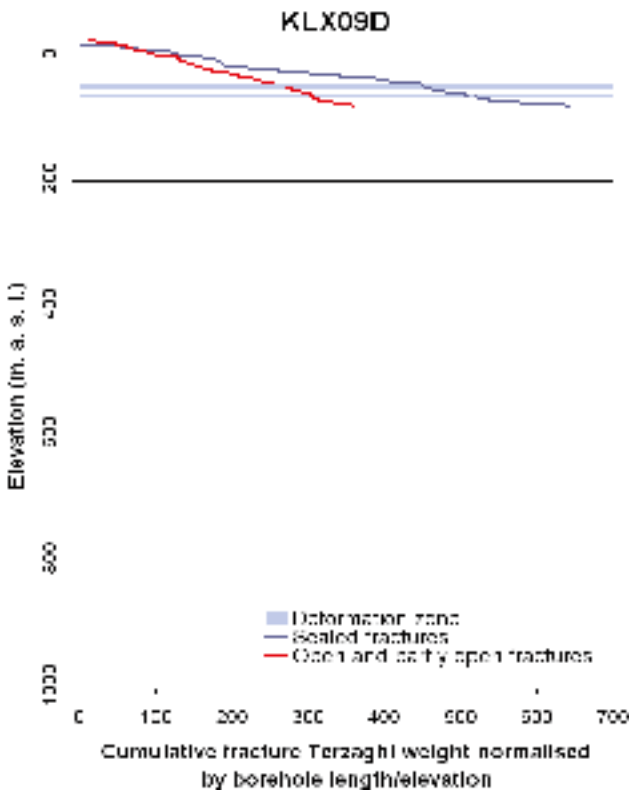
KLX09D
Elevation (m. a. s. l.)
Deformation zone
Sealed fractures
Open and partly open fractures
Cumulative fracture Terzaghi weight normalised
by borehole length/elevation

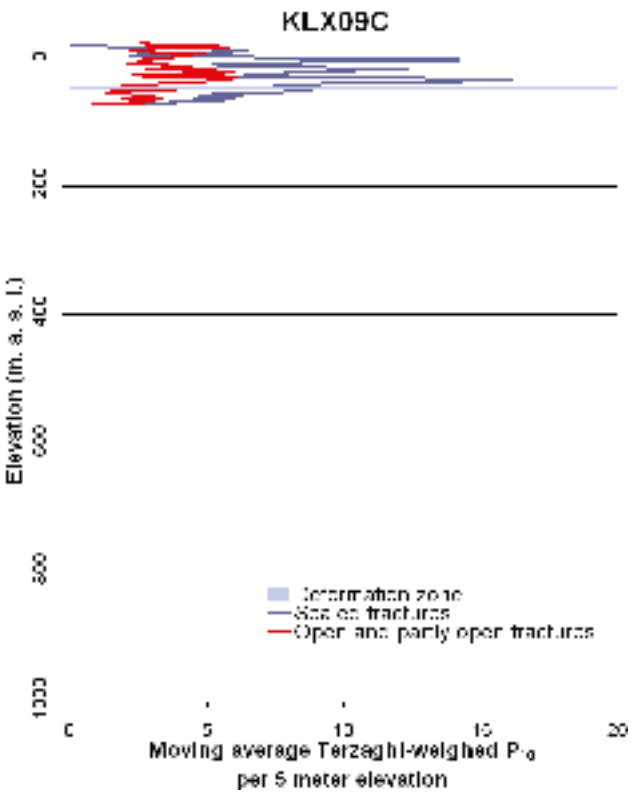
KLX09C
Elevation (m. a. s. l.)
Deformation zone
Sealed fractures
Open and partly open fractures
Moving average Terzaghi-weighed P10
per 5 meter elevation

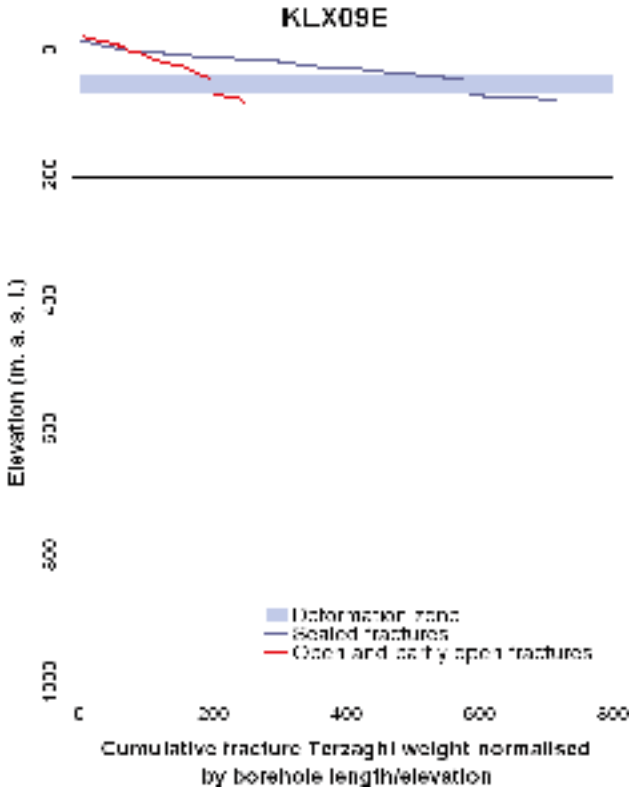
KLX09E
Elevation (m. a. s. l.)
Deformation zone
Sealed fractures
Open and partly open fractures
Cumulative fracture Terzaghi weight normalised
by borehole length/elevation

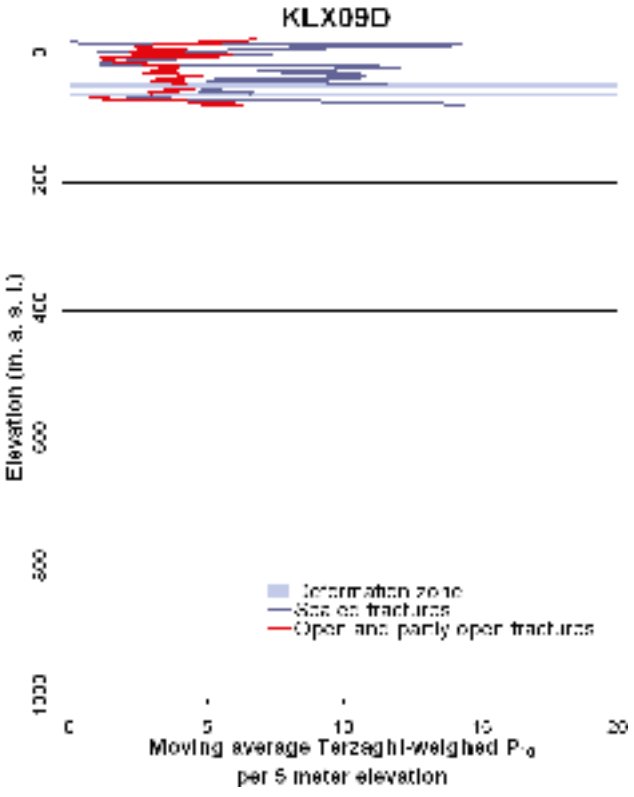
KLX09D
Elevation (m. a. s. l.)
Deformation zone
Sealed fractures
Open and partly open fractures
Moving average Terzaghi-weighed P10
per 5 meter elevation

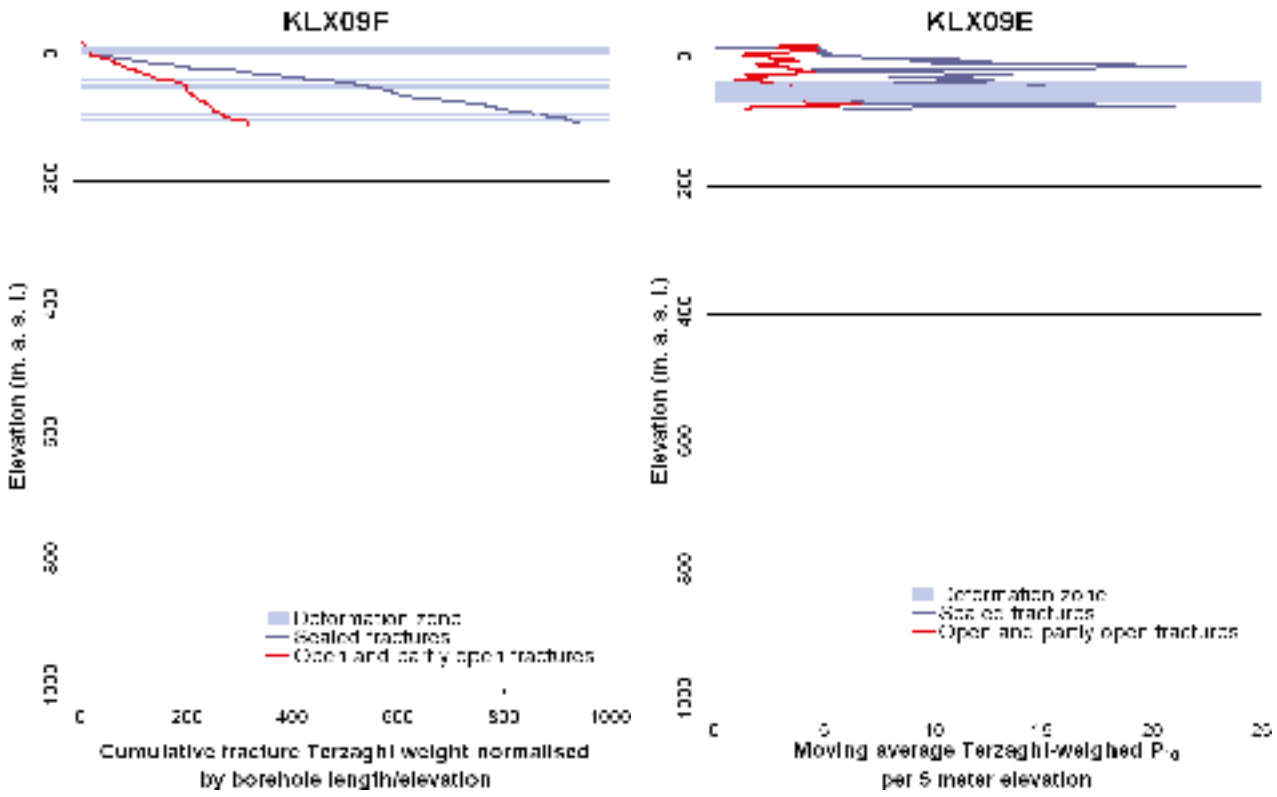
KLX09F
KLX09E
Elevation (m. a. s. l.)
Cumulative fracture Terzaghi weight normalised
by borehole length/elevation
Moving average Terzaghi-weighed P10
per 5 meter elevation
Deformation zone
Sealed fractures
Open and partly open fractures

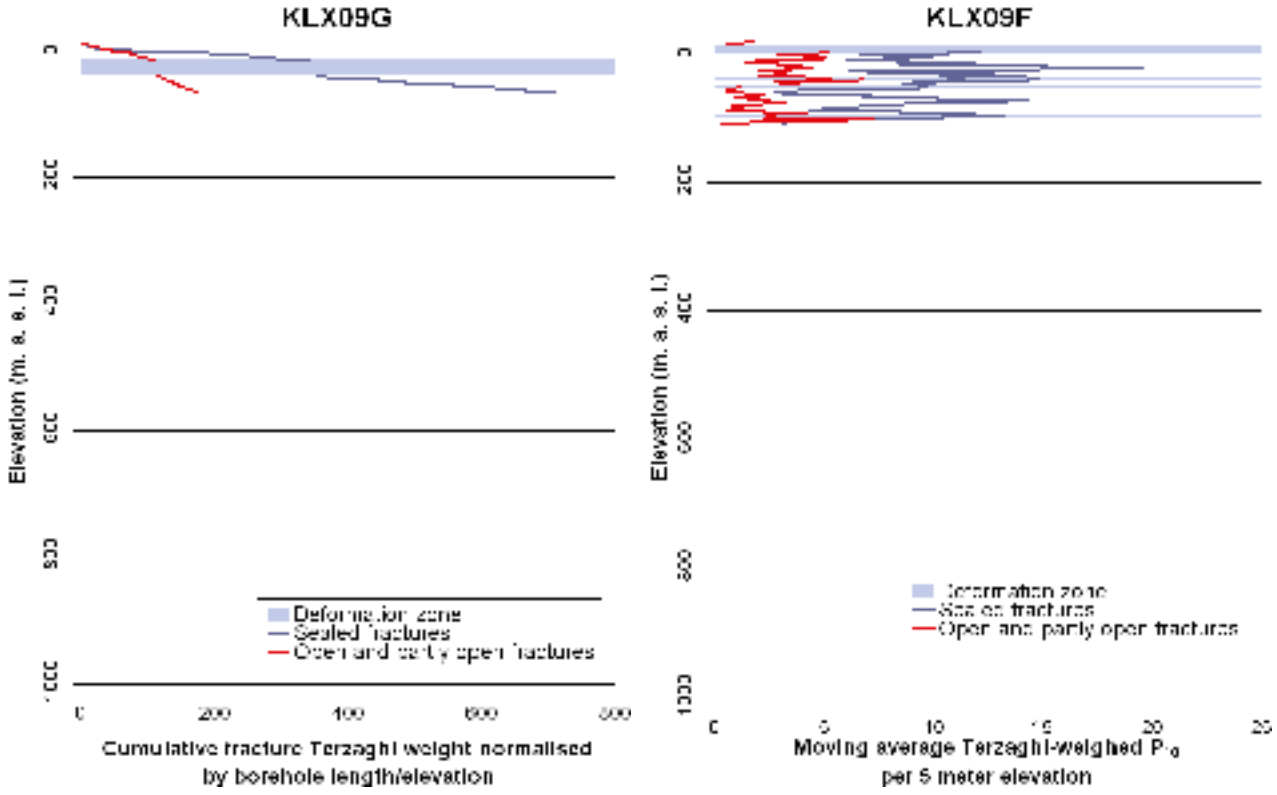
KLX09G
KLX09F
Elevation (m. a. s. l.)
Cumulative fracture Terzaghi weight normalised
by borehole length/elevation
Moving average Terzaghi-weighed P10
per 5 meter elevation
Deformation zone
Sealed fractures
Open and partly open fractures

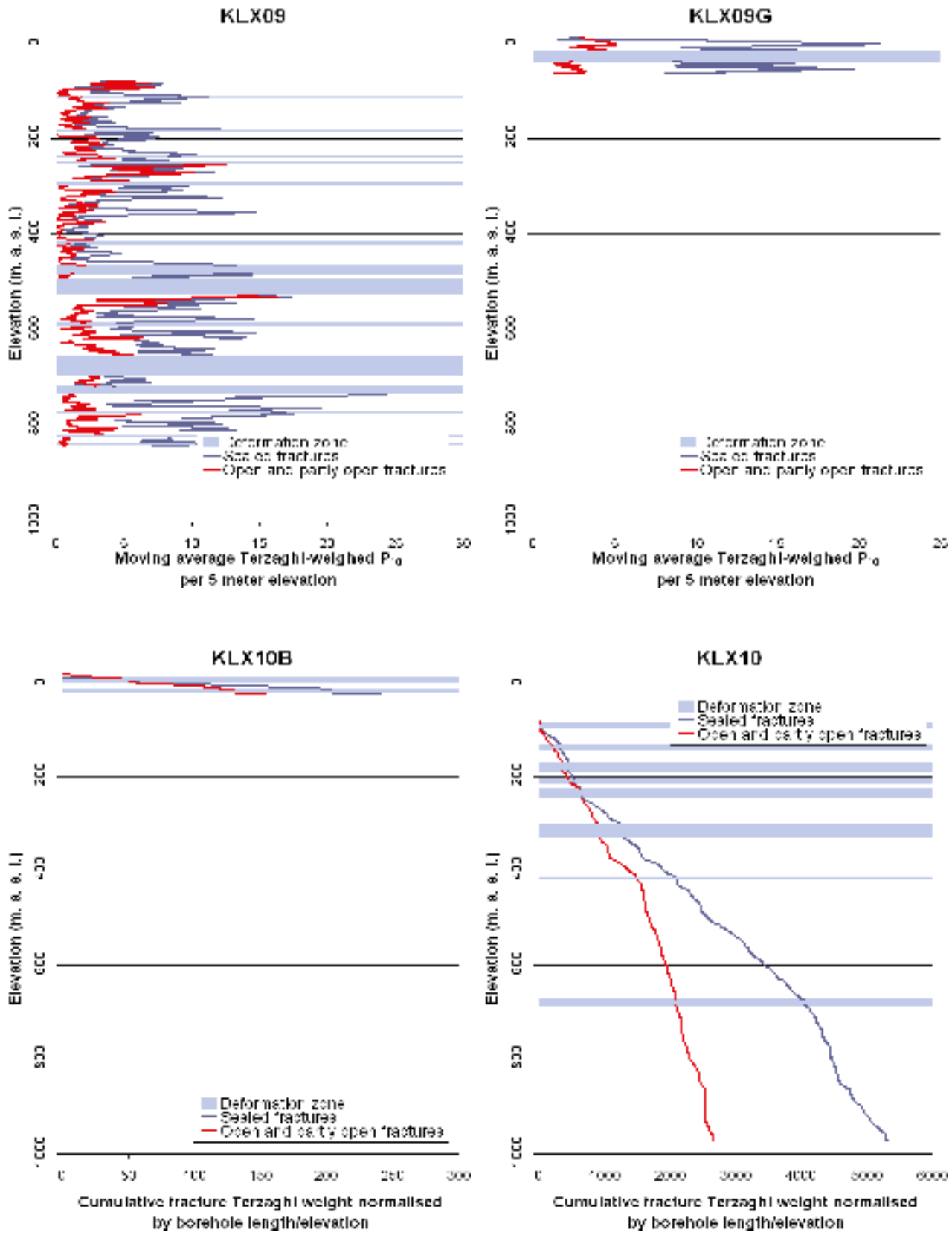
KLX09
KLX09G
KLX10B
KLX10
Elevation (m. a. s. l.)
Moving average Terzaghi-weighed P10
per 5 meter elevation
Cumulative fracture Terzaghi weight normalised
by borehole length/elevation
Deformation zone
Sealed fractures
Open and partly open fractures

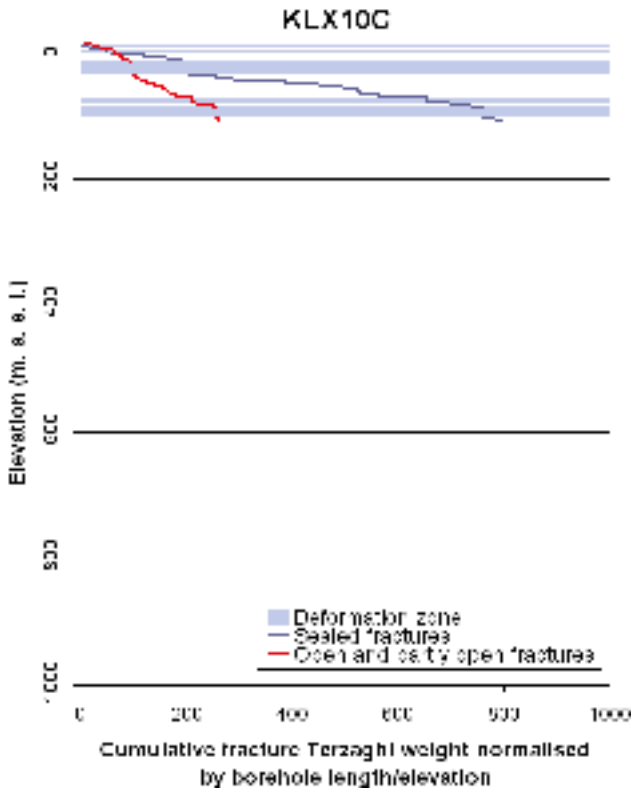
KLX10C
Elevation (m. a. s. l.)
Deformation zone
Sealed fractures
Open and partly open fractures
Cumulative fracture Terzaghi weight normalised
by borehole length/elevation

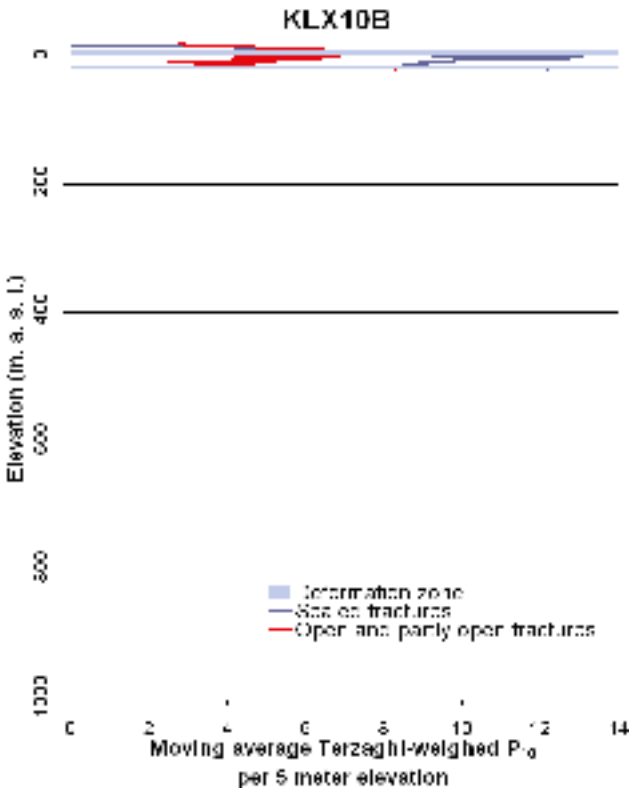
KLX10B
Elevation (m. a. s. l.)
Deformation zone
Sealed fractures
Open and partly open fractures
Moving average Terzaghi-weighed P-0
per 5 meter elevation

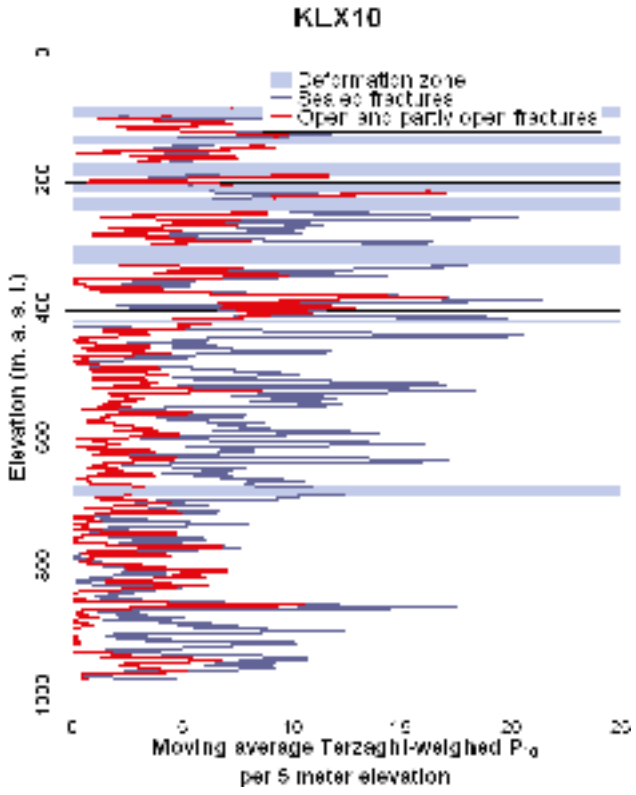
KLX10
Elevation (m. a. s. l.)
Deformation zone
Sealed fractures
Open and partly open fractures
Moving average Terzaghi-weighed P-0
per 5 meter elevation

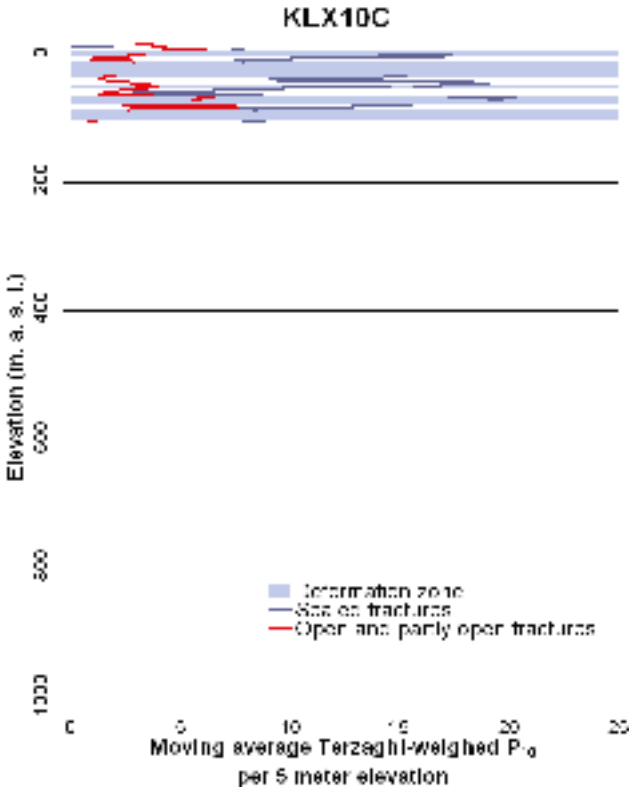
KLX10C
Elevation (m. a. s. l.)
Deformation zone
Sealed fractures
Open and partly open fractures
Moving average Terzaghi-weighed P-0
per 5 meter elevation

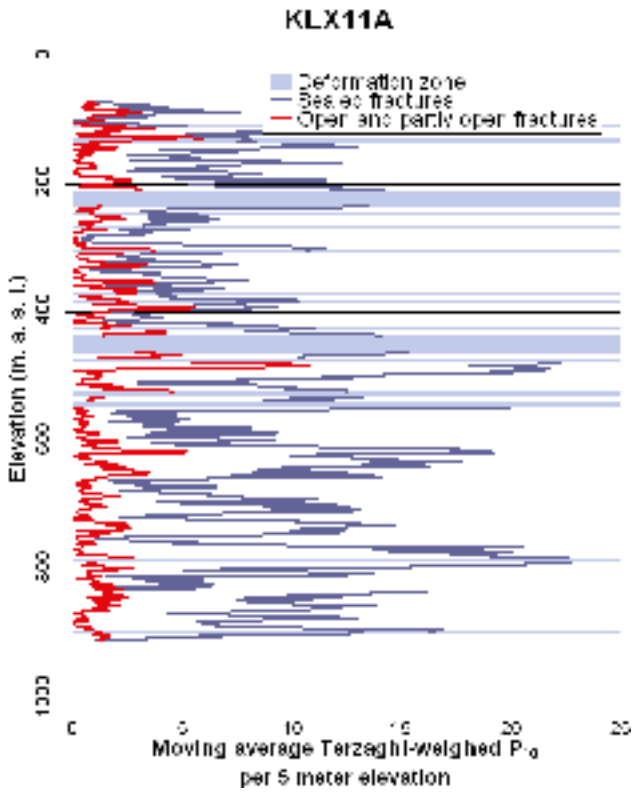
KLX11A
Deformation zone
Sealed fractures
Open and partly open fractures
Elevation (m. a. s. l.)
Moving average Terzaghi-weighed P10
per 5 meter elevation

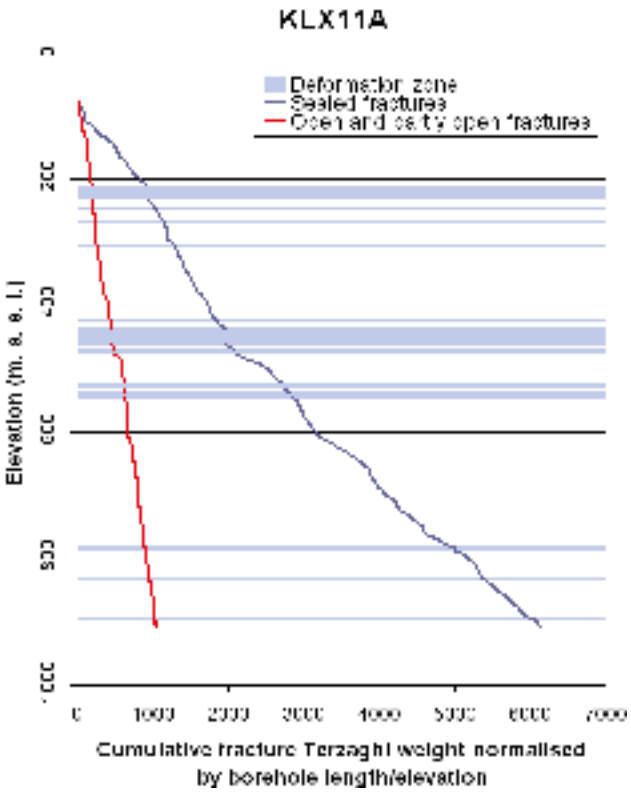
KLX11A
Deformation zone
Sealed fractures
Open and partly open fractures
Elevation (m. a. s. l.)
Cumulative fracture Terzaghi weight normalised
by borehole length/elevation

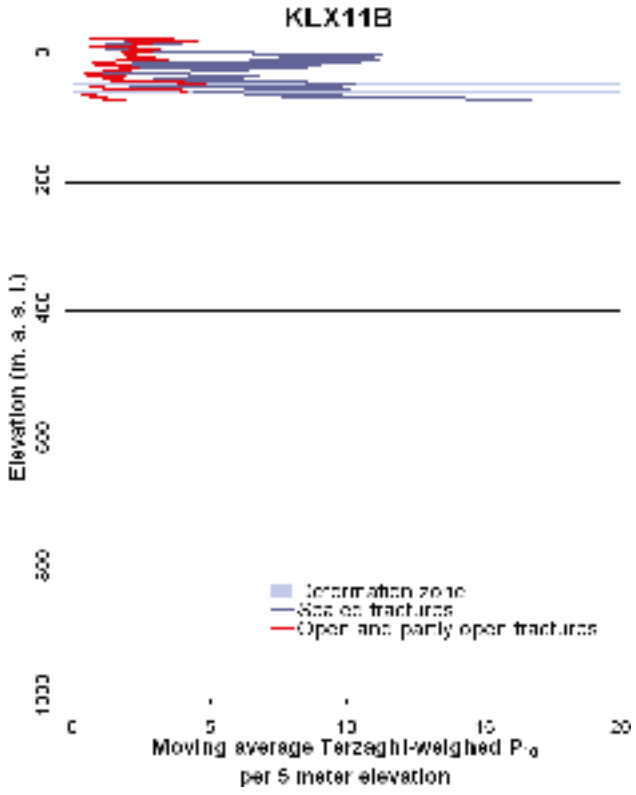
KLX11B
Deformation zone
Sealed fractures
Open and partly open fractures
Elevation (m. a. s. l.)
Moving average Terzaghi-weighed P10
per 5 meter elevation

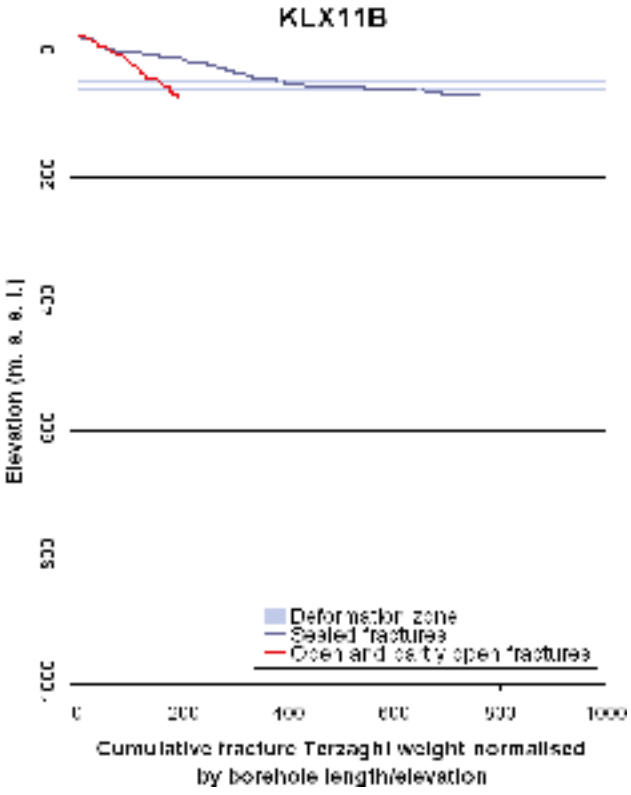
KLX11B
Deformation zone
Sealed fractures
Open and partly open fractures
Elevation (m. a. s. l.)
Cumulative fracture Terzaghi weight normalised
by borehole length/elevation

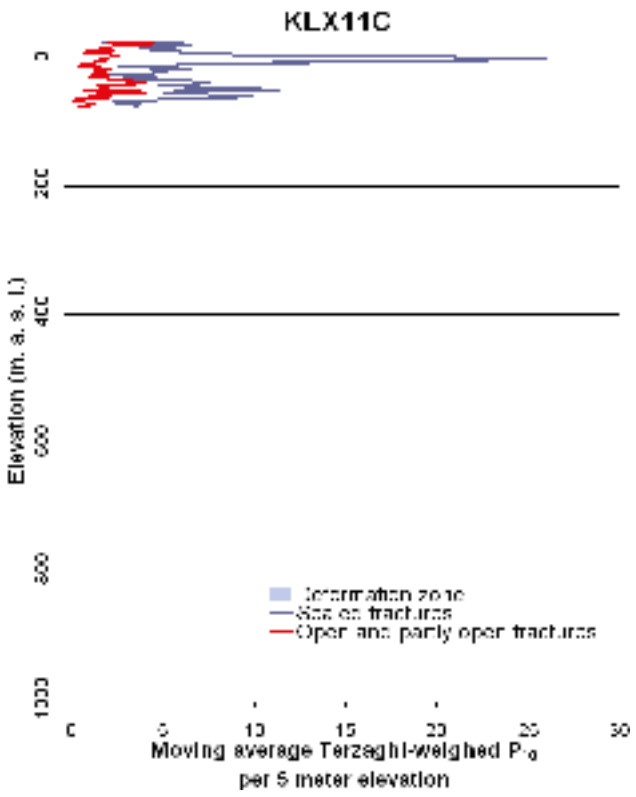
KLX11C
Elevation (m. a. s. l.)
Deformation zone
Sealed fractures
Open and partly open fractures
Moving average Terzaghi-weighed P10
per 5 meter elevation

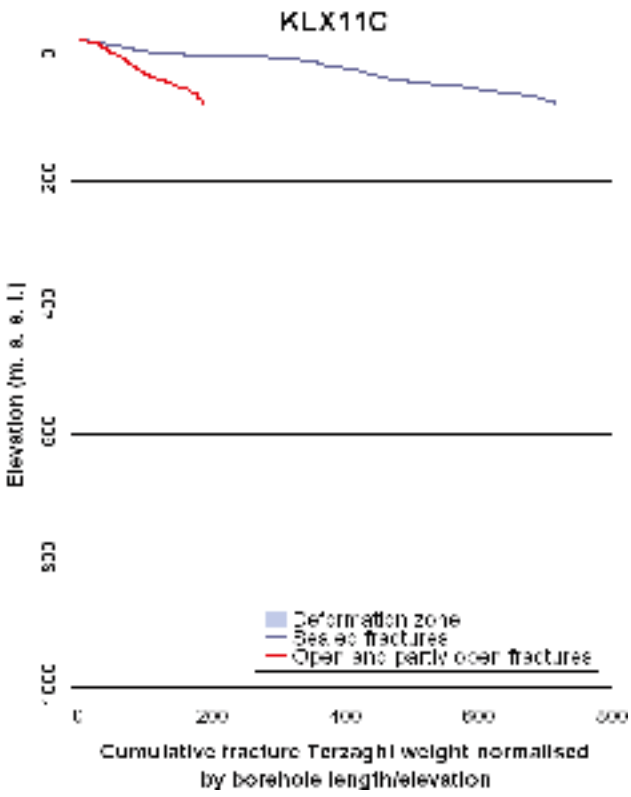
KLX11C
Elevation (m. a. s. l.)
Deformation zone
Sealed fractures
Open and partly open fractures
Cumulative fracture Terzaghi weight normalised
by borehole length/elevation

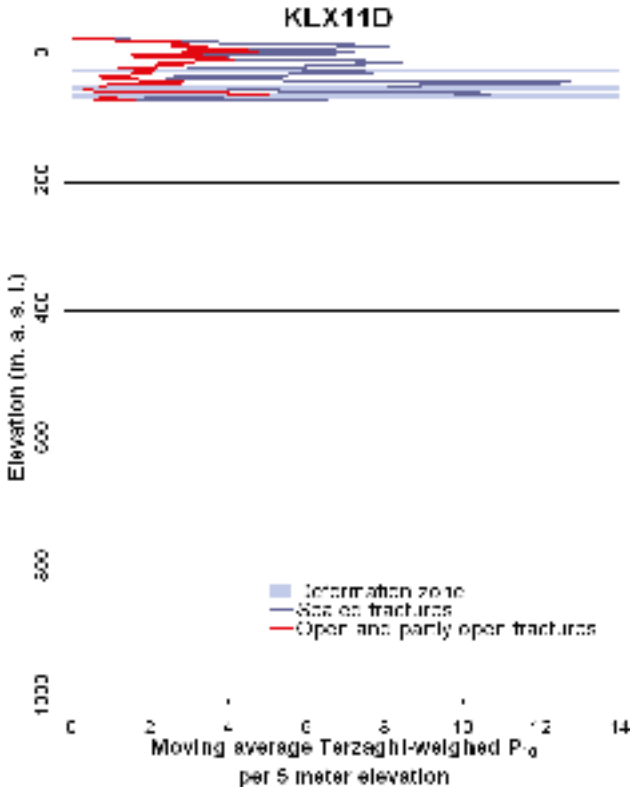
KLX11D
Elevation (m. a. s. l.)
Deformation zone
Sealed fractures
Open and partly open fractures
Moving average Terzaghi-weighed P10
per 5 meter elevation

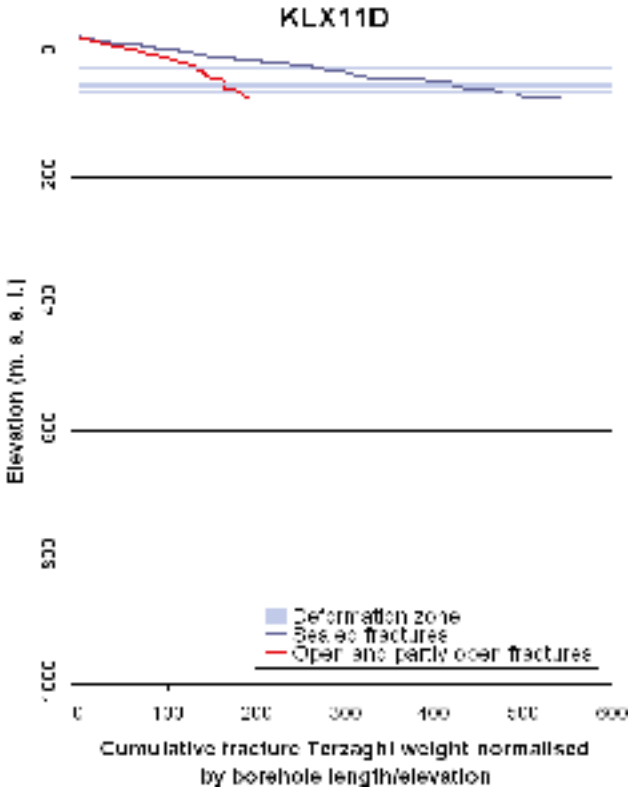
KLX11D
Elevation (m. a. s. l.)
Deformation zone
Sealed fractures
Open and partly open fractures
Cumulative fracture Terzaghi weight normalised
by borehole length/elevation

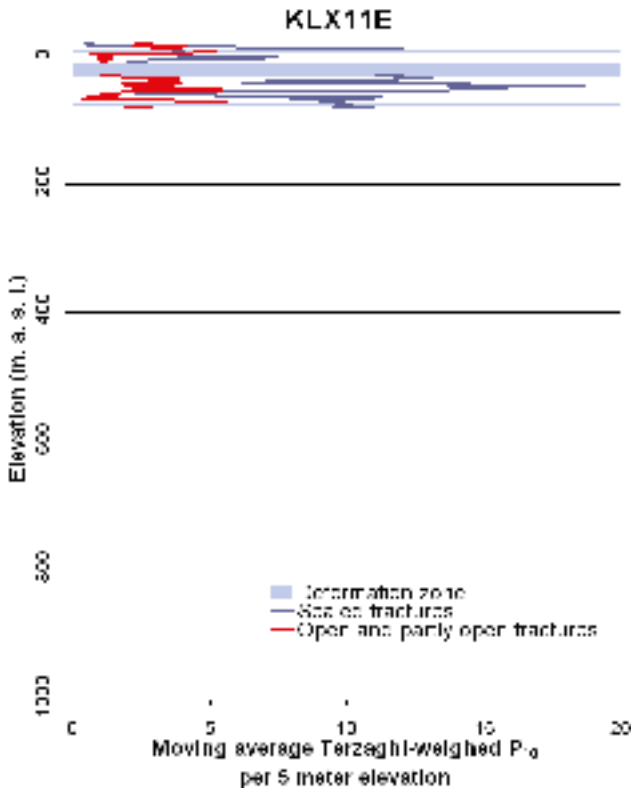
KLX11E
Elevation (m. a. s. l.)
Deformation zone
Sealed fractures
Open and partly open fractures
Moving average Terzaghi-weighed P10
per 5 meter elevation

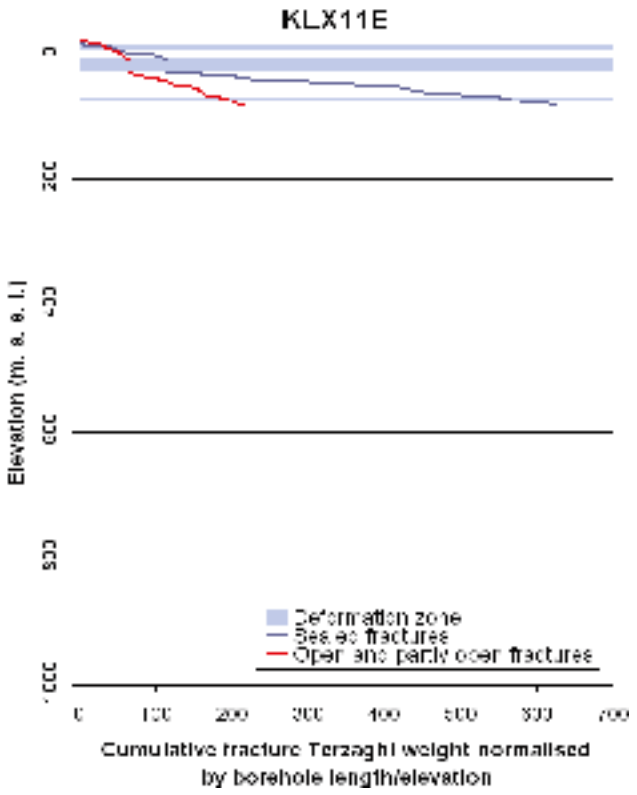
KLX11E
Elevation (m. a. s. l.)
Deformation zone
Sealed fractures
Open and partly open fractures
Cumulative fracture Terzaghi weight normalised
by borehole length/elevation

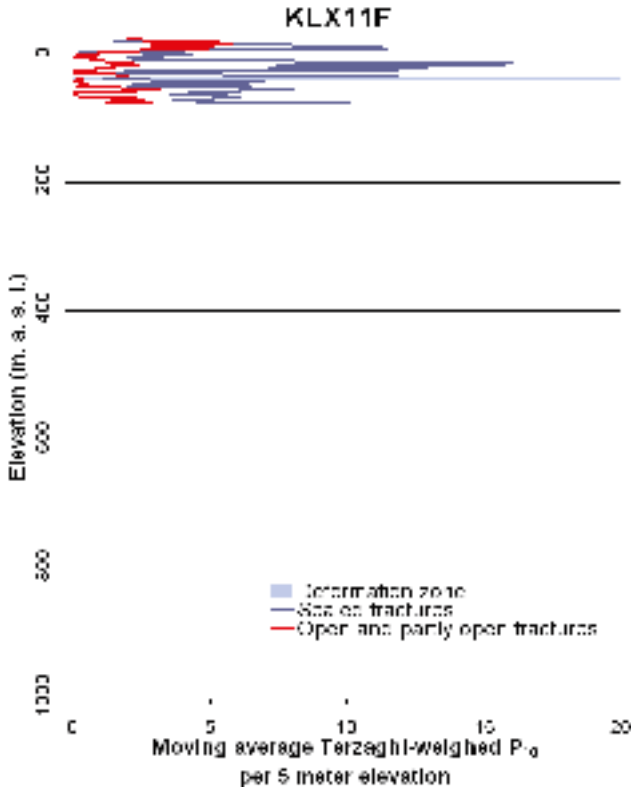
KLX11F
Elevation (m. a. s. l.)
Deformation zone
Sealed fractures
Open and partly open fractures
Moving average Terzaghi-weighed P10
per 5 meter elevation

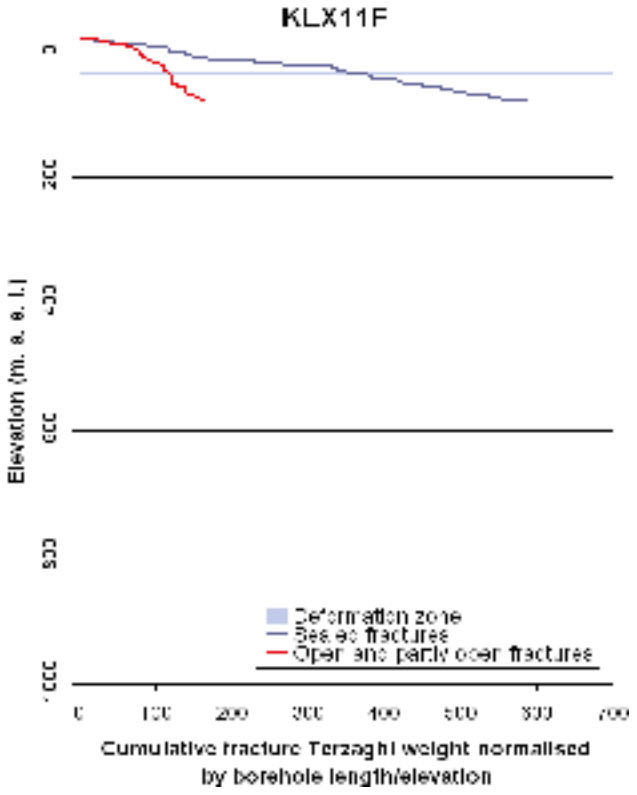
KLX11F
Elevation (m. a. s. l.)
Deformation zone
Sealed fractures
Open and partly open fractures
Cumulative fracture Terzaghi weight normalised
by borehole length/elevation

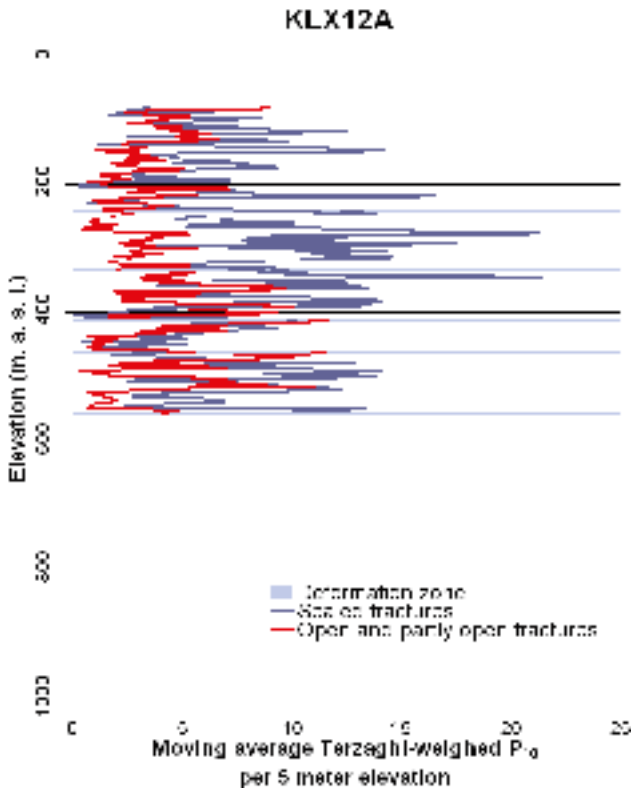
KLX12A
Elevation (m. a. s. l.)
Deformation zone
Sealed fractures
Open and partly open fractures
Moving average Terzaghi-weighed P10
per 5 meter elevation

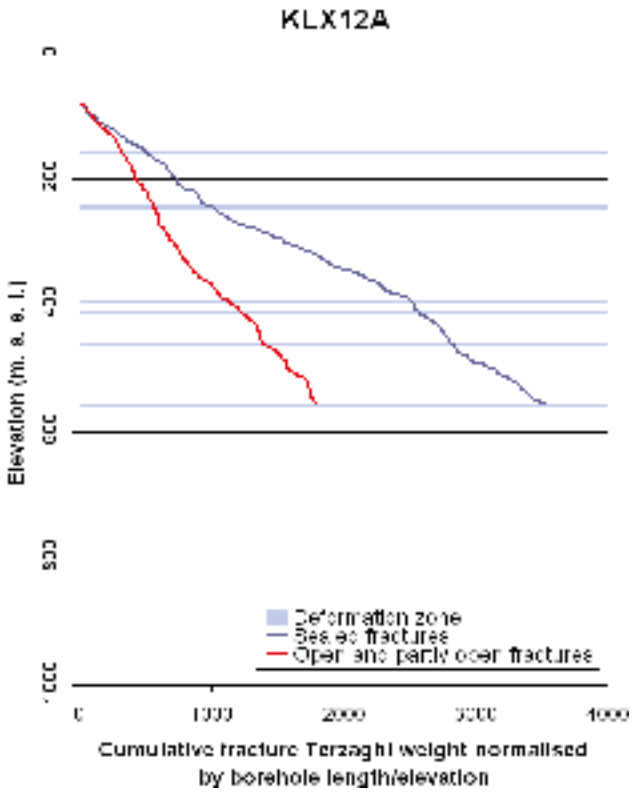
KLX12A
Elevation (m. a. s. l.)
Deformation zone
Sealed fractures
Open and partly open fractures
Cumulative fracture Terzaghi weight normalised
by borehole length/elevation

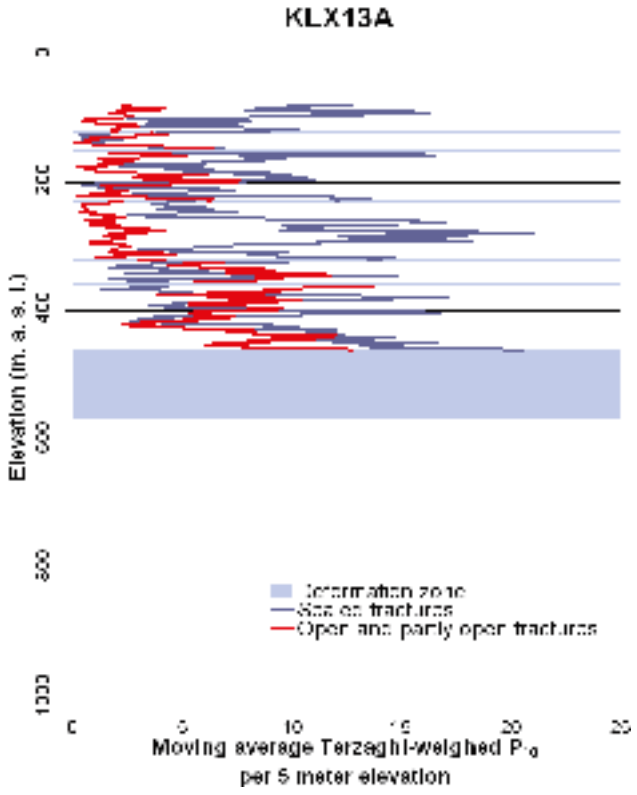
KLX13A
Elevation (m. a. s. l.)
Deformation zone
Sealed fractures
Open and partly open fractures
Moving average Terzaghi-weighed P10
per 5 meter elevation

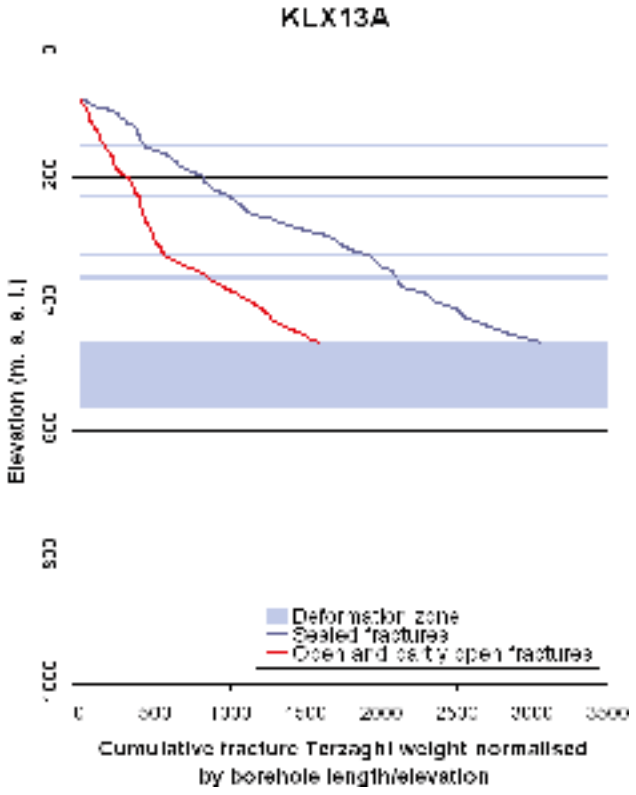
KLX13A
Elevation (m. a. s. l.)
Deformation zone
Sealed fractures
Open and partly open fractures
Cumulative fracture Terzaghi weight normalised
by borehole length/elevation

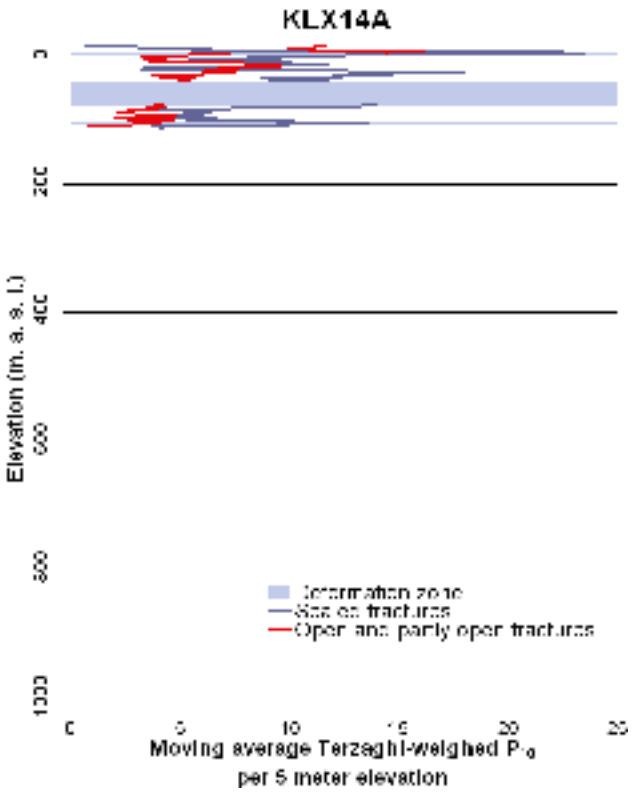
KLX14A
Elevation (m. a. s. l.)
Moving average Terzaghi-weighed P10
per 5 meter elevation

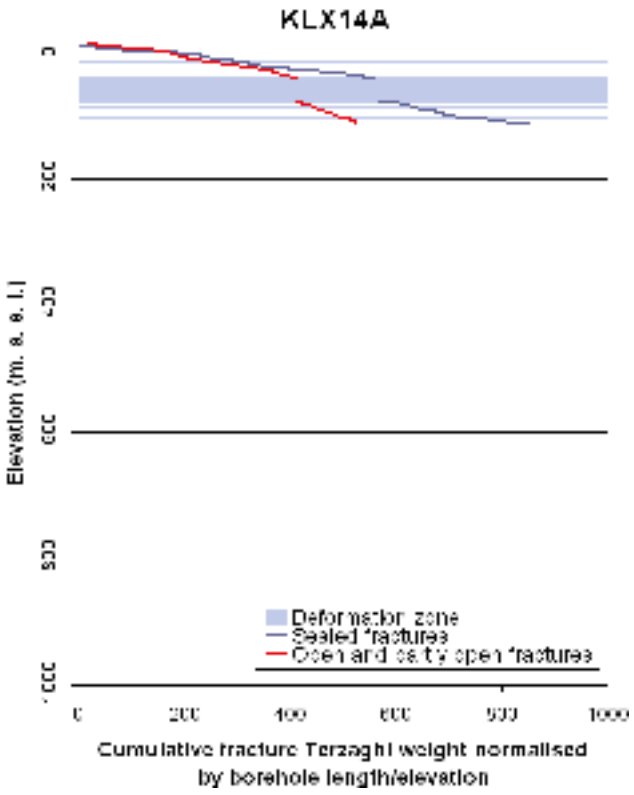
KLX14A
Elevation (m. a. s. l.)
Deformation zone
Sealed fractures
Open and partly open fractures
Cumulative fracture Terzaghi weight normalised
by borehole length/elevation

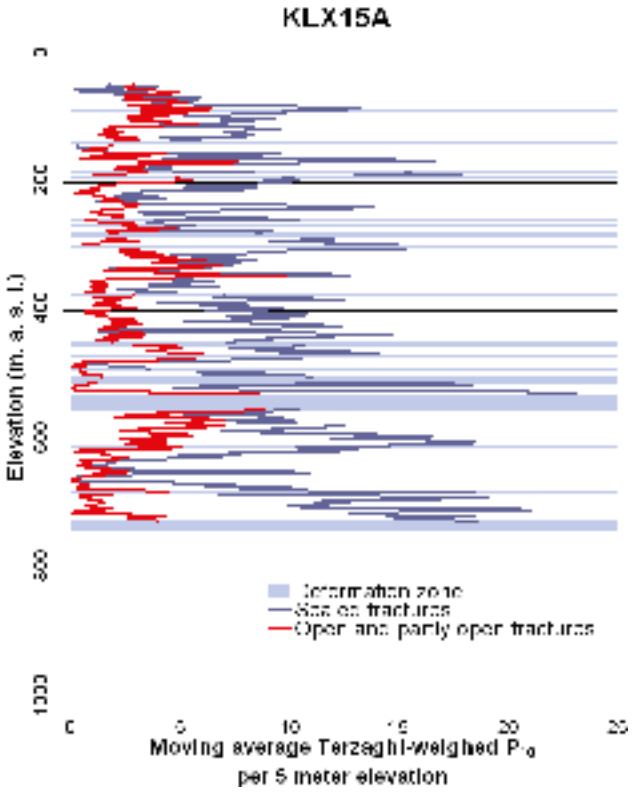
KLX15A
Elevation (m. a. s. l.)
Moving average Terzaghi-weighed P10
per 5 meter elevation

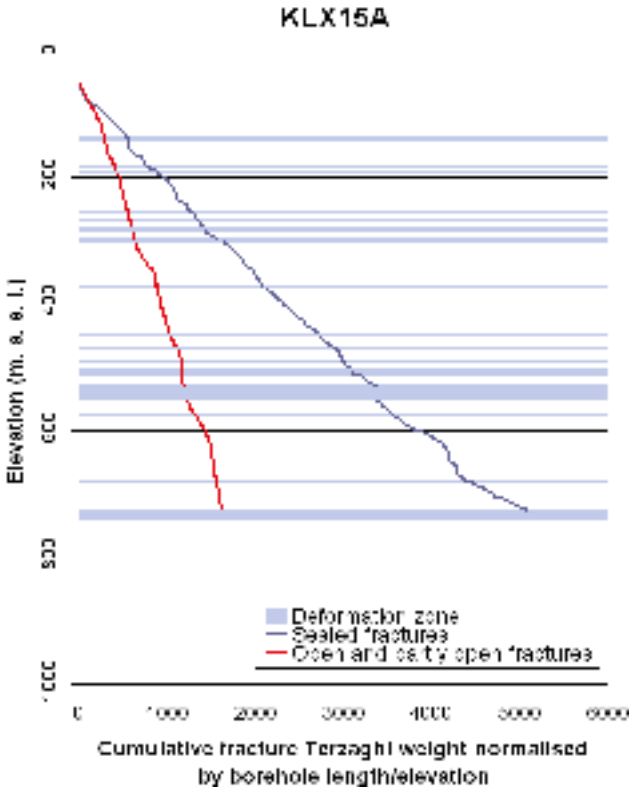
KLX15A
Elevation (m. a. s. l.)
Deformation zone
Sealed fractures
Open and partly open fractures
Cumulative fracture Terzaghi weight normalised
by borehole length/elevation

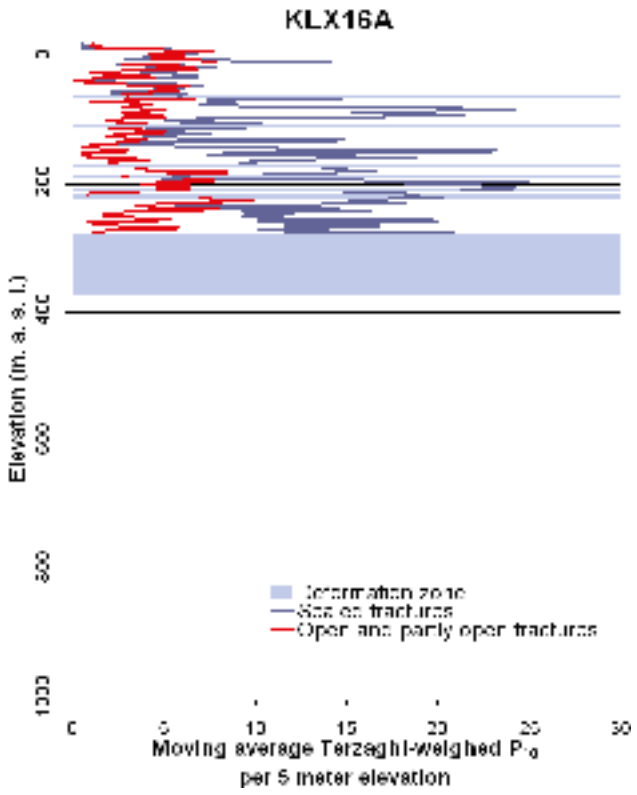
KLX16A
Elevation (m. a. s. l.)
Moving average Terzaghi-weighed P10
per 5 meter elevation

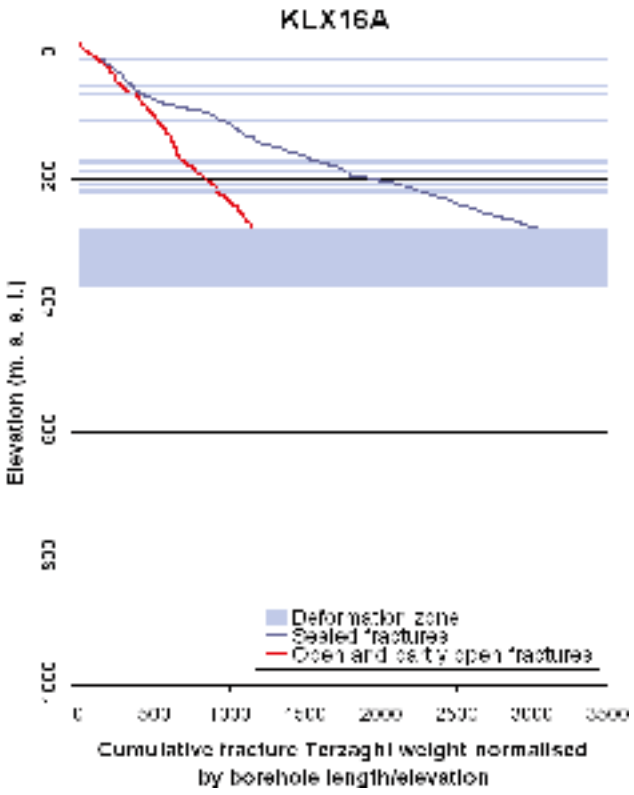
KLX16A
Elevation (m. a. s. l.)
Deformation zone
Sealed fractures
Open and partly open fractures
Cumulative fracture Terzaghi weight normalised
by borehole length/elevation

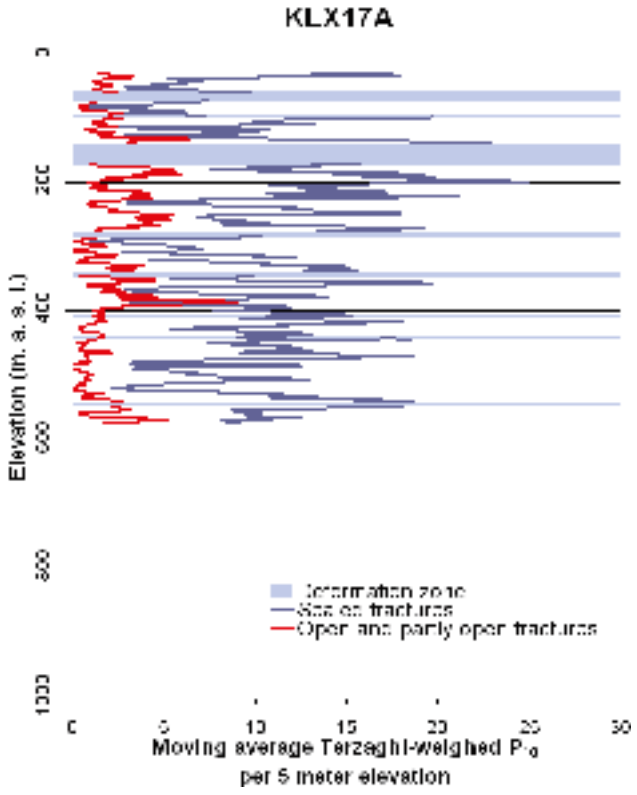
KLX17A
Elevation (m. a. s. l.)
Moving average Terzaghi-weighed P10
per 5 meter elevation

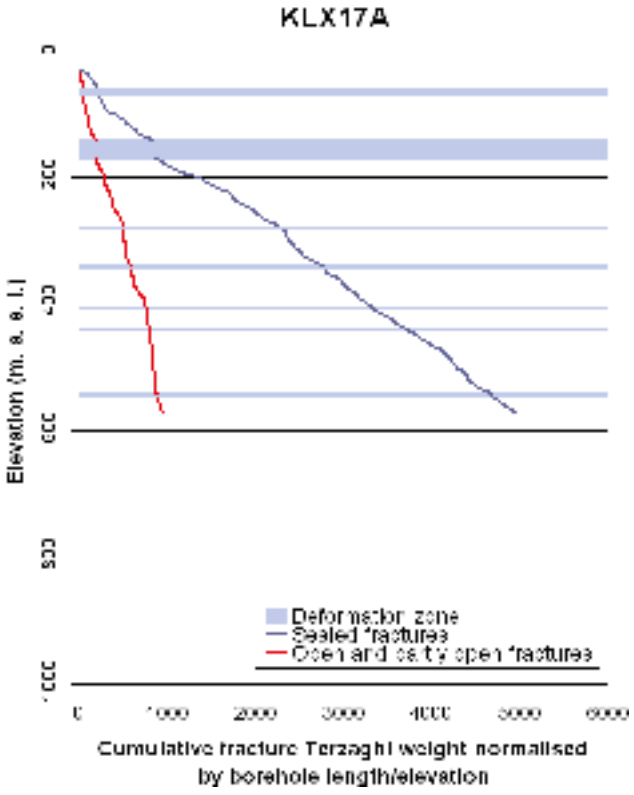
KLX17A
Elevation (m. a. s. l.)
Deformation zone
Sealed fractures
Open and partly open fractures
Cumulative fracture Terzaghi weight normalised
by borehole length/elevation

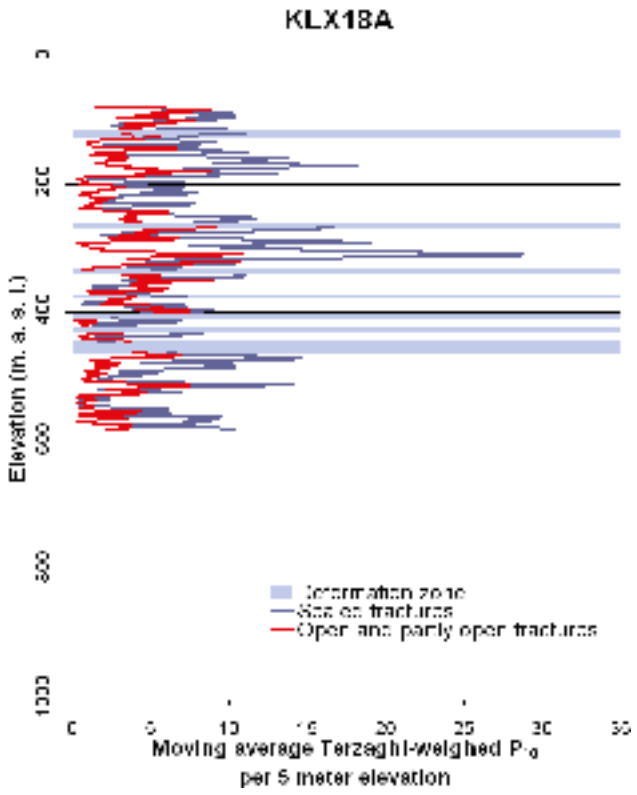
KLX18A
Elevation (m. a. s. l.)
Moving average Terzaghi-weighed P10
per 5 meter elevation

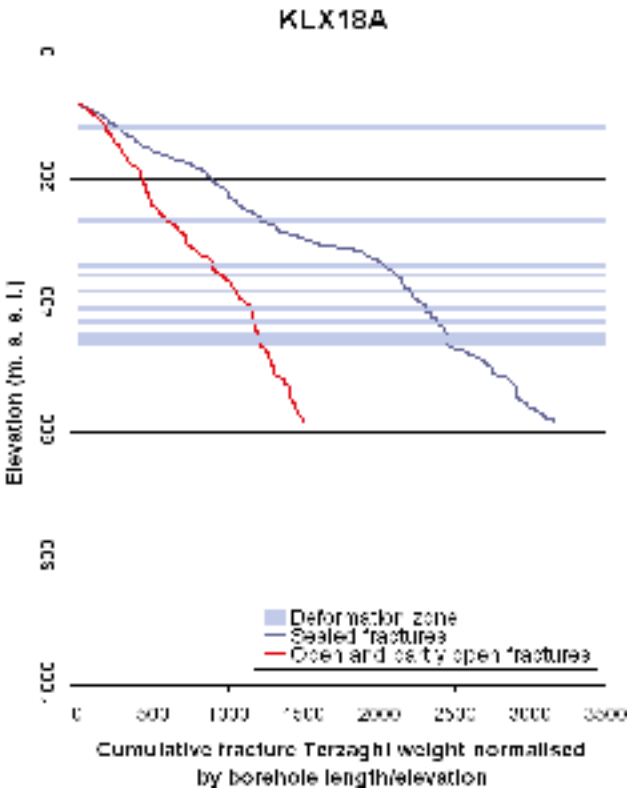
KLX18A
Elevation (m. a. s. l.)
Deformation zone
Sealed fractures
Open and partly open fractures
Cumulative fracture Terzaghi weight normalised
by borehole length/elevation

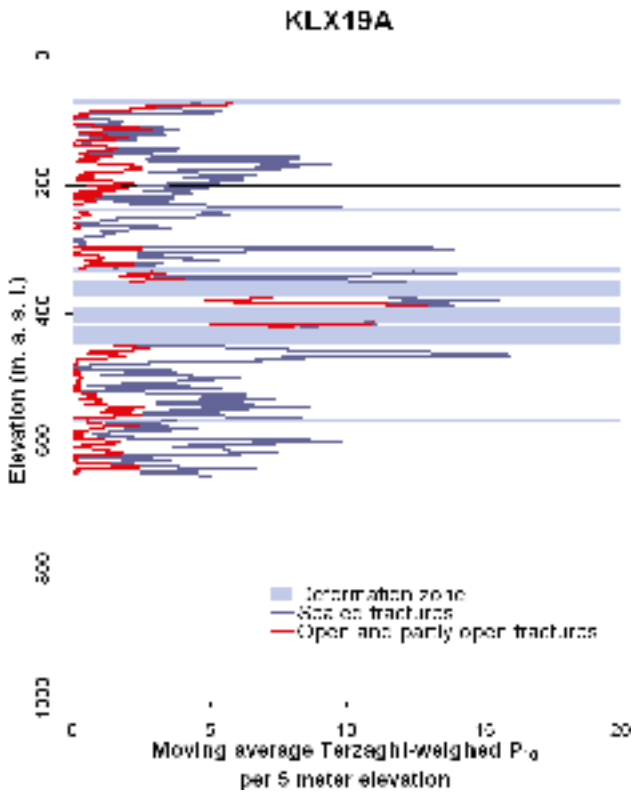
KLX19A
Elevation (m. a. s. l.)
Deformation zone
Sealed fractures
Open and partly open fractures
Moving average Terzaghi-weighed P10
per 5 meter elevation

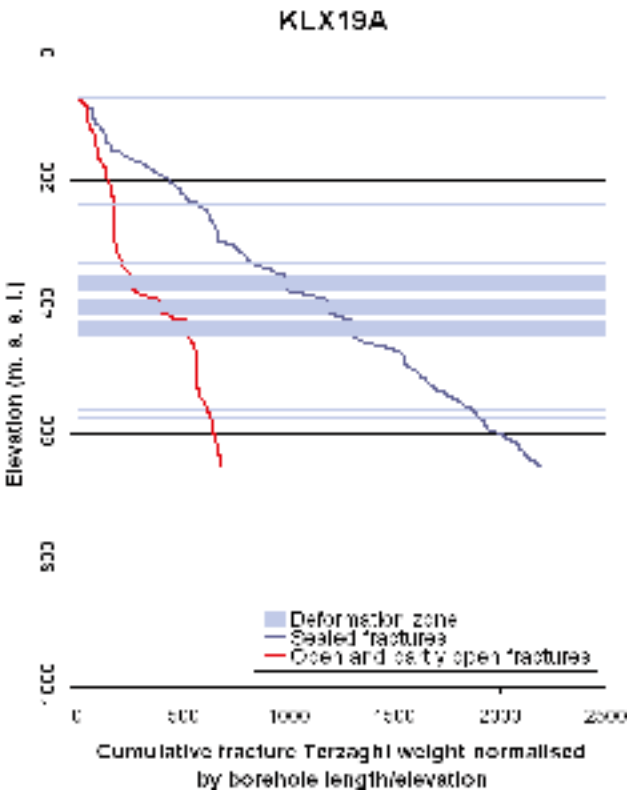
KLX19A
Elevation (m. a. s. l.)
Deformation zone
Sealed fractures
Open and partly open fractures
Cumulative fracture Terzaghi weight normalised
by borehole length/elevation

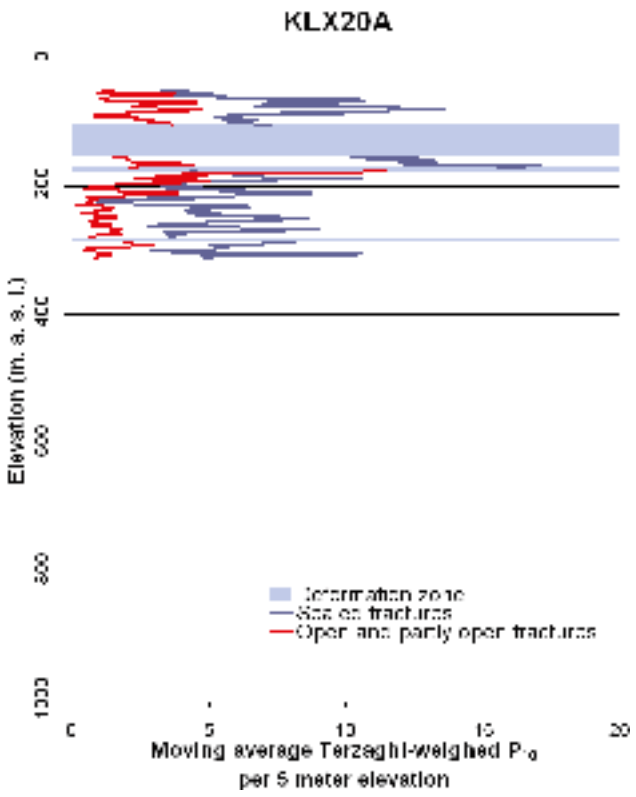
KLX20A
Elevation (m. a. s. l.)
Moving average Terzaghi-weighed P10
per 5 meter elevation

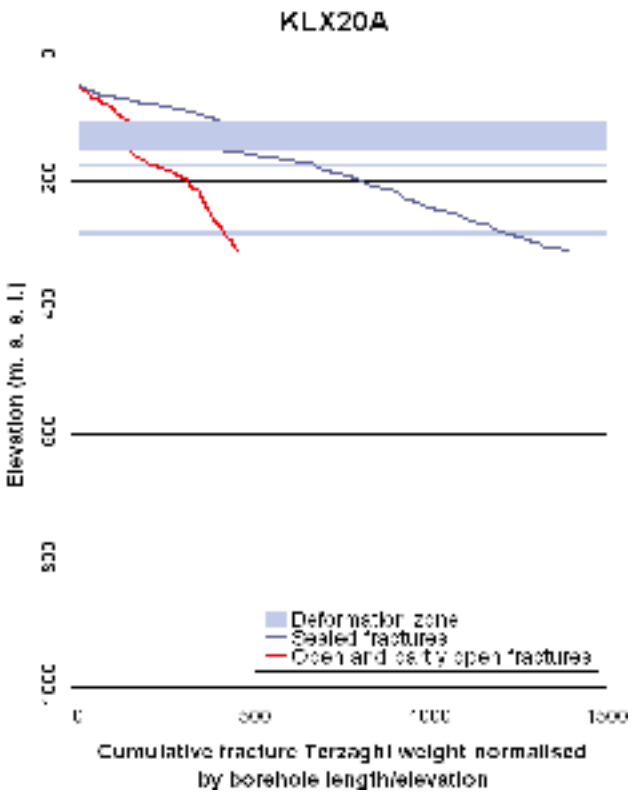
KLX20A
Elevation (m. a. s. l.)
Cumulative fracture Terzaghi weight normalised
by borehole length/elevation

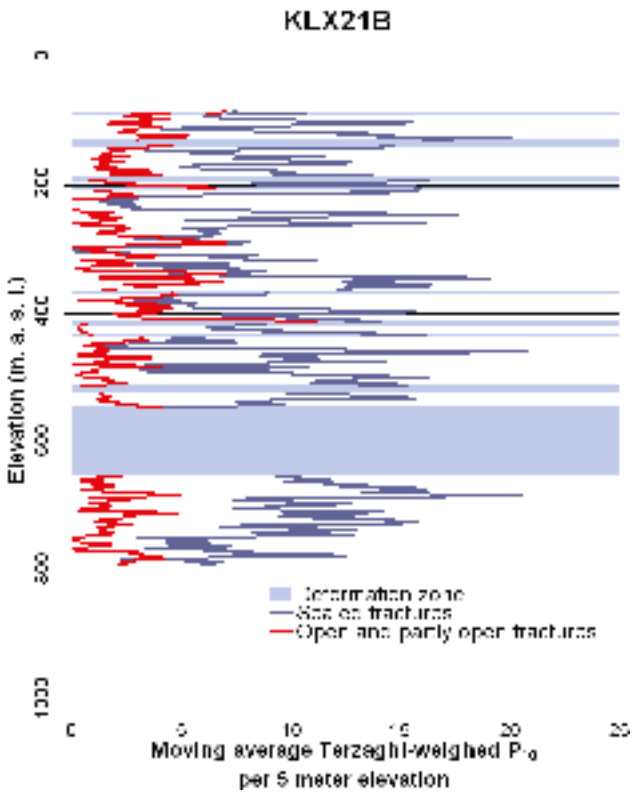
KLX21B
Elevation (m. a. s. l.)
Moving average Terzaghi-weighed P10
per 5 meter elevation

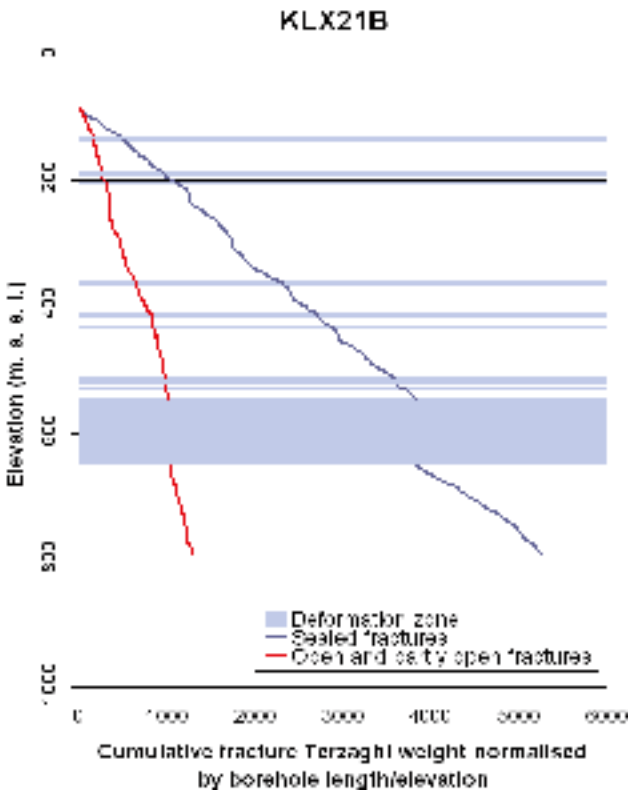
KLX21B
Elevation (m. a. s. l.)
Cumulative fracture Terzaghi weight normalised
by borehole length/elevation

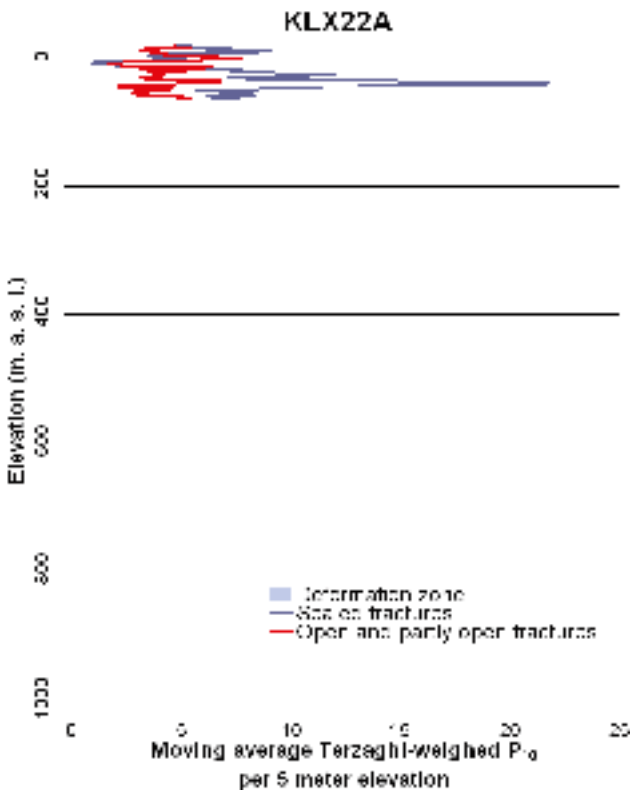
KLX22A
Elevation (m. a. s. l.)
Moving average Terzaghi-weighed P10
per 5 meter elevation
Deformation zone
Sealed fractures
Open and partly open fractures

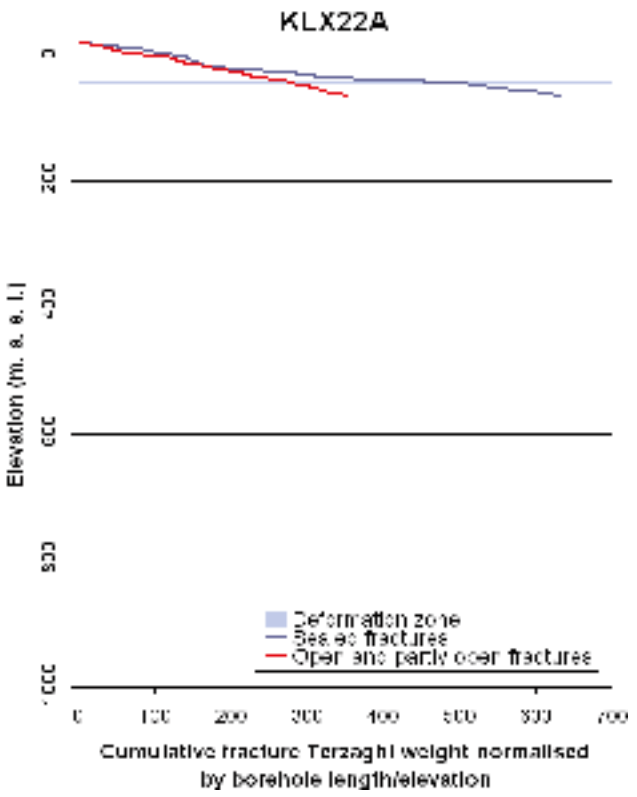
KLX22A
Elevation (m. a. s. l.)
Cumulative fracture Terzaghi weight normalised
by borehole length/elevation
Deformation zone
Sealed fractures
Open and partly open fractures

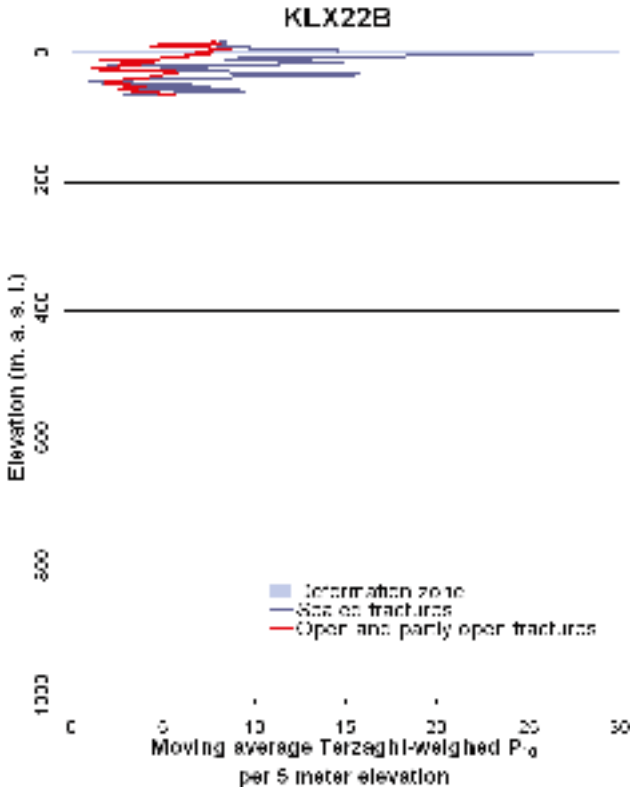
KLX22B
Elevation (m. a. s. l.)
Moving average Terzaghi-weighed P10
per 5 meter elevation
Deformation zone
Sealed fractures
Open and partly open fractures

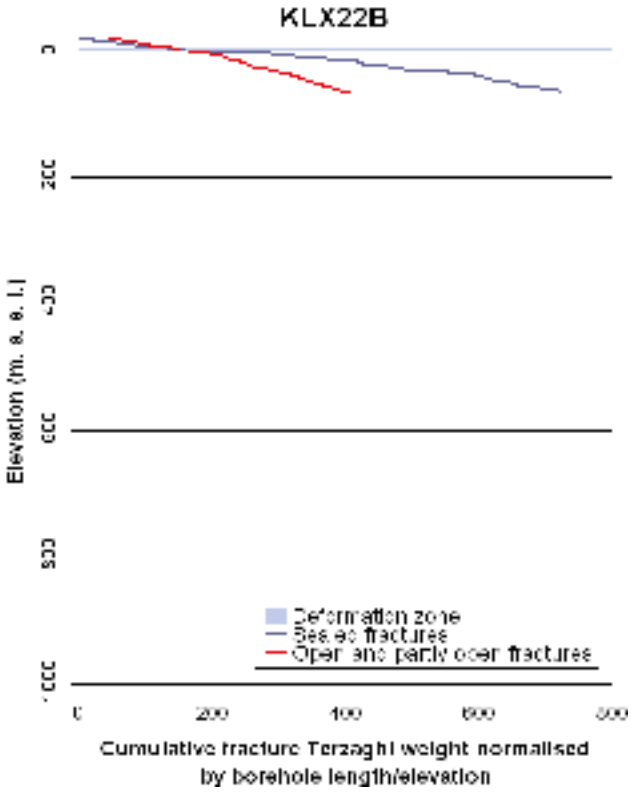
KLX22B
Elevation (m. a. s. l.)
Cumulative fracture Terzaghi weight normalised
by borehole length/elevation
Deformation zone
Sealed fractures
Open and partly open fractures

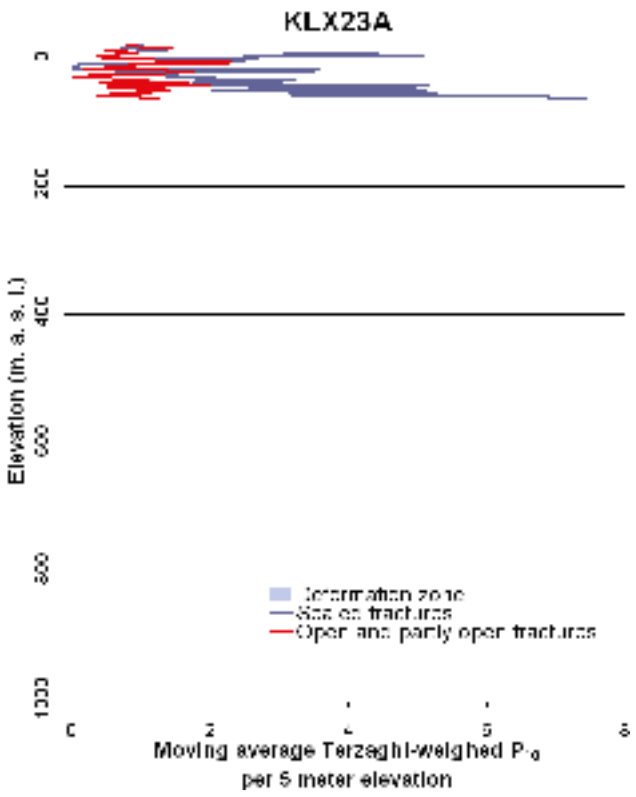
KLX23A
Elevation (m. a. s. l.)
Deformation zone
Sealed fractures
Open and partly open fractures
Moving average Terzaghi-weighed P10
per 5 meter elevation

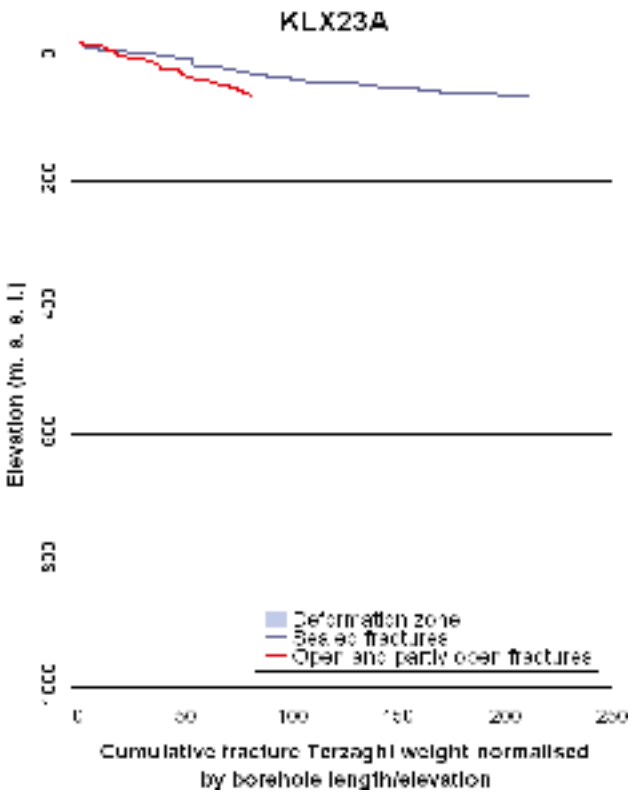
KLX23A
Elevation (m. a. s. l.)
Deformation zone
Sealed fractures
Open and partly open fractures
Cumulative fracture Terzaghi weight normalised
by borehole length/elevation

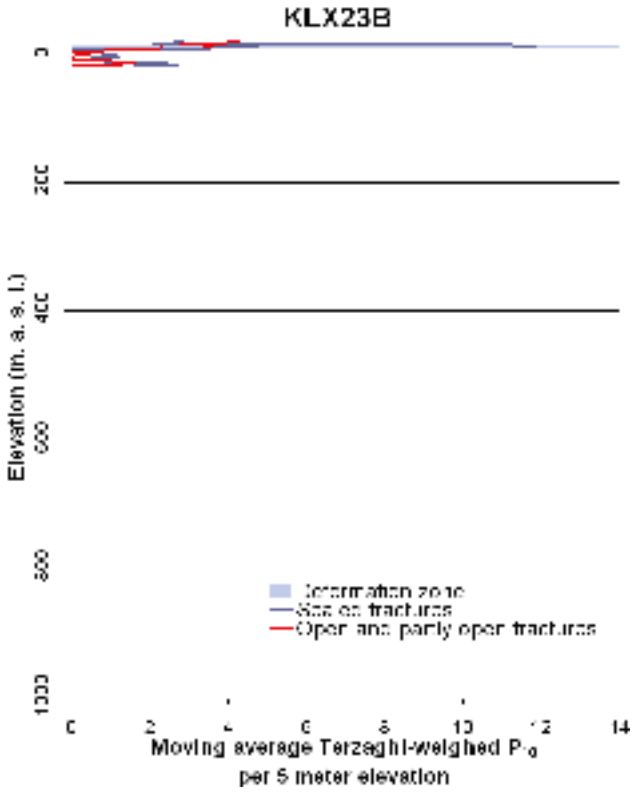
KLX23B
Elevation (m. a. s. l.)
Deformation zone
Sealed fractures
Open and partly open fractures
Moving average Terzaghi-weighed P10
per 5 meter elevation

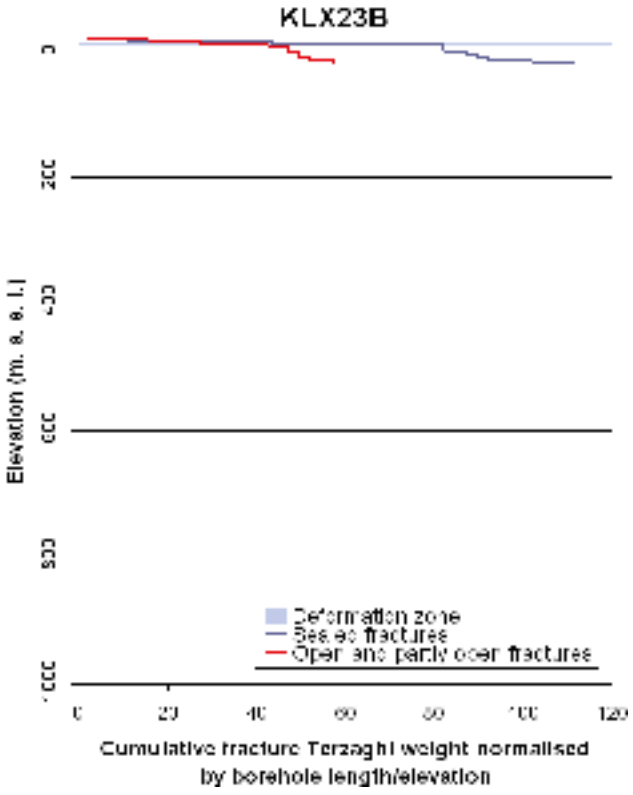
KLX23B
Elevation (m. a. s. l.)
Deformation zone
Sealed fractures
Open and partly open fractures
Cumulative fracture Terzaghi weight normalised
by borehole length/elevation

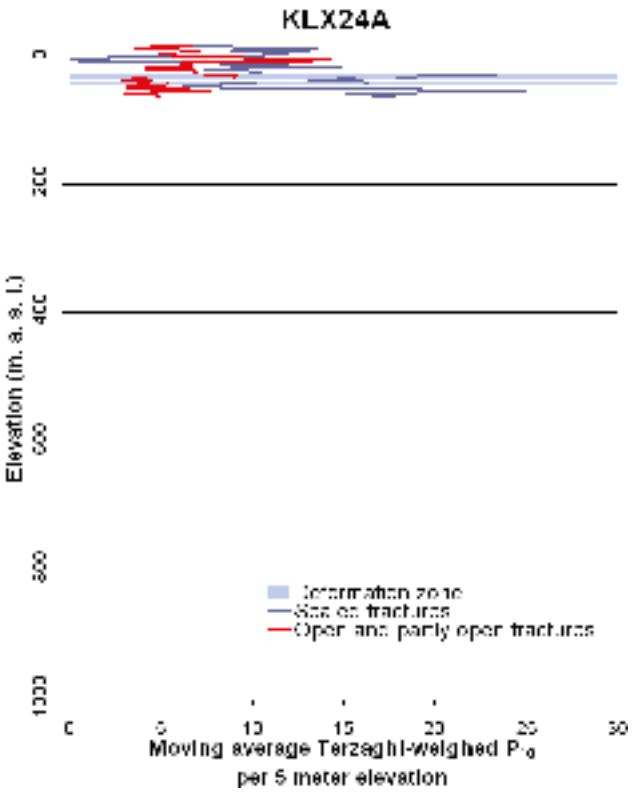
KLX24A
Elevation (m. a. s. l.)
Deformation zone
Sealed fractures
Open and partly open fractures
Moving average Terzaghi-weighed P10
per 5 meter elevation

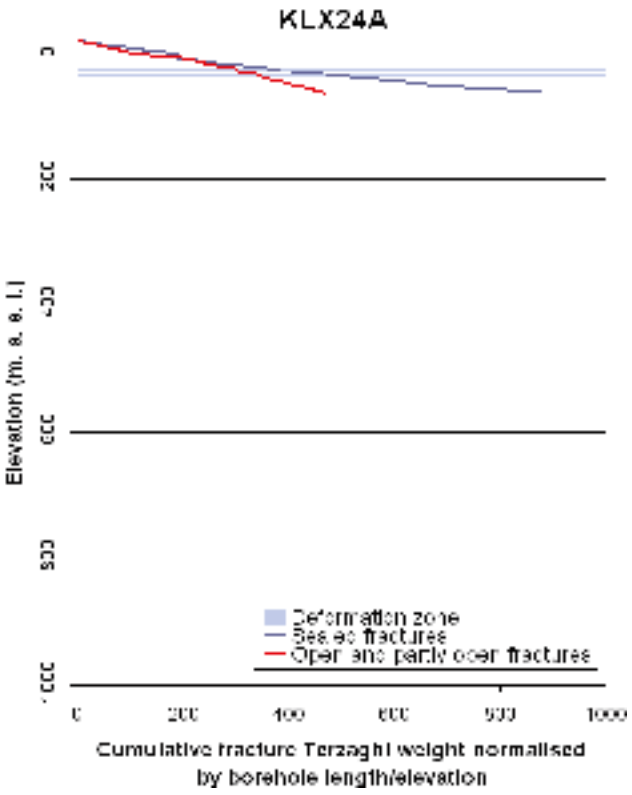
KLX24A
Elevation (m. a. s. l.)
Deformation zone
Sealed fractures
Open and partly open fractures
Cumulative fracture Terzaghi weight normalised
by borehole length/elevation

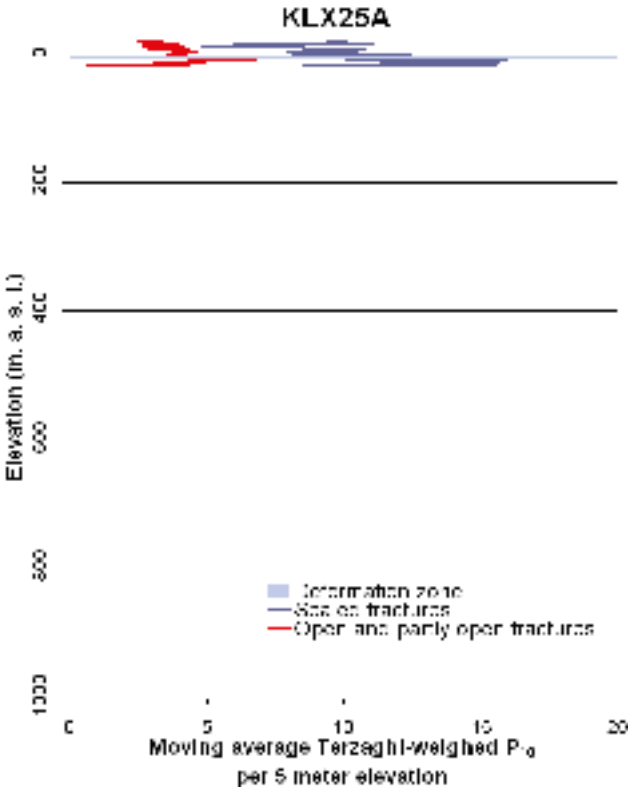
KLX25A
Elevation (m. a. s. l.)
Deformation zone
Sealed fractures
Open and partly open fractures
Moving average Terzaghi-weighed P10
per 5 meter elevation

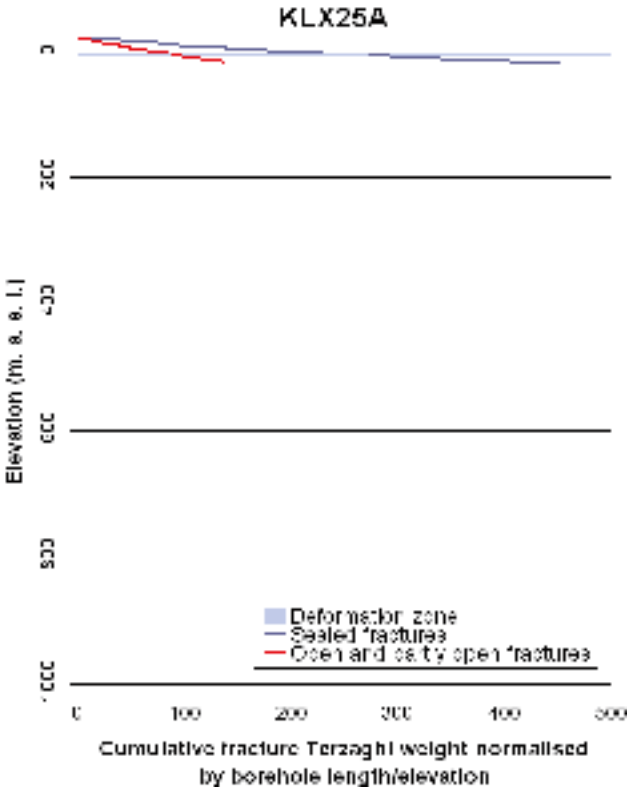
KLX25A
Elevation (m. a. s. l.)
Deformation zone
Sealed fractures
Open and partly open fractures
Cumulative fracture Terzaghi weight normalised
by borehole length/elevation

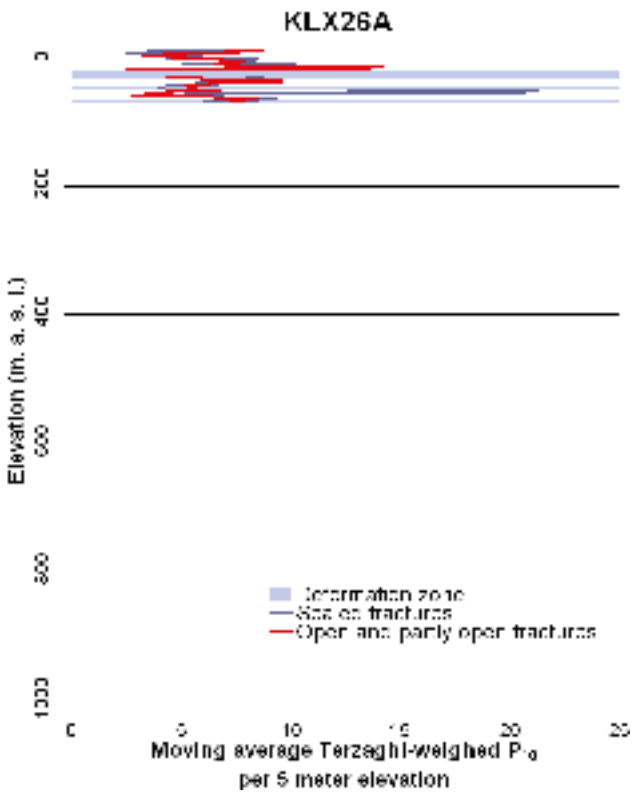
KLX26A
Elevation (m. a. s. l.)
Moving average Terzaghi-weighed P10
per 5 meter elevation

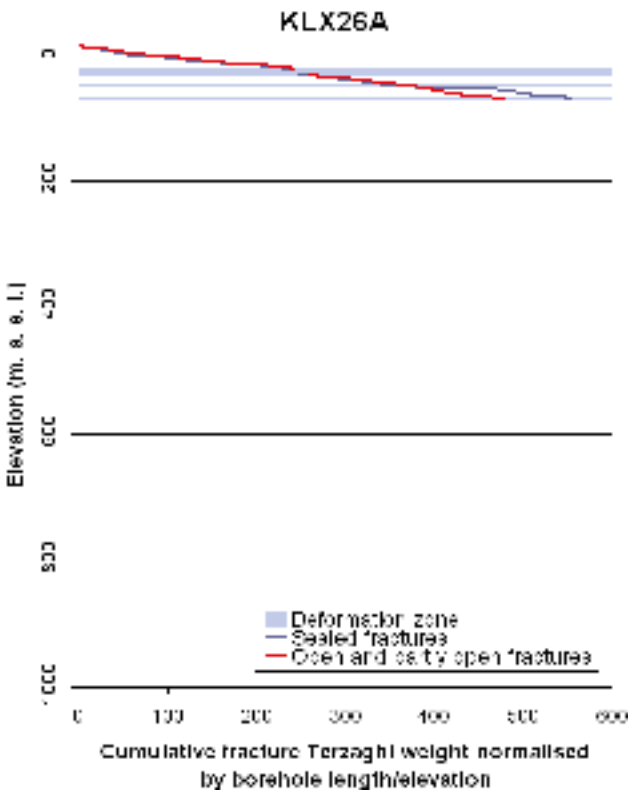
KLX26A
Elevation (m. a. s. l.)
Cumulative fracture Terzaghi weight normalised
by borehole length/elevation

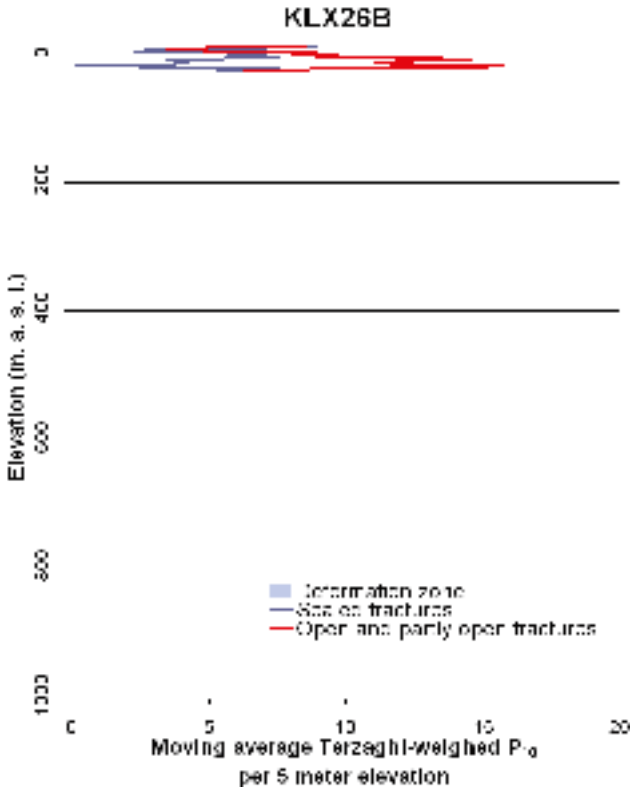
KLX26B
Elevation (m. a. s. l.)
Moving average Terzaghi-weighed P10
per 5 meter elevation

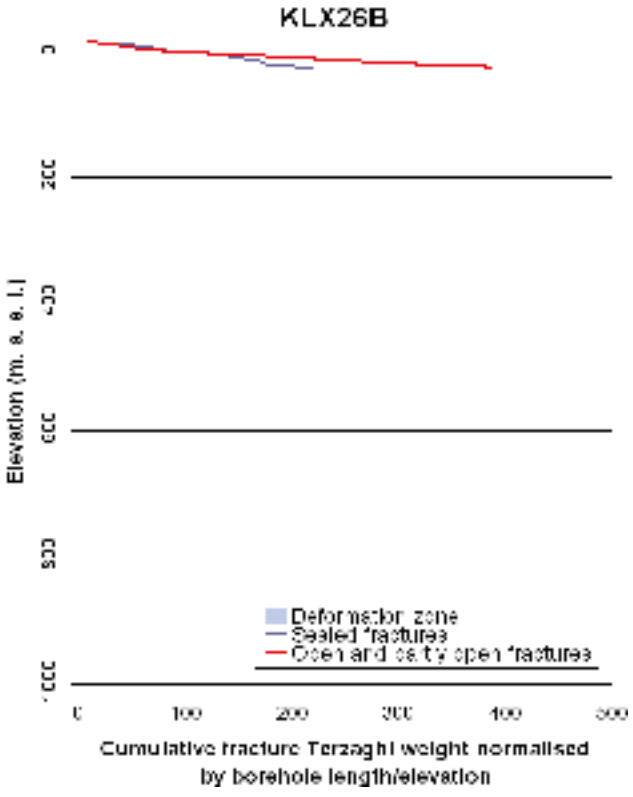
KLX26B
Elevation (m. a. s. l.)
Cumulative fracture Terzaghi weight normalised
by borehole length/elevation

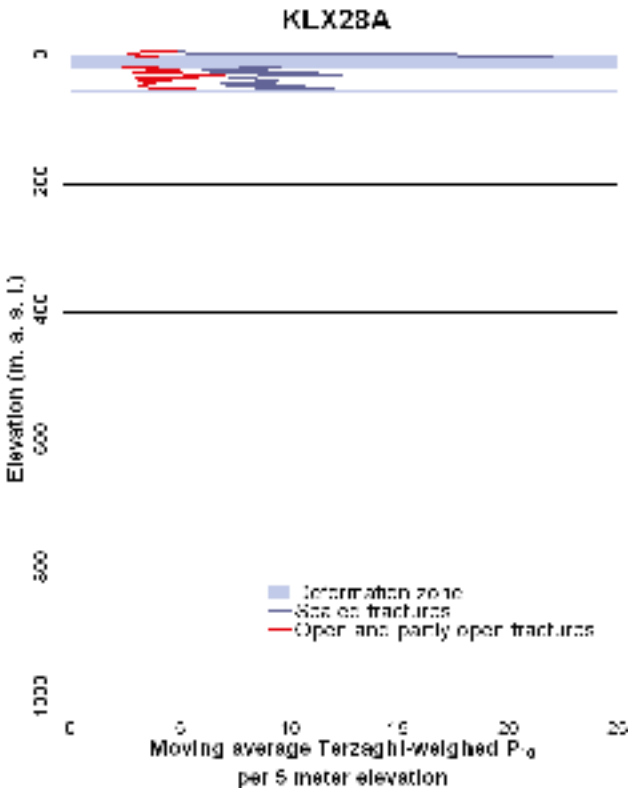
KLX28A
Elevation (m. a. s. l.)
Moving average Terzaghi-weighed P10
per 5 meter elevation

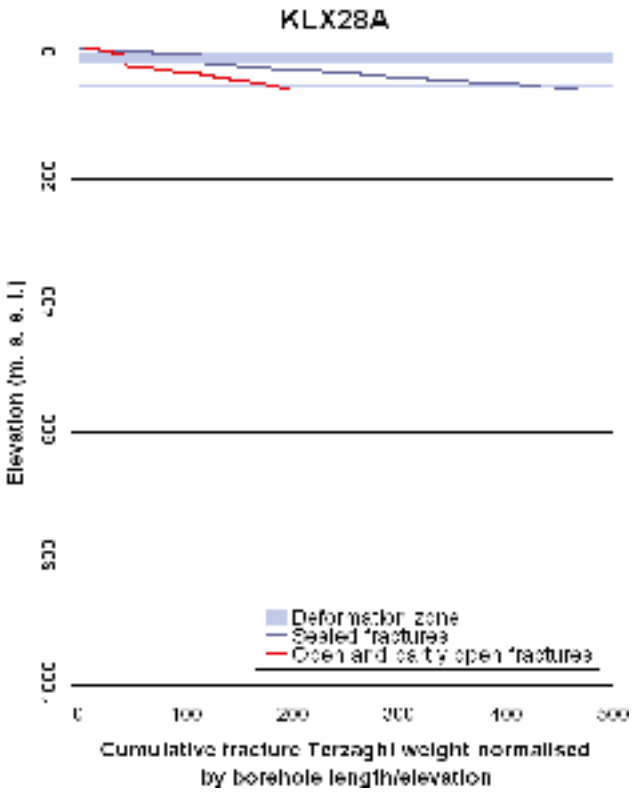
KLX28A
Elevation (m. a. s. l.)
Deformation zone
Sealed fractures
Open and partly open fractures
Cumulative fracture Terzaghi weight normalised
by borehole length/elevation

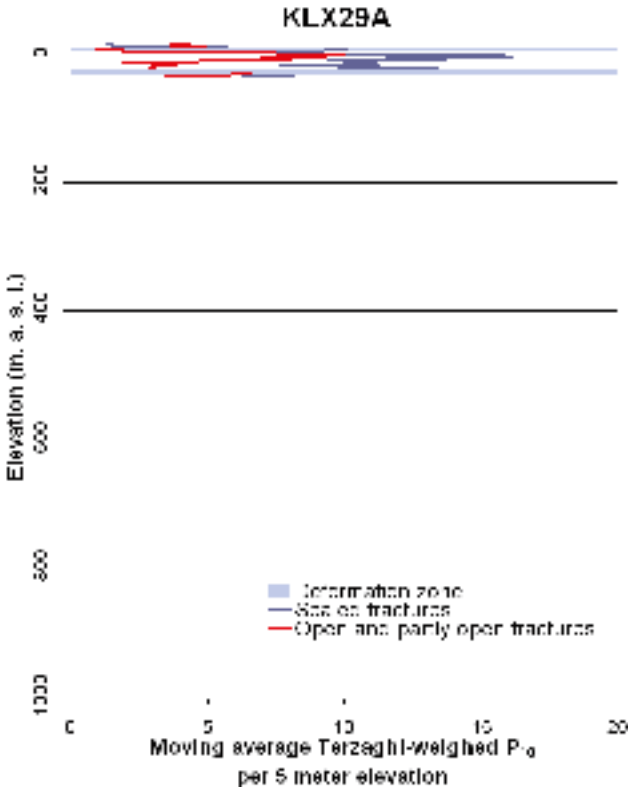
KLX29A
Elevation (m. a. s. l.)
Moving average Terzaghi-weighed P10
per 5 meter elevation

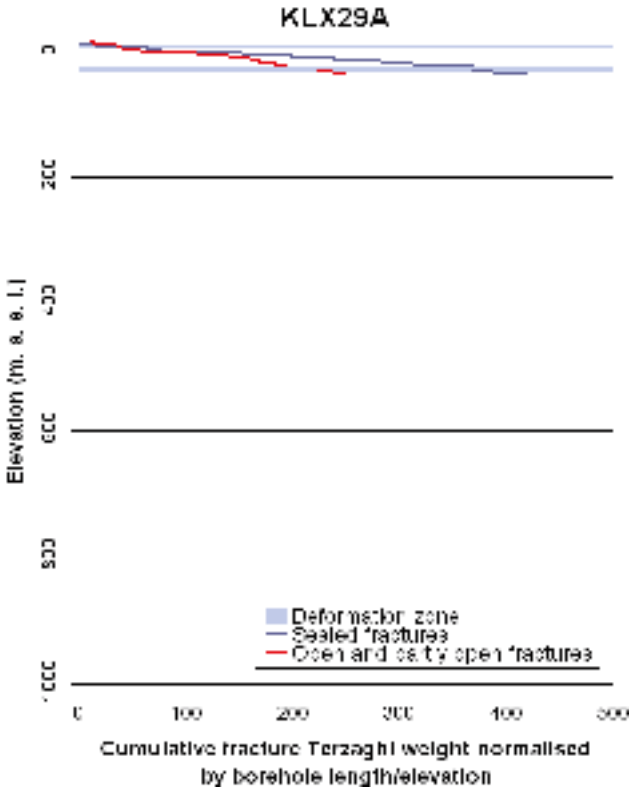
KLX29A
Elevation (m. a. s. l.)
Deformation zone
Sealed fractures
Open and partly open fractures
Cumulative fracture Terzaghi weight normalised
by borehole length/elevation

References

Davy P, Darcel C, Bour O, Munier R, de Dreuzy J R, 2006. A note on the angular correction applied to fracture intensity profiles along drill core. Journal of Geophysical Research, Vol. 111, No. B11408.

La Pointe P, Fox A, Hermanson J, Öhman J, 2008. Geological discrete fracture network model for the Laxemar site. Site Descriptive Modelling, SDM Site Laxemar. SKB R-08-55, Svensk Kärnbränslehantering AB.

Mauldon M, Mauldon J G, 1997. Fracture sampling on a cylinder; from scanlines to boreholes and tunnels, Rock Mechanics and Rock Engineering, Vol. 30, No. 3, pp. 129–144.

Priest S D, 1993. Discontinuity analysis for rock engineering, Chapman & Hall, New York, USA. ISBN 978-0412476006.

Terzaghi R D, 1965. Sources of error in joint surveys. Geotechnique, Vol. 15, pp. 287–304

Yow J L, 1987. Technical Note: Blind zones in the acquisition of discontinuity orientation data, International Journal of Rock Mechanics and Mining Science and Geomechanics Abstracts, Vol. 24, No. 5, pp. 317–318.

Appendix 5a

Fracture orientation in boreholes (Kamb contouring)

Fracture orientations have been plotted for each cored borehole in Laxemar. The compilation is intended for users who would like to review fracture orientation borehole by borehole. Each stereoplot shows total fracture orientation (open and sealed) outside deformation zones identified in the extended single hole interpretation. The stereoplots shows fracture orientations as pole plots on lower hemisphere, equal area Schmidt projections using Kamp contouring /Kamb 1959/.

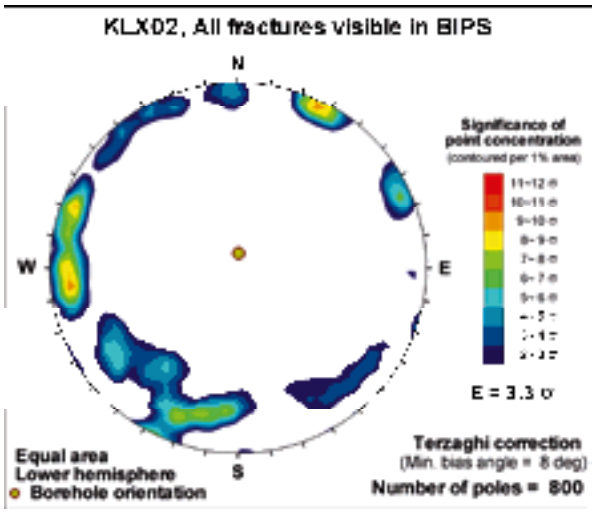
KLX02, All fractures visible in BIPS
N
W
E
S
Significance of point concentration
(contoured per 1% area)
E = 3.3 σ
Equal area
Lower hemisphere
Borehole orientation
Terzaghi correction
(Min. bias angle = 8 deg)
Number of poles = 800

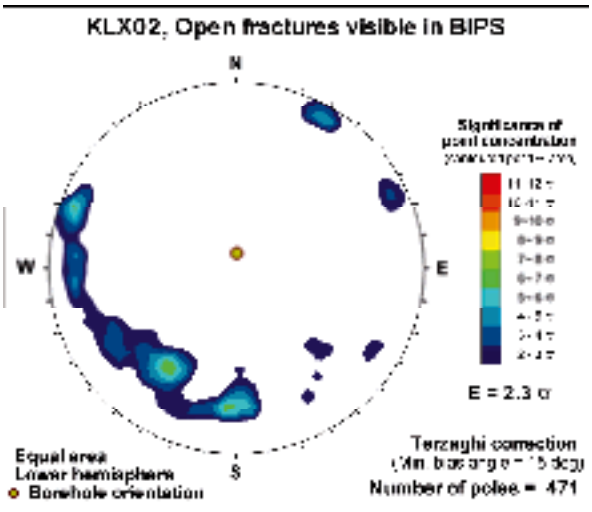
KLX02, Open fractures visible in BIPS
N
W
E
S
E = 2.3 σ
Equal area
Lower hemisphere
Borehole orientation
Number of poles = 471

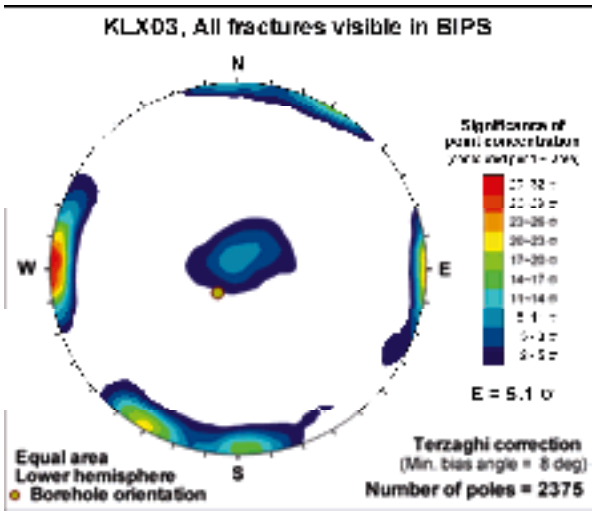
KLX03, All fractures visible in BIPS
N
W
E
S
E = 5.1 σ
Equal area
Lower hemisphere
Borehole orientation
Terzaghi correction
(Min. bias angle = 8 deg)
Number of poles = 2375

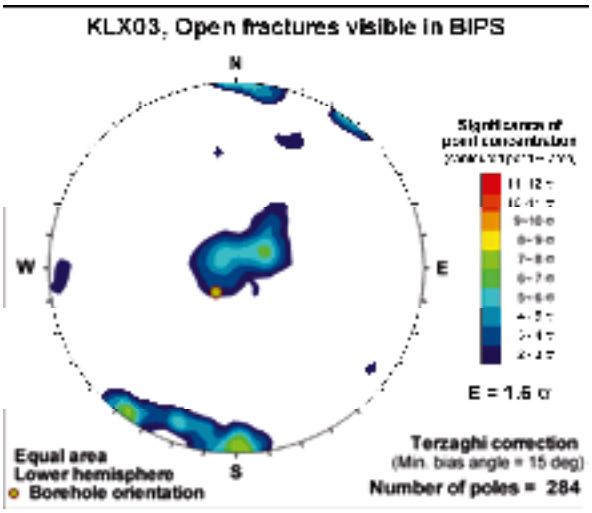
KLX03, Open fractures visible in BIPS
N
W
E
S
E = 1.6 σ
Equal area
Lower hemisphere
Borehole orientation
Terzaghi correction
(Min. bias angle = 15 deg)
Number of poles = 284

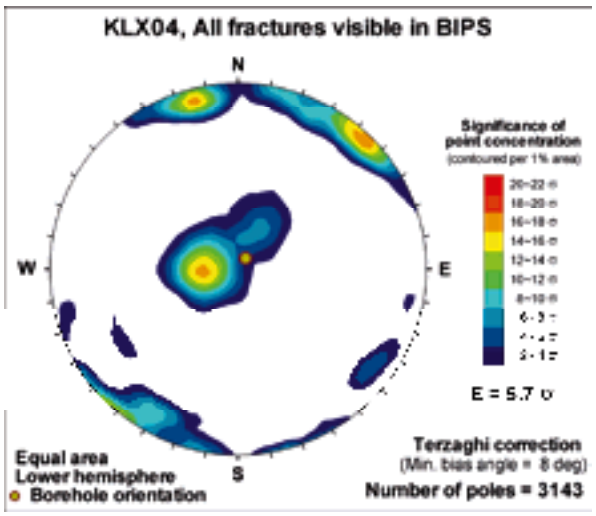
KLX04, All fractures visible in BIPS
N
W
E
S
Significance of point concentration
(contoured per 1% area)
E = 5.7 σ
Equal area
Lower hemisphere
Borehole orientation
Terzaghi correction
(Min. bias angle = 8 deg)
Number of poles = 3143

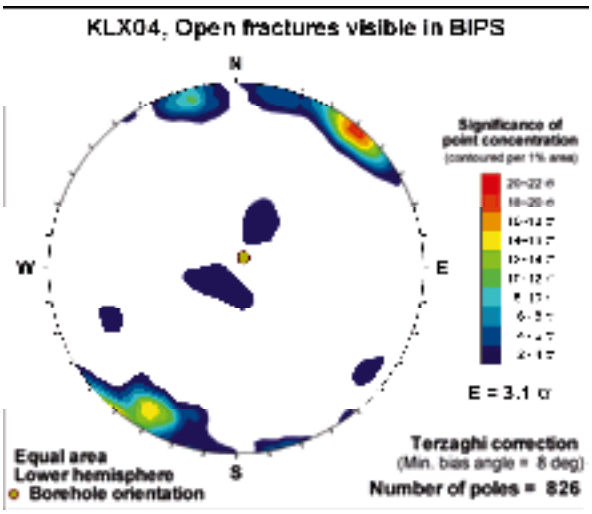
KLX04, Open fractures visible in BIPS
N
W
E
S
E = 3.1 σ
Equal area
Lower hemisphere
Borehole orientation
Terzaghi correction
(Min. bias angle = 8 deg)
Number of poles = 826

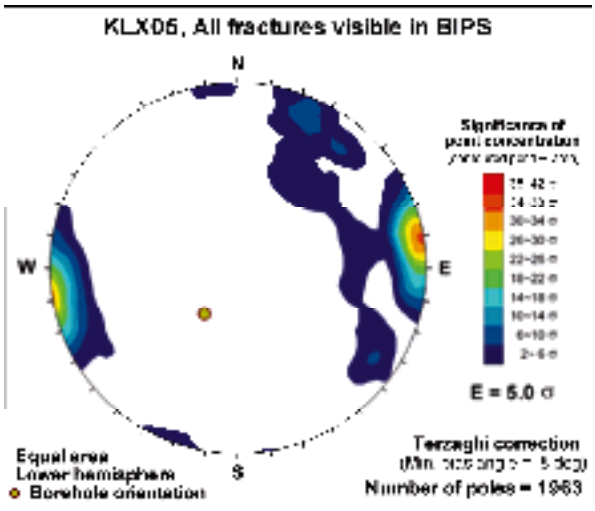
KLX06, All fractures visible in BIPS
N
W
E
S
Significance of point concentration
E = 5.0 σ
Terzaghi correction
Number of poles = 1963
Equal area
Lower hemisphere
Borehole orientation

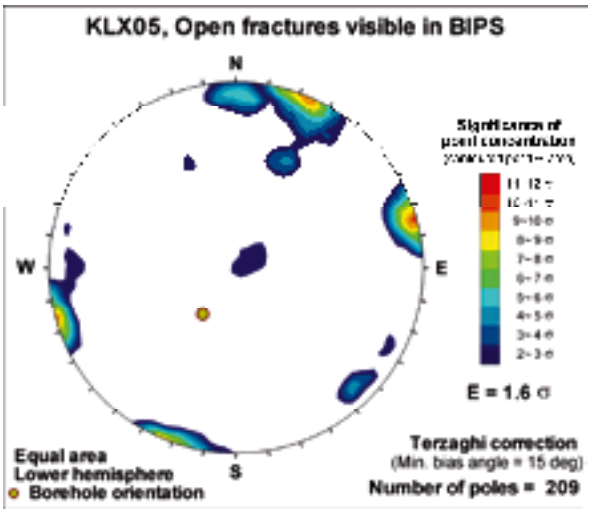
KLX05, Open fractures visible in BIPS
N
W
E
S
Significance of point concentration
E = 1.6 σ
Terzaghi correction
(Min. bias angle = 15 deg)
Number of poles = 209
Equal area
Lower hemisphere
Borehole orientation

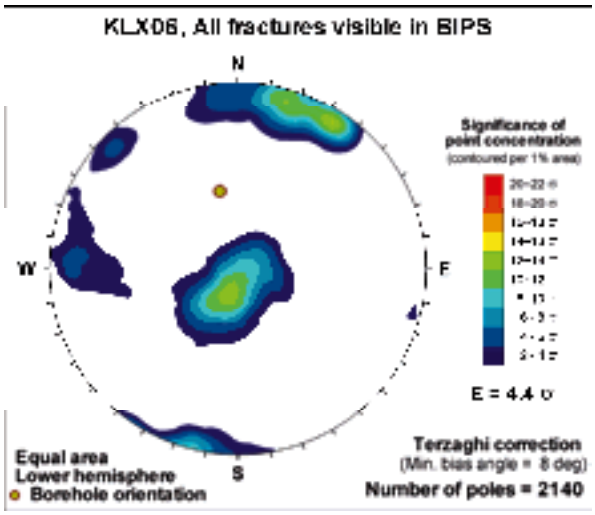
KLX06, All fractures visible in BIPS
N
W
E
S
Significance of point concentration
(contoured per 1% area)
E = 4.4 σ
Terzaghi correction
(Min. bias angle = 8 deg)
Number of poles = 2140
Equal area
Lower hemisphere
Borehole orientation

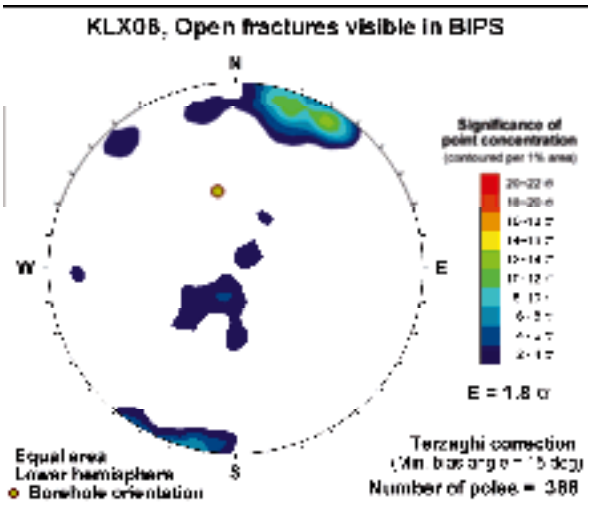
KLX06, Open fractures visible in BIPS
N
W
E
S
Significance of point concentration
(contoured per 1% area)
E = 1.8 σ
Terzaghi correction
Number of poles = 388
Equal area
Lower hemisphere
Borehole orientation

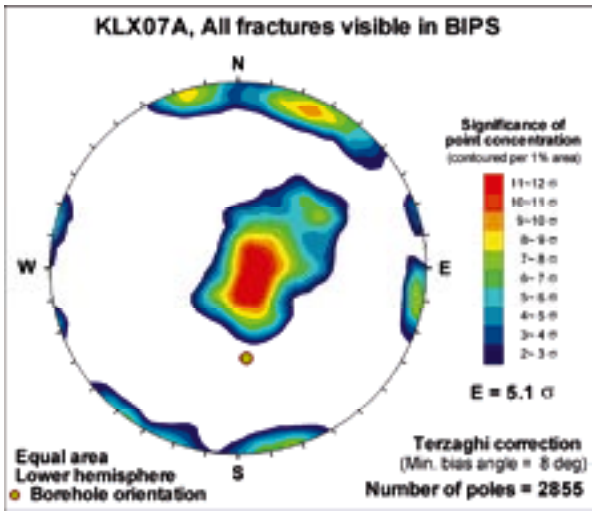
KLX07A, All fractures visible in BIPS
N
W
E
S
Significance of point concentration
(contoured per 1% area)
E = 5.1 σ
Terzaghi correction
(Min. bias angle = 8 deg)
Number of poles = 2855
Equal area
Lower hemisphere
Borehole orientation

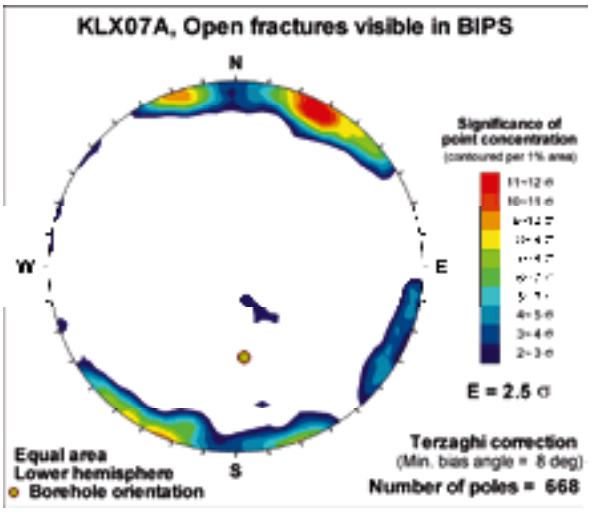
KLX07A, Open fractures visible in BIPS
N
W
E
S
Significance of point concentration
(contoured per 1% area)
E = 2.5 σ
Terzaghi correction
(Min. bias angle = 8 deg)
Number of poles = 668
Equal area
Lower hemisphere
Borehole orientation

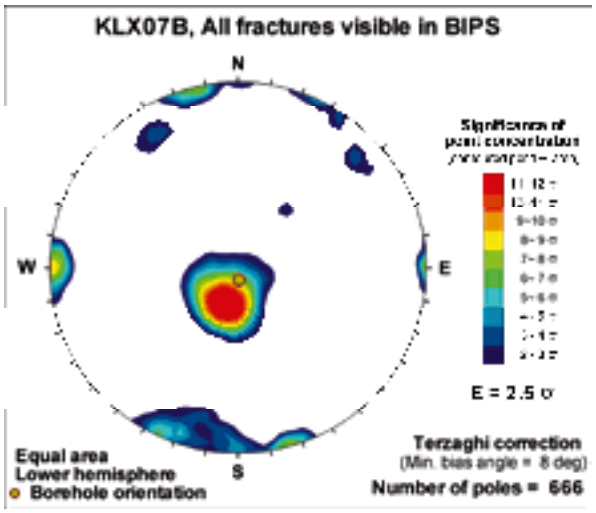
KLX07B, All fractures visible in BIPS
N
W
E
S
E = 2.5 σ
Equal area
Lower hemisphere
Borehole orientation
Terzaghi correction
(Min. bias angle = 8 deg)
Number of poles = 666

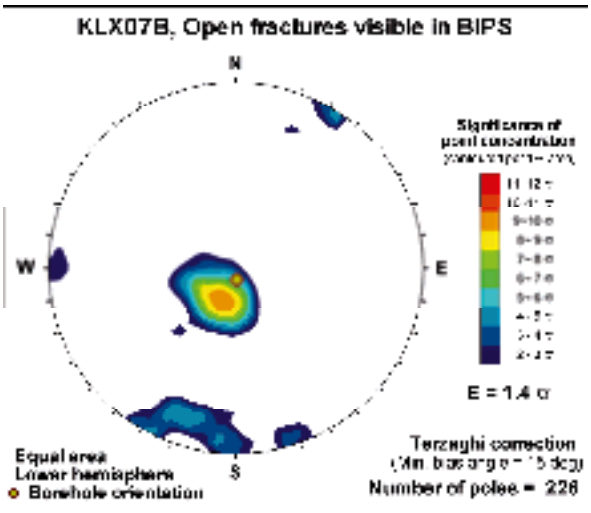
KLX07B, Open fractures visible in BIPS
N
W
E
S
E = 1.4 σ
Equal area
Lower hemisphere
Borehole orientation
Terzaghi correction
Number of poles = 228

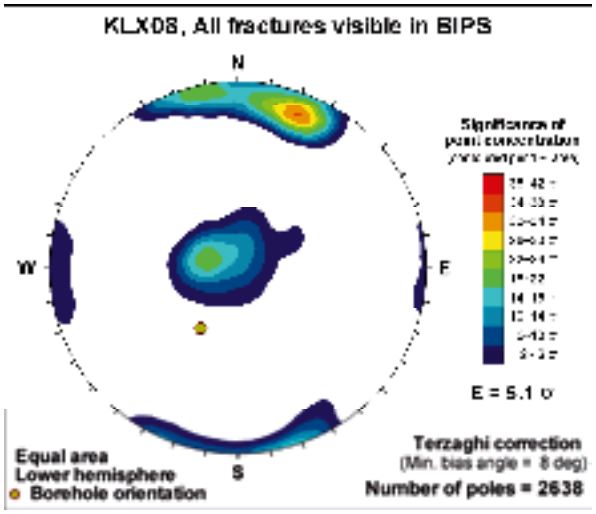
KLX08, All fractures visible in BIPS
N
W
E
S
E = 5.1 σ
Equal area
Lower hemisphere
Borehole orientation
Terzaghi correction
(Min. bias angle = 8 deg)
Number of poles = 2638

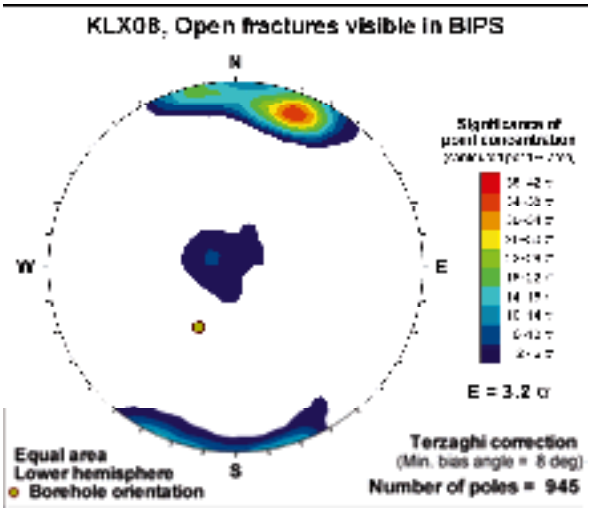
KLX08, Open fractures visible in BIPS
N
W
E
S
E = 3.2 σ
Equal area
Lower hemisphere
Borehole orientation
Terzaghi correction
(Min. bias angle = 8 deg)
Number of poles = 945

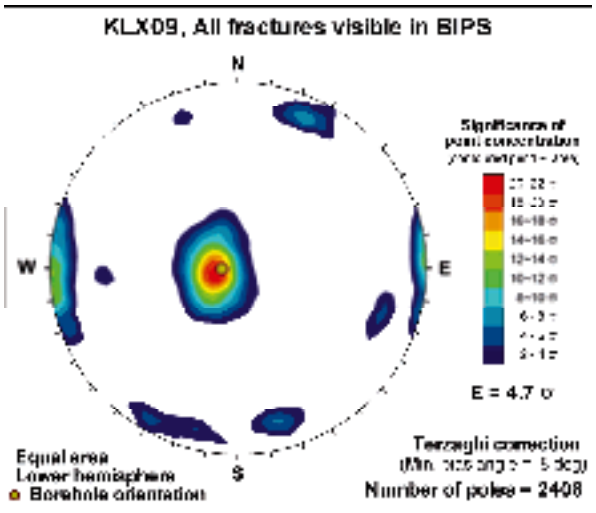
KLX09, All fractures visible in BIPS
N
W
E
S
E = 4.7 σ
Equal area
Lower hemisphere
Borehole orientation
Terzaghi correction
Number of poles = 2408

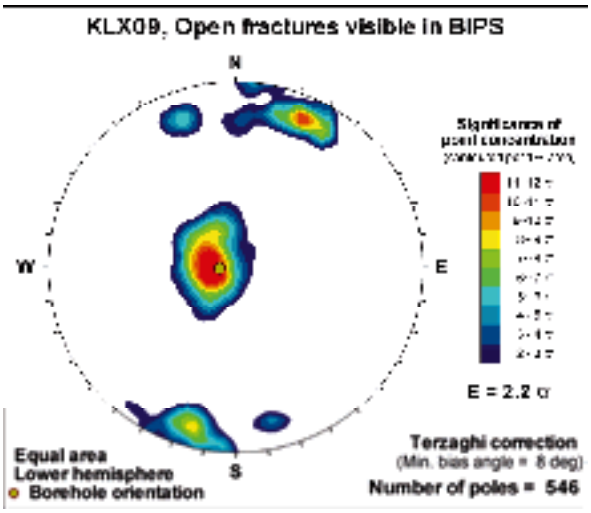
KLX09, Open fractures visible in BIPS
N
W
E
S
E = 2.2 σ
Equal area
Lower hemisphere
Borehole orientation
Terzaghi correction
(Min. bias angle = 8 deg)
Number of poles = 546

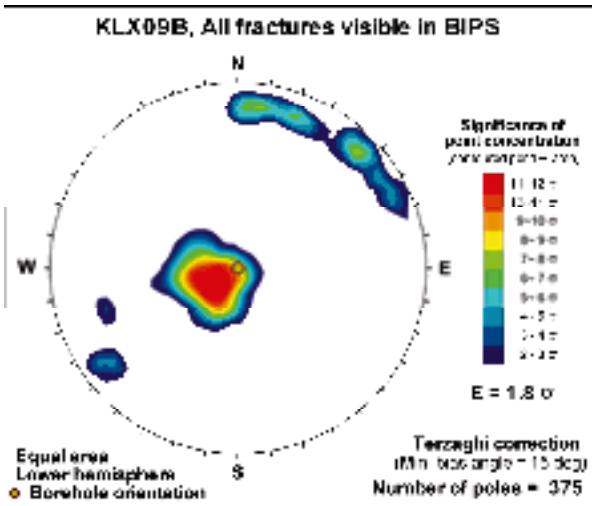
KLX09B, All fractures visible in BIPS
N
W
E
S
E = 1.8 σ
Terzaghi correction
Number of poles = 375
Equal area
Lower hemisphere
Borehole orientation

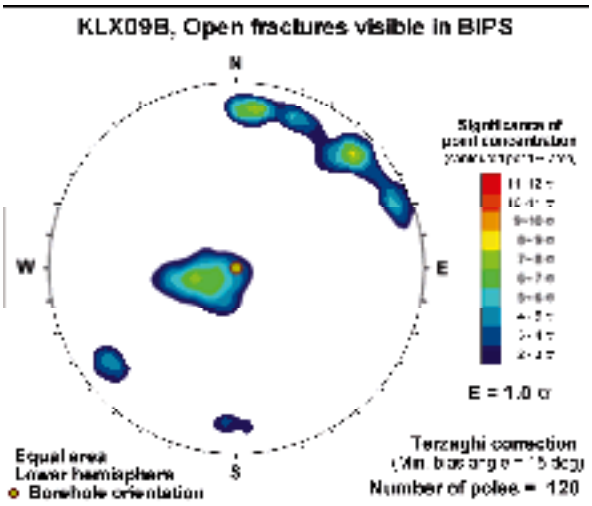
KLX09B, Open fractures visible in BIPS
N
W
E
S
E = 1.0 σ
Terzaghi correction
Number of poles = 120
Equal area
Lower hemisphere
Borehole orientation

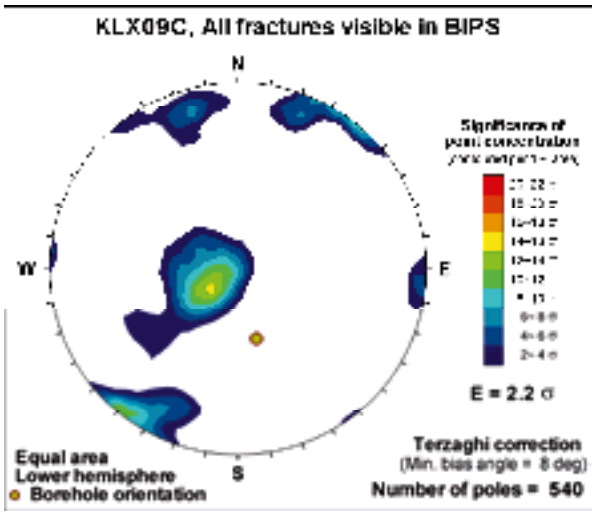
KLX09C, All fractures visible in BIPS
N
W
E
S
E = 2.2 σ
Terzaghi correction
(Min. bias angle = 8 deg)
Number of poles = 540
Equal area
Lower hemisphere
Borehole orientation

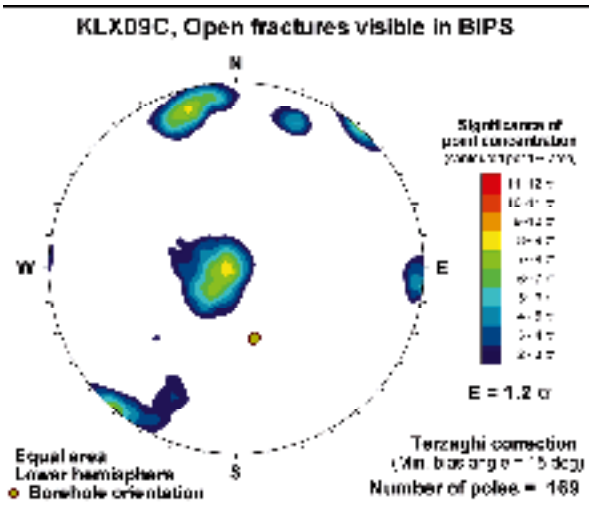
KLX09C, Open fractures visible in BIPS
N
W
E
S
E = 1.2 σ
Terzaghi correction
Number of poles = 169
Equal area
Lower hemisphere
Borehole orientation

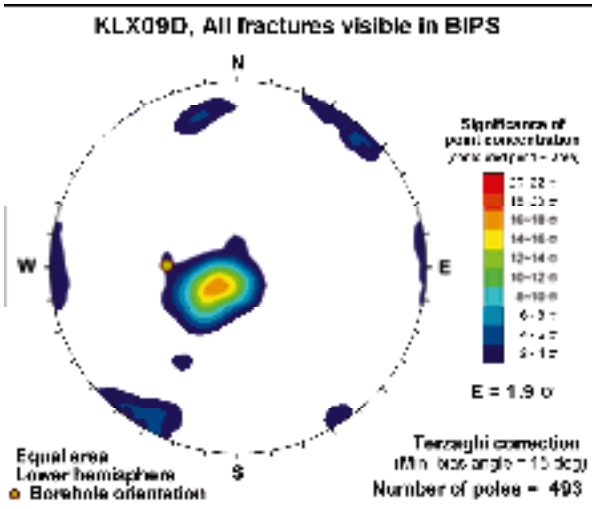
KLX09D, All fractures visible in BIPS
N
W
E
S
E = 1.9 σ
Terzaghi correction
Number of poles = 493
Equal area
Lower hemisphere
Borehole orientation

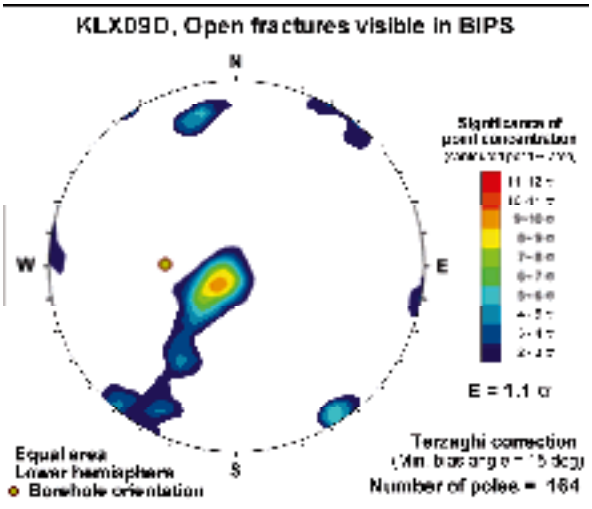
KLX09D, Open fractures visible in BIPS
N
W
E
S
E = 1.1 σ
Terzaghi correction
Number of poles = 164
Equal area
Lower hemisphere
Borehole orientation

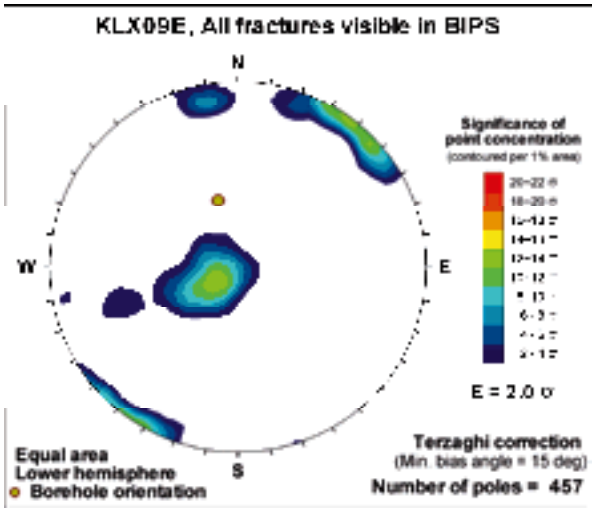
KLX09E, All fractures visible in BIPS
N
W
E
S
Significance of point concentration
(contoured per 1% area)
E = 2.0 σ
Equal area
Lower hemisphere
Borehole orientation
Terzaghi correction
(Min. bias angle = 15 deg)
Number of poles = 457

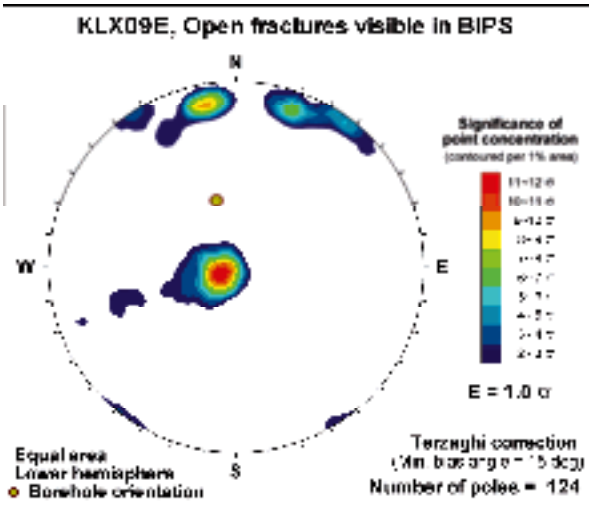
KLX09E, Open fractures visible in BIPS
N
W
E
S
Significance of point concentration
(contoured per 1% area)
E = 1.0 σ
Equal area
Lower hemisphere
Borehole orientation
Terzaghi correction
(Min. bias angle = 15 deg)
Number of poles = 124

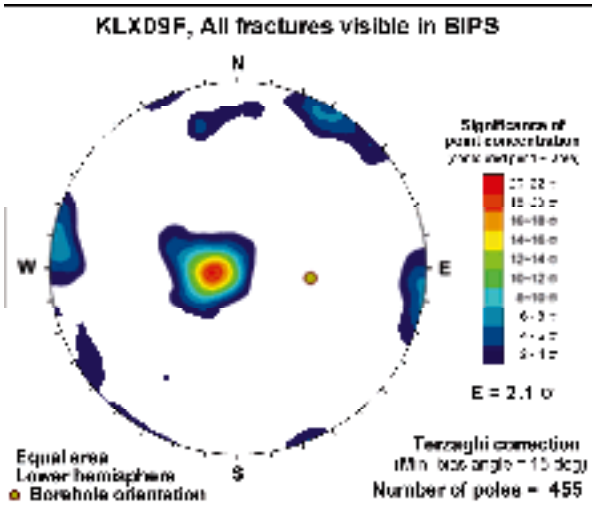
KLX09F, All fractures visible in BIPS
N
W
E
S
E = 2.1 σ
Equal area
Lower hemisphere
Borehole orientation
Terzaghi correction
(Min. bias angle = 15 deg)
Number of poles = 455

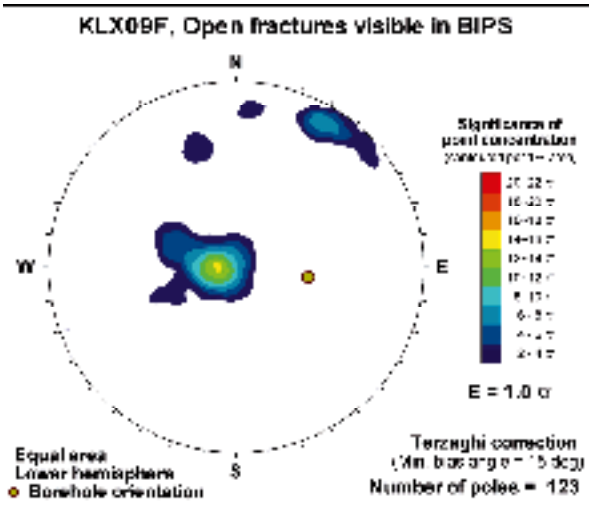
KLX09F, Open fractures visible in BIPS
N
W
E
S
E = 1.0 σ
Equal area
Lower hemisphere
Borehole orientation
Terzaghi correction
(Min. bias angle = 15 deg)
Number of poles = 123

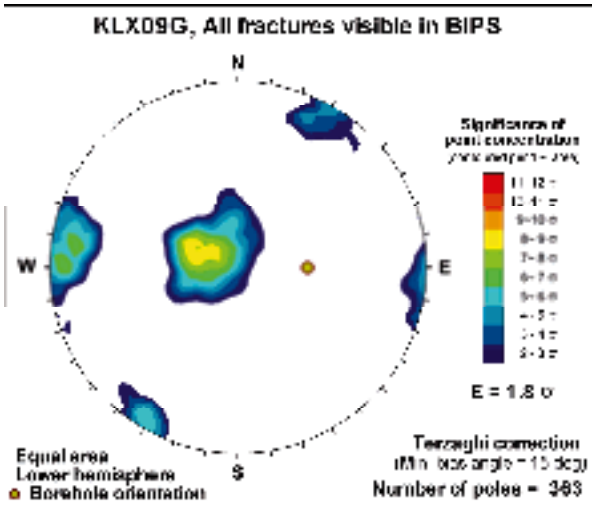
KLX09G, All fractures visible in BIPS
N
W
E
S
E = 1.8 σ
Equal area
Lower hemisphere
Borehole orientation
Terzaghi correction
(Min. bias angle = 15 deg)
Number of poles = 383

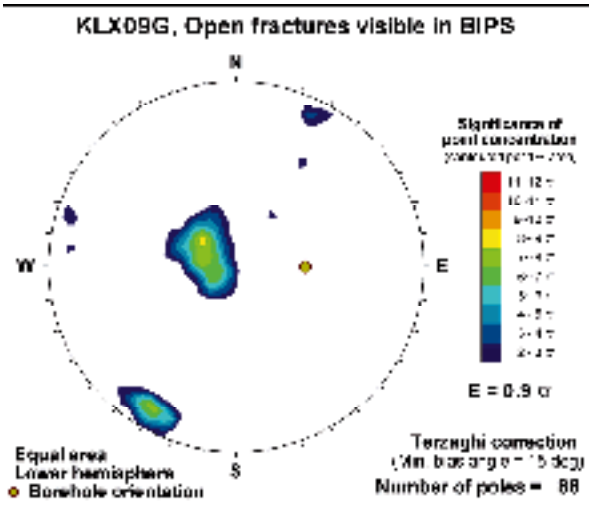
KLX09G, Open fractures visible in BIPS
N
W
E
S
E = 0.9 σ
Equal area
Lower hemisphere
Borehole orientation
Terzaghi correction
(Min. bias angle = 15 deg)
Number of poles = 88

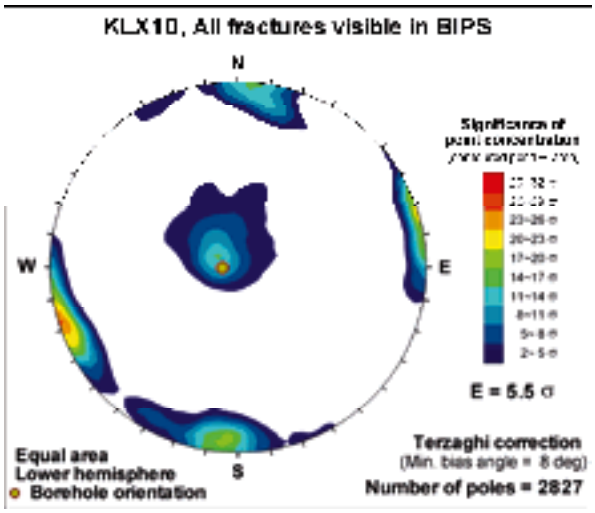
KLX10, All fractures visible in BIPS
N
W
E
S
E = 5.5 σ
Terzaghi correction
(Min. bias angle = 8 deg)
Number of poles = 2827
Equal area
Lower hemisphere
Borehole orientation

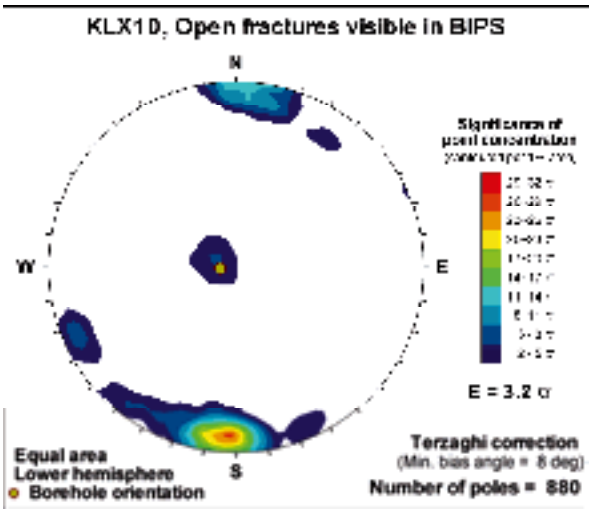
KLX10, Open fractures visible in BIPS
N
W
E
S
E = 3.2 σ
Terzaghi correction
(Min. bias angle = 8 deg)
Number of poles = 880
Equal area
Lower hemisphere
Borehole orientation

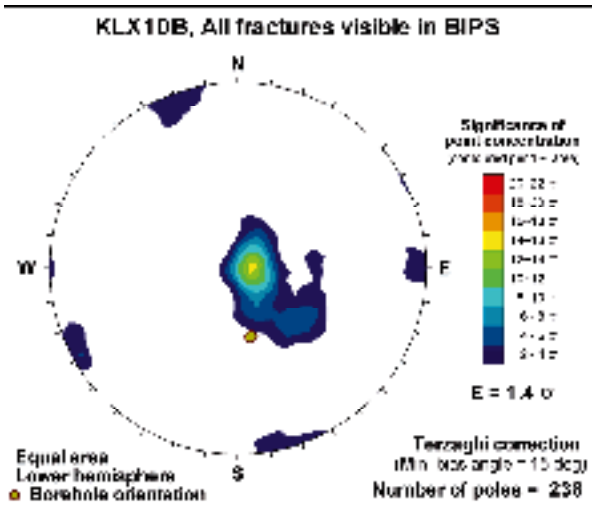
KLX10B, All fractures visible in BIPS
N
W
E
S
E = 1.4 σ
Terzaghi correction
Number of poles = 238
Equal area
Lower hemisphere
Borehole orientation

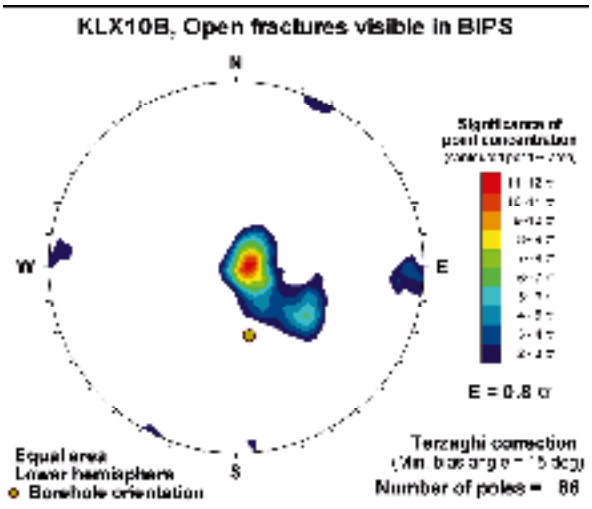
KLX10B, Open fractures visible in BIPS
N
W
E
S
E = 0.8 σ
Terzaghi correction
Number of poles = 86
Equal area
Lower hemisphere
Borehole orientation

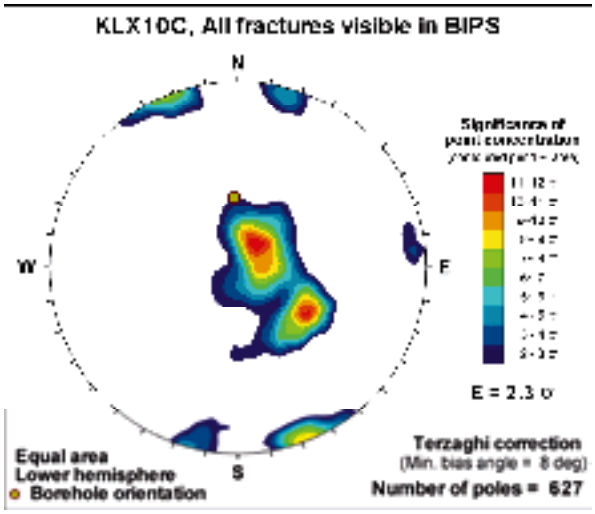
KLX10C, All fractures visible in BIPS
N
W
E
S
E = 2.3 σ
Terzaghi correction
(Min. bias angle = 8 deg)
Number of poles = 627
Equal area
Lower hemisphere
Borehole orientation

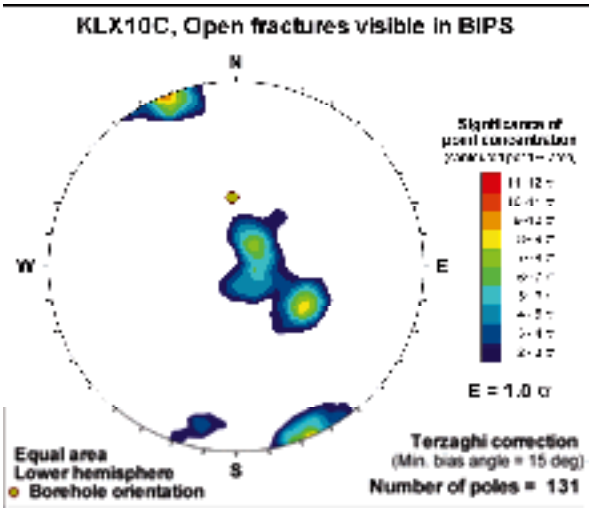
KLX10C, Open fractures visible in BIPS
N
W
E
S
E = 1.0 σ
Terzaghi correction
(Min. bias angle = 15 deg)
Number of poles = 131
Equal area
Lower hemisphere
Borehole orientation

KLX11A, All fractures visible in BIPS

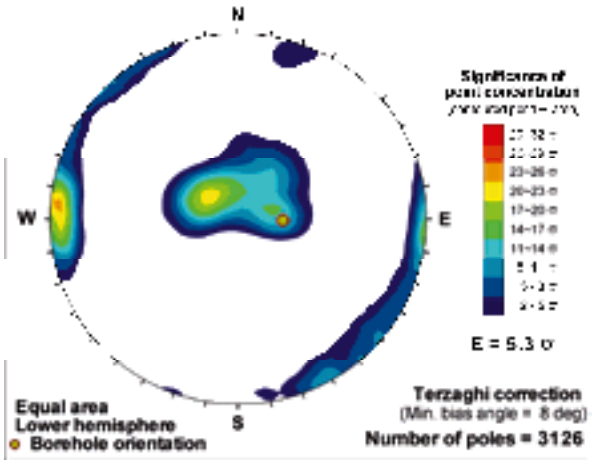

KLX11A, Open fractures visible in BIPS

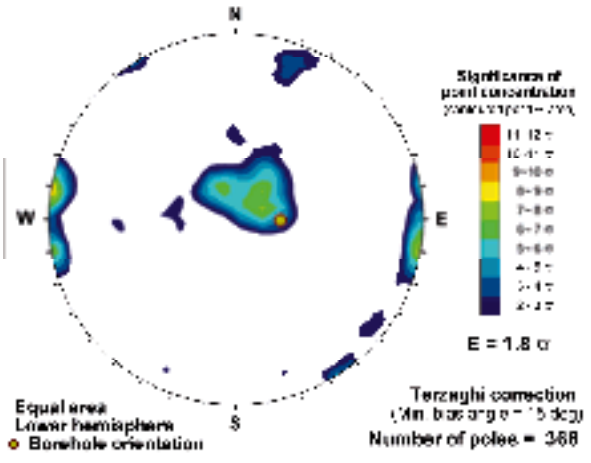

KLX11B, All fractures visible in BIPS

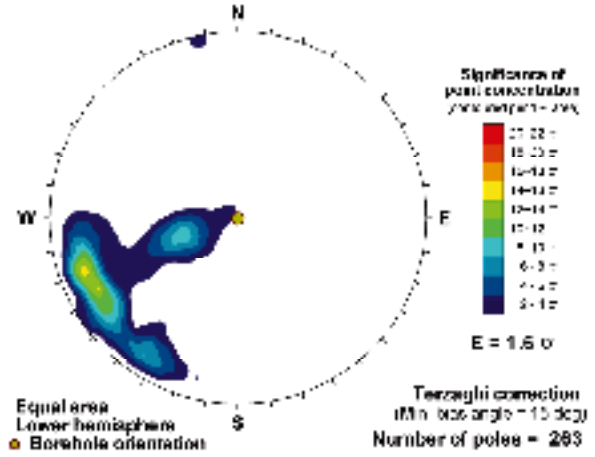

KLX11B, Open fractures visible in BIPS

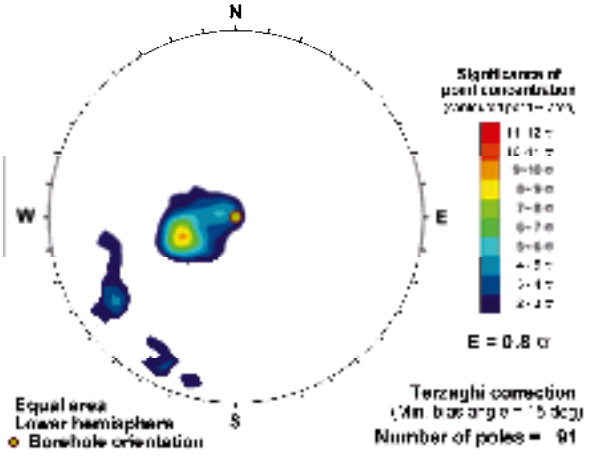

KLX11C, All fractures visible in BIPS

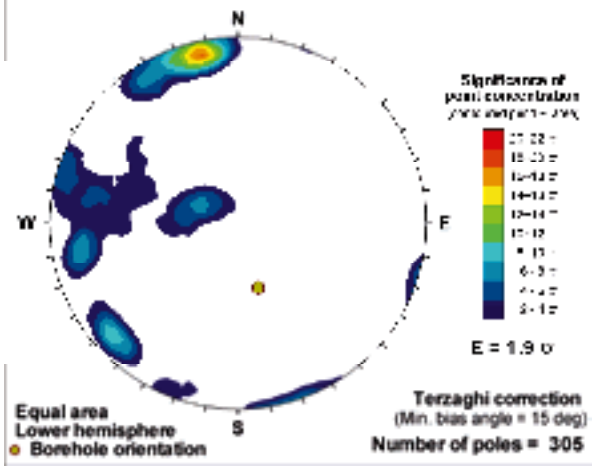

KLX11C, Open fractures visible in BIPS

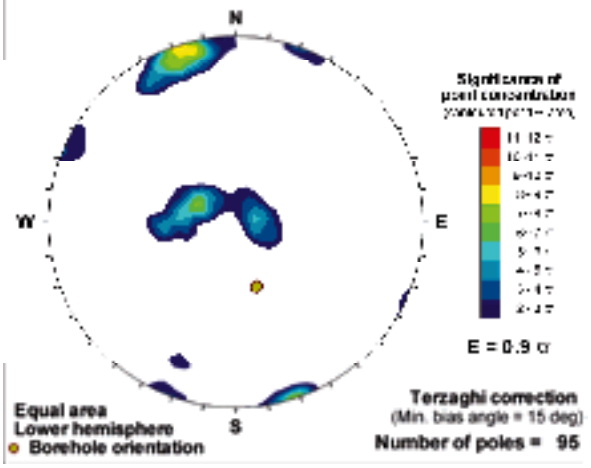

KLX11D, All fractures visible in BIPS

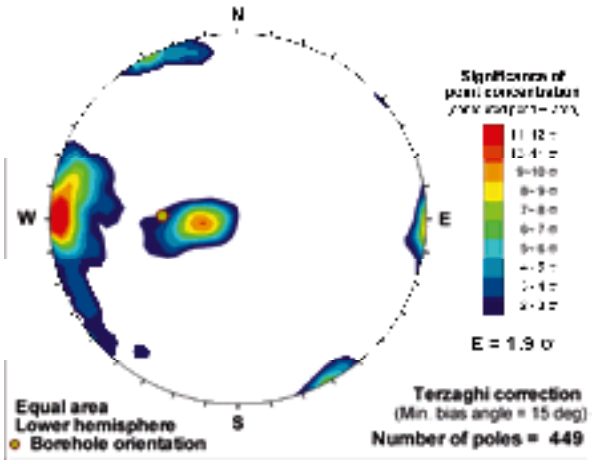

KLX11D, Open fractures visible in BIPS

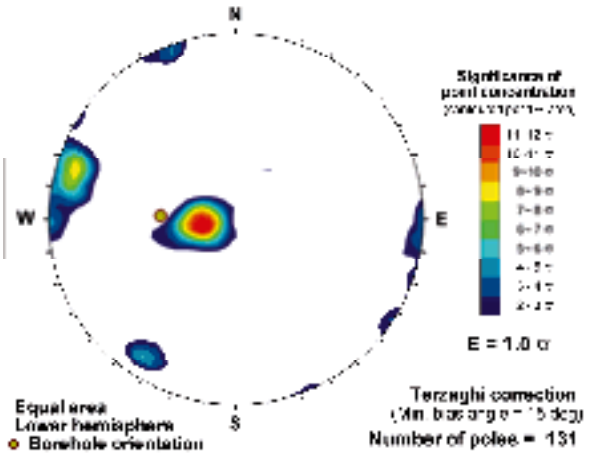

KLX11E, All fractures visible in BIPS

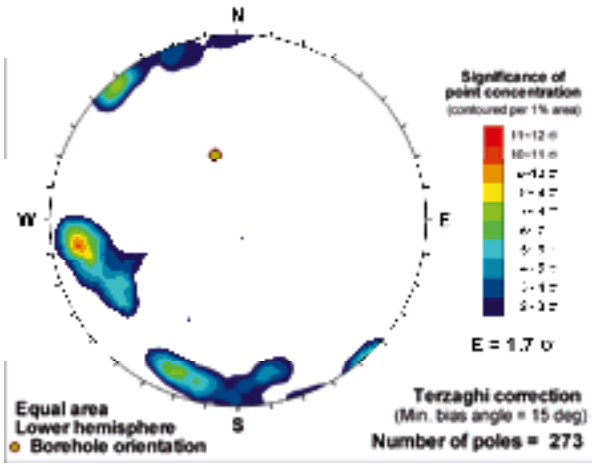

KLX11E, Open fractures visible in BIPS

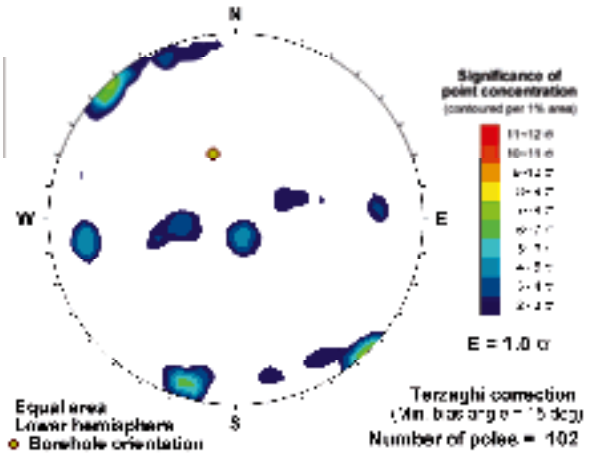

KLX11F, All fractures visible in BIPS

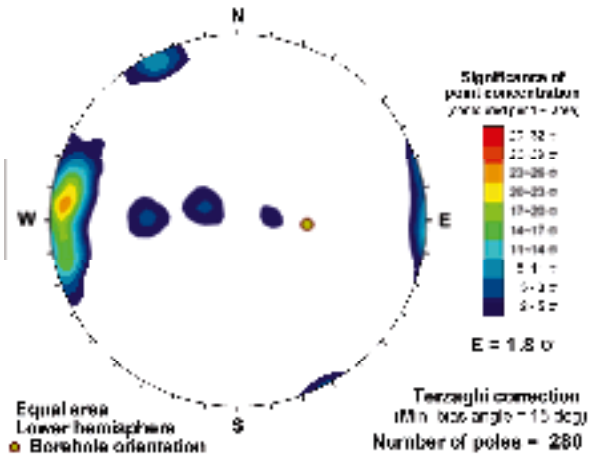

KLX11F, Open fractures visible in BIPS

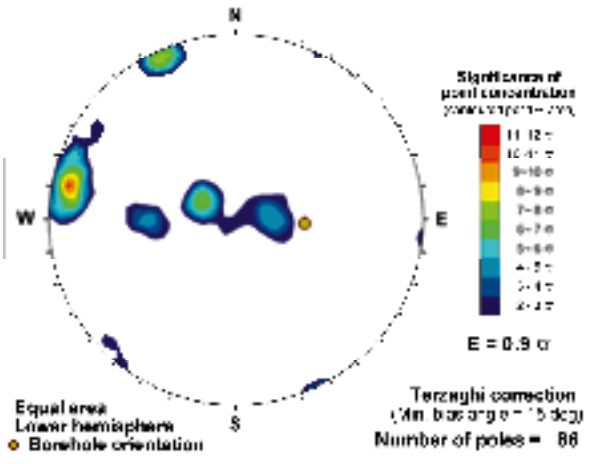

KLX12A, All fractures visible in BIPS

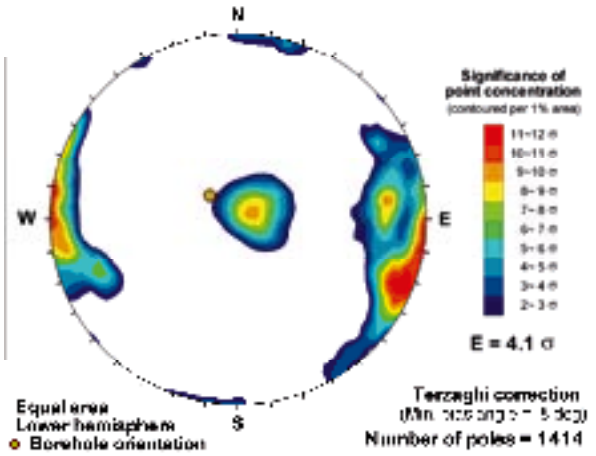

KLX12A, Open fractures visible in BIPS

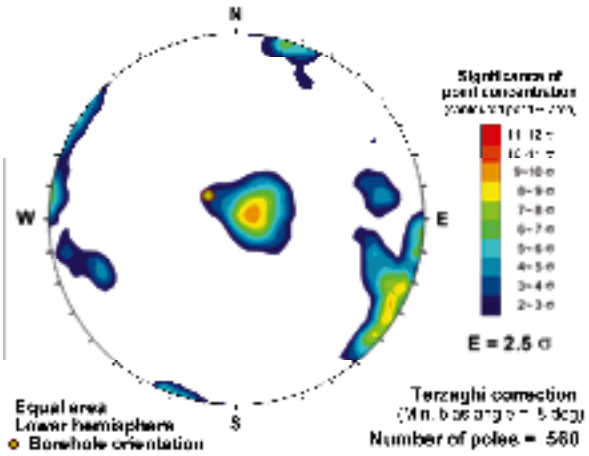

KLX13A, All fractures visible in BIPS

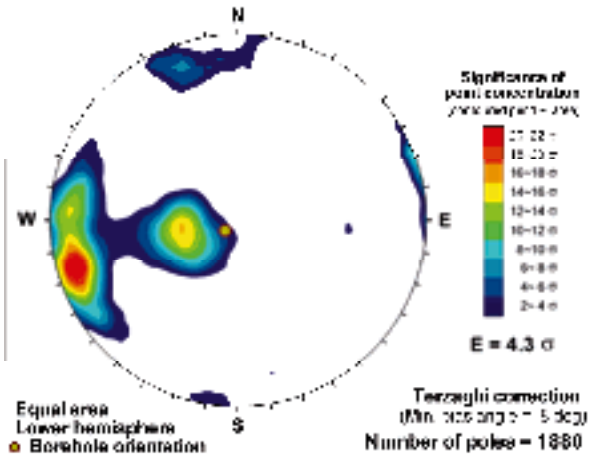

KLX13A, Open fractures visible in BIPS

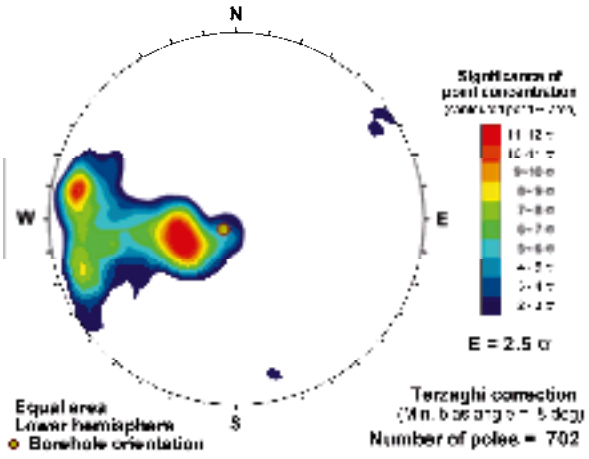

KLX14A, All fractures visible in BIPS

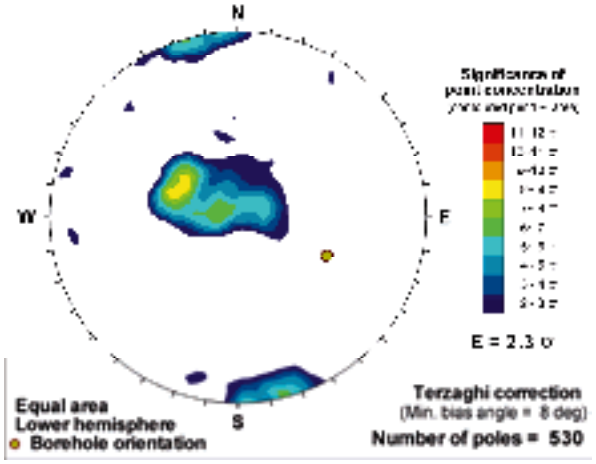

KLX14A, Open fractures visible in BIPS

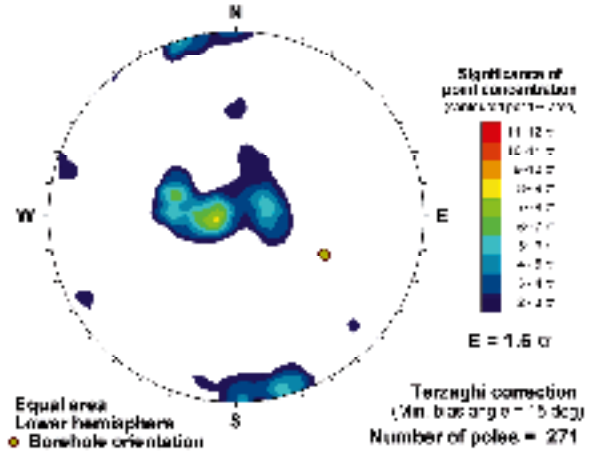

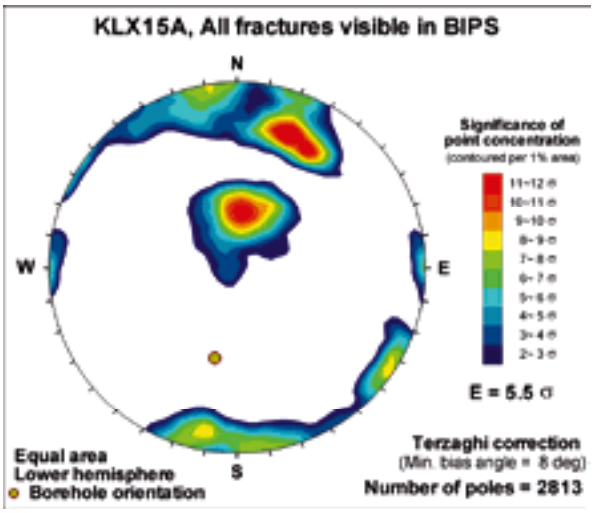
KLX15A, All fractures visible in BIPS
N
W
E
S
Significance of point concentration
(contoured per 1% area)
E = 5.5 σ
Equal area
Lower hemisphere
Borehole orientation
Terzaghi correction
(Min. bias angle = 8 deg)
Number of poles = 2813

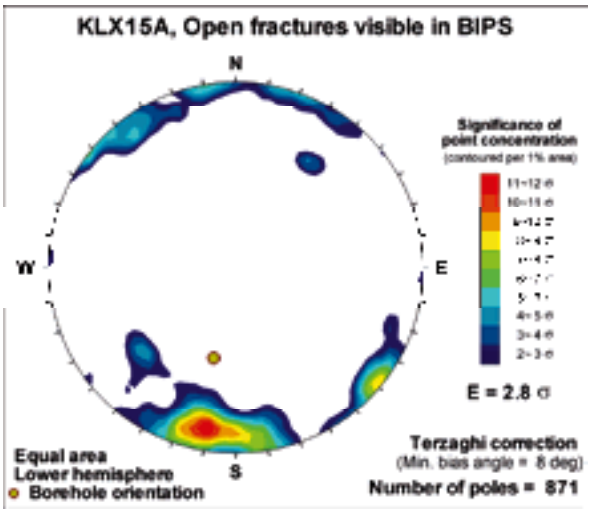
KLX15A, Open fractures visible in BIPS
N
W
E
S
Significance of point concentration
(contoured per 1% area)
E = 2.8 σ
Equal area
Lower hemisphere
Borehole orientation
Terzaghi correction
(Min. bias angle = 8 deg)
Number of poles = 871

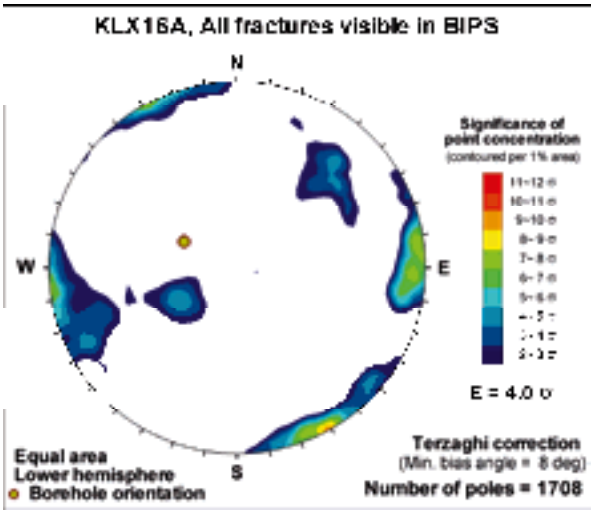
KLX16A, All fractures visible in BIPS
N
W
E
S
Significance of point concentration
(contoured per 1% area)
E = 4.0 σ
Equal area
Lower hemisphere
Borehole orientation
Terzaghi correction
(Min. bias angle = 8 deg)
Number of poles = 1708

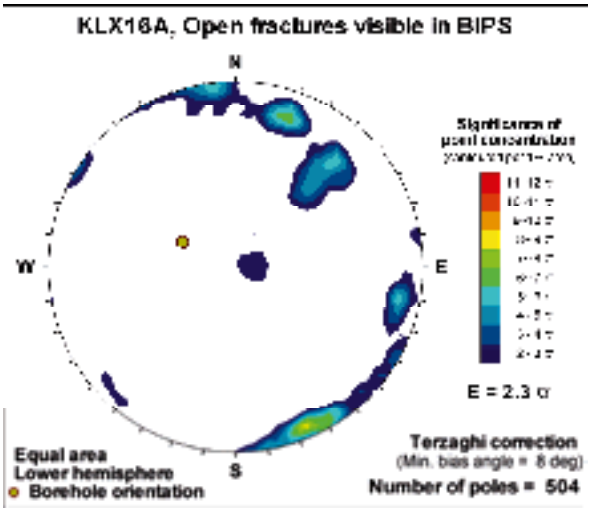
KLX16A, Open fractures visible in BIPS
N
W
E
S
E = 2.3 σ
Equal area
Lower hemisphere
Borehole orientation
Terzaghi correction
(Min. bias angle = 8 deg)
Number of poles = 504

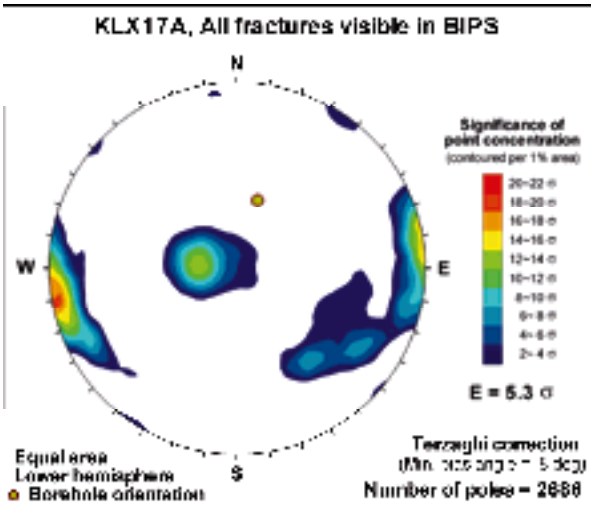
KLX17A, All fractures visible in BIPS
N
W
E
S
Significance of point concentration
(contoured per 1% area)
E = 5.3 σ
Equal area
Lower hemisphere
Borehole orientation
Number of poles = 2688

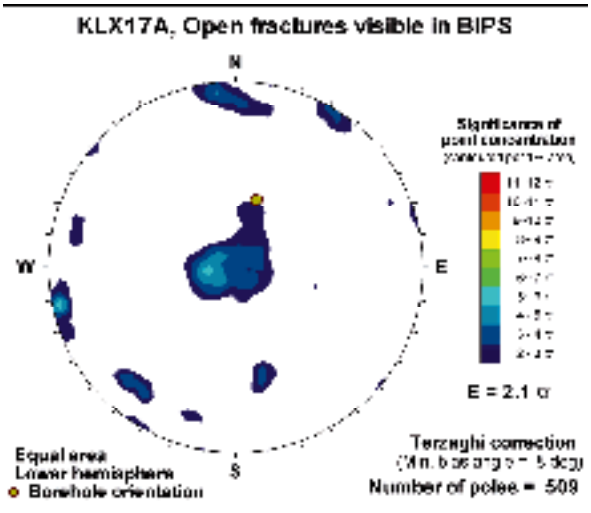
KLX17A, Open fractures visible in BIPS
N
W
E
S
E = 2.1 σ
Equal area
Lower hemisphere
Borehole orientation
Number of poles = 509

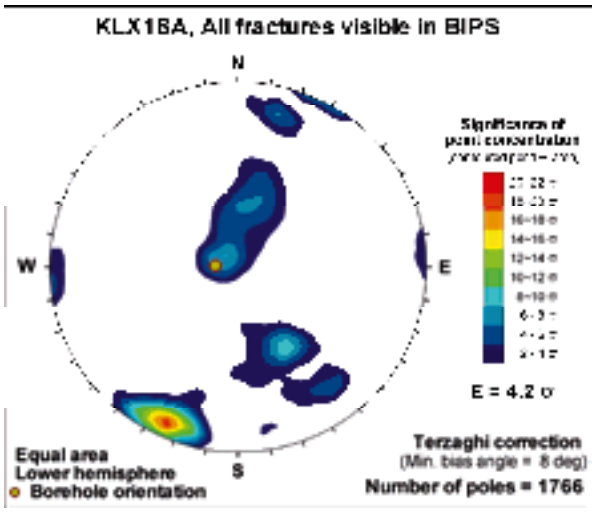
KLX18A, All fractures visible in BIPS
N
W
E
S
E = 4.2 σ
Equal area
Lower hemisphere
Borehole orientation
Terzaghi correction
(Min. bias angle = 8 deg)
Number of poles = 1766

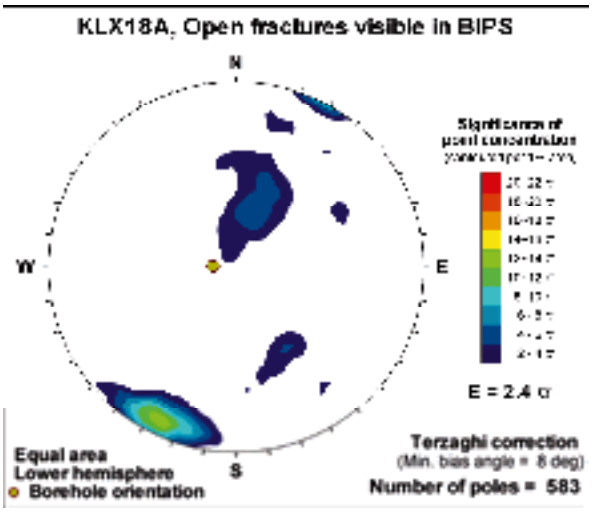
KLX18A, Open fractures visible in BIPS
N
W
E
S
E = 2.4 σ
Equal area
Lower hemisphere
Borehole orientation
Terzaghi correction
(Min. bias angle = 8 deg)
Number of poles = 583

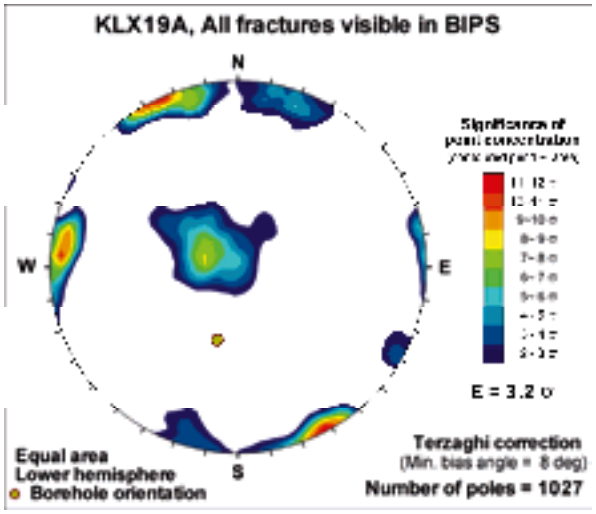
KLX19A, All fractures visible in BIPS
N
W
E
S
E = 3.2 σ
Equal area
Lower hemisphere
Borehole orientation
Terzaghi correction
(Min. bias angle = 8 deg)
Number of poles = 1027

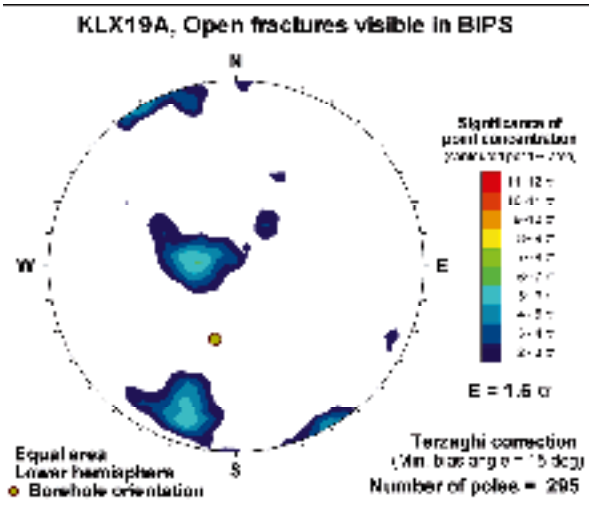
KLX19A, Open fractures visible in BIPS
N
W
E
S
E = 1.6 σ
Equal area
Lower hemisphere
Borehole orientation
Terzaghi correction
Number of poles = 295

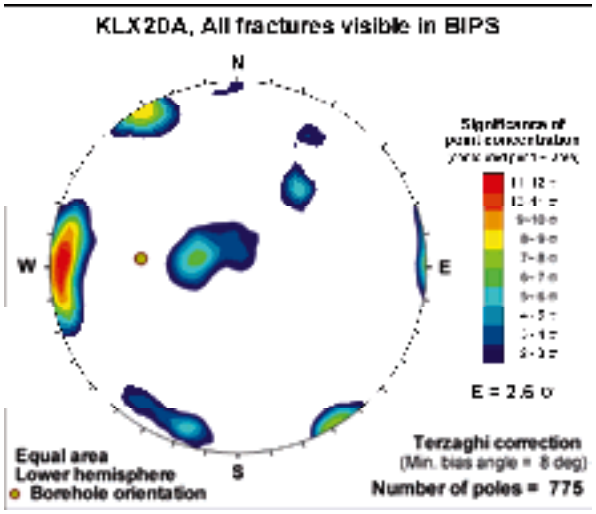
KLX20A, All fractures visible in BIPS
N
W
E
S
E = 2.6 σ
Equal area
Lower hemisphere
Borehole orientation
Terzaghi correction
(Min. bias angle = 8 deg)
Number of poles = 775

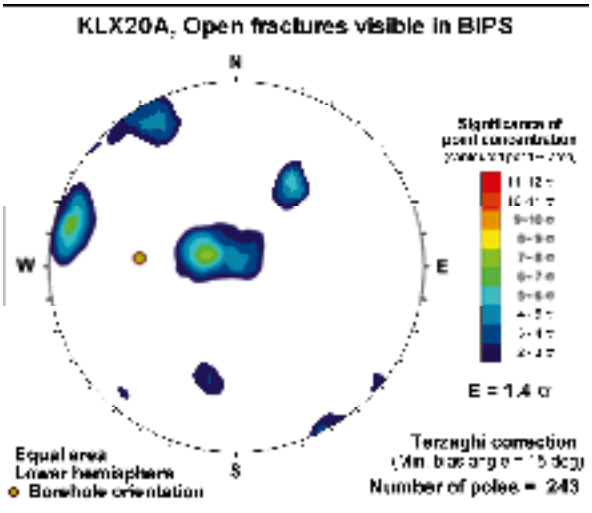
KLX20A, Open fractures visible in BIPS
N
W
E
S
E = 1.4 σ
Equal area
Lower hemisphere
Borehole orientation
Terzaghi correction
Number of poles = 243

KLX21B, All fractures visible in BIPS

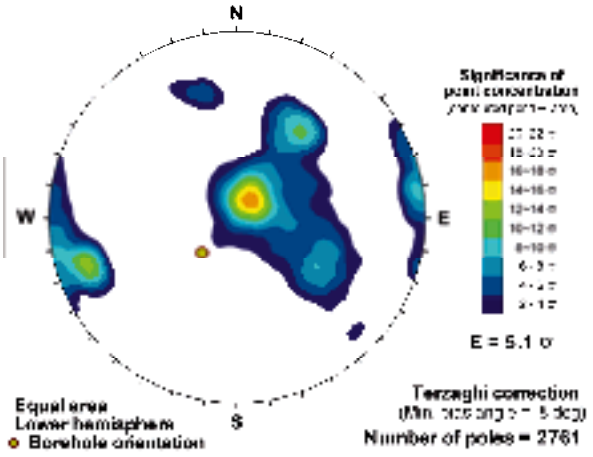

KLX21B, Open fractures visible in BIPS

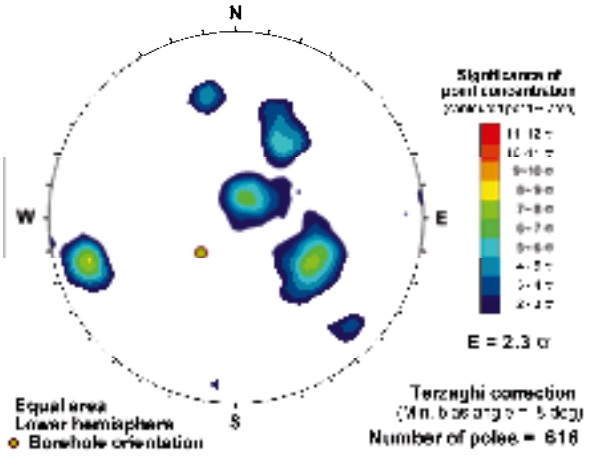

KLX22A, All fractures visible in BIPS

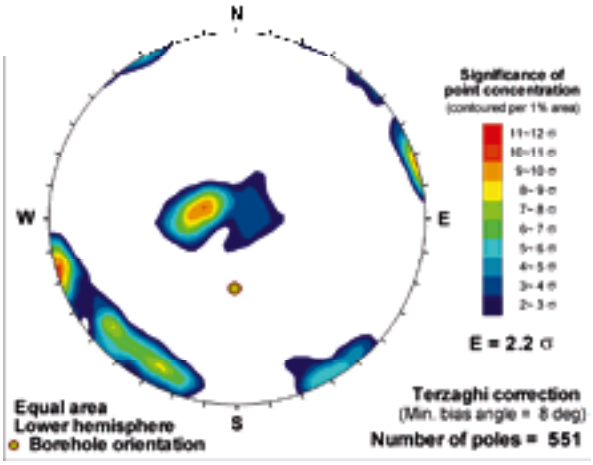

KLX22A, Open fractures visible in BIPS

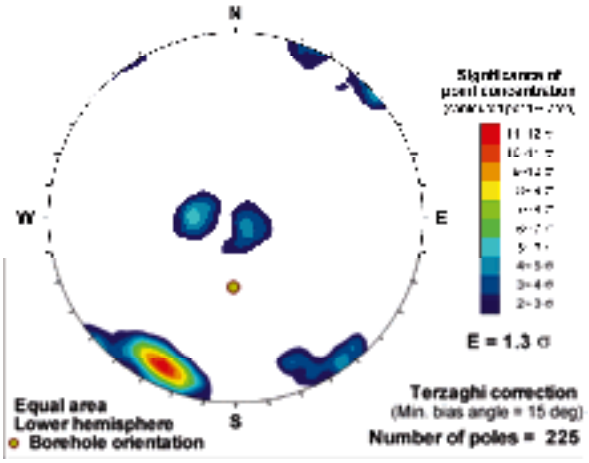

KLX22B, All fractures visible in BIPS

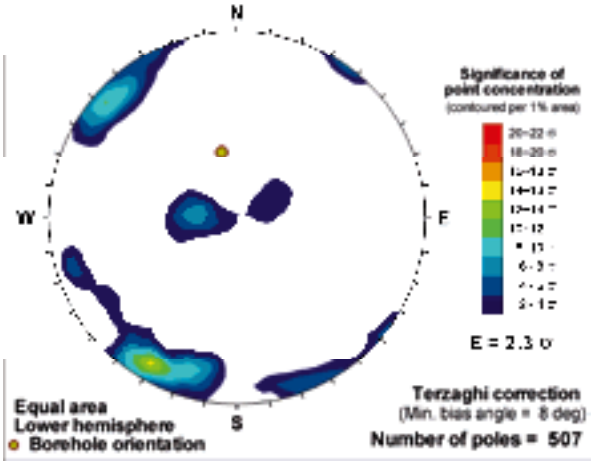

KLX22B, Open fractures visible in BIPS

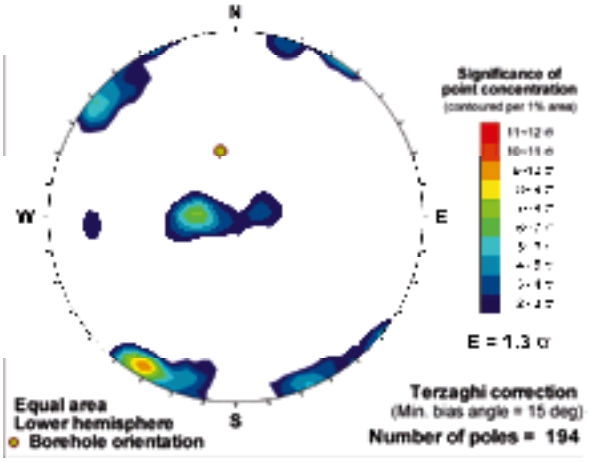

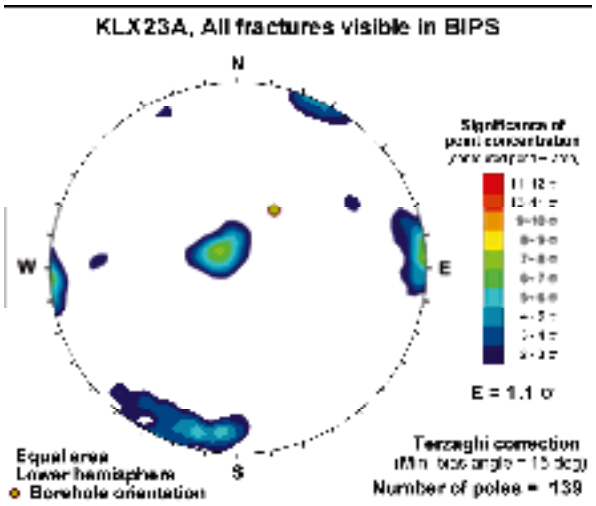
KLX23A, All fractures visible in BIPS
N
W
E
S
Significance of point concentration
E = 1.1 σ
Equal area
Lower hemisphere
Borehole orientation
Terzaghi correction
Number of poles = 139

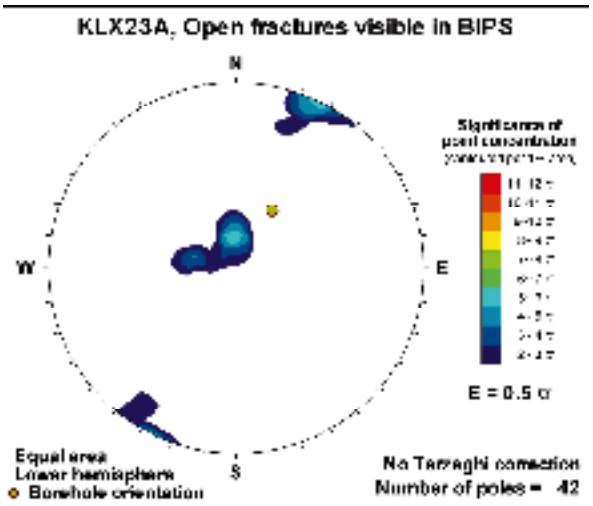
KLX23A, Open fractures visible in BIPS
N
W
E
S
Significance of point concentration
E = 0.5 σ
Equal area
Lower hemisphere
Borehole orientation
No Terzaghi correction
Number of poles = 42

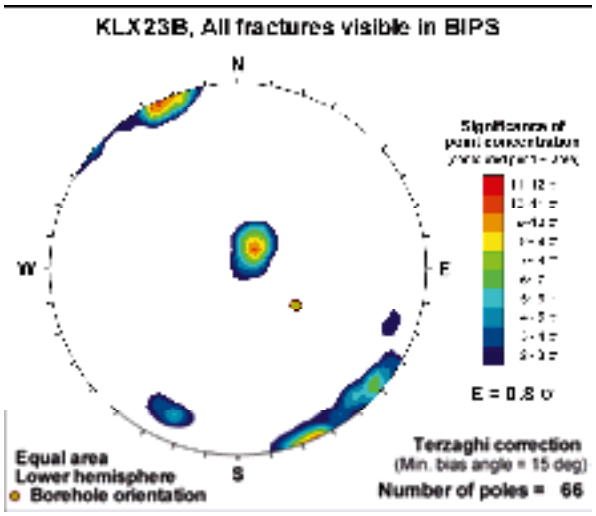
KLX23B, All fractures visible in BIPS
N
W
E
S
Significance of point concentration
E = 0.8 σ
Equal area
Lower hemisphere
Borehole orientation
Terzaghi correction
(Min. bias angle = 15 deg)
Number of poles = 66

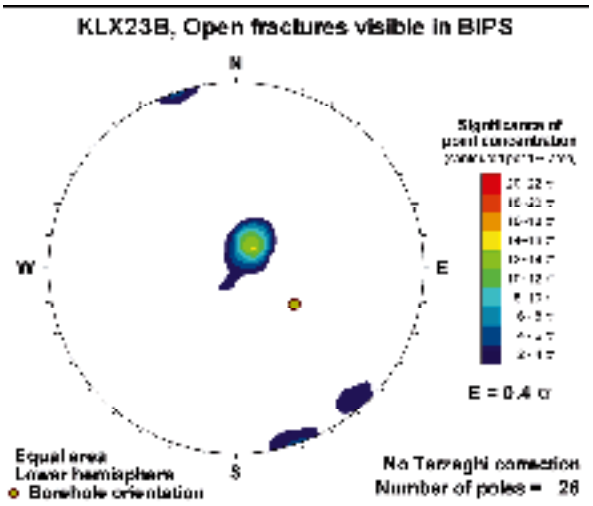
KLX23B, Open fractures visible in BIPS
N
W
E
S
Significance of point concentration
E = 0.4 σ
Equal area
Lower hemisphere
Borehole orientation
No Terzaghi correction
Number of poles = 28

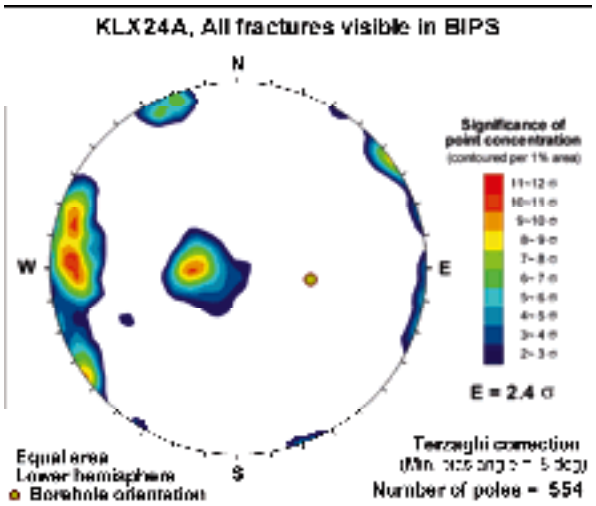
KLX24A, All fractures visible in BIPS
N
W
E
S
Significance of point concentration
(contoured per 1% area)
E = 2.4 σ
Equal area
Lower hemisphere
Borehole orientation
Terzaghi correction
Number of poles = 554

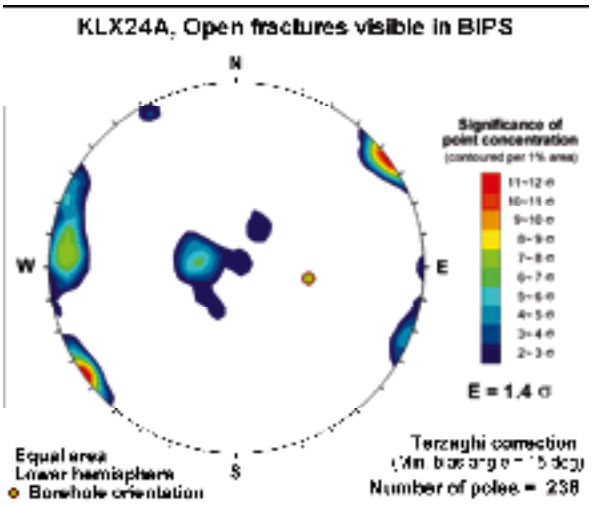
KLX24A, Open fractures visible in BIPS
N
W
E
S
Significance of point concentration
(contoured per 1% area)
E = 1.4 σ
Equal area
Lower hemisphere
Borehole orientation
Terzaghi correction
Number of poles = 238

KLX25A, All fractures visible in BIPS

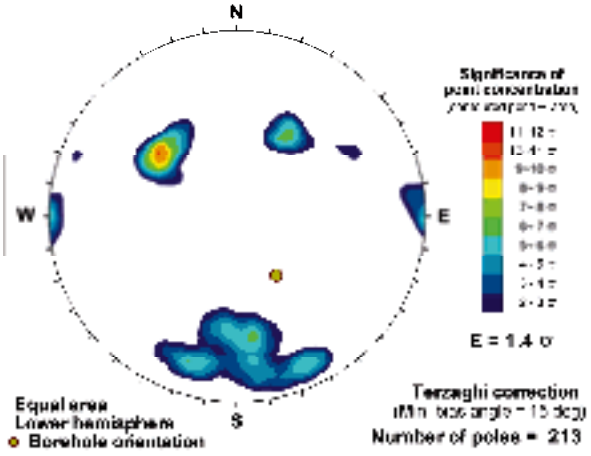

KLX25A, Open fractures visible in BIPS

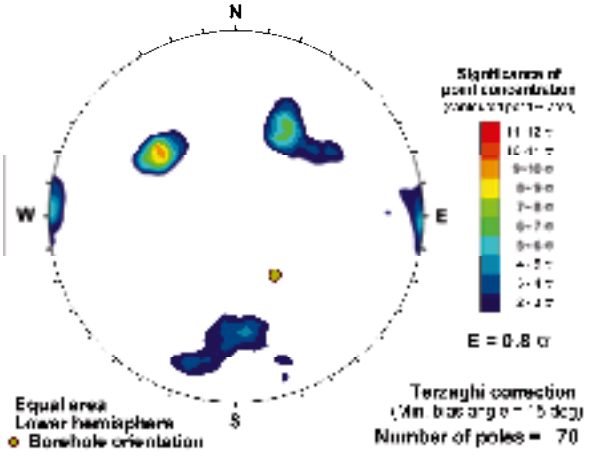

KLX26A, All fractures visible in BIPS

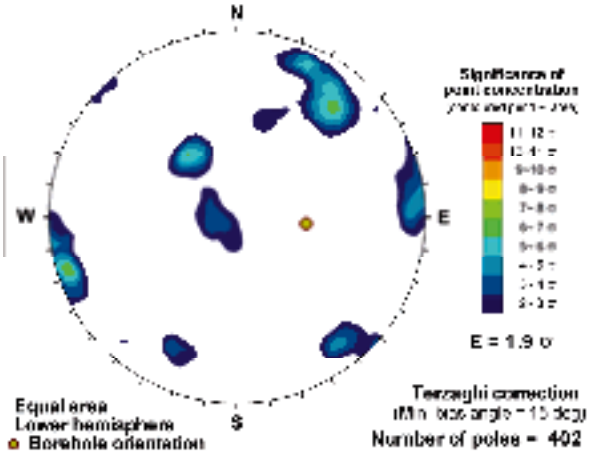

KLX26A, Open fractures visible in BIPS

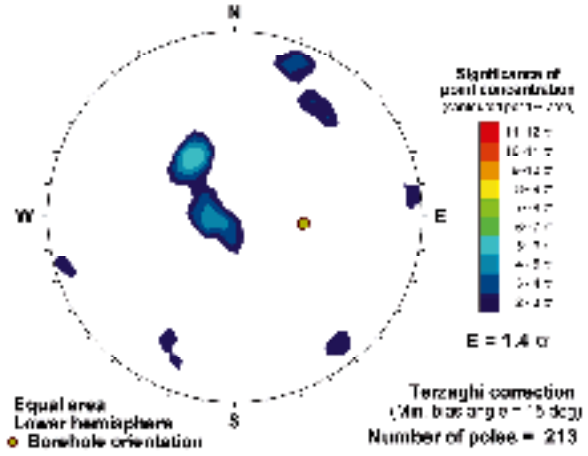

KLX26B, All fractures visible in BIPS

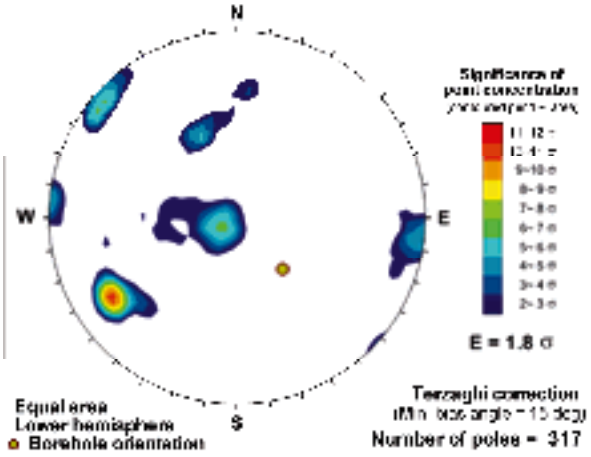

KLX26B, Open fractures visible in BIPS

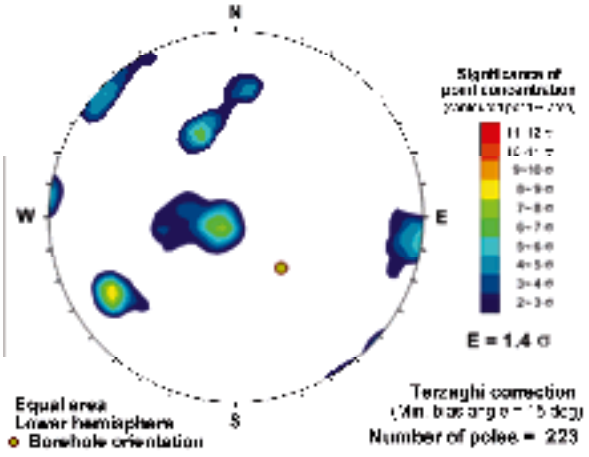

KLX28A, All fractures visible in BIPS

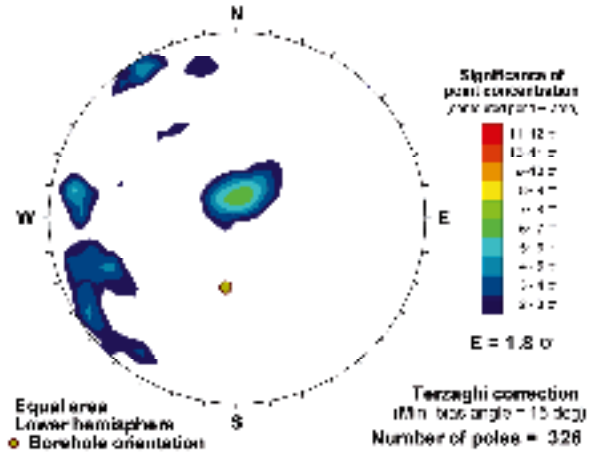

KLX28A, Open fractures visible in BIPS

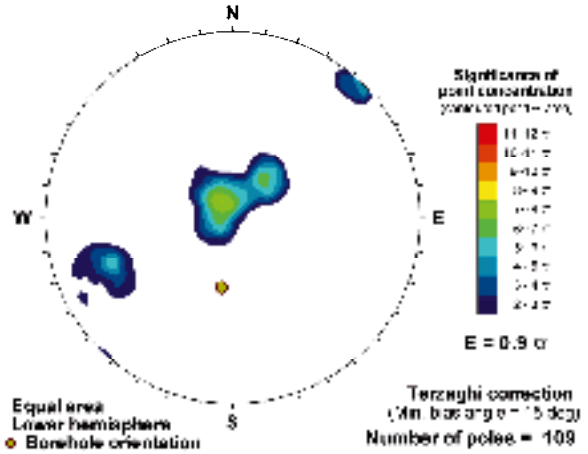

KLX29A, All fractures visible in BIPS

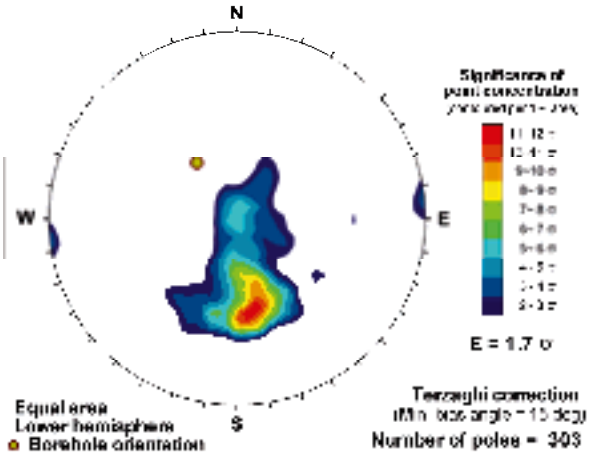

KLX29A, Open fractures visible in BIPS

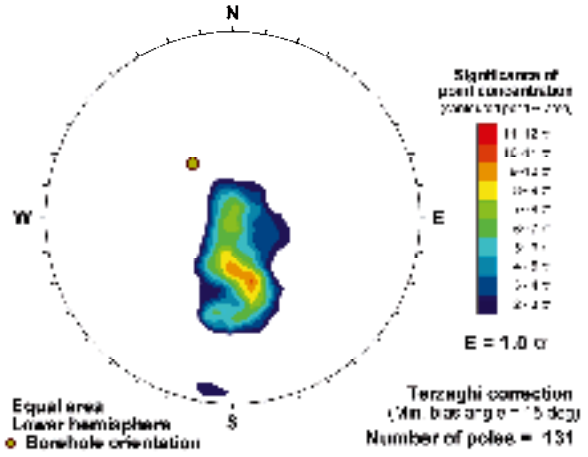

Appendix 5b

Fracture orientation in 30 m bins (Fisher concentration)

Fracture orientations have been plotted for each cored borehole in Laxemar in 30 m elevation intervals. The compilation is intended for users who would like to review fracture orientation on certain elevation levels in Laxemar. Each stereoplot shows total fracture orientation (open and sealed) outside deformation zones identified in the extended single hole interpretation. The stereoplots shows fracture orientations as pole plots on lower hemisphere, equal area Schmidt projections /Schmidt 1917/ with Fisher concentrations /Fisher 1953/ shown as a percentage of the total number of poles per 1.0% of the stereonet area.

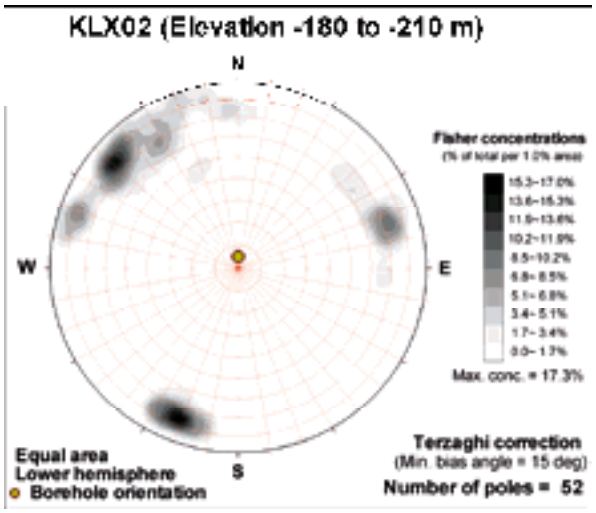
KLX02 (Elevation -180 to -210 m)
N
W
E
S
Fisher concentrations
(% of total per 1.0% area)
15.3–17.0%
13.6–15.3%
11.9–13.6%
10.2–11.9%
8.5–10.2%
6.8–8.5%
5.1–6.8%
3.4–5.1%
1.7–3.4%
0.0–1.7%
Max. conc. = 17.3%
Equal area
Lower hemisphere
Borehole orientation
Terzaghi correction
(Min. bias angle = 15 deg)
Number of poles = 52

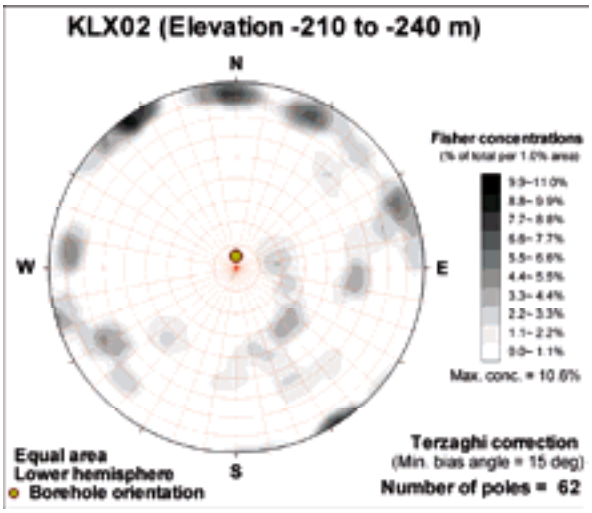
KLX02 (Elevation -210 to -240 m)
N
W
E
S
Fisher concentrations
(% of total per 1.0% area)
9.9–11.0%
8.8–9.9%
7.7–8.8%
6.6–7.7%
5.5–6.6%
4.4–5.5%
3.3–4.4%
2.2–3.3%
1.1–2.2%
0.0–1.1%
Max. conc. = 10.6%
Equal area
Lower hemisphere
Borehole orientation
Terzaghi correction
(Min. bias angle = 15 deg)
Number of poles = 62

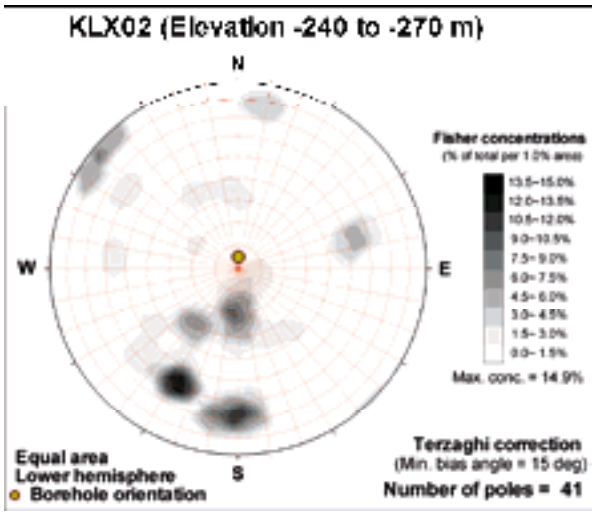
KLX02 (Elevation -240 to -270 m)
N
W
E
S
Fisher concentrations
(% of total per 1.0% area)
13.5–15.0%
12.0–13.5%
10.5–12.0%
9.0–10.5%
7.5–9.0%
6.0–7.5%
4.5–6.0%
3.0–4.5%
1.5–3.0%
0.0–1.5%
Max. conc. = 14.9%
Equal area
Lower hemisphere
Borehole orientation
Terzaghi correction
(Min. bias angle = 15 deg)
Number of poles = 41

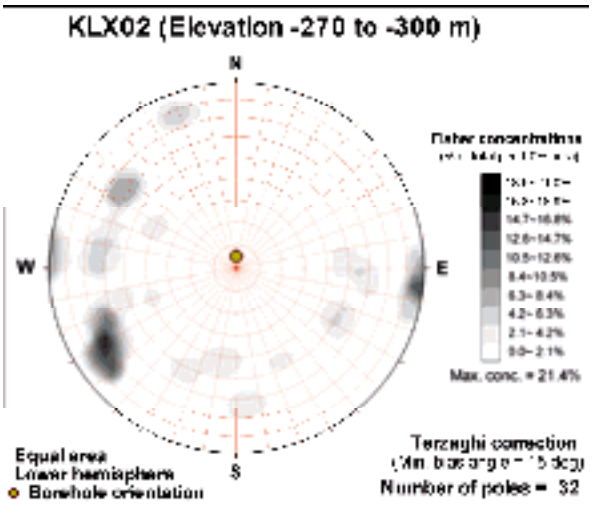
KLX02 (Elevation -270 to -300 m)
N
W
E
S
Max. conc. = 21.4%
Equal area
Lower hemisphere
Borehole orientation
Number of poles = 32

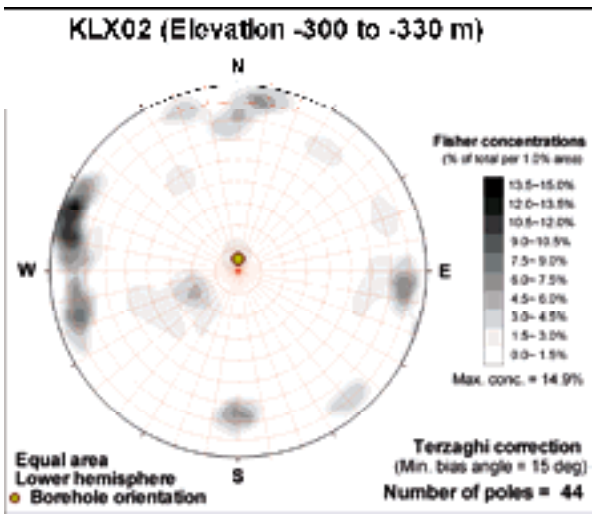
KLX02 (Elevation -300 to -330 m)
N
W
E
S
Fisher concentrations
(% of total per 1.0% area)
13.5–15.0%
12.0–13.5%
10.5–12.0%
9.0–10.5%
7.5–9.0%
6.0–7.5%
4.5–6.0%
3.0–4.5%
1.5–3.0%
0.0–1.5%
Max. conc. = 14.9%
Equal area
Lower hemisphere
Borehole orientation
Terzaghi correction
(Min. bias angle = 15 deg)
Number of poles = 44

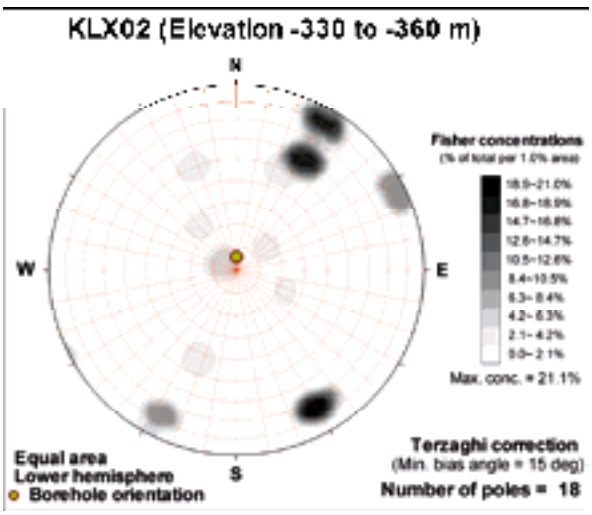
KLX02 (Elevation -330 to -360 m)
N
W
E
S
Fisher concentrations
(% of total per 1.0% area)
18.9–21.0%
16.8–18.9%
14.7–16.8%
12.6–14.7%
10.5–12.6%
8.4–10.5%
6.3–8.4%
4.2–6.3%
2.1–4.2%
0.0–2.1%
Max. conc. = 21.1%
Equal area
Lower hemisphere
Borehole orientation
Terzaghi correction
(Min. bias angle = 15 deg)
Number of poles = 18

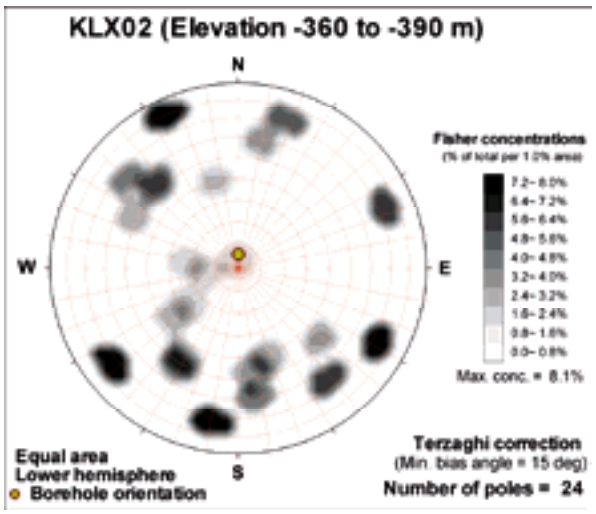
KLX02 (Elevation -360 to -390 m)
N
W
E
S
Fisher concentrations
(% of total per 1.0% area)
7.2– 8.0%
6.4– 7.2%
5.6– 6.4%
4.8– 5.6%
4.0– 4.8%
3.2– 4.0%
2.4– 3.2%
1.6– 2.4%
0.8– 1.6%
0.0– 0.8%
Max. conc. = 8.1%
Equal area
Lower hemisphere
Borehole orientation
Terzaghi correction
(Min. bias angle = 15 deg)
Number of poles = 24

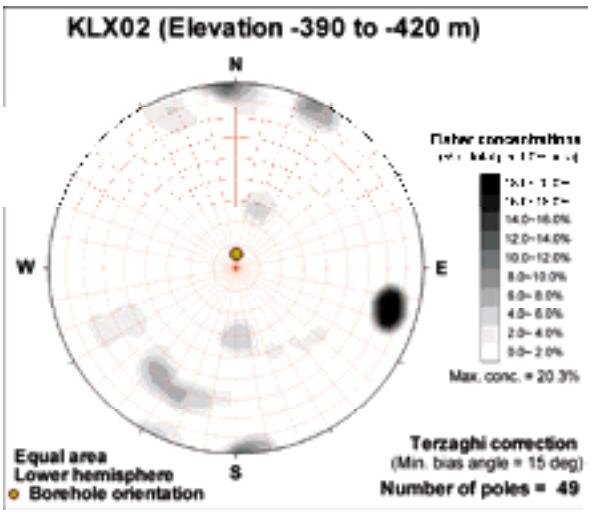
KLX02 (Elevation -390 to -420 m)
N
W
E
S
Max. conc. = 20.3%
Equal area
Lower hemisphere
Borehole orientation
Terzaghi correction
(Min. bias angle = 15 deg)
Number of poles = 49

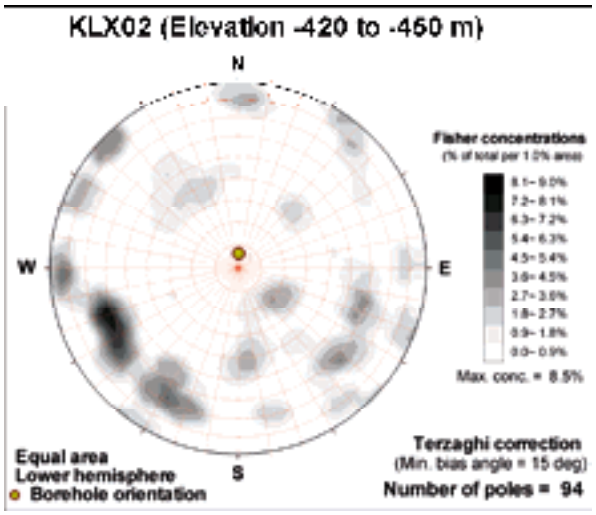
KLX02 (Elevation -420 to -460 m)
N
W
E
S
Fisher concentrations
(% of total per 1.0% area)
8.1– 9.0%
7.2– 8.1%
6.3– 7.2%
5.4– 6.3%
4.5– 5.4%
3.6– 4.5%
2.7– 3.6%
1.8– 2.7%
0.9– 1.8%
0.0– 0.9%
Max. conc. = 8.5%
Equal area
Lower hemisphere
Borehole orientation
Terzaghi correction
(Min. bias angle = 15 deg)
Number of poles = 94

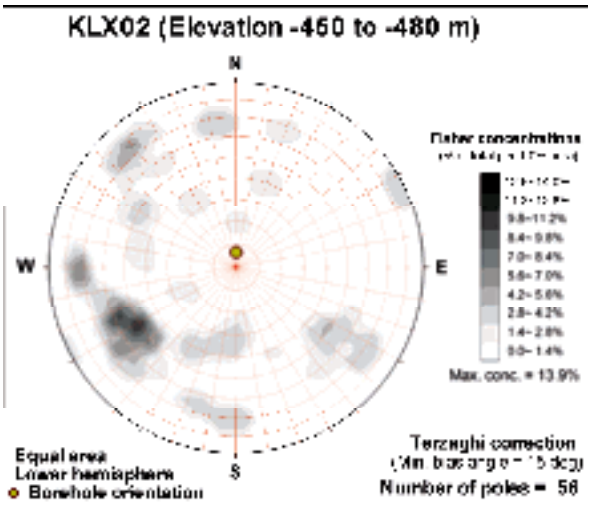
KLX02 (Elevation -460 to -480 m)
N
W
E
S
Max. conc. = 13.9%
Equal area
Lower hemisphere
Borehole orientation
Number of poles = 58

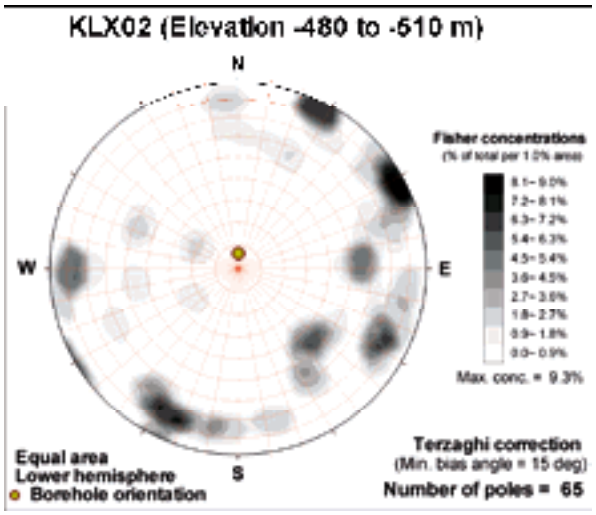
KLX02 (Elevation -480 to -510 m)
N
W
E
S
Fisher concentrations
(% of total per 1.0% area)
8.1– 9.0%
7.2– 8.1%
6.3– 7.2%
5.4– 6.3%
4.5– 5.4%
3.6– 4.5%
2.7– 3.6%
1.8– 2.7%
0.9– 1.8%
0.0– 0.9%
Max. conc. = 9.3%
Equal area
Lower hemisphere
Borehole orientation
Terzaghi correction
(Min. bias angle = 15 deg)
Number of poles = 65

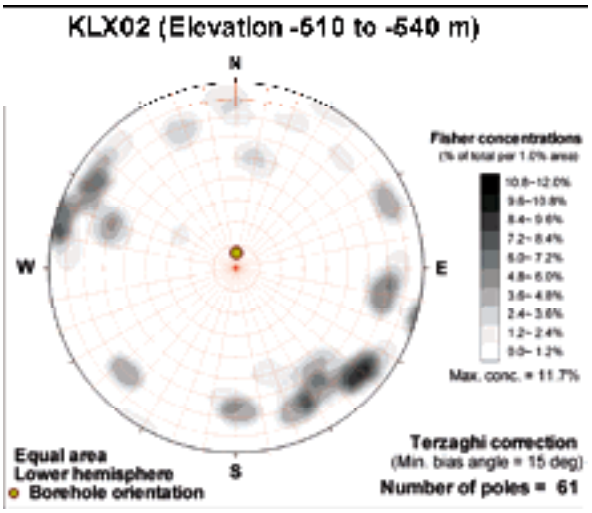
KLX02 (Elevation -510 to -540 m)
N
W
E
S
Fisher concentrations
(% of total per 1.0% area)
10.8–12.0%
9.6–10.8%
8.4– 9.6%
7.2– 8.4%
6.0– 7.2%
4.8– 6.0%
3.6– 4.8%
2.4– 3.6%
1.2– 2.4%
0.0– 1.2%
Max. conc. = 11.7%
Equal area
Lower hemisphere
Borehole orientation
Terzaghi correction
(Min. bias angle = 15 deg)
Number of poles = 61

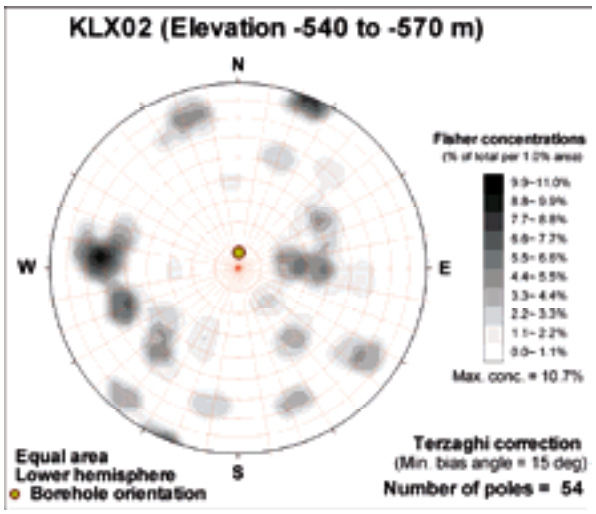
KLX02 (Elevation -540 to -570 m)
N
W
E
S
Fisher concentrations
(% of total per 1.0% area)
9.9–11.0%
8.8–9.9%
7.7–8.8%
6.6–7.7%
5.5–6.6%
4.4–5.5%
3.3–4.4%
2.2–3.3%
1.1–2.2%
0.0–1.1%
Max. conc. = 10.7%
Equal area
Lower hemisphere
Borehole orientation
Terzaghi correction
(Min. bias angle = 15 deg)
Number of poles = 54

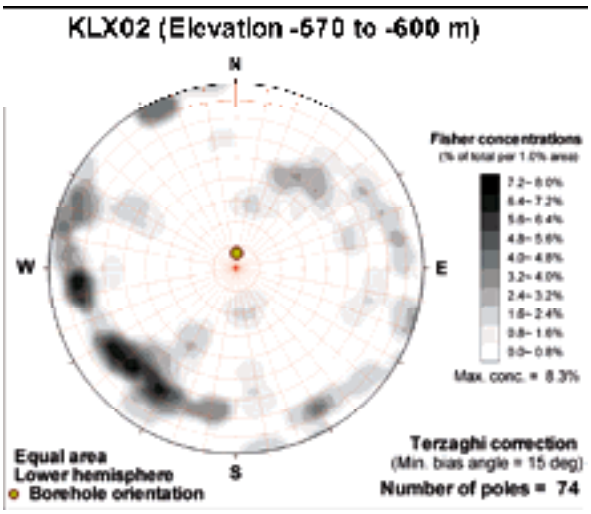
KLX02 (Elevation -570 to -600 m)
N
W
E
S
Fisher concentrations
(% of total per 1.0% area)
7.2–8.0%
6.4–7.2%
5.6–6.4%
4.8–5.6%
4.0–4.8%
3.2–4.0%
2.4–3.2%
1.6–2.4%
0.8–1.6%
0.0–0.8%
Max. conc. = 8.3%
Equal area
Lower hemisphere
Borehole orientation
Terzaghi correction
(Min. bias angle = 15 deg)
Number of poles = 74

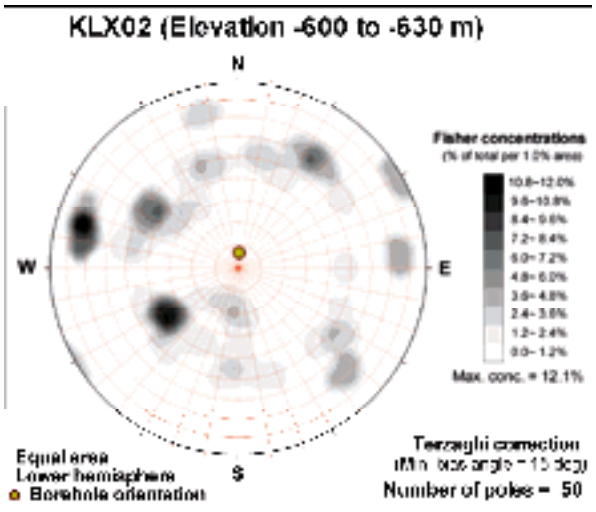
KLX02 (Elevation -600 to -630 m)
N
W
E
S
Fisher concentrations
(% of total per 1.0% area)
10.8–12.0%
9.6–10.8%
8.4–9.6%
7.2–8.4%
6.0–7.2%
4.8–6.0%
3.6–4.8%
2.4–3.6%
1.2–2.4%
0.0–1.2%
Max. conc. = 12.1%
Equal area
Lower hemisphere
Borehole orientation
Terzaghi correction
(Min. bias angle = 15 deg)
Number of poles = 50

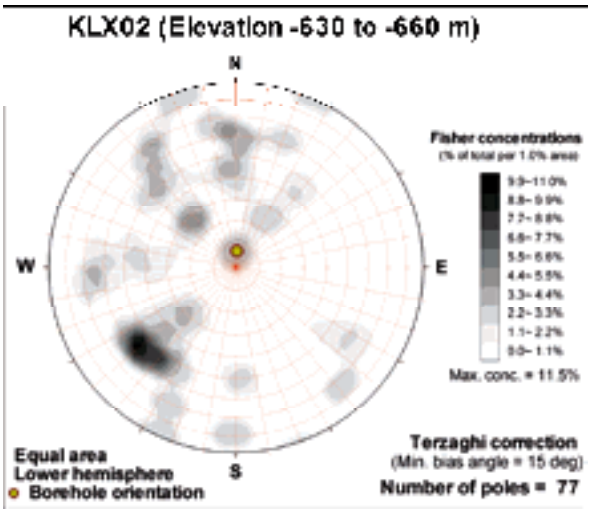
KLX02 (Elevation -630 to -660 m)
N
W
E
S
Fisher concentrations
(% of total per 1.0% area)
9.9–11.0%
8.8–9.9%
7.7–8.8%
6.6–7.7%
5.5–6.6%
4.4–5.5%
3.3–4.4%
2.2–3.3%
1.1–2.2%
0.0–1.1%
Max. conc. = 11.5%
Equal area
Lower hemisphere
Borehole orientation
Terzaghi correction
(Min. bias angle = 15 deg)
Number of poles = 77

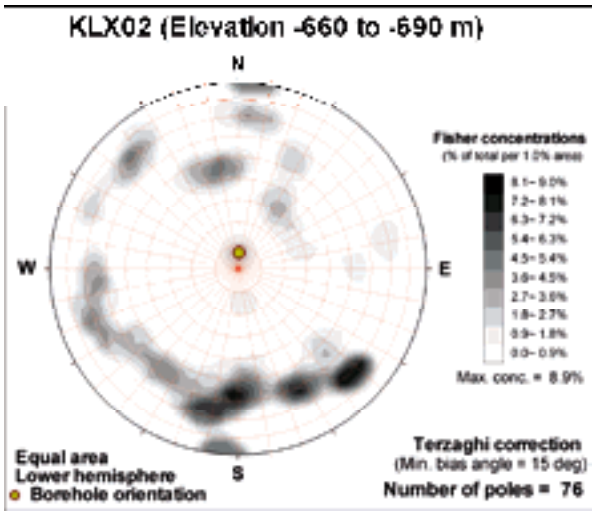
KLX02 (Elevation -660 to -690 m)
N
W
E
S
Fisher concentrations
(% of total per 1.0% area)
8.1–9.0%
7.2–8.1%
6.3–7.2%
5.4–6.3%
4.5–5.4%
3.6–4.5%
2.7–3.6%
1.8–2.7%
0.9–1.8%
0.0–0.9%
Max. conc. = 8.9%
Equal area
Lower hemisphere
Borehole orientation
Terzaghi correction
(Min. bias angle = 15 deg)
Number of poles = 76

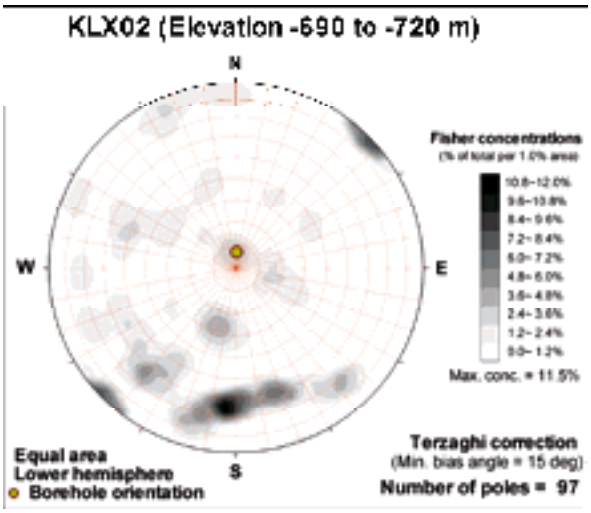
KLX02 (Elevation -690 to -720 m)
N
W
E
S
Fisher concentrations
(% of total per 1.0% area)
10.8–12.0%
9.6–10.8%
8.4–9.6%
7.2–8.4%
6.0–7.2%
4.8–6.0%
3.6–4.8%
2.4–3.6%
1.2–2.4%
0.0–1.2%
Max. conc. = 11.5%
Equal area
Lower hemisphere
Borehole orientation
Terzaghi correction
(Min. bias angle = 15 deg)
Number of poles = 97

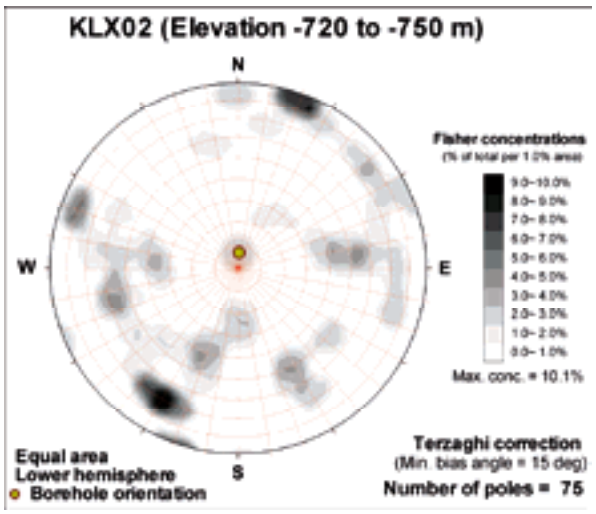
KLX02 (Elevation -720 to -750 m)
N
W
E
S
Fisher concentrations
(% of total per 1.0% area)
9.0–10.0%
8.0–9.0%
7.0–8.0%
6.0–7.0%
5.0–6.0%
4.0–5.0%
3.0–4.0%
2.0–3.0%
1.0–2.0%
0.0–1.0%
Max. conc. = 10.1%
Equal area
Lower hemisphere
Borehole orientation
Terzaghi correction
(Min. bias angle = 15 deg)
Number of poles = 75

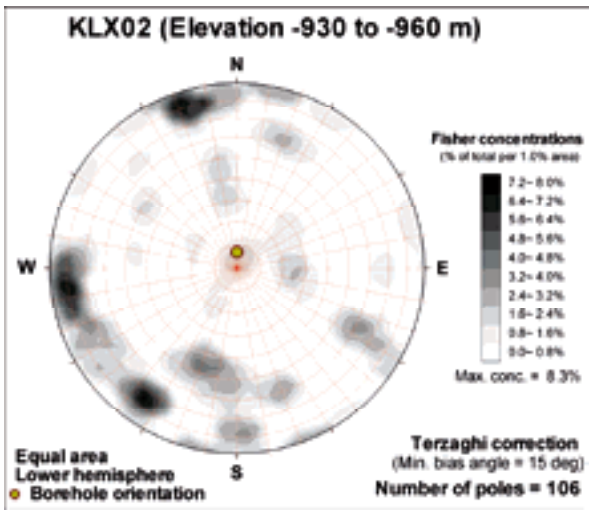
KLX02 (Elevation -930 to -960 m)
N
W
E
S
Fisher concentrations
(% of total per 1.0% area)
7.2–8.0%
6.4–7.2%
5.6–6.4%
4.8–5.6%
4.0–4.8%
3.2–4.0%
2.4–3.2%
1.6–2.4%
0.8–1.6%
0.0–0.8%
Max. conc. = 8.3%
Equal area
Lower hemisphere
Borehole orientation
Terzaghi correction
(Min. bias angle = 15 deg)
Number of poles = 106

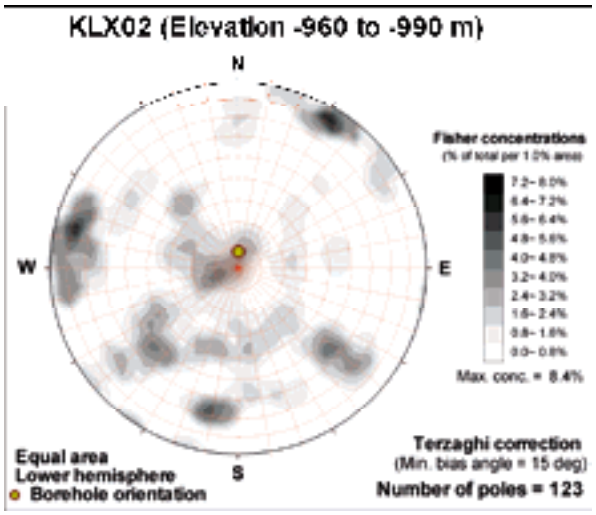
KLX02 (Elevation -960 to -990 m)
N
W
E
S
Fisher concentrations
(% of total per 1.0% area)
7.2–8.0%
6.4–7.2%
5.6–6.4%
4.8–5.6%
4.0–4.8%
3.2–4.0%
2.4–3.2%
1.6–2.4%
0.8–1.6%
0.0–0.8%
Max. conc. = 8.4%
Equal area
Lower hemisphere
Borehole orientation
Terzaghi correction
(Min. bias angle = 15 deg)
Number of poles = 123

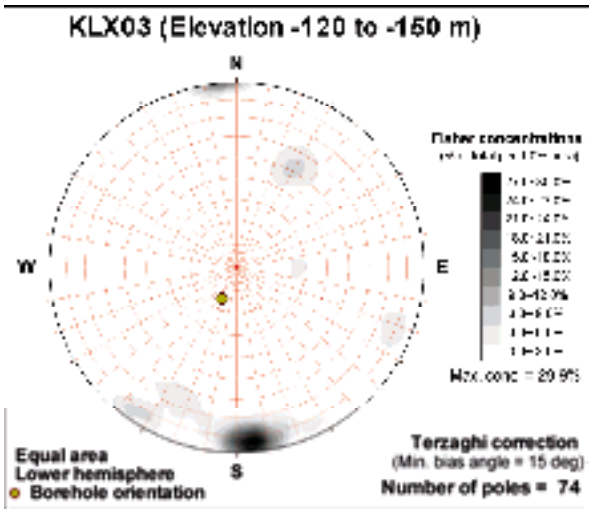
KLX03 (Elevation -120 to -150 m)
N
W
E
S
Equal area
Lower hemisphere
Borehole orientation
Terzaghi correction
(Min. bias angle = 15 deg)
Number of poles = 74

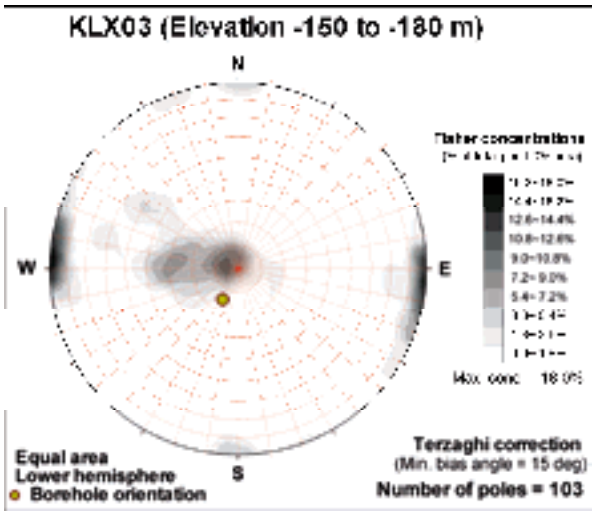
KLX03 (Elevation -150 to -180 m)
N
W
E
S
Equal area
Lower hemisphere
Borehole orientation
Terzaghi correction
(Min. bias angle = 15 deg)
Number of poles = 103

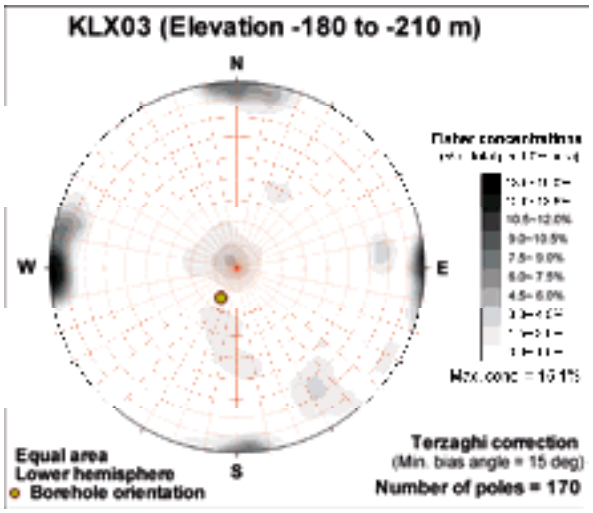
KLX03 (Elevation -180 to -210 m)
N
W
E
S
Equal area
Lower hemisphere
Borehole orientation
Terzaghi correction
(Min. bias angle = 15 deg)
Number of poles = 170

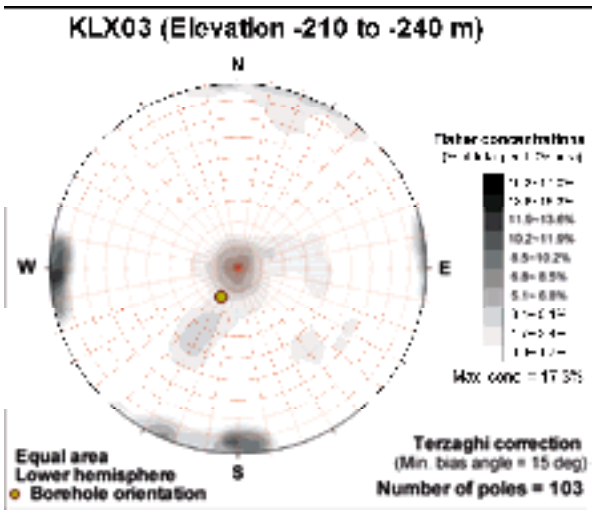
KLX03 (Elevation -210 to -240 m)
N
W
E
S
Fisher concentrations
Max. conc = 17.5%
Equal area
Lower hemisphere
Borehole orientation
Terzaghi correction
(Min. bias angle = 15 deg)
Number of poles = 103

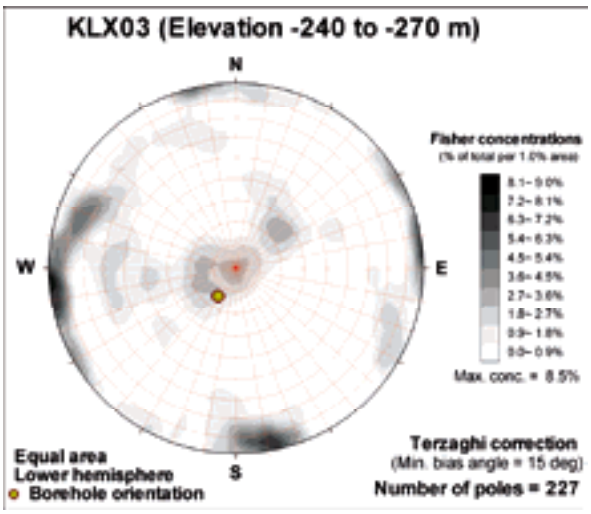
KLX03 (Elevation -240 to -270 m)
N
W
E
S
Fisher concentrations
Max. conc. = 8.5%
Equal area
Lower hemisphere
Borehole orientation
Terzaghi correction
(Min. bias angle = 15 deg)
Number of poles = 227

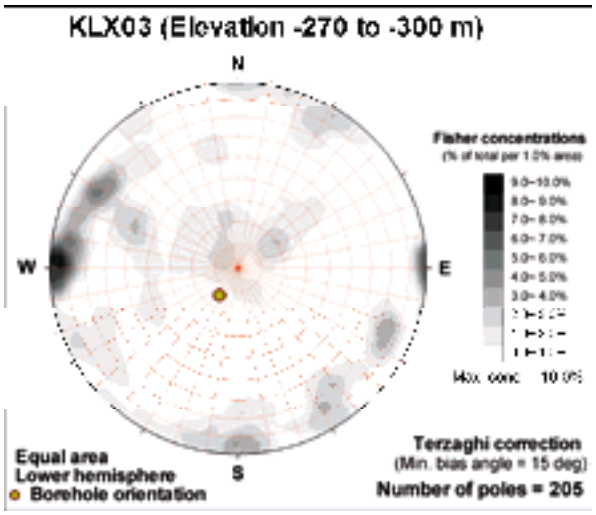
KLX03 (Elevation -270 to -300 m)
N
W
E
S
Fisher concentrations
Equal area
Lower hemisphere
Borehole orientation
Terzaghi correction
(Min. bias angle = 15 deg)
Number of poles = 205

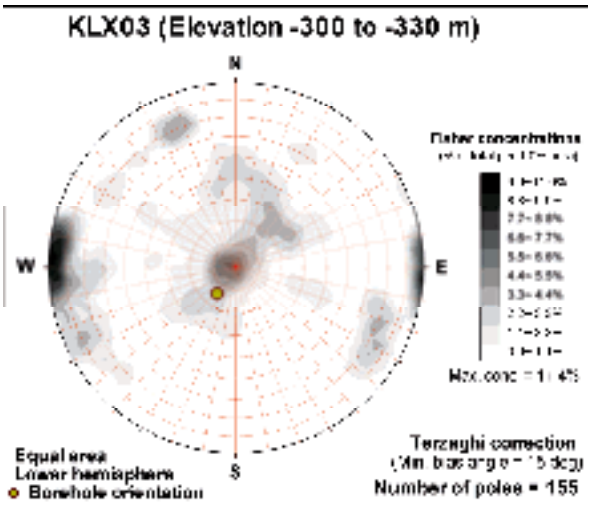
KLX03 (Elevation -300 to -330 m)
N
W
E
S
Fisher concentrations
Equal area
Lower hemisphere
Borehole orientation
Terzaghi correction
Number of poles = 155

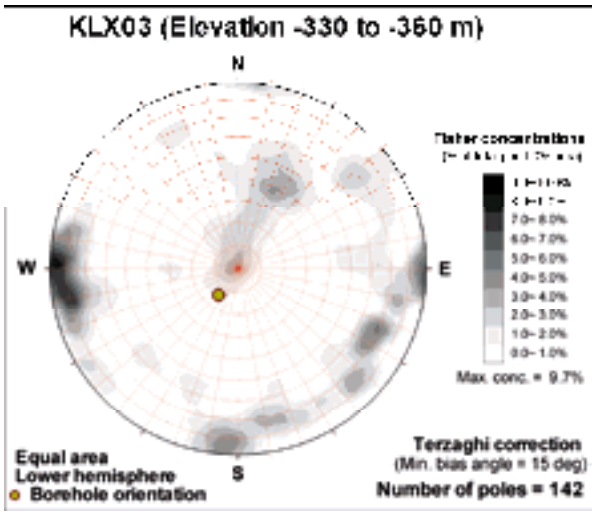
KLX03 (Elevation -330 to -360 m)
N
W
E
S
Fisher concentrations
Max. conc. = 9.7%
Equal area
Lower hemisphere
Borehole orientation
Terzaghi correction
(Min. bias angle = 15 deg)
Number of poles = 142

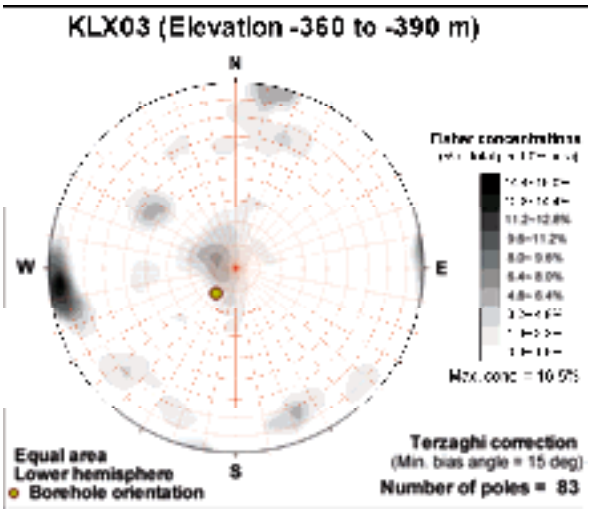
KLX03 (Elevation -360 to -390 m)
N
W
E
S
Fisher concentrations
Equal area
Lower hemisphere
Borehole orientation
Terzaghi correction
(Min. bias angle = 15 deg)
Number of poles = 83

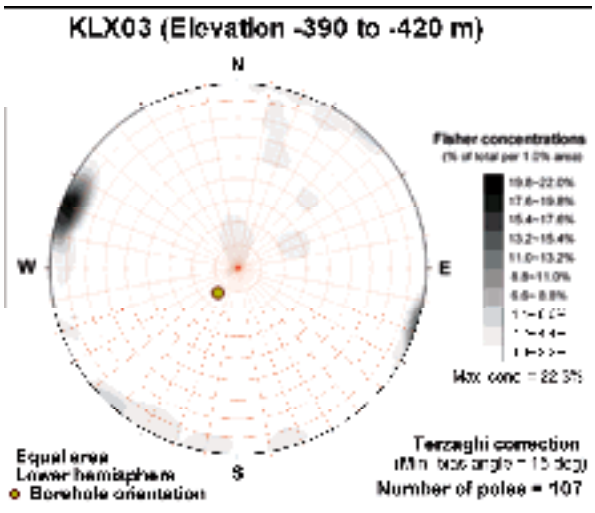
KLX03 (Elevation -390 to -420 m)
N
W
E
S
Fisher concentrations
(% of total per 1.0% area)
Max. conc = 22.3%
Equal area
Lower hemisphere
Borehole orientation
Terzaghi correction
(Min. bias angle = 15 deg)
Number of poles = 107

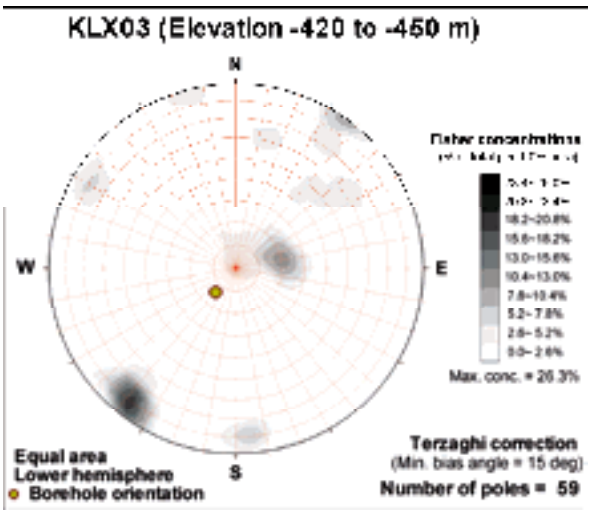
KLX03 (Elevation -420 to -450 m)
N
W
E
S
Max. conc. = 26.3%
Equal area
Lower hemisphere
Borehole orientation
Terzaghi correction
(Min. bias angle = 15 deg)
Number of poles = 59

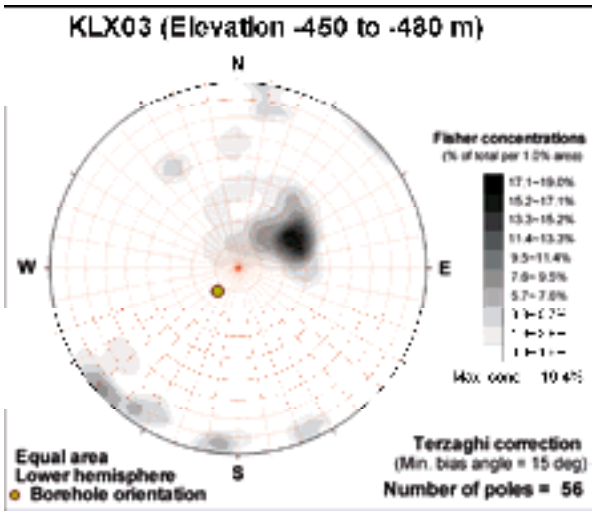
KLX03 (Elevation -450 to -480 m)
N
W
E
S
Fisher concentrations
(% of total per 1.0% area)
Equal area
Lower hemisphere
Borehole orientation
Terzaghi correction
(Min. bias angle = 15 deg)
Number of poles = 56

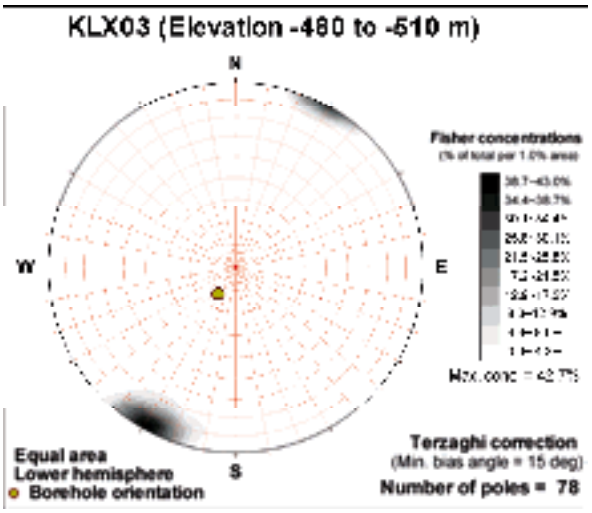
KLX03 (Elevation -480 to -510 m)
N
W
E
S
Fisher concentrations
(% of total per 1.0% area)
Equal area
Lower hemisphere
Borehole orientation
Terzaghi correction
(Min. bias angle = 15 deg)
Number of poles = 78

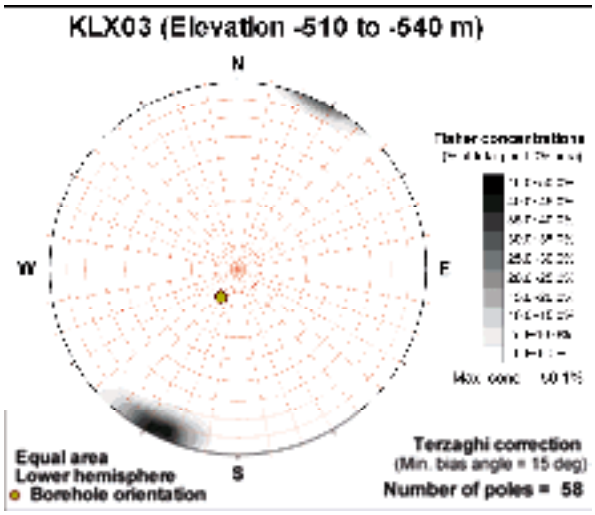
KLX03 (Elevation -510 to -540 m)
N
W
E
S
Equal area
Lower hemisphere
Borehole orientation
Terzaghi correction
(Min. bias angle = 15 deg)
Number of poles = 58

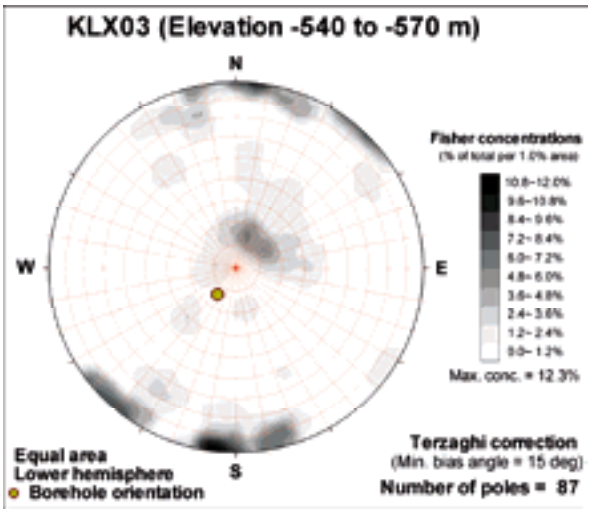
KLX03 (Elevation -540 to -570 m)
N
W
E
S
Fisher concentrations
(% of total per 1.0% area)
Max. conc. = 12.3%
Equal area
Lower hemisphere
Borehole orientation
Terzaghi correction
(Min. bias angle = 15 deg)
Number of poles = 87

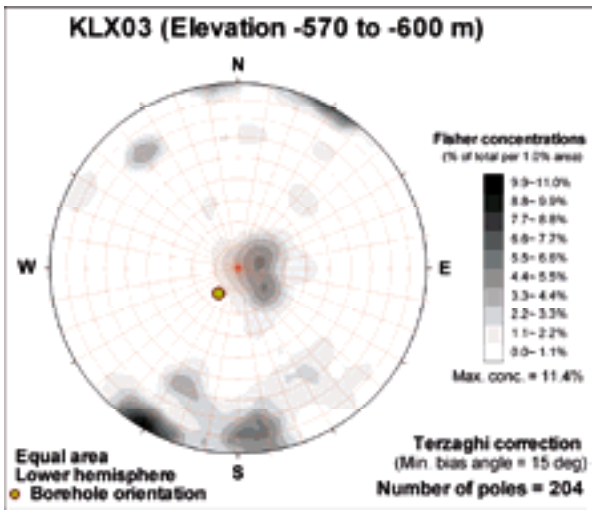
KLX03 (Elevation -570 to -600 m)
N
W
E
S
Fisher concentrations
(% of total per 1.0% area)
9.9–11.0%
8.8–9.9%
7.7–8.8%
6.6–7.7%
5.5–6.6%
4.4–5.5%
3.3–4.4%
2.2–3.3%
1.1–2.2%
0.0–1.1%
Max. conc. = 11.4%
Equal area
Lower hemisphere
Borehole orientation
Terzaghi correction
(Min. bias angle = 15 deg)
Number of poles = 204

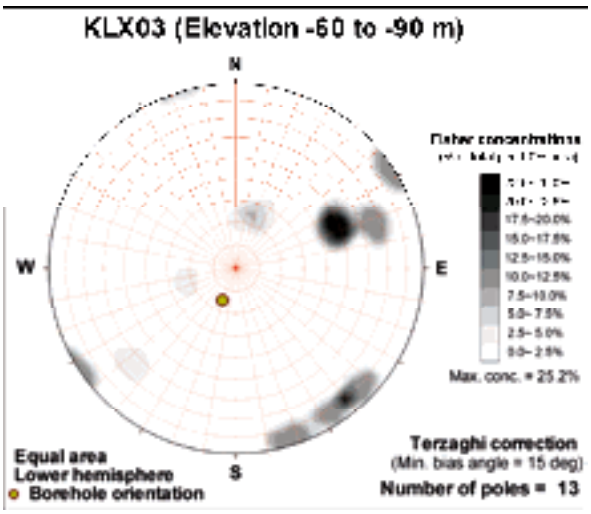
KLX03 (Elevation -60 to -90 m)
N
W
E
S
Fisher concentrations
Max. conc. = 25.2%
Equal area
Lower hemisphere
Borehole orientation
Terzaghi correction
(Min. bias angle = 15 deg)
Number of poles = 13

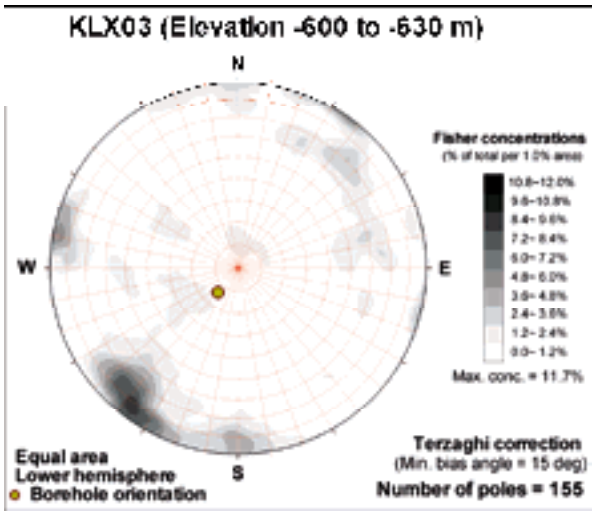
KLX03 (Elevation -600 to -630 m)
N
W
E
S
Fisher concentrations
(% of total per 1.0% area)
10.8–12.0%
9.6–10.8%
8.4–9.6%
7.2–8.4%
6.0–7.2%
4.8–6.0%
3.6–4.8%
2.4–3.6%
1.2–2.4%
0.0–1.2%
Max. conc. = 11.7%
Equal area
Lower hemisphere
Borehole orientation
Terzaghi correction
(Min. bias angle = 15 deg)
Number of poles = 155

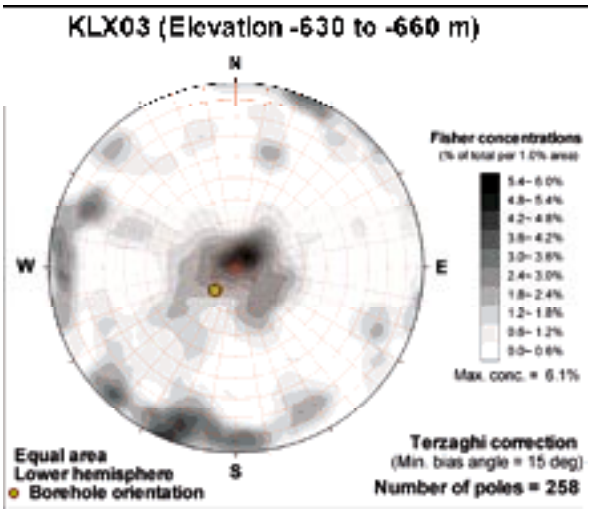
KLX03 (Elevation -630 to -660 m)
N
W
E
S
Fisher concentrations
(% of total per 1.0% area)
5.4–6.0%
4.8–5.4%
4.2–4.8%
3.6–4.2%
3.0–3.6%
2.4–3.0%
1.8–2.4%
1.2–1.8%
0.6–1.2%
0.0–0.6%
Max. conc. = 6.1%
Equal area
Lower hemisphere
Borehole orientation
Terzaghi correction
(Min. bias angle = 15 deg)
Number of poles = 258

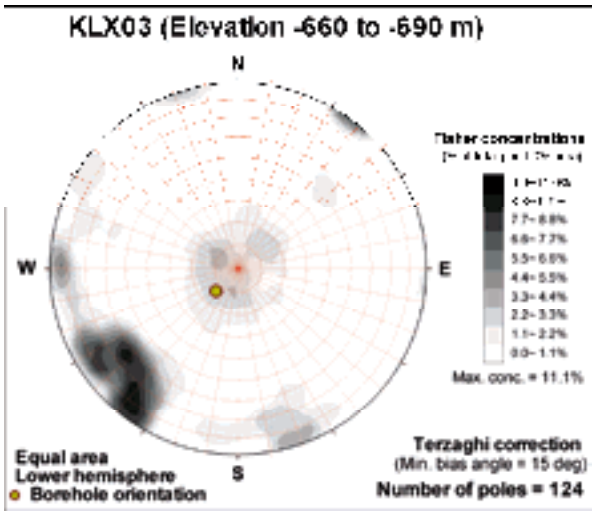
KLX03 (Elevation -660 to -690 m)
N
W
E
S
Fisher concentrations
7.7–8.8%
6.6–7.7%
5.5–6.6%
4.4–5.5%
3.3–4.4%
2.2–3.3%
1.1–2.2%
0.0–1.1%
Max. conc. = 11.1%
Equal area
Lower hemisphere
Borehole orientation
Terzaghi correction
(Min. bias angle = 15 deg)
Number of poles = 124

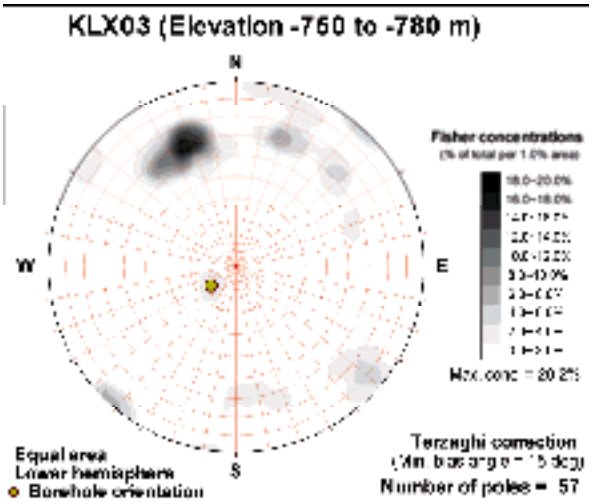
KLX03 (Elevation -750 to -780 m)
N
W
E
S
Fisher concentrations
(% of total per 1.0% area)
Max. conc. = 20.2%
Equal area
Lower hemisphere
Borehole orientation
Terzaghi correction
(Min. bias angle = 15 deg)
Number of poles = 57

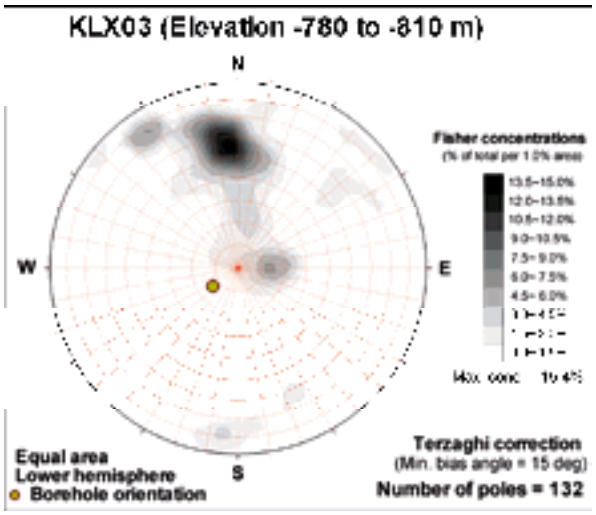
KLX03 (Elevation -780 to -810 m)
N
W
E
S
Fisher concentrations
(% of total per 1.0% area)
Max. conc. = 19.4%
Equal area
Lower hemisphere
Borehole orientation
Terzaghi correction
(Min. bias angle = 15 deg)
Number of poles = 132

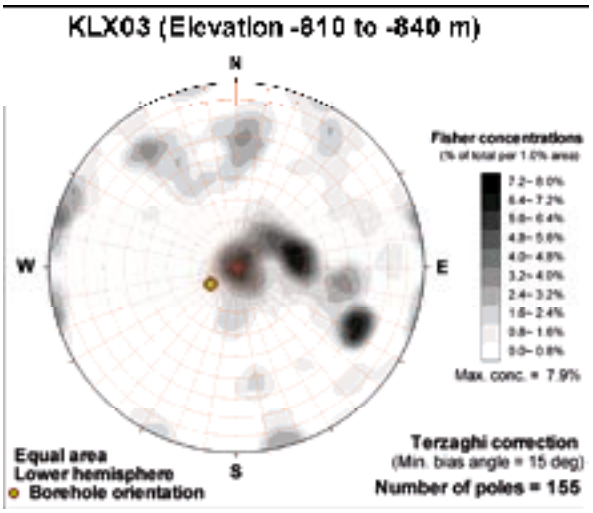
KLX03 (Elevation -810 to -840 m)
N
W
E
S
Fisher concentrations
(% of total per 1.0% area)
Max. conc. = 7.9%
Equal area
Lower hemisphere
Borehole orientation
Terzaghi correction
(Min. bias angle = 15 deg)
Number of poles = 155

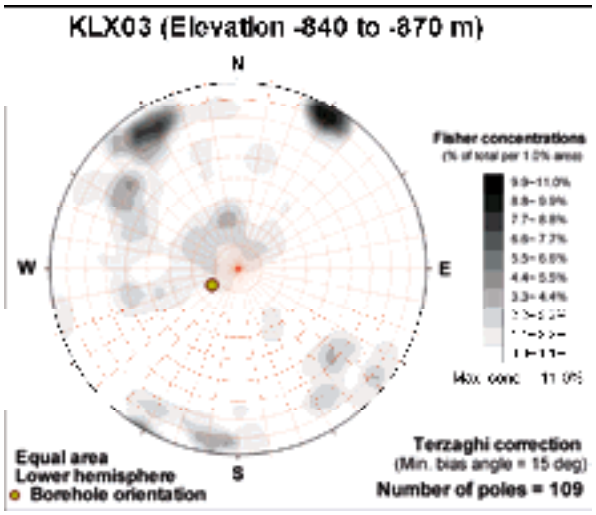
KLX03 (Elevation -840 to -870 m)
N
W
E
S
Fisher concentrations
(% of total per 1.0% area)
Max. conc. = 11.0%
Equal area
Lower hemisphere
Borehole orientation
Terzaghi correction
(Min. bias angle = 15 deg)
Number of poles = 109

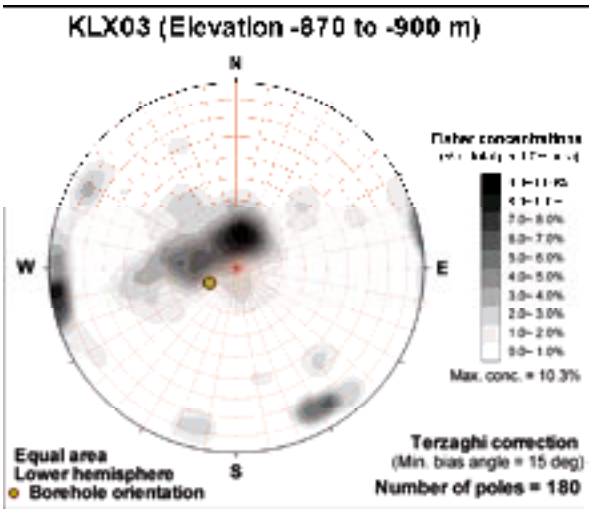
KLX03 (Elevation -870 to -900 m)
N
W
E
S
Max. conc. = 10.3%
Equal area
Lower hemisphere
Borehole orientation
Terzaghi correction
(Min. bias angle = 15 deg)
Number of poles = 180

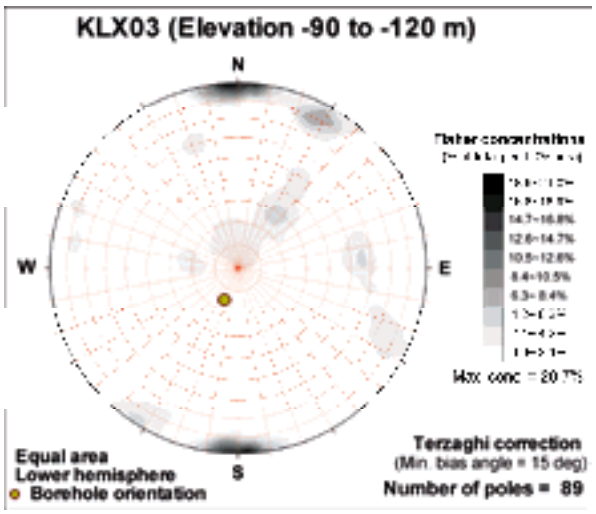
KLX03 (Elevation -90 to -120 m)
N
W
E
S
Fisher concentrations
Max. conc. = 20.7%
Equal area
Lower hemisphere
Borehole orientation
Terzaghi correction
(Min. bias angle = 15 deg)
Number of poles = 89

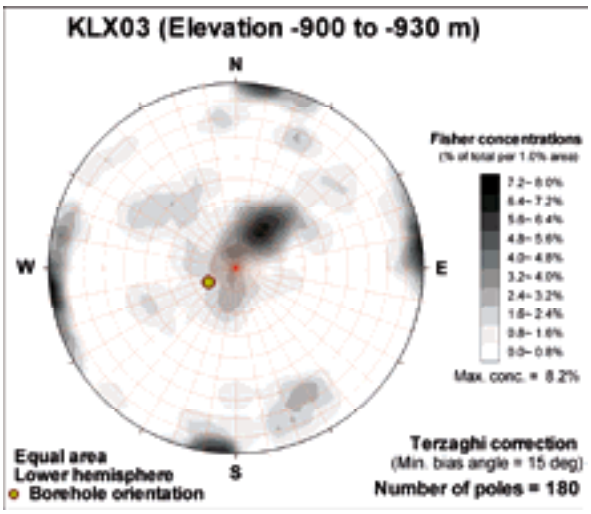
KLX03 (Elevation -900 to -930 m)
N
W
E
S
Fisher concentrations
Max. conc. = 8.2%
Equal area
Lower hemisphere
Borehole orientation
Terzaghi correction
(Min. bias angle = 15 deg)
Number of poles = 180

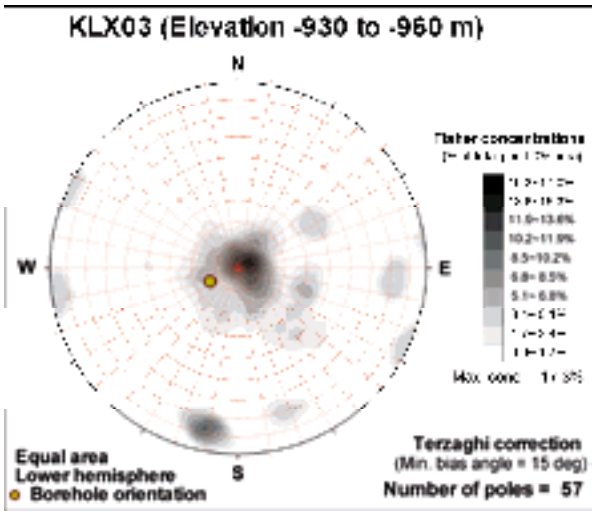
KLX03 (Elevation -930 to -960 m)
N
W
E
S
Fisher concentrations
Equal area
Lower hemisphere
Borehole orientation
Terzaghi correction
(Min. bias angle = 15 deg)
Number of poles = 57

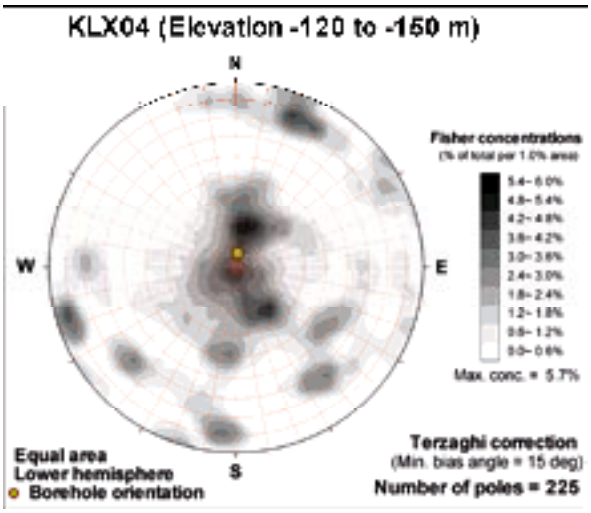
KLX04 (Elevation -120 to -150 m)
N
W
E
S
Fisher concentrations
Max. conc. = 5.7%
Equal area
Lower hemisphere
Borehole orientation
Terzaghi correction
(Min. bias angle = 15 deg)
Number of poles = 225

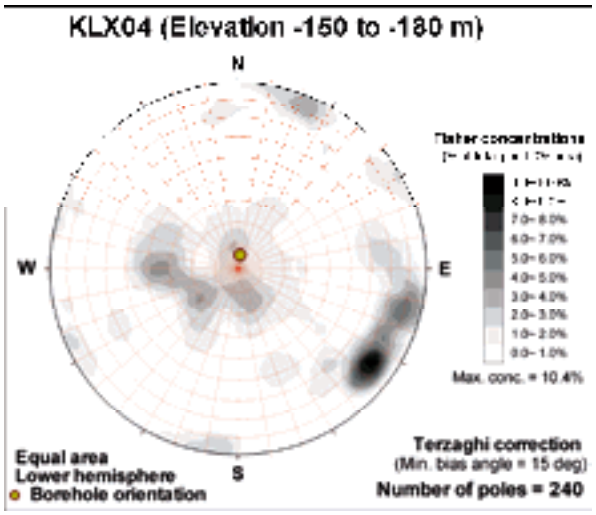
KLX04 (Elevation -150 to -180 m)
N
W
E
S
Fisher concentrations
Max. conc. = 10.4%
Equal area
Lower hemisphere
Borehole orientation
Terzaghi correction
(Min. bias angle = 15 deg)
Number of poles = 240

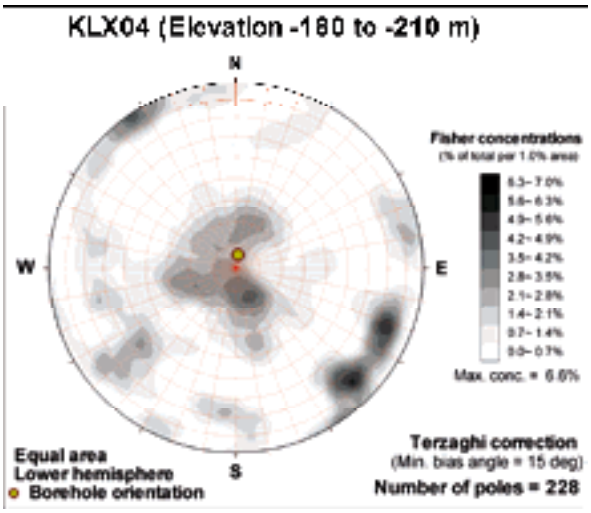
KLX04 (Elevation -180 to -210 m)
N
W
E
S
Fisher concentrations
Max. conc. = 6.6%
Equal area
Lower hemisphere
Borehole orientation
Terzaghi correction
(Min. bias angle = 15 deg)
Number of poles = 228

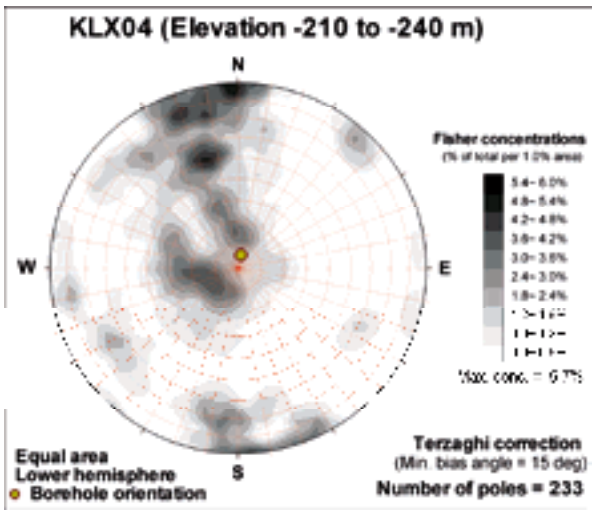
KLX04 (Elevation -210 to -240 m)
N
W
E
S
Fisher concentrations
Equal area
Lower hemisphere
Borehole orientation
Terzaghi correction
(Min. bias angle = 15 deg)
Number of poles = 233

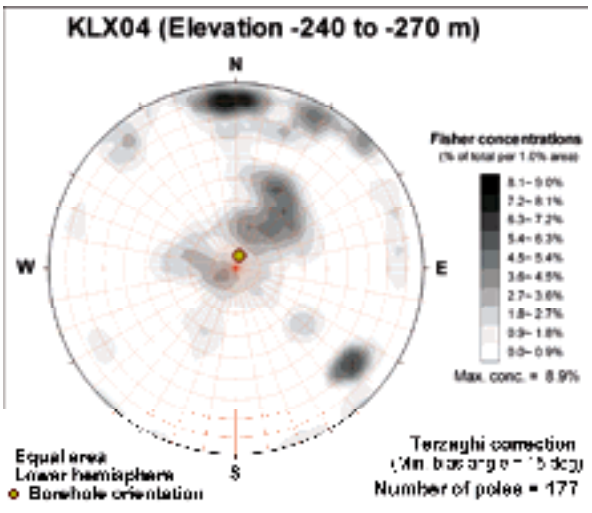
KLX04 (Elevation -240 to -270 m)
N
W
E
S
Fisher concentrations
Max. conc. = 8.9%
Equal area
Lower hemisphere
Borehole orientation
Terzaghi correction
Number of poles = 177

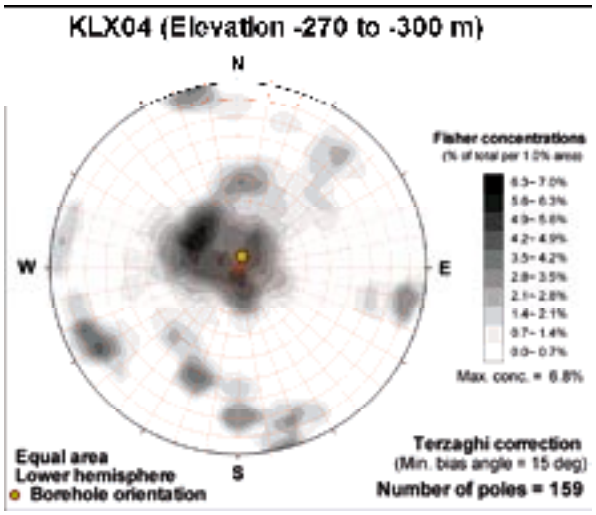
KLX04 (Elevation -270 to -300 m)
N
W
E
S
Fisher concentrations
Max. conc. = 6.8%
Equal area
Lower hemisphere
Borehole orientation
Terzaghi correction
(Min. bias angle = 15 deg)
Number of poles = 159

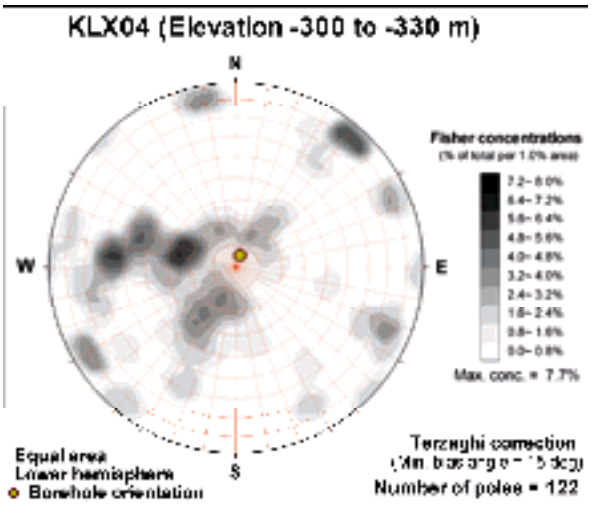
KLX04 (Elevation -300 to -330 m)
N
W
E
S
Fisher concentrations
Max. conc. = 7.7%
Equal area
Lower hemisphere
Borehole orientation
Terzaghi correction
Number of poles = 122

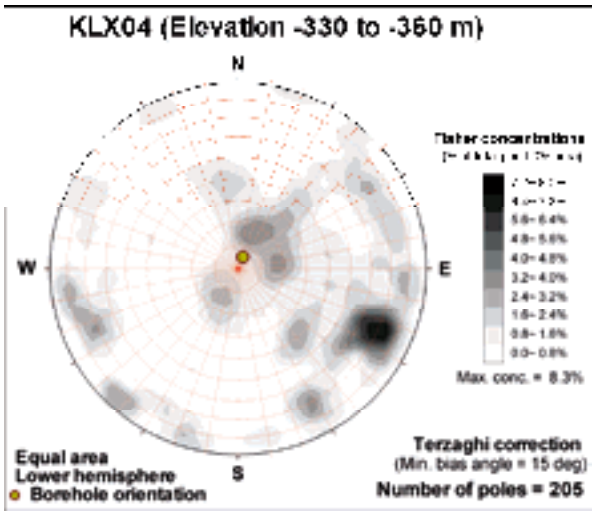
KLX04 (Elevation -330 to -360 m)
N
W
E
S
Max. conc. = 8.3%
Equal area
Lower hemisphere
Borehole orientation
Terzaghi correction
(Min. bias angle = 15 deg)
Number of poles = 205

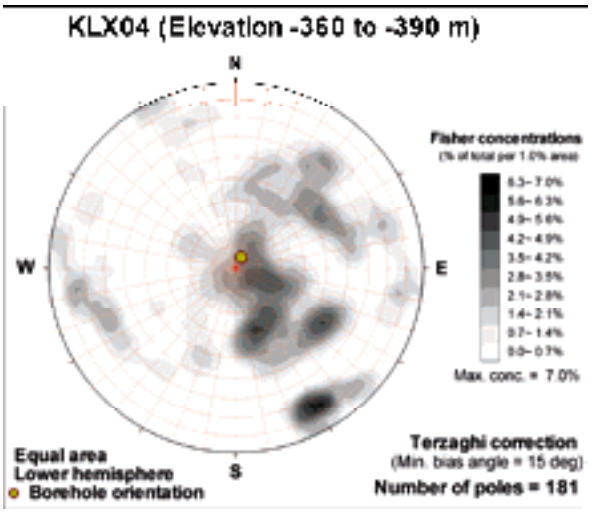
KLX04 (Elevation -360 to -390 m)
N
W
E
S
Fisher concentrations
Max. conc. = 7.0%
Equal area
Lower hemisphere
Borehole orientation
Terzaghi correction
(Min. bias angle = 15 deg)
Number of poles = 181

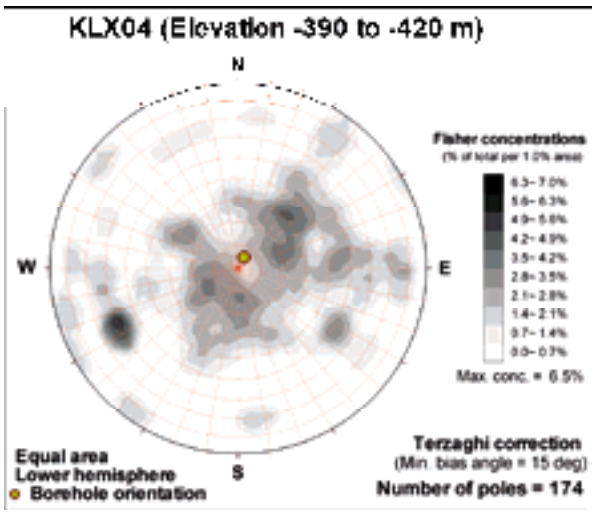
KLX04 (Elevation -390 to -420 m)
N
W
E
S
Fisher concentrations
(% of total per 1.0% area)
6.3–7.0%
5.6–6.3%
4.9–5.6%
4.2–4.9%
3.5–4.2%
2.8–3.5%
2.1–2.8%
1.4–2.1%
0.7–1.4%
0.0–0.7%
Max. conc. = 6.5%
Equal area
Lower hemisphere
Borehole orientation
Terzaghi correction
(Min. bias angle = 15 deg)
Number of poles = 174

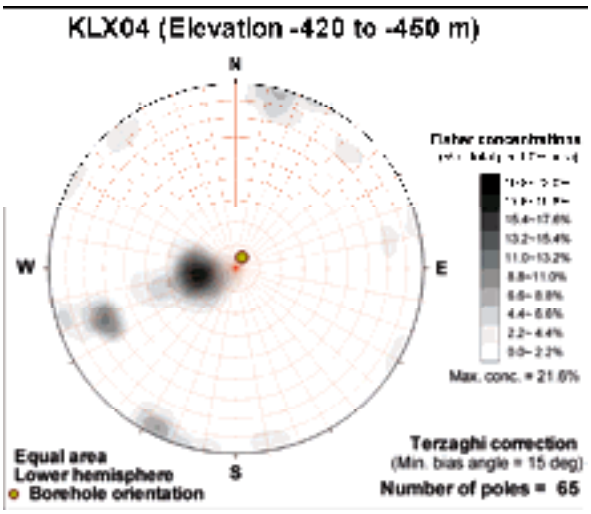
KLX04 (Elevation -420 to -450 m)
N
W
E
S
Max. conc. = 21.6%
Equal area
Lower hemisphere
Borehole orientation
Terzaghi correction
(Min. bias angle = 15 deg)
Number of poles = 65

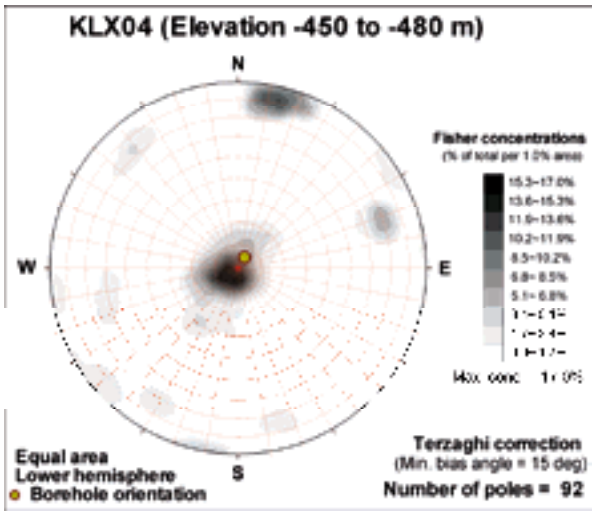
KLX04 (Elevation -450 to -480 m)
N
W
E
S
Fisher concentrations
(% of total per 1.0% area)
Equal area
Lower hemisphere
Borehole orientation
Terzaghi correction
(Min. bias angle = 15 deg)
Number of poles = 92

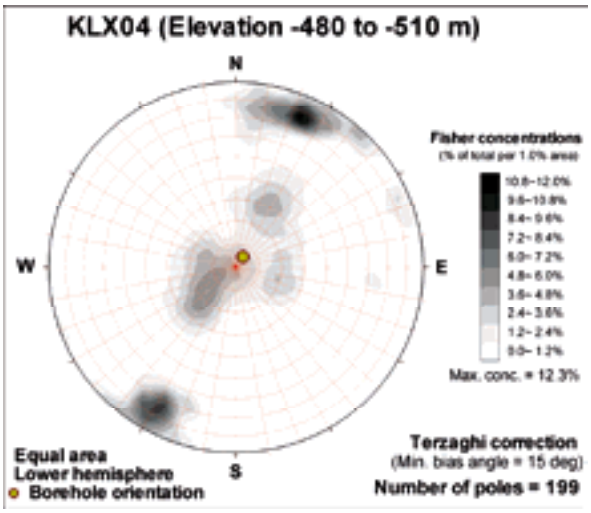
KLX04 (Elevation -480 to -510 m)
N
W
E
S
Fisher concentrations
(% of total per 1.0% area)
Max. conc. = 12.3%
Equal area
Lower hemisphere
Borehole orientation
Terzaghi correction
(Min. bias angle = 15 deg)
Number of poles = 199

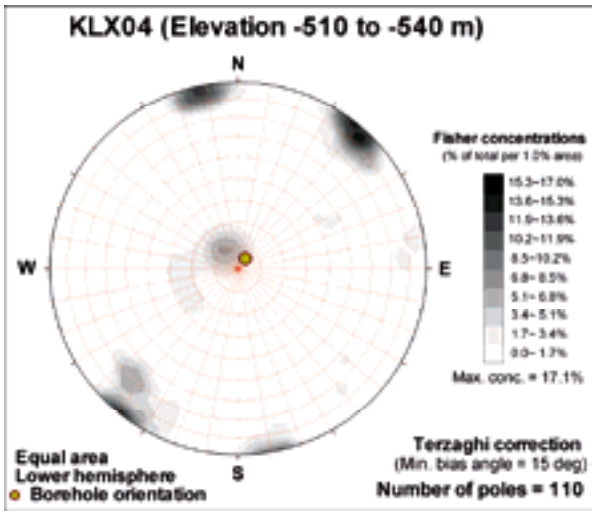
KLX04 (Elevation -510 to -540 m)
N
W
E
S
Fisher concentrations
(% of total per 1.0% area)
Max. conc. = 17.1%
Equal area
Lower hemisphere
Borehole orientation
Terzaghi correction
(Min. bias angle = 15 deg)
Number of poles = 110

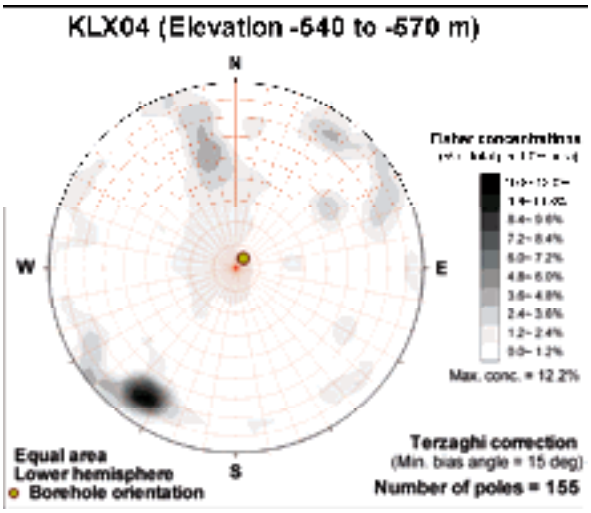
KLX04 (Elevation -540 to -570 m)
N
W
E
S
Max. conc. = 12.2%
Equal area
Lower hemisphere
Borehole orientation
Terzaghi correction
(Min. bias angle = 15 deg)
Number of poles = 155

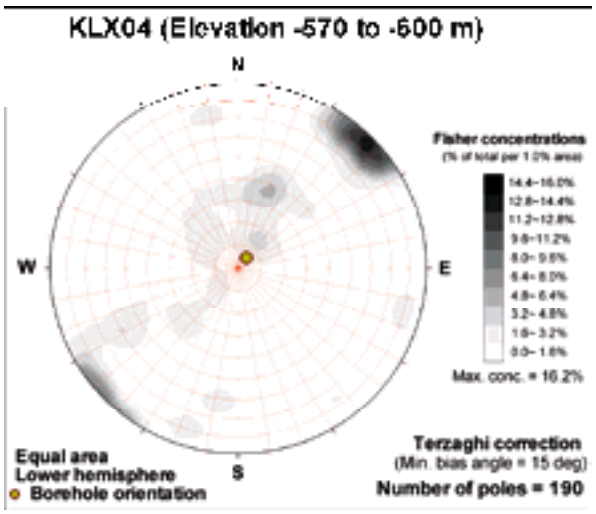
KLX04 (Elevation -570 to -600 m)
N
W
E
S
Fisher concentrations
(% of total per 1.0% area)
14.4–16.0%
12.8–14.4%
11.2–12.8%
9.6–11.2%
8.0–9.6%
6.4–8.0%
4.8–6.4%
3.2–4.8%
1.6–3.2%
0.0–1.6%
Max. conc. = 16.2%
Equal area
Lower hemisphere
Borehole orientation
Terzaghi correction
(Min. bias angle = 15 deg)
Number of poles = 190

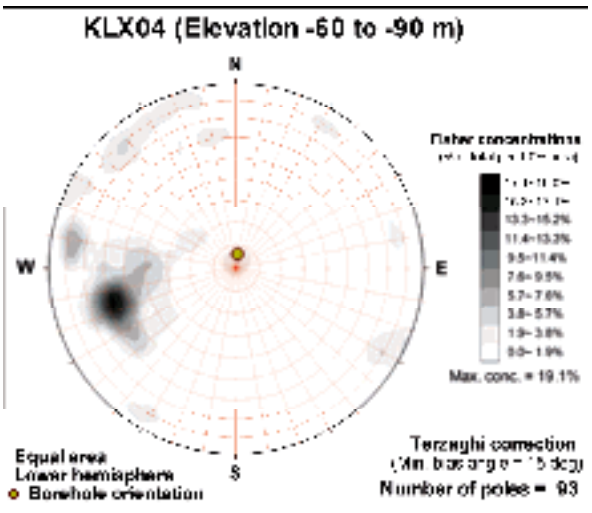
KLX04 (Elevation -60 to -90 m)
N
W
E
S
Max. conc. = 19.1%
Equal area
Lower hemisphere
Borehole orientation
Number of poles = 93

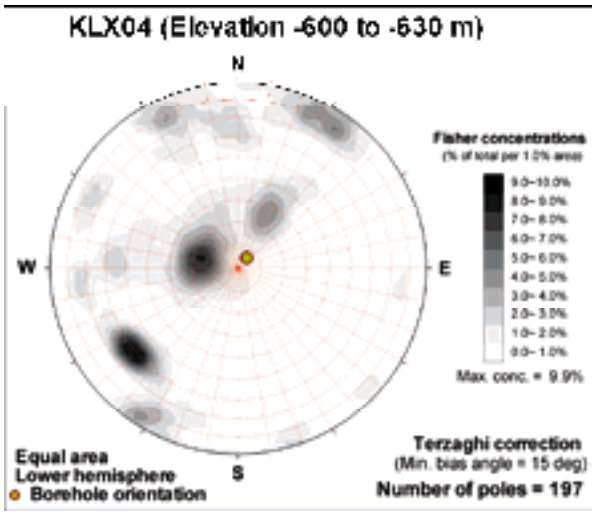
KLX04 (Elevation -600 to -630 m)
N
W
E
S
Fisher concentrations
(% of total per 1.0% area)
9.0–10.0%
8.0–9.0%
7.0–8.0%
6.0–7.0%
5.0–6.0%
4.0–5.0%
3.0–4.0%
2.0–3.0%
1.0–2.0%
0.0–1.0%
Max. conc. = 9.9%
Equal area
Lower hemisphere
Borehole orientation
Terzaghi correction
(Min. bias angle = 15 deg)
Number of poles = 197

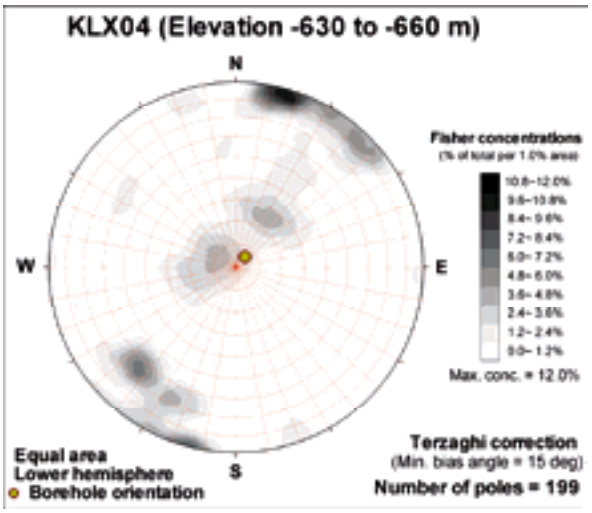
KLX04 (Elevation -630 to -660 m)
N
W
E
S
Fisher concentrations
(% of total per 1.0% area)
10.8–12.0%
9.6–10.8%
8.4–9.6%
7.2–8.4%
6.0–7.2%
4.8–6.0%
3.6–4.8%
2.4–3.6%
1.2–2.4%
0.0–1.2%
Max. conc. = 12.0%
Equal area
Lower hemisphere
Borehole orientation
Terzaghi correction
(Min. bias angle = 15 deg)
Number of poles = 199

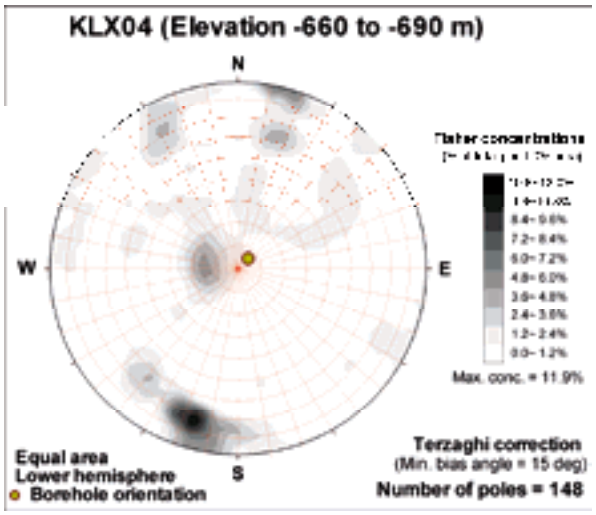
KLX04 (Elevation -660 to -690 m)
N
W
E
S
Max. conc. = 11.9%
Equal area
Lower hemisphere
Borehole orientation
Terzaghi correction
(Min. bias angle = 15 deg)
Number of poles = 148

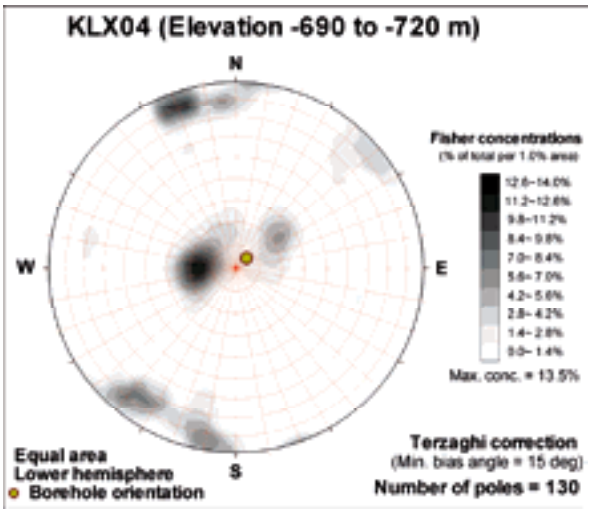
KLX04 (Elevation -690 to -720 m)
N
W
E
S
Fisher concentrations
(% of total per 1.0% area)
12.6–14.0%
11.2–12.6%
9.8–11.2%
8.4–9.8%
7.0–8.4%
5.6–7.0%
4.2–5.6%
2.8–4.2%
1.4–2.8%
0.0–1.4%
Max. conc. = 13.5%
Equal area
Lower hemisphere
Borehole orientation
Terzaghi correction
(Min. bias angle = 15 deg)
Number of poles = 130

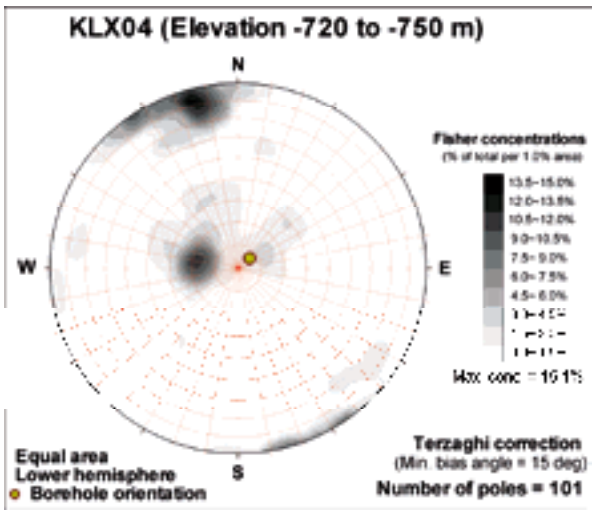
KLX04 (Elevation -720 to -750 m)
N
W
E
S
Fisher concentrations
Equal area
Lower hemisphere
Borehole orientation
Terzaghi correction
(Min. bias angle = 15 deg)
Number of poles = 101

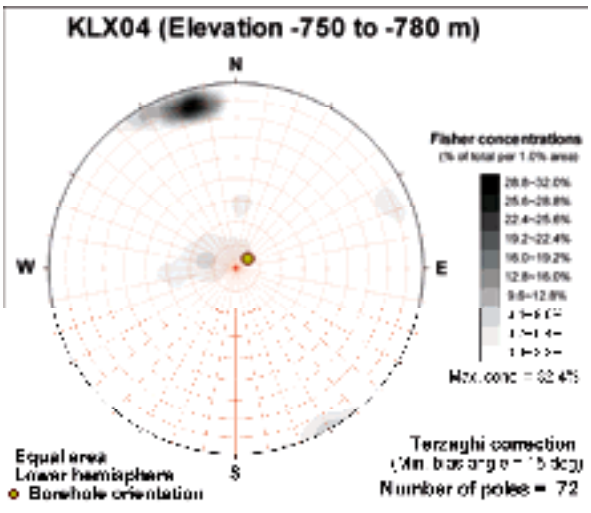
KLX04 (Elevation -750 to -780 m)
N
W
E
S
Fisher concentrations
Equal area
Lower hemisphere
Borehole orientation
Terzaghi correction
Number of poles = 72

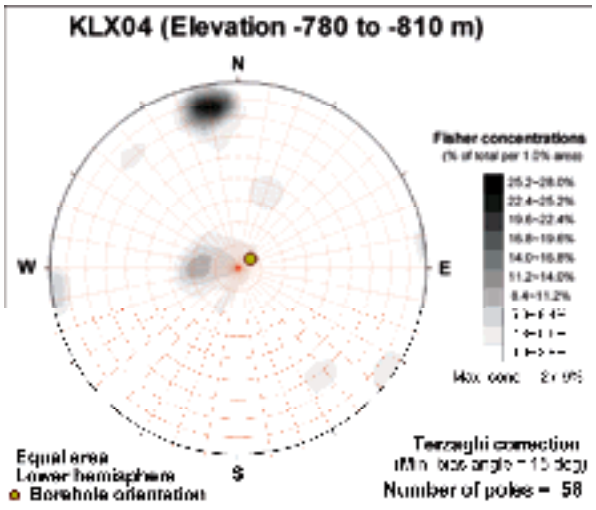
KLX04 (Elevation -780 to -810 m)
N
W
E
S
Fisher concentrations
Equal area
Lower hemisphere
Borehole orientation
Terzaghi correction
Number of poles = 58

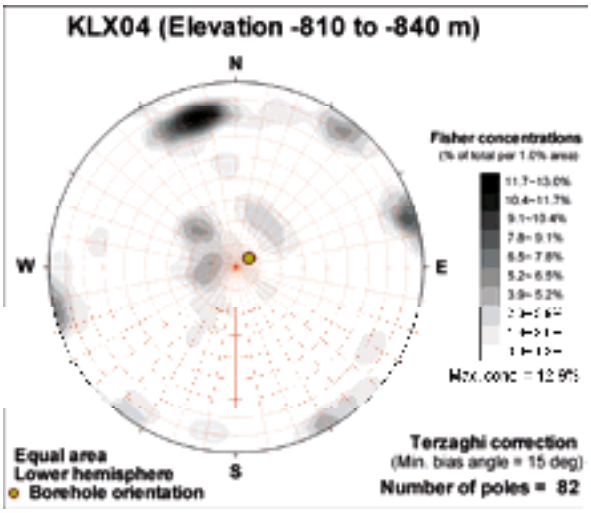
KLX04 (Elevation -810 to -840 m)
N
W
E
S
Fisher concentrations
Equal area
Lower hemisphere
Borehole orientation
Terzaghi correction
(Min. bias angle = 15 deg)
Number of poles = 82

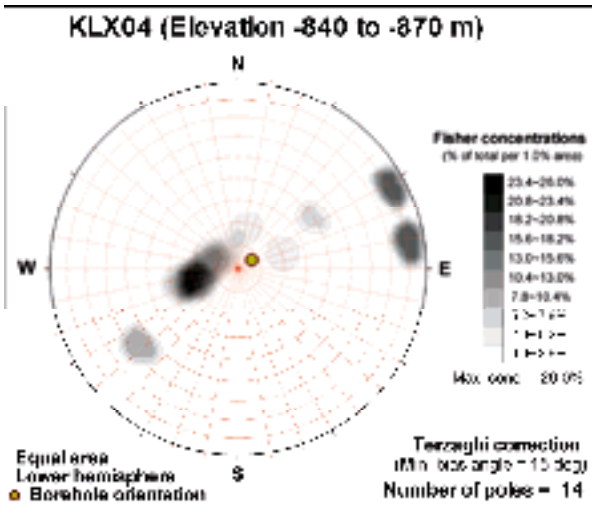
KLX04 (Elevation -840 to -870 m)
N
W
E
S
Fisher concentrations
Equal area
Lower hemisphere
Borehole orientation
Terzaghi correction
Number of poles = 14

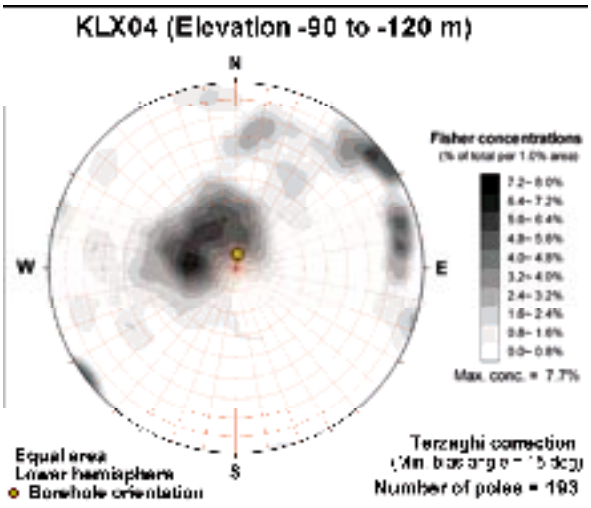
KLX04 (Elevation -90 to -120 m)
N
W
E
S
Fisher concentrations
Equal area
Lower hemisphere
Borehole orientation
Terzaghi correction
Number of poles = 193

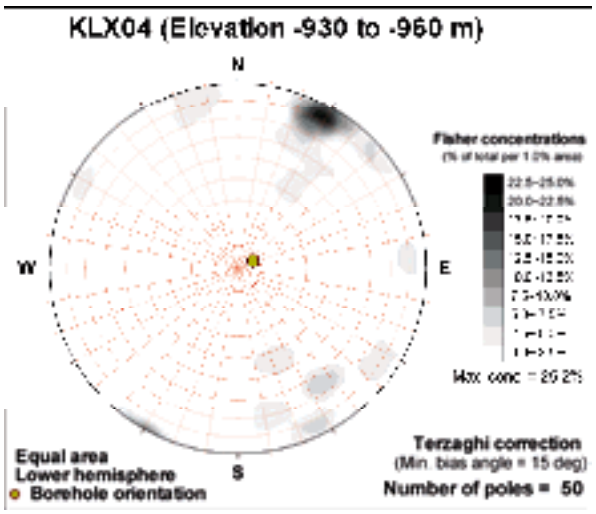
KLX04 (Elevation -930 to -960 m)
N
W
E
S
Fisher concentrations
Max. conc = 20.2%
Equal area
Lower hemisphere
Borehole orientation
Terzaghi correction
(Min. bias angle = 15 deg)
Number of poles = 50

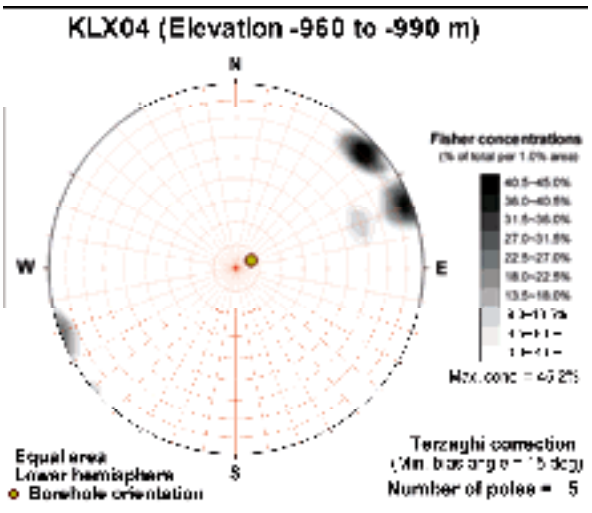
KLX04 (Elevation -960 to -990 m)
N
W
E
S
Fisher concentrations
Equal area
Lower hemisphere
Borehole orientation
Terzaghi correction
Number of poles = 5

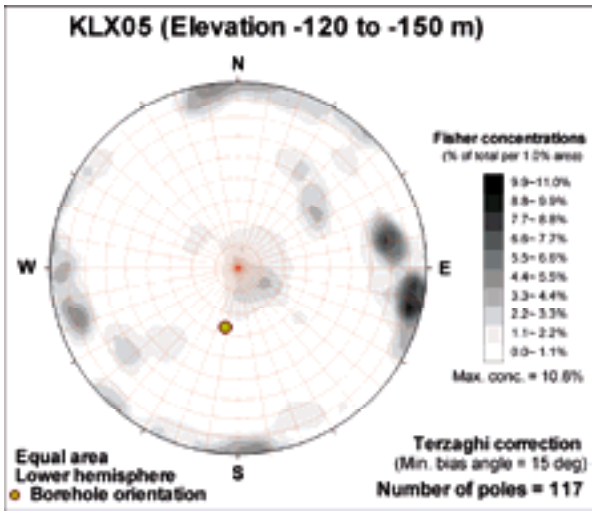
KLX05 (Elevation -120 to -150 m)
N
W
E
S
Fisher concentrations
Max. conc. = 10.6%
Equal area
Lower hemisphere
Borehole orientation
Terzaghi correction
(Min. bias angle = 15 deg)
Number of poles = 117

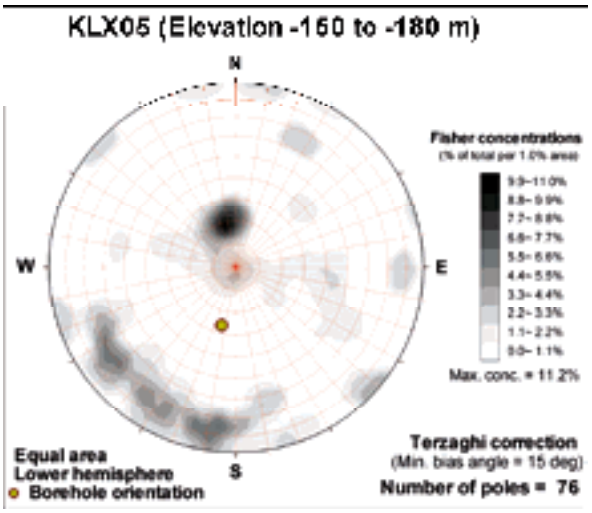
KLX05 (Elevation -150 to -180 m)
N
W
E
S
Fisher concentrations
Max. conc. = 11.2%
Equal area
Lower hemisphere
Borehole orientation
Terzaghi correction
(Min. bias angle = 15 deg)
Number of poles = 76

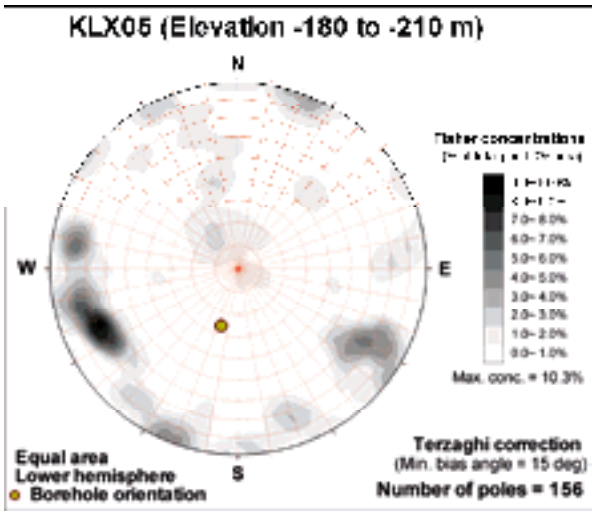
KLX05 (Elevation -180 to -210 m)
N
W
E
S
Max. conc. = 10.3%
Equal area
Lower hemisphere
Borehole orientation
Terzaghi correction
(Min. bias angle = 15 deg)
Number of poles = 156

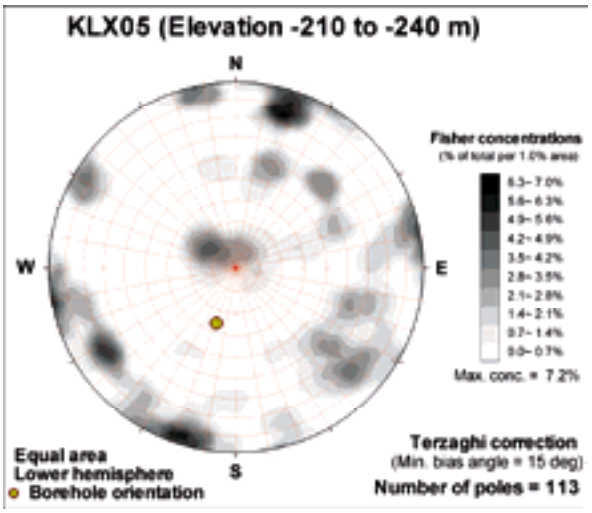
KLX05 (Elevation -210 to -240 m)
N
W
E
S
Fisher concentrations
Max. conc. = 7.2%
Equal area
Lower hemisphere
Borehole orientation
Terzaghi correction
(Min. bias angle = 15 deg)
Number of poles = 113

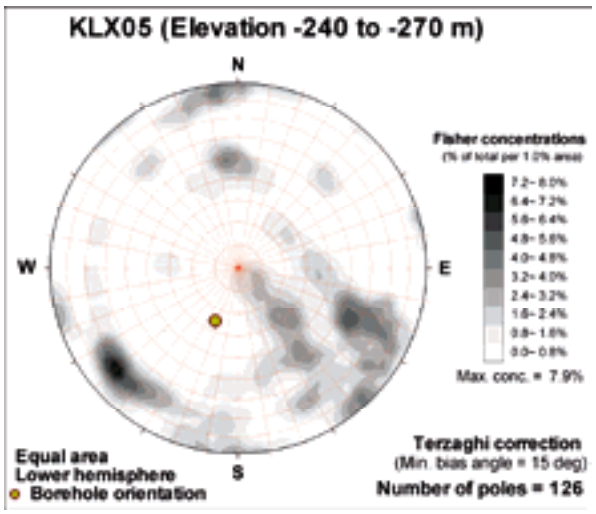
KLX05 (Elevation -240 to -270 m)
N
W
E
S
Fisher concentrations
(% of total per 1.0% area)
Max. conc. = 7.9%
Equal area
Lower hemisphere
Borehole orientation
Terzaghi correction
(Min. bias angle = 15 deg)
Number of poles = 126

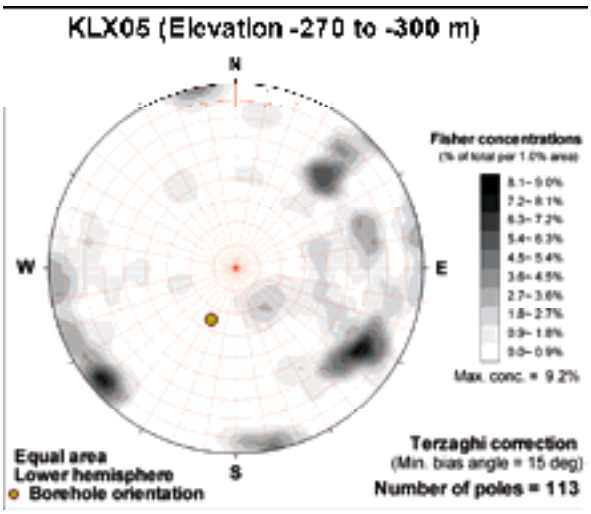
KLX05 (Elevation -270 to -300 m)
N
W
E
S
Fisher concentrations
(% of total per 1.0% area)
Max. conc. = 9.2%
Equal area
Lower hemisphere
Borehole orientation
Terzaghi correction
(Min. bias angle = 15 deg)
Number of poles = 113

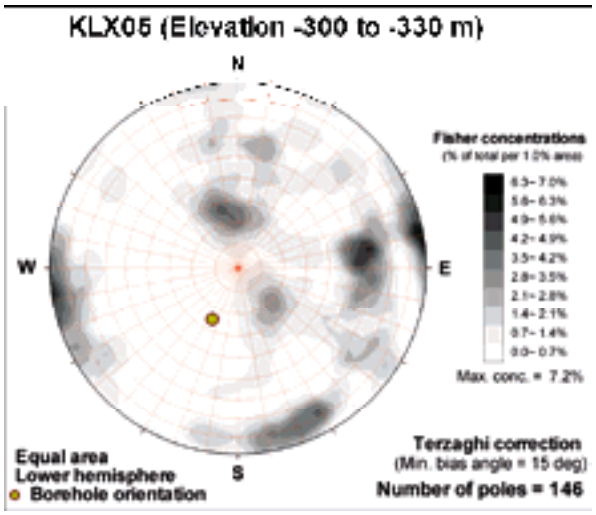
KLX05 (Elevation -300 to -330 m)
N
W
E
S
Fisher concentrations
(% of total per 1.0% area)
Max. conc. = 7.2%
Equal area
Lower hemisphere
Borehole orientation
Terzaghi correction
(Min. bias angle = 15 deg)
Number of poles = 146

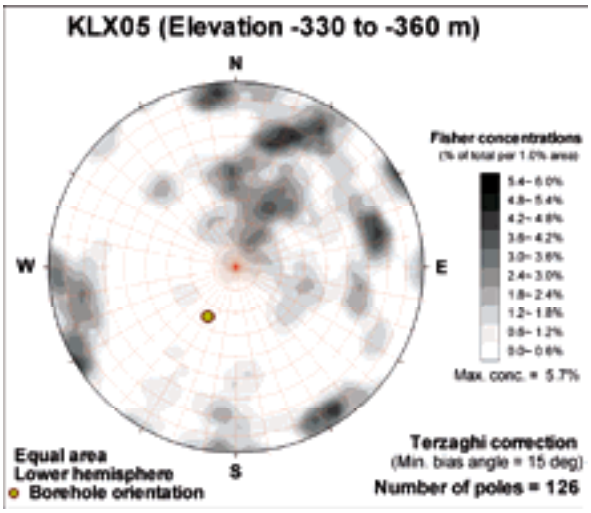
KLX05 (Elevation -330 to -360 m)
N
W
E
S
Fisher concentrations
(% of total per 1.0% area)
Max. conc. = 5.7%
Equal area
Lower hemisphere
Borehole orientation
Terzaghi correction
(Min. bias angle = 15 deg)
Number of poles = 126

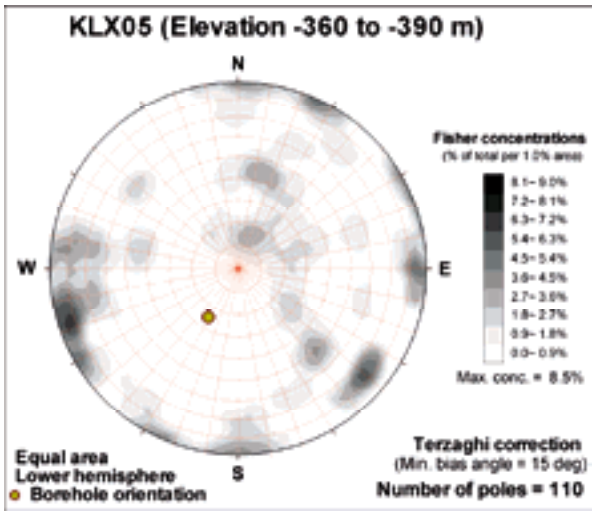
KLX05 (Elevation -360 to -390 m)
N
W
E
S
Fisher concentrations
(% of total per 1.0% area)
Max. conc. = 8.5%
Equal area
Lower hemisphere
Borehole orientation
Terzaghi correction
(Min. bias angle = 15 deg)
Number of poles = 110

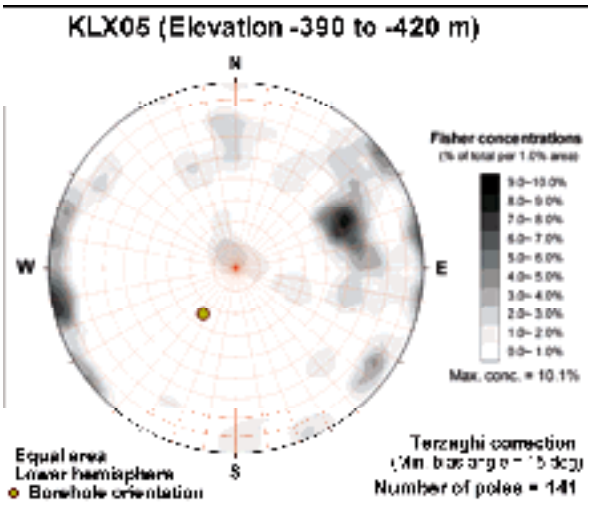
KLX05 (Elevation -390 to -420 m)
N
W
E
S
Fisher concentrations
(% of total per 1.0% area)
Max. conc. = 10.1%
Equal area
Lower hemisphere
Borehole orientation
Terzaghi correction
Number of poles = 141

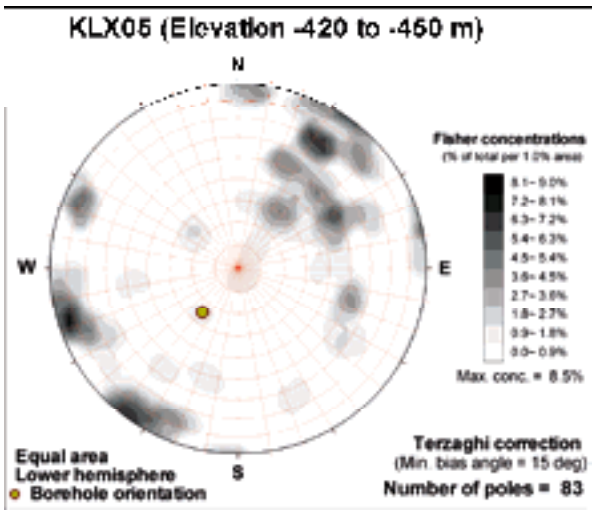
KLX05 (Elevation -420 to -450 m)
N
W
E
S
Fisher concentrations
Max. conc. = 8.5%
Equal area
Lower hemisphere
Borehole orientation
Terzaghi correction
(Min. bias angle = 15 deg)
Number of poles = 83

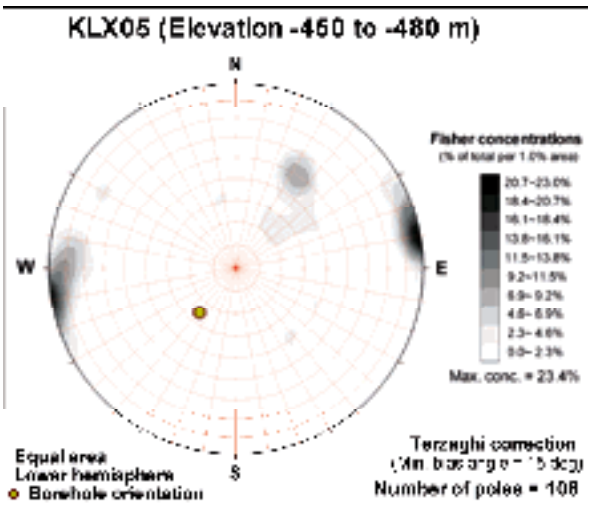
KLX05 (Elevation -450 to -480 m)
N
W
E
S
Fisher concentrations
Max. conc. = 23.4%
Equal area
Lower hemisphere
Borehole orientation
Terzaghi correction
Number of poles = 108

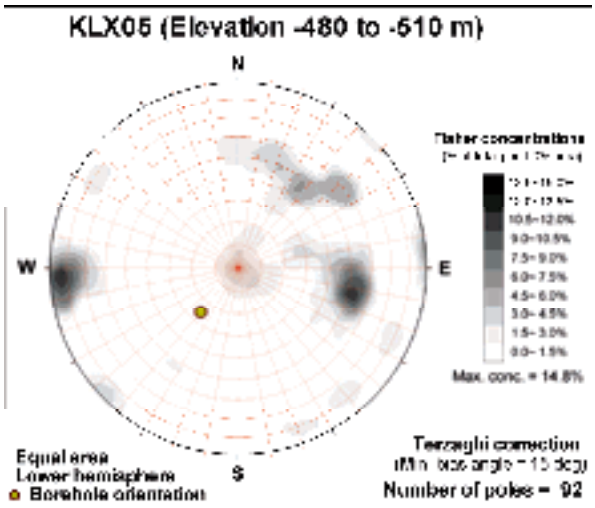
KLX05 (Elevation -480 to -510 m)
N
W
E
S
Max. conc. = 14.8%
Equal area
Lower hemisphere
Borehole orientation
Terzaghi correction
Number of poles = 92

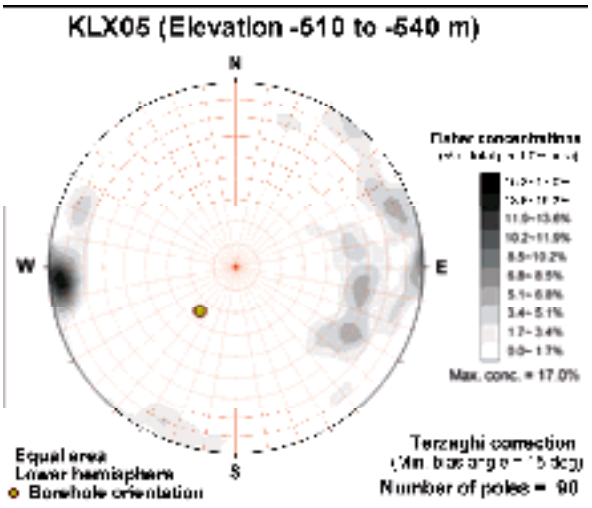
KLX05 (Elevation -510 to -540 m)
N
W
E
S
Max. conc. = 17.0%
Equal area
Lower hemisphere
Borehole orientation
Terzaghi correction
Number of poles = 90

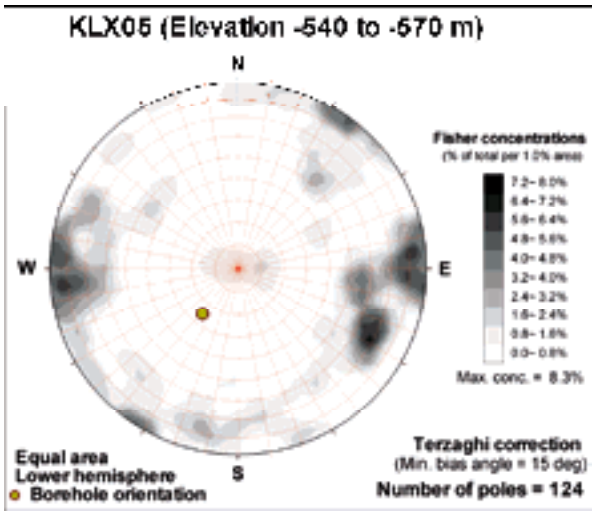
KLX05 (Elevation -540 to -570 m)
N
W
E
S
Fisher concentrations
Max. conc. = 8.3%
Equal area
Lower hemisphere
Borehole orientation
Terzaghi correction
(Min. bias angle = 15 deg)
Number of poles = 124

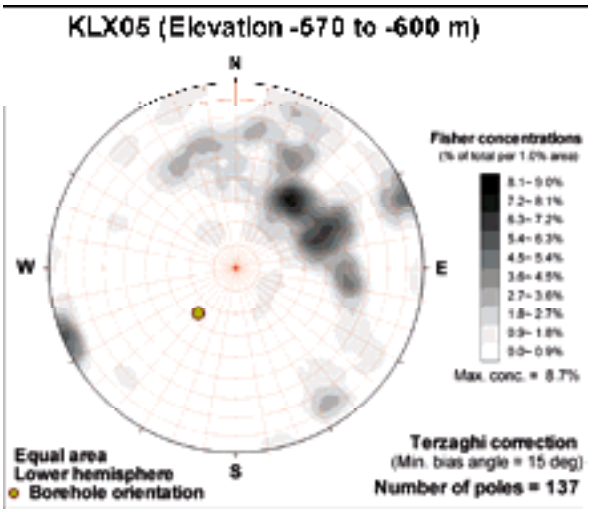
KLX05 (Elevation -570 to -600 m)
N
W
E
S
Fisher concentrations
Max. conc. = 8.7%
Equal area
Lower hemisphere
Borehole orientation
Terzaghi correction
(Min. bias angle = 15 deg)
Number of poles = 137

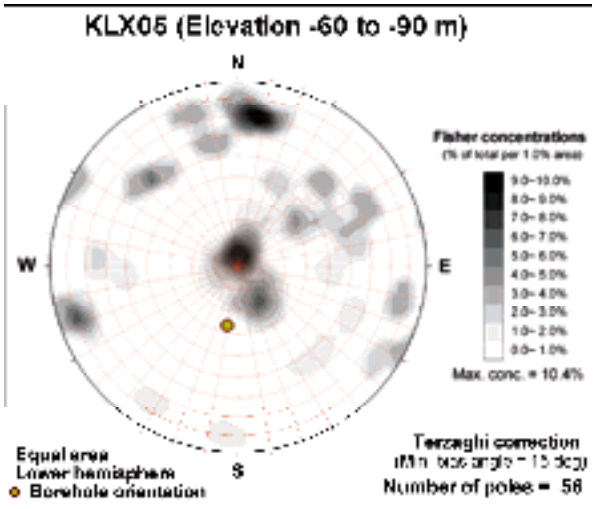
KLX05 (Elevation -60 to -90 m)
N
W
E
S
Fisher concentrations
(% of total per 1.0% area)
9.0–10.0%
8.0–9.0%
7.0–8.0%
6.0–7.0%
5.0–6.0%
4.0–5.0%
3.0–4.0%
2.0–3.0%
1.0–2.0%
0.0–1.0%
Max. conc. = 10.4%
Equal area
Lower hemisphere
Borehole orientation
Terzaghi correction
(Min. bias angle = 15 deg)
Number of poles = 58

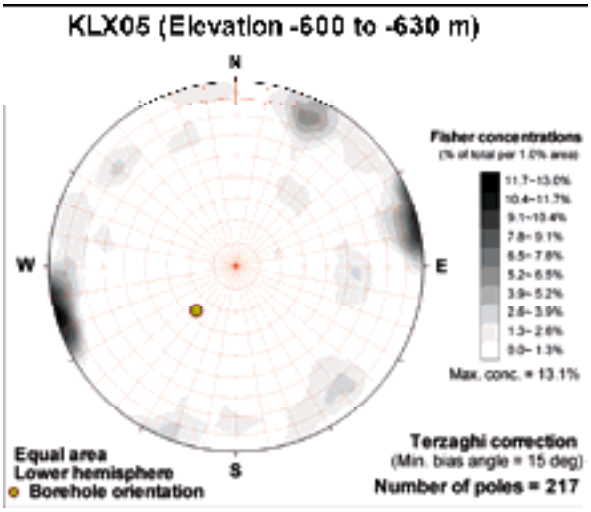
KLX05 (Elevation -600 to -630 m)
N
W
E
S
Fisher concentrations
(% of total per 1.0% area)
11.7–13.0%
10.4–11.7%
9.1–10.4%
7.8–9.1%
6.5–7.8%
5.2–6.5%
3.9–5.2%
2.6–3.9%
1.3–2.6%
0.0–1.3%
Max. conc. = 13.1%
Equal area
Lower hemisphere
Borehole orientation
Terzaghi correction
(Min. bias angle = 15 deg)
Number of poles = 217

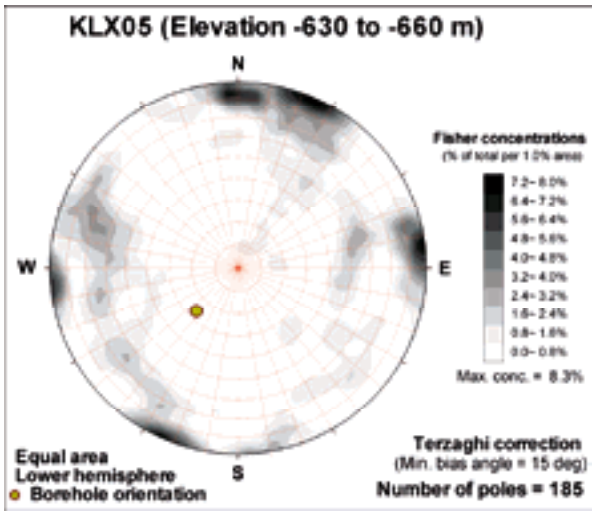
KLX05 (Elevation -630 to -660 m)
N
W
E
S
Fisher concentrations
(% of total per 1.0% area)
7.2–8.0%
6.4–7.2%
5.6–6.4%
4.8–5.6%
4.0–4.8%
3.2–4.0%
2.4–3.2%
1.6–2.4%
0.8–1.6%
0.0–0.8%
Max. conc. = 8.3%
Equal area
Lower hemisphere
Borehole orientation
Terzaghi correction
(Min. bias angle = 15 deg)
Number of poles = 185

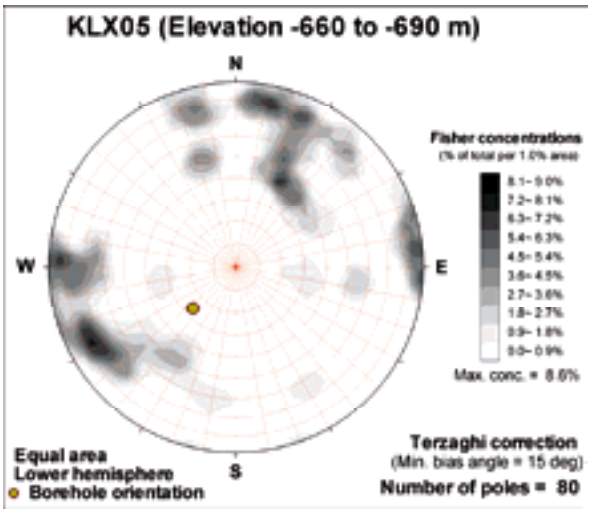
KLX05 (Elevation -660 to -690 m)
N
W
E
S
Fisher concentrations
(% of total per 1.0% area)
8.1–9.0%
7.2–8.1%
6.3–7.2%
5.4–6.3%
4.5–5.4%
3.6–4.5%
2.7–3.6%
1.8–2.7%
0.9–1.8%
0.0–0.9%
Max. conc. = 8.6%
Equal area
Lower hemisphere
Borehole orientation
Terzaghi correction
(Min. bias angle = 15 deg)
Number of poles = 80

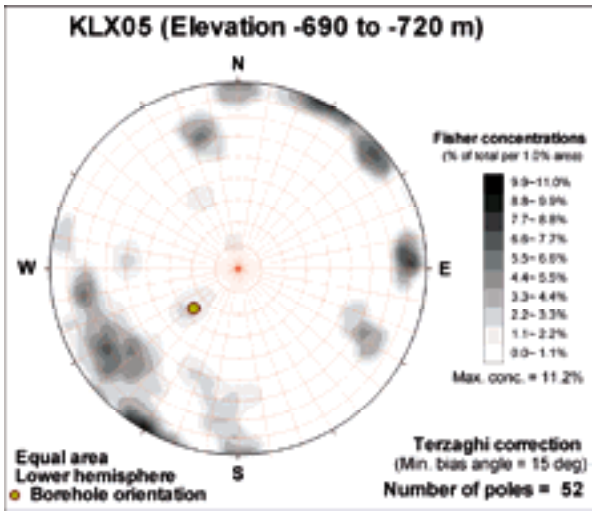
KLX05 (Elevation -690 to -720 m)
N
W
E
S
Fisher concentrations
(% of total per 1.0% area)
9.9–11.0%
8.8–9.9%
7.7–8.8%
6.6–7.7%
5.5–6.6%
4.4–5.5%
3.3–4.4%
2.2–3.3%
1.1–2.2%
0.0–1.1%
Max. conc. = 11.2%
Equal area
Lower hemisphere
Borehole orientation
Terzaghi correction
(Min. bias angle = 15 deg)
Number of poles = 52

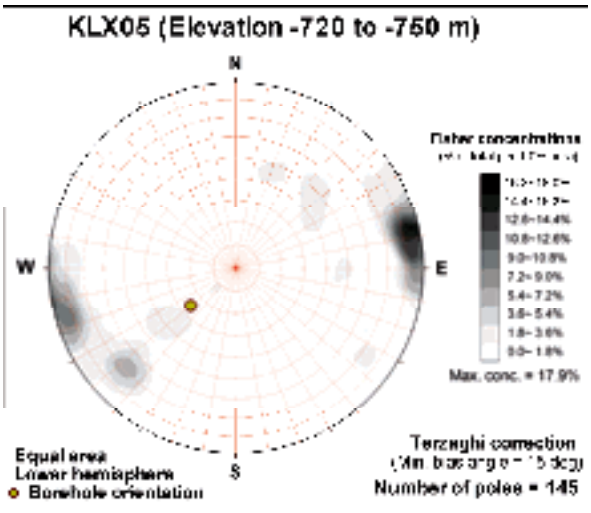
KLX05 (Elevation -720 to -750 m)
N
W
E
S
Max. conc. = 17.9%
Equal area
Lower hemisphere
Borehole orientation
Number of poles = 145

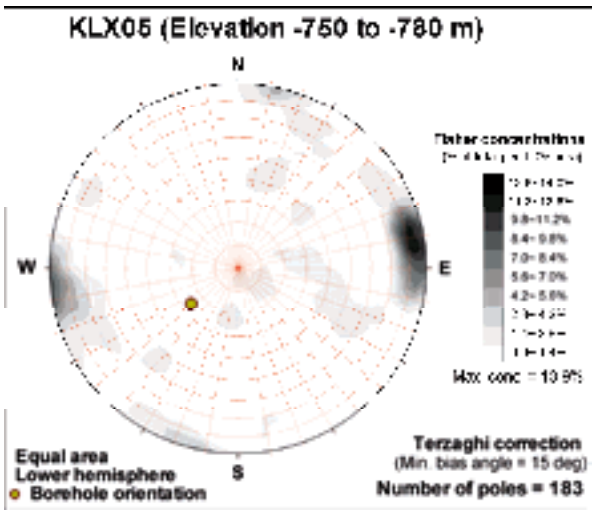
KLX05 (Elevation -750 to -780 m)
N
W
E
S
Fisher concentrations
Max. conc. = 10.9%
Equal area
Lower hemisphere
Borehole orientation
Terzaghi correction
(Min. bias angle = 15 deg)
Number of poles = 183

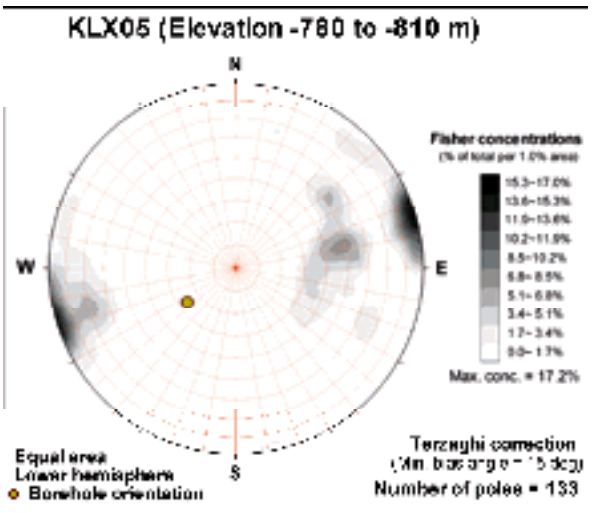
KLX05 (Elevation -780 to -810 m)
N
W
E
S
Fisher concentrations
Max. conc. = 17.2%
Equal area
Lower hemisphere
Borehole orientation
Terzaghi correction
(Min. bias angle = 15 deg)
Number of poles = 133

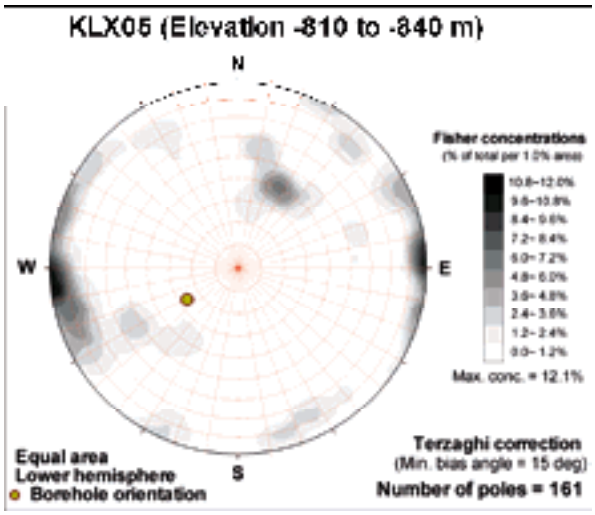
KLX05 (Elevation -810 to -840 m)
N
W
E
S
Fisher concentrations
Max. conc. = 12.1%
Equal area
Lower hemisphere
Borehole orientation
Terzaghi correction
(Min. bias angle = 15 deg)
Number of poles = 161

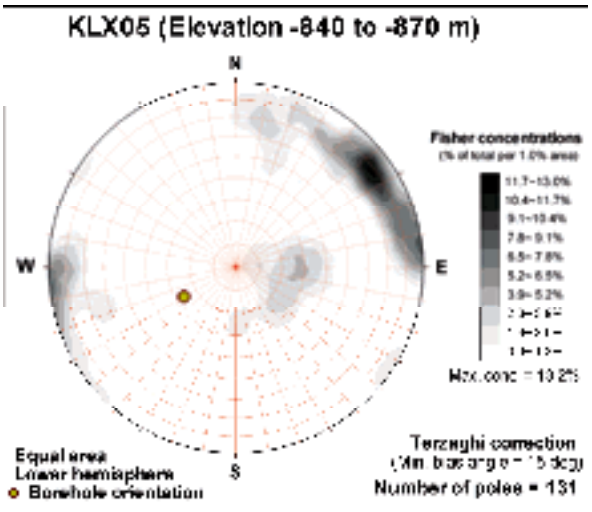
KLX05 (Elevation -840 to -870 m)
N
W
E
S
Fisher concentrations
Equal area
Lower hemisphere
Borehole orientation
Terzaghi correction
Number of poles = 131

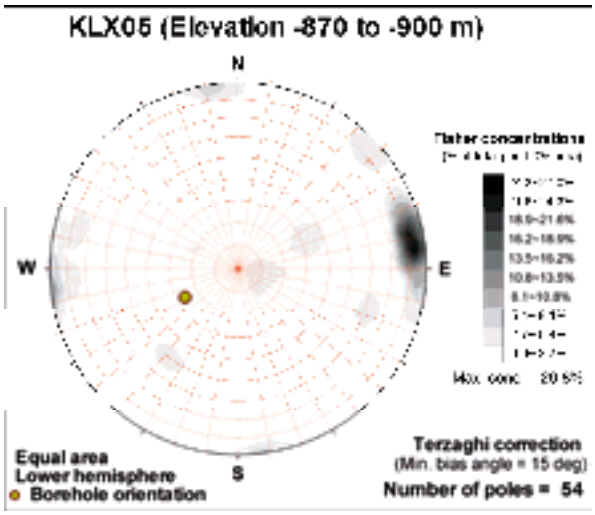
KLX05 (Elevation -870 to -900 m)
N
W
E
S
Fisher concentrations
Equal area
Lower hemisphere
Borehole orientation
Terzaghi correction
(Min. bias angle = 15 deg)
Number of poles = 54

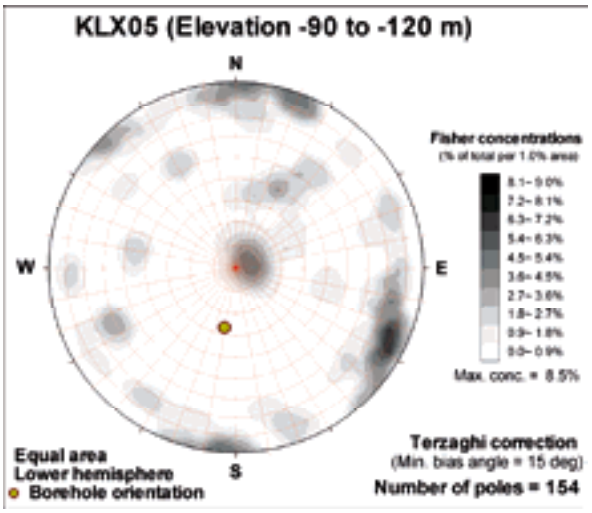
KLX05 (Elevation -90 to -120 m)
N
W
E
S
Fisher concentrations
Max. conc. = 8.5%
Equal area
Lower hemisphere
Borehole orientation
Terzaghi correction
(Min. bias angle = 15 deg)
Number of poles = 154

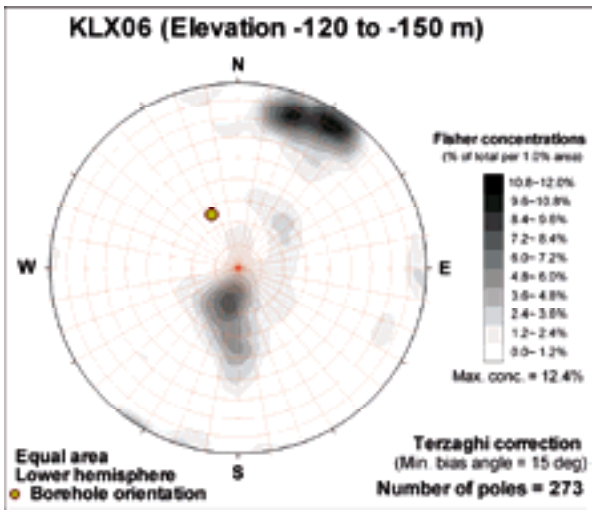
KLX06 (Elevation -120 to -150 m)
N
W
E
S
Fisher concentrations
(% of total per 1.0% area)
10.8–12.0%
9.6–10.8%
8.4–9.6%
7.2–8.4%
6.0–7.2%
4.8–6.0%
3.6–4.8%
2.4–3.6%
1.2–2.4%
0.0–1.2%
Max. conc. = 12.4%
Equal area
Lower hemisphere
Borehole orientation
Terzaghi correction
(Min. bias angle = 15 deg)
Number of poles = 273

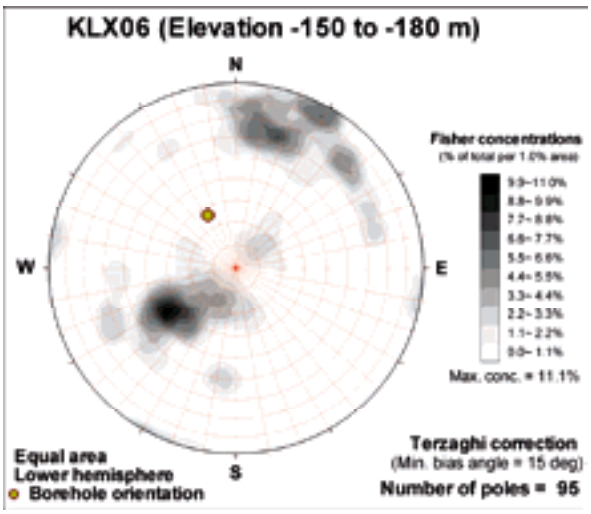
KLX06 (Elevation -150 to -180 m)
N
W
E
S
Fisher concentrations
(% of total per 1.0% area)
9.9–11.0%
8.8–9.9%
7.7–8.8%
6.6–7.7%
5.5–6.6%
4.4–5.5%
3.3–4.4%
2.2–3.3%
1.1–2.2%
0.0–1.1%
Max. conc. = 11.1%
Equal area
Lower hemisphere
Borehole orientation
Terzaghi correction
(Min. bias angle = 15 deg)
Number of poles = 95

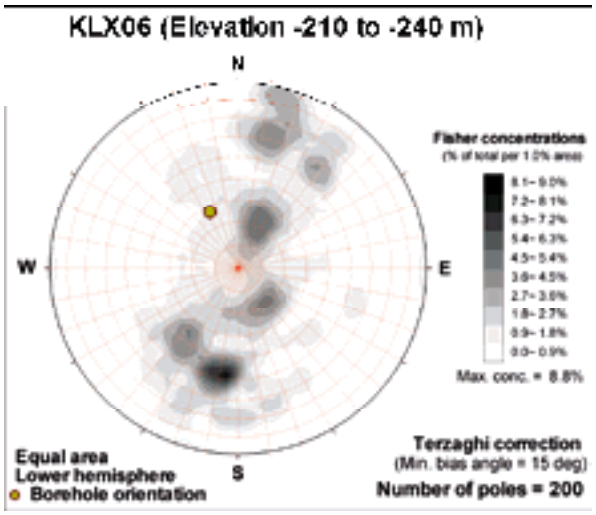
KLX06 (Elevation -210 to -240 m)
N
W
E
S
Fisher concentrations
(% of total per 1.0% area)
8.1–9.0%
7.2–8.1%
6.3–7.2%
5.4–6.3%
4.5–5.4%
3.6–4.5%
2.7–3.6%
1.8–2.7%
0.9–1.8%
0.0–0.9%
Max. conc. = 8.8%
Equal area
Lower hemisphere
Borehole orientation
Terzaghi correction
(Min. bias angle = 15 deg)
Number of poles = 200

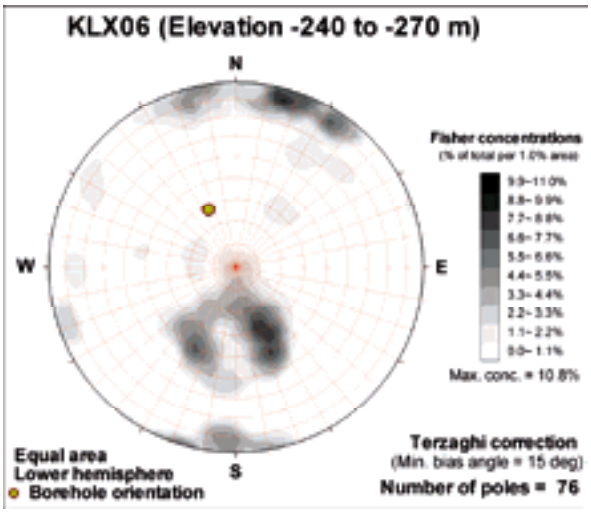
KLX06 (Elevation -240 to -270 m)
N
W
E
S
Fisher concentrations
(% of total per 1.0% area)
9.9–11.0%
8.8–9.9%
7.7–8.8%
6.6–7.7%
5.5–6.6%
4.4–5.5%
3.3–4.4%
2.2–3.3%
1.1–2.2%
0.0–1.1%
Max. conc. = 10.8%
Equal area
Lower hemisphere
Borehole orientation
Terzaghi correction
(Min. bias angle = 15 deg)
Number of poles = 76

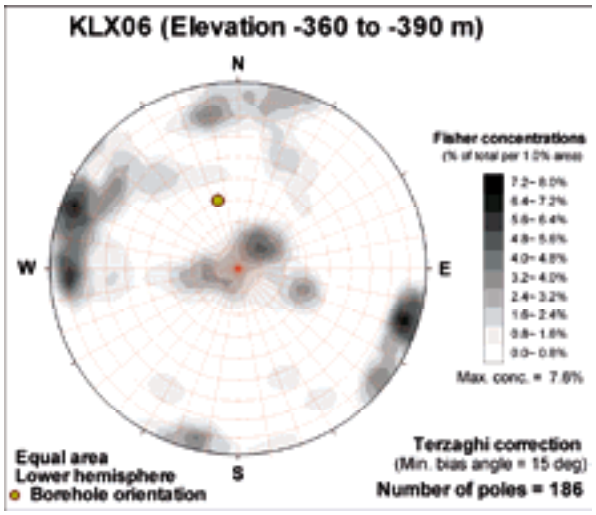
KLX06 (Elevation -360 to -390 m)
N
W
E
S
Fisher concentrations
(% of total per 1.0% area)
7.2–8.0%
6.4–7.2%
5.6–6.4%
4.8–5.6%
4.0–4.8%
3.2–4.0%
2.4–3.2%
1.6–2.4%
0.8–1.6%
0.0–0.8%
Max. conc. = 7.8%
Equal area
Lower hemisphere
Borehole orientation
Terzaghi correction
(Min. bias angle = 15 deg)
Number of poles = 186

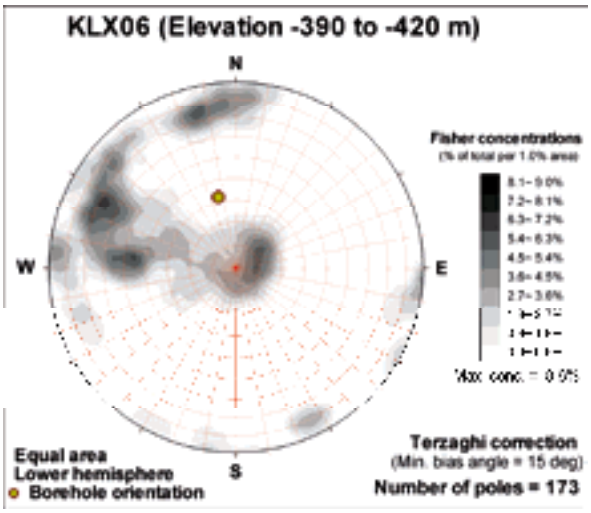
KLX06 (Elevation -390 to -420 m)
N
W
E
S
Fisher concentrations
(% of total per 1.0% area)
8.1–9.0%
7.2–8.1%
6.3–7.2%
5.4–6.3%
4.5–5.4%
3.6–4.5%
2.7–3.6%
Equal area
Lower hemisphere
Borehole orientation
Terzaghi correction
(Min. bias angle = 15 deg)
Number of poles = 173

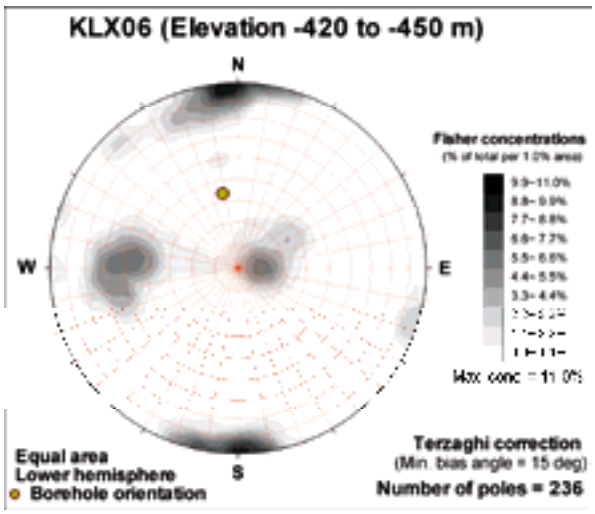
KLX06 (Elevation -420 to -450 m)
N
W
E
S
Fisher concentrations
(% of total per 1.0% area)
Equal area
Lower hemisphere
Borehole orientation
Terzaghi correction
(Min. bias angle = 15 deg)
Number of poles = 236

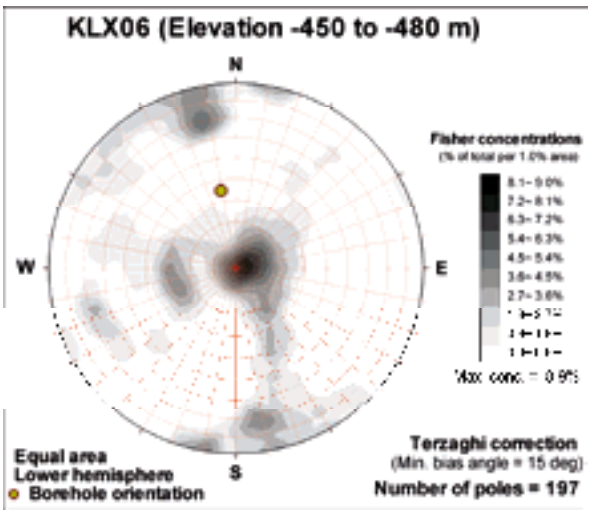
KLX06 (Elevation -450 to -480 m)
N
W
E
S
Fisher concentrations
(% of total per 1.0% area)
Equal area
Lower hemisphere
Borehole orientation
Terzaghi correction
(Min. bias angle = 15 deg)
Number of poles = 197

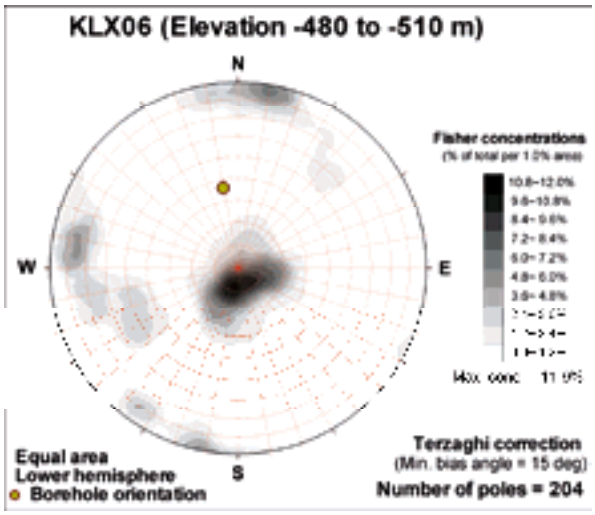
KLX06 (Elevation -480 to -510 m)
N
W
E
S
Fisher concentrations
(% of total per 1.0% area)
Equal area
Lower hemisphere
Borehole orientation
Terzaghi correction
(Min. bias angle = 15 deg)
Number of poles = 204

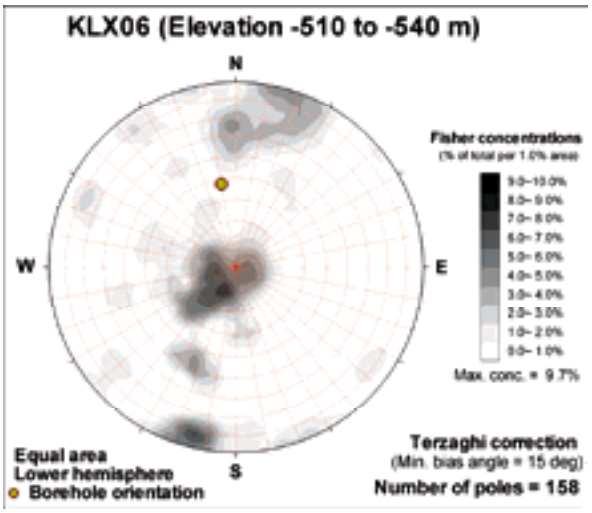
KLX06 (Elevation -510 to -540 m)
N
W
E
S
Fisher concentrations
(% of total per 1.0% area)
Max. conc. = 9.7%
Equal area
Lower hemisphere
Borehole orientation
Terzaghi correction
(Min. bias angle = 15 deg)
Number of poles = 158

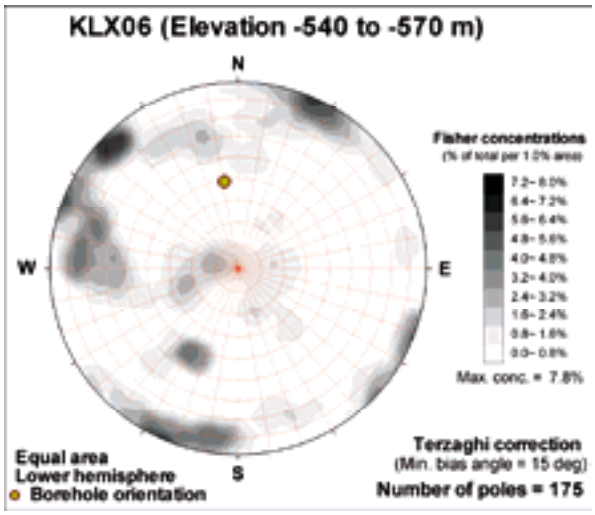
KLX06 (Elevation -540 to -570 m)
N
W
E
S
Fisher concentrations
(% of total per 1.0% area)
Max. conc. = 7.8%
Equal area
Lower hemisphere
Borehole orientation
Terzaghi correction
(Min. bias angle = 15 deg)
Number of poles = 175

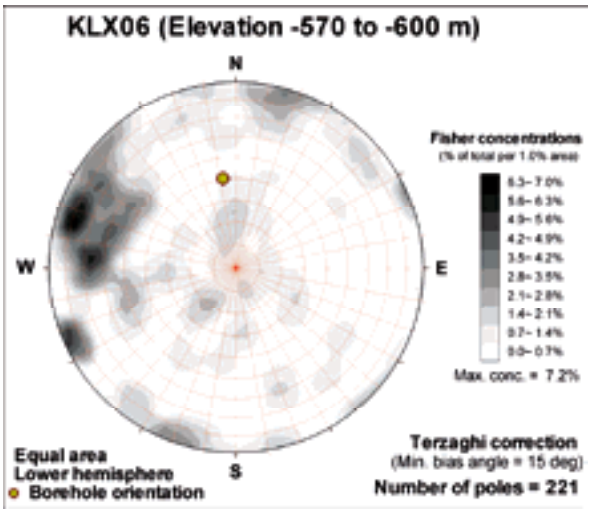
KLX06 (Elevation -570 to -600 m)
N
W
E
S
Fisher concentrations
(% of total per 1.0% area)
Max. conc. = 7.2%
Equal area
Lower hemisphere
Borehole orientation
Terzaghi correction
(Min. bias angle = 15 deg)
Number of poles = 221

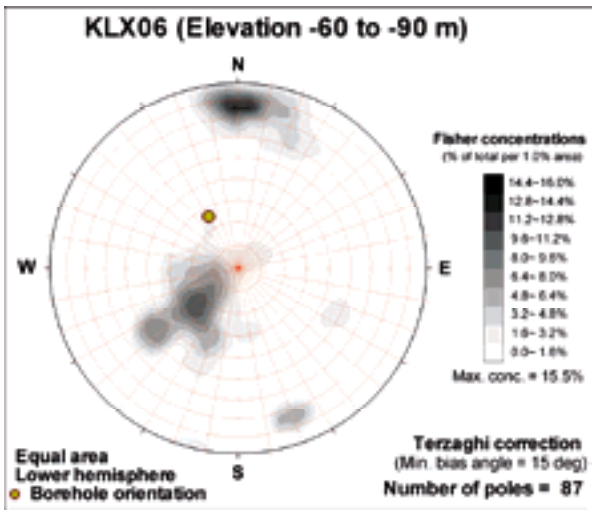
KLX06 (Elevation -60 to -90 m)
N
W
E
S
Fisher concentrations
(% of total per 1.0% area)
14.4–16.0%
12.8–14.4%
11.2–12.8%
9.6–11.2%
8.0– 9.6%
6.4– 8.0%
4.8– 6.4%
3.2– 4.8%
1.6– 3.2%
0.0– 1.6%
Max. conc. = 15.5%
Equal area
Lower hemisphere
Borehole orientation
Terzaghi correction
(Min. bias angle = 15 deg)
Number of poles = 87

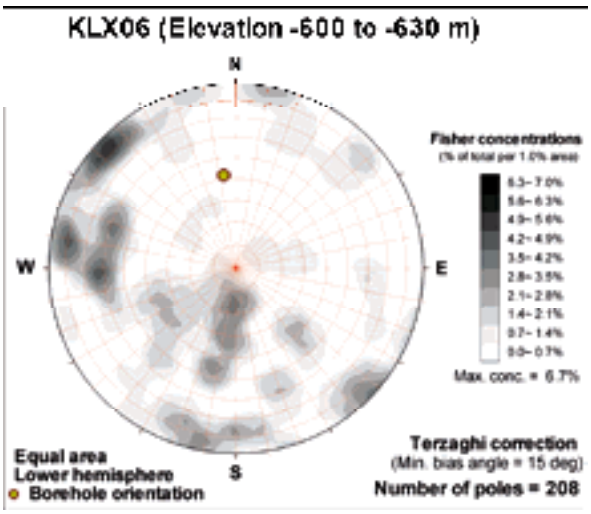
KLX06 (Elevation -600 to -630 m)
N
W
E
S
Fisher concentrations
(% of total per 1.0% area)
6.3– 7.0%
5.6– 6.3%
4.9– 5.6%
4.2– 4.9%
3.5– 4.2%
2.8– 3.5%
2.1– 2.8%
1.4– 2.1%
0.7– 1.4%
0.0– 0.7%
Max. conc. = 6.7%
Equal area
Lower hemisphere
Borehole orientation
Terzaghi correction
(Min. bias angle = 15 deg)
Number of poles = 208

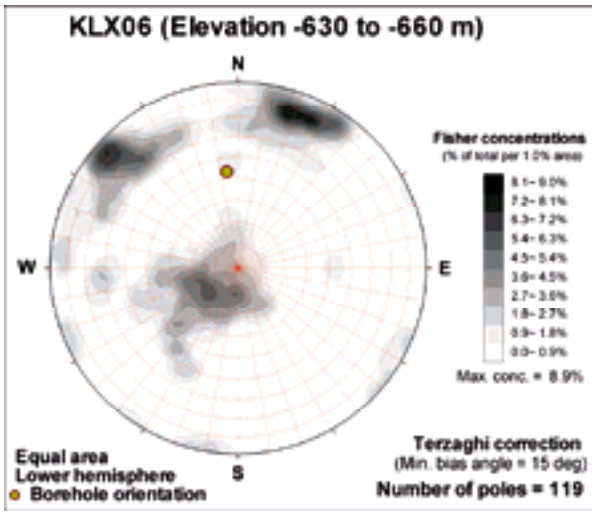
KLX06 (Elevation -630 to -660 m)
N
W
E
S
Fisher concentrations
(% of total per 1.0% area)
8.1– 9.0%
7.2– 8.1%
6.3– 7.2%
5.4– 6.3%
4.5– 5.4%
3.6– 4.5%
2.7– 3.6%
1.8– 2.7%
0.9– 1.8%
0.0– 0.9%
Max. conc. = 8.9%
Equal area
Lower hemisphere
Borehole orientation
Terzaghi correction
(Min. bias angle = 15 deg)
Number of poles = 119

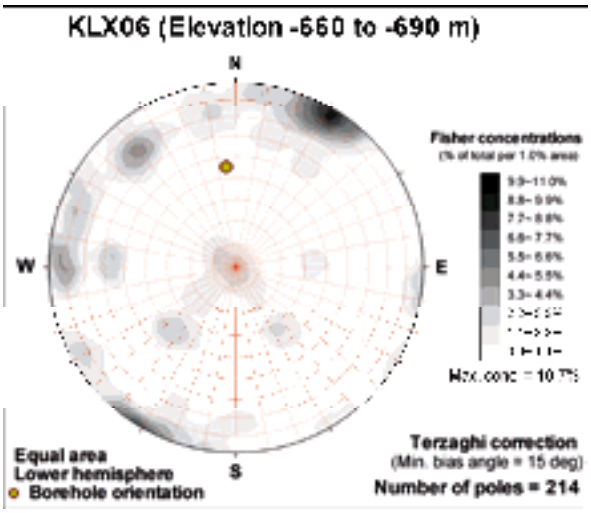
KLX06 (Elevation -660 to -690 m)
N
W
E
S
Fisher concentrations
(% of total per 1.0% area)
9.9–11.0%
8.8– 9.9%
7.7– 8.8%
6.6– 7.7%
5.5– 6.6%
4.4– 5.5%
3.3– 4.4%
Equal area
Lower hemisphere
Borehole orientation
Terzaghi correction
(Min. bias angle = 15 deg)
Number of poles = 214

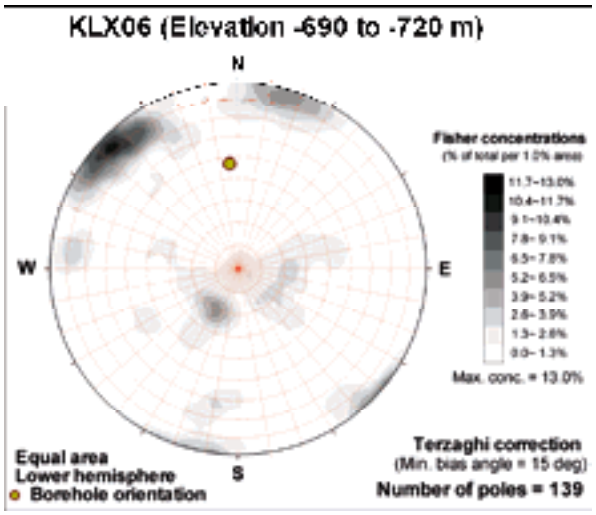
KLX06 (Elevation -690 to -720 m)
N
W
E
S
Fisher concentrations
(% of total per 1.0% area)
11.7–13.0%
10.4–11.7%
9.1–10.4%
7.8– 9.1%
6.5– 7.8%
5.2– 6.5%
3.9– 5.2%
2.6– 3.9%
1.3– 2.6%
0.0– 1.3%
Max. conc. = 13.0%
Equal area
Lower hemisphere
Borehole orientation
Terzaghi correction
(Min. bias angle = 15 deg)
Number of poles = 139

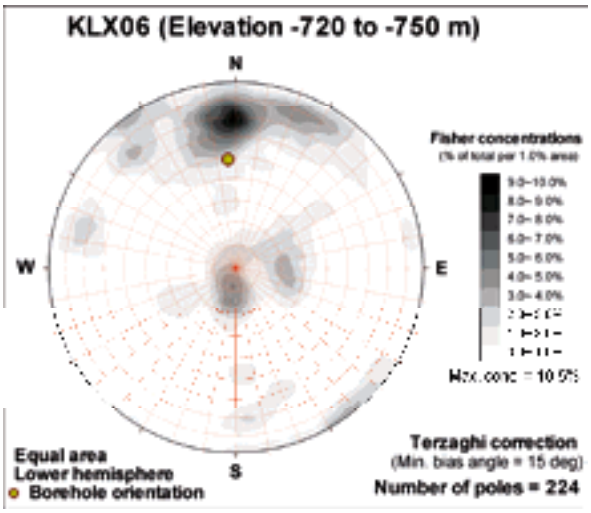
KLX06 (Elevation -720 to -750 m)
N
W
E
S
Fisher concentrations
(% of total per 1.0% area)
9.0–10.0%
8.0– 9.0%
7.0– 8.0%
6.0– 7.0%
5.0– 6.0%
4.0– 5.0%
3.0– 4.0%
Equal area
Lower hemisphere
Borehole orientation
Terzaghi correction
(Min. bias angle = 15 deg)
Number of poles = 224

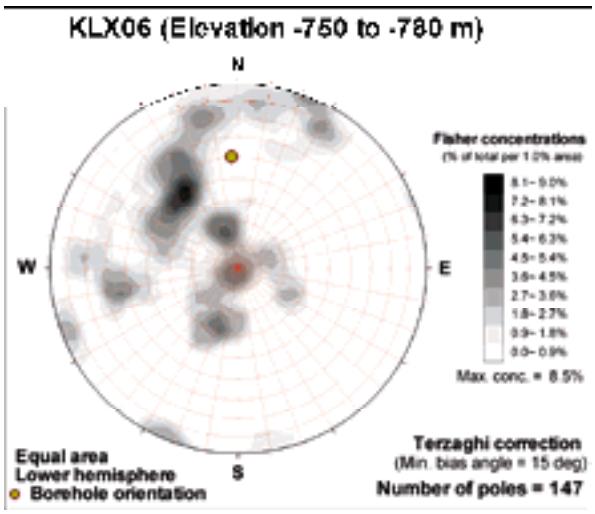
KLX06 (Elevation -750 to -780 m)
N
W
E
S
Fisher concentrations
(% of total per 1.0% area)
8.1– 9.0%
7.2– 8.1%
6.3– 7.2%
5.4– 6.3%
4.5– 5.4%
3.6– 4.5%
2.7– 3.6%
1.8– 2.7%
0.9– 1.8%
0.0– 0.9%
Max. conc. = 8.5%
Equal area
Lower hemisphere
Borehole orientation
Terzaghi correction
(Min. bias angle = 15 deg)
Number of poles = 147

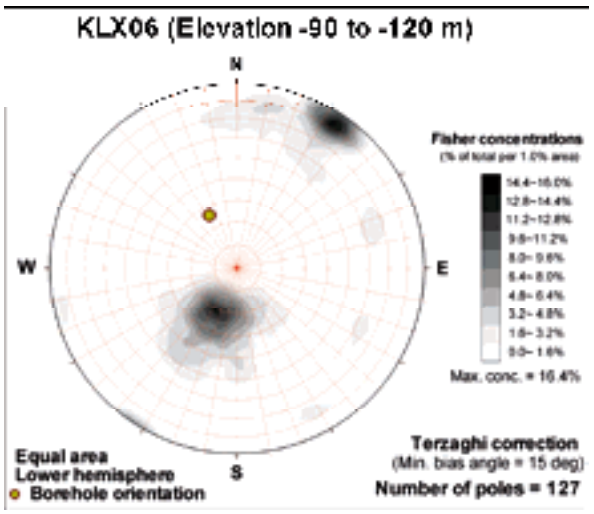
KLX06 (Elevation -90 to -120 m)
N
W
E
S
Fisher concentrations
(% of total per 1.0% area)
14.4– 16.0%
12.8– 14.4%
11.2– 12.8%
9.6– 11.2%
8.0– 9.6%
6.4– 8.0%
4.8– 6.4%
3.2– 4.8%
1.6– 3.2%
0.0– 1.6%
Max. conc. = 16.4%
Equal area
Lower hemisphere
Borehole orientation
Terzaghi correction
(Min. bias angle = 15 deg)
Number of poles = 127

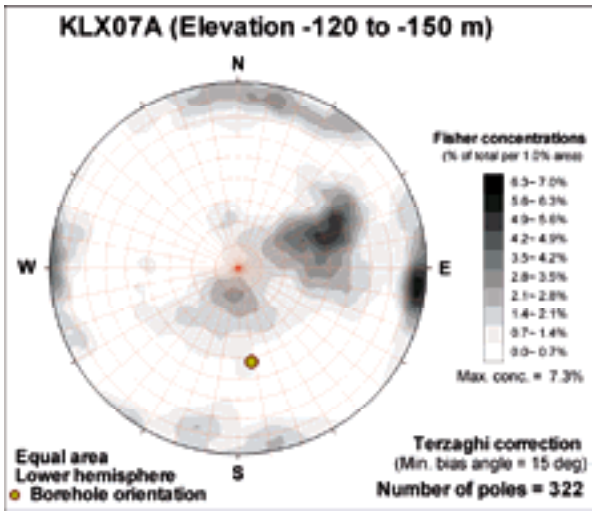
KLX07A (Elevation -120 to -150 m)
N
W
E
S
Fisher concentrations
(% of total per 1.0% area)
6.3– 7.0%
5.6– 6.3%
4.9– 5.6%
4.2– 4.9%
3.5– 4.2%
2.8– 3.5%
2.1– 2.8%
1.4– 2.1%
0.7– 1.4%
0.0– 0.7%
Max. conc. = 7.3%
Equal area
Lower hemisphere
Borehole orientation
Terzaghi correction
(Min. bias angle = 15 deg)
Number of poles = 322

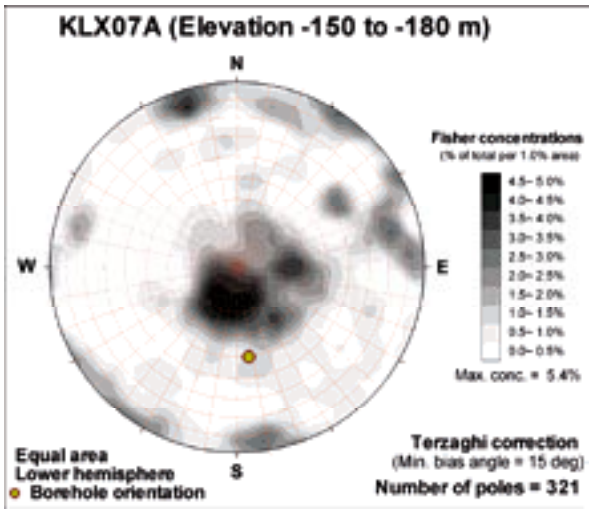
KLX07A (Elevation -150 to -180 m)
N
W
E
S
Fisher concentrations
(% of total per 1.0% area)
4.5– 5.0%
4.0– 4.5%
3.5– 4.0%
3.0– 3.5%
2.5– 3.0%
2.0– 2.5%
1.5– 2.0%
1.0– 1.5%
0.5– 1.0%
0.0– 0.5%
Max. conc. = 5.4%
Equal area
Lower hemisphere
Borehole orientation
Terzaghi correction
(Min. bias angle = 15 deg)
Number of poles = 321

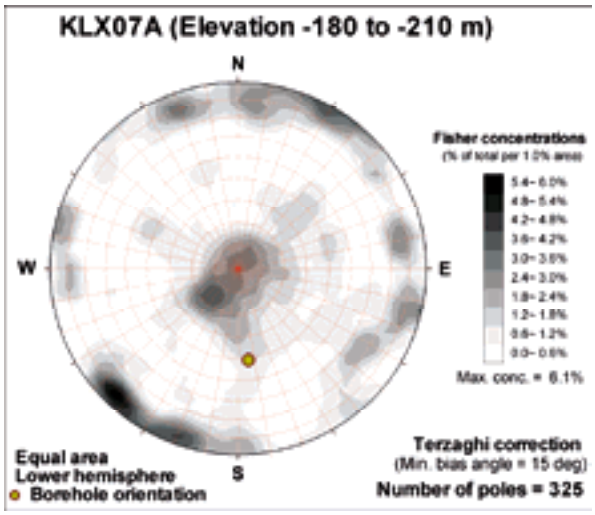
KLX07A (Elevation -180 to -210 m)
N
W
E
S
Fisher concentrations
(% of total per 1.0% area)
5.4– 6.0%
4.8– 5.4%
4.2– 4.8%
3.6– 4.2%
3.0– 3.6%
2.4– 3.0%
1.8– 2.4%
1.2– 1.8%
0.6– 1.2%
0.0– 0.6%
Max. conc. = 6.1%
Equal area
Lower hemisphere
Borehole orientation
Terzaghi correction
(Min. bias angle = 15 deg)
Number of poles = 325

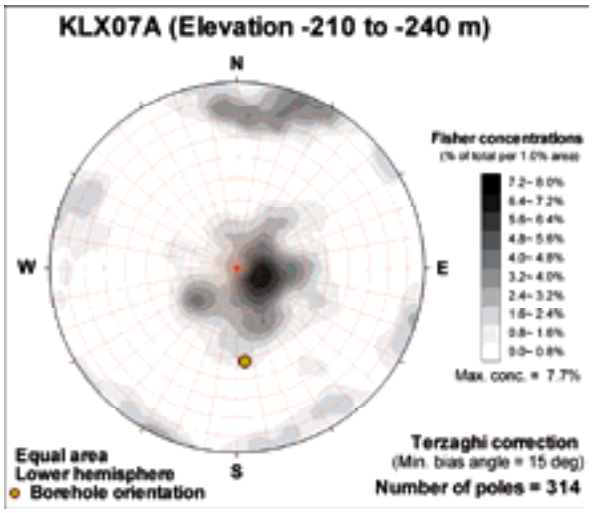
KLX07A (Elevation -210 to -240 m)
N
W
E
S
Fisher concentrations
(% of total per 1.0% area)
7.2– 8.0%
6.4– 7.2%
5.6– 6.4%
4.8– 5.6%
4.0– 4.8%
3.2– 4.0%
2.4– 3.2%
1.6– 2.4%
0.8– 1.6%
0.0– 0.8%
Max. conc. = 7.7%
Equal area
Lower hemisphere
Borehole orientation
Terzaghi correction
(Min. bias angle = 15 deg)
Number of poles = 314

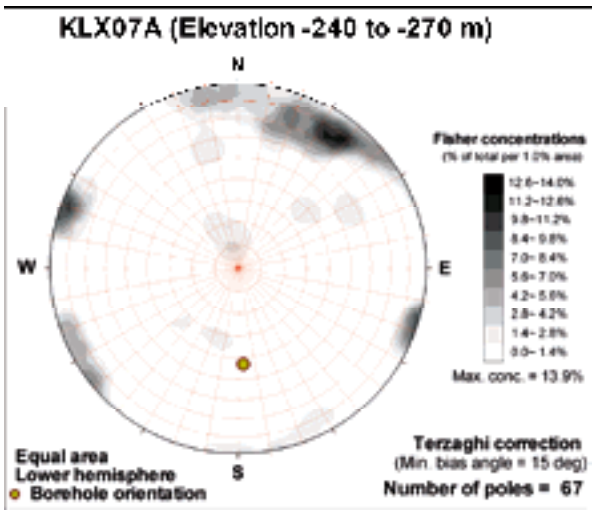
KLX07A (Elevation -240 to -270 m)
N
W
E
S
Fisher concentrations
(% of total per 1.0% area)
12.6–14.0%
11.2–12.6%
9.8–11.2%
8.4–9.8%
7.0–8.4%
5.6–7.0%
4.2–5.6%
2.8–4.2%
1.4–2.8%
0.0–1.4%
Max. conc. = 13.9%
Equal area
Lower hemisphere
Borehole orientation
Terzaghi correction
(Min. bias angle = 15 deg)
Number of poles = 67

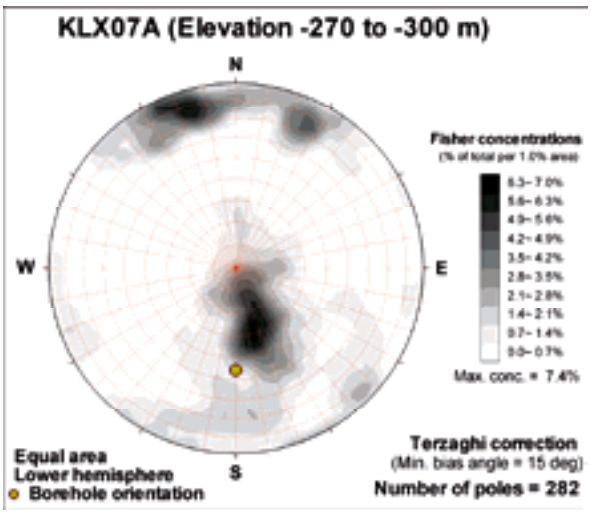
KLX07A (Elevation -270 to -300 m)
N
W
E
S
Fisher concentrations
(% of total per 1.0% area)
6.3–7.0%
5.6–6.3%
4.9–5.6%
4.2–4.9%
3.5–4.2%
2.8–3.5%
2.1–2.8%
1.4–2.1%
0.7–1.4%
0.0–0.7%
Max. conc. = 7.4%
Equal area
Lower hemisphere
Borehole orientation
Terzaghi correction
(Min. bias angle = 15 deg)
Number of poles = 282

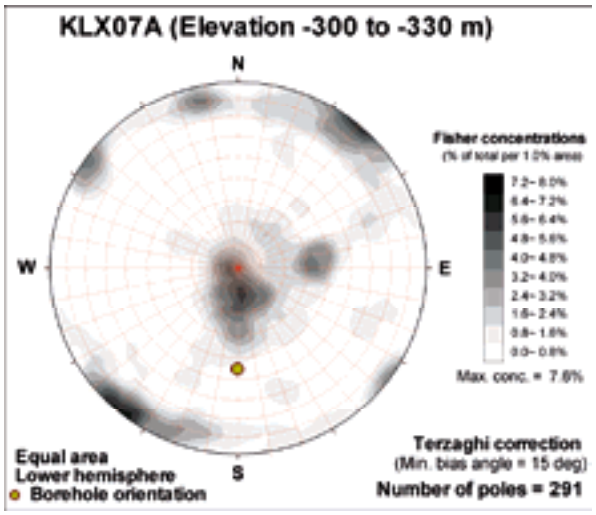
KLX07A (Elevation -300 to -330 m)
N
W
E
S
Fisher concentrations
(% of total per 1.0% area)
7.2–8.0%
6.4–7.2%
5.6–6.4%
4.8–5.6%
4.0–4.8%
3.2–4.0%
2.4–3.2%
1.6–2.4%
0.8–1.6%
0.0–0.8%
Max. conc. = 7.6%
Equal area
Lower hemisphere
Borehole orientation
Terzaghi correction
(Min. bias angle = 15 deg)
Number of poles = 291

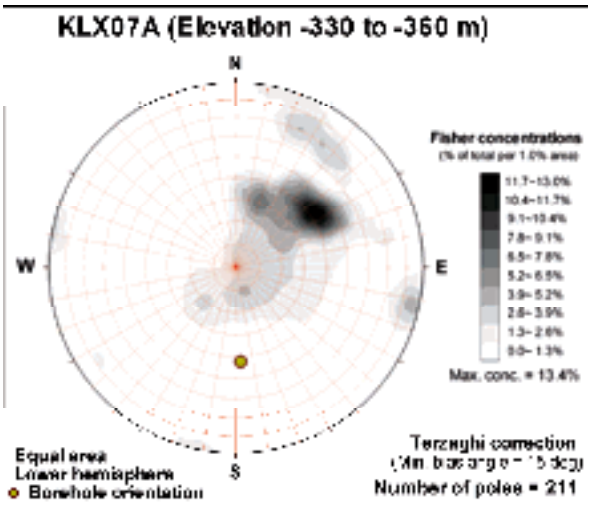
KLX07A (Elevation -330 to -360 m)
N
W
E
S
Fisher concentrations
(% of total per 1.0% area)
11.7–13.0%
10.4–11.7%
9.1–10.4%
7.8–9.1%
6.5–7.8%
5.2–6.5%
3.9–5.2%
2.6–3.9%
1.3–2.6%
0.0–1.3%
Max. conc. = 13.4%
Equal area
Lower hemisphere
Borehole orientation
Terzaghi correction
(Min. bias angle = 15 deg)
Number of poles = 211

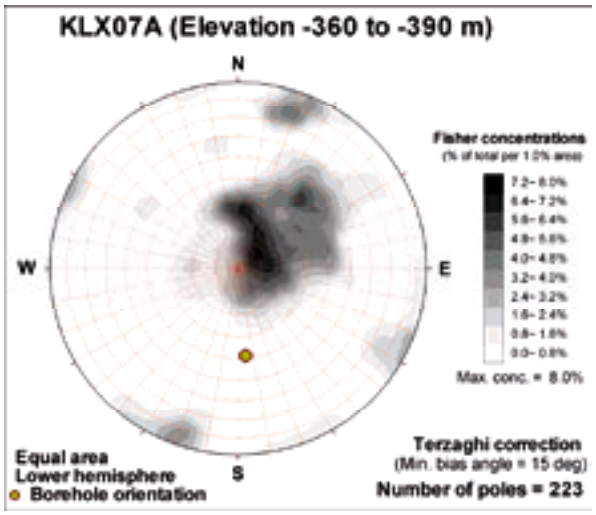
KLX07A (Elevation -360 to -390 m)
N
W
E
S
Fisher concentrations
(% of total per 1.0% area)
7.2–8.0%
6.4–7.2%
5.6–6.4%
4.8–5.6%
4.0–4.8%
3.2–4.0%
2.4–3.2%
1.6–2.4%
0.8–1.6%
0.0–0.8%
Max. conc. = 8.0%
Equal area
Lower hemisphere
Borehole orientation
Terzaghi correction
(Min. bias angle = 15 deg)
Number of poles = 223

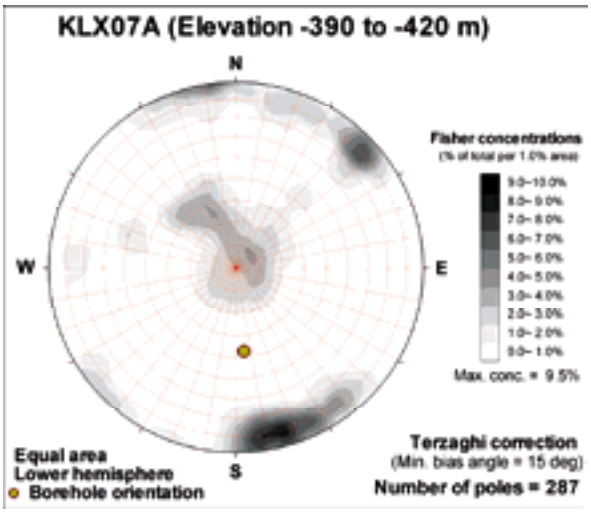
KLX07A (Elevation -390 to -420 m)
N
W
E
S
Fisher concentrations
(% of total per 1.0% area)
9.0–10.0%
8.0–9.0%
7.0–8.0%
6.0–7.0%
5.0–6.0%
4.0–5.0%
3.0–4.0%
2.0–3.0%
1.0–2.0%
0.0–1.0%
Max. conc. = 9.5%
Equal area
Lower hemisphere
Borehole orientation
Terzaghi correction
(Min. bias angle = 15 deg)
Number of poles = 287

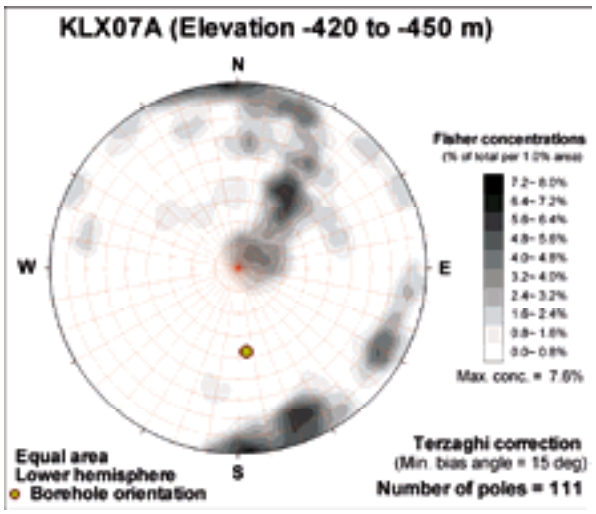
KLX07A (Elevation -420 to -450 m)
N
W
E
S
Fisher concentrations
(% of total per 1.0% area)
7.2–8.0%
6.4–7.2%
5.6–6.4%
4.8–5.6%
4.0–4.8%
3.2–4.0%
2.4–3.2%
1.6–2.4%
0.8–1.6%
0.0–0.8%
Max. conc. = 7.6%
Equal area
Lower hemisphere
Borehole orientation
Terzaghi correction
(Min. bias angle = 15 deg)
Number of poles = 111

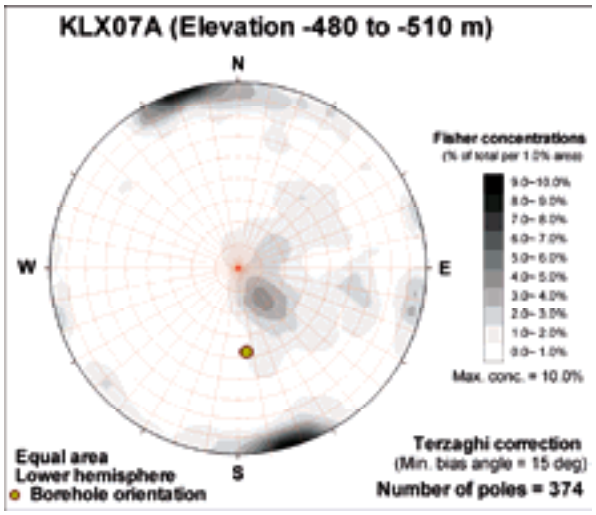
KLX07A (Elevation -480 to -510 m)
N
W
E
S
Fisher concentrations
(% of total per 1.0% area)
9.0–10.0%
8.0–9.0%
7.0–8.0%
6.0–7.0%
5.0–6.0%
4.0–5.0%
3.0–4.0%
2.0–3.0%
1.0–2.0%
0.0–1.0%
Max. conc. = 10.0%
Equal area
Lower hemisphere
Borehole orientation
Terzaghi correction
(Min. bias angle = 15 deg)
Number of poles = 374

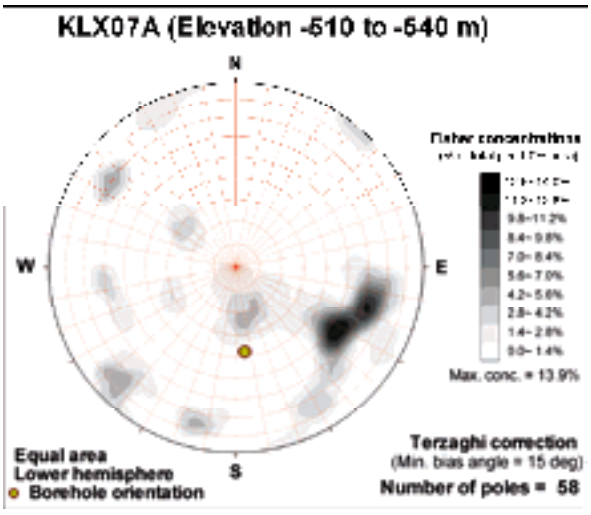
KLX07A (Elevation -510 to -540 m)
N
W
E
S
Max. conc. = 13.9%
Equal area
Lower hemisphere
Borehole orientation
Terzaghi correction
(Min. bias angle = 15 deg)
Number of poles = 58

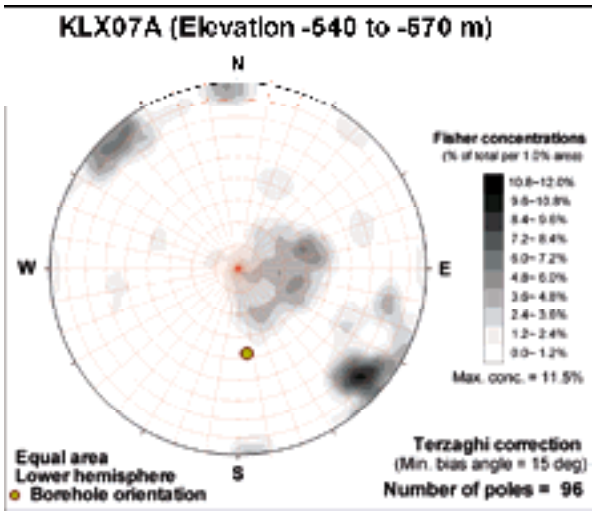
KLX07A (Elevation -540 to -570 m)
N
W
E
S
Fisher concentrations
(% of total per 1.0% area)
10.8–12.0%
9.6–10.8%
8.4–9.6%
7.2–8.4%
6.0–7.2%
4.8–6.0%
3.6–4.8%
2.4–3.6%
1.2–2.4%
0.0–1.2%
Max. conc. = 11.5%
Equal area
Lower hemisphere
Borehole orientation
Terzaghi correction
(Min. bias angle = 15 deg)
Number of poles = 96

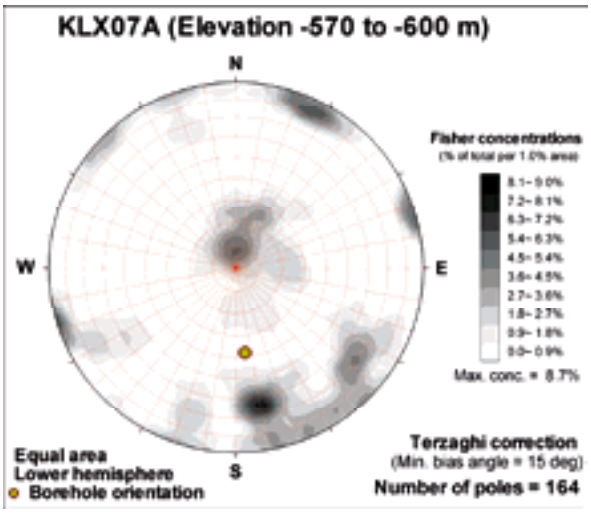
KLX07A (Elevation -570 to -600 m)
N
W
E
S
Fisher concentrations
(% of total per 1.0% area)
8.1–9.0%
7.2–8.1%
6.3–7.2%
5.4–6.3%
4.5–5.4%
3.6–4.5%
2.7–3.6%
1.8–2.7%
0.9–1.8%
0.0–0.9%
Max. conc. = 8.7%
Equal area
Lower hemisphere
Borehole orientation
Terzaghi correction
(Min. bias angle = 15 deg)
Number of poles = 164

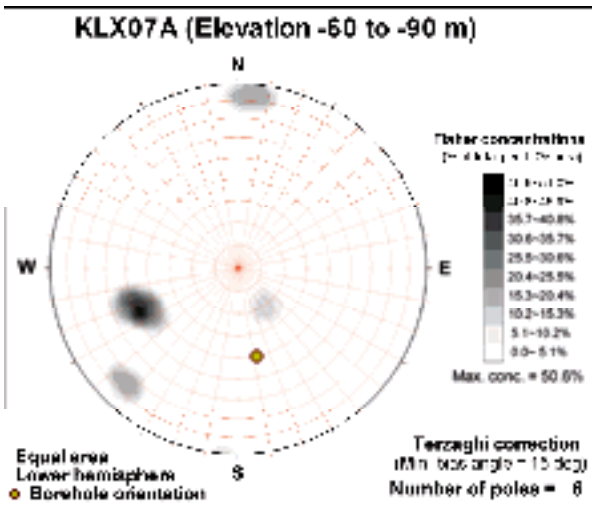
KLX07A (Elevation -60 to -90 m)
N
W
E
S
Equal area
Lower hemisphere
Borehole orientation
Terzaghi correction
Number of poles = 6

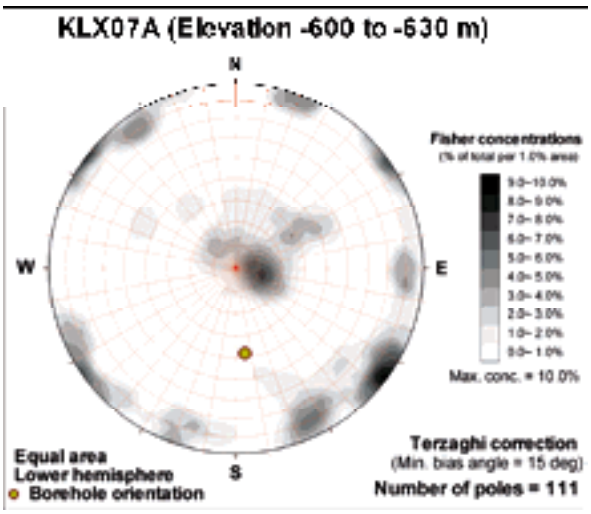
KLX07A (Elevation -600 to -630 m)
N
W
E
S
Fisher concentrations
Max. conc. = 10.0%
Equal area
Lower hemisphere
Borehole orientation
Terzaghi correction
(Min. bias angle = 15 deg)
Number of poles = 111

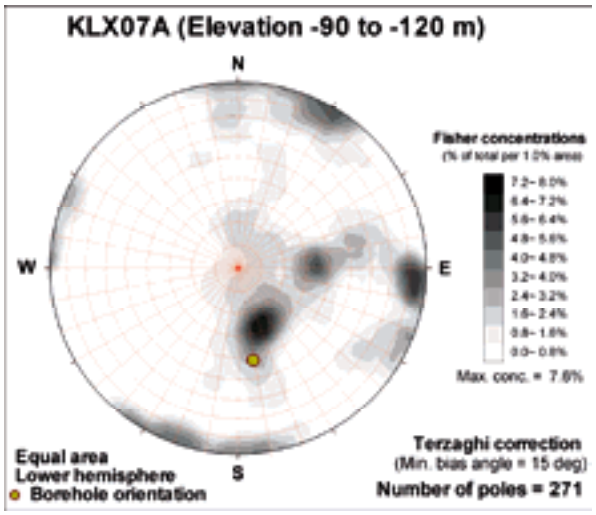
KLX07A (Elevation -90 to -120 m)
N
W
E
S
Fisher concentrations
Max. conc. = 7.8%
Equal area
Lower hemisphere
Borehole orientation
Terzaghi correction
(Min. bias angle = 15 deg)
Number of poles = 271

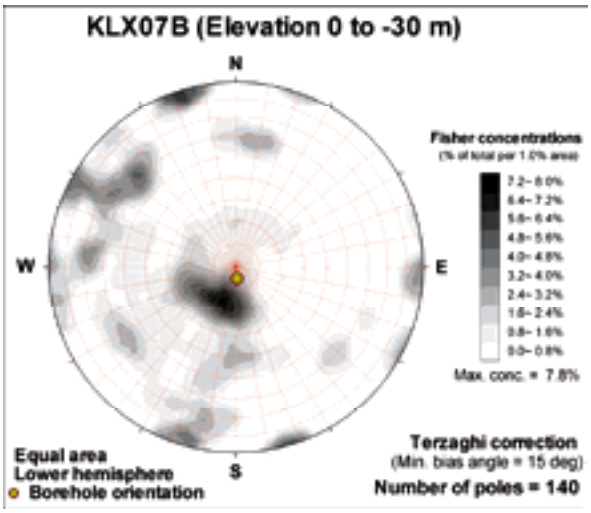
KLX07B (Elevation 0 to -30 m)
N
W
E
S
Fisher concentrations
Max. conc. = 7.8%
Equal area
Lower hemisphere
Borehole orientation
Terzaghi correction
(Min. bias angle = 15 deg)
Number of poles = 140

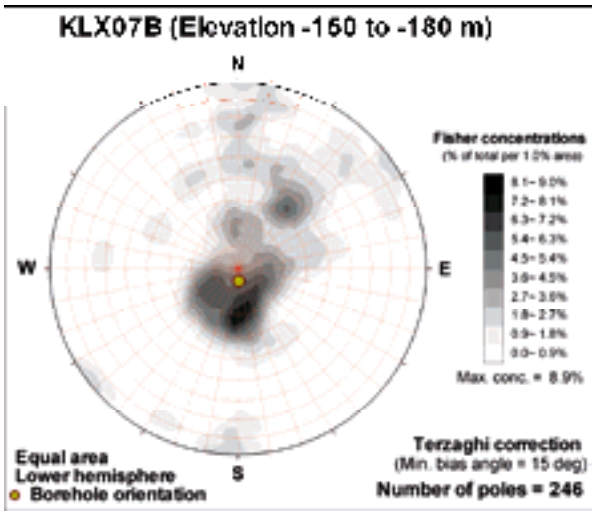
KLX07B (Elevation -150 to -180 m)
N
W
E
S
Fisher concentrations
Max. conc. = 8.9%
Equal area
Lower hemisphere
Borehole orientation
Terzaghi correction
(Min. bias angle = 15 deg)
Number of poles = 246

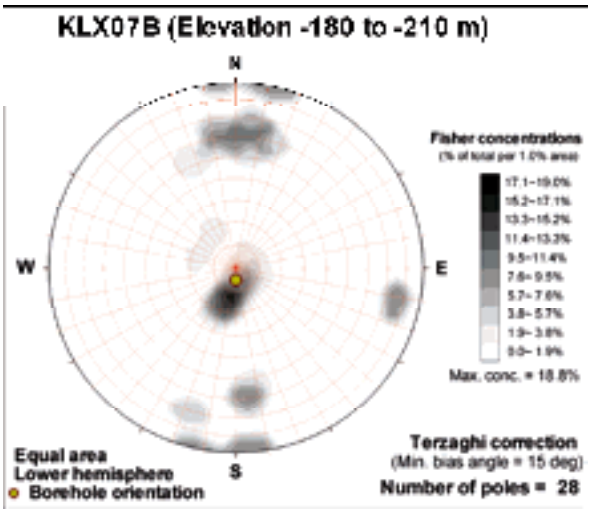
KLX07B (Elevation -180 to -210 m)
N
W
E
S
Fisher concentrations
Max. conc. = 18.8%
Equal area
Lower hemisphere
Borehole orientation
Terzaghi correction
(Min. bias angle = 15 deg)
Number of poles = 28

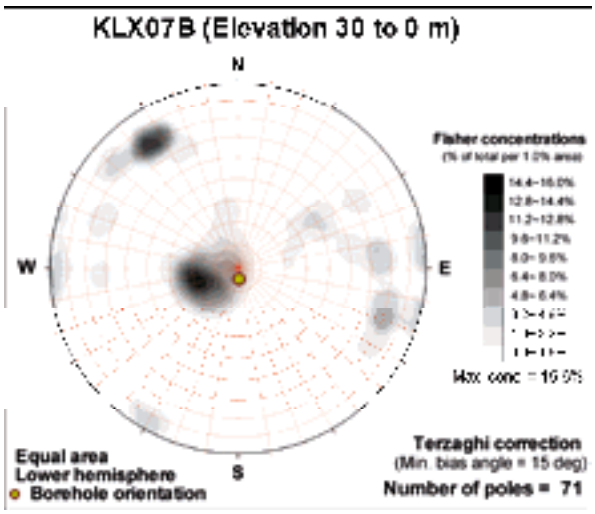
KLX07B (Elevation 30 to 0 m)
N
W
E
S
Fisher concentrations
(% of total per 1.0% area)
Max. conc. = 16.9%
Equal area
Lower hemisphere
Borehole orientation
Terzaghi correction
(Min. bias angle = 15 deg)
Number of poles = 71

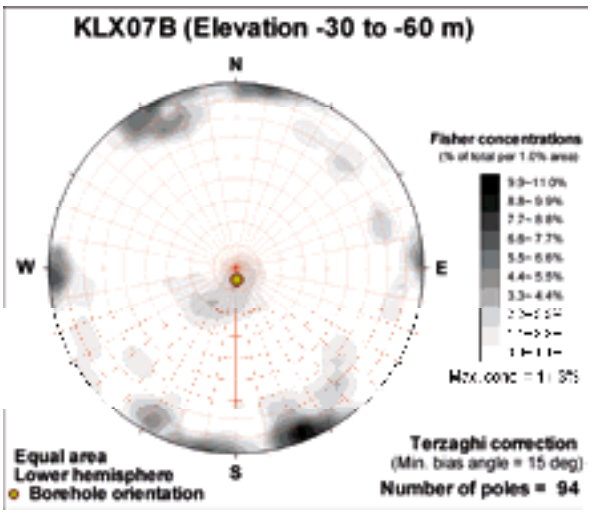
KLX07B (Elevation -30 to -60 m)
N
W
E
S
Fisher concentrations
(% of total per 1.0% area)
Equal area
Lower hemisphere
Borehole orientation
Terzaghi correction
(Min. bias angle = 15 deg)
Number of poles = 94

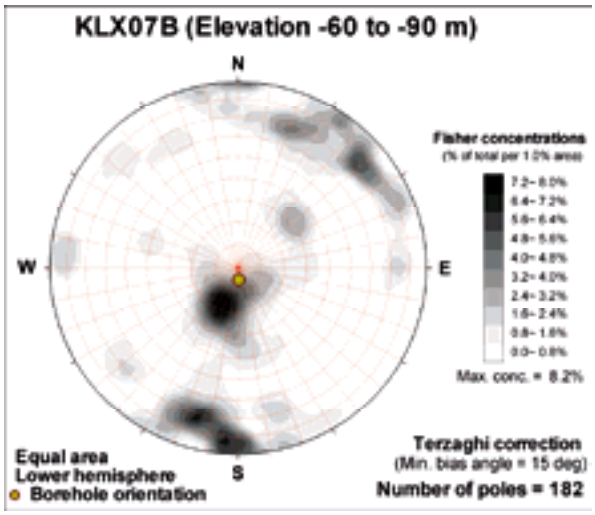
KLX07B (Elevation -60 to -90 m)
N
W
E
S
Fisher concentrations
(% of total per 1.0% area)
Max. conc. = 8.2%
Equal area
Lower hemisphere
Borehole orientation
Terzaghi correction
(Min. bias angle = 15 deg)
Number of poles = 182

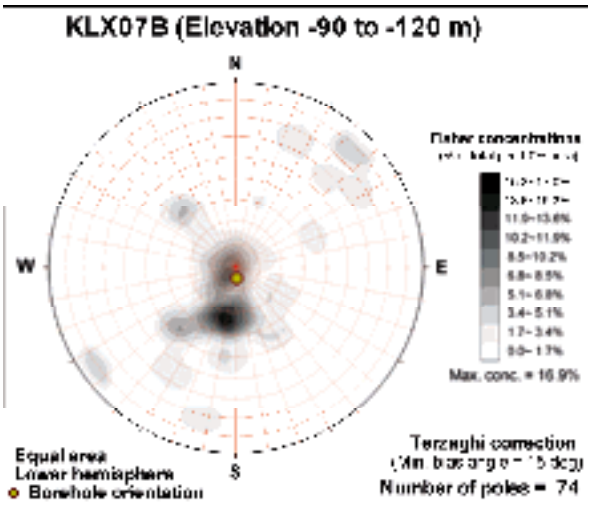
KLX07B (Elevation -90 to -120 m)
N
W
E
S
Max. conc. = 16.9%
Equal area
Lower hemisphere
Borehole orientation
Number of poles = 74

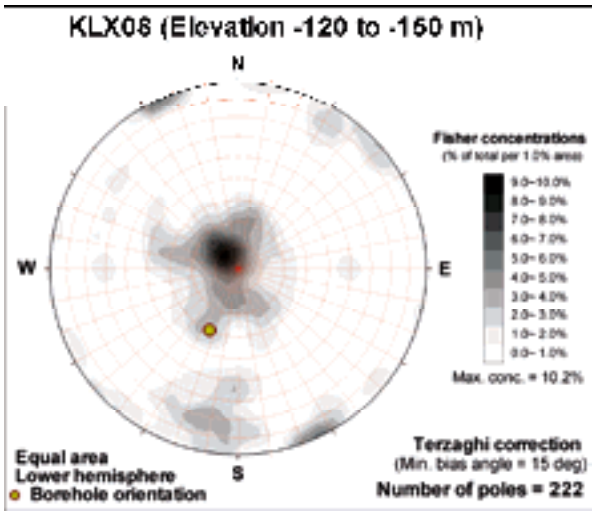
KLX08 (Elevation -120 to -150 m)
N
W
E
S
Fisher concentrations
(% of total per 1.0% area)
Max. conc. = 10.2%
Equal area
Lower hemisphere
Borehole orientation
Terzaghi correction
(Min. bias angle = 15 deg)
Number of poles = 222

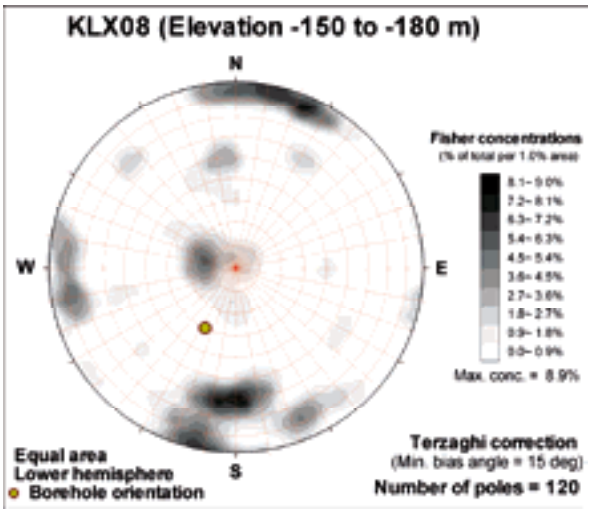
KLX08 (Elevation -150 to -180 m)
N
W
E
S
Fisher concentrations
(% of total per 1.0% area)
Max. conc. = 8.9%
Equal area
Lower hemisphere
Borehole orientation
Terzaghi correction
(Min. bias angle = 15 deg)
Number of poles = 120

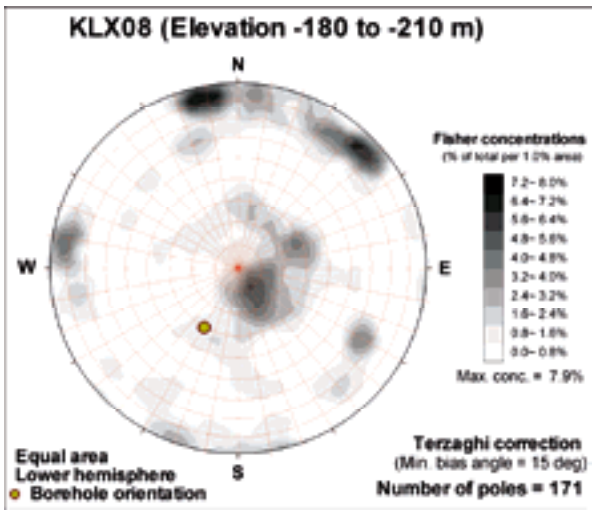
KLX08 (Elevation -180 to -210 m)
N
W
E
S
Fisher concentrations
(% of total per 1.0% area)
7.2- 8.0%
6.4- 7.2%
5.6- 6.4%
4.8- 5.6%
4.0- 4.8%
3.2- 4.0%
2.4- 3.2%
1.6- 2.4%
0.8- 1.6%
0.0- 0.8%
Max. conc. = 7.9%
Equal area
Lower hemisphere
Borehole orientation
Terzaghi correction
(Min. bias angle = 15 deg)
Number of poles = 171

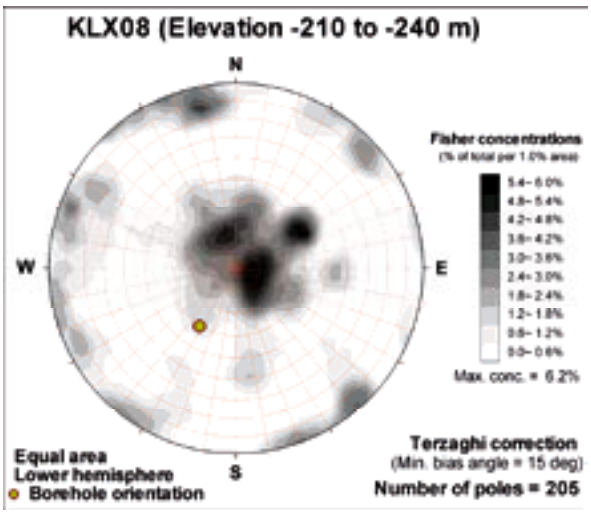
KLX08 (Elevation -210 to -240 m)
N
W
E
S
Fisher concentrations
(% of total per 1.0% area)
5.4- 6.0%
4.8- 5.4%
4.2- 4.8%
3.6- 4.2%
3.0- 3.6%
2.4- 3.0%
1.8- 2.4%
1.2- 1.8%
0.6- 1.2%
0.0- 0.6%
Max. conc. = 6.2%
Equal area
Lower hemisphere
Borehole orientation
Terzaghi correction
(Min. bias angle = 15 deg)
Number of poles = 205

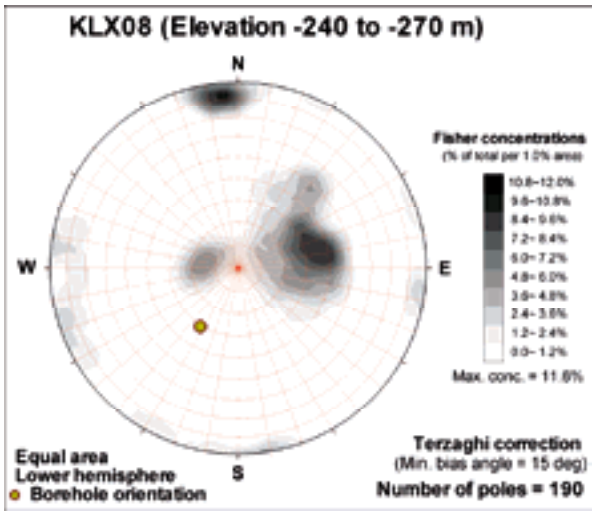
KLX08 (Elevation -240 to -270 m)
N
W
E
S
Fisher concentrations
(% of total per 1.0% area)
10.8-12.0%
9.6-10.8%
8.4- 9.6%
7.2- 8.4%
6.0- 7.2%
4.8- 6.0%
3.6- 4.8%
2.4- 3.6%
1.2- 2.4%
0.0- 1.2%
Max. conc. = 11.6%
Equal area
Lower hemisphere
Borehole orientation
Terzaghi correction
(Min. bias angle = 15 deg)
Number of poles = 190

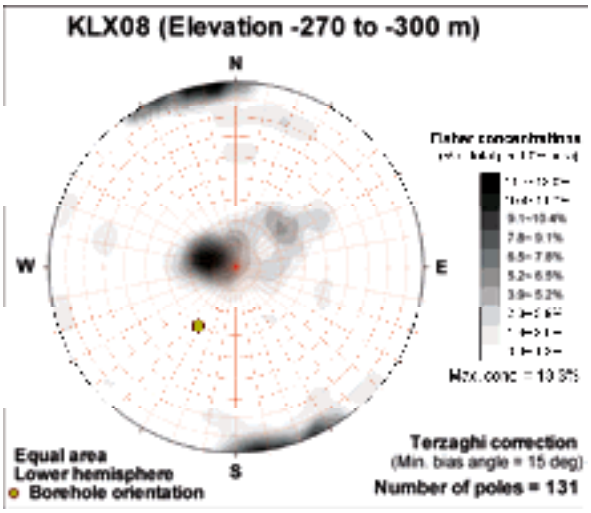
KLX08 (Elevation -270 to -300 m)
N
W
E
S
Equal area
Lower hemisphere
Borehole orientation
Terzaghi correction
(Min. bias angle = 15 deg)
Number of poles = 131

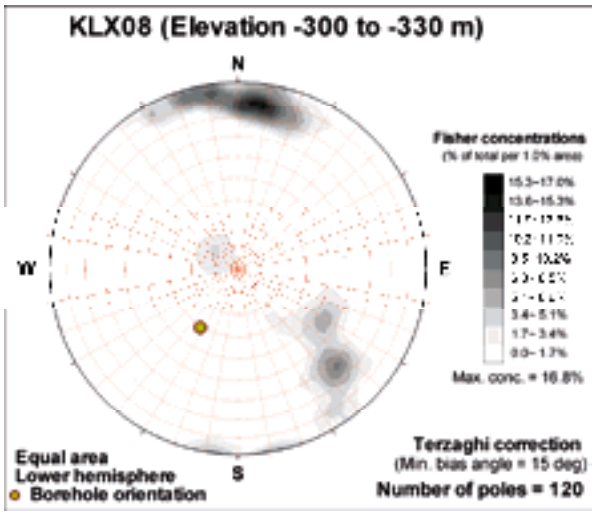
KLX08 (Elevation -300 to -330 m)
N
W
E
S
Fisher concentrations
(% of total per 1.0% area)
15.3-17.0%
13.6-15.3%
10.2-11.9%
8.5-10.2%
6.8- 8.5%
5.1- 6.8%
3.4- 5.1%
1.7- 3.4%
0.0- 1.7%
Max. conc. = 16.8%
Equal area
Lower hemisphere
Borehole orientation
Terzaghi correction
(Min. bias angle = 15 deg)
Number of poles = 120

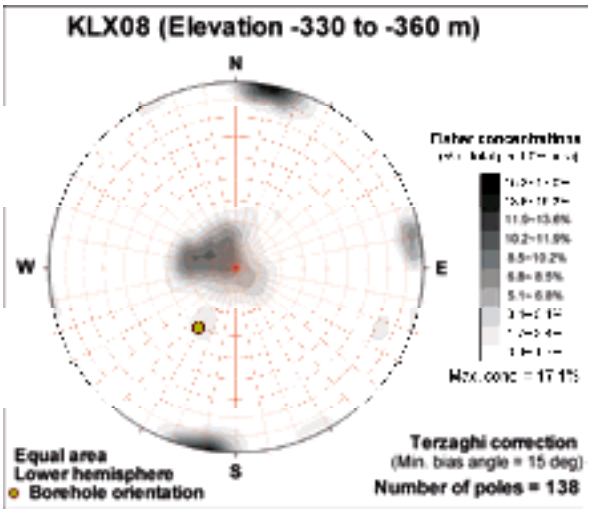
KLX08 (Elevation -330 to -360 m)
N
W
E
S
Fisher concentrations
11.9-13.6%
10.2-11.9%
8.5-10.2%
6.8- 8.5%
5.1- 6.8%
Equal area
Lower hemisphere
Borehole orientation
Terzaghi correction
(Min. bias angle = 15 deg)
Number of poles = 138

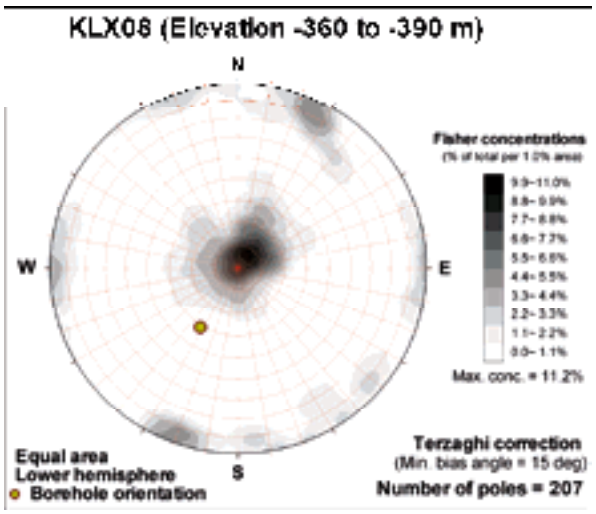
KLX08 (Elevation -360 to -390 m)
N
W
E
S
Fisher concentrations
(% of total per 1.0% area)
9.9–11.0%
8.8–9.9%
7.7–8.8%
6.6–7.7%
5.5–6.6%
4.4–5.5%
3.3–4.4%
2.2–3.3%
1.1–2.2%
0.0–1.1%
Max. conc. = 11.2%
Equal area
Lower hemisphere
Borehole orientation
Terzaghi correction
(Min. bias angle = 15 deg)
Number of poles = 207

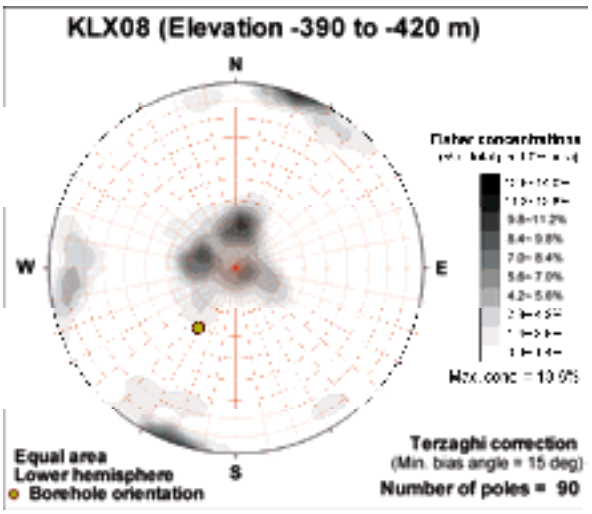
KLX08 (Elevation -390 to -420 m)
N
W
E
S
Fisher concentrations
Equal area
Lower hemisphere
Borehole orientation
Terzaghi correction
(Min. bias angle = 15 deg)
Number of poles = 90

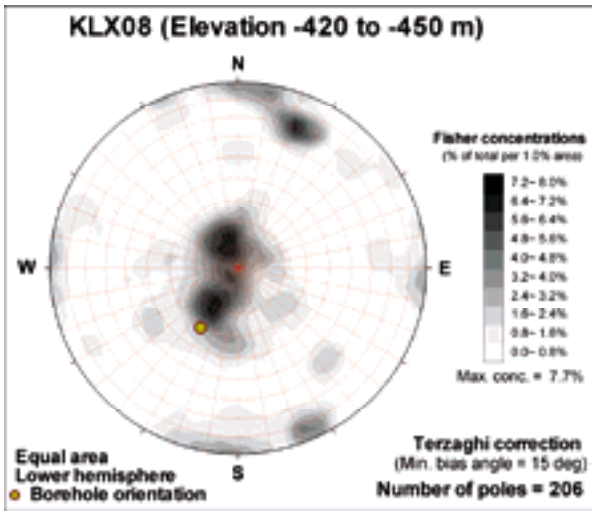
KLX08 (Elevation -420 to -450 m)
N
W
E
S
Fisher concentrations
(% of total per 1.0% area)
7.2–8.0%
6.4–7.2%
5.6–6.4%
4.8–5.6%
4.0–4.8%
3.2–4.0%
2.4–3.2%
1.6–2.4%
0.8–1.6%
0.0–0.8%
Max. conc. = 7.7%
Equal area
Lower hemisphere
Borehole orientation
Terzaghi correction
(Min. bias angle = 15 deg)
Number of poles = 206

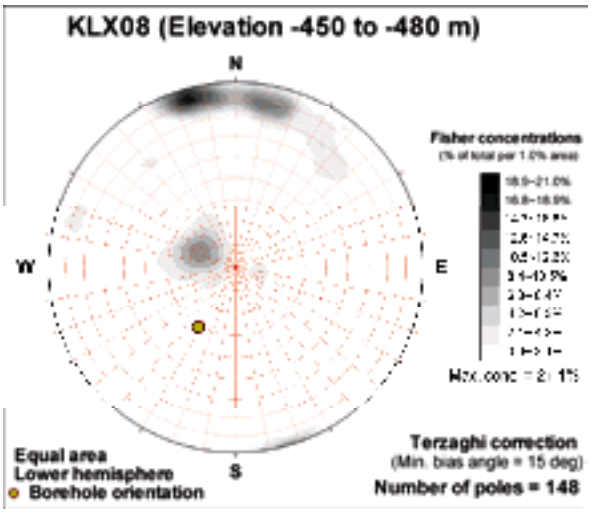
KLX08 (Elevation -450 to -480 m)
N
W
E
S
Fisher concentrations
(% of total per 1.0% area)
Equal area
Lower hemisphere
Borehole orientation
Terzaghi correction
(Min. bias angle = 15 deg)
Number of poles = 148

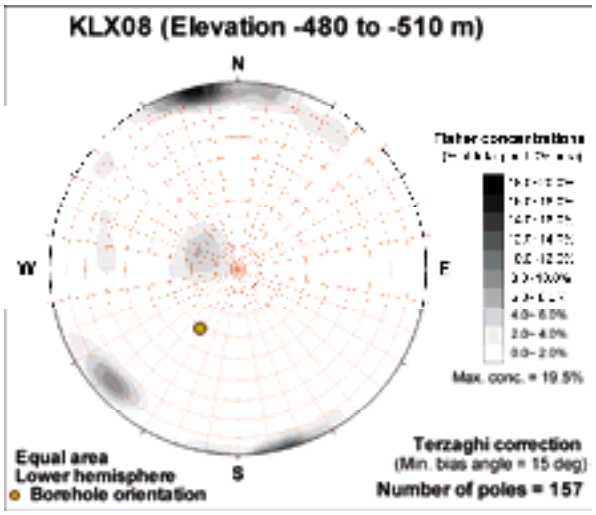
KLX08 (Elevation -480 to -510 m)
N
W
E
S
Max. conc. = 19.5%
Equal area
Lower hemisphere
Borehole orientation
Terzaghi correction
(Min. bias angle = 15 deg)
Number of poles = 157

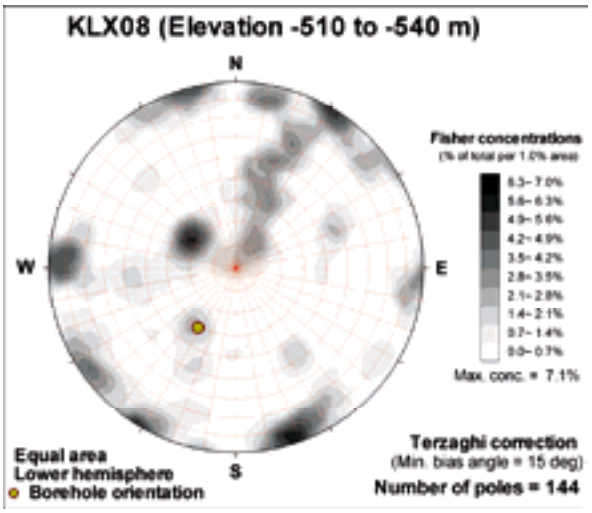
KLX08 (Elevation -510 to -540 m)
N
W
E
S
Fisher concentrations
(% of total per 1.0% area)
6.3–7.0%
5.6–6.3%
4.9–5.6%
4.2–4.9%
3.5–4.2%
2.8–3.5%
2.1–2.8%
1.4–2.1%
0.7–1.4%
0.0–0.7%
Max. conc. = 7.1%
Equal area
Lower hemisphere
Borehole orientation
Terzaghi correction
(Min. bias angle = 15 deg)
Number of poles = 144

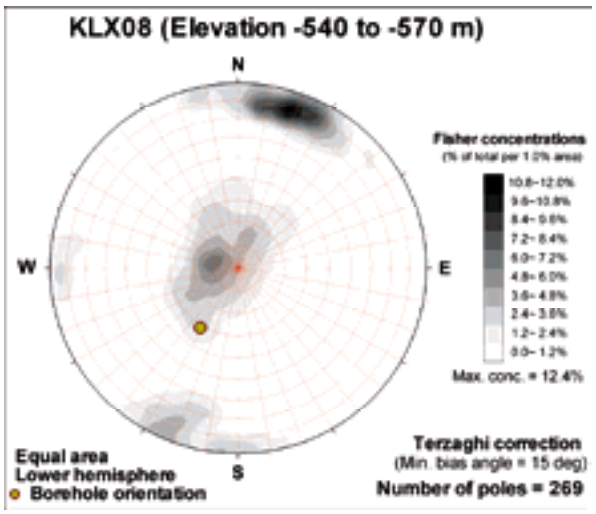
KLX08 (Elevation -540 to -570 m)
N
W
E
S
Fisher concentrations
(% of total per 1.0% area)
10.8–12.0%
9.6–10.8%
8.4–9.6%
7.2–8.4%
6.0–7.2%
4.8–6.0%
3.6–4.8%
2.4–3.6%
1.2–2.4%
0.0–1.2%
Max. conc. = 12.4%
Equal area
Lower hemisphere
Borehole orientation
Terzaghi correction
(Min. bias angle = 15 deg)
Number of poles = 269

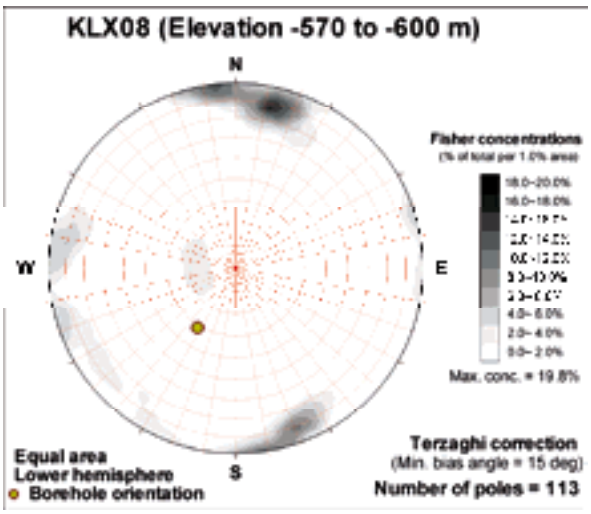
KLX08 (Elevation -570 to -600 m)
N
W
E
S
Fisher concentrations
(% of total per 1.0% area)
18.0–20.0%
16.0–18.0%
14.0–16.0%
12.0–14.0%
10.0–12.0%
8.0–10.0%
6.0–8.0%
4.0–6.0%
2.0–4.0%
0.0–2.0%
Max. conc. = 19.8%
Equal area
Lower hemisphere
Borehole orientation
Terzaghi correction
(Min. bias angle = 15 deg)
Number of poles = 113

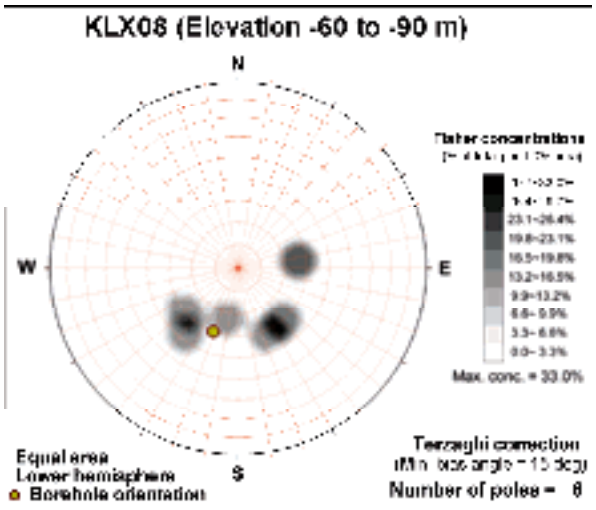
KLX08 (Elevation -60 to -90 m)
N
W
E
S
Fisher concentrations
(% of total per 1.0% area)
26.4–29.7%
23.1–26.4%
19.8–23.1%
16.5–19.8%
13.2–16.5%
9.9–13.2%
6.6–9.9%
3.3–6.6%
0.0–3.3%
Max. conc. = 33.0%
Equal area
Lower hemisphere
Borehole orientation
Terzaghi correction
(Min. bias angle = 15 deg)
Number of poles = 8

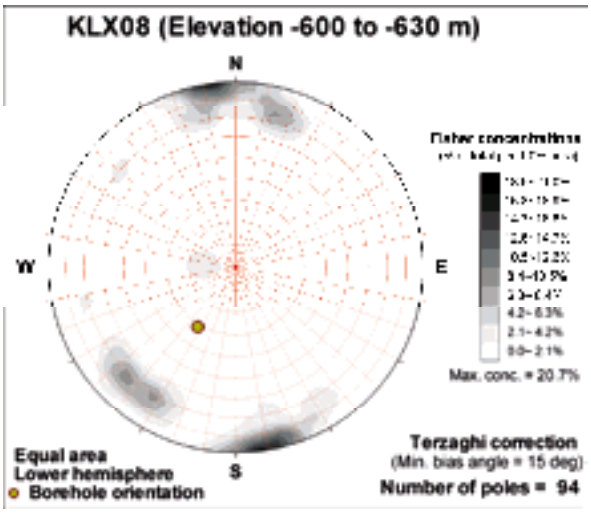
KLX08 (Elevation -600 to -630 m)
N
W
E
S
Fisher concentrations
(% of total per 1.0% area)
18.8–20.7%
16.9–18.8%
15.0–16.9%
13.1–15.0%
11.3–13.1%
9.4–11.3%
7.5–9.4%
5.6–7.5%
3.8–5.6%
1.9–3.8%
0.0–1.9%
Max. conc. = 20.7%
Equal area
Lower hemisphere
Borehole orientation
Terzaghi correction
(Min. bias angle = 15 deg)
Number of poles = 94

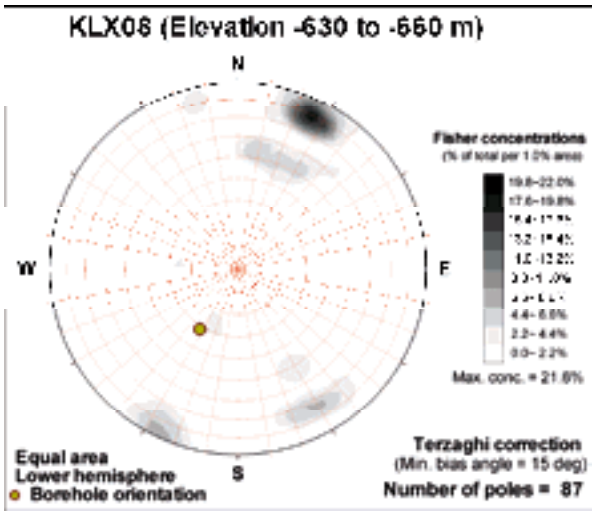
KLX08 (Elevation -630 to -660 m)
N
W
E
S
Fisher concentrations
(% of total per 1.0% area)
19.6–22.0%
17.6–19.6%
15.7–17.6%
13.7–15.7%
11.8–13.7%
9.8–11.8%
7.8–9.8%
5.9–7.8%
3.9–5.9%
2.0–3.9%
0.0–2.0%
Max. conc. = 21.6%
Equal area
Lower hemisphere
Borehole orientation
Terzaghi correction
(Min. bias angle = 15 deg)
Number of poles = 87

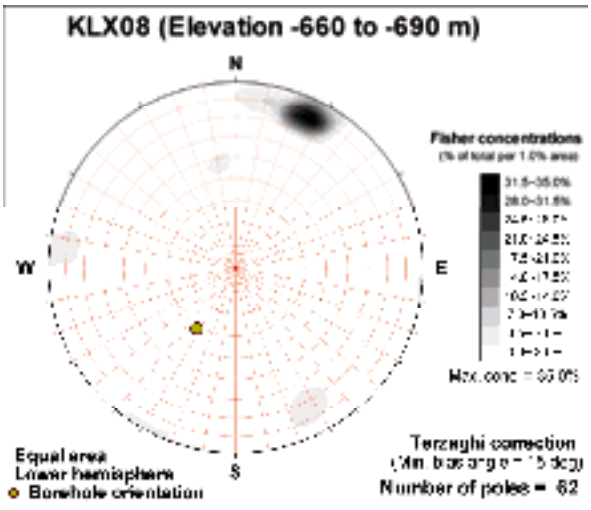
KLX08 (Elevation -660 to -690 m)
N
W
E
S
Fisher concentrations
(% of total per 1.0% area)
31.5–35.0%
28.0–31.5%
24.5–28.0%
21.0–24.5%
17.5–21.0%
14.0–17.5%
10.5–14.0%
7.0–10.5%
3.5–7.0%
0.0–3.5%
Max. conc. = 35.0%
Equal area
Lower hemisphere
Borehole orientation
Terzaghi correction
(Min. bias angle = 15 deg)
Number of poles = 62

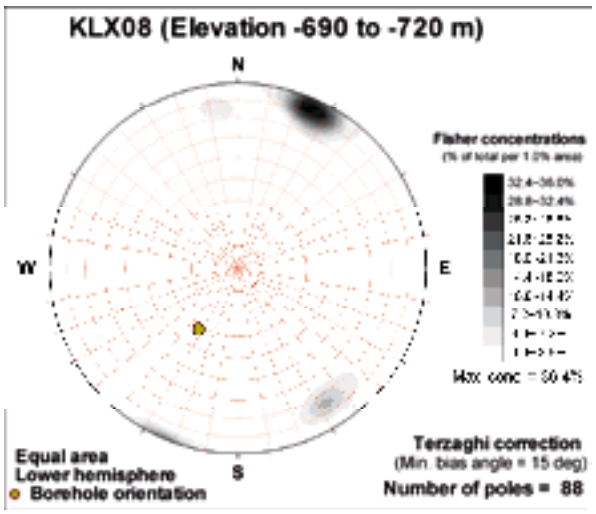
KLX08 (Elevation -690 to -720 m)
N
W
E
S
Fisher concentrations
(% of total per 1.0% area)
Max. conc = 50.4%
Equal area
Lower hemisphere
Borehole orientation
Terzaghi correction
(Min. bias angle = 15 deg)
Number of poles = 88

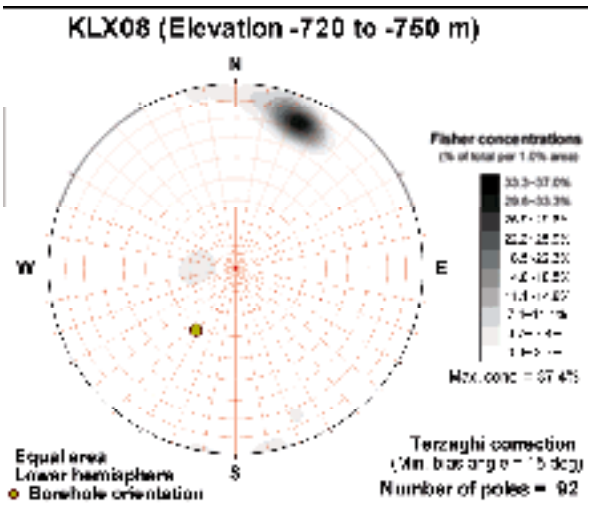
KLX08 (Elevation -720 to -750 m)
N
W
E
S
Fisher concentrations
(% of total per 1.0% area)
Max. conc = 67.4%
Equal area
Lower hemisphere
Borehole orientation
Terzaghi correction
Number of poles = 92

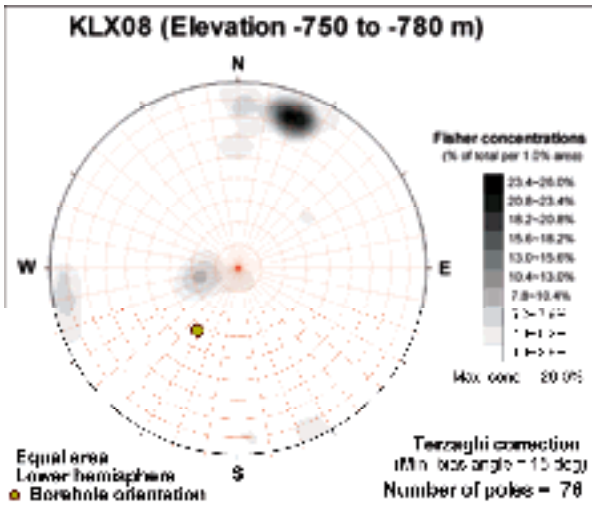
KLX08 (Elevation -750 to -780 m)
N
W
E
S
Fisher concentrations
(% of total per 1.0% area)
Equal area
Lower hemisphere
Borehole orientation
Terzaghi correction
Number of poles = 78

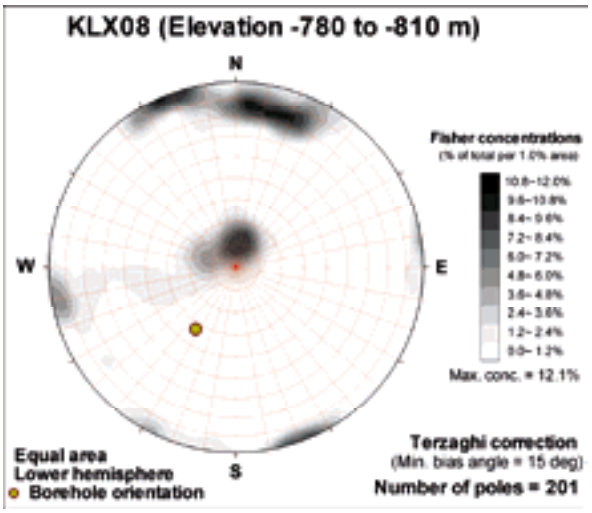
KLX08 (Elevation -780 to -810 m)
N
W
E
S
Fisher concentrations
(% of total per 1.0% area)
Max. conc. = 12.1%
Equal area
Lower hemisphere
Borehole orientation
Terzaghi correction
(Min. bias angle = 15 deg)
Number of poles = 201

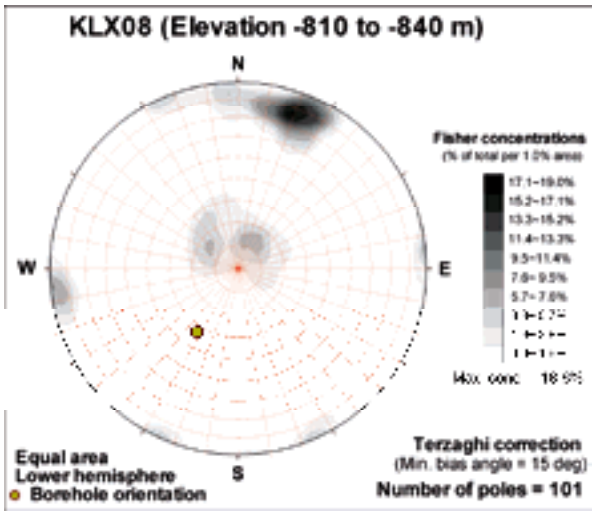
KLX08 (Elevation -810 to -840 m)
N
W
E
S
Fisher concentrations
(% of total per 1.0% area)
Equal area
Lower hemisphere
Borehole orientation
Terzaghi correction
(Min. bias angle = 15 deg)
Number of poles = 101

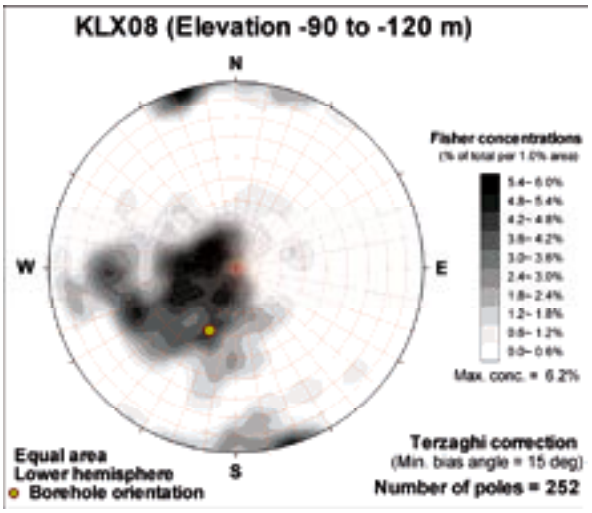
KLX08 (Elevation -90 to -120 m)
N
W
E
S
Fisher concentrations
(% of total per 1.0% area)
Max. conc. = 6.2%
Equal area
Lower hemisphere
Borehole orientation
Terzaghi correction
(Min. bias angle = 15 deg)
Number of poles = 252

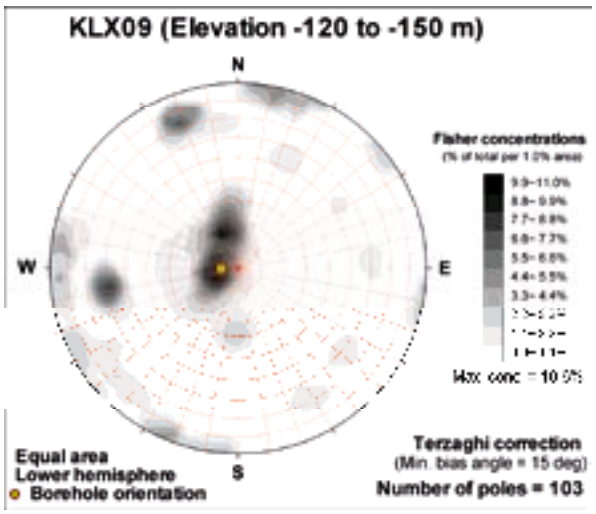
KLX09 (Elevation -120 to -150 m)
N
W
E
S
Fisher concentrations
(% of total per 1.0% area)
Max. conc. = 10.9%
Equal area
Lower hemisphere
Borehole orientation
Terzaghi correction
(Min. bias angle = 15 deg)
Number of poles = 103

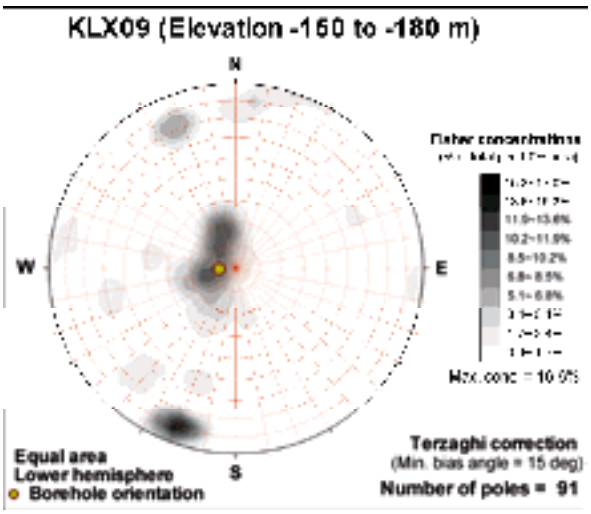
KLX09 (Elevation -150 to -180 m)
N
W
E
S
Max. conc. = 10.9%
Equal area
Lower hemisphere
Borehole orientation
Terzaghi correction
(Min. bias angle = 15 deg)
Number of poles = 91

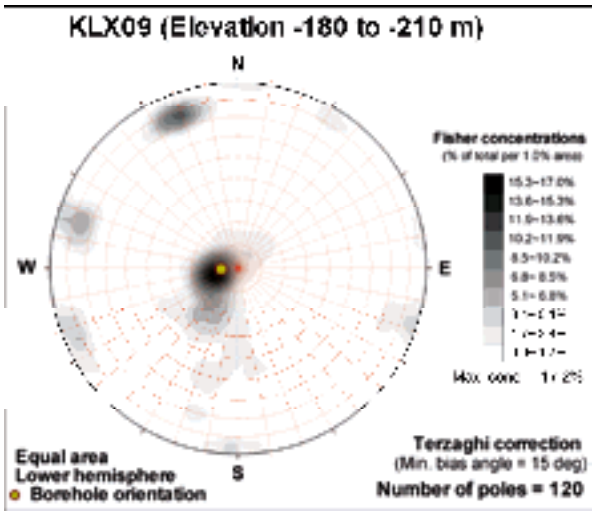
KLX09 (Elevation -180 to -210 m)
N
W
E
S
Fisher concentrations
(% of total per 1.0% area)
Equal area
Lower hemisphere
Borehole orientation
Terzaghi correction
(Min. bias angle = 15 deg)
Number of poles = 120

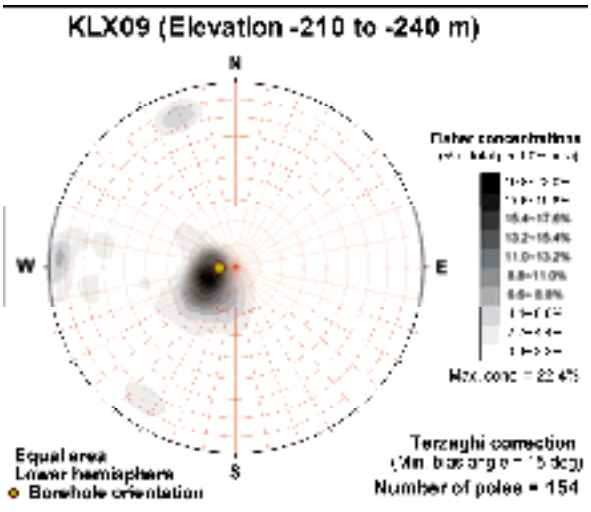
KLX09 (Elevation -210 to -240 m)
N
W
E
S
Equal area
Lower hemisphere
Borehole orientation
Number of poles = 154

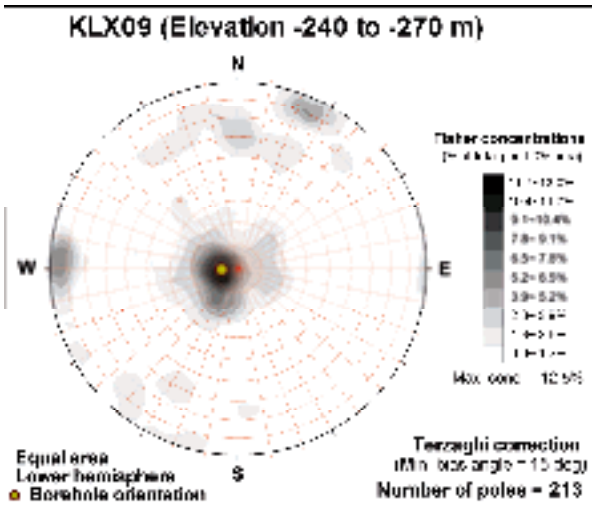
KLX09 (Elevation -240 to -270 m)
N
W
E
S
Fisher concentrations
Equal area
Lower hemisphere
Borehole orientation
Terzaghi correction
Number of poles = 213

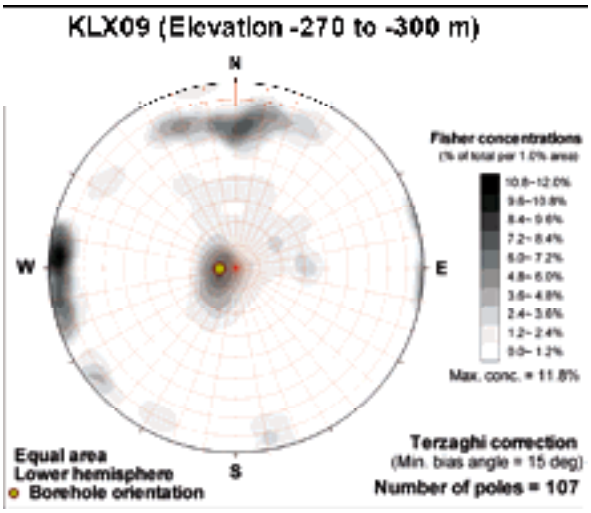
KLX09 (Elevation -270 to -300 m)
N
W
E
S
Fisher concentrations
(% of total per 1.0% area)
Max. conc. = 11.8%
Equal area
Lower hemisphere
Borehole orientation
Terzaghi correction
(Min. bias angle = 15 deg)
Number of poles = 107

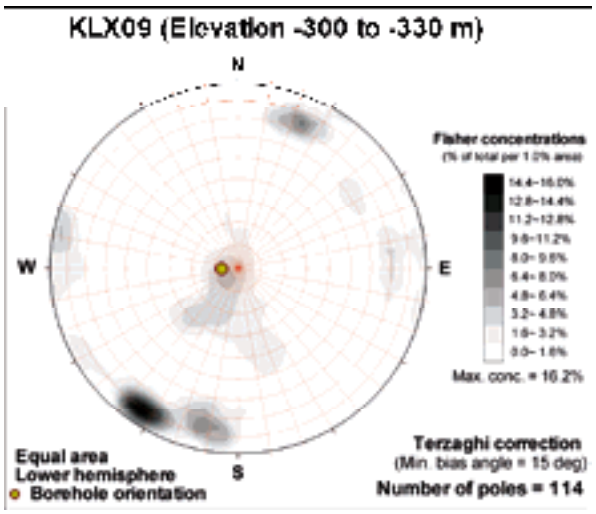
KLX09 (Elevation -300 to -330 m)
N
W
E
S
Fisher concentrations
(% of total per 1.0% area)
14.4–16.0%
12.8–14.4%
11.2–12.8%
9.6–11.2%
8.0–9.6%
6.4–8.0%
4.8–6.4%
3.2–4.8%
1.6–3.2%
0.0–1.6%
Max. conc. = 16.2%
Equal area
Lower hemisphere
Borehole orientation
Terzaghi correction
(Min. bias angle = 15 deg)
Number of poles = 114

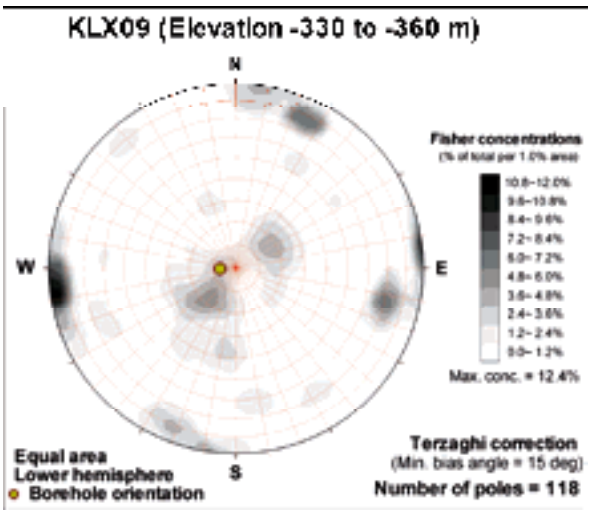
KLX09 (Elevation -330 to -360 m)
N
W
E
S
Fisher concentrations
(% of total per 1.0% area)
10.8–12.0%
9.6–10.8%
8.4–9.6%
7.2–8.4%
6.0–7.2%
4.8–6.0%
3.6–4.8%
2.4–3.6%
1.2–2.4%
0.0–1.2%
Max. conc. = 12.4%
Equal area
Lower hemisphere
Borehole orientation
Terzaghi correction
(Min. bias angle = 15 deg)
Number of poles = 118

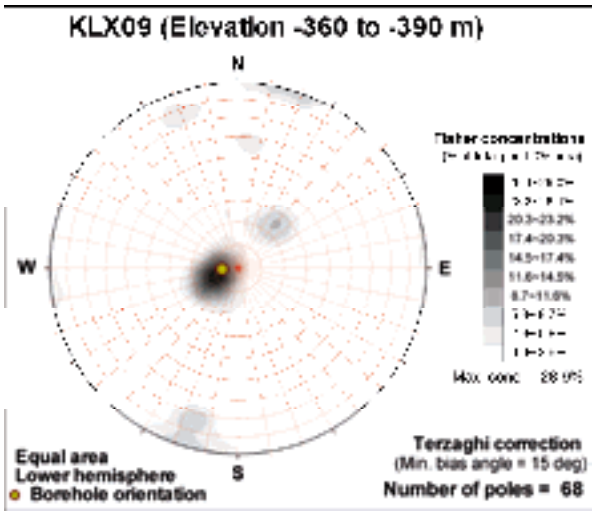
KLX09 (Elevation -360 to -390 m)
N
W
E
S
Fisher concentrations
20.3–23.2%
17.4–20.3%
14.5–17.4%
11.6–14.5%
8.7–11.6%
Equal area
Lower hemisphere
Borehole orientation
Terzaghi correction
(Min. bias angle = 15 deg)
Number of poles = 68

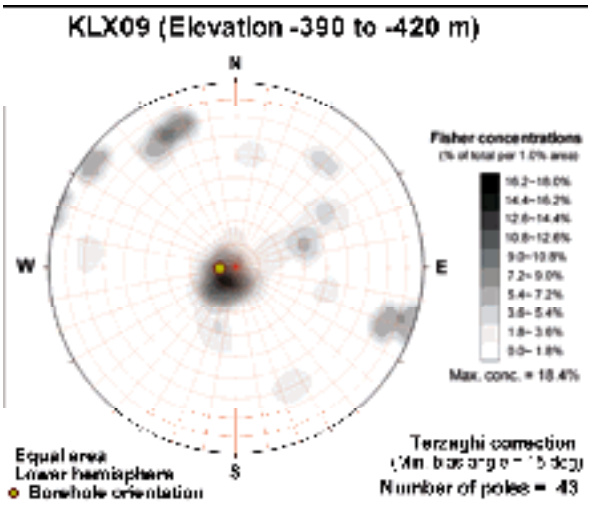
KLX09 (Elevation -390 to -420 m)
N
W
E
S
Fisher concentrations
(% of total per 1.0% area)
16.2–18.0%
14.4–16.2%
12.6–14.4%
10.8–12.6%
9.0–10.8%
7.2–9.0%
5.4–7.2%
3.6–5.4%
1.8–3.6%
0.0–1.8%
Max. conc. = 18.4%
Equal area
Lower hemisphere
Borehole orientation
Terzaghi correction
Number of poles = 43

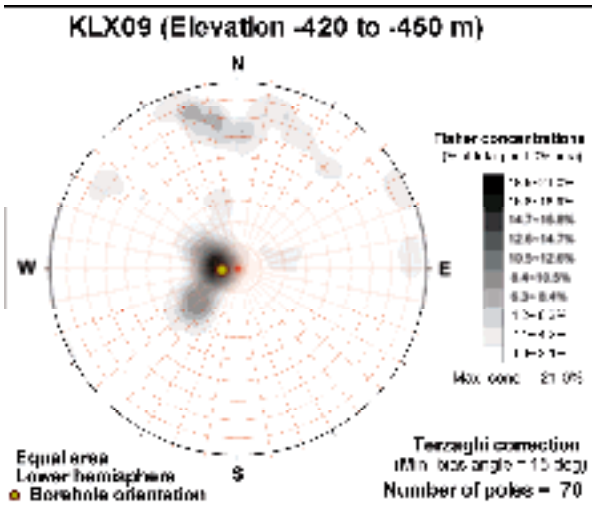
KLX09 (Elevation -420 to -460 m)
N
W
E
S
Fisher concentrations
14.7–16.8%
12.6–14.7%
10.5–12.6%
8.4–10.5%
6.3–8.4%
Equal area
Lower hemisphere
Borehole orientation
Terzaghi correction
Number of poles = 70

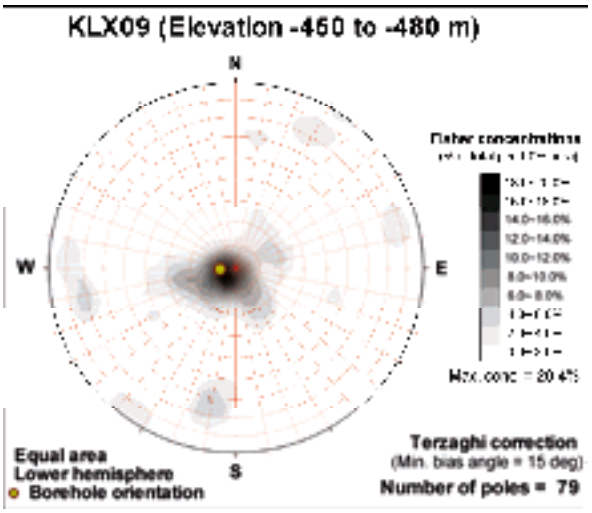
KLX09 (Elevation -460 to -480 m)
N
W
E
S
Fisher concentrations
16.0–18.0%
14.0–16.0%
12.0–14.0%
10.0–12.0%
8.0–10.0%
6.0–8.0%
Equal area
Lower hemisphere
Borehole orientation
Terzaghi correction
(Min. bias angle = 15 deg)
Number of poles = 79

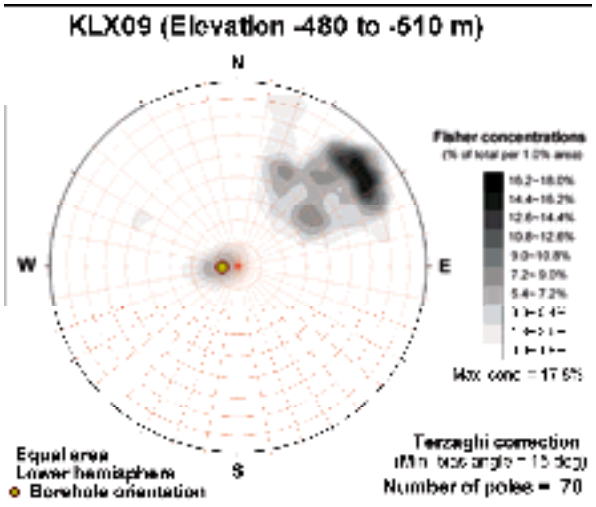
KLX09 (Elevation -480 to -510 m)
N
W
E
S
Fisher concentrations
(% of total per 1.0% area)
Max. conc. = 17.6%
Equal area
Lower hemisphere
Borehole orientation
Terzaghi correction
(Min. bias angle = 15 deg)
Number of poles = 70

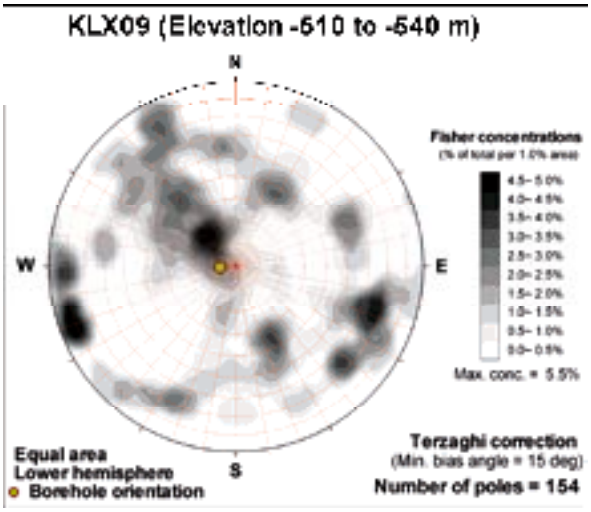
KLX09 (Elevation -510 to -540 m)
N
W
E
S
Fisher concentrations
(% of total per 1.0% area)
Max. conc. = 5.5%
Equal area
Lower hemisphere
Borehole orientation
Terzaghi correction
(Min. bias angle = 15 deg)
Number of poles = 154

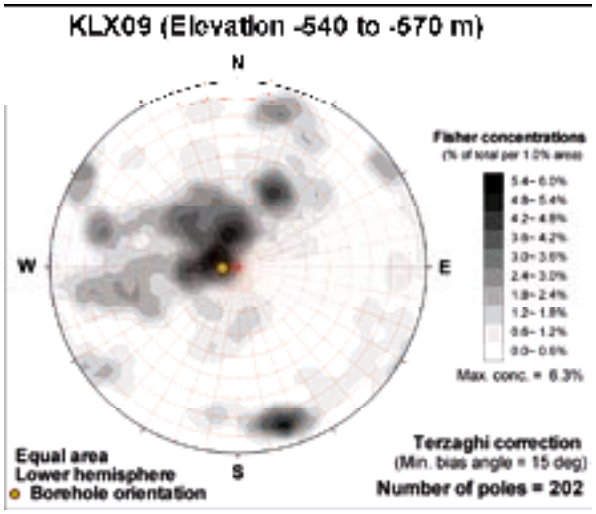
KLX09 (Elevation -540 to -570 m)
N
W
E
S
Fisher concentrations
(% of total per 1.0% area)
Max. conc. = 6.3%
Equal area
Lower hemisphere
Borehole orientation
Terzaghi correction
(Min. bias angle = 15 deg)
Number of poles = 202

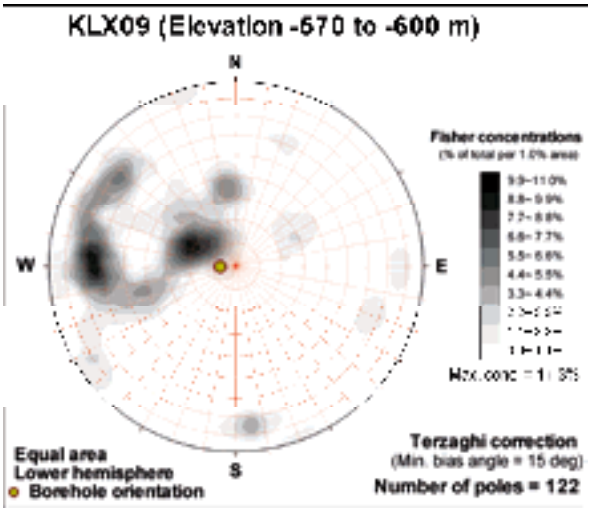
KLX09 (Elevation -570 to -600 m)
N
W
E
S
Fisher concentrations
(% of total per 1.0% area)
Equal area
Lower hemisphere
Borehole orientation
Terzaghi correction
(Min. bias angle = 15 deg)
Number of poles = 122

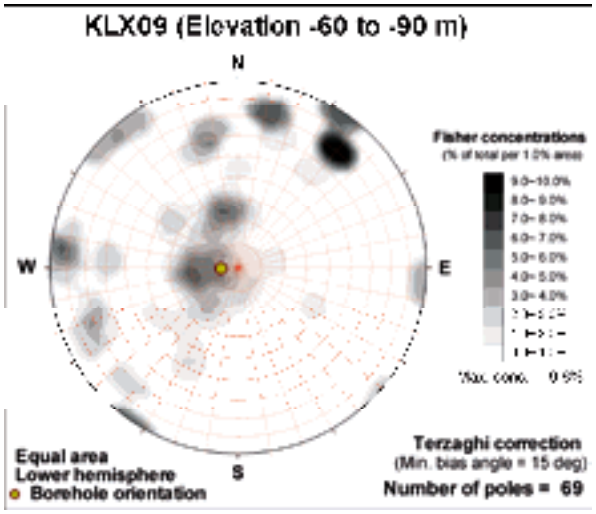
KLX09 (Elevation -60 to -90 m)
N
W
E
S
Fisher concentrations
(% of total per 1.0% area)
Equal area
Lower hemisphere
Borehole orientation
Terzaghi correction
(Min. bias angle = 15 deg)
Number of poles = 69

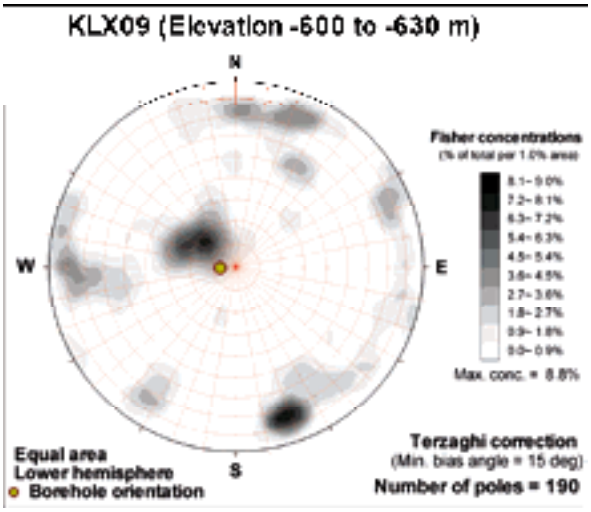
KLX09 (Elevation -600 to -630 m)
N
W
E
S
Fisher concentrations
(% of total per 1.0% area)
Max. conc. = 8.8%
Equal area
Lower hemisphere
Borehole orientation
Terzaghi correction
(Min. bias angle = 15 deg)
Number of poles = 190

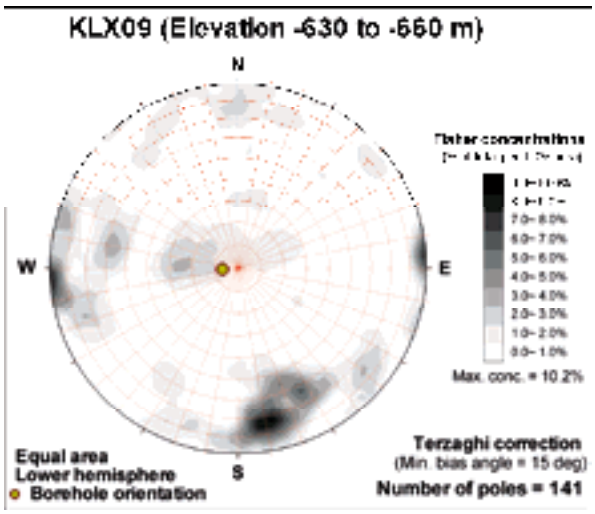
KLX09 (Elevation -630 to -660 m)
N
W
E
S
Fisher concentrations
Max. conc. = 10.2%
Equal area
Lower hemisphere
Borehole orientation
Terzaghi correction
(Min. bias angle = 15 deg)
Number of poles = 141

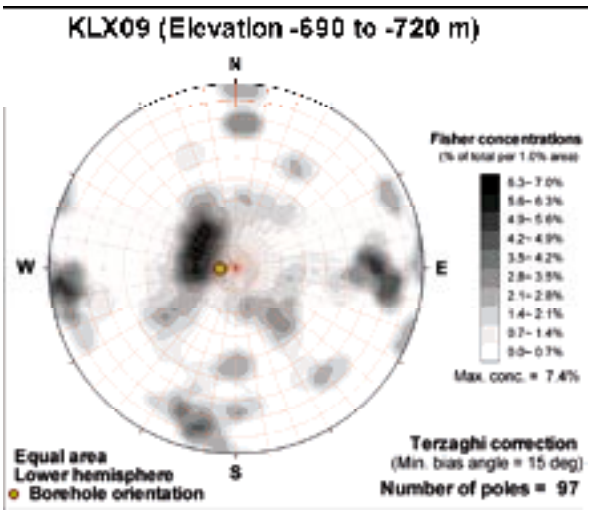
KLX09 (Elevation -690 to -720 m)
N
W
E
S
Fisher concentrations
Max. conc. = 7.4%
Equal area
Lower hemisphere
Borehole orientation
Terzaghi correction
(Min. bias angle = 15 deg)
Number of poles = 97

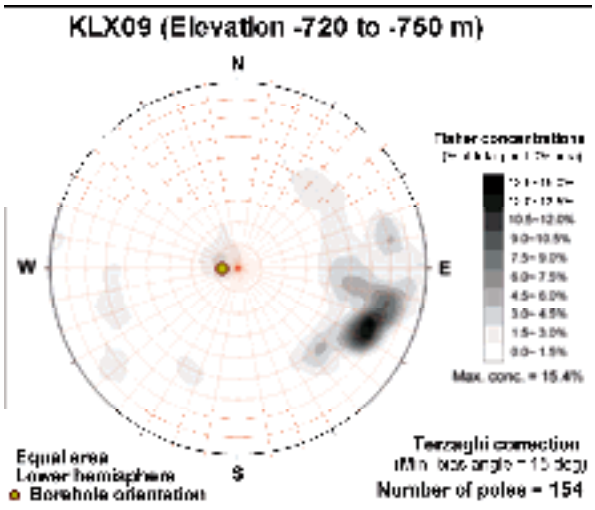
KLX09 (Elevation -720 to -750 m)
N
W
E
S
Fisher concentrations
Max. conc. = 15.4%
Equal area
Lower hemisphere
Borehole orientation
Terzaghi correction
(Min. bias angle = 15 deg)
Number of poles = 154

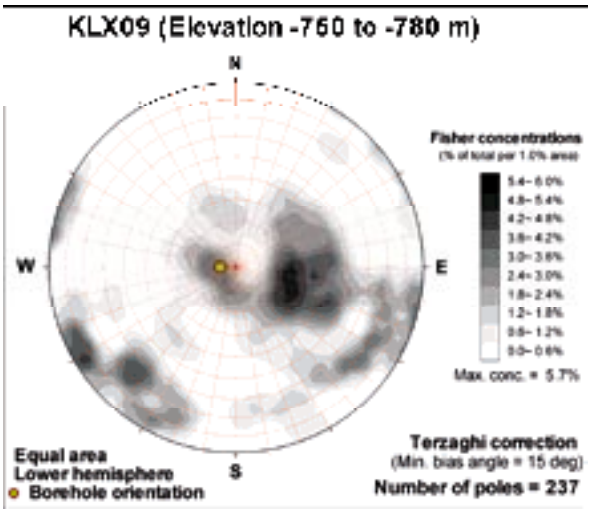
KLX09 (Elevation -750 to -780 m)
N
W
E
S
Fisher concentrations
Max. conc. = 5.7%
Equal area
Lower hemisphere
Borehole orientation
Terzaghi correction
(Min. bias angle = 15 deg)
Number of poles = 237

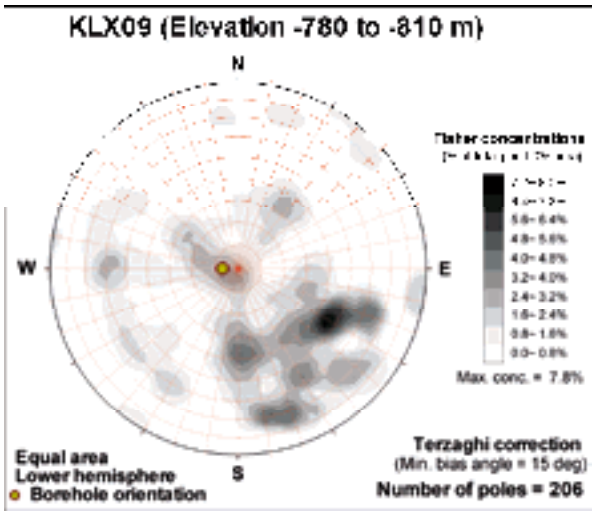
KLX09 (Elevation -780 to -810 m)
N
W
E
S
Fisher concentrations
Max. conc. = 7.8%
Equal area
Lower hemisphere
Borehole orientation
Terzaghi correction
(Min. bias angle = 15 deg)
Number of poles = 206

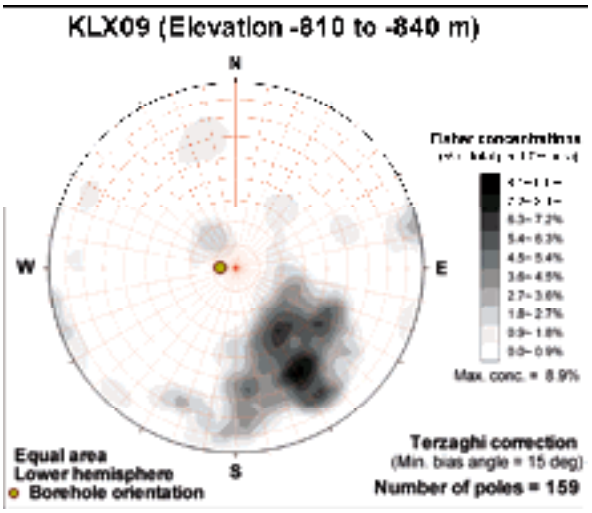
KLX09 (Elevation -810 to -840 m)
N
W
E
S
Fisher concentrations
Max. conc. = 8.9%
Equal area
Lower hemisphere
Borehole orientation
Terzaghi correction
(Min. bias angle = 15 deg)
Number of poles = 159

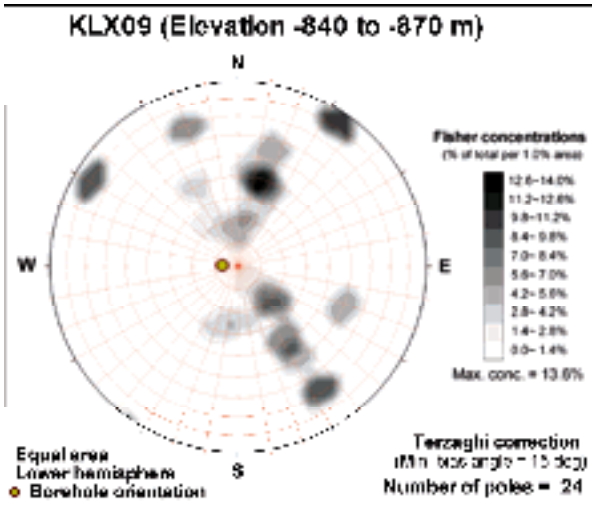
KLX09 (Elevation -840 to -870 m)
N
W
E
S
Fisher concentrations
Max. conc. = 13.6%
Equal area
Lower hemisphere
Borehole orientation
Terzaghi correction
Number of poles = 24

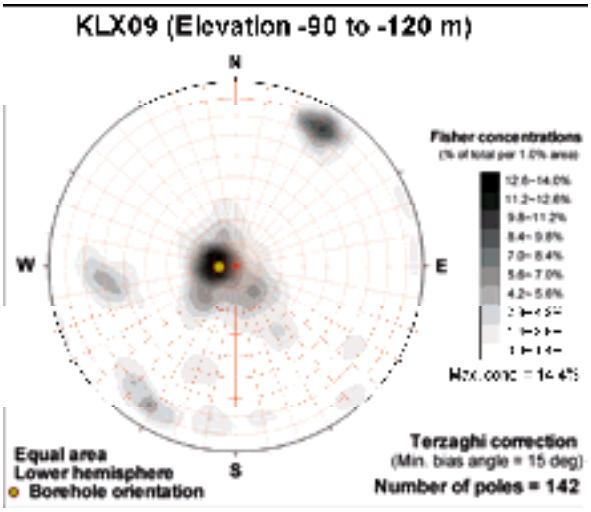
KLX09 (Elevation -90 to -120 m)
N
W
E
S
Fisher concentrations
Equal area
Lower hemisphere
Borehole orientation
Terzaghi correction
(Min. bias angle = 15 deg)
Number of poles = 142

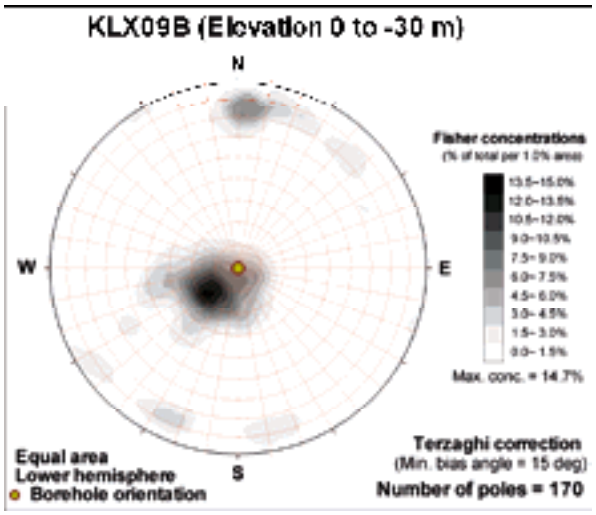
KLX09B (Elevation 0 to -30 m)
N
W
E
S
Fisher concentrations
Max. conc. = 14.7%
Equal area
Lower hemisphere
Borehole orientation
Terzaghi correction
(Min. bias angle = 15 deg)
Number of poles = 170

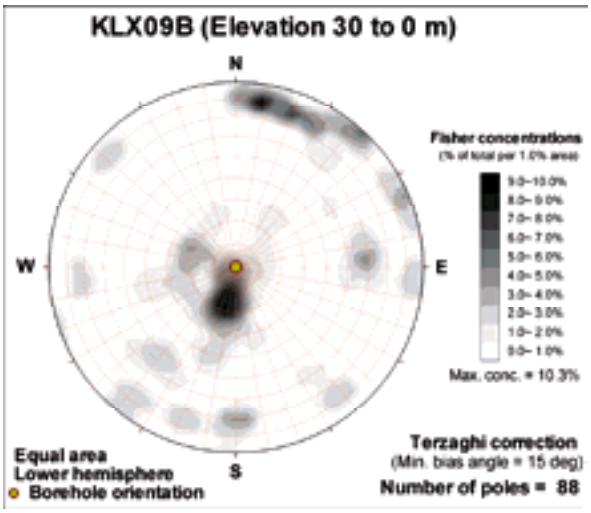
KLX09B (Elevation 30 to 0 m)
N
W
E
S
Fisher concentrations
Max. conc. = 10.3%
Equal area
Lower hemisphere
Borehole orientation
Terzaghi correction
(Min. bias angle = 15 deg)
Number of poles = 88

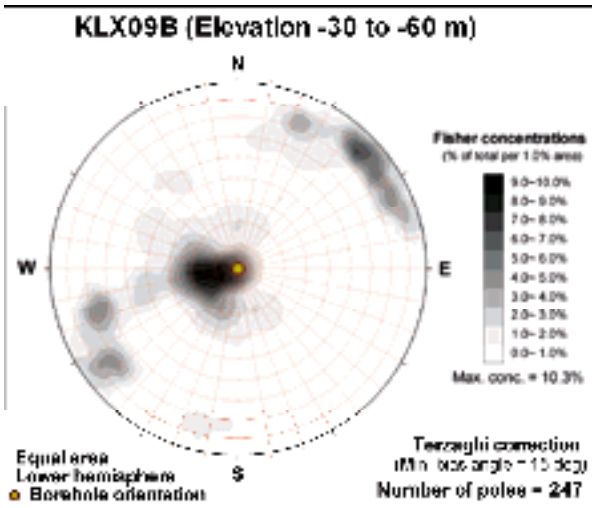
KLX09B (Elevation -30 to -60 m)
N
W
E
S
Fisher concentrations
Max. conc. = 10.3%
Equal area
Lower hemisphere
Borehole orientation
Terzaghi correction
(Min. bias angle = 15 deg)
Number of poles = 247

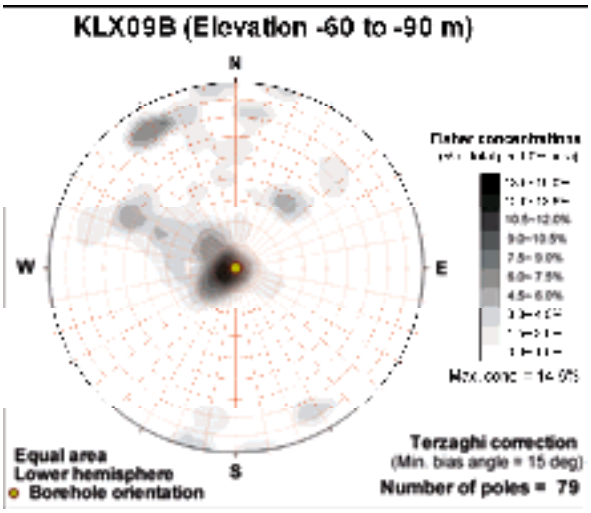
KLX09B (Elevation -60 to -90 m)
N
W
E
S
Equal area
Lower hemisphere
Borehole orientation
Terzaghi correction
(Min. bias angle = 15 deg)
Number of poles = 79

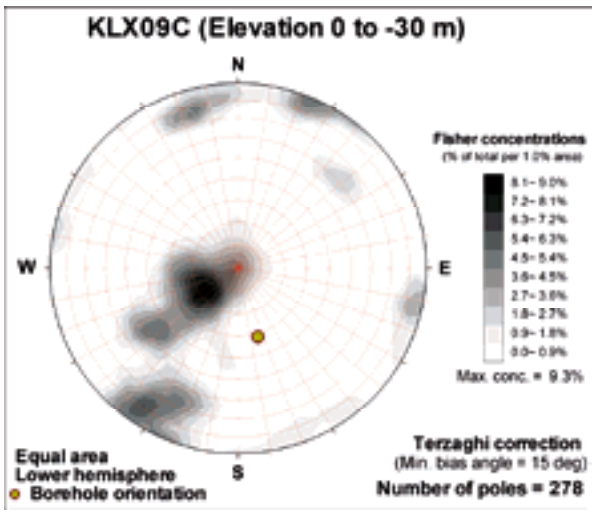
KLX09C (Elevation 0 to -30 m)
N
W
E
S
Fisher concentrations
(% of total per 1.0% area)
8.1–9.0%
7.2–8.1%
6.3–7.2%
5.4–6.3%
4.5–5.4%
3.6–4.5%
2.7–3.6%
1.8–2.7%
0.9–1.8%
0.0–0.9%
Max. conc. = 9.3%
Equal area
Lower hemisphere
Borehole orientation
Terzaghi correction
(Min. bias angle = 15 deg)
Number of poles = 278

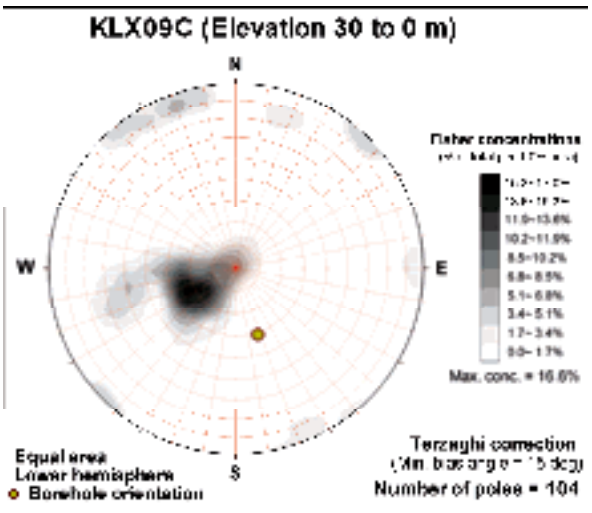
KLX09C (Elevation 30 to 0 m)
N
W
E
S
Max. conc. = 16.6%
Equal area
Lower hemisphere
Borehole orientation
Terzaghi correction
Number of poles = 104

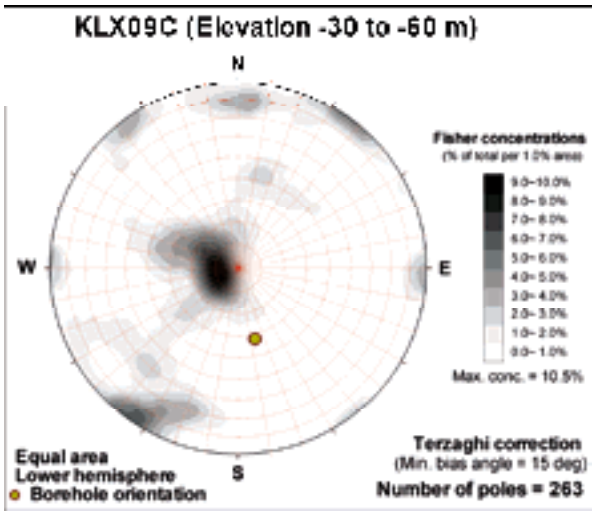
KLX09C (Elevation -30 to -60 m)
N
W
E
S
Fisher concentrations
(% of total per 1.0% area)
9.0–10.0%
8.0–9.0%
7.0–8.0%
6.0–7.0%
5.0–6.0%
4.0–5.0%
3.0–4.0%
2.0–3.0%
1.0–2.0%
0.0–1.0%
Max. conc. = 10.5%
Equal area
Lower hemisphere
Borehole orientation
Terzaghi correction
(Min. bias angle = 15 deg)
Number of poles = 263

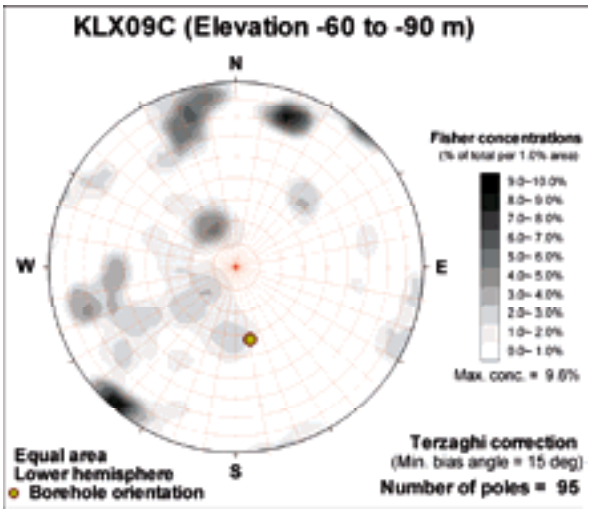
KLX09C (Elevation -60 to -90 m)
N
W
E
S
Fisher concentrations
(% of total per 1.0% area)
9.0–10.0%
8.0–9.0%
7.0–8.0%
6.0–7.0%
5.0–6.0%
4.0–5.0%
3.0–4.0%
2.0–3.0%
1.0–2.0%
0.0–1.0%
Max. conc. = 9.6%
Equal area
Lower hemisphere
Borehole orientation
Terzaghi correction
(Min. bias angle = 15 deg)
Number of poles = 95

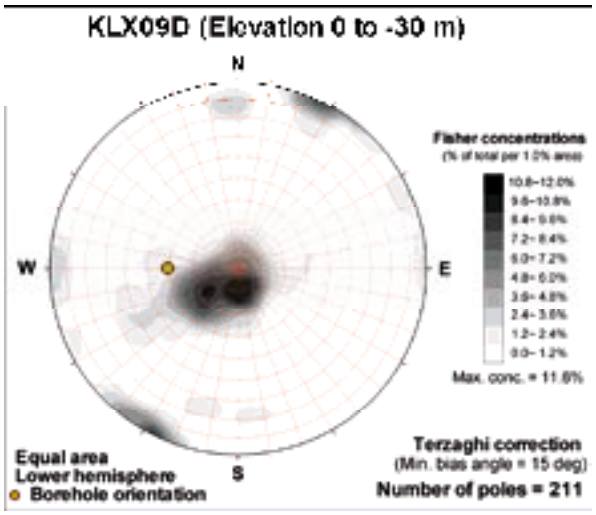
KLX09D (Elevation 0 to -30 m)
N
W
E
S
Fisher concentrations
(% of total per 1.0% area)
10.8–12.0%
9.6–10.8%
8.4–9.6%
7.2–8.4%
6.0–7.2%
4.8–6.0%
3.6–4.8%
2.4–3.6%
1.2–2.4%
0.0–1.2%
Max. conc. = 11.6%
Equal area
Lower hemisphere
Borehole orientation
Terzaghi correction
(Min. bias angle = 15 deg)
Number of poles = 211

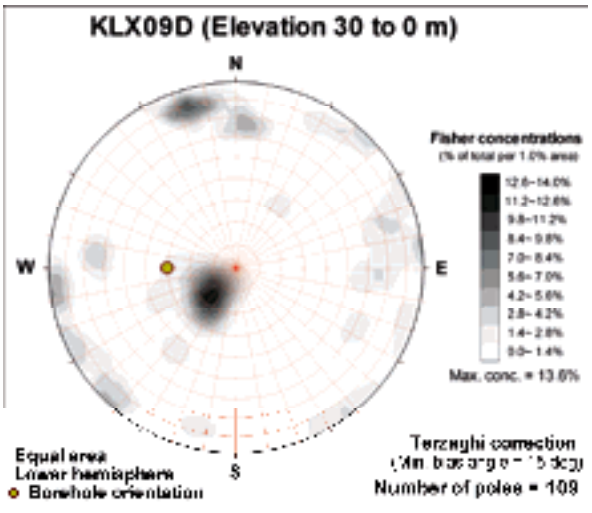
KLX09D (Elevation 30 to 0 m)
N
W
E
S
Fisher concentrations
(% of total per 1.0% area)
12.6–14.0%
11.2–12.6%
9.8–11.2%
8.4–9.8%
7.0–8.4%
5.6–7.0%
4.2–5.6%
2.8–4.2%
1.4–2.8%
0.0–1.4%
Max. conc. = 13.6%
Equal area
Lower hemisphere
Borehole orientation
Terzaghi correction
Number of poles = 109

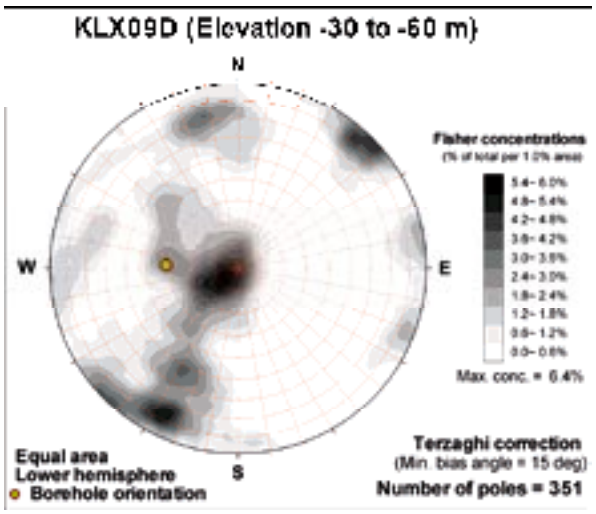
KLX09D (Elevation -30 to -60 m)
N
W
E
S
Fisher concentrations
(% of total per 1.0% area)
5.4- 6.0%
4.8- 5.4%
4.2- 4.8%
3.6- 4.2%
3.0- 3.6%
2.4- 3.0%
1.8- 2.4%
1.2- 1.8%
0.6- 1.2%
0.0- 0.6%
Max. conc. = 6.4%
Equal area
Lower hemisphere
Borehole orientation
Terzaghi correction
(Min. bias angle = 15 deg)
Number of poles = 351

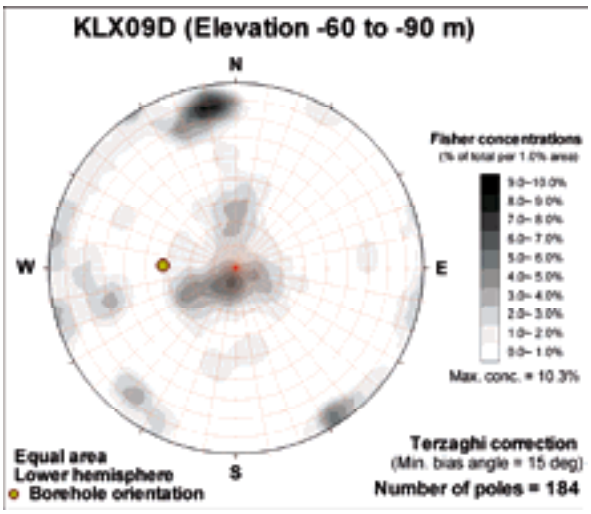
KLX09D (Elevation -60 to -90 m)
N
W
E
S
Fisher concentrations
(% of total per 1.0% area)
9.0-10.0%
8.0- 9.0%
7.0- 8.0%
6.0- 7.0%
5.0- 6.0%
4.0- 5.0%
3.0- 4.0%
2.0- 3.0%
1.0- 2.0%
0.0- 1.0%
Max. conc. = 10.3%
Equal area
Lower hemisphere
Borehole orientation
Terzaghi correction
(Min. bias angle = 15 deg)
Number of poles = 184

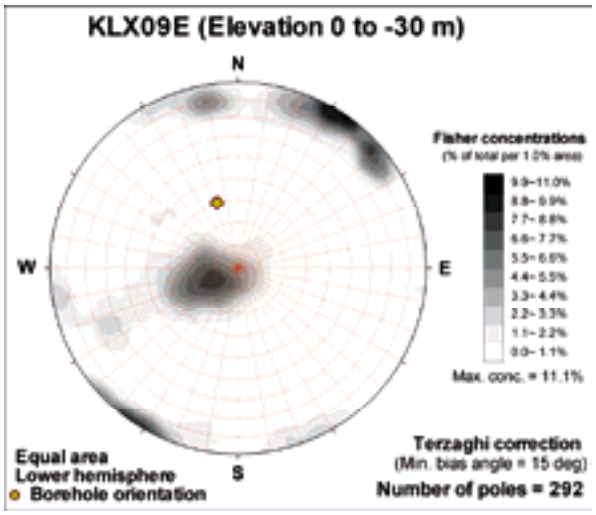
KLX09E (Elevation 0 to -30 m)
N
W
E
S
Fisher concentrations
(% of total per 1.0% area)
9.9-11.0%
8.8- 9.9%
7.7- 8.8%
6.6- 7.7%
5.5- 6.6%
4.4- 5.5%
3.3- 4.4%
2.2- 3.3%
1.1- 2.2%
0.0- 1.1%
Max. conc. = 11.1%
Equal area
Lower hemisphere
Borehole orientation
Terzaghi correction
(Min. bias angle = 15 deg)
Number of poles = 292

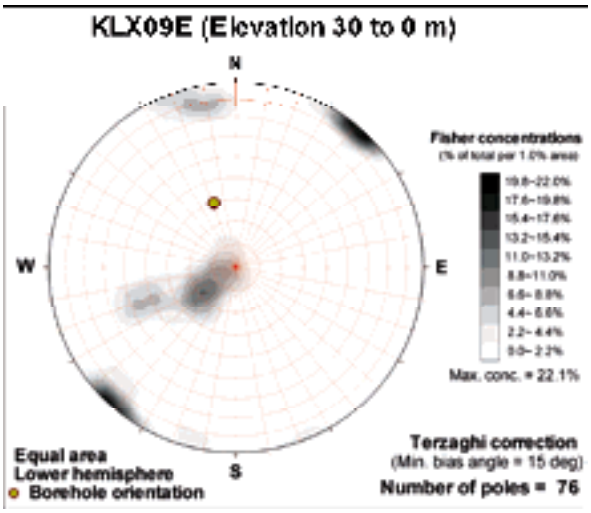
KLX09E (Elevation 30 to 0 m)
N
W
E
S
Fisher concentrations
(% of total per 1.0% area)
19.8-22.0%
17.6-19.8%
15.4-17.6%
13.2-15.4%
11.0-13.2%
8.8-11.0%
6.6- 8.8%
4.4- 6.6%
2.2- 4.4%
0.0- 2.2%
Max. conc. = 22.1%
Equal area
Lower hemisphere
Borehole orientation
Terzaghi correction
(Min. bias angle = 15 deg)
Number of poles = 76

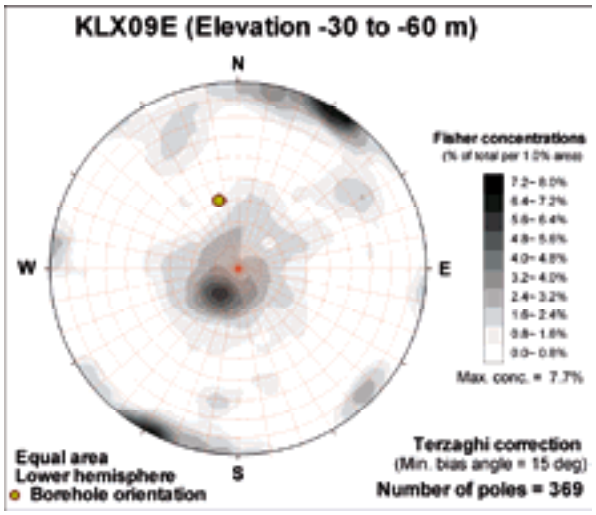
KLX09E (Elevation -30 to -60 m)
N
W
E
S
Fisher concentrations
(% of total per 1.0% area)
7.2- 8.0%
6.4- 7.2%
5.6- 6.4%
4.8- 5.6%
4.0- 4.8%
3.2- 4.0%
2.4- 3.2%
1.6- 2.4%
0.8- 1.6%
0.0- 0.8%
Max. conc. = 7.7%
Equal area
Lower hemisphere
Borehole orientation
Terzaghi correction
(Min. bias angle = 15 deg)
Number of poles = 369

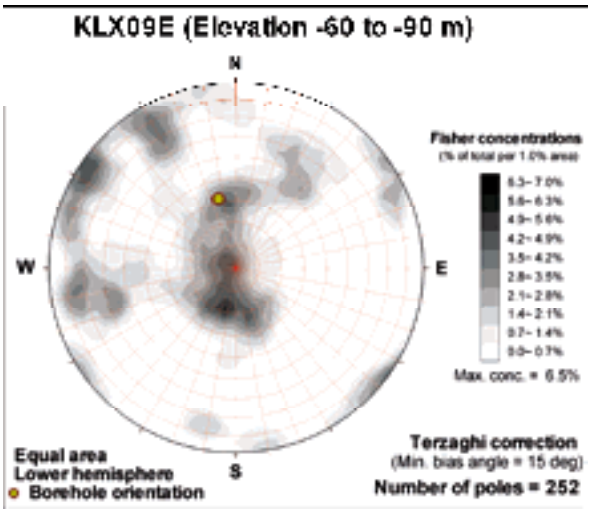
KLX09E (Elevation -60 to -90 m)
N
W
E
S
Fisher concentrations
(% of total per 1.0% area)
6.3- 7.0%
5.6- 6.3%
4.9- 5.6%
4.2- 4.9%
3.5- 4.2%
2.8- 3.5%
2.1- 2.8%
1.4- 2.1%
0.7- 1.4%
0.0- 0.7%
Max. conc. = 6.5%
Equal area
Lower hemisphere
Borehole orientation
Terzaghi correction
(Min. bias angle = 15 deg)
Number of poles = 252

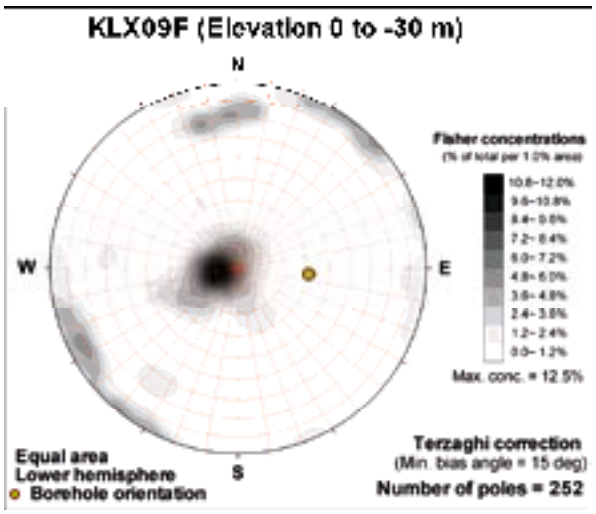
KLX09F (Elevation 0 to -30 m)
N
W
E
S
Fisher concentrations
(% of total per 1.0% area)
Max. conc. = 12.5%
Equal area
Lower hemisphere
Borehole orientation
Terzaghi correction
(Min. bias angle = 15 deg)
Number of poles = 252

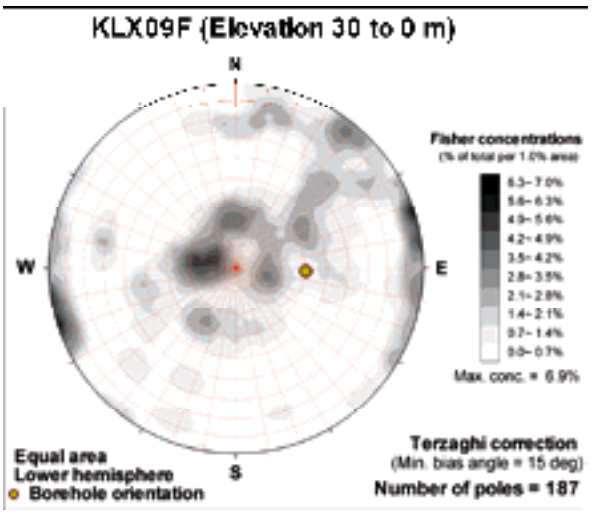
KLX09F (Elevation 30 to 0 m)
N
W
E
S
Fisher concentrations
(% of total per 1.0% area)
Max. conc. = 6.9%
Equal area
Lower hemisphere
Borehole orientation
Terzaghi correction
(Min. bias angle = 15 deg)
Number of poles = 187

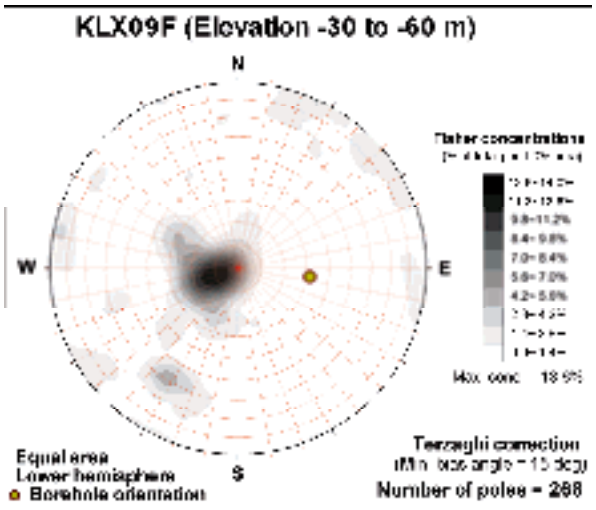
KLX09F (Elevation -30 to -60 m)
N
W
E
S
Fisher concentrations
Equal area
Lower hemisphere
Borehole orientation
Terzaghi correction
(Min. bias angle = 15 deg)
Number of poles = 268

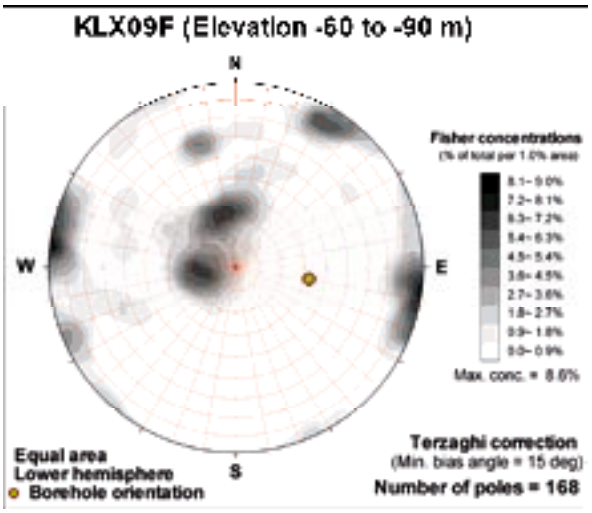
KLX09F (Elevation -60 to -90 m)
N
W
E
S
Fisher concentrations
(% of total per 1.0% area)
Max. conc. = 8.6%
Equal area
Lower hemisphere
Borehole orientation
Terzaghi correction
(Min. bias angle = 15 deg)
Number of poles = 168

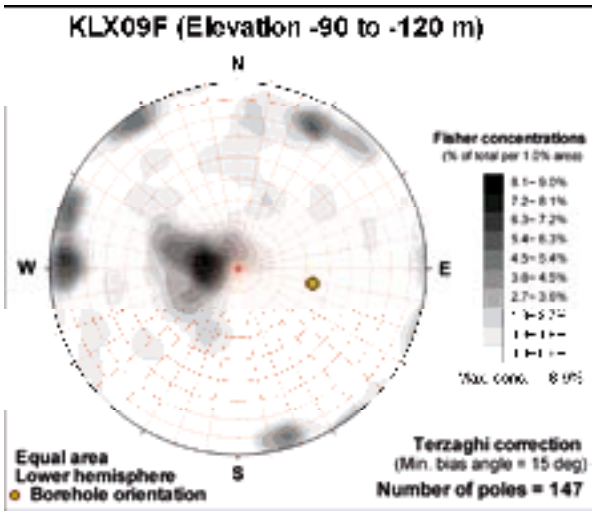
KLX09F (Elevation -90 to -120 m)
N
W
E
S
Fisher concentrations
(% of total per 1.0% area)
Equal area
Lower hemisphere
Borehole orientation
Terzaghi correction
(Min. bias angle = 15 deg)
Number of poles = 147

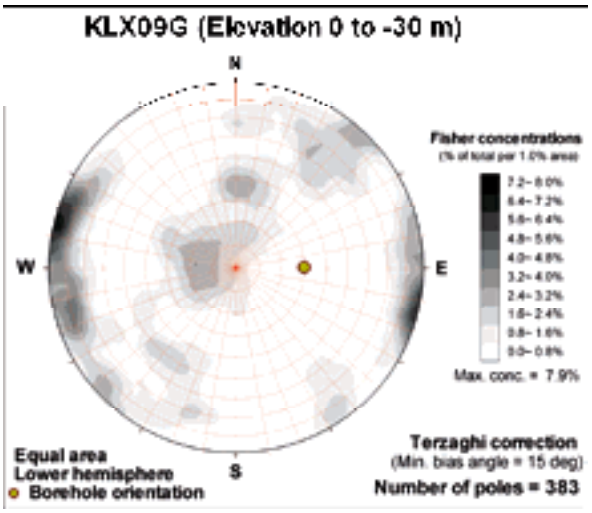
KLX09G (Elevation 0 to -30 m)
N
W
E
S
Fisher concentrations
(% of total per 1.0% area)
Max. conc. = 7.9%
Equal area
Lower hemisphere
Borehole orientation
Terzaghi correction
(Min. bias angle = 15 deg)
Number of poles = 383

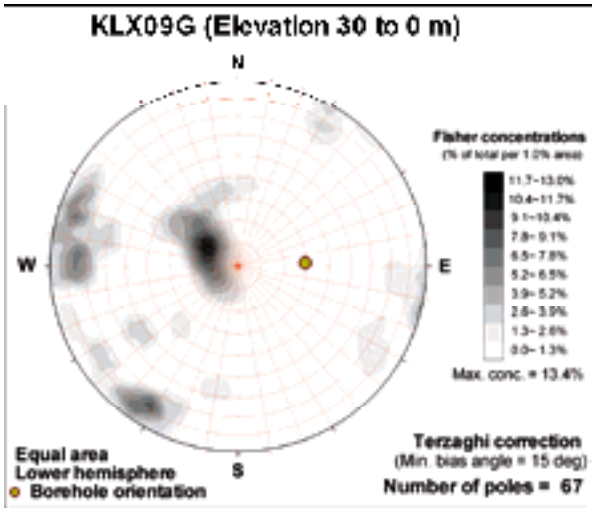
KLX09G (Elevation 30 to 0 m)
N
W
E
S
Fisher concentrations
(% of total per 1.0% area)
11.7–13.0%
10.4–11.7%
9.1–10.4%
7.8–9.1%
6.5–7.8%
5.2–6.5%
3.9–5.2%
2.6–3.9%
1.3–2.6%
0.0–1.3%
Max. conc. = 13.4%
Equal area
Lower hemisphere
Borehole orientation
Terzaghi correction
(Min. bias angle = 15 deg)
Number of poles = 67

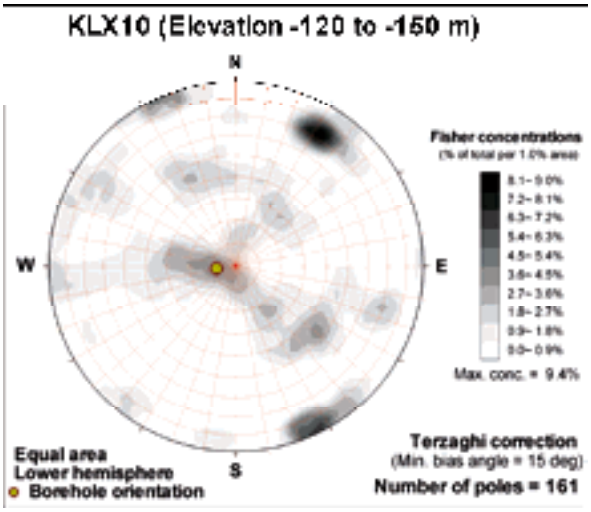
KLX10 (Elevation -120 to -150 m)
N
W
E
S
Fisher concentrations
(% of total per 1.0% area)
8.1–9.0%
7.2–8.1%
6.3–7.2%
5.4–6.3%
4.5–5.4%
3.6–4.5%
2.7–3.6%
1.8–2.7%
0.9–1.8%
0.0–0.9%
Max. conc. = 9.4%
Equal area
Lower hemisphere
Borehole orientation
Terzaghi correction
(Min. bias angle = 15 deg)
Number of poles = 161

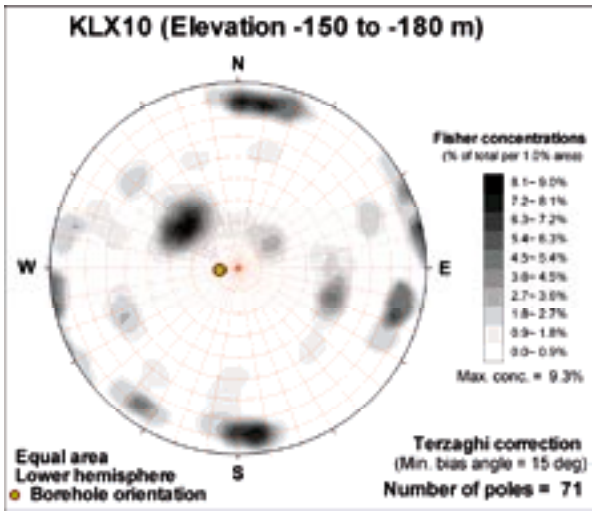
KLX10 (Elevation -150 to -180 m)
N
W
E
S
Fisher concentrations
(% of total per 1.0% area)
8.1–9.0%
7.2–8.1%
6.3–7.2%
5.4–6.3%
4.5–5.4%
3.6–4.5%
2.7–3.6%
1.8–2.7%
0.9–1.8%
0.0–0.9%
Max. conc. = 9.3%
Equal area
Lower hemisphere
Borehole orientation
Terzaghi correction
(Min. bias angle = 15 deg)
Number of poles = 71

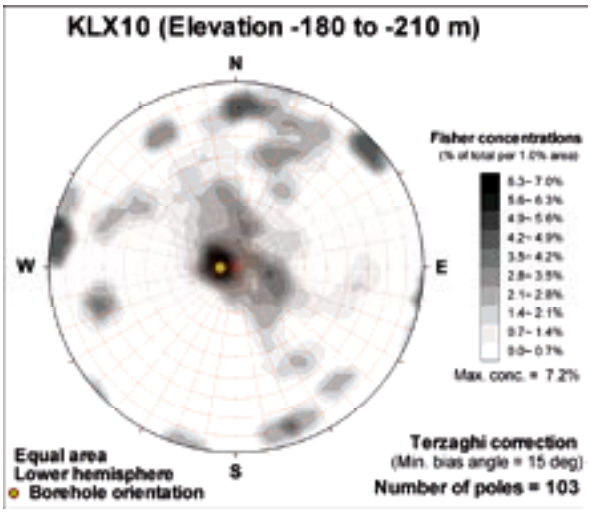
KLX10 (Elevation -180 to -210 m)
N
W
E
S
Fisher concentrations
(% of total per 1.0% area)
6.3–7.0%
5.6–6.3%
4.9–5.6%
4.2–4.9%
3.5–4.2%
2.8–3.5%
2.1–2.8%
1.4–2.1%
0.7–1.4%
0.0–0.7%
Max. conc. = 7.2%
Equal area
Lower hemisphere
Borehole orientation
Terzaghi correction
(Min. bias angle = 15 deg)
Number of poles = 103

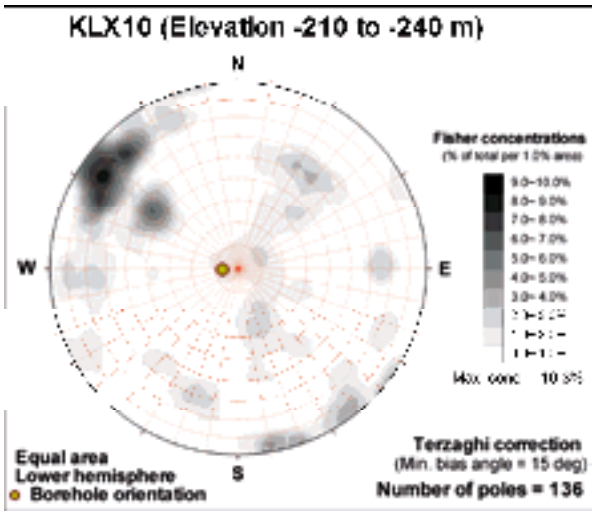
KLX10 (Elevation -210 to -240 m)
N
W
E
S
Fisher concentrations
(% of total per 1.0% area)
9.0–10.0%
8.0–9.0%
7.0–8.0%
6.0–7.0%
5.0–6.0%
4.0–5.0%
3.0–4.0%
Equal area
Lower hemisphere
Borehole orientation
Terzaghi correction
(Min. bias angle = 15 deg)
Number of poles = 136

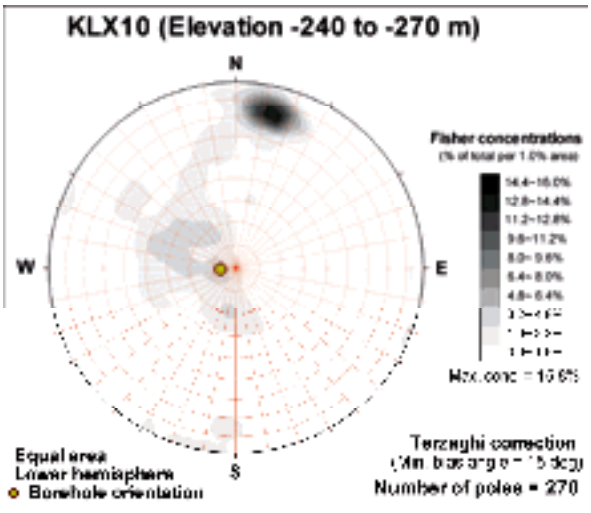
KLX10 (Elevation -240 to -270 m)
N
W
E
S
Fisher concentrations
(% of total per 1.0% area)
12.8–14.4%
11.2–12.8%
9.6–11.2%
8.0–9.6%
6.4–8.0%
4.8–6.4%
Equal area
Lower hemisphere
Borehole orientation
Terzaghi correction
Number of poles = 270

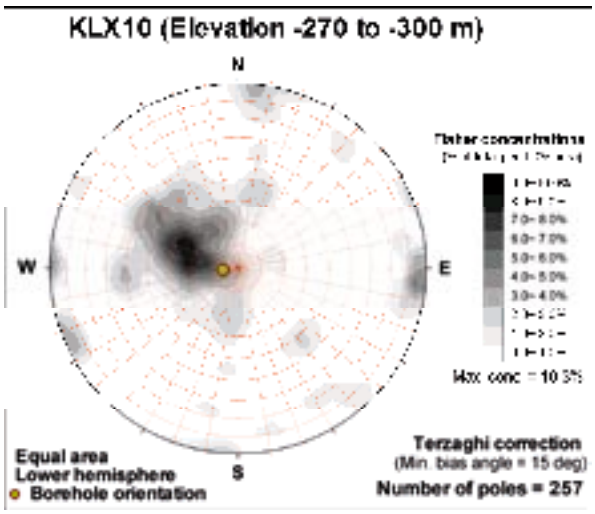
KLX10 (Elevation -270 to -300 m)
N
W
E
S
Fisher concentrations
Max. conc. = 10.3%
Equal area
Lower hemisphere
Borehole orientation
Terzaghi correction
(Min. bias angle = 15 deg)
Number of poles = 257

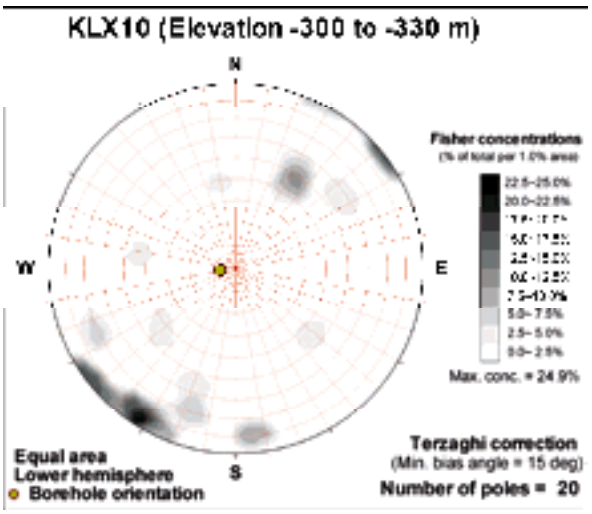
KLX10 (Elevation -300 to -330 m)
N
W
E
S
Fisher concentrations
Max. conc. = 24.9%
Equal area
Lower hemisphere
Borehole orientation
Terzaghi correction
(Min. bias angle = 15 deg)
Number of poles = 20

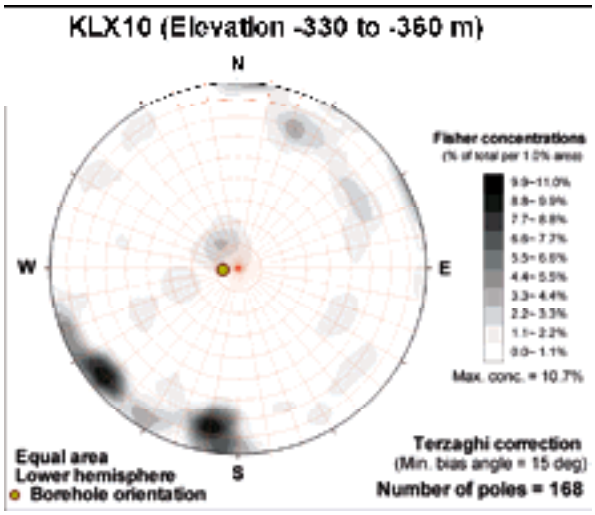
KLX10 (Elevation -330 to -360 m)
N
W
E
S
Fisher concentrations
Max. conc. = 10.7%
Equal area
Lower hemisphere
Borehole orientation
Terzaghi correction
(Min. bias angle = 15 deg)
Number of poles = 168

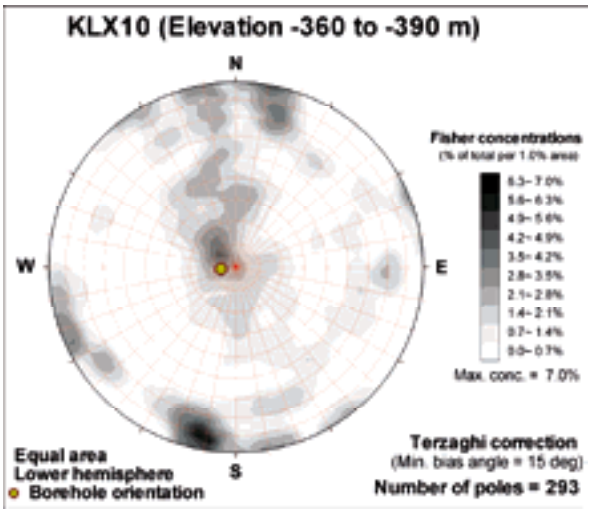
KLX10 (Elevation -360 to -390 m)
N
W
E
S
Fisher concentrations
Max. conc. = 7.0%
Equal area
Lower hemisphere
Borehole orientation
Terzaghi correction
(Min. bias angle = 15 deg)
Number of poles = 293

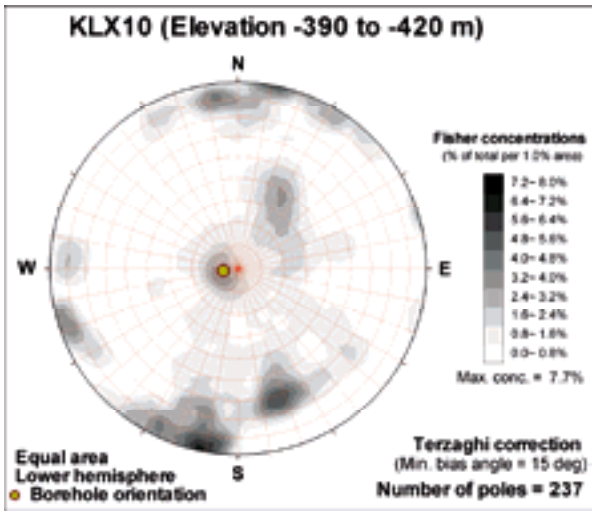
KLX10 (Elevation -390 to -420 m)
N
W
E
S
Fisher concentrations
Max. conc. = 7.7%
Equal area
Lower hemisphere
Borehole orientation
Terzaghi correction
(Min. bias angle = 15 deg)
Number of poles = 237

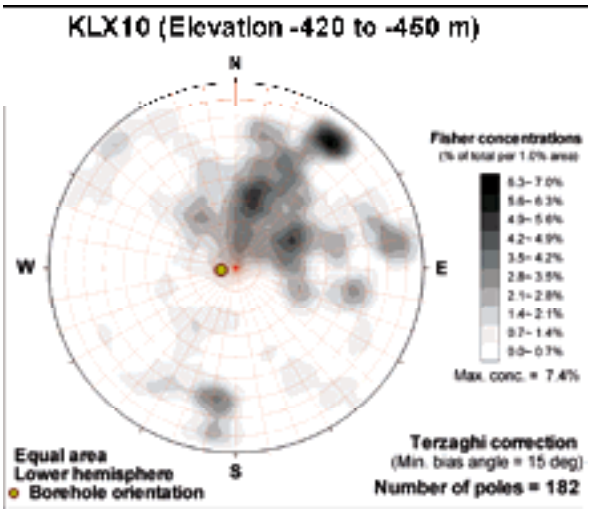
KLX10 (Elevation -420 to -450 m)
N
W
E
S
Fisher concentrations
Max. conc. = 7.4%
Equal area
Lower hemisphere
Borehole orientation
Terzaghi correction
(Min. bias angle = 15 deg)
Number of poles = 182

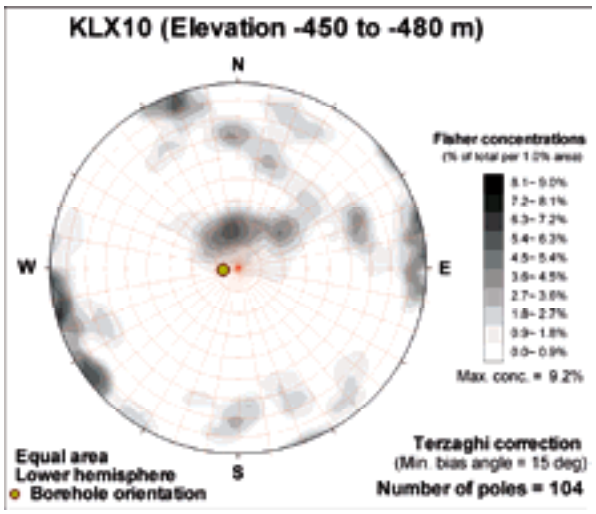
KLX10 (Elevation -450 to -480 m)
N
W
E
S
Fisher concentrations
(% of total per 1.0% area)
Max. conc. = 9.2%
Equal area
Lower hemisphere
Borehole orientation
Terzaghi correction
(Min. bias angle = 15 deg)
Number of poles = 104

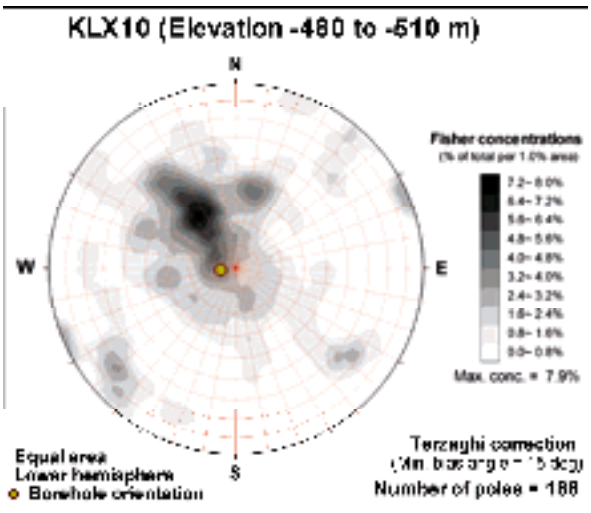
KLX10 (Elevation -480 to -510 m)
N
W
E
S
Fisher concentrations
(% of total per 1.0% area)
Max. conc. = 7.9%
Equal area
Lower hemisphere
Borehole orientation
Number of poles = 188

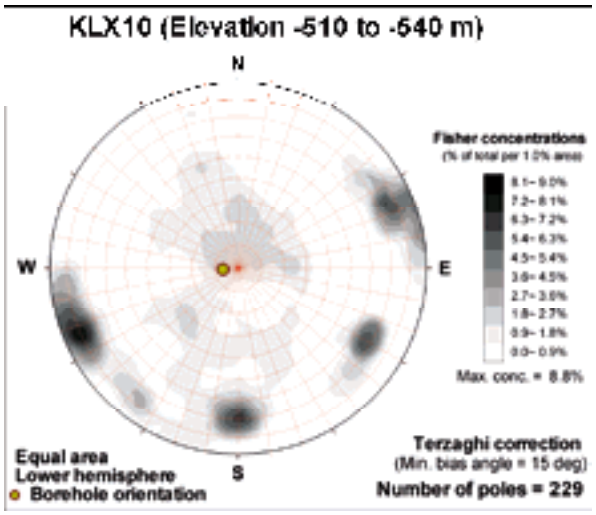
KLX10 (Elevation -510 to -540 m)
N
W
E
S
Fisher concentrations
(% of total per 1.0% area)
Max. conc. = 8.8%
Equal area
Lower hemisphere
Borehole orientation
Terzaghi correction
(Min. bias angle = 15 deg)
Number of poles = 229

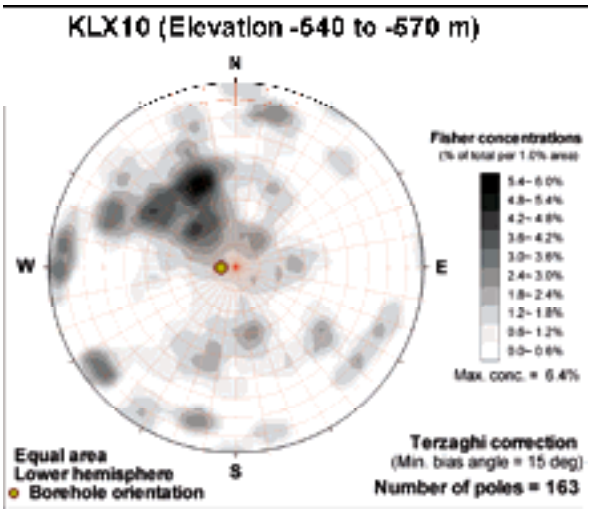
KLX10 (Elevation -540 to -570 m)
N
W
E
S
Fisher concentrations
(% of total per 1.0% area)
Max. conc. = 6.4%
Equal area
Lower hemisphere
Borehole orientation
Terzaghi correction
(Min. bias angle = 15 deg)
Number of poles = 163

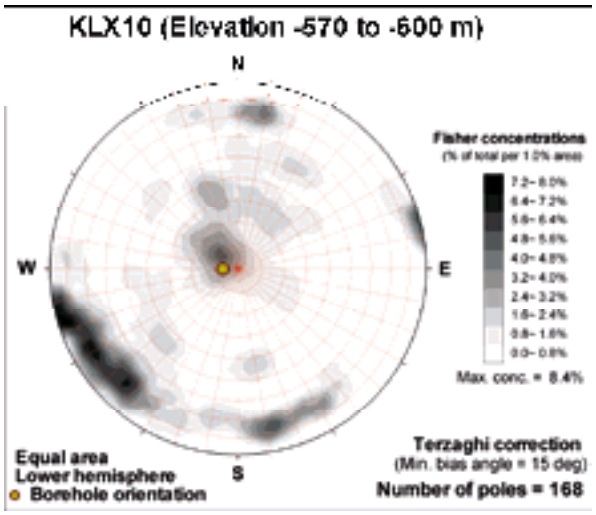
KLX10 (Elevation -570 to -600 m)
N
W
E
S
Fisher concentrations
(% of total per 1.0% area)
Max. conc. = 8.4%
Equal area
Lower hemisphere
Borehole orientation
Terzaghi correction
(Min. bias angle = 15 deg)
Number of poles = 168

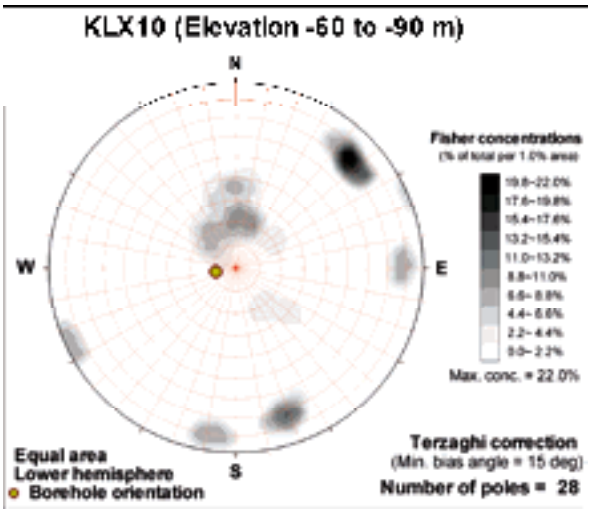
KLX10 (Elevation -60 to -90 m)
N
W
E
S
Fisher concentrations
(% of total per 1.0% area)
Max. conc. = 22.0%
Equal area
Lower hemisphere
Borehole orientation
Terzaghi correction
(Min. bias angle = 15 deg)
Number of poles = 28

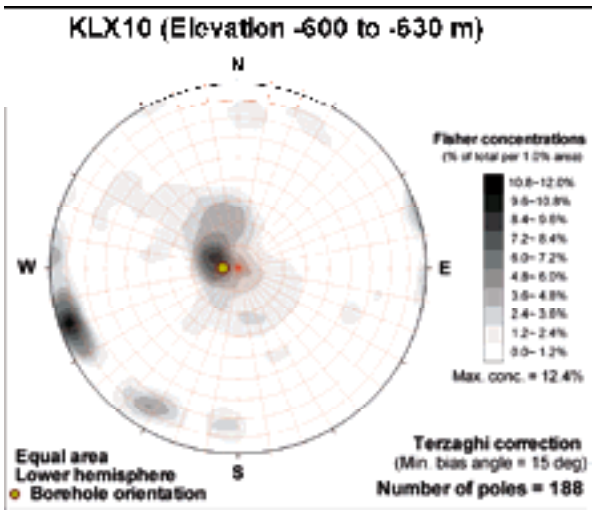
KLX10 (Elevation -600 to -630 m)
N
W
E
S
Fisher concentrations
(% of total per 1.0% area)
Max. conc. = 12.4%
Equal area
Lower hemisphere
Borehole orientation
Terzaghi correction
(Min. bias angle = 15 deg)
Number of poles = 188

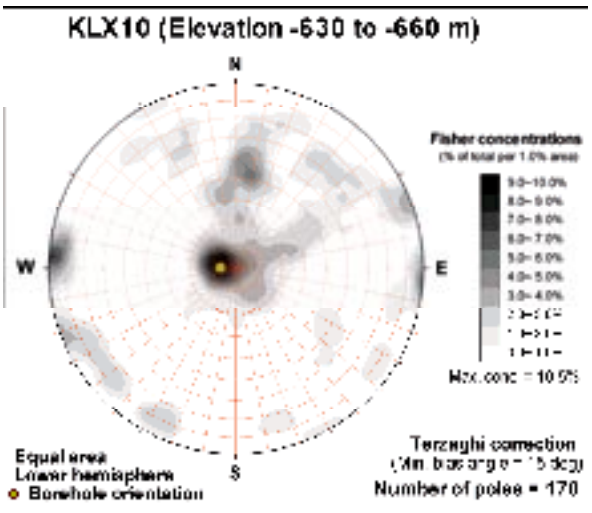
KLX10 (Elevation -630 to -660 m)
N
W
E
S
Fisher concentrations
(% of total per 1.0% area)
Equal area
Lower hemisphere
Borehole orientation
Terzaghi correction
Number of poles = 170

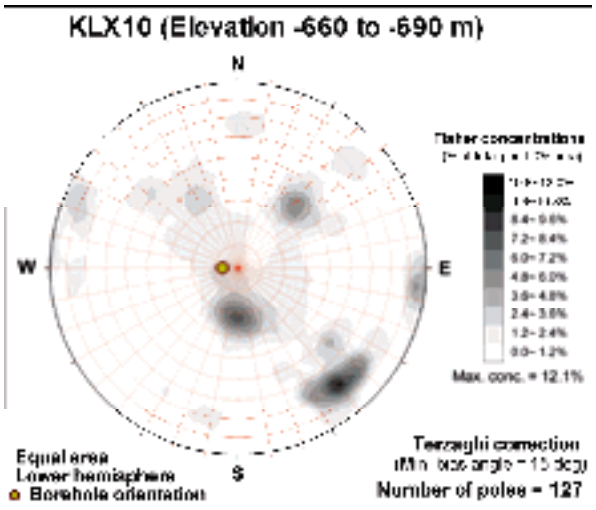
KLX10 (Elevation -660 to -690 m)
N
W
E
S
Max. conc. = 12.1%
Equal area
Lower hemisphere
Borehole orientation
Terzaghi correction
(Min. bias angle = 15 deg)
Number of poles = 127

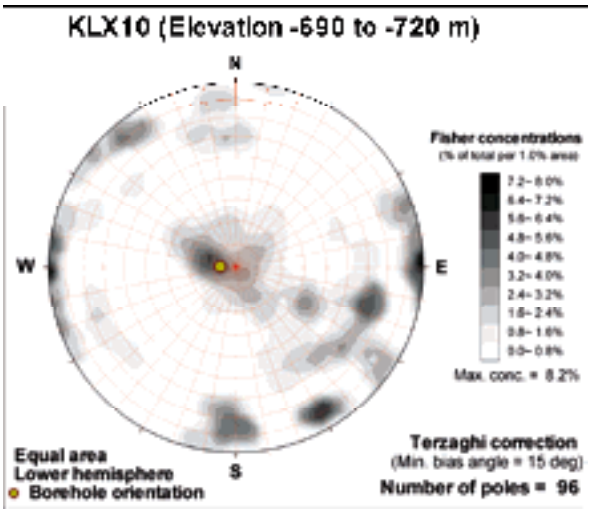
KLX10 (Elevation -690 to -720 m)
N
W
E
S
Fisher concentrations
(% of total per 1.0% area)
Max. conc. = 8.2%
Equal area
Lower hemisphere
Borehole orientation
Terzaghi correction
(Min. bias angle = 15 deg)
Number of poles = 96

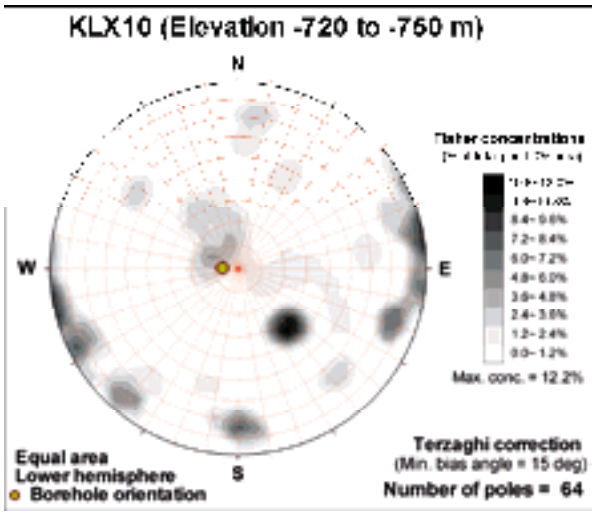
KLX10 (Elevation -720 to -760 m)
N
W
E
S
Max. conc. = 12.2%
Equal area
Lower hemisphere
Borehole orientation
Terzaghi correction
(Min. bias angle = 15 deg)
Number of poles = 64

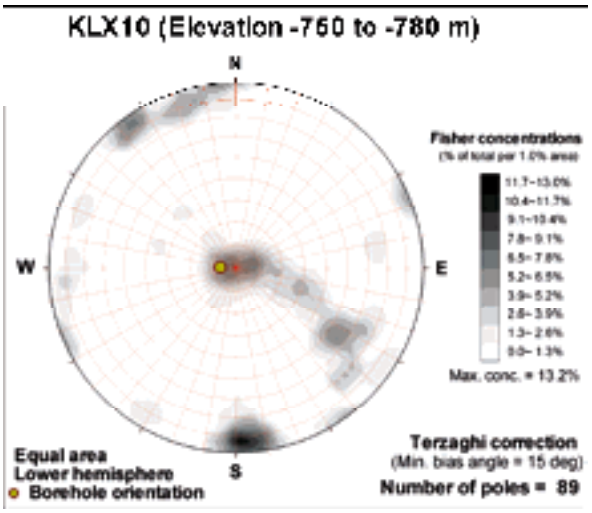
KLX10 (Elevation -760 to -780 m)
N
W
E
S
Fisher concentrations
(% of total per 1.0% area)
Max. conc. = 13.2%
Equal area
Lower hemisphere
Borehole orientation
Terzaghi correction
(Min. bias angle = 15 deg)
Number of poles = 89

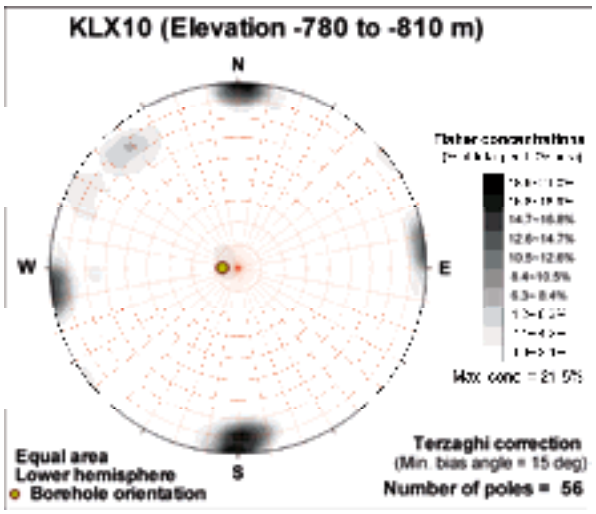
KLX10 (Elevation -780 to -810 m)
N
W
E
S
Fisher concentrations
Max. conc. = 21.5%
Equal area
Lower hemisphere
Borehole orientation
Terzaghi correction
(Min. bias angle = 15 deg)
Number of poles = 56

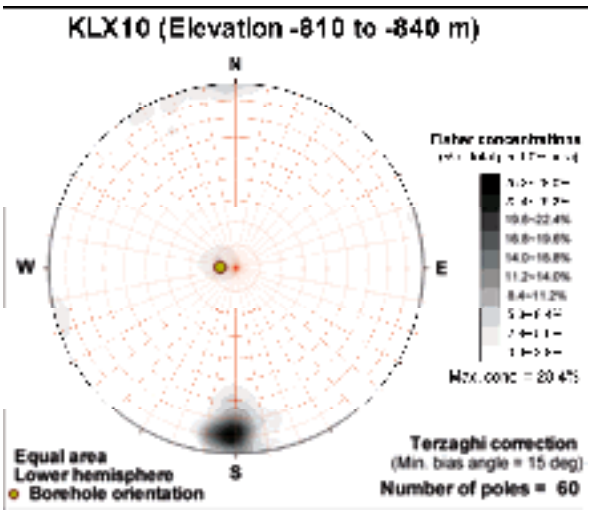
KLX10 (Elevation -810 to -840 m)
N
W
E
S
Fisher concentrations
Max. conc. = 20.4%
Equal area
Lower hemisphere
Borehole orientation
Terzaghi correction
(Min. bias angle = 15 deg)
Number of poles = 60

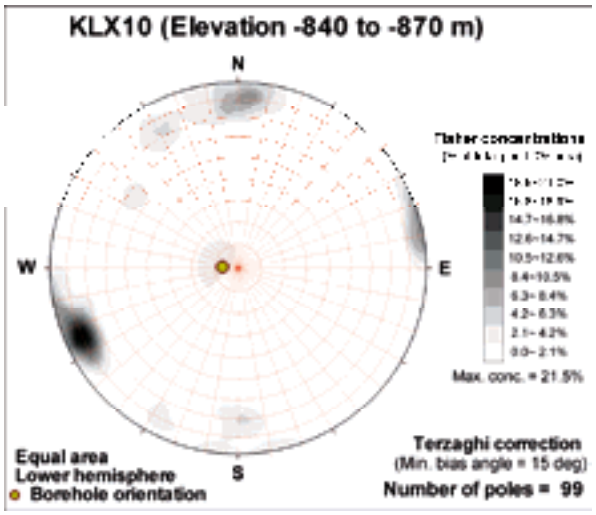
KLX10 (Elevation -840 to -870 m)
N
W
E
S
Fisher concentrations
Max. conc. = 21.5%
Equal area
Lower hemisphere
Borehole orientation
Terzaghi correction
(Min. bias angle = 15 deg)
Number of poles = 99

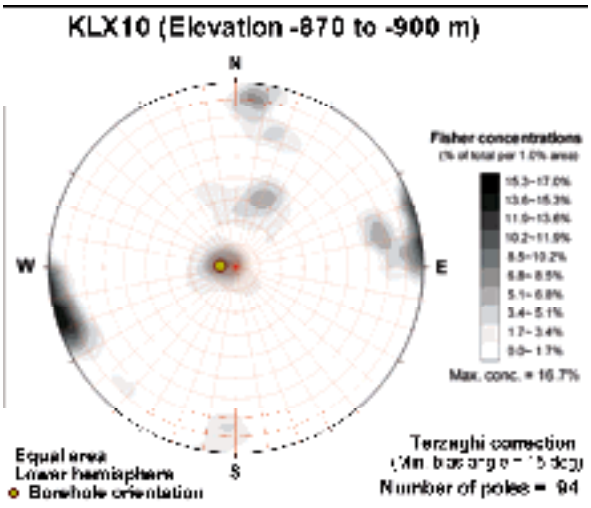
KLX10 (Elevation -870 to -900 m)
N
W
E
S
Fisher concentrations
Max. conc. = 16.7%
Equal area
Lower hemisphere
Borehole orientation
Terzaghi correction
Number of poles = 94

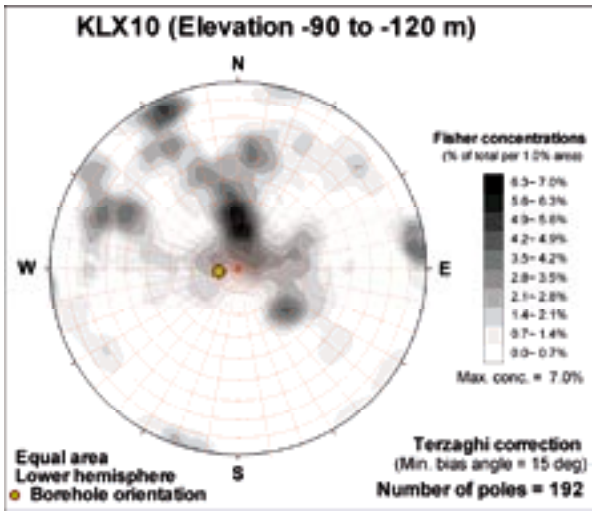
KLX10 (Elevation -90 to -120 m)
N
W
E
S
Fisher concentrations
Max. conc. = 7.0%
Equal area
Lower hemisphere
Borehole orientation
Terzaghi correction
(Min. bias angle = 15 deg)
Number of poles = 192

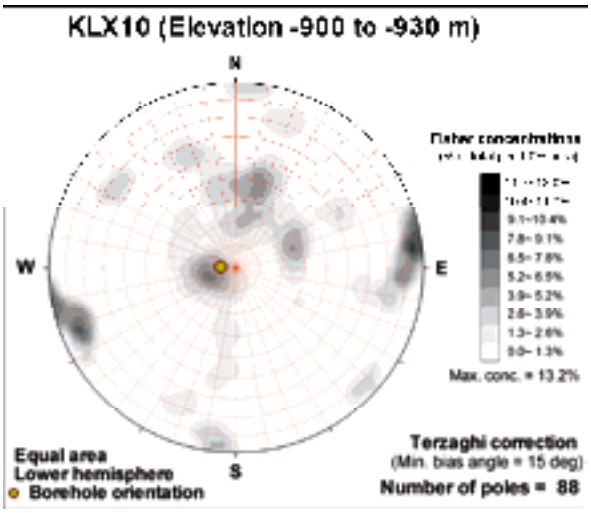
KLX10 (Elevation -900 to -930 m)
N
W
E
S
Fisher concentrations
Max. conc. = 13.2%
Equal area
Lower hemisphere
Borehole orientation
Terzaghi correction
(Min. bias angle = 15 deg)
Number of poles = 88

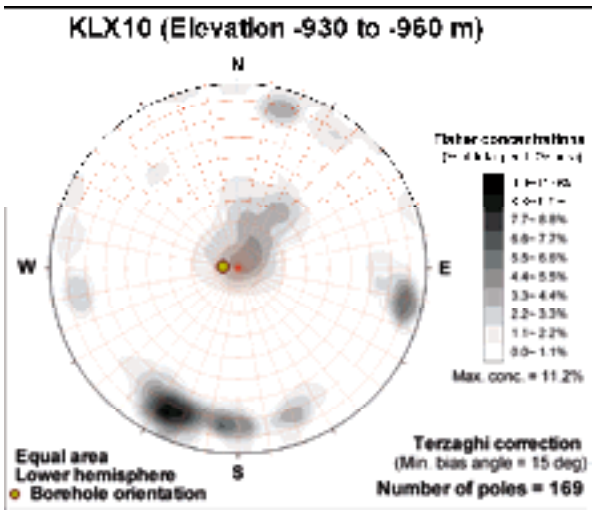
KLX10 (Elevation -930 to -960 m)
N
W
E
S
Fisher concentrations
Max. conc. = 11.2%
Equal area
Lower hemisphere
Borehole orientation
Terzaghi correction
(Min. bias angle = 15 deg)
Number of poles = 169

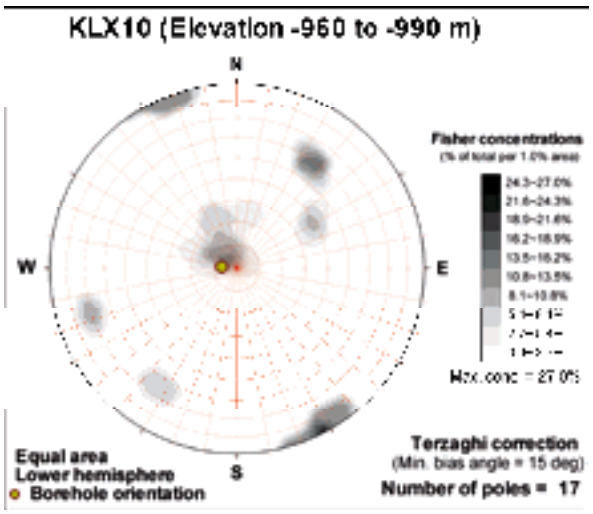
KLX10 (Elevation -960 to -990 m)
N
W
E
S
Fisher concentrations
Equal area
Lower hemisphere
Borehole orientation
Terzaghi correction
(Min. bias angle = 15 deg)
Number of poles = 17

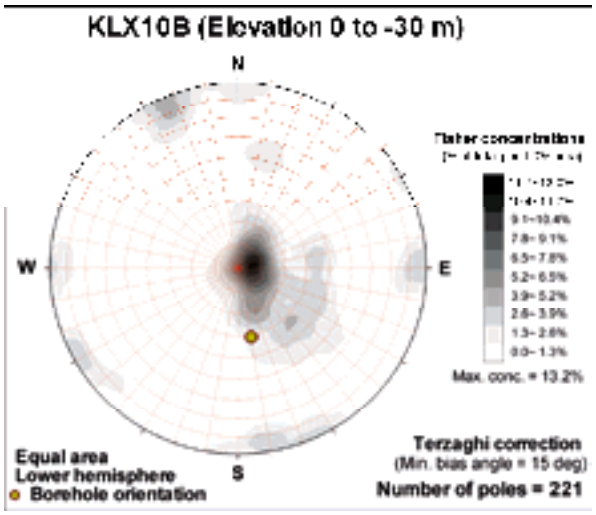
KLX10B (Elevation 0 to -30 m)
N
W
E
S
Fisher concentrations
Max. conc. = 13.2%
Equal area
Lower hemisphere
Borehole orientation
Terzaghi correction
(Min. bias angle = 15 deg)
Number of poles = 221

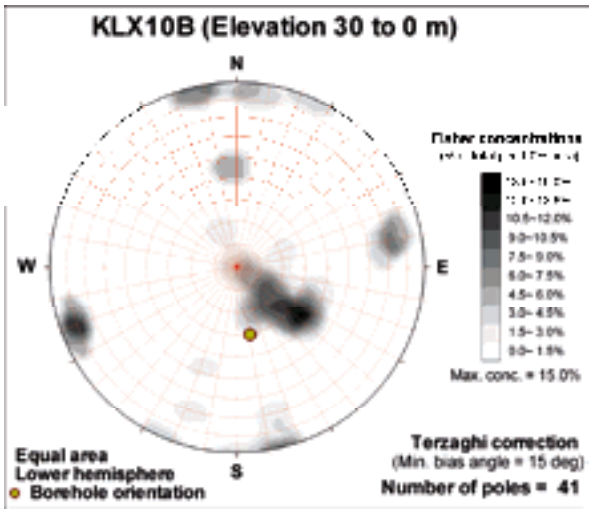
KLX10B (Elevation 30 to 0 m)
N
W
E
S
Fisher concentrations
Max. conc. = 15.0%
Equal area
Lower hemisphere
Borehole orientation
Terzaghi correction
(Min. bias angle = 15 deg)
Number of poles = 41

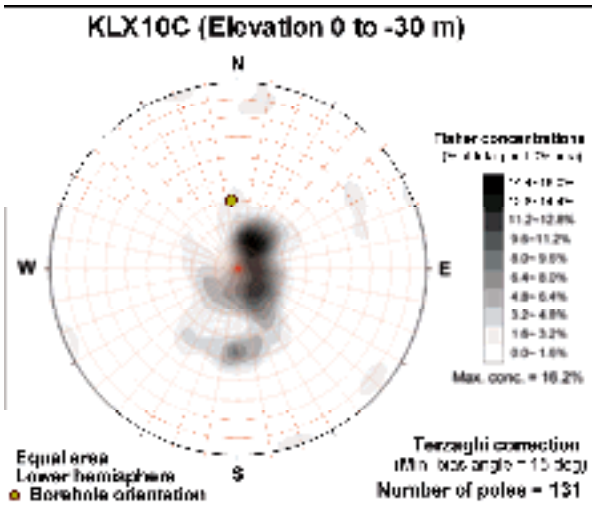
KLX10C (Elevation 0 to -30 m)
N
W
E
S
Fisher concentrations
Max. conc. = 16.2%
Equal area
Lower hemisphere
Borehole orientation
Terzaghi correction
(Min. bias angle = 15 deg)
Number of poles = 131

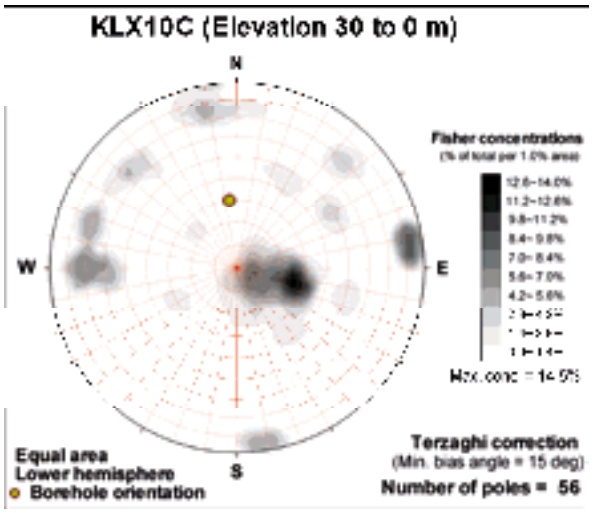
KLX10C (Elevation 30 to 0 m)
N
W
E
S
Fisher concentrations
Equal area
Lower hemisphere
Borehole orientation
Terzaghi correction
(Min. bias angle = 15 deg)
Number of poles = 56

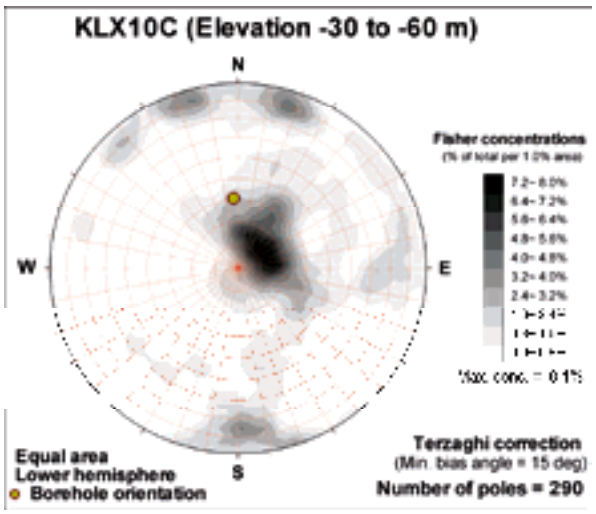
KLX10C (Elevation -30 to -60 m)
N
W
E
S
Fisher concentrations
Equal area
Lower hemisphere
Borehole orientation
Terzaghi correction
(Min. bias angle = 15 deg)
Number of poles = 290

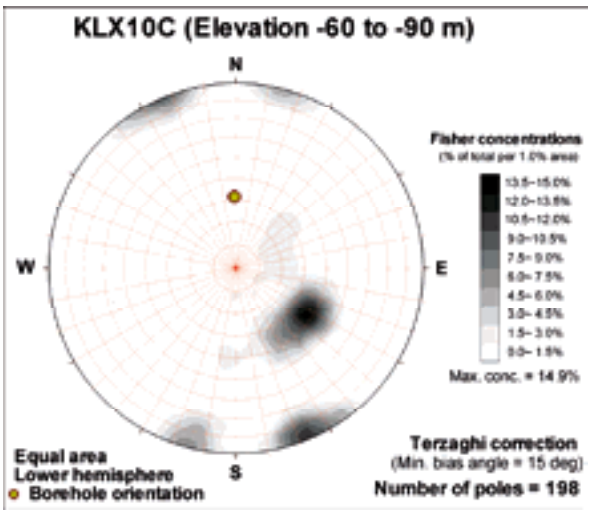
KLX10C (Elevation -60 to -90 m)
N
W
E
S
Fisher concentrations
Max. conc. = 14.9%
Equal area
Lower hemisphere
Borehole orientation
Terzaghi correction
(Min. bias angle = 15 deg)
Number of poles = 198

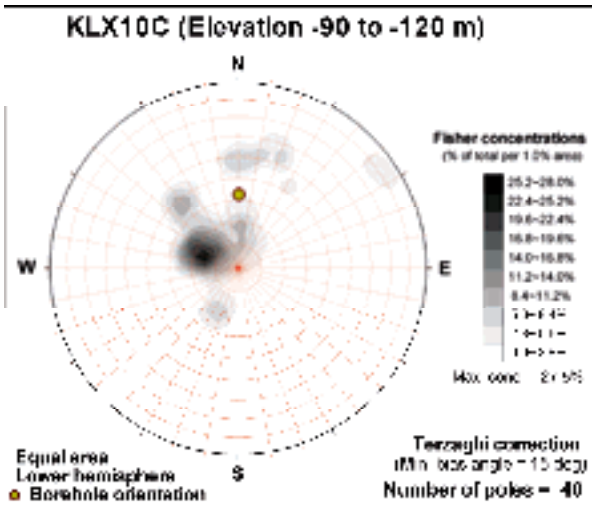
KLX10C (Elevation -90 to -120 m)
N
W
E
S
Fisher concentrations
Equal area
Lower hemisphere
Borehole orientation
Terzaghi correction
(Min. bias angle = 15 deg)
Number of poles = 40

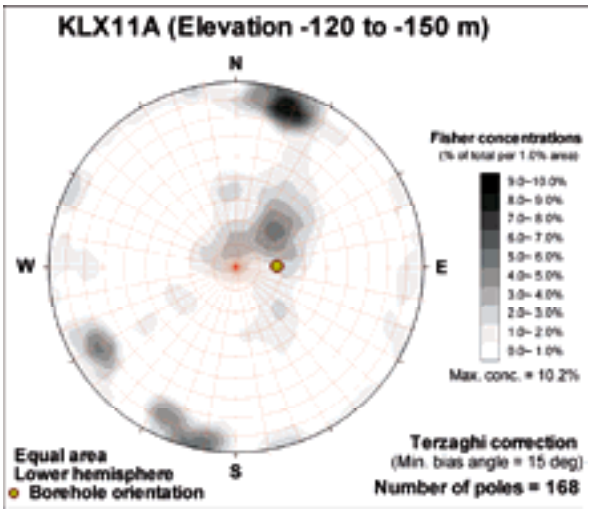
KLX11A (Elevation -120 to -150 m)
N
W
E
S
Fisher concentrations
Max. conc. = 10.2%
Equal area
Lower hemisphere
Borehole orientation
Terzaghi correction
(Min. bias angle = 15 deg)
Number of poles = 168

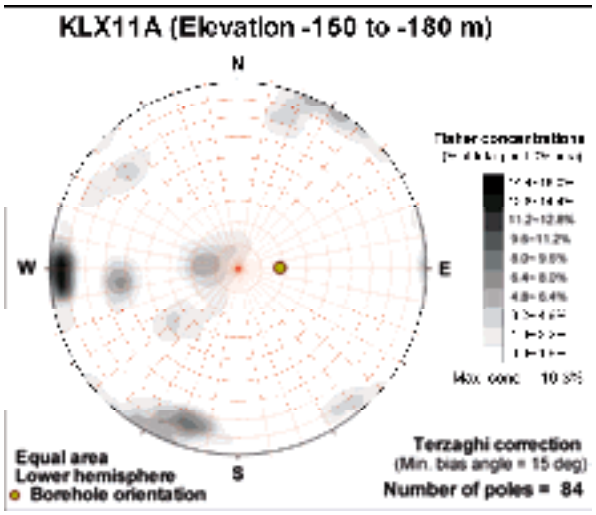
KLX11A (Elevation -150 to -180 m)
N
W
E
S
Fisher concentrations
Equal area
Lower hemisphere
Borehole orientation
Terzaghi correction
(Min. bias angle = 15 deg)
Number of poles = 84

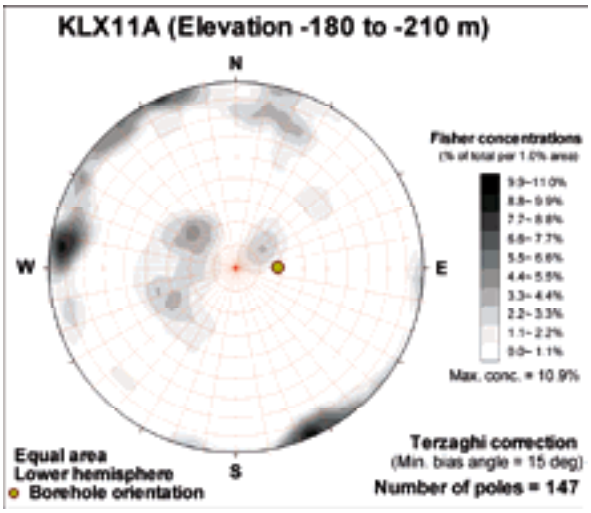
KLX11A (Elevation -180 to -210 m)
N
W
E
S
Fisher concentrations
Max. conc. = 10.9%
Equal area
Lower hemisphere
Borehole orientation
Terzaghi correction
(Min. bias angle = 15 deg)
Number of poles = 147

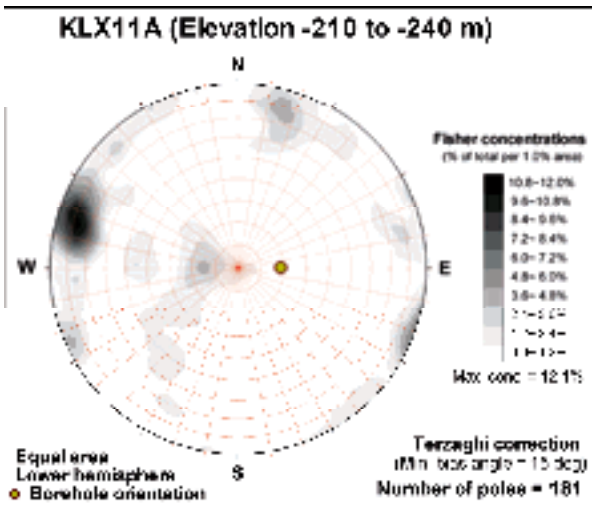
KLX11A (Elevation -210 to -240 m)
N
W
E
S
Fisher concentrations
(% of total per 1.0% area)
Max. conc. = 12.1%
Equal area
Lower hemisphere
Borehole orientation
Terzaghi correction
(Min. bias angle = 15 deg)
Number of poles = 181

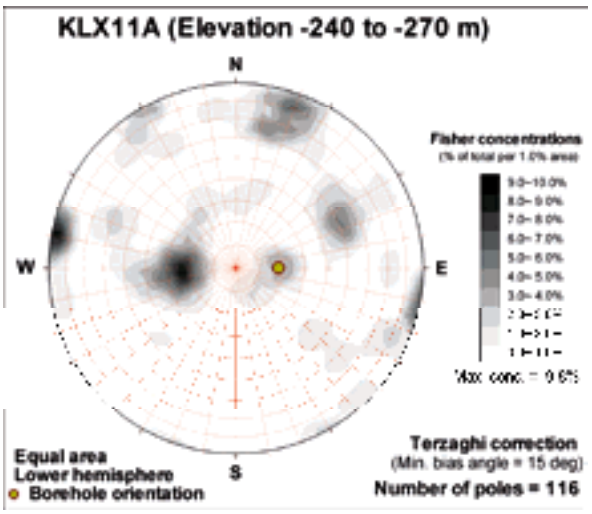
KLX11A (Elevation -240 to -270 m)
N
W
E
S
Fisher concentrations
(% of total per 1.0% area)
Equal area
Lower hemisphere
Borehole orientation
Terzaghi correction
(Min. bias angle = 15 deg)
Number of poles = 116

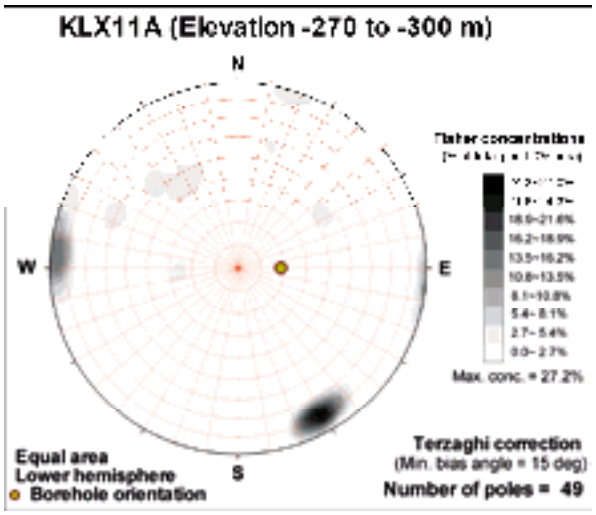
KLX11A (Elevation -270 to -300 m)
N
W
E
S
Max. conc. = 27.2%
Equal area
Lower hemisphere
Borehole orientation
Terzaghi correction
(Min. bias angle = 15 deg)
Number of poles = 49

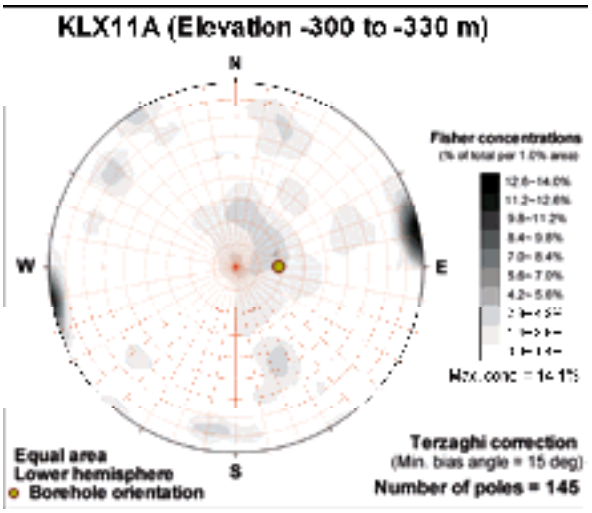
KLX11A (Elevation -300 to -330 m)
N
W
E
S
Fisher concentrations
(% of total per 1.0% area)
Equal area
Lower hemisphere
Borehole orientation
Terzaghi correction
(Min. bias angle = 15 deg)
Number of poles = 145

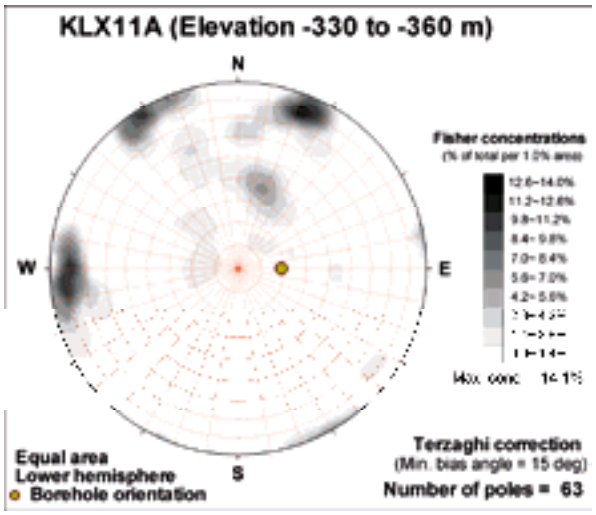
KLX11A (Elevation -330 to -360 m)
N
W
E
S
Fisher concentrations
(% of total per 1.0% area)
Equal area
Lower hemisphere
Borehole orientation
Terzaghi correction
(Min. bias angle = 15 deg)
Number of poles = 63

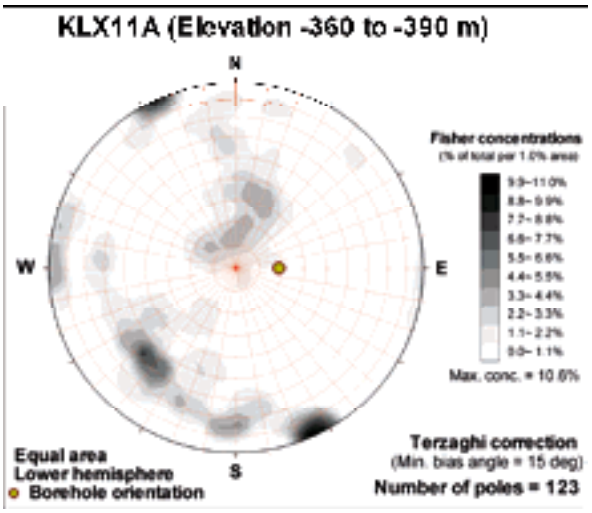
KLX11A (Elevation -360 to -390 m)
N
W
E
S
Fisher concentrations
(% of total per 1.0% area)
Max. conc. = 10.6%
Equal area
Lower hemisphere
Borehole orientation
Terzaghi correction
(Min. bias angle = 15 deg)
Number of poles = 123

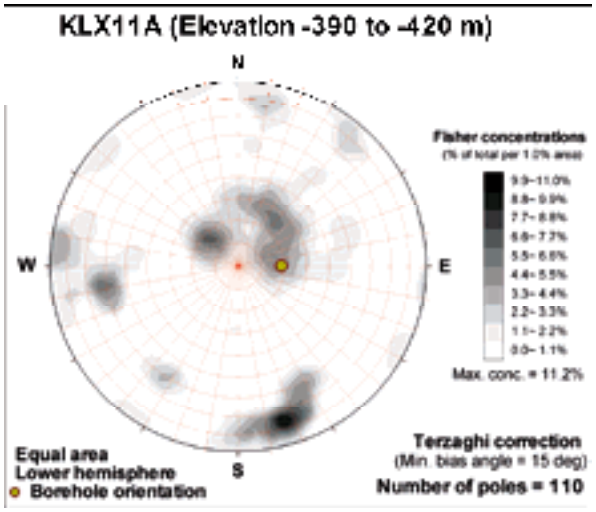
KLX11A (Elevation -390 to -420 m)
N
W
E
S
Fisher concentrations
Max. conc. = 11.2%
Equal area
Lower hemisphere
Borehole orientation
Terzaghi correction
(Min. bias angle = 15 deg)
Number of poles = 110

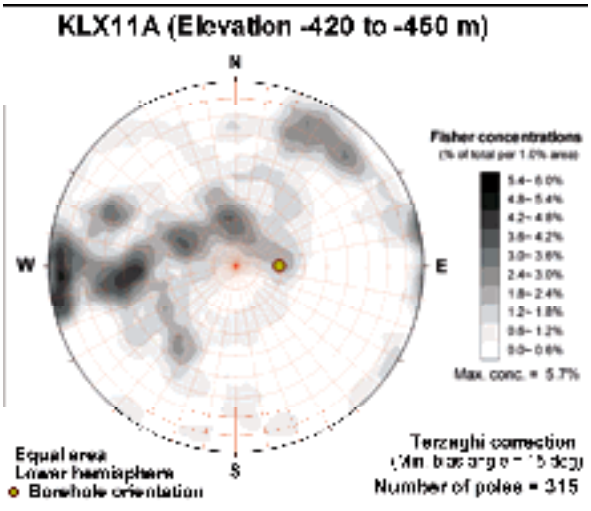
KLX11A (Elevation -420 to -460 m)
N
W
E
S
Fisher concentrations
Max. conc. = 5.7%
Equal area
Lower hemisphere
Borehole orientation
Terzaghi correction
Number of poles = 315

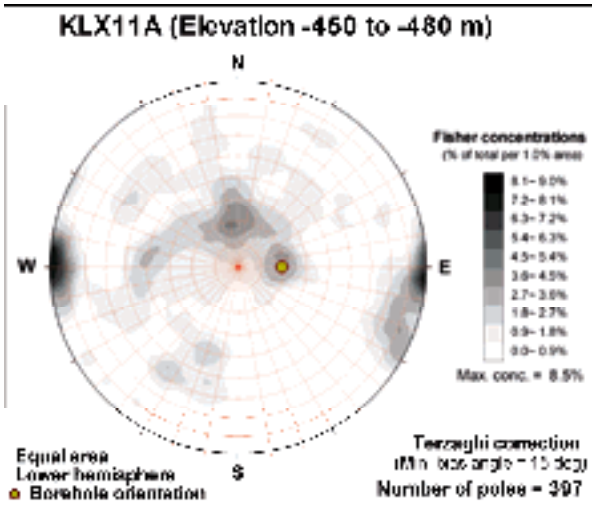
KLX11A (Elevation -460 to -480 m)
N
W
E
S
Fisher concentrations
Max. conc. = 8.5%
Equal area
Lower hemisphere
Borehole orientation
Terzaghi correction
Number of poles = 397

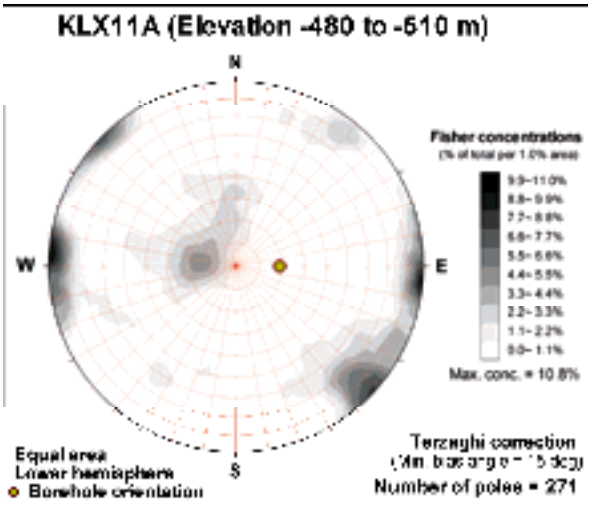
KLX11A (Elevation -480 to -510 m)
N
W
E
S
Fisher concentrations
Max. conc. = 10.8%
Equal area
Lower hemisphere
Borehole orientation
Terzaghi correction
Number of poles = 271

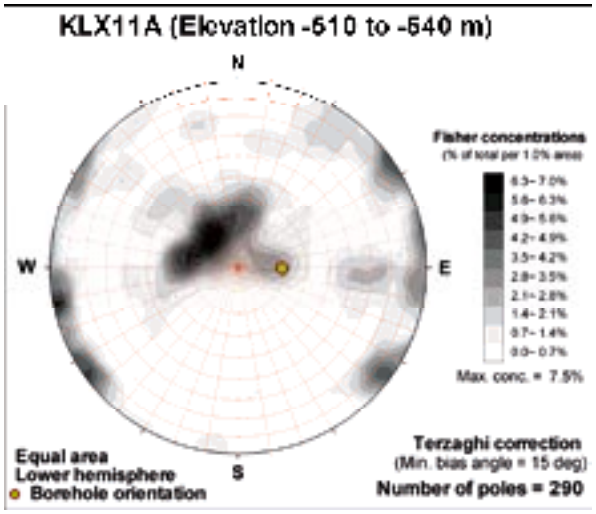
KLX11A (Elevation -510 to -540 m)
N
W
E
S
Fisher concentrations
Max. conc. = 7.5%
Equal area
Lower hemisphere
Borehole orientation
Terzaghi correction
(Min. bias angle = 15 deg)
Number of poles = 290

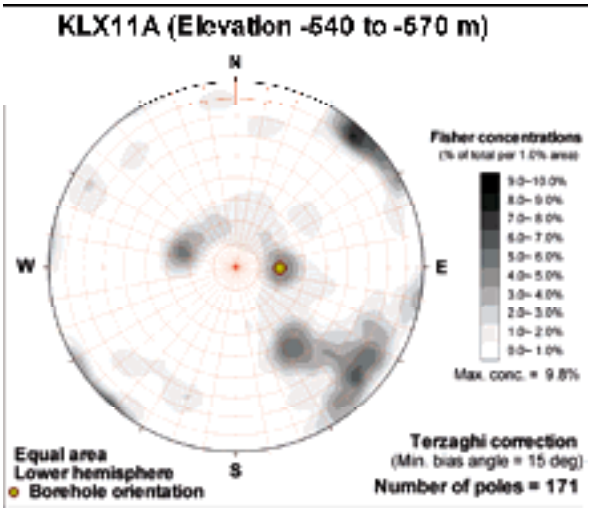
KLX11A (Elevation -540 to -570 m)
N
W
E
S
Fisher concentrations
Max. conc. = 9.8%
Equal area
Lower hemisphere
Borehole orientation
Terzaghi correction
(Min. bias angle = 15 deg)
Number of poles = 171

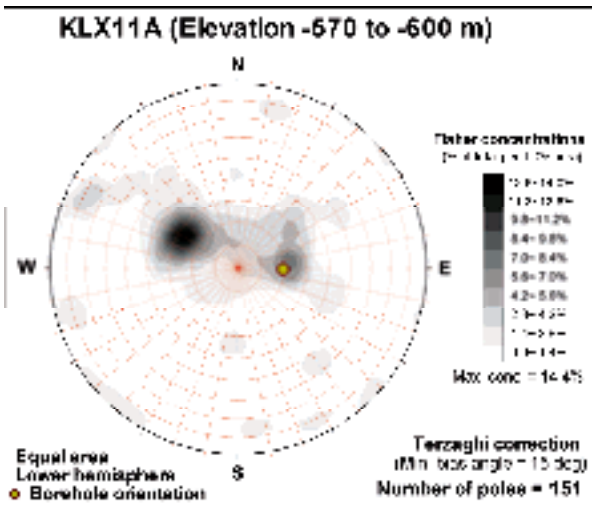
KLX11A (Elevation -570 to -600 m)
N
W
E
S
Fisher concentrations
Max. conc = 14.4%
Equal area
Lower hemisphere
Borehole orientation
Terzaghi correction
(Min. bias angle = 15 deg)
Number of poles = 151

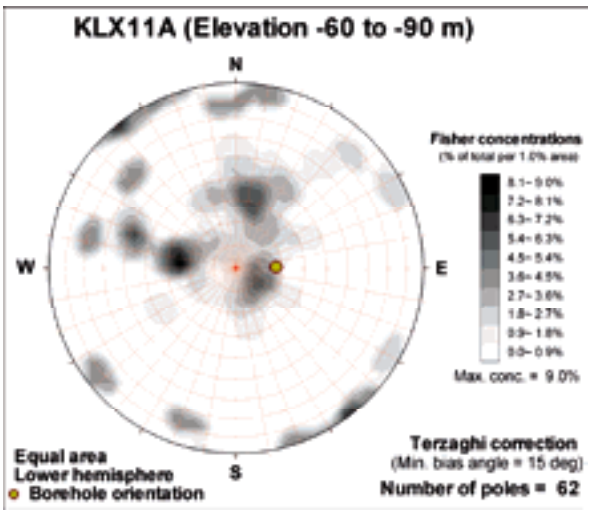
KLX11A (Elevation -60 to -90 m)
N
W
E
S
Fisher concentrations
Max. conc. = 9.0%
Equal area
Lower hemisphere
Borehole orientation
Terzaghi correction
(Min. bias angle = 15 deg)
Number of poles = 62

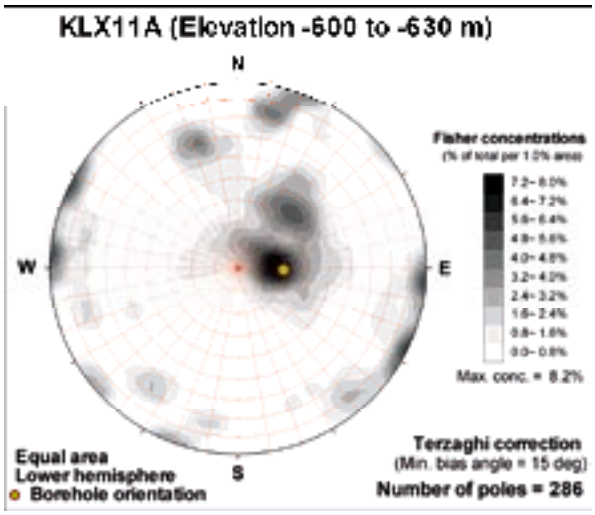
KLX11A (Elevation -600 to -630 m)
N
W
E
S
Fisher concentrations
Max. conc. = 8.2%
Equal area
Lower hemisphere
Borehole orientation
Terzaghi correction
(Min. bias angle = 15 deg)
Number of poles = 286

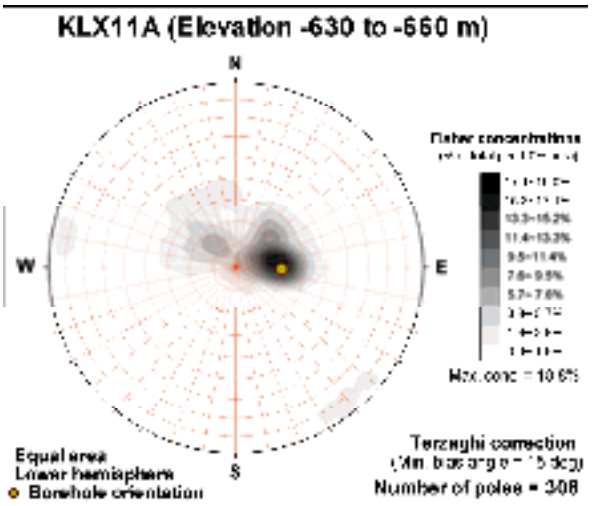
KLX11A (Elevation -630 to -660 m)
N
W
E
S
Equal area
Lower hemisphere
Borehole orientation
Terzaghi correction
Number of poles = 308

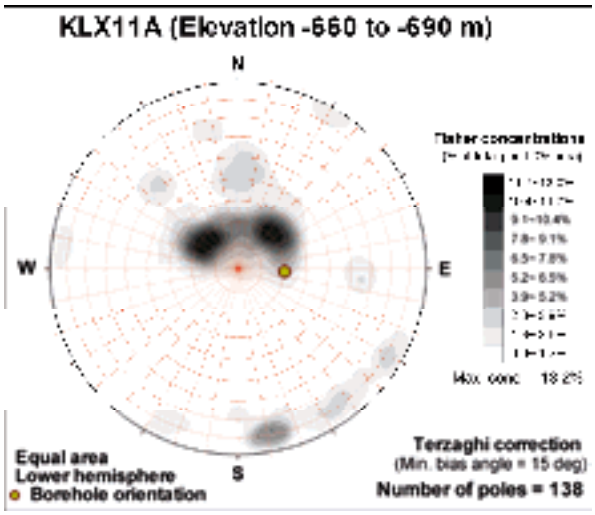
KLX11A (Elevation -660 to -690 m)
N
W
E
S
Fisher concentrations
Equal area
Lower hemisphere
Borehole orientation
Terzaghi correction
(Min. bias angle = 15 deg)
Number of poles = 138

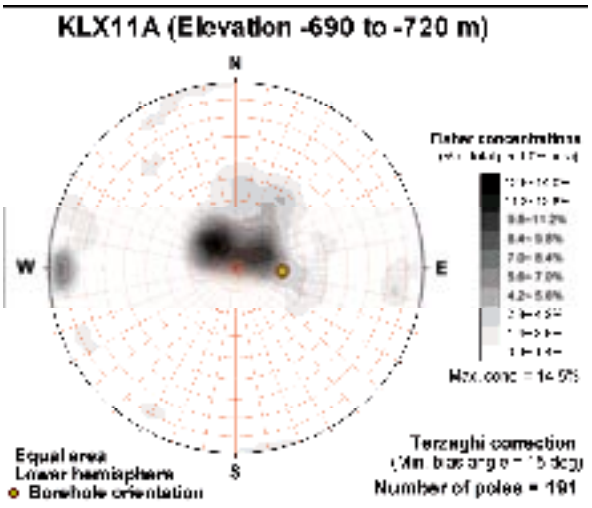
KLX11A (Elevation -690 to -720 m)
N
W
E
S
Equal area
Lower hemisphere
Borehole orientation
Terzaghi correction
Number of poles = 191

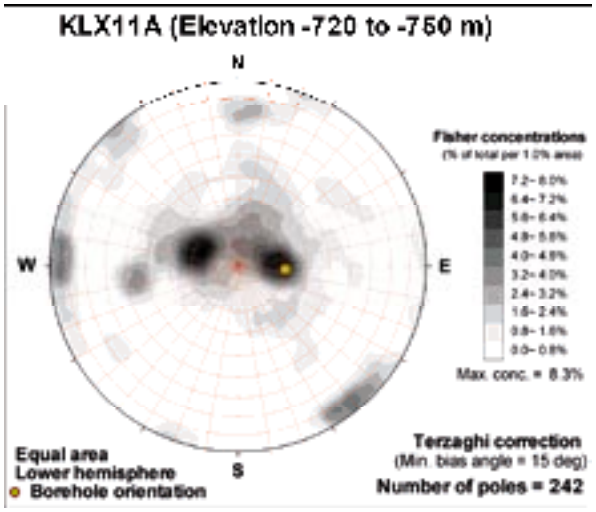
KLX11A (Elevation -720 to -750 m)
N
W
E
S
Fisher concentrations
Max. conc. = 8.3%
Equal area
Lower hemisphere
Borehole orientation
Terzaghi correction
(Min. bias angle = 15 deg)
Number of poles = 242

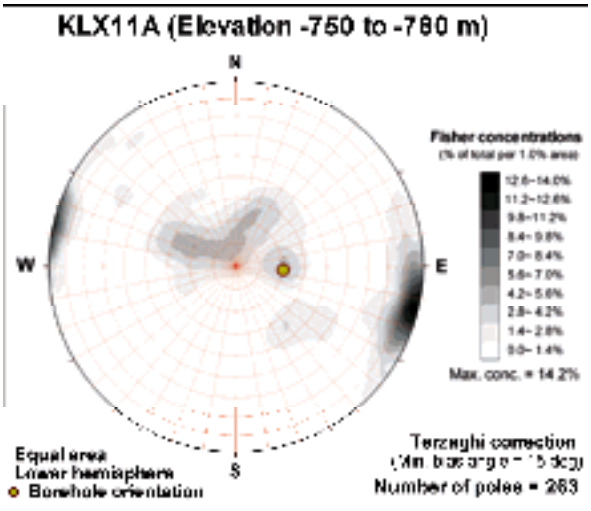
KLX11A (Elevation -750 to -780 m)
N
W
E
S
Fisher concentrations
Max. conc. = 14.2%
Equal area
Lower hemisphere
Borehole orientation
Number of poles = 263

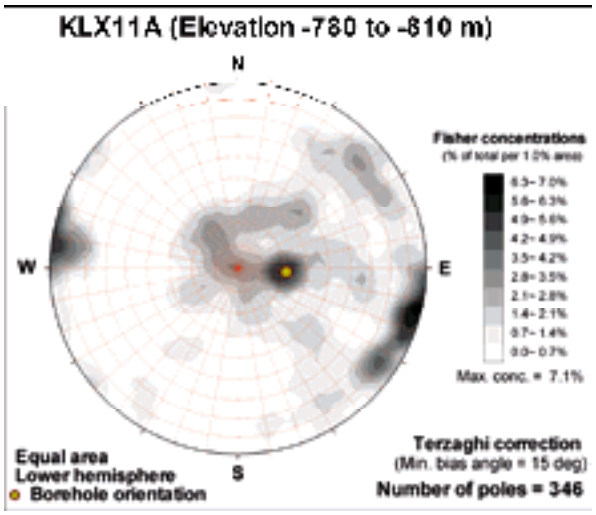
KLX11A (Elevation -780 to -810 m)
N
W
E
S
Fisher concentrations
Max. conc. = 7.1%
Equal area
Lower hemisphere
Borehole orientation
Terzaghi correction
(Min. bias angle = 15 deg)
Number of poles = 346

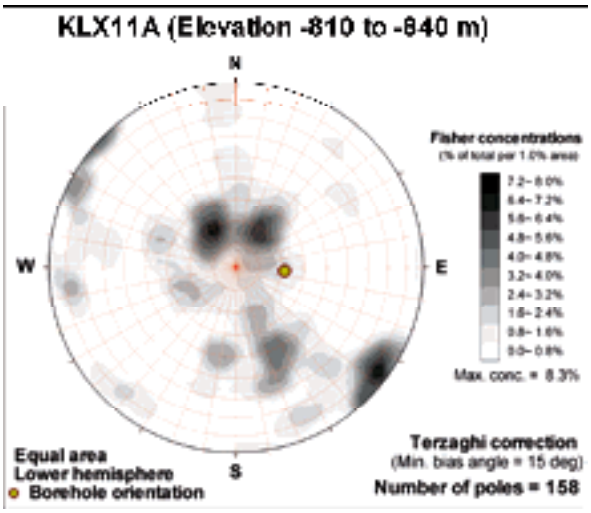
KLX11A (Elevation -810 to -840 m)
N
W
E
S
Fisher concentrations
Max. conc. = 8.3%
Equal area
Lower hemisphere
Borehole orientation
Terzaghi correction
(Min. bias angle = 15 deg)
Number of poles = 158

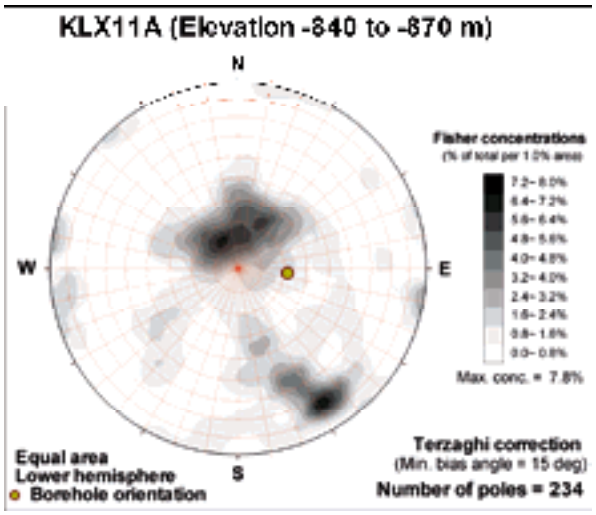
KLX11A (Elevation -840 to -870 m)
N
W
E
S
Fisher concentrations
Max. conc. = 7.8%
Equal area
Lower hemisphere
Borehole orientation
Terzaghi correction
(Min. bias angle = 15 deg)
Number of poles = 234

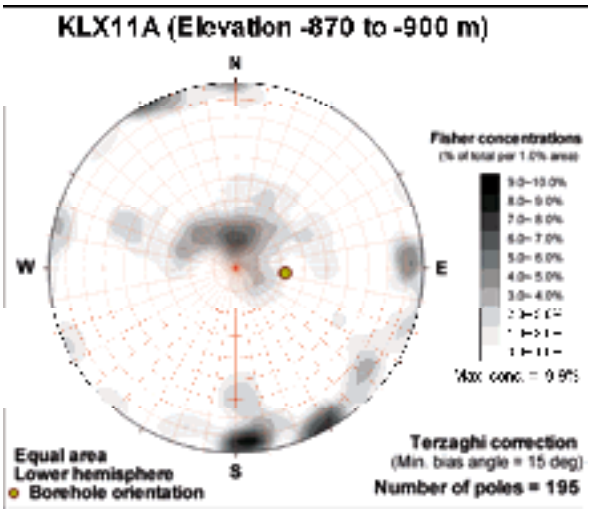
KLX11A (Elevation -870 to -900 m)
N
W
E
S
Fisher concentrations
Equal area
Lower hemisphere
Borehole orientation
Terzaghi correction
(Min. bias angle = 15 deg)
Number of poles = 195

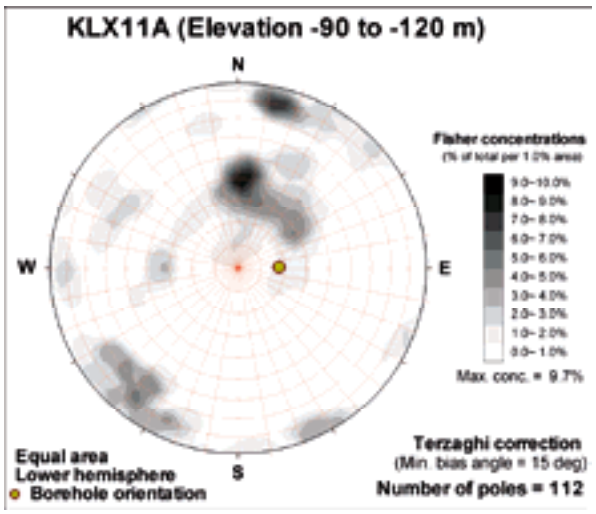
KLX11A (Elevation -90 to -120 m)
N
W
E
S
Fisher concentrations
(% of total per 1.0% area)
9.0–10.0%
8.0–9.0%
7.0–8.0%
6.0–7.0%
5.0–6.0%
4.0–5.0%
3.0–4.0%
2.0–3.0%
1.0–2.0%
0.0–1.0%
Max. conc. = 9.7%
Equal area
Lower hemisphere
Borehole orientation
Terzaghi correction
(Min. bias angle = 15 deg)
Number of poles = 112

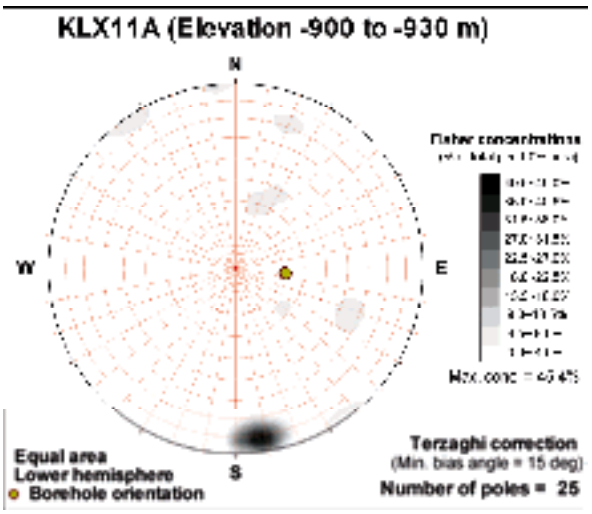
KLX11A (Elevation -900 to -930 m)
N
W
E
S
Equal area
Lower hemisphere
Borehole orientation
Terzaghi correction
(Min. bias angle = 15 deg)
Number of poles = 25

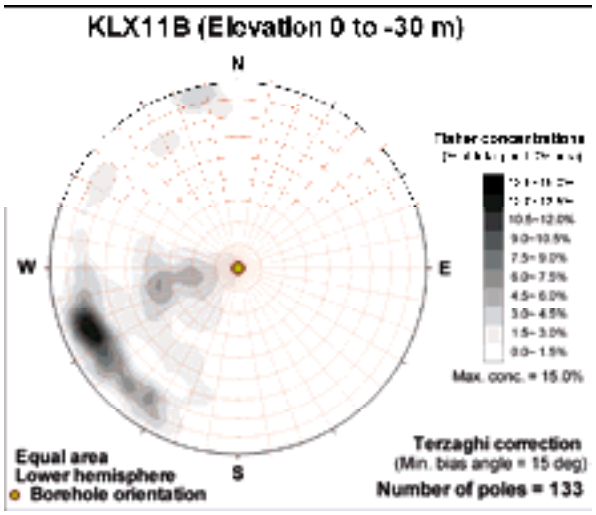
KLX11B (Elevation 0 to -30 m)
N
W
E
S
Max. conc. = 15.0%
Equal area
Lower hemisphere
Borehole orientation
Terzaghi correction
(Min. bias angle = 15 deg)
Number of poles = 133

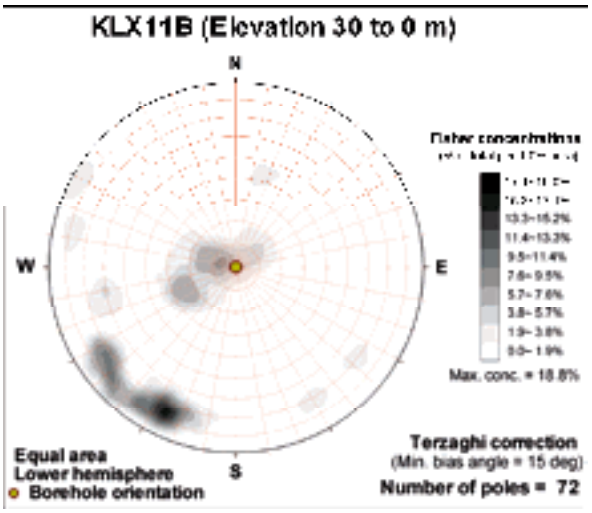
KLX11B (Elevation 30 to 0 m)
N
W
E
S
Max. conc. = 18.8%
Equal area
Lower hemisphere
Borehole orientation
Terzaghi correction
(Min. bias angle = 15 deg)
Number of poles = 72

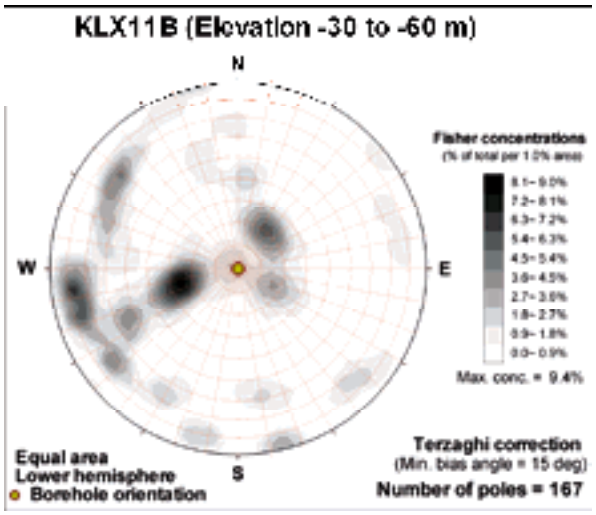
KLX11B (Elevation -30 to -60 m)
N
W
E
S
Fisher concentrations
(% of total per 1.0% area)
Max. conc. = 9.4%
Equal area
Lower hemisphere
Borehole orientation
Terzaghi correction
(Min. bias angle = 15 deg)
Number of poles = 167

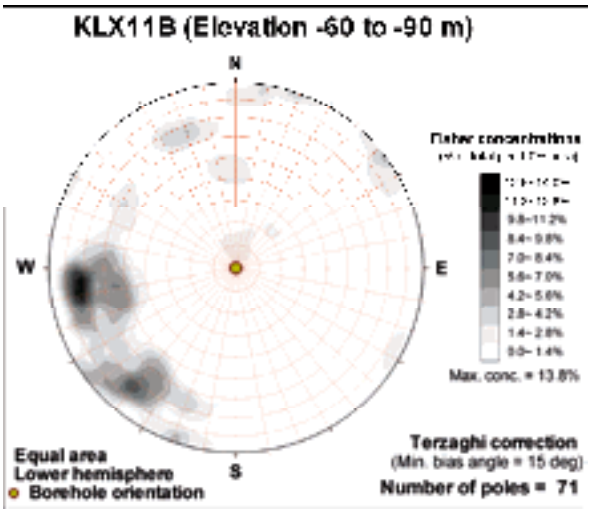
KLX11B (Elevation -60 to -90 m)
N
W
E
S
Max. conc. = 13.8%
Equal area
Lower hemisphere
Borehole orientation
Terzaghi correction
(Min. bias angle = 15 deg)
Number of poles = 71

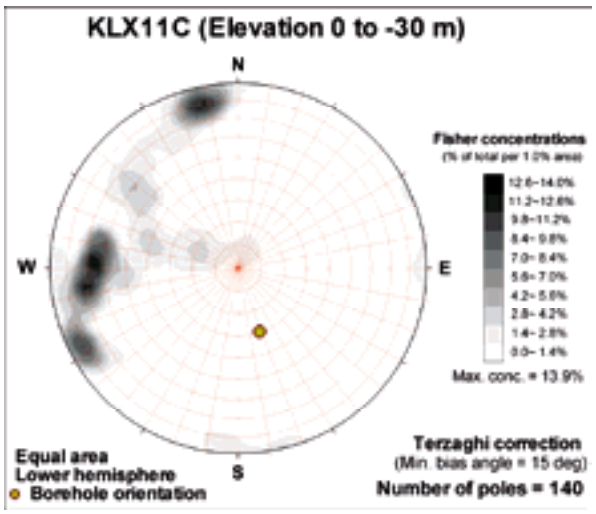
KLX11C (Elevation 0 to -30 m)
N
W
E
S
Fisher concentrations
Max. conc. = 13.9%
Equal area
Lower hemisphere
Borehole orientation
Terzaghi correction
(Min. bias angle = 15 deg)
Number of poles = 140

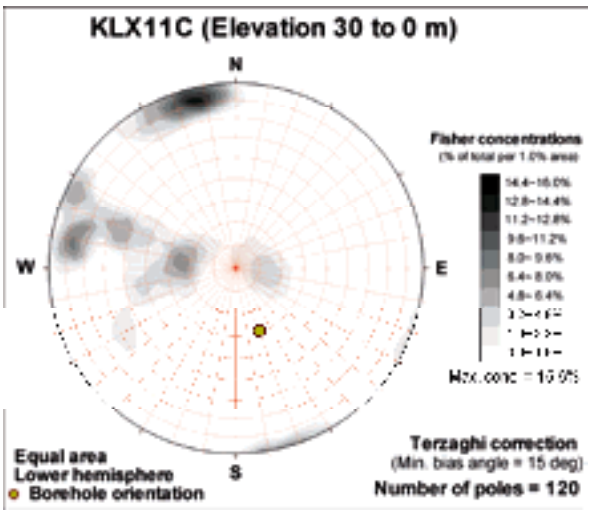
KLX11C (Elevation 30 to 0 m)
N
W
E
S
Fisher concentrations
Equal area
Lower hemisphere
Borehole orientation
Terzaghi correction
(Min. bias angle = 15 deg)
Number of poles = 120

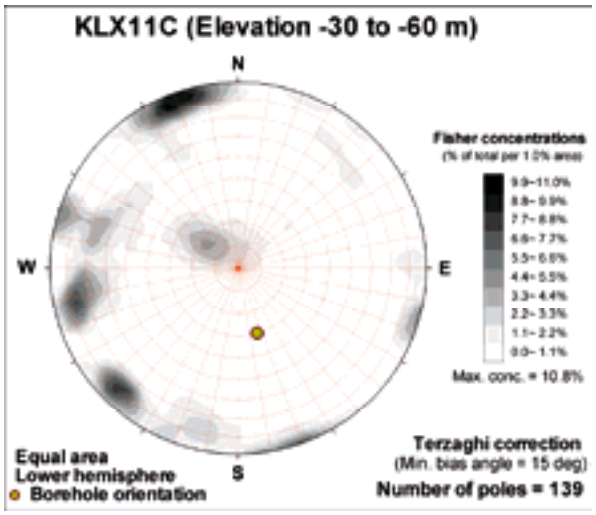
KLX11C (Elevation -30 to -60 m)
N
W
E
S
Fisher concentrations
Max. conc. = 10.8%
Equal area
Lower hemisphere
Borehole orientation
Terzaghi correction
(Min. bias angle = 15 deg)
Number of poles = 139

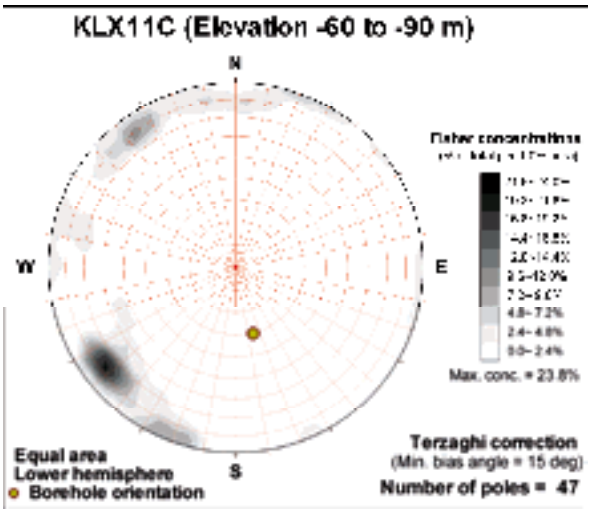
KLX11C (Elevation -60 to -90 m)
N
W
E
S
Max. conc. = 23.8%
Equal area
Lower hemisphere
Borehole orientation
Terzaghi correction
(Min. bias angle = 15 deg)
Number of poles = 47

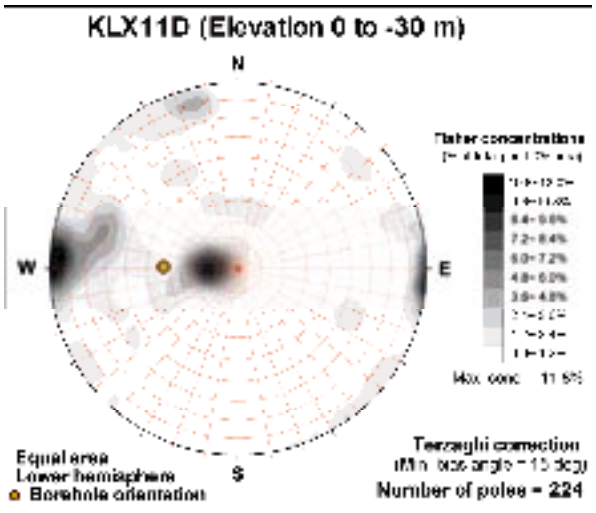
KLX11D (Elevation 0 to -30 m)
N
W
E
S
Equal area
Lower hemisphere
Borehole orientation
Terzaghi correction
Number of poles = 224

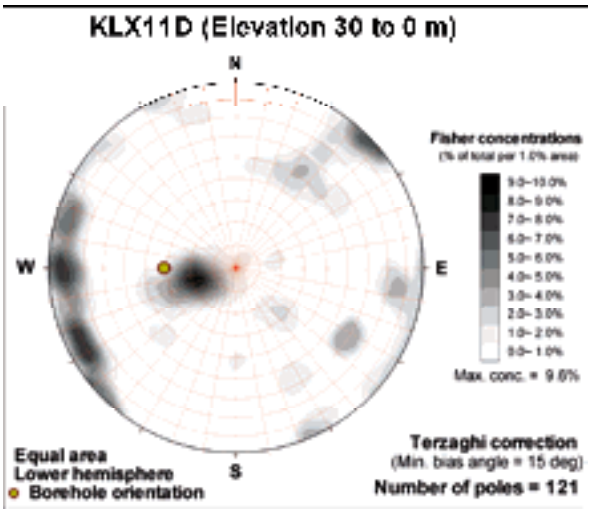
KLX11D (Elevation 30 to 0 m)
N
W
E
S
Fisher concentrations
Max. conc. = 9.6%
Equal area
Lower hemisphere
Borehole orientation
Terzaghi correction
(Min. bias angle = 15 deg)
Number of poles = 121

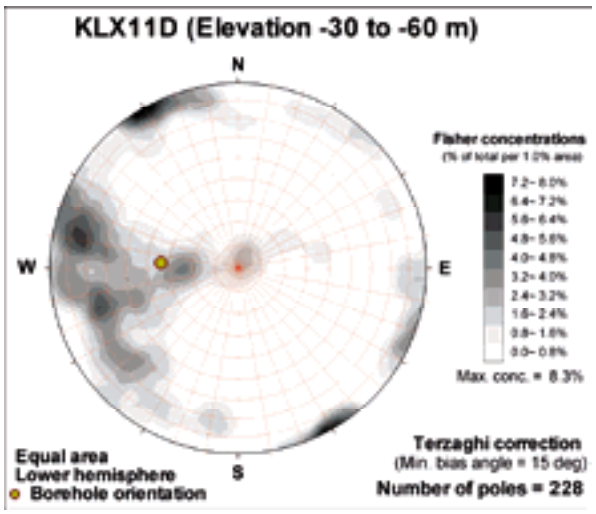
KLX11D (Elevation -30 to -60 m)
N
W
E
S
Fisher concentrations
(% of total per 1.0% area)
7.2–8.0%
6.4–7.2%
5.6–6.4%
4.8–5.6%
4.0–4.8%
3.2–4.0%
2.4–3.2%
1.6–2.4%
0.8–1.6%
0.0–0.8%
Max. conc. = 8.3%
Equal area
Lower hemisphere
Borehole orientation
Terzaghi correction
(Min. bias angle = 15 deg)
Number of poles = 228

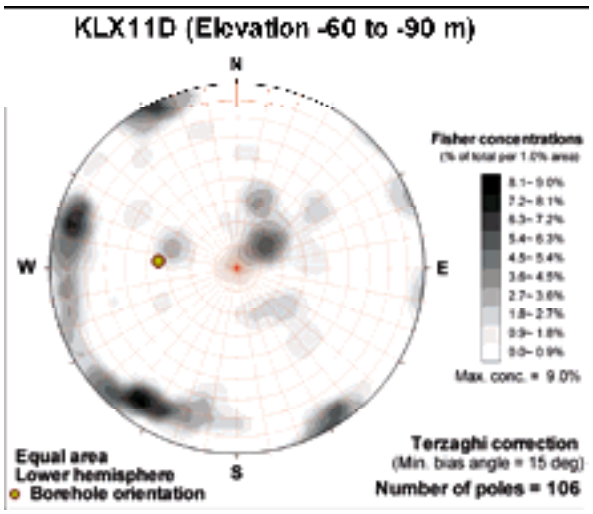
KLX11D (Elevation -60 to -90 m)
N
W
E
S
Fisher concentrations
(% of total per 1.0% area)
8.1–9.0%
7.2–8.1%
6.3–7.2%
5.4–6.3%
4.5–5.4%
3.6–4.5%
2.7–3.6%
1.8–2.7%
0.9–1.8%
0.0–0.9%
Max. conc. = 9.0%
Equal area
Lower hemisphere
Borehole orientation
Terzaghi correction
(Min. bias angle = 15 deg)
Number of poles = 106

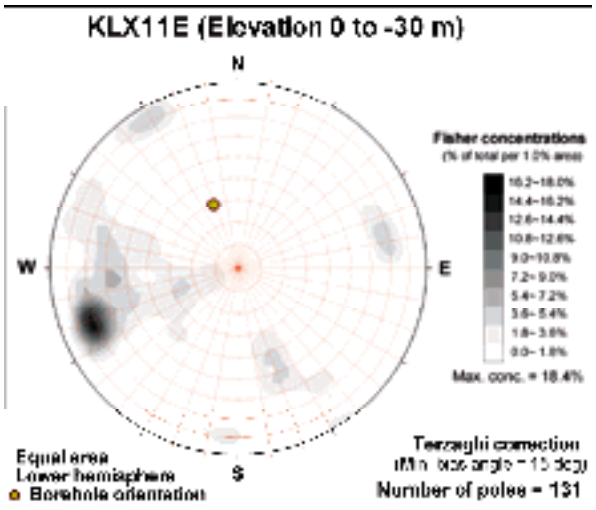
KLX11E (Elevation 0 to -30 m)
N
W
E
S
Fisher concentrations
(% of total per 1.0% area)
16.2–18.0%
14.4–16.2%
12.6–14.4%
10.8–12.6%
9.0–10.8%
7.2–9.0%
5.4–7.2%
3.6–5.4%
1.8–3.6%
0.0–1.8%
Max. conc. = 18.4%
Equal area
Lower hemisphere
Borehole orientation
Terzaghi correction
(Min. bias angle = 15 deg)
Number of poles = 131

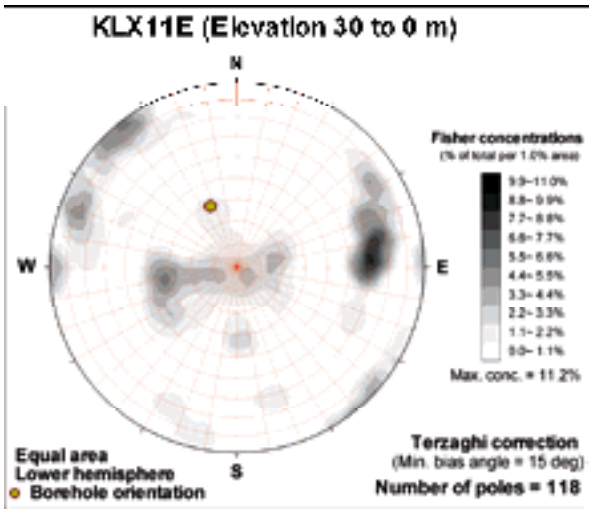
KLX11E (Elevation 30 to 0 m)
N
W
E
S
Fisher concentrations
(% of total per 1.0% area)
9.9–11.0%
8.8–9.9%
7.7–8.8%
6.6–7.7%
5.5–6.6%
4.4–5.5%
3.3–4.4%
2.2–3.3%
1.1–2.2%
0.0–1.1%
Max. conc. = 11.2%
Equal area
Lower hemisphere
Borehole orientation
Terzaghi correction
(Min. bias angle = 15 deg)
Number of poles = 118

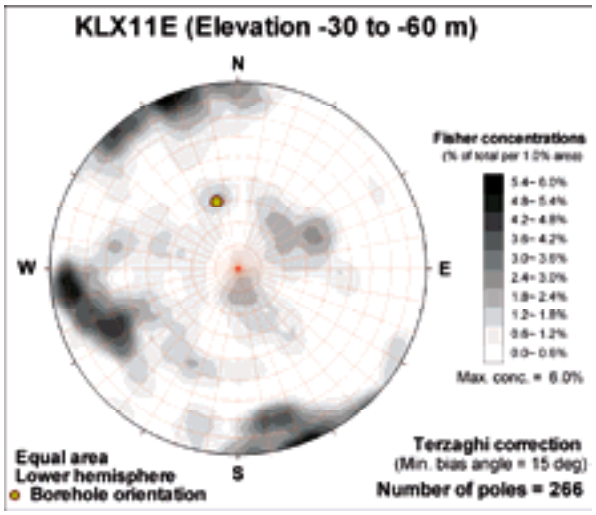
KLX11E (Elevation -30 to -60 m)
N
W
E
S
Fisher concentrations
(% of total per 1.0% area)
5.4–6.0%
4.8–5.4%
4.2–4.8%
3.6–4.2%
3.0–3.6%
2.4–3.0%
1.8–2.4%
1.2–1.8%
0.6–1.2%
0.0–0.6%
Max. conc. = 6.0%
Equal area
Lower hemisphere
Borehole orientation
Terzaghi correction
(Min. bias angle = 15 deg)
Number of poles = 266

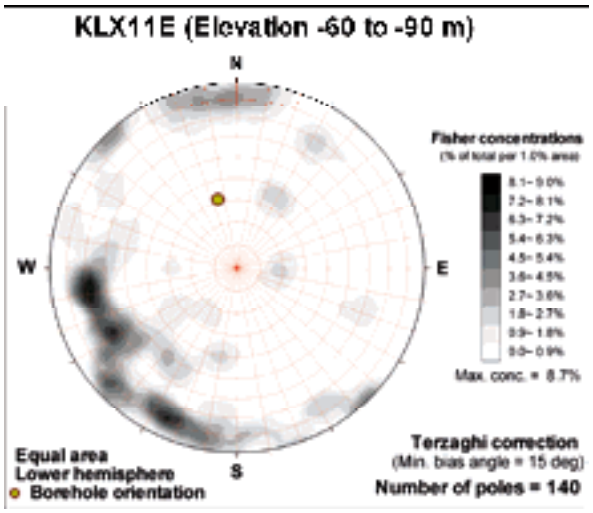
KLX11E (Elevation -60 to -90 m)
N
W
E
S
Fisher concentrations
(% of total per 1.0% area)
8.1–9.0%
7.2–8.1%
6.3–7.2%
5.4–6.3%
4.5–5.4%
3.6–4.5%
2.7–3.6%
1.8–2.7%
0.9–1.8%
0.0–0.9%
Max. conc. = 8.7%
Equal area
Lower hemisphere
Borehole orientation
Terzaghi correction
(Min. bias angle = 15 deg)
Number of poles = 140

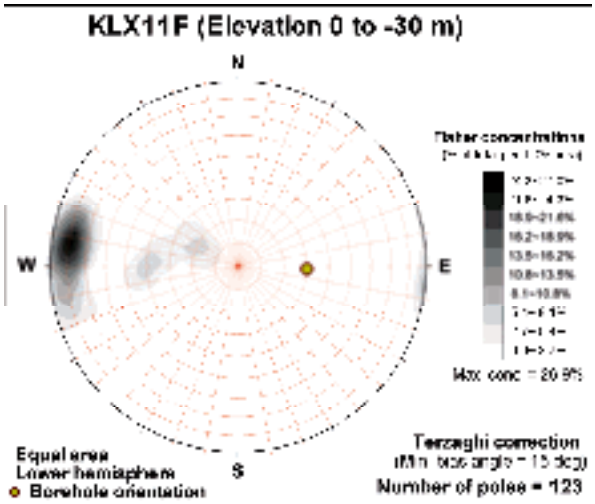
KLX11F (Elevation 0 to -30 m)
N
W
E
S
Fisher concentrations
Max. conc. = 20.9%
Equal area
Lower hemisphere
Borehole orientation
Terzaghi correction
Number of poles = 123

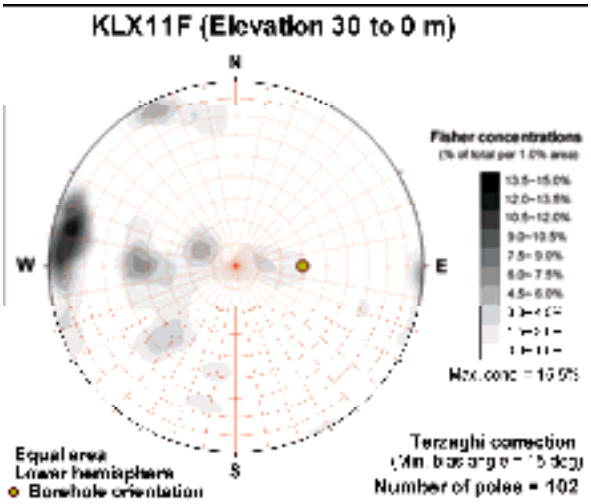
KLX11F (Elevation 30 to 0 m)
N
W
E
S
Fisher concentrations
Equal area
Lower hemisphere
Borehole orientation
Terzaghi correction
Number of poles = 102

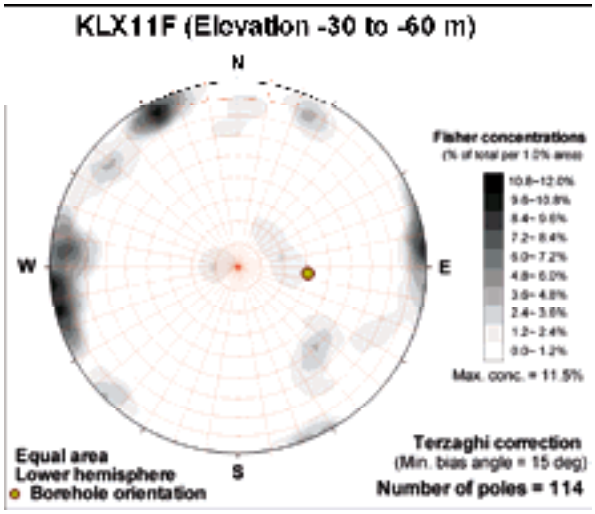
KLX11F (Elevation -30 to -60 m)
N
W
E
S
Fisher concentrations
Max. conc. = 11.5%
Equal area
Lower hemisphere
Borehole orientation
Terzaghi correction
(Min. bias angle = 15 deg)
Number of poles = 114

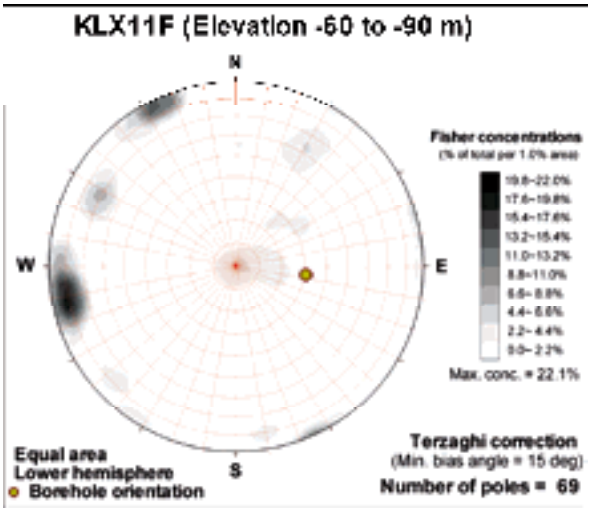
KLX11F (Elevation -60 to -90 m)
N
W
E
S
Fisher concentrations
Max. conc. = 22.1%
Equal area
Lower hemisphere
Borehole orientation
Terzaghi correction
(Min. bias angle = 15 deg)
Number of poles = 69

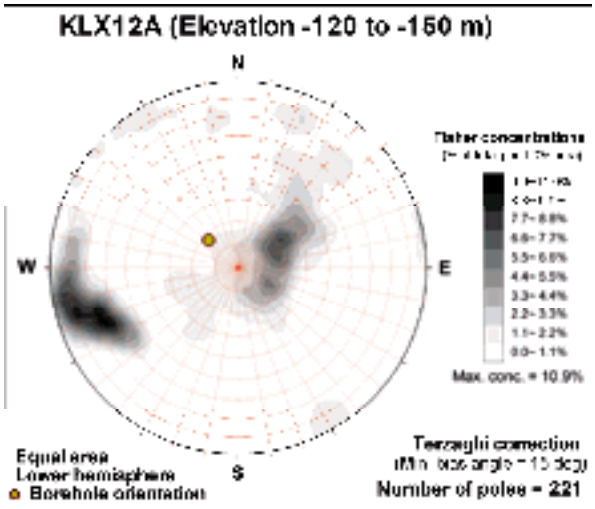
KLX12A (Elevation -120 to -150 m)
N
W
E
S
Fisher concentrations
Max. conc. = 10.9%
Equal area
Lower hemisphere
Borehole orientation
Terzaghi correction
Number of poles = 221

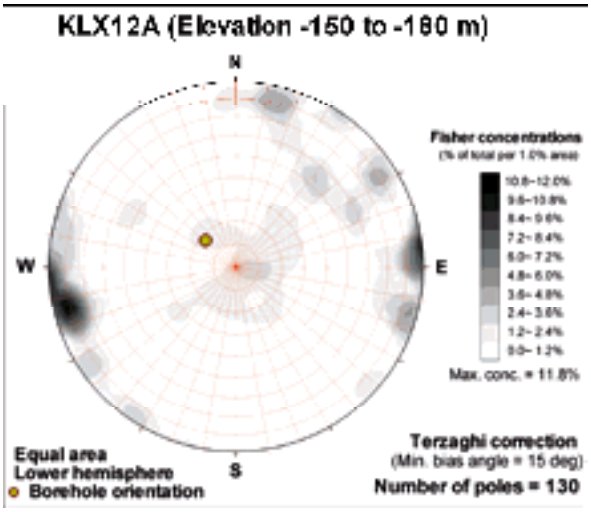
KLX12A (Elevation -150 to -180 m)
N
W
E
S
Fisher concentrations
Max. conc. = 11.8%
Equal area
Lower hemisphere
Borehole orientation
Terzaghi correction
(Min. bias angle = 15 deg)
Number of poles = 130

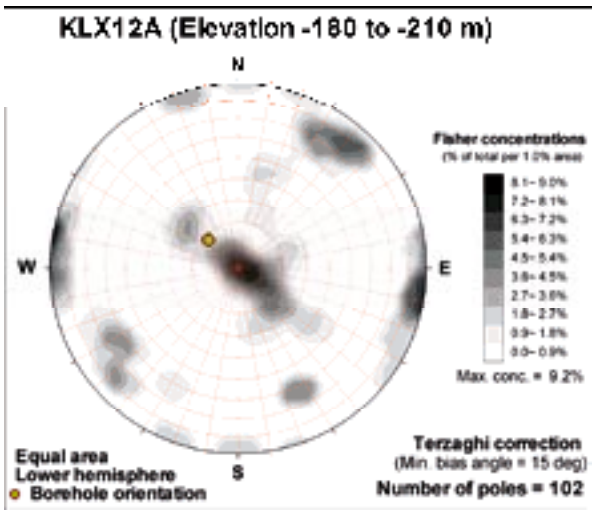
KLX12A (Elevation -180 to -210 m)
N
W
E
S
Fisher concentrations
(% of total per 1.0% area)
8.1– 9.0%
7.2– 8.1%
6.3– 7.2%
5.4– 6.3%
4.5– 5.4%
3.6– 4.5%
2.7– 3.6%
1.8– 2.7%
0.9– 1.8%
0.0– 0.9%
Max. conc. = 9.2%
Equal area
Lower hemisphere
Borehole orientation
Terzaghi correction
(Min. bias angle = 15 deg)
Number of poles = 102

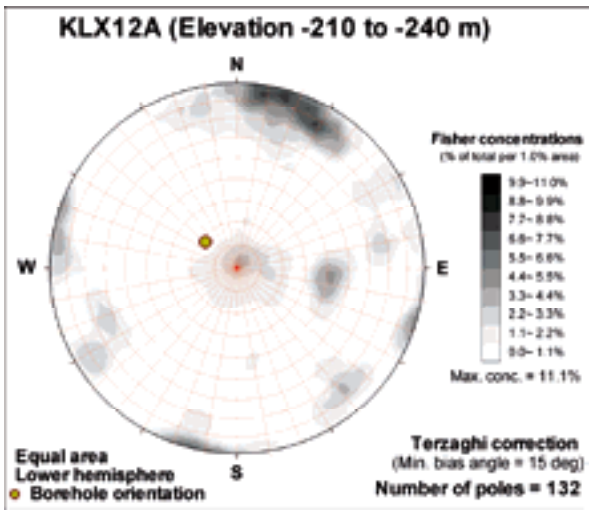
KLX12A (Elevation -210 to -240 m)
N
W
E
S
Fisher concentrations
(% of total per 1.0% area)
9.9–11.0%
8.8– 9.9%
7.7– 8.8%
6.6– 7.7%
5.5– 6.6%
4.4– 5.5%
3.3– 4.4%
2.2– 3.3%
1.1– 2.2%
0.0– 1.1%
Max. conc. = 11.1%
Equal area
Lower hemisphere
Borehole orientation
Terzaghi correction
(Min. bias angle = 15 deg)
Number of poles = 132

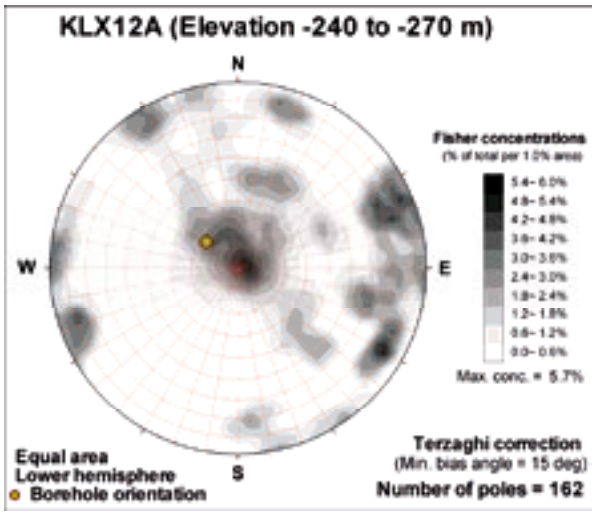
KLX12A (Elevation -240 to -270 m)
N
W
E
S
Fisher concentrations
(% of total per 1.0% area)
5.4– 6.0%
4.8– 5.4%
4.2– 4.8%
3.6– 4.2%
3.0– 3.6%
2.4– 3.0%
1.8– 2.4%
1.2– 1.8%
0.6– 1.2%
0.0– 0.6%
Max. conc. = 5.7%
Equal area
Lower hemisphere
Borehole orientation
Terzaghi correction
(Min. bias angle = 15 deg)
Number of poles = 162

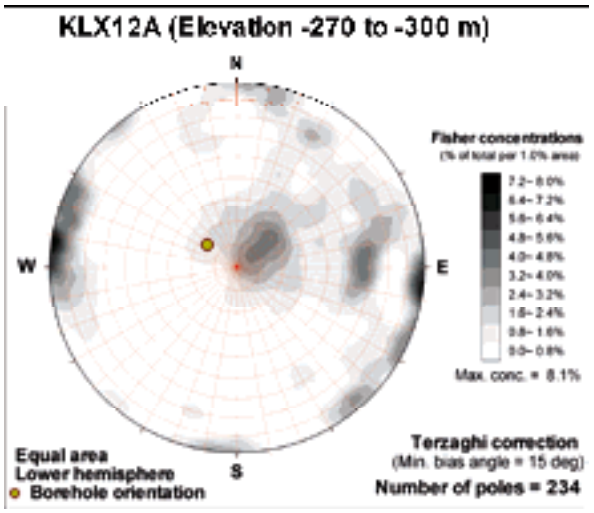
KLX12A (Elevation -270 to -300 m)
N
W
E
S
Fisher concentrations
(% of total per 1.0% area)
7.2– 8.0%
6.4– 7.2%
5.6– 6.4%
4.8– 5.6%
4.0– 4.8%
3.2– 4.0%
2.4– 3.2%
1.6– 2.4%
0.8– 1.6%
0.0– 0.8%
Max. conc. = 8.1%
Equal area
Lower hemisphere
Borehole orientation
Terzaghi correction
(Min. bias angle = 15 deg)
Number of poles = 234

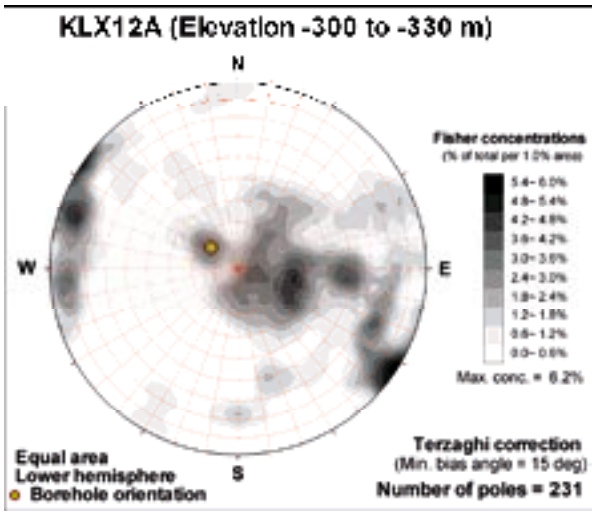
KLX12A (Elevation -300 to -330 m)
N
W
E
S
Fisher concentrations
(% of total per 1.0% area)
5.4– 6.0%
4.8– 5.4%
4.2– 4.8%
3.6– 4.2%
3.0– 3.6%
2.4– 3.0%
1.8– 2.4%
1.2– 1.8%
0.6– 1.2%
0.0– 0.6%
Max. conc. = 6.2%
Equal area
Lower hemisphere
Borehole orientation
Terzaghi correction
(Min. bias angle = 15 deg)
Number of poles = 231

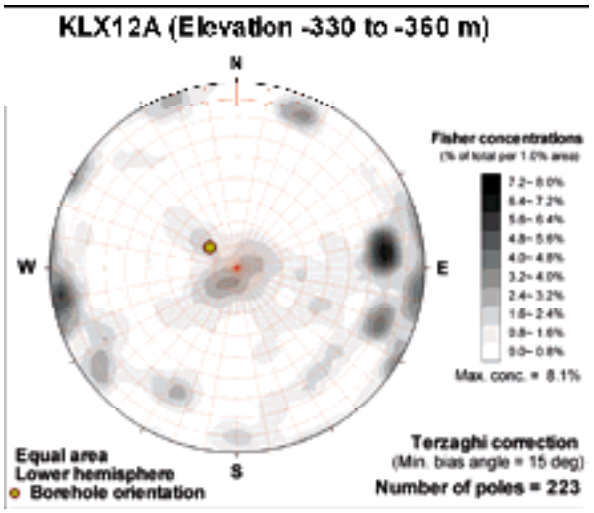
KLX12A (Elevation -330 to -360 m)
N
W
E
S
Fisher concentrations
(% of total per 1.0% area)
7.2– 8.0%
6.4– 7.2%
5.6– 6.4%
4.8– 5.6%
4.0– 4.8%
3.2– 4.0%
2.4– 3.2%
1.6– 2.4%
0.8– 1.6%
0.0– 0.8%
Max. conc. = 8.1%
Equal area
Lower hemisphere
Borehole orientation
Terzaghi correction
(Min. bias angle = 15 deg)
Number of poles = 223

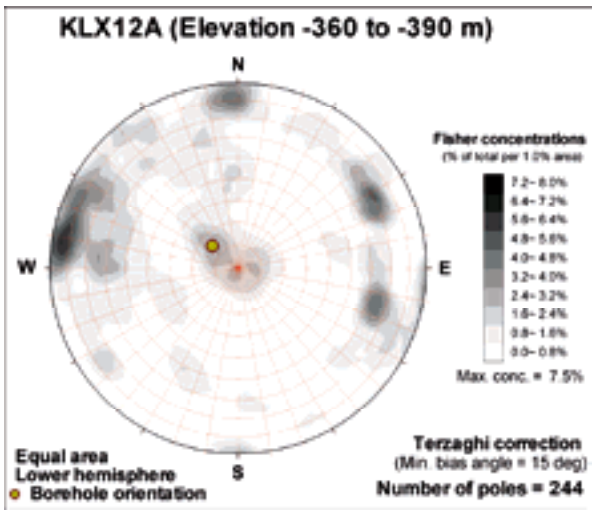
KLX12A (Elevation -360 to -390 m)
N
W
E
S
Fisher concentrations
Max. conc. = 7.5%
Equal area
Lower hemisphere
Borehole orientation
Terzaghi correction
(Min. bias angle = 15 deg)
Number of poles = 244

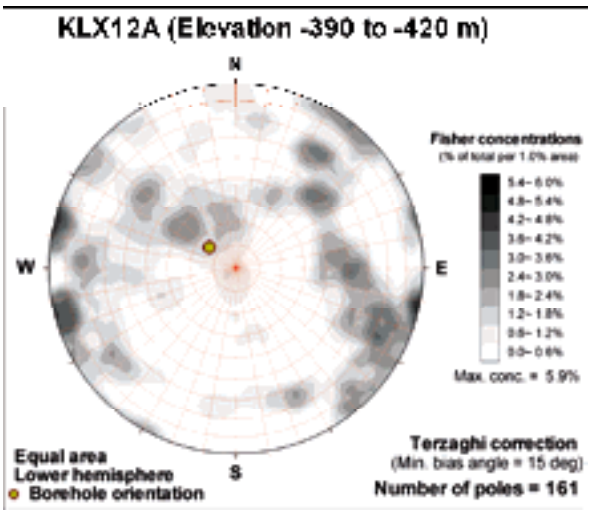
KLX12A (Elevation -390 to -420 m)
N
W
E
S
Fisher concentrations
Max. conc. = 5.9%
Equal area
Lower hemisphere
Borehole orientation
Terzaghi correction
(Min. bias angle = 15 deg)
Number of poles = 161

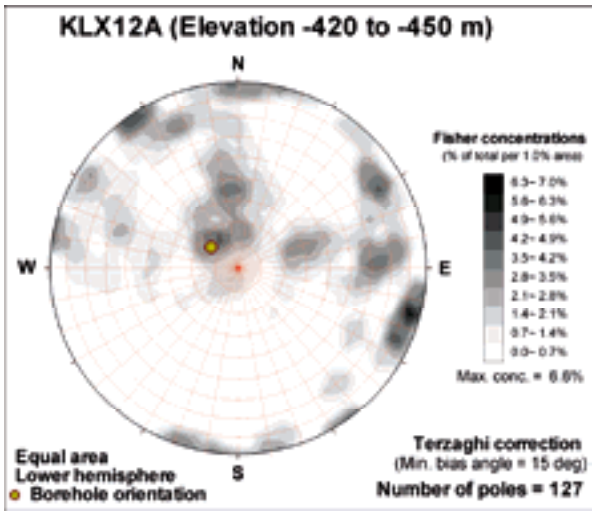
KLX12A (Elevation -420 to -450 m)
N
W
E
S
Fisher concentrations
Max. conc. = 6.8%
Equal area
Lower hemisphere
Borehole orientation
Terzaghi correction
(Min. bias angle = 15 deg)
Number of poles = 127

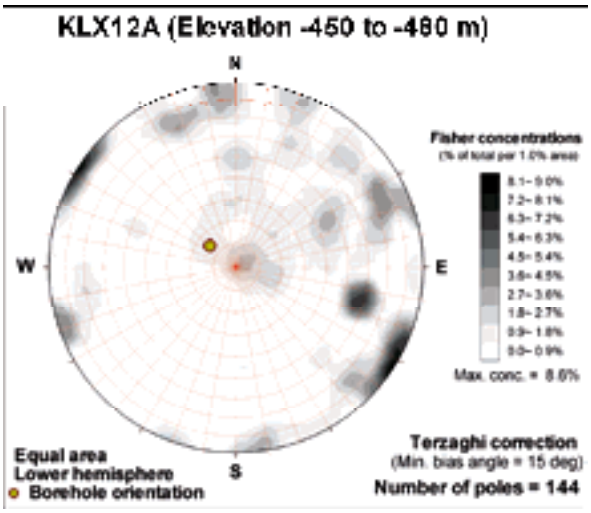
KLX12A (Elevation -450 to -480 m)
N
W
E
S
Fisher concentrations
Max. conc. = 8.6%
Equal area
Lower hemisphere
Borehole orientation
Terzaghi correction
(Min. bias angle = 15 deg)
Number of poles = 144

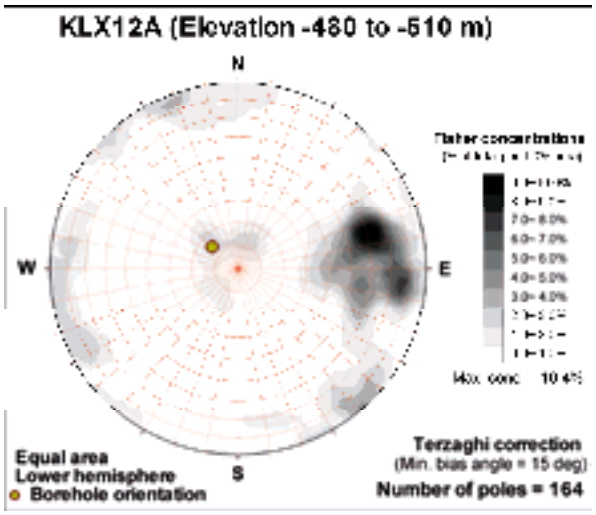
KLX12A (Elevation -480 to -510 m)
N
W
E
S
Equal area
Lower hemisphere
Borehole orientation
Terzaghi correction
(Min. bias angle = 15 deg)
Number of poles = 164

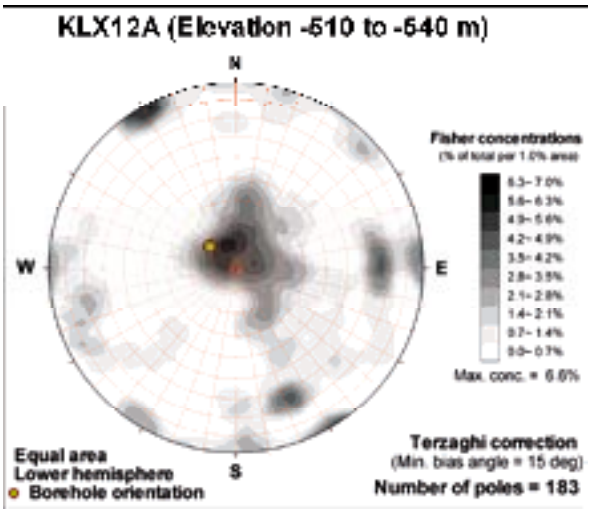
KLX12A (Elevation -510 to -540 m)
N
W
E
S
Fisher concentrations
Max. conc. = 6.6%
Equal area
Lower hemisphere
Borehole orientation
Terzaghi correction
(Min. bias angle = 15 deg)
Number of poles = 183

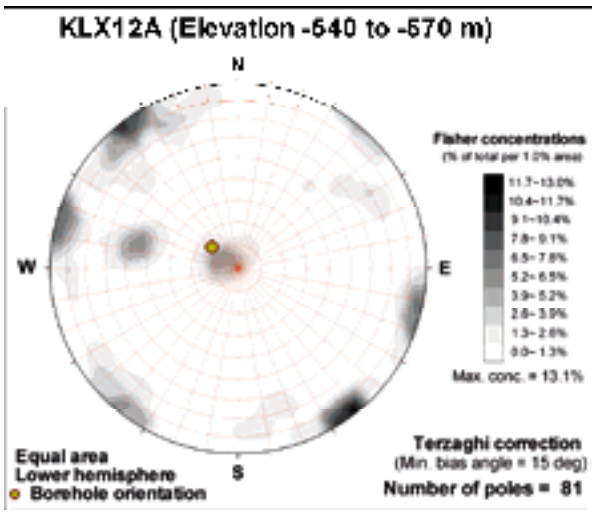
KLX12A (Elevation -540 to -570 m)
N
W
E
S
Fisher concentrations
(% of total per 1.0% area)
Max. conc. = 13.1%
Equal area
Lower hemisphere
Borehole orientation
Terzaghi correction
(Min. bias angle = 15 deg)
Number of poles = 81

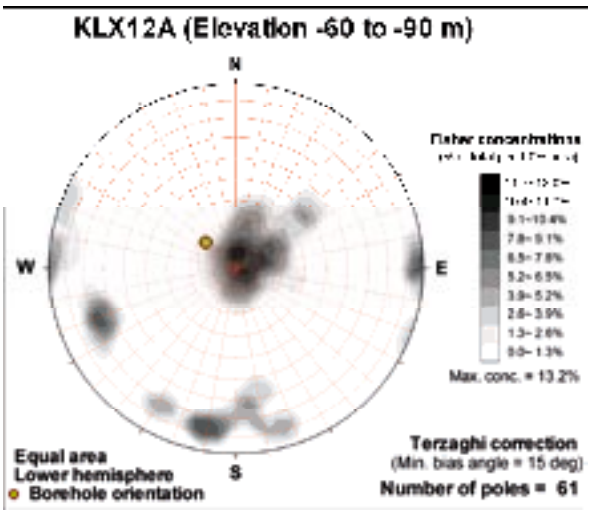
KLX12A (Elevation -60 to -90 m)
N
W
E
S
Max. conc. = 13.2%
Equal area
Lower hemisphere
Borehole orientation
Terzaghi correction
(Min. bias angle = 15 deg)
Number of poles = 61

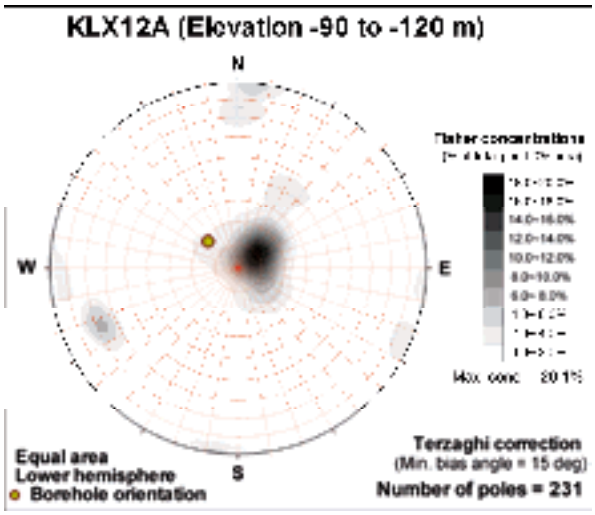
KLX12A (Elevation -90 to -120 m)
N
W
E
S
Equal area
Lower hemisphere
Borehole orientation
Terzaghi correction
(Min. bias angle = 15 deg)
Number of poles = 231

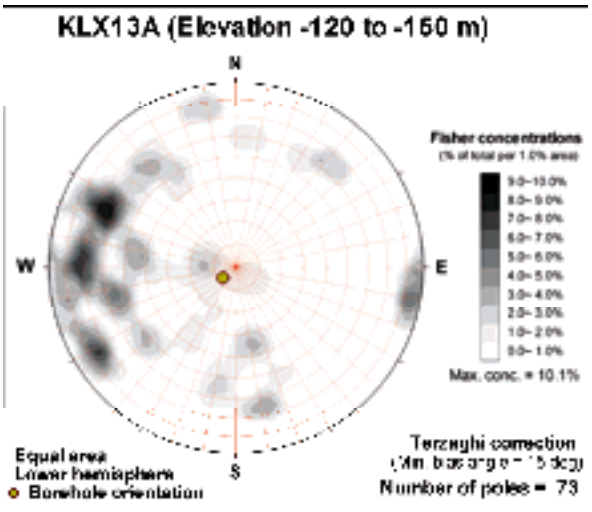
KLX13A (Elevation -120 to -150 m)
N
W
E
S
Max. conc. = 10.1%
Equal area
Lower hemisphere
Borehole orientation
Number of poles = 73

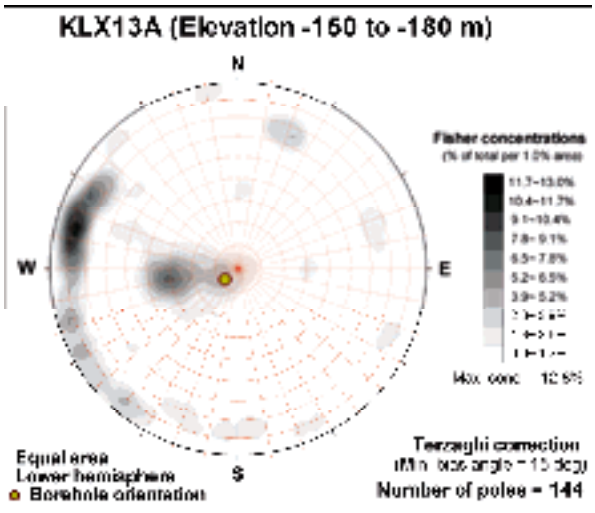
KLX13A (Elevation -150 to -180 m)
N
W
E
S
Equal area
Lower hemisphere
Borehole orientation
Number of poles = 144

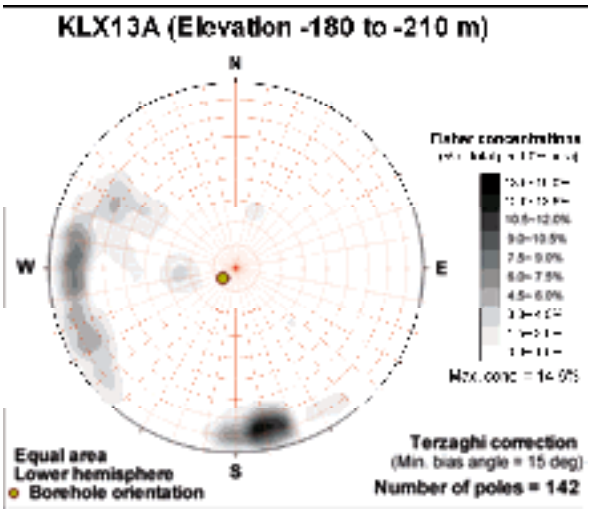
KLX13A (Elevation -180 to -210 m)
N
W
E
S
Equal area
Lower hemisphere
Borehole orientation
Terzaghi correction
(Min. bias angle = 15 deg)
Number of poles = 142

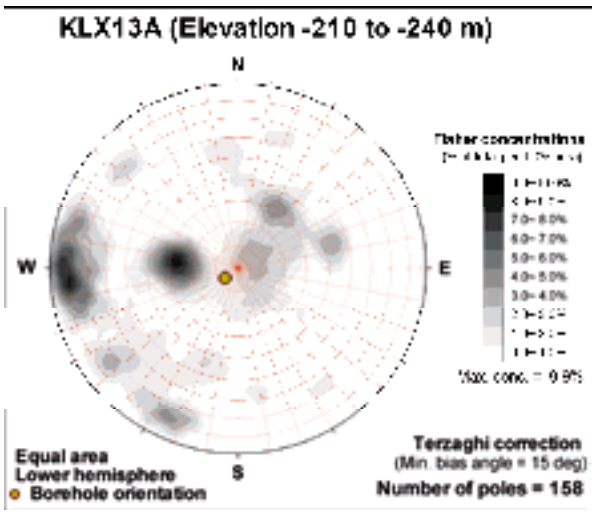
KLX13A (Elevation -210 to -240 m)
N
W
E
S
Fisher concentrations
Max. conc. = 9.9%
Equal area
Lower hemisphere
Borehole orientation
Terzaghi correction
(Min. bias angle = 15 deg)
Number of poles = 158

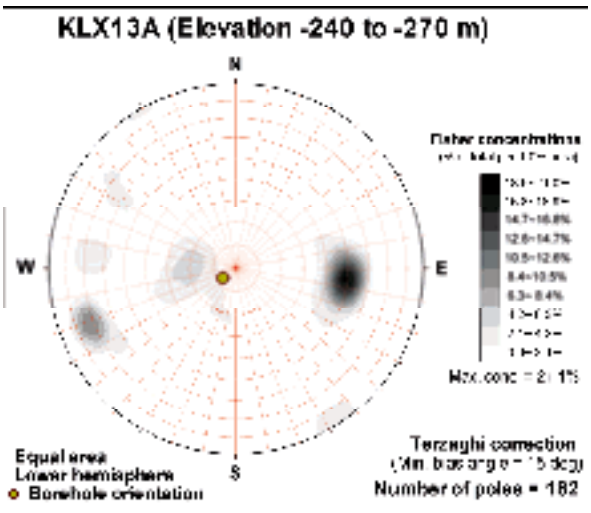
KLX13A (Elevation -240 to -270 m)
N
W
E
S
Fisher concentrations
Equal area
Lower hemisphere
Borehole orientation
Terzaghi correction
Number of poles = 182

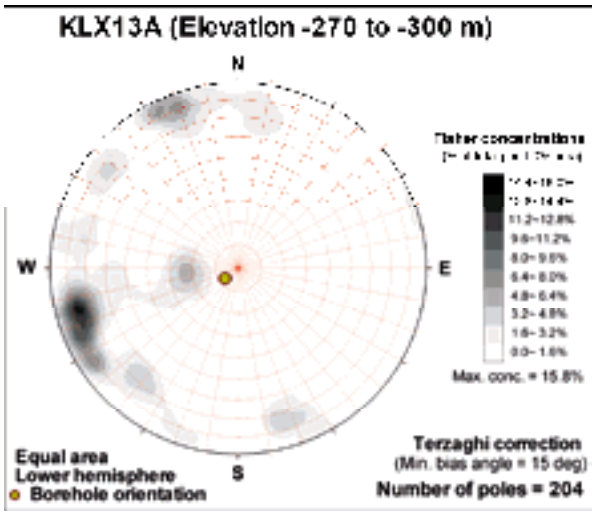
KLX13A (Elevation -270 to -300 m)
N
W
E
S
Fisher concentrations
Max. conc. = 15.8%
Equal area
Lower hemisphere
Borehole orientation
Terzaghi correction
(Min. bias angle = 15 deg)
Number of poles = 204

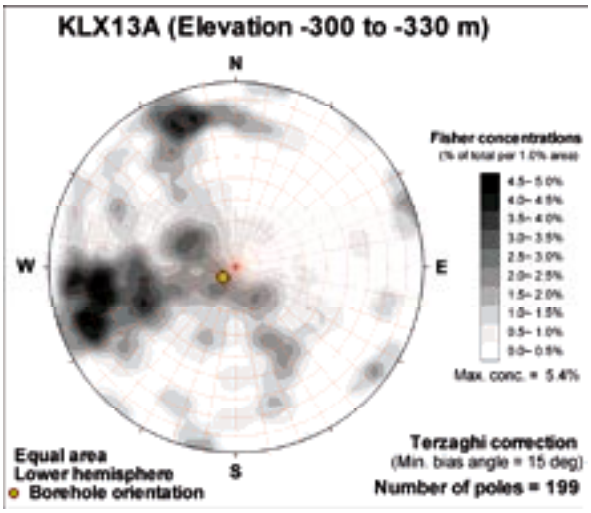
KLX13A (Elevation -300 to -330 m)
N
W
E
S
Fisher concentrations
Max. conc. = 5.4%
Equal area
Lower hemisphere
Borehole orientation
Terzaghi correction
(Min. bias angle = 15 deg)
Number of poles = 199

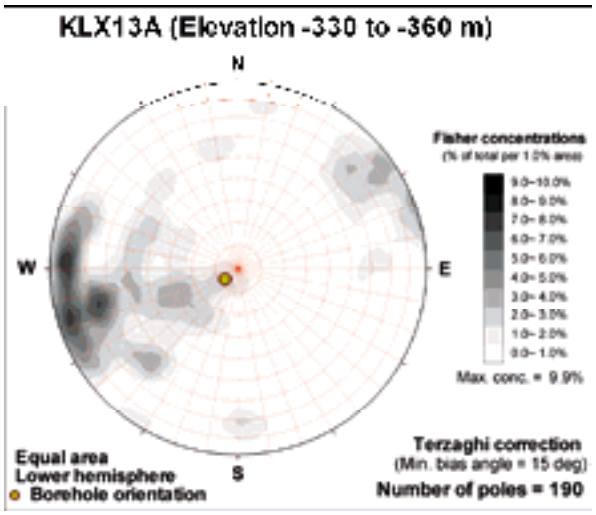
KLX13A (Elevation -330 to -360 m)
N
W
E
S
Fisher concentrations
Max. conc. = 9.9%
Equal area
Lower hemisphere
Borehole orientation
Terzaghi correction
(Min. bias angle = 15 deg)
Number of poles = 190

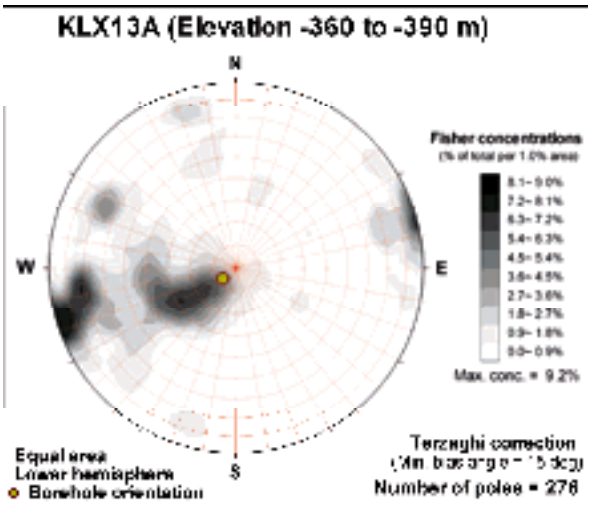
KLX13A (Elevation -360 to -390 m)
N
W
E
S
Fisher concentrations
Max. conc. = 9.2%
Equal area
Lower hemisphere
Borehole orientation
Terzaghi correction
Number of poles = 278

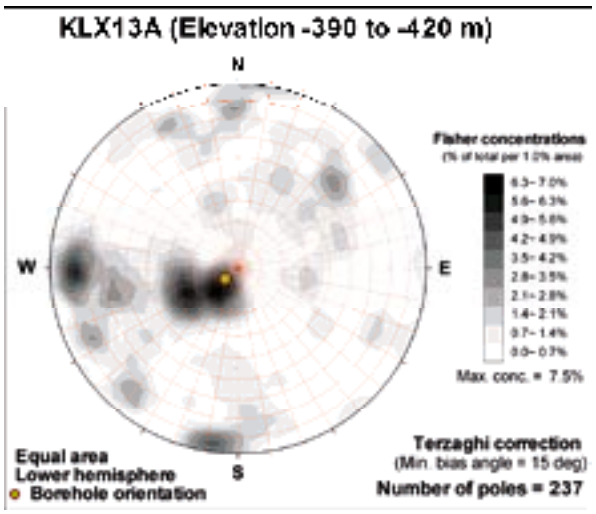
KLX13A (Elevation -390 to -420 m)
N
W
E
S
Fisher concentrations
(% of total per 1.0% area)
6.3–7.0%
5.6–6.3%
4.9–5.6%
4.2–4.9%
3.5–4.2%
2.8–3.5%
2.1–2.8%
1.4–2.1%
0.7–1.4%
0.0–0.7%
Max. conc. = 7.5%
Equal area
Lower hemisphere
Borehole orientation
Terzaghi correction
(Min. bias angle = 15 deg)
Number of poles = 237

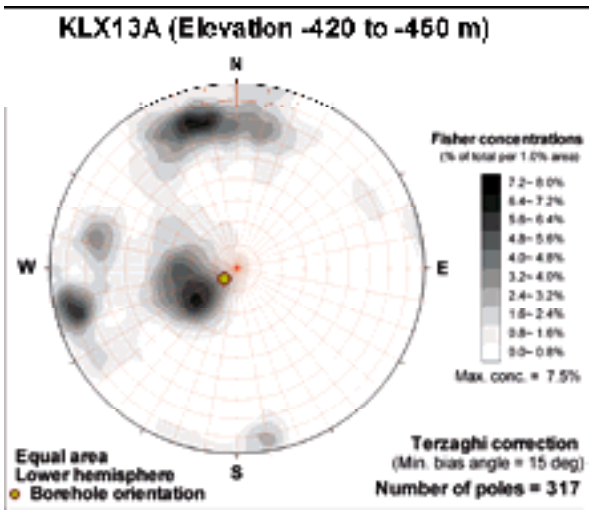
KLX13A (Elevation -420 to -460 m)
N
W
E
S
Fisher concentrations
(% of total per 1.0% area)
7.2–8.0%
6.4–7.2%
5.6–6.4%
4.8–5.6%
4.0–4.8%
3.2–4.0%
2.4–3.2%
1.6–2.4%
0.8–1.6%
0.0–0.8%
Max. conc. = 7.5%
Equal area
Lower hemisphere
Borehole orientation
Terzaghi correction
(Min. bias angle = 15 deg)
Number of poles = 317

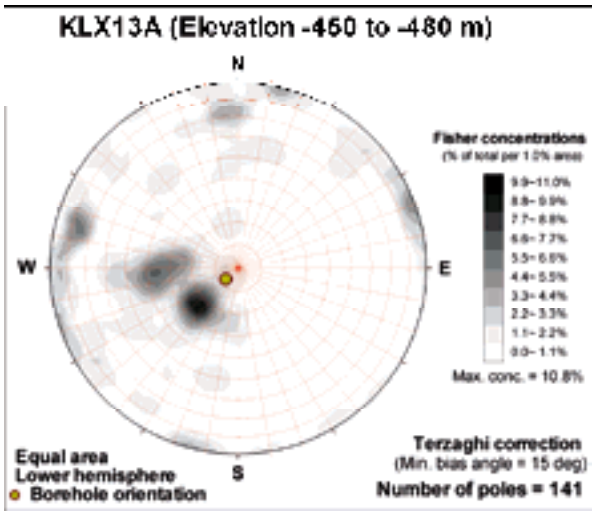
KLX13A (Elevation -460 to -480 m)
N
W
E
S
Fisher concentrations
(% of total per 1.0% area)
9.9–11.0%
8.8–9.9%
7.7–8.8%
6.6–7.7%
5.5–6.6%
4.4–5.5%
3.3–4.4%
2.2–3.3%
1.1–2.2%
0.0–1.1%
Max. conc. = 10.8%
Equal area
Lower hemisphere
Borehole orientation
Terzaghi correction
(Min. bias angle = 15 deg)
Number of poles = 141

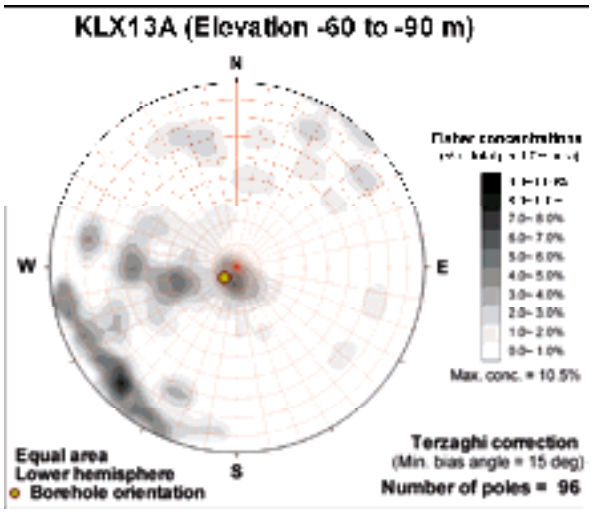
KLX13A (Elevation -60 to -90 m)
N
W
E
S
Max. conc. = 10.5%
Equal area
Lower hemisphere
Borehole orientation
Terzaghi correction
(Min. bias angle = 15 deg)
Number of poles = 96

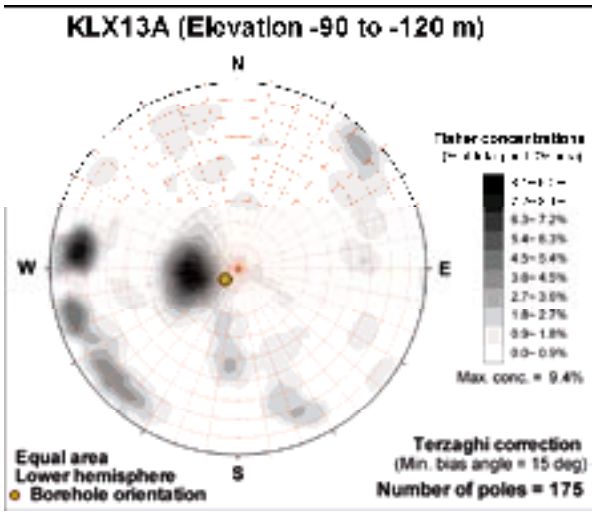
KLX13A (Elevation -90 to -120 m)
N
W
E
S
Max. conc. = 9.4%
Equal area
Lower hemisphere
Borehole orientation
Terzaghi correction
(Min. bias angle = 15 deg)
Number of poles = 175

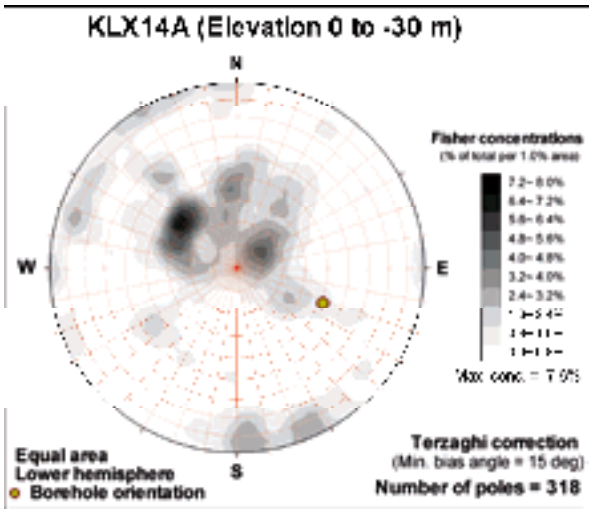
KLX14A (Elevation 0 to -30 m)
N
W
E
S
Fisher concentrations
(% of total per 1.0% area)
7.2–8.0%
6.4–7.2%
5.6–6.4%
4.8–5.6%
4.0–4.8%
3.2–4.0%
2.4–3.2%
Equal area
Lower hemisphere
Borehole orientation
Terzaghi correction
(Min. bias angle = 15 deg)
Number of poles = 318

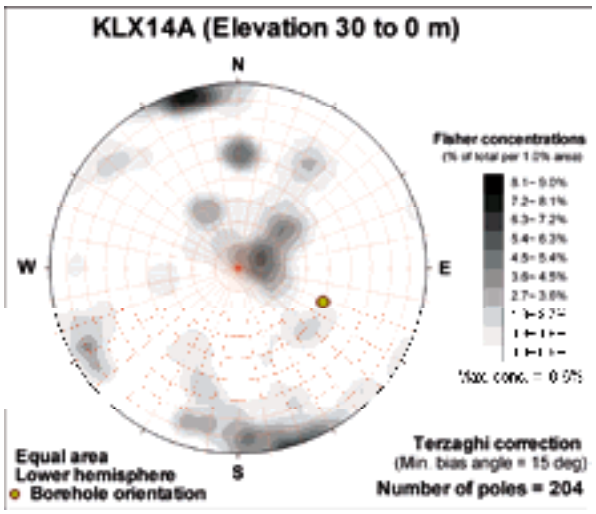
KLX14A (Elevation 30 to 0 m)
N
W
E
S
Fisher concentrations
Equal area
Lower hemisphere
Borehole orientation
Terzaghi correction
(Min. bias angle = 15 deg)
Number of poles = 204

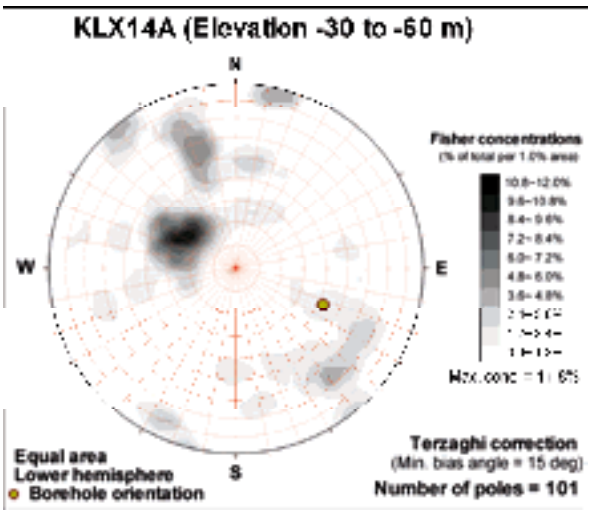
KLX14A (Elevation -30 to -60 m)
N
W
E
S
Fisher concentrations
Equal area
Lower hemisphere
Borehole orientation
Terzaghi correction
(Min. bias angle = 15 deg)
Number of poles = 101

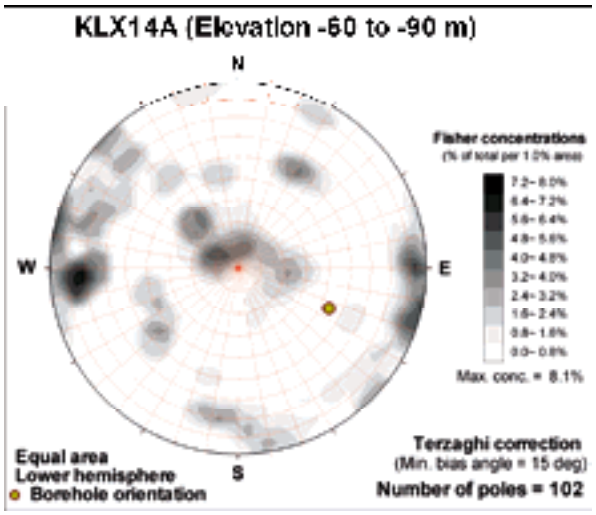
KLX14A (Elevation -60 to -90 m)
N
W
E
S
Fisher concentrations
Max. conc. = 8.1%
Equal area
Lower hemisphere
Borehole orientation
Terzaghi correction
(Min. bias angle = 15 deg)
Number of poles = 102

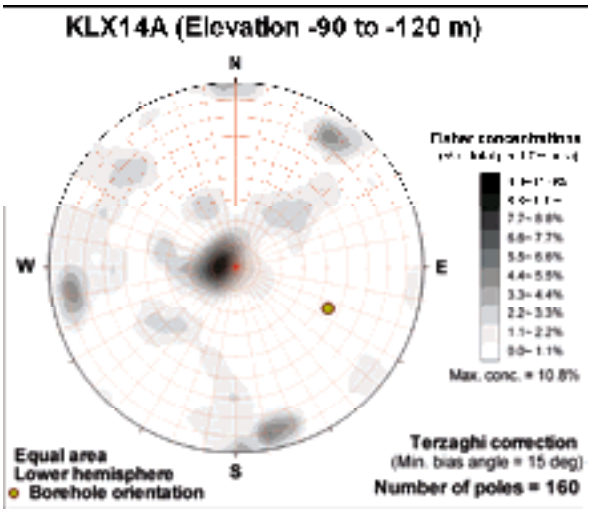
KLX14A (Elevation -90 to -120 m)
N
W
E
S
Max. conc. = 10.8%
Equal area
Lower hemisphere
Borehole orientation
Terzaghi correction
(Min. bias angle = 15 deg)
Number of poles = 160

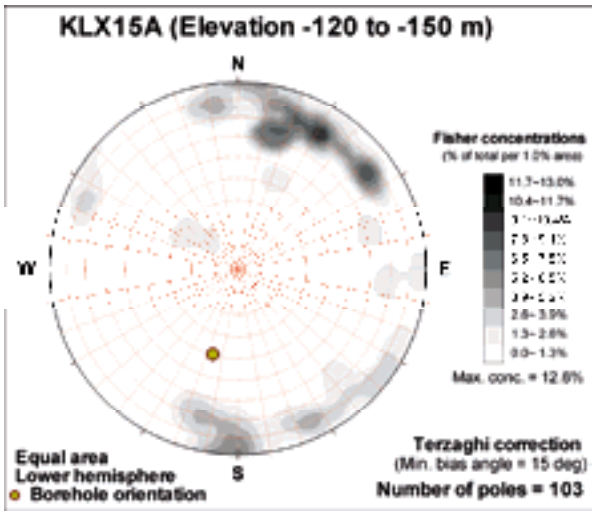
KLX15A (Elevation -120 to -150 m)
N
W
E
S
Fisher concentrations
Max. conc. = 12.8%
Equal area
Lower hemisphere
Borehole orientation
Terzaghi correction
(Min. bias angle = 15 deg)
Number of poles = 103

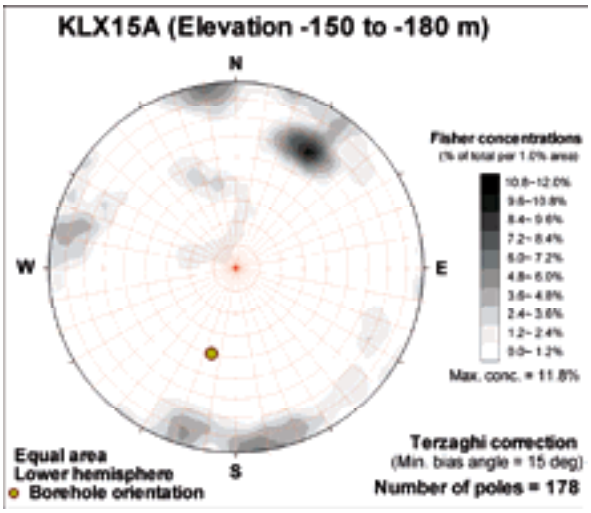
KLX15A (Elevation -150 to -180 m)
N
W
E
S
Fisher concentrations
Max. conc. = 11.8%
Equal area
Lower hemisphere
Borehole orientation
Terzaghi correction
(Min. bias angle = 15 deg)
Number of poles = 178

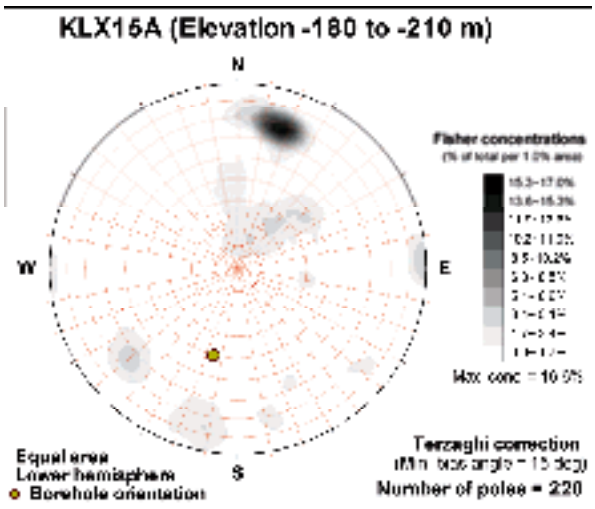
KLX15A (Elevation -180 to -210 m)
N
W
E
S
Fisher concentrations
Equal area
Lower hemisphere
Borehole orientation
Terzaghi correction
Number of poles = 220

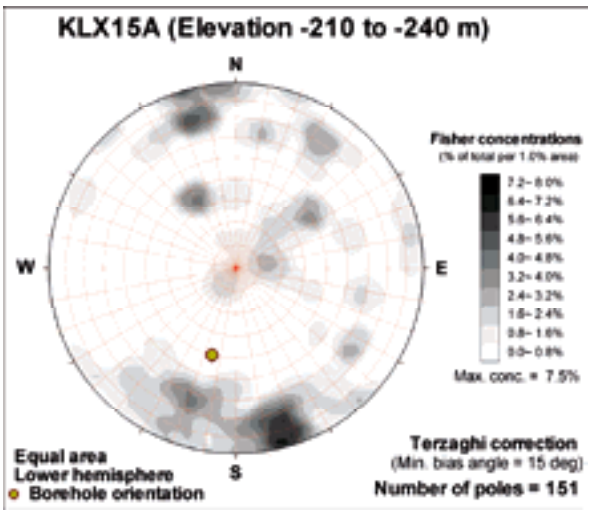
KLX15A (Elevation -210 to -240 m)
N
W
E
S
Fisher concentrations
Max. conc. = 7.5%
Equal area
Lower hemisphere
Borehole orientation
Terzaghi correction
(Min. bias angle = 15 deg)
Number of poles = 151

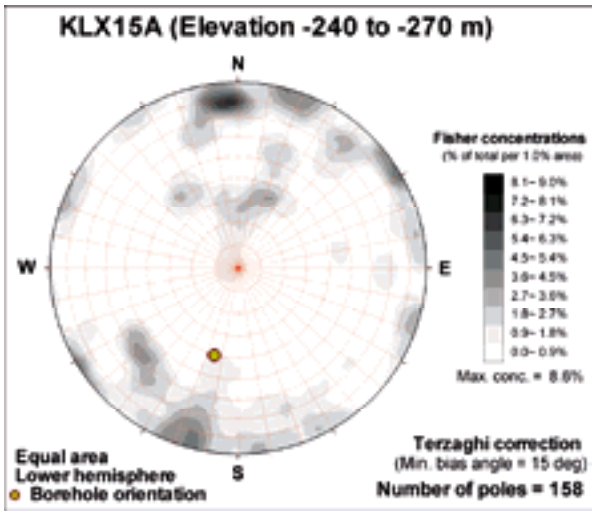
KLX15A (Elevation -240 to -270 m)
N
W
E
S
Fisher concentrations
Max. conc. = 8.6%
Equal area
Lower hemisphere
Borehole orientation
Terzaghi correction
(Min. bias angle = 15 deg)
Number of poles = 158

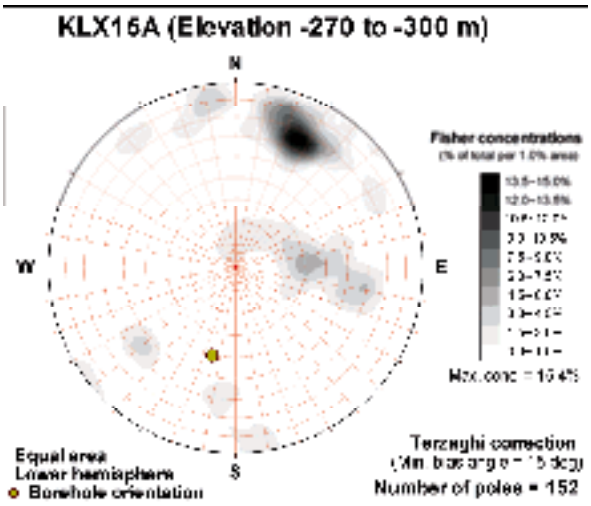
KLX15A (Elevation -270 to -300 m)
N
W
E
S
Fisher concentrations
Equal area
Lower hemisphere
Borehole orientation
Terzaghi correction
Number of poles = 152

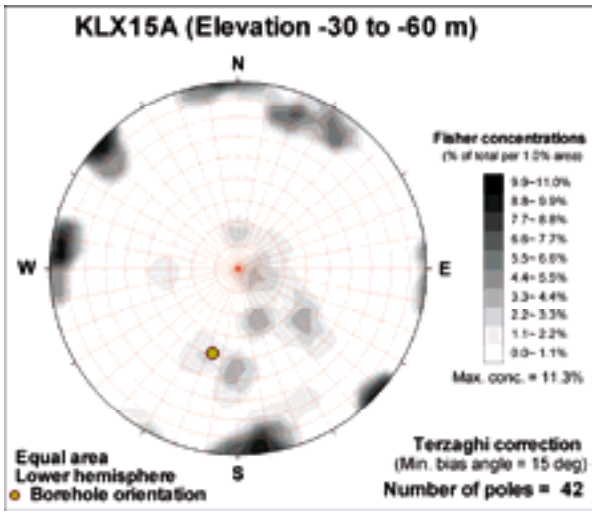
KLX15A (Elevation -30 to -60 m)
N
W
E
S
Fisher concentrations
Max. conc. = 11.3%
Equal area
Lower hemisphere
Borehole orientation
Terzaghi correction
(Min. bias angle = 15 deg)
Number of poles = 42

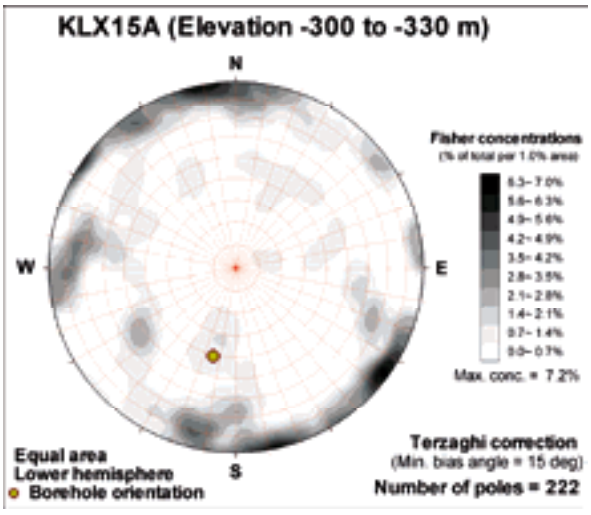
KLX15A (Elevation -300 to -330 m)
N
W
E
S
Fisher concentrations
Max. conc. = 7.2%
Equal area
Lower hemisphere
Borehole orientation
Terzaghi correction
(Min. bias angle = 15 deg)
Number of poles = 222

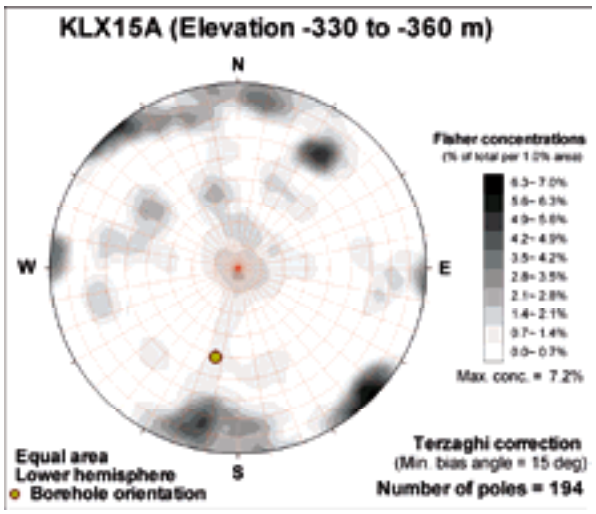
KLX15A (Elevation -330 to -360 m)
N
W
E
S
Fisher concentrations
(% of total per 1.0% area)
6.3– 7.0%
5.6– 6.3%
4.9– 5.6%
4.2– 4.9%
3.5– 4.2%
2.8– 3.5%
2.1– 2.8%
1.4– 2.1%
0.7– 1.4%
0.0– 0.7%
Max. conc. = 7.2%
Equal area
Lower hemisphere
Borehole orientation
Terzaghi correction
(Min. bias angle = 15 deg)
Number of poles = 194

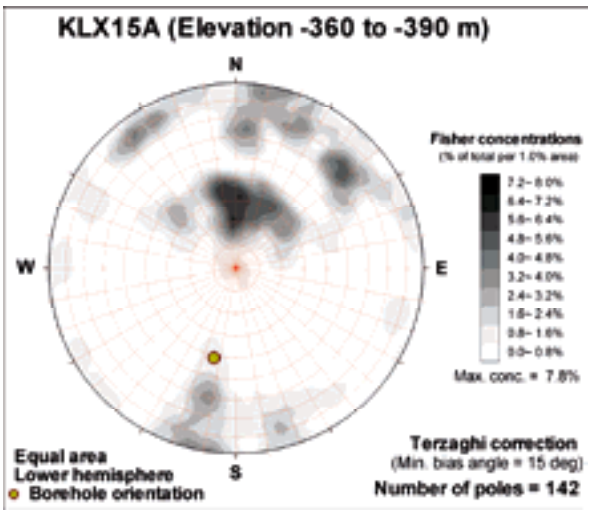
KLX15A (Elevation -360 to -390 m)
N
W
E
S
Fisher concentrations
(% of total per 1.0% area)
7.2– 8.0%
6.4– 7.2%
5.6– 6.4%
4.8– 5.6%
4.0– 4.8%
3.2– 4.0%
2.4– 3.2%
1.6– 2.4%
0.8– 1.6%
0.0– 0.8%
Max. conc. = 7.8%
Equal area
Lower hemisphere
Borehole orientation
Terzaghi correction
(Min. bias angle = 15 deg)
Number of poles = 142

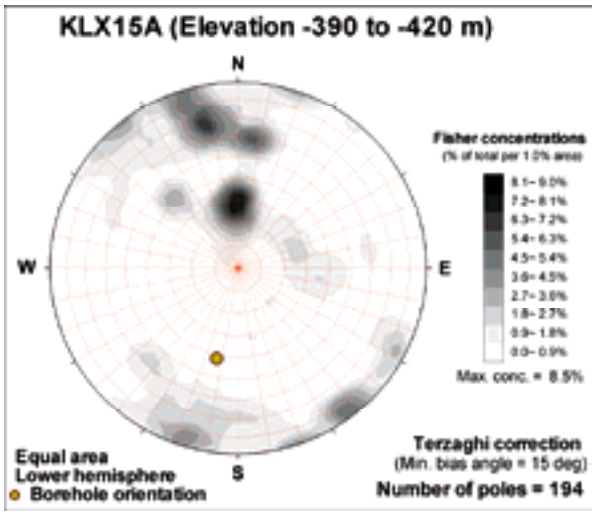
KLX15A (Elevation -390 to -420 m)
N
W
E
S
Fisher concentrations
(% of total per 1.0% area)
8.1– 9.0%
7.2– 8.1%
6.3– 7.2%
5.4– 6.3%
4.5– 5.4%
3.6– 4.5%
2.7– 3.6%
1.8– 2.7%
0.9– 1.8%
0.0– 0.9%
Max. conc. = 8.5%
Equal area
Lower hemisphere
Borehole orientation
Terzaghi correction
(Min. bias angle = 15 deg)
Number of poles = 194

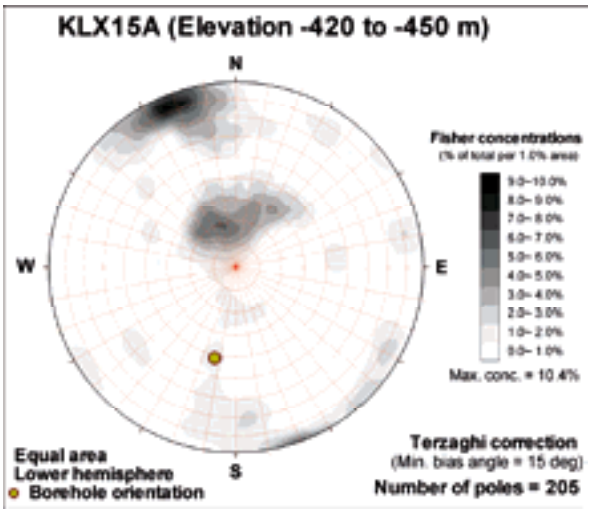
KLX15A (Elevation -420 to -450 m)
N
W
E
S
Fisher concentrations
(% of total per 1.0% area)
9.0–10.0%
8.0– 9.0%
7.0– 8.0%
6.0– 7.0%
5.0– 6.0%
4.0– 5.0%
3.0– 4.0%
2.0– 3.0%
1.0– 2.0%
0.0– 1.0%
Max. conc. = 10.4%
Equal area
Lower hemisphere
Borehole orientation
Terzaghi correction
(Min. bias angle = 15 deg)
Number of poles = 205

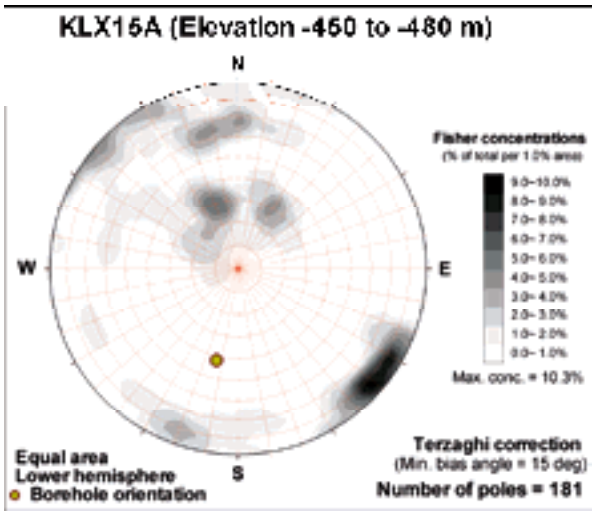
KLX15A (Elevation -450 to -480 m)
N
W
E
S
Fisher concentrations
(% of total per 1.0% area)
9.0–10.0%
8.0– 9.0%
7.0– 8.0%
6.0– 7.0%
5.0– 6.0%
4.0– 5.0%
3.0– 4.0%
2.0– 3.0%
1.0– 2.0%
0.0– 1.0%
Max. conc. = 10.3%
Equal area
Lower hemisphere
Borehole orientation
Terzaghi correction
(Min. bias angle = 15 deg)
Number of poles = 181

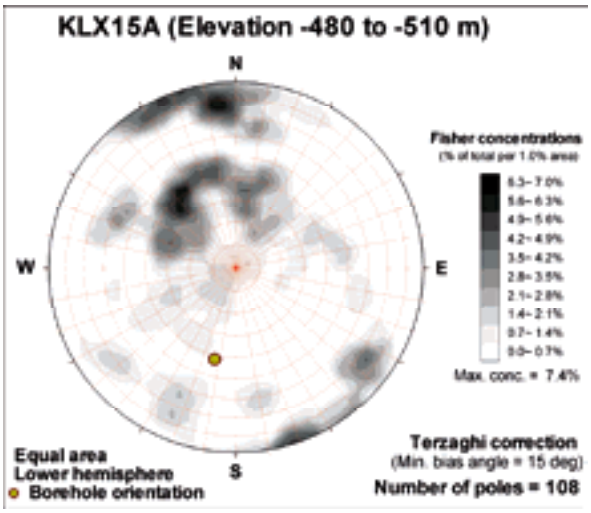
KLX15A (Elevation -480 to -510 m)
N
W
E
S
Fisher concentrations
(% of total per 1.0% area)
6.3– 7.0%
5.6– 6.3%
4.9– 5.6%
4.2– 4.9%
3.5– 4.2%
2.8– 3.5%
2.1– 2.8%
1.4– 2.1%
0.7– 1.4%
0.0– 0.7%
Max. conc. = 7.4%
Equal area
Lower hemisphere
Borehole orientation
Terzaghi correction
(Min. bias angle = 15 deg)
Number of poles = 108

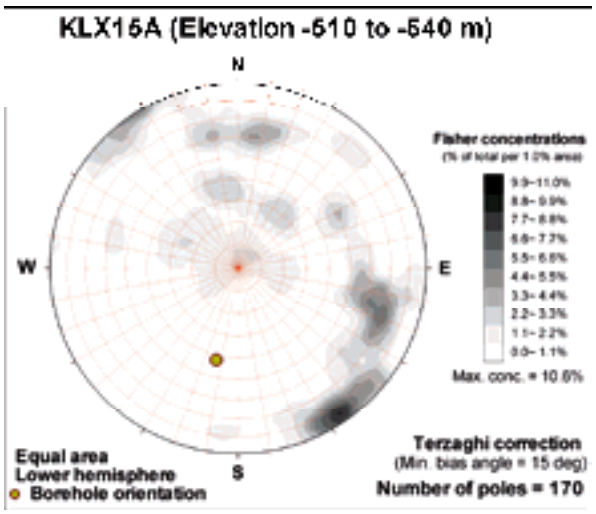
KLX15A (Elevation -510 to -540 m)
N
W
E
S
Fisher concentrations
(% of total per 1.0% area)
9.9–11.0%
8.8–9.9%
7.7–8.8%
6.6–7.7%
5.5–6.6%
4.4–5.5%
3.3–4.4%
2.2–3.3%
1.1–2.2%
0.0–1.1%
Max. conc. = 10.6%
Equal area
Lower hemisphere
Borehole orientation
Terzaghi correction
(Min. bias angle = 15 deg)
Number of poles = 170

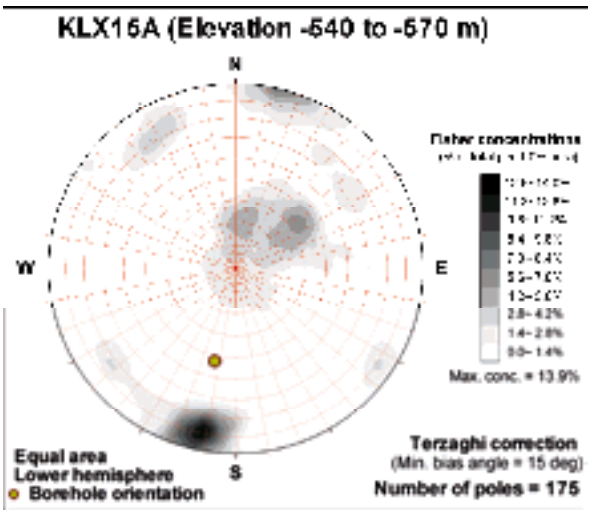
KLX15A (Elevation -540 to -570 m)
N
W
E
S
Max. conc. = 13.9%
Equal area
Lower hemisphere
Borehole orientation
Terzaghi correction
(Min. bias angle = 15 deg)
Number of poles = 175

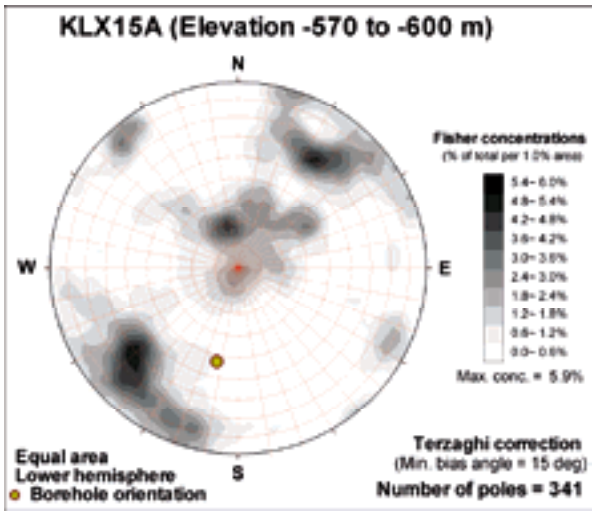
KLX15A (Elevation -570 to -600 m)
N
W
E
S
Fisher concentrations
(% of total per 1.0% area)
5.4–6.0%
4.8–5.4%
4.2–4.8%
3.6–4.2%
3.0–3.6%
2.4–3.0%
1.8–2.4%
1.2–1.8%
0.6–1.2%
0.0–0.6%
Max. conc. = 5.9%
Equal area
Lower hemisphere
Borehole orientation
Terzaghi correction
(Min. bias angle = 15 deg)
Number of poles = 341

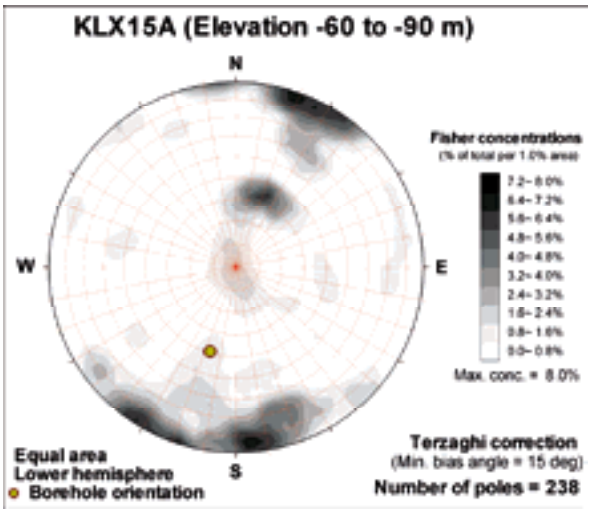
KLX15A (Elevation -60 to -90 m)
N
W
E
S
Fisher concentrations
(% of total per 1.0% area)
7.2–8.0%
6.4–7.2%
5.6–6.4%
4.8–5.6%
4.0–4.8%
3.2–4.0%
2.4–3.2%
1.6–2.4%
0.8–1.6%
0.0–0.8%
Max. conc. = 8.0%
Equal area
Lower hemisphere
Borehole orientation
Terzaghi correction
(Min. bias angle = 15 deg)
Number of poles = 238

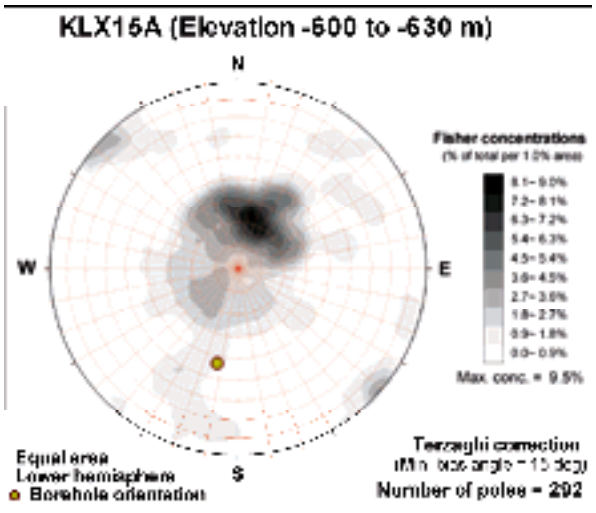
KLX15A (Elevation -600 to -630 m)
N
W
E
S
Fisher concentrations
(% of total per 1.0% area)
8.1–9.0%
7.2–8.1%
6.3–7.2%
5.4–6.3%
4.5–5.4%
3.6–4.5%
2.7–3.6%
1.8–2.7%
0.9–1.8%
0.0–0.9%
Max. conc. = 9.5%
Equal area
Lower hemisphere
Borehole orientation
Terzaghi correction
(Min. bias angle = 15 deg)
Number of poles = 292

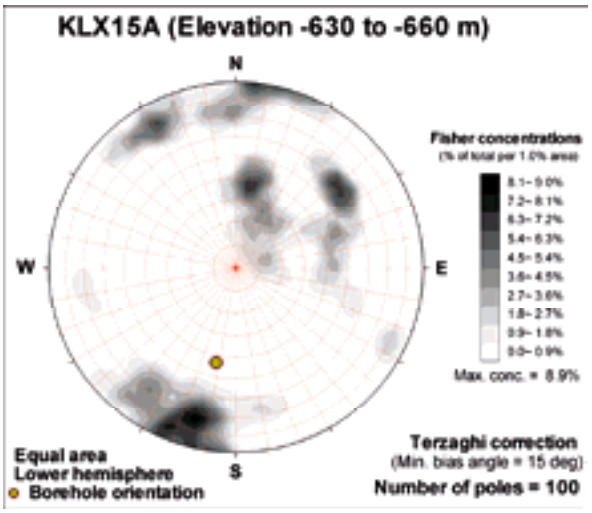
KLX15A (Elevation -630 to -660 m)
N
W
E
S
Fisher concentrations
(% of total per 1.0% area)
8.1–9.0%
7.2–8.1%
6.3–7.2%
5.4–6.3%
4.5–5.4%
3.6–4.5%
2.7–3.6%
1.8–2.7%
0.9–1.8%
0.0–0.9%
Max. conc. = 8.9%
Equal area
Lower hemisphere
Borehole orientation
Terzaghi correction
(Min. bias angle = 15 deg)
Number of poles = 100

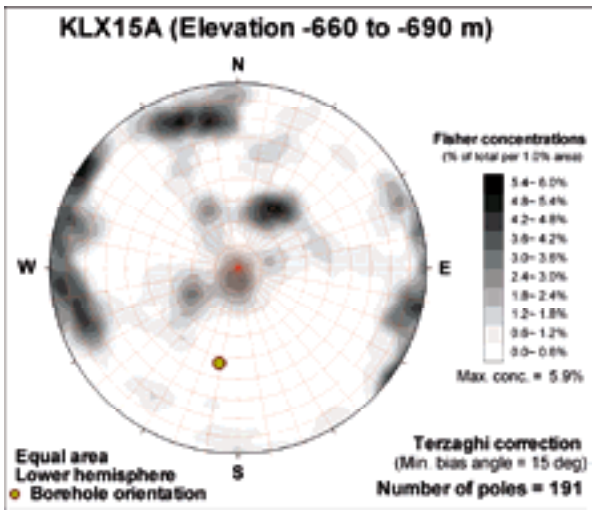
KLX15A (Elevation -660 to -690 m)
N
W
E
S
Fisher concentrations
(% of total per 1.0% area)
Max. conc. = 5.9%
Equal area
Lower hemisphere
Borehole orientation
Terzaghi correction
(Min. bias angle = 15 deg)
Number of poles = 191

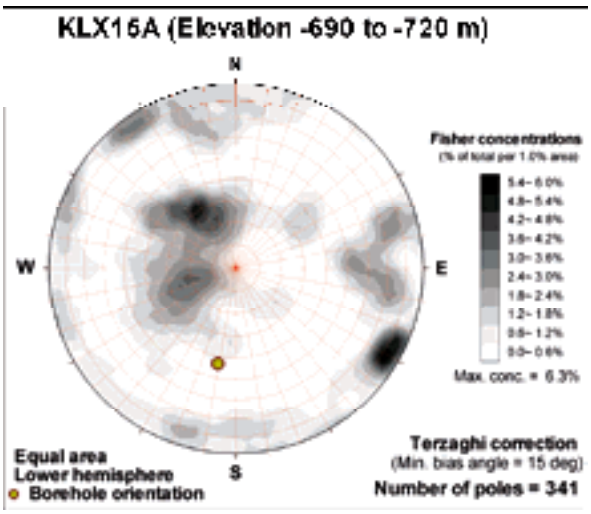
KLX15A (Elevation -690 to -720 m)
N
W
E
S
Fisher concentrations
(% of total per 1.0% area)
Max. conc. = 6.3%
Equal area
Lower hemisphere
Borehole orientation
Terzaghi correction
(Min. bias angle = 15 deg)
Number of poles = 341

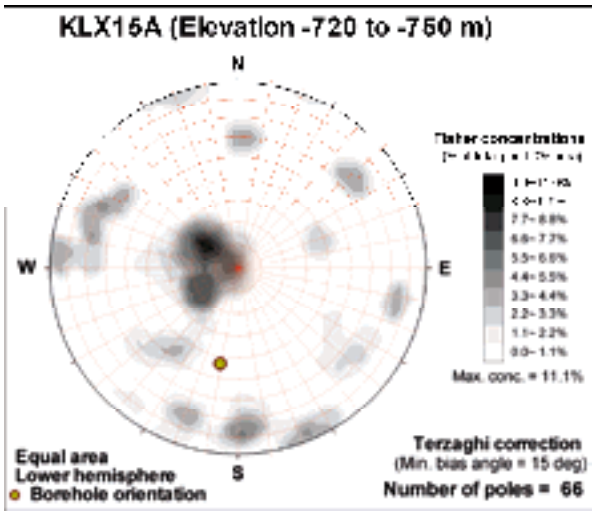
KLX15A (Elevation -720 to -750 m)
N
W
E
S
Max. conc. = 11.1%
Equal area
Lower hemisphere
Borehole orientation
Terzaghi correction
(Min. bias angle = 15 deg)
Number of poles = 66

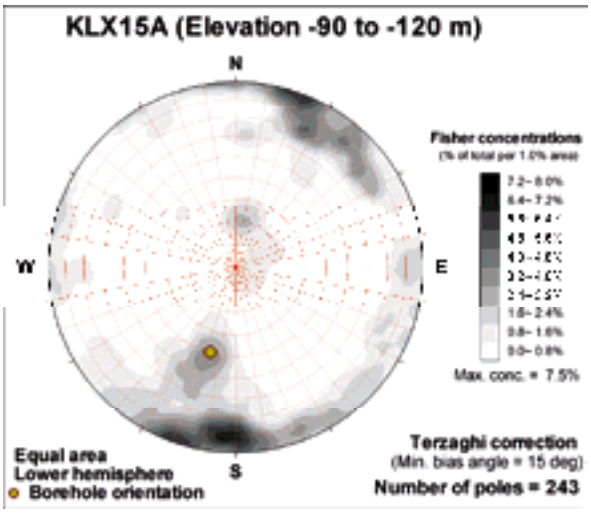
KLX15A (Elevation -90 to -120 m)
N
W
E
S
Fisher concentrations
(% of total per 1.0% area)
Max. conc. = 7.5%
Equal area
Lower hemisphere
Borehole orientation
Terzaghi correction
(Min. bias angle = 15 deg)
Number of poles = 243

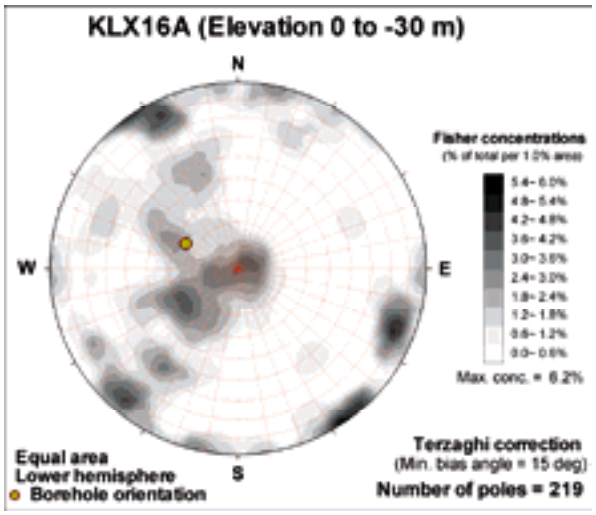
KLX16A (Elevation 0 to -30 m)
N
W
E
S
Fisher concentrations
(% of total per 1.0% area)
Max. conc. = 6.2%
Equal area
Lower hemisphere
Borehole orientation
Terzaghi correction
(Min. bias angle = 15 deg)
Number of poles = 219

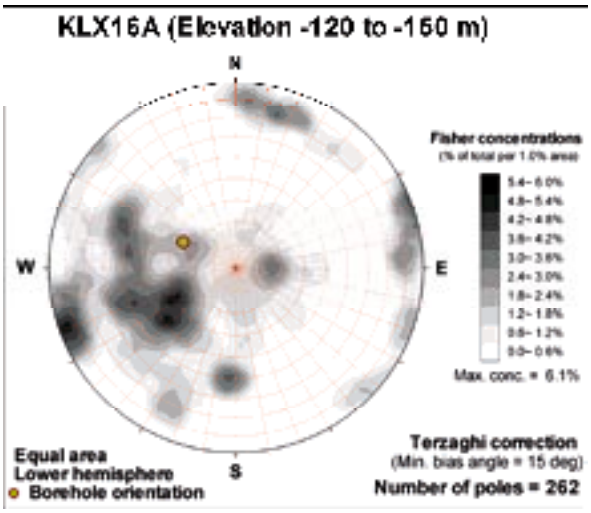
KLX16A (Elevation -120 to -150 m)
N
W
E
S
Fisher concentrations
(% of total per 1.0% area)
Max. conc. = 6.1%
Equal area
Lower hemisphere
Borehole orientation
Terzaghi correction
(Min. bias angle = 15 deg)
Number of poles = 262

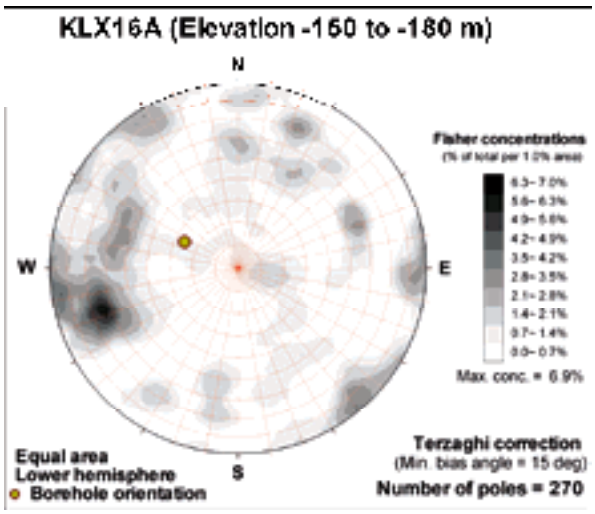
KLX16A (Elevation -150 to -180 m)
N
W
E
S
Fisher concentrations
(% of total per 1.0% area)
6.3–7.0%
5.6–6.3%
4.9–5.6%
4.2–4.9%
3.5–4.2%
2.8–3.5%
2.1–2.8%
1.4–2.1%
0.7–1.4%
0.0–0.7%
Max. conc. = 6.9%
Equal area
Lower hemisphere
Borehole orientation
Terzaghi correction
(Min. bias angle = 15 deg)
Number of poles = 270

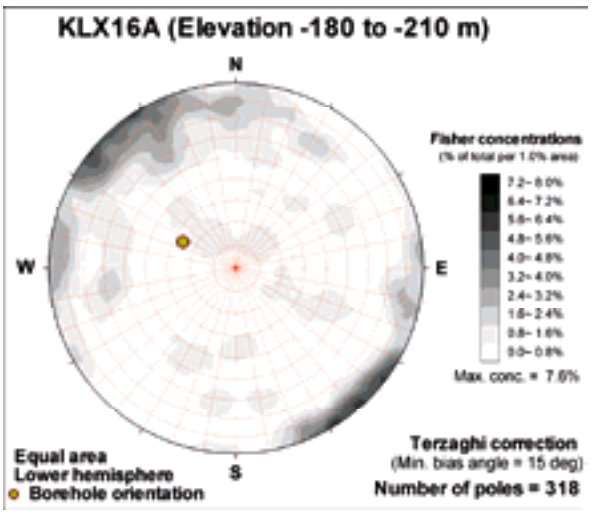
KLX16A (Elevation -180 to -210 m)
N
W
E
S
Fisher concentrations
(% of total per 1.0% area)
7.2–8.0%
6.4–7.2%
5.6–6.4%
4.8–5.6%
4.0–4.8%
3.2–4.0%
2.4–3.2%
1.6–2.4%
0.8–1.6%
0.0–0.8%
Max. conc. = 7.6%
Equal area
Lower hemisphere
Borehole orientation
Terzaghi correction
(Min. bias angle = 15 deg)
Number of poles = 318

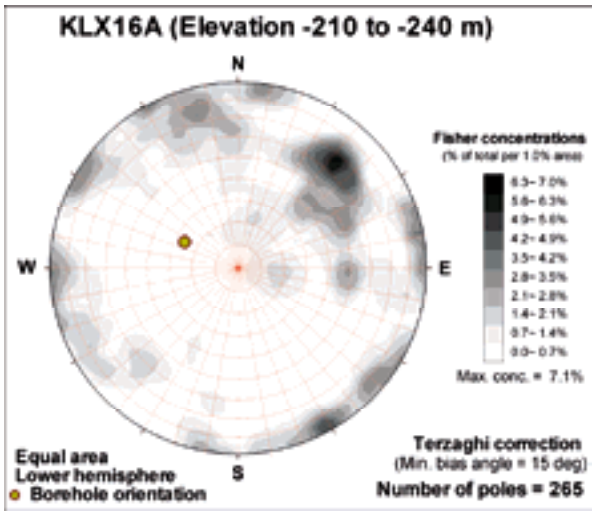
KLX16A (Elevation -210 to -240 m)
N
W
E
S
Fisher concentrations
(% of total per 1.0% area)
6.3–7.0%
5.6–6.3%
4.9–5.6%
4.2–4.9%
3.5–4.2%
2.8–3.5%
2.1–2.8%
1.4–2.1%
0.7–1.4%
0.0–0.7%
Max. conc. = 7.1%
Equal area
Lower hemisphere
Borehole orientation
Terzaghi correction
(Min. bias angle = 15 deg)
Number of poles = 265

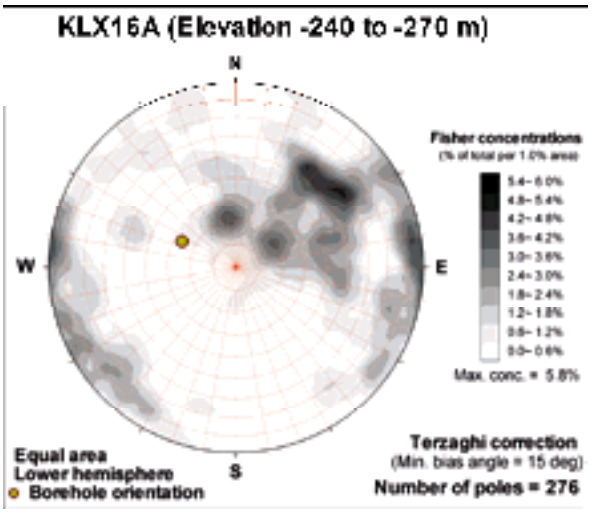
KLX16A (Elevation -240 to -270 m)
N
W
E
S
Fisher concentrations
(% of total per 1.0% area)
5.4–6.0%
4.8–5.4%
4.2–4.8%
3.6–4.2%
3.0–3.6%
2.4–3.0%
1.8–2.4%
1.2–1.8%
0.6–1.2%
0.0–0.6%
Max. conc. = 5.8%
Equal area
Lower hemisphere
Borehole orientation
Terzaghi correction
(Min. bias angle = 15 deg)
Number of poles = 276

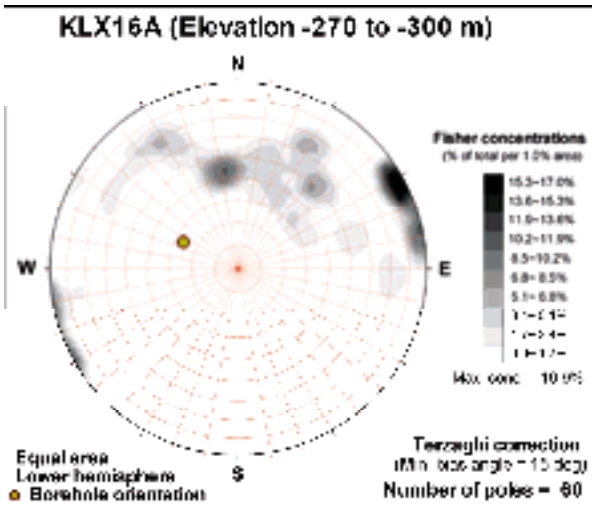
KLX16A (Elevation -270 to -300 m)
N
W
E
S
Fisher concentrations
(% of total per 1.0% area)
15.3–17.0%
13.6–15.3%
11.9–13.6%
10.2–11.9%
8.5–10.2%
6.8–8.5%
5.1–6.8%
Equal area
Lower hemisphere
Borehole orientation
Number of poles = 80

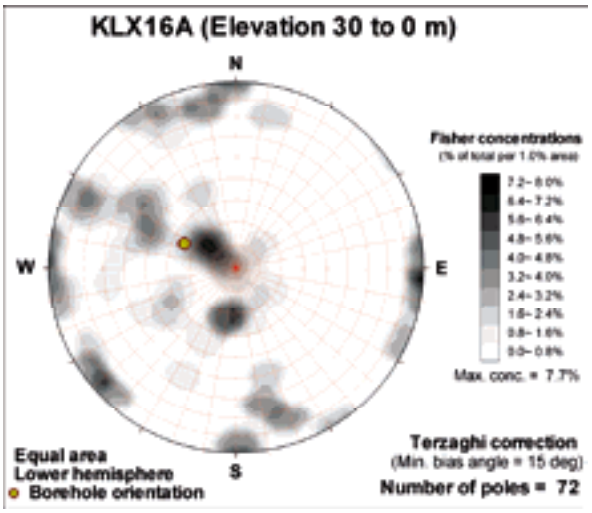
KLX16A (Elevation 30 to 0 m)
N
W
E
S
Fisher concentrations
(% of total per 1.0% area)
7.2–8.0%
6.4–7.2%
5.6–6.4%
4.8–5.6%
4.0–4.8%
3.2–4.0%
2.4–3.2%
1.6–2.4%
0.8–1.6%
0.0–0.8%
Max. conc. = 7.7%
Equal area
Lower hemisphere
Borehole orientation
Terzaghi correction
(Min. bias angle = 15 deg)
Number of poles = 72

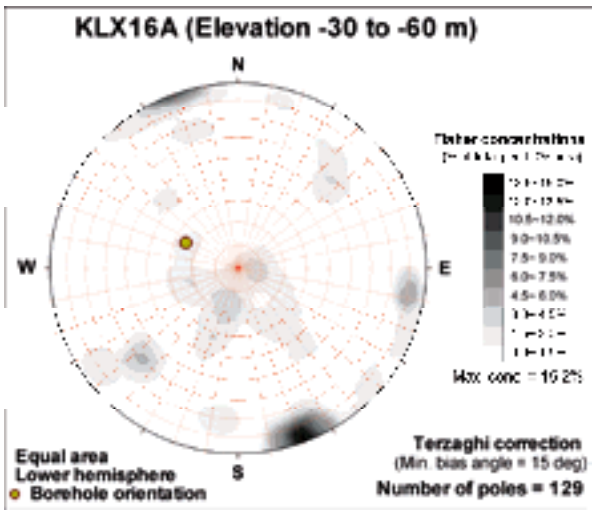
KLX16A (Elevation -30 to -60 m)
N
W
E
S
Fisher concentrations
Max. conc. = 10.2%
Equal area
Lower hemisphere
Borehole orientation
Terzaghi correction
(Min. bias angle = 15 deg)
Number of poles = 129

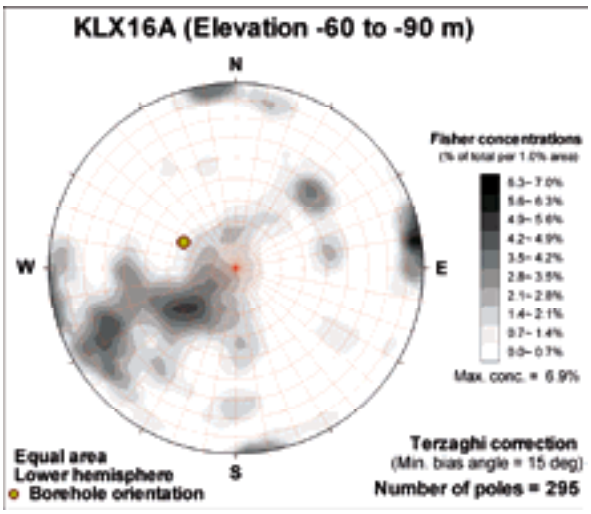
KLX16A (Elevation -60 to -90 m)
N
W
E
S
Fisher concentrations
Max. conc. = 6.9%
Equal area
Lower hemisphere
Borehole orientation
Terzaghi correction
(Min. bias angle = 15 deg)
Number of poles = 295

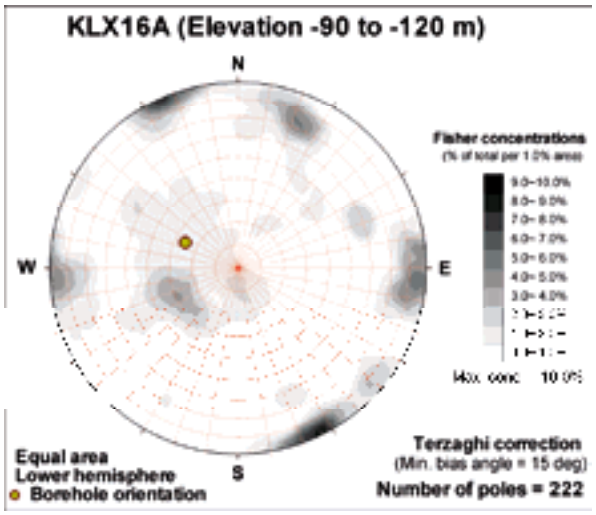
KLX16A (Elevation -90 to -120 m)
N
W
E
S
Fisher concentrations
Equal area
Lower hemisphere
Borehole orientation
Terzaghi correction
(Min. bias angle = 15 deg)
Number of poles = 222

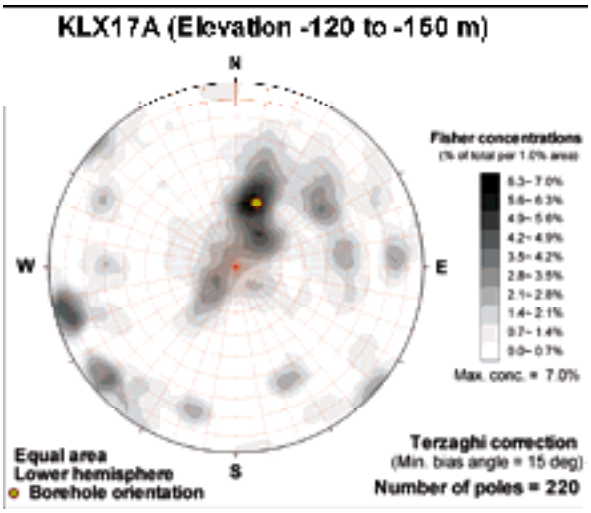
KLX17A (Elevation -120 to -150 m)
N
W
E
S
Fisher concentrations
Max. conc. = 7.0%
Equal area
Lower hemisphere
Borehole orientation
Terzaghi correction
(Min. bias angle = 15 deg)
Number of poles = 220

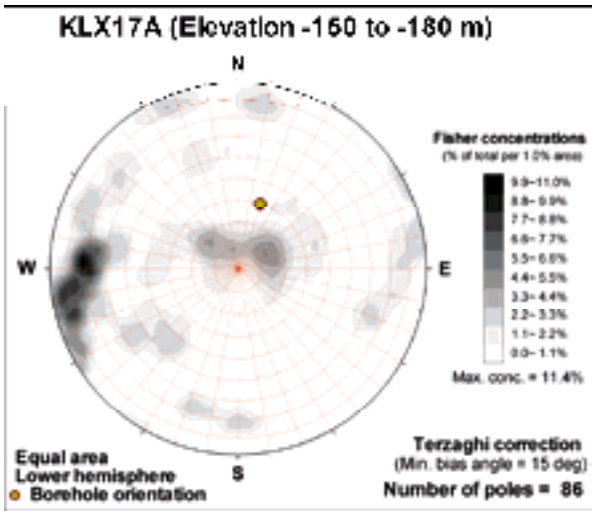
KLX17A (Elevation -150 to -180 m)
N
W
E
S
Fisher concentrations
Max. conc. = 11.4%
Equal area
Lower hemisphere
Borehole orientation
Terzaghi correction
(Min. bias angle = 15 deg)
Number of poles = 86

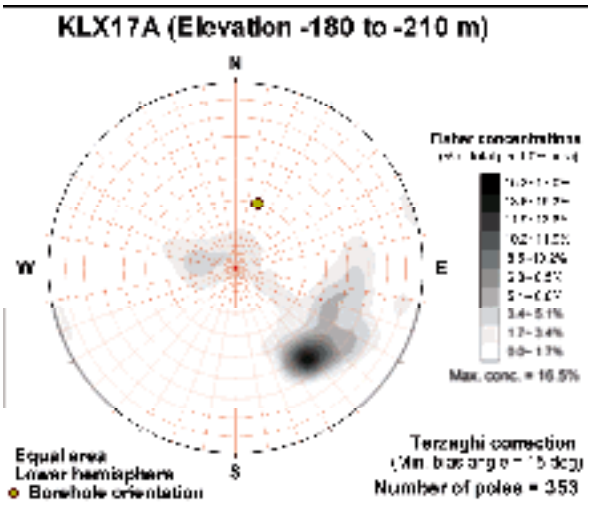
KLX17A (Elevation -180 to -210 m)
N
W
E
S
Max. conc. = 16.5%
Equal area
Lower hemisphere
Borehole orientation
Number of poles = 353

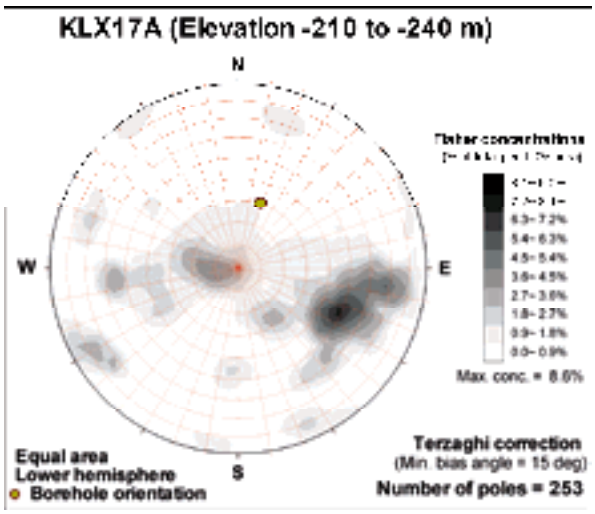
KLX17A (Elevation -210 to -240 m)
N
W
E
S
Fisher concentrations
Max. conc. = 8.6%
Equal area
Lower hemisphere
Borehole orientation
Terzaghi correction
(Min. bias angle = 15 deg)
Number of poles = 253

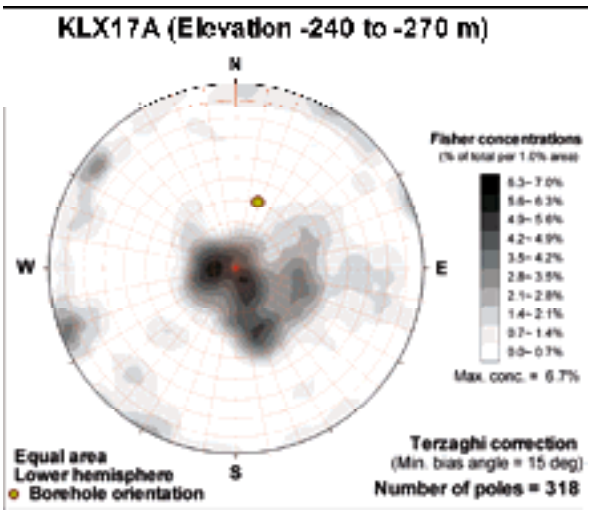
KLX17A (Elevation -240 to -270 m)
N
W
E
S
Fisher concentrations
Max. conc. = 6.7%
Equal area
Lower hemisphere
Borehole orientation
Terzaghi correction
(Min. bias angle = 15 deg)
Number of poles = 318

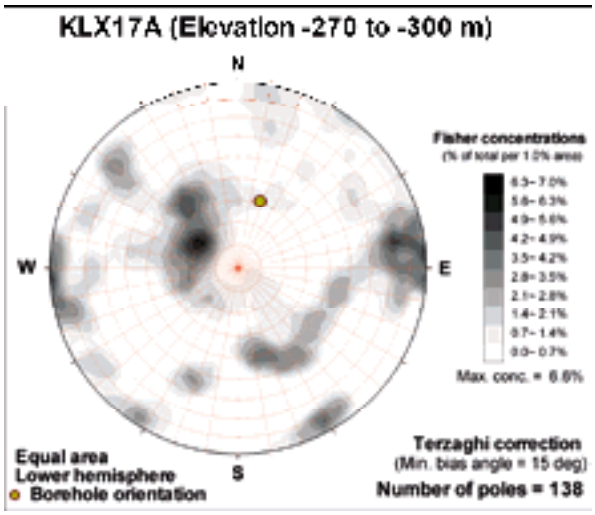
KLX17A (Elevation -270 to -300 m)
N
W
E
S
Fisher concentrations
Max. conc. = 6.6%
Equal area
Lower hemisphere
Borehole orientation
Terzaghi correction
(Min. bias angle = 15 deg)
Number of poles = 138

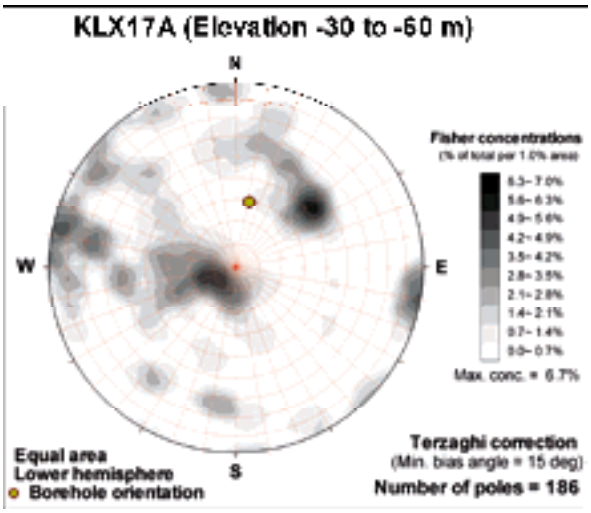
KLX17A (Elevation -30 to -60 m)
N
W
E
S
Fisher concentrations
Max. conc. = 6.7%
Equal area
Lower hemisphere
Borehole orientation
Terzaghi correction
(Min. bias angle = 15 deg)
Number of poles = 186

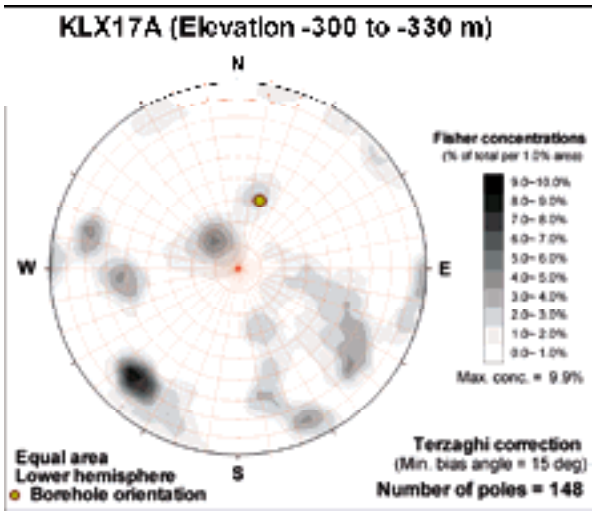
KLX17A (Elevation -300 to -330 m)
N
W
E
S
Fisher concentrations
Max. conc. = 9.9%
Equal area
Lower hemisphere
Borehole orientation
Terzaghi correction
(Min. bias angle = 15 deg)
Number of poles = 148

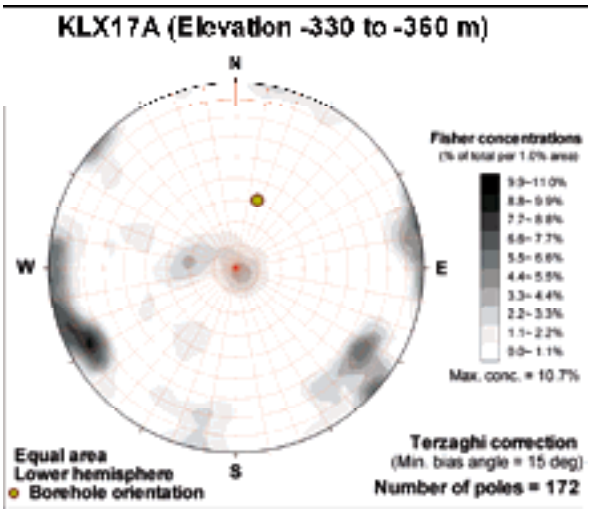
KLX17A (Elevation -330 to -360 m)
N
W
E
S
Fisher concentrations
Max. conc. = 10.7%
Equal area
Lower hemisphere
Borehole orientation
Terzaghi correction
(Min. bias angle = 15 deg)
Number of poles = 172

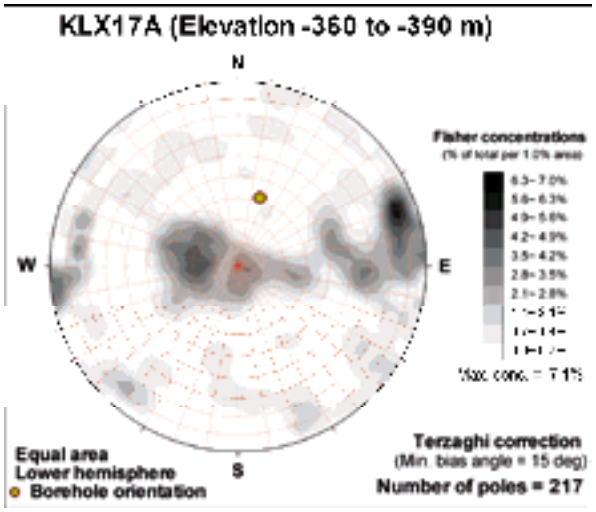
KLX17A (Elevation -360 to -390 m)
N
W
E
S
Fisher concentrations
Equal area
Lower hemisphere
Borehole orientation
Terzaghi correction
(Min. bias angle = 15 deg)
Number of poles = 217

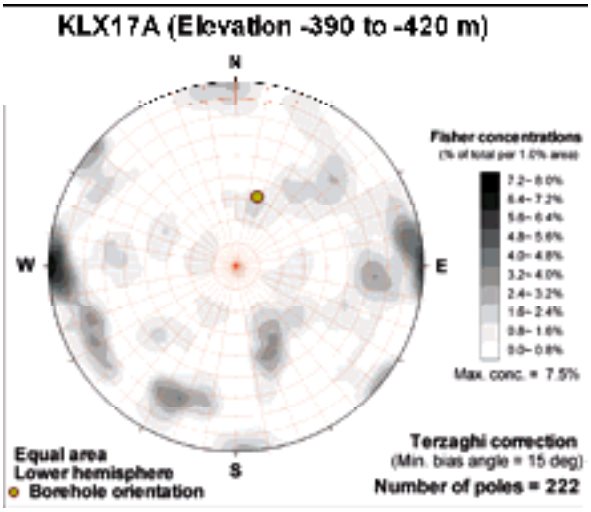
KLX17A (Elevation -390 to -420 m)
N
W
E
S
Fisher concentrations
Max. conc. = 7.5%
Equal area
Lower hemisphere
Borehole orientation
Terzaghi correction
(Min. bias angle = 15 deg)
Number of poles = 222

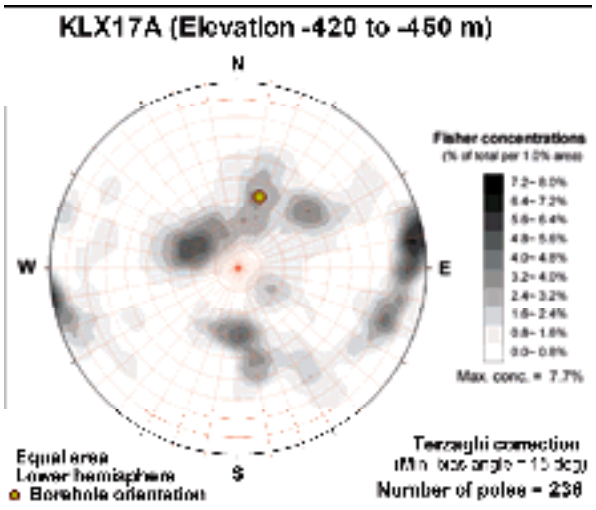
KLX17A (Elevation -420 to -450 m)
N
W
E
S
Fisher concentrations
Max. conc. = 7.7%
Equal area
Lower hemisphere
Borehole orientation
Terzaghi correction
Number of poles = 238

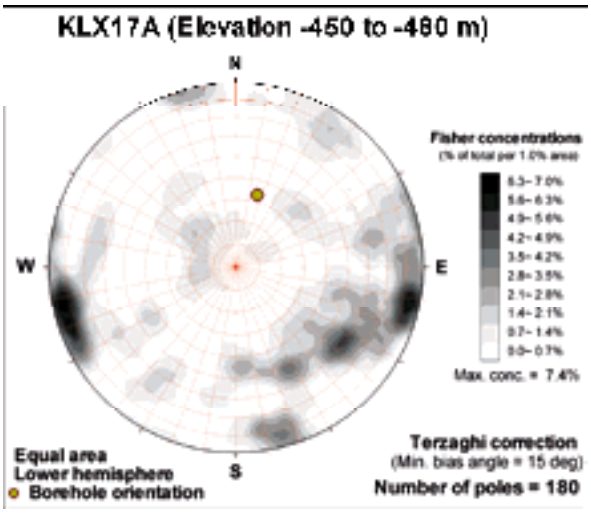
KLX17A (Elevation -450 to -480 m)
N
W
E
S
Fisher concentrations
Max. conc. = 7.4%
Equal area
Lower hemisphere
Borehole orientation
Terzaghi correction
(Min. bias angle = 15 deg)
Number of poles = 180

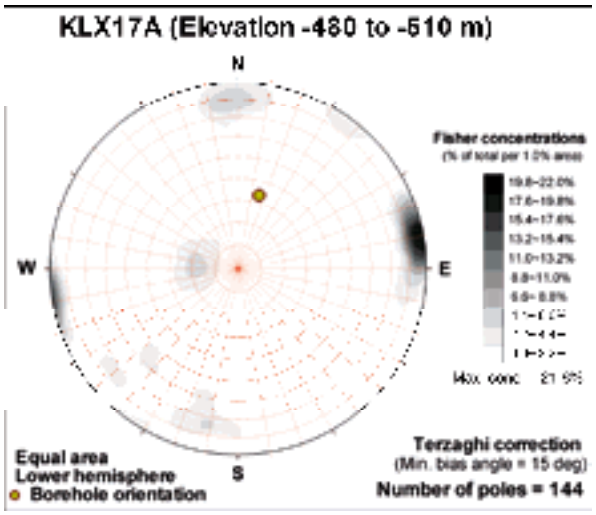
KLX17A (Elevation -480 to -510 m)
N
W
E
S
Fisher concentrations
Equal area
Lower hemisphere
Borehole orientation
Terzaghi correction
(Min. bias angle = 15 deg)
Number of poles = 144

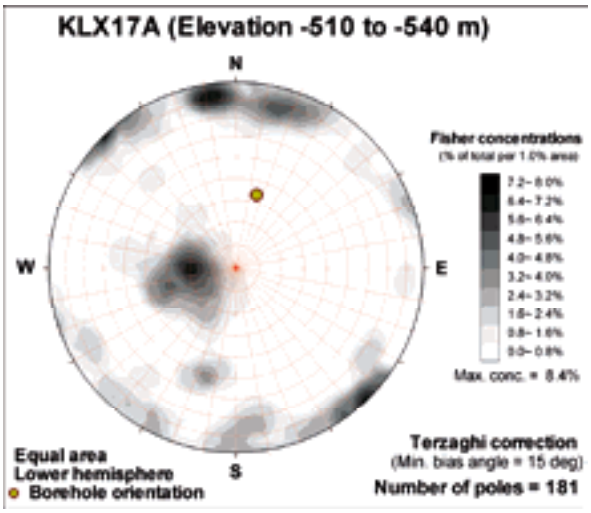
KLX17A (Elevation -510 to -540 m)
N
W
E
S
Fisher concentrations
Max. conc. = 8.4%
Equal area
Lower hemisphere
Borehole orientation
Terzaghi correction
(Min. bias angle = 15 deg)
Number of poles = 181

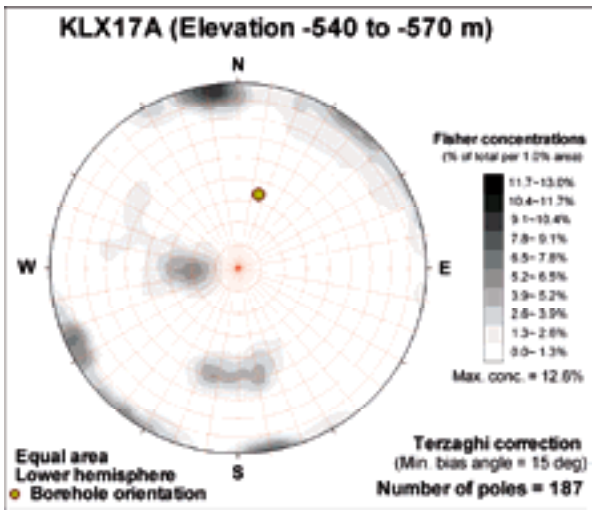
KLX17A (Elevation -540 to -570 m)
N
W
E
S
Fisher concentrations
(% of total per 1.0% area)
11.7–13.0%
10.4–11.7%
9.1–10.4%
7.8–9.1%
6.5–7.8%
5.2–6.5%
3.9–5.2%
2.6–3.9%
1.3–2.6%
0.0–1.3%
Max. conc. = 12.6%
Equal area
Lower hemisphere
Borehole orientation
Terzaghi correction
(Min. bias angle = 15 deg)
Number of poles = 187

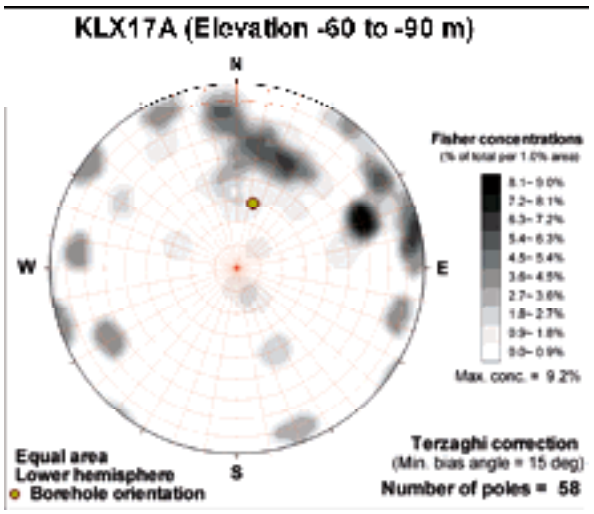
KLX17A (Elevation -60 to -90 m)
N
W
E
S
Fisher concentrations
(% of total per 1.0% area)
8.1–9.0%
7.2–8.1%
6.3–7.2%
5.4–6.3%
4.5–5.4%
3.6–4.5%
2.7–3.6%
1.8–2.7%
0.9–1.8%
0.0–0.9%
Max. conc. = 9.2%
Equal area
Lower hemisphere
Borehole orientation
Terzaghi correction
(Min. bias angle = 15 deg)
Number of poles = 58

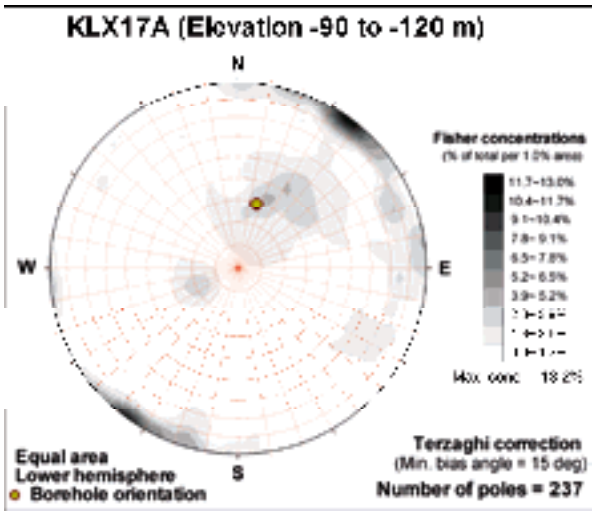
KLX17A (Elevation -90 to -120 m)
N
W
E
S
Fisher concentrations
(% of total per 1.0% area)
11.7–13.0%
10.4–11.7%
9.1–10.4%
7.8–9.1%
6.5–7.8%
5.2–6.5%
3.9–5.2%
Equal area
Lower hemisphere
Borehole orientation
Terzaghi correction
(Min. bias angle = 15 deg)
Number of poles = 237

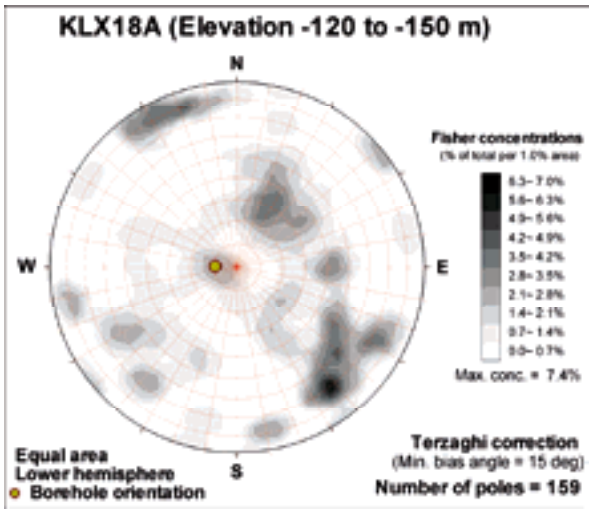
KLX18A (Elevation -120 to -150 m)
N
W
E
S
Fisher concentrations
(% of total per 1.0% area)
6.3–7.0%
5.6–6.3%
4.9–5.6%
4.2–4.9%
3.5–4.2%
2.8–3.5%
2.1–2.8%
1.4–2.1%
0.7–1.4%
0.0–0.7%
Max. conc. = 7.4%
Equal area
Lower hemisphere
Borehole orientation
Terzaghi correction
(Min. bias angle = 15 deg)
Number of poles = 159

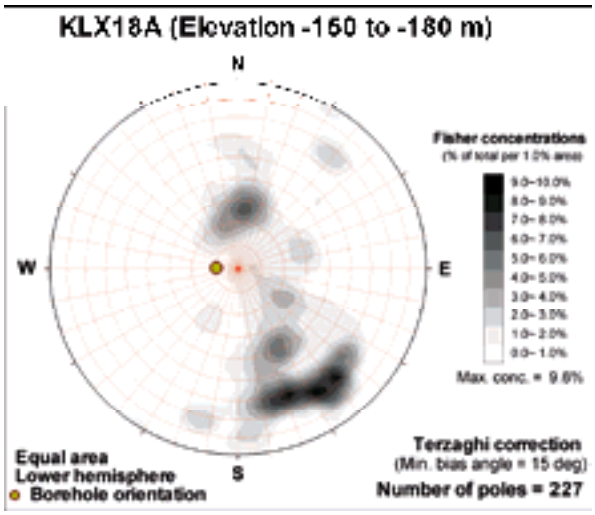
KLX18A (Elevation -150 to -180 m)
N
W
E
S
Fisher concentrations
(% of total per 1.0% area)
9.0–10.0%
8.0–9.0%
7.0–8.0%
6.0–7.0%
5.0–6.0%
4.0–5.0%
3.0–4.0%
2.0–3.0%
1.0–2.0%
0.0–1.0%
Max. conc. = 9.6%
Equal area
Lower hemisphere
Borehole orientation
Terzaghi correction
(Min. bias angle = 15 deg)
Number of poles = 227

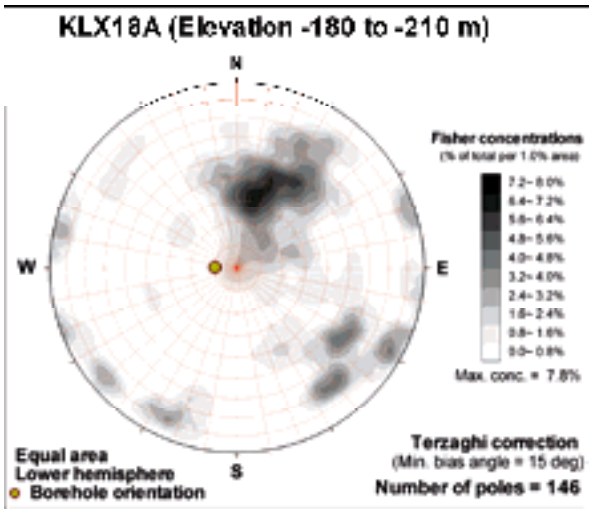
KLX18A (Elevation -180 to -210 m)
N
W
E
S
Fisher concentrations
(% of total per 1.0% area)
7.2–8.0%
6.4–7.2%
5.6–6.4%
4.8–5.6%
4.0–4.8%
3.2–4.0%
2.4–3.2%
1.6–2.4%
0.8–1.6%
0.0–0.8%
Max. conc. = 7.8%
Equal area
Lower hemisphere
Borehole orientation
Terzaghi correction
(Min. bias angle = 15 deg)
Number of poles = 146

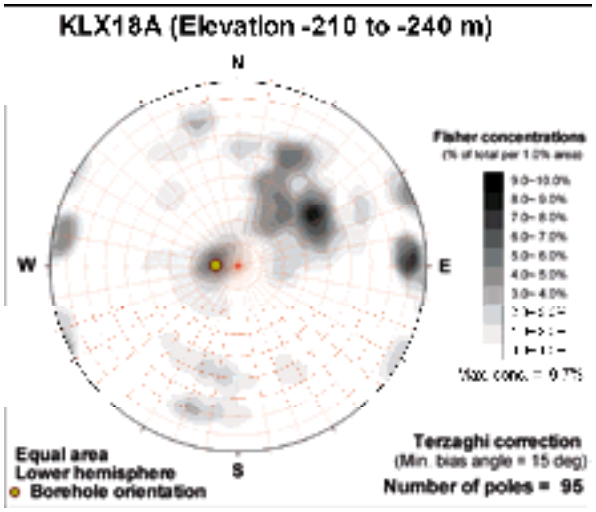
KLX18A (Elevation -210 to -240 m)
N
W
E
S
Fisher concentrations
(% of total per 1.0% area)
Max. conc. = 9.7%
Equal area
Lower hemisphere
Borehole orientation
Terzaghi correction
(Min. bias angle = 15 deg)
Number of poles = 95

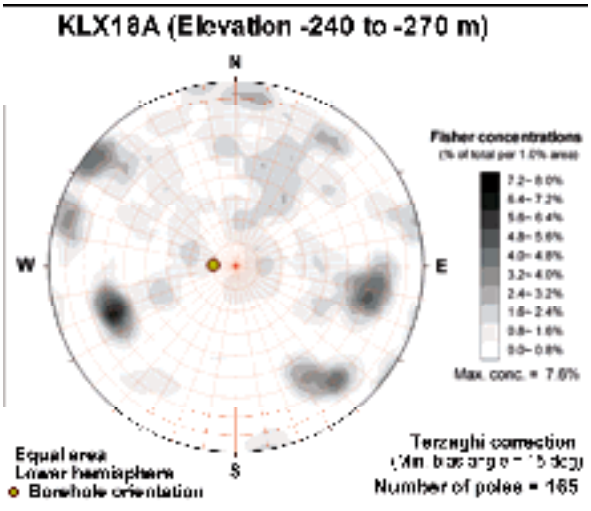
KLX18A (Elevation -240 to -270 m)
N
W
E
S
Fisher concentrations
(% of total per 1.0% area)
Max. conc. = 7.6%
Equal area
Lower hemisphere
Borehole orientation
Terzaghi correction
Number of poles = 165

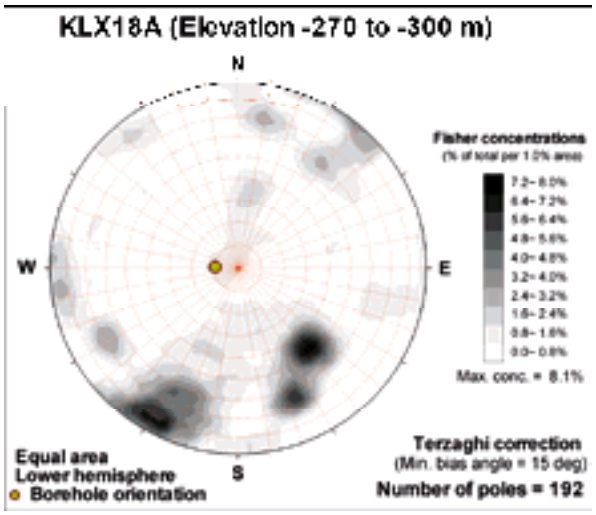
KLX18A (Elevation -270 to -300 m)
N
W
E
S
Fisher concentrations
(% of total per 1.0% area)
Max. conc. = 8.1%
Equal area
Lower hemisphere
Borehole orientation
Terzaghi correction
(Min. bias angle = 15 deg)
Number of poles = 192

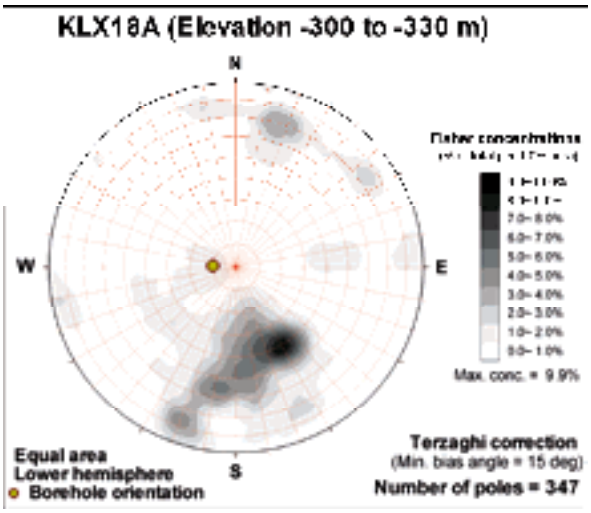
KLX18A (Elevation -300 to -330 m)
N
W
E
S
Max. conc. = 9.9%
Equal area
Lower hemisphere
Borehole orientation
Terzaghi correction
(Min. bias angle = 15 deg)
Number of poles = 347

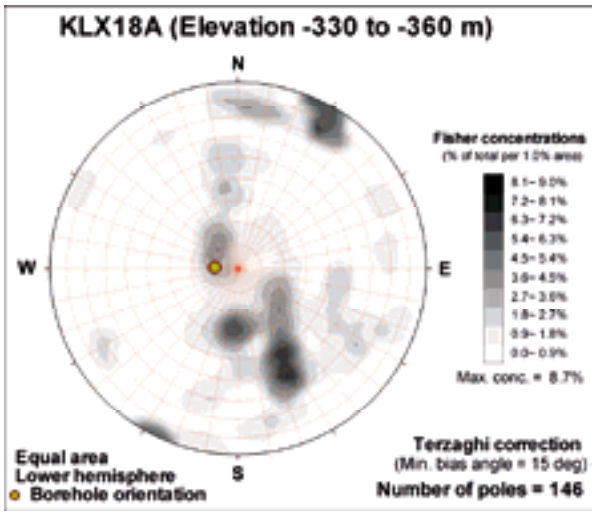
KLX18A (Elevation -330 to -360 m)
N
W
E
S
Fisher concentrations
(% of total per 1.0% area)
Max. conc. = 8.7%
Equal area
Lower hemisphere
Borehole orientation
Terzaghi correction
(Min. bias angle = 15 deg)
Number of poles = 146

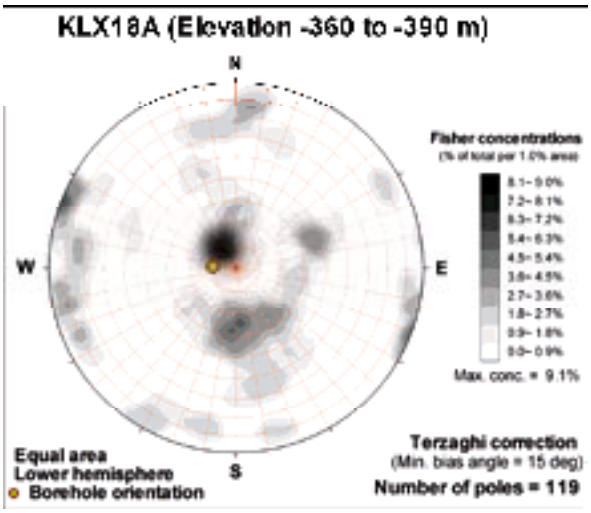
KLX18A (Elevation -360 to -390 m)
N
W
E
S
Fisher concentrations
(% of total per 1.0% area)
Max. conc. = 9.1%
Equal area
Lower hemisphere
Borehole orientation
Terzaghi correction
(Min. bias angle = 15 deg)
Number of poles = 119

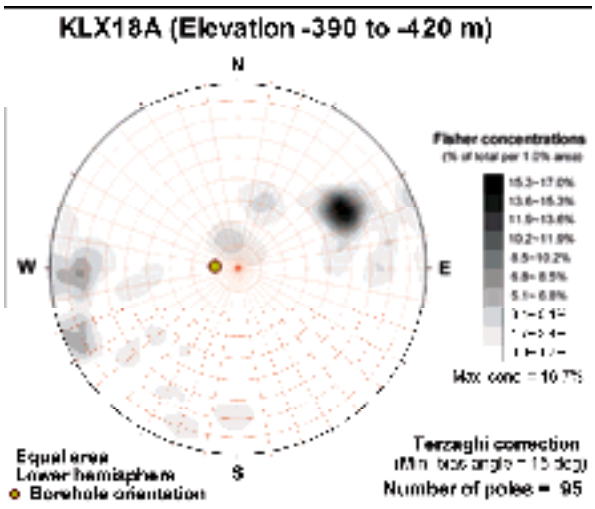
KLX18A (Elevation -390 to -420 m)
N
W
E
S
Fisher concentrations
Max. conc. = 10.7%
Equal area
Lower hemisphere
Borehole orientation
Terzaghi correction
(Min. bias angle = 15 deg)
Number of poles = 95

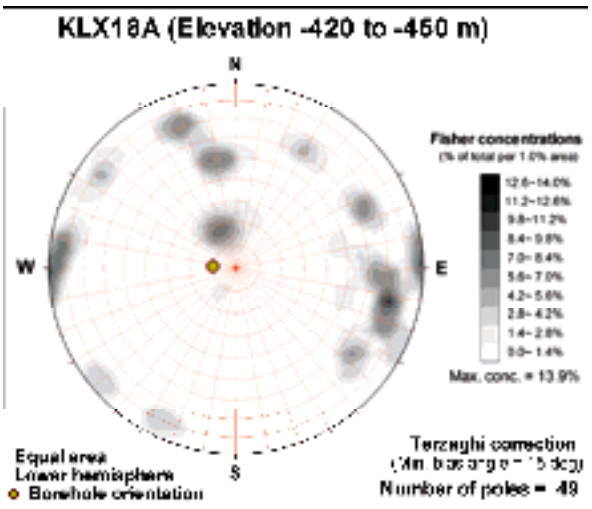
KLX18A (Elevation -420 to -450 m)
N
W
E
S
Fisher concentrations
Max. conc. = 13.9%
Equal area
Lower hemisphere
Borehole orientation
Terzaghi correction
(Min. bias angle = 15 deg)
Number of poles = 49

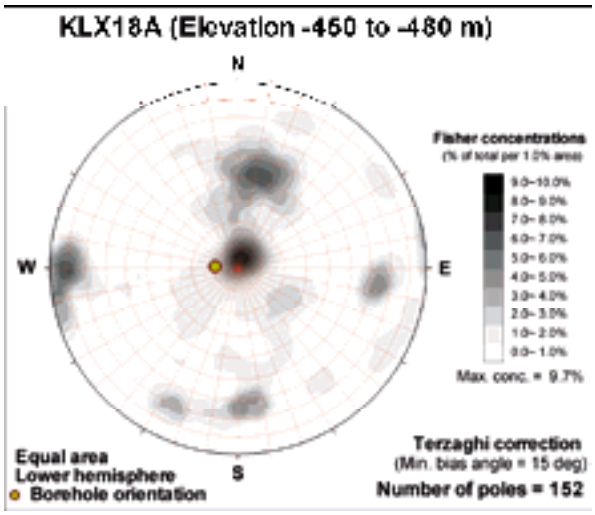
KLX18A (Elevation -450 to -480 m)
N
W
E
S
Fisher concentrations
Max. conc. = 9.7%
Equal area
Lower hemisphere
Borehole orientation
Terzaghi correction
(Min. bias angle = 15 deg)
Number of poles = 152

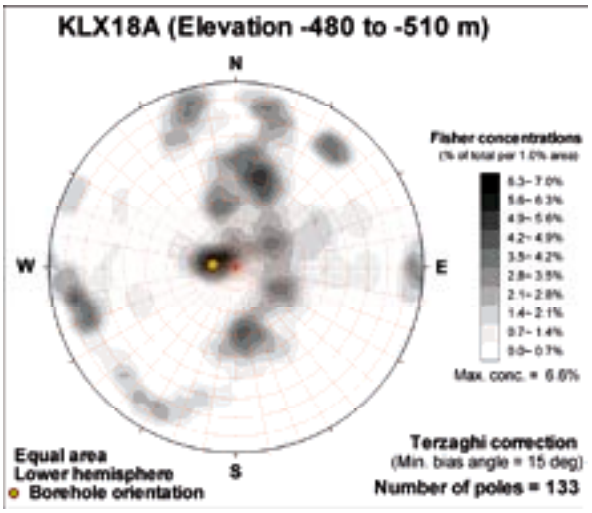
KLX18A (Elevation -480 to -510 m)
N
W
E
S
Fisher concentrations
Max. conc. = 6.6%
Equal area
Lower hemisphere
Borehole orientation
Terzaghi correction
(Min. bias angle = 15 deg)
Number of poles = 133

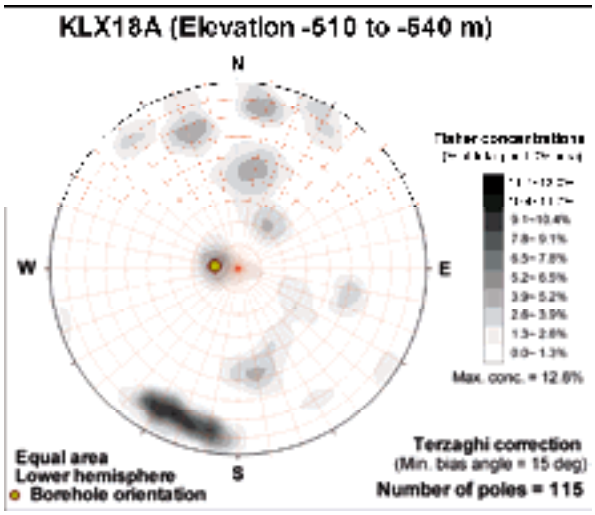
KLX18A (Elevation -510 to -540 m)
N
W
E
S
Max. conc. = 12.6%
Equal area
Lower hemisphere
Borehole orientation
Terzaghi correction
(Min. bias angle = 15 deg)
Number of poles = 115

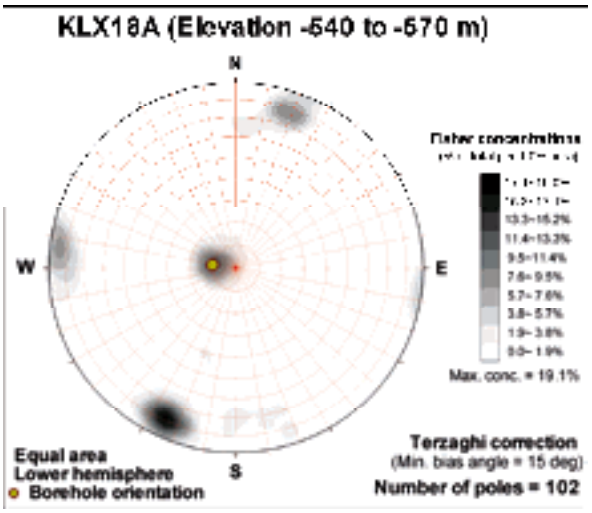
KLX18A (Elevation -540 to -570 m)
N
W
E
S
Max. conc. = 19.1%
Equal area
Lower hemisphere
Borehole orientation
Terzaghi correction
(Min. bias angle = 15 deg)
Number of poles = 102

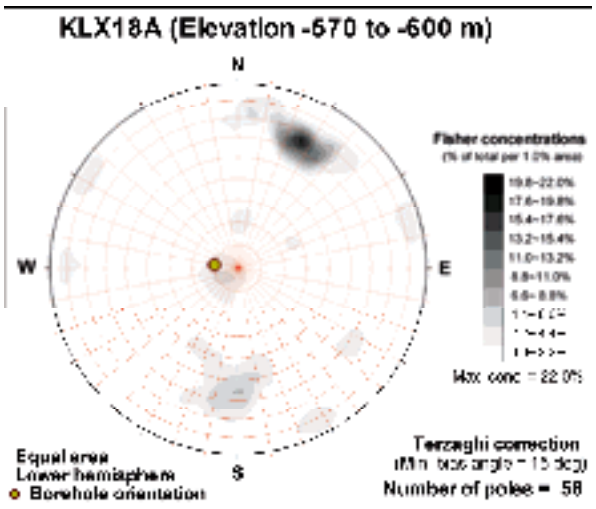
KLX18A (Elevation -570 to -600 m)
N
W
E
S
Fisher concentrations
(% of total per 1.0% area)
Max. conc. = 22.0%
Equal area
Lower hemisphere
Borehole orientation
Terzaghi correction
(Min. bias angle = 15 deg)
Number of poles = 58

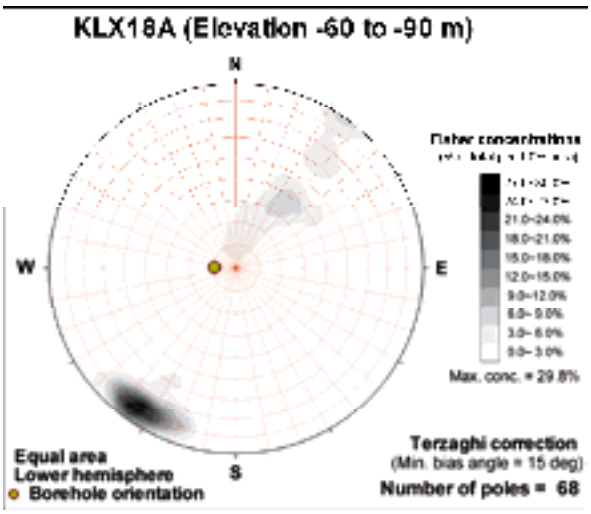
KLX18A (Elevation -60 to -90 m)
N
W
E
S
Fisher concentrations
Max. conc. = 29.8%
Equal area
Lower hemisphere
Borehole orientation
Terzaghi correction
(Min. bias angle = 15 deg)
Number of poles = 68

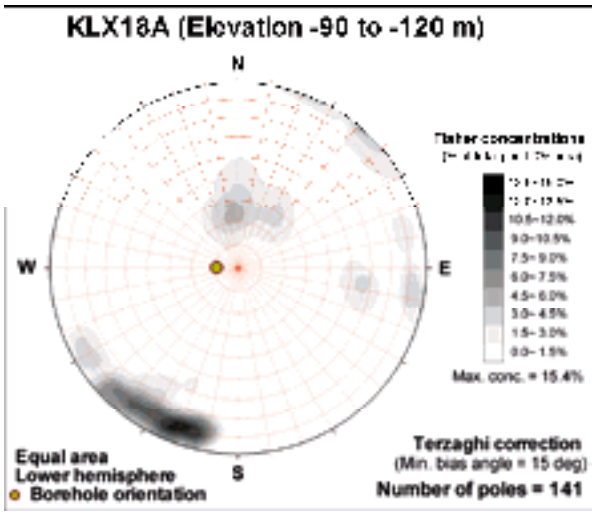
KLX18A (Elevation -90 to -120 m)
N
W
E
S
Fisher concentrations
Max. conc. = 15.4%
Equal area
Lower hemisphere
Borehole orientation
Terzaghi correction
(Min. bias angle = 15 deg)
Number of poles = 141

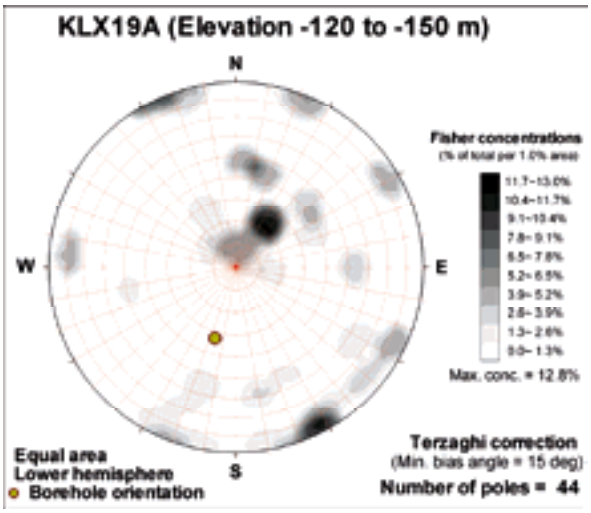
KLX19A (Elevation -120 to -150 m)
N
W
E
S
Fisher concentrations
(% of total per 1.0% area)
Max. conc. = 12.8%
Equal area
Lower hemisphere
Borehole orientation
Terzaghi correction
(Min. bias angle = 15 deg)
Number of poles = 44

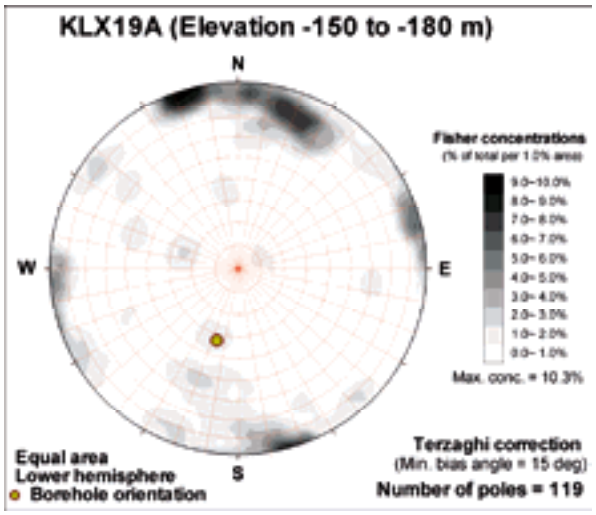
KLX19A (Elevation -150 to -180 m)
N
W
E
S
Fisher concentrations
(% of total per 1.0% area)
Max. conc. = 10.3%
Equal area
Lower hemisphere
Borehole orientation
Terzaghi correction
(Min. bias angle = 15 deg)
Number of poles = 119

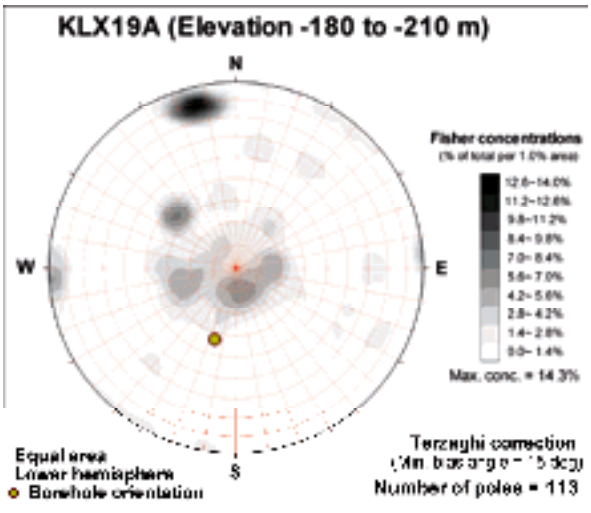
KLX19A (Elevation -180 to -210 m)
N
W
E
S
Fisher concentrations
(% of total per 1.0% area)
Max. conc. = 14.3%
Equal area
Lower hemisphere
Borehole orientation
Terzaghi correction
Number of poles = 113

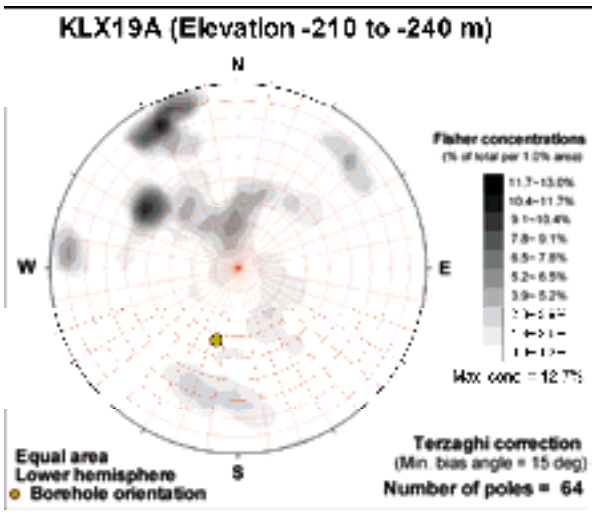
KLX19A (Elevation -210 to -240 m)
N
W
E
S
Fisher concentrations
(% of total per 1.0% area)
Max. conc = 12.7%
Equal area
Lower hemisphere
Borehole orientation
Terzaghi correction
(Min. bias angle = 15 deg)
Number of poles = 64

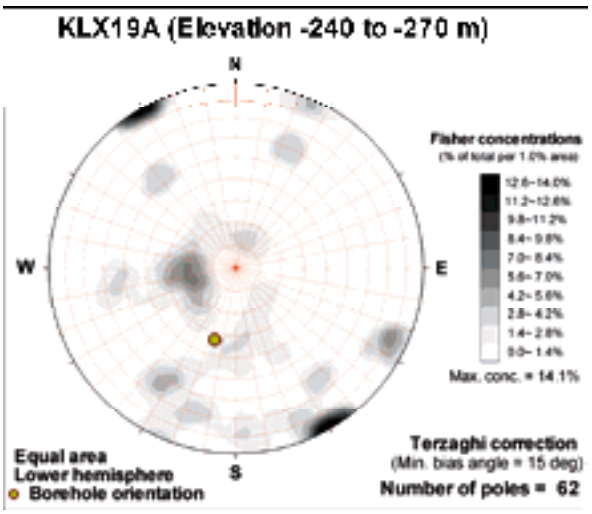
KLX19A (Elevation -240 to -270 m)
N
W
E
S
Fisher concentrations
(% of total per 1.0% area)
Max. conc. = 14.1%
Equal area
Lower hemisphere
Borehole orientation
Terzaghi correction
(Min. bias angle = 15 deg)
Number of poles = 62

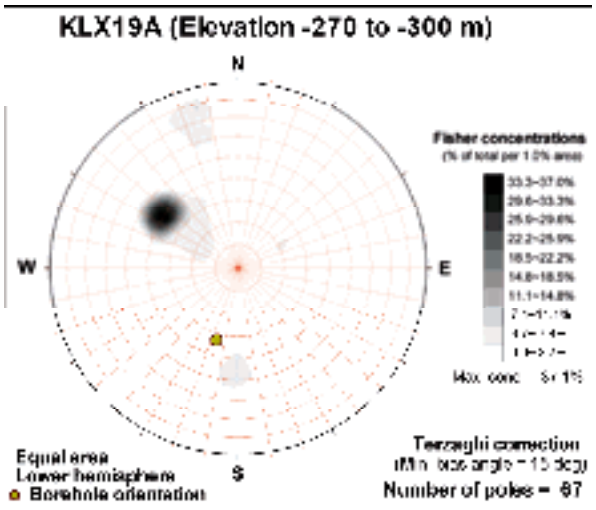
KLX19A (Elevation -270 to -300 m)
N
W
E
S
Fisher concentrations
(% of total per 1.0% area)
Equal area
Lower hemisphere
Borehole orientation
Terzaghi correction
(Min. bias angle = 15 deg)
Number of poles = 67

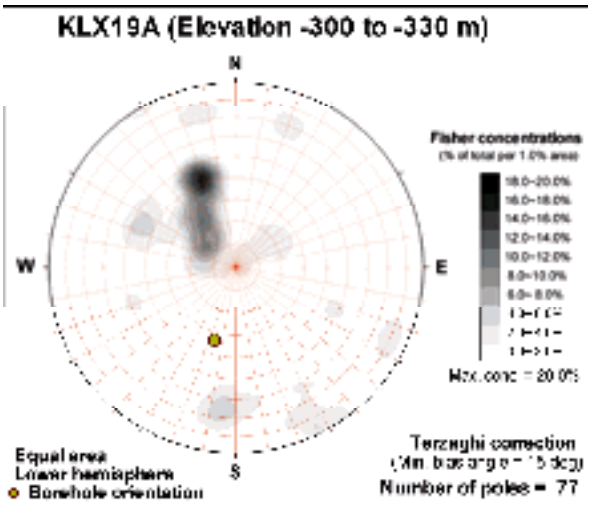
KLX19A (Elevation -300 to -330 m)
N
W
E
S
Fisher concentrations
(% of total per 1.0% area)
Equal area
Lower hemisphere
Borehole orientation
Terzaghi correction
(Min. bias angle = 15 deg)
Number of poles = 77

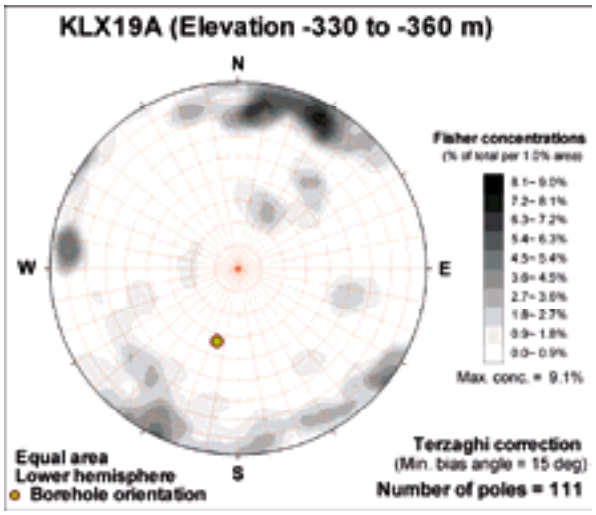
KLX19A (Elevation -330 to -360 m)
N
W
E
S
Fisher concentrations
(% of total per 1.0% area)
Max. conc. = 9.1%
Equal area
Lower hemisphere
Borehole orientation
Terzaghi correction
(Min. bias angle = 15 deg)
Number of poles = 111

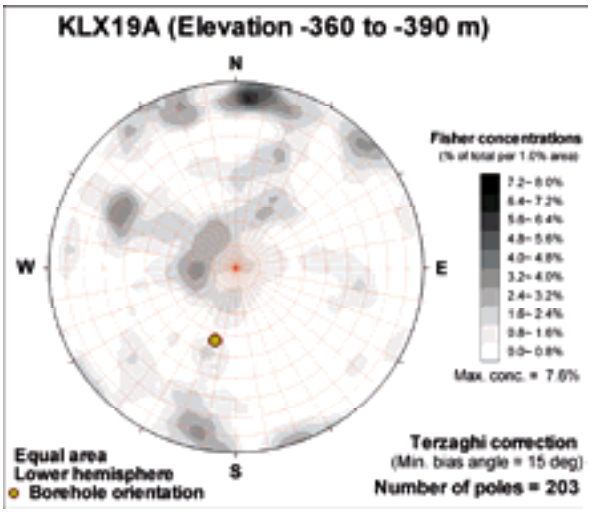
KLX19A (Elevation -360 to -390 m)
N
W
E
S
Fisher concentrations
(% of total per 1.0% area)
Max. conc. = 7.6%
Equal area
Lower hemisphere
Borehole orientation
Terzaghi correction
(Min. bias angle = 15 deg)
Number of poles = 203

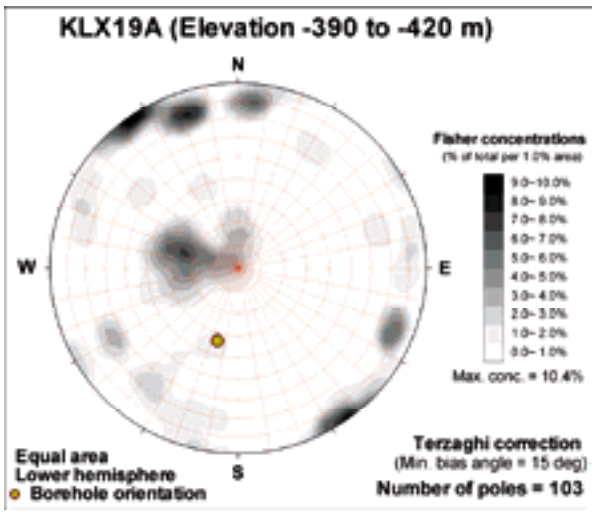
KLX19A (Elevation -390 to -420 m)
N
W
E
S
Fisher concentrations
(% of total per 1.0% area)
9.0–10.0%
8.0–9.0%
7.0–8.0%
6.0–7.0%
5.0–6.0%
4.0–5.0%
3.0–4.0%
2.0–3.0%
1.0–2.0%
0.0–1.0%
Max. conc. = 10.4%
Equal area
Lower hemisphere
Borehole orientation
Terzaghi correction
(Min. bias angle = 15 deg)
Number of poles = 103

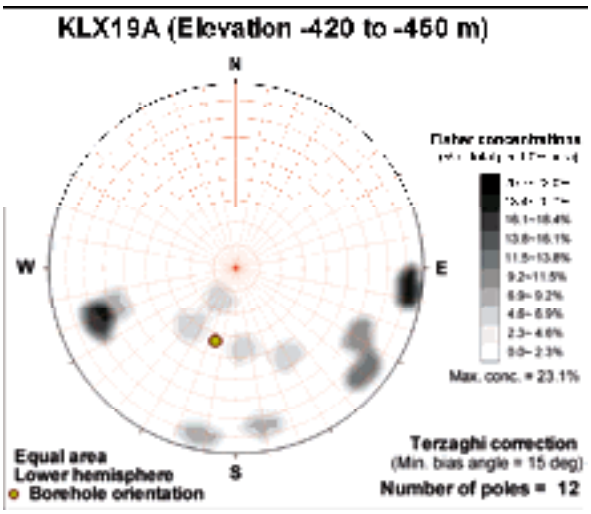
KLX19A (Elevation -420 to -460 m)
N
W
E
S
Max. conc. = 23.1%
Equal area
Lower hemisphere
Borehole orientation
Terzaghi correction
(Min. bias angle = 15 deg)
Number of poles = 12

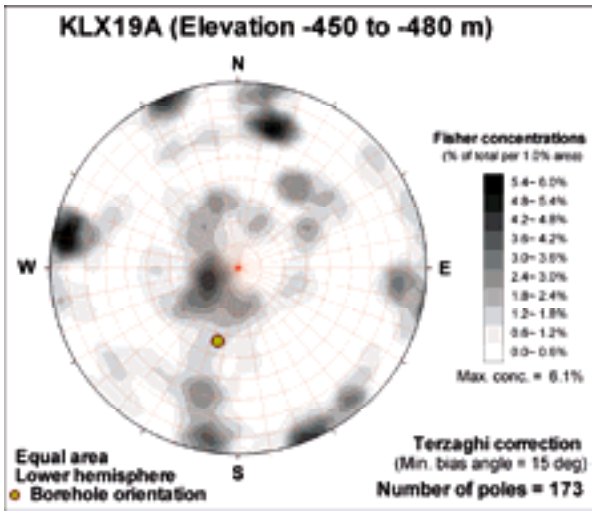
KLX19A (Elevation -450 to -480 m)
N
W
E
S
Fisher concentrations
(% of total per 1.0% area)
5.4–6.0%
4.8–5.4%
4.2–4.8%
3.6–4.2%
3.0–3.6%
2.4–3.0%
1.8–2.4%
1.2–1.8%
0.6–1.2%
0.0–0.6%
Max. conc. = 6.1%
Equal area
Lower hemisphere
Borehole orientation
Terzaghi correction
(Min. bias angle = 15 deg)
Number of poles = 173

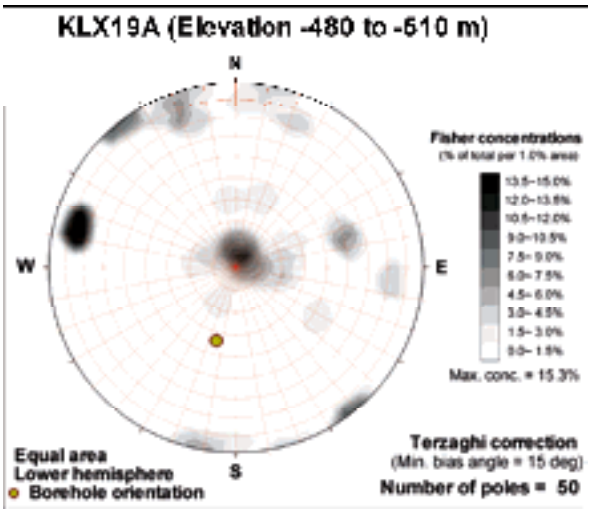
KLX19A (Elevation -480 to -510 m)
N
W
E
S
Fisher concentrations
(% of total per 1.0% area)
13.5–15.0%
12.0–13.5%
10.5–12.0%
9.0–10.5%
7.5–9.0%
6.0–7.5%
4.5–6.0%
3.0–4.5%
1.5–3.0%
0.0–1.5%
Max. conc. = 15.3%
Equal area
Lower hemisphere
Borehole orientation
Terzaghi correction
(Min. bias angle = 15 deg)
Number of poles = 50

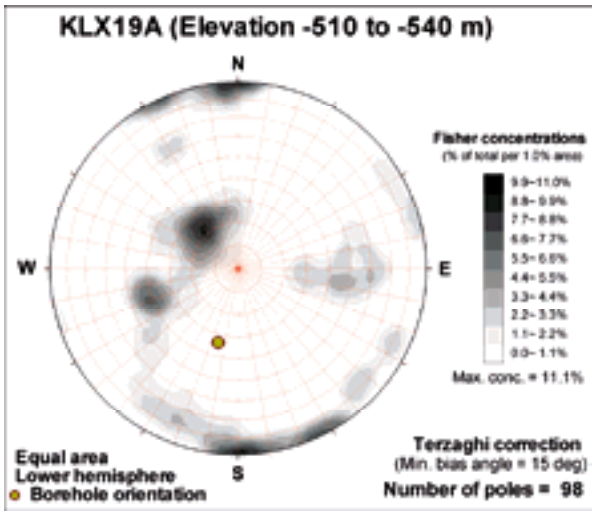
KLX19A (Elevation -510 to -540 m)
N
W
E
S
Fisher concentrations
(% of total per 1.0% area)
9.9–11.0%
8.8–9.9%
7.7–8.8%
6.6–7.7%
5.5–6.6%
4.4–5.5%
3.3–4.4%
2.2–3.3%
1.1–2.2%
0.0–1.1%
Max. conc. = 11.1%
Equal area
Lower hemisphere
Borehole orientation
Terzaghi correction
(Min. bias angle = 15 deg)
Number of poles = 98

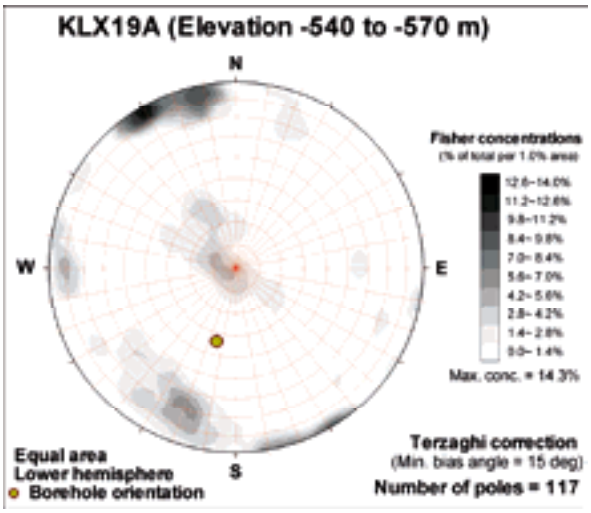
KLX19A (Elevation -540 to -570 m)
N
W
E
S
Fisher concentrations
(% of total per 1.0% area)
12.6–14.0%
11.2–12.6%
9.8–11.2%
8.4–9.8%
7.0–8.4%
5.6–7.0%
4.2–5.6%
2.8–4.2%
1.4–2.8%
0.0–1.4%
Max. conc. = 14.3%
Equal area
Lower hemisphere
Borehole orientation
Terzaghi correction
(Min. bias angle = 15 deg)
Number of poles = 117

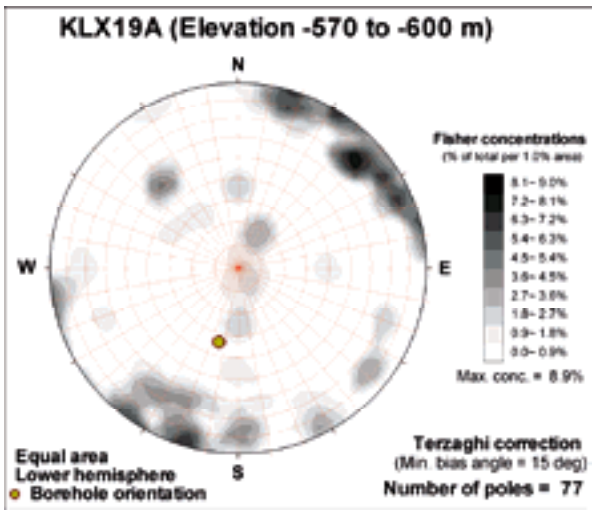
KLX19A (Elevation -570 to -600 m)
N
W
E
S
Fisher concentrations
(% of total per 1.0% area)
8.1–9.0%
7.2–8.1%
6.3–7.2%
5.4–6.3%
4.5–5.4%
3.6–4.5%
2.7–3.6%
1.8–2.7%
0.9–1.8%
0.0–0.9%
Max. conc. = 8.9%
Equal area
Lower hemisphere
Borehole orientation
Terzaghi correction
(Min. bias angle = 15 deg)
Number of poles = 77

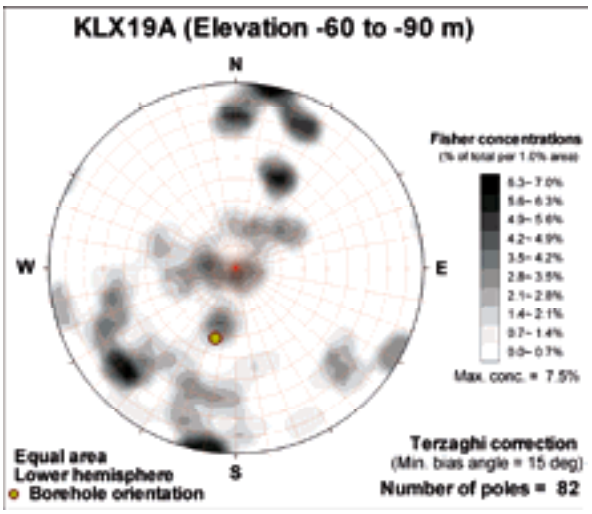
KLX19A (Elevation -60 to -90 m)
N
W
E
S
Fisher concentrations
(% of total per 1.0% area)
6.3–7.0%
5.6–6.3%
4.9–5.6%
4.2–4.9%
3.5–4.2%
2.8–3.5%
2.1–2.8%
1.4–2.1%
0.7–1.4%
0.0–0.7%
Max. conc. = 7.5%
Equal area
Lower hemisphere
Borehole orientation
Terzaghi correction
(Min. bias angle = 15 deg)
Number of poles = 82

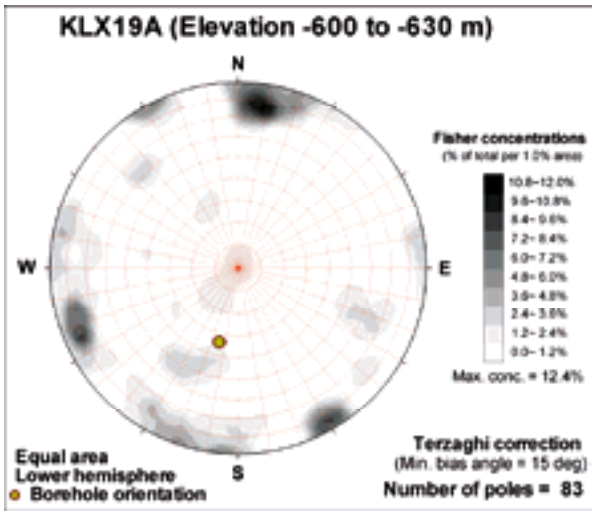
KLX19A (Elevation -600 to -630 m)
N
W
E
S
Fisher concentrations
(% of total per 1.0% area)
10.8–12.0%
9.6–10.8%
8.4–9.6%
7.2–8.4%
6.0–7.2%
4.8–6.0%
3.6–4.8%
2.4–3.6%
1.2–2.4%
0.0–1.2%
Max. conc. = 12.4%
Equal area
Lower hemisphere
Borehole orientation
Terzaghi correction
(Min. bias angle = 15 deg)
Number of poles = 83

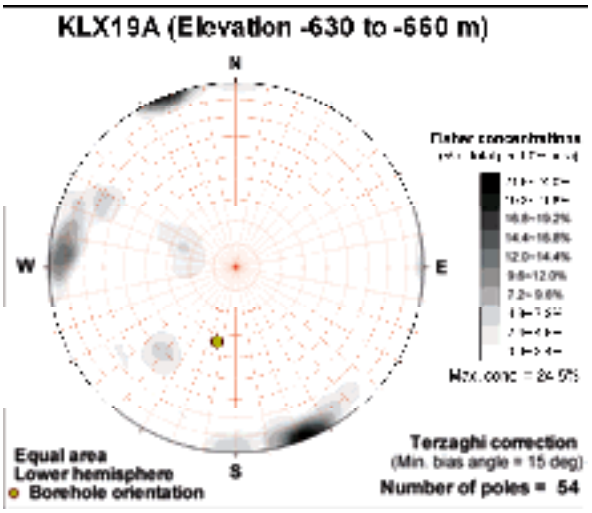
KLX19A (Elevation -630 to -660 m)
N
W
E
S
Equal area
Lower hemisphere
Borehole orientation
Terzaghi correction
(Min. bias angle = 15 deg)
Number of poles = 54

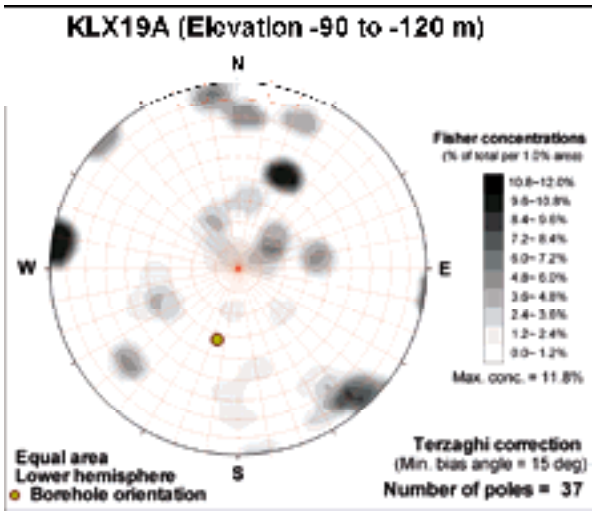
KLX19A (Elevation -90 to -120 m)
N
W
E
S
Fisher concentrations
(% of total per 1.0% area)
10.8–12.0%
9.6–10.8%
8.4–9.6%
7.2–8.4%
6.0–7.2%
4.8–6.0%
3.6–4.8%
2.4–3.6%
1.2–2.4%
0.0–1.2%
Max. conc. = 11.8%
Equal area
Lower hemisphere
Borehole orientation
Terzaghi correction
(Min. bias angle = 15 deg)
Number of poles = 37

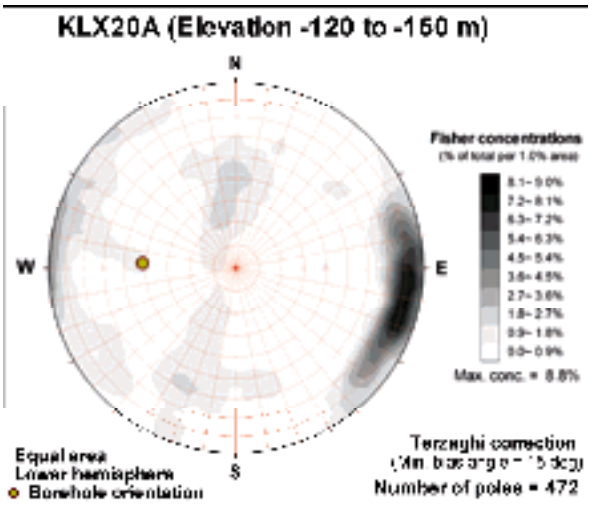
KLX20A (Elevation -120 to -150 m)
N
W
E
S
Fisher concentrations
(% of total per 1.0% area)
8.1–9.0%
7.2–8.1%
6.3–7.2%
5.4–6.3%
4.5–5.4%
3.6–4.5%
2.7–3.6%
1.8–2.7%
0.9–1.8%
0.0–0.9%
Max. conc. = 8.8%
Equal area
Lower hemisphere
Borehole orientation
Terzaghi correction
Number of poles = 472

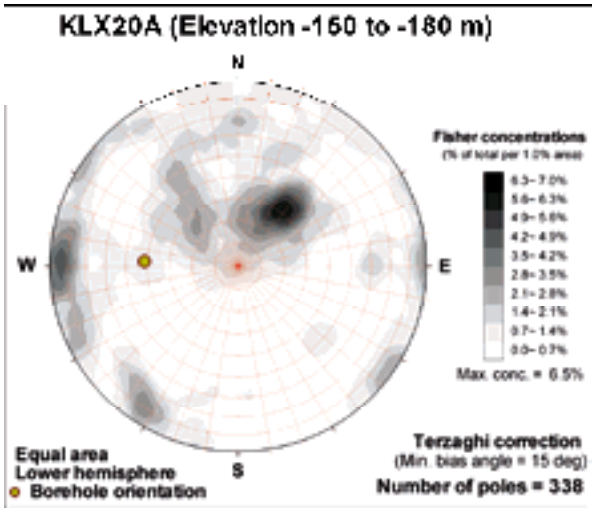
KLX20A (Elevation -150 to -180 m)
N
W
E
S
Fisher concentrations
(% of total per 1.0% area)
6.3- 7.0%
5.6- 6.3%
4.9- 5.6%
4.2- 4.9%
3.5- 4.2%
2.8- 3.5%
2.1- 2.8%
1.4- 2.1%
0.7- 1.4%
0.0- 0.7%
Max. conc. = 6.5%
Equal area
Lower hemisphere
Borehole orientation
Terzaghi correction
(Min. bias angle = 15 deg)
Number of poles = 338

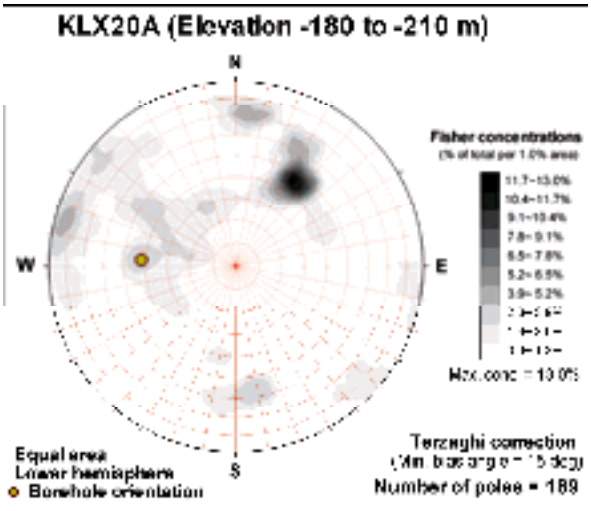
KLX20A (Elevation -180 to -210 m)
N
W
E
S
Fisher concentrations
(% of total per 1.0% area)
Equal area
Lower hemisphere
Borehole orientation
Terzaghi correction
Number of poles = 189

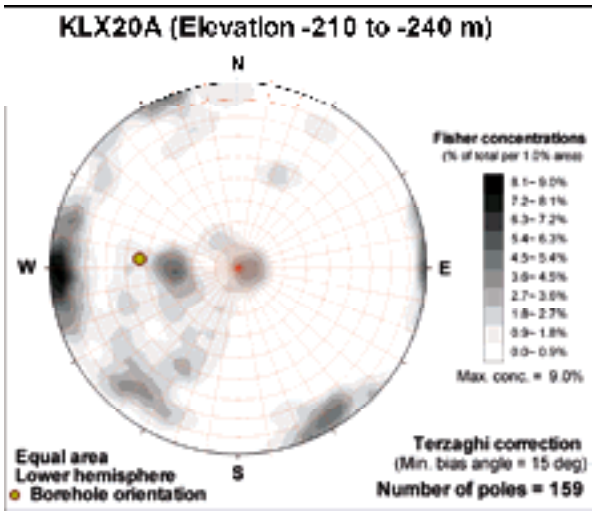
KLX20A (Elevation -210 to -240 m)
N
W
E
S
Fisher concentrations
(% of total per 1.0% area)
8.1- 9.0%
7.2- 8.1%
6.3- 7.2%
5.4- 6.3%
4.5- 5.4%
3.6- 4.5%
2.7- 3.6%
1.8- 2.7%
0.9- 1.8%
0.0- 0.9%
Max. conc. = 9.0%
Equal area
Lower hemisphere
Borehole orientation
Terzaghi correction
(Min. bias angle = 15 deg)
Number of poles = 159

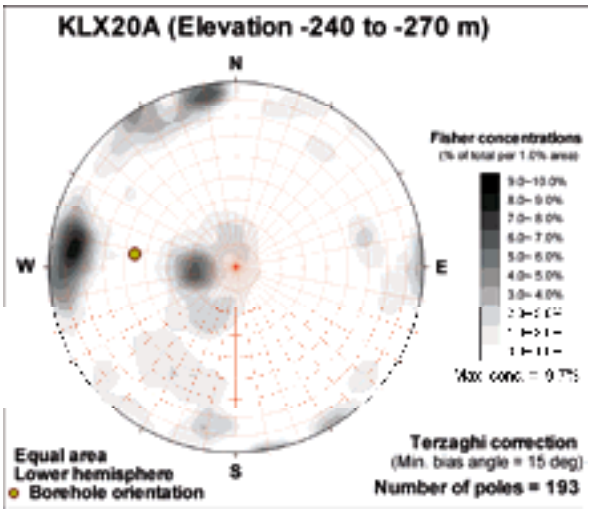
KLX20A (Elevation -240 to -270 m)
N
W
E
S
Fisher concentrations
(% of total per 1.0% area)
Equal area
Lower hemisphere
Borehole orientation
Terzaghi correction
(Min. bias angle = 15 deg)
Number of poles = 193

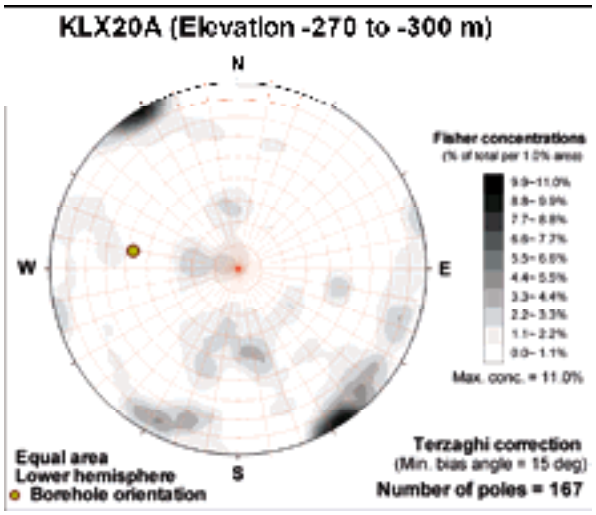
KLX20A (Elevation -270 to -300 m)
N
W
E
S
Fisher concentrations
(% of total per 1.0% area)
9.9-11.0%
8.8- 9.9%
7.7- 8.8%
6.6- 7.7%
5.5- 6.6%
4.4- 5.5%
3.3- 4.4%
2.2- 3.3%
1.1- 2.2%
0.0- 1.1%
Max. conc. = 11.0%
Equal area
Lower hemisphere
Borehole orientation
Terzaghi correction
(Min. bias angle = 15 deg)
Number of poles = 167

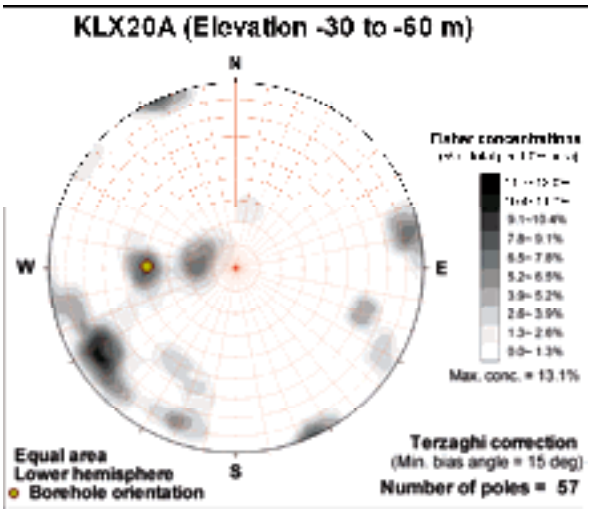
KLX20A (Elevation -30 to -60 m)
N
W
E
S
9.1-10.4%
7.8- 9.1%
6.5- 7.8%
5.2- 6.5%
3.9- 5.2%
2.6- 3.9%
1.3- 2.6%
0.0- 1.3%
Max. conc. = 13.1%
Equal area
Lower hemisphere
Borehole orientation
Terzaghi correction
(Min. bias angle = 15 deg)
Number of poles = 57

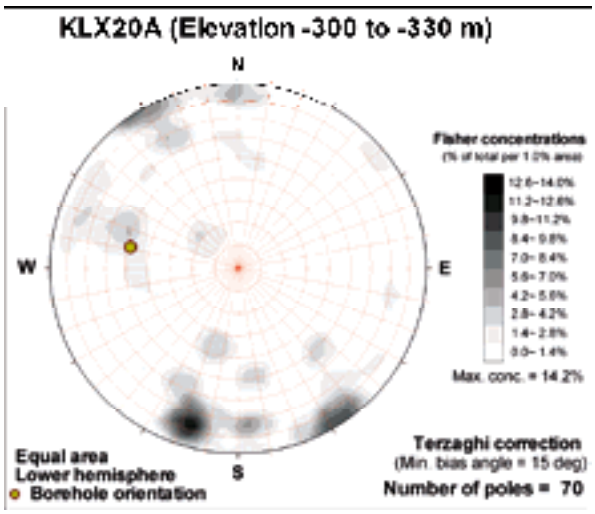
KLX20A (Elevation -300 to -330 m)
N
W
E
S
Fisher concentrations
(% of total per 1.0% area)
Max. conc. = 14.2%
Equal area
Lower hemisphere
Borehole orientation
Terzaghi correction
(Min. bias angle = 15 deg)
Number of poles = 70

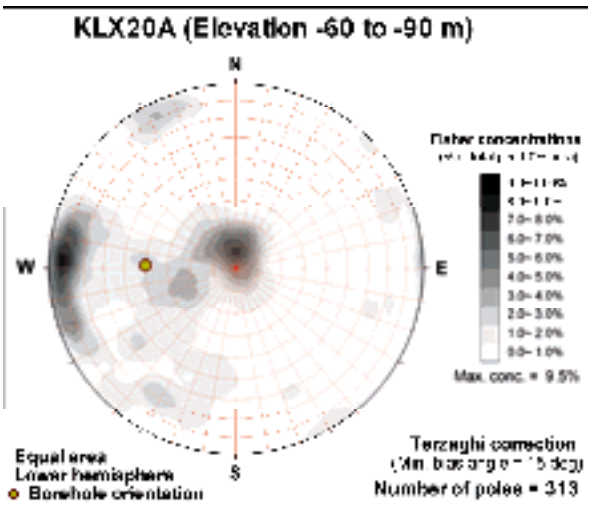
KLX20A (Elevation -60 to -90 m)
N
W
E
S
Max. conc. = 9.5%
Equal area
Lower hemisphere
Borehole orientation
Number of poles = 313

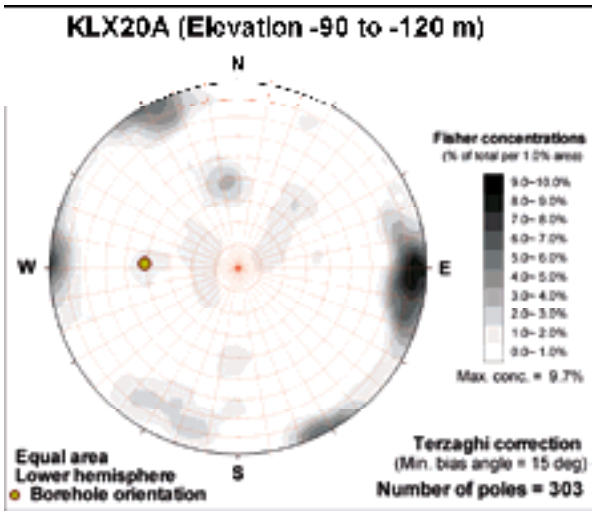
KLX20A (Elevation -90 to -120 m)
N
W
E
S
Fisher concentrations
(% of total per 1.0% area)
Max. conc. = 9.7%
Equal area
Lower hemisphere
Borehole orientation
Terzaghi correction
(Min. bias angle = 15 deg)
Number of poles = 303

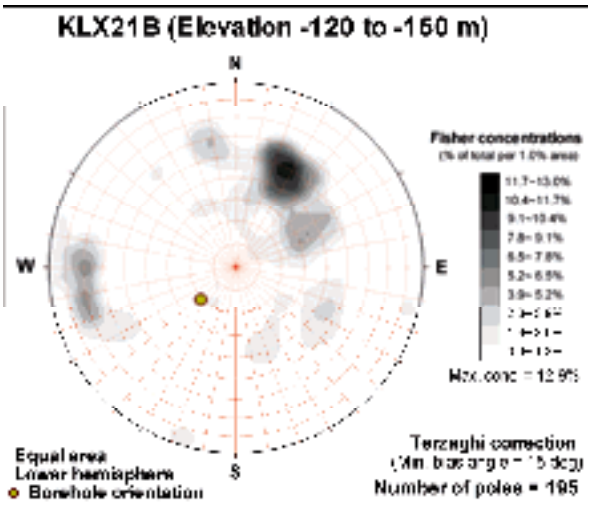
KLX21B (Elevation -120 to -150 m)
N
W
E
S
Fisher concentrations
(% of total per 1.0% area)
Equal area
Lower hemisphere
Borehole orientation
Number of poles = 195

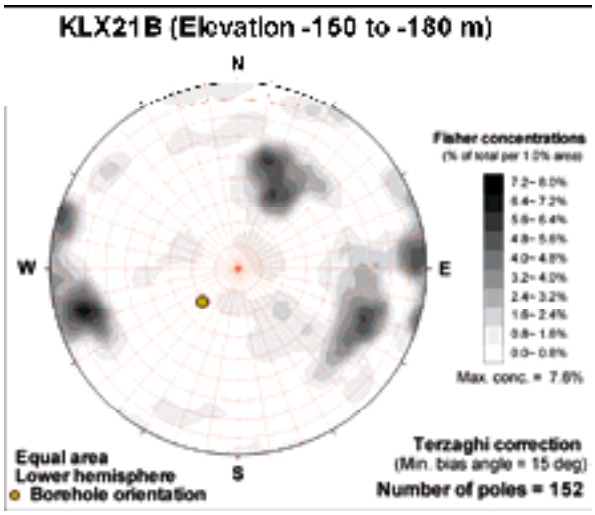
KLX21B (Elevation -150 to -180 m)
N
W
E
S
Fisher concentrations
(% of total per 1.0% area)
Max. conc. = 7.6%
Equal area
Lower hemisphere
Borehole orientation
Terzaghi correction
(Min. bias angle = 15 deg)
Number of poles = 152

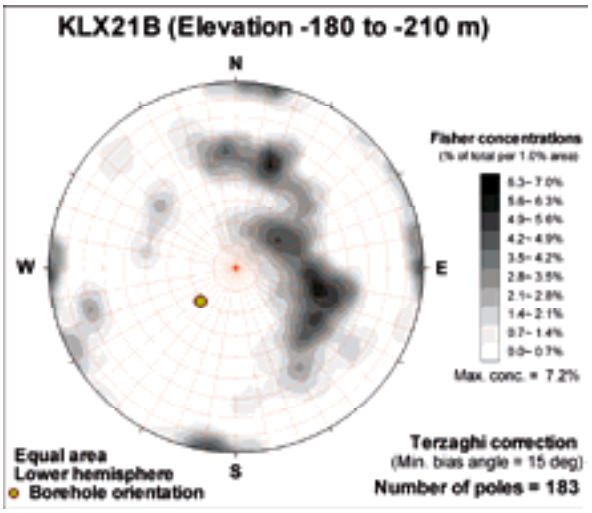
KLX21B (Elevation -180 to -210 m)
N
W
E
S
Fisher concentrations
(% of total per 1.0% area)
Max. conc. = 7.2%
Equal area
Lower hemisphere
Borehole orientation
Terzaghi correction
(Min. bias angle = 15 deg)
Number of poles = 183

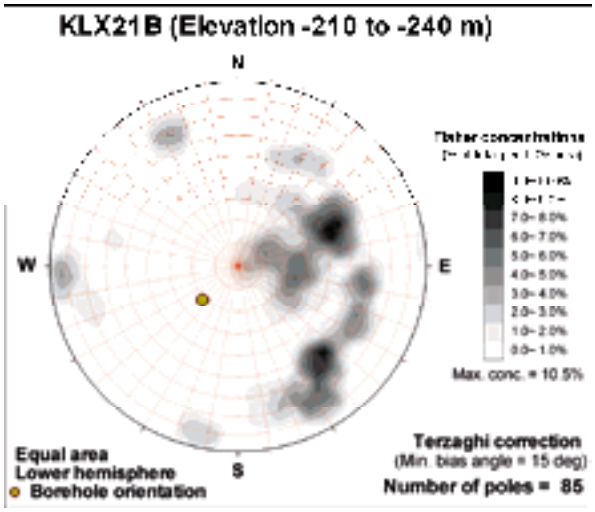
KLX21B (Elevation -210 to -240 m)
N
W
E
S
Fisher concentrations
Max. conc. = 10.5%
Equal area
Lower hemisphere
Borehole orientation
Terzaghi correction
(Min. bias angle = 15 deg)
Number of poles = 85

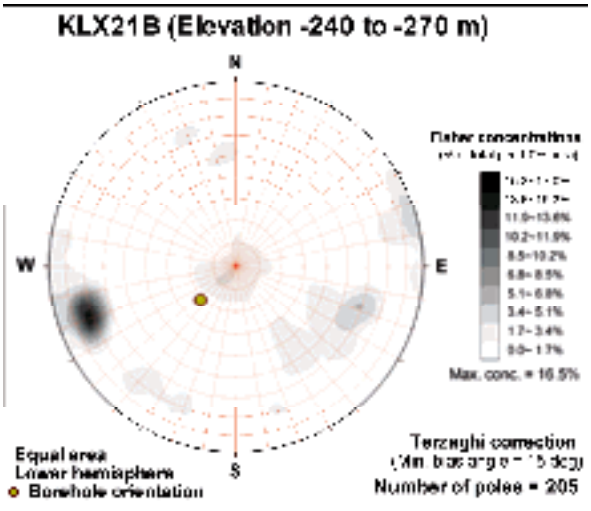
KLX21B (Elevation -240 to -270 m)
N
W
E
S
Fisher concentrations
Max. conc. = 16.5%
Equal area
Lower hemisphere
Borehole orientation
Terzaghi correction
Number of poles = 205

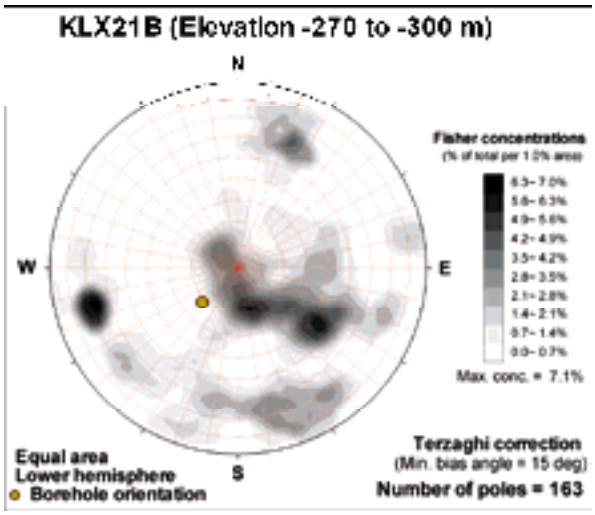
KLX21B (Elevation -270 to -300 m)
N
W
E
S
Fisher concentrations
Max. conc. = 7.1%
Equal area
Lower hemisphere
Borehole orientation
Terzaghi correction
(Min. bias angle = 15 deg)
Number of poles = 163

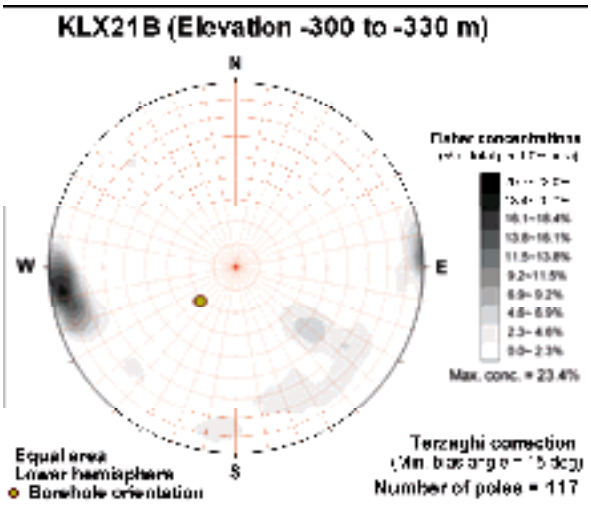
KLX21B (Elevation -300 to -330 m)
N
W
E
S
Fisher concentrations
Max. conc. = 23.4%
Equal area
Lower hemisphere
Borehole orientation
Terzaghi correction
Number of poles = 117

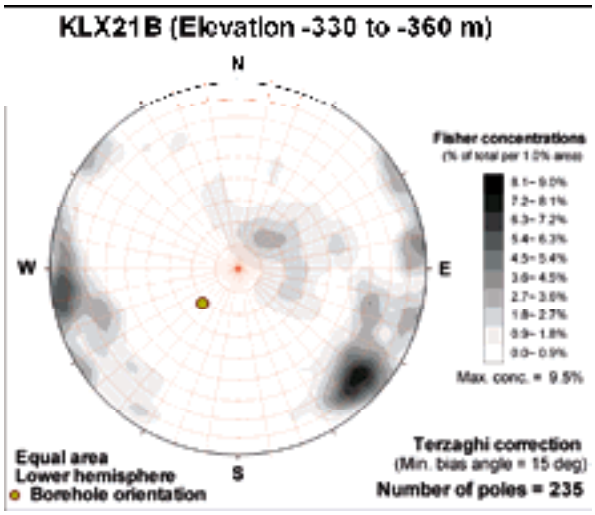
KLX21B (Elevation -330 to -360 m)
N
W
E
S
Fisher concentrations
Max. conc. = 9.5%
Equal area
Lower hemisphere
Borehole orientation
Terzaghi correction
(Min. bias angle = 15 deg)
Number of poles = 235

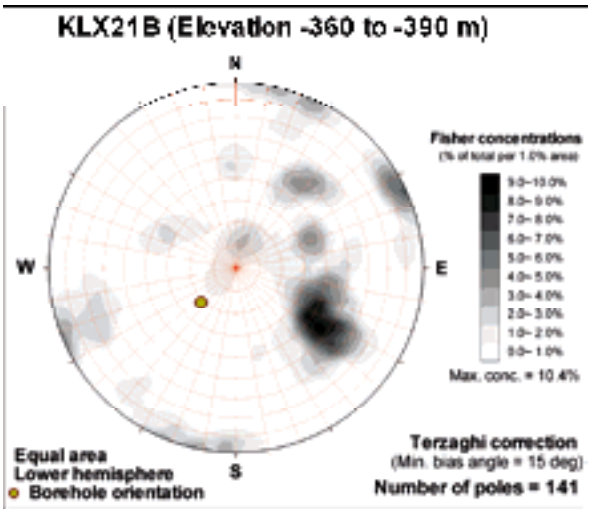
KLX21B (Elevation -360 to -390 m)
N
W
E
S
Fisher concentrations
Max. conc. = 10.4%
Equal area
Lower hemisphere
Borehole orientation
Terzaghi correction
(Min. bias angle = 15 deg)
Number of poles = 141

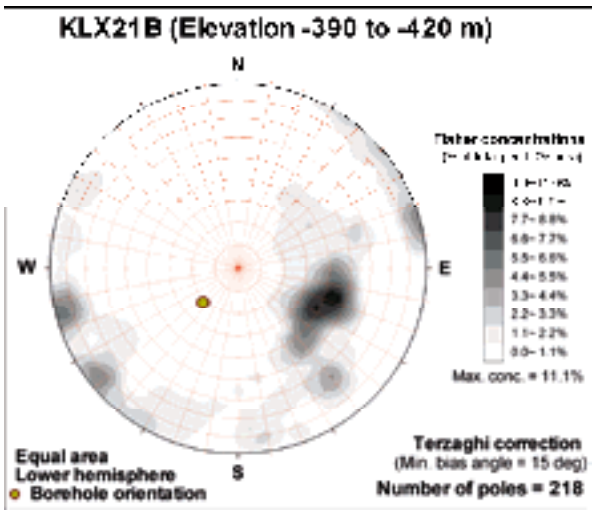
KLX21B (Elevation -390 to -420 m)
N
W
E
S
Fisher concentrations
Max. conc. = 11.1%
Equal area
Lower hemisphere
Borehole orientation
Terzaghi correction
(Min. bias angle = 15 deg)
Number of poles = 218

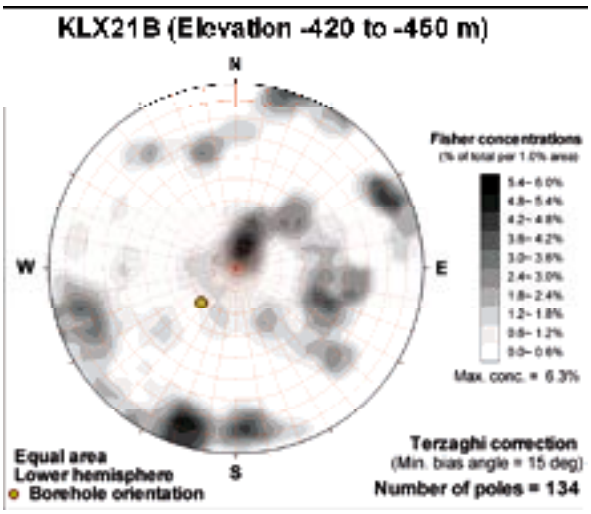
KLX21B (Elevation -420 to -460 m)
N
W
E
S
Fisher concentrations
Max. conc. = 6.3%
Equal area
Lower hemisphere
Borehole orientation
Terzaghi correction
(Min. bias angle = 15 deg)
Number of poles = 134

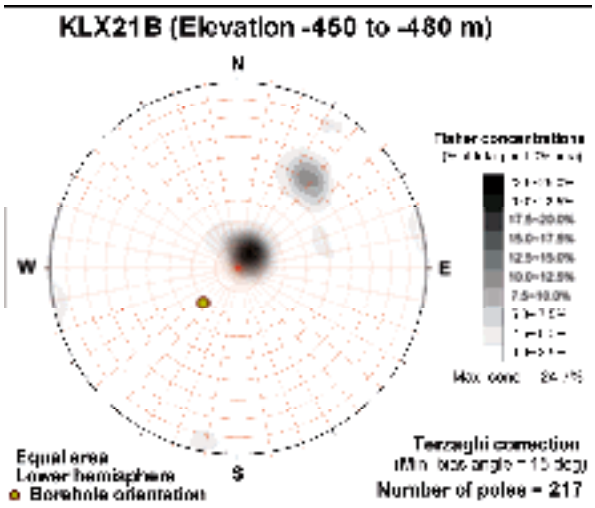
KLX21B (Elevation -460 to -480 m)
N
W
E
S
Fisher concentrations
Equal area
Lower hemisphere
Borehole orientation
Terzaghi correction
Number of poles = 217

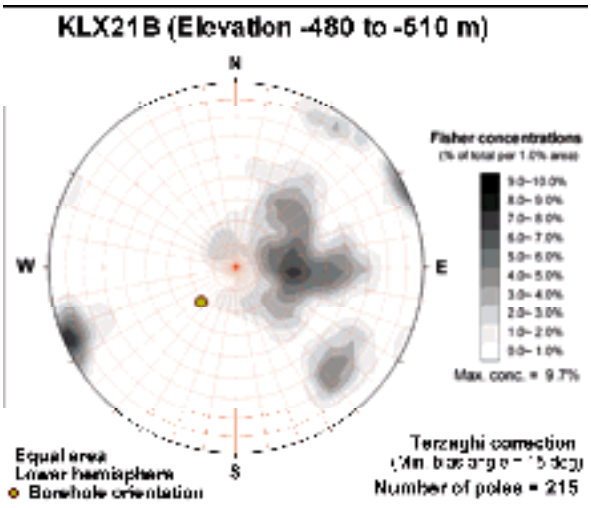
KLX21B (Elevation -480 to -510 m)
N
W
E
S
Fisher concentrations
Max. conc. = 9.7%
Equal area
Lower hemisphere
Borehole orientation
Terzaghi correction
Number of poles = 215

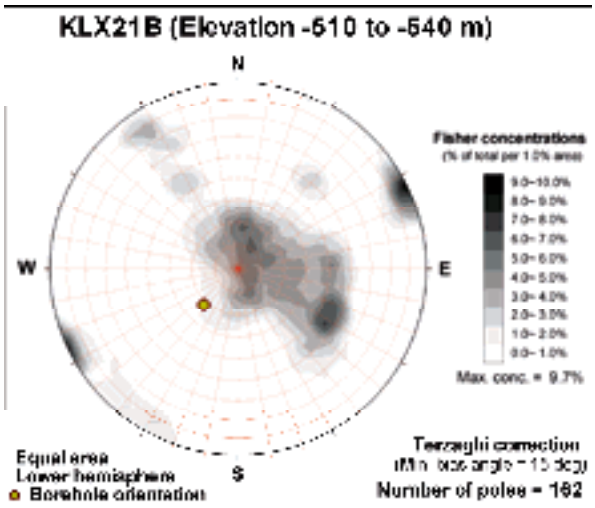
KLX21B (Elevation -510 to -540 m)
N
W
E
S
Fisher concentrations
Max. conc. = 9.7%
Equal area
Lower hemisphere
Borehole orientation
Terzaghi correction
Number of poles = 182

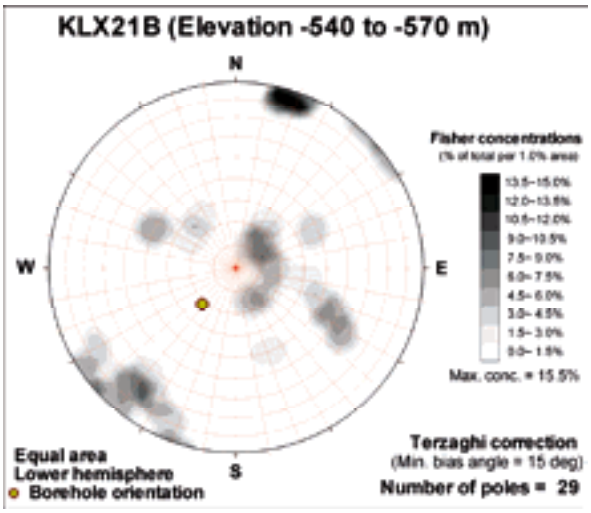
KLX21B (Elevation -540 to -570 m)
N
W
E
S
Fisher concentrations
Max. conc. = 15.5%
Equal area
Lower hemisphere
Borehole orientation
Terzaghi correction
(Min. bias angle = 15 deg)
Number of poles = 29

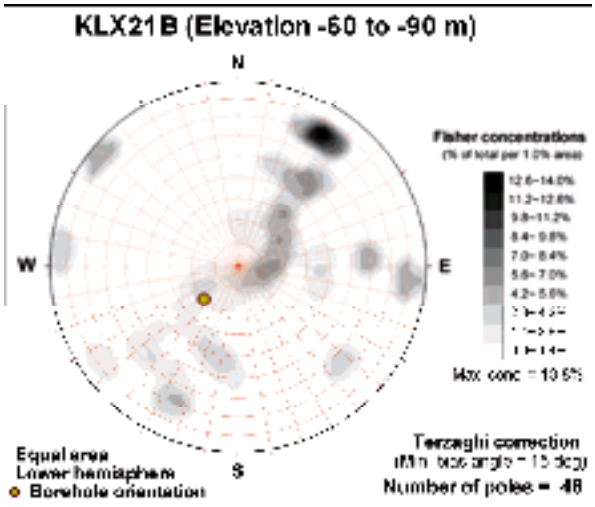
KLX21B (Elevation -60 to -90 m)
N
W
E
S
Fisher concentrations
Max. conc. = 10.6%
Equal area
Lower hemisphere
Borehole orientation
Terzaghi correction
(Min. bias angle = 15 deg)
Number of poles = 48

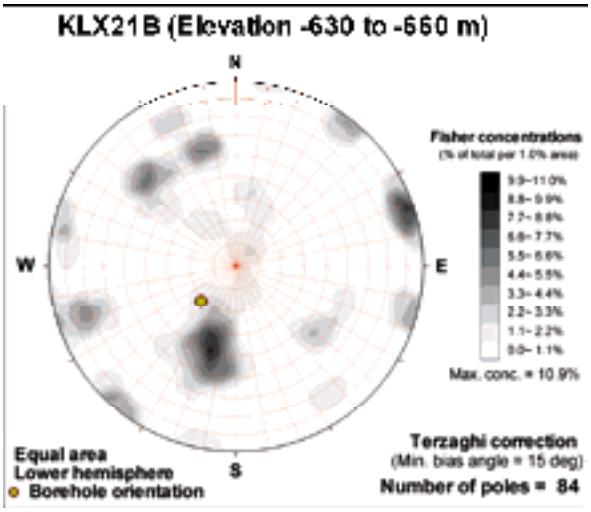
KLX21B (Elevation -630 to -660 m)
N
W
E
S
Fisher concentrations
Max. conc. = 10.9%
Equal area
Lower hemisphere
Borehole orientation
Terzaghi correction
(Min. bias angle = 15 deg)
Number of poles = 84

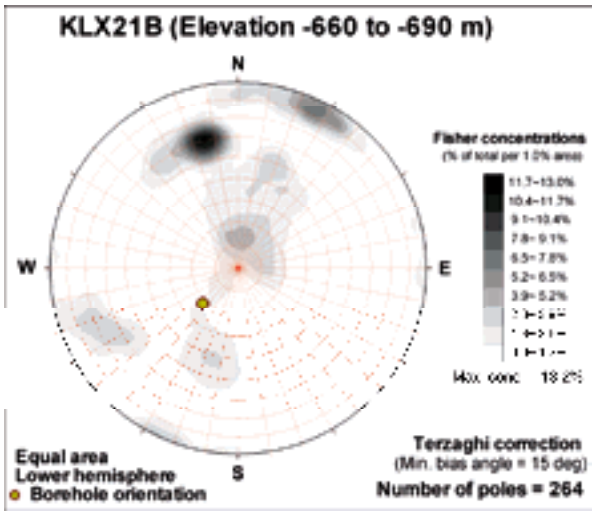
KLX21B (Elevation -660 to -690 m)
N
W
E
S
Fisher concentrations
Equal area
Lower hemisphere
Borehole orientation
Terzaghi correction
(Min. bias angle = 15 deg)
Number of poles = 264

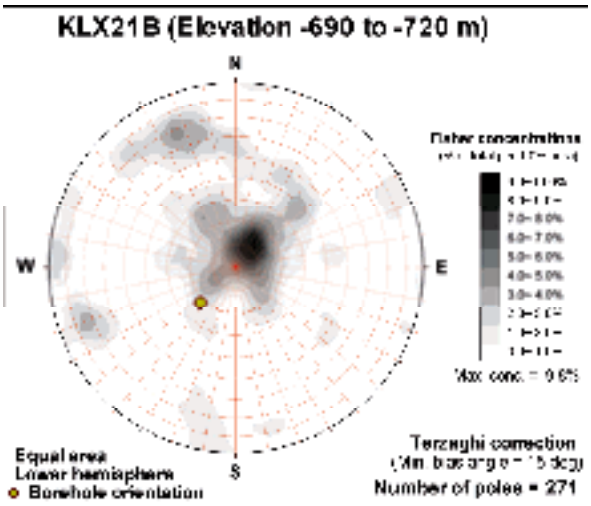
KLX21B (Elevation -690 to -720 m)
N
W
E
S
Equal area
Lower hemisphere
Borehole orientation
Terzaghi correction
Number of poles = 271

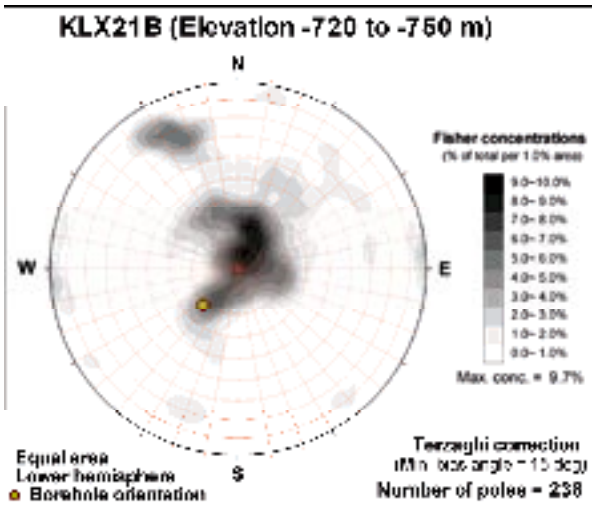
KLX21B (Elevation -720 to -750 m)
N
W
E
S
Fisher concentrations
Max. conc. = 9.7%
Equal area
Lower hemisphere
Borehole orientation
Terzaghi correction
(Min. bias angle = 15 deg)
Number of poles = 238

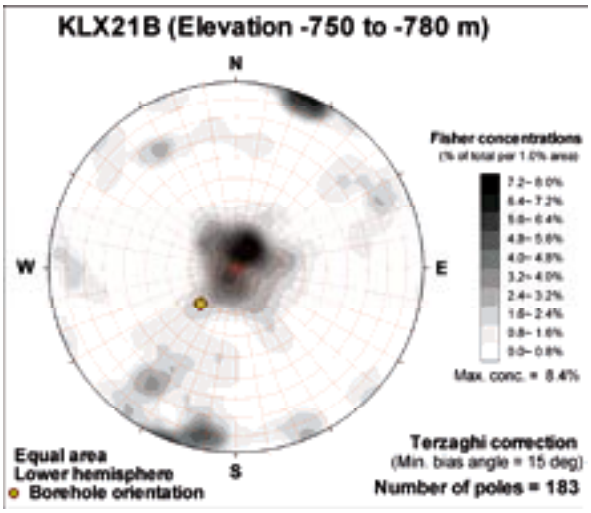
KLX21B (Elevation -750 to -780 m)
N
W
E
S
Fisher concentrations
Max. conc. = 8.4%
Equal area
Lower hemisphere
Borehole orientation
Terzaghi correction
(Min. bias angle = 15 deg)
Number of poles = 183

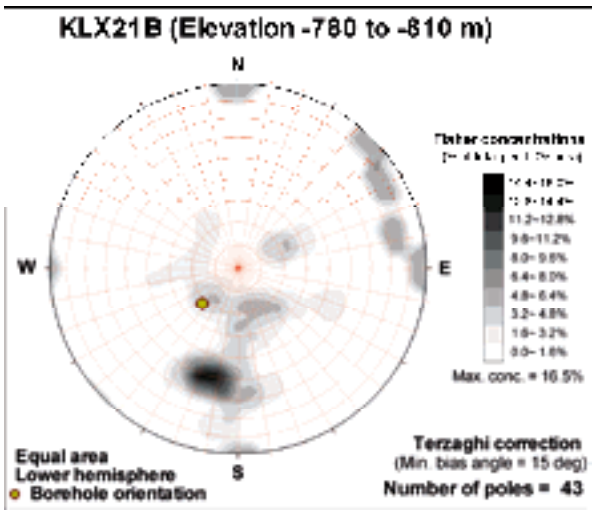
KLX21B (Elevation -780 to -810 m)
N
W
E
S
Fisher concentrations
Max. conc. = 16.5%
Equal area
Lower hemisphere
Borehole orientation
Terzaghi correction
(Min. bias angle = 15 deg)
Number of poles = 43

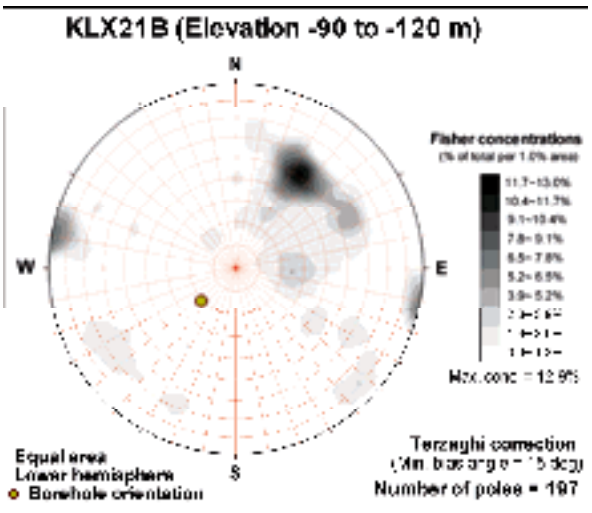
KLX21B (Elevation -90 to -120 m)
N
W
E
S
Fisher concentrations
Equal area
Lower hemisphere
Borehole orientation
Terzaghi correction
Number of poles = 197

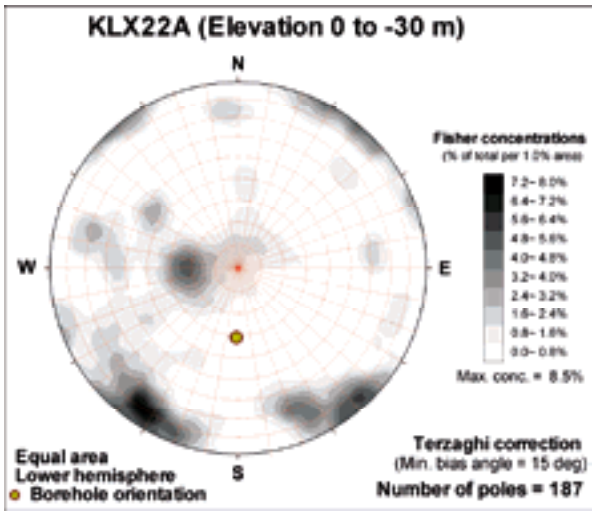
KLX22A (Elevation 0 to -30 m)
N
W
E
S
Fisher concentrations
Max. conc. = 8.5%
Equal area
Lower hemisphere
Borehole orientation
Terzaghi correction
(Min. bias angle = 15 deg)
Number of poles = 187

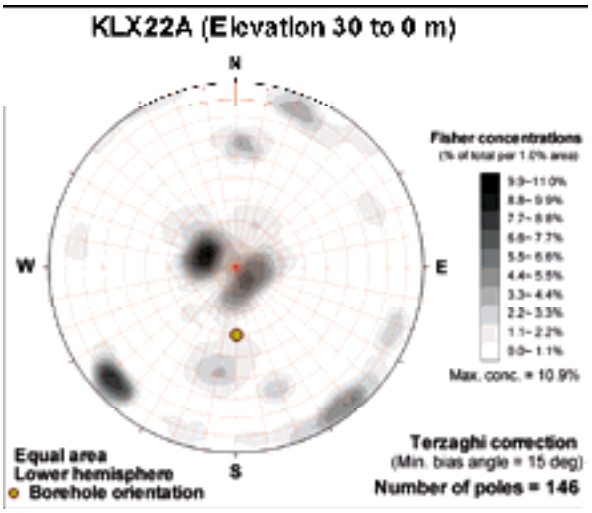
KLX22A (Elevation 30 to 0 m)
N
W
E
S
Fisher concentrations
Max. conc. = 10.9%
Equal area
Lower hemisphere
Borehole orientation
Terzaghi correction
(Min. bias angle = 15 deg)
Number of poles = 146

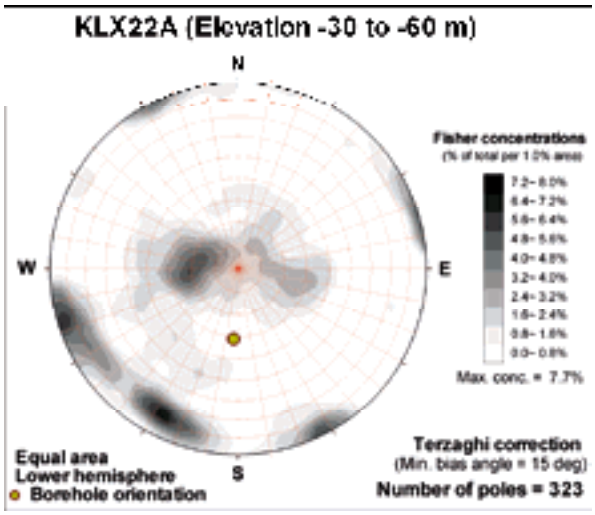
KLX22A (Elevation -30 to -60 m)
N
W
E
S
Fisher concentrations
Max. conc. = 7.7%
Equal area
Lower hemisphere
Borehole orientation
Terzaghi correction
(Min. bias angle = 15 deg)
Number of poles = 323

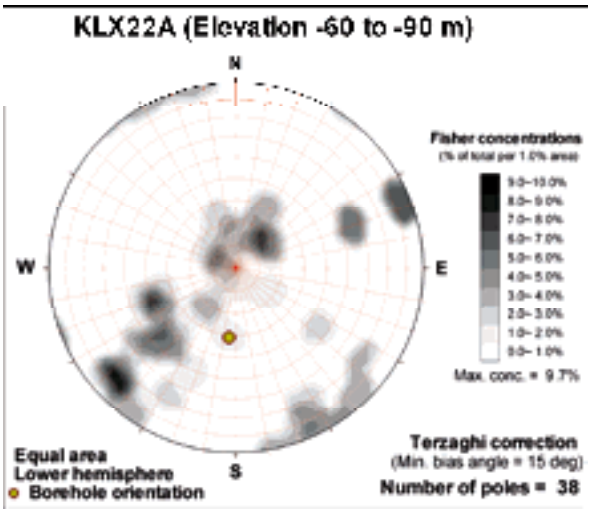
KLX22A (Elevation -60 to -90 m)
N
W
E
S
Fisher concentrations
Max. conc. = 9.7%
Equal area
Lower hemisphere
Borehole orientation
Terzaghi correction
(Min. bias angle = 15 deg)
Number of poles = 38

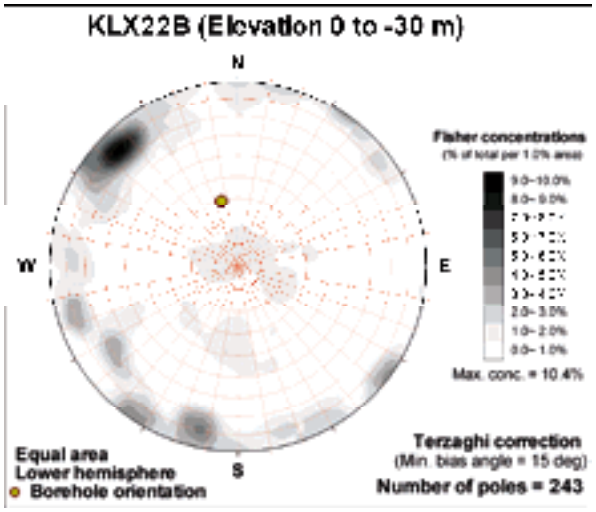
KLX22B (Elevation 0 to -30 m)
N
W
E
S
Fisher concentrations
(% of total per 1.0% area)
9.0–10.0%
8.0–9.0%
7.0–8.0%
6.0–7.0%
5.0–6.0%
4.0–5.0%
3.0–4.0%
2.0–3.0%
1.0–2.0%
0.0–1.0%
Max. conc. = 10.4%
Equal area
Lower hemisphere
Borehole orientation
Terzaghi correction
(Min. bias angle = 15 deg)
Number of poles = 243

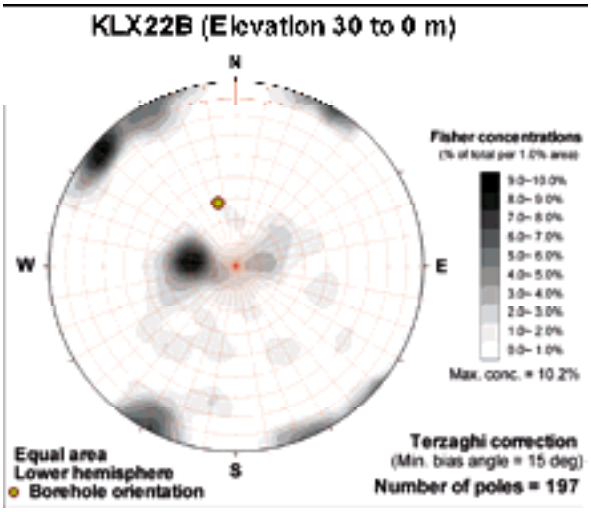
KLX22B (Elevation 30 to 0 m)
N
W
E
S
Fisher concentrations
(% of total per 1.0% area)
9.0–10.0%
8.0–9.0%
7.0–8.0%
6.0–7.0%
5.0–6.0%
4.0–5.0%
3.0–4.0%
2.0–3.0%
1.0–2.0%
0.0–1.0%
Max. conc. = 10.2%
Equal area
Lower hemisphere
Borehole orientation
Terzaghi correction
(Min. bias angle = 15 deg)
Number of poles = 197

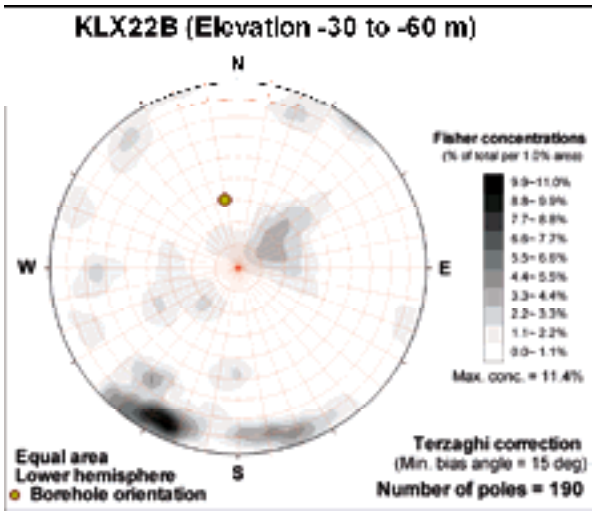
KLX22B (Elevation -30 to -60 m)
N
W
E
S
Fisher concentrations
(% of total per 1.0% area)
9.9–11.0%
8.8–9.9%
7.7–8.8%
6.6–7.7%
5.5–6.6%
4.4–5.5%
3.3–4.4%
2.2–3.3%
1.1–2.2%
0.0–1.1%
Max. conc. = 11.4%
Equal area
Lower hemisphere
Borehole orientation
Terzaghi correction
(Min. bias angle = 15 deg)
Number of poles = 190

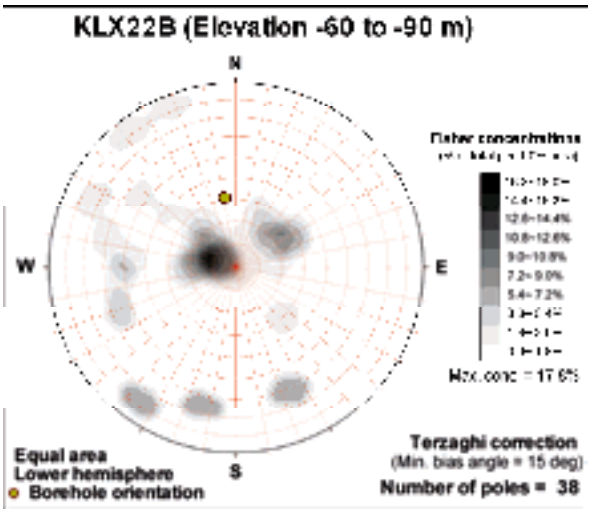
KLX22B (Elevation -60 to -90 m)
N
W
E
S
12.6–14.4%
10.8–12.6%
9.0–10.8%
7.2–9.0%
5.4–7.2%
Equal area
Lower hemisphere
Borehole orientation
Terzaghi correction
(Min. bias angle = 15 deg)
Number of poles = 38

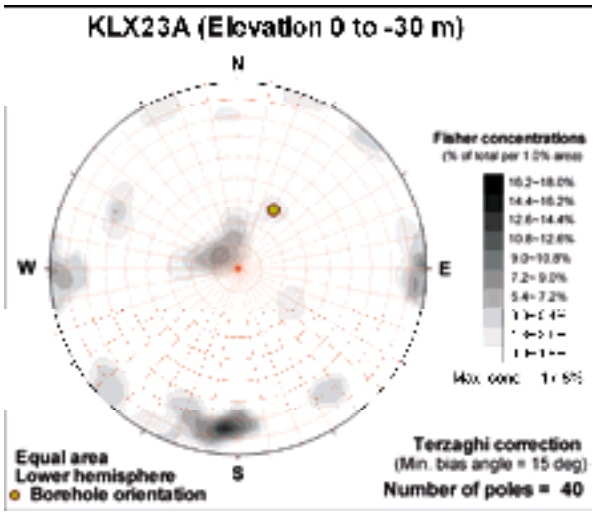
KLX23A (Elevation 0 to -30 m)
N
W
E
S
Fisher concentrations
(% of total per 1.0% area)
16.2–18.0%
14.4–16.2%
12.6–14.4%
10.8–12.6%
9.0–10.8%
7.2–9.0%
5.4–7.2%
Equal area
Lower hemisphere
Borehole orientation
Terzaghi correction
(Min. bias angle = 15 deg)
Number of poles = 40

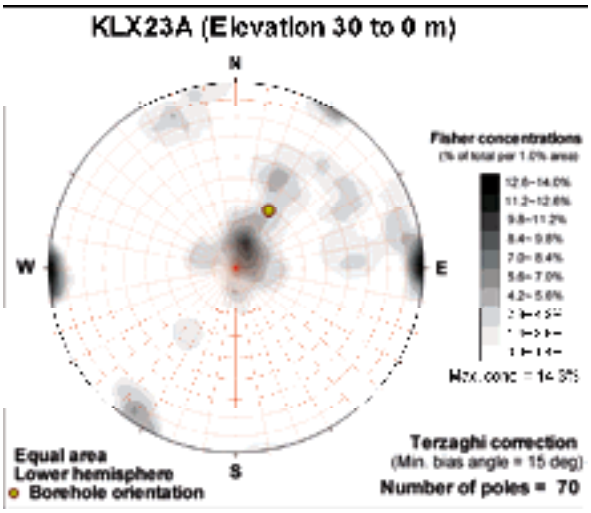
KLX23A (Elevation 30 to 0 m)
N
W
E
S
Fisher concentrations
(% of total per 1.0% area)
12.6–14.0%
11.2–12.6%
9.8–11.2%
8.4–9.8%
7.0–8.4%
5.6–7.0%
4.2–5.6%
Equal area
Lower hemisphere
Borehole orientation
Terzaghi correction
(Min. bias angle = 15 deg)
Number of poles = 70

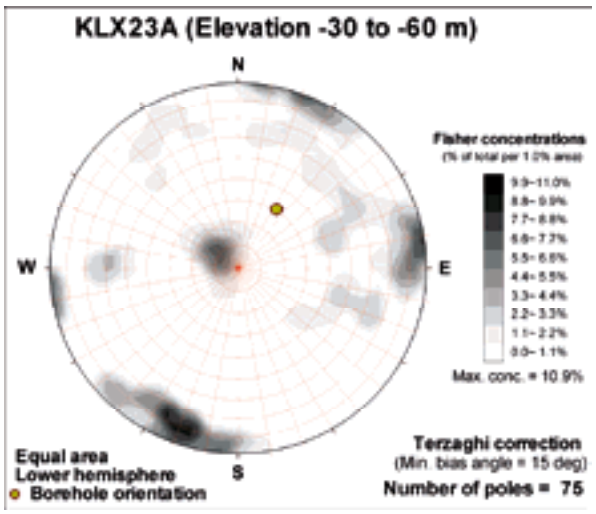
KLX23A (Elevation -30 to -60 m)
N
W
E
S
Fisher concentrations
(% of total per 1.0% area)
9.9–11.0%
8.8–9.9%
7.7–8.8%
6.6–7.7%
5.5–6.6%
4.4–5.5%
3.3–4.4%
2.2–3.3%
1.1–2.2%
0.0–1.1%
Max. conc. = 10.9%
Equal area
Lower hemisphere
Borehole orientation
Terzaghi correction
(Min. bias angle = 15 deg)
Number of poles = 75

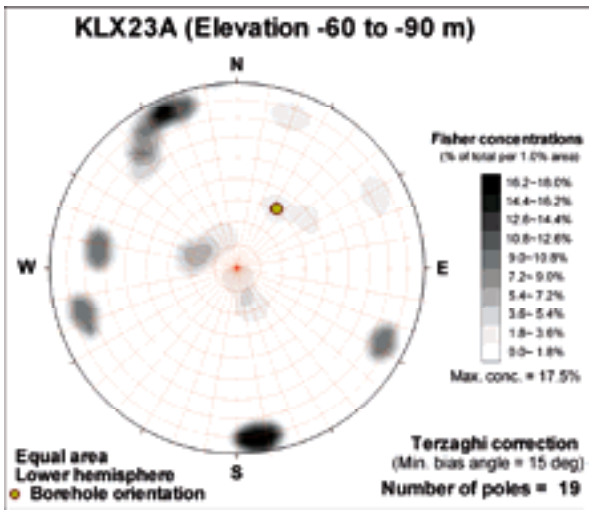
KLX23A (Elevation -60 to -90 m)
N
W
E
S
Fisher concentrations
(% of total per 1.0% area)
16.2–18.0%
14.4–16.2%
12.6–14.4%
10.8–12.6%
9.0–10.8%
7.2–9.0%
5.4–7.2%
3.6–5.4%
1.8–3.6%
0.0–1.8%
Max. conc. = 17.5%
Equal area
Lower hemisphere
Borehole orientation
Terzaghi correction
(Min. bias angle = 15 deg)
Number of poles = 19

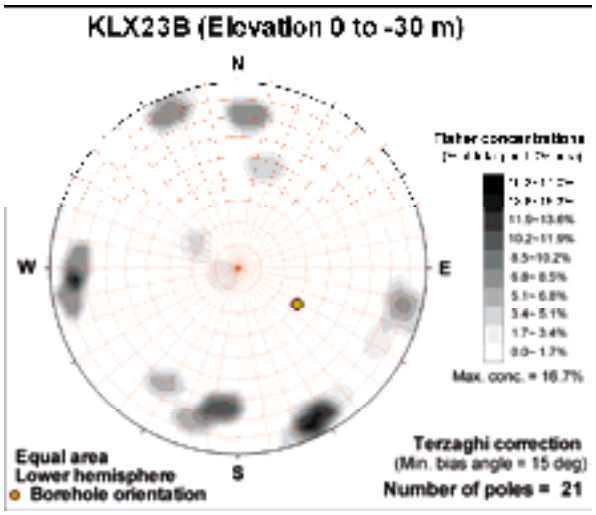
KLX23B (Elevation 0 to -30 m)
N
W
E
S
11.9–13.6%
10.2–11.9%
8.5–10.2%
6.8–8.5%
5.1–6.8%
3.4–5.1%
1.7–3.4%
0.0–1.7%
Max. conc. = 16.7%
Equal area
Lower hemisphere
Borehole orientation
Terzaghi correction
(Min. bias angle = 15 deg)
Number of poles = 21

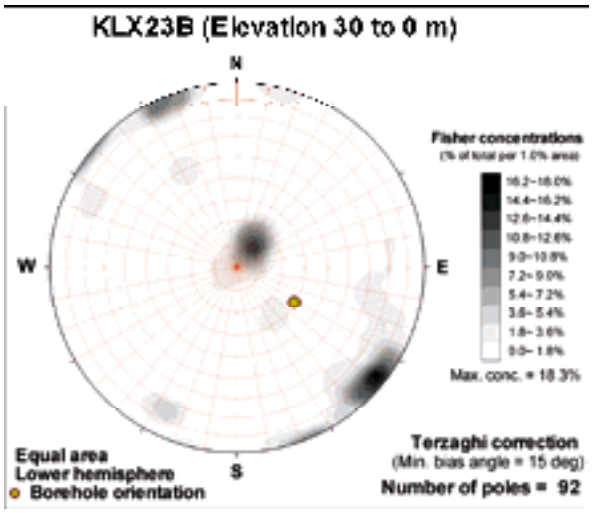
KLX23B (Elevation 30 to 0 m)
N
W
E
S
Fisher concentrations
(% of total per 1.0% area)
16.2–18.0%
14.4–16.2%
12.6–14.4%
10.8–12.6%
9.0–10.8%
7.2–9.0%
5.4–7.2%
3.6–5.4%
1.8–3.6%
0.0–1.8%
Max. conc. = 18.3%
Equal area
Lower hemisphere
Borehole orientation
Terzaghi correction
(Min. bias angle = 15 deg)
Number of poles = 92

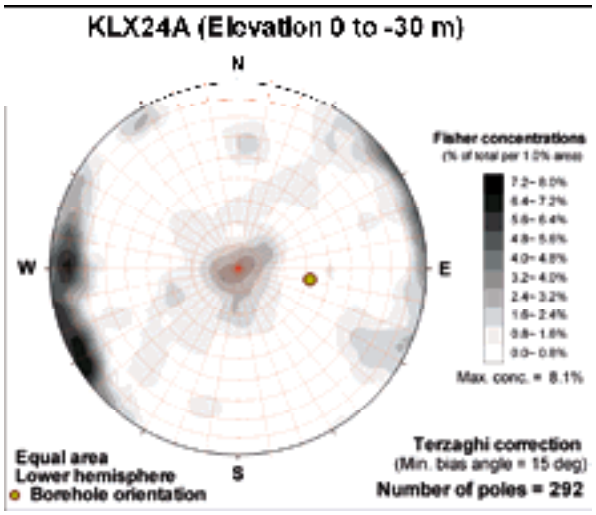
KLX24A (Elevation 0 to -30 m)
N
W
E
S
Fisher concentrations
(% of total per 1.0% area)
7.2–8.0%
6.4–7.2%
5.6–6.4%
4.8–5.6%
4.0–4.8%
3.2–4.0%
2.4–3.2%
1.6–2.4%
0.8–1.6%
0.0–0.8%
Max. conc. = 8.1%
Equal area
Lower hemisphere
Borehole orientation
Terzaghi correction
(Min. bias angle = 15 deg)
Number of poles = 292

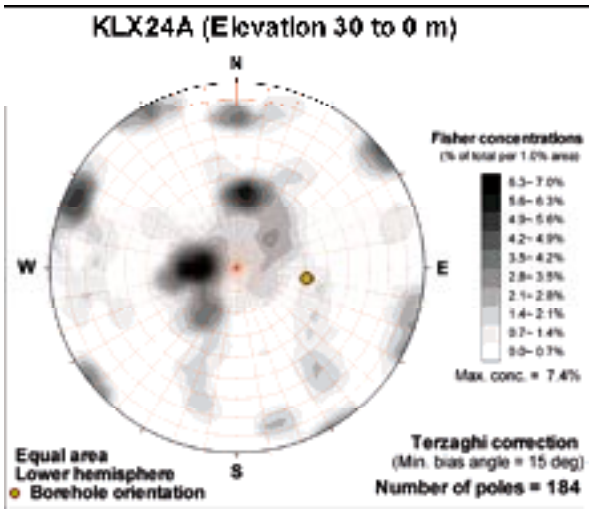
KLX24A (Elevation 30 to 0 m)
N
W
E
S
Fisher concentrations
(% of total per 1.0% area)
6.3–7.0%
5.6–6.3%
4.9–5.6%
4.2–4.9%
3.5–4.2%
2.8–3.5%
2.1–2.8%
1.4–2.1%
0.7–1.4%
0.0–0.7%
Max. conc. = 7.4%
Equal area
Lower hemisphere
Borehole orientation
Terzaghi correction
(Min. bias angle = 15 deg)
Number of poles = 184

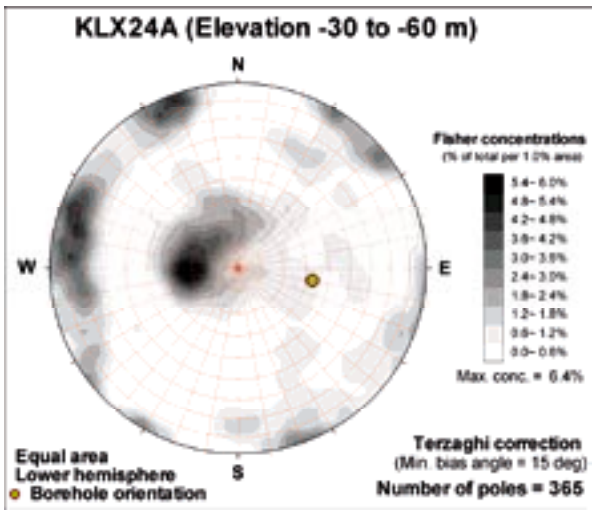
KLX24A (Elevation -30 to -60 m)
N
W
E
S
Fisher concentrations
(% of total per 1.0% area)
Max. conc. = 6.4%
Equal area
Lower hemisphere
Borehole orientation
Terzaghi correction
(Min. bias angle = 15 deg)
Number of poles = 365

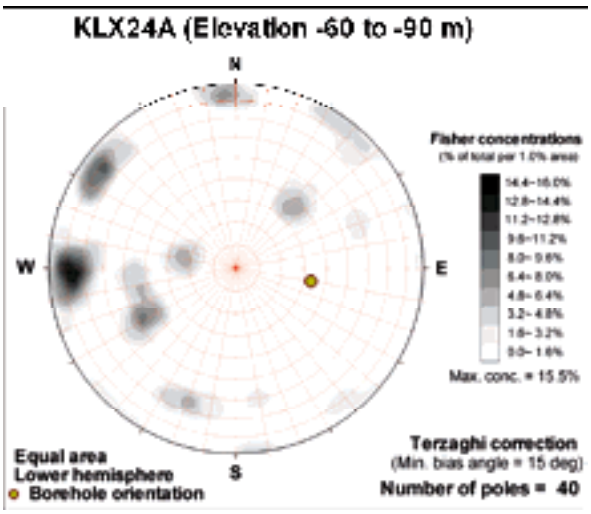
KLX24A (Elevation -60 to -90 m)
N
W
E
S
Fisher concentrations
(% of total per 1.0% area)
Max. conc. = 15.5%
Equal area
Lower hemisphere
Borehole orientation
Terzaghi correction
(Min. bias angle = 15 deg)
Number of poles = 40

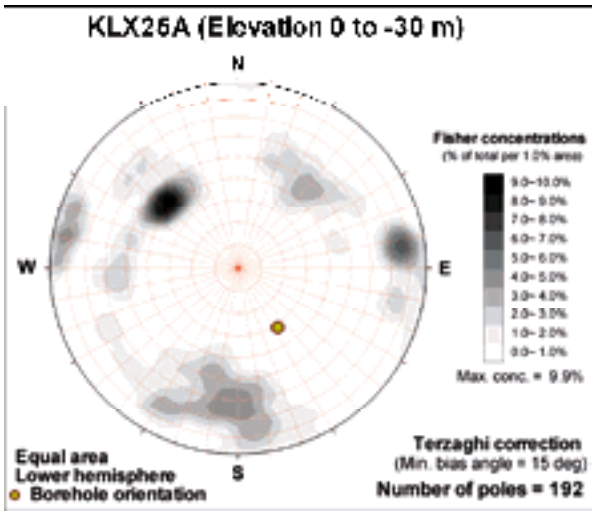
KLX25A (Elevation 0 to -30 m)
N
W
E
S
Fisher concentrations
(% of total per 1.0% area)
Max. conc. = 9.9%
Equal area
Lower hemisphere
Borehole orientation
Terzaghi correction
(Min. bias angle = 15 deg)
Number of poles = 192

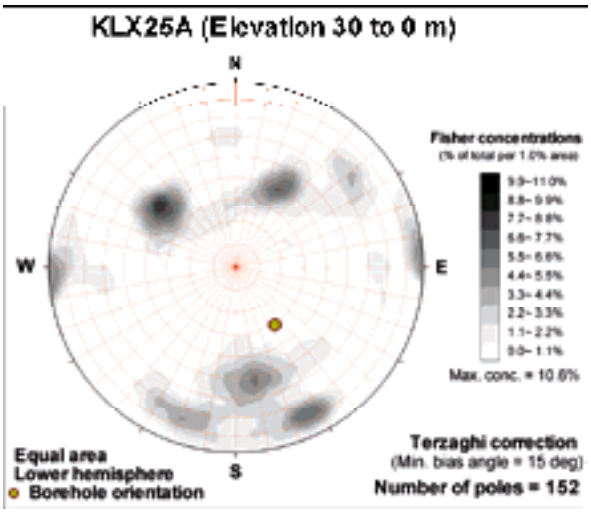
KLX25A (Elevation 30 to 0 m)
N
W
E
S
Fisher concentrations
(% of total per 1.0% area)
Max. conc. = 10.6%
Equal area
Lower hemisphere
Borehole orientation
Terzaghi correction
(Min. bias angle = 15 deg)
Number of poles = 152

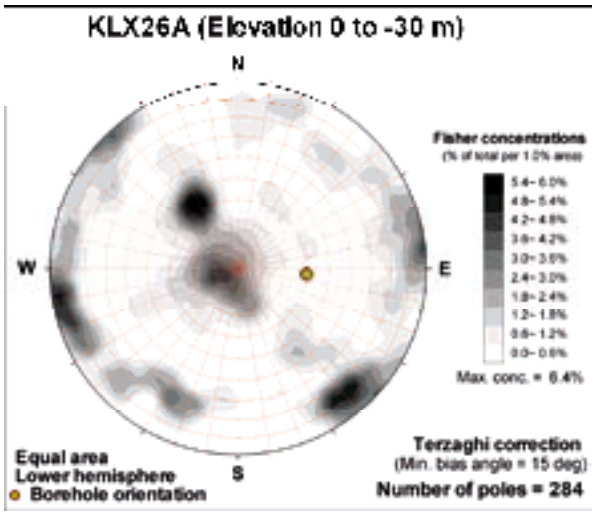
KLX26A (Elevation 0 to -30 m)
N
W
E
S
Fisher concentrations
(% of total per 1.0% area)
Max. conc. = 6.4%
Equal area
Lower hemisphere
Borehole orientation
Terzaghi correction
(Min. bias angle = 15 deg)
Number of poles = 284

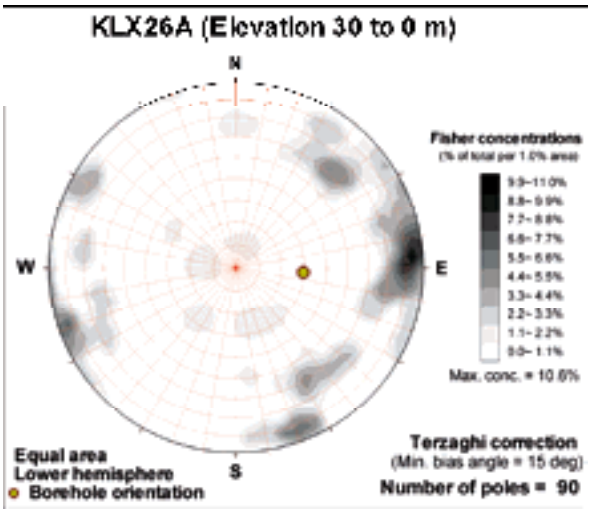
KLX26A (Elevation 30 to 0 m)
N
W
E
S
Fisher concentrations
(% of total per 1.0% area)
Max. conc. = 10.6%
Equal area
Lower hemisphere
Borehole orientation
Terzaghi correction
(Min. bias angle = 15 deg)
Number of poles = 90

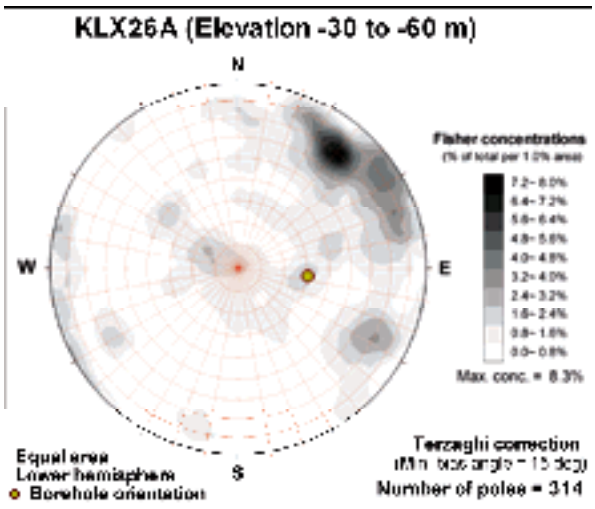
KLX26A (Elevation -30 to -60 m)
N
W
E
S
Fisher concentrations
(% of total per 1.0% area)
7.2– 8.0%
6.4– 7.2%
5.6– 6.4%
4.8– 5.6%
4.0– 4.8%
3.2– 4.0%
2.4– 3.2%
1.6– 2.4%
0.8– 1.6%
0.0– 0.8%
Max. conc. = 8.3%
Equal area
Lower hemisphere
Borehole orientation
Terzaghi correction
(Min. bias angle = 15 deg)
Number of poles = 314

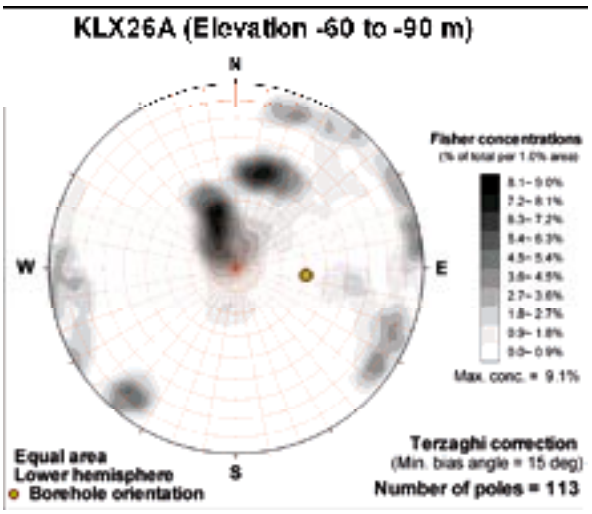
KLX26A (Elevation -60 to -90 m)
N
W
E
S
Fisher concentrations
(% of total per 1.0% area)
8.1– 9.0%
7.2– 8.1%
6.3– 7.2%
5.4– 6.3%
4.5– 5.4%
3.6– 4.5%
2.7– 3.6%
1.8– 2.7%
0.9– 1.8%
0.0– 0.9%
Max. conc. = 9.1%
Equal area
Lower hemisphere
Borehole orientation
Terzaghi correction
(Min. bias angle = 15 deg)
Number of poles = 113

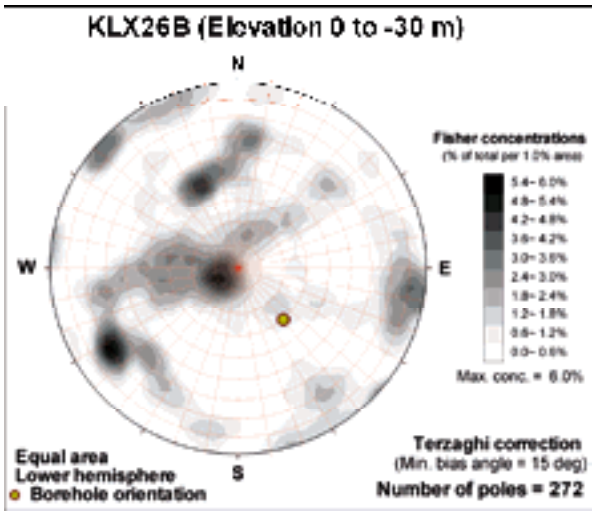
KLX26B (Elevation 0 to -30 m)
N
W
E
S
Fisher concentrations
(% of total per 1.0% area)
5.4– 6.0%
4.8– 5.4%
4.2– 4.8%
3.6– 4.2%
3.0– 3.6%
2.4– 3.0%
1.8– 2.4%
1.2– 1.8%
0.6– 1.2%
0.0– 0.6%
Max. conc. = 6.0%
Equal area
Lower hemisphere
Borehole orientation
Terzaghi correction
(Min. bias angle = 15 deg)
Number of poles = 272

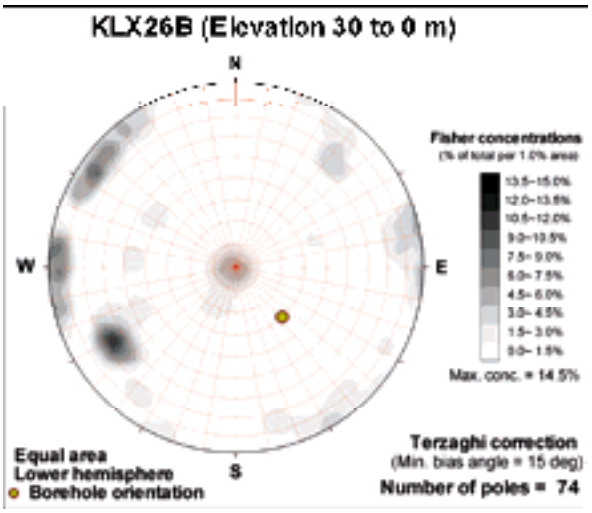
KLX26B (Elevation 30 to 0 m)
N
W
E
S
Fisher concentrations
(% of total per 1.0% area)
13.5–15.0%
12.0–13.5%
10.5–12.0%
9.0–10.5%
7.5– 9.0%
6.0– 7.5%
4.5– 6.0%
3.0– 4.5%
1.5– 3.0%
0.0– 1.5%
Max. conc. = 14.5%
Equal area
Lower hemisphere
Borehole orientation
Terzaghi correction
(Min. bias angle = 15 deg)
Number of poles = 74

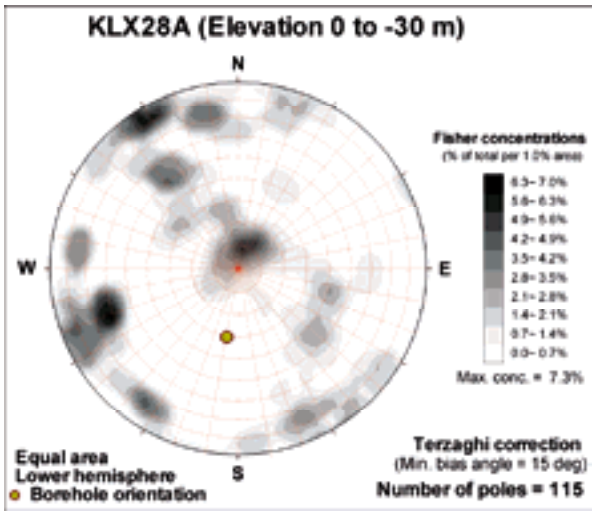
KLX28A (Elevation 0 to -30 m)
N
W
E
S
Fisher concentrations
(% of total per 1.0% area)
6.3– 7.0%
5.6– 6.3%
4.9– 5.6%
4.2– 4.9%
3.5– 4.2%
2.8– 3.5%
2.1– 2.8%
1.4– 2.1%
0.7– 1.4%
0.0– 0.7%
Max. conc. = 7.3%
Equal area
Lower hemisphere
Borehole orientation
Terzaghi correction
(Min. bias angle = 15 deg)
Number of poles = 115

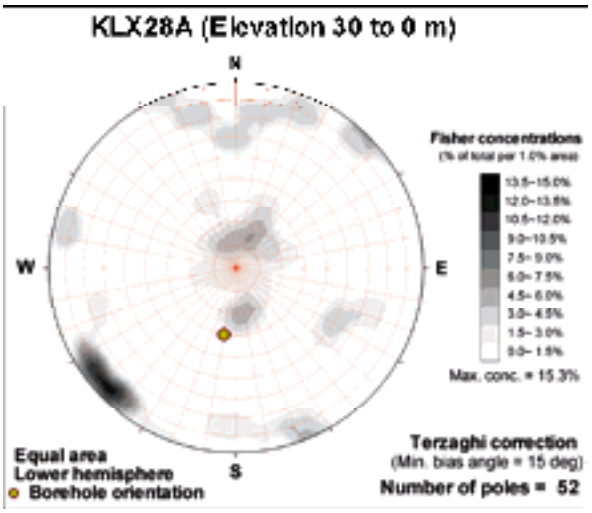
KLX28A (Elevation 30 to 0 m)
N
W
E
S
Fisher concentrations
(% of total per 1.0% area)
13.5–15.0%
12.0–13.5%
10.5–12.0%
9.0–10.5%
7.5– 9.0%
6.0– 7.5%
4.5– 6.0%
3.0– 4.5%
1.5– 3.0%
0.0– 1.5%
Max. conc. = 15.3%
Equal area
Lower hemisphere
Borehole orientation
Terzaghi correction
(Min. bias angle = 15 deg)
Number of poles = 52

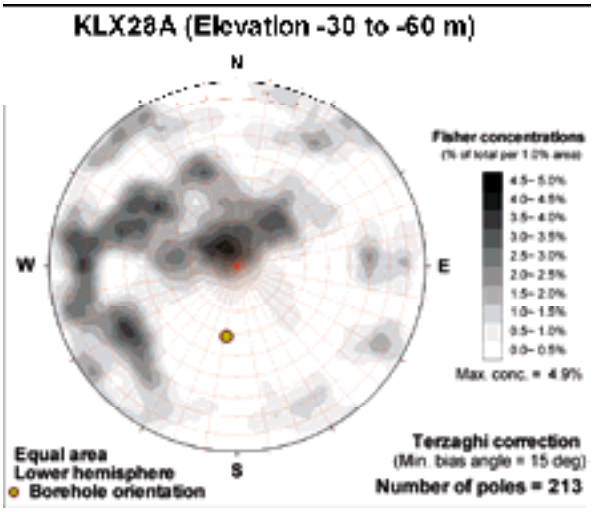
KLX28A (Elevation -30 to -60 m)
N
W
E
S
Fisher concentrations
Max. conc. = 4.9%
Equal area
Lower hemisphere
Borehole orientation
Terzaghi correction
(Min. bias angle = 15 deg)
Number of poles = 213

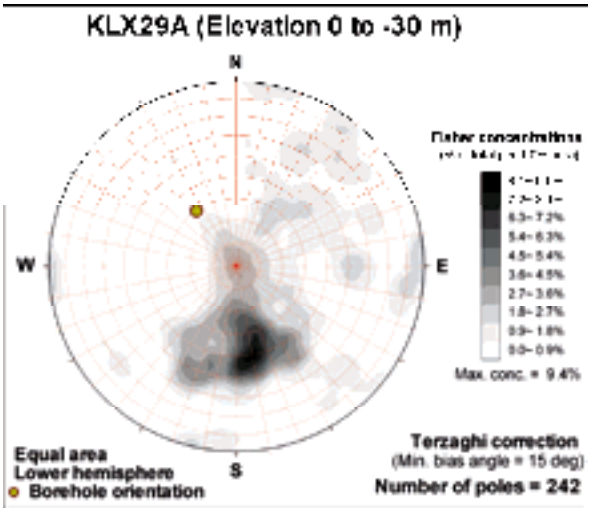
KLX29A (Elevation 0 to -30 m)
N
W
E
S
Fisher concentrations
Max. conc. = 9.4%
Equal area
Lower hemisphere
Borehole orientation
Terzaghi correction
(Min. bias angle = 15 deg)
Number of poles = 242

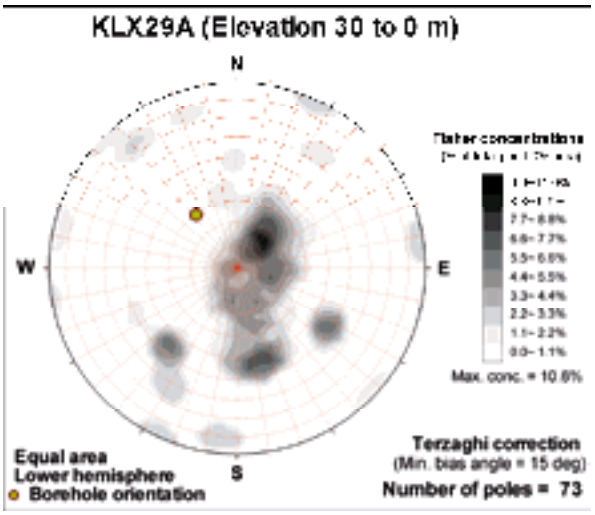
KLX29A (Elevation 30 to 0 m)
N
W
E
S
Fisher concentrations
Max. conc. = 10.6%
Equal area
Lower hemisphere
Borehole orientation
Terzaghi correction
(Min. bias angle = 15 deg)
Number of poles = 73

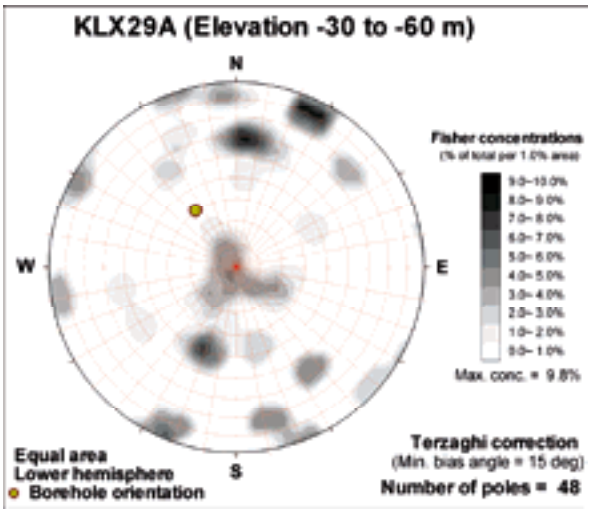
KLX29A (Elevation -30 to -60 m)
N
W
E
S
Fisher concentrations
Max. conc. = 9.8%
Equal area
Lower hemisphere
Borehole orientation
Terzaghi correction
(Min. bias angle = 15 deg)
Number of poles = 48

Appendix 6

WellCad plots for geological and hydrogeological data – Percussion boreholes

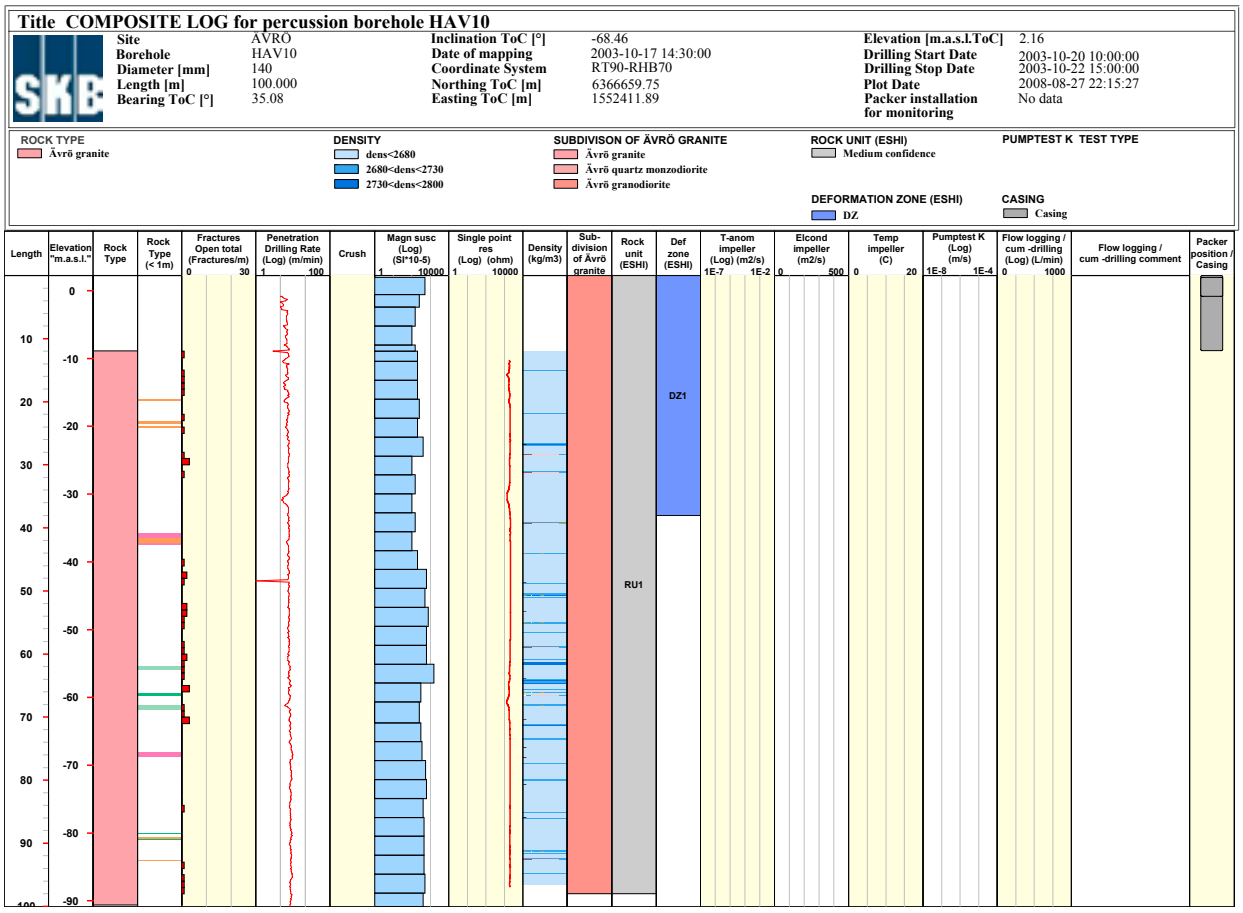

Title COMPOSITE LOG for percussion borehole HAV11

Site	AVRO	**Inclination ToC [°]**	-59.60	**Elevation [m.a.s.l.ToC]**	2.38
Borehole	HAV11	**Date of mapping**	2004-06-07 00:00:00	**Drilling Start Date**	2004-06-07 14:50:00
Diameter [mm]	140	**Coordinate System**	RT90-RHB70	**Drilling Stop Date**	2004-06-14 09:00:00
Length [m]	220.500	**Northing ToC [m]**	6366565.25	**Plot Date**	2008-08-27 22:15:27
Bearing ToC [°]	113.47	**Easting ToC [m]**	1553040.90	**Packer installation for monitoring**	No data

ROCK TYPE
- Fine-grained granite
- Granite
- Ävrö granite
- Quartz monzodiorite

DENSITY

SUBDIVISON OF ÄVRÖ GRANITE
- Ävrö granite
- Ävrö quartz monzodiorite
- Ävrö granodiorite

ROCK UNIT (ESHI)

DEFORMATION ZONE (ESHI)

PUMPTEST K TEST TYPE
- 1B: Pumpingtest-submersible Pump

CASING
- Casing

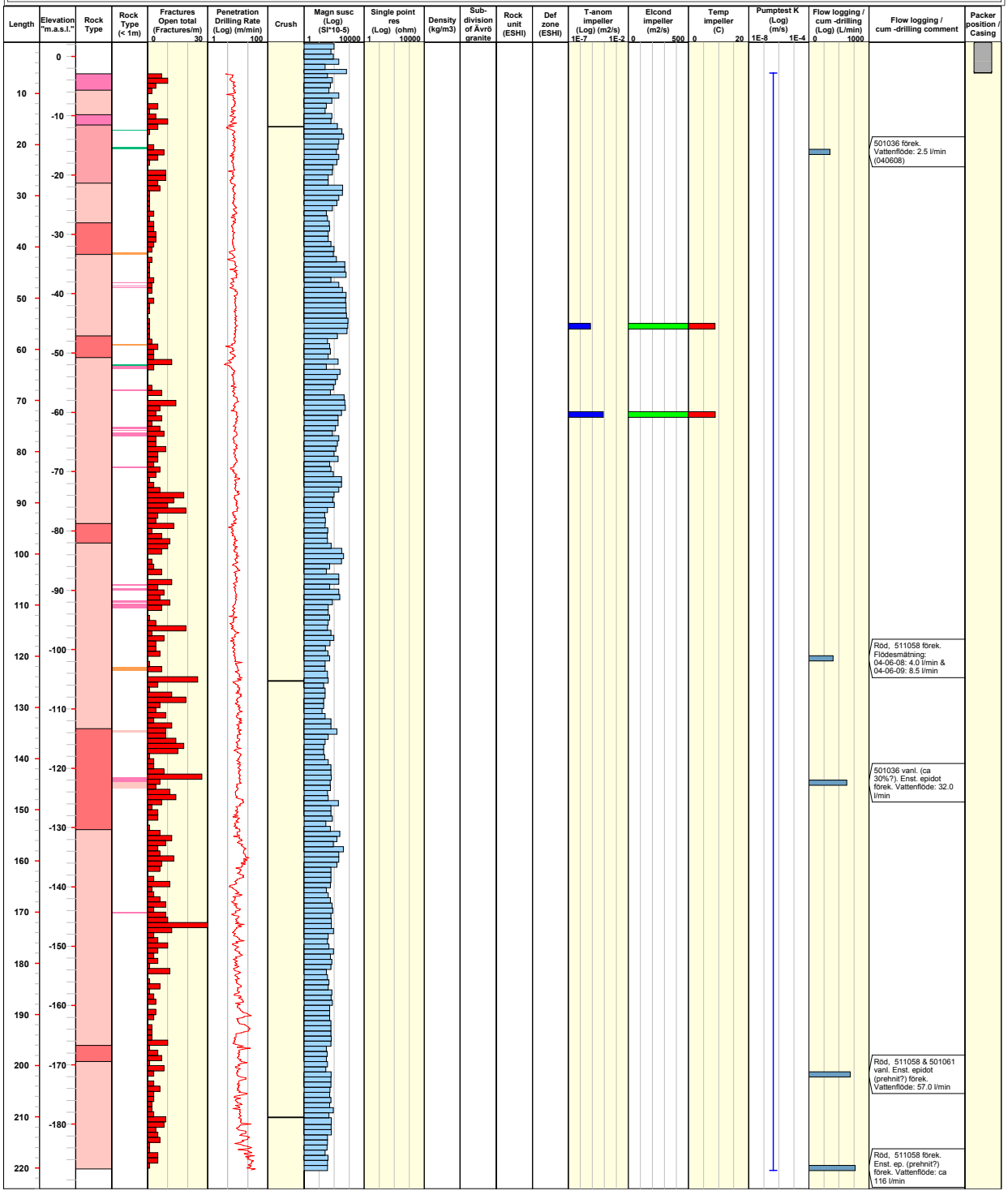

Title COMPOSITE LOG for percussion borehole HAV12

Site	AVRO	**Inclination ToC [°]**	-58.78	**Elevation [m.a.s.l.ToC]**	9.33
Borehole	HAV12	**Date of mapping**	2004-05-12 00:00:00	**Drilling Start Date**	2004-05-12 06:00:00
Diameter [mm]	140	**Coordinate System**	RT90-RHB70	**Drilling Stop Date**	2004-05-19 08:00:00
Length [m]	157.800	**Northing ToC [m]**	6367765.05	**Plot Date**	2008-08-27 22:15:27
Bearing ToC [°]	0.27	**Easting ToC [m]**	1553194.46	**Packer installation for monitoring**	No data

ROCK TYPE
- Fine-grained granite
- Ävrö granite
- Fine-grained diorite-gabbro

DENSITY

SUBDIVISON OF ÄVRÖ GRANITE
- Ävrö granite
- Ävrö quartz monzodiorite
- Ävrö granodiorite

ROCK UNIT (ESHI)

DEFORMATION ZONE (ESHI)

PUMPTEST K TEST TYPE
- 1B: Pumpingtest-submersible Pump

CASING
- Casing

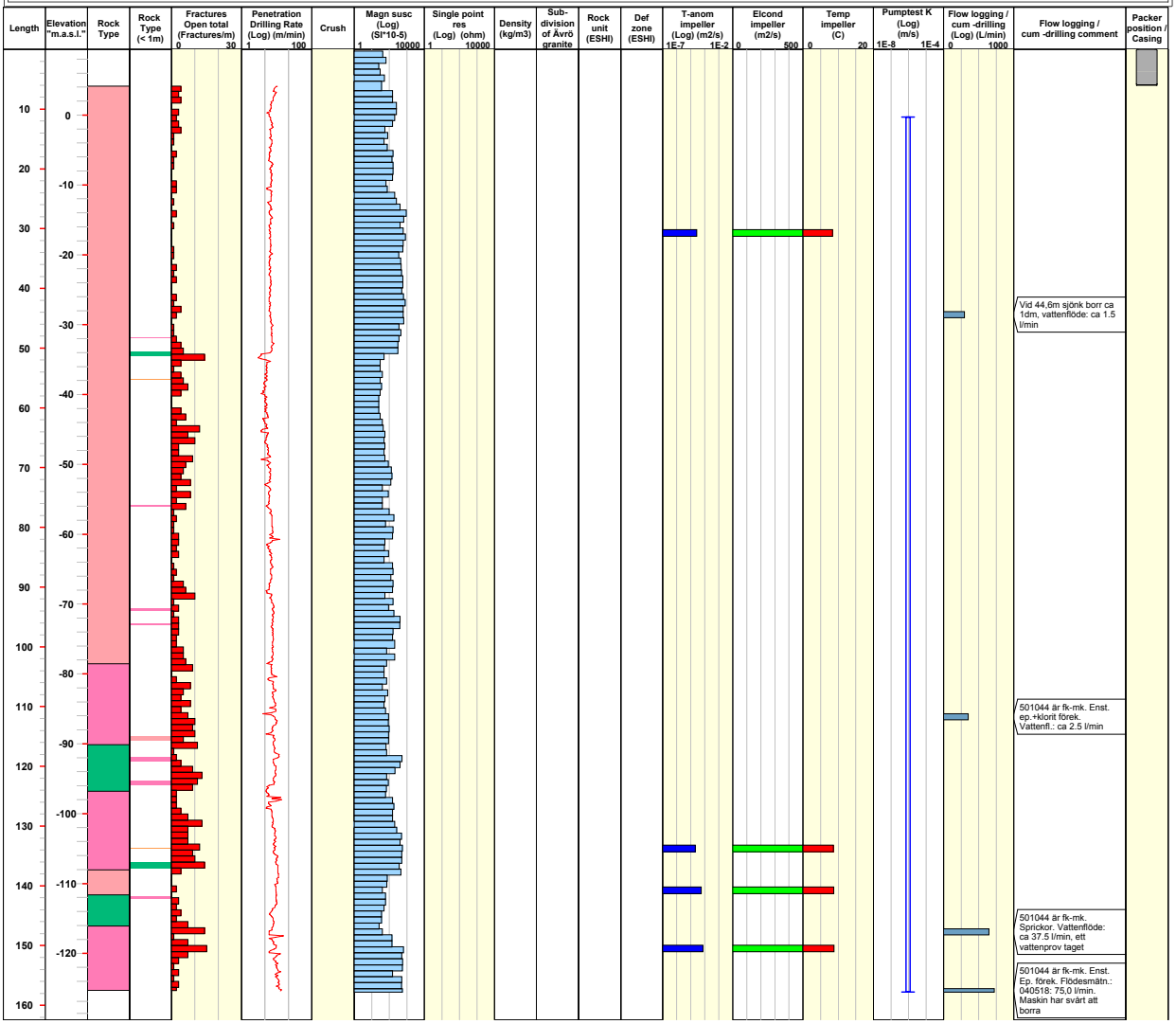

Title COMPOSITE LOG for percussion borehole HAV13

Site	AVRO	**Inclination ToC [°]**	-58.80	**Elevation [m.a.s.l.ToC]**	2.15
Borehole	HAV13	**Date of mapping**	2004-05-24 00:00:00	**Drilling Start Date**	2004-05-24 08:00:00
Diameter [mm]	140	**Coordinate System**	RT90-RHB70	**Drilling Stop Date**	2004-05-27 13:00:00
Length [m]	142.200	**Northing ToC [m]**	6367627.04	**Plot Date**	2008-08-27 22:15:27
Bearing ToC [°]	0.08	**Easting ToC [m]**	1552682.20	**Packer installation for monitoring**	No data

ROCK TYPE
- Fine-grained granite
- Ävrö granite

DENSITY

SUBDIVISON OF ÄVRÖ GRANITE
- Ävrö granite
- Ävrö quartz monzodiorite
- Ävrö granodiorite

ROCK UNIT (ESHI)

DEFORMATION ZONE (ESHI)

PUMPTEST K TEST TYPE

CASING
- Casing

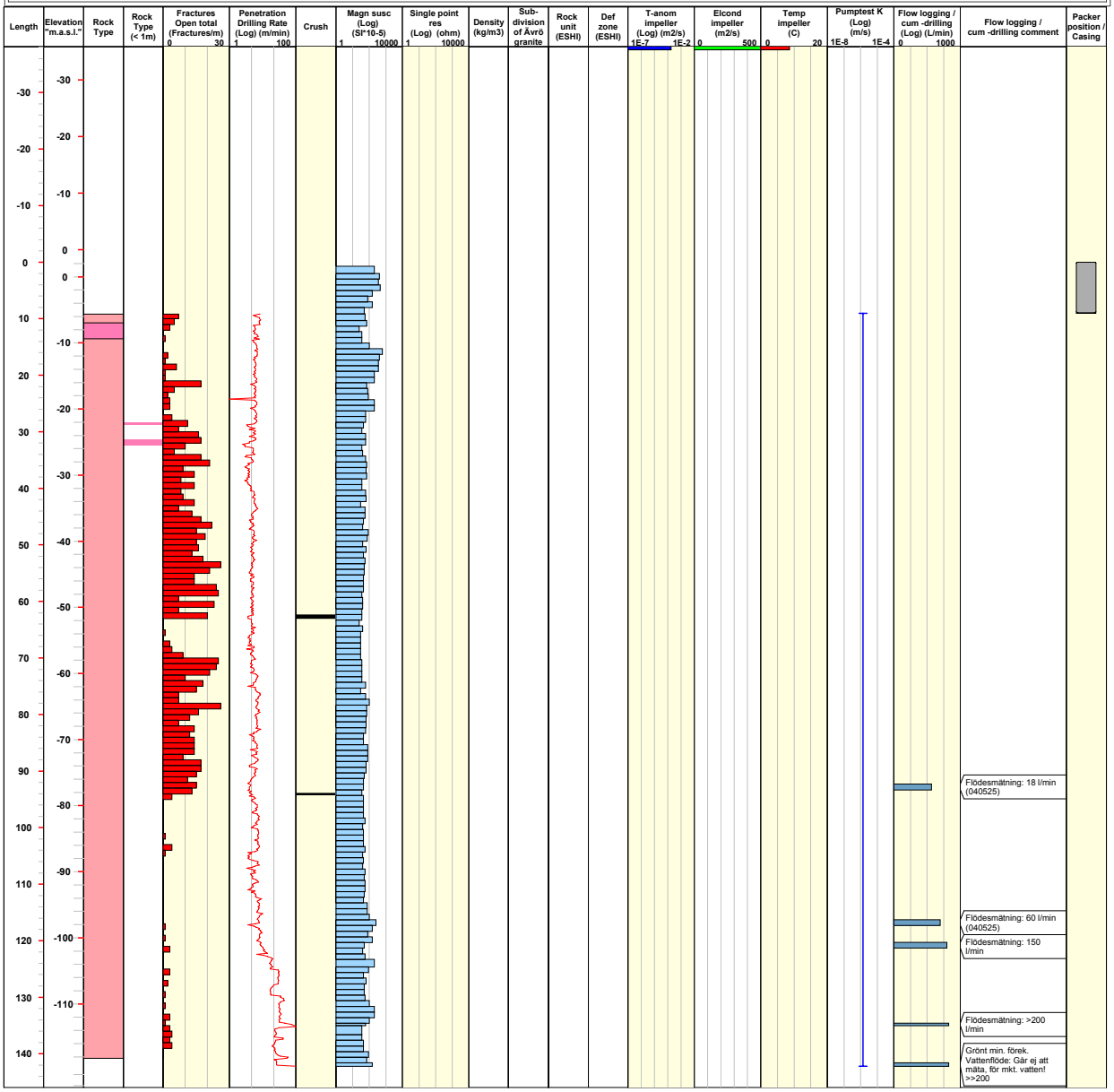

Title COMPOSITE LOG for percussion borehole HAV14

Site	AVRO	**Inclination ToC [°]**	-60.41	**Elevation [m.a.s.l.ToC]**	7.69
Borehole	HAV14	**Date of mapping**	2004-06-01 00:00:00	**Drilling Start Date**	2004-06-01 11:50:00
Diameter [mm]	136	**Coordinate System**	RT90-RHB70	**Drilling Stop Date**	2004-06-04 10:00:00
Length [m]	182.400	**Northing ToC [m]**	6367227.16	**Plot Date**	2008-08-27 22:15:27
Bearing ToC [°]	271.46	**Easting ToC [m]**	1552350.59	**Packer installation for monitoring**	No data

ROCK TYPE
- Fine-grained granite
- Pegmatite
- Ävrö granite
- Diorite / Gabbro
- Fine-grained diorite-gabbro

DENSITY

SUBDIVISON OF ÄVRÖ GRANITE
- Ävrö granite
- Ävrö quartz monzodiorite
- Ävrö granodiorite

ROCK UNIT (ESHI)

DEFORMATION ZONE (ESHI)

PUMPTEST K TEST TYPE
- 1B: Pumpingtest-submersible Pump

CASING
- Casing

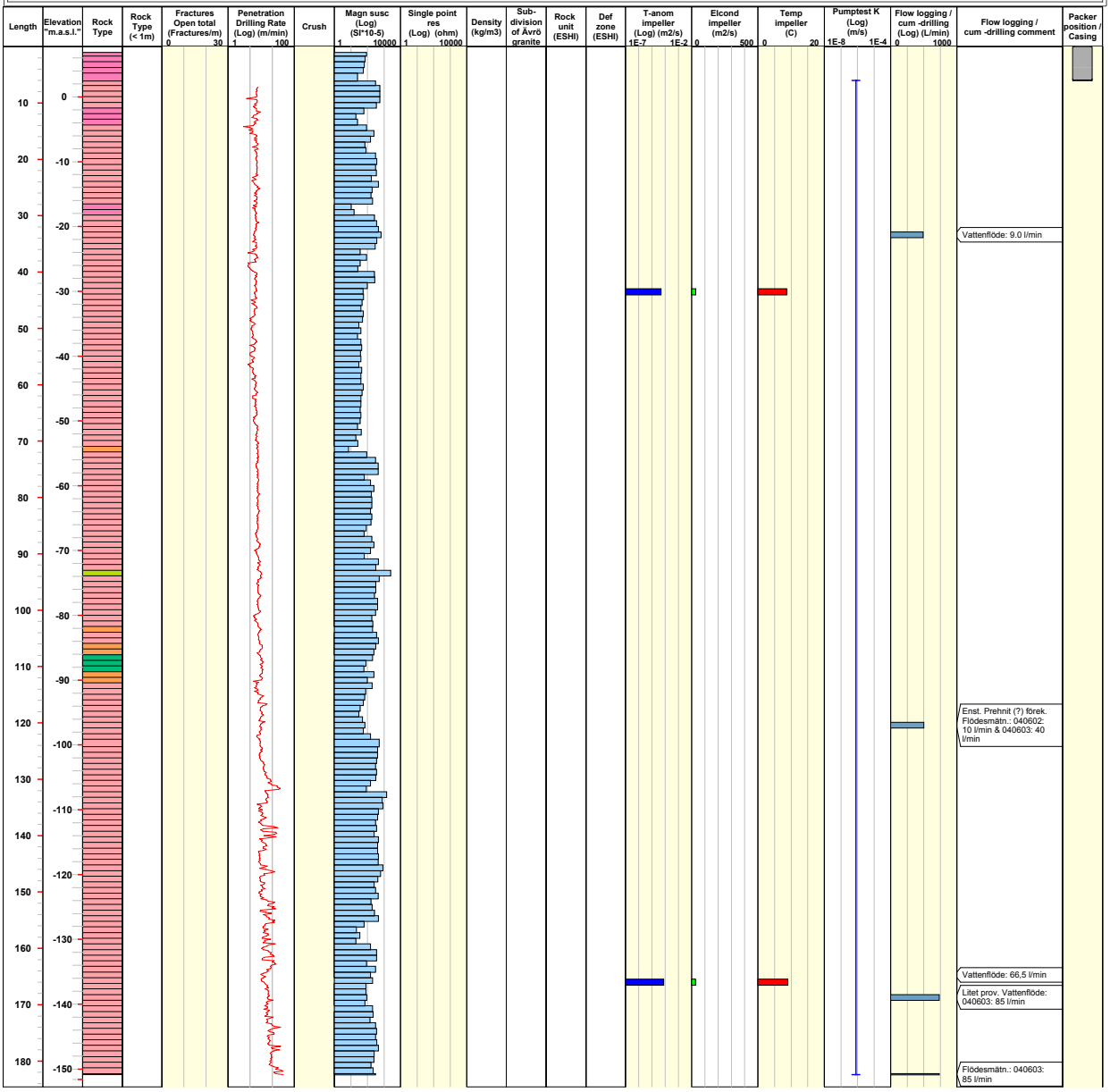

Title COMPOSITE LOG for percussion borehole HAV10

Site	AVRO	**Inclination ToC [°]**	-68.46	**Elevation [m.a.s.l.ToC]**	2.16
Borehole	HAV10	**Date of mapping**	2003-10-17 14:30:00	**Drilling Start Date**	2003-10-20 10:00:00
Diameter [mm]	140	**Coordinate System**	RT90-RHB70	**Drilling Stop Date**	2003-10-22 15:00:00
Length [m]	100.000	**Northing ToC [m]**	6366659.75	**Plot Date**	2008-08-27 22:15:27
Bearing ToC [°]	35.08	**Easting ToC [m]**	1552411.89	**Packer installation for monitoring**	No data

ROCK TYPE
- Ävrö granite

DENSITY
- dens<2680
- 2680<dens<2730
- 2730<dens<2800

SUBDIVISON OF ÄVRÖ GRANITE
- Ävrö granite
- Ävrö quartz monzodiorite
- Ävrö granodiorite

ROCK UNIT (ESHI)
- Medium confidence

DEFORMATION ZONE (ESHI)
- DZ

PUMPTEST K TEST TYPE

CASING
- Casing

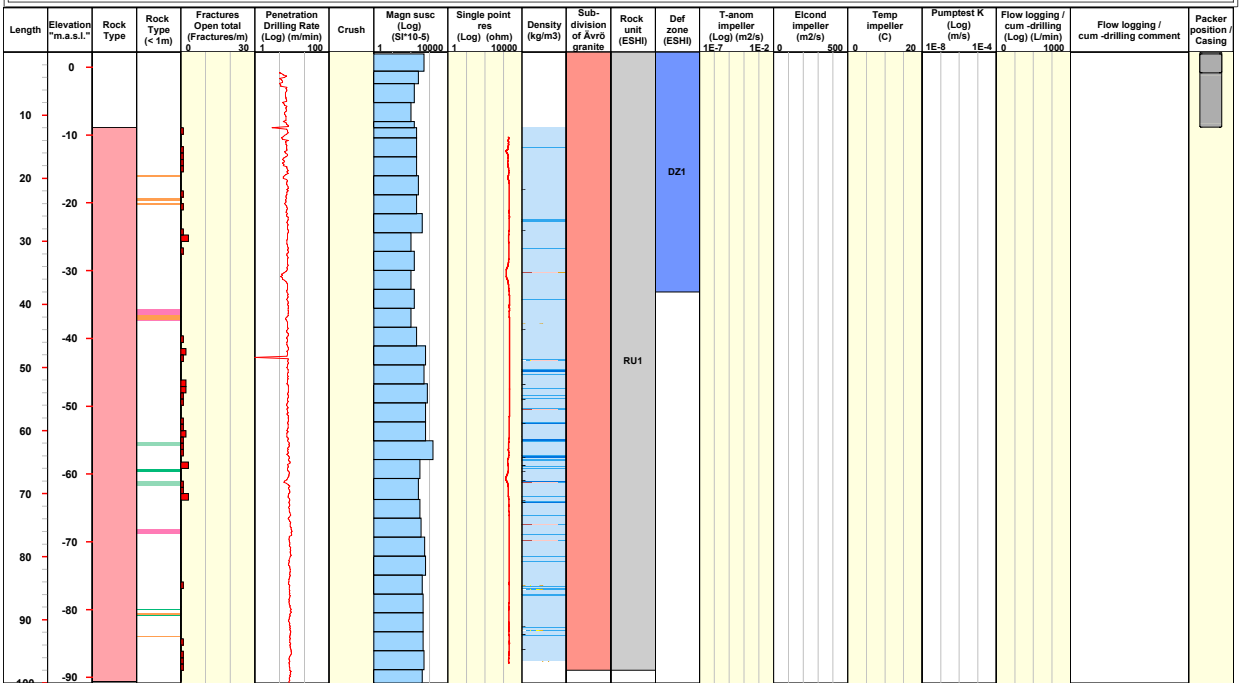

Title COMPOSITE LOG for percussion borehole HLX10

Site	LAXEMAR	**Inclination ToC [°]**	-68.68	**Elevation [m.a.s.l.ToC]**	11.67
Borehole	HLX10	**Date of mapping**	1992-09-30 00:00:00	**Drilling Start Date**	1992-09-30 00:00:00
Diameter [mm]	137	**Coordinate System**	RT90-RHB70	**Drilling Stop Date**	1992-09-30 00:00:00
Length [m]	85.000	**Northing ToC [m]**	6366634.98	**Plot Date**	2008-08-24 22:12:09
Bearing ToC [°]	176.67	**Easting ToC [m]**	1549140.19	**Packer installation for monitoring**	No data

ROCK TYPE — Ävrö granite

DENSITY

SUBDIVISON OF ÄVRÖ GRANITE

ROCK UNIT (ESHI)

DEFORMATION ZONE (ESHI)

PUMPTEST K TEST TYPE — 1B: Pumpingtest-submersible Pump

CASING — Casing

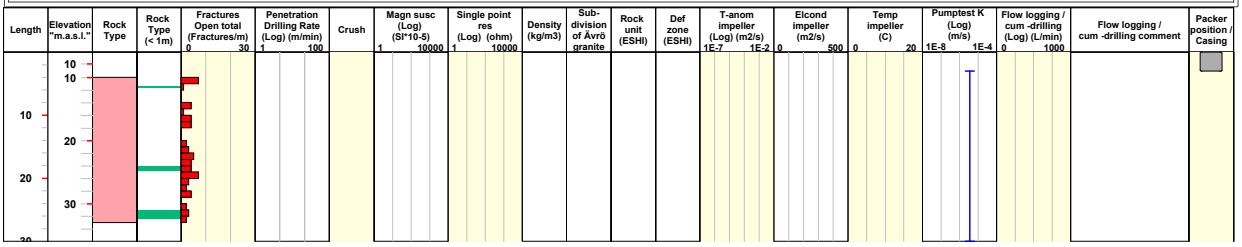

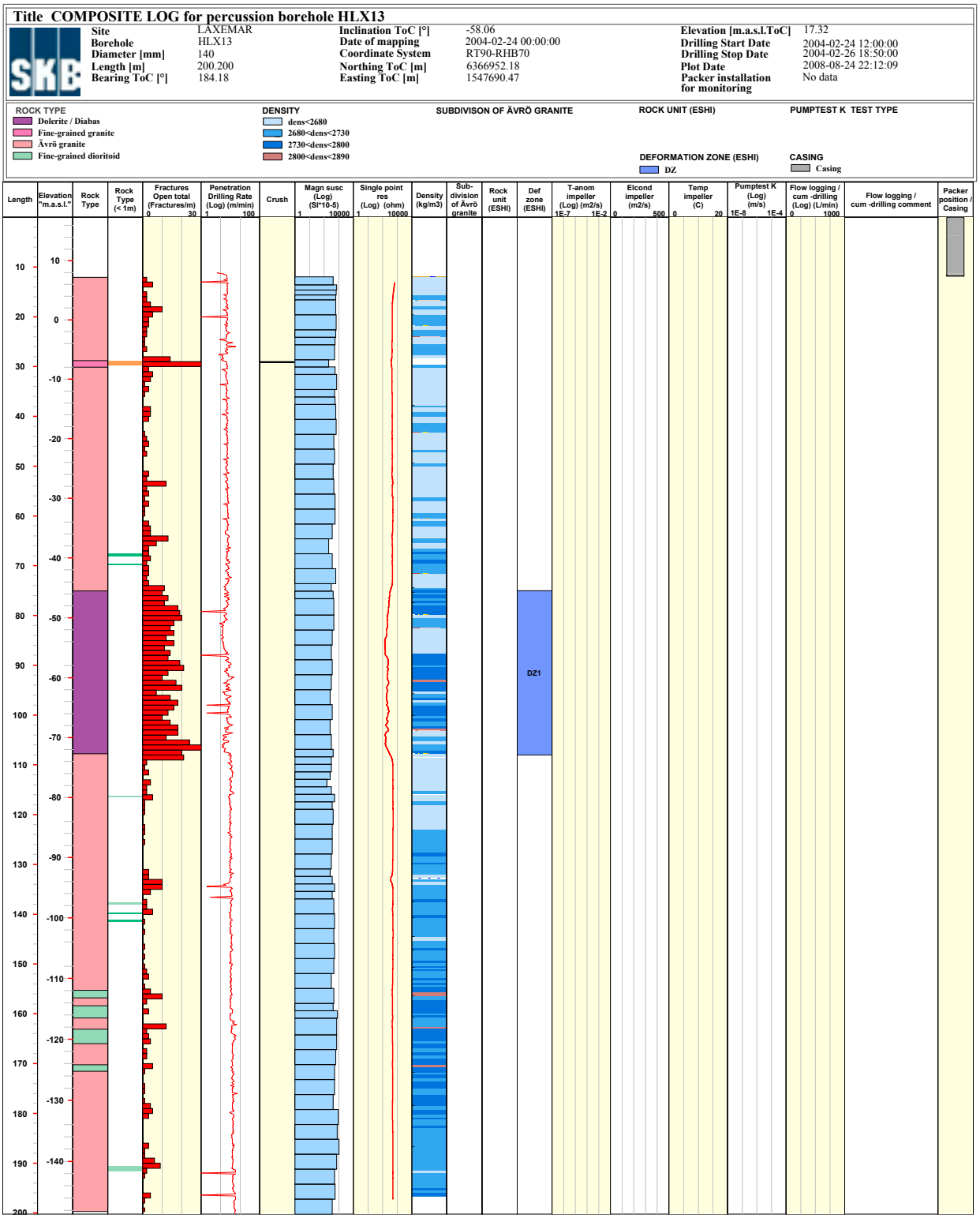
Title COMPOSITE LOG for percussion borehole HLX13
Site LAXEMAR
Borehole HLX13
Diameter [mm] 140
Length [m] 200.200
Bearing ToC [°] 184.18
Inclination ToC [°] -58.06
Date of mapping 2004-02-24 00:00:00
Coordinate System RT90-RHB70
Northing ToC [m] 6366952.18
Easting ToC [m] 1547690.47
Elevation [m.a.s.l.ToC] 17.32
Drilling Start Date 2004-02-24 12:00:00
Drilling Stop Date 2004-02-26 18:50:00
Plot Date 2008-08-24 22:12:09
Packer installation for monitoring No data
ROCK TYPE
Dolerite / Diabas
Fine-grained granite
Ävrö granite
Fine-grained dioritoid
DENSITY
dens<2680
2680<dens<2730
2730<dens<2800
2800<dens<2890
SUBDIVISON OF ÄVRÖ GRANITE
ROCK UNIT (ESHI)
PUMPTEST K TEST TYPE
DEFORMATION ZONE (ESHI)
DZ
CASING
Casing
Length
Elevation "m.a.s.l."
Rock Type
Rock Type (< 1m)
Fractures Open total (Fractures/m)
Penetration Drilling Rate (Log) (m/min)
Crush
Magn susc (Log) (SI*10-5)
Single point res (Log) (ohm)
Density (kg/m3)
Sub-division of Ävrö granite
Rock unit (ESHI)
Def zone (ESHI)
T-anom impeller (Log) (m2/s)
Elcond impeller (m2/s)
Temp impeller (C)
Pumptest K (Log) (m/s)
Flow logging / cum -drilling (Log) (L/min)
Flow logging / cum -drilling comment
Packer position / Casing
DZ1

Title COMPOSITE LOG for percussion borehole HLX14

Site	LAXEMAR	**Inclination ToC [°]**	-68.64	**Elevation [m.a.s.l.ToC]**	17.09
Borehole	HLX14	**Date of mapping**	2004-03-08 00:00:00	**Drilling Start Date**	2004-03-08 10:00:00
Diameter [mm]	139	**Coordinate System**	RT90-RHB70	**Drilling Stop Date**	2004-03-11 10:00:00
Length [m]	115.900	**Northing ToC [m]**	7208.67	**Plot Date**	2008-08-24 22:12:09
Bearing ToC [°]	101.70	**Easting ToC [m]**	-1694.65	**Packer installation for monitoring**	2004-11-15 10:30:00

ROCK TYPE LAXEMAR
- Ävrö granite
- Fine-grained dioritoid

DENSITY

SUBDIVISON OF ÄVRÖ GRANITE

ROCK UNIT (ESHI)

PUMPTEST K TEST TYPE
- 1B: Pumpingtest-submersible Pump

DEFORMATION ZONE (ESHI)

CASING
- Casing

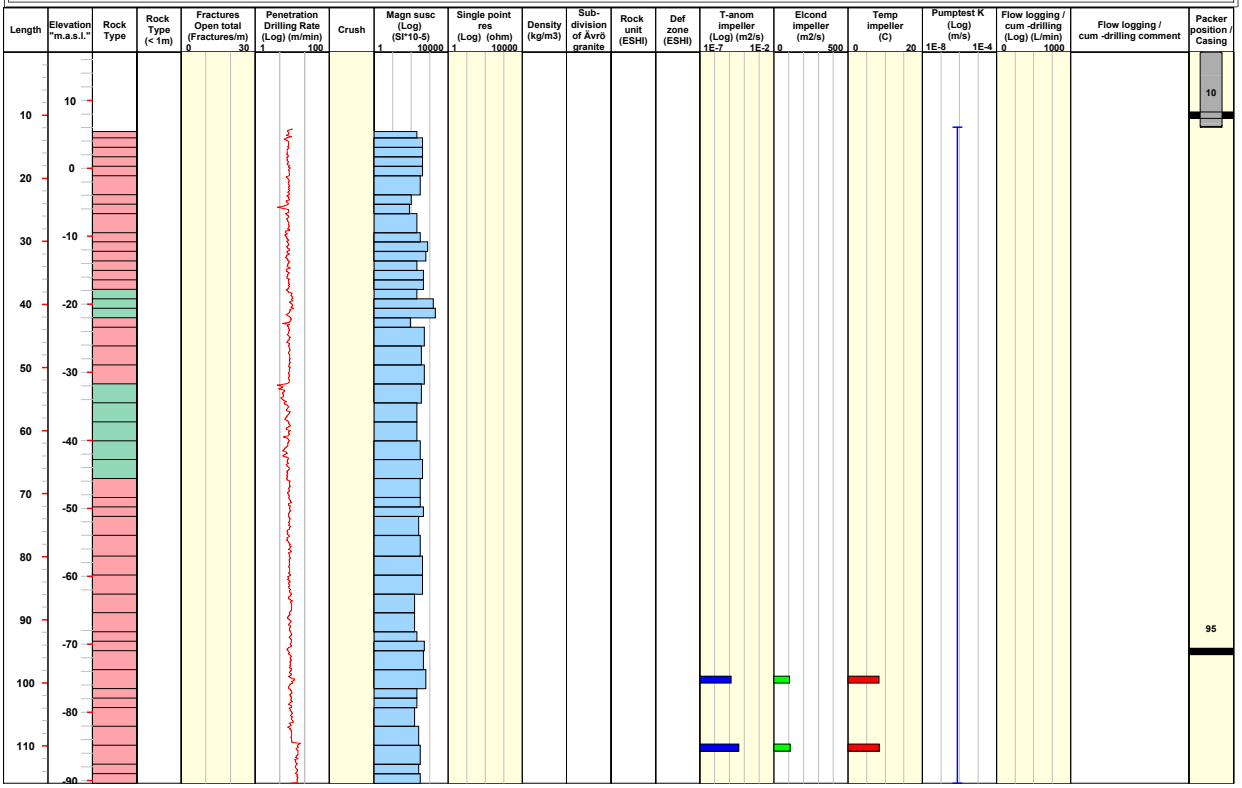

Title COMPOSITE LOG for percussion borehole HLX15

Site	LAXEMAR	**Inclination ToC [°]**	-58.36	**Elevation [m.a.s.l.ToC]**	4.74
Borehole	HLX15	**Date of mapping**	2004-04-27 00:00:00	**Drilling Start Date**	2004-04-27 07:00:00
Diameter [mm]	137	**Coordinate System**	RT90-RHB70	**Drilling Stop Date**	2004-04-29 09:30:00
Length [m]	151.900	**Northing ToC [m]**	6365361.16	**Plot Date**	2008-08-24 22:12:09
Bearing ToC [°]	184.65	**Easting ToC [m]**	1548664.06	**Packer installation for monitoring**	No data

ROCK TYPE
- Pegmatite
- Granite
- Quartz monzodiorite
- Soil

DENSITY
- dens<2680
- 2680<dens<2730
- 2730<dens<2800
- 2800<dens<2890

SUBDIVISON OF ÄVRÖ GRANITE

ROCK UNIT (ESHI)
- Medium confidence

DEFORMATION ZONE (ESHI)

PUMPTEST K TEST TYPE

CASING
- Casing

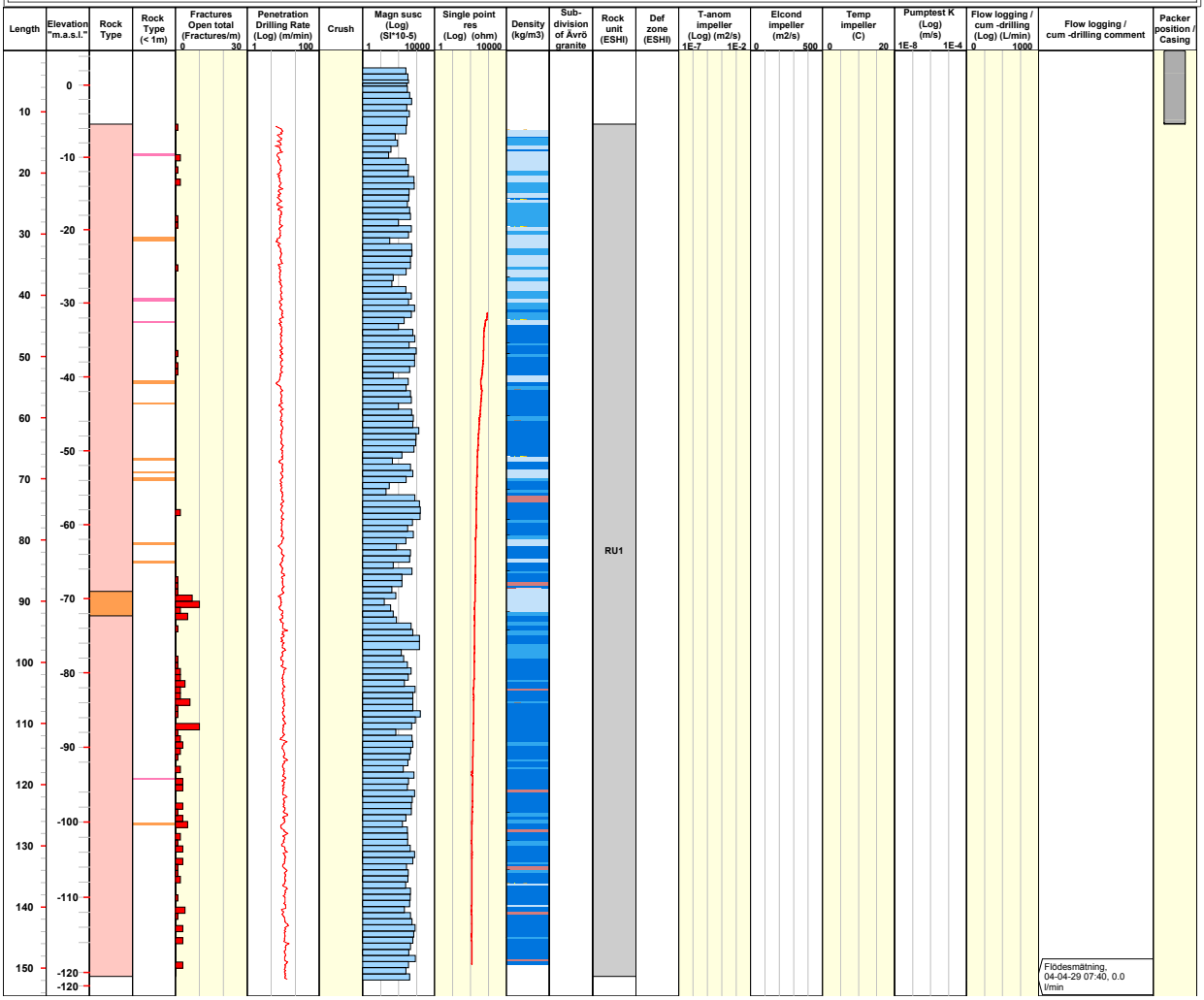

Title COMPOSITE LOG for percussion borehole HLX16

Site	LAXEMAR	**Inclination ToC [°]**	-58.09	**Elevation [m.a.s.l.ToC]**	3.58
Borehole	HLX16	**Date of mapping**	2004-06-22 00:00:00	**Drilling Start Date**	2004-06-22 10:15:00
Diameter [mm]	138	**Coordinate System**	RT90-RHB70	**Drilling Stop Date**	2004-06-24 09:15:00
Length [m]	202.200	**Northing ToC [m]**	6366024.61	**Plot Date**	2008-08-24 22:12:09
Bearing ToC [°]	139.90	**Easting ToC [m]**	1549914.93	**Packer installation for monitoring**	No data

ROCK TYPE
- Fine-grained granite
- Ävrö granite
- Diorite / Gabbro
- Fine-grained diorite-gabbro

DENSITY

SUBDIVISON OF ÄVRÖ GRANITE
- Ävrö granite
- Ävrö quartz monzodiorite
- Ävrö granodiorite

ROCK UNIT (ESHI)

DEFORMATION ZONE (ESHI)

PUMPTEST K TEST TYPE

CASING
- Casing

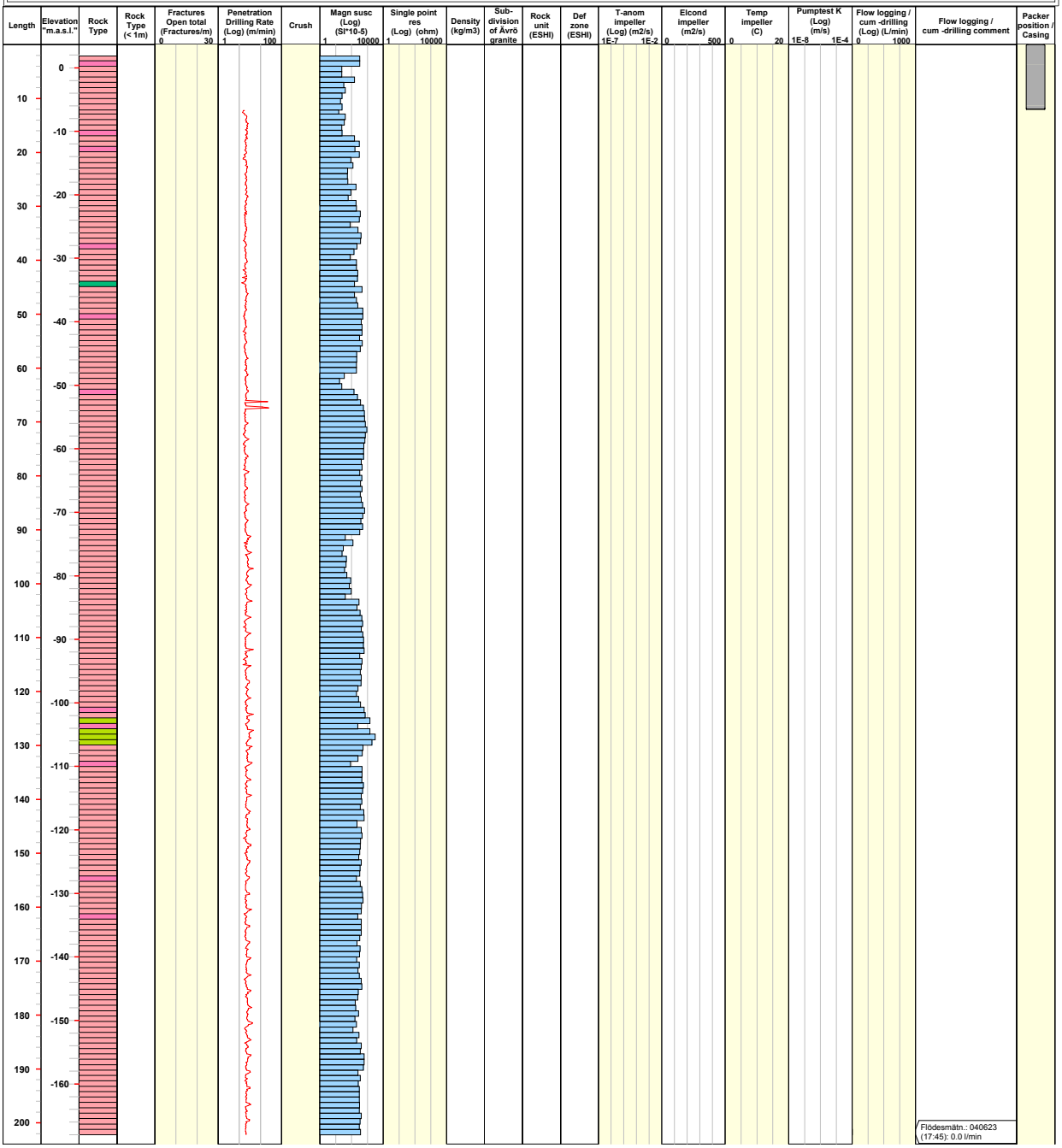

Title COMPOSITE LOG for percussion borehole HLX17

Site	LAXEMAR	**Inclination ToC [°]**	-59.48	**Elevation [m.a.s.l.ToC]**	3.28
Borehole	HLX17	**Date of mapping**	2004-06-28 00:00:00	**Drilling Start Date**	2004-06-28 14:30:00
Diameter [mm]	139	**Coordinate System**	RT90-RHB70	**Drilling Stop Date**	2004-07-01 09:00:00
Length [m]	202.200	**Northing ToC [m]**	6365950.70	**Plot Date**	2008-08-24 22:12:09
Bearing ToC [°]	310.94	**Easting ToC [m]**	1550040.80	**Packer installation for monitoring**	No data

ROCK TYPE
- Fine-grained granite
- Ävrö granite
- Diorite / Gabbro

DENSITY
- dens<2680
- 2680<dens<2730
- 2730<dens<2800
- 2800<dens<2890

SUBDIVISON OF ÄVRÖ GRANITE
- Ävrö granite
- Ävrö quartz monzodiorite
- Ävrö granodiorite

ROCK UNIT (ESHI)
- Medium confidence

DEFORMATION ZONE (ESHI)

PUMPTEST K TEST TYPE

CASING
- Casing

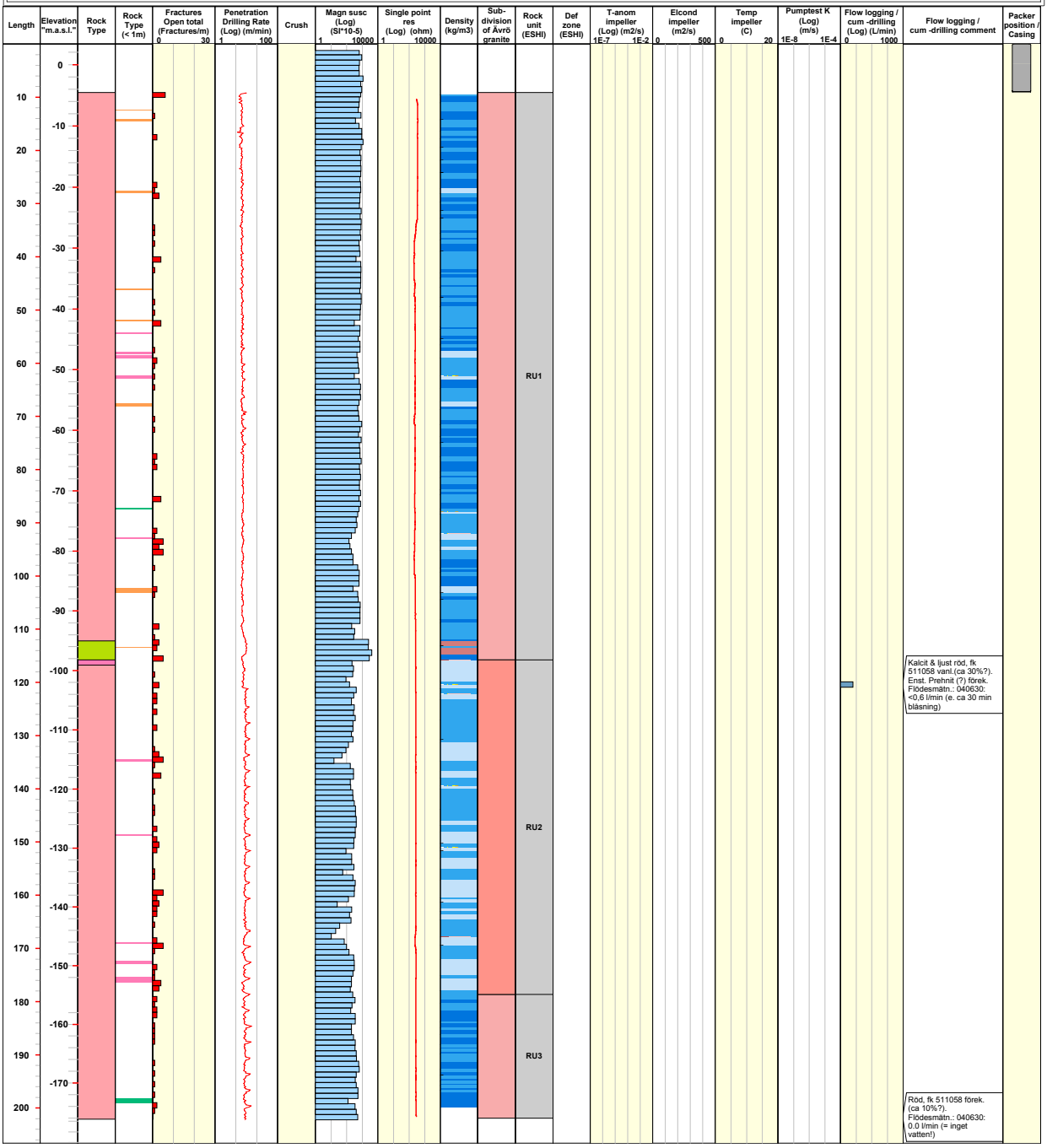

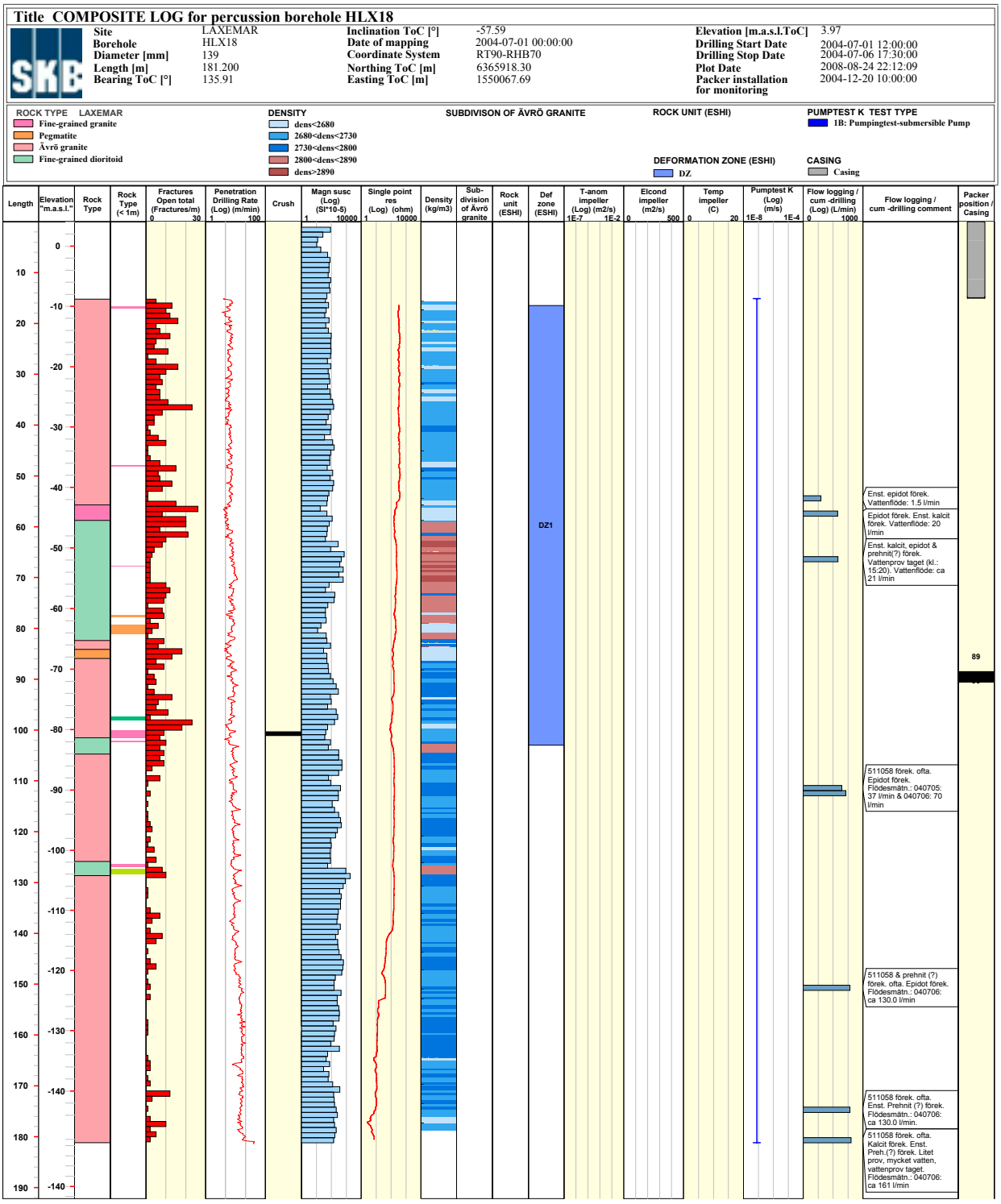
Title COMPOSITE LOG for percussion borehole HLX18
Site LAXEMAR
Borehole HLX18
Diameter [mm] 139
Length [m] 181.200
Bearing ToC [°] 135.91
Inclination ToC [°] -57.59
Date of mapping 2004-07-01 00:00:00
Coordinate System RT90-RHB70
Northing ToC [m] 6365918.30
Easting ToC [m] 1550067.69
Elevation [m.a.s.l.ToC] 3.97
Drilling Start Date 2004-07-01 12:00:00
Drilling Stop Date 2004-07-06 17:30:00
Plot Date 2008-08-24 22:12:09
Packer installation for monitoring 2004-12-20 10:00:00
ROCK TYPE LAXEMAR
Fine-grained granite
Pegmatite
Ävrö granite
Fine-grained dioritoid
DENSITY
dens<2680
2680<dens<2730
2730<dens<2800
2800<dens<2890
dens>2890
SUBDIVISON OF ÄVRÖ GRANITE
ROCK UNIT (ESHI)
DEFORMATION ZONE (ESHI)
DZ
PUMPTEST K TEST TYPE
1B: Pumpingtest-submersible Pump
CASING
Casing
Length
Elevation "m.a.s.l."
Rock Type
Rock Type (< 1m)
Fractures Open total (Fractures/m)
Penetration Drilling Rate (Log) (m/min)
Crush
Magn susc (Log) (SI*10-5)
Single point res (Log) (ohm)
Density (kg/m3)
Sub-division of Ävrö granite
Rock unit (ESHI)
Def zone (ESHI)
T-anom impeller (Log) (m2/s)
Elcond impeller (m2/s)
Temp impeller (C)
Pumptest K (Log) (m/s)
Flow logging / cum -drilling (Log) (L/min)
Flow logging / cum -drilling comment
Packer position / Casing
DZ1
Enst. epidot förek. Vattenflöde: 1.5 l/min
Epidot förek. Enst. kalcit förek. Vattenflöde: 20 l/min
Enst. kalcit, epidot & prehnit(?) förek. Vattenprov taget (kl.: 15:20). Vattenflöde: ca 21 l/min
89
511058 förek. ofta. Epidot förek. Flödesmätn.: 040705: 37 l/min & 040706: 70 l/min
511058 & prehnit (?) förek. ofta. Epidot förek. Flödesmätn.: 040706: ca 130.0 l/min
511058 förek. ofta. Enst. Prehnit (?) förek. Flödesmätn.: 040706: ca 130.0 l/min.
511058 förek. ofta. Kalcit förek. Enst. Preh.(?) förek. Litet prov, mycket vatten, vattenprov taget. Flödesmätn.: 040706: ca 161 l/min

Title COMPOSITE LOG for percussion borehole HLX19

Site	LAXEMAR	**Inclination ToC [°]**	-57.89	**Elevation [m.a.s.l.ToC]**	5.88
Borehole	HLX19	**Date of mapping**	2003-09-30 18:30:00	**Drilling Start Date**	2004-08-10 13:30:00
Diameter [mm]	137	**Coordinate System**	RT90-RHB70	**Drilling Stop Date**	2004-08-12 20:15:00
Length [m]	202.200	**Northing ToC [m]**	6365757.06	**Plot Date**	2008-08-24 22:12:09
Bearing ToC [°]	130.04	**Easting ToC [m]**	1550090.91	**Packer installation for monitoring**	No data

ROCK TYPE
- Fine-grained granite
- Pegmatite
- Ävrö granite
- Diorite / Gabbro
- Fine-grained diorite-gabbro

DENSITY
- dens<2680
- 2680<dens<2730
- 2730<dens<2800
- 2800<dens<2890
- dens>2890

SUBDIVISON OF ÄVRÖ GRANITE

ROCK UNIT (ESHI)

DEFORMATION ZONE (ESHI)
- DZ

PUMPTEST K TEST TYPE

CASING
- Casing

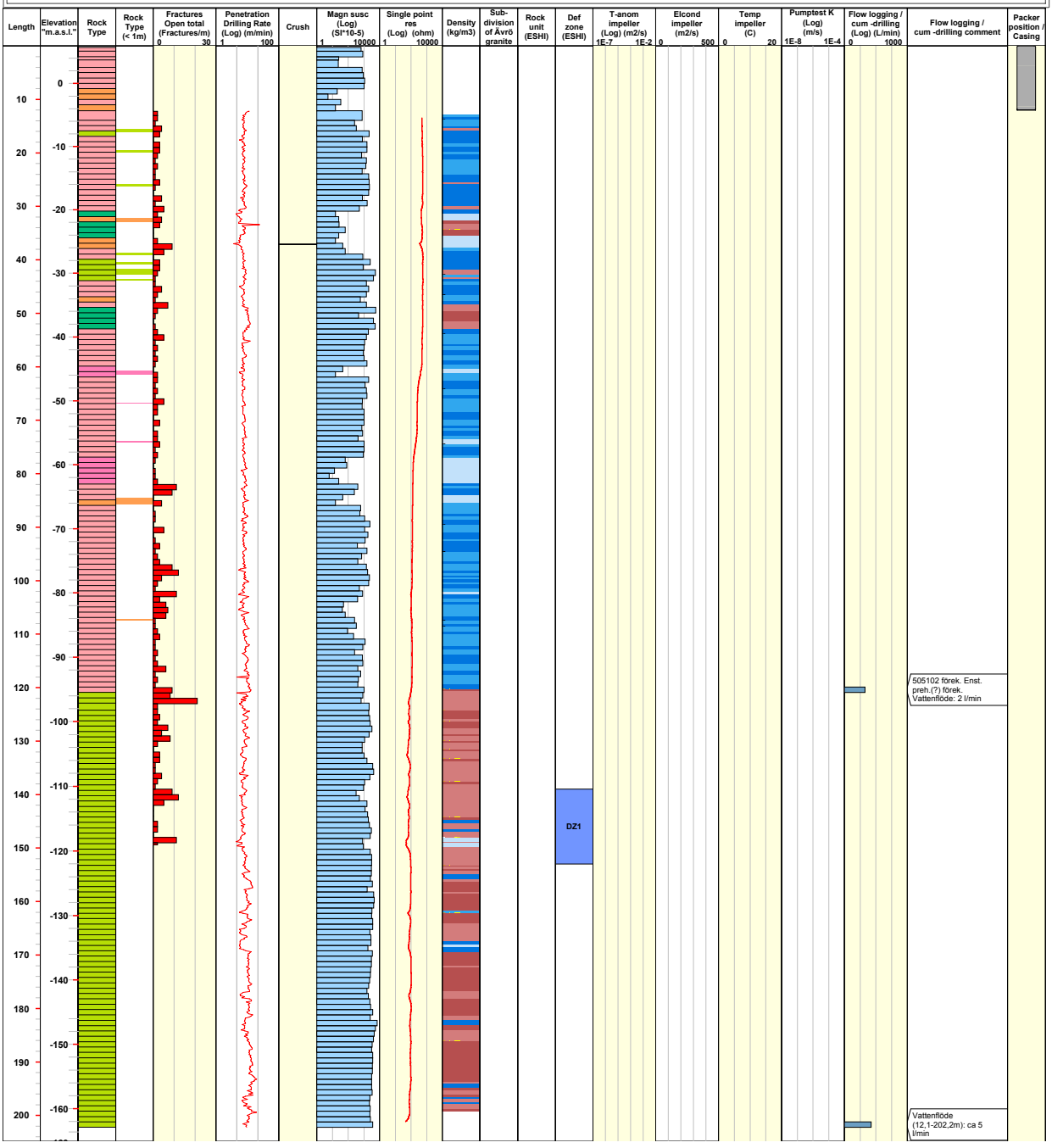

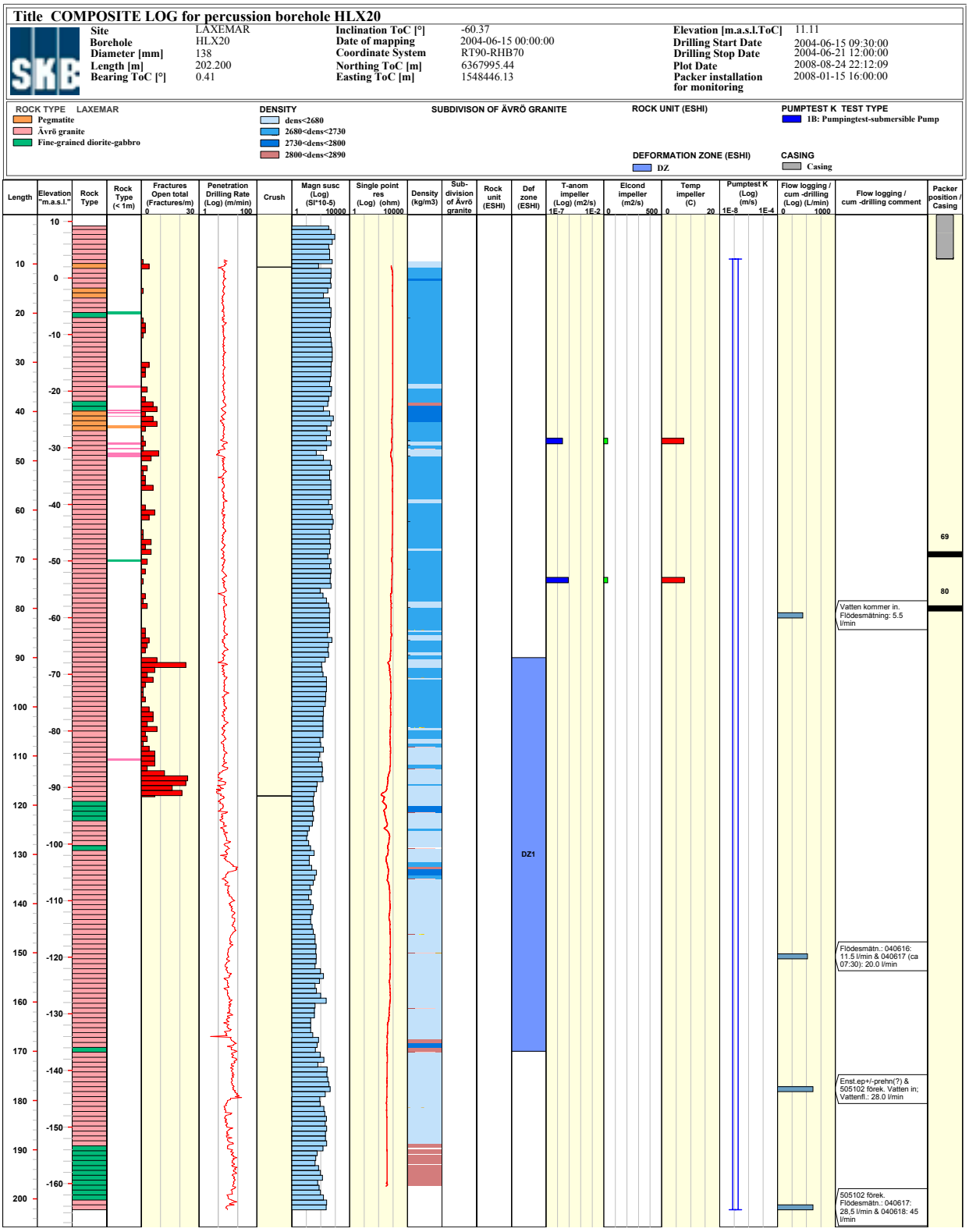
Title COMPOSITE LOG for percussion borehole HLX20
Site LAXEMAR
Borehole HLX20
Diameter [mm] 138
Length [m] 202.200
Bearing ToC [°] 0.41
Inclination ToC [°] -60.37
Date of mapping 2004-06-15 00:00:00
Coordinate System RT90-RHB70
Northing ToC [m] 6367995.44
Easting ToC [m] 1548446.13
Elevation [m.a.s.l.ToC] 11.11
Drilling Start Date 2004-06-15 09:30:00
Drilling Stop Date 2004-06-21 12:00:00
Plot Date 2008-08-24 22:12:09
Packer installation for monitoring 2008-01-15 16:00:00
ROCK TYPE LAXEMAR
Pegmatite
Ävrö granite
Fine-grained diorite-gabbro
DENSITY
dens<2680
2680<dens<2730
2730<dens<2800
2800<dens<2890
SUBDIVISON OF ÄVRÖ GRANITE
ROCK UNIT (ESHI)
DEFORMATION ZONE (ESHI)
DZ
PUMPTEST K TEST TYPE
1B: Pumpingtest-submersible Pump
CASING
Casing
Length
Elevation "m.a.s.l."
Rock Type
Rock Type (< 1m)
Fractures Open total (Fractures/m)
Penetration Drilling Rate (Log) (m/min)
Crush
Magn susc (Log) (SI*10-5)
Single point res (Log) (ohm)
Density (kg/m3)
Sub-division of Ävrö granite
Rock unit (ESHI)
Def zone (ESHI)
T-anom impeller (Log) (m2/s)
Elcond impeller (m2/s)
Temp impeller (C)
Pumptest K (Log) (m/s)
Flow logging / cum -drilling (Log) (L/min)
Flow logging / cum -drilling comment
Packer position / Casing
DZ1
69
80
Vatten kommer in. Flödesmätning: 5.5 l/min
Flödesmätn.: 040616: 11.5 l/min & 040617 (ca 07:30): 20.0 l/min
Enst.ep+/-prehn(?) & 505102 förek. Vatten in; Vattenfl.: 28.0 l/min
505102 förek. Flödesmätn.: 040617: 28,5 l/min & 040618: 45 l/min

Title COMPOSITE LOG for percussion borehole HLX21

Site	LAXEMAR	**Inclination ToC [°]**	-56.98	**Elevation [m.a.s.l.ToC]**	10.24
Borehole	HLX21	**Date of mapping**	2004-08-30 00:00:00	**Drilling Start Date**	2004-08-30 08:00:00
Diameter [mm]	138	**Coordinate System**	RT90-RHB70	**Drilling Stop Date**	2004-09-02 09:00:00
Length [m]	150.300	**Northing ToC [m]**	6366567.93	**Plot Date**	2008-08-24 22:12:09
Bearing ToC [°]	185.54	**Easting ToC [m]**	1549632.41	**Packer installation for monitoring**	2004-11-03 15:10:00

ROCK TYPE LAXEMAR
- Fine-grained granite
- Pegmatite
- Ävrö granite

DENSITY
- dens<2680
- 2680<dens<2730

SUBDIVISON OF ÄVRÖ GRANITE
- Ävrö granite
- Ävrö quartz monzodiorite
- Ävrö granodiorite

ROCK UNIT (ESHI)
- Medium confidence

PUMPTEST K TEST TYPE
- 1B: Pumpingtest-submersible Pump

DEFORMATION ZONE (ESHI)
- DZ

CASING
- Casing

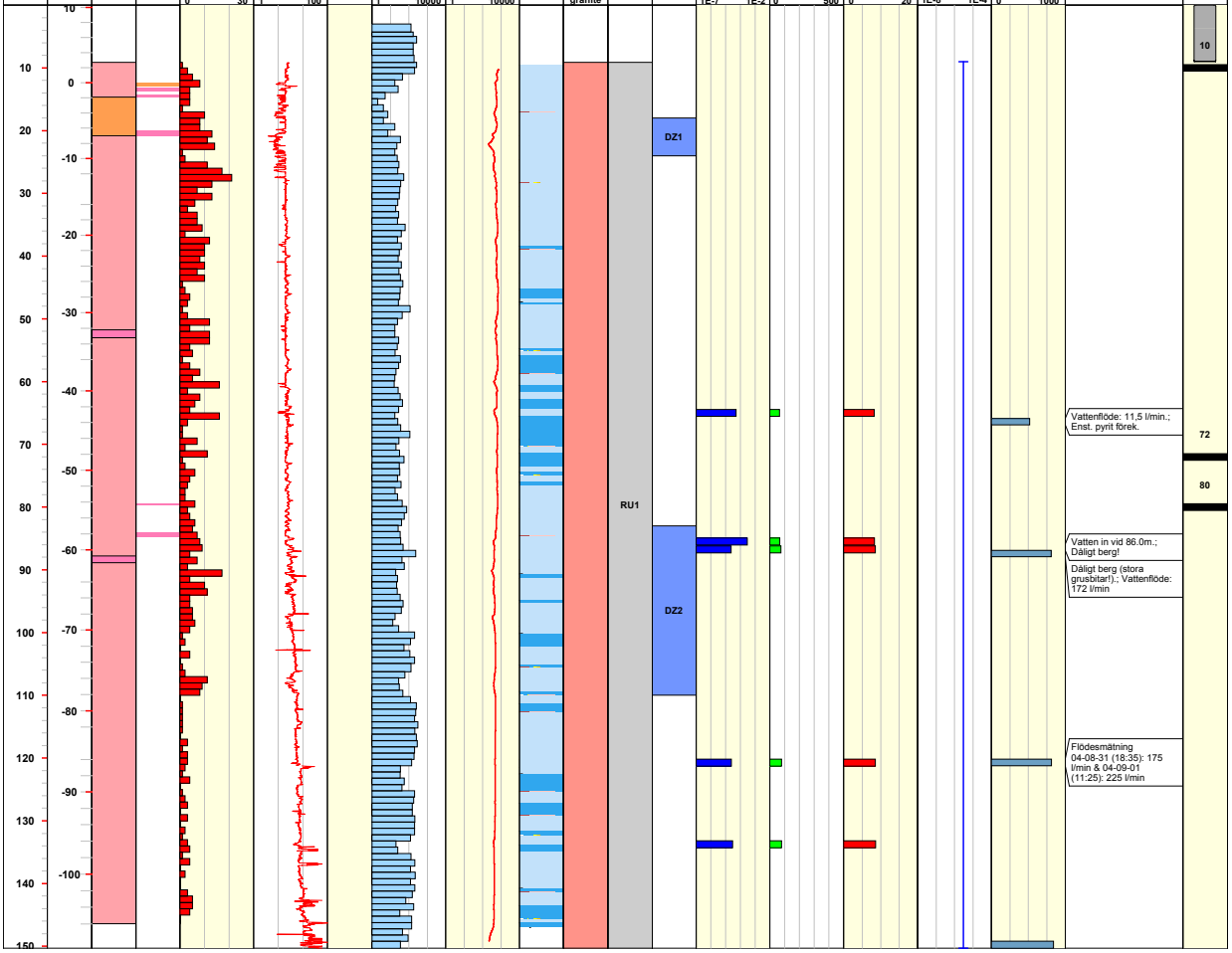

Title COMPOSITE LOG for percussion borehole HLX22

Site	LAXEMAR	**Inclination ToC [°]**	-59.43	**Elevation [m.a.s.l.ToC]**	10.06
Borehole	HLX22	**Date of mapping**	2004-08-23 00:00:00	**Drilling Start Date**	2004-08-23 15:30:00
Diameter [mm]	138	**Coordinate System**	RT90-RHB70	**Drilling Stop Date**	2004-08-26 09:30:00
Length [m]	163.200	**Northing ToC [m]**	6366487.83	**Plot Date**	2008-08-24 22:12:09
Bearing ToC [°]	13.45	**Easting ToC [m]**	1549661.54	**Packer installation for monitoring**	2004-12-17 08:00:00

ROCK TYPE LAXEMAR
- Fine-grained granite
- Ävrö granite

DENSITY
- dens<2680
- 2680<dens<2730
- 2800<dens<2890

SUBDIVISON OF ÄVRÖ GRANITE
- Ävrö granite
- Ävrö quartz monzodiorite
- Ävrö granodiorite

ROCK UNIT (ESHI)
- Medium confidence

DEFORMATION ZONE (ESHI)
- DZ

PUMPTEST K TEST TYPE

CASING
- Casing

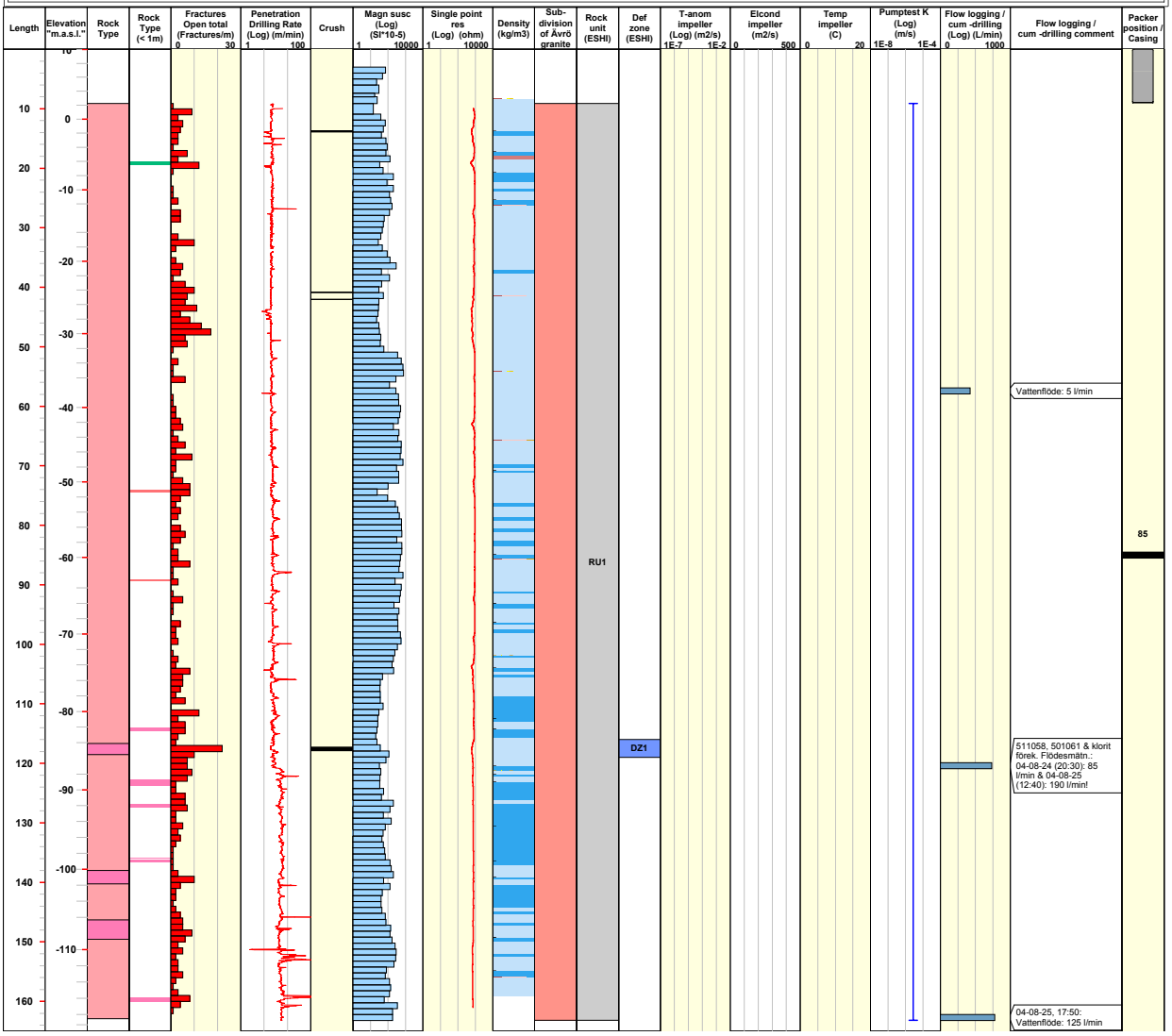

Title COMPOSITE LOG for percussion borehole HLX23

Site	LAXEMAR	**Inclination ToC [°]**	-58.17	**Elevation [m.a.s.l.ToC]**	14.62
Borehole	HLX23	**Date of mapping**	2004-09-13 00:00:00	**Drilling Start Date**	2004-09-13 12:30:00
Diameter [mm]	139	**Coordinate System**	RT90-RHB70	**Drilling Stop Date**	2004-09-16 10:00:00
Length [m]	160.200	**Northing ToC [m]**	6366577.19	**Plot Date**	2008-08-24 22:12:09
Bearing ToC [°]	182.89	**Easting ToC [m]**	1548888.72	**Packer installation for monitoring**	2004-12-10 09:30:00

ROCK TYPE LAXEMAR
- Fine-grained granite
- Ävrö granite
- Fine-grained diorite-gabbro

DENSITY
- dens<2680
- 2680<dens<2730
- 2730<dens<2800
- 2800<dens<2890

SUBDIVISON OF ÄVRÖ GRANITE
- Ävrö granite
- Ävrö quartz monzodiorite
- Ävrö granodiorite

ROCK UNIT (ESHI)
- Medium confidence

DEFORMATION ZONE (ESHI)
- DZ

PUMPTEST K TEST TYPE

CASING
- Casing

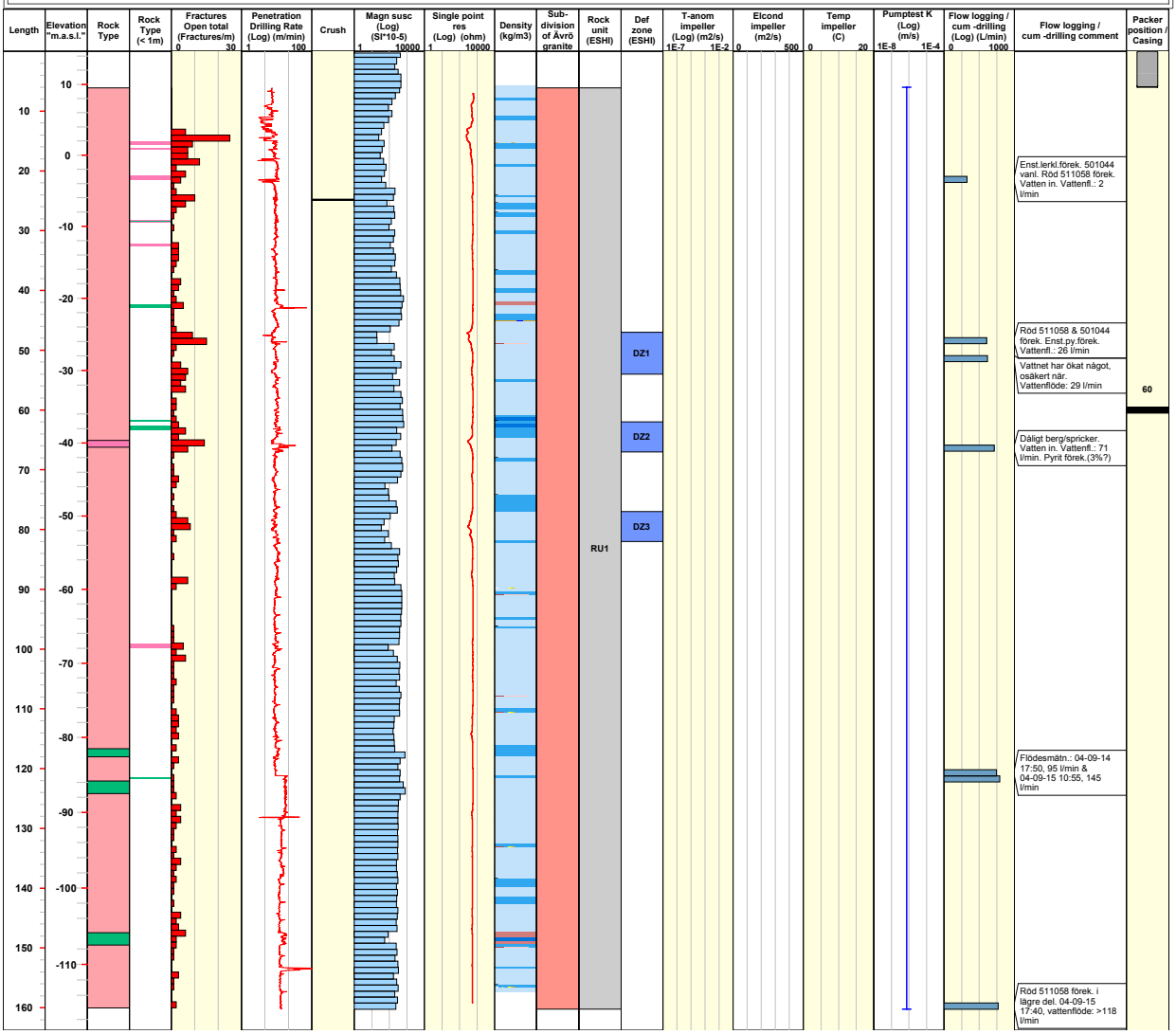

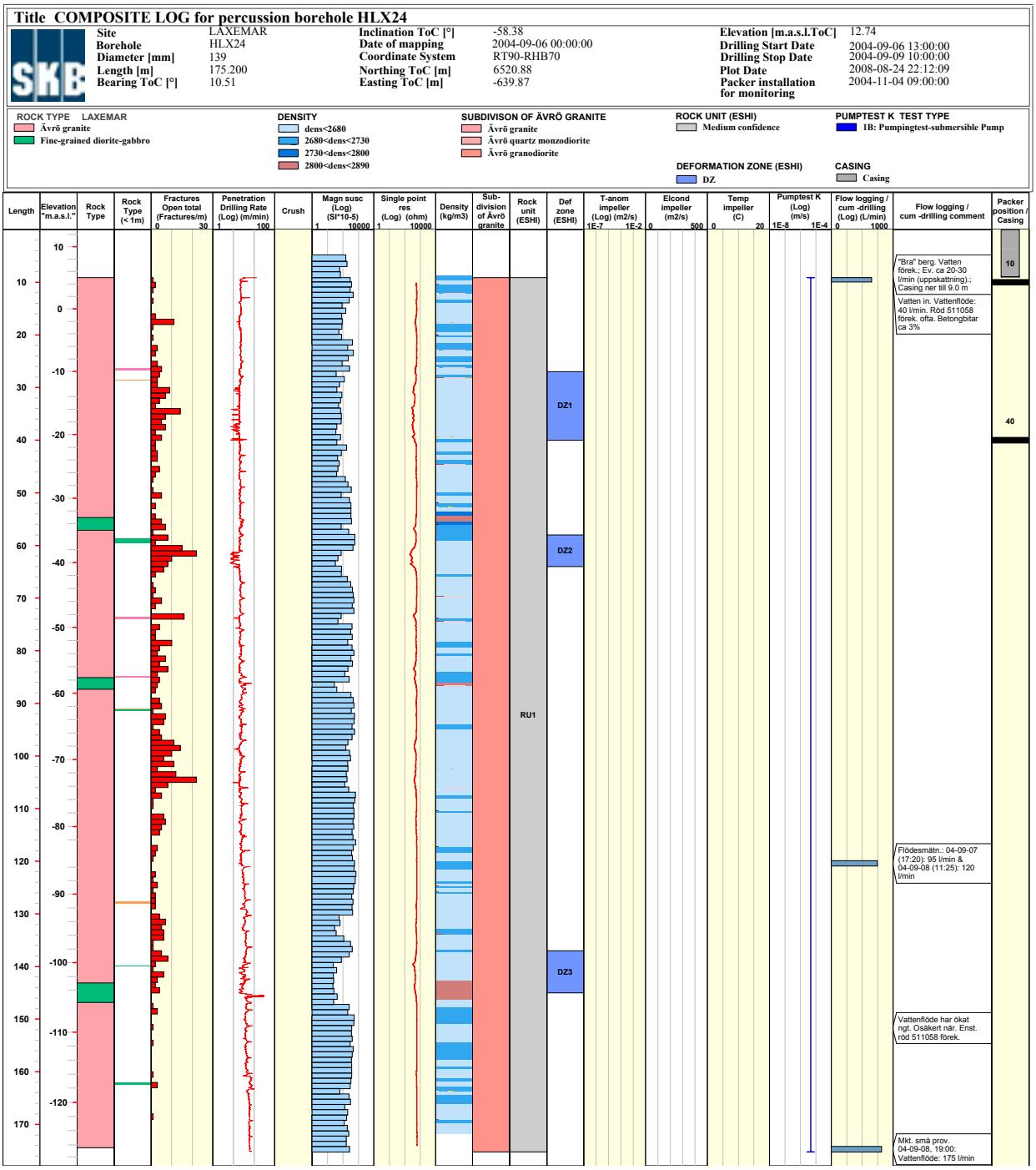
Title COMPOSITE LOG for percussion borehole HLX24
Site LAXEMAR
Borehole HLX24
Diameter [mm] 139
Length [m] 175.200
Bearing ToC [°] 10.51
Inclination ToC [°] -58.38
Date of mapping 2004-09-06 00:00:00
Coordinate System RT90-RHB70
Northing ToC [m] 6520.88
Easting ToC [m] -639.87
Elevation [m.a.s.l.ToC] 12.74
Drilling Start Date 2004-09-06 13:00:00
Drilling Stop Date 2004-09-09 10:00:00
Plot Date 2008-08-24 22:12:09
Packer installation for monitoring 2004-11-04 09:00:00
ROCK TYPE LAXEMAR
Ävrö granite
Fine-grained diorite-gabbro
DENSITY
dens<2680
2680<dens<2730
2730<dens<2800
2800<dens<2890
SUBDIVISON OF ÄVRÖ GRANITE
Ävrö granite
Ävrö quartz monzodiorite
Ävrö granodiorite
ROCK UNIT (ESHI)
Medium confidence
DEFORMATION ZONE (ESHI)
DZ
PUMPTEST K TEST TYPE
1B: Pumpingtest-submersible Pump
CASING
Casing
Length
Elevation "m.a.s.l."
Rock Type
Rock Type (< 1m)
Fractures Open total (Fractures/m) 0 30
Penetration Drilling Rate (Log) (m/min) 1 100
Crush
Magn susc (Log) (SI*10-5) 1 10000
Single point res (Log) (ohm) 1 10000
Density (kg/m3)
Sub-division of Ävrö granite
Rock unit (ESHI)
Def zone (ESHI)
T-anom impeller (Log) (m2/s) 1E-7 1E-2
Elcond impeller (m2/s) 0 500
Temp impeller (C) 0 20
Pumptest K (Log) (m/s) 1E-8 1E-4
Flow logging / cum -drilling (Log) (L/min) 0 1000
Flow logging / cum -drilling comment
Packer position / Casing
10
0
-10
-20
-30
-40
-50
-60
-70
-80
-90
-100
-110
-120
DZ1
DZ2
DZ3
RU1
"Bra" berg. Vatten förek.; Ev. ca 20-30 l/min (uppskattning).; Casing ner till 9.0 m
Vatten in. Vattenflöde: 40 l/min. Röd 511058 förek. ofta. Betongbitar ca 3%
Flödesmätn.: 04-09-07 (17:20): 95 l/min & 04-09-08 (11:25): 120 l/min
Vattenflöde har ökat ngt. Osäkert när. Enst. röd 511058 förek.
Mkt. små prov. 04-09-08, 19:00: Vattenflöde: 175 l/min
10
40

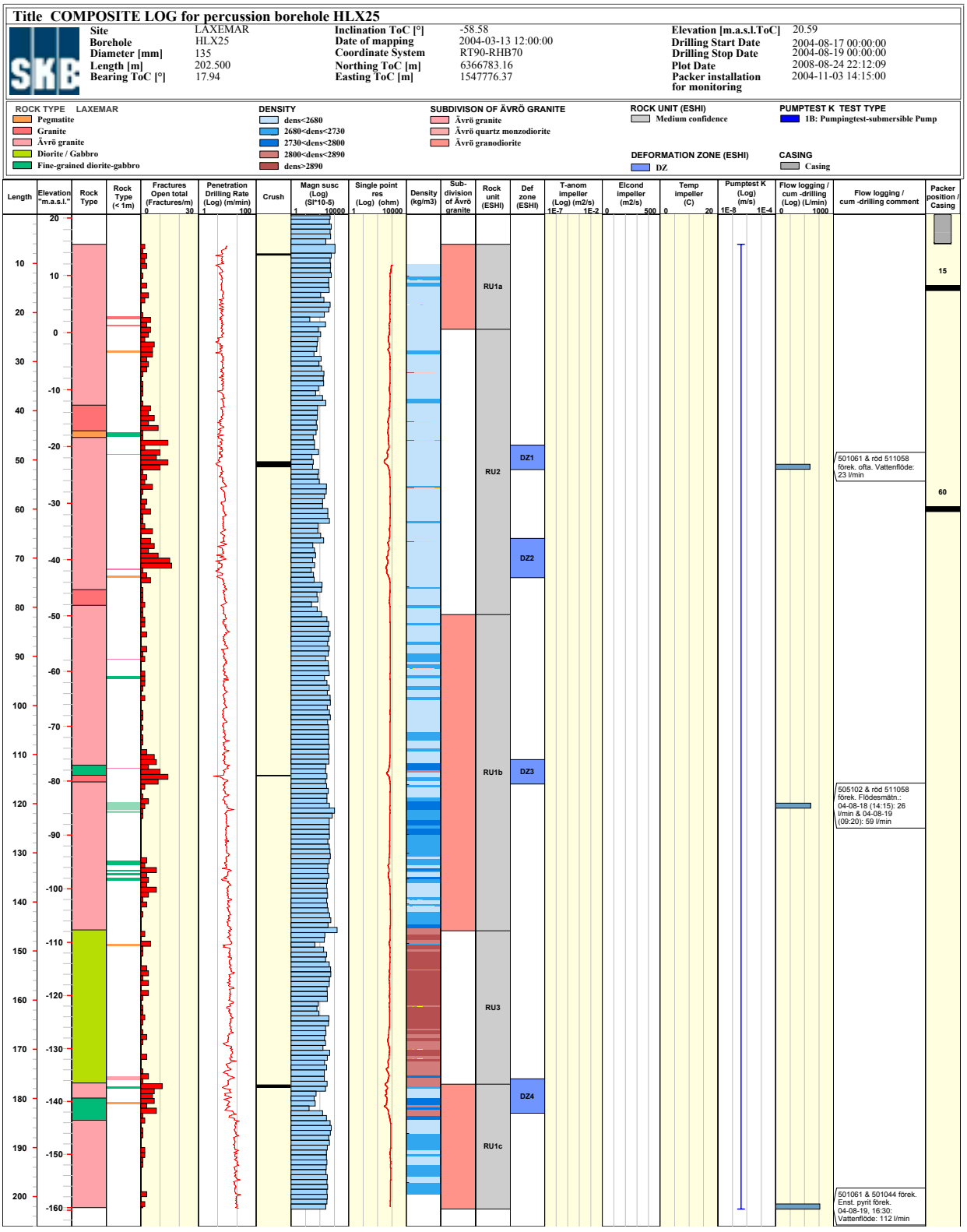
Title COMPOSITE LOG for percussion borehole HLX25
Site LAXEMAR
Borehole HLX25
Diameter [mm] 135
Length [m] 202.500
Bearing ToC [°] 17.94
Inclination ToC [°] -58.58
Date of mapping 2004-03-13 12:00:00
Coordinate System RT90-RHB70
Northing ToC [m] 6366783.16
Easting ToC [m] 1547776.37
Elevation [m.a.s.l.ToC] 20.59
Drilling Start Date 2004-08-17 00:00:00
Drilling Stop Date 2004-08-19 00:00:00
Plot Date 2008-08-24 22:12:09
Packer installation for monitoring 2004-11-03 14:15:00
ROCK TYPE LAXEMAR
Pegmatite
Granite
Ävrö granite
Diorite / Gabbro
Fine-grained diorite-gabbro
DENSITY
dens<2680
2680<dens<2730
2730<dens<2800
2800<dens<2890
dens>2890
SUBDIVISON OF ÄVRÖ GRANITE
Ävrö granite
Ävrö quartz monzodiorite
Ävrö granodiorite
ROCK UNIT (ESHI)
Medium confidence
DEFORMATION ZONE (ESHI)
DZ
PUMPTEST K TEST TYPE
1B: Pumpingtest-submersible Pump
CASING
Casing
Length
Elevation "m.a.s.l."
Rock Type
Rock Type (< 1m)
Fractures Open total (Fractures/m)
Penetration Drilling Rate (Log) (m/min)
Crush
Magn susc (Log) (SI*10-5)
Single point res (Log) (ohm)
Density (kg/m3)
Sub-division of Ävrö granite
Rock unit (ESHI)
Def zone (ESHI)
T-anom impeller (Log) (m2/s)
Elcond impeller (m2/s)
Temp impeller (C)
Pumptest K (Log) (m/s)
Flow logging / cum -drilling (Log) (L/min)
Flow logging / cum -drilling comment
Packer position / Casing
RU1a
RU2
RU1b
RU3
RU1c
DZ1
DZ2
DZ3
DZ4
501061 & rod 511058 förek. ofta. Vattenflöde: 23 l/min
505102 & rod 511058 förek. Flödesmätn.: 04-08-18 (14:15): 26 l/min & 04-08-19 (09:20): 59 l/min
501061 & 501044 förek. Enst. pyrit förek. 04-08-19, 16:30: Vattenflöde: 112 l/min
15
60

Title COMPOSITE LOG for percussion borehole HLX26

Site	LAXEMAR	**Inclination ToC [°]**	-60.41	**Elevation [m.a.s.l.ToC]**	6.41
Borehole	HLX26	**Date of mapping**	2004-09-23 00:00:00	**Drilling Start Date**	2004-09-23 16:40:00
Diameter [mm]	137	**Coordinate System**	RT90-RHB70	**Drilling Stop Date**	2004-09-28 18:00:00
Length [m]	151.200	**Northing ToC [m]**	6365277.89	**Plot Date**	2008-08-24 22:12:09
Bearing ToC [°]	12.37	**Easting ToC [m]**	1548600.57	**Packer installation for monitoring**	2004-11-04 10:25:00

ROCK TYPE LAXEMAR
- Fine-grained granite
- Quartz monzodiorite
- Fine-grained diorite-gabbro

DENSITY
- dens<2680
- 2680<dens<2730
- 2730<dens<2800

SUBDIVISON OF ÄVRÖ GRANITE

ROCK UNIT (ESHI)
- Medium confidence

DEFORMATION ZONE (ESHI)
- DZ

PUMPTEST K TEST TYPE

CASING
- Casing

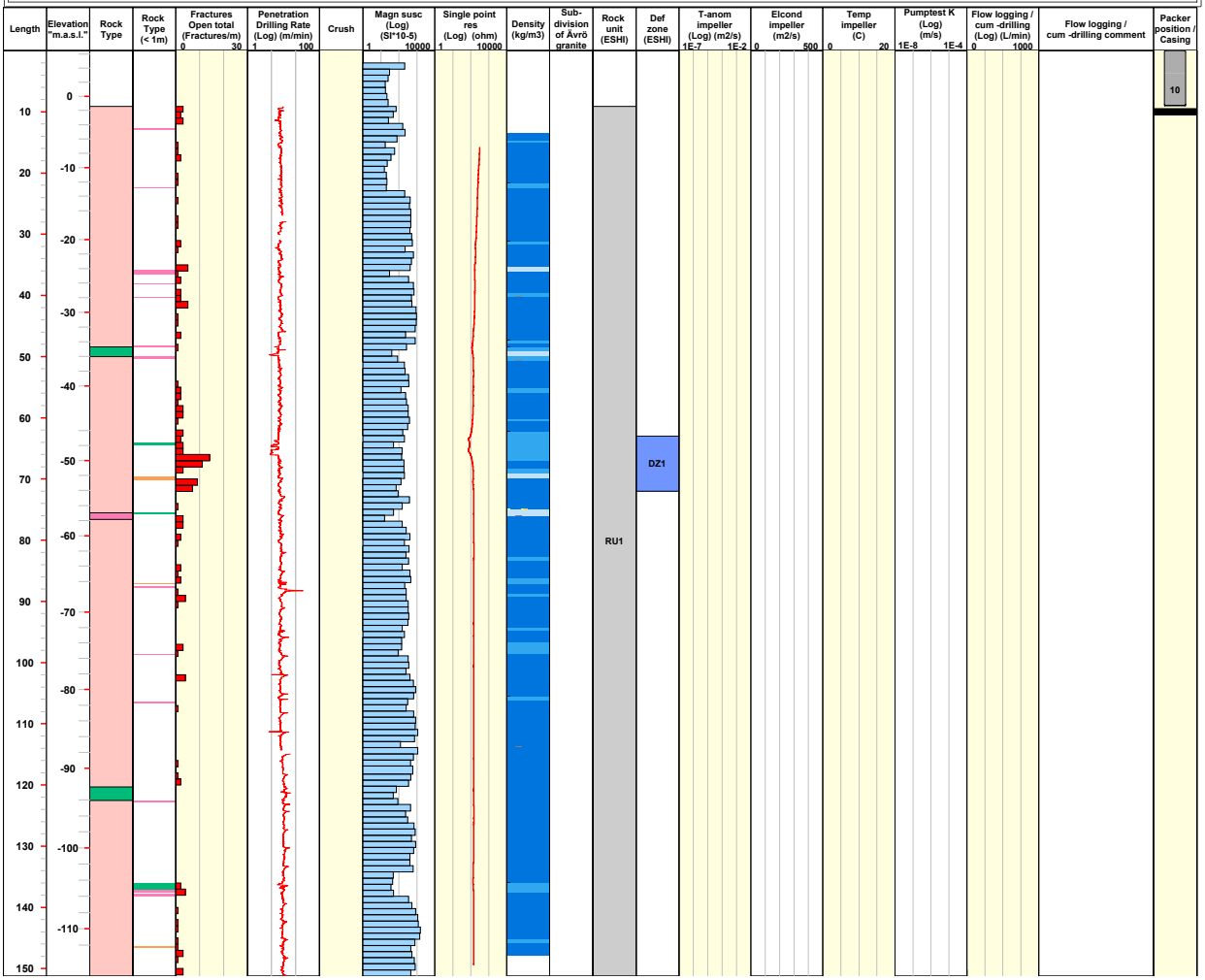

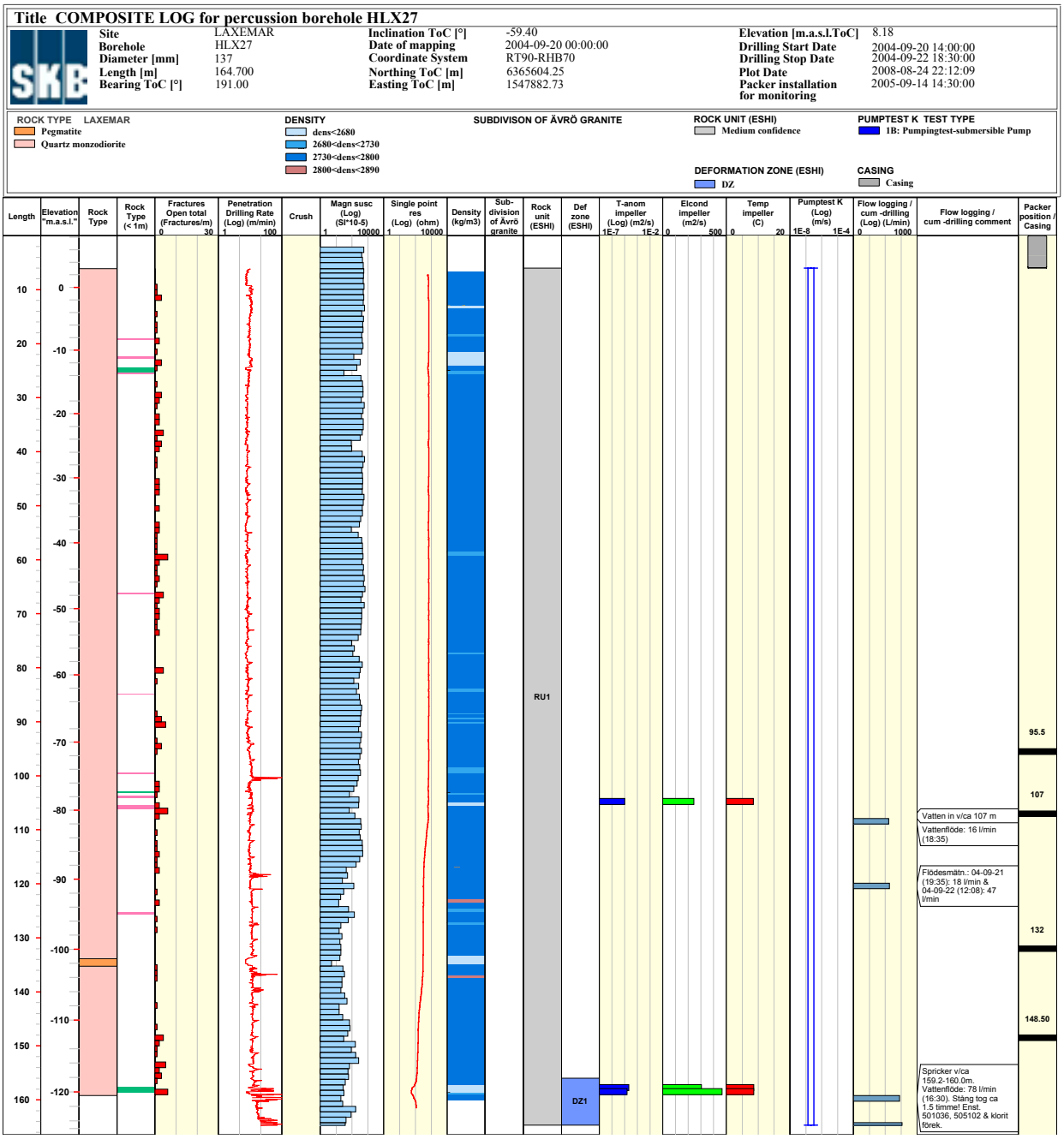
Title COMPOSITE LOG for percussion borehole HLX27
Site LAXEMAR
Borehole HLX27
Diameter [mm] 137
Length [m] 164.700
Bearing ToC [°] 191.00
Inclination ToC [°] -59.40
Date of mapping 2004-09-20 00:00:00
Coordinate System RT90-RHB70
Northing ToC [m] 6365604.25
Easting ToC [m] 1547882.73
Elevation [m.a.s.l.ToC] 8.18
Drilling Start Date 2004-09-20 14:00:00
Drilling Stop Date 2004-09-22 18:30:00
Plot Date 2008-08-24 22:12:09
Packer installation for monitoring 2005-09-14 14:30:00
ROCK TYPE LAXEMAR
Pegmatite
Quartz monzodiorite
DENSITY
dens<2680
2680<dens<2730
2730<dens<2800
2800<dens<2890
SUBDIVISON OF ÄVRÖ GRANITE
ROCK UNIT (ESHI)
Medium confidence
DEFORMATION ZONE (ESHI)
DZ
PUMPTEST K TEST TYPE
1B: Pumpingtest-submersible Pump
CASING
Casing
Length
Elevation "m.a.s.l."
Rock Type
Rock Type (< 1m)
Fractures Open total (Fractures/m)
Penetration Drilling Rate (Log) (m/min)
Crush
Magn susc (Log) (SI*10-5)
Single point res (Log) (ohm)
Density (kg/m3)
Sub-division of Ävrö granite
Rock unit (ESHI)
Def zone (ESHI)
T-anom impeller (Log) (m2/s)
Elcond impeller (m2/s)
Temp impeller (C)
Pumptest K (Log) (m/s)
Flow logging / cum -drilling (Log) (L/min)
Flow logging / cum -drilling comment
Packer position / Casing
RU1
DZ1
95.5
107
132
148.50
Vatten in v/ca 107 m
Vattenflöde: 16 l/min (18:35)
Flödesmätn.: 04-09-21 (19:35): 18 l/min & 04-09-22 (12:08): 47 l/min
Spricker v/ca 159.2-160.0m. Vattenflöde: 78 l/min (16:30). Stäng tog ca 1.5 timme! Enst. 501036, 505102 & klorit förek.

Title COMPOSITE LOG for percussion borehole HLX28

Site	LAXEMAR	**Inclination ToC [°]**	-59.48	**Elevation [m.a.s.l.ToC]**	13.35
Borehole	HLX28	**Date of mapping**	2004-09-29 00:00:00	**Drilling Start Date**	2004-09-29 13:40:00
Diameter [mm]	136	**Coordinate System**	RT90-RHB70	**Drilling Stop Date**	2004-10-02 07:30:00
Length [m]	154.200	**Northing ToC [m]**	6365860.89	**Plot Date**	2008-08-24 22:12:09
Bearing ToC [°]	201.38	**Easting ToC [m]**	1546834.52	**Packer installation for monitoring**	2007-09-12 00:00:00

ROCK TYPE LAXEMAR
- Fine-grained granite
- Quartz monzodiorite
- Fine-grained diorite-gabbro

DENSITY
- dens<2680
- 2680<dens<2730
- 2730<dens<2800
- 2800<dens<2890

SUBDIVISON OF ÄVRÖ GRANITE

ROCK UNIT (ESHI)
- Medium confidence

DEFORMATION ZONE (ESHI)
- DZ

PUMPTEST K TEST TYPE
- 1B: Pumpingtest-submersible Pump

CASING
- Casing

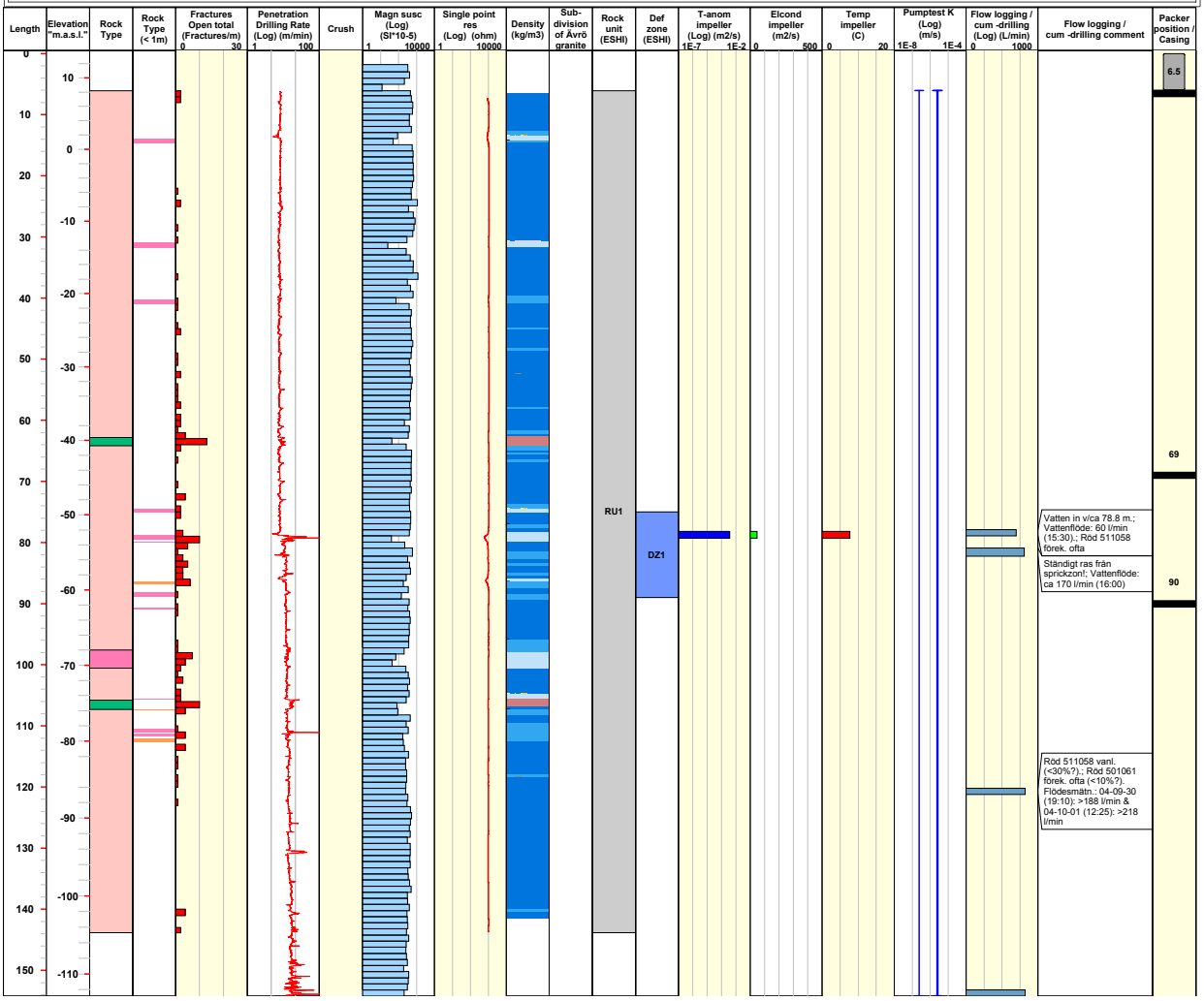

Title COMPOSITE LOG for percussion borehole HLX29

Site	LAXEMAR	**Coordinate System**	RT90-RHB70	**Packer installation for monitoring**	
Borehole	HLX29	**Northing ToC [m]**	6365725.42		
Diameter [mm]	137	**Easting ToC [m]**	1546733.19		
Length [m]	12.900	**Elevation [m.a.s.l.ToC]**	10.63		
Bearing ToC [°]	22.34	**Drilling Start Date**	2004-10-02 13:30:00		
Inclination ToC [°]	-56.95	**Drilling Stop Date**	2004-10-03 13:00:00		
Date of mapping	2004-10-02 00:00:00	**Plot Date**	2008-08-24 22:12:09		

ROCK TYPE
- Fine-grained granite
- Quartz monzodiorite

ROCK UNIT (ESHI) | DEFORMATION ZONE (ESHI) | PUMPTEST K TEST TYPE

CASING
- Casing

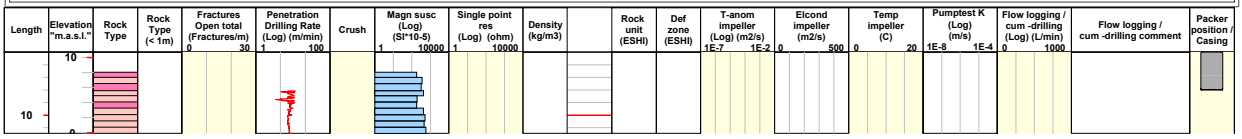

Title COMPOSITE LOG for percussion borehole HLX30

Site	LAXEMAR	**Inclination ToC [°]**	-61.03	**Elevation [m.a.s.l.ToC]**	12.11
Borehole	HLX30	**Date of mapping**	2004-11-26 00:00:00	**Drilling Start Date**	2004-11-26 07:00:00
Diameter [mm]	139	**Coordinate System**	RT90-RHB70	**Drilling Stop Date**	2004-11-30 17:00:00
Length [m]	163.400	**Northing ToC [m]**	6366729.92	**Plot Date**	2008-08-24 22:12:09
Bearing ToC [°]	55.82	**Easting ToC [m]**	1548026.78	**Packer installation for monitoring**	2004-12-01 14:15:00

ROCK TYPE LAXEMAR
- Ävrö granite
- Fine-grained diorite-gabbro

DENSITY
- dens<2680
- 2680<dens<2730
- 2730<dens<2800
- 2800<dens<2890

SUBDIVISON OF ÄVRÖ GRANITE
- Ävrö granite
- Ävrö quartz monzodiorite
- Ävrö granodiorite

ROCK UNIT (ESHI)
- Medium confidence

DEFORMATION ZONE (ESHI)
- DZ

PUMPTEST K TEST TYPE

CASING
- Casing

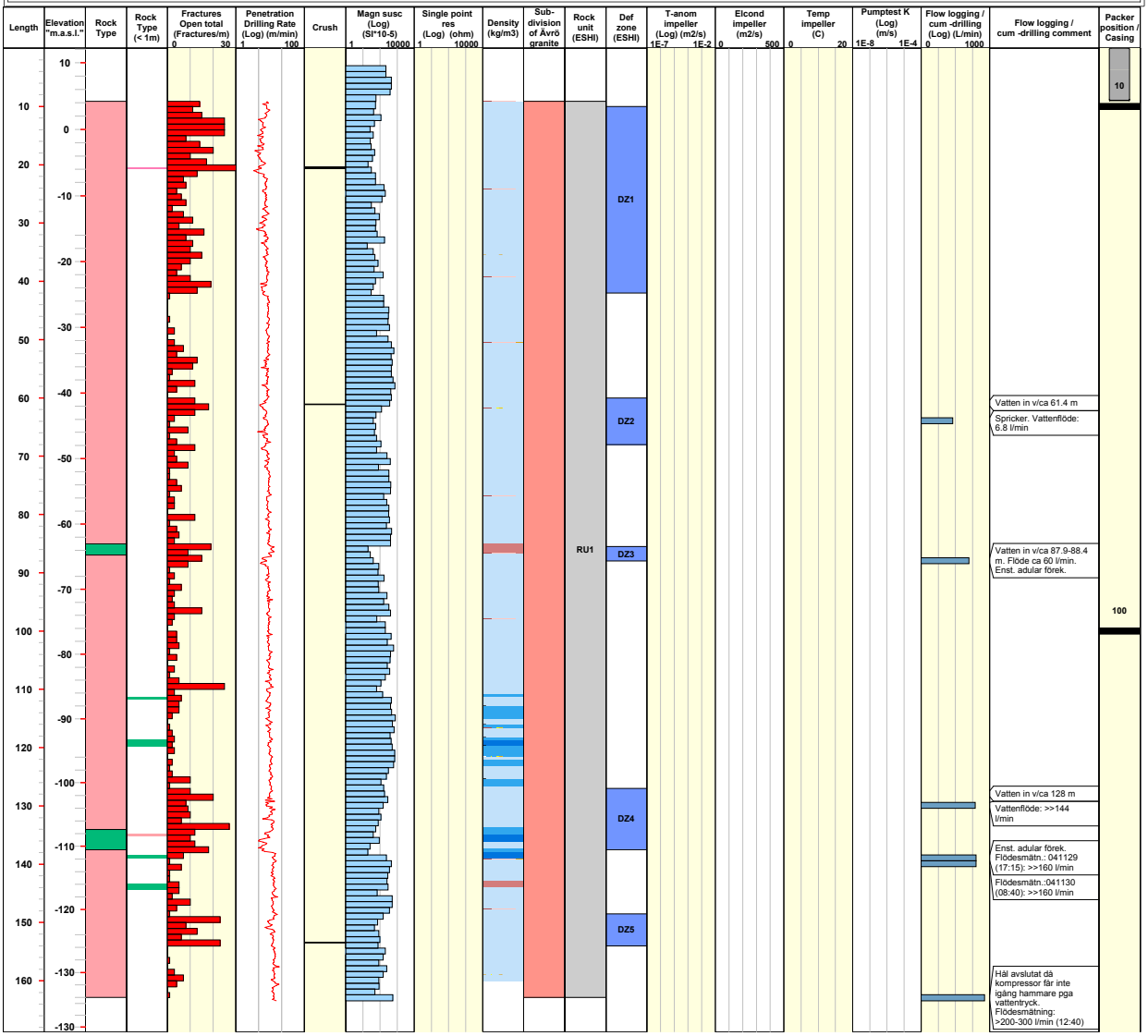

Title COMPOSITE LOG for percussion borehole HLX31

Site	LAXEMAR	**Inclination ToC [°]**	-58.75	**Elevation [m.a.s.l.ToC]**	12.09
Borehole	HLX31	**Date of mapping**	2004-12-01 00:00:00	**Drilling Start Date**	2004-12-01 07:00:00
Diameter [mm]	139	**Coordinate System**	RT90-RHB70	**Drilling Stop Date**	2004-12-03 12:00:00
Length [m]	133.200	**Northing ToC [m]**	6366773.69	**Plot Date**	2008-08-24 22:12:09
Bearing ToC [°]	231.77	**Easting ToC [m]**	1548172.31	**Packer installation for monitoring**	2004-12-17 14:43:00

ROCK TYPE LAXEMAR
- Ävrö granite

DENSITY
- dens<2680
- 2680<dens<2730

SUBDIVISON OF ÄVRÖ GRANITE
- Ävrö granite
- Ävrö quartz monzodiorite
- Ävrö granodiorite

ROCK UNIT (ESHI)
- Medium confidence

PUMPTEST K TEST TYPE

DEFORMATION ZONE (ESHI)
- DZ

CASING
- Casing

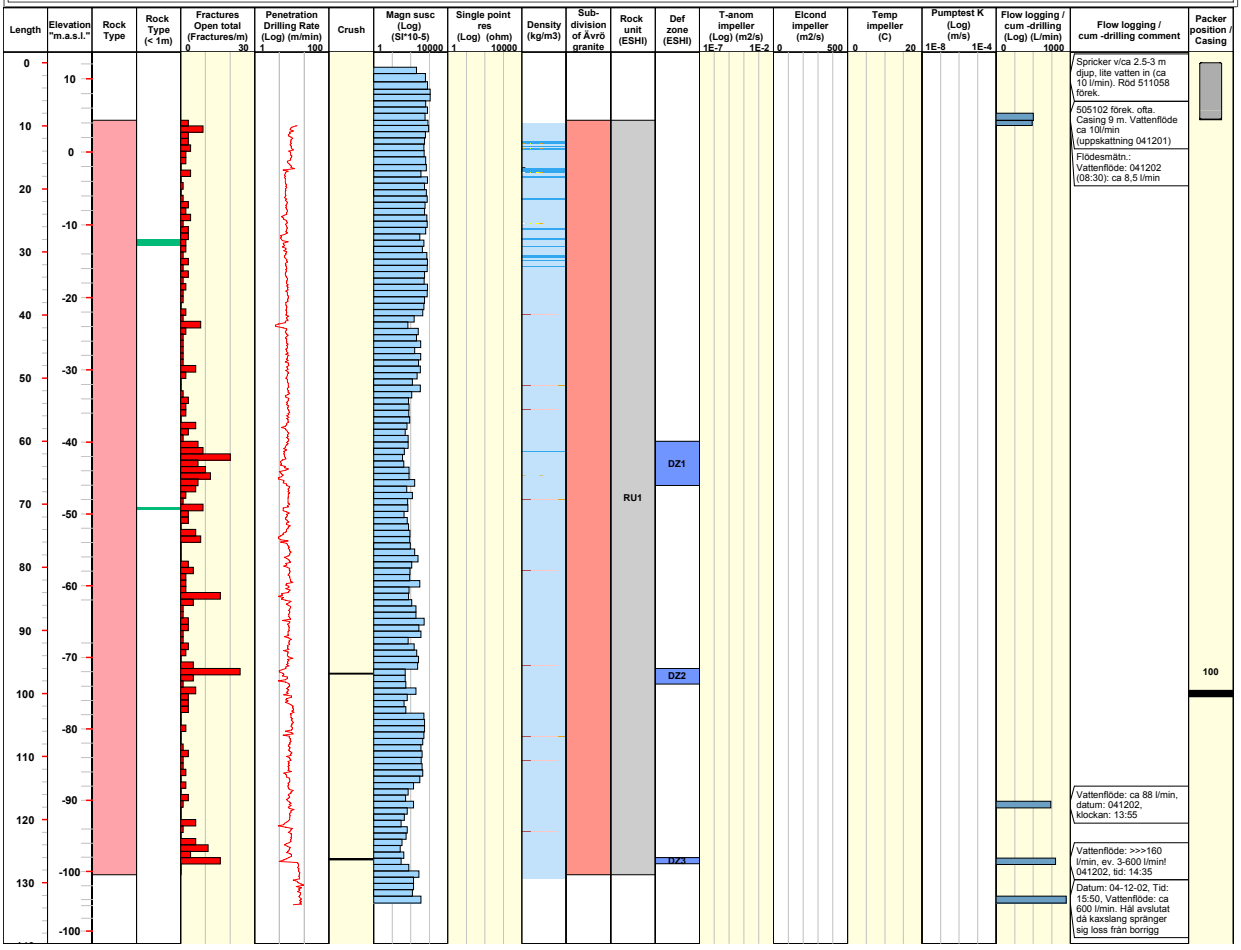

Title COMPOSITE LOG for percussion borehole HLX32

Site	LAXEMAR	**Inclination ToC [°]**	-58.66	**Elevation [m.a.s.l.ToC]**	10.77
Borehole	HLX32	**Date of mapping**	2005-01-03 08:00:00	**Drilling Start Date**	2005-01-04 12:00:00
Diameter [mm]	140	**Coordinate System**	RT90-RHB70	**Drilling Stop Date**	2005-01-11 12:30:00
Length [m]	162.600	**Northing ToC [m]**	6365724.97	**Plot Date**	2008-08-24 22:12:09
Bearing ToC [°]	28.59	**Easting ToC [m]**	1546734.41	**Packer installation for monitoring**	2005-09-15 08:40:00

ROCK TYPE LAXEMAR
- Fine-grained granite
- Quartz monzodiorite
- Fine-grained diorite-gabbro

DENSITY
- dens<2680
- 2680<dens<2730
- 2730<dens<2800

SUBDIVISON OF ÄVRÖ GRANITE
- Ävrö granite
- Ävrö quartz monzodiorite
- Ävrö granodiorite

ROCK UNIT (ESHI)
- Medium confidence

DEFORMATION ZONE (ESHI)
- DZ

PUMPTEST K TEST TYPE
- 1B: Pumpingtest-submersible Pump

CASING
- Casing

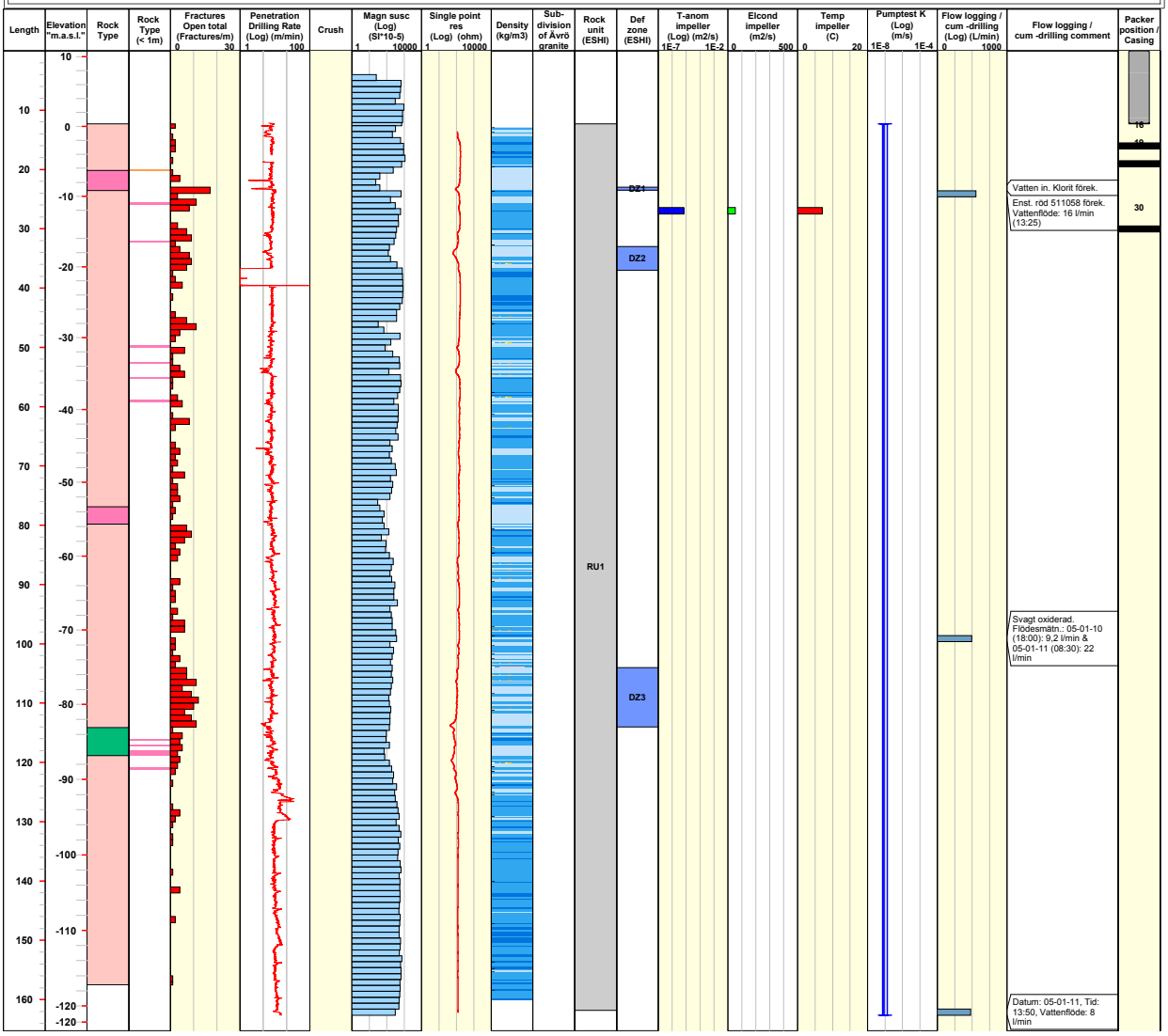

Title COMPOSITE LOG for percussion borehole HLX33

Site	LAXEMAR	**Inclination ToC [°]**	-58.80	**Elevation [m.a.s.l.ToC]**	12.13
Borehole	HLX33	**Date of mapping**	2004-12-17 00:00:00	**Drilling Start Date**	2004-12-17 07:00:00
Diameter [mm]	139	**Coordinate System**	RT90-RHB70	**Drilling Stop Date**	2004-12-20 19:15:00
Length [m]	202.100	**Northing ToC [m]**	6366470.93	**Plot Date**	2008-08-24 22:12:09
Bearing ToC [°]	21.77	**Easting ToC [m]**	1548562.75	**Packer installation for monitoring**	2004-12-22 14:51:00

ROCK TYPE LAXEMAR
- Ävrö granite
- Fine-grained diorite-gabbro

DENSITY
- dens<2680
- 2680<dens<2730
- 2730<dens<2800
- 2800<dens<2890

SUBDIVISON OF ÄVRÖ GRANITE
- Ävrö granite
- Ävrö quartz monzodiorite
- Ävrö granodiorite

ROCK UNIT (ESHI)
- Medium confidence

DEFORMATION ZONE (ESHI)
- DZ

PUMPTEST K TEST TYPE
- 1B: Pumpingtest-submersible Pump

CASING
- Casing

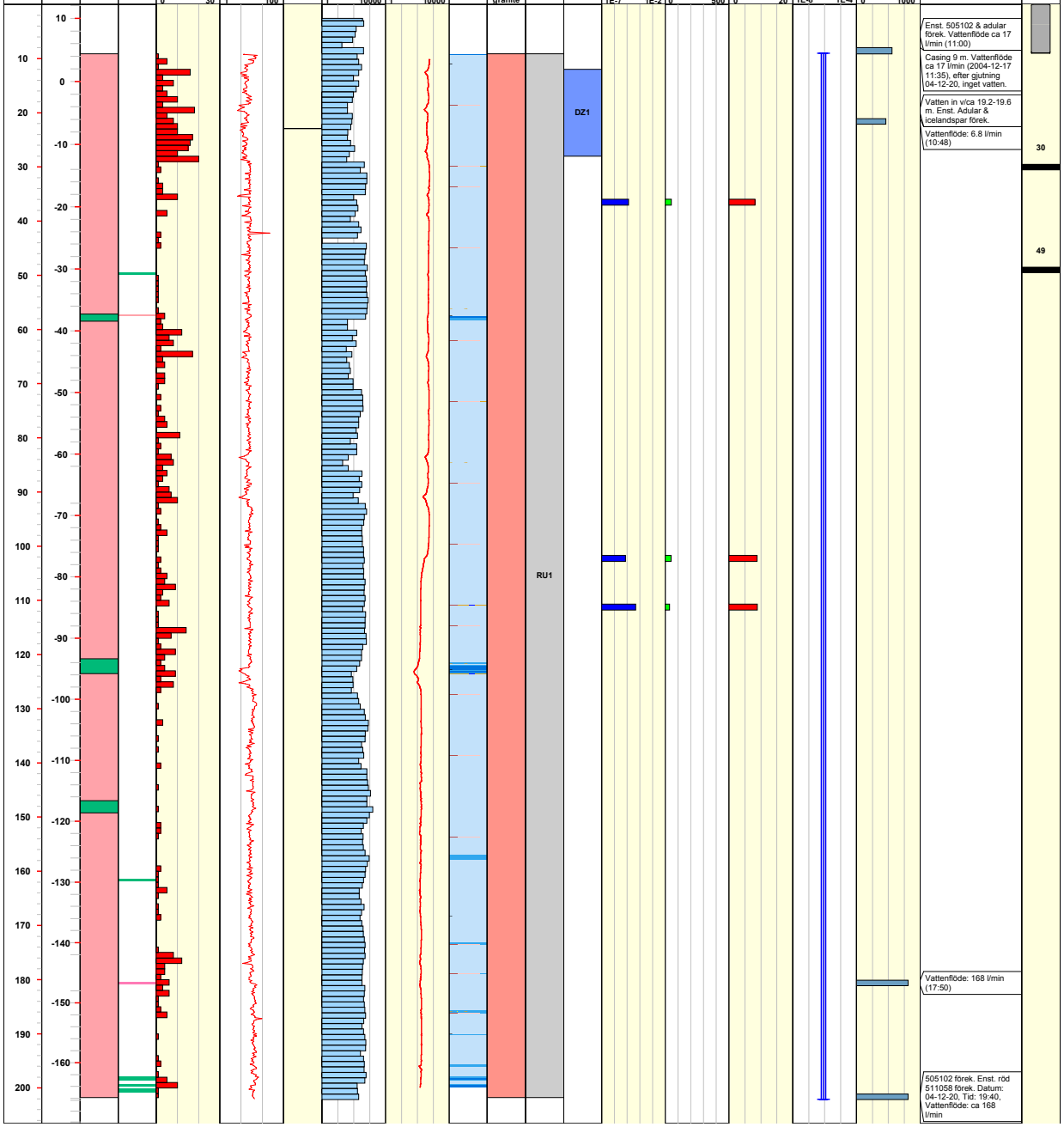

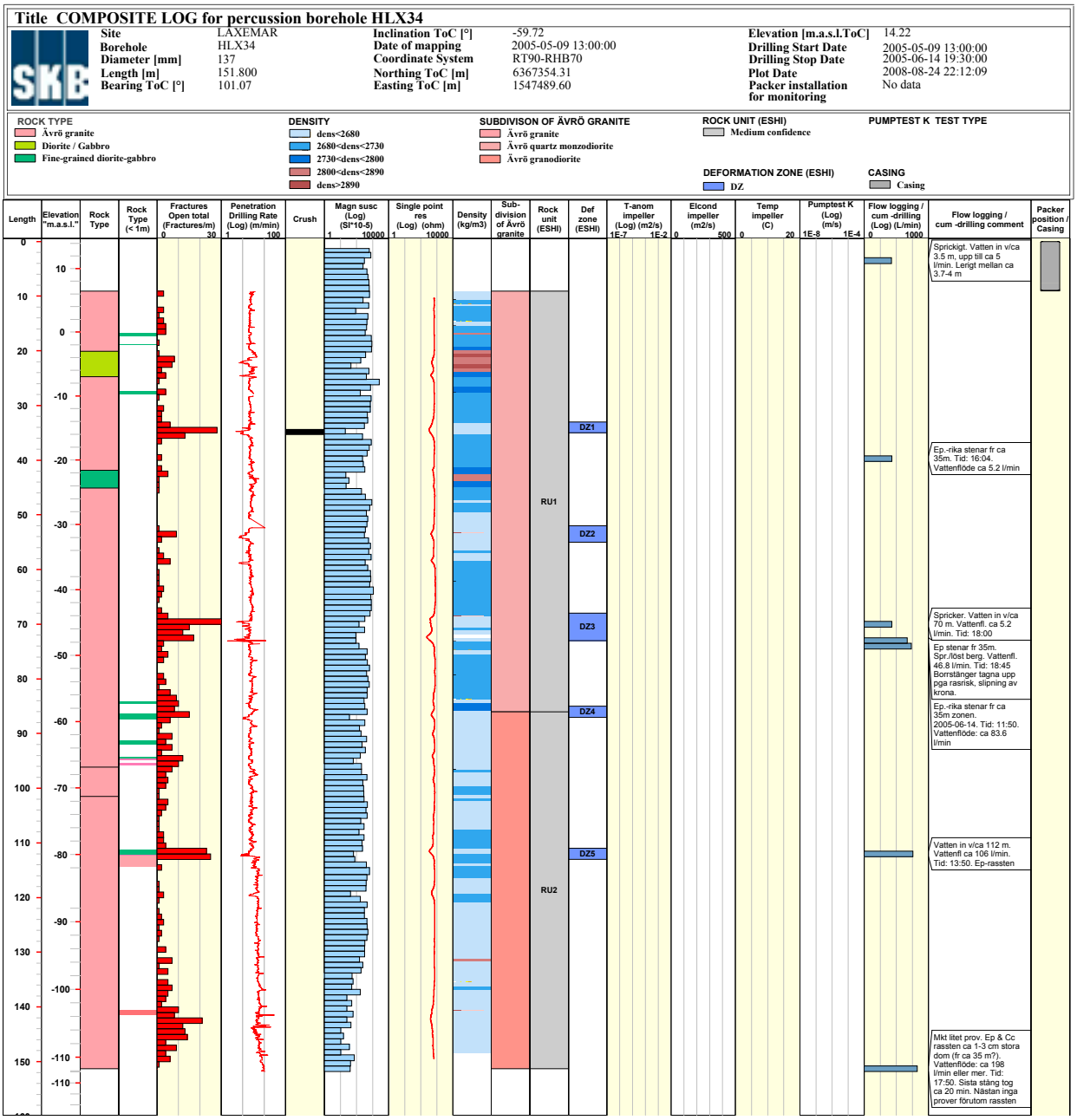
Title COMPOSITE LOG for percussion borehole HLX34
Site LAXEMAR
Borehole HLX34
Diameter [mm] 137
Length [m] 151.800
Bearing ToC [°] 101.07
Inclination ToC [°] -59.72
Date of mapping 2005-05-09 13:00:00
Coordinate System RT90-RHB70
Northing ToC [m] 6367354.31
Easting ToC [m] 1547489.60
Elevation [m.a.s.l.ToC] 14.22
Drilling Start Date 2005-05-09 13:00:00
Drilling Stop Date 2005-06-14 19:30:00
Plot Date 2008-08-24 22:12:09
Packer installation for monitoring No data
ROCK TYPE
Ävrö granite
Diorite / Gabbro
Fine-grained diorite-gabbro
DENSITY
dens<2680
2680<dens<2730
2730<dens<2800
2800<dens<2890
dens>2890
SUBDIVISON OF ÄVRÖ GRANITE
Ävrö granite
Ävrö quartz monzodiorite
Ävrö granodiorite
ROCK UNIT (ESHI)
Medium confidence
DEFORMATION ZONE (ESHI)
DZ
PUMPTEST K TEST TYPE
CASING
Casing
Length
Elevation "m.a.s.l."
Rock Type
Rock Type (< 1m)
Fractures Open total (Fractures/m)
Penetration Drilling Rate (Log) (m/min)
Crush
Magn susc (Log) (SI*10-5)
Single point res (Log) (ohm)
Density (kg/m3)
Sub-division of Ävrö granite
Rock unit (ESHI)
Def zone (ESHI)
T-anom impeller (Log) (m2/s)
Elcond impeller (m2/s)
Temp impeller (C)
Pumptest K (Log) (m/s)
Flow logging / cum -drilling (Log) (L/min)
Flow logging / cum -drilling comment
Packer position / Casing
RU1
RU2
DZ1
DZ2
DZ3
DZ4
DZ5
Sprickigt. Vatten in v/ca 3.5 m, upp till ca 5 l/min. Lerigt mellan ca 3.7-4 m
Ep.-rika stenar fr ca 35m. Tid: 16:04. Vattenflöde ca 5.2 l/min
Spricker. Vatten in v/ca 70 m. Vattenfl. ca 5.2 l/min. Tid: 18:00
Ep stenar fr 35m. Spr./löst berg. Vattenfl. 46.8 l/min. Tid: 18:45 Borrstänger lagna upp pga rasrisk, slipning av krona.
Ep.-rika stenar fr ca 35m zonen. 2005-06-14. Tid: 11:50. Vattenflöde: ca 83.6 l/min
Vatten in v/ca 112 m. Vattenfl ca 106 l/min. Tid: 13:50. Ep-rassten
Mkt litet prov. Ep & Cc rassten ca 1-3 cm stora dom (fr ca 35 m?). Vattenflöde: ca 198 l/min eller mer. Tid: 17:50. Sista stång tog ca 20 min. Nästan inga prover förutom rassten

Title COMPOSITE LOG for percussion borehole HLX35

Site	LAXEMAR	**Inclination ToC [°]**	-60.12	**Elevation [m.a.s.l.ToC]**	14.37
Borehole	HLX35	**Date of mapping**	2005-05-28 00:00:00	**Drilling Start Date**	2005-05-28 07:00:00
Diameter [mm]	140	**Coordinate System**	RT90-RHB70	**Drilling Stop Date**	2005-06-02 20:00:00
Length [m]	151.800	**Northing ToC [m]**	6367193.97	**Plot Date**	2008-08-24 22:12:09
Bearing ToC [°]	102.22	**Easting ToC [m]**	1547437.84	**Packer installation for monitoring**	2005-06-03 14:10:00

ROCK TYPE LAXEMAR
- Ävrö granite
- Fine-grained diorite-gabbro

DENSITY
- dens<2680
- 2680<dens<2730
- 2730<dens<2800
- 2800<dens<2890
- dens>2890

SUBDIVISON OF ÄVRÖ GRANITE
- Ävrö granite
- Ävrö quartz monzodiorite
- Ävrö granodiorite

ROCK UNIT (ESHI)
- Medium confidence

DEFORMATION ZONE (ESHI)
- DZ

PUMPTEST K TEST TYPE
- 1B: Pumpingtest-submersible Pump

CASING
- Casing

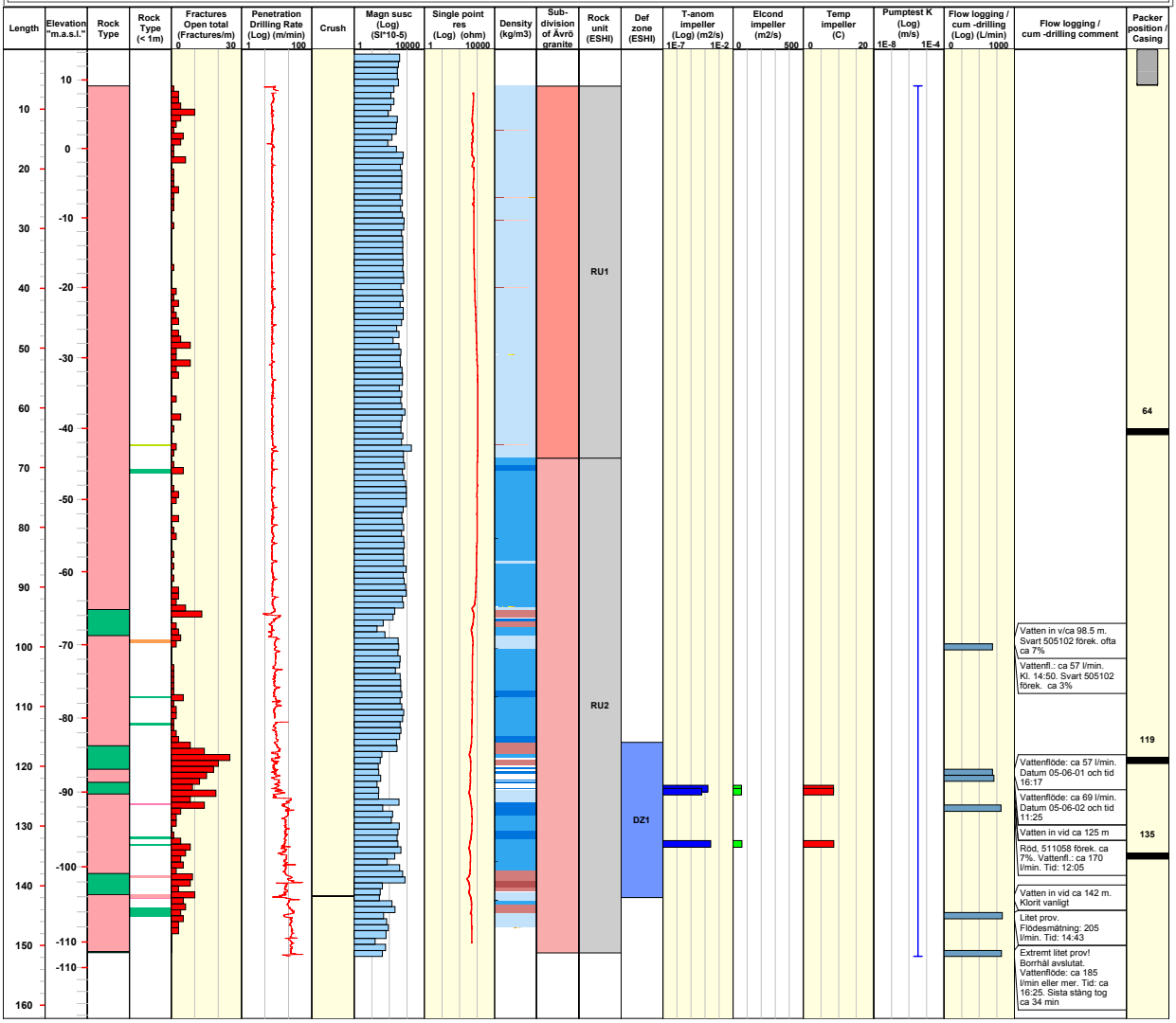

Title COMPOSITE LOG for percussion borehole HLX36

Site	LAXEMAR	**Inclination ToC [°]**	-59.01	**Elevation [m.a.s.l.ToC]**	15.49
Borehole	HLX36	**Date of mapping**	2005-09-20 00:00:00	**Drilling Start Date**	2005-09-20 07:00:00
Diameter [mm]	140	**Coordinate System**	RT90-RHB70	**Drilling Stop Date**	2005-09-22 07:00:00
Length [m]	199.800	**Northing ToC [m]**	6366172.12	**Plot Date**	2008-08-24 22:12:09
Bearing ToC [°]	270.61	**Easting ToC [m]**	1546558.50	**Packer installation for monitoring**	2006-11-13 15:40:00

ROCK TYPE LAXEMAR
- Dolerite / Diabas
- Fine-grained granite
- Quartz monzodiorite

DENSITY
- dens<2680
- 2680<dens<2730
- 2730<dens<2800
- 2800<dens<2890
- dens>2890

SUBDIVISON OF ÄVRÖ GRANITE

ROCK UNIT (ESHI)
- Medium confidence

DEFORMATION ZONE (ESHI)
- DZ

PUMPTEST K TEST TYPE

CASING
- Casing

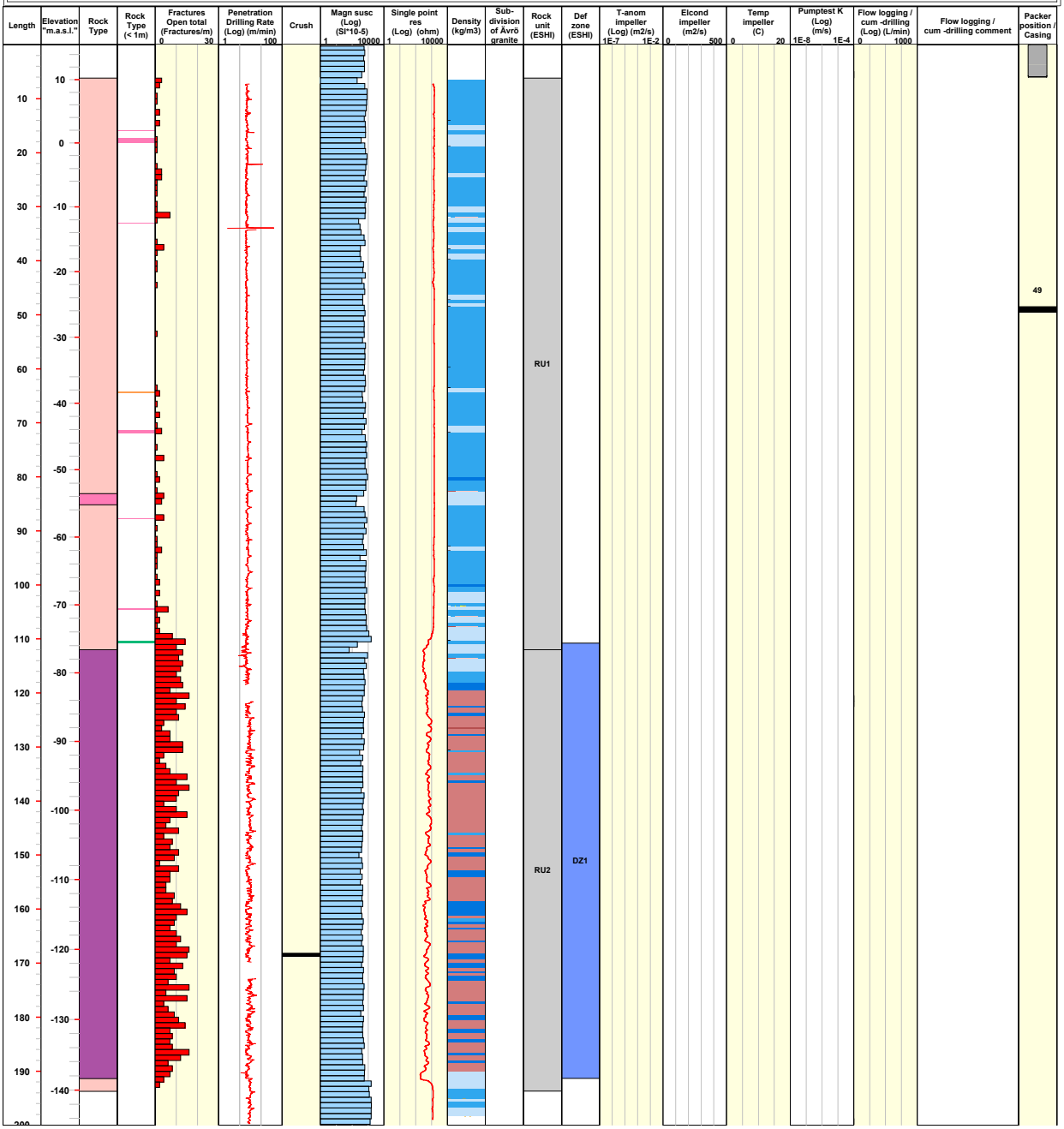

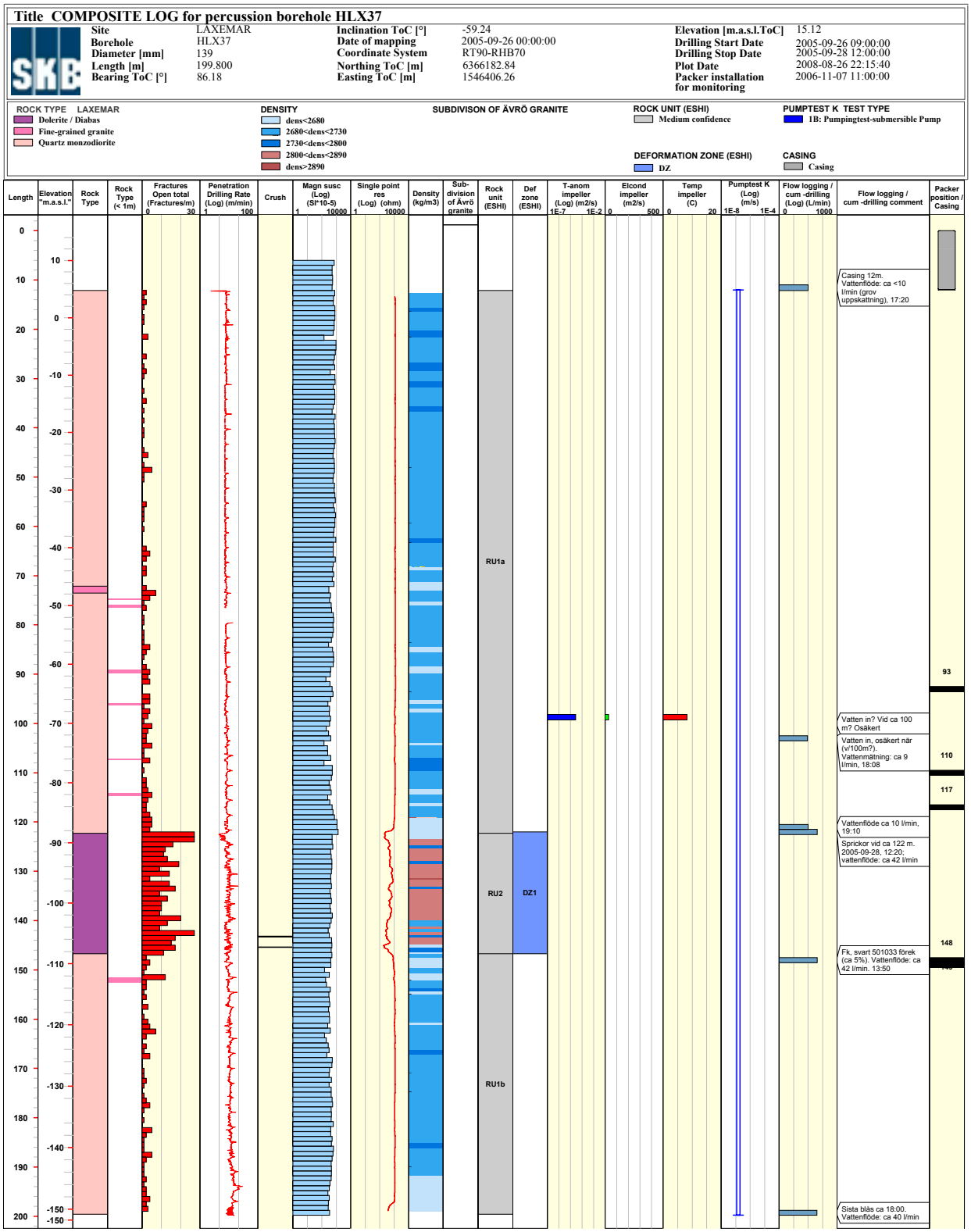
Title COMPOSITE LOG for percussion borehole HLX37
Site LAXEMAR
Borehole HLX37
Diameter [mm] 139
Length [m] 199.800
Bearing ToC [°] 86.18
Inclination ToC [°] -59.24
Date of mapping 2005-09-26 00:00:00
Coordinate System RT90-RHB70
Northing ToC [m] 6366182.84
Easting ToC [m] 1546406.26
Elevation [m.a.s.l.ToC] 15.12
Drilling Start Date 2005-09-26 09:00:00
Drilling Stop Date 2005-09-28 12:00:00
Plot Date 2008-08-26 22:15:40
Packer installation for monitoring 2006-11-07 11:00:00
ROCK TYPE LAXEMAR
Dolerite / Diabas
Fine-grained granite
Quartz monzodiorite
DENSITY
dens<2680
2680<dens<2730
2730<dens<2800
2800<dens<2890
dens>2890
SUBDIVISON OF ÄVRÖ GRANITE
ROCK UNIT (ESHI)
Medium confidence
DEFORMATION ZONE (ESHI)
DZ
PUMPTEST K TEST TYPE
1B: Pumpingtest-submersible Pump
CASING
Casing
Length
Elevation "m.a.s.l."
Rock Type
Rock Type (< 1m)
Fractures Open total (Fractures/m)
Penetration Drilling Rate (Log) (m/min)
Crush
Magn susc (Log) (SI*10-5)
Single point res (Log) (ohm)
Density (kg/m3)
Sub-division of Ävrö granite
Rock unit (ESHI)
Def zone (ESHI)
T-anom impeller (Log) (m2/s)
Elcond impeller (m2/s)
Temp impeller (C)
Pumptest K (Log) (m/s)
Flow logging / cum -drilling (Log) (L/min)
Flow logging / cum -drilling comment
Packer position / Casing
RU1a
RU2
DZ1
RU1b
Casing 12m. Vattenflöde: ca <10 l/min (grov uppskattning), 17:20
Vatten in? Vid ca 100 m? Osäkert
Vatten in, osäkert när (v/100m?). Vattenmätning: ca 9 l/min, 18:08
Vattenflöde ca 10 l/min, 19:10
Sprickor vid ca 122 m. 2005-09-28, 12:20; vattenflöde: ca 42 l/min
Fk, svart 501033 förek (ca 5%). Vattenflöde: ca 42 l/min. 13:50
Sista blås ca 18:00. Vattenflöde: ca 40 l/min
93
110
117
148

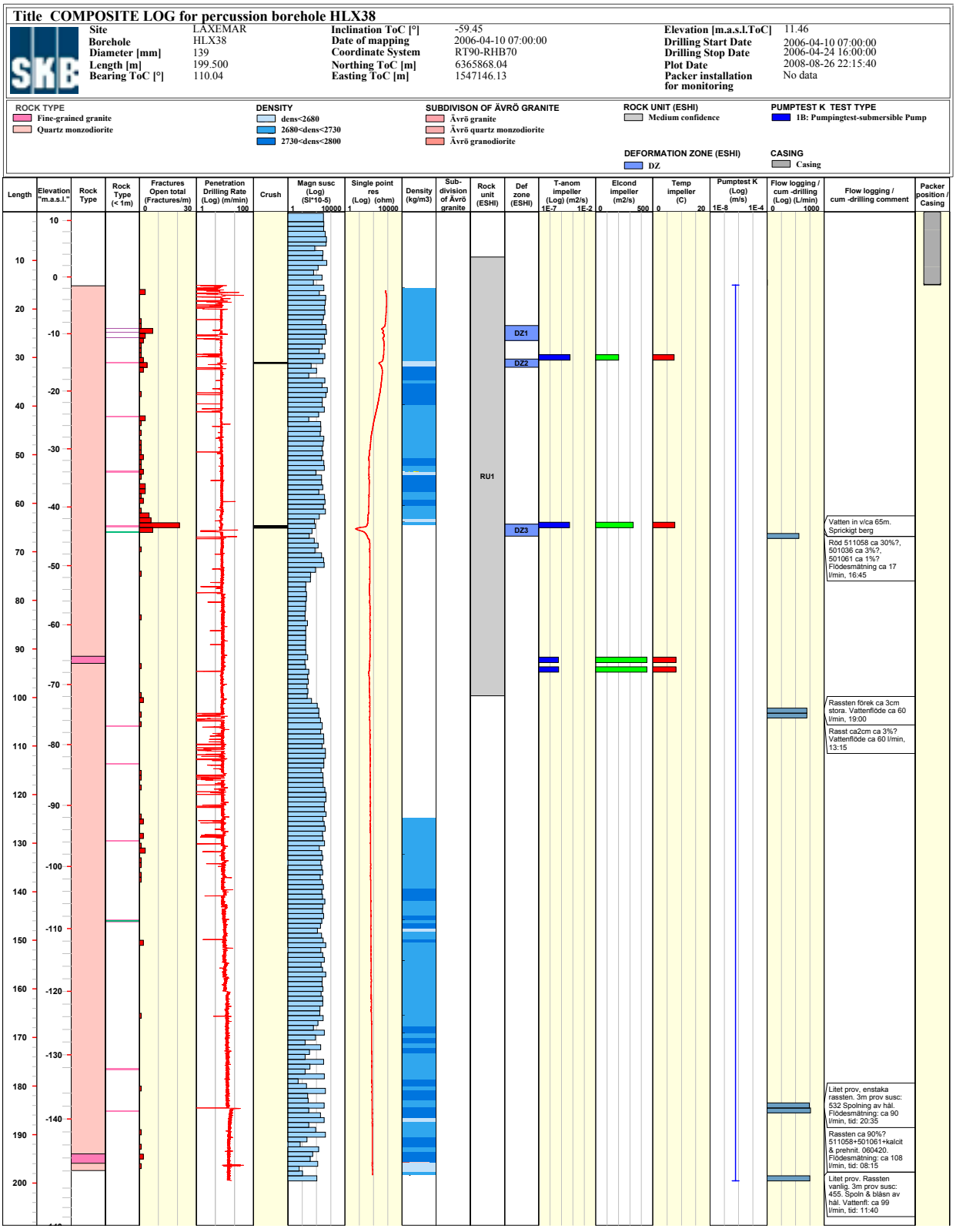
Title COMPOSITE LOG for percussion borehole HLX38
Site LAXEMAR
Borehole HLX38
Diameter [mm] 139
Length [m] 199.500
Bearing ToC [°] 110.04
Inclination ToC [°] -59.45
Date of mapping 2006-04-10 07:00:00
Coordinate System RT90-RHB70
Northing ToC [m] 6365868.04
Easting ToC [m] 1547146.13
Elevation [m.a.s.l.ToC] 11.46
Drilling Start Date 2006-04-10 07:00:00
Drilling Stop Date 2006-04-24 16:00:00
Plot Date 2008-08-26 22:15:40
Packer installation for monitoring No data
ROCK TYPE
Fine-grained granite
Quartz monzodiorite
DENSITY
dens<2680
2680<dens<2730
2730<dens<2800
SUBDIVISON OF ÄVRÖ GRANITE
Ävrö granite
Ävrö quartz monzodiorite
Ävrö granodiorite
ROCK UNIT (ESHI)
Medium confidence
DEFORMATION ZONE (ESHI)
DZ
PUMPTEST K TEST TYPE
1B: Pumpingtest-submersible Pump
CASING
Casing
Length
Elevation "m.a.s.l."
Rock Type
Rock Type (< 1m)
Fractures Open total (Fractures/m)
Penetration Drilling Rate (Log) (m/min)
Crush
Magn susc (Log) (SI*10-5)
Single point res (Log) (ohm)
Density (kg/m3)
Sub-division of Ävrö granite
Rock unit (ESHI)
Def zone (ESHI)
T-anom impeller (Log) (m2/s)
Elcond impeller (m2/s)
Temp impeller (C)
Pumptest K (Log) (m/s)
Flow logging / cum -drilling (Log) (L/min)
Flow logging / cum -drilling comment
Packer position / Casing
DZ1
DZ2
DZ3
RU1
Vatten in v/ca 65m. Sprickigt berg
Röd 511058 ca 30%?, 501036 ca 3%?, 501061 ca 1%? Flödesmätning ca 17 l/min, 16:45
Rassten förek ca 3cm stora. Vattenflöde ca 60 l/min, 19:00
Rasst ca2cm ca 3%? Vattenflöde ca 60 l/min, 13:15
Litet prov, enstaka rassten. 3m prov susc: 532 Spolning av hål. Flödesmätning: ca 90 l/min, tid: 20:35
Rassten ca 90%? 511058+501061+kalcit & prehnit. 060420. Flödesmätning: ca 108 l/min, tid: 08:15
Litet prov. Rassten vanlig. 3m prov susc: 455. Spoln & blåsn av hål. Vattenfl: ca 99 l/min, tid: 11:40

Title COMPOSITE LOG for percussion borehole HLX39

Site	LAXEMAR	**Inclination ToC [°]**	-59.34	**Elevation [m.a.s.l.ToC]**	26.97
Borehole	HLX39	**Date of mapping**	2006-06-07 00:00:00	**Drilling Start Date**	2006-06-07 11:40:00
Diameter [mm]	138	**Coordinate System**	RT90-RHB70	**Drilling Stop Date**	2006-06-14 12:00:00
Length [m]	199.300	**Northing ToC [m]**	6366887.05	**Plot Date**	2008-08-26 22:15:40
Bearing ToC [°]	14.29	**Easting ToC [m]**	1546880.53	**Packer installation for monitoring**	2008-01-15 00:00:00

ROCK TYPE LAXEMAR
- Fine-grained granite
- Ävrö granite
- Diorite / Gabbro
- Fine-grained diorite-gabbro

DENSITY
- dens<2680
- 2680<dens<2730
- 2730<dens<2800
- 2800<dens<2890

SUBDIVISON OF ÄVRÖ GRANITE
- Ävrö granite
- Ävrö quartz monzodiorite
- Ävrö granodiorite

ROCK UNIT (ESHI)
- Medium confidence

DEFORMATION ZONE (ESHI)
- DZ

PUMPTEST K TEST TYPE
- 1B: Pumpingtest-submersible Pump

CASING
- Casing

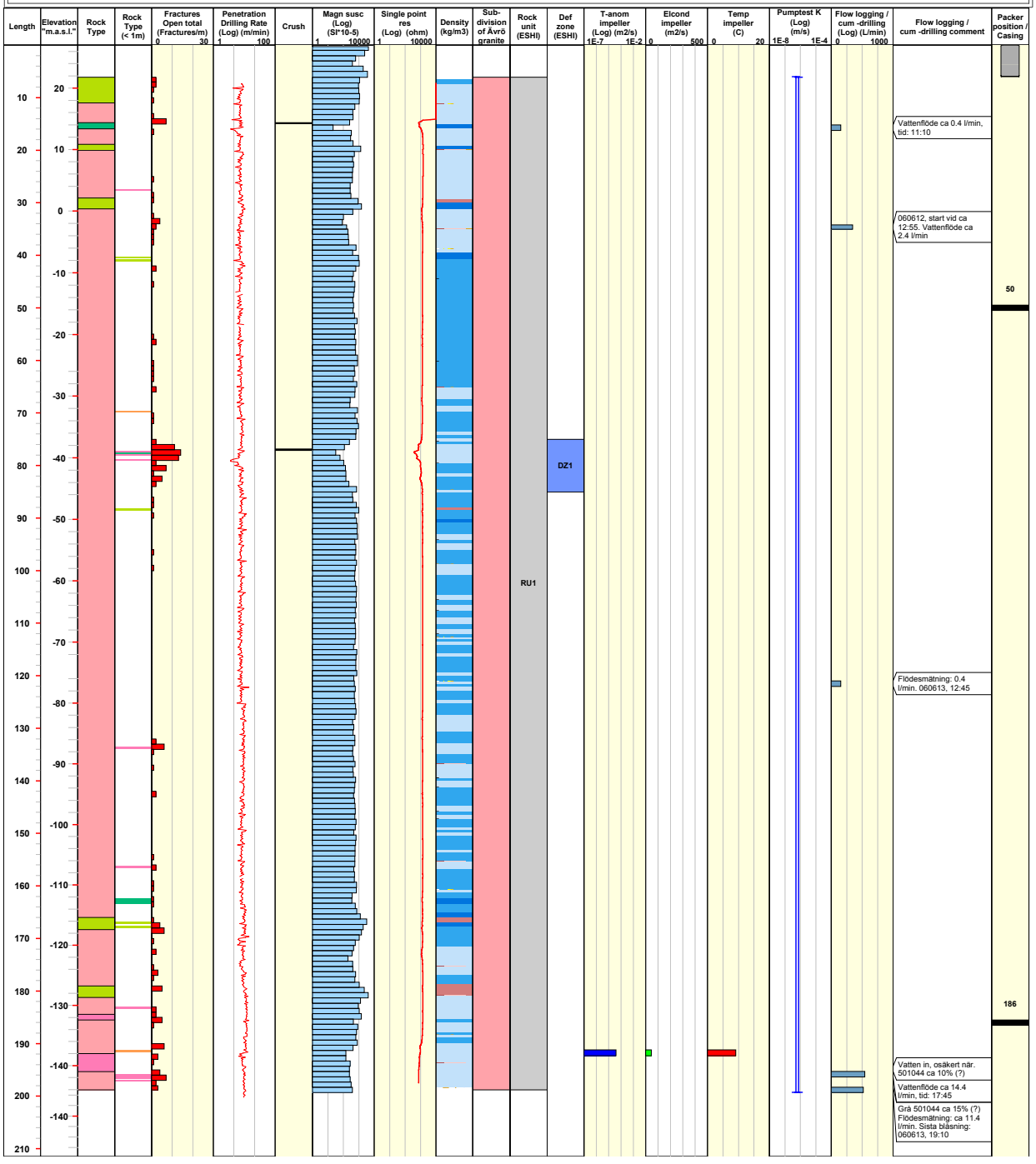

Title COMPOSITE LOG for percussion borehole HLX40

Site	LAXEMAR	**Inclination ToC [°]**	-59.81	**Elevation [m.a.s.l.ToC]**	25.67
Borehole	HLX40	**Date of mapping**	2006-05-02 00:00:00	**Drilling Start Date**	2006-05-02 16:15:00
Diameter [mm]	138	**Coordinate System**	RT90-RHB70	**Drilling Stop Date**	2006-05-09 12:30:00
Length [m]	199.500	**Northing ToC [m]**	6366905.94	**Plot Date**	2008-08-26 22:15:40
Bearing ToC [°]	11.03	**Easting ToC [m]**	1546943.99	**Packer installation for monitoring**	No data

ROCK TYPE
- Fine-grained granite
- Pegmatite
- Ävrö granite
- Diorite / Gabbro

DENSITY
- dens<2680
- 2680<dens<2730
- 2730<dens<2800

SUBDIVISON OF ÄVRÖ GRANITE
- Ävrö granite
- Ävrö quartz monzodiorite
- Ävrö granodiorite

ROCK UNIT (ESHI)
- Medium confidence

DEFORMATION ZONE (ESHI)
- DZ

PUMPTEST K TEST TYPE

CASING
- Casing

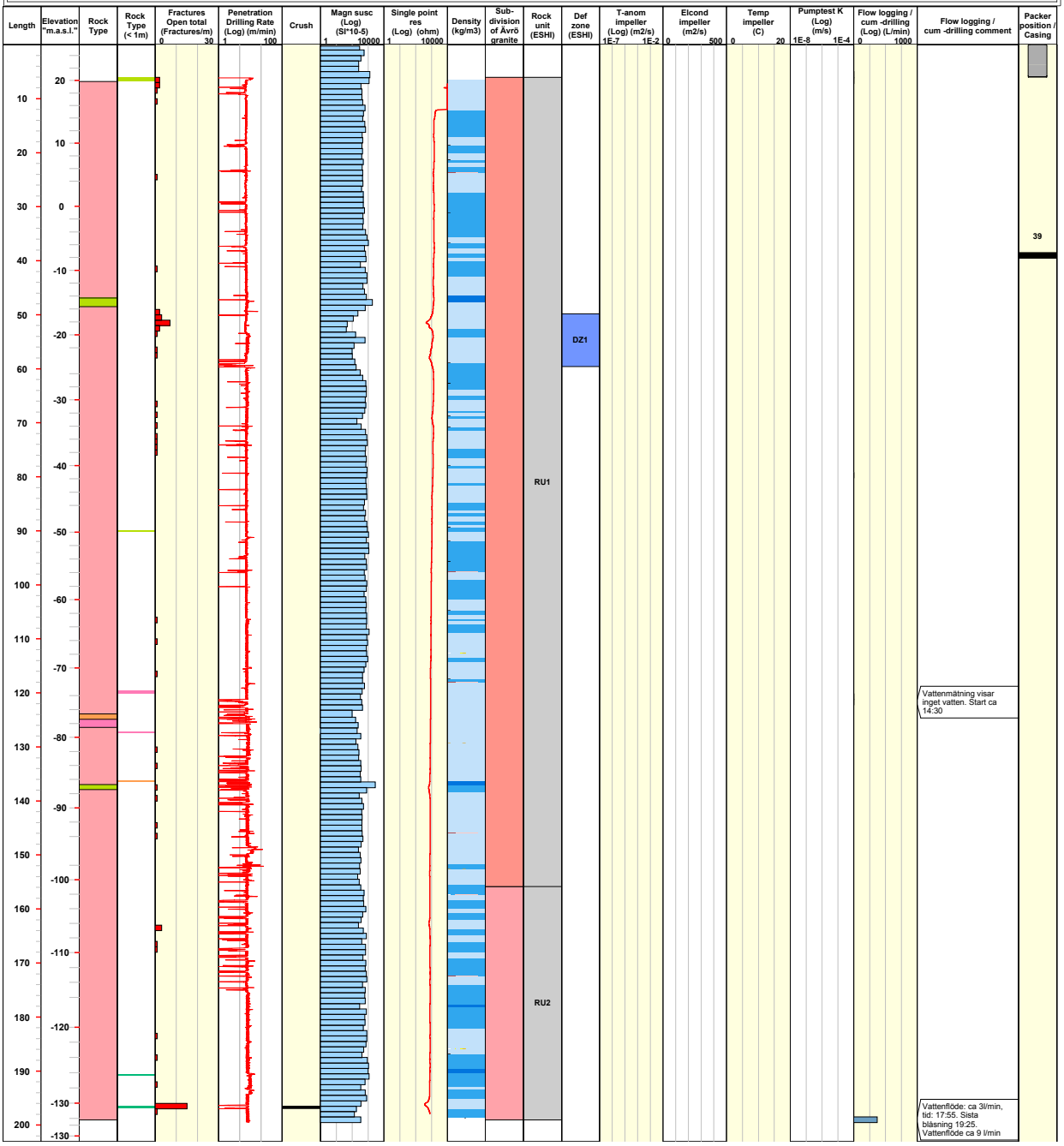

Title COMPOSITE LOG for percussion borehole HLX41

Site	LAXEMAR	**Inclination ToC [°]**	-59.14	**Elevation [m.a.s.l.ToC]**	21.73
Borehole	HLX41	**Date of mapping**	2006-05-22 12:00:00	**Drilling Start Date**	2006-05-22 12:00:00
Diameter [mm]	139	**Coordinate System**	RT90-RHB70	**Drilling Stop Date**	2006-06-01 11:00:00
Length [m]	199.500	**Northing ToC [m]**	6367012.38	**Plot Date**	2008-08-26 22:15:40
Bearing ToC [°]	208.29	**Easting ToC [m]**	1547017.66	**Packer installation for monitoring**	No data

ROCK TYPE
- Fine-grained granite
- Ävrö granite
- Diorite / Gabbro

DENSITY
- dens<2680
- 2680<dens<2730
- 2730<dens<2800
- 2800<dens<2890
- dens>2890

SUBDIVISON OF ÄVRÖ GRANITE
- Ävrö granite
- Ävrö quartz monzodiorite
- Ävrö granodiorite

ROCK UNIT (ESHI)
- Medium confidence

DEFORMATION ZONE (ESHI)

PUMPTEST K TEST TYPE

CASING
- Casing

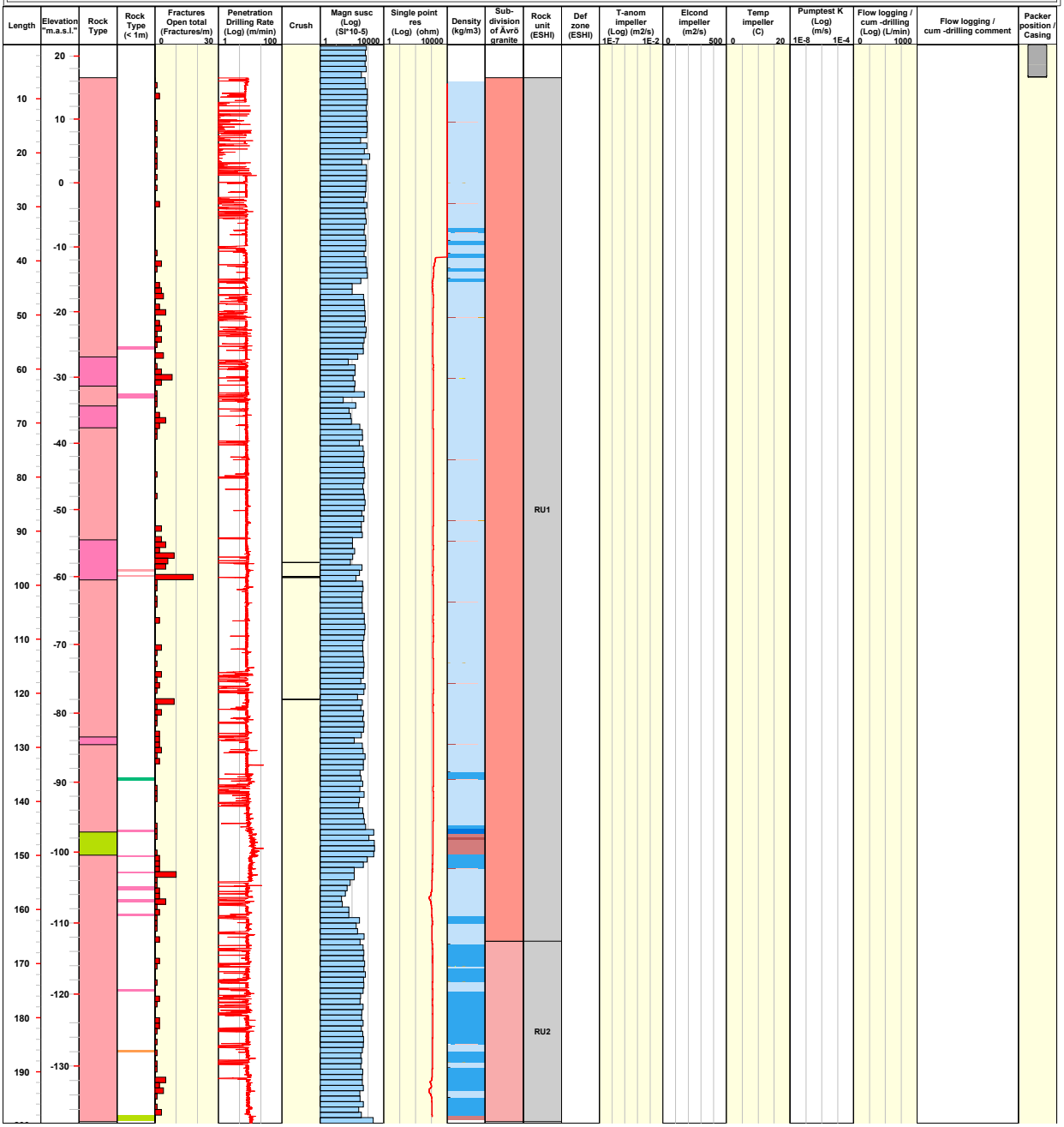

Title COMPOSITE LOG for percussion borehole HLX42

Site	LAXEMAR	**Inclination ToC [°]**	-57.20	**Elevation [m.a.s.l.ToC]**	12.81
Borehole	HLX42	**Date of mapping**	2006-11-13 00:00:00	**Drilling Start Date**	2006-11-13 13:30:00
Diameter [mm]	139	**Coordinate System**	RT90-RHB70	**Drilling Stop Date**	2006-11-16 19:00:00
Length [m]	152.600	**Northing ToC [m]**	6364826.22	**Plot Date**	2008-08-26 22:15:40
Bearing ToC [°]	321.51	**Easting ToC [m]**	1547446.78	**Packer installation for monitoring**	2006-11-22 10:00:00

ROCK TYPE LAXEMAR
- Fine-grained granite
- Pegmatite
- Quartz monzodiorite
- Fine-grained diorite-gabbro

DENSITY

SUBDIVISON OF ÄVRÖ GRANITE

ROCK UNIT (ESHI)
- Medium confidence

PUMPTEST K TEST TYPE
- 1B: Pumpingtest-submersible Pump

DEFORMATION ZONE (ESHI)

CASING
- Casing

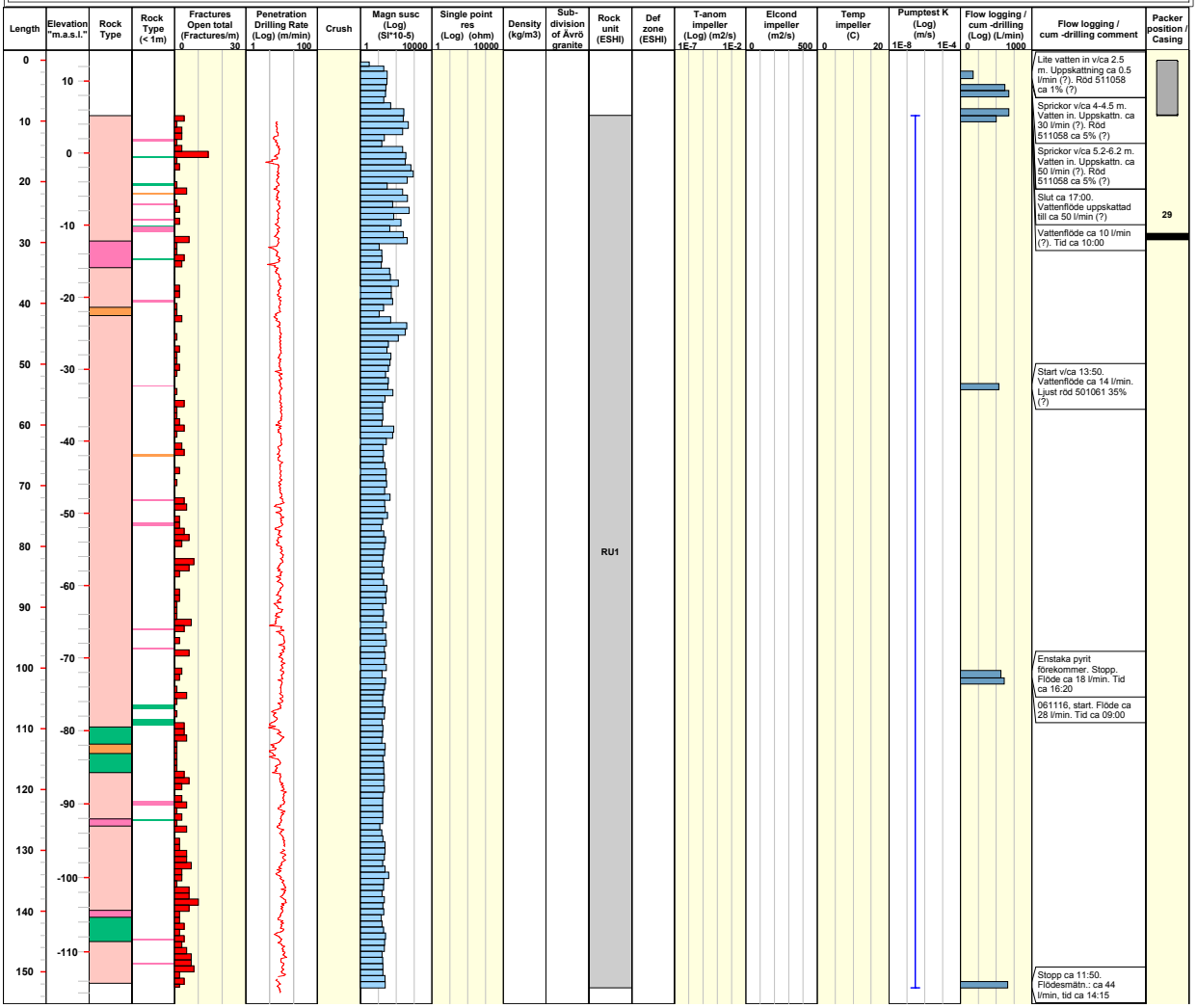

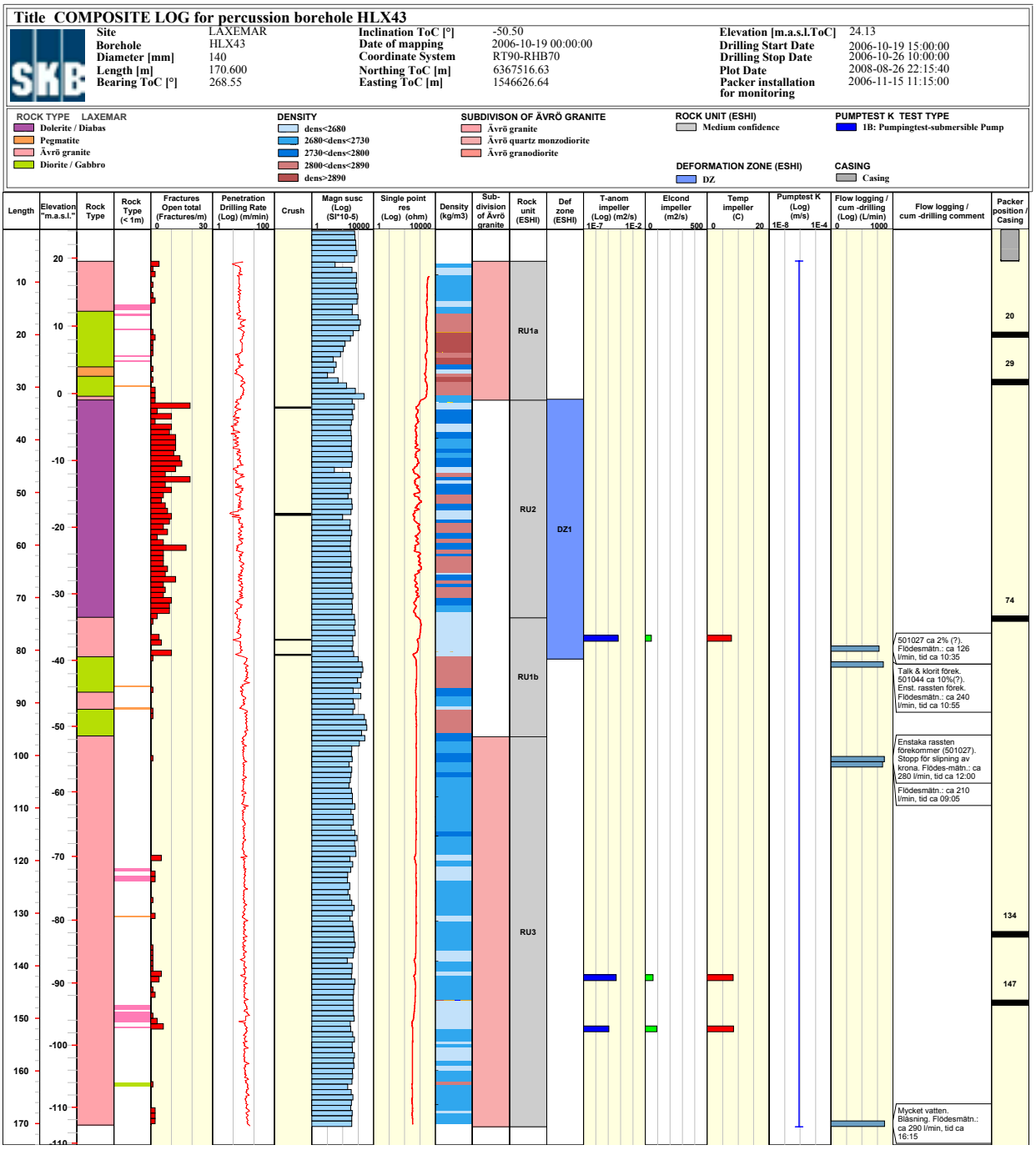
Title COMPOSITE LOG for percussion borehole HLX43
Site LAXEMAR
Borehole HLX43
Diameter [mm] 140
Length [m] 170.600
Bearing ToC [°] 268.55
Inclination ToC [°] -50.50
Date of mapping 2006-10-19 00:00:00
Coordinate System RT90-RHB70
Northing ToC [m] 6367516.63
Easting ToC [m] 1546626.64
Elevation [m.a.s.l.ToC] 24.13
Drilling Start Date 2006-10-19 15:00:00
Drilling Stop Date 2006-10-26 10:00:00
Plot Date 2008-08-26 22:15:40
Packer installation for monitoring 2006-11-15 11:15:00
ROCK TYPE LAXEMAR
Dolerite / Diabas
Pegmatite
Ävrö granite
Diorite / Gabbro
DENSITY
dens<2680
2680<dens<2730
2730<dens<2800
2800<dens<2890
dens>2890
SUBDIVISON OF ÄVRÖ GRANITE
Ävrö granite
Ävrö quartz monzodiorite
Ävrö granodiorite
ROCK UNIT (ESHI)
Medium confidence
PUMPTEST K TEST TYPE
1B: Pumpingtest-submersible Pump
DEFORMATION ZONE (ESHI)
DZ
CASING
Casing
Length
Elevation "m.a.s.l."
Rock Type
Rock Type (< 1m)
Fractures Open total (Fractures/m)
Penetration Drilling Rate (Log) (m/min)
Crush
Magn susc (Log) (SI*10-5)
Single point res (Log) (ohm)
Density (kg/m3)
Sub-division of Ävrö granite
Rock unit (ESHI)
Def zone (ESHI)
T-anom impeller (Log) (m2/s)
Elcond impeller (m2/s)
Temp impeller (C)
Pumptest K (Log) (m/s)
Flow logging / cum -drilling (Log) (L/min)
Flow logging / cum -drilling comment
Packer position / Casing
RU1a
RU2
RU1b
RU3
DZ1
501027 ca 2% (?). Flödesmätn.: ca 126 l/min, tid ca 10:35
Talk & klorit förek. 501044 ca 10%(?). Enst. rassten förek. Flödesmätn.: ca 240 l/min, tid ca 10:55
Enstaka rassten förekommer (501027). Stopp för slipning av krona. Flödes-mätn.: ca 280 l/min, tid ca 12:00
Flödesmätn.: ca 210 l/min, tid ca 09:05
Mycket vatten. Blåsning. Flödesmätn.: ca 290 l/min, tid ca 16:15
20
29
74
134
147

Title COMPOSITE LOG for percussion borehole HSH01

Site	SIMPEVARP	**Inclination ToC [°]**	-69.98	**Elevation [m.a.s.l.ToC]**	2.79
Borehole	HSH01	**Date of mapping**	2002-06-24 16:00:00	**Drilling Start Date**	2002-06-24 16:00:00
Diameter [mm]	140	**Coordinate System**	RT90-RHB70	**Drilling Stop Date**	2002-07-02 17:30:00
Length [m]	200.000	**Northing ToC [m]**	6366216.95	**Plot Date**	2008-08-27 22:15:27
Bearing ToC [°]	4.99	**Easting ToC [m]**	1552545.76	**Packer installation for monitoring**	2004-04-01 13:15:00

ROCK TYPE SIMPEVARP
- Fine-grained granite
- Granite
- Quartz monzodiorite
- Fine-grained dioritoid

DENSITY

SUBDIVISON OF ÄVRÖ GRANITE
- Ävrö granite
- Ävrö quartz monzodiorite
- Ävrö granodiorite

ROCK UNIT (ESHI)
- Medium confidence

PUMPTEST K TEST TYPE

DEFORMATION ZONE (ESHI)
- DZ

CASING
- Casing

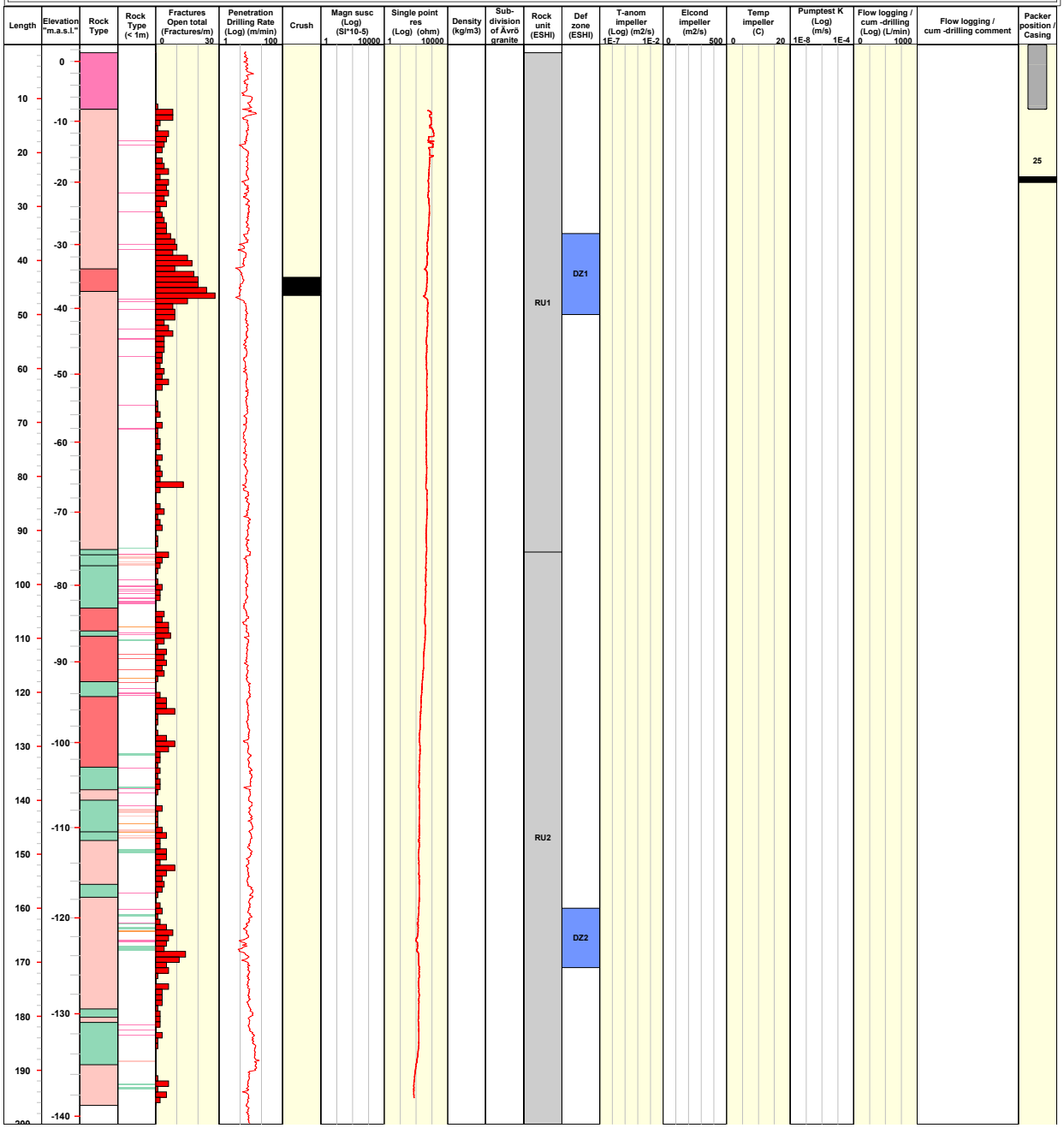

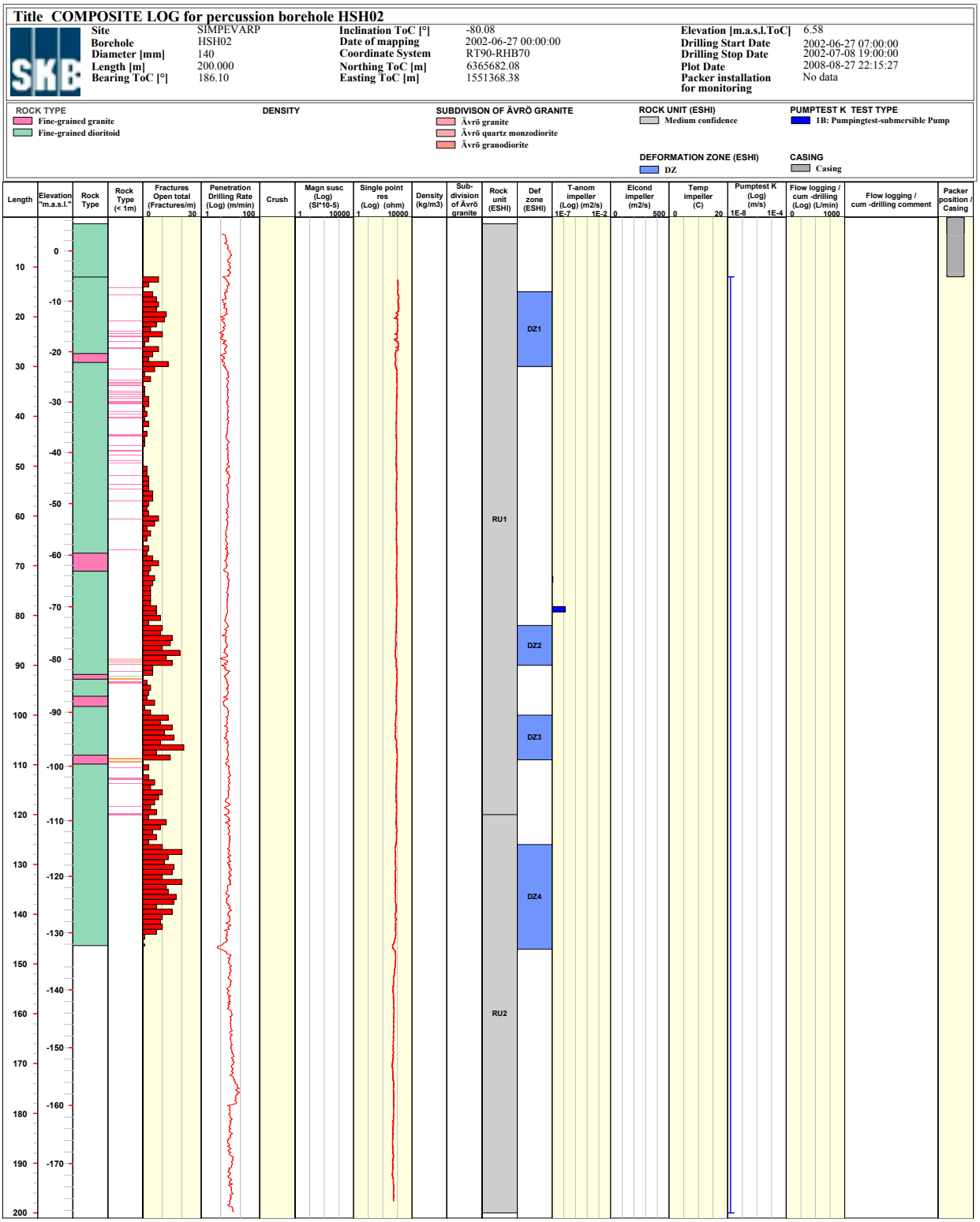
Title COMPOSITE LOG for percussion borehole HSH02
Site SIMPEVARP
Borehole HSH02
Diameter [mm] 140
Length [m] 200.000
Bearing ToC [°] 186.10
Inclination ToC [°] -80.08
Date of mapping 2002-06-27 00:00:00
Coordinate System RT90-RHB70
Northing ToC [m] 6365682.08
Easting ToC [m] 1551368.38
Elevation [m.a.s.l.ToC] 6.58
Drilling Start Date 2002-06-27 07:00:00
Drilling Stop Date 2002-07-08 19:00:00
Plot Date 2008-08-27 22:15:27
Packer installation for monitoring No data
ROCK TYPE
Fine-grained granite
Fine-grained dioritoid
DENSITY
SUBDIVISON OF ÄVRÖ GRANITE
Ävrö granite
Ävrö quartz monzodiorite
Ävrö granodiorite
ROCK UNIT (ESHI)
Medium confidence
PUMPTEST K TEST TYPE
1B: Pumpingtest-submersible Pump
DEFORMATION ZONE (ESHI)
DZ
CASING
Casing
Length
Elevation "m.a.s.l."
Rock Type
Rock Type (< 1m)
Fractures Open total (Fractures/m)
Penetration Drilling Rate (Log) (m/min)
Crush
Magn susc (Log) (SI*10-5)
Single point res (Log) (ohm)
Density (kg/m3)
Sub-division of Ävrö granite
Rock unit (ESHI)
Def zone (ESHI)
T-anom impeller (Log) (m2/s)
Elcond impeller (m2/s)
Temp impeller (C)
Pumptest K (Log) (m/s)
Flow logging / cum -drilling (Log) (L/min)
Flow logging / cum -drilling comment
Packer position / Casing
DZ1
DZ2
DZ3
DZ4
RU1
RU2

Title COMPOSITE LOG for percussion borehole HSH03

Site	SIMPEVARP	**Inclination ToC [°]**	-79.48	**Elevation [m.a.s.l.ToC]**	2.45
Borehole	HSH03	**Date of mapping**	2002-07-02 17:30:00	**Drilling Start Date**	2002-07-02 17:30:00
Diameter [mm]	139	**Coordinate System**	RT90-RHB70	**Drilling Stop Date**	2002-07-09 19:00:00
Length [m]	201.000	**Northing ToC [m]**	6366213.13	**Plot Date**	2008-08-27 22:15:27
Bearing ToC [°]	218.94	**Easting ToC [m]**	1552544.57	**Packer installation for monitoring**	No data

ROCK TYPE
- Granite
- Ävrö granite
- Quartz monzodiorite

DENSITY

SUBDIVISON OF ÄVRÖ GRANITE

ROCK UNIT (ESHI)
- Medium confidence

PUMPTEST K TEST TYPE
- 1B: Pumpingtest-submersible Pump

DEFORMATION ZONE (ESHI)
- DZ

CASING
- Casing

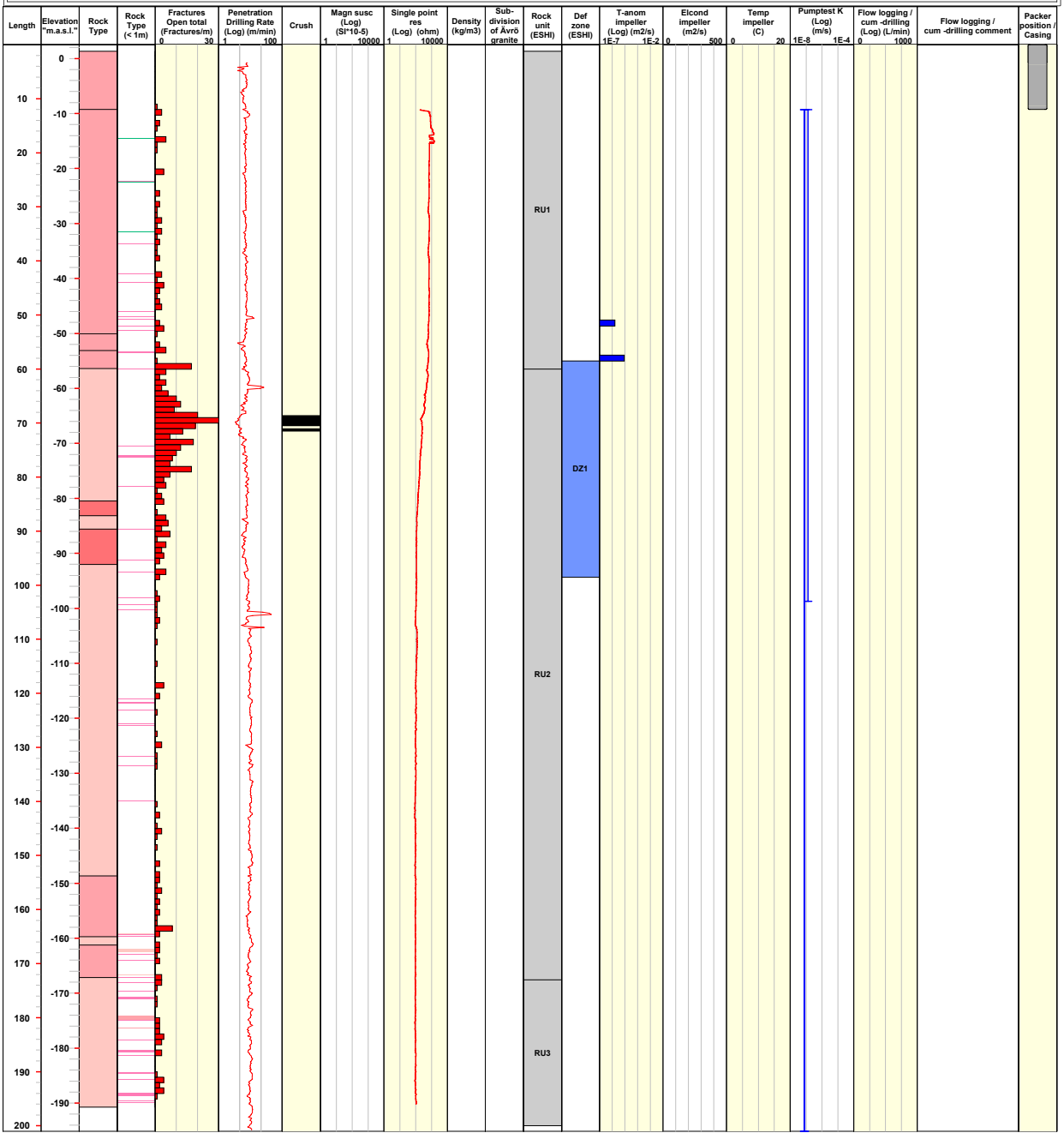

Appendix 7

PFL-f transmissivities versus Geological Extended Single-hole Interpretation(ESHI)

The Geological Extended Single-hole Interpretation (ESHI) of the drilled cores defines Rock Units (RU) and deformations zones (DZ) along the borehole that is used for further analysis by different disciplines. In this appendix the transmissivities and orientations of PFL-f features are shown together with ESHI. In the plots of PFL-f features elevation (elevation, or “level” in the plots, corresponds to the Z coordinate in the RH70/RHB70 system) the orientations of the PFL-f are shown as strike/dip. The pole plots show the Pole Vector, with orientation trend/dip, to each fracture that has a measured PFL-f feature.

Borehole KLX02.

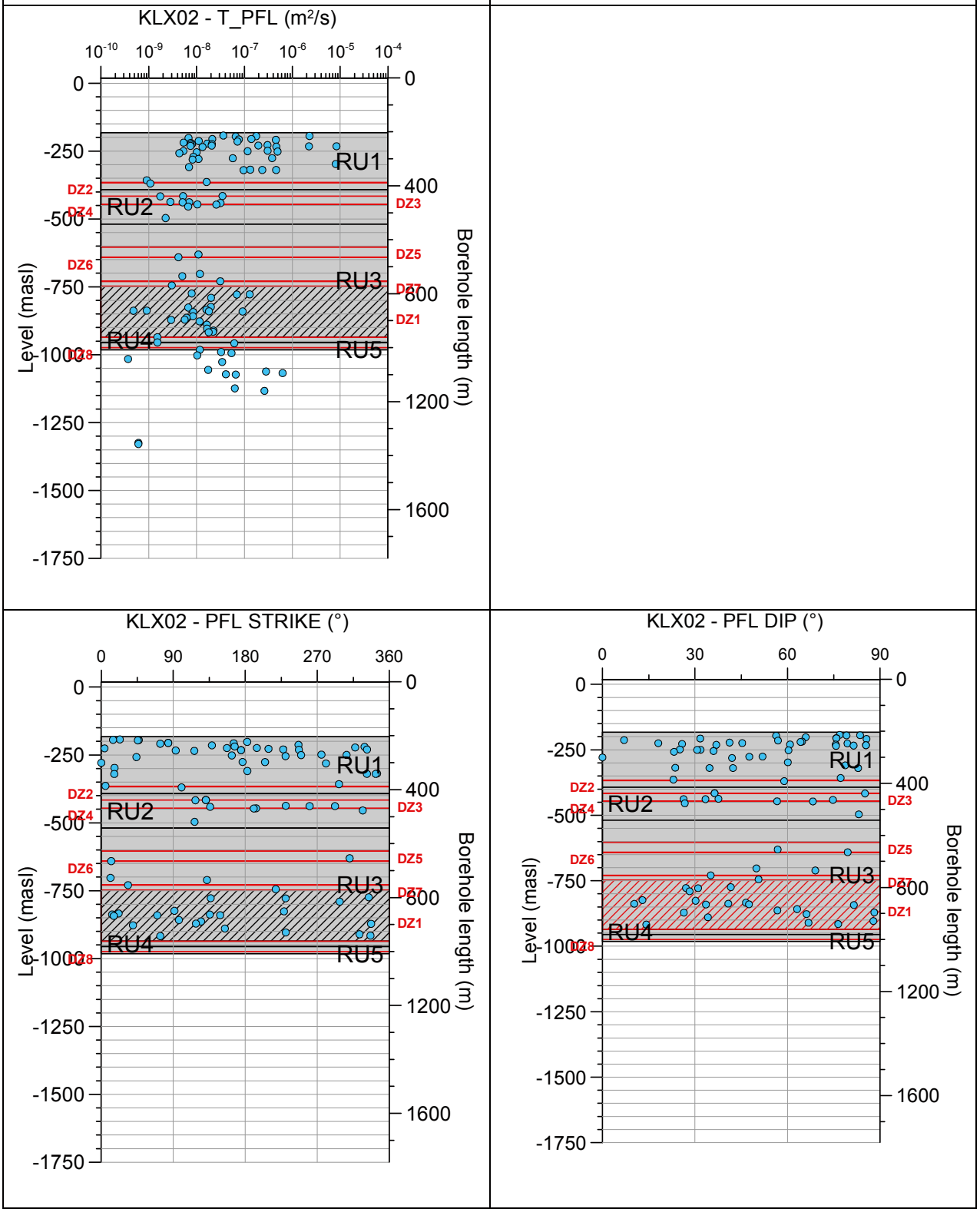

Comment: Transmissivity values and positions in the borehole of the PFL-f features in KLX02 are more uncertain compared to other boreholes as the measurements in KLX02 were made before Site Investigations started with different methodology. Below ca 1,000 m bh-length there are no oriented fractures.

Borehole KLX02. Poles for PFL-f feature planes outside deformation zones (ESHI).

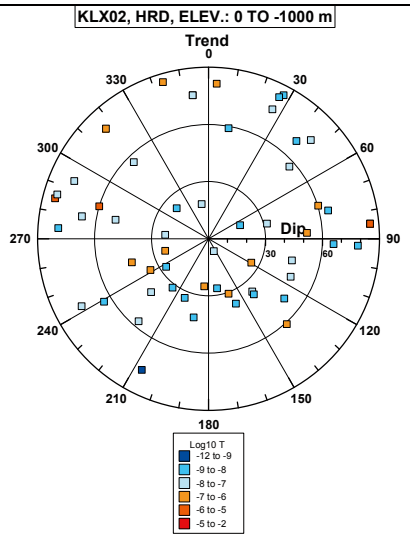

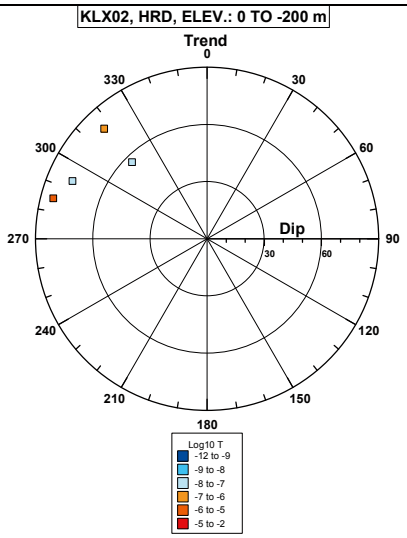

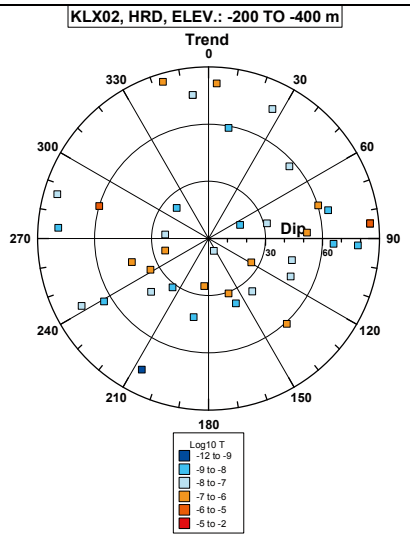

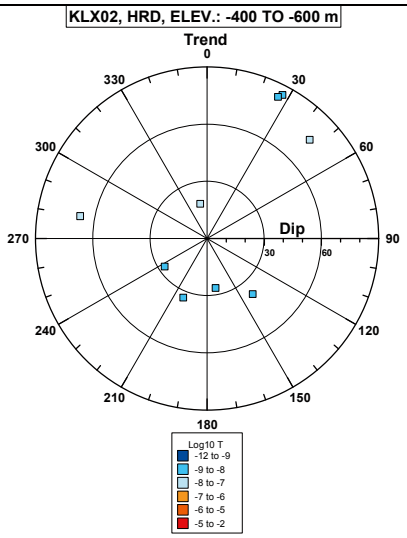

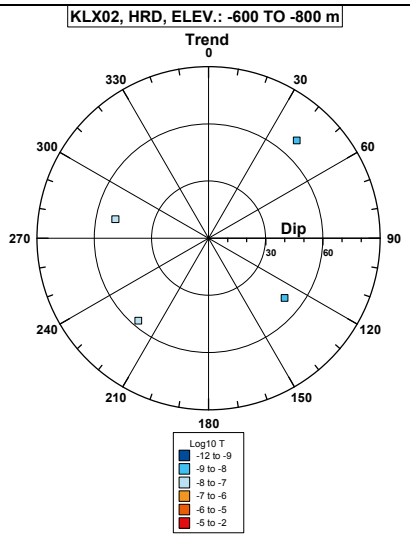

Borehole KLX02. Poles for PFL-f feature planes in deformation zones (ESHI).

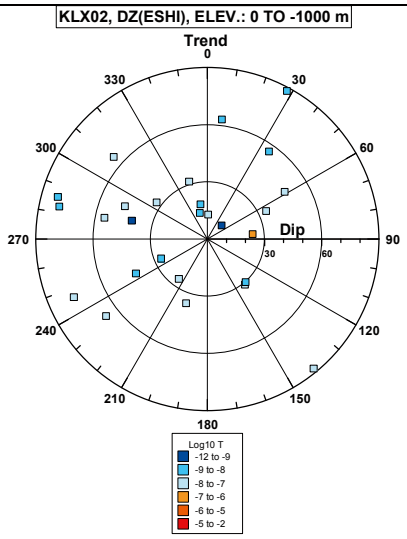

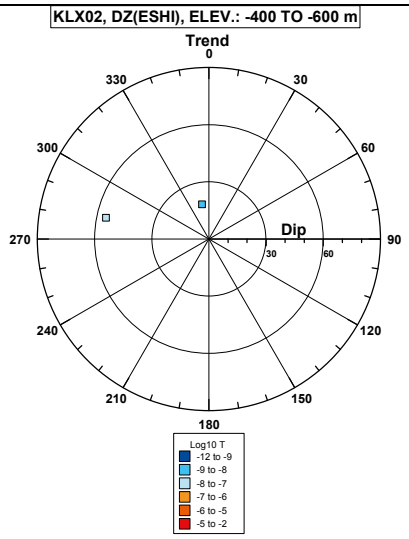

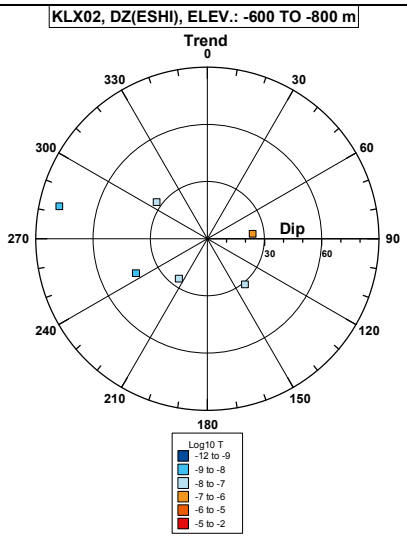

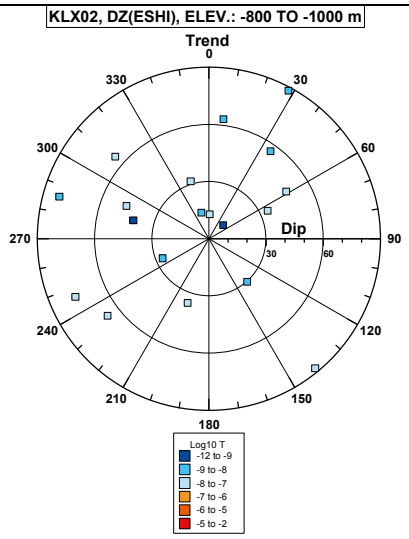

Borehole KLX03.

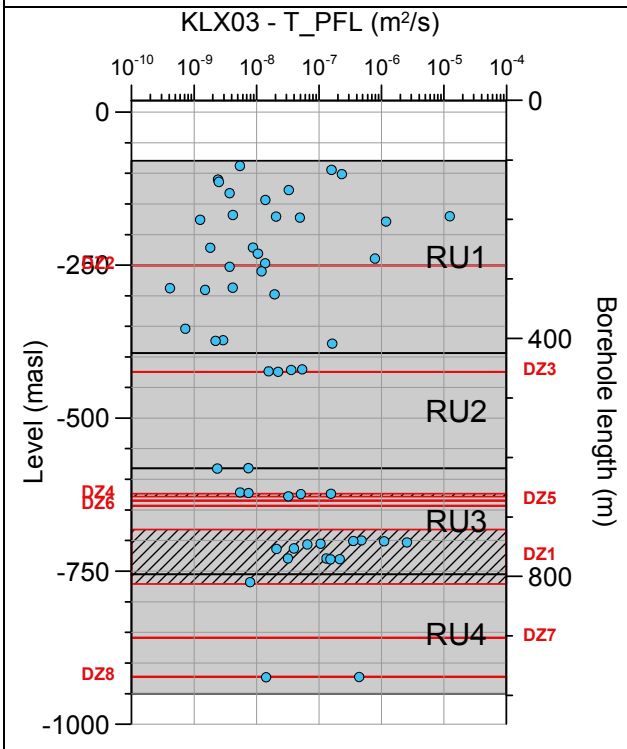

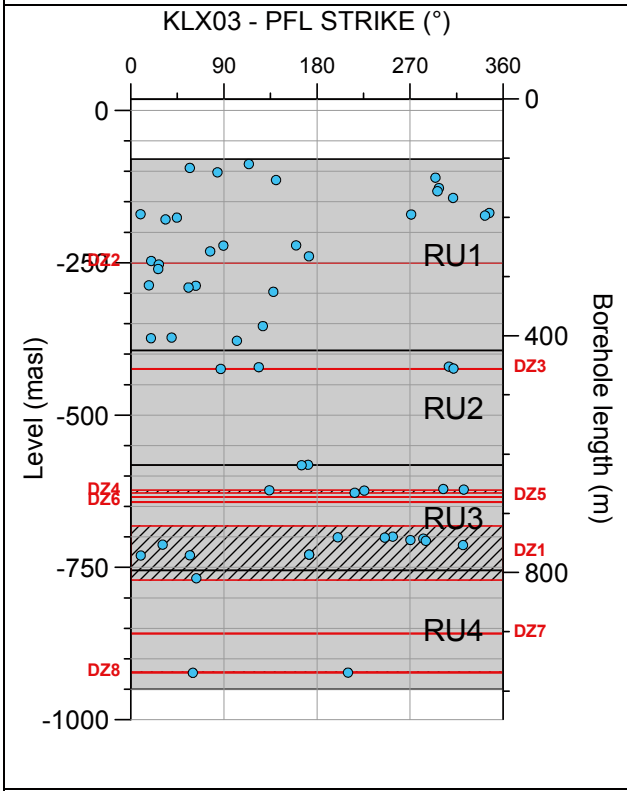

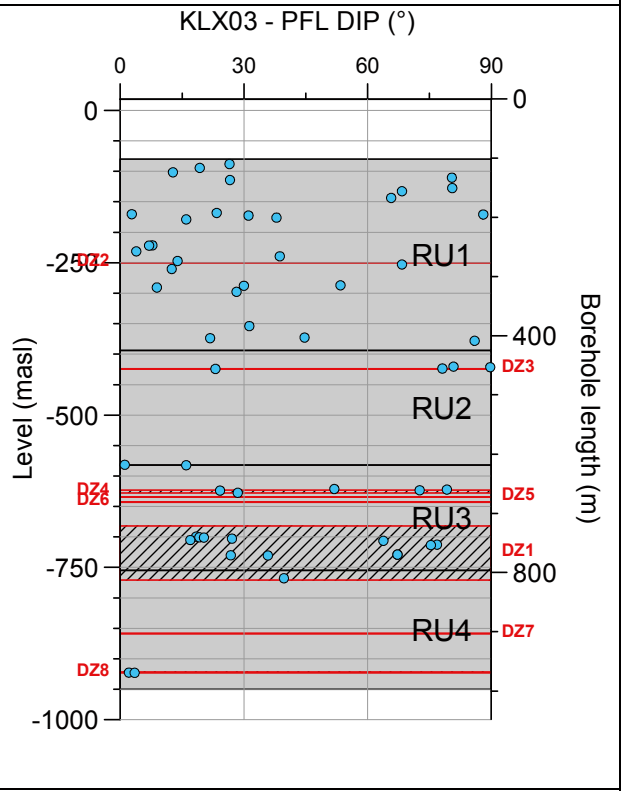

Comment:

Borehole KLX03. Poles for PFL-f feature planes outside deformation zones (ESHI).

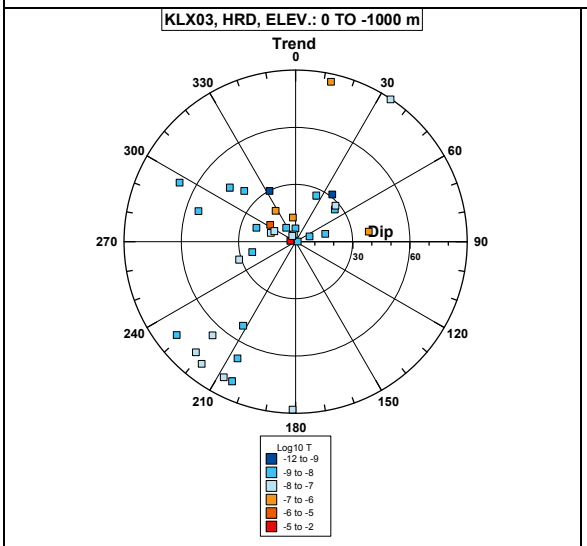

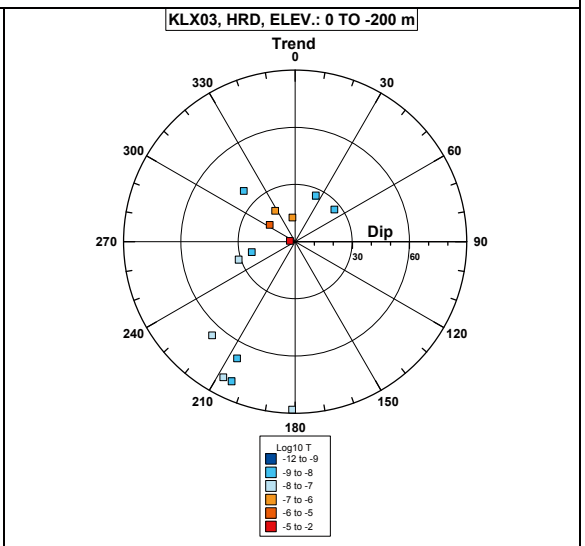

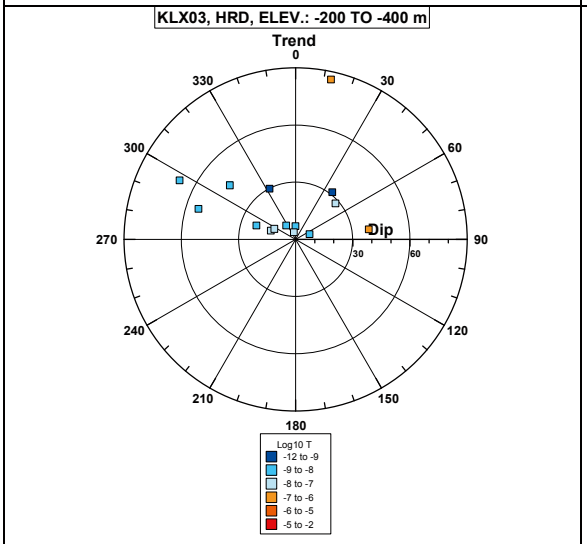

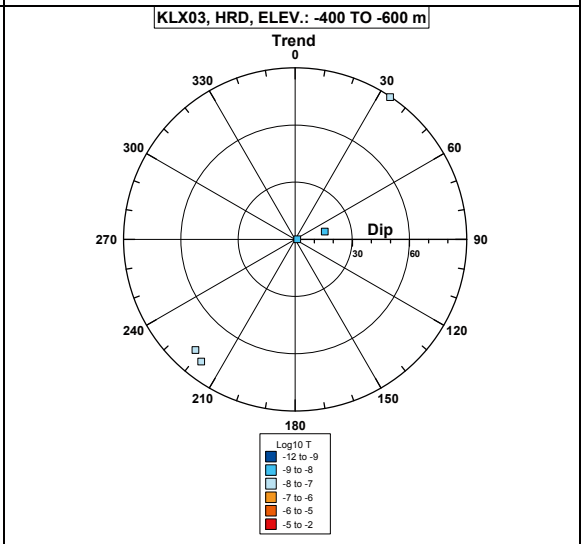

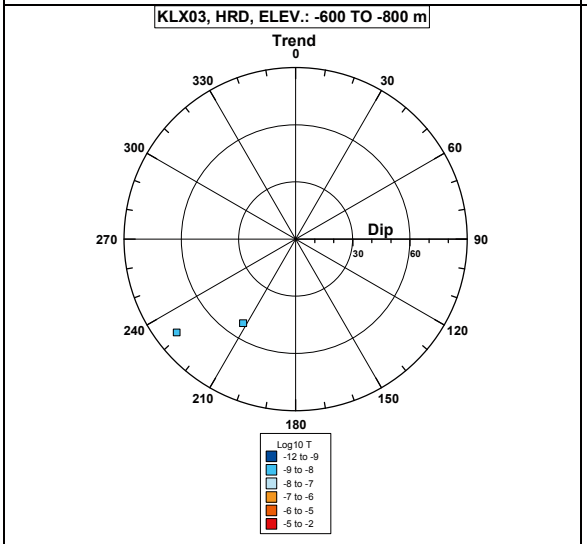

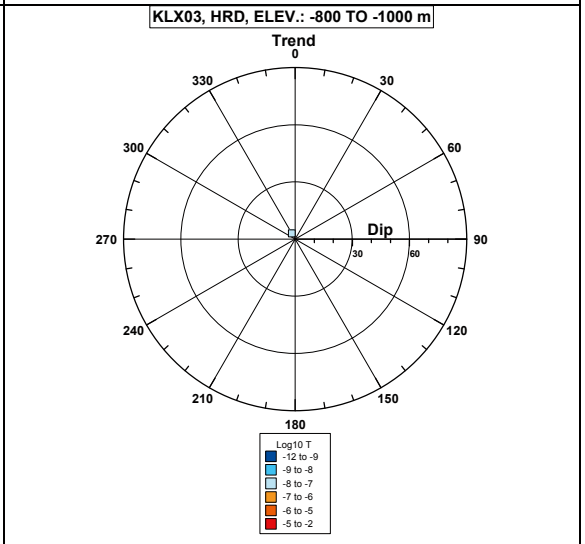

Borehole KLX03. Poles for PFL-f feature planes in deformation zones (ESHI).

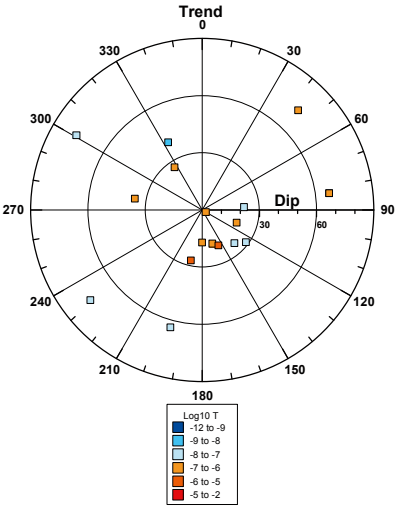

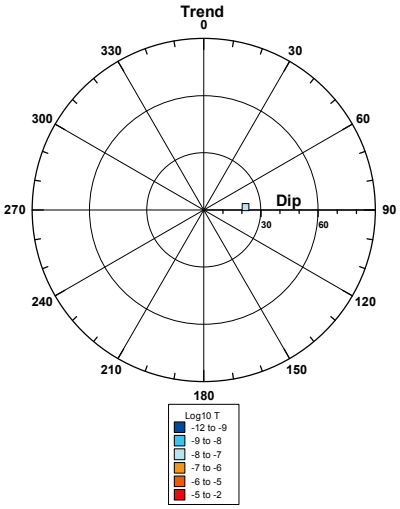

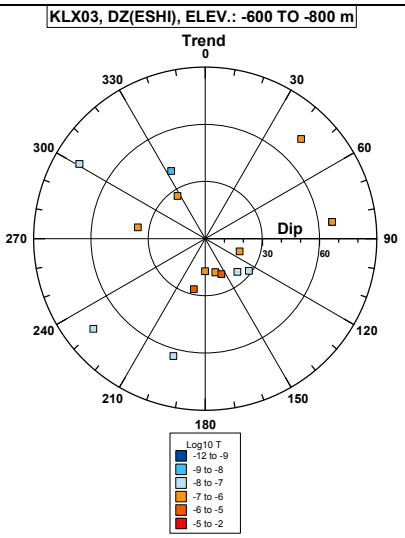

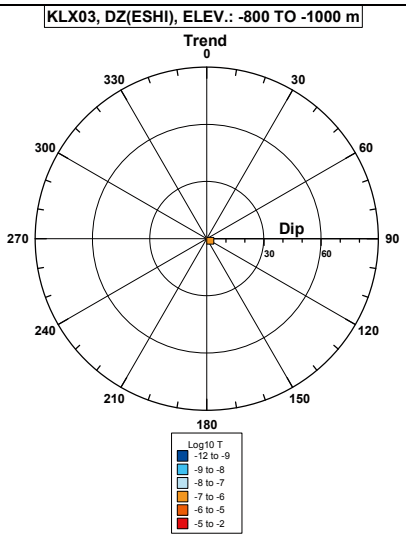

Borehole KLX04.

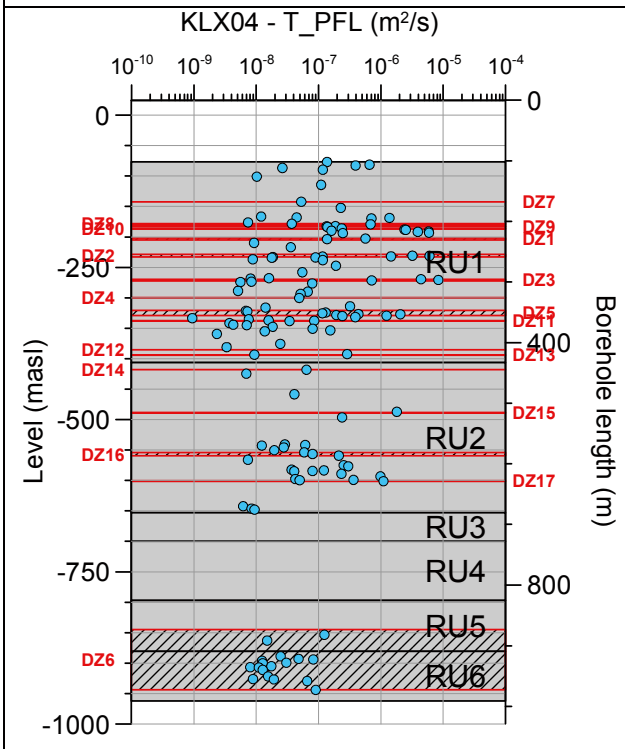

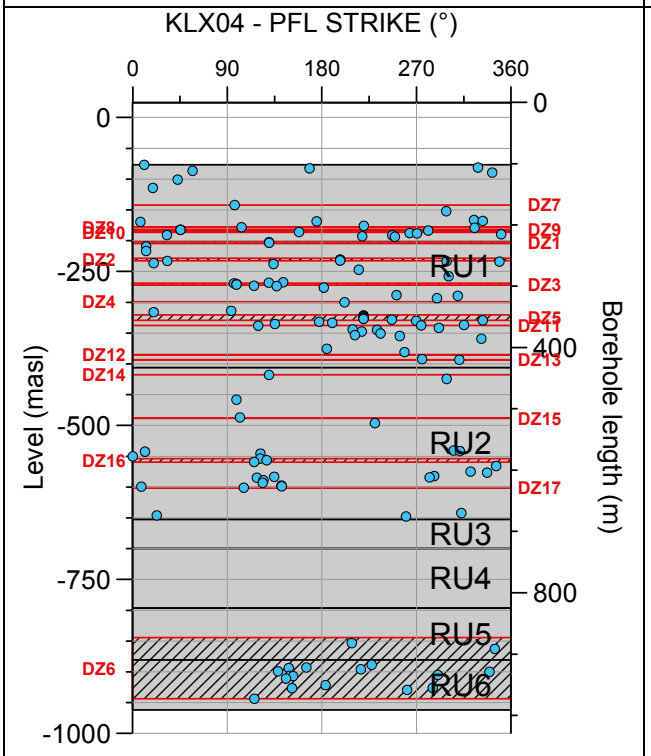

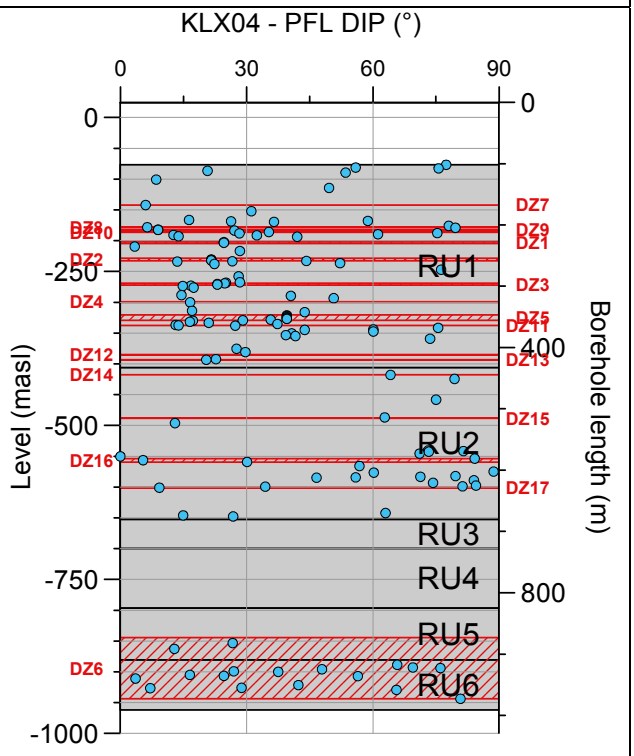

Comment:

Borehole KLX04. Poles for PFL-f feature planes outside deformation zones (ESHI).

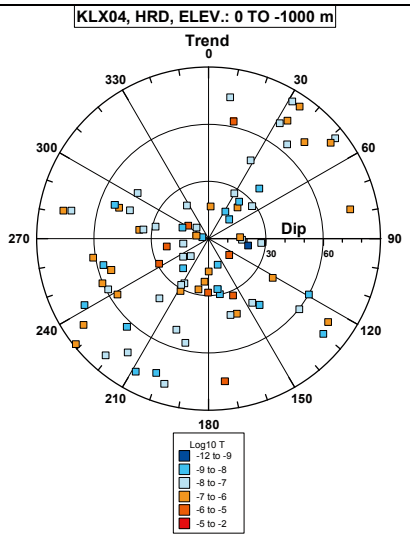

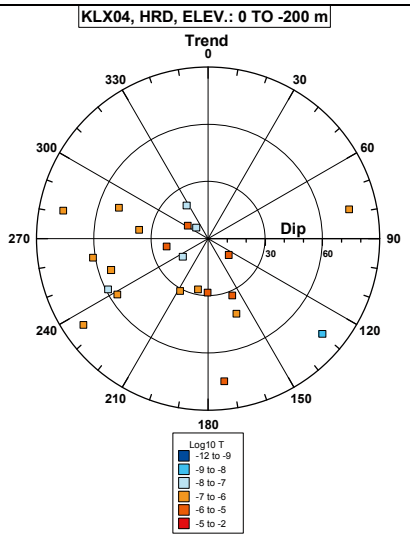

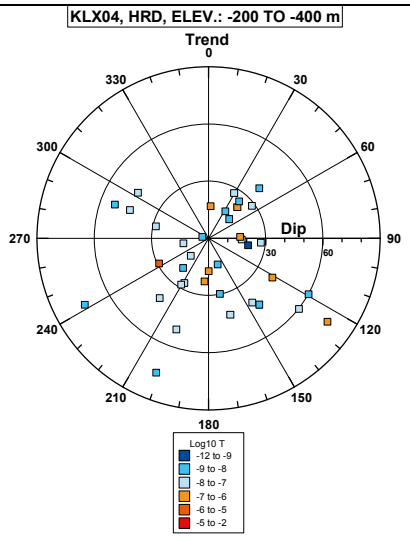

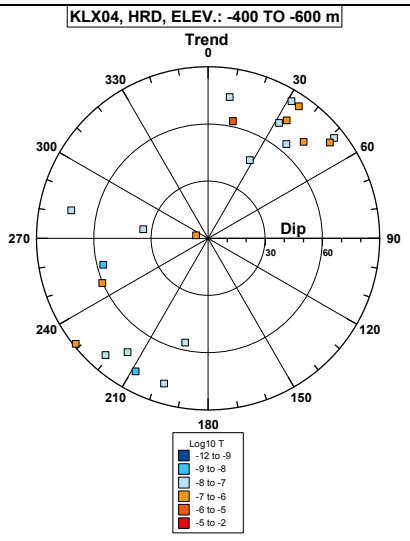

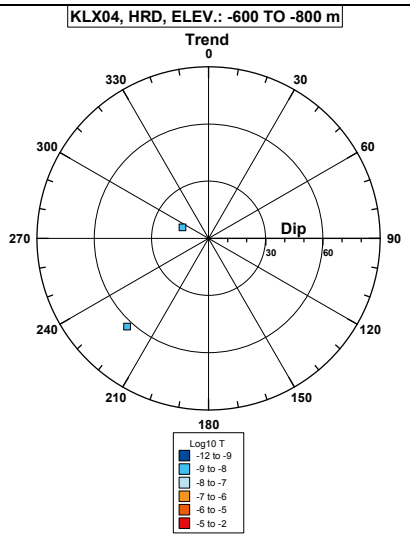

Borehole KLX04. Poles for PFL-f feature planes in deformation zones (ESHI).

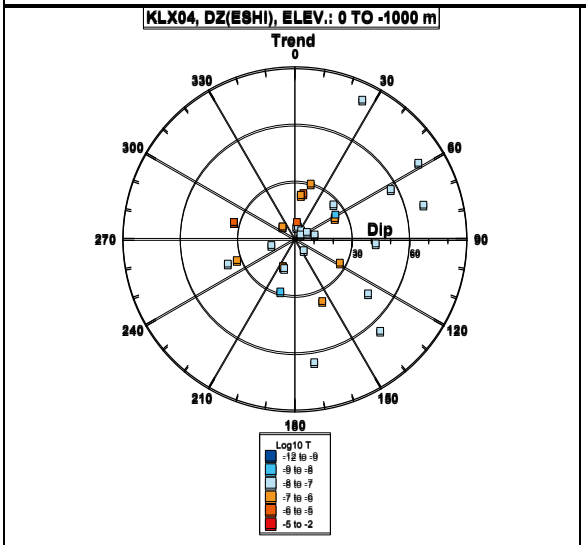

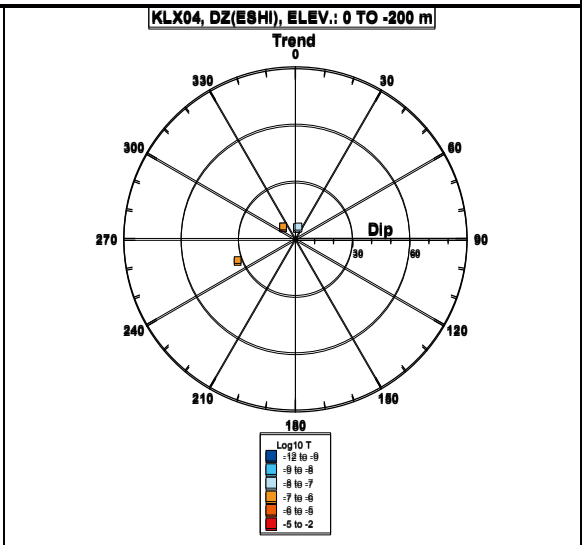

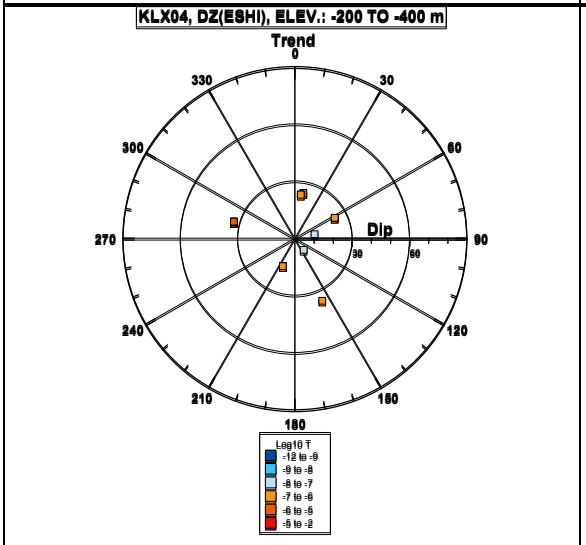

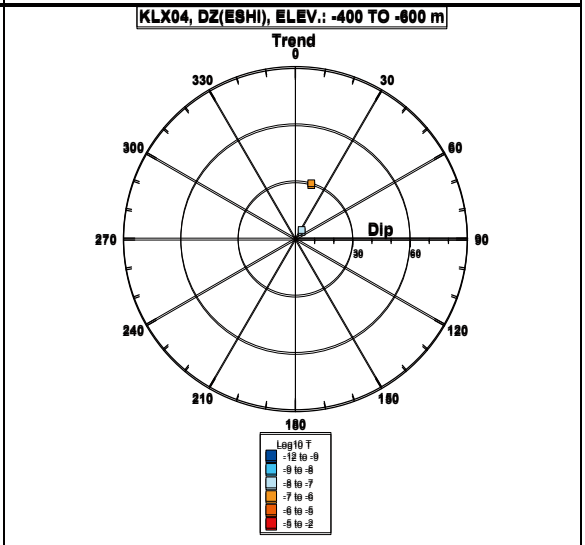

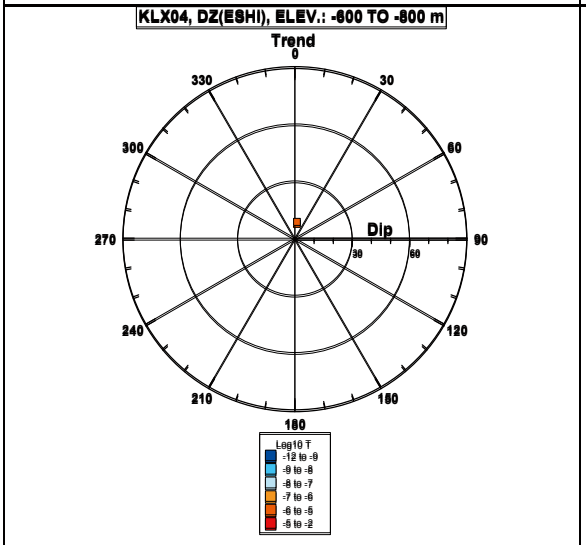

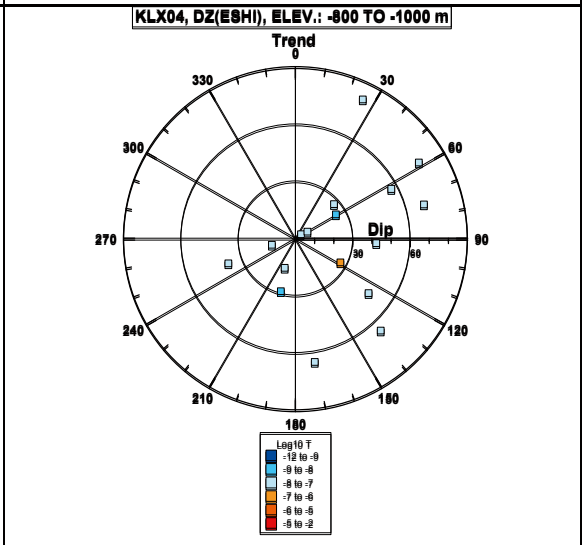

Borehole KLX05.

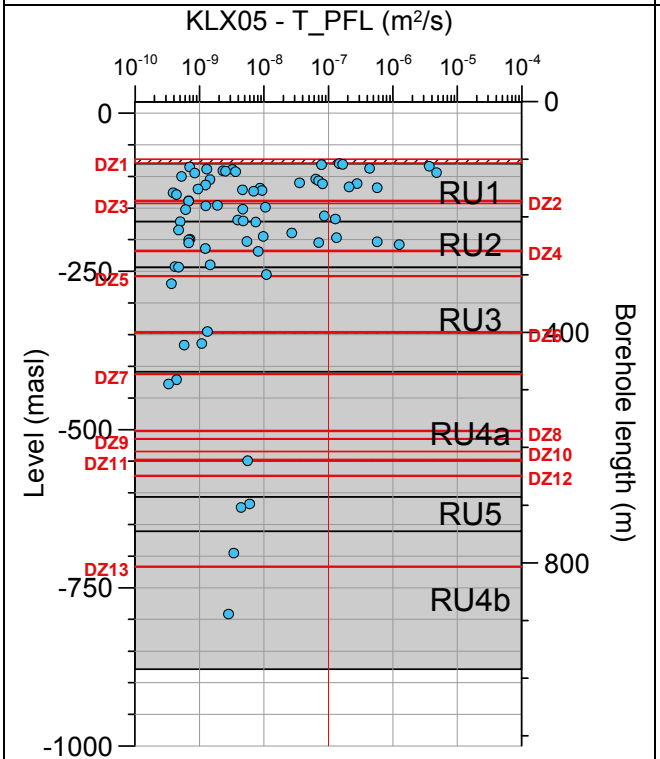

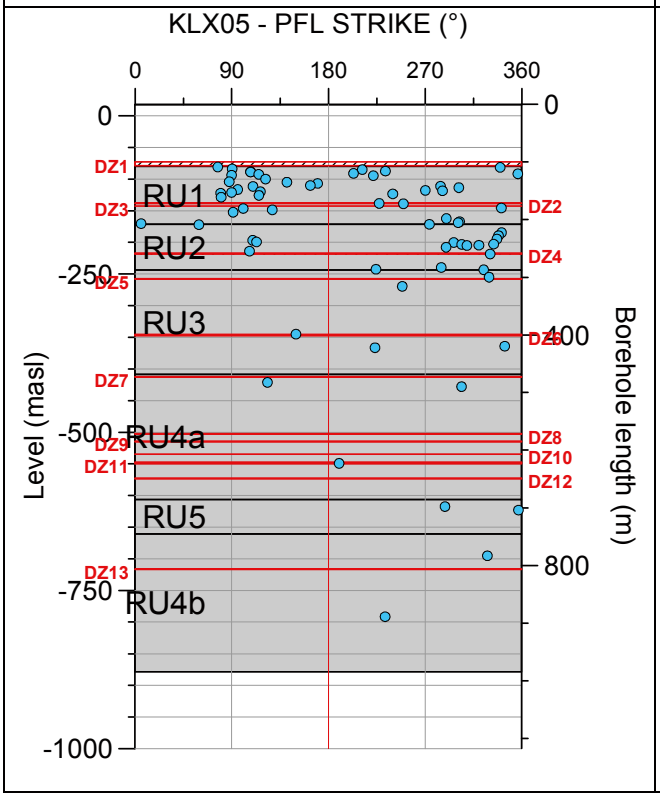

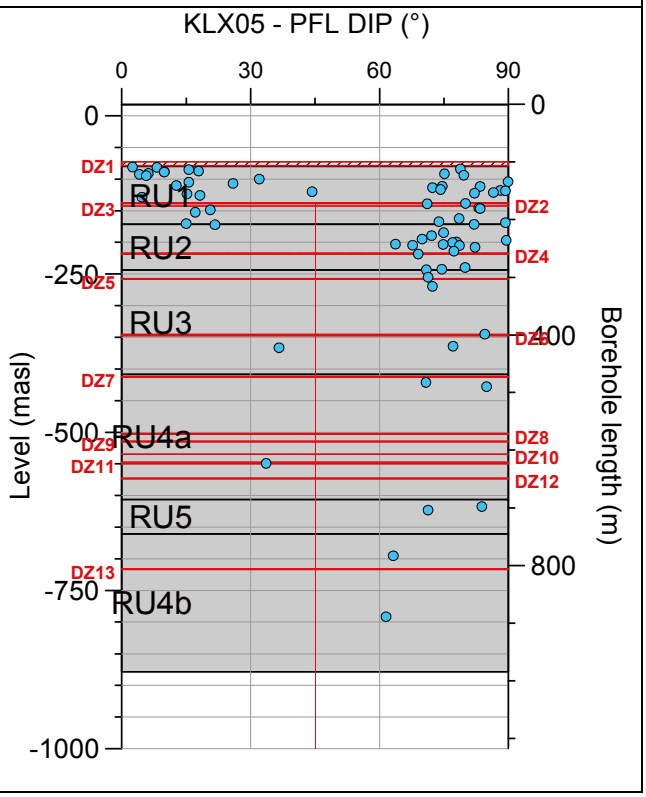

Comment:

Borehole KLX05. Poles for PFL-f feature planes outside deformation zones (ESHI).

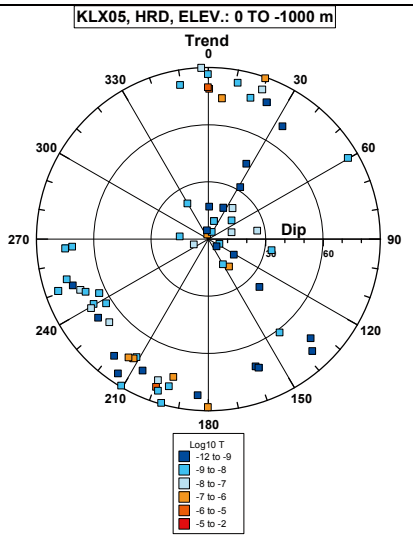

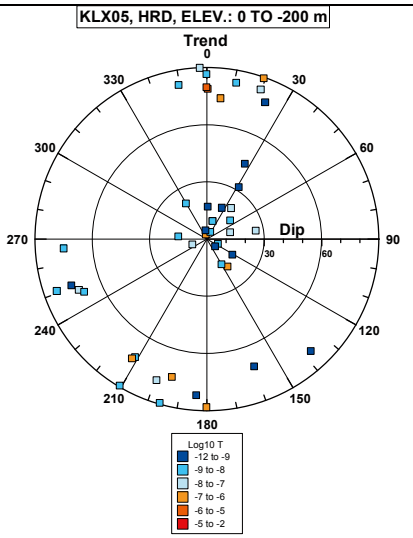

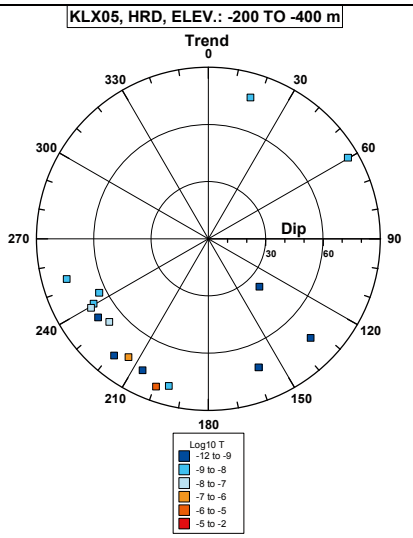

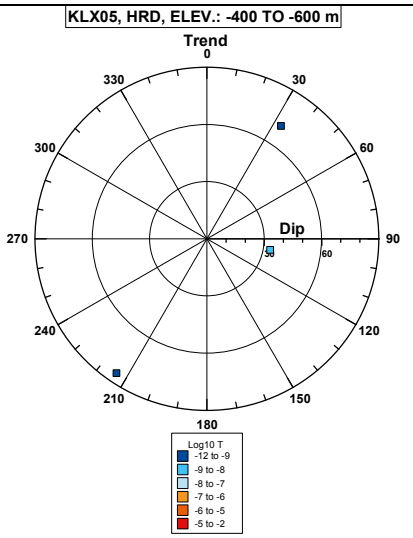

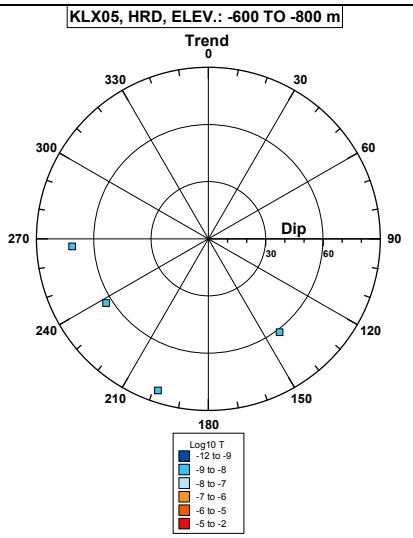

Borehole KLX05. Poles for PFL-f feature planes in deformation zones (ESHI).
No interpreted deformation zones (ESHI) in the borehole.

Borehole KLX06.

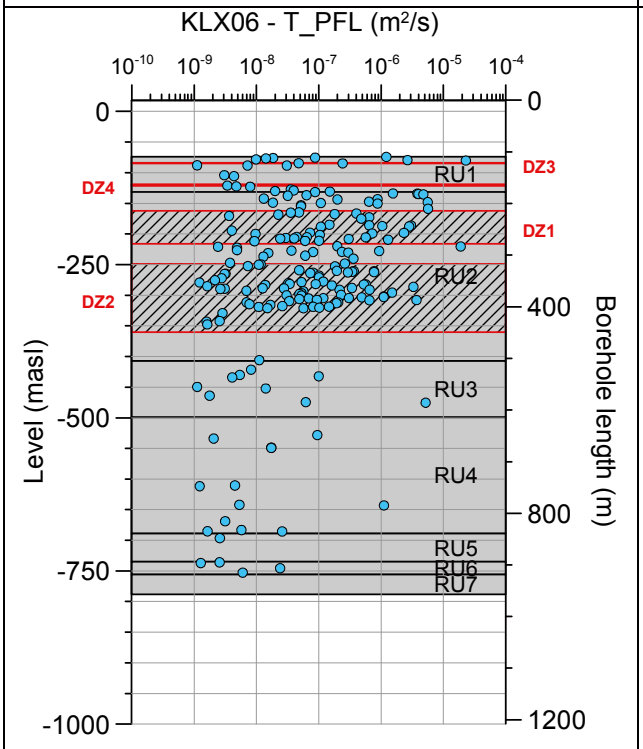

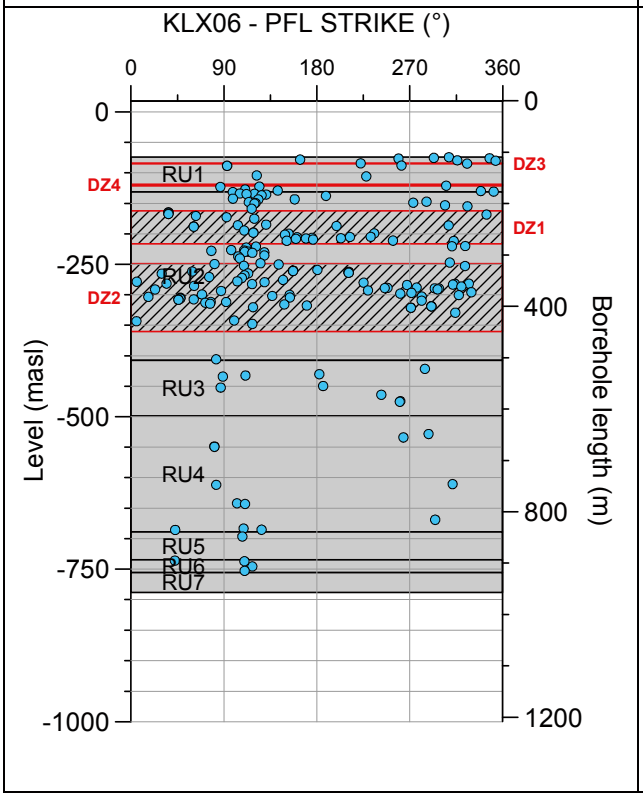

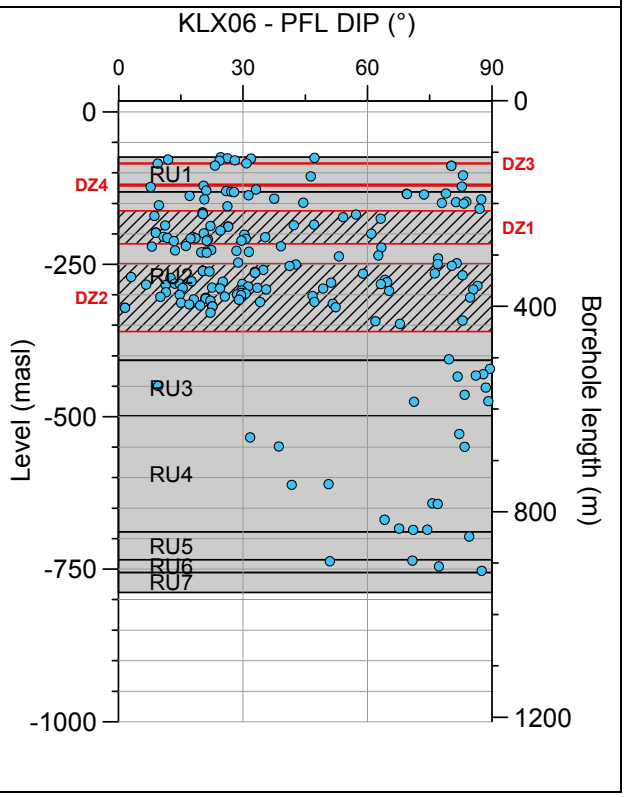

Comment:

Borehole KLX06. Poles for PFL-f feature planes outside deformation zones (ESHI).

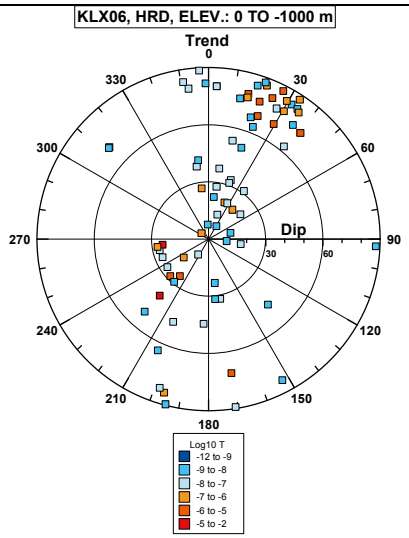

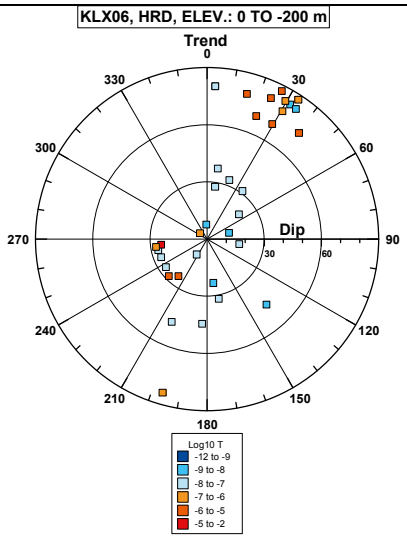

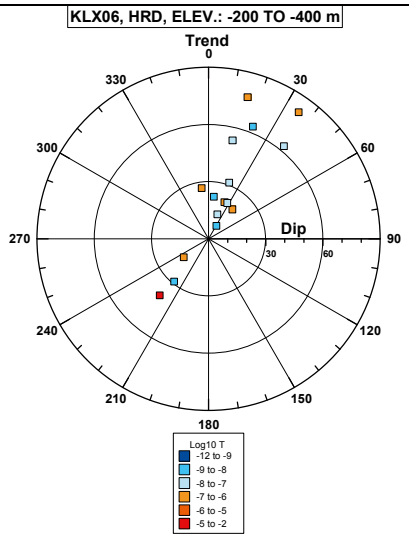

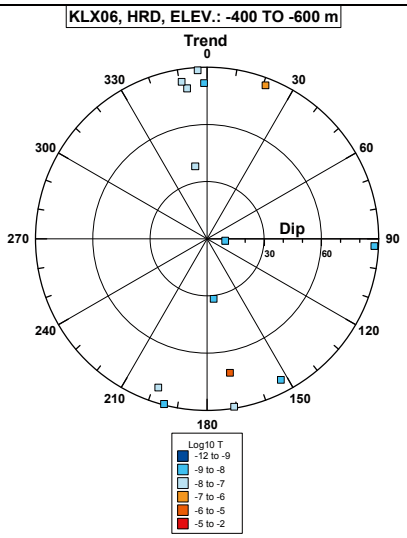

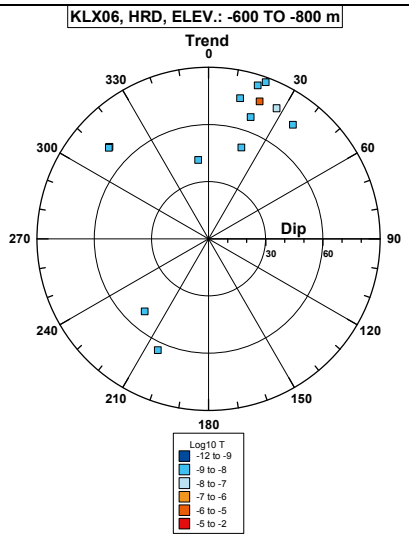

Borehole KLX06. Poles for PFL-f feature planes in deformation zones (ESHI).

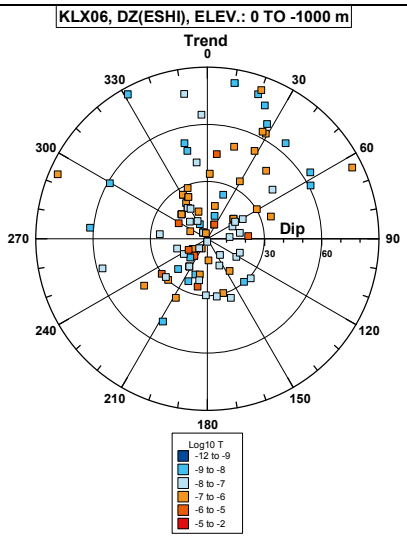

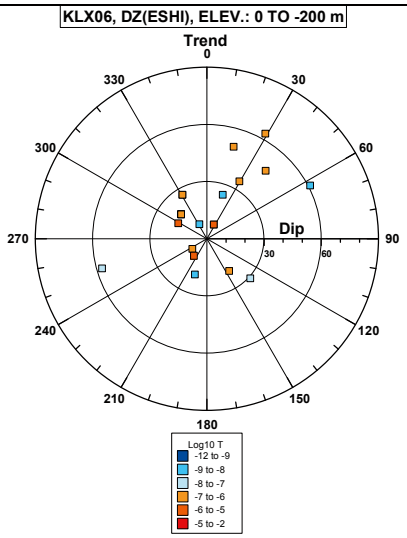

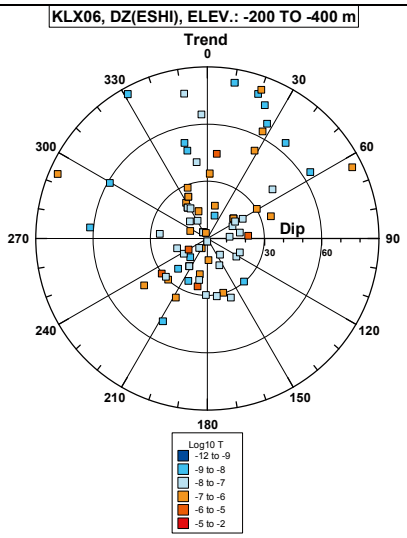

Borehole KLX07A.

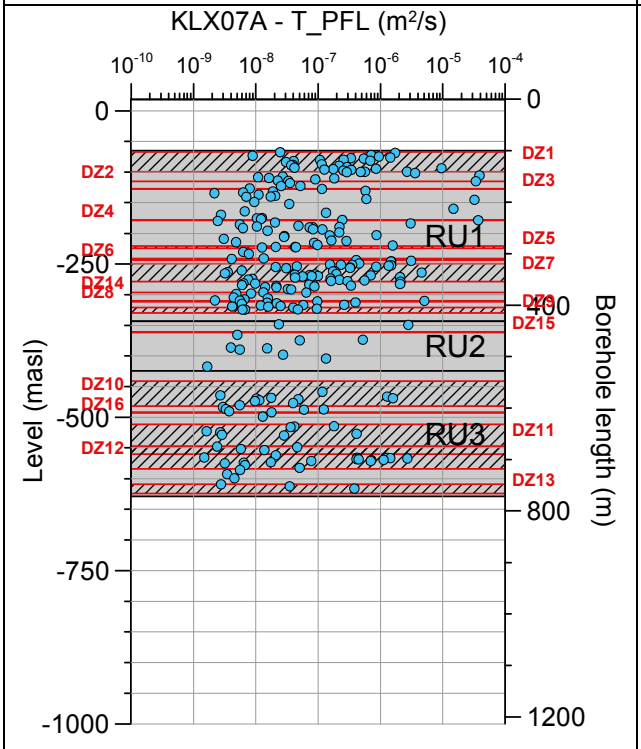

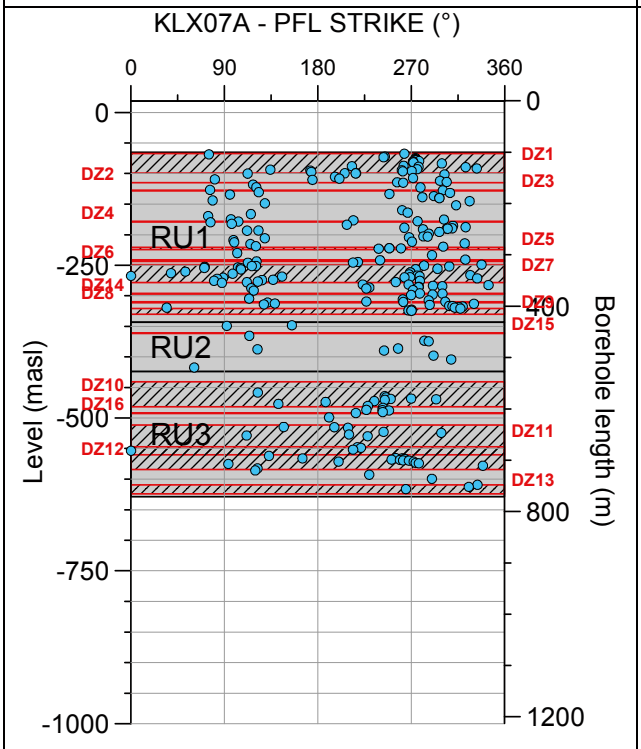

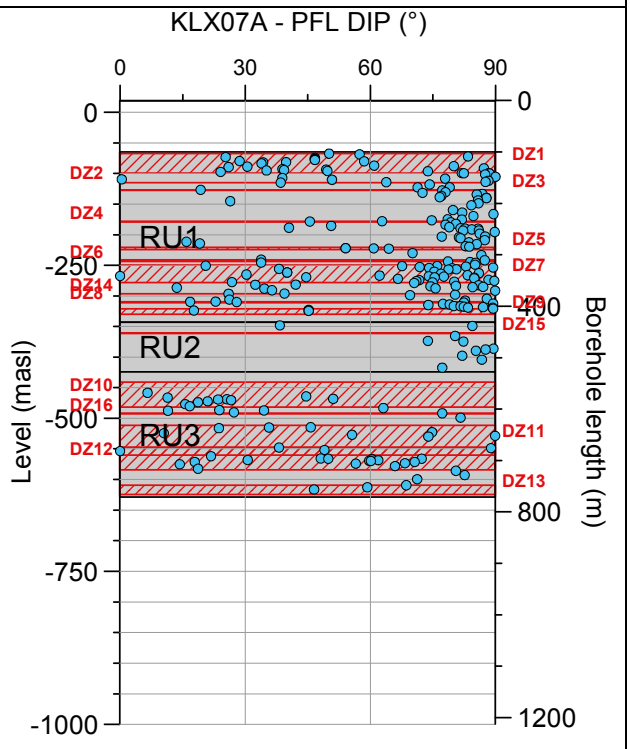

Comment:

Borehole KLX07A. Poles for PFL-f feature planes outside deformation zones (ESHI).

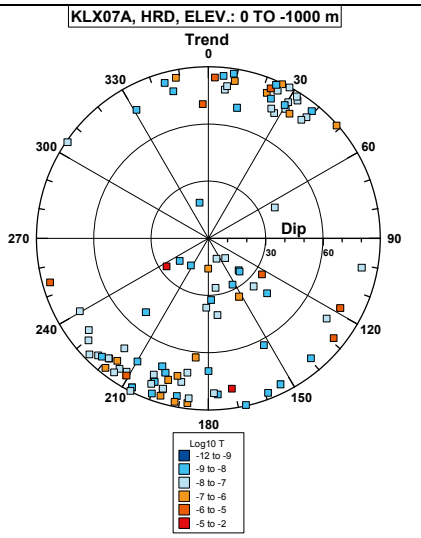

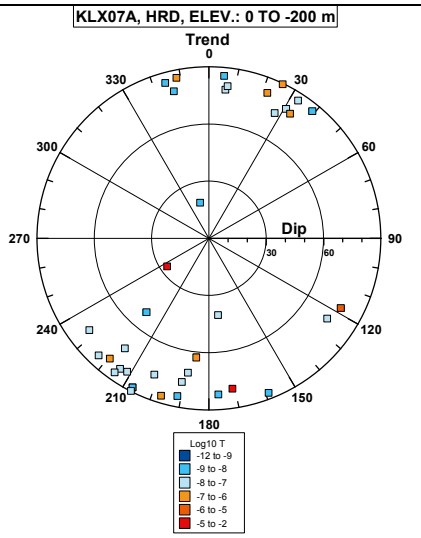

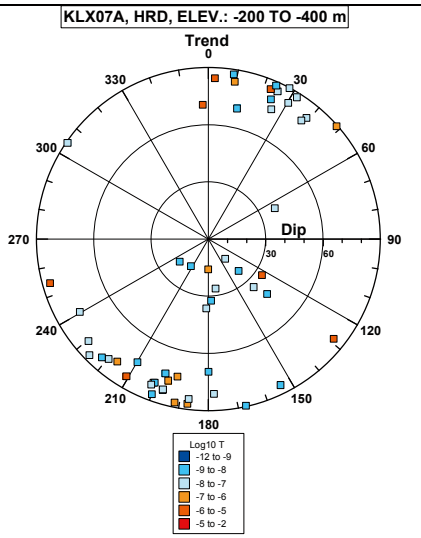

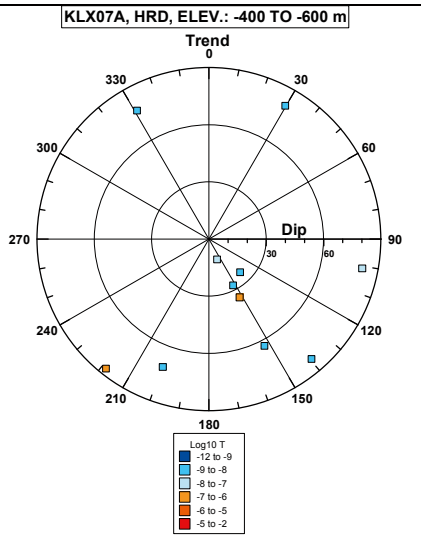

Borehole KLX07A. Poles for PFL-f feature planes in deformation zones (ESHI).

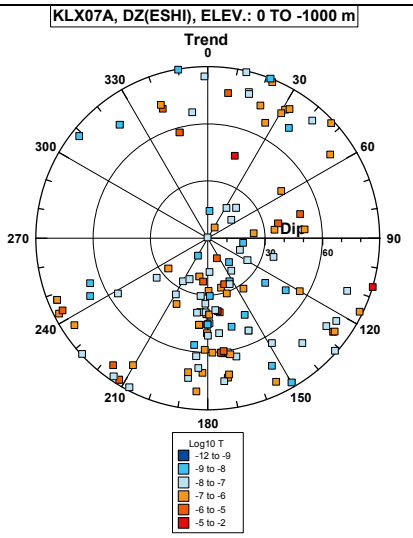

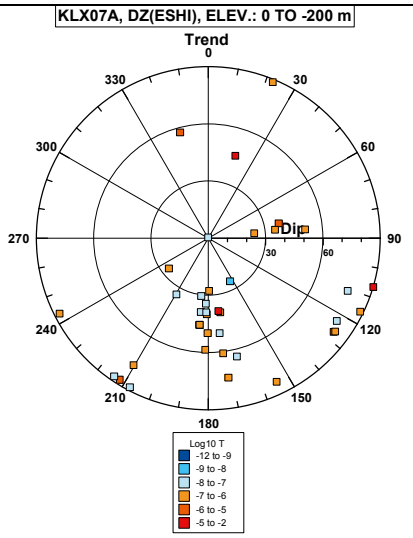

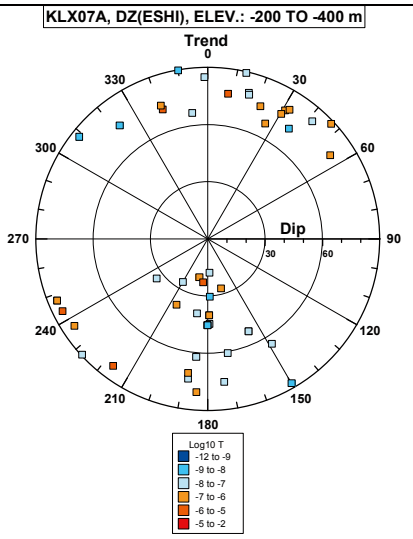

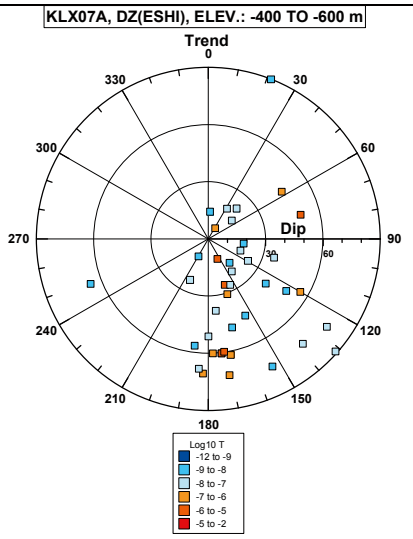

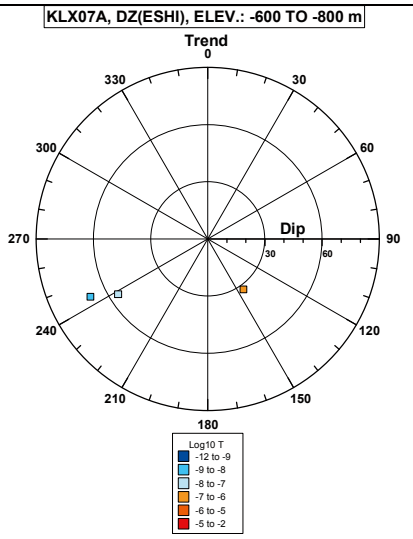

Borehole KLX07B.

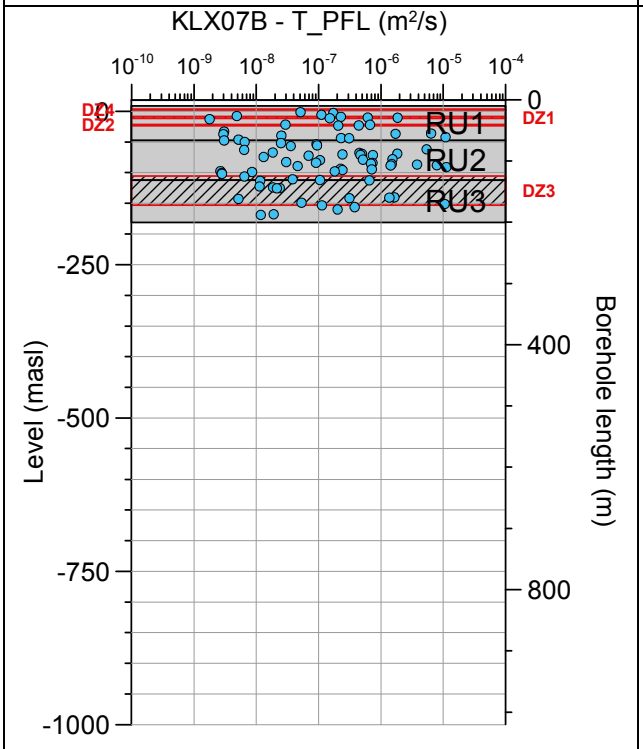

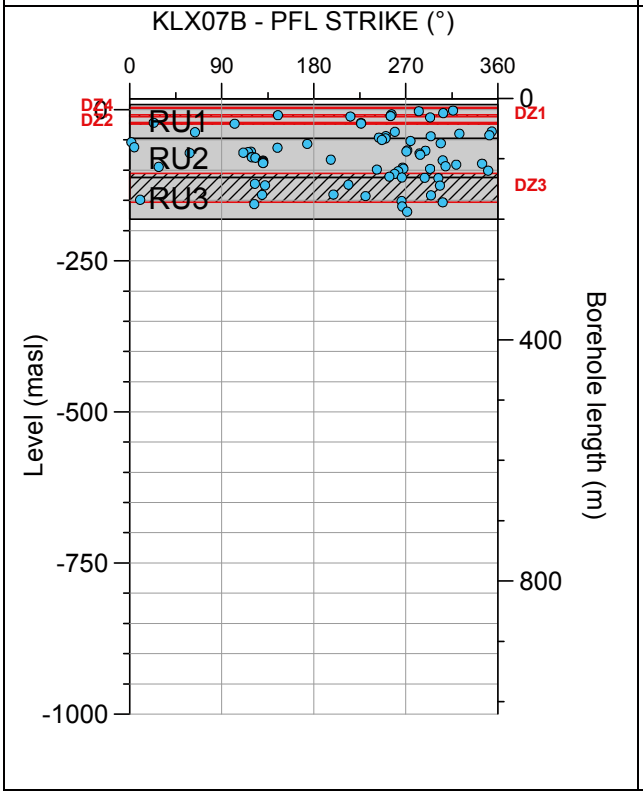

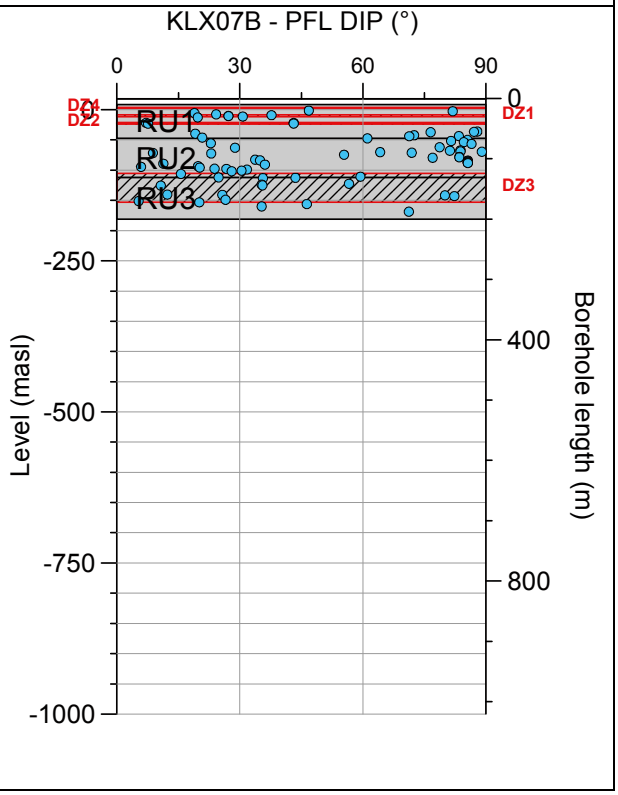

Comment:

Borehole KLX07B. Poles for PFL-f feature planes outside deformation zones (ESHI).

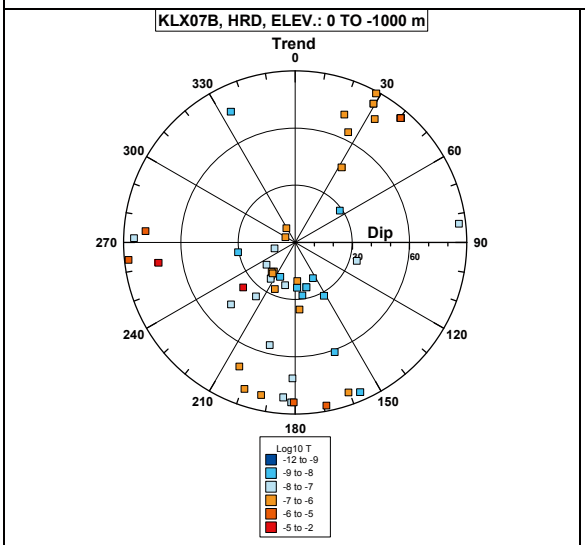

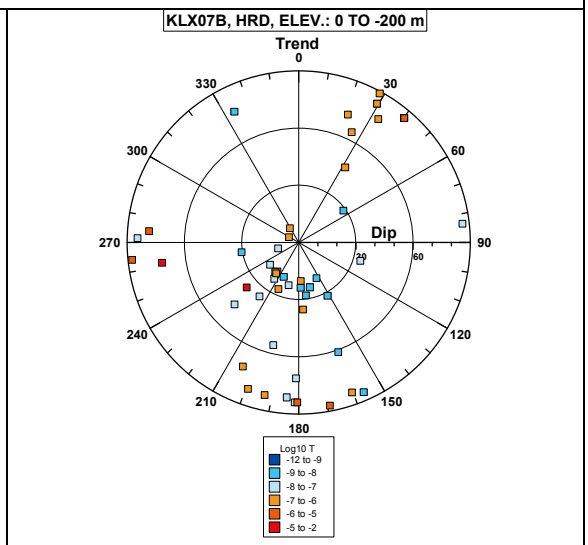

Borehole KLX07B. Poles for PFL-f feature planes in deformation zones (ESHI).

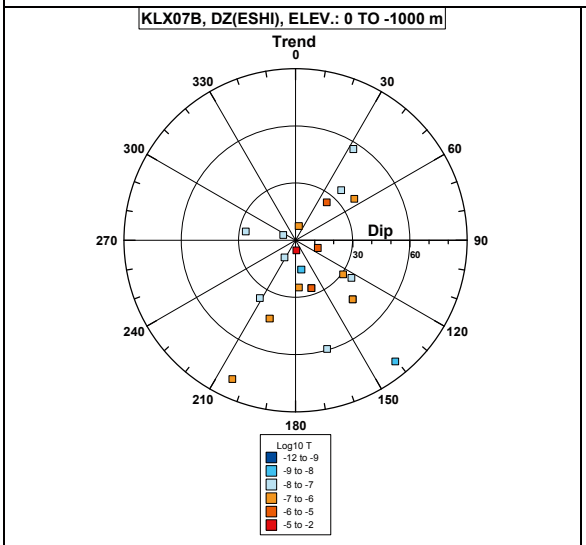

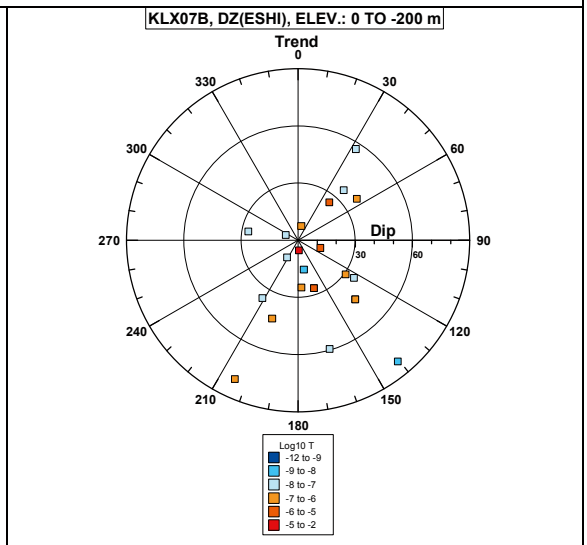

Borehole KLX08.

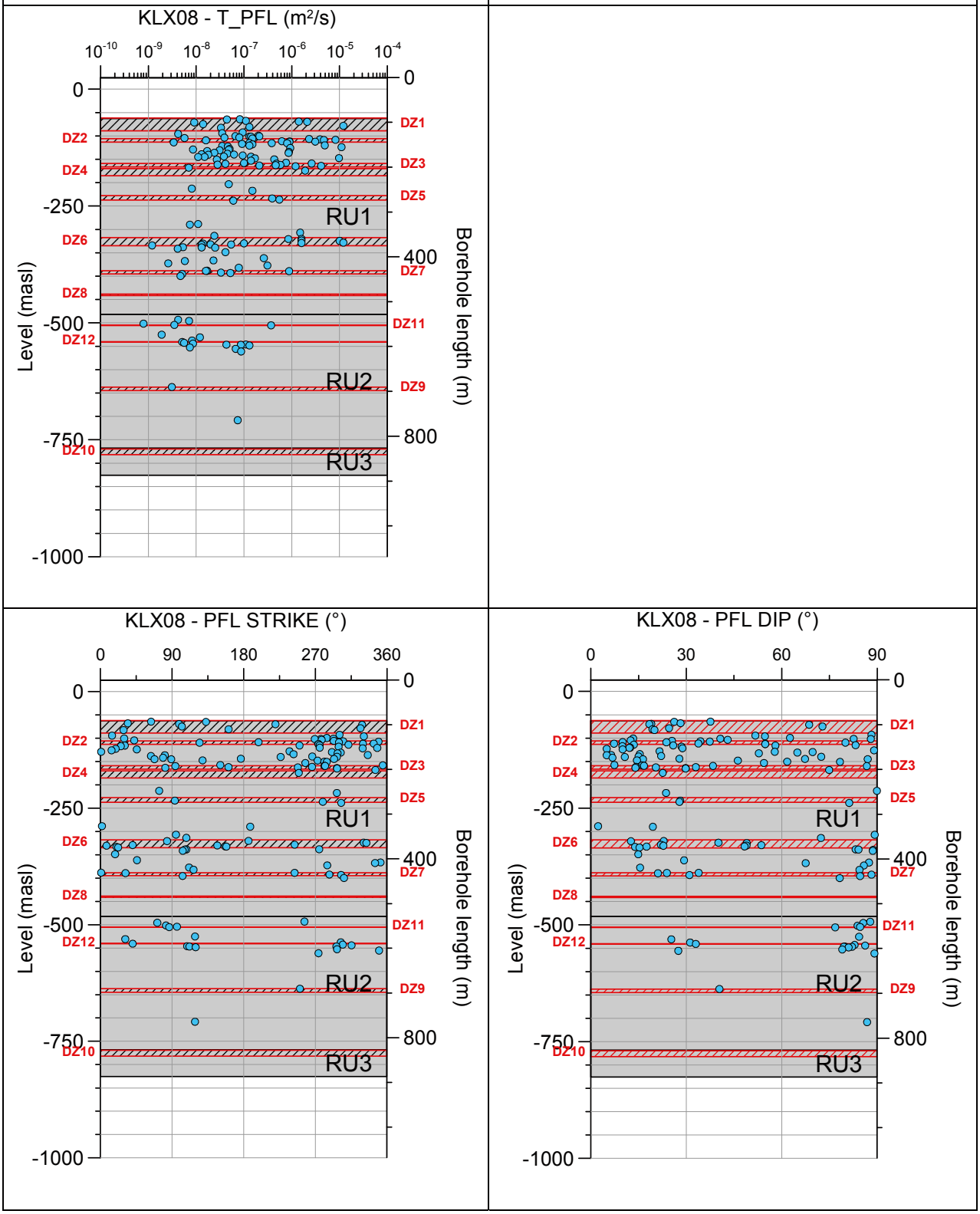

Comment:

Borehole KLX08. Poles for PFL-f feature planes outside deformation zones (ESHI).

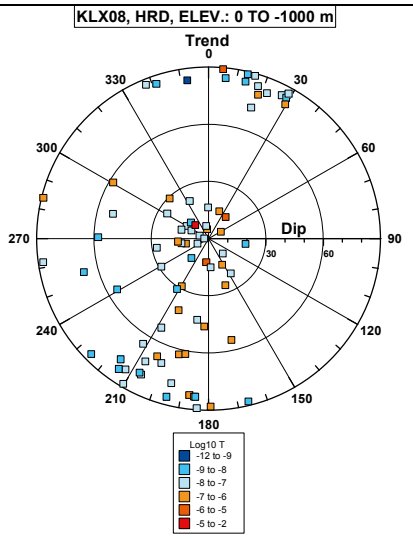

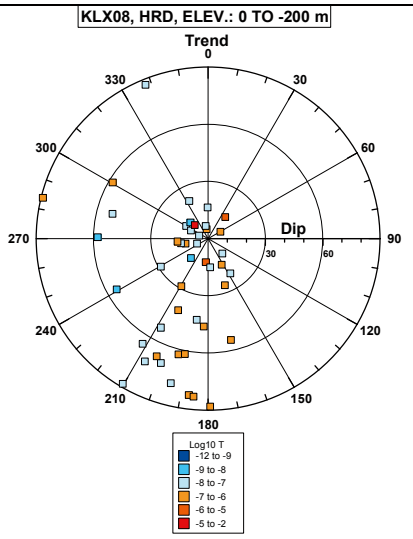

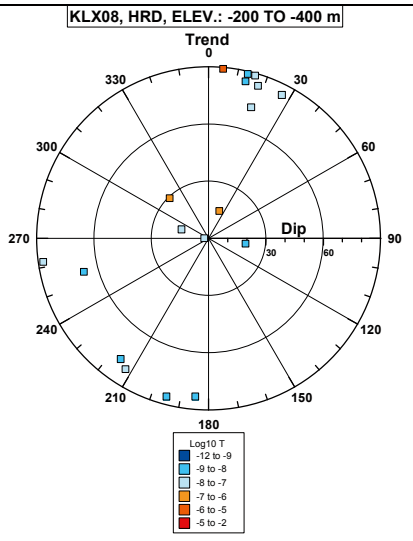

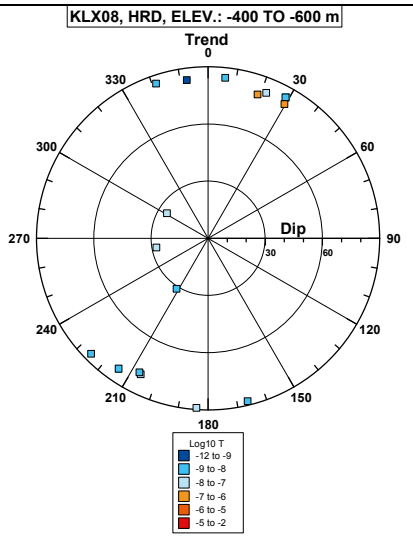

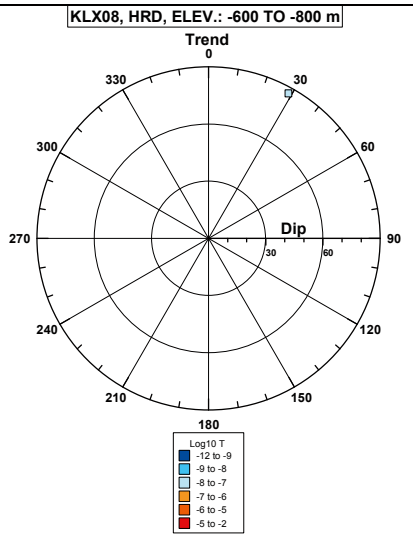

Borehole KLX08. Poles for PFL-f feature planes in deformation zones (ESHI).

KLX08, DZ(ESHI), ELEV.: 0 TO -1000 m

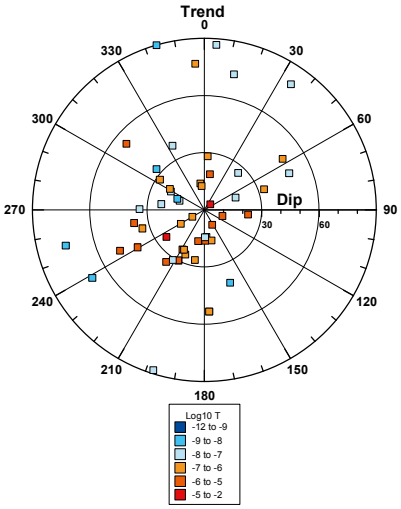

KLX08, DZ(ESHI), ELEV.: 0 TO -200 m

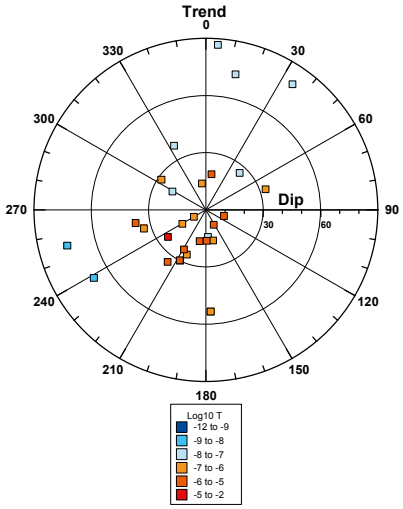

KLX08, DZ(ESHI), ELEV.: -200 TO -400 m

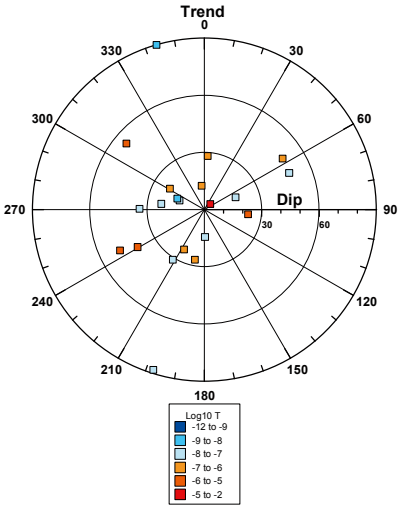

KLX08, DZ(ESHI), ELEV.: -400 TO -600 m

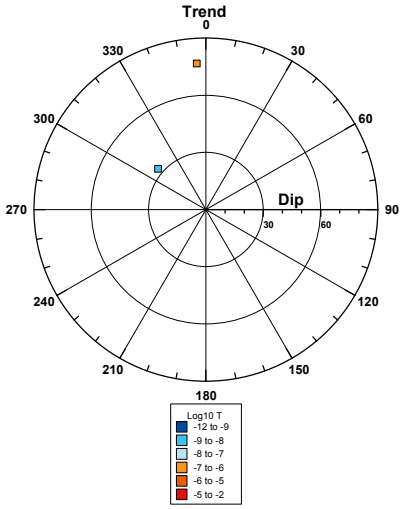

KLX08, DZ(ESHI), ELEV.: -600 TO -800 m

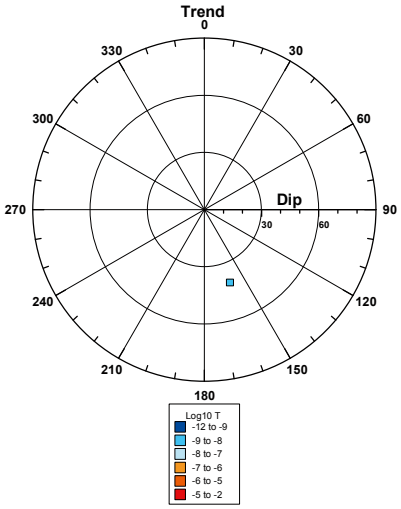

Borehole KLX09.

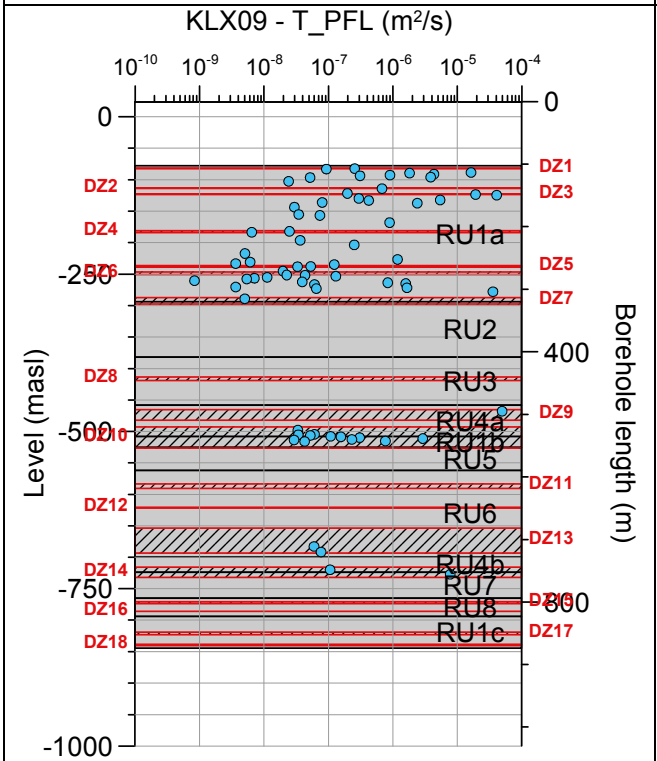

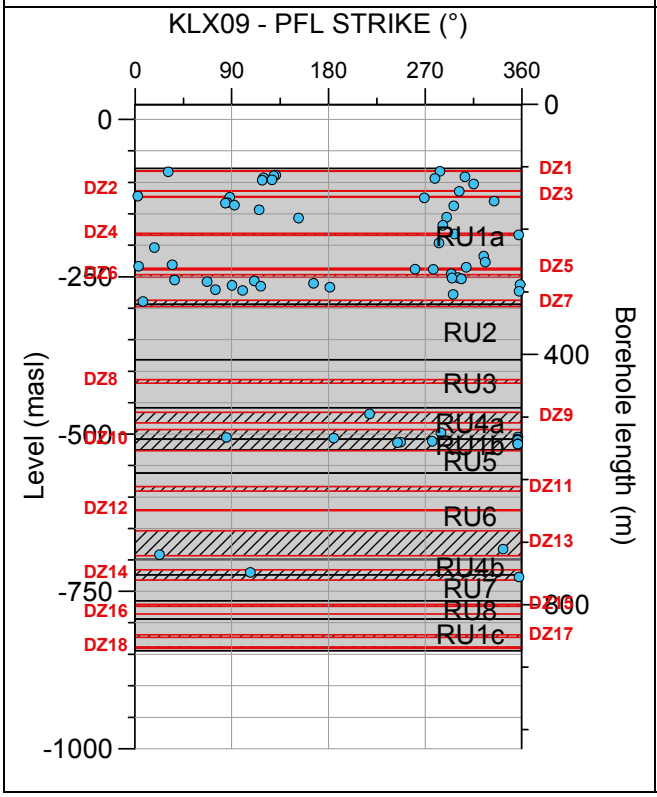

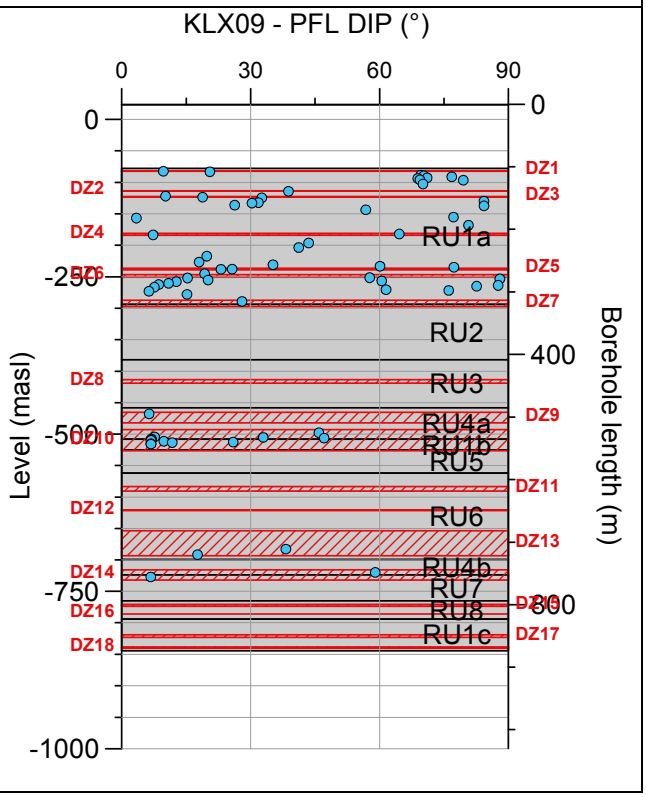

Comment:

Borehole KLX09. Poles for PFL-f feature planes outside deformation zones (ESHI).

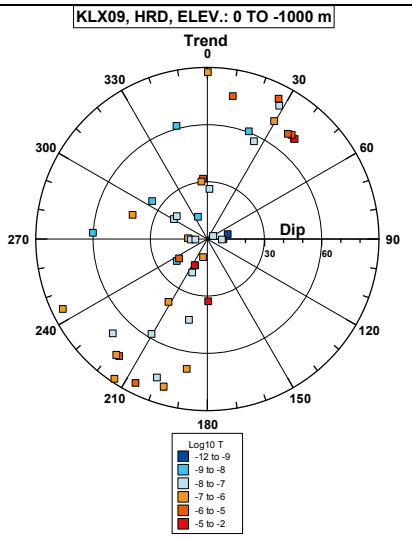

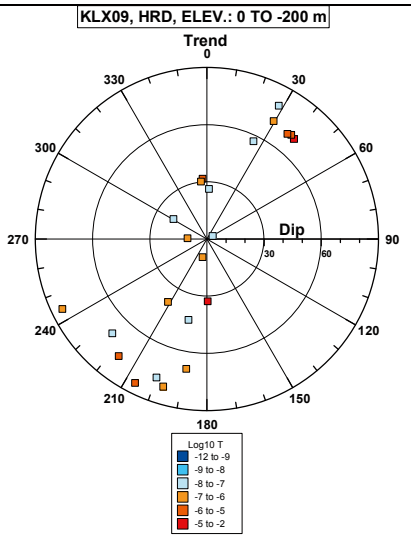

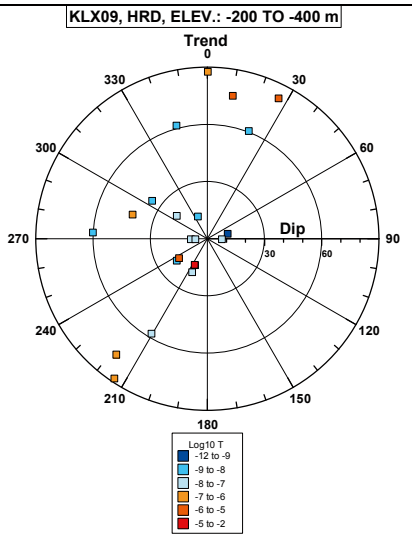

Borehole KLX09. Poles for PFL-f feature planes in deformation zones (ESHI).

KLX09, DZ(ESHI), ELEV.: 0 TO -1000 m

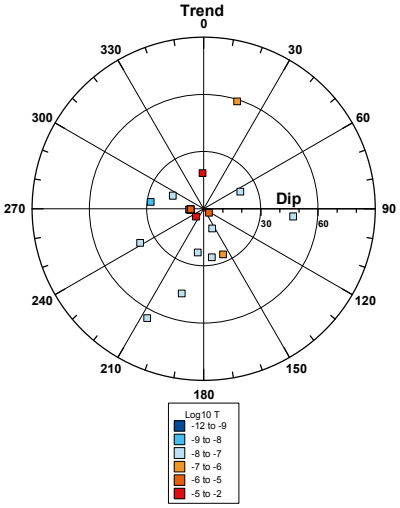

KLX09, DZ(ESHI), ELEV.: 0 TO -200 m

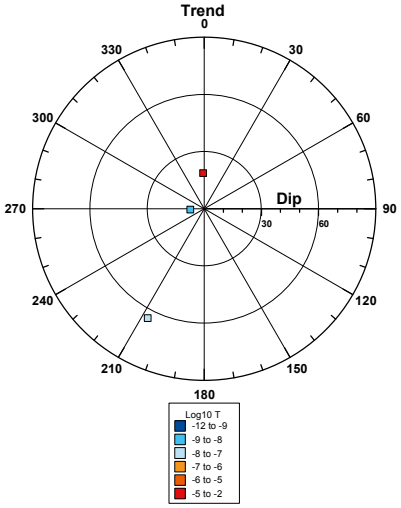

KLX09, DZ(ESHI), ELEV.: -200 TO -400 m

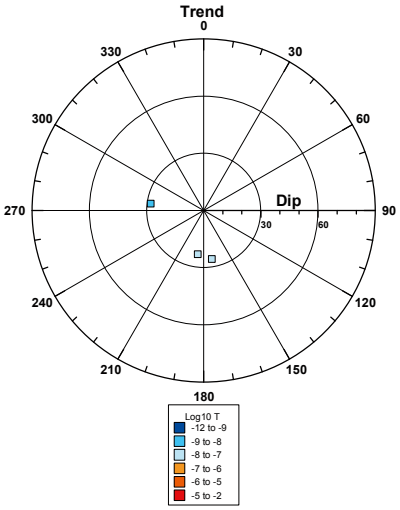

KLX09, DZ(ESHI), ELEV.: -400 TO -600 m

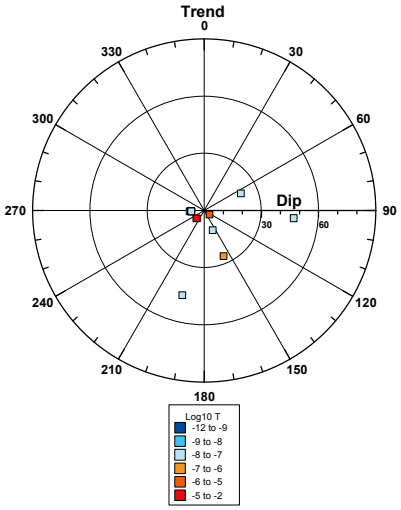

KLX09, DZ(ESHI), ELEV.: -600 TO -800 m

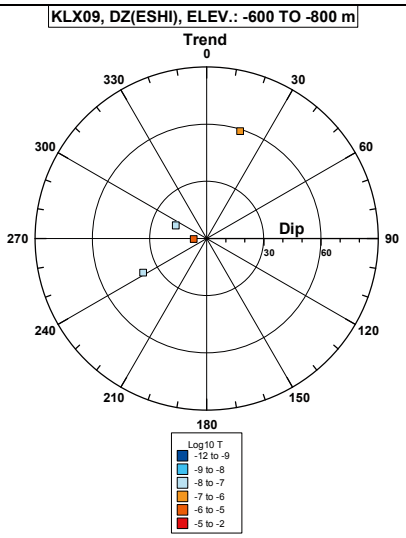

Borehole KLX09B.

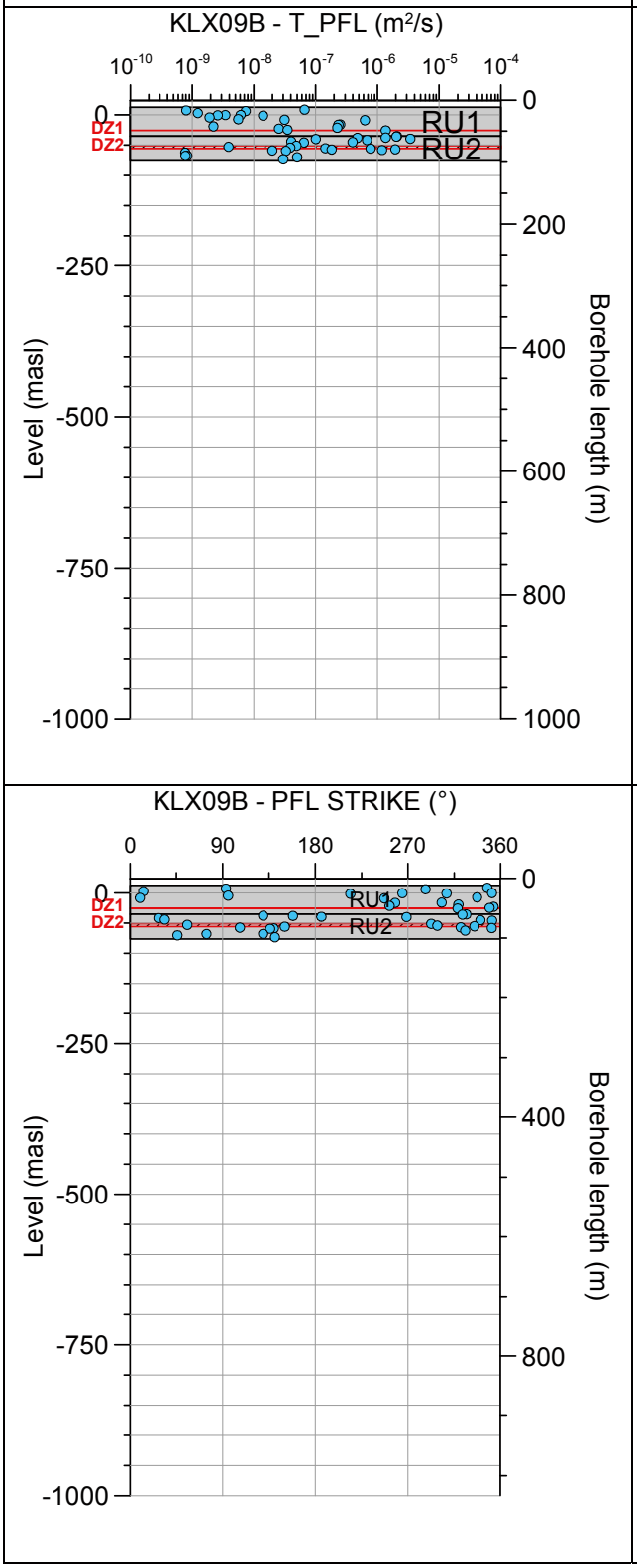

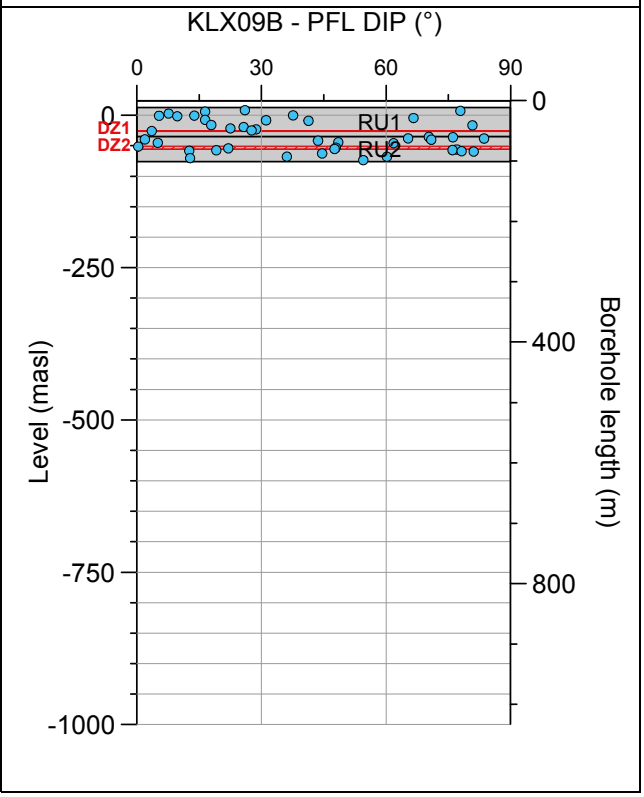

Comment:

Borehole KLX09B. Poles for PFL-f feature planes outside deformation zones (ESHI).

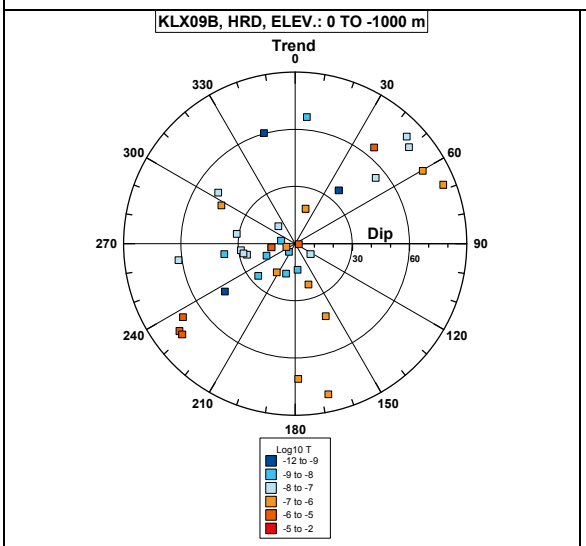

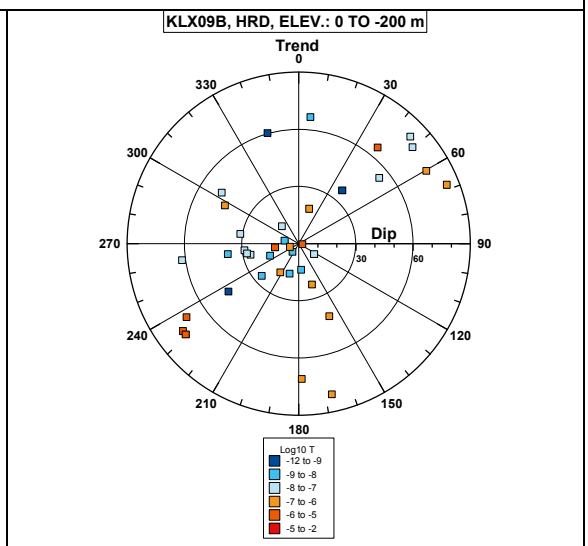

Borehole KLX09B. Poles for PFL-f feature planes in deformation zones (ESHI).

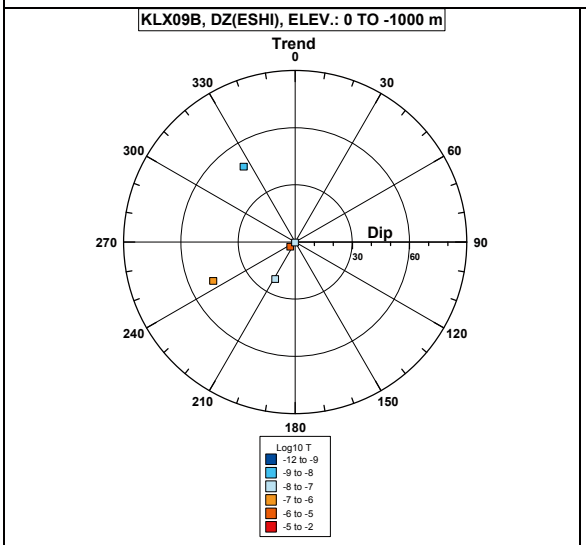

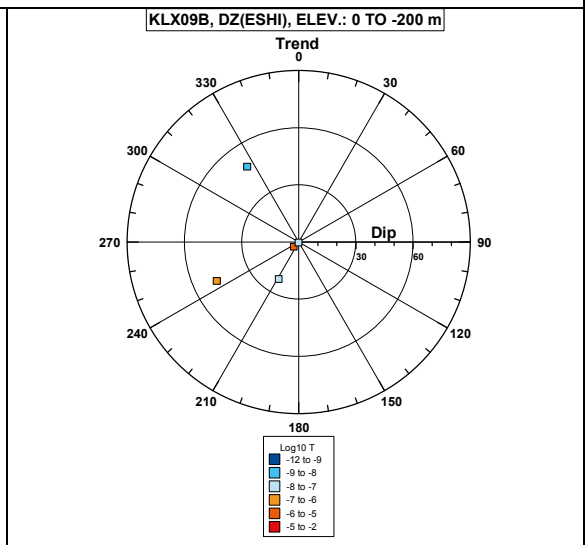

Borehole KLX09C.

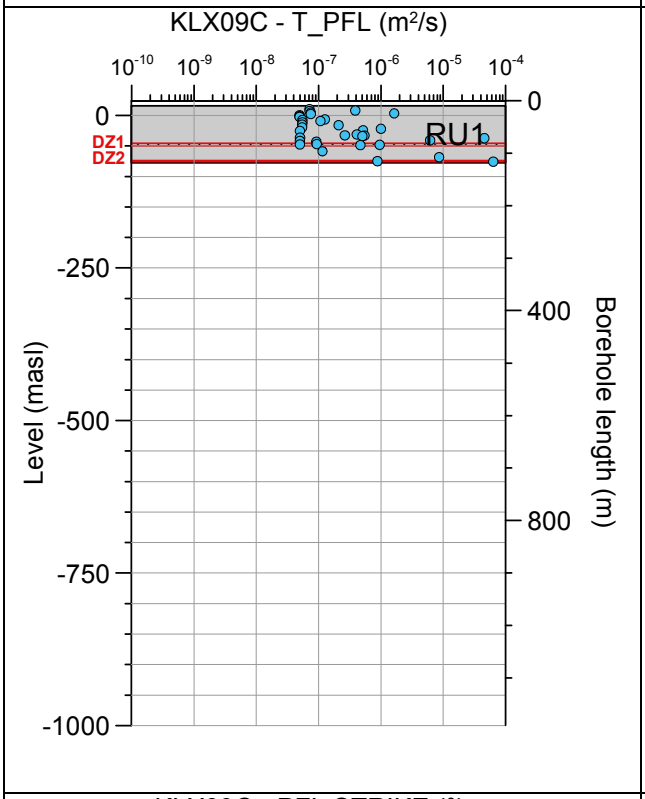

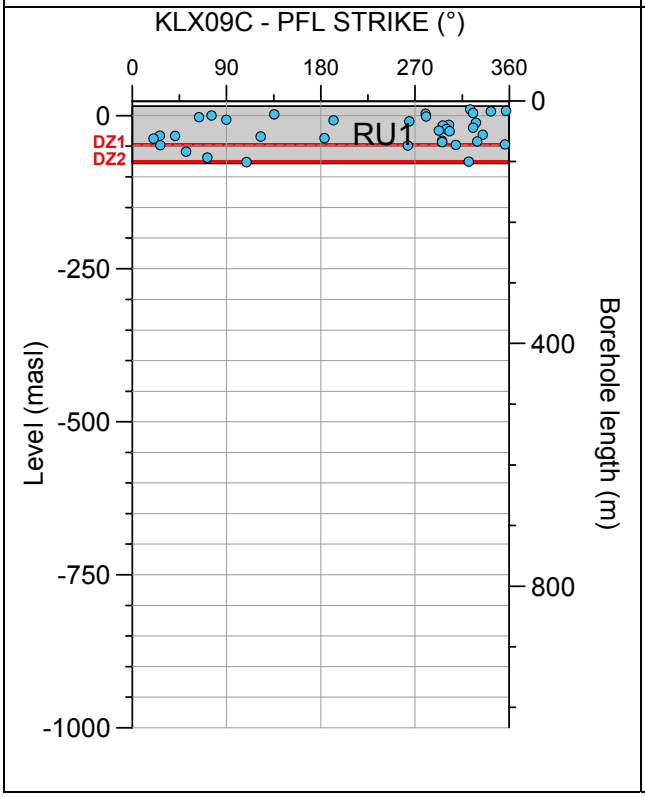

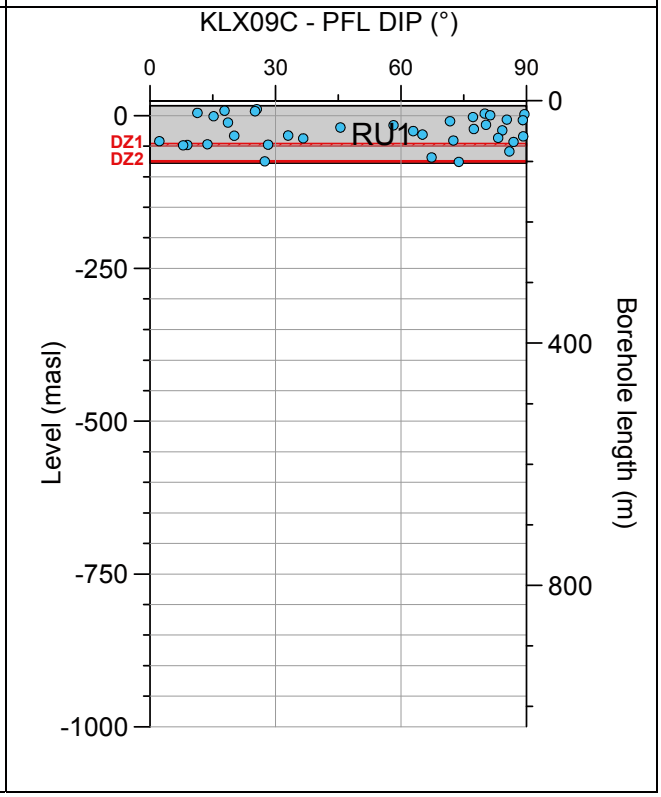

Comment:

Borehole KLX09C. Poles for PFL-f feature planes outside deformation zones (ESHI).

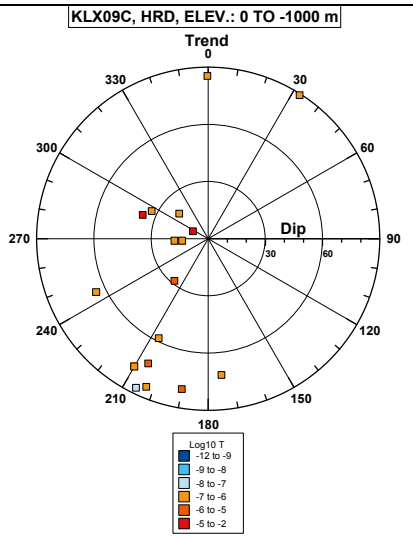

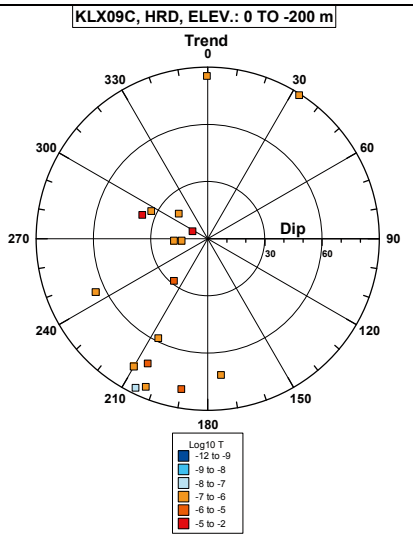

Borehole KLX09C. Poles for PFL-f feature planes in deformation zones (ESHI).

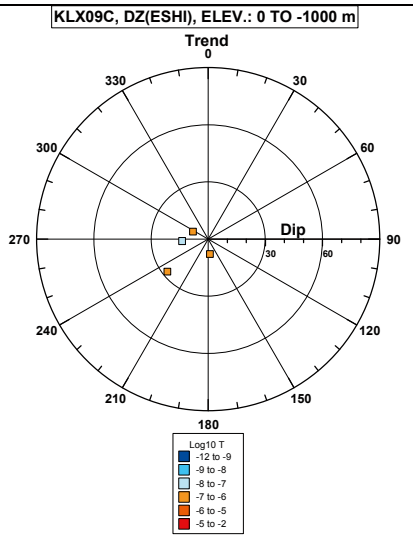

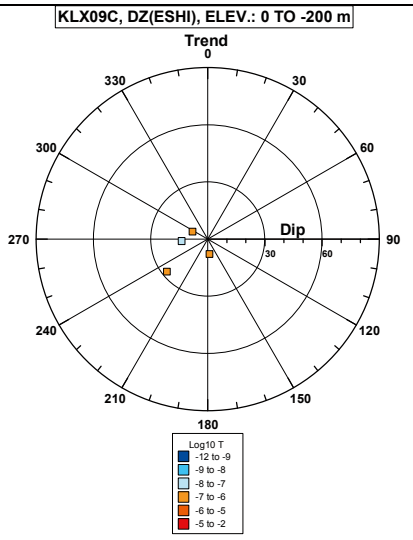

Borehole KLX09D.

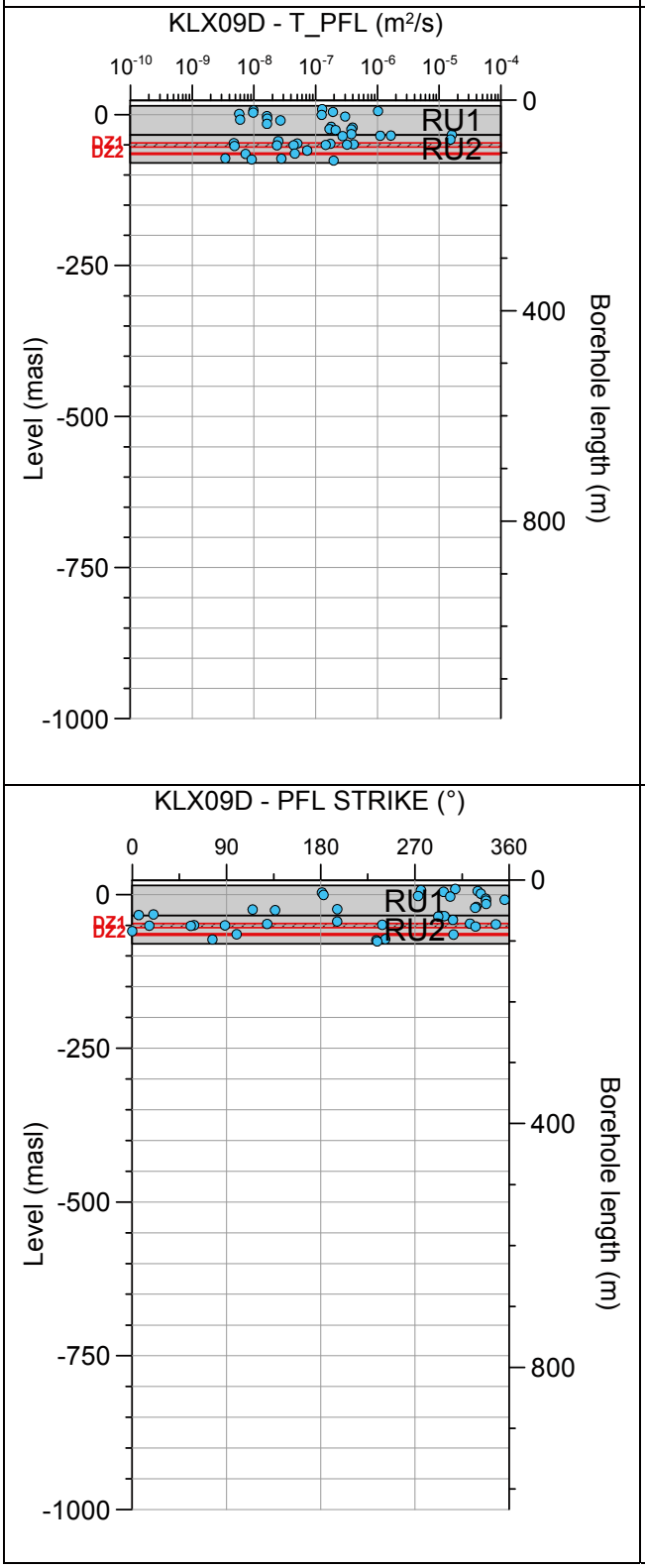

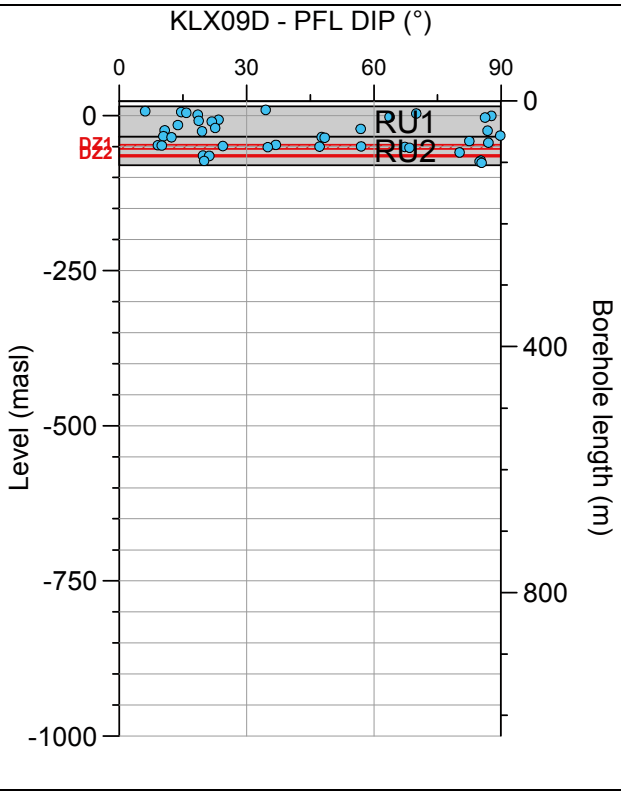

Comment:

Borehole KLX09D. Poles for PFL-f feature planes outside deformation zones (ESHI).

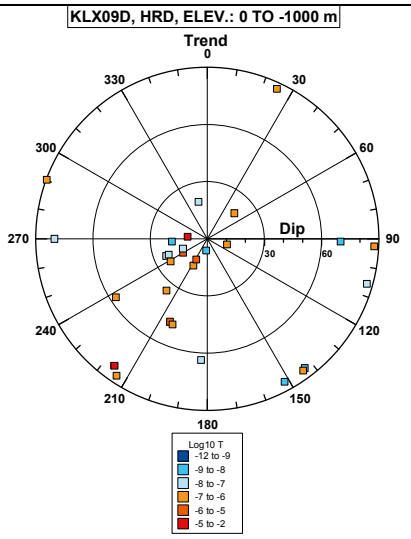

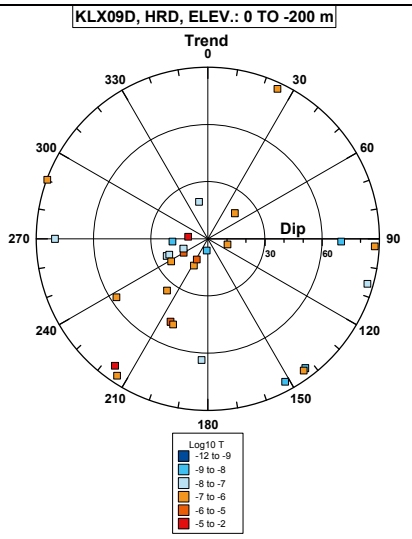

Borehole KLX09D. Poles for PFL-f feature planes in deformation zones (ESHI).

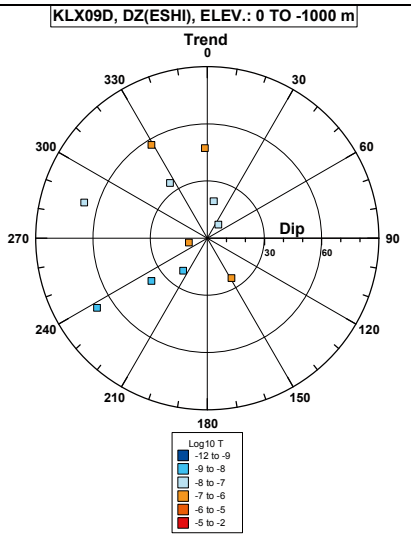

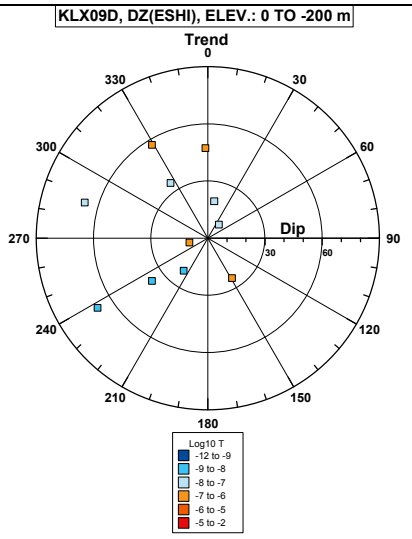

Borehole KLX09E.

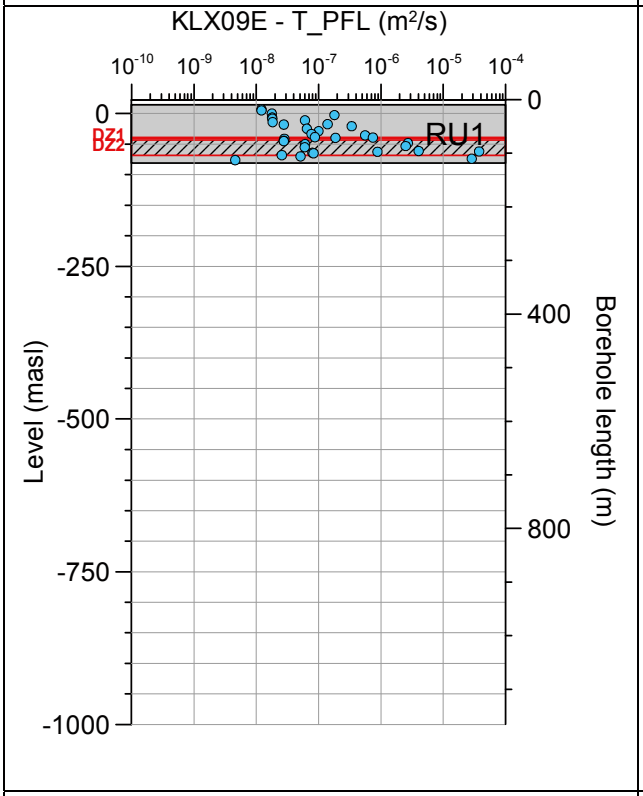

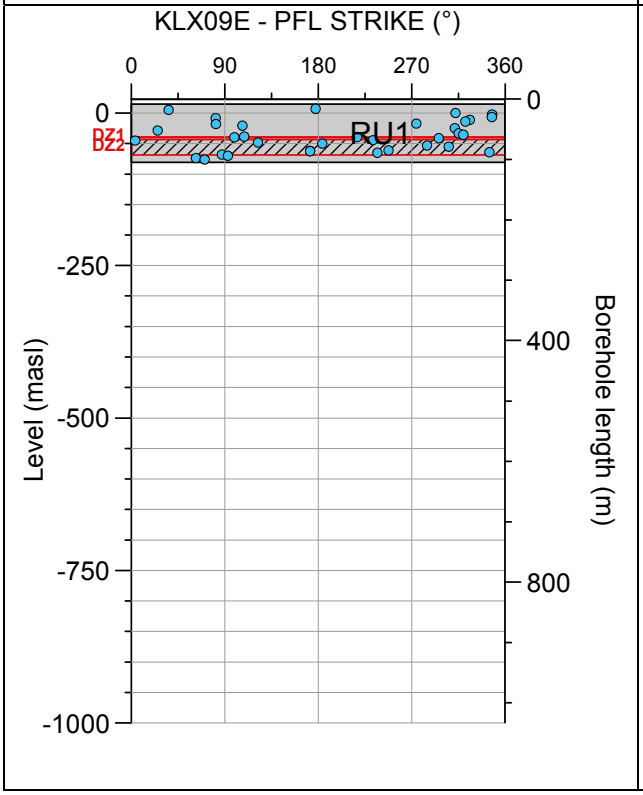

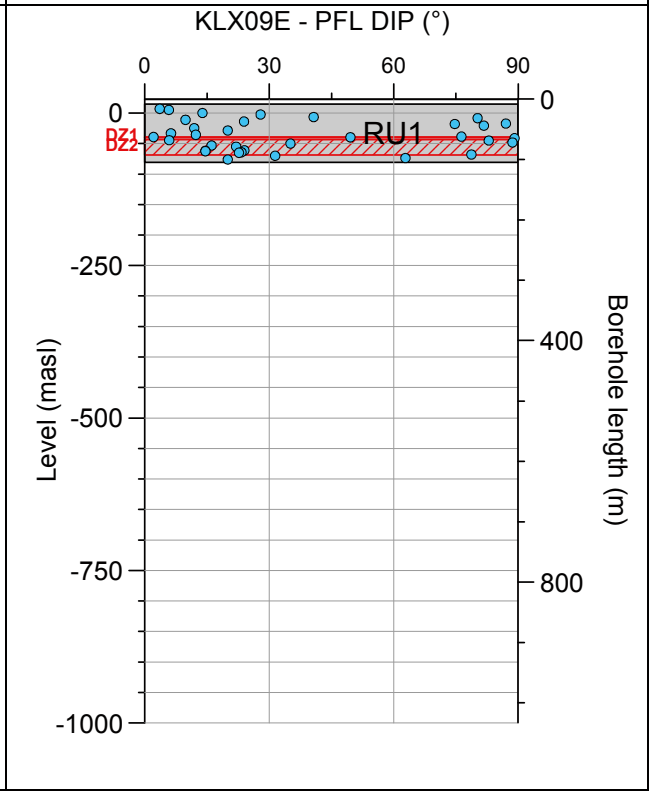

Comment:

Borehole KLX09E. Poles for PFL-f feature planes outside deformation zones (ESHI).

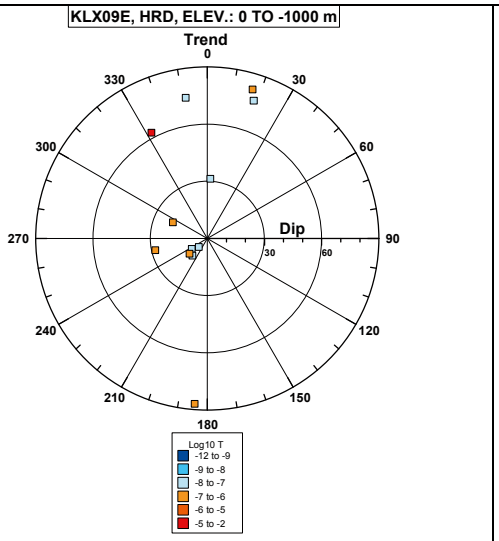

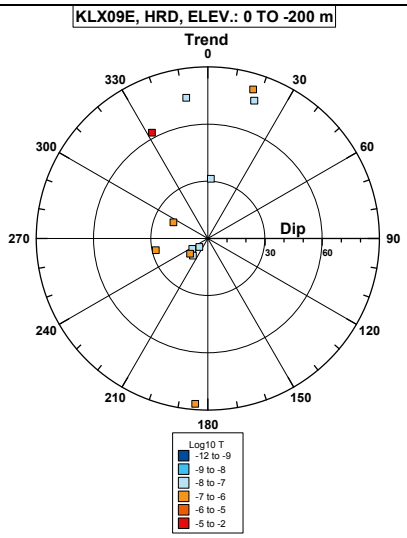

Borehole KLX09E. Poles for PFL-f feature planes in deformation zones (ESHI).

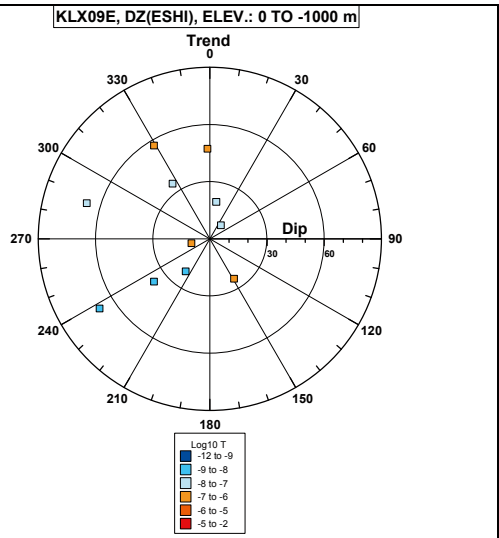

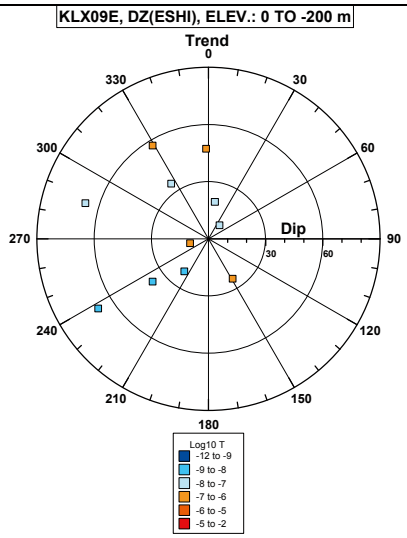

Borehole KLX09F.

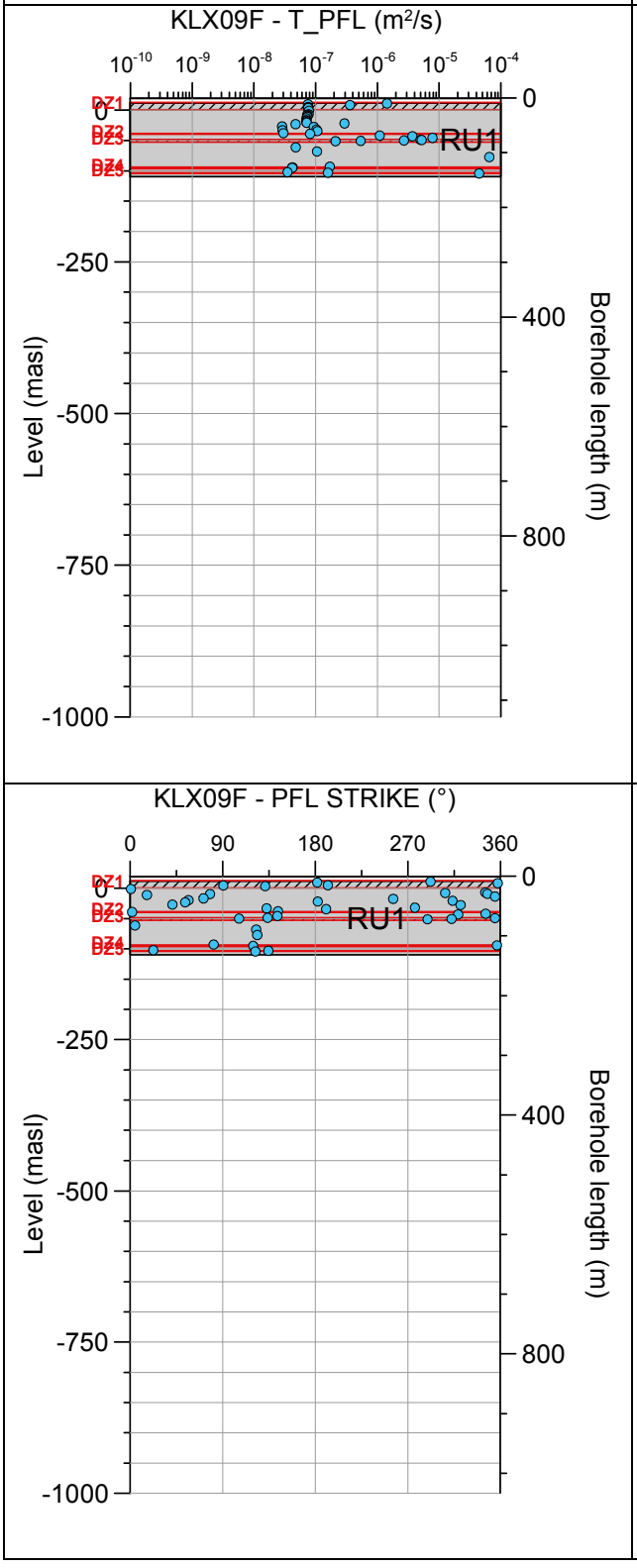

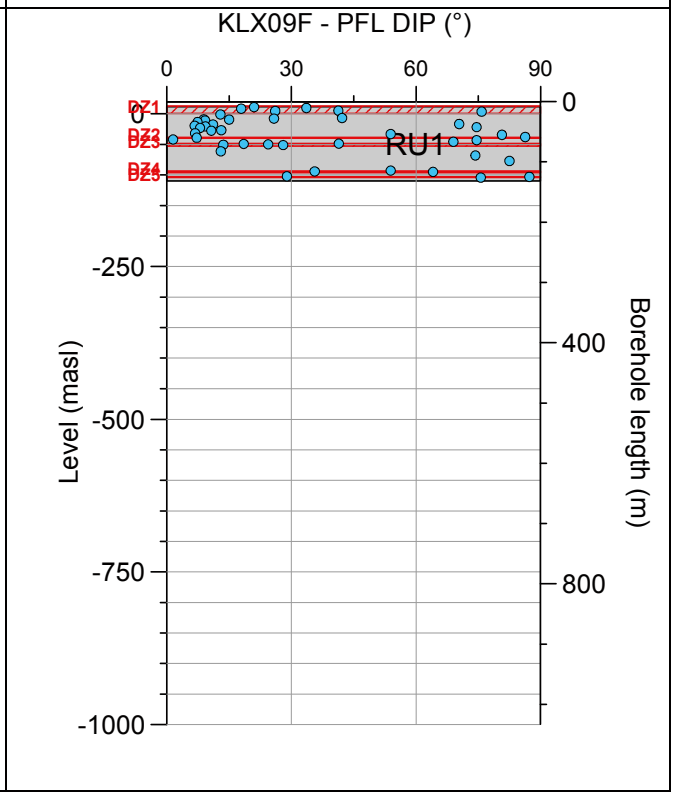

Comment:

Borehole KLX09F. Poles for PFL-f feature planes outside deformation zones (ESHI).

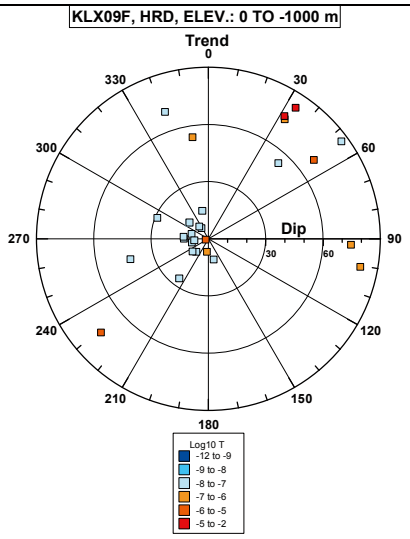

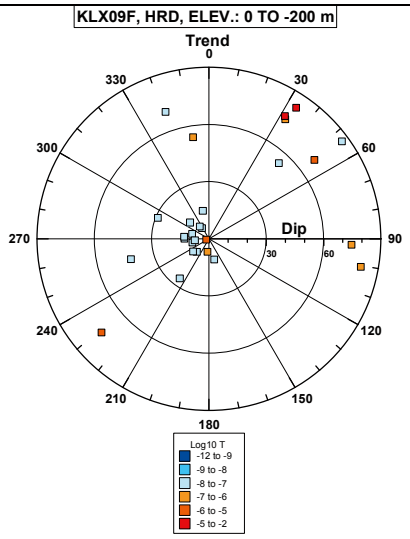

Borehole KLX09F. Poles for PFL-f feature planes in deformation zones (ESHI).

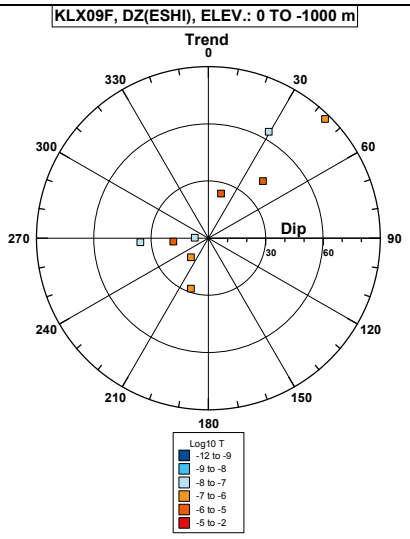

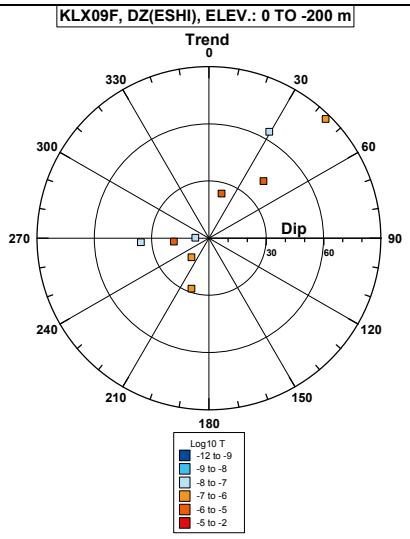

Borehole KLX09G.

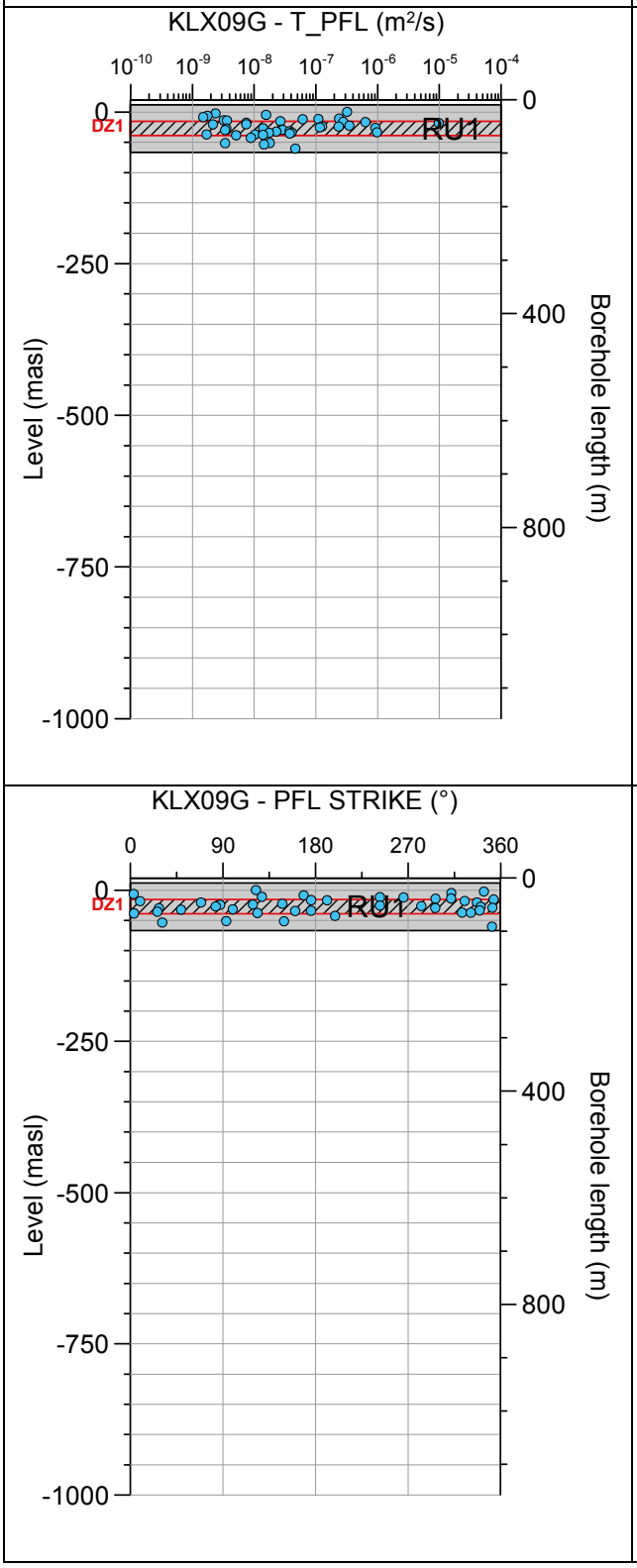

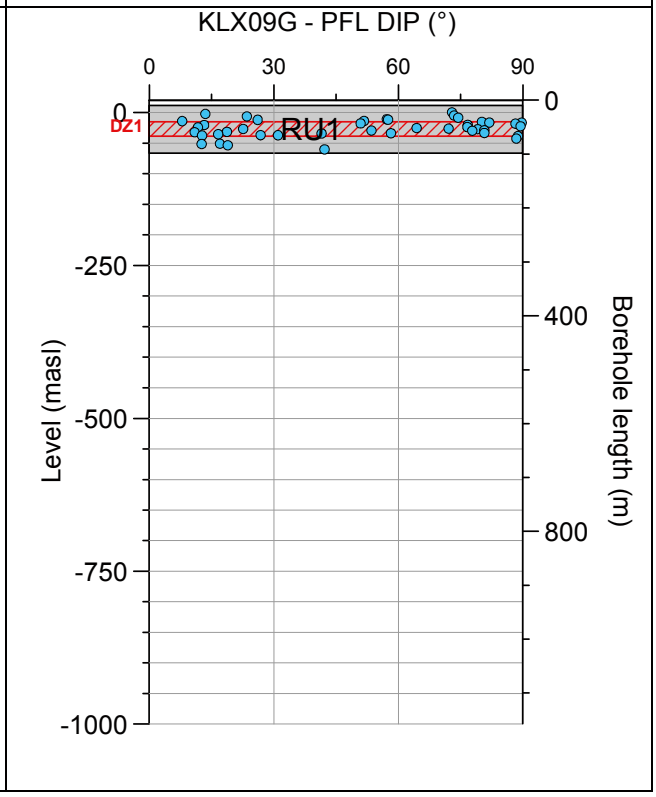

Comment:

Borehole KLX09G. Poles for PFL-f feature planes outside deformation zones (ESHI).

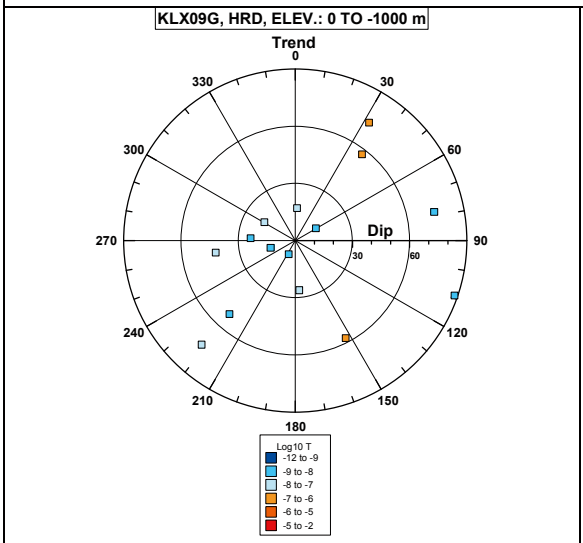

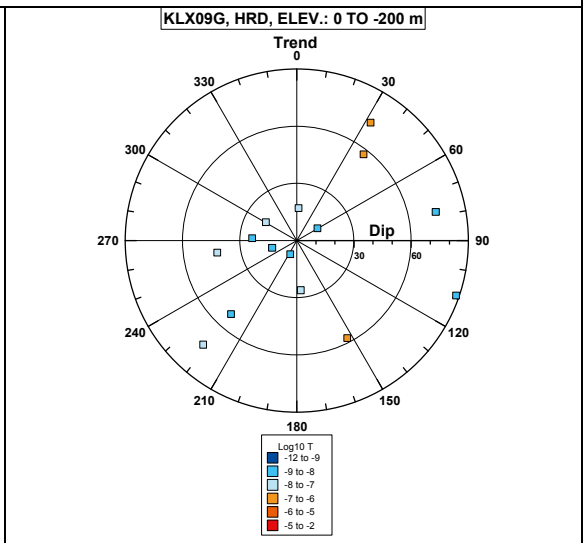

Borehole KLX09G. Poles for PFL-f feature planes in deformation zones (ESHI).

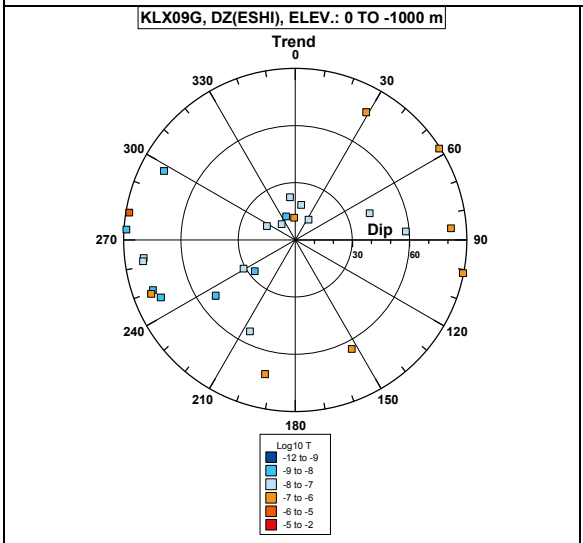

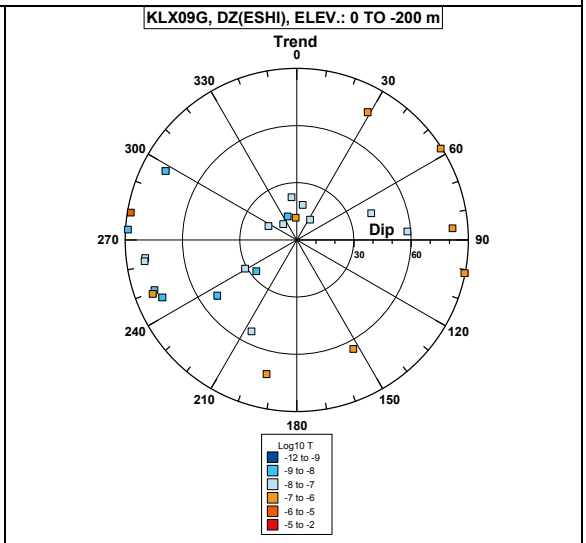

Borehole KLX10.

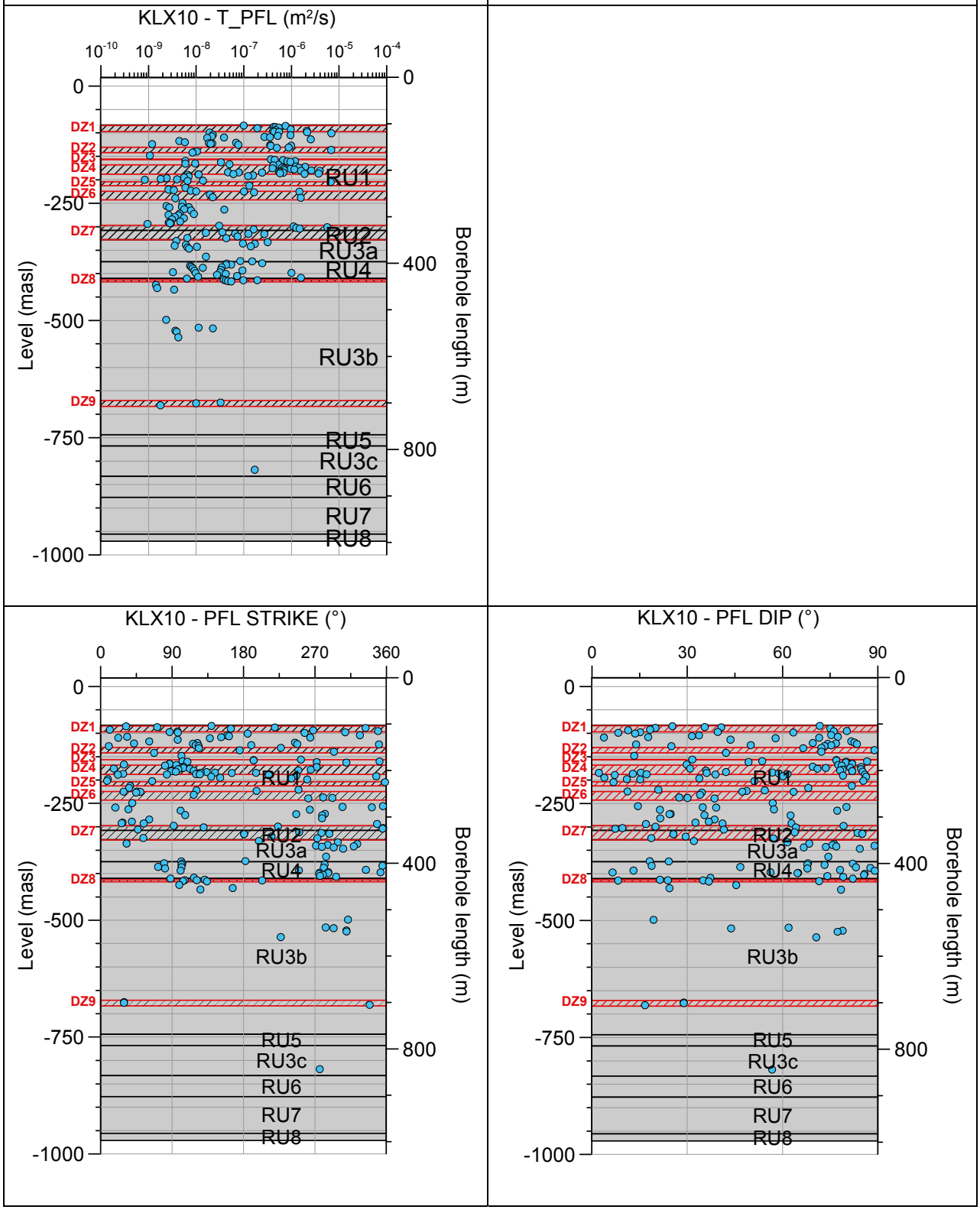

Comment:

Borehole KLX10. Poles for PFL-f feature planes outside deformation zones (ESHI).

KLX10, HRD, ELEV.: 0 TO -1000 m

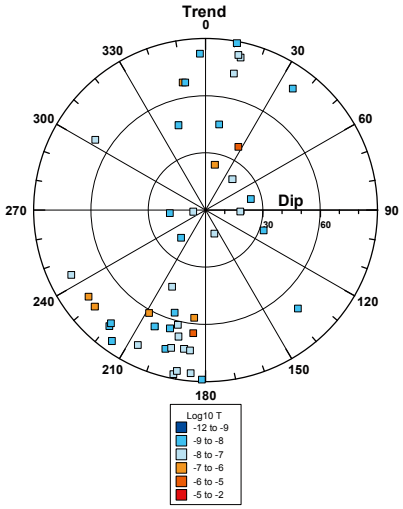

KLX10, HRD, ELEV.: 0 TO -200 m

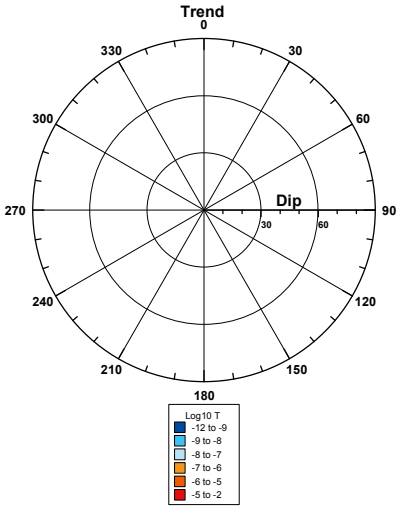

KLX10, HRD, ELEV.: -200 TO -400 m

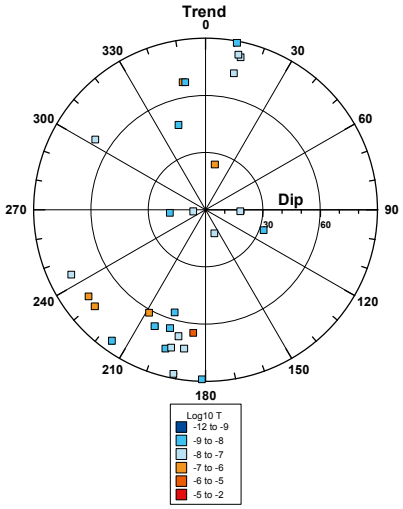

KLX10, HRD, ELEV.: -400 TO -600 m

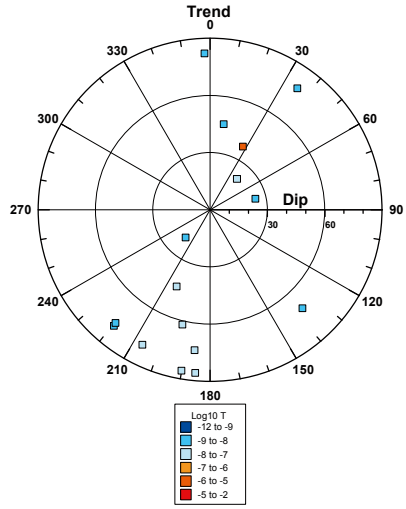

KLX10, HRD, ELEV.: -800 TO -1000 m

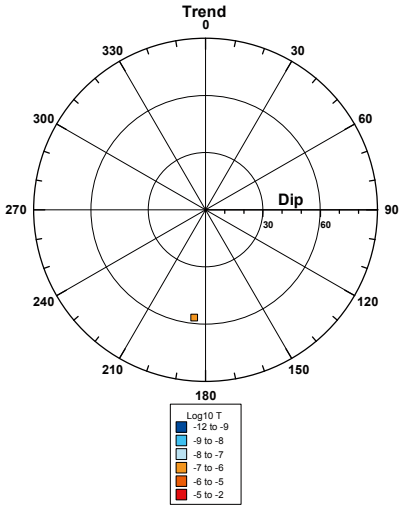

Borehole KLX10. Poles for PFL-f feature planes in deformation zones (ESHI).

KLX10, DZ(ESHI), ELEV.: 0 TO -1000 m

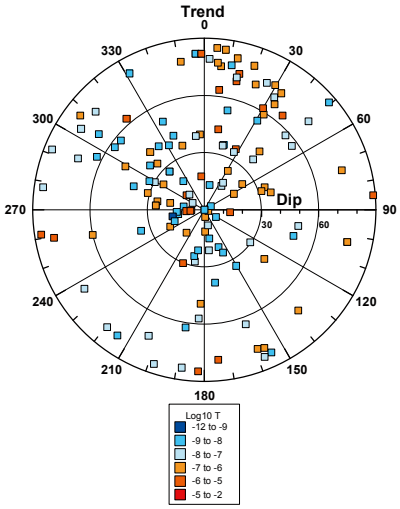

KLX10, DZ(ESHI), ELEV.: 0 TO -200 m

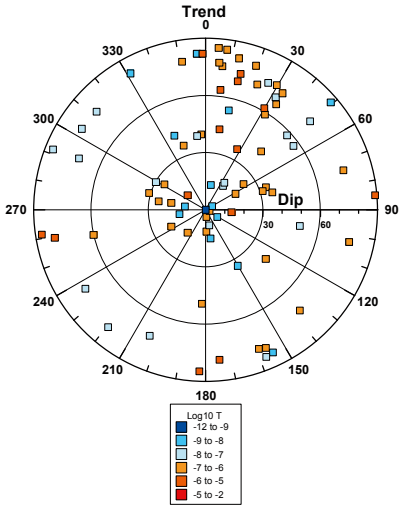

KLX10, DZ(ESHI), ELEV.: -200 TO -400 m

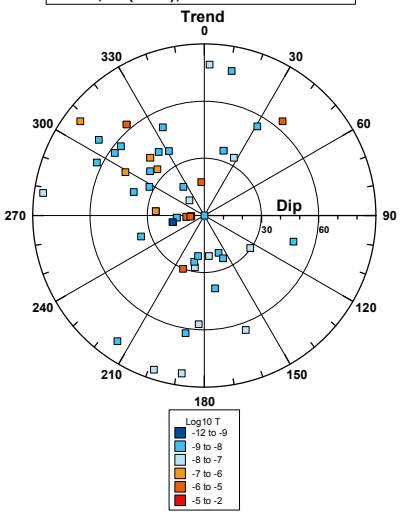

KLX10, DZ(ESHI), ELEV.: -400 TO -600 m

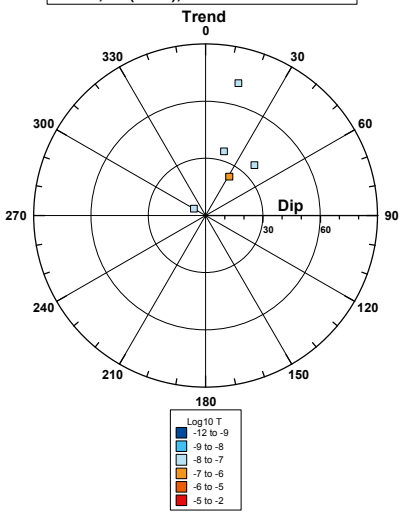

KLX10, DZ(ESHI), ELEV.: -600 TO -800 m

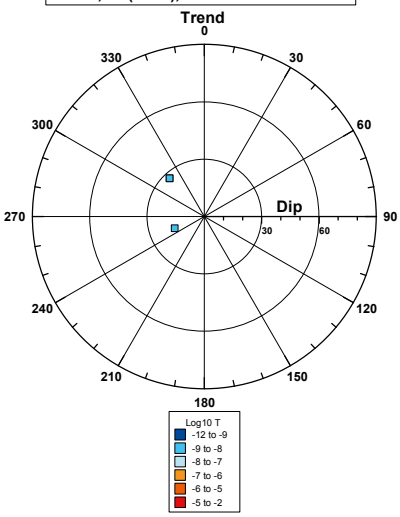

Borehole KLX10B.

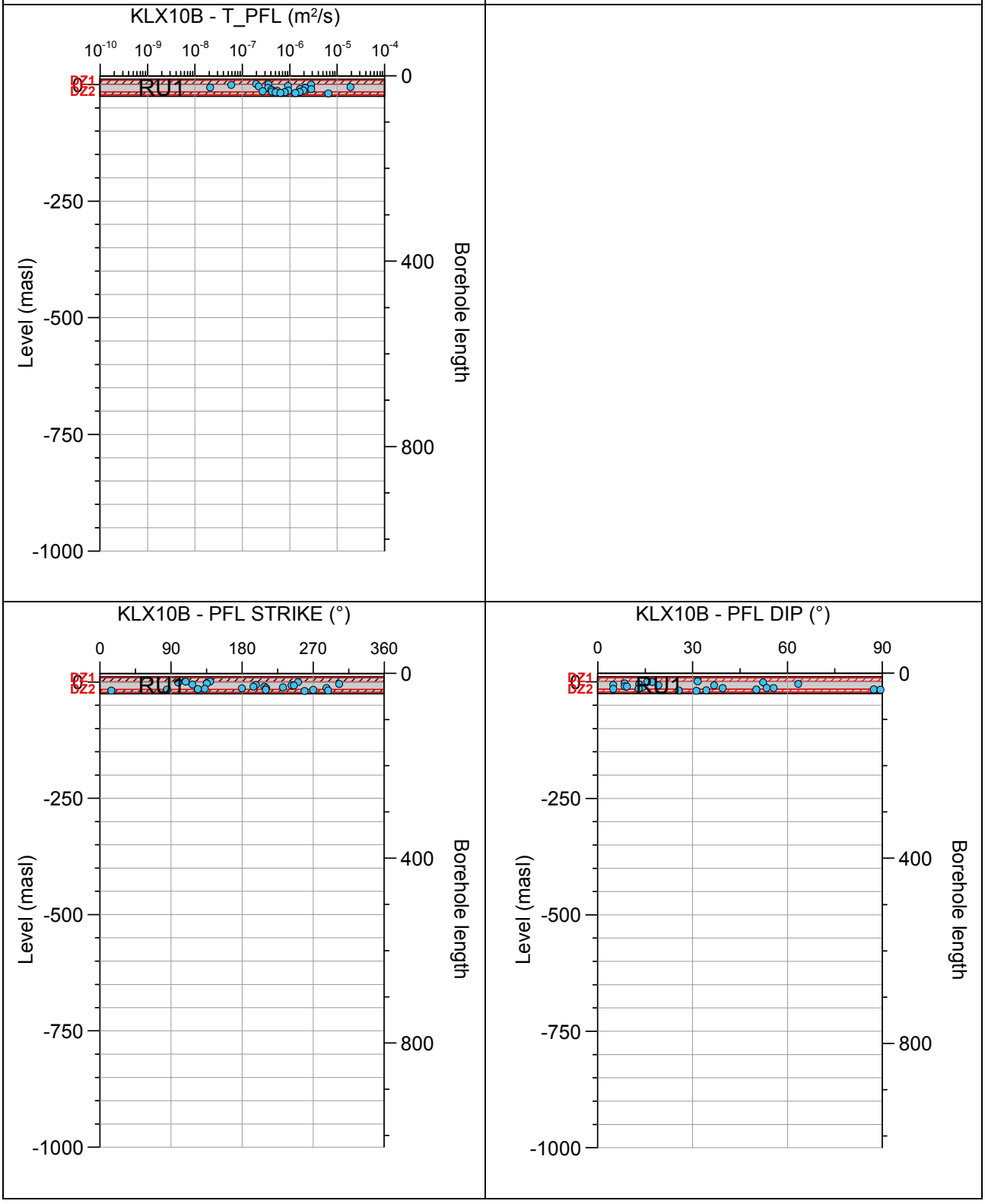

Comment:

Borehole KLX10B. Poles for PFL-f feature planes outside deformation zones (ESHI).

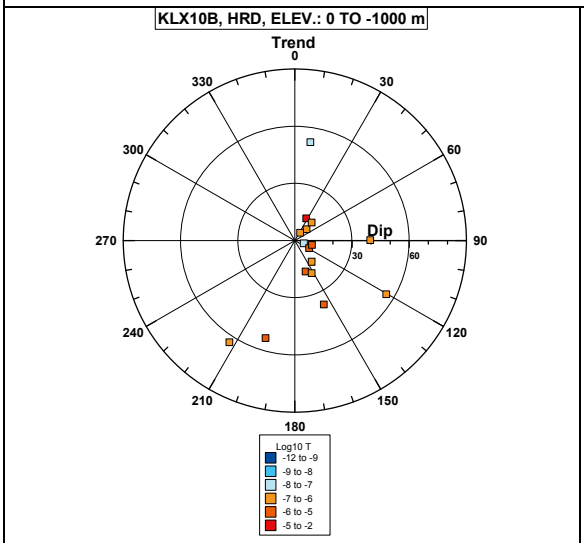

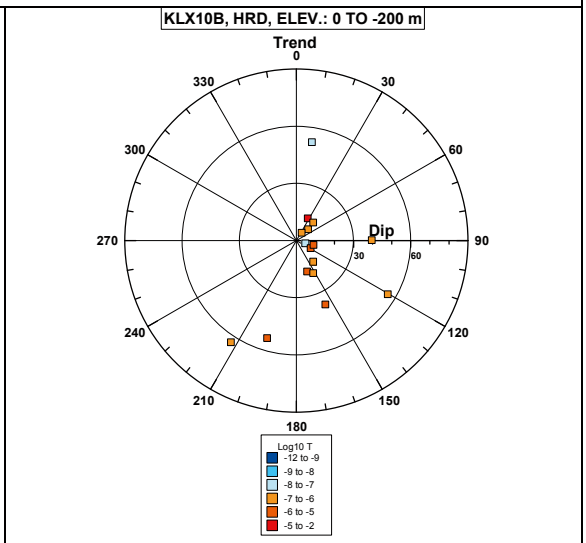

Borehole KLX10B. Poles for PFL-f feature planes in deformation zones (ESHI).

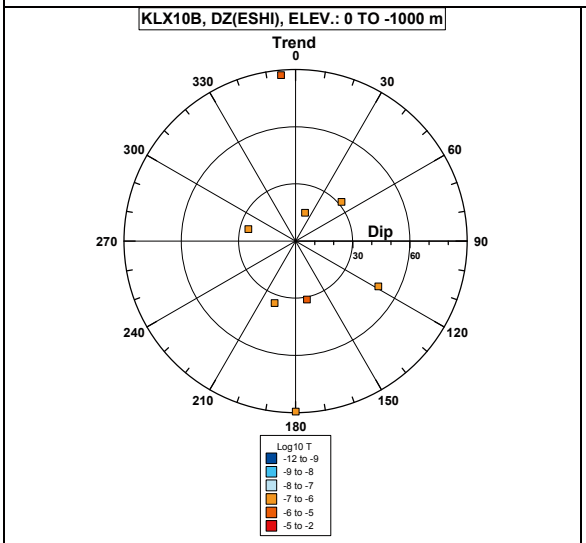

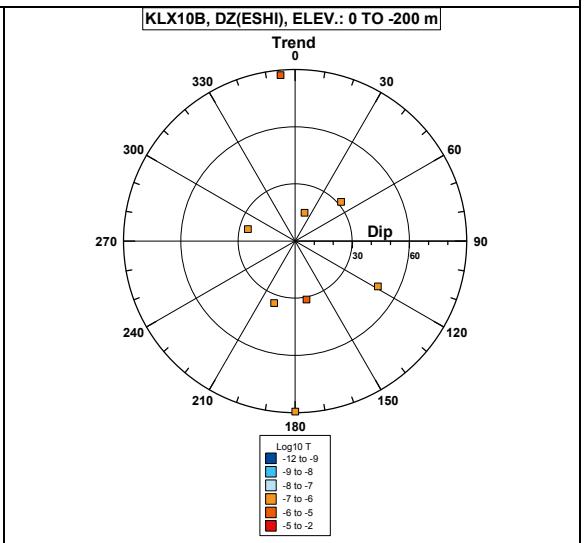

Borehole KLX10C.

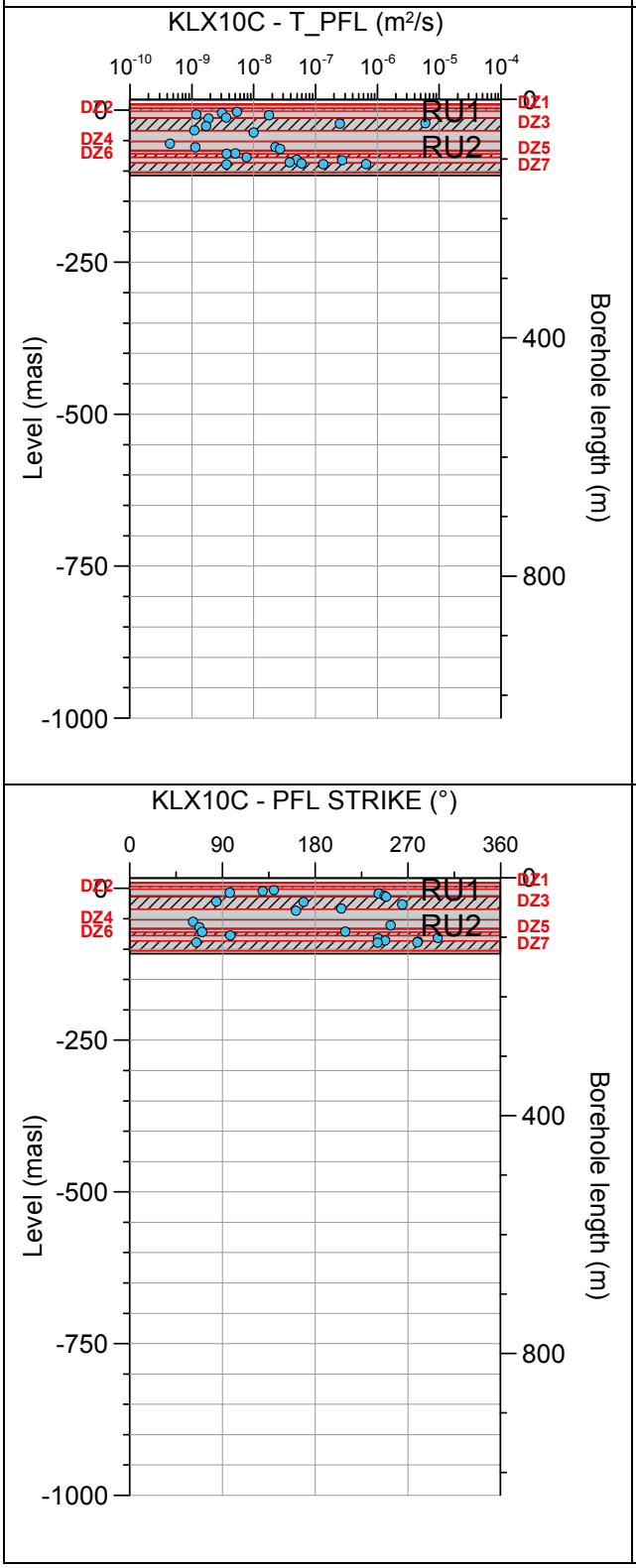

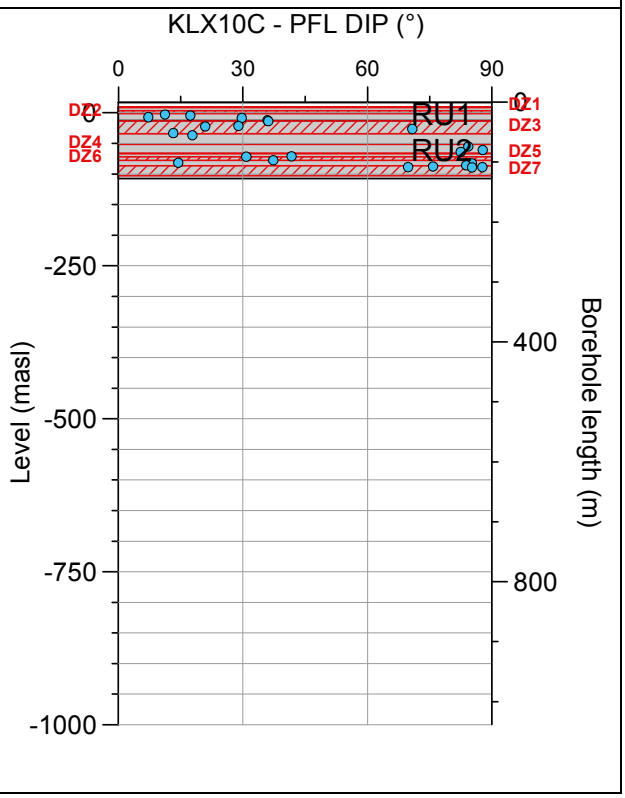

Comment:

Borehole KLX10C. Poles for PFL-f feature planes outside deformation zones (ESHI).

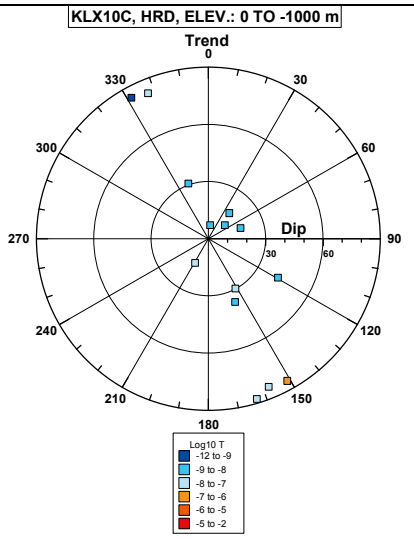

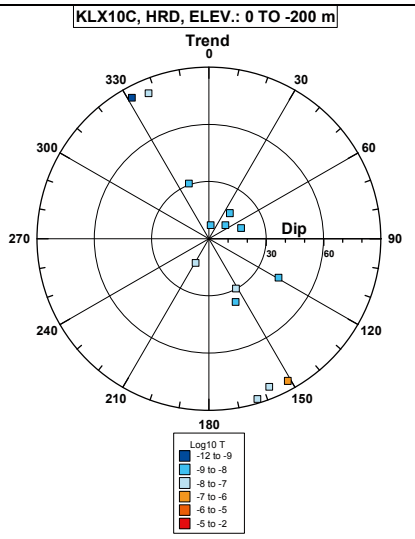

Borehole KLX10C. Poles for PFL-f feature planes in deformation zones (ESHI).

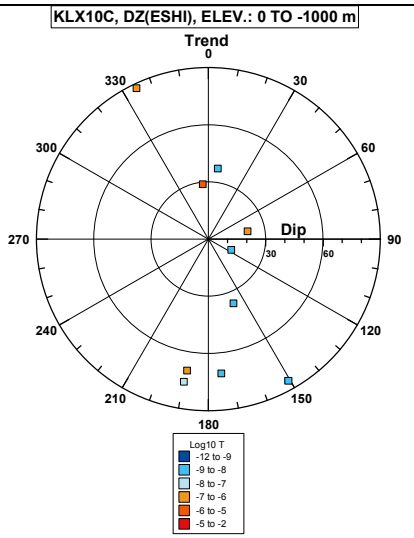

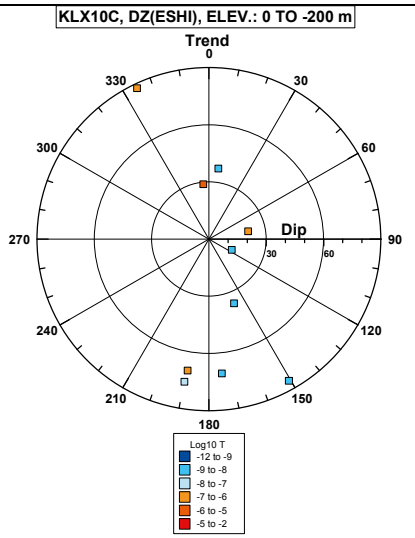

Borehole KLX11A.

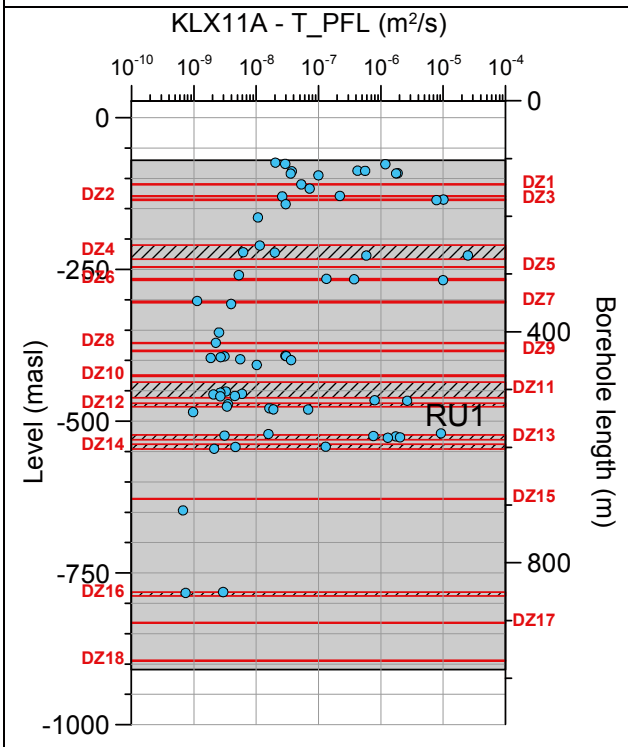

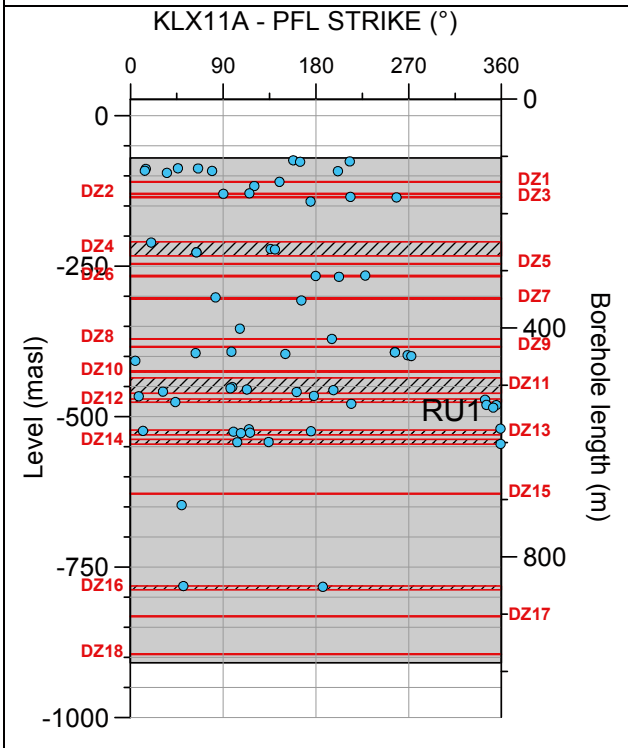

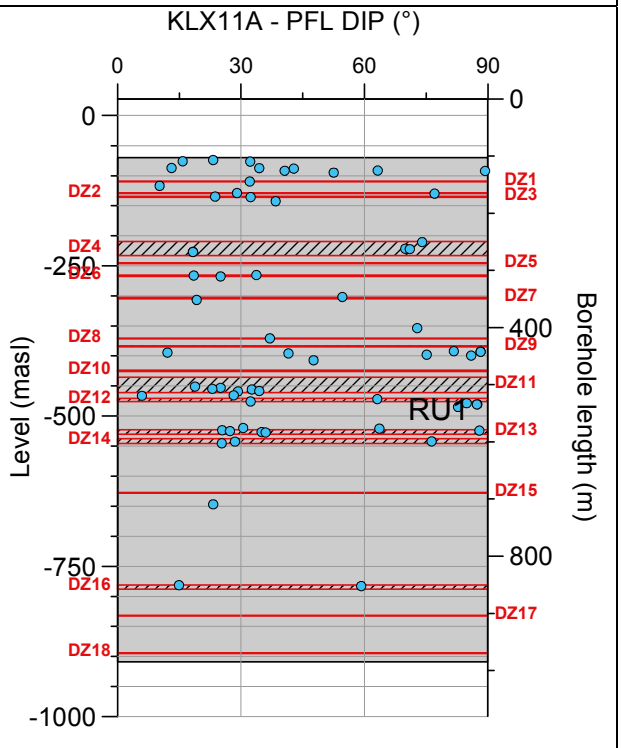

Comment:

Borehole KLX11A. Poles for PFL-f feature planes outside deformation zones (ESHI).

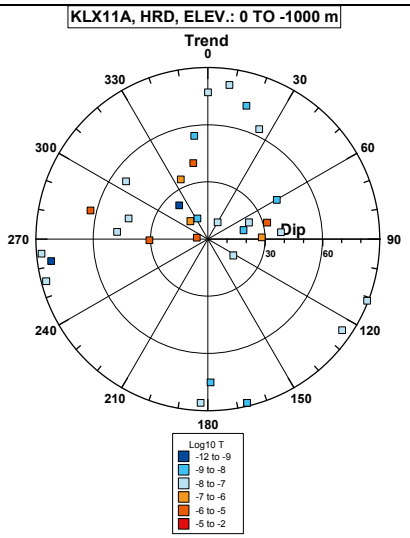

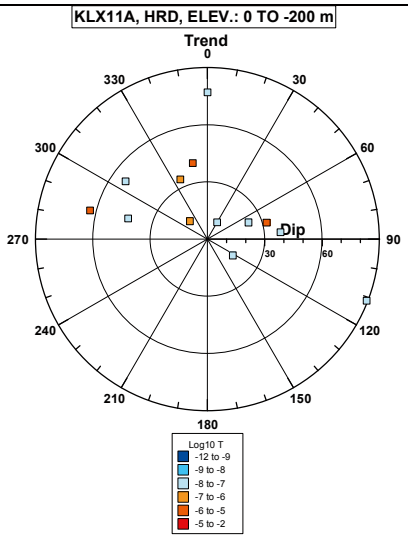

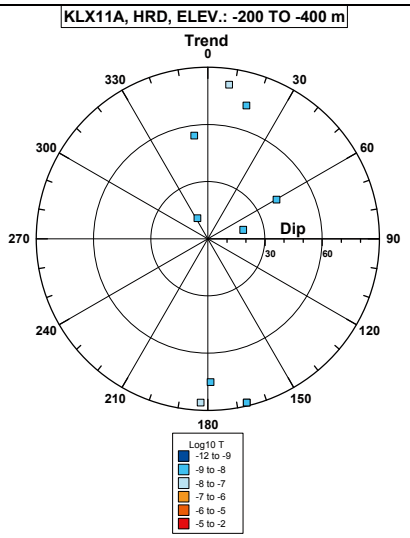

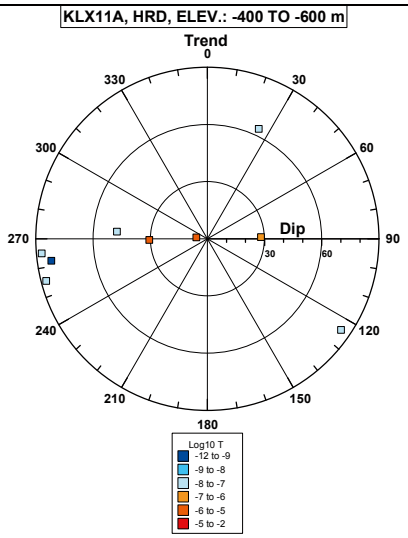

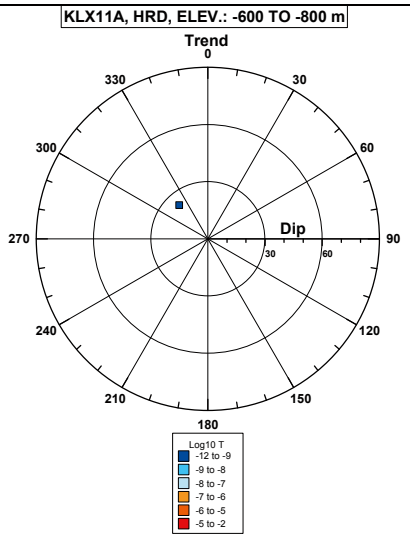

Borehole KLX11A. Poles for PFL-f feature planes in deformation zones (ESHI).

KLX11A, HRD, ELEV.: 0 TO -1000 m

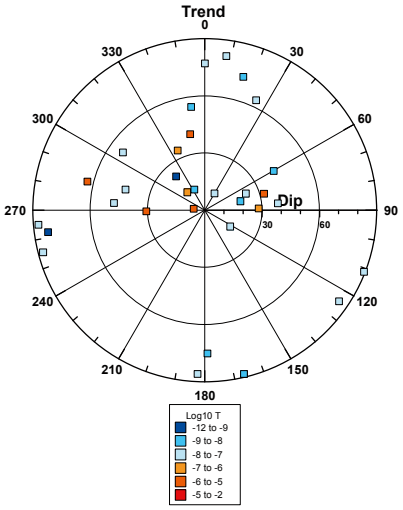

KLX11A, DZ(ESHI), ELEV.: 0 TO -200 m

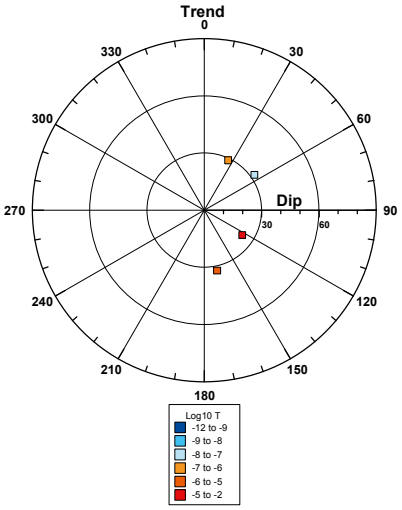

KLX11A, DZ(ESHI), ELEV.: -200 TO -400 m

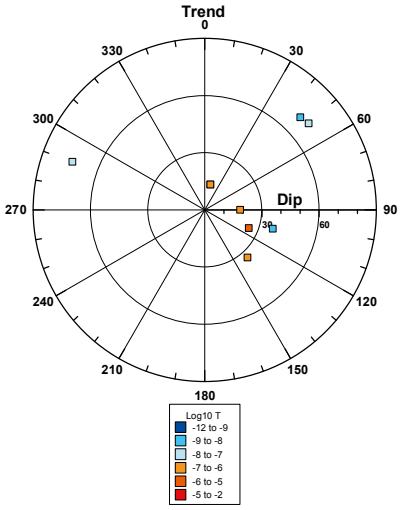

KLX11A, DZ(ESHI), ELEV.: -400 TO -600 m

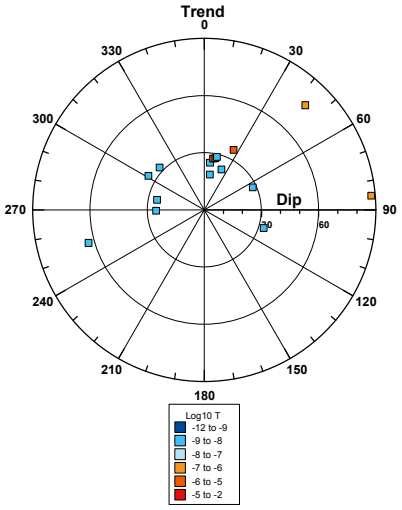

KLX11A, DZ(ESHI), ELEV.: -600 TO -800 m

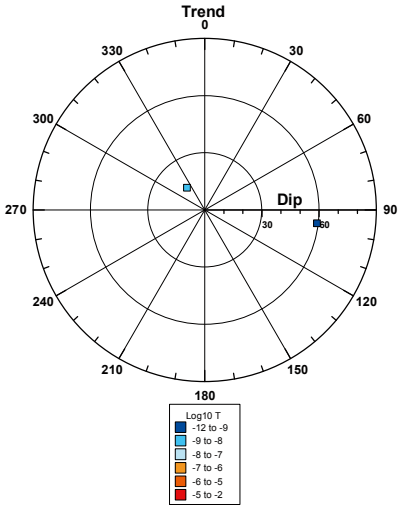

Borehole KLX11B.

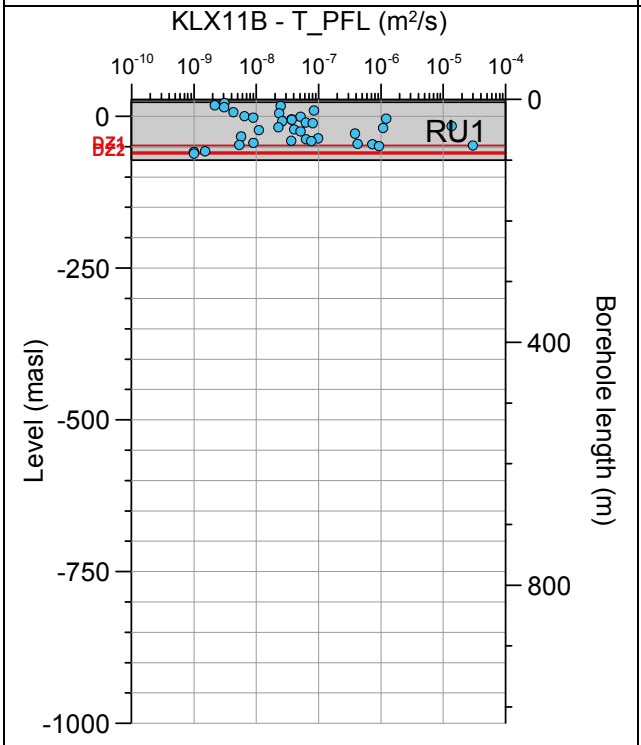

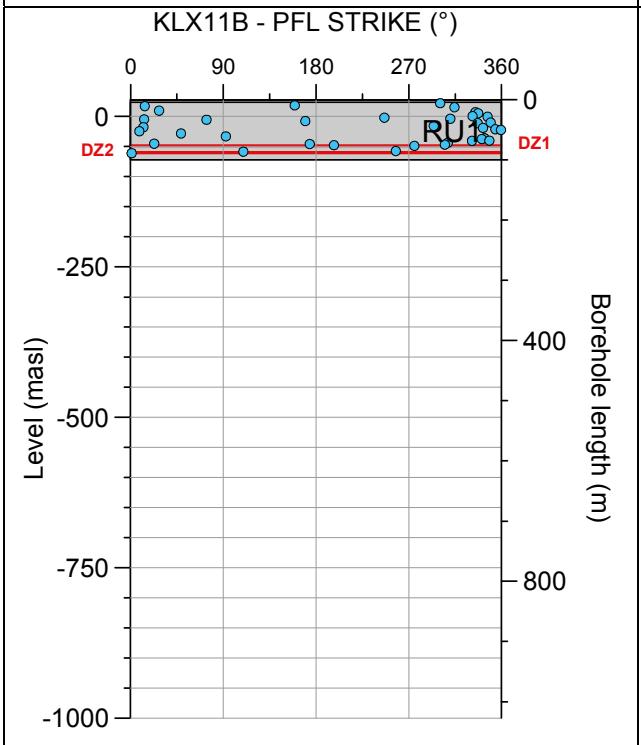

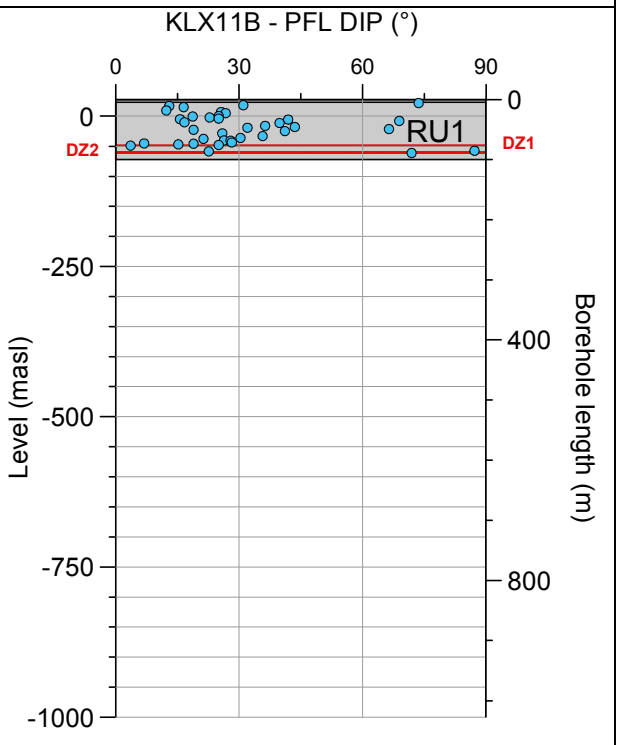

Comment:

Borehole KLX11B. Poles for PFL-f feature planes outside deformation zones (ESHI).

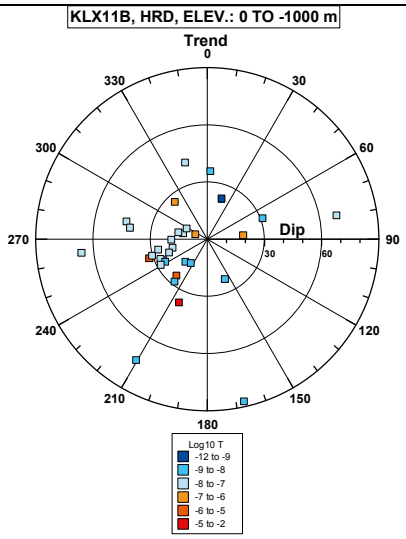

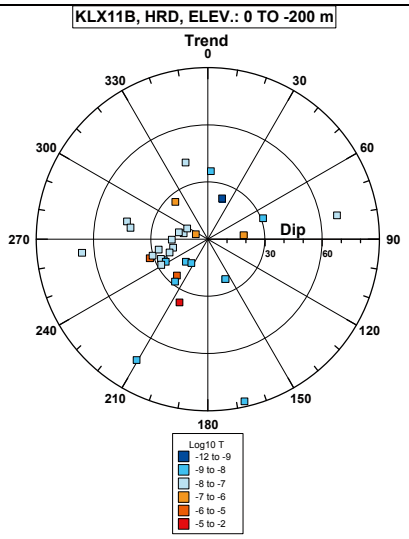

Borehole KLX11B. Poles for PFL-f feature planes in deformation zones (ESHI).

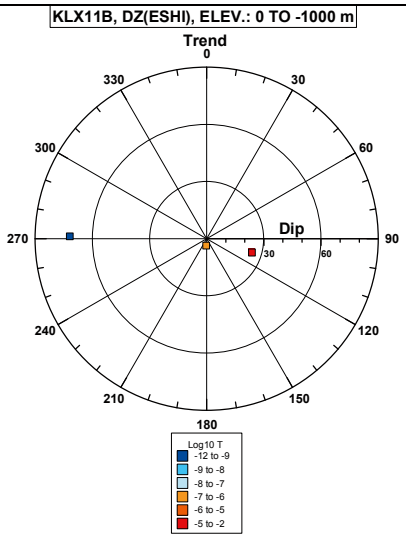

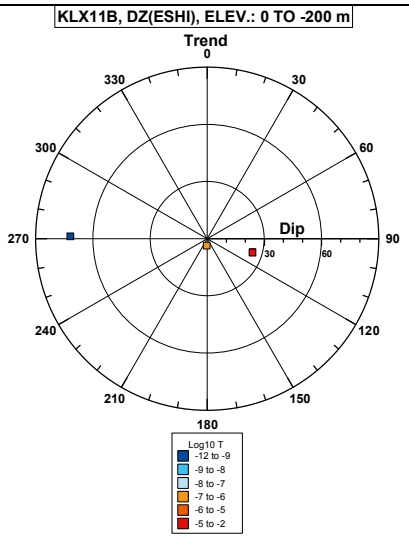

Borehole KLX11C.

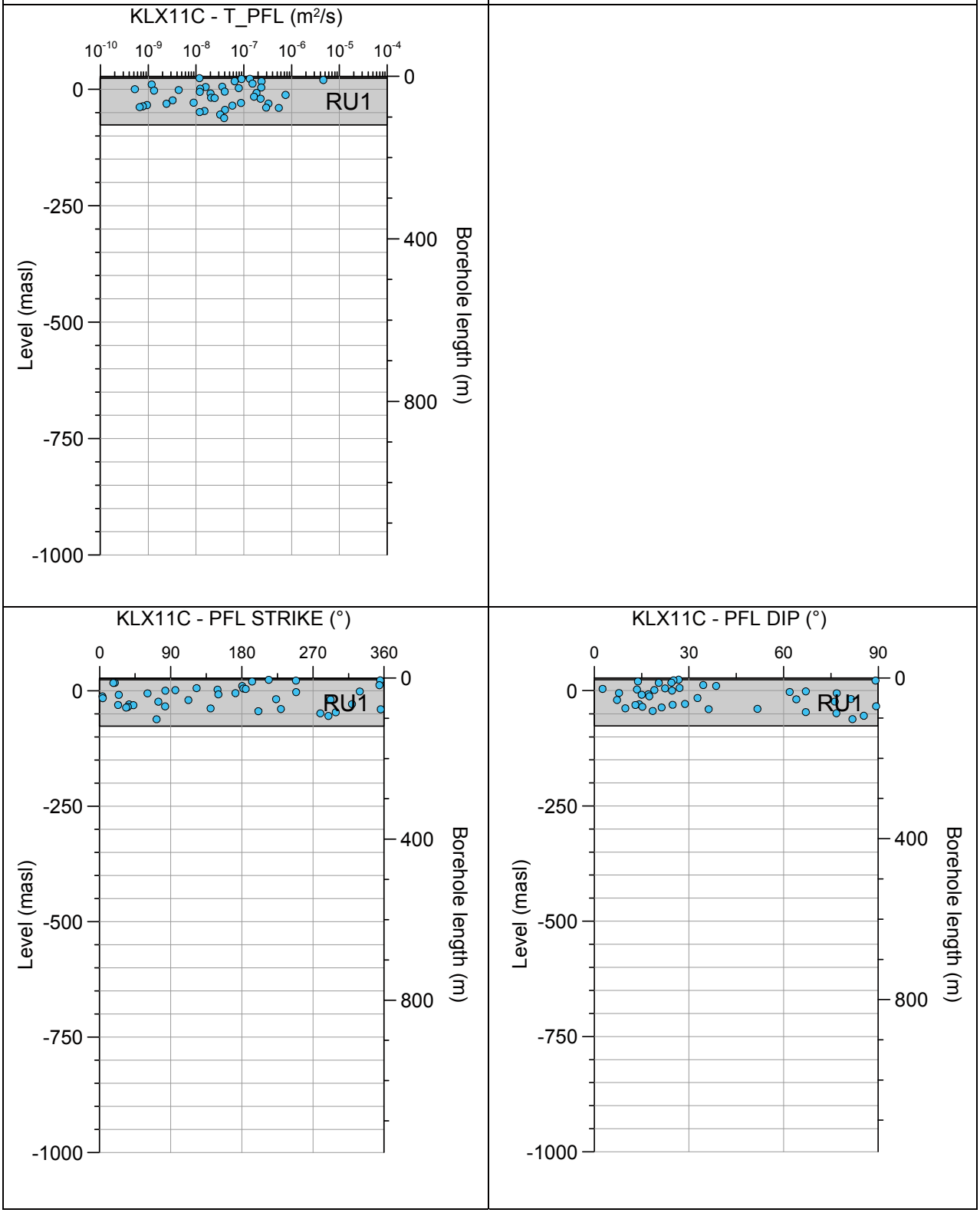

Comment:

Borehole KLX11C. Poles for PFL-f feature planes outside deformation zones (ESHI).

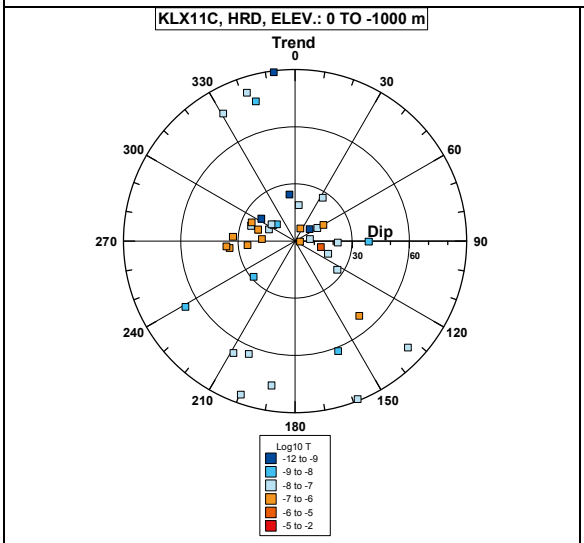

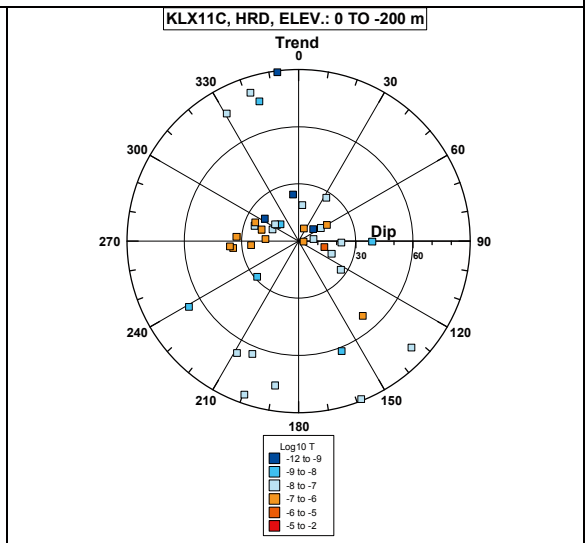

Borehole KLX11C. Poles for PFL-f feature planes in deformation zones (ESHI).

No interpreted deformation zones (ESHI) in the borehole.

Borehole KLX11D.

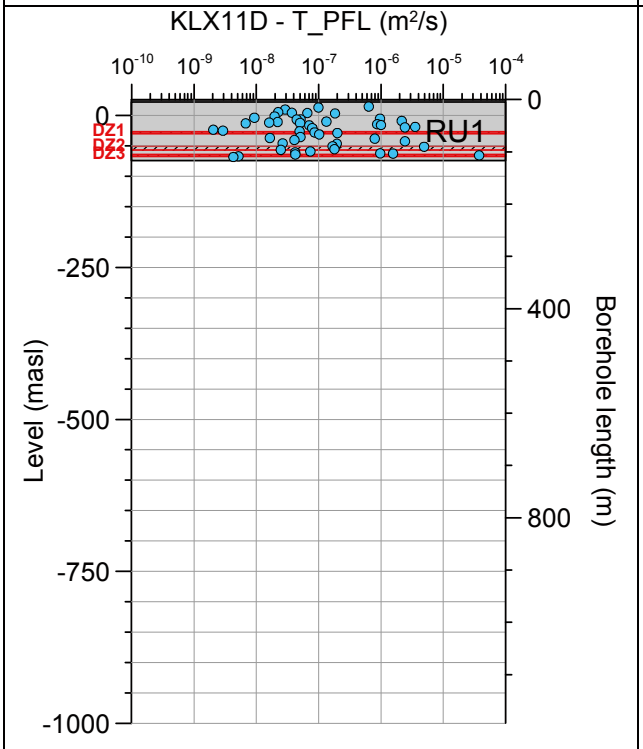

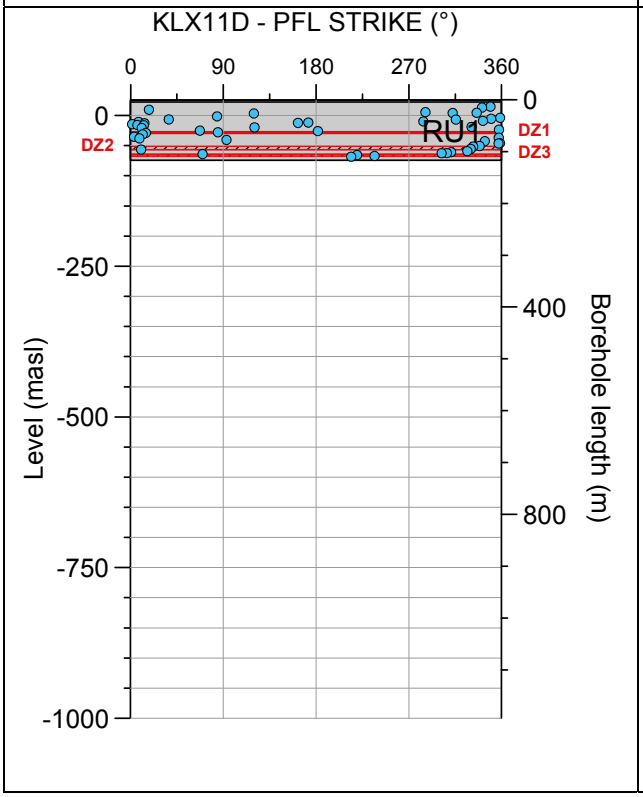

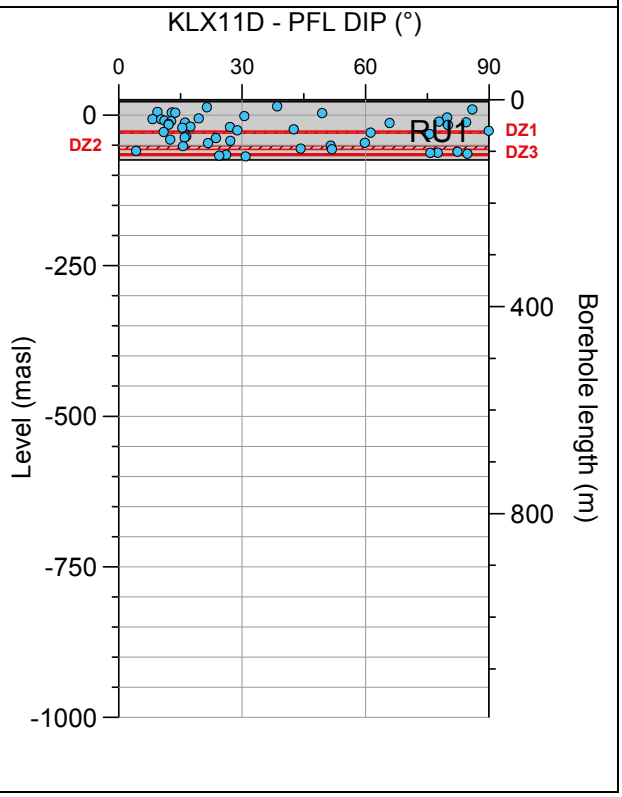

Comment:

Borehole KLX11D. Poles for PFL-f feature planes outside deformation zones (ESHI).

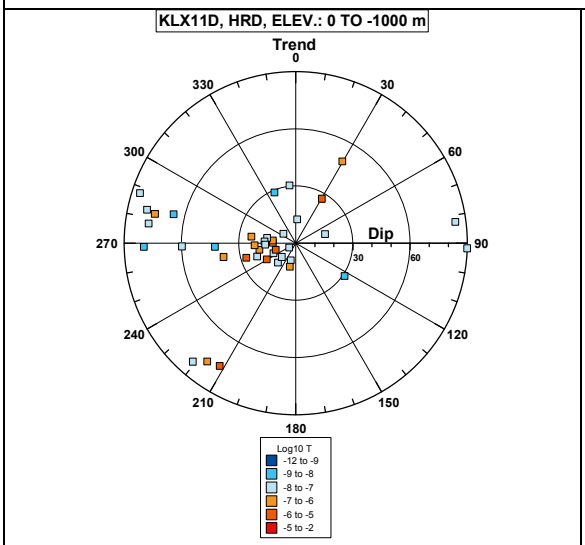

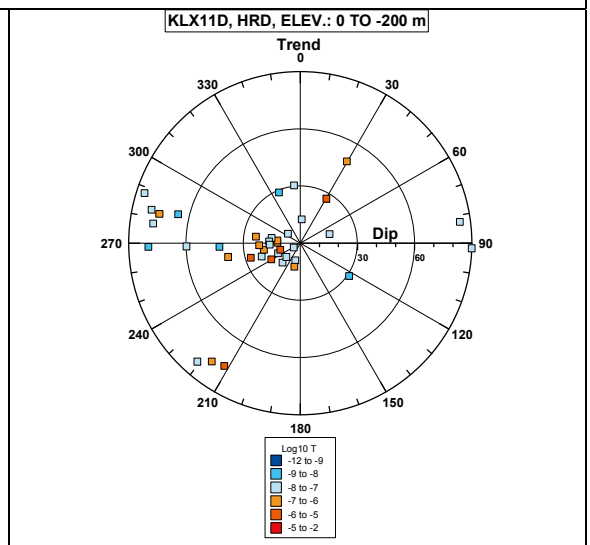

Borehole KLX11D. Poles for PFL-f feature planes in deformation zones (ESHI).

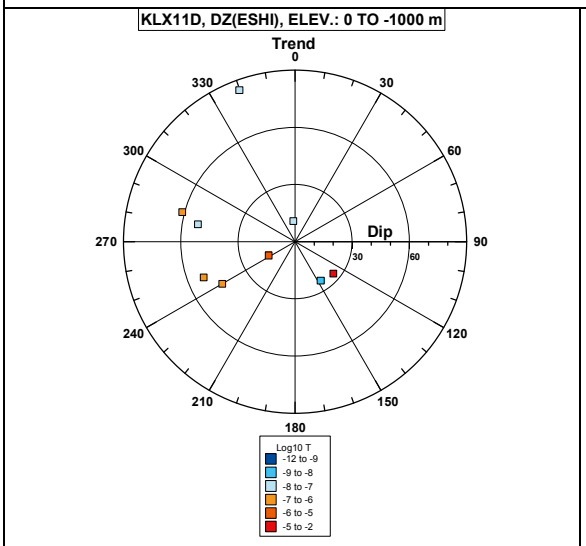

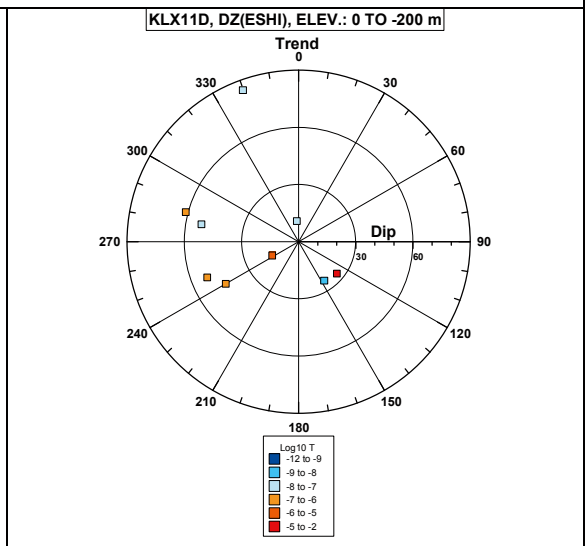

Borehole KLX11E.

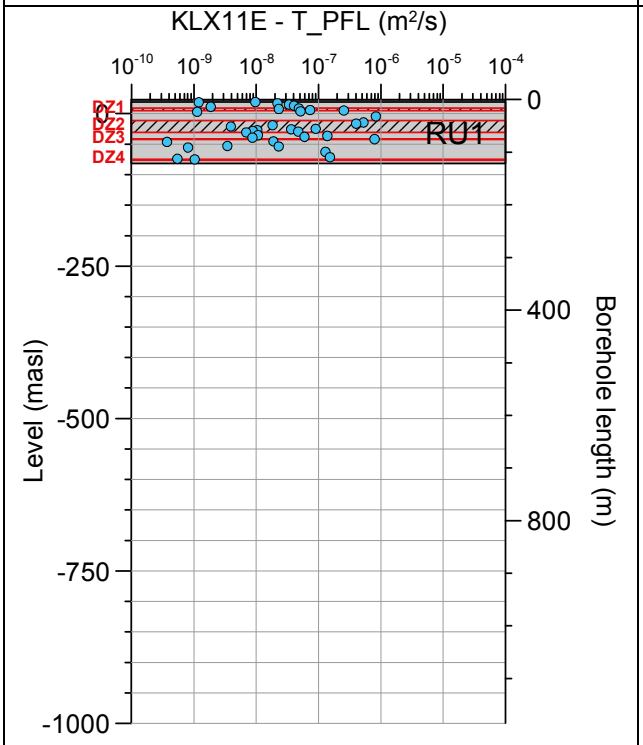

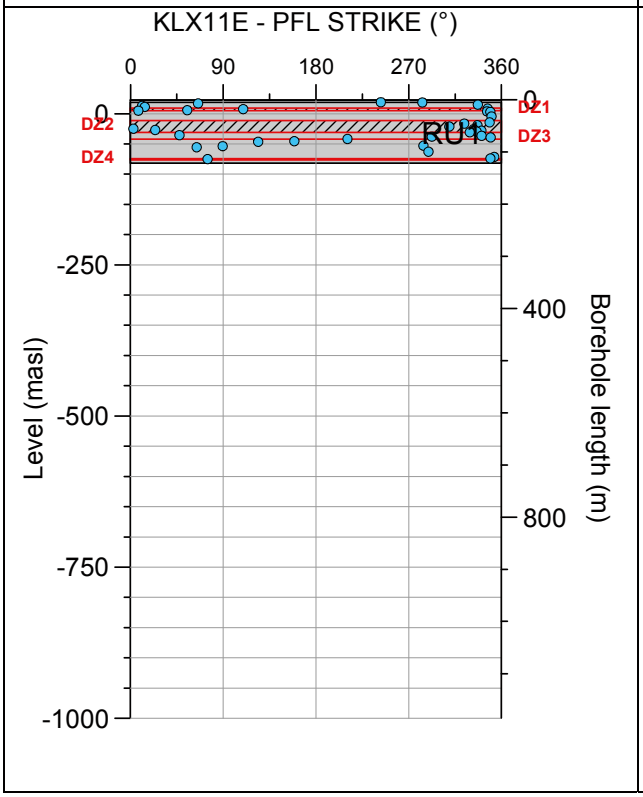

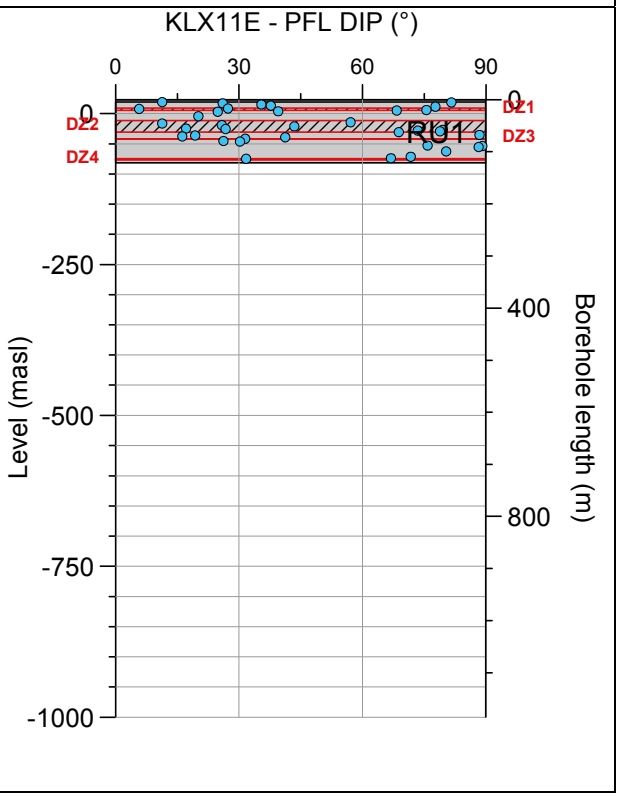

Comment:

Borehole KLX11E. Poles for PFL-f feature planes outside deformation zones (ESHI).

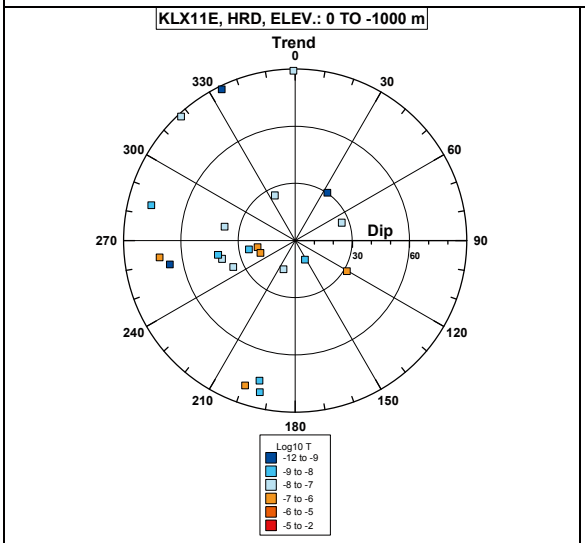

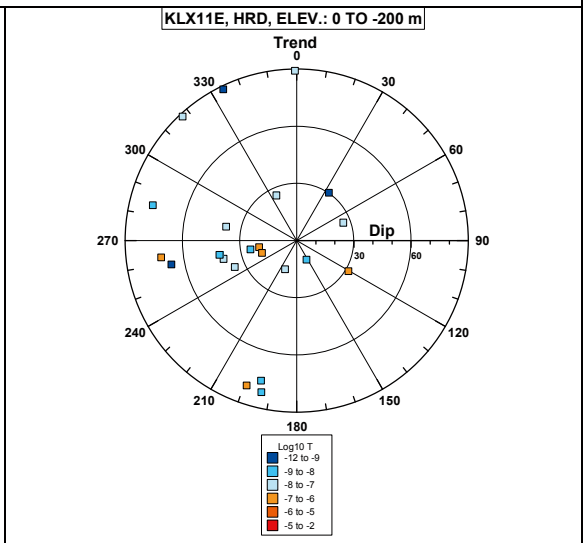

Borehole KLX11E. Poles for PFL-f feature planes in deformation zones (ESHI).

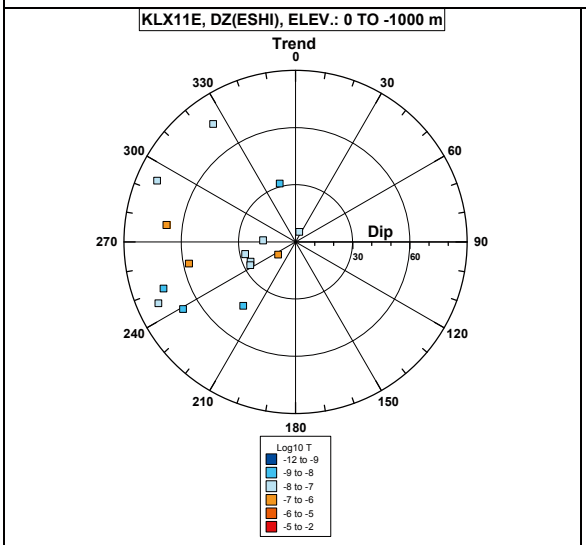

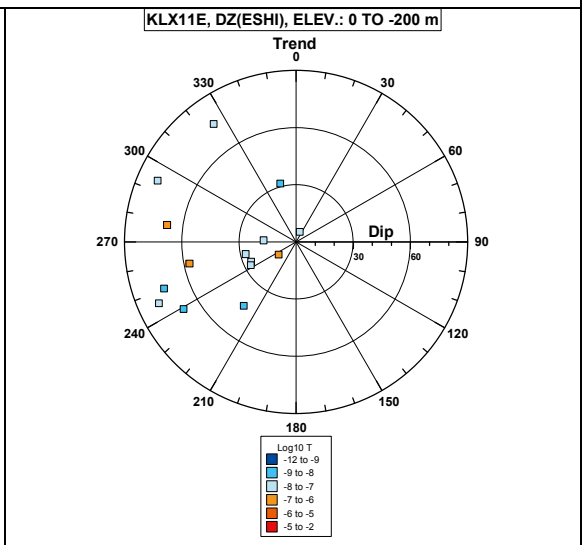

Borehole KLX11F.

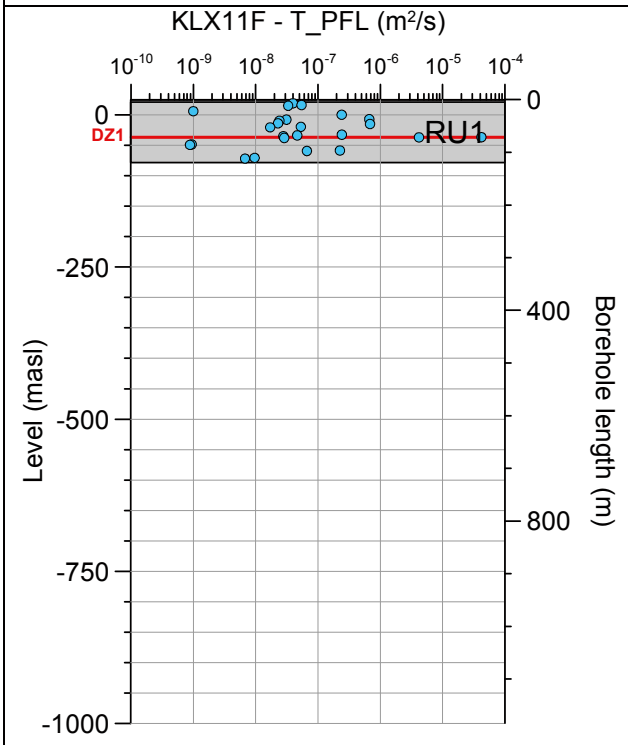

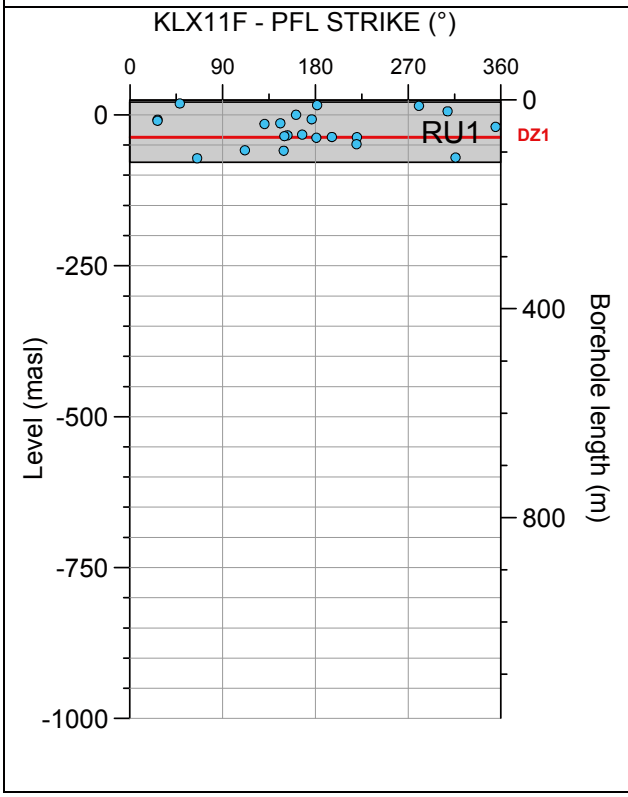

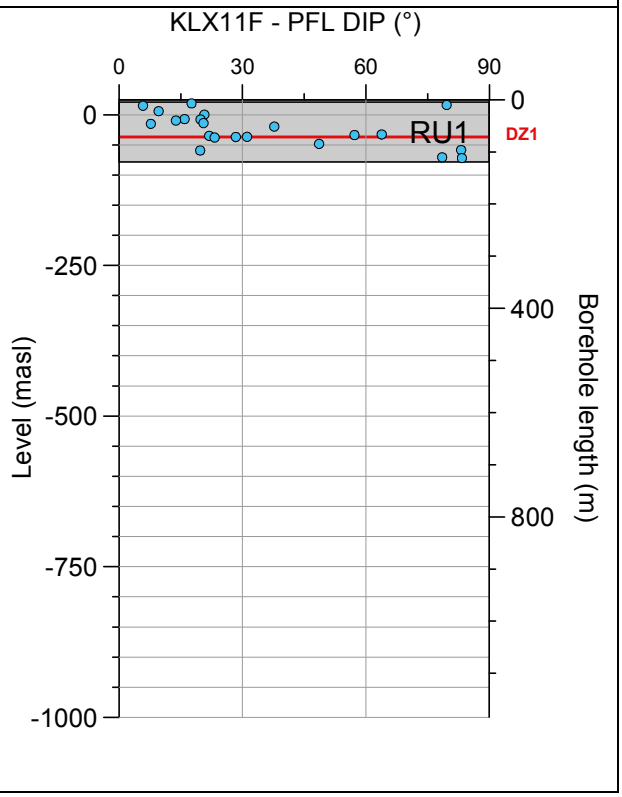

Comment:

Borehole KLX11F. Poles for PFL-f feature planes outside deformation zones (ESHI).

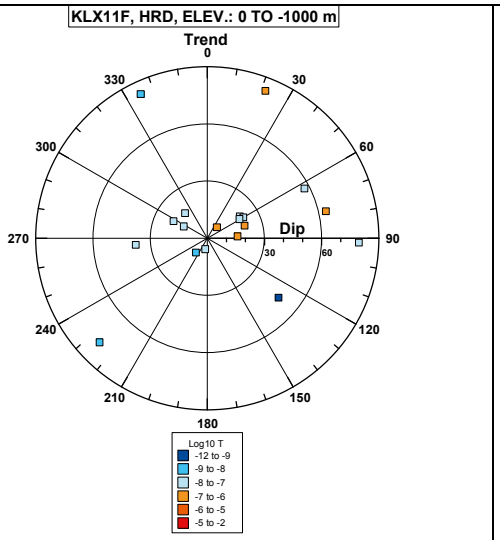

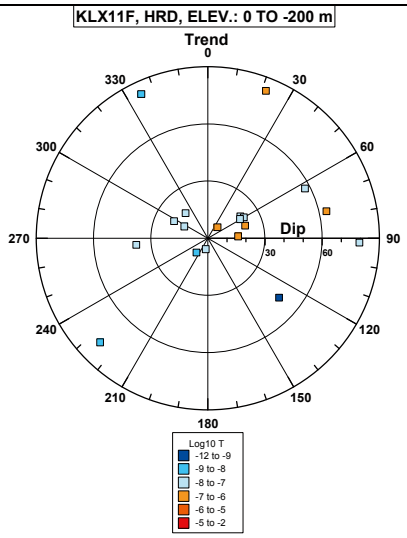

Borehole KLX11F. Poles for PFL-f feature planes in deformation zones (ESHI).

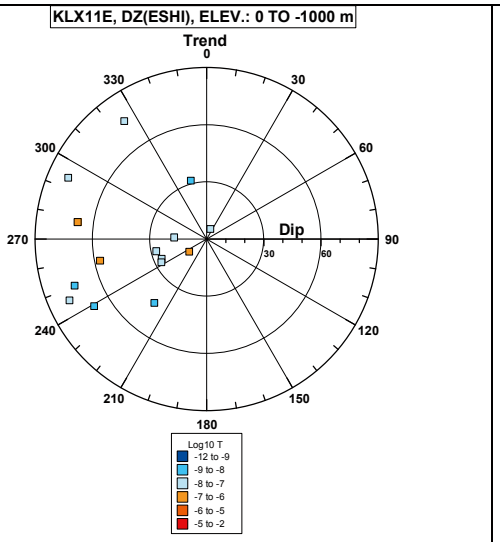

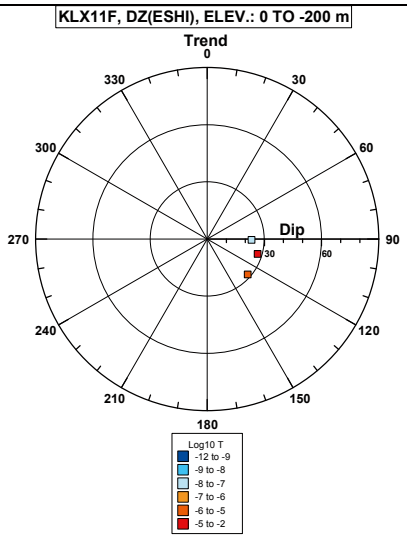

Borehole KLX12A.

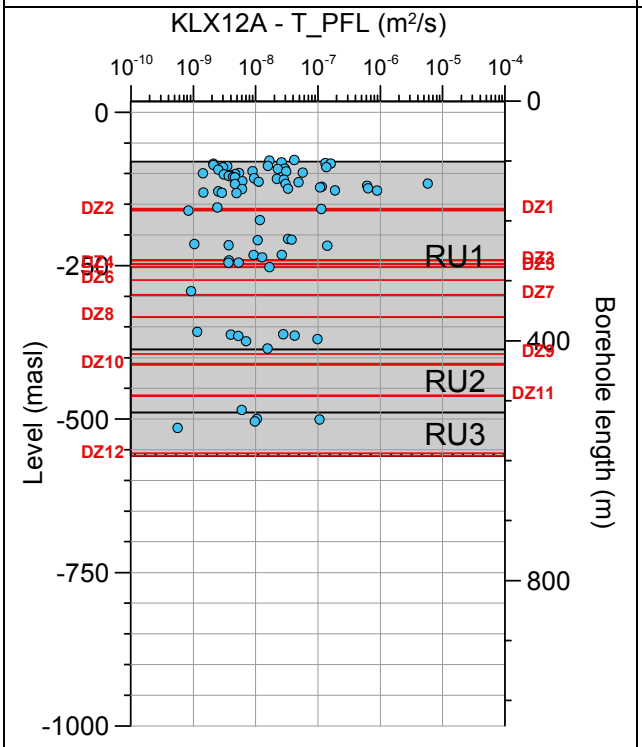

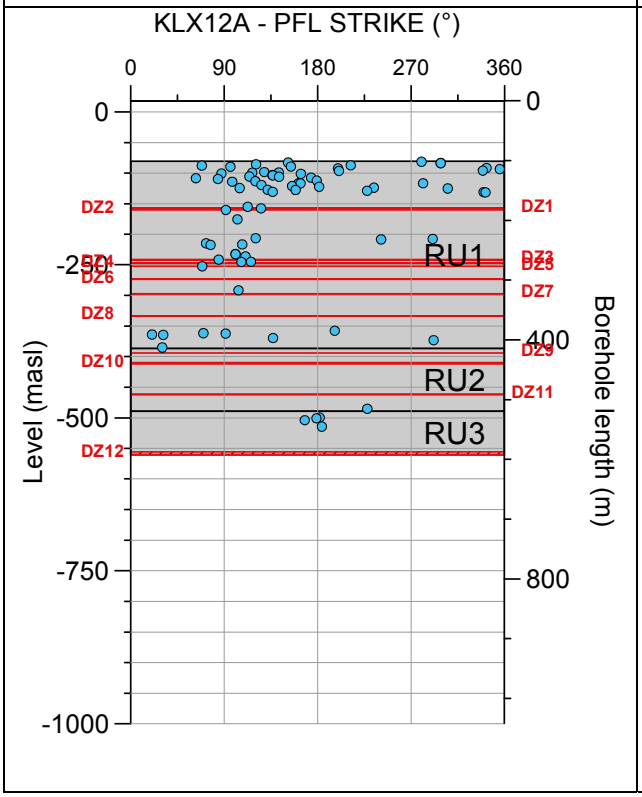

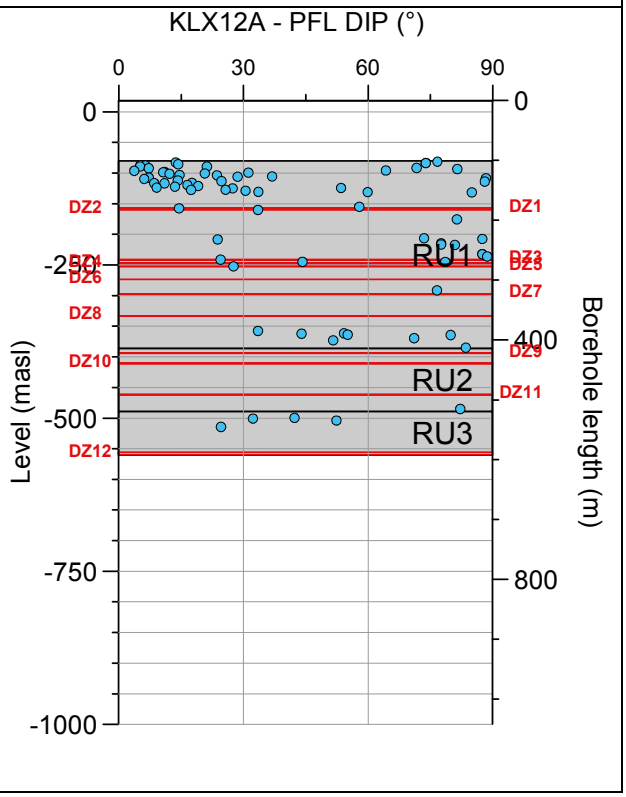

Comment:

Borehole KLX12A. Poles for PFL-f feature planes outside deformation zones (ESHI).

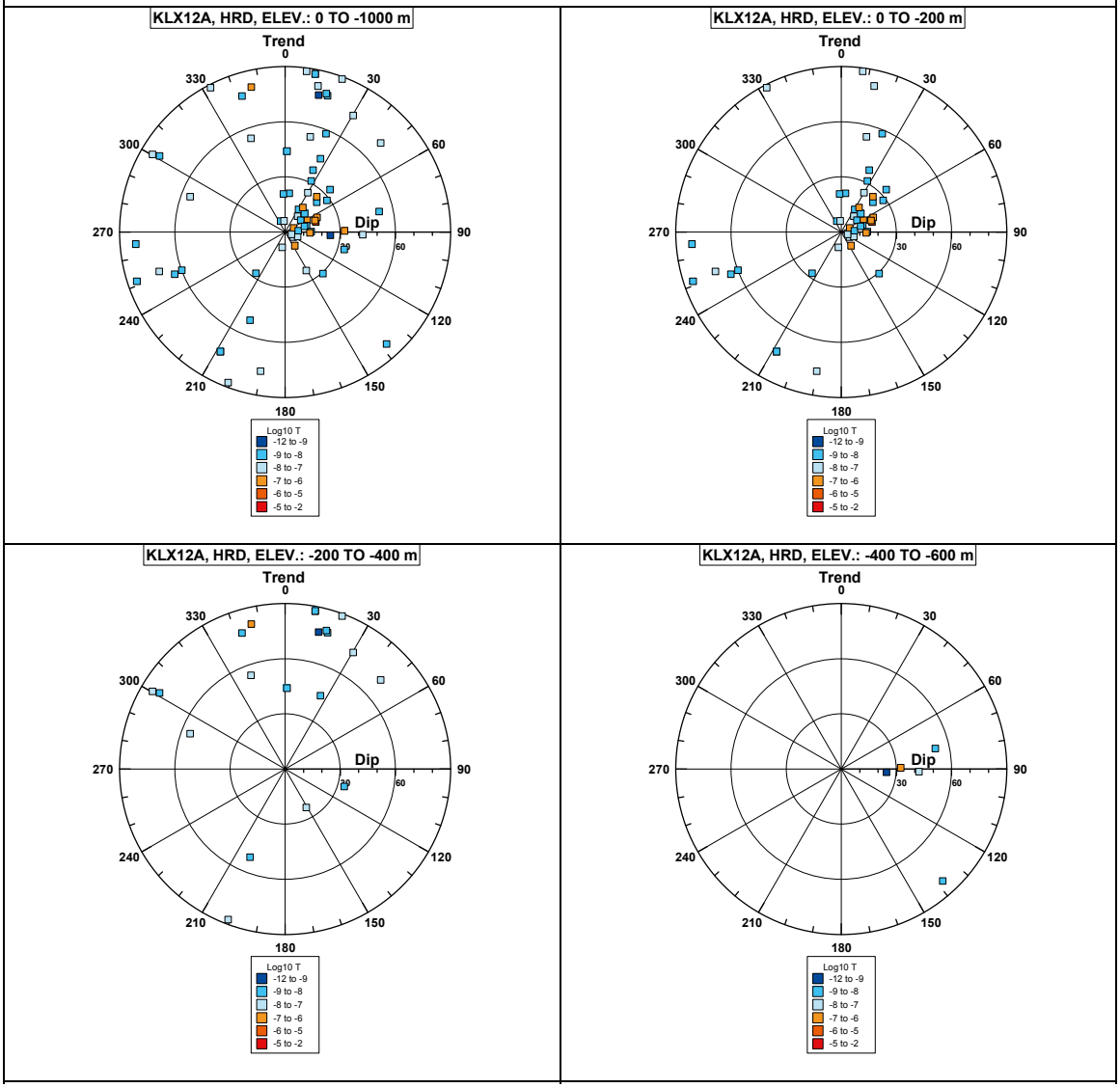

Borehole KLX12A. Poles for PFL-f feature planes in deformation zones (ESHI).

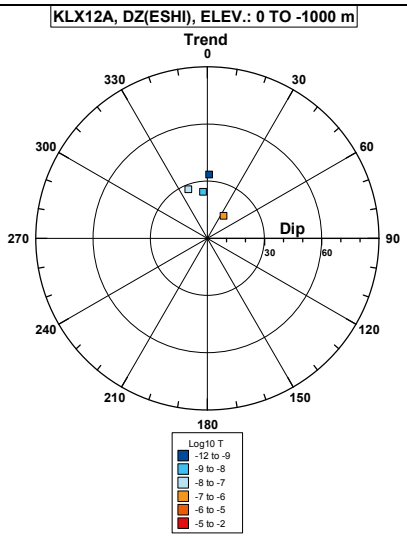

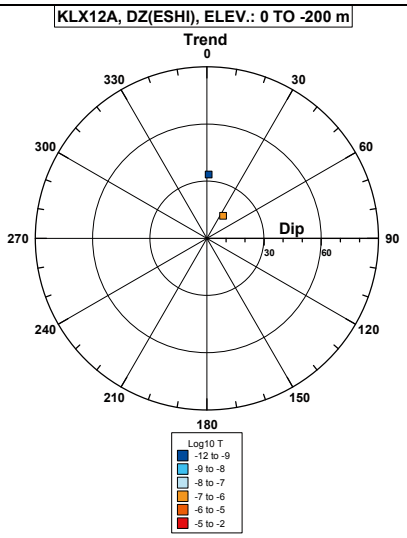

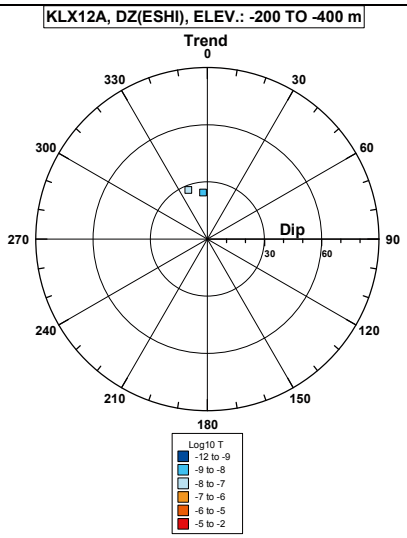

Borehole KLX13A.

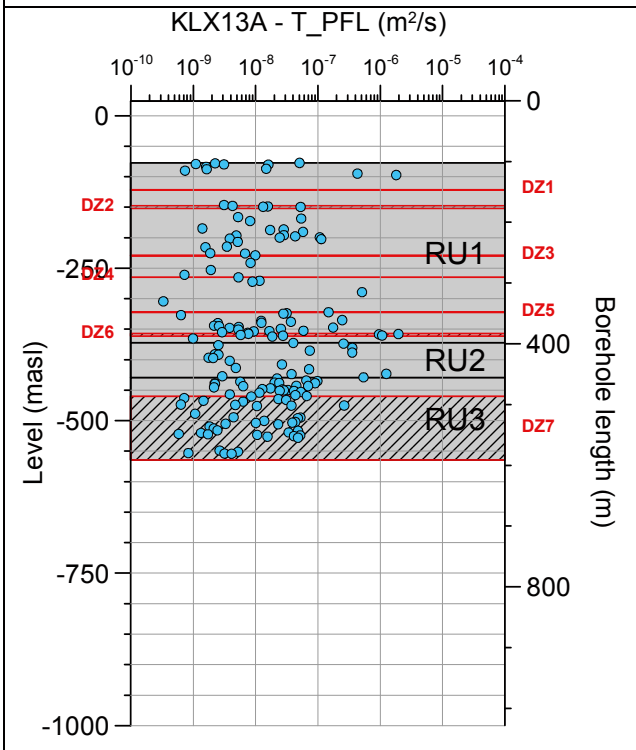

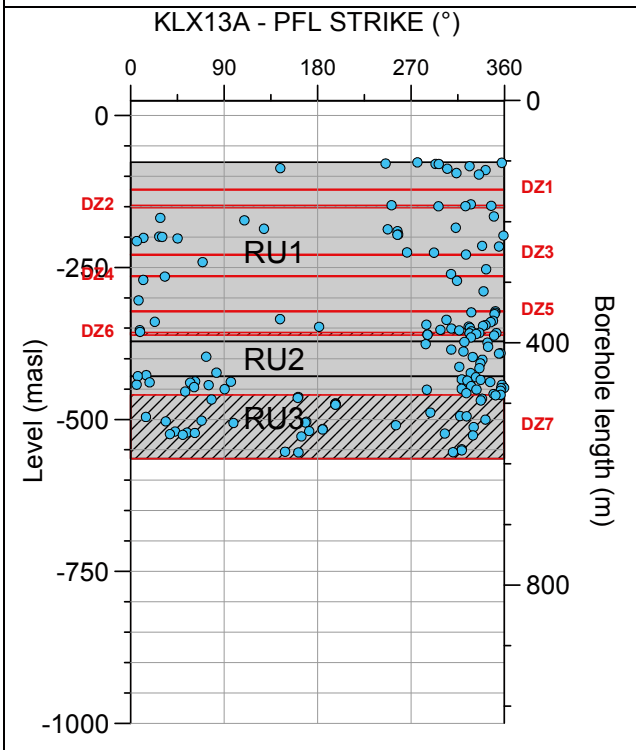

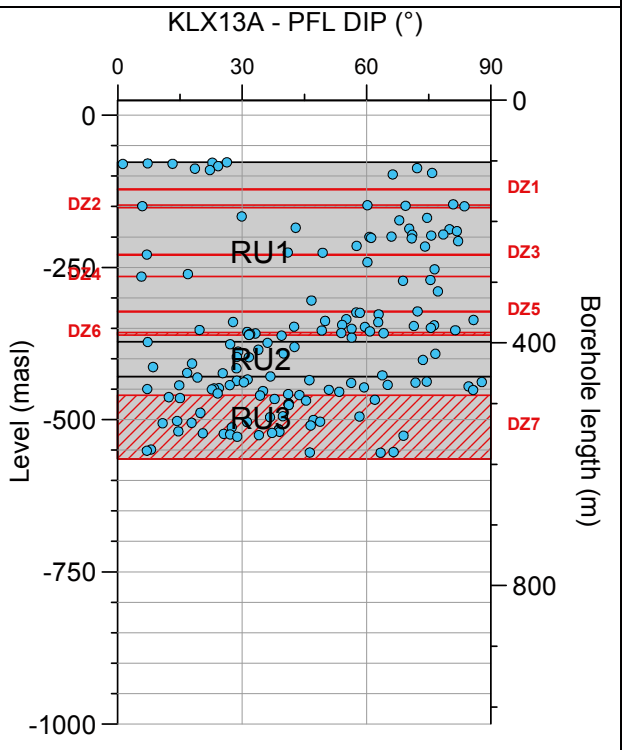

Comment:

Borehole KLX13A. Poles for PFL-f feature planes outside deformation zones (ESHI).

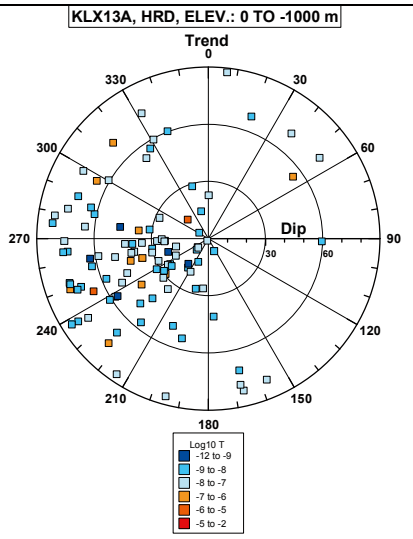

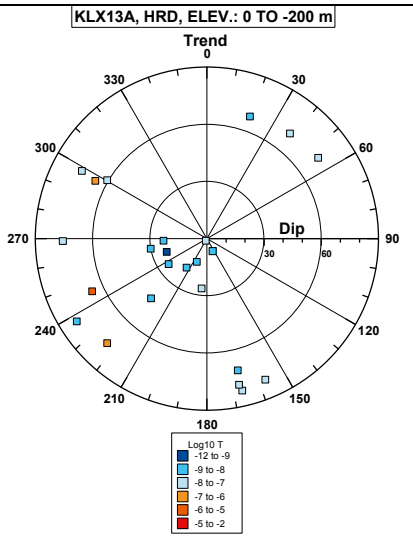

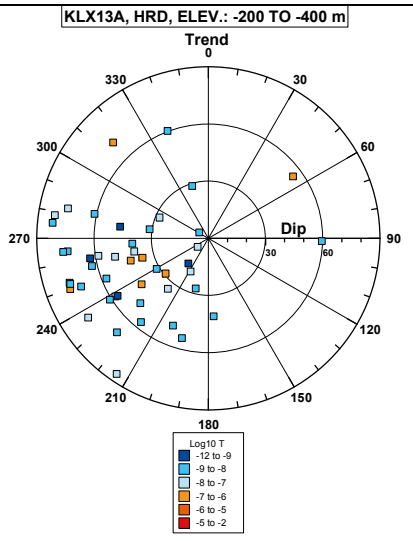

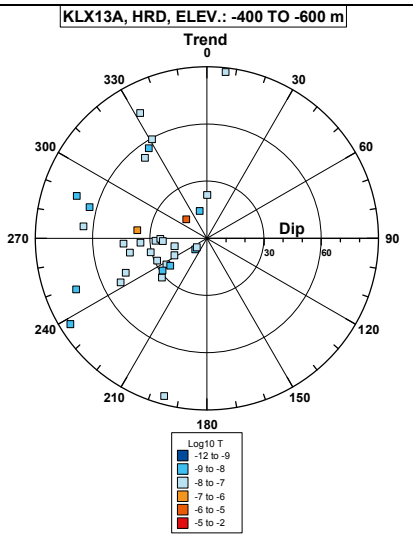

Borehole KLX13A. Poles for PFL-f feature planes in deformation zones (ESHI).

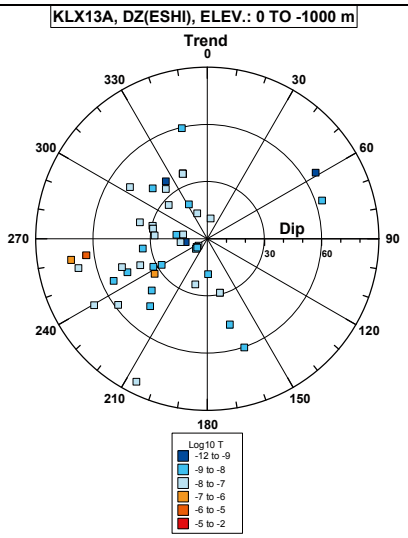

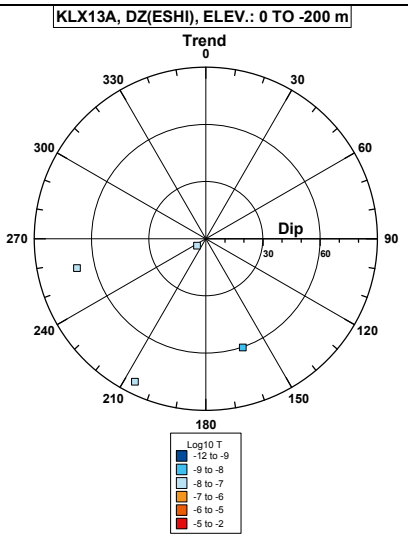

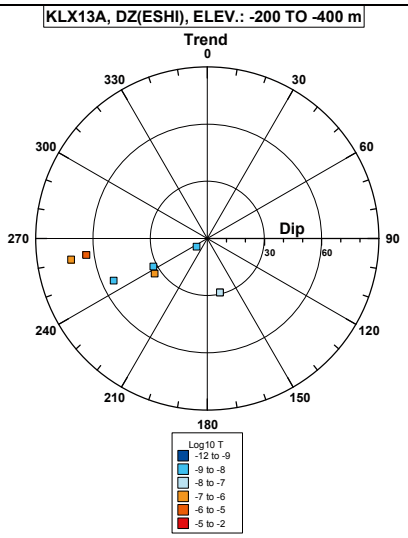

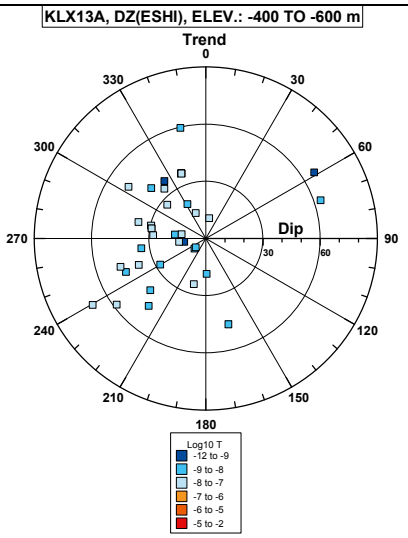

Borehole KLX14A.

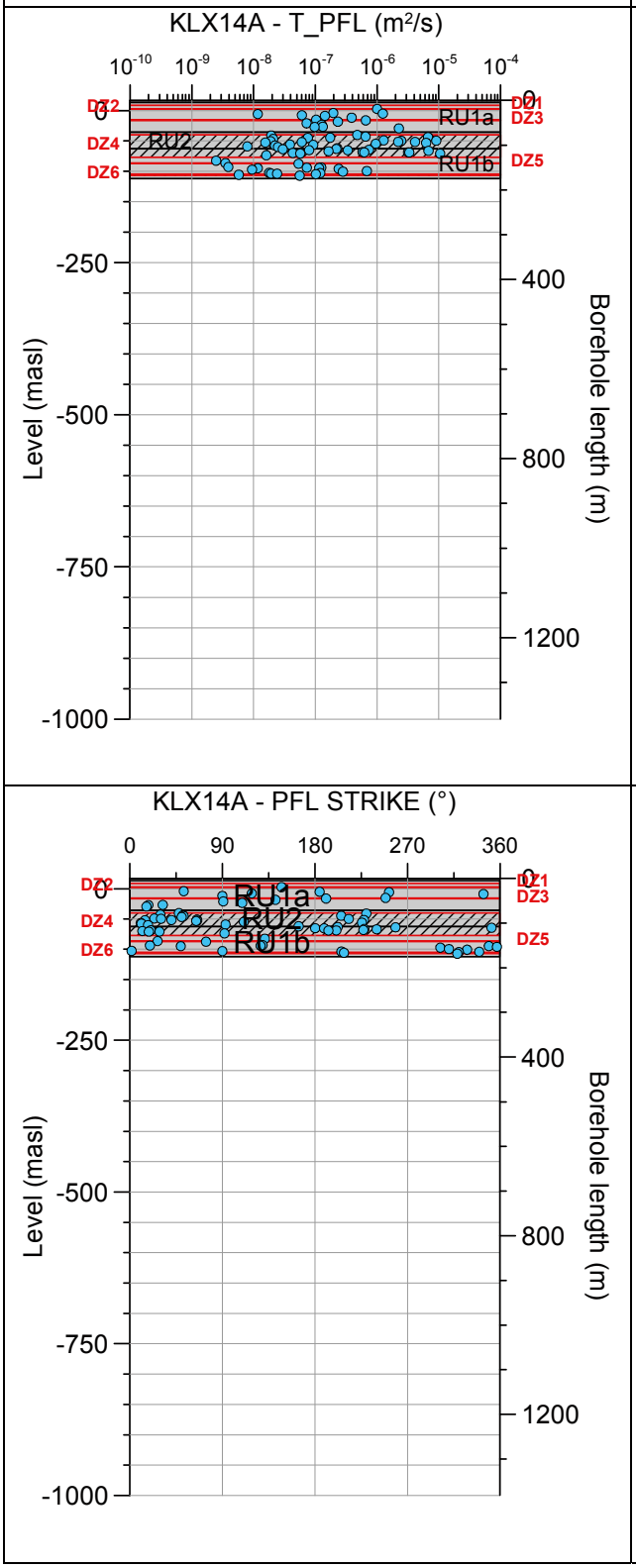

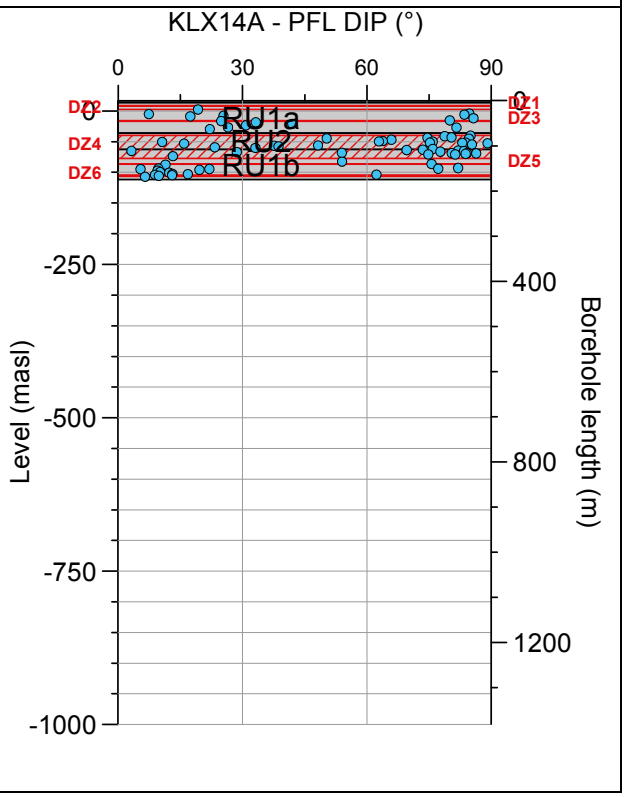

Comment:

Borehole KLX14A. Poles for PFL-f feature planes outside deformation zones (ESHI).

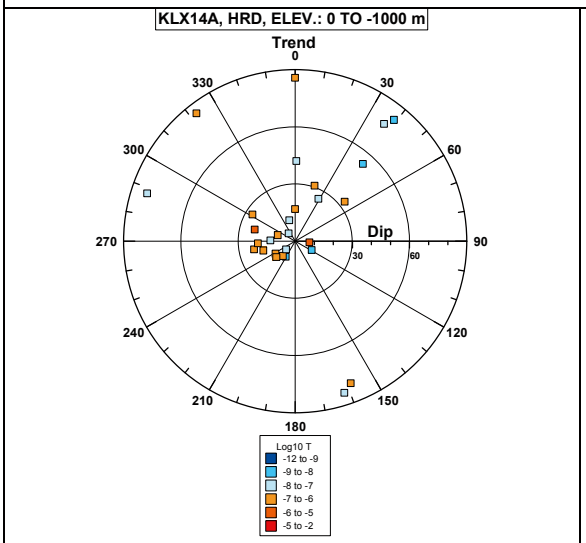

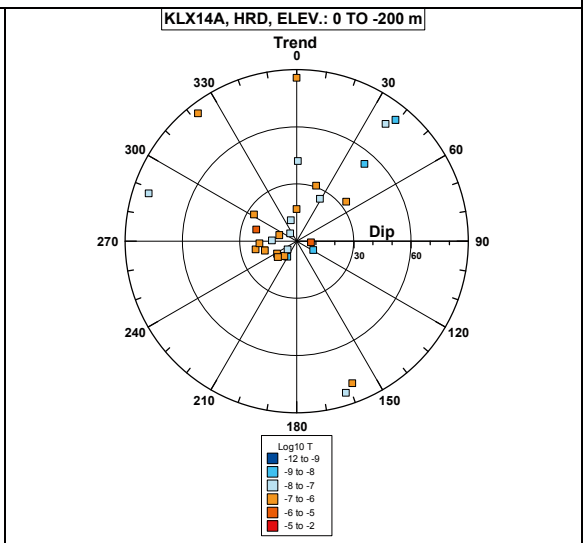

Borehole KLX14A. Poles for PFL-f feature planes in deformation zones (ESHI).

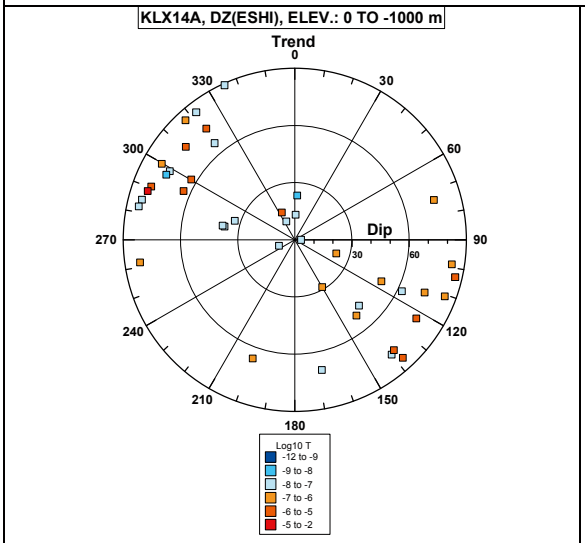

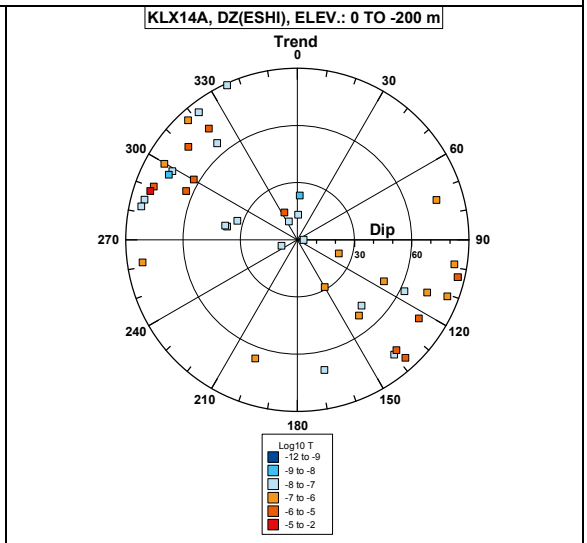

Borehole KLX15A.

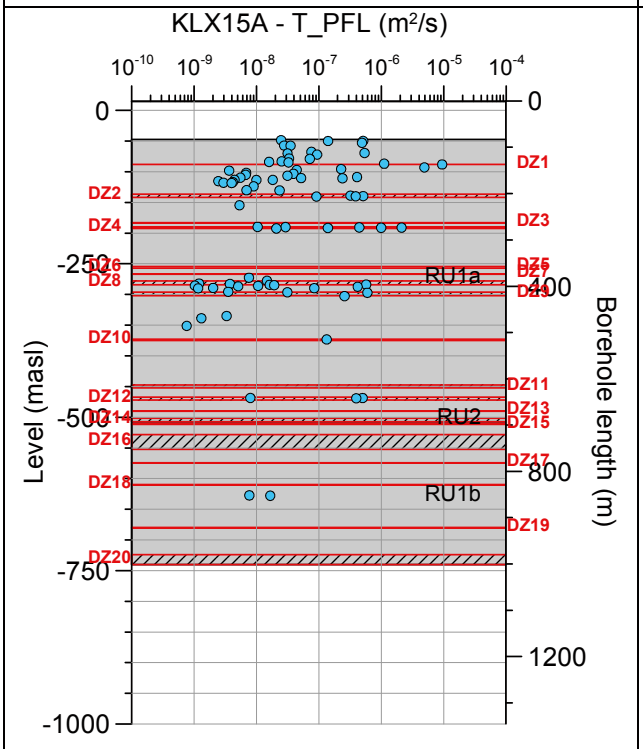

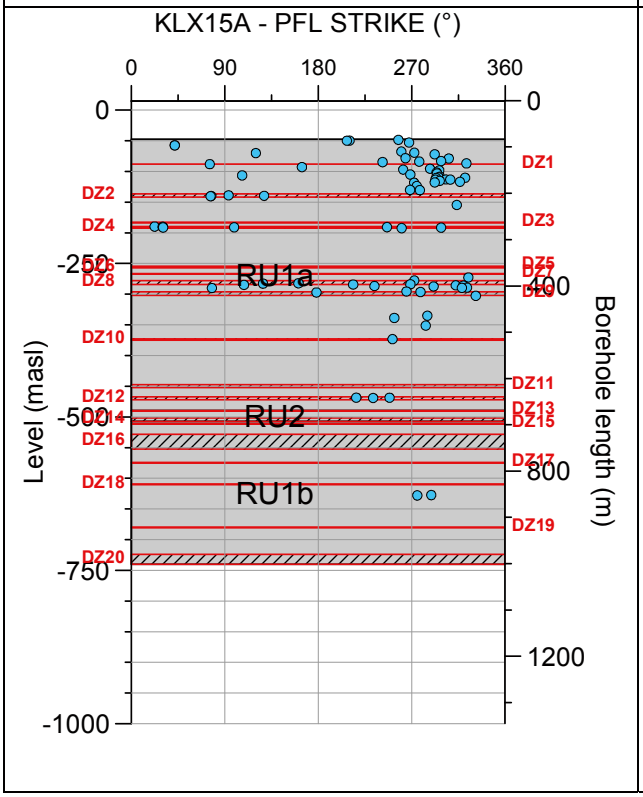

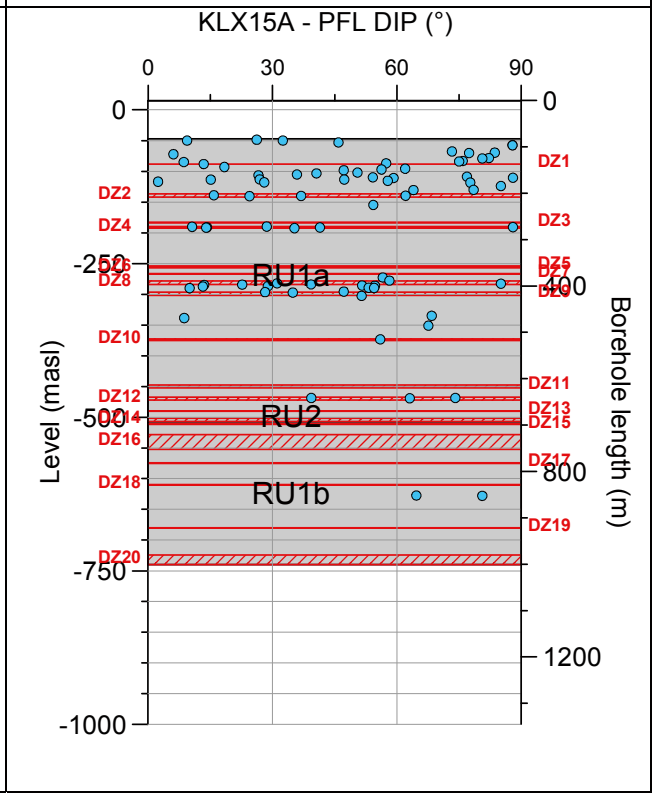

Comment:

Borehole KLX15A. Poles for PFL-f feature planes outside deformation zones (ESHI).

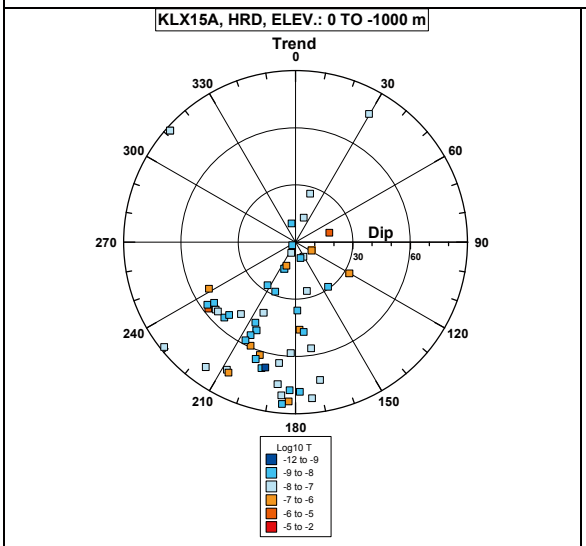

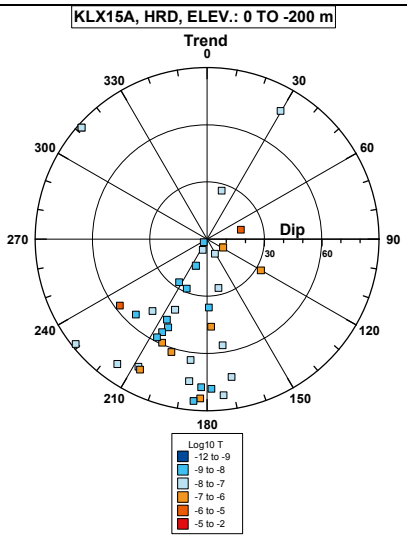

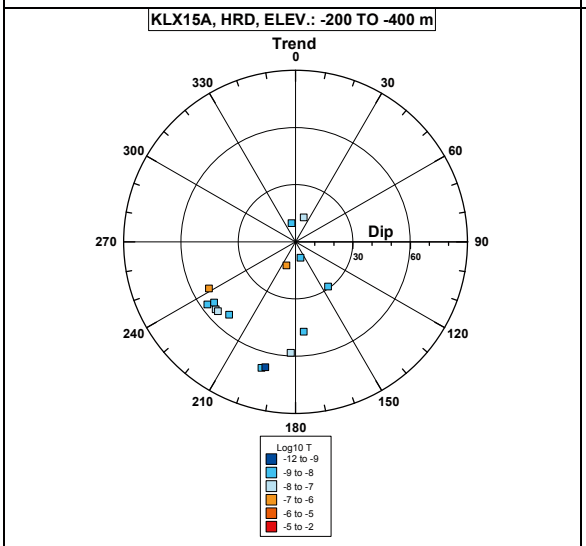

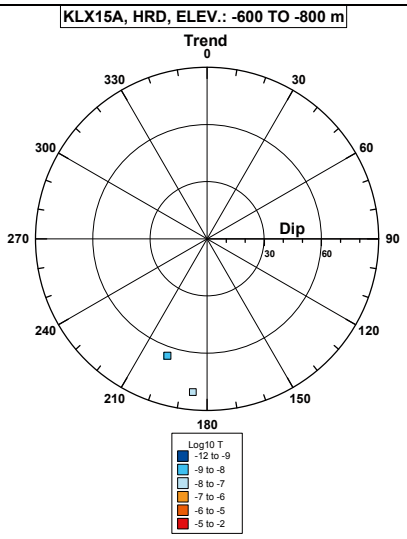

Borehole KLX15A. Poles for PFL-f feature planes in deformation zones (ESHI).

KLX15A, DZ(ESHI), ELEV.: 0 TO -1000 m

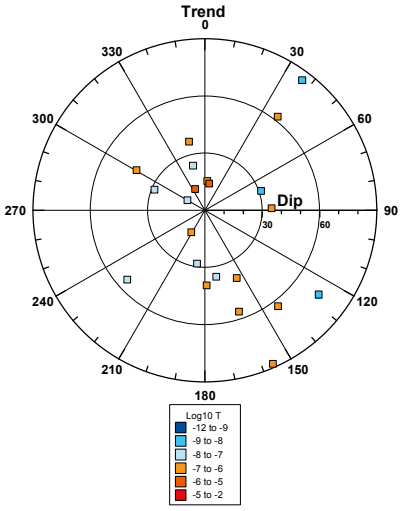

KLX15A, DZ(ESHI), ELEV.: 0 TO -200 m

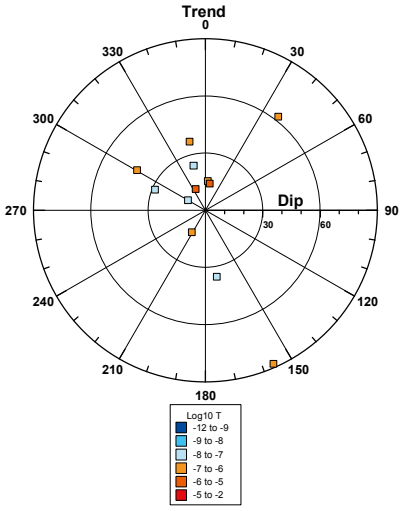

KLX15A, DZ(ESHI), ELEV.: -200 TO -400 m

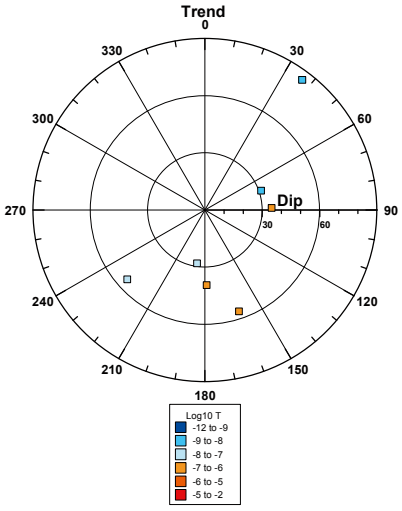

KLX15A, DZ(ESHI), ELEV.: -400 TO -600 m

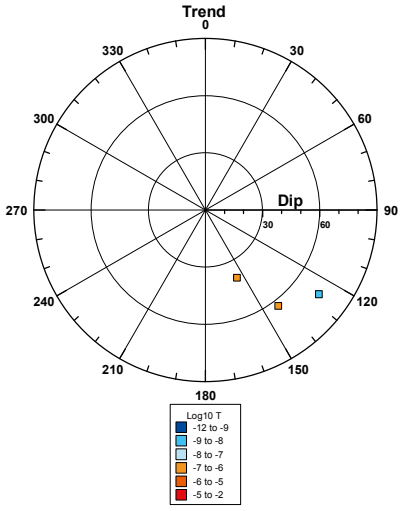

Borehole KLX16A.

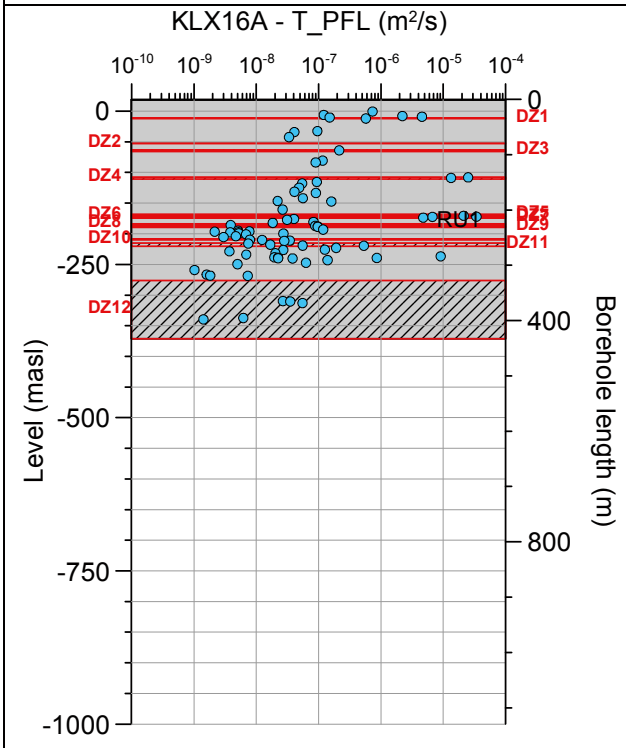

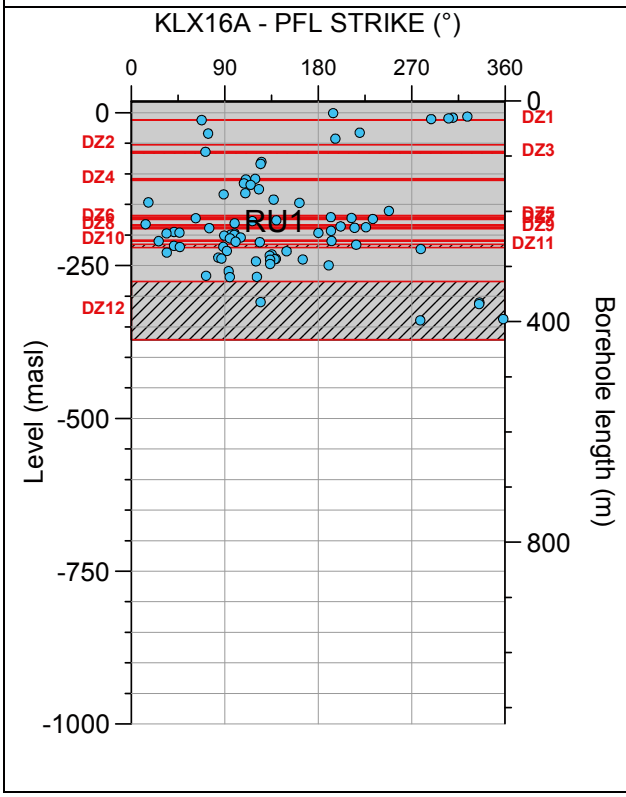

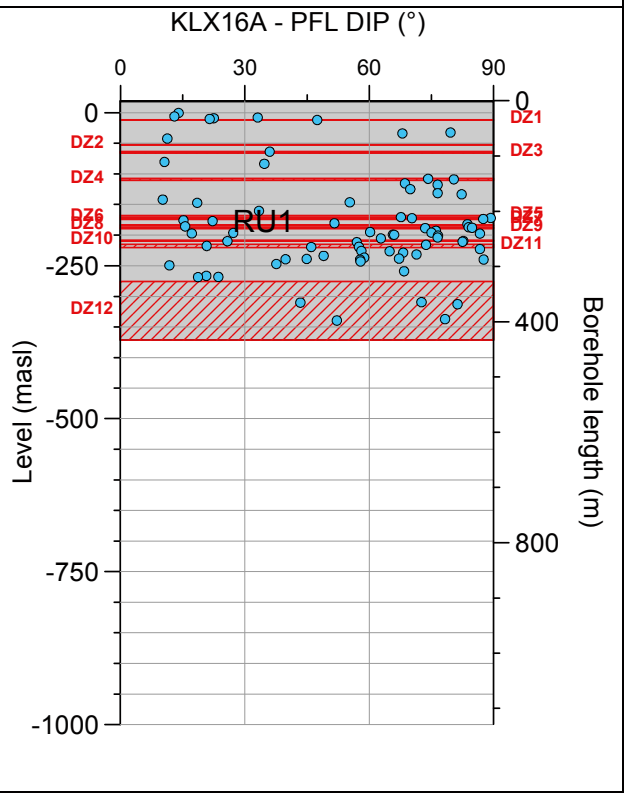

Comment:

Borehole KLX16A. Poles for PFL-f feature planes outside deformation zones (ESHI).

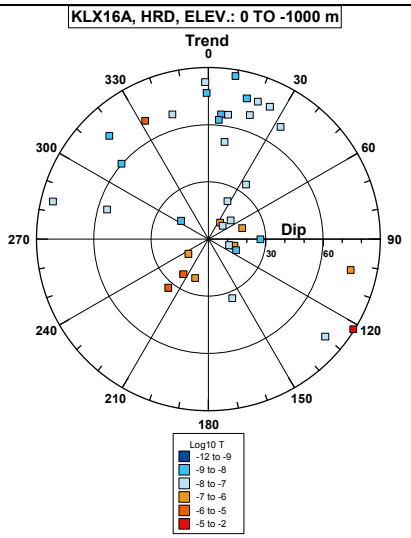

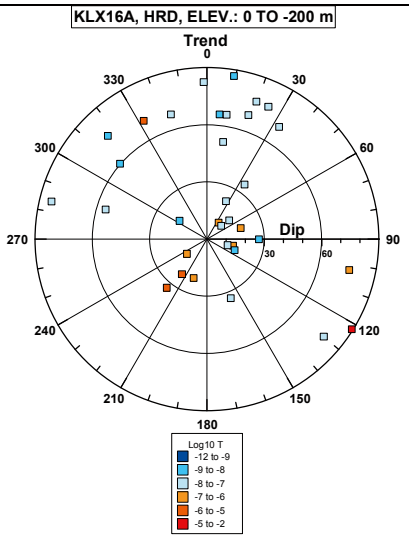

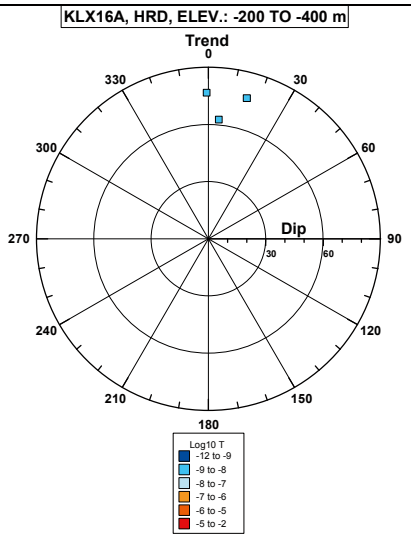

Borehole KLX16A. Poles for PFL-f feature planes in deformation zones (ESHI).

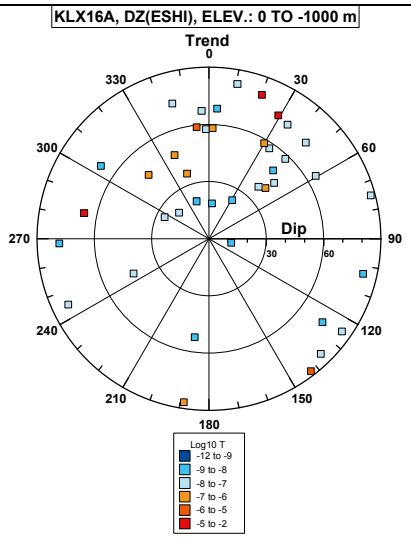

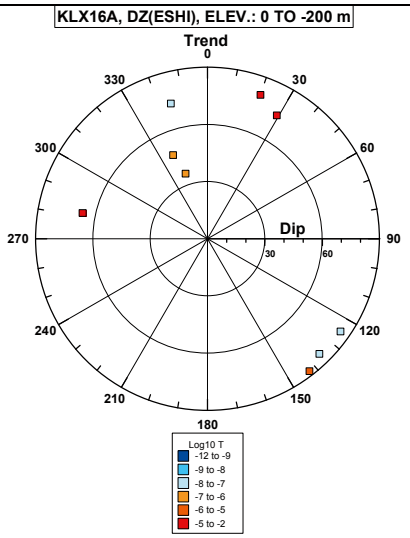

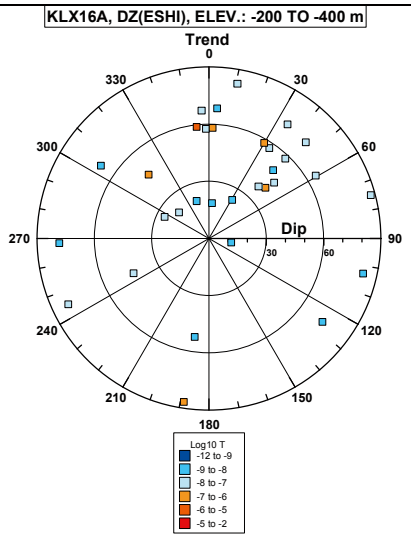

Borehole KLX17A.

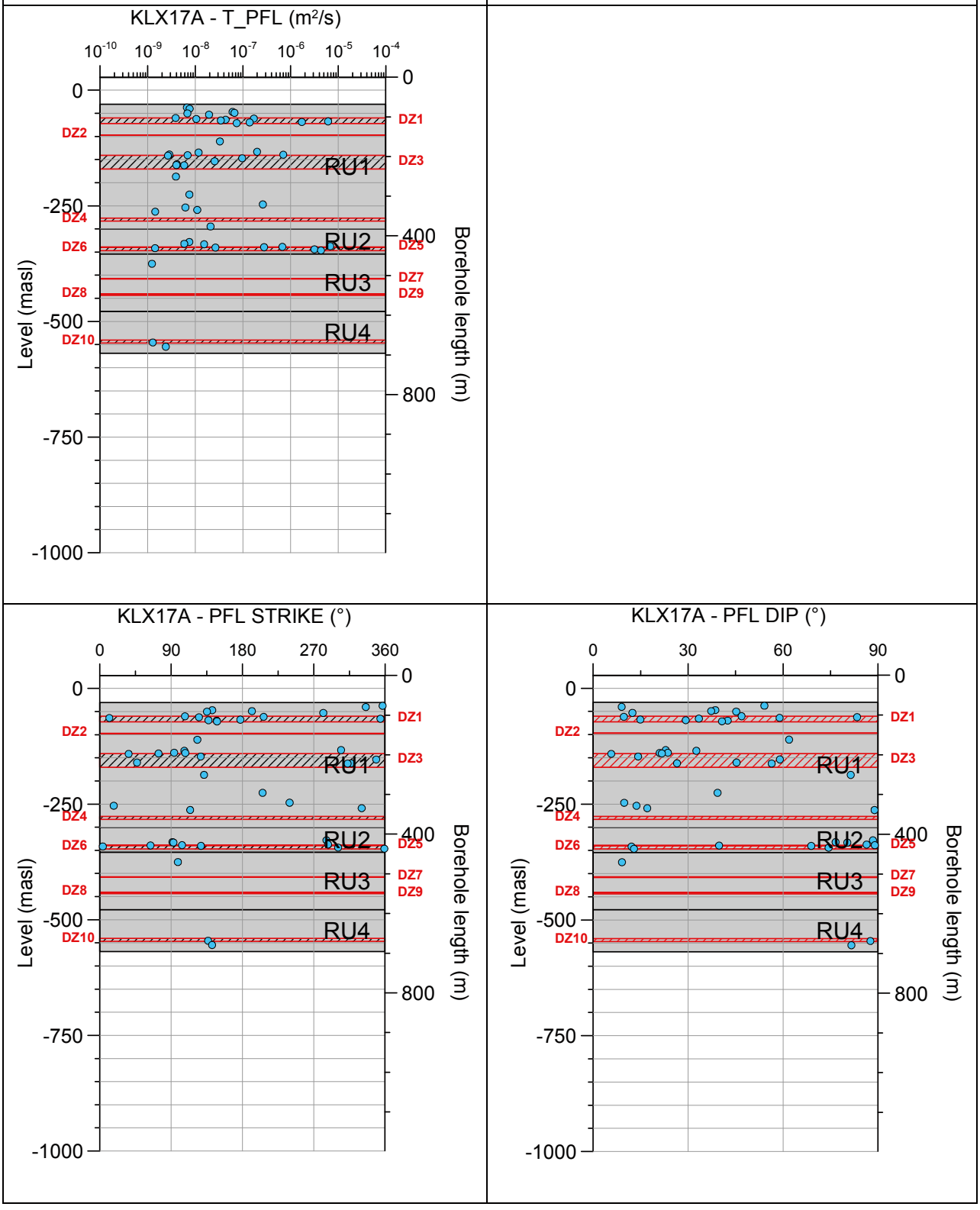

Comment:

Borehole KLX17A. Poles for PFL-f feature planes outside deformation zones (ESHI).

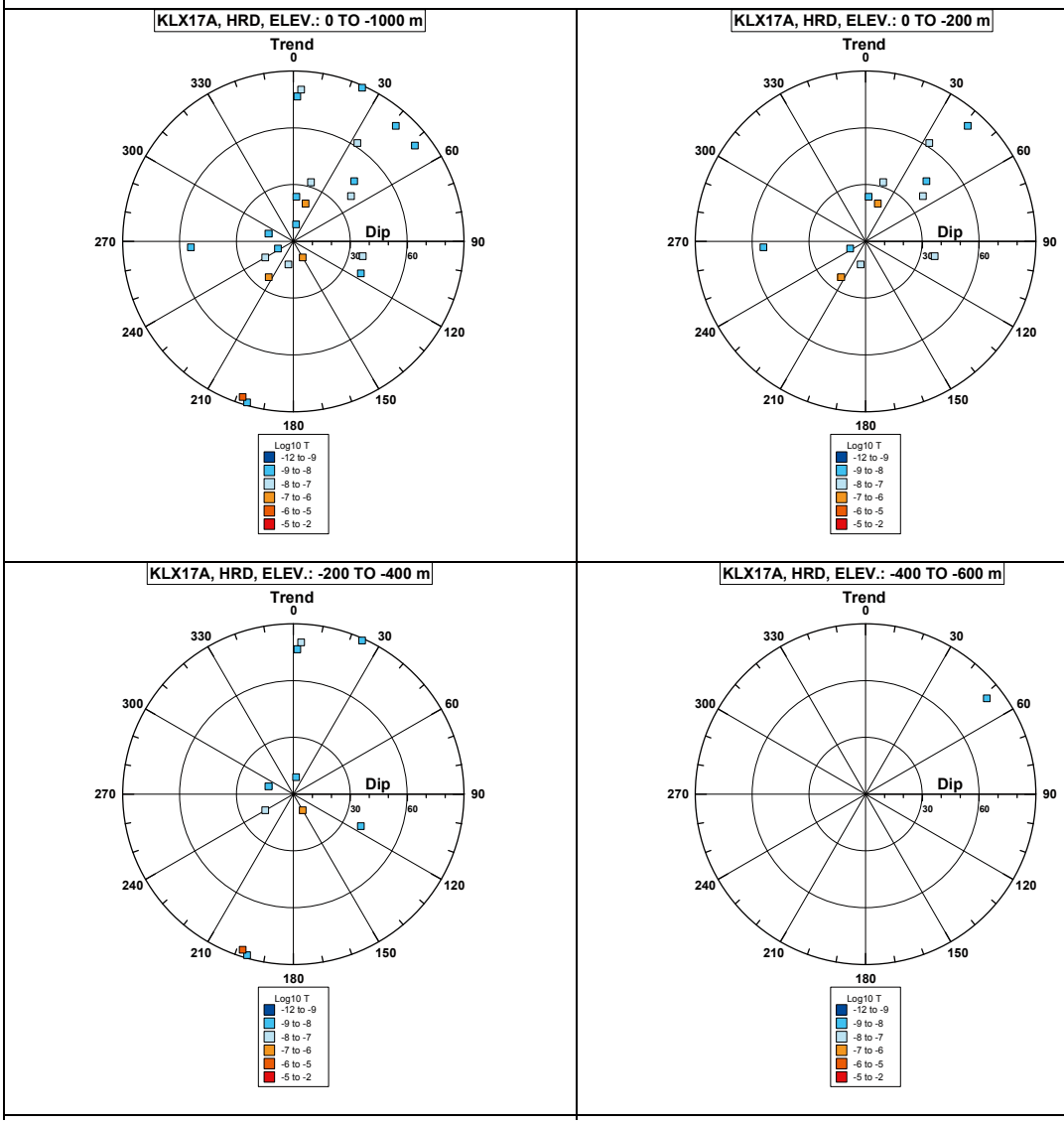

Borehole KLX17A. Poles for PFL-f feature planes in deformation zones (ESHI).

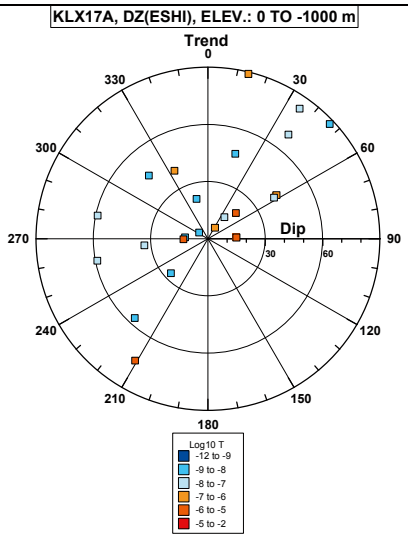

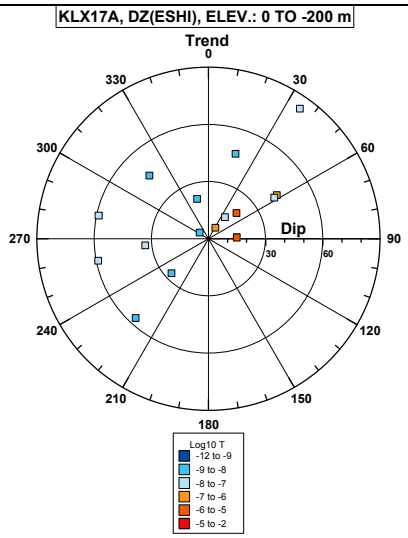

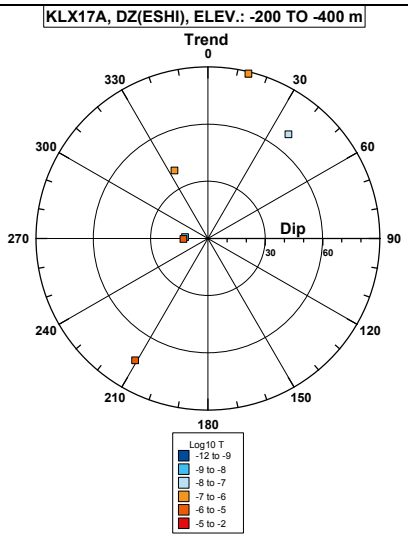

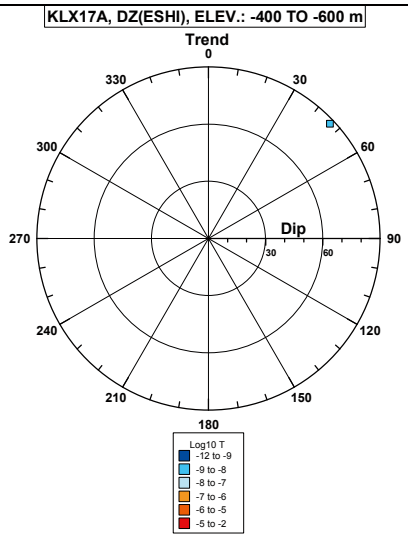

Borehole KLX18A.

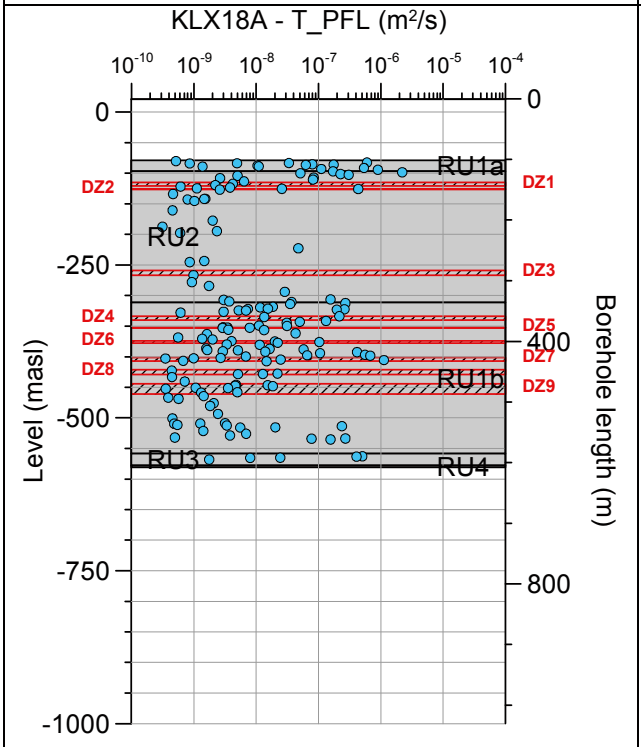

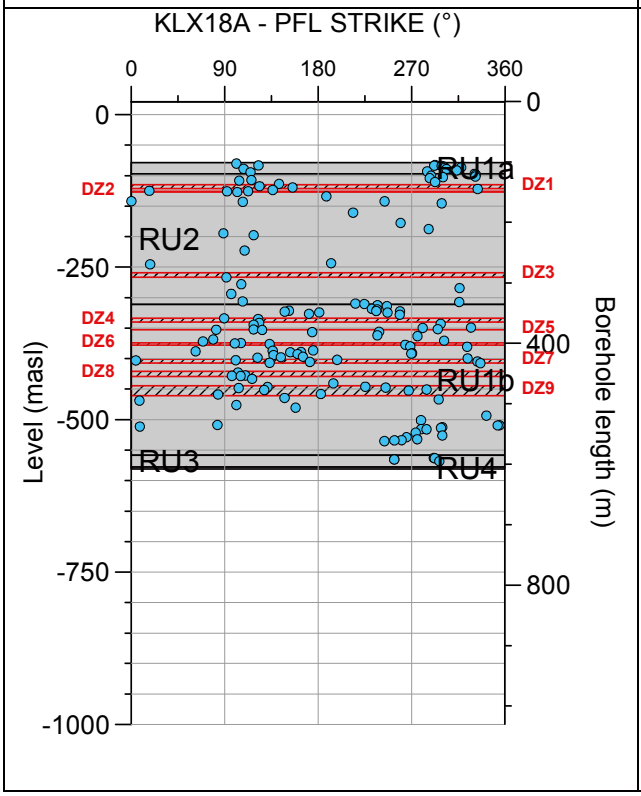

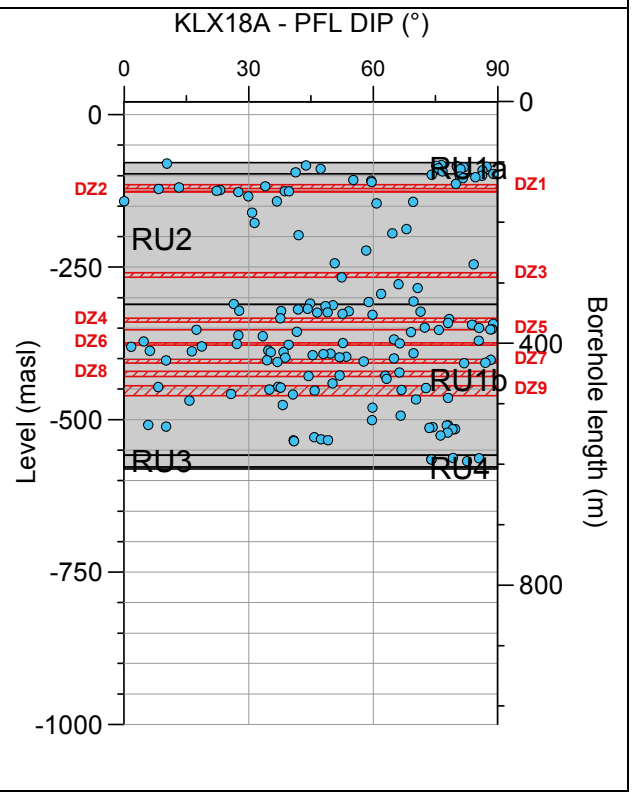

Comment:

Borehole KLX18A. Poles for PFL-f feature planes outside deformation zones (ESHI).

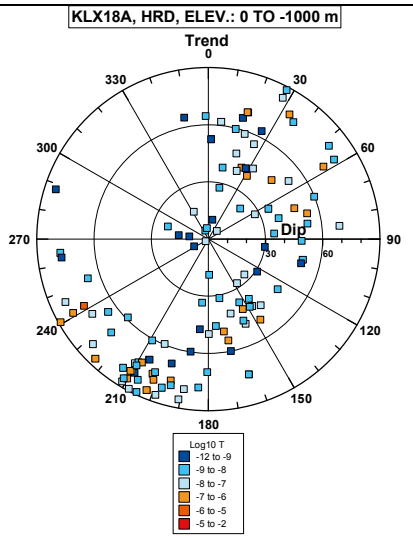

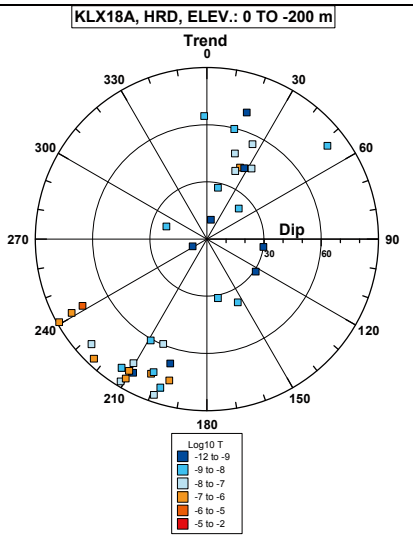

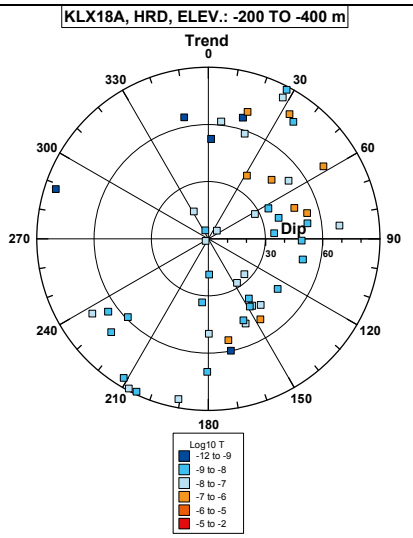

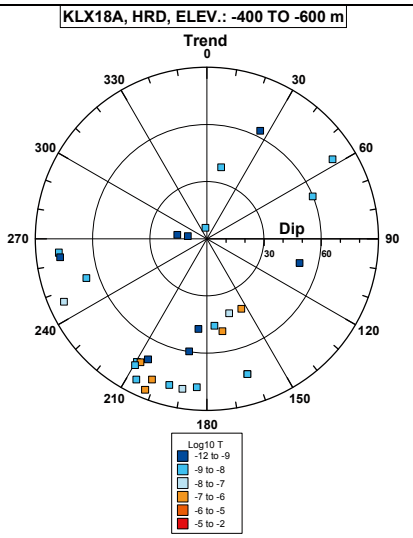

Borehole KLX18A. Poles for PFL-f feature planes in deformation zones (ESHI).

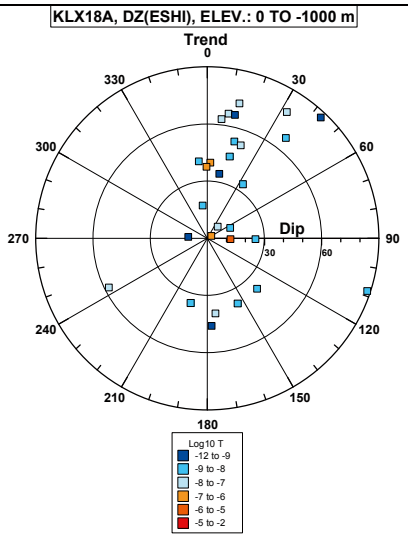

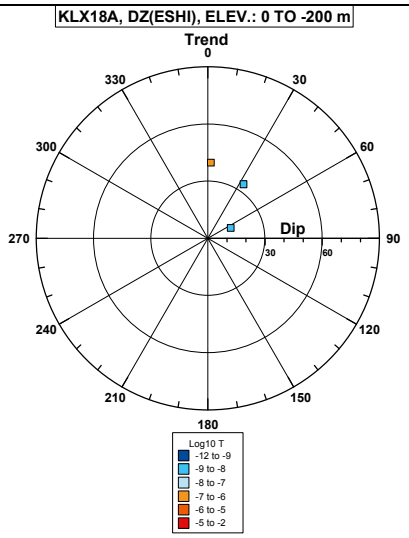

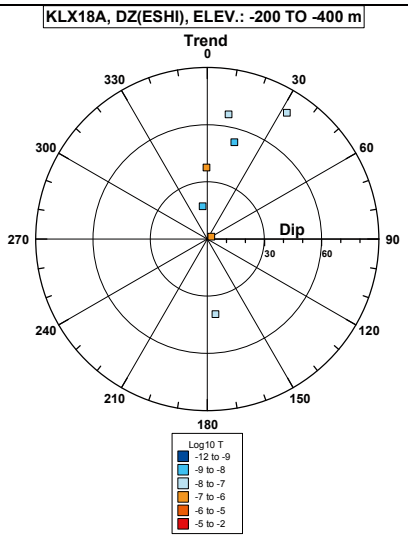

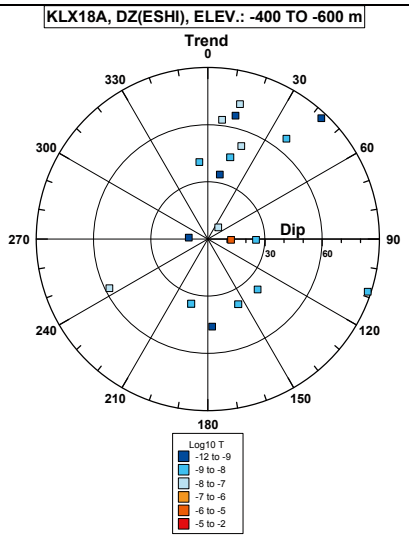

Borehole KLX19A.

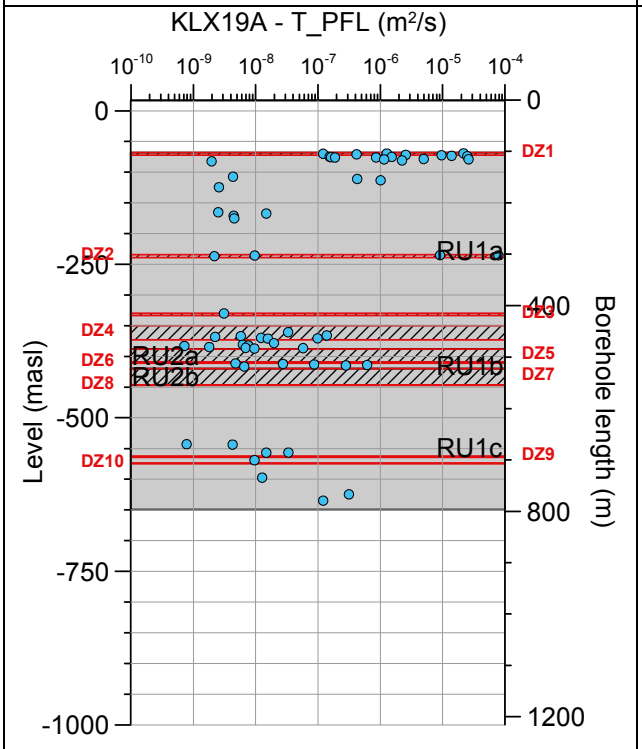

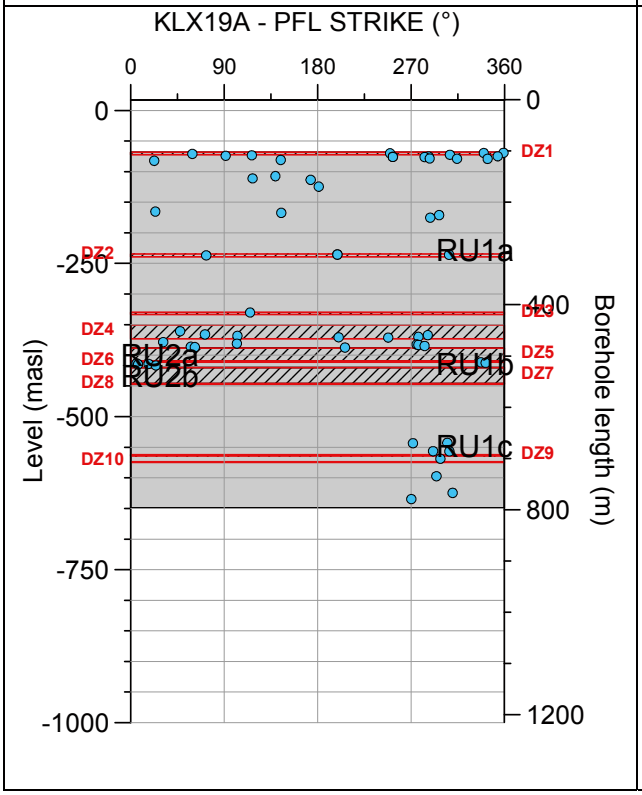

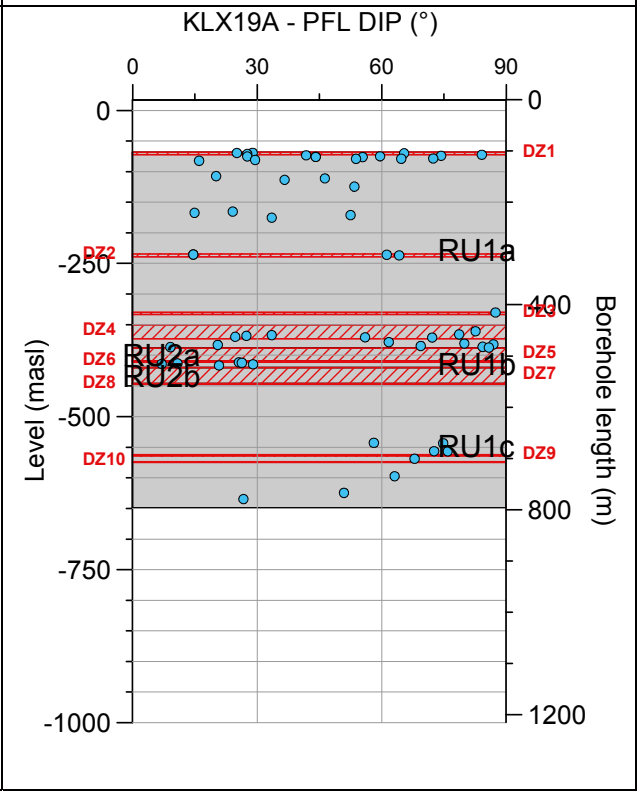

Comment:

Borehole KLX19A. Poles for PFL-f feature planes outside deformation zones (ESHI).

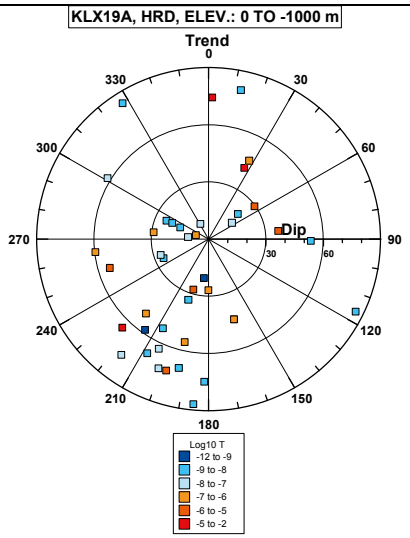

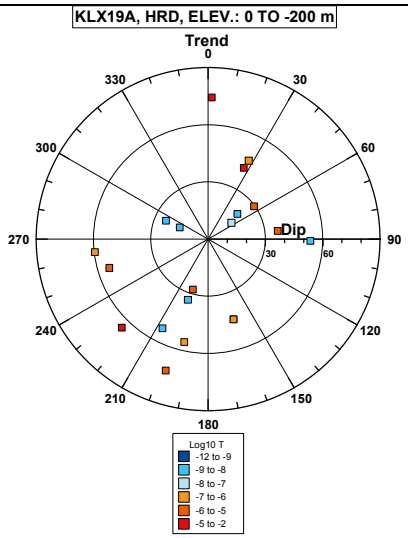

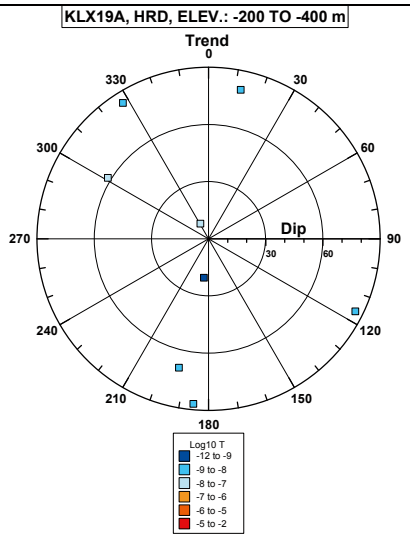

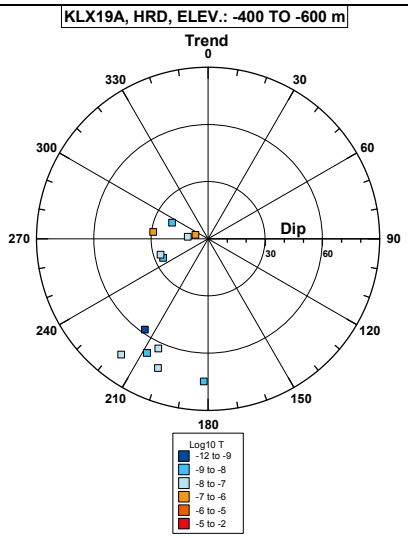

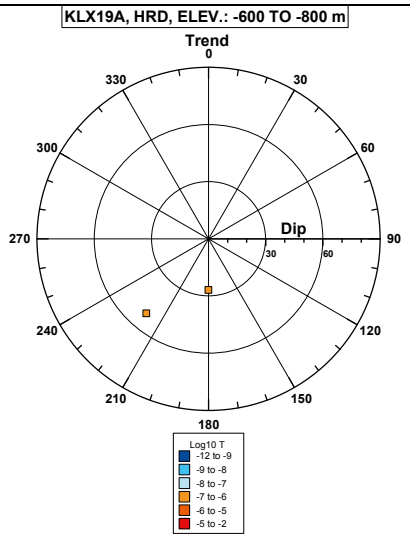

Borehole KLX19A. Poles for PFL-f feature planes in deformation zones (ESHI).

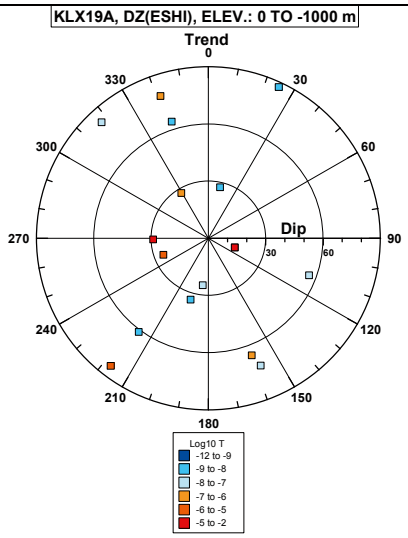

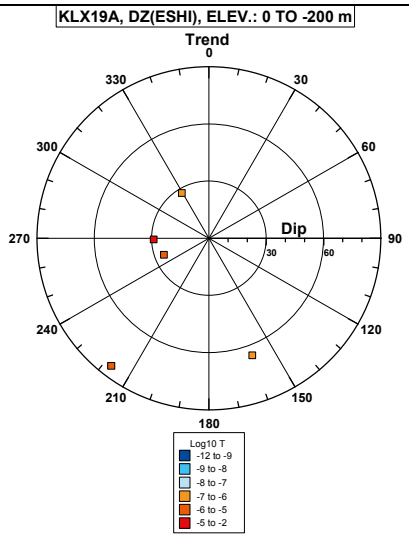

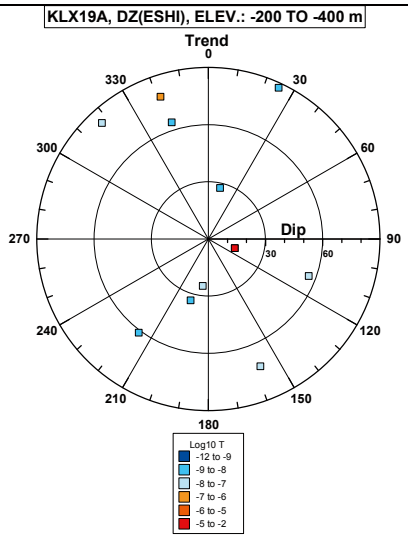

Borehole KLX20A.

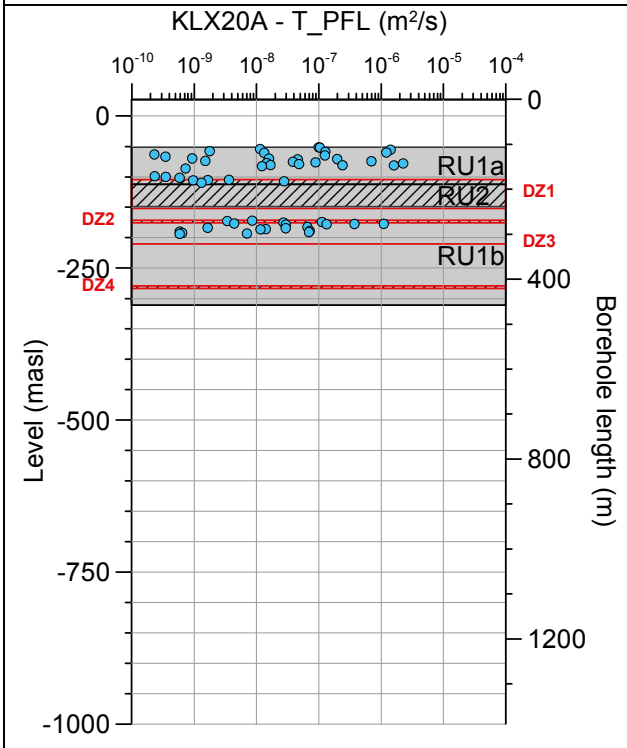

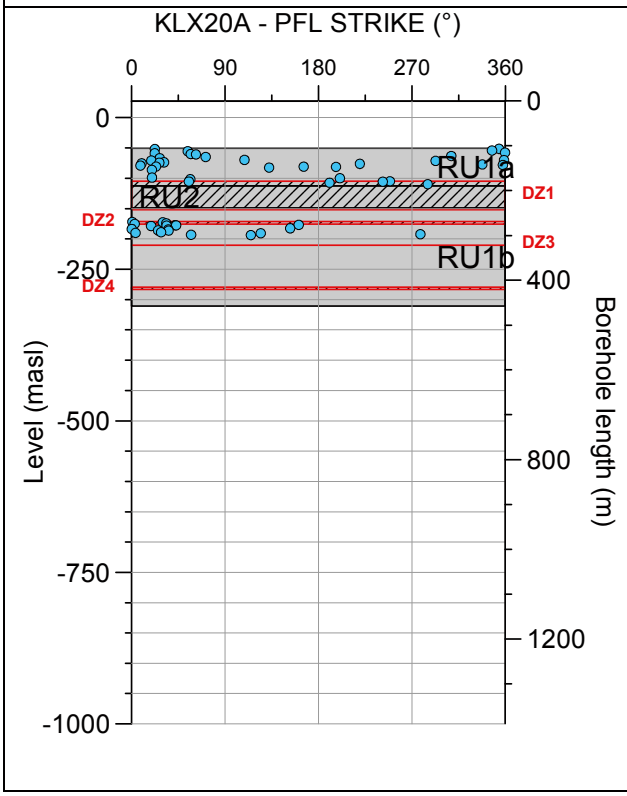

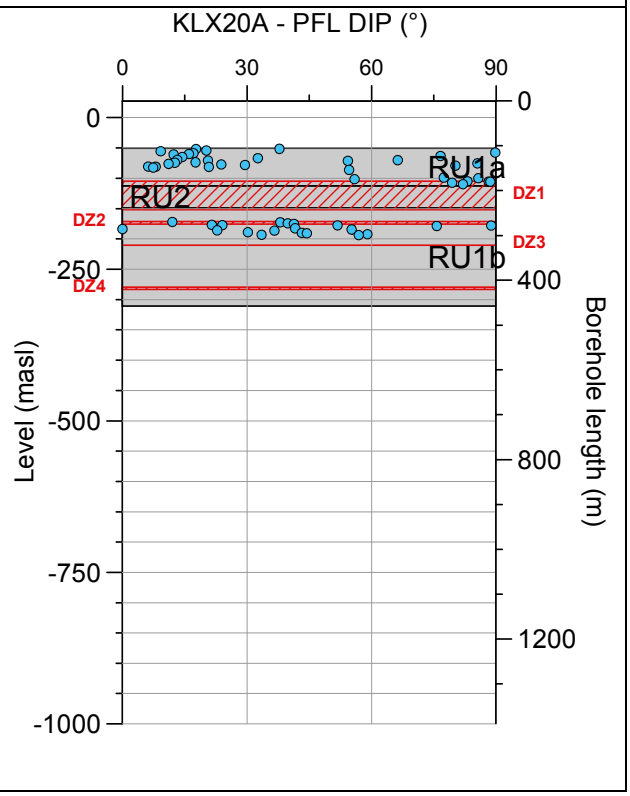

Comment:

Borehole KLX20A. Poles for PFL-f feature planes outside deformation zones (ESHI).

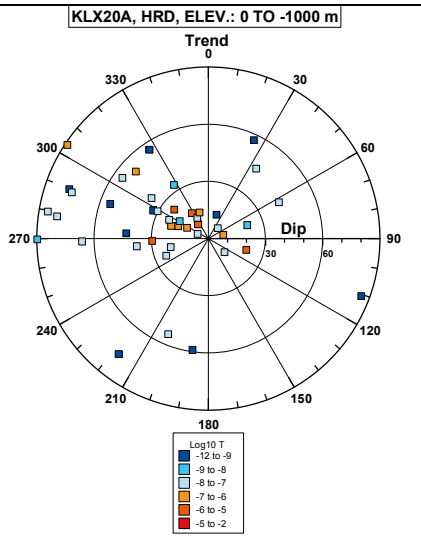

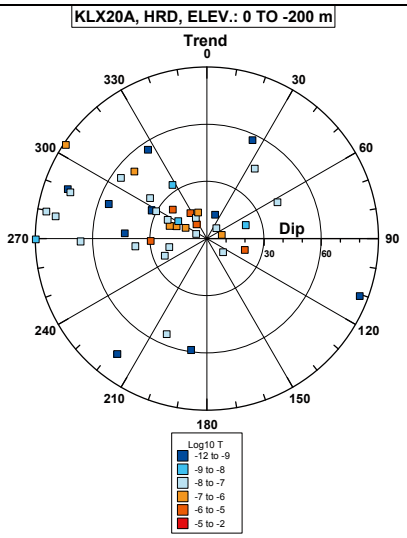

Borehole KLX20A. Poles for PFL-f feature planes in deformation zones (ESHI).

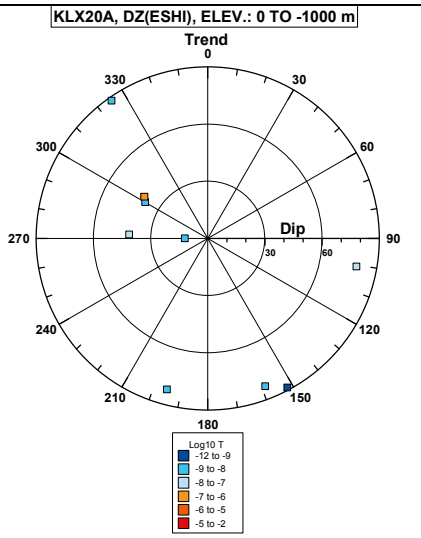

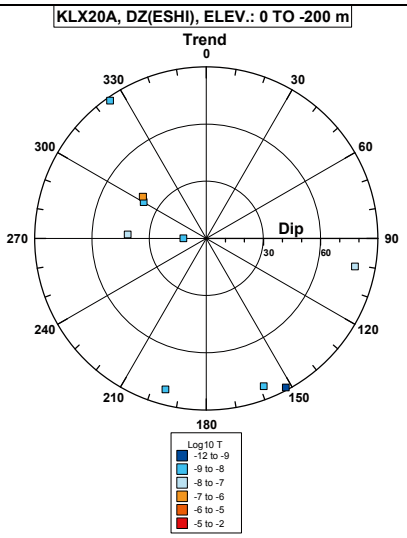

Borehole KLX21B.

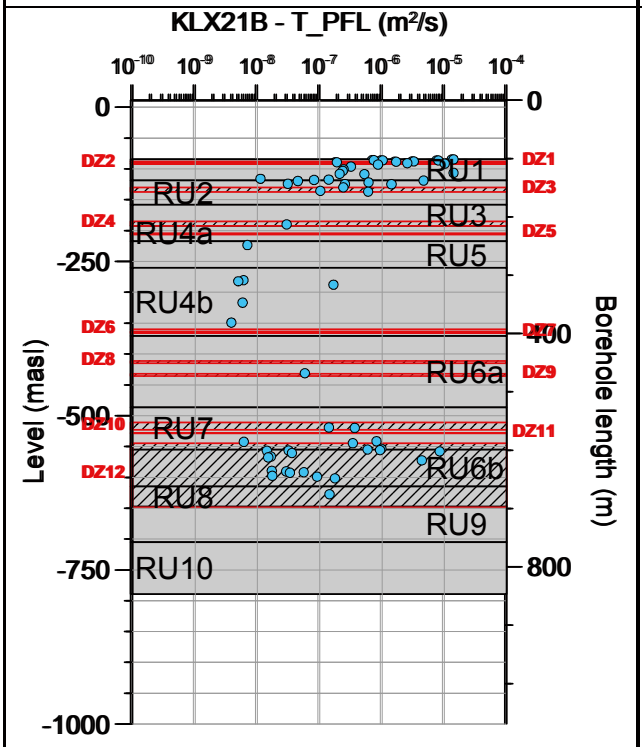

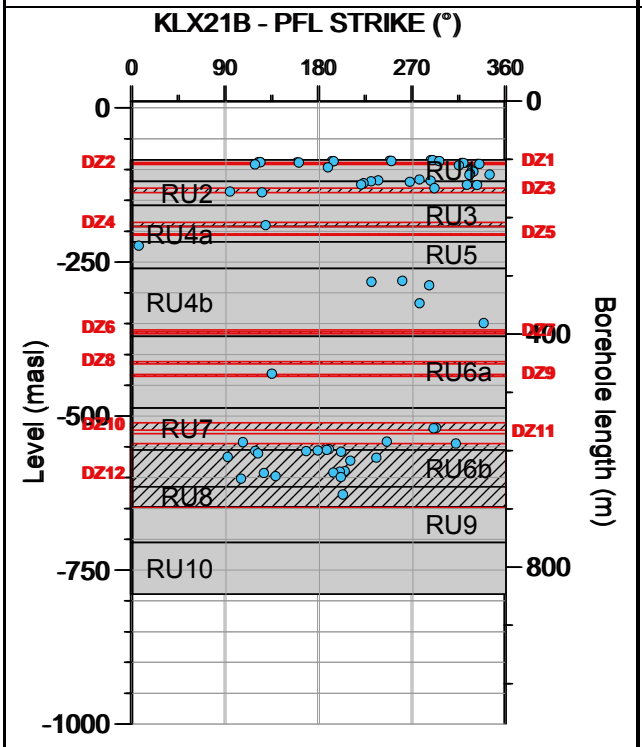

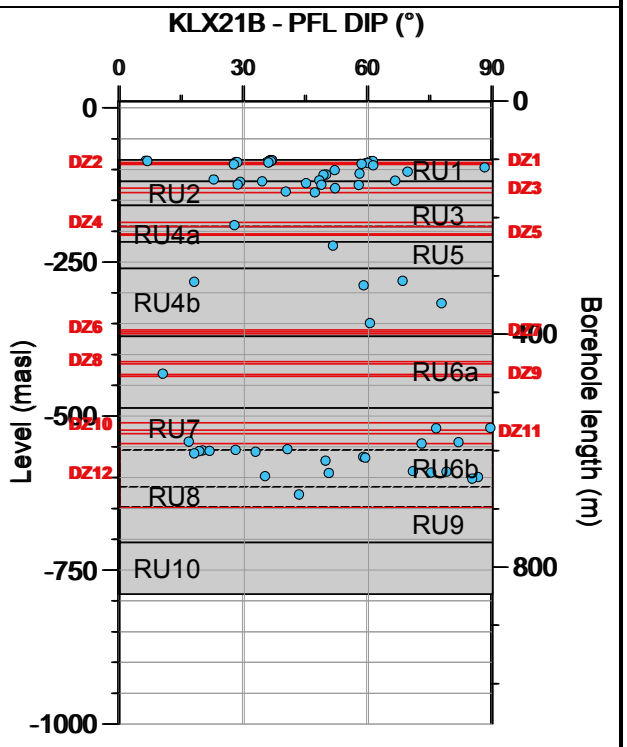

Comment:

Borehole KLX21B. Poles for PFL-f feature planes outside deformation zones (ESHI).

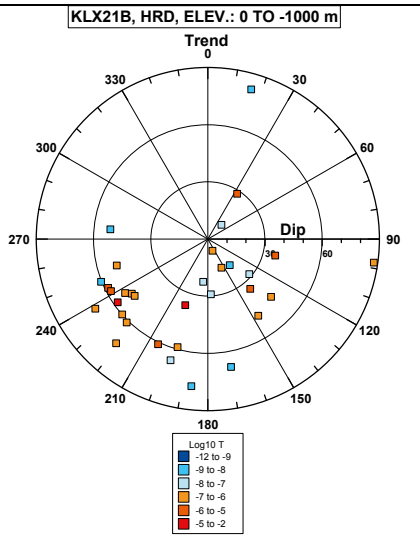

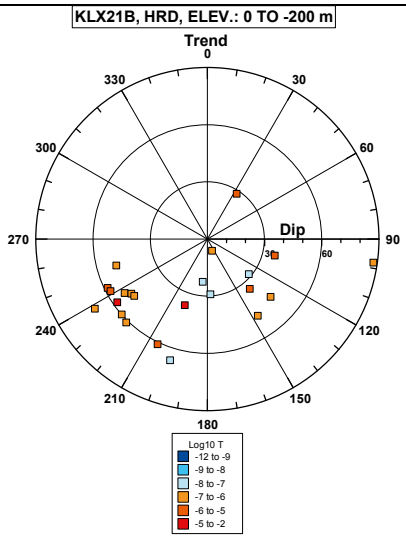

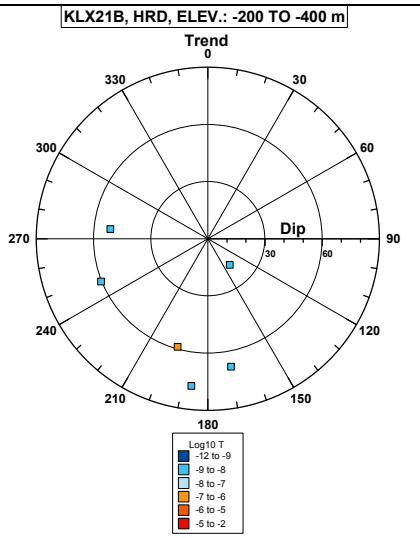

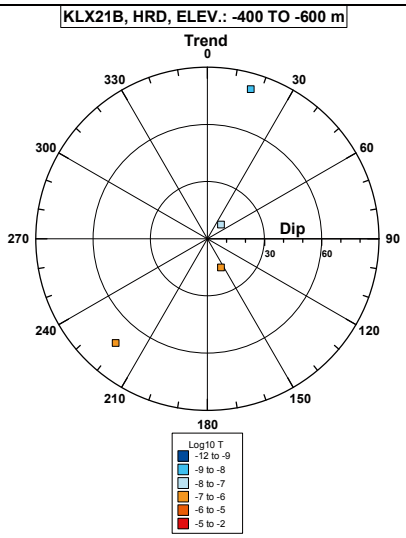

Borehole KLX21B. Poles for PFL-f feature planes in deformation zones (ESHI).

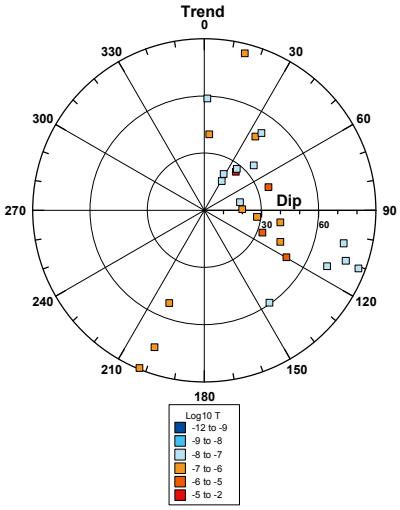

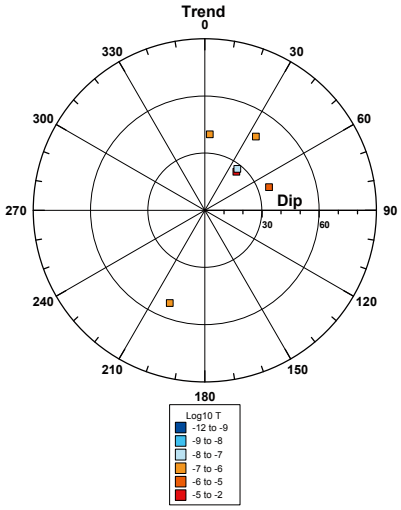

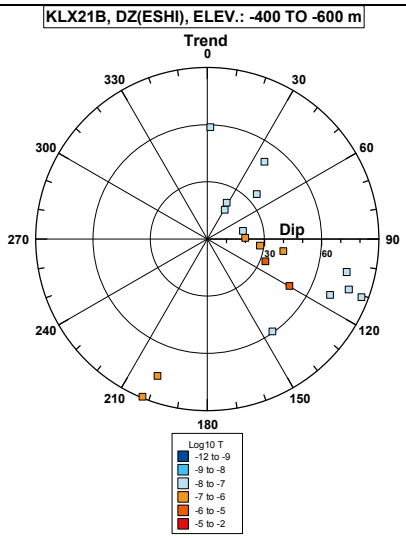

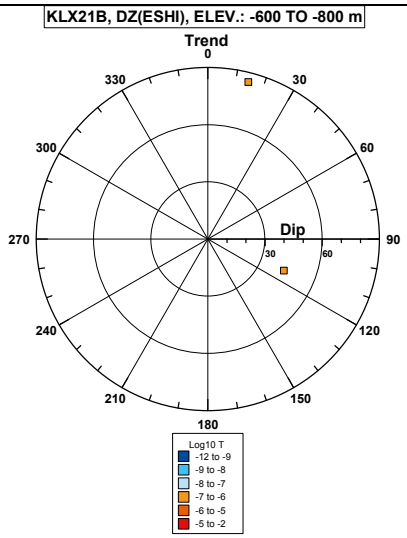

Borehole KLX22A.

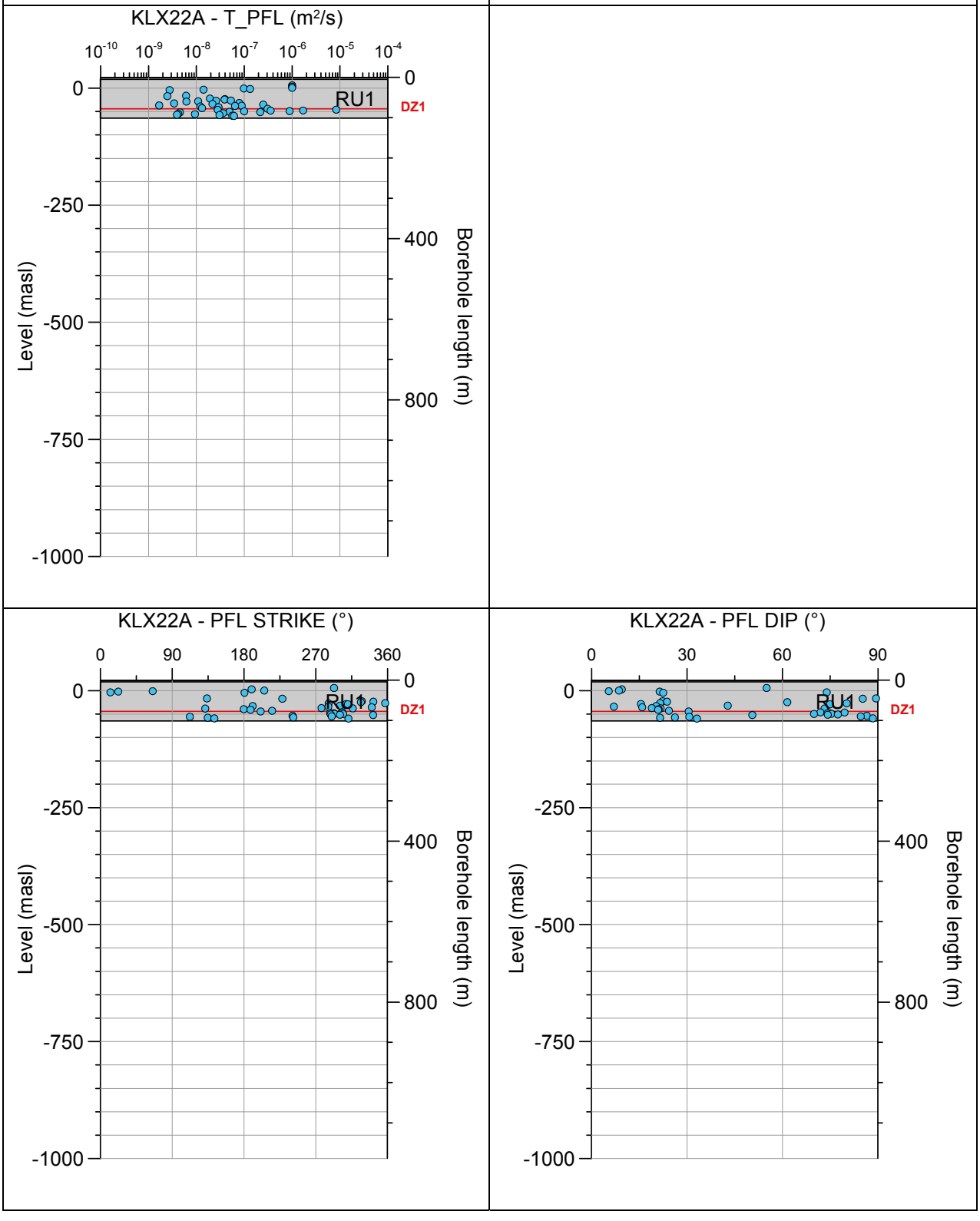

Comment:

Borehole KLX22A. Poles for PFL-f feature planes outside deformation zones (ESHI).

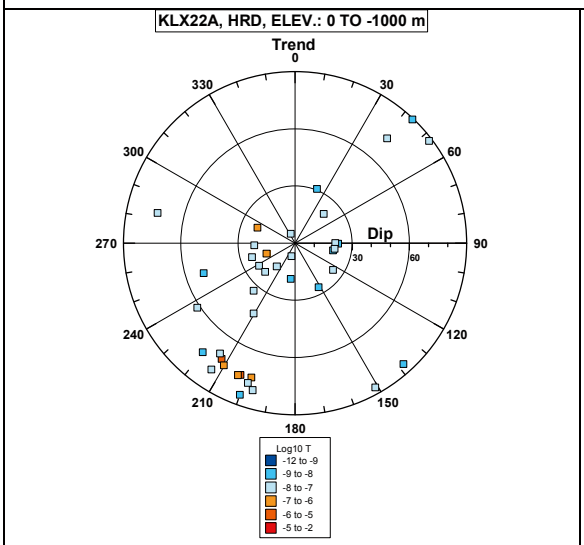

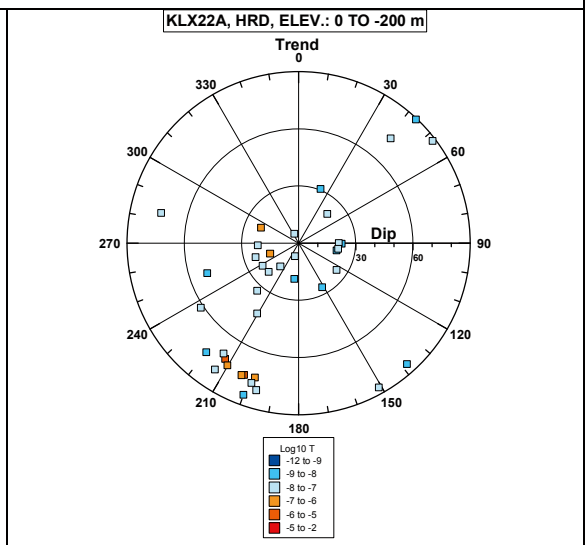

Borehole KLX22A. Poles for PFL-f feature planes in deformation zones (ESHI).

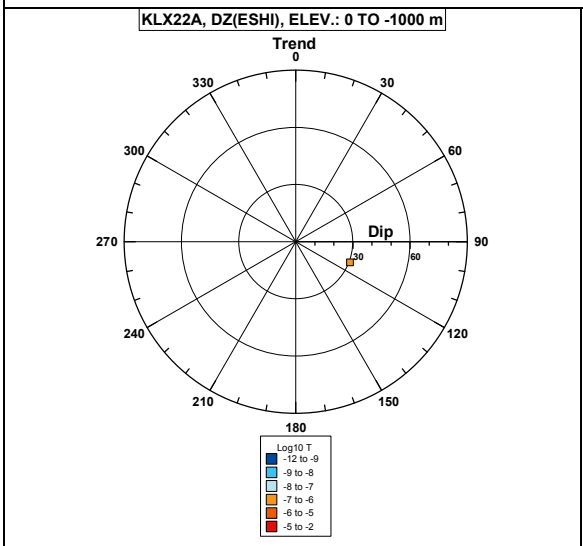

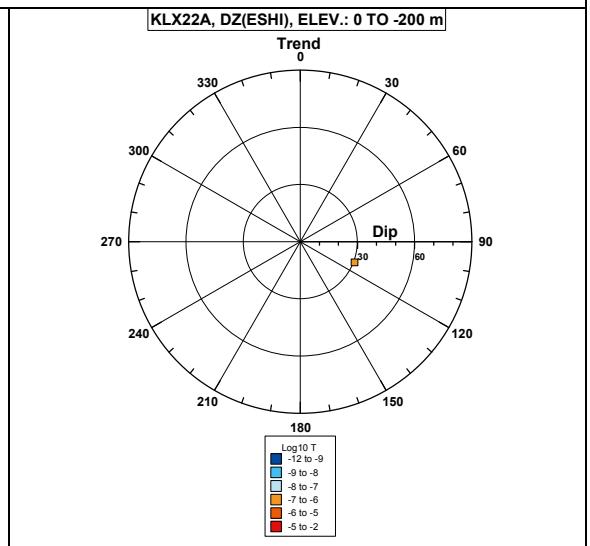

Borehole KLX22B.

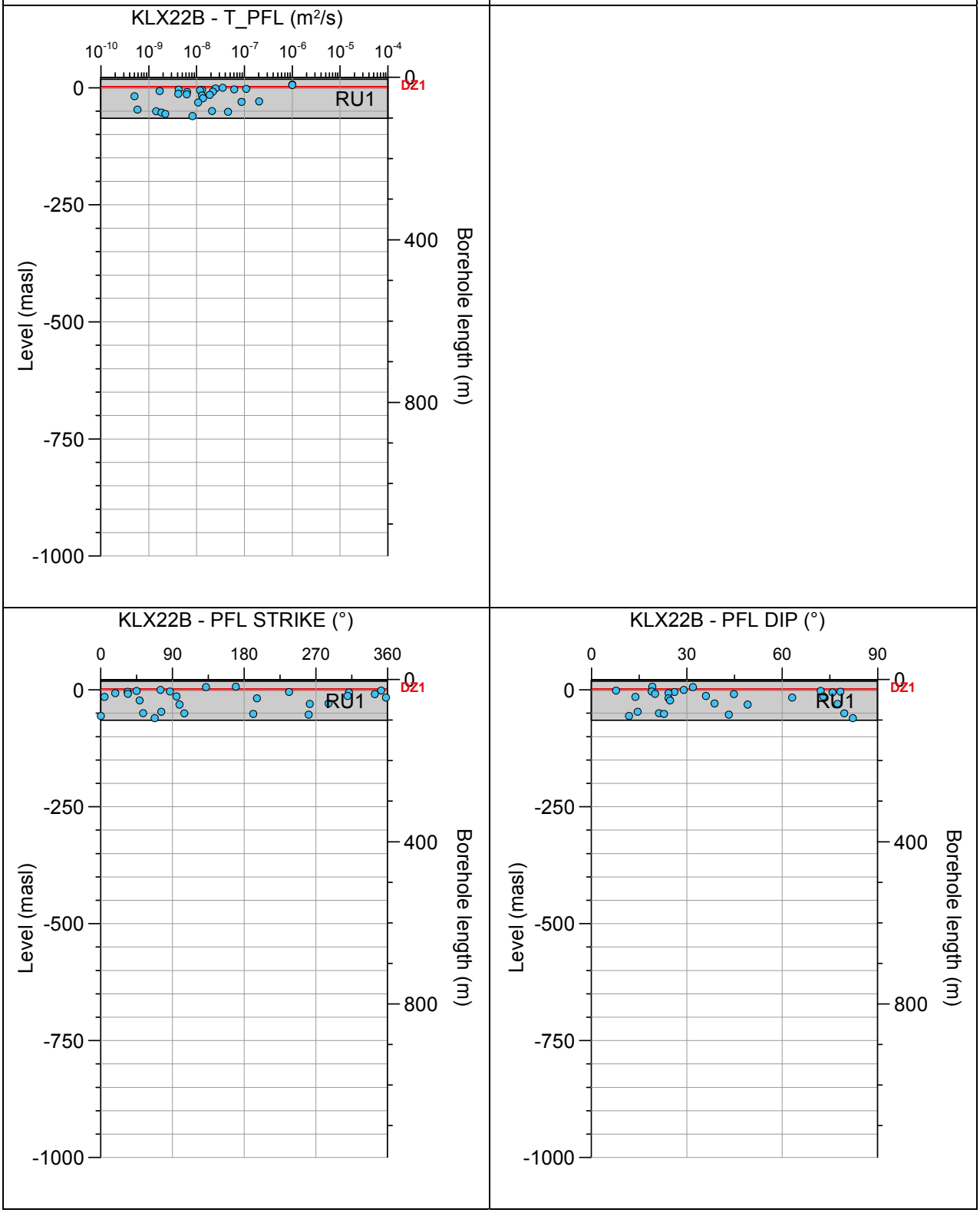

Comment:

Borehole KLX22B. Poles for PFL-f feature planes outside deformation zones (ESHI).

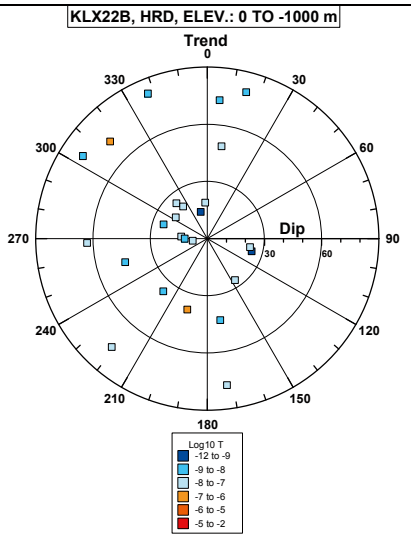

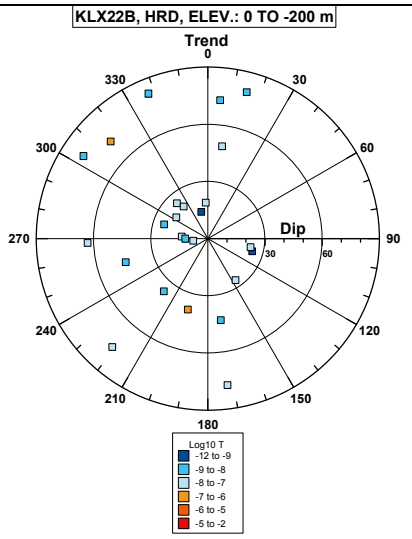

Borehole KLX22B. Poles for PFL-f feature planes in deformation zones (ESHI).

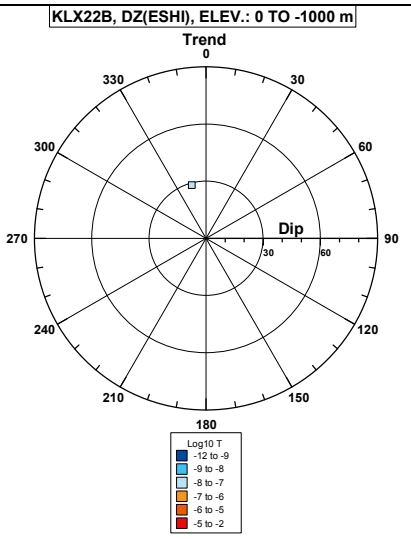

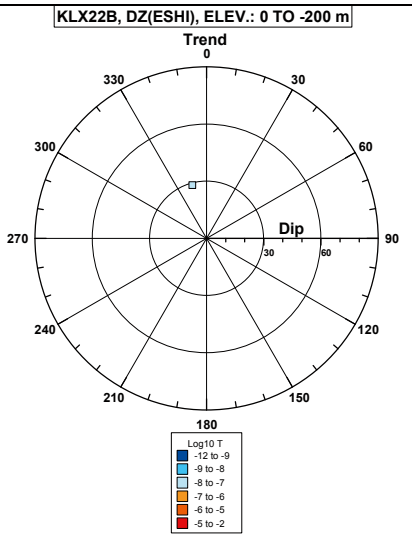

Borehole KLX23A.

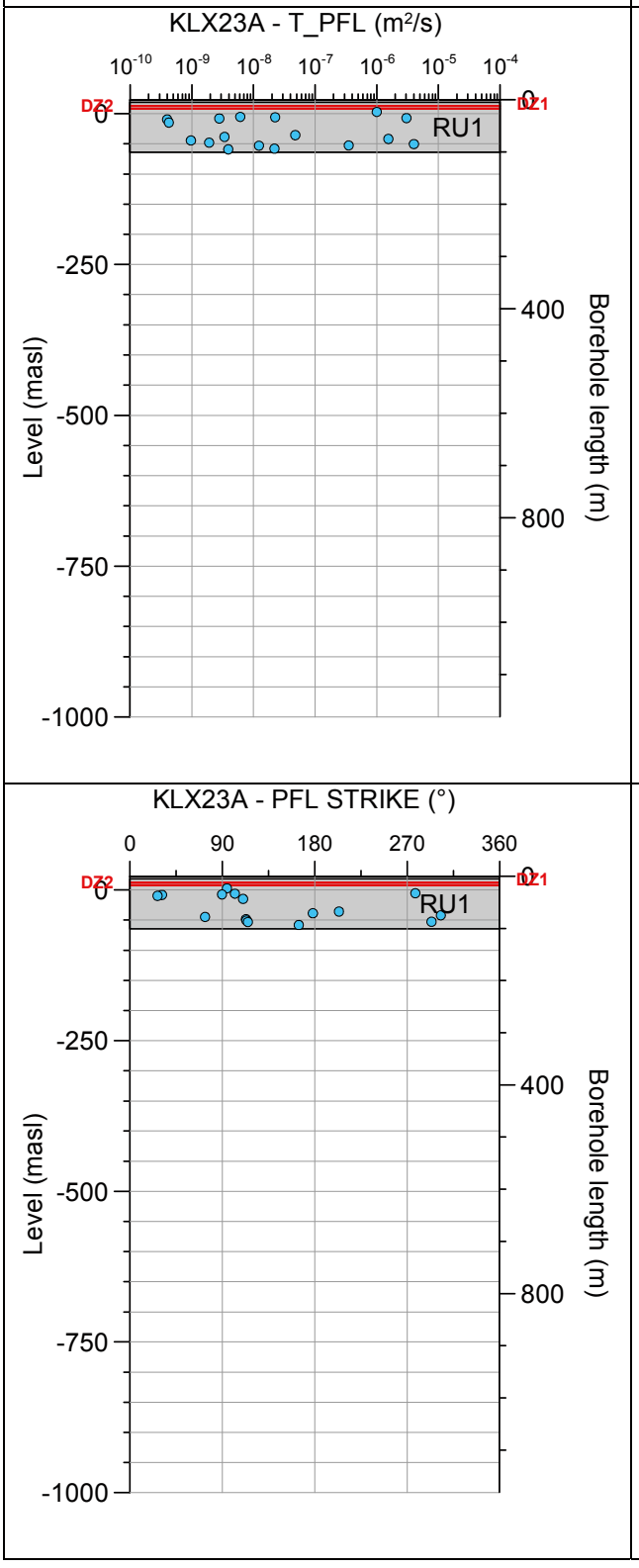

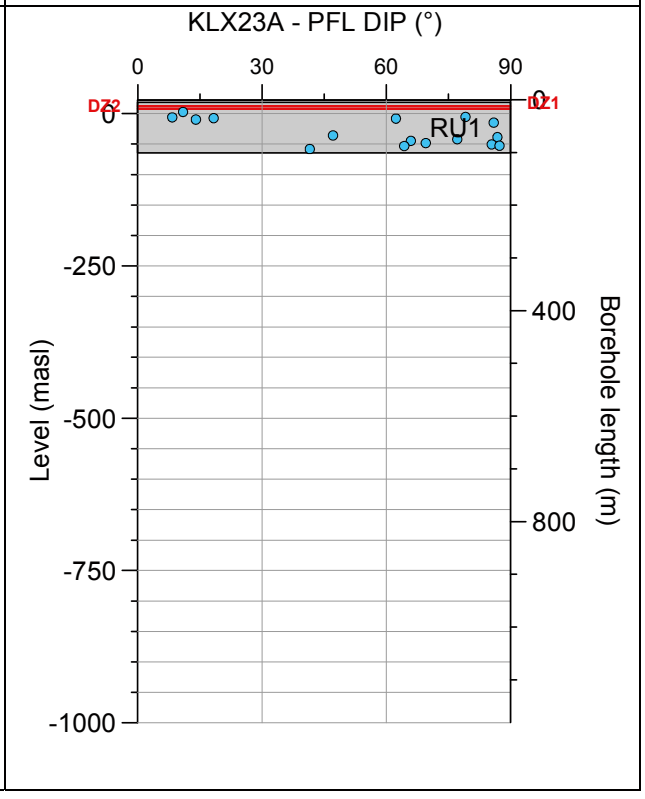

Comment:

Borehole KLX23A. Poles for PFL-f feature planes outside deformation zones (ESHI).

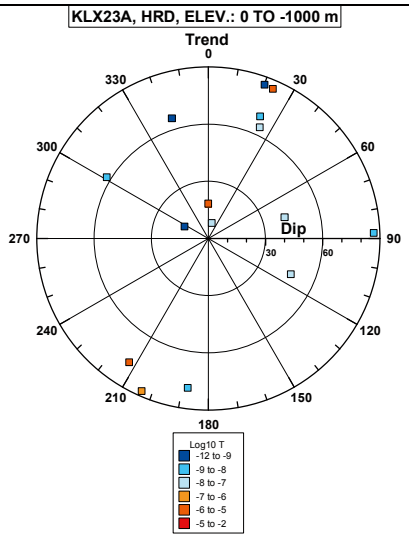

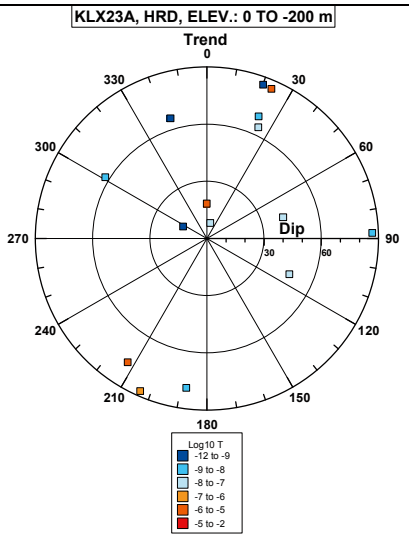

Borehole KLX23A. Poles for PFL-f feature planes in deformation zones (ESHI).

No interpreted deformation zones (ESHI) in the borehole.

Borehole KLX23B.

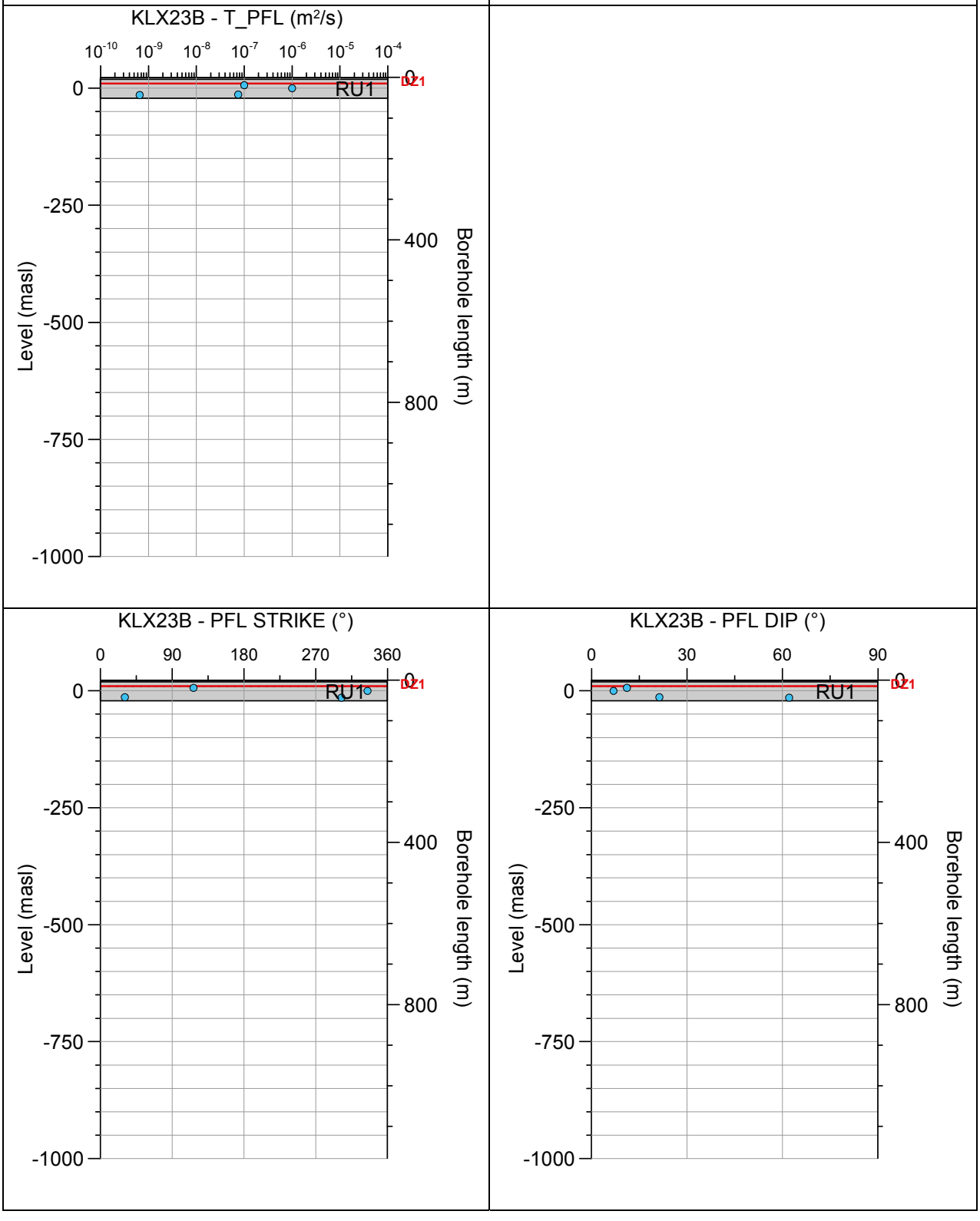

Comment:

Borehole KLX23B. Poles for PFL-f feature planes outside deformation zones (ESHI).

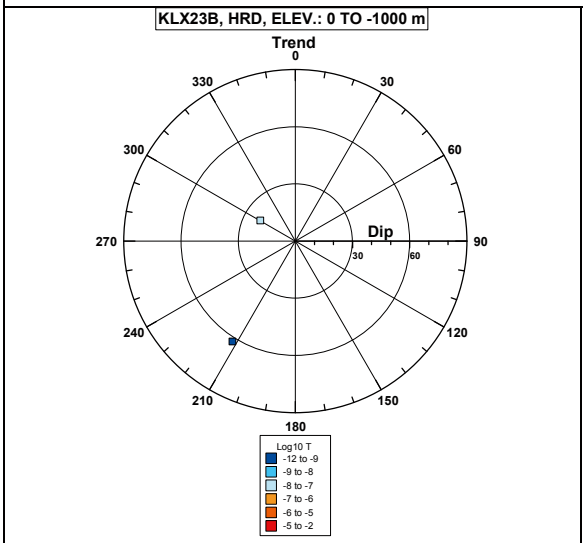

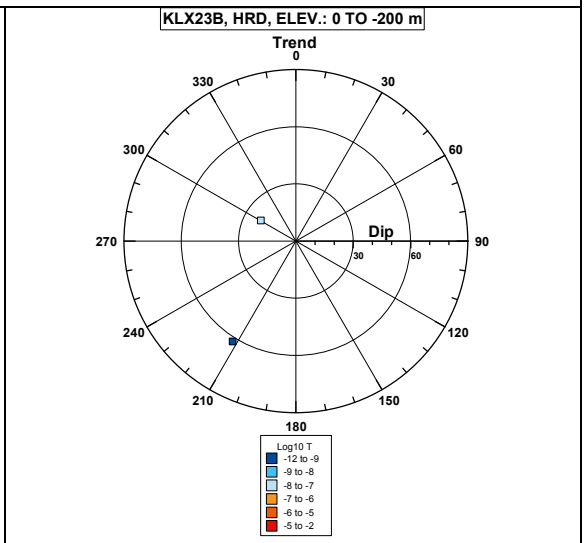

Borehole KLX23B. Poles for PFL-f feature planes in deformation zones (ESHI).

No interpreted deformation zones (ESHI) in the borehole.

Borehole KLX24A.

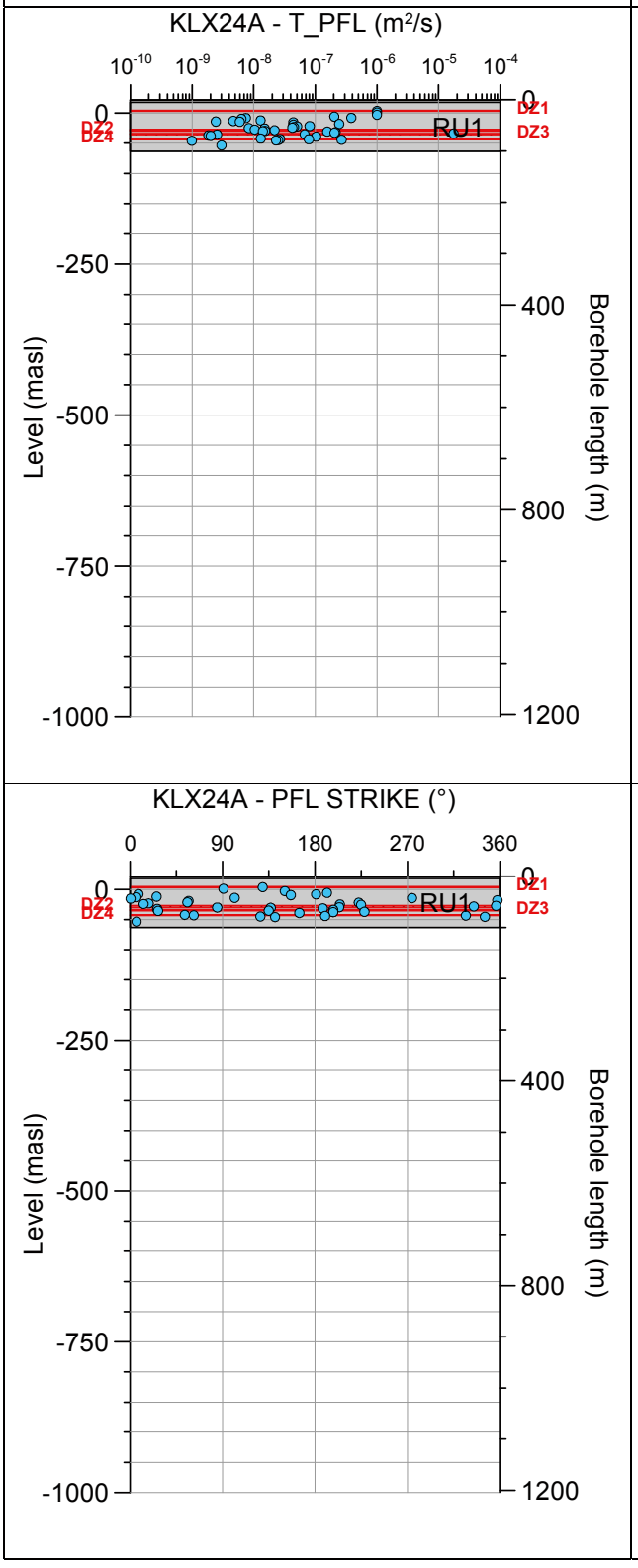

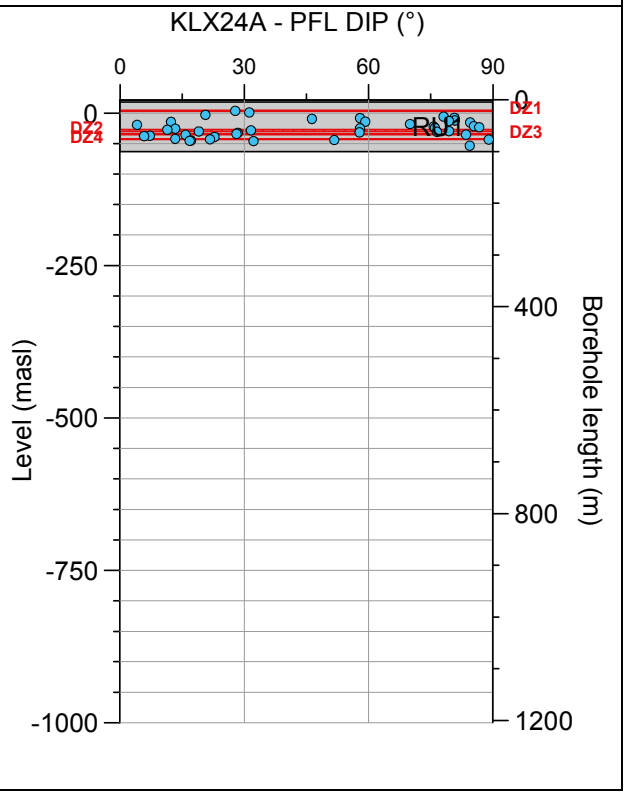

Comment:

Borehole KLX24A. Poles for PFL-f feature planes outside deformation zones (ESHI).

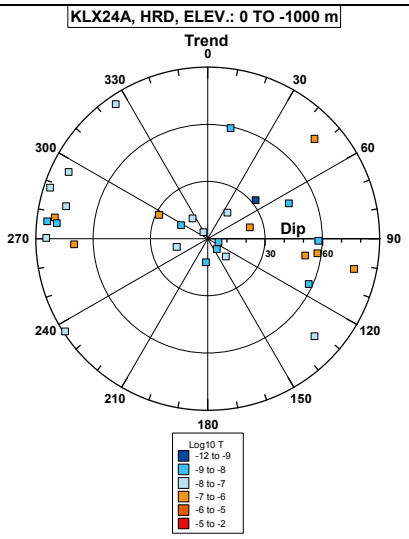

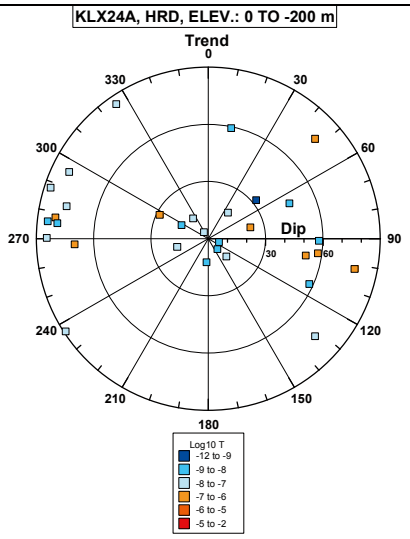

Borehole KLX24A. Poles for PFL-f feature planes in deformation zones (ESHI).

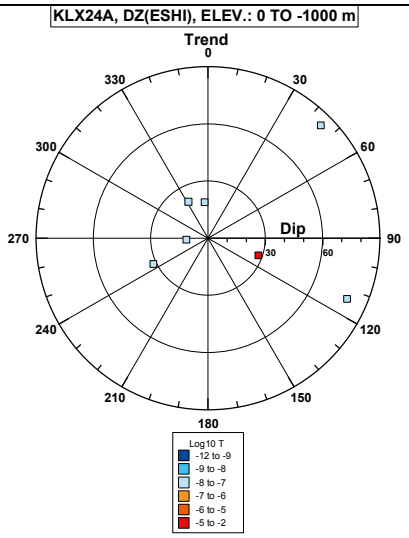

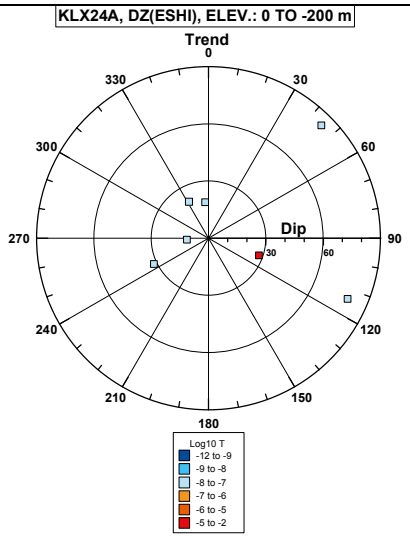

Borehole KLX25A.

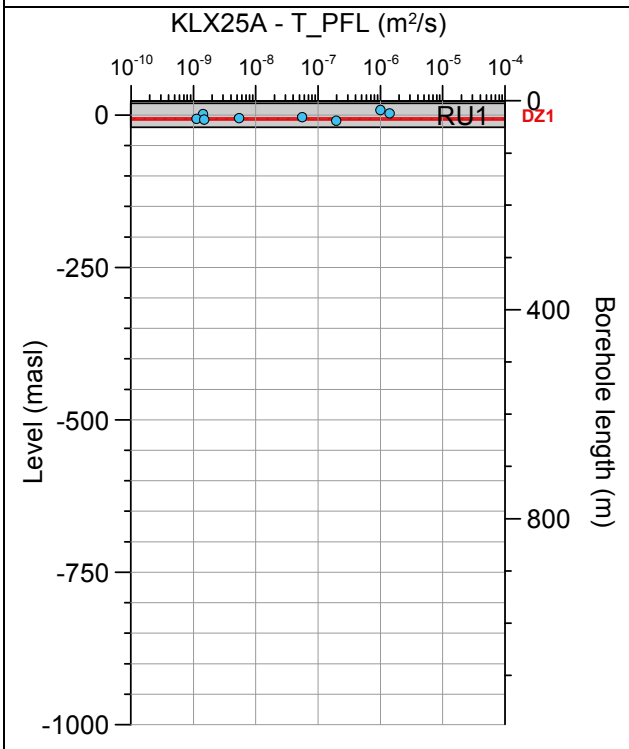

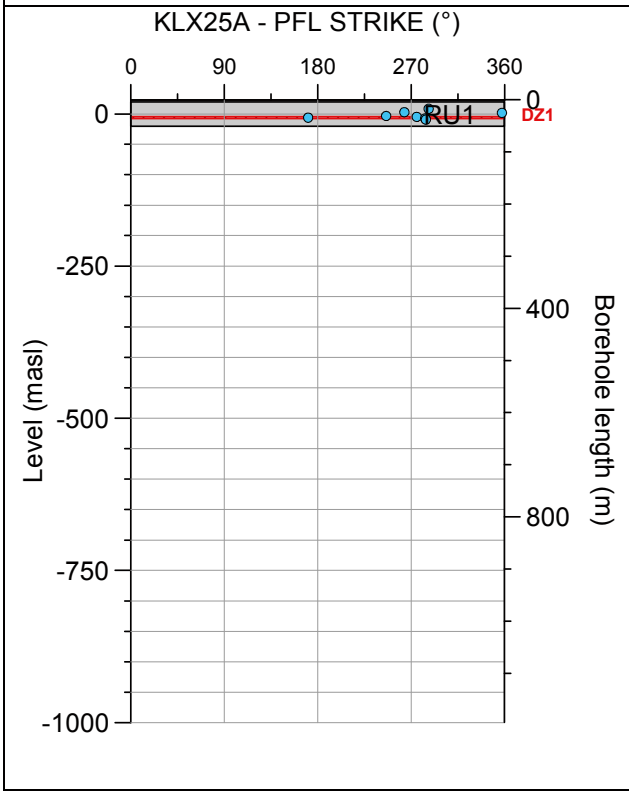

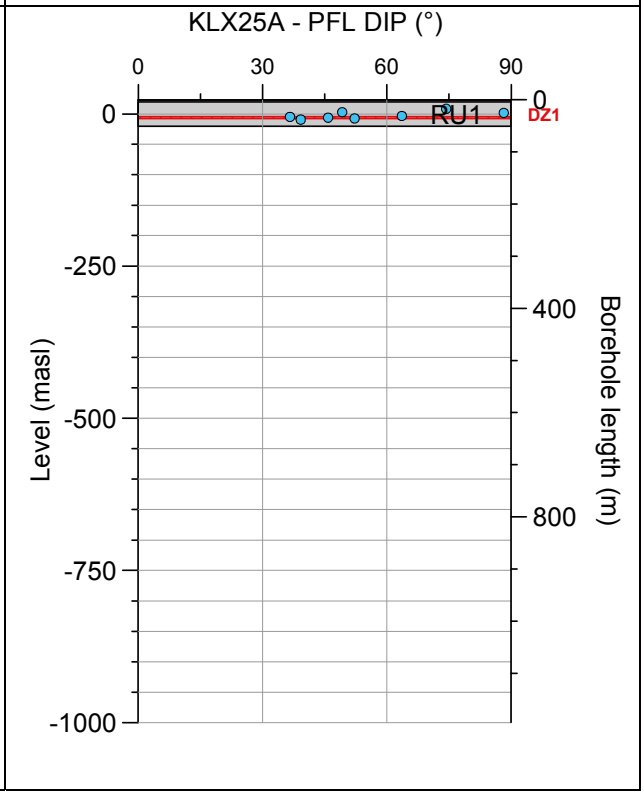

Comment:

Borehole KLX25A. Poles for PFL-f feature planes outside deformation zones (ESHI).

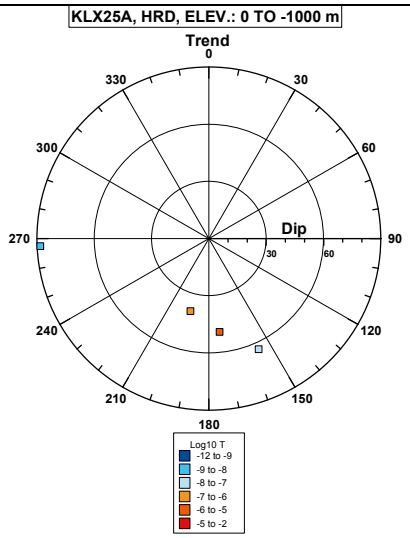

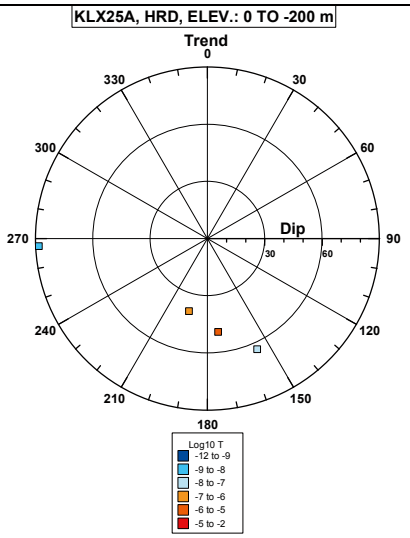

Borehole KLX25A. Poles for PFL-f feature planes in deformation zones (ESHI).

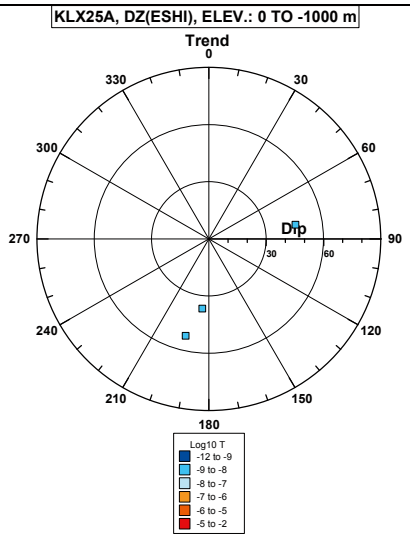

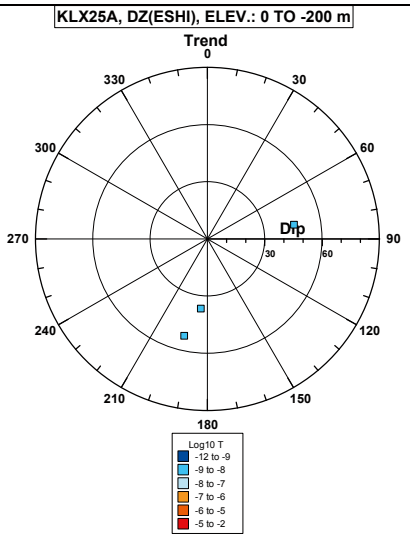

Borehole KLX26A.

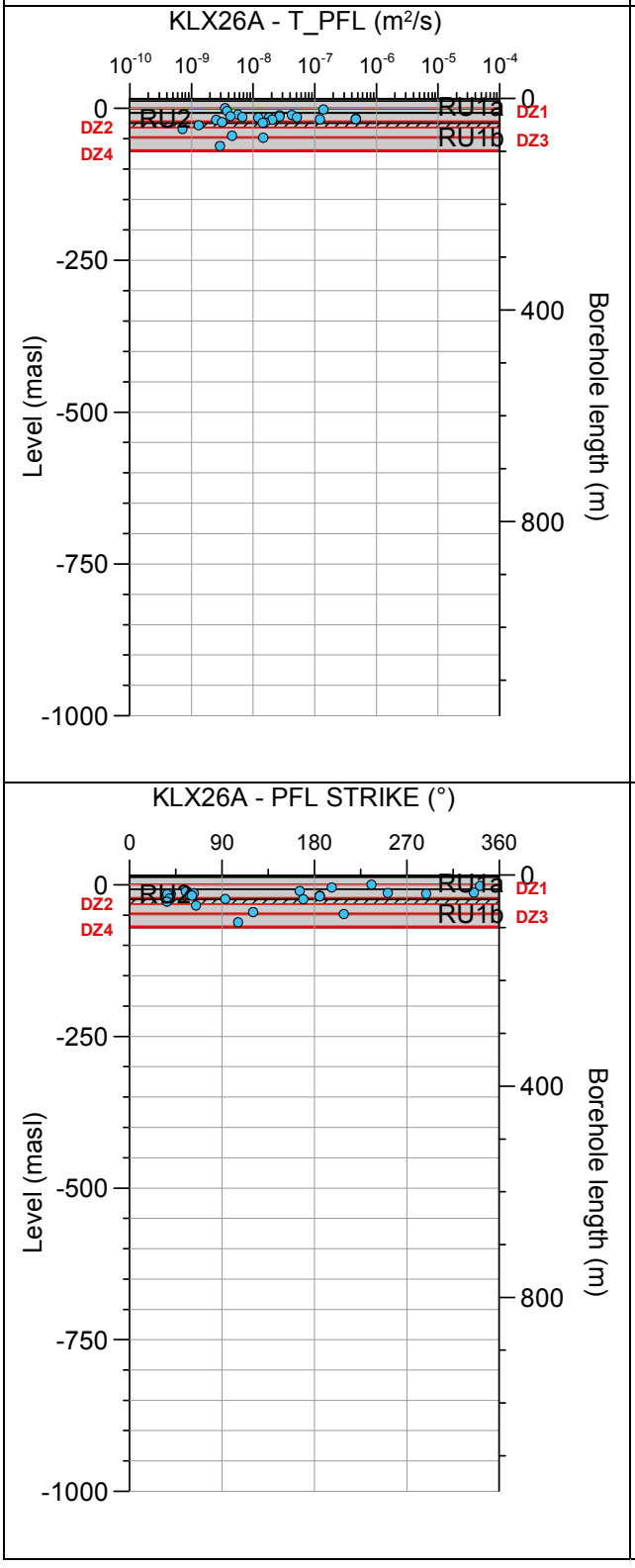

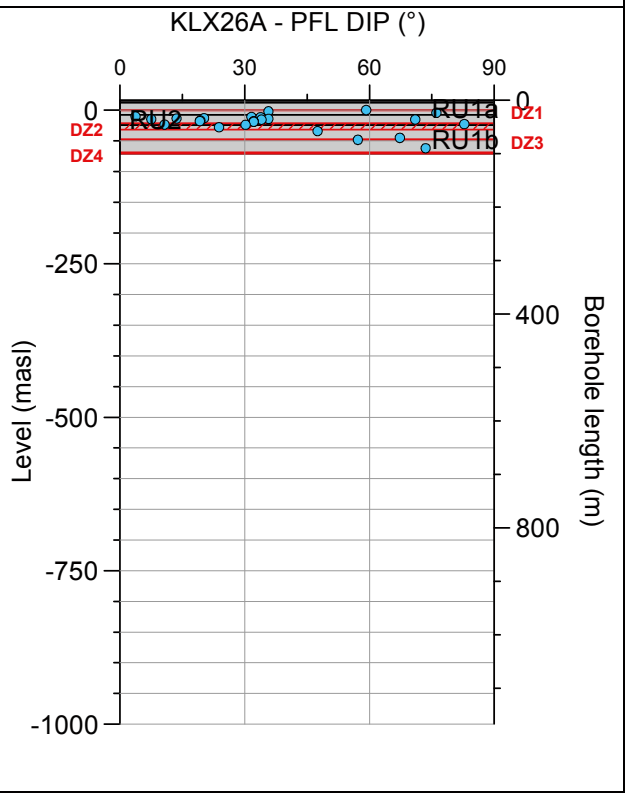

Comment:

Borehole KLX26A. Poles for PFL-f feature planes outside deformation zones (ESHI).

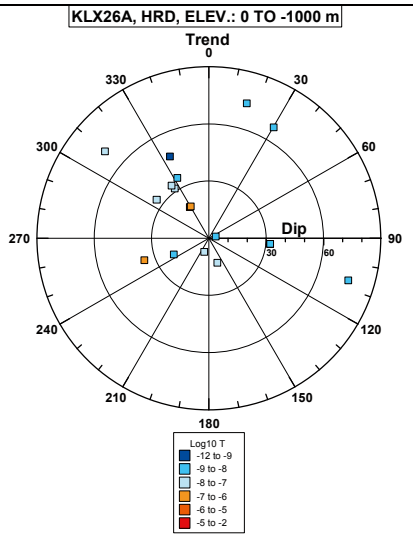

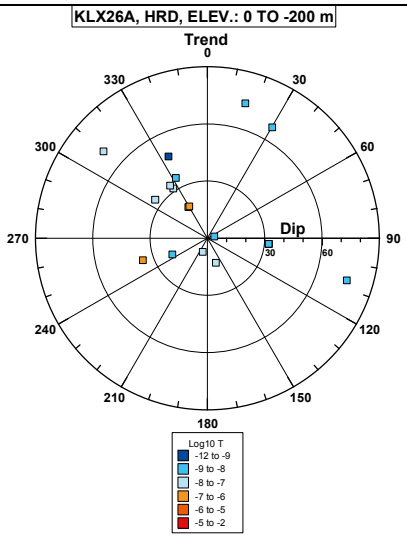

Borehole KLX26A. Poles for PFL-f feature planes in deformation zones (ESHI).

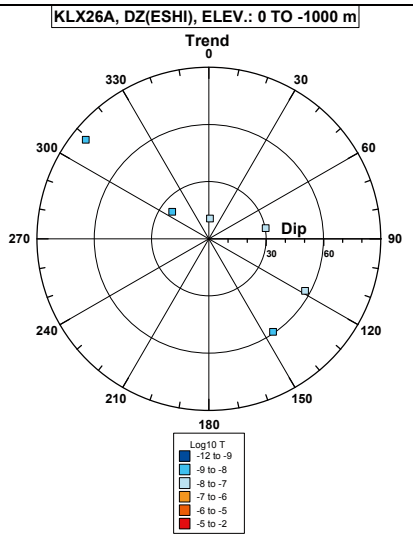

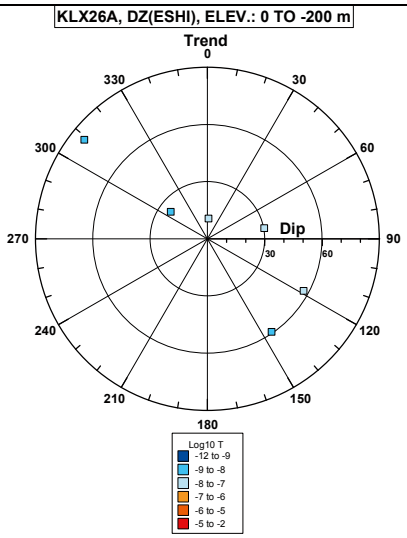

Borehole KLX26B.

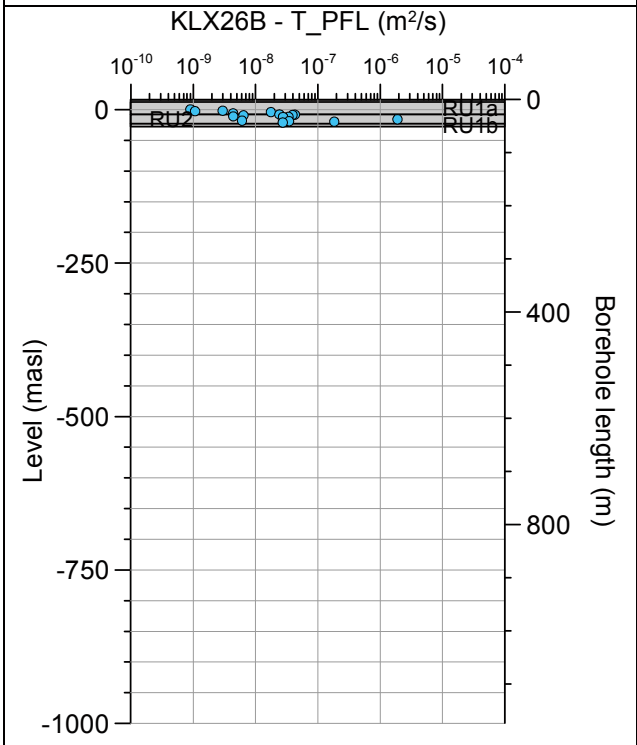

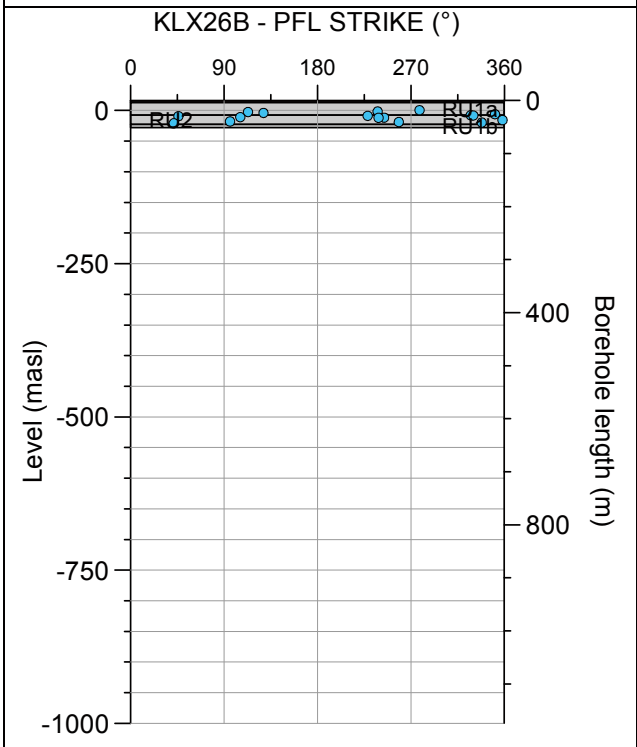

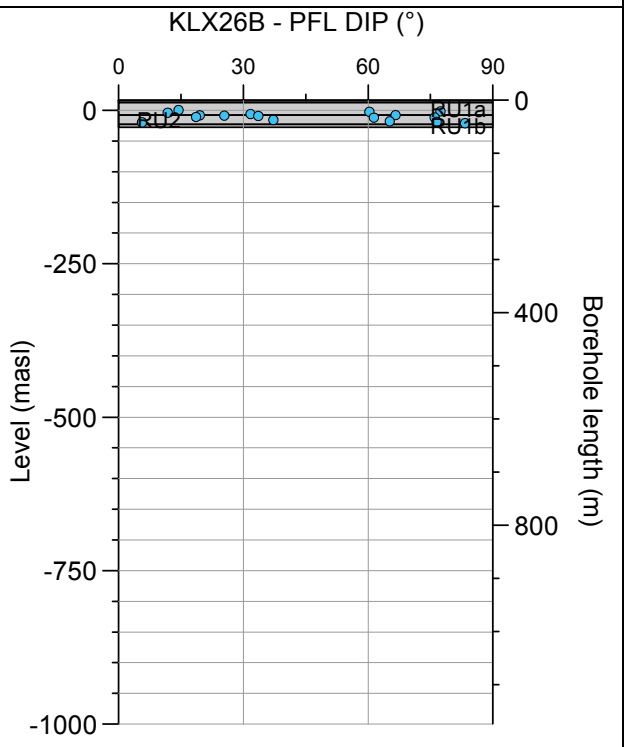

Comment:

Borehole KLX26B. Poles for PFL-f feature planes outside deformation zones (ESHI).

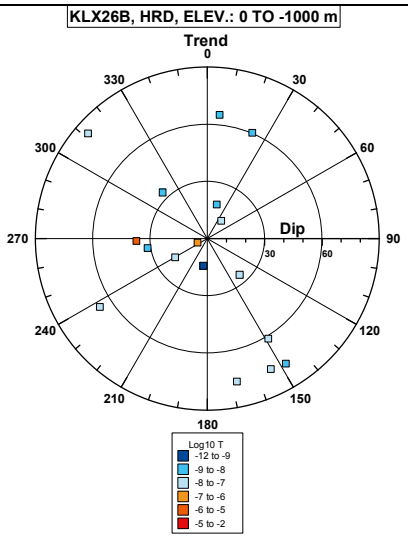

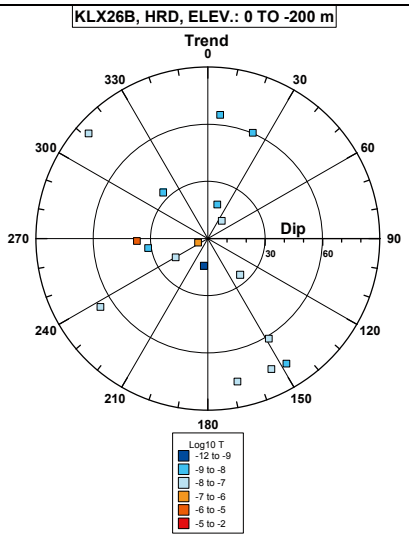

Borehole KLX26B. Poles for PFL-f feature planes in deformation zones (ESHI).

No interpreted deformation zones (ESHI) in the borehole.

Borehole KLX28A.

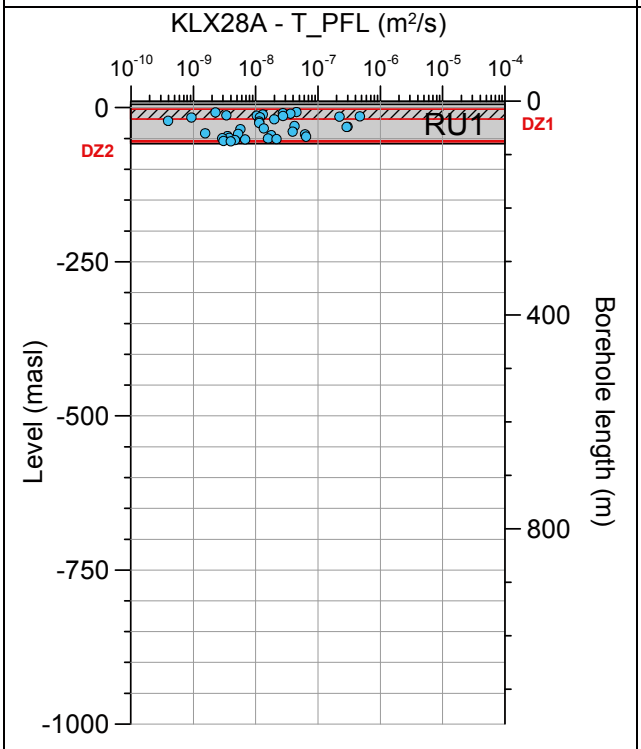

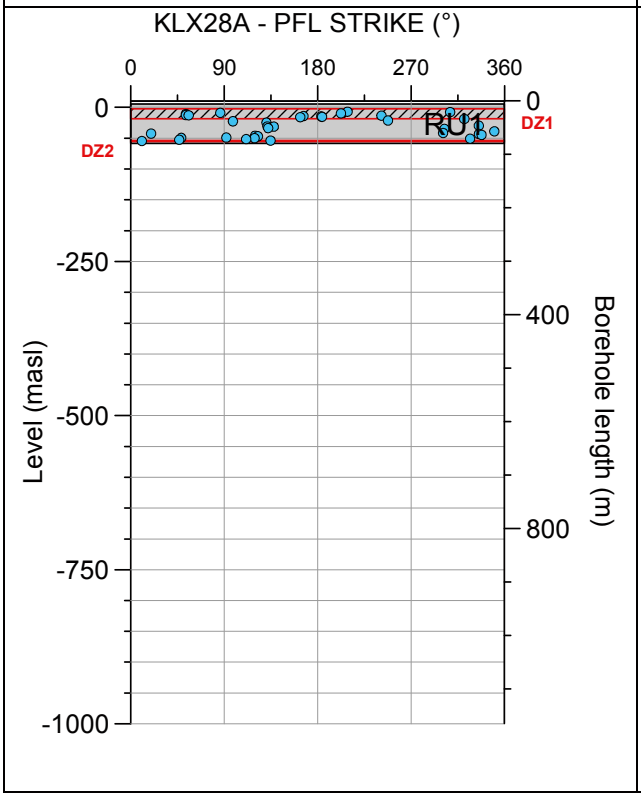

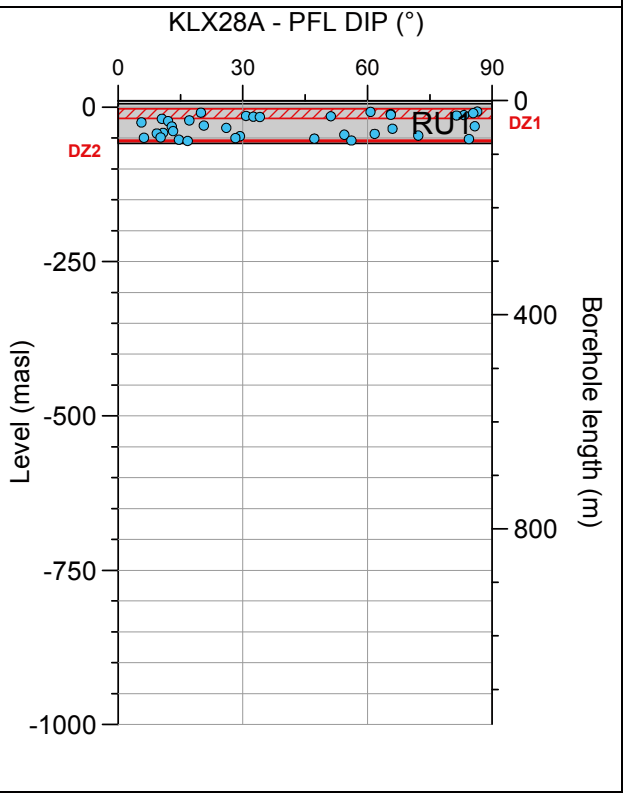

Comment:

Borehole KLX28A. Poles for PFL-f feature planes outside deformation zones (ESHI).

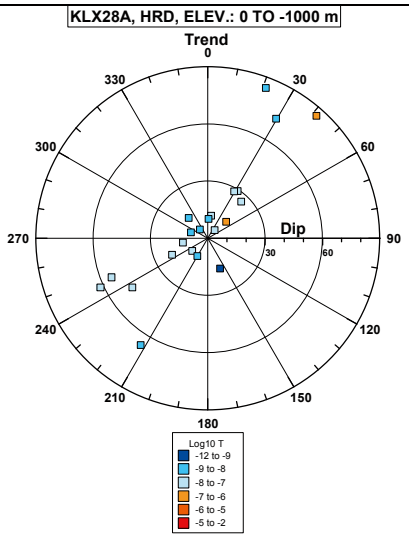

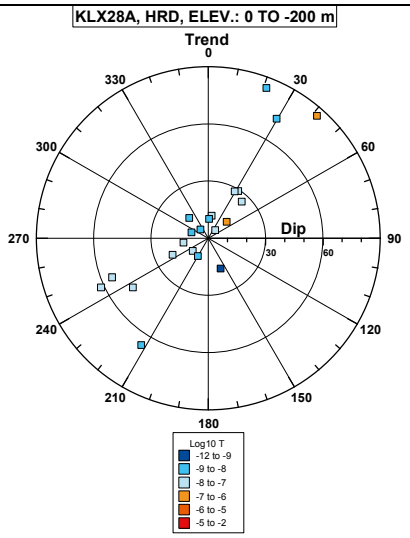

Borehole KLX28A. Poles for PFL-f feature planes in deformation zones (ESHI).

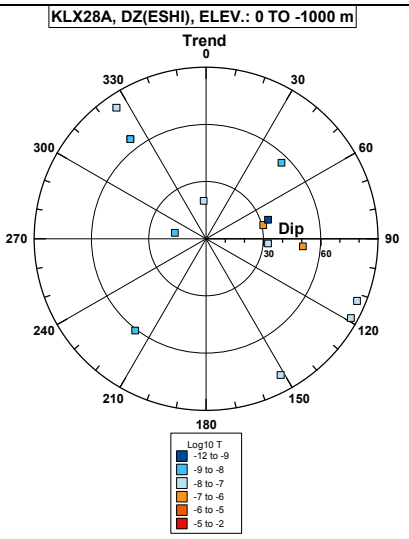

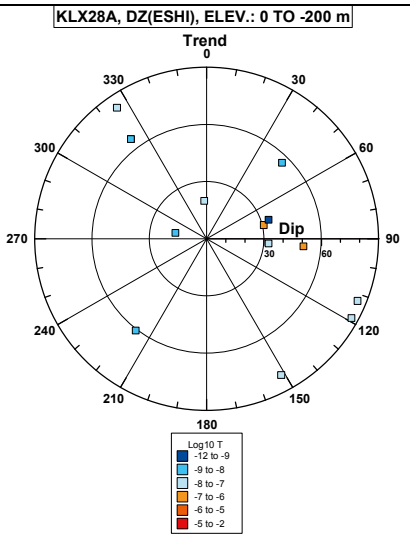

Borehole KLX29A.

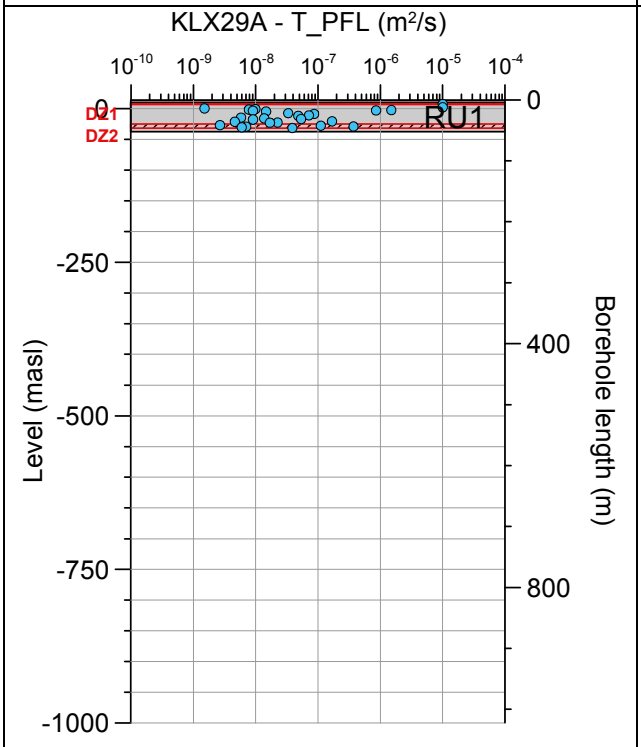

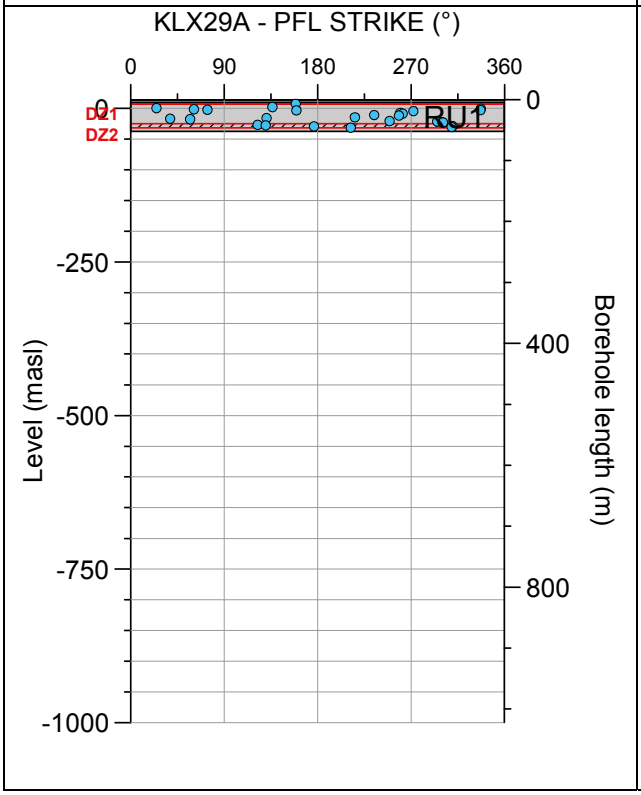

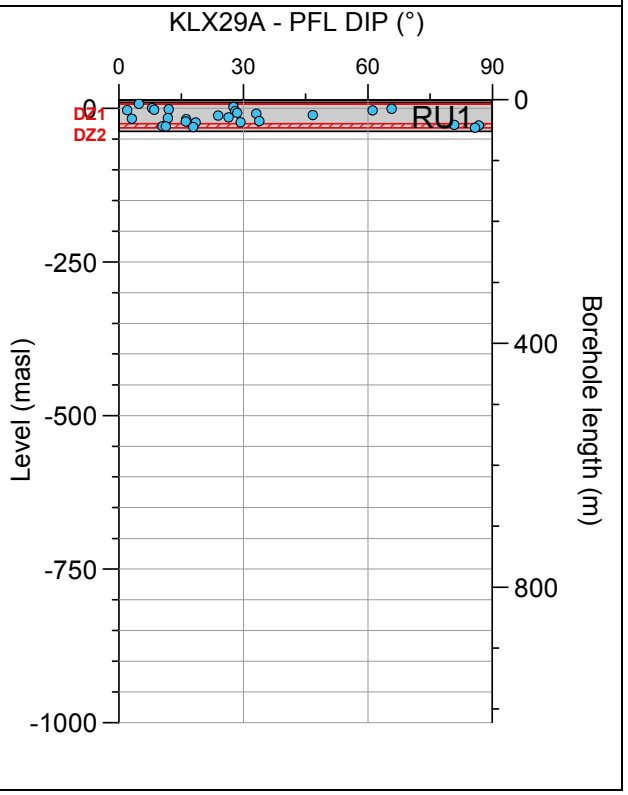

Comment:

Borehole KLX29A. Poles for PFL-f feature planes outside deformation zones (ESHI).

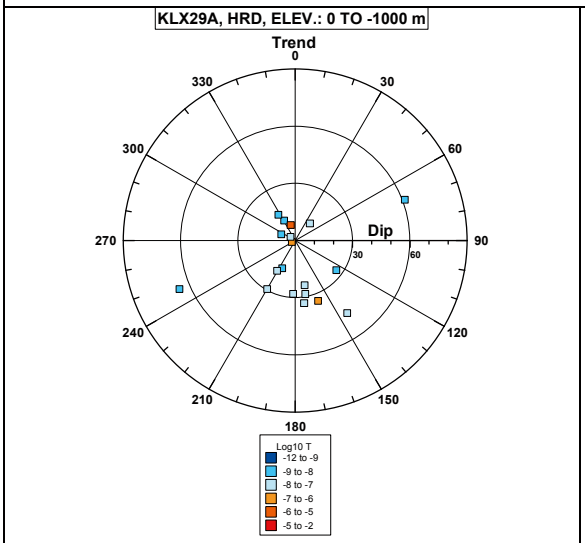

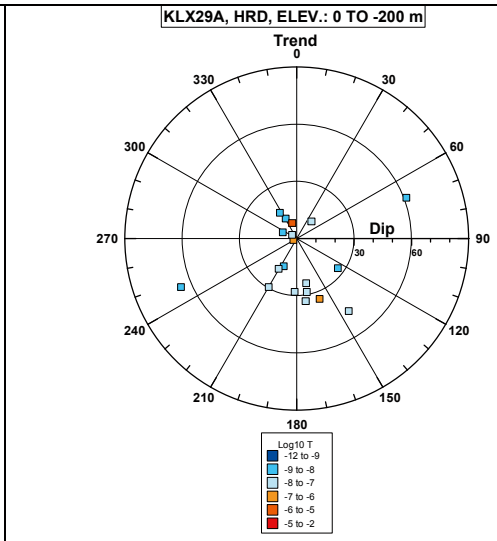

Borehole KLX29A. Poles for PFL-f feature planes in deformation zones (ESHI).